NAM

Report on the Second Workshop on Mmax for Seismic Hazard and Risk Analysis in the Groningen Gas Field

(Full Report)

13-17 June 2022

The Infinity Building, Amsterdam

General Introduction

In probabilistic seismic hazard and risk analyses, Mmax is the largest earthquake magnitude considered physically possible within a given seismic source. For hazard studies for natural seismicity, Mmax is generally found not to exert a very strong influence on the estimates of hazard estimates. However, for hazard assessments related to induced earthquakes, where the possibility of the largest potential events being only incrementally larger than the observed earthquakes must be considered, the impact of Mmax can be appreciable. Additionally, estimates of Mmax for induced seismicity can influence the perception of the risk associated with continuation of the industrial operations causing the earthquakes. For both natural and induced seismicity, estimates of Mmax always carry considerable epistemic uncertainty, hence these estimates are presented as distributions of possible values rather than unique values.

In light of these considerations, and the potentially controversial nature of Mmax estimates for Groningen, the NAM Hazard and Risk Analysis engaged an international panel of experts to determine a distribution of Mmax values based on all of the available information and a number of proponent models. The panel members were selected on the basis of experience and expertise is seismic hazard analysis (for natural and/or induced seismicity), the characterisation of induced seismicity, and the estimation of Mmax for seismic hazard analyses. This expert panel was chaired by Kevin Coppersmith and included Jon Ake, Hilmar Bungum, Torsten Dahm, Ian Main, Art McGarr, Ivan Wong and Bob Youngs. To inform the evaluation of the available data, methods and models by this expert panel, a workshop was organised in Amsterdam by NAM in March 2016. Over several days, experts presented data and measurements from the Groningen field and several presenters put forward proponent models for Mmax. Following the workshop presentations, the expert panel deliberated on the information presented and then proposed a distribution of Mmax values to be used in the ongoing seismic hazard and risk calculations.

Four years later, NAM organised a small meeting to review the additional information and modelling that had been conducted following the issue of the 2016 Mmax report, to determine whether there would be value in re-visiting the assessment of the maximum magnitude for the Groningen field. The conclusion was that there was sufficient new information available justify a second Mmax workshop. Happily, all eight members of the original expert panel agreed to participate in this new meeting and NAM began preparations for a workshop in Amsterdam in November 2020. Due to the Covid-19 pandemic, the event was postponed until October 2021, but then had to be postponed for a second time because of the coronavirus restrictions that were still in place. The workshop was finally held in Amsterdam in week 13-17 June 2022, with the participation of many Dutch and international experts who made presentations over the course of four days. Each participant in the workshop was given full access to an extensive database of geological, geophysical, seismological and operational data for the field. Following the 4-day workshop, the expert panel then met for a day to discuss the information presented and discussed, and then continued their evaluation remotely over the ensuing weeks.

The June 2022 workshop and the subsequent discussions within the expert panel have resulted in a new distribution of Mmax for Groningen earthquakes. The full details of the new distribution and its technical bases are explained in the panel's report. The distribution has moved to the left (i.e., to smaller magnitudes) with respect to the earlier evaluation by the panel in 2016, as illustrated in the figure below. The upper tail has been truncated and the probability of Mmax being no larger than **M** 5 has risen from 60% to 77%. The median Mmax estimate is now **M** ~4.5 and the weighted mean estimate of Mmax has decreased from **M** 5.0 to **M** 4.6.

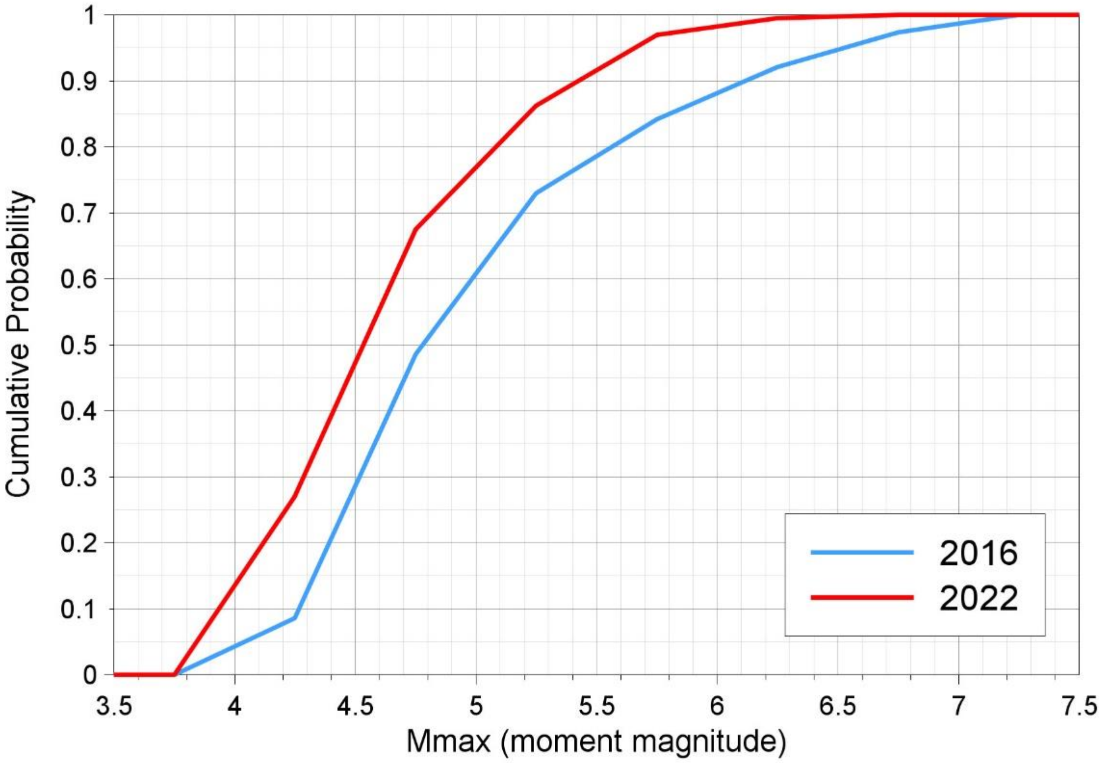

In following pages, we include the expert panel's report, the final workshop agenda, and list of participants, and all of the presentations delivered at the workshop. We express our sincere gratitude to the members of the expert panel for undertaking this important task, to all the workshop participants who contributed to this process, and to Steve Oates at Shell for compiling the databases that were shared with all workshop participants in preparation for the event.

We believe that the proposed distribution on Mmax should now be adopted in all future seismic hazard and risk analyses for the Groningen field. As always, it is important to understand these values as the probabilities associated with the appropriate upper bounds on earthquake magnitudes that could be reached—and *not* as probabilities of such events occurring.

The expert panel report makes a number of recommendations for additional work that could be undertaken to further refine the estimate of Mmax for Groningen, and it is strongly recommended that all of these be considered in ongoing work to quantify the induced seismic hazard and risk in the field.

Groningen Mmax Workshop II

Infinity Building, South Amsterdam, The Netherlands

13-17 June 2022.

Groningen Mmax Workshop II

13-17 June 2022, Infinity Building, South Amsterdam, The Netherlands

Background

For several years, NAM has been developing and refining a seismic hazard and risk model as part of the response to induced earthquakes occurring in the Groningen gas field. As part of these efforts, a workshop was conducted in March 2016 to address the question of the maximum earthquake magnitude, Mmax, that should be considered in the seismic hazard and risk modelling. An international panel of experts was appointed to make the assessment of Mmax for Groningen, informed by the presentations made at the workshop. In the time that has elapsed since the first Mmax workshop was conducted, considerable additional information has become available in the form of new data and new models, such that it is now considered worthwhile re-visiting the issue.

Objectives

The same expert panel, chaired by Kevin Coppersmith and comprising Jon Ake, Hilmar Bungum, Torsten Dahm, Ian Main, Art McGarr, Ivan Wong and Bob Youngs, has been reconvened, and a new workshop scheduled to take place in Amsterdam during the week 13-17 June 2022.

As in 2016, the purpose of the workshop is to inform the expert panel through a series of presentations, questions posed by the panel members and other participants, as well as the general discussion, all of which complements data and publications provided to all participants beforehand. The expert panel is charged with three specific tasks:

1. To clearly define the concept of Mmax in relation to seismicity in the Groningen field and for application in probabilistic seismic hazard and risk analyses.
2. To define a distribution of Mmax values and their associated probabilities, in the form of as discrete logic tree with alternative Mmax values and associated branch weights.
3. To clearly distinguish between induced earthquakes and triggered earthquakes in the formulation of the logic tree, such that the hazard and risk analyses could consider the two types of seismicity separately.
4. To determine if the proposed Mmax distribution compatible with the existing PSHRA framework for Groningen, including the V6 seismological model and the logic tree.

Roles and Responsibilities

The intention is to run the Workshop following the broad principles of the SSHAC (Senior Seismic Hazard Analysis Committee) guidelines for hazard assessment, following the current implementation guidelines (https://www.nrc.gov/reading-rm/doc-collections/nuregs/staff/sr2213/index.html). The Expert Panel effectively assume the role of the Technical Integration (TI) Team charged with objectively and impartially developing a logic-tree for Mmax that captures the centre, the body, and the range of technically defensible interpretations of the available data, methods, and models. The Expert Panel therefore collectively have intellectual ownership of the distribution of Mmax values implied by the final logic tree. Presenters at the workshop provide input to the Panel's deliberations either as Resource Experts, who impartially share data, observations, and analyses, or as Proponent Experts, who advocate for a specific model or interpretation. Some other participants may contribute to the process of technical challenge and defence through questions and discussions. Finally, there are observers, who will be able to watch the dynamics of the presentations and ensuing discussions both from a technical perspective and in terms of the process that is followed. A list of the participants is included at the end of this document.

Schedule and Organisation

The workshop will last for 4 days, following the agenda outlined below. The final day—Friday 17th June 2022—will be reserved for a closed meeting of the Expert Panel to have exploratory discussions and prepare the planning for the preparation of their report and final recommendations. The panel will be requested to subsequently provide detailed documentation explaining the reasoning behind the proposed values and associated weights on the Mmax logic-tree.

During the workshop, a space will be provided for the panel to hold break out meetings as needed, and the panel will also have the right to request additional information or clarifications from the participants and presenters when it is identified that such addenda will enrich their evaluations.

Monday 13th June: Intro/Groningen field/Tectonic Mmax/Induced and triggered earthquakes

Start	End	Speaker	Presentation
8:30	9:00	Julian Bommer	Welcome. Introductions. Background and objectives of workshop.
09:00	09:15	Ministerie EZK	Importance of Mmax for the Groningen seismic risk assessment
9:15	10:15	Clemens Visser	Geology of the field. Past, present and future gas production.
10:15	10:45		*Coffee break*
10:45	11:30	Rob van Eijs	Subsidence and compaction of the gas field
11:30	12:15	Bob Youngs	Definition & estimation of Mmax for tectonic earthquakes
12:15	13:15		*Lunch*
13:15	14:00	Helen Crowley	Mmax values for (tectonic) seismic hazard and risk in Europe
14:00	14:45	Matt Weingarten	Induced earthquakes related to gas production
14:45	15:15		*Coffee break*
15:15	16:30	Gillian Foulger	Induced & triggered earthquakes globally: larger events
16:30	17:00	All	General discussion

Tuesday 14th June: Groningen seismicity and fault ruptures

Start	End	Speaker	Presentation
8:30	9:15	Bernard Dost	History of seismic monitoring in the Groningen field
9:15	10:30	Steve Oates	Groningen earthquakes: focal depths and fault ruptures
10:30	11:00		*Coffee break*
11:00	11:45	Chris Spiers	Properties of Groningen reservoir and fault rocks
11:45	12:30	Rick Wentinck	Geomechanical model of fault rupture in the Groningen field
12:30	13:30		*Lunch*
13:30	14:45	Jean-P. Ampuero	Physics-based models of natural and induced seismicity
14:45	15:15		*Coffee break*
15:15	16:30	Mark Zoback	Crustal stresses and earthquake triggering
16:30	17:00	All	General discussion

Wednesday 15th June: Groningen event-size distribution & Statistical estimates of Mmax

Start	End	Speaker	Presentation
8:30	9:30	Stephen Bourne	Groningen seismological model and earthquake recurrence
9:30	10:15	Laura Gulia	Re-assessment of earthquake distribution for Groningen
10:15	10:45		*Coffee break*
10:45	11:30	Jean-Ph. Avouac	Recurrence model for Groningen earthquakes
11:30	12:15	Zak Varty	Recurrence model for Groningen earthquakes
12:15	13:15		*Lunch*
13:15	14:00	A Muntendam-Bos	Groningen induced event-size distribution
14:00	14:45	Sander Osinga	Taper from recurrence relationship to Mmax
14:45	15:15		*Coffee break*
15:15	16:30	Gert Zöller	Proponent assessment for Mmax in the Groningen field
16:30	17:15	Nepomuk Boitz	Proponent assessment for Mmax in the Groningen field
17:15	18:00	All	General discussion

Thursday 16th June: Proponent models for Mmax

Start	End	Speaker	Presentation
8:30	9:15	David Dempsey*	Proponent assessment for Mmax in the Groningen field
9:15	10:0	Andrzej Kijko*	Proponent assessment for Mmax in the Groningen field
10:00	10:30		*Coffee break*
10:30	11:15	Leo Eisner	Proponent assessment for Mmax in the Groningen field
11:15	12:00	Charles Vlek	Proponent assessment for Mmax in the Groningen field
12:00	13:00		*Lunch*
13:00	13:45	Stephen Bourne	Proponent assessment for Mmax in the Groningen field
13:45	14:45	Loes Buijze	Proponent assessment for Mmax in the Groningen field
14:45	15:15		*Coffee break*
15:15	15:45	Ylona van Dinther	DEEPnl research project on Mmax in the Groningen field
15:45	16:30	All	General discussion

* remote presentation

#	Name	Affiliation	Days
1	Jon Ake	Independent	Mon-Fri
2	Hilmar Bungum	Independent	Mon-Fri
3	Kevin Coppersmith	Coppersmith Consulting Inc.	Mon-Fri
4	Torsten Dham	GFZ-Potsdam	Mon-Fri
5	Ian Main	University of Edinburgh	Mon-Fri
6	Art McGarr	USGS	Mon-Fri
7	Ivan Wong	Lettis Consultants International	Mon-Fri
8	Bob Youngs	Wood Environment & Infrastructure	Mon-Fri
9	Jan van Elk	NAM	Mon-Fri
10	Dirk Doornhof	NAM	Mon-Thurs
11	Clemens Visser	NAM	Mon-Thurs
12	Rob van Eijs	NAM	Mon-Thurs
13	Bernard Dost	KNMI	Mon-Thurs
14	Stephen Bourne	Shell	Mon-Thurs
15	Steve Oates	Shell	Mon-Thurs
16	Mark Zoback	Stanford University	Mon-Thurs
17	Rick Wentinck	Independent consultant	Mon-Thurs
18	Chris Spiers	Utrecht University	Mon-Thurs
19	Laura Gulia	Independent consultant	Mon-Thurs
20	Helen Crowley	Independent consultant	Monday
21	Julian Bommer	Independent consultant	Mon-Thurs
22	Jean-Paul Ampuero	GEOAZUR	Mon-Thurs
23	Huihui Weng	GEOAZUR	Mon-Thurs
24	Jean-Philippe Avouac	Caltech	Mon-Thurs
25	Matteo Acosta	Caltech	Mon-Thurs
26	Zak Varty	Lancaster University	Mon-Thurs
27	Gillian Foulger	Durham University	Mon-Thurs
28	Matthew Weingarten	San Diego State University	Mon-Thurs
29	Gert Zöller	Potsdam University	Mon-Thurs
30	Loes Buijze	University Utrecht & TNO	Mon-Thurs
31	Serge Shapiro	Free University of Berlin	Mon-Thurs
32	Nepomuck Boitz	Free University of Berlin	Mon-Thurs
33	Leo Eisner	Seismik	Mon-Thurs
34	Charles Vlek	University of Groningen	Wed-Thurs
35	David Dempsey	University of Auckland	Thursday (remote)
36	Andrzej Kijko	University of Pretoria	Thursday (remote)
37	Annemarie Muntendam-Bos	SodM	Mon-Thurs
38	Niels Grobbe	SodM	Mon-Thurs
39	Jorien van der Wal	SodM	Mon-Thurs
40	Jaap Breunese	TNO	Mon-Thurs
41	Dirk Kraaijpoel	TNO	Mon-Thurs
42	Sander Osinga	TNO	Mon-Thurs
43	Frans Aben	TNO	Mon-Thurs
44	Bouko Vogelaar	TNO	Mon-Thurs
45	Maarten Pluymaekers	TNO	Mon-Thurs
46	Ylona van Dinther	Utrecht University	Wed-Thurs
47	Vincent van der Heiden	Utrecht University	Mon-Thurs
48	Pauline Kruiver	KNMI	Mon-Thurs
49	Karin van Thienen-Visser	Ministry of Economic Affairs and Climate	Mon-Thurs
50	Frank Wilschut	Ministry of Economic Affairs and Climate	Monday
51	Dirk Doornhof	Independent consultant	Mon-Thurs
52	Femke Vossepoel	TU Delft / KEM Panel	Tues-Wed
53	Ipo Ritsema	Deltares / KEM panel	Mon-Thurs
54	Iunio Iervolino	University of Naples / KEM panel	Mon-Thurs
55	Pierre-Yves Bard	University of Grenoble / KEM panel	Mon-Wed
56	Stefan Wiemer	SED, ETHZ / KEM panel	Mon-Tues
57	André Niemeijer	Utrecht University	Mon-Thurs

Second Report from the Expert Panel on Maximum Magnitude Estimates for Probabilistic Seismic Hazard and Risk Modelling in Groningen Gas Field

9 September 2022

Second Report from the Expert Panel on Maximum Magnitude Estimates for Probabilistic Seismic Hazard and Risk Modelling in Groningen Gas Field

9 September 2022

Introduction

This report describes the second assessment of maximum magnitude (Mmax) made by the Groningen Mmax Panel, which is charged with developing a distribution of Mmax for the Groningen gas field that is appropriate for use in a probabilistic seismic hazard analysis (PSHA) and subsequent probabilistic risk analyses (PRA). The first assessment by the Panel was made in 2016 (Groningen Mmax Panel, 2016) and the same Panel was reassembled to make another assessment in light of significant new data and information that have been developed for the project. To provide the Panel with the applicable new information, the Groningen Mmax Workshop II was held in Amsterdam on 13-17 June 2022. The agenda for that workshop and all presentation materials were provided to the Panel. The presentations and several supporting documents from the literature form the fundamental basis for the Panel's updated assessment. The members of the Panel offer their sincere appreciation for the presentations made at the workshop and for the efforts by the organizers to provide information to the Panel. In particular, the stellar work of Dr Julian Bommer in conducting, facilitating, and organizing the workshop is gratefully acknowledged.

The intended product and context for the assessment of Mmax is the same as it was during the first assessment in 2016. The definition of Mmax is in the context of its common use in seismic source characterization for PSHA. For example, as defined in USNRC (2012a, Chapter 11): Mmax is "*the largest earthquake that a seismic source is assessed to be capable of generating. The maximum magnitude is the upper bound to recurrence curves*." Mmax, as it is defined for PSHA and used here, is a time-independent upper bound. This assessment applies only to the seismicity interpreted to be caused by gas extraction from the Groningen field and is not intended to be an assessment for the maximum magnitude of naturally occurring tectonic earthquakes in the region. The Mmax is assessed as a time-independent parameter and is understood to describe an upper bound during the lifetime of a reservoir given the specific usage and production, in our case for Groningen. If the usage and production would change, another distribution for Mmax may need to be derived. The assessment of Mmax is a required input of all PSHAs. Such assessments are done routinely for purposes of engineering hazard analyses, risk analyses, and safety assessments.

This assessment of Mmax for the Groningen field is intended to capture the center, body, and range of technically defensible interpretations (CBR of TDI; see Section 3.1 of USNRC 2012b for explanation of this concept). This means that the Panel has focused on developing an Mmax distribution that includes epistemic uncertainties and is based on a consideration of tectonic and operational factors relating to the Groningen field, analyses of observed seismicity, earthquake physics, analogues, and experience in developing Mmax for PSHAs in other studies. We view our charge as not requiring statistical proof that our Mmax distribution is correct; rather, we are providing a technically-defensible distribution whose shape and limits reflect the Panel's knowledge and assessment of the uncertainties after due consideration of the available pertinent information. (See comments at the end of this document pertaining to the process followed by the Panel).

Note that the assessment, like all assessments for purposes of seismic hazard analysis, is intended to be a description of the <u>future</u> hazards. This assessment takes into consideration the features, events, and processes that have happened in the past (e.g., the locations, rates, and sizes of past earthquakes), but it is also takes account of processes or events that have not (yet) been observed at Groningen but have some chance of occurrence based on comparisons to analogous case histories. This is especially true for rare phenomena like Mmax that may not have been witnessed in the relatively short observational record.

The Panel would like to acknowledge and compliment the significant work done by and for the Groningen Mmax project since the 2016 workshop. The new data and analyses conducted during this period are useful in reducing uncertainties in key aspects pertaining to Mmax. These include: characteristics of the field, spatial and temporal distributions of seismicity, geodetic strain, better defined conceptual and rheological models, etc. The Panel is pleased to note that the new information and actions, on the whole, were consistent with the recommendations made in the Panel's 2016 report.

Logic Trees

The logic tree that expresses the Panel's updated assessment of Mmax for the Groningen field is given in Figure 1 and displays the key epistemic uncertainties. The first node of the logic tree expresses the two basic processes that describe the sources of potential future seismicity related to the Groningen field. The first branch indicates that the seismicity at Groningen is and will be related to induced seismicity alone; that is, related to the processes that are currently believed to occur because of the compaction of the reservoir due to withdrawal of gas. This seismicity is assumed to be localized to the region affected by the pore pressure reduction.

The second branch represents the occurrence of induced seismicity as well as seismicity that is triggered by the operations of the gas withdrawal. As in the 2016 report, the Panel adopts the terminology given in McGarr et al. (2002): "*As used here, the adjective 'induced' describes seismicity resulting from an activity that causes a stress change that is comparable in magnitude to the ambient shear stress acting on a fault to cause slip, whereas 'triggered' is used if the stress change is only a small fraction of the ambient level (e.g., Bossu, 1996; McGarr and Simpson, 1997)*." In contrast to induced earthquake activity, triggered seismicity includes earthquakes whose ruptures extend significantly beyond the region affected by the compaction associated with gas production. As indicated during the discussions at the workshop, it can be concluded that triggered seismicity has not been witnessed so far at Groningen, but the possibility of its occurrence cannot be eliminated based on the existing data.

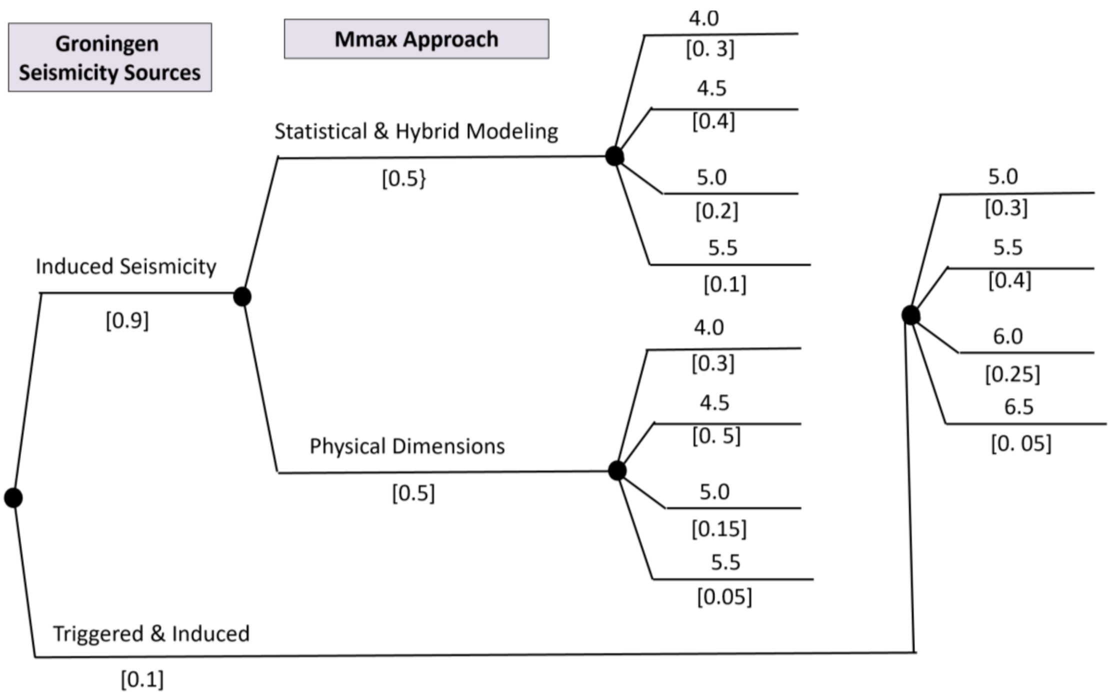

Figure 1. Logic tree showing the major elements of the assessment of Mmax for the Groningen field. Alternative branches are identified at each node and weights are assigned to each branch. The end point for each branch is the estimated maximum magnitude to the nearest half unit and its probability (in brackets).

The weights associated with the two branches of the first node of the logic tree are the following:

Induced	[0.9]
Triggered & induced	[0.1]

The weights reflect a strong belief that the future seismicity of the Groningen field area will occur as induced seismicity but with an acknowledgment that we cannot preclude the possibility that the future seismicity will include both induced and triggered components. The reasons for these weights are the following. There is abundant evidence that the current seismicity within the Groningen area is the result of gas extraction processes and associated compaction within the reservoir. For example, high-resolution earthquake hypocenters confirm that nearly all of the observed seismicity initiates within the reservoir horizon. Normal-faulting related to compaction in the reservoir units is identified based on earthquake focal mechanisms. Geodetic data confirm subsidence at the surface of several tens of centimeters as the reservoir is compacted and the spatial coincidence with such subsidence and the extraction region is clear. The data that have been collected in the past several years since the Panel last met, as presented and discussed at the workshop have led to a more highly resolved spatial and temporal picture of persistent induced seismicity. Thus, the Panel gives high weight to the notion that such activity will continue.

In contrast, the branch of the logic tree that represents the potential occurrence of both induced and triggered events is given low weight for several reasons. As already noted, there is reasonable evidence that the current observed seismicity does not include earthquakes that would readily be considered as triggered events, although the period of observation (five or six decades) is relatively short. Triggered events are commonly associated with locations or regions characterized by the presence of more active tectonics as shown, for example, by the presence of Quaternary faults, deformation related to active faults or tectonic background seismicity. Such is not the case in the Groningen region, which lies within what is considered to be a stable continental region (SCR) well away from plate boundaries and observed Quaternary deformation. Although faults and evidence of ancient fault movements lie within the Carboniferous units beneath the reservoir and in nearby regions away from the reservoir, there is no evidence from seismicity or other tectonic indicators that these units display evidence of near-critical stresses that would be susceptible to triggering by the operations of the gas field. In fact, the historical record of seismicity that predates the presence of the gas extraction operation is remarkably quiescent. For example, the only event in the region found in the European historical catalogue spanning the period 1000-1899 (*https://emidius.eu/epica/*) is an event dated October 27, 1225, which is indicated without specific location from only one source in the chronicle of the monastery of Witterwierum. Given this information, the Panel regards the basis for the 1225 "event" being an earthquake as equivocal.

Despite the abundant evidence that triggered events are likely not included in the current catalogue of events in the Groningen region and that evidence does not appear to be present for critical stresses within the Carboniferous units beneath the reservoir (inferred not from *in situ* measurements but rather from absence of documented rupture initiations), the Panel finds that the potential for triggering cannot be definitively ruled out. Gas extraction fields worldwide have arguably given rise to triggered seismicity, so this possibility should be considered. As a result, the potential for triggered seismicity as well as induced seismicity is included in the logic tree with a low weight.

The second node of the logic tree expresses the uncertainty in the approach to be taken to assess Mmax, given that induced seismicity is the mechanism for future earthquakes in the region. The two alternative approaches and their weights are the following:

Statistical and hybrid modeling	[0.5]
Physical dimensions	[0.5]

Statistical modeling of observed seismicity is a major activity that has been employed using the Groningen seismicity catalogue and was the subject of several presentations at the workshop. Hybrid modeling incorporates data related to stresses within the reservoir and uses accepted failure criteria, such as Coulomb failure criteria or frictional constitutive relations (e.g. rate-state), with physical modeling of stresses within the reservoir and simulations to predict the spatial and temporal characteristics of seismicity that would be expected. This includes modeling focused on the maximum magnitudes of forecast seismicity. As shown in the presentations at the workshop, such modeling is typically calibrated and verified by comparisons to seismicity models. We call these approaches “hybrid” and include them together with purely statistical approaches in the logic tree. The hybrid models are those that consider scenarios where earthquakes sizes may grow significantly larger than the field dimensions of the reservoir under production.

The seismicity and hybrid modeling approaches were discussed extensively at the workshop and various magnitude assessments were provided that incorporate the observed seismicity over the period of observation of the reservoir—generally in the period from about 1991 to the present. For instance, presentations by Buijze et al., Ampuero et al. and van Dinther et al. used physics-based models and numerical simulations to simulate rupture scenarios for different settings. Estimates of maximal magnitudes, if presented, are in the range of moment magnitude **M** 4.1 and 4.6. However, complex rupture geometries due to interaction of faults and possible jumps of slip between faults were not yet considered, which could lead to magnitude estimates that are somewhat larger. Based on the range of results from these models and taking account of the relatively short period of seismicity observation, the Panel arrived at a distribution of Mmax for the statistical and hybrid modeling branch shown in the logic tree in Figure 1.

An alternative approach to assessing Mmax, given the induced seismicity branch, is the consideration of the dimensions of ruptures that might occur within the reservoir. This approach considers the maximum dimensions, in terms of length and width, that fault ruptures postulated to occur within the reservoir might have. The approach uses the current knowledge of the structure of the reservoir, the spatial patterns of observed seismicity (e.g., whether or not the seismicity exists beneath the reservoir in the Carboniferous units or above the reservoir in the Zechstein units), as well as the locations, patterns, and mechanisms of mapped faults within the reservoir. From these data, dimensions of possible ruptures are estimated and they, in turn, are used to estimate the associated magnitudes. For example, Stephen Bourne presented an assessment of the maximum possible fault rupture widths that might be credible given the available data and argued that empirical scaling relationships between rupture width and magnitude could be used to assess Mmax for earthquakes occurring within the repository. Rupture dimensions has been used for many years to assess Mmax for fault sources and a wide array of empirical scaling relationships exist in the literature for this purpose.

The physical dimensions branch of the logic tree includes a consideration of physical constraints on the stress perturbation induced by the reservoir usage together with rheological models and existing fault structures. During the Groningen Mmax Panel 2016 workshop the argument was discussed that the total strain energy that may build-up during the life-time of field production may be released in a single event – a scenario that is highly unlikely and questionable. At the 2022 workshop, the presentations by van Eijs et al. (day 1) and Spiers et al. (day 2) presented new results for Groningen showing that only 30-60% of the built-up deformation is elastically stored. Moreover, the stored elastic energy is released by a population of earthquakes that follow a frequency-magnitude distribution, not just by a single event. Therefore, the simplistic approach of relating the total volume change to Mmax is not considered further in this assessment. Instead, to develop the distribution, the Panel considered the potential dimensions of ruptures that might occur within the reservoir as constrained by the thickness of the reservoir, the style of faulting, possible lengths of ruptures that would initiate within the reservoir and not extend significantly outside of it. This could also involve complex ruptures or uncommon aspect ratio and rupture geometries, as partly observed for induced seismicity. An example of a complex or uncommon induced event rupture is, among others, the Ekofisk oil field Mw 4.4 rupture (for example, Dahm et al., 2015), or the Mw 5.5 Pohang (Grigoli et al 2018) or the Mw 5.1 Fairfield Oklahoma earthquake (see e.g., Lopez-Comino and Cesca, 2018).

The Panel then considered possible scaling relationships that would be applicable, such as rupture length, width, and area for normal faulting (Thingbaijam et al., 2017; Leonard, 2014 for SCR and dip slip faulting) and the magnitudes that would be calculated for the given rupture dimensions. These explorations suggest that magnitudes as large as **M** 5 to 5.5 are possible, but they would require very unusual rupture shapes with high length to width aspect ratios. Thus, the weights assigned to **M** 5 and to 5.5 for the induced rupture dimensions branch are very low but they are not zero.

The Panel considered the statistical/hybrid and rupture dimensions approaches as potential means of assessing Mmax in the induced seismicity branch, and concluded that they should be assigned equal weight. Based on the presentations at the workshop, it is apparent that the statistical and hybrid modeling approaches have been and are currently the focus of many of the studies of Groningen seismicity, but the use of rupture dimensions to constrain maximum magnitudes also covers plausible scenarios of earthquakes not included in the catalogue of observed earthquakes. Given the value of both approaches, the Panel concluded that they should be equally weighted in the logic tree for Mmax.

The Mmax distribution assessed by the Panel for the case where both induced and triggered seismicity are assumed to occur is shown in the logic tree (Figure 1). The two fundamental concepts used in assessing Mmax for this branch were the dimensions of rupture that might be applicable if seismicity was not constrained to the reservoir and appropriate analogues to the Groningen gas field and their associated observed earthquakes.

The Panel considered the possibility that triggering processes might also entail the triggering of faults within the Carboniferous units beneath the reservoir and/or structures that would extend beyond the strict margins of the reservoir into the aquifer areas and perhaps beyond. These possibilities would, obviously, lead to larger rupture dimensions than ruptures confined to the reservoir itself.

The consideration of appropriate analogues to the Groningen gas field is an important activity and must be carefully done. In general, the Panel found that the Groningen-specific data and information—particularly that gathered since the last workshop—were very useful in defining the important attributes of the field and, in turn, in defining the criteria that must be fulfilled in order to be considered an appropriate analogue. For example, identified aspects of the Groningen gas field to be considered in drawing analogies to other fields are the following:

- Gas extraction only, no injection
- Stable continental region tectonically
- Essentially no seismicity pre-operation, suggesting low tectonic stresses
- Normal faulting regime
- No Quaternary active faults in reservoir or in nearby region affected by the stress perturbation
- Observed seismicity confined to reservoir

Given these attributes and reviewing the updated information on possible analogues in the database, there are very few, if any, close analogues that would allow for a high degree of confidence in their use in the Panel's Mmax assessment. This is especially true for the case where the Groningen seismicity source is assessed to be induced only and even the case where triggering is assumed to occur.

The characteristics of the Groningen field are in many respects unique and, as a result, the use of some of the well-known possibly triggered earthquakes such as those at Gazli was found by the Panel to be inappropriate. This is because their use would violate so many of the criteria given above to draw meaningful and defensible analogies such that the earthquake magnitudes at the locations could be confidently "imported" to the Groningen field to help populate the Mmax distribution. Disregarding the clearly indefensible cases, the consideration of analogues did expand the Mmax distribution to include some larger triggered events and these are reflected in the distribution. For instance, the maximal observed magnitude at the Lacq gas field was **M** 4.2, the maximal magnitude of **M** 4.4 (e.g. Dahm et al., 2007) of the Rotenburg/Söhlingen/Völkerson gas fields in North Germany, which occurred in a similar tectonic setting and Rotliegend reservoir formation. In general, there are only a few case histories that might offer some support for triggered earthquakes associated with gas extraction.

Mmax Distributions

Given the approaches and assessments in the logic tree, various estimates of Mmax were developed by the Panel, as shown in Figure 1. The directly assessed conditional Mmax distributions in the logic trees are discussed in this section as well as the total or unconditional Mmax distribution across the entire logic tree.

Groningen Seismicity Source Alternatives

Although the branches of the logic tree have very different weights, the conditional Mmax distributions (conditioned as having a weight of 1.0 for each branch) can be compared for the two models of seismicity for Groningen, as shown in Figure 2. The Mmax distributions overlap at about **M** 5 but are otherwise quite different. The induced seismicity model leads to lower Mmax values because the approaches used are very specific to the Groningen field and generally do not include scenarios that would entail magnitudes much larger than are modeled using observed seismicity or rupture dimensions that extend beyond the immediate reservoir. In contrast, the triggered branch includes the consideration of earthquake ruptures that extend beyond the immediate field as well as the consideration of analogues in other regions that include the possibility of triggered earthquakes.

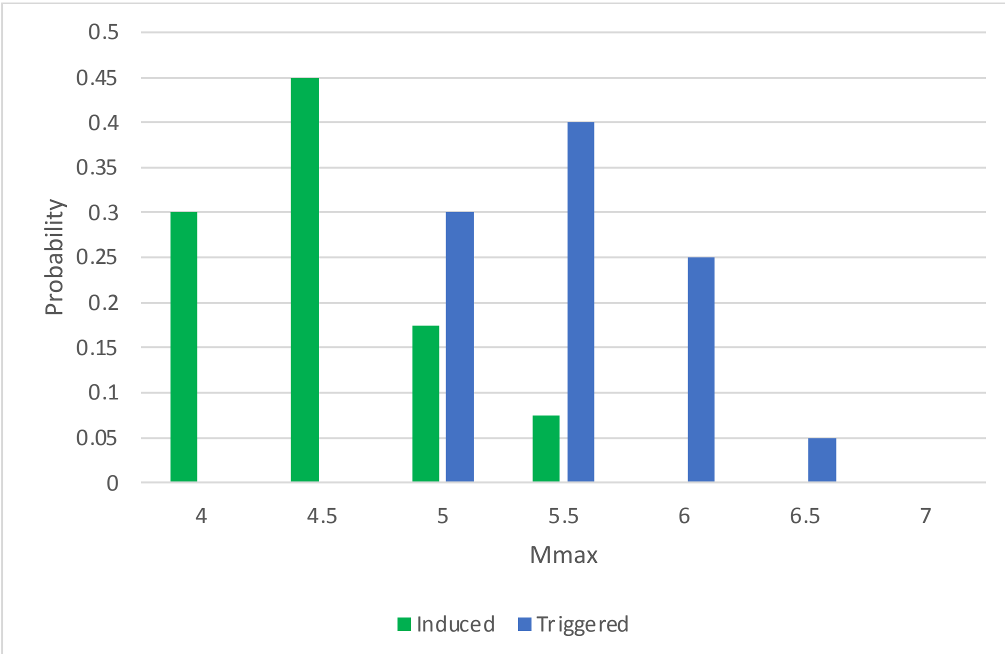

Figure 2. Conditional probability distribution for Mmax for the two models of Groningen seismicity: "induced seismicity only" (green) and "triggered and induced seismicity" (blue). The conditional distributions are normalized to a weight of 1.0 for each model for ease of comparison.

Mmax Approach, Given Induced Seismicity

As discussed above, the Panel made direct assessments of the Mmax distributions that express the epistemic uncertainties in the Mmax approach taken, given the induced seismicity branch of the logic tree. The resulting conditional Mmax distributions for the two branches are shown as probability distributions in Figure 3. Somewhat surprisingly, the Mmax distributions for the two approaches to characterizing the induced seismicity Mmax are very similar even though they are based on very different conceptual models and employ different types of data.

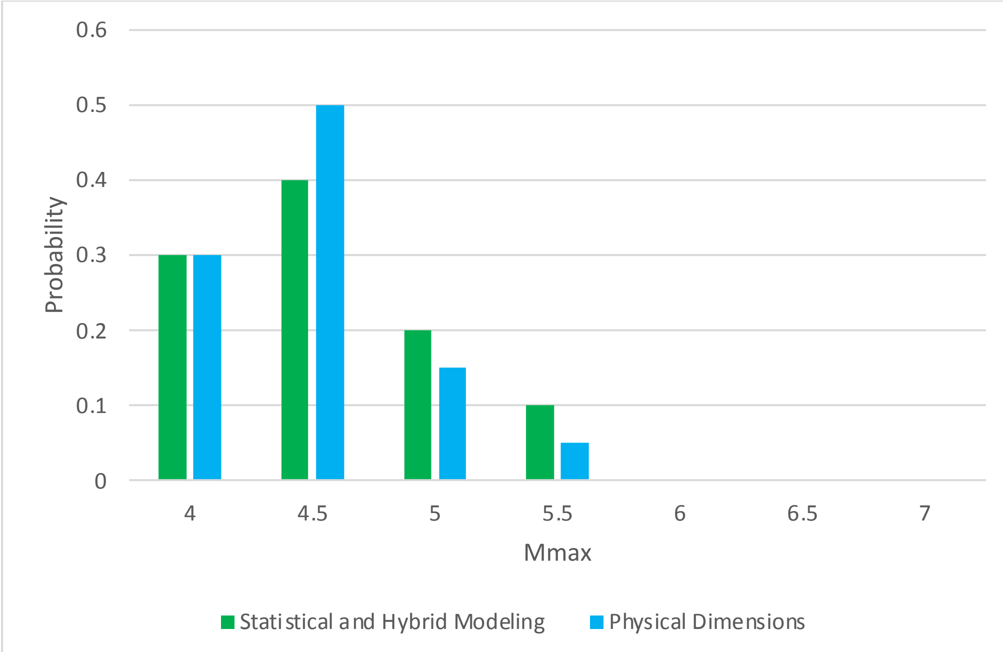

Figure 3. Conditional probability distribution of the Mmax distribution for the Groningen seismicity for the combined statistical and hybrid modelling approach (green) or the physical dimensions approach (blue), after normalising each to a total probability of 1.0.

Unconditional Mmax Distribution

In addition to the Mmax distributions assessed directly by the Panel, the logic trees and associated weights on the branches allow for calculation of the total (unconditional) Mmax distribution across all of the elements of the logic tree. That Mmax distribution is shown in Figure 4 and is compared to the Mmax distribution developed by the Panel in 2016.

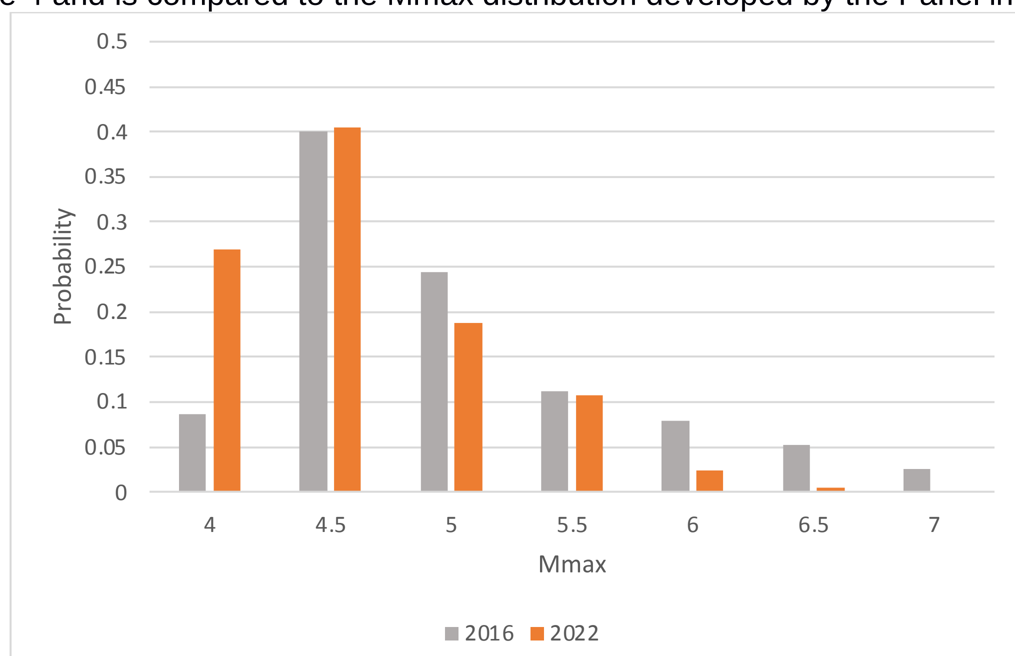

Figure 4. Probability distribution for Mmax for the Groningen seismicity source integrated across all elements of the logic tree. Shown is the distribution for the current study (orange) as well as the distribution for the 2016 study (grey).

As can be seen, the Mmax distribution spans a range of magnitudes from **M** 4.0 to 6.5, with the bulk of the probability mass in the range of **M** 4.0 to 5.0. In comparison to the 2016 distribution, there is considerably more weight at the **M** 4.0 level. This is largely because the magnitude assessments using modeling of the observed seismicity and evidence for ruptures to be confined to the reservoir are given more credibility than they were in 2016 due to the improved data and understanding of the reservoir. Another significant difference lies at the larger magnitudes of **M** 6.0 to 7.0. The consideration of appropriate analogues as well as the better understanding of the Groningen characteristics led to the rejection of analogues that were not judged to be defensible. Thus, in general, the new data and studies conducted over the past six years have led to a reduction in the uncertainties and this is reflected in the Mmax distribution itself.

Table 1 Assessed discrete Mmax distribution shown in Figure 4.

M	Weight
4.0	0.27
4.5	0.405
5.0	0.1875
5.5	0.1075
6.0	0.025
6.5	0.005
7.0	0

The assessed Mmax distribution is represented discretely by the probability mass function (PMF) shown above with values centered in 0.5 magnitude unit bins. In addition, a continuous cumulative distribution function (CDF) is provided in Table 2. The CDF is constructed by assigning the probability mass in each discrete magnitude bin uniformly over the 0.5 magnitude unit bin width centered on the magnitudes shown in Figure 3 and listed in Table 1. The resulting CDF is shown in Figure 5.

Table 2. CDF of Mmax distribution shown in Figure 5.

M	Cumulative Probability
3.75	0
4.25	0.27
4.75	0.675
5.25	0.8625
5.75	0.97
6.25	0.995
6.75	1

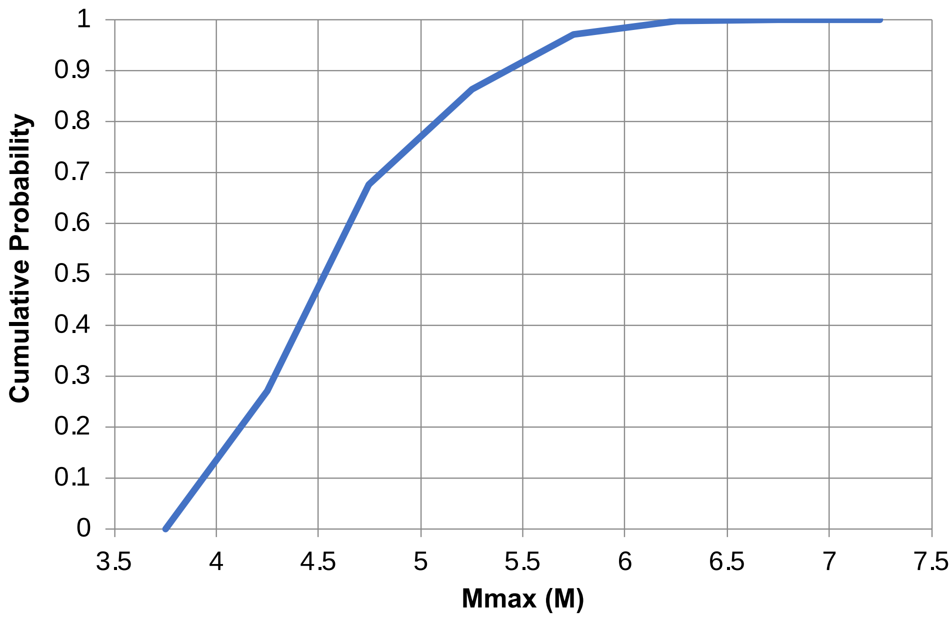

Figure 5: Assessed Mmax CDF.

Recommendations

Assuming that studies pertaining to seismic hazard will continue in the future at Groningen, the Panel offers the following recommendations.

- We commend the project for continuing to improve the resolution of seismicity studies that allow the detailed assessment of the locations of induced seismicity within the reservoir. With respect to the seismogenic potential of the geologic units beneath the reservoir horizon, reduction of uncertainty would best be done by obtaining information on the stress state of the Carboniferous units. Such information could shed light on the triggering of potential of faults within this unit that may be related to the gas extraction process.

- Consider applying state of the art high-resolution data mining and machine learning techniques, including automated phase picking and double-difference hypocentral location, to analyze the seismicity from full-waveform digital data. Based on applications elsewhere, this is likely to better resolve the locations of hypocenters and determine whether events are located outside of the reservoir. It is also likely to reduce the magnitude of completeness, and hence reduce the uncertainty in the frequency-magnitude parameters by having a broader dynamic range and number of observations.

- Conduct detailed studies to look at the geometry of the faults that are implied by the seismicity (e g. dips of faults from focal mechanisms and source inversions), detailed geometries can be used for constraining potential rupture dimensions.

- Consider using Groningen as a test case for prospective operational earthquake forecasting by submitting competing hypotheses for future seismicity, for instance to Collaboratory for the Study of Earthquake Predictability (CSEP) testing platform. Alternatively, an independent testing platform for induced seismicity may be developed at Groningen. Typically, this will involve submitting five year forward predictions for alternative event rate models developed using the extensive Groningen database, including a suite of purely statistical and hybrid forecasting models. This will also allow a more rigorous hypothesis test than retrospective ‘out of sample’ analyses.

A Note Regarding Process

Throughout the process of developing these assessments of Mmax for the Groningen gas field, reference has been made to how the approach used “follows the broad principles of the SSHAC guidelines for hazard assessment, following the current implementation guidelines.” This is true from the standpoint of broadly defining the products, roles of participants, the need to capture the CBR of TDI, and consideration of alternative data, models, and methods. However, once one moves from the “broad principles” and the “general spirit” of a SSHAC process to the details of exactly what is required in regulatory implementation guidance, the process used for the assessment of Mmax for Groningen falls far short of the requirements for a SSHAC project—even the lowest SSHAC Level 1 process level. We offer our perceptions regarding this issue in Attachment A because it has been raised in the materials provided to the Panel, such as the workshop agendas, summaries of the first workshop process (Bommer & Van Elk, 2017), and the recent commentary provided in Bommer (2022). Although the Panel argues that the technical assessment of Mmax documented in this report is defensible, the assessment would be much more robust if it was an integrated component of a full SSHAC study of seismic hazard and risk for Groningen.

References

Bommer, J.J., (2022). Earthquake hazard and risk analysis for natural and induced seismicity: towards objective assessments in the face of uncertainty. *Bulletin of Earthquake Engineering*, *20*(6), pp.2825-3069.

Bommer, J.J. and Van Elk, J., (2017). Comment on “The maximum possible and maximum expected earthquake magnitude for production-induced earthquakes at the gas field in Groningen, the Netherlands” by Gert Zöller and Matthias Holschneider. *Bulletin of the Seismological Society of America*, Vol. 107, No. 3, pp. 1564-1567.

Bossu, R. (1996). PhD Thesis, University Joseph Fourier, Grenoble.

Dahm, T., Krüger, F., Stammler, K., Klinge, K., Kind, R., Wylegalla, K., & Grasso, J. R. (2007). The 2004 Mw 4.4 Rotenburg, Northern Germany, earthquake and its possible relationship with gas recovery. *Bulletin of the Seismological Society of America*, *97*(3), 691-704.

Dahm, T., S. Cesca, S. Hainzl, T. Braun, and F. Krüger (2015), Discrimination between induced, triggered, and natural earth-quakes close to hydro-carbon reservoirs: A probabilistic approach based on the modeling of depletion-induced stress changes and seismological source parameters, *J. Geophys. Res. Solid Earth*, 120, doi:10.1002/2014JB011778

Grigoli, F., Cesca, S., Rinaldi, A.P., Manconi, A., Lopez-Comino, J.A., Clinton, J.F., Westaway, R., Cauzzi, C., Dahm, T. and Wiemer, S., (2018). The November 2017 M w 5.5 Pohang earthquake: A possible case of induced seismicity in South Korea. *Science*, *360*(6392), pp.1003-1006.

Groningen Mmax Panel (2016). *Report from the Expert Panel on Maximum Magnitude Estimates for Probabilistic Seismic Hazard and Risk Modelling in Groningen Gas Field*, 25 April 2016, 13p.

Leonard, M. (2014). Self-consistent earthquake fault-scaling relations: Update and extension to stable continental strike-slip faults. *Bulletin of the Seismological Society of America*, *104*(6), 2953-2965.

López-Comino, J. A., & Cesca, S. (2018). Source complexity of an injection induced event: The 2016 Mw 5.1 Fairview, Oklahoma earthquake. *Geophysical Research Letters*, *45*(9), 4025-4032.

McGarr, A. and D. Simpson (1997). In: *Rockbursts and Seismicity in Mines*. pp. 385-396, Balkema.

McGarr, A., D. Simpson, and L. Seeber (2002), *Case histories of induced and triggered seismicity.* In International Handbook of Earthquake and Engineering Seismology, vol. 81A, pp. 647–661, Academic Press, San Francisco, Calif.

Pijnenburg, R. P. J., Verberne, B. A., Hangx, S. J. T., & Spiers, C. J. (2019). Inelastic deformation of the Slochteren sandstone: Stress-strain relations and implications for induced seismicity in the Groningen gas field. *Journal of Geophysical Research: Solid Earth*, 124, 5254–5282. https://doi.org/10.1029/2019JB017366

Thingbaijam, K. K. S., Martin Mai, P., & Goda, K. (2017). New Empirical Earthquake Source-Scaling Laws. *Bulletin of the Seismological Society of America*, *107*(5), 2225-2246.

USNRC (U.S. Nuclear Regulatory Commission). (2012a). *Central and Eastern United States Seismic Source Characterization for Nuclear Facilities*. NUREG-2115, Washington, D.C.

USNRC (U.S. Nuclear Regulatory Commission). (2012b). *Practical Implementation Guidelines for SSHAC Level 3 and 4 Hazard Studies*. NUREG-2117, Rev. 1, Washington, D.C.

Respectfully submitted,

Members of the Expert Panel on Maximum Magnitude Estimates for Probabilistic Seismic Hazard and Risk Modelling in Groningen Gas Field

Kevin Coppersmith, Chair

Jon Ake

Hilmar Bungum

Torsten Dahm

Art McGarr

Ian Main

Ivan Wong

Bob Youngs

Attachment A
Comments Regarding Process

Throughout the process of developing these assessments of Mmax for the Groningen gas field, reference has been made to how the approach used “follows the broad principles of the SSHAC guidelines for hazard assessment, following the current implementation guidelines.” While this is true from the standpoint of broadly defining the products as needing to capture the CBR of TDI, the general role of the Panel as technical integrators, and the resource and proponent experts providing their data and interpretations in a workshop environment that encourages the “challenge and defense” that has marked SSHAC workshops for other projects. But once one moves from the “broad principles” and the “general spirit” of a SSHAC process to the details of exactly what is required in regulatory implementation guidance, the process used for the assessment of Mmax for Groningen falls far short of the requirements for a SSHAC project—even the lowest SSHAC Level 1 process level. We offer our perceptions regarding this issue because it has been raised in the materials provided to the Panel, such as the workshop agendas, summaries of the first workshop process (Bommer & Van Elk, 2017), and the recent commentary provided in Bommer (2022).

In the interest of time and space in this document, we will provide our views on just a few of the clear departures between this Groningen Mmax study and accepted practice for a SSHAC study—particularly a study conducted at SSHAC Level 2 or 3. These example departures relate to the development and evaluation of a project database, the integration phase of a SSHAC project including feedback, and participatory peer review.

Development and Evaluation of Project Database

The first phase of a SSHAC process includes the identification, compilation and evaluation of the data that the Technical Integration (TI) team identifies as being pertinent to the assessments that they will be making. Typically, a comprehensive database is developed and is made available to the TI team for their consideration in a manner that allows for adequate time and evaluation—typically over a period of months. As the project proceeds, the project database continues to be supplemented with new information identified by the TI team and/or new data collected specifically for the project to reduce uncertainties in the ultimate assessments. The evaluation of the database is an important activity that allows the TI team to consider the alternative datasets, models and methods that have been proposed by the larger technical community.

In the case of the Groningen Mmax project, the expert panel faced the challenge of entering the project in 2016—and coming back into the project after 6 years in 2022—and attempting to absorb and evaluate a vast amount of new information, identified by others, in a very short period of time. This does not conform to the SSHAC principle of subject-matter experts becoming experts on the specific application through exposure to the available data, methods, and models over several months of data compilation and collection, evaluation, and integration.

Integration Phase of the Project Including Feedback

After the data, models, and methods have been evaluated during the evaluation phase of a SSHAC project, the model-building or integration phase is conducted. The models that are built provide the technical assessments required for the technical products of the study and the uncertainties are quantified such that the products reflect the CBR of TDI. Typically, the model-building process is a collaborative process involving all members of the TI team as they assess the important technical approaches that will be followed, the viability of alternative models and methods in light of the available data, and the proper representation of uncertainties given current knowledge. This process typically requires multiple meetings of the team, side calculations to understand the processes and uncertainties, and consideration of feedback regarding the potential hazard significance of the assessments being made. Feedback also provides a basis for prioritization of the model-building process to focus on the assessments that are most important to the hazard results and on the uncertainties that contribution most to the hazard uncertainties.

The model-building process for the Groningen Mmax assessment was contracted to essentially a single one-day meeting of the Panel to consider the data and assessments made by project participants, followed by remote correspondence amongst the Panel members to consider the range of possible assessments and the technical defense of the uncertainties quantified. No feedback was provided regarding hazard significance or implications of the uncertainties quantified to their subsequent use in risk analyses. As a result, the Panel was left to estimate the potential importance of the elements of their assessments based on their own experience on other projects.

Participatory Peer Review

A hallmark of a SSHAC process is the continual peer review that occurs from a participatory peer review panel (PPRP) throughout the course of the project. A PPRP must have the experience and range of expertise that the TI teams possess in order to provide their commentary and feedback throughout the project. In addition, the PPRP is charged with ensuring that a defensible SSHAC process has been followed such that the products of the study capture the CBR of TDI. Experience has shown that the rigorous process of peer review not only improves the quality and defensibility of the products of a SSHAC hazard assessment, it provides the regulatory assurance that is required to enhance public acceptance.

No peer review process was invoked in the Groningen Mmax assessment process. The Panel was provided with the applicable data and the charge to develop and document an Mmax distribution that could be used for future hazard and risk assessments. Independent peer review would have ensured that the process followed was defensible and that the technical assessments made properly capture the CBR of TDI. Such peer review would likely enhance the regulatory and public acceptance of the Panel’s assessments and conclusions.

Conclusions Regarding Process

Although the Panel argues that the technical assessment of Mmax documented in this report is defensible, the assessment would be much more robust if it was an integrated component of a full SSHAC study of seismic hazard and risk for Groningen. It is our understanding the attempt to apply SSHAC to this critical and controversial problem was proposed but was frustrated by the regulator (summarized in Bommer, 2022). However, if the decision to close the field is ever reversed and the hazard and risk study is ever restarted, the Panel would strongly recommend that the study be conducted as a SSHAC process.

Groningen Mmax Workshop II

Infinity Building, South Amsterdam, The Netherlands

13-17 June 2022,

Presentations

Workshop on Maximum Magnitude of earthquakes in Groningen

DAY 1

Monday 13th June: Intro/Groningen field/Tectonic Mmax/Induced and triggered earthquakes

Start	End	Speaker	Presentation
8:30	9:00	Julian Bommer	Welcome. Introductions. Background and objectives of workshop.
09:00	09:15	Ministerie EZK	Importance of Mmax for the Groningen seismic risk assessment
9:15	10:15	Clemens Visser	Geology of the field. Past, present and future gas production.
10:15	10:45		*Coffee break*
10:45	11:30	Rob van Eijs	Subsidence and compaction of the gas field
11:30	12:15	Bob Youngs	Definition & estimation of Mmax for tectonic earthquakes
12:15	13:15		*Lunch*
13:15	14:00	Helen Crowley	Mmax values for (tectonic) seismic hazard and risk in Europe
14:00	14:45	Matt Weingarten	Induced earthquakes related to gas production
14:45	15:15		*Coffee break*
15:15	16:30	Gillian Foulger	Induced & triggered earthquakes globally: larger events
16:30	17:00	All	General discussion

Background and Objectives of the Workshop

Julian J Bommer

Welcome to Amsterdam!

Thank you all for being here and for your patience with organisation of this event
(*and for those under contract to NAM, thank for your forbearance with the contracting process*)

Those under contract should charge their time and expenses through the IQN system

There is absolutely no requirement for confidentiality in relation to this workshop, indeed you are actively encouraged to publish any work undertaken for this event and to disseminate your findings in the scientific literature
(*an acknowledgement to NAM, where appropriate, would be appreciated*)

Those who do publish their findings on Mmax in the Groningen field should feel free to also charge the time spent on producing these papers

The Final Event in NAM's Scientific Study Programme

NAM has been asked to close their scientific study programme, hence work on the ground-motion prediction and site response models, and on the fragility and consequence models, has been terminated; the work on the seismic source model has also been discontinued apart from this workshop focused on Mmax, which was originally scheduled to have happened a long time ago but which fell foul of the pandemic:

~~16-18 November 2020~~

~~18-21 October 2021~~

13-16 June 2022

We're finally here – and hopefully it will have been worth the wait

What is the Purpose of this Workshop?

To provide an opportunity for the Expert Panel on Mmax to review and possibly revise their proposed Mmax model for Groningen from March 2016, in the light of new data and analyses

Following the principles of the SSHAC (Senior Seismic Hazard Analysis Committee) process, the model will be a logic-tree with alternative values of Mmax to which relative weights are assigned, with the objective of capturing the centre, the body, and the range of technically defensible interpretations of the available data, methods and models

The Expert Panel's deliberations will be informed by the presentations during the workshop, their questions to the presenters, and also the discussions amongst all the participants, but they are the sole intellectual authors of the final Mmax model

Kevin Coppersmith

Member of original SSHAC, leader of SSHAC PSHA projects around the world

Jon Ake

Formerly at USNRC, expert on PSHA and induced seismicity

Hilmar Bungum

Formerly at NORSAR, expert on PSHA in low seismicity areas

Torsten Dahm

Professor at GFZ Potsdam, expert on induced seismicity

Ian Main

Professor at Edinburgh University, expert on rock mechanics and seismology

Art McGarr

US Geological Survey, pioneering expert in the field of induced seismicity

Ivan Wong

Extensive experience in PSHA for natural and induced seismicity

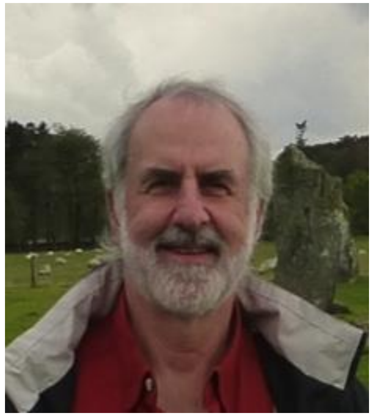

Bob Youngs

Extensive experience in PSHA and estimation of Mmax for tectonic earthquakes

Is Mmax important?

Mmax is the largest earthquake magnitude considered in probabilistic seismic hazard and risk analyses

Mmax is generally considered to represent the largest earthquake that could occur on a given seismic source in the current tectonic regime

A great deal of attention has been given to the estimation of Mmax for tectonic earthquakes, especially in regions of low seismicity, although it is a parameter that does not exert a very strong influence on hazard estimates except for long-period spectral accelerations and low annual exceedance frequencies

Mmax in PSHA for crustal earthquakes usually takes values in the range 6.5 - 8.0

And, infrequent earthquakes sample fewer standard deviations of GMPE

Tendency for ground-motion amplitudes to saturate at larger magnitudes

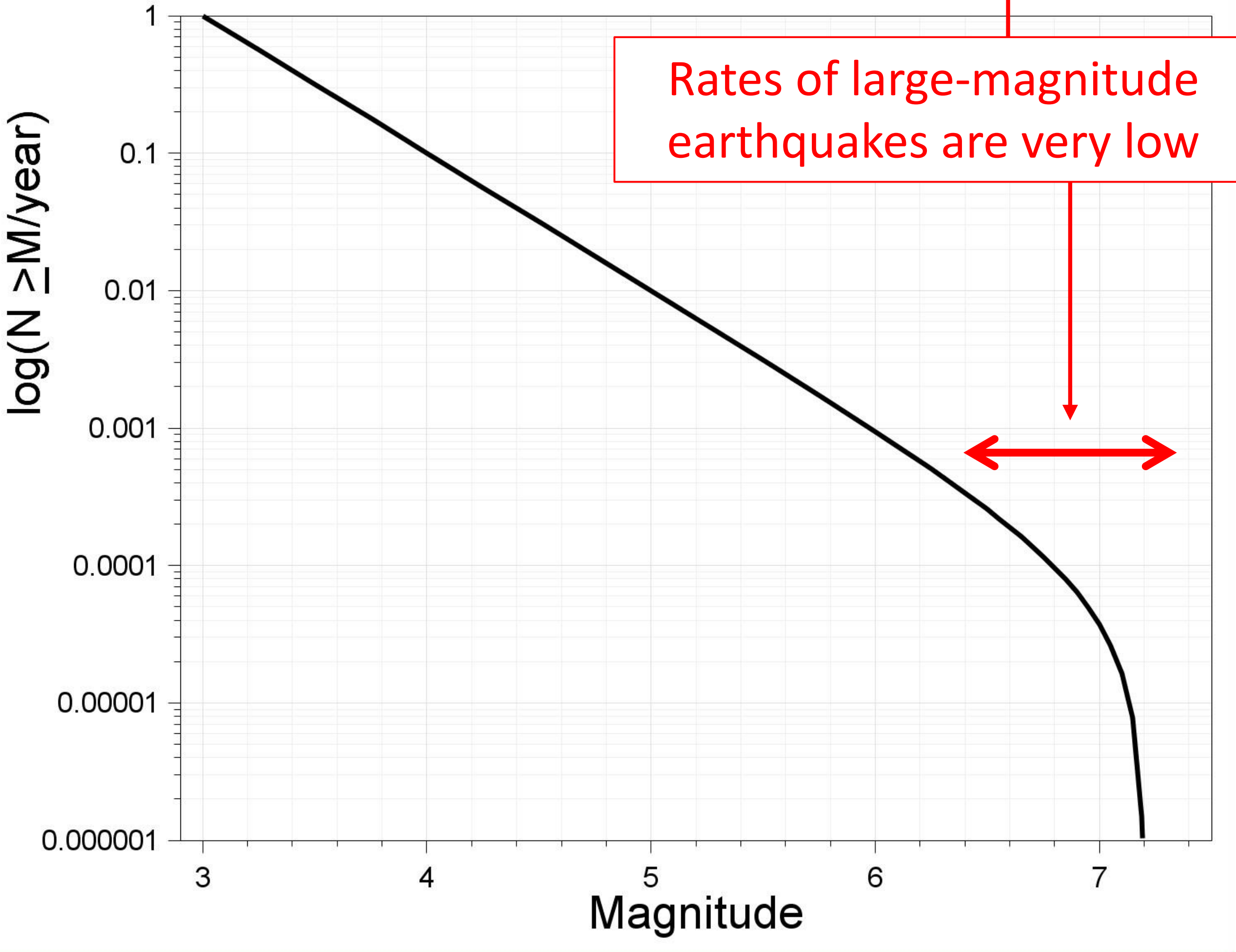

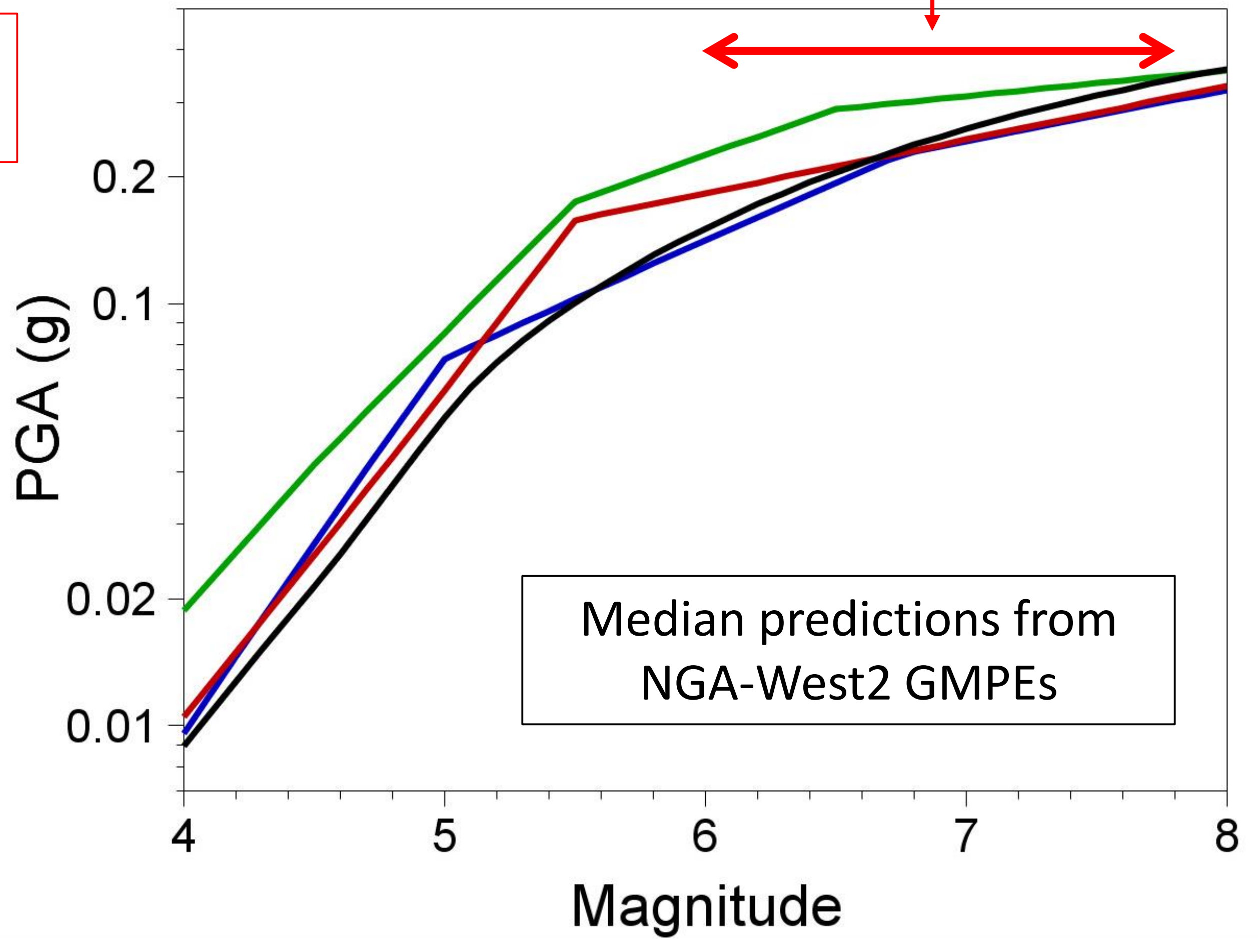

Consequently, hazard estimates – especially when dominated by seismic sources close to the site – are generally dominated by moderate magnitudes hence the influence of Mmax is small

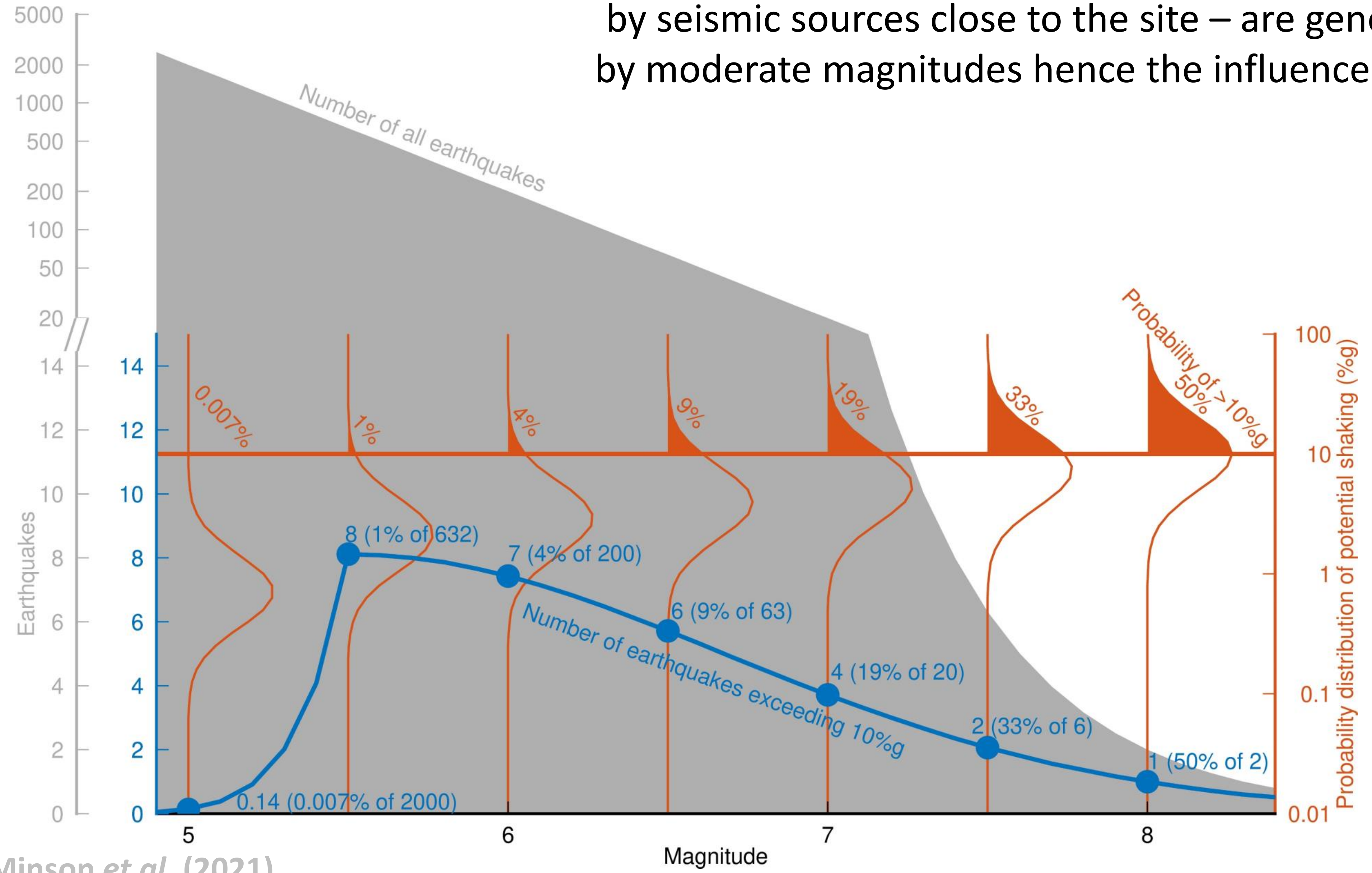

Minson *et al*. (2021)

Mmax for Induced Seismicity

Whereas Mmax exerts only a modest influence on hazard estimates for natural seismicity, it can be a very important – even critical – parameter when assessing the hazard due to induced earthquakes

At a USGS workshop in 2014 to discuss the inclusion of induced seismicity in the US national hazard maps "*Participants at the workshop felt that the USGS induced seismicity models should consider the possibility of triggering large regional earthquakes and should consider the same maximum magnitude distribution as was used for the tectonic earthquakes in the NSHM model which has a mean of 7.0 but extends from M6.5 to M7.95 with low weights at the ends of the distribution*".

For cases of genuinely induced rather than triggered seismicity, such as Groningen, such an approach could be considered very conservative since it would mean that in all hazard runs, events of **almost 3 units of magnitude larger than the biggest observed earthquake** to date would be considered in every realisation of future seismicity

Mmax for Groningen (1/4)

1995

KNMI estimated M **3.3** from trend in cumulative energy and M **3.5** ± 0.5 from geological considerations

1998

KNMI estimated M **3.7** from trend in cumulative energy, M **3.8** from bounded Gutenberg-Richter relationship (mean + σ) and M **3.5** ± 0.5 from geological considerations

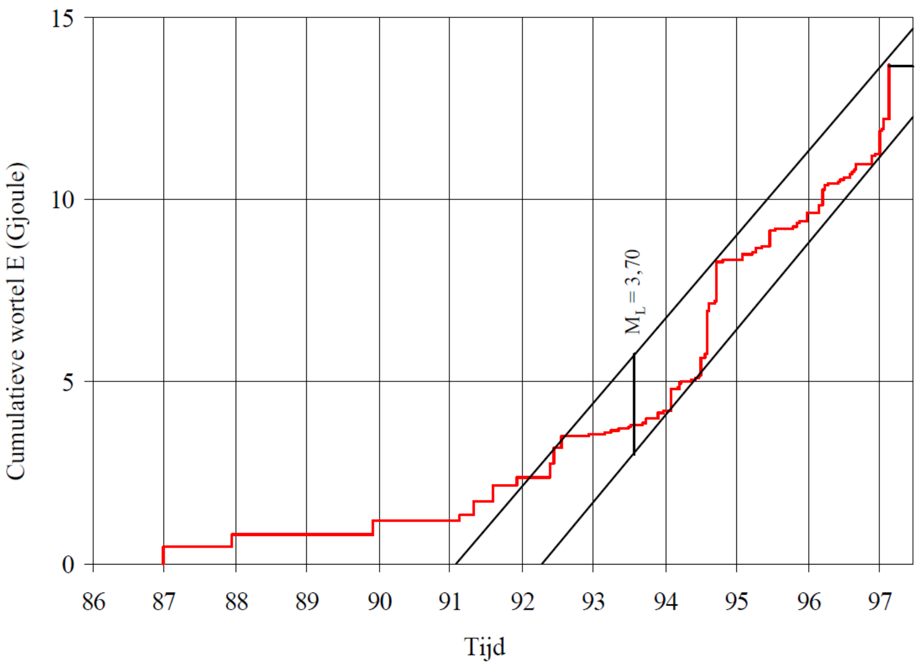

Distribution from 1,000 Monte Carlo simulations

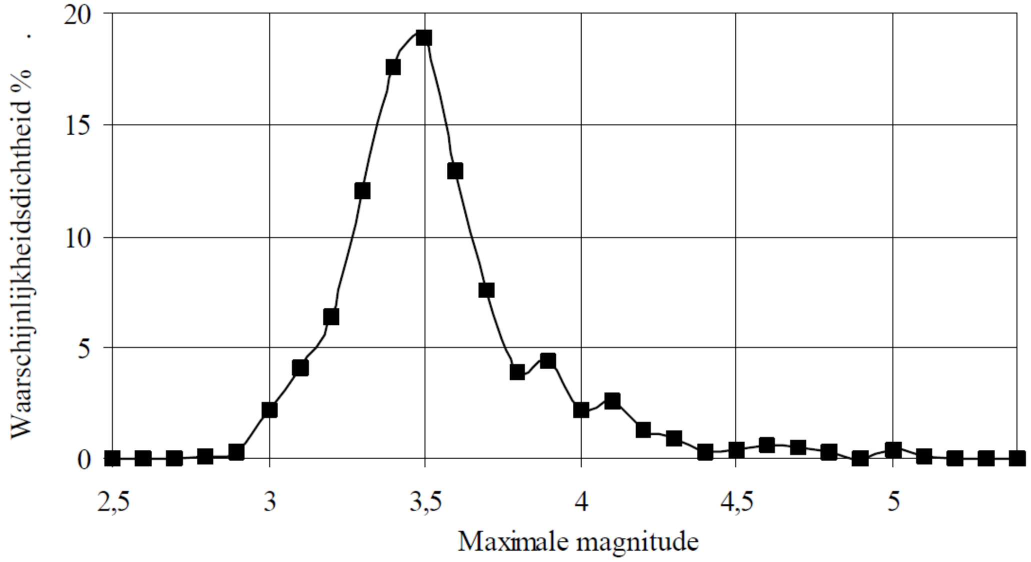

Mmax for Groningen (2/4)

2004

KNMI applied a Bayesian approach to the earthquake catalogue from 1986 to 2003, estimating a mean value of M **3.6** and an 84-percentile value of M **3.9**

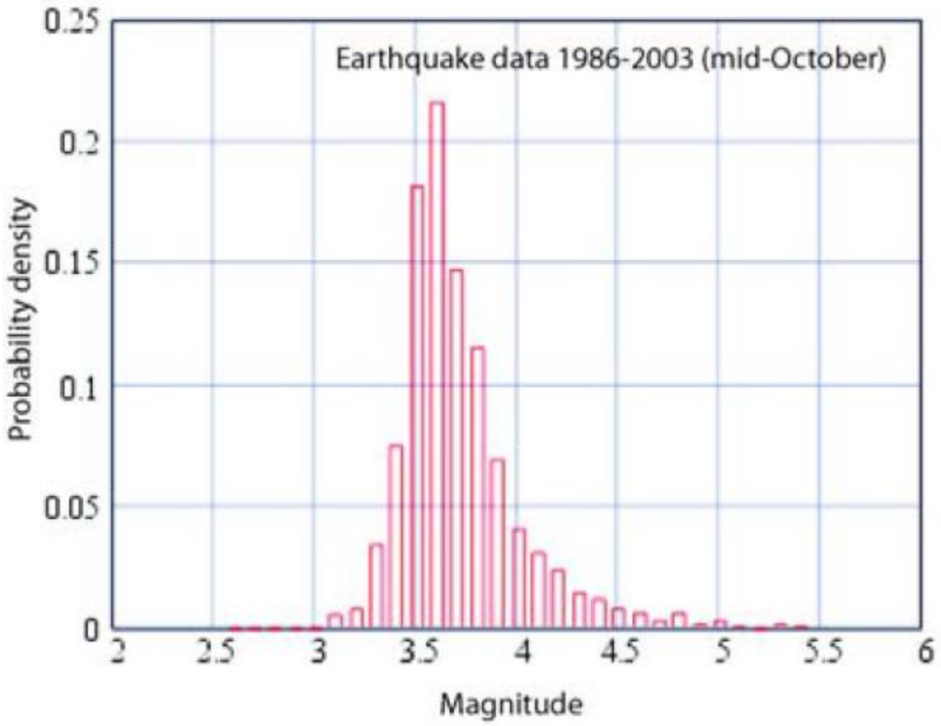

2010

KNMI estimated M **3.7** from trend in cumulative energy, M **3.9** from bounded Gutenberg-Richter relationship (mean + σ) and M **3.5** ± 0.5 from geological considerations

Mmax for Groningen (3/4)

2013

KNMI concluded that based only on statistics of the earthquake catalogue, no reliable estimate of a maximum probable earthquake in Groningen could be obtained

Pending more reliable constraints from geological information and geomechanical modelling, KNMI decided to adopt a conservative upper limit on Mmax of **M** 5.0

Considering fault ruptures confined to the reservoir and with a maximum aspect ratio of 20, KNMI estimated a maximum magnitude of **M** 4.9

Analyses by TNO determined estimates of **M** ~5 for faults confined to the reservoir, and M ~ 5.8 for ruptures that could extend to 5 km depth within the Carboniferous

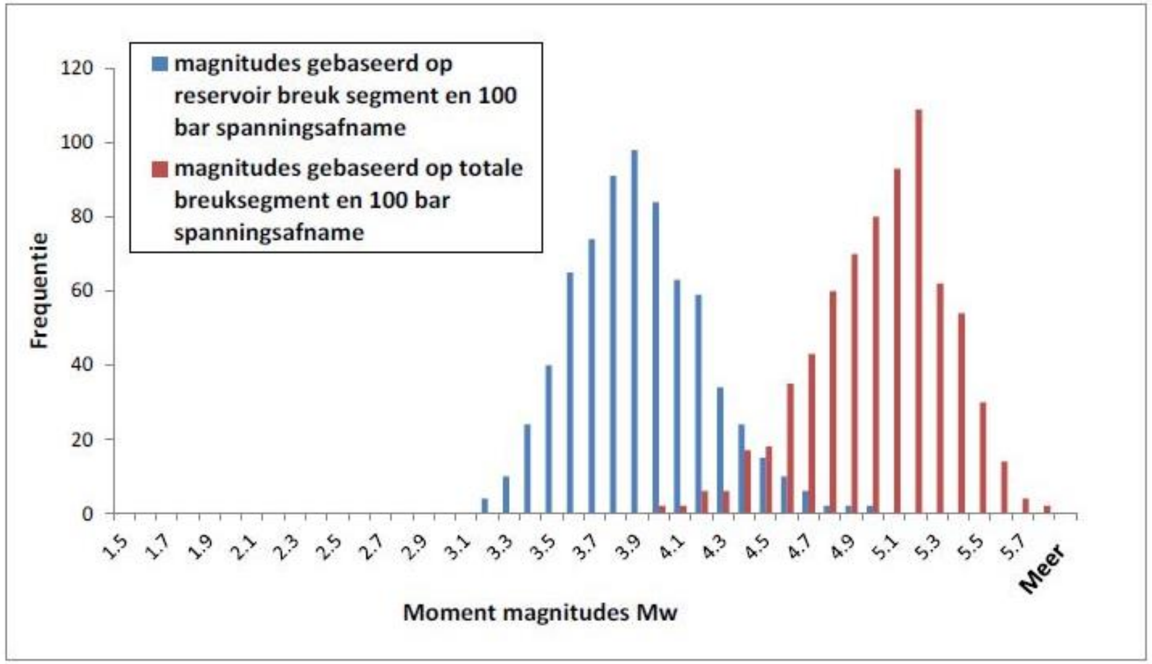

Mmax for Groningen (4/4)

2013

A report by SodM issued in January 2013 discussed possible values for Mmax of **M** 4.5, **M** 5.0 and **M** 6.0

For the seismic hazard and risk model, NAM adopted a maximum magnitude of **M** 6.5, derived from the assumption that all the strain accumulated from full production of the reservoir is released seismically in single event

Internal discussions of the implications of this model led to the decision to appoint an Expert Panel to make an independent assessment of an appropriate distribution for this parameter

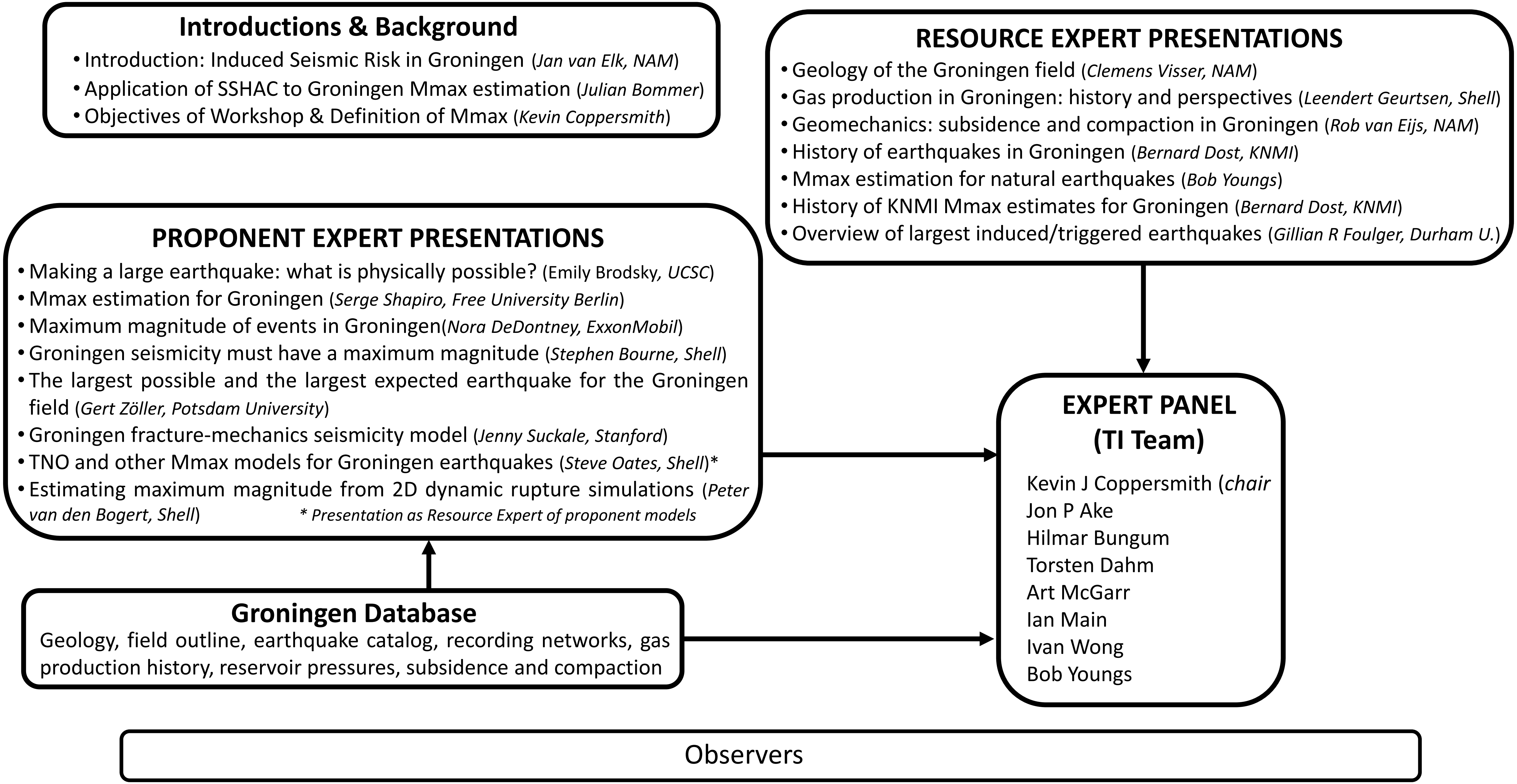
Introductions & Background
• Introduction: Induced Seismic Risk in Groningen (Jan van Elk, NAM)
• Application of SSHAC to Groningen Mmax estimation (Julian Bommer)
• Objectives of Workshop & Definition of Mmax (Kevin Coppersmith)
RESOURCE EXPERT PRESENTATIONS
• Geology of the Groningen field (Clemens Visser, NAM)
• Gas production in Groningen: history and perspectives (Leendert Geurtsen, Shell)
• Geomechanics: subsidence and compaction in Groningen (Rob van Eijs, NAM)
• History of earthquakes in Groningen (Bernard Dost, KNMI)
• Mmax estimation for natural earthquakes (Bob Youngs)
• History of KNMI Mmax estimates for Groningen (Bernard Dost, KNMI)
• Overview of largest induced/triggered earthquakes (Gillian R Foulger, Durham U.)
PROPONENT EXPERT PRESENTATIONS
• Making a large earthquake: what is physically possible? (Emily Brodsky, UCSC)
• Mmax estimation for Groningen (Serge Shapiro, Free University Berlin)
• Maximum magnitude of events in Groningen(Nora DeDontney, ExxonMobil)
• Groningen seismicity must have a maximum magnitude (Stephen Bourne, Shell)
• The largest possible and the largest expected earthquake for the Groningen field (Gert Zöller, Potsdam University)
• Groningen fracture-mechanics seismicity model (Jenny Suckale, Stanford)
• TNO and other Mmax models for Groningen earthquakes (Steve Oates, Shell)*
• Estimating maximum magnitude from 2D dynamic rupture simulations (Peter van den Bogert, Shell)
* Presentation as Resource Expert of proponent models
EXPERT PANEL
(TI Team)
Kevin J Coppersmith (chair
Jon P Ake
Hilmar Bungum
Torsten Dahm
Art McGarr
Ian Main
Ivan Wong
Bob Youngs
Groningen Database
Geology, field outline, earthquake catalog, recording networks, gas production history, reservoir pressures, subsidence and compaction
Observers

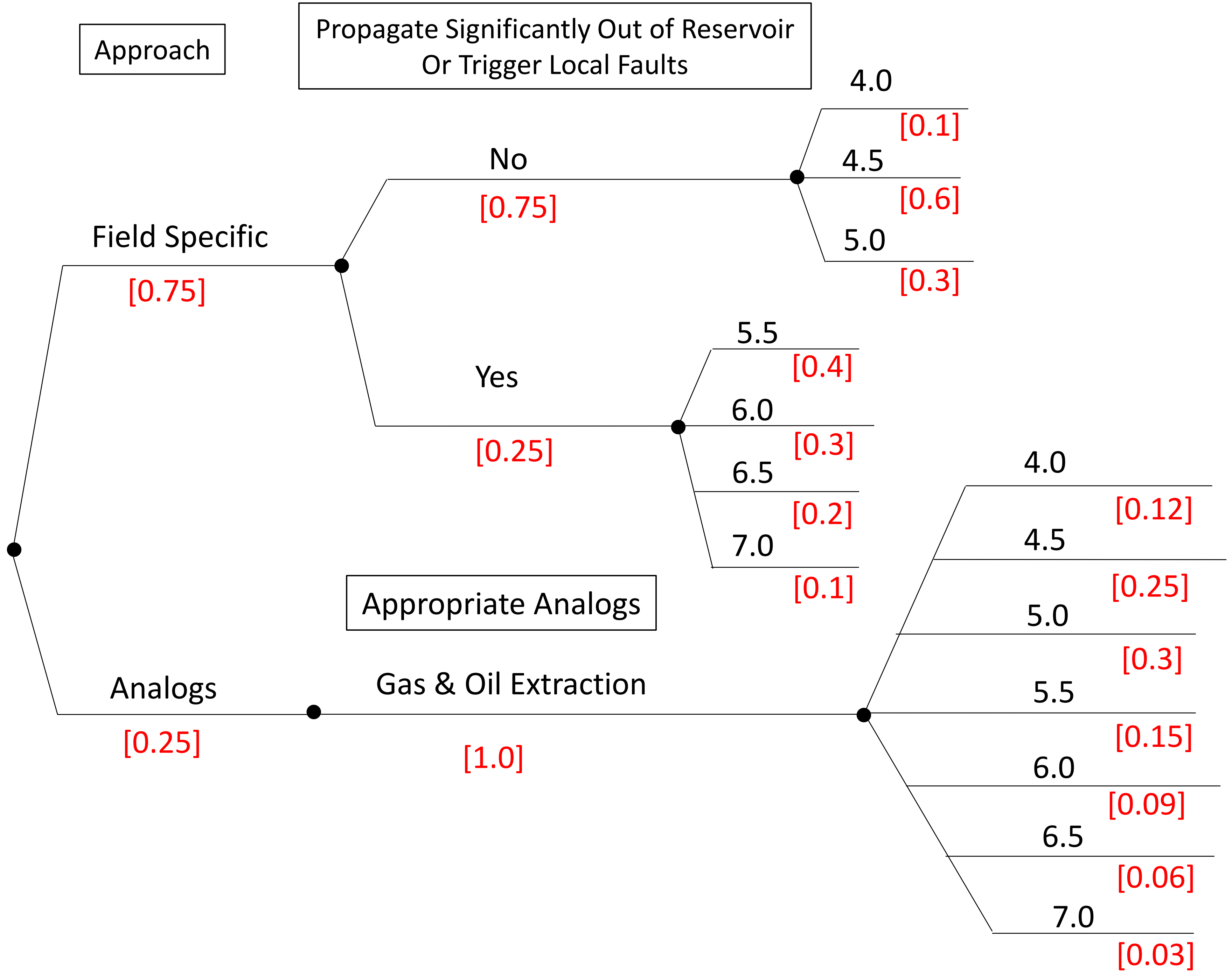

Approach
Propagate Significantly Out of Reservoir Or Trigger Local Faults
Field Specific
[0.75]
No
[0.75]
4.0
[0.1]
4.5
[0.6]
5.0
[0.3]
Yes
[0.25]
5.5
[0.4]
6.0
[0.3]
6.5
[0.2]
7.0
[0.1]
Appropriate Analogs
Analogs
[0.25]
Gas & Oil Extraction
[1.0]
4.0
[0.12]
4.5
[0.25]
5.0
[0.3]
5.5
[0.15]
6.0
[0.09]
6.5
[0.06]
7.0
[0.03]

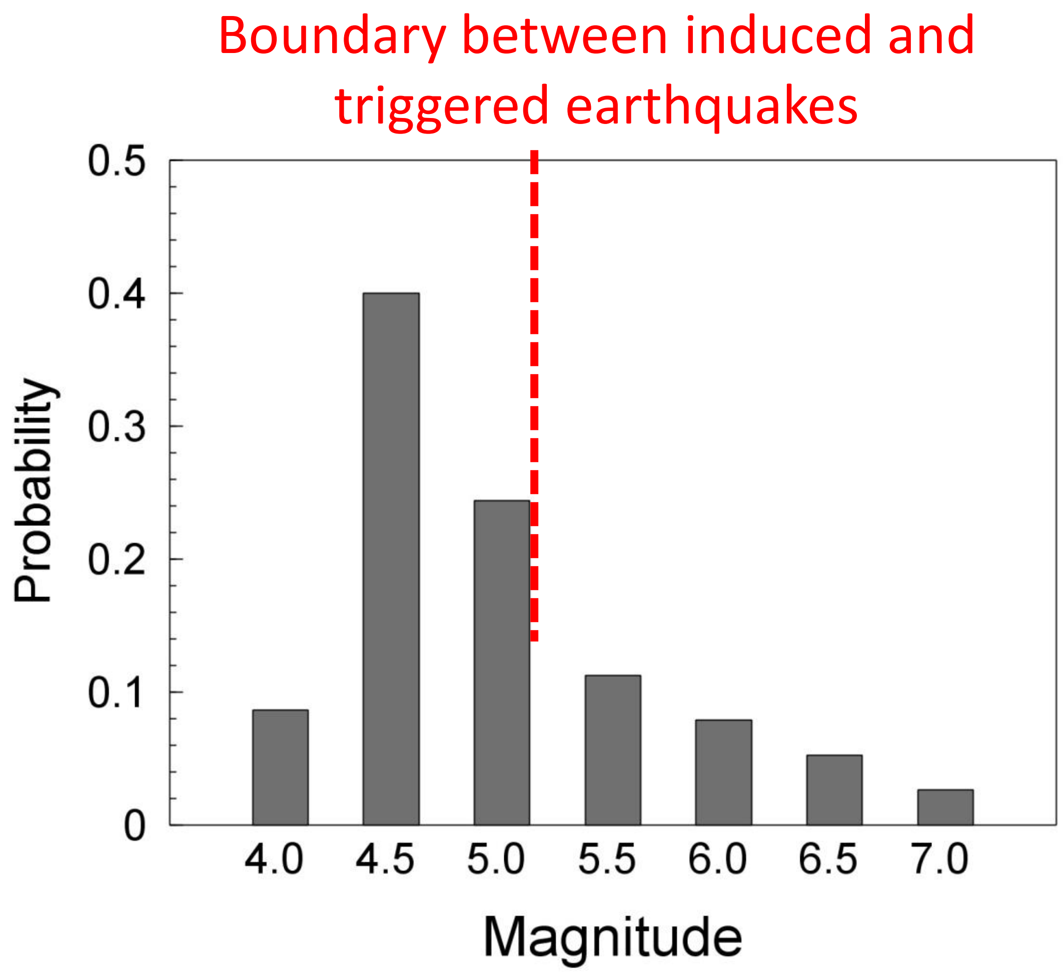

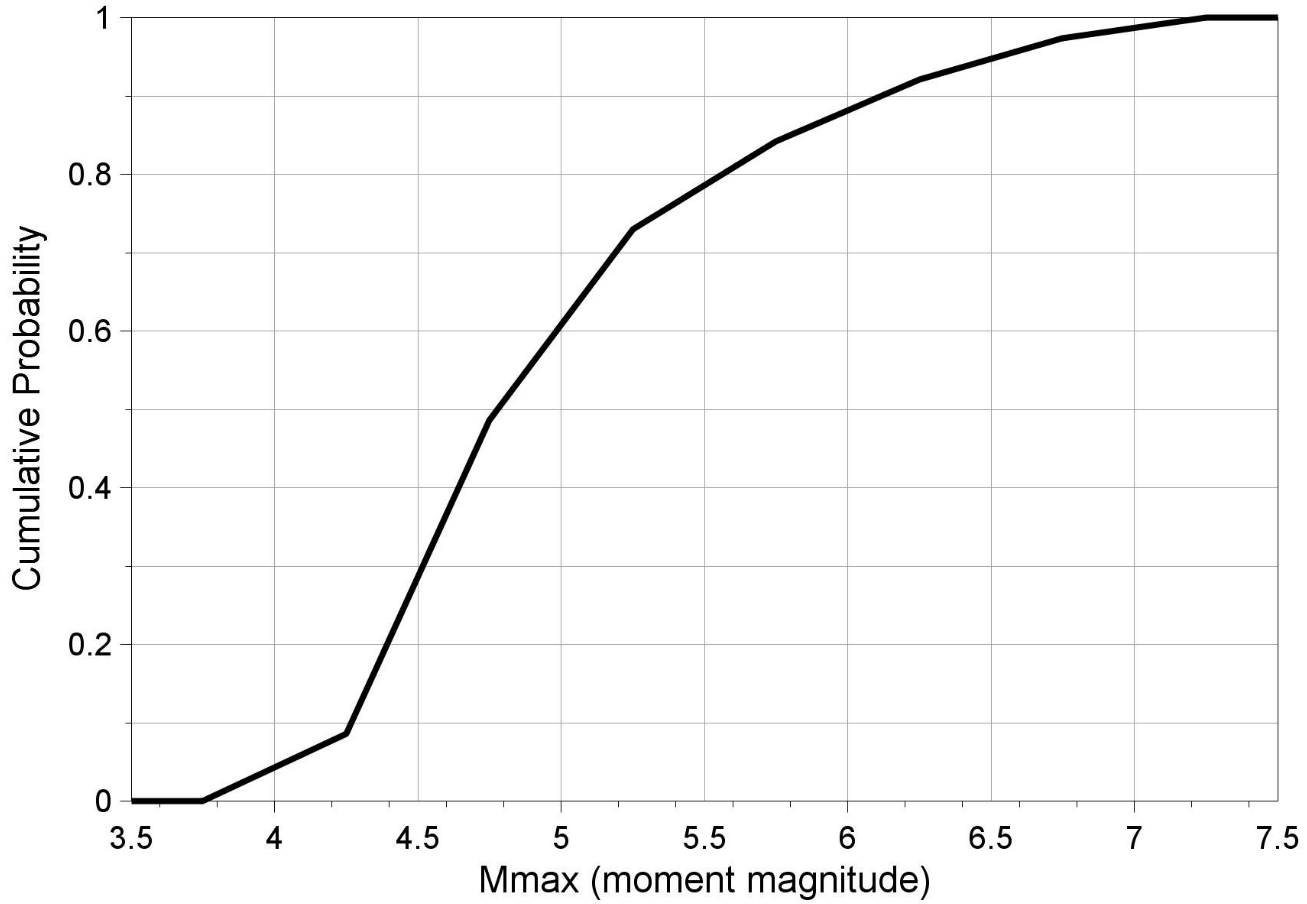

Six years later, there is a wealth of additional data available and many new analyses have been conducted, prompting consideration of whether this distribution requires updating

Monday 13th June: Intro/Groningen field/Tectonic Mmax/Induced and triggered earthquakes

Start	End	Speaker	Presentation
8:30	9:00	Julian Bommer	Welcome. Introductions. Background and objectives of workshop.
09:00	09:15	Ministerie EZK	Importance of Mmax for the Groningen seismic risk assessment
9:15	10:15	Clemens Visser	Geology of the field. Past, present and future gas production.
10:15	10:45		*Coffee break*
10:45	11:30	Rob van Eijs	Subsidence and compaction of the gas field
11:30	12:15	Bob Youngs	Definition & estimation of Mmax for tectonic earthquakes
12:15	13:15		*Lunch*
13:15	14:00	Helen Crowley	Mmax values for (tectonic) seismic hazard and risk in Europe
14:00	14:45	Matt Weingarten	Induced earthquakes related to gas production
14:45	15:15		*Coffee break*
15:15	16:30	Gillian Foulger	Induced & triggered earthquakes globally: larger events
16:30	17:00	All	General discussion

Tuesday 14th June: Groningen seismicity and fault ruptures

Start	End	Speaker	Presentation
8:30	9:15	Bernard Dost	History of seismic monitoring in the Groningen field
9:15	10:30	Steve Oates	Groningen earthquakes: focal depths and fault ruptures
10:30	11:00		*Coffee break*
11:00	11:45	Chris Spiers	Properties of Groningen reservoir and fault rocks
11:45	12:30	Rick Wentinck	Geomechanical model of fault rupture in the Groningen field
12:30	13:30		*Lunch*
13:30	14:45	Jean-P. Ampuero	Physics-based models of natural and induced seismicity
14:45	15:15		*Coffee break*
15:15	16:30	Mark Zoback	Crustal stresses and earthquake triggering
16:30	17:00	All	General discussion

Wednesday 15th June: Groningen event-size distribution & Statistical estimates of Mmax

Start	End	Speaker	Presentation
8:30	9:30	Stephen Bourne	Groningen seismological model and earthquake recurrence
9:30	10:15	Laura Gulia	Re-assessment of earthquake distribution for Groningen
10:15	10:45		*Coffee break*
10:45	11:30	Jean-Ph. Avouac	Recurrence model for Groningen earthquakes
11:30	12:15	Zak Varty	Recurrence model for Groningen earthquakes
12:15	13:15		*Lunch*
13:15	14:00	A Muntendam-Bos	Groningen induced event-size distribution
14:00	14:45	Sander Osinga	Taper from recurrence relationship to Mmax
14:45	15:15		*Coffee break*
15:15	16:30	Gert Zöller	Proponent assessment for Mmax in the Groningen field
16:30	17:15	Nepomuk Boitz	Proponent assessment for Mmax in the Groningen field
17:15	18:00	All	General discussion

Thursday 16th June: Proponent models for Mmax

Start	End	Speaker	Presentation
8:30	9:15	David Dempsey*	Proponent assessment for Mmax in the Groningen field
9:15	10:0	Andrzej Kijko*	Proponent assessment for Mmax in the Groningen field
10:00	10:30		*Coffee break*
10:30	11:15	Leo Eisner	Proponent assessment for Mmax in the Groningen field
11:15	12:00	Charles Vlek	Proponent assessment for Mmax in the Groningen field
12:00	13:00		*Lunch*
13:00	13:45	Stephen Bourne	Proponent assessment for Mmax in the Groningen field
13:45	14:45	Loes Buijze	Proponent assessment for Mmax in the Groningen field
14:45	15:15		*Coffee break*
15:15	15:45	Ylona van Dinther	DEEPnl research project on Mmax in the Groningen field
15:45	16:30	All	General discussion

* remote presentation

On Friday 17th June, when we all are back home or starting our journeys, the Expert Panel will enter their “enclave” to deliberate on information and ideas presented and discussed during the Workshop and whether this warrants an update of the Mmax distribution proposed 6 years ago

While priority will be given to the Expert Panel to address questions to presenters, discussion amongst all of the participants is encouraged provided (1) it remains strictly focused on the topic of the workshop, namely Mmax and the shape of the upper end of the magnitude-frequency relationship for Groningen, and (2) all exchanges are courteous and respectful

You are reminded that we must have a copy of your presentation both for the record and also for reference by the Expert Panel on Friday

Let’s enjoy a lively, informative and productive Workshop!

Ministerie van Economische Zaken
en Klimaat

Introduction EZK

Karin van Thienen-Visser

Introduction

- Dr. Karin van Thienen-Visser
  - Ministry of Economic Affairs and Climate Policy (Dutch: EZK)
  - Coordinating specialist advisor deep subsurface
    - ‘translate’ scientific insights into policy in the Netherlands
    - Coordinate knowledge program on the effects of mining (KEM) since 2019
  - Background
    - PhD in seismology 2008 (Utrecht University)
    - 11 years working in Geomechanics and Seismology at TNO (subsidence and induced seismicity due to mining).

EZK policy on Groningen SHRA since 2016

- Decision to transfer SHRA to public domain
  - 2017: TNO was contracted to separately implement SHRA for Groningen
  - 2020: Agreements on governance between EZK, SSM, TNO, (NAM)
  - 2021: Special KEM subpanel for model development SHRA (joining in workshop)
  - 2021: First SHRA performed by TNO for annual production decision by minister of EZK
- Further scientific development of SHRA
  - Ensure finalization of NAM's Study and Data Acquisition Plan, supervised by SSM; including this workshop
  - Assignments to TNO (following advice SSM, KEM subpanel)
  - Studies as part of KEM programme
  - Note: SHRA analysis will also be needed after stop of gas production

Expectations of this workshop for EZK

- A revisit on the elements that have implications for the expected (maximum) magnitudes and their occurence rates
- Pleased that scope of the workshop has been broadened to:
  - Mmax distribution
  - Use of taper
  - Compatibility existing SHRA
- Pleased that the workshop is now taking place.
- Workshop fits in our policy of public SHRA development

What will we do with the results

- SSHAC panel will write their report to NAM
- NAM will include results in (close-out) SDAP report to SSM and EZK
- EZK will assign TNO to implement results in public SHRA
- EZK will decide on model versions to be used in following SHRA calculations, after proposal TNO and consulting SSM and KEM subpanel

INTRODUCTION TO THE GEOLOGY OF THE GRONINGEN FIELD

MAY 2022

FIT4FUTURE

PRESENTATION OUTLINE

- Introduction to Groningen
- Discovery and historical overview
- Tectonic setting
- Depositional setting
- Reservoir model
- Gas production

GENERAL INTRODUCTION

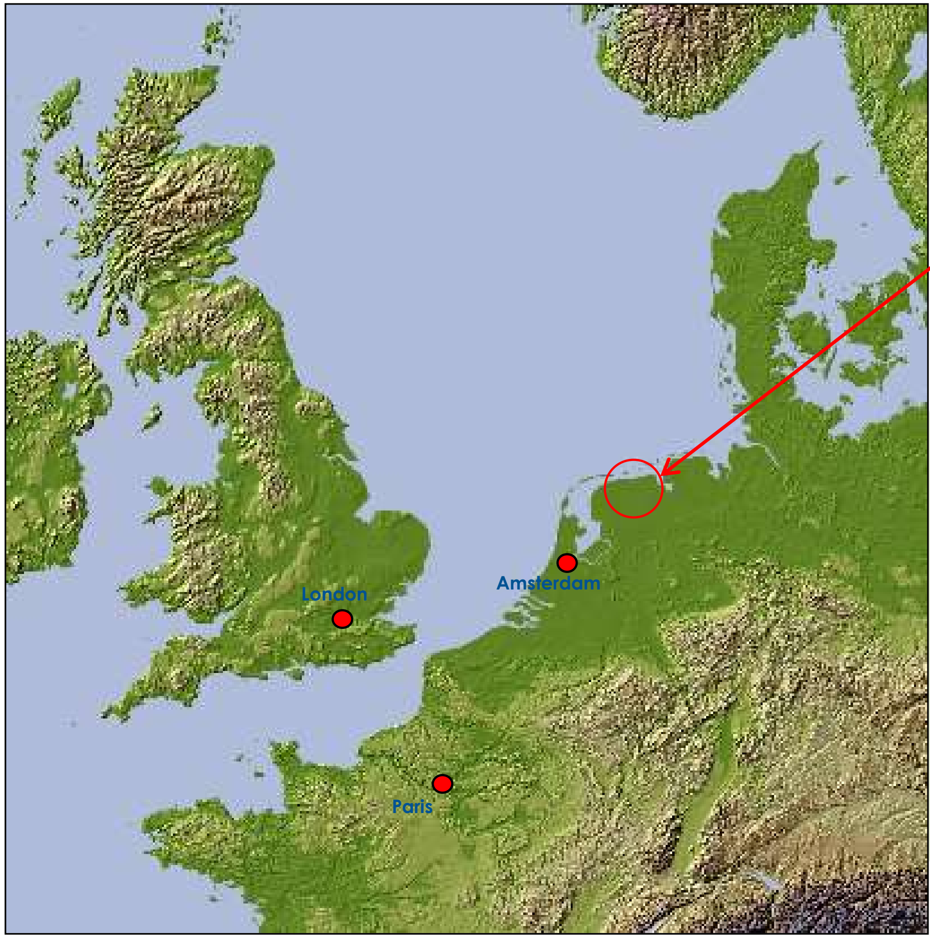

Groningen area

Discovery well Slochteren-1, drilled in1959

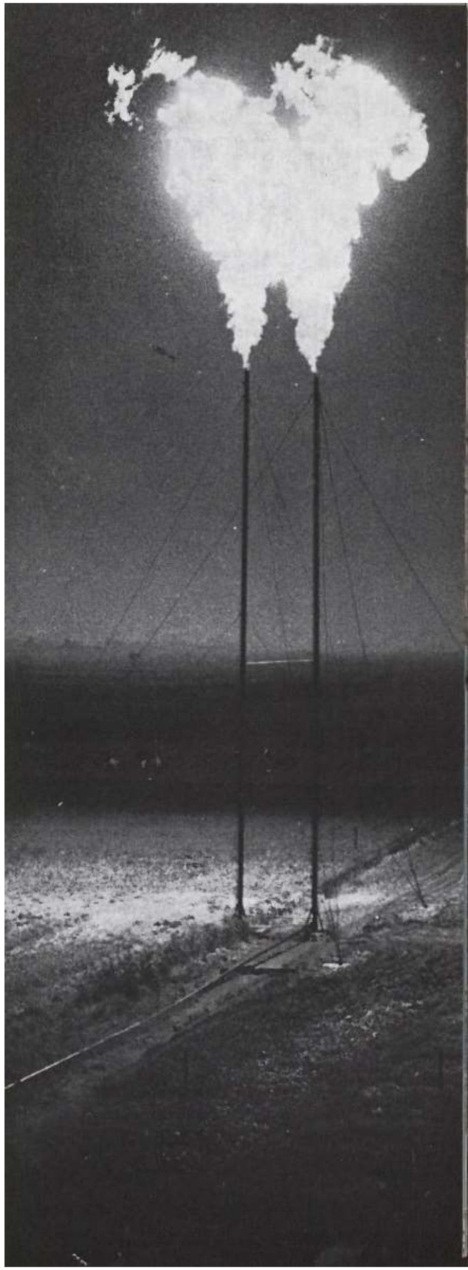

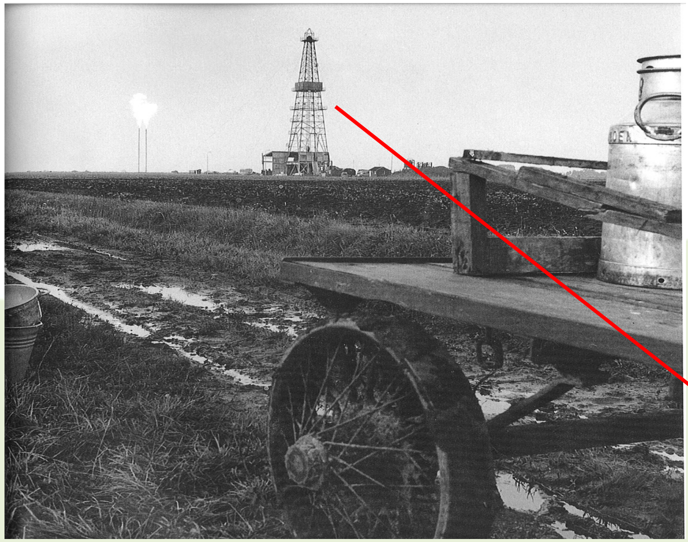

A few numbers:	
Area	862 km2
Discovered	1959
Wells drilled	333
Producing wells in 2012	253
Water injection wells	2
In-place volumes	2900 Bcm
Net-to-Gross	0.88 - 0.98
Porosity	0.11 – 0.18
Permeability	1 – 1000 mD
Gas saturation	0 – 0.83

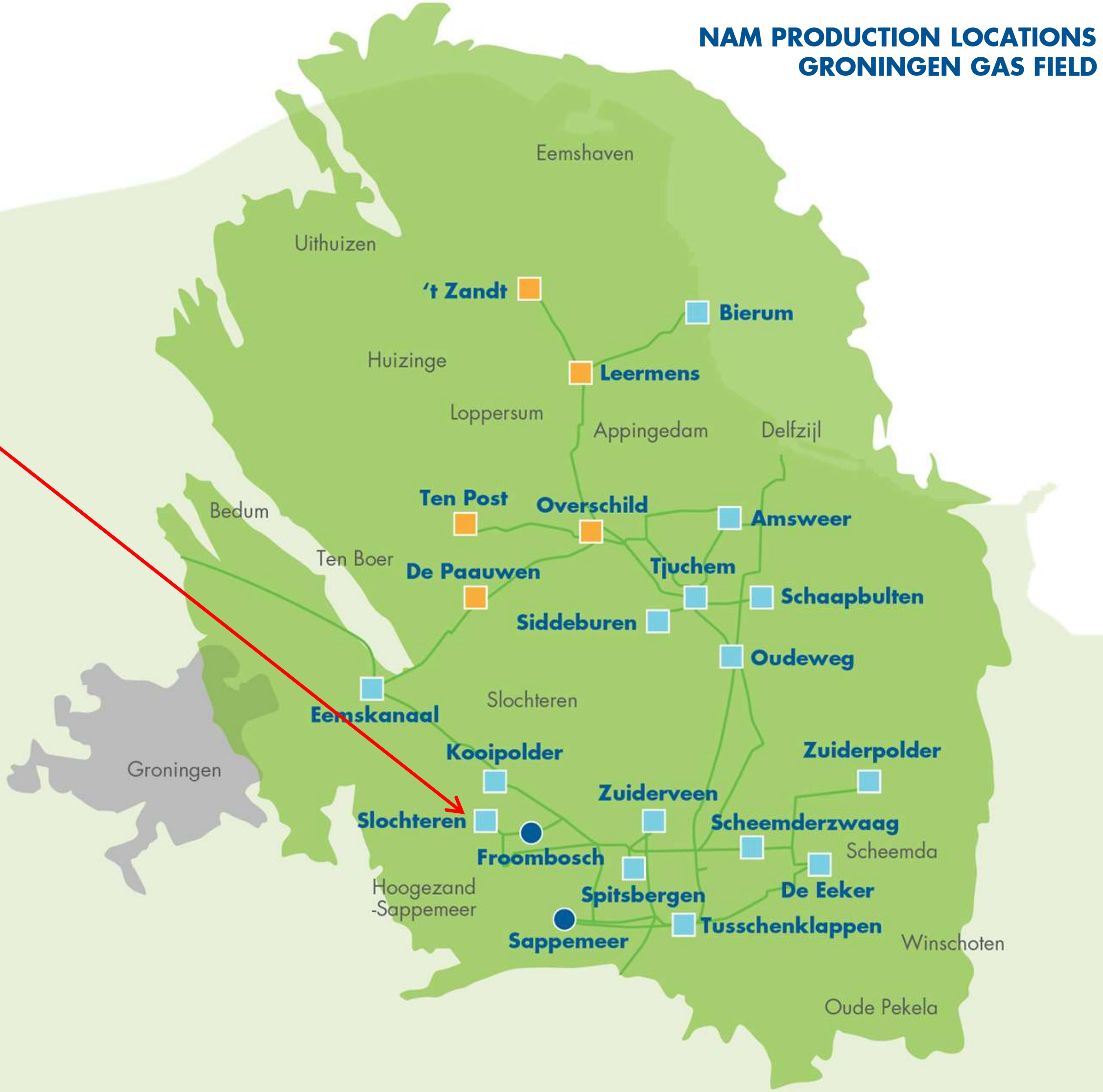

1930's: Start of exploration activities

Gravimetric surveys by the Bataafsche Petroleum Maatschappij

1940's and early 1950's: In search for Zechstein carbonate oil accumulations

<u>HAR-1 (1952)</u>
Target: Permian Zechstein carbonate
Also 200m of water-bearing Slochteren

<u>TBR-1 (1955)</u>
Stopped in shaley upper part Rotliegend

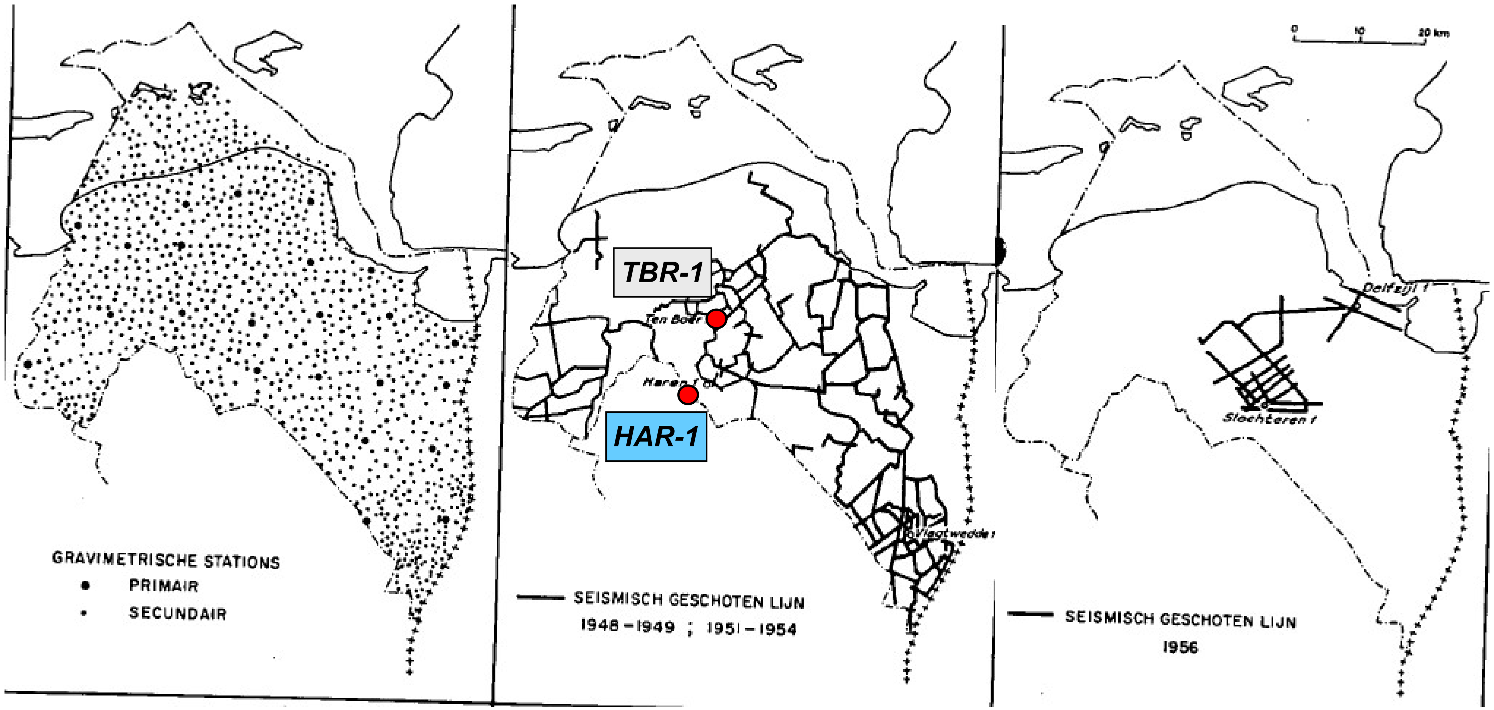

1950's exploration

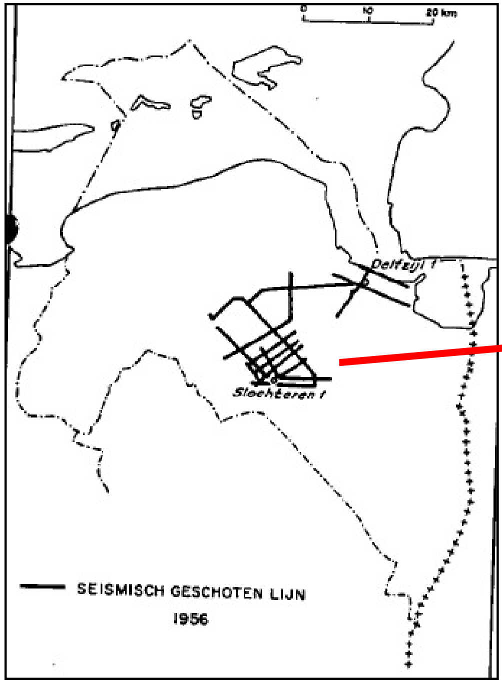

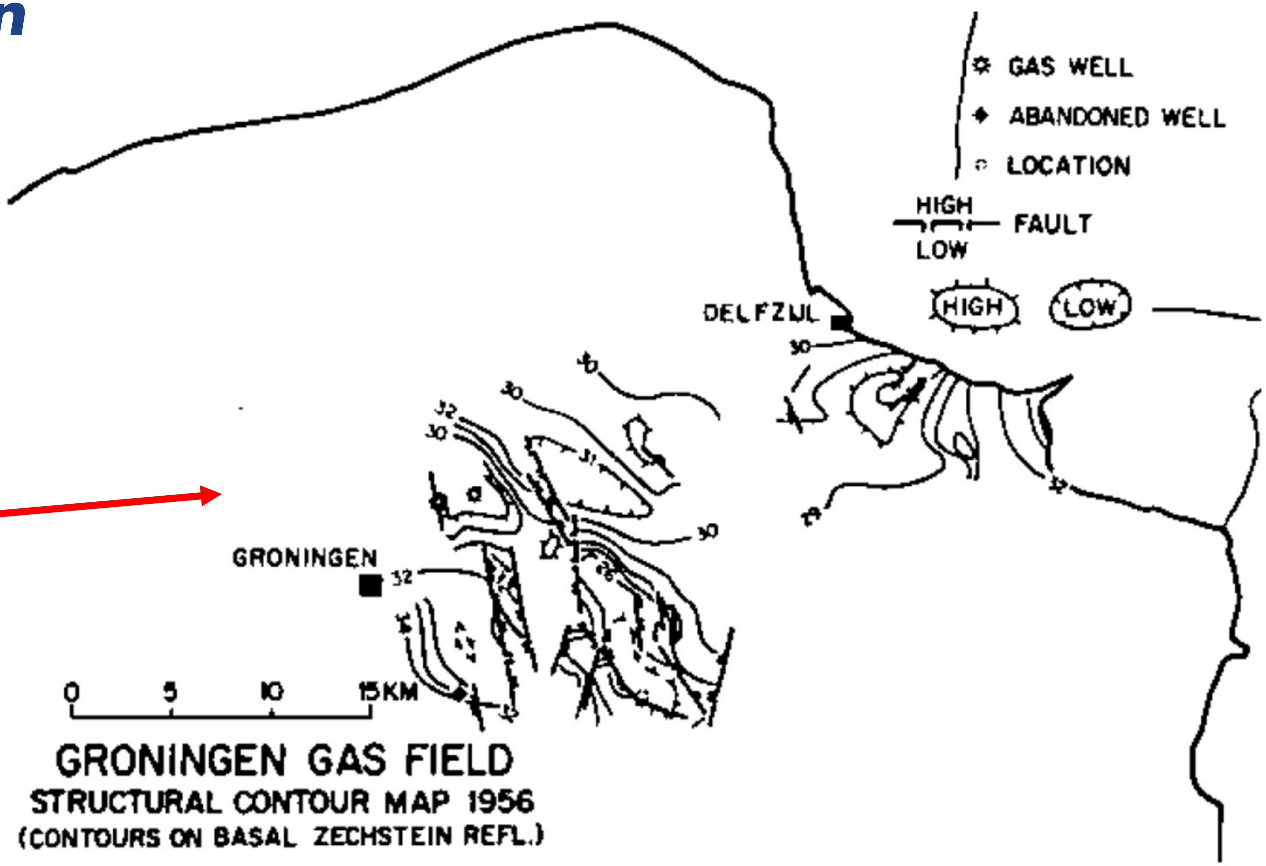

Fig. 3. — Carte en isobathes à la base du Zechstein du champ de Groningen (1956)

FIT4FUTURE

1950's exploration

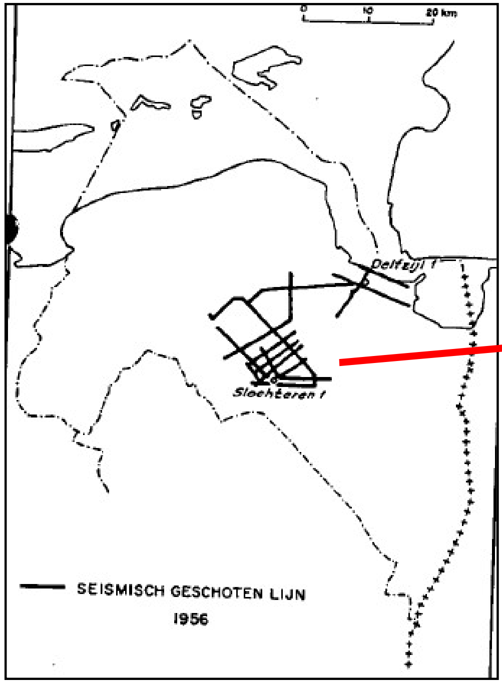

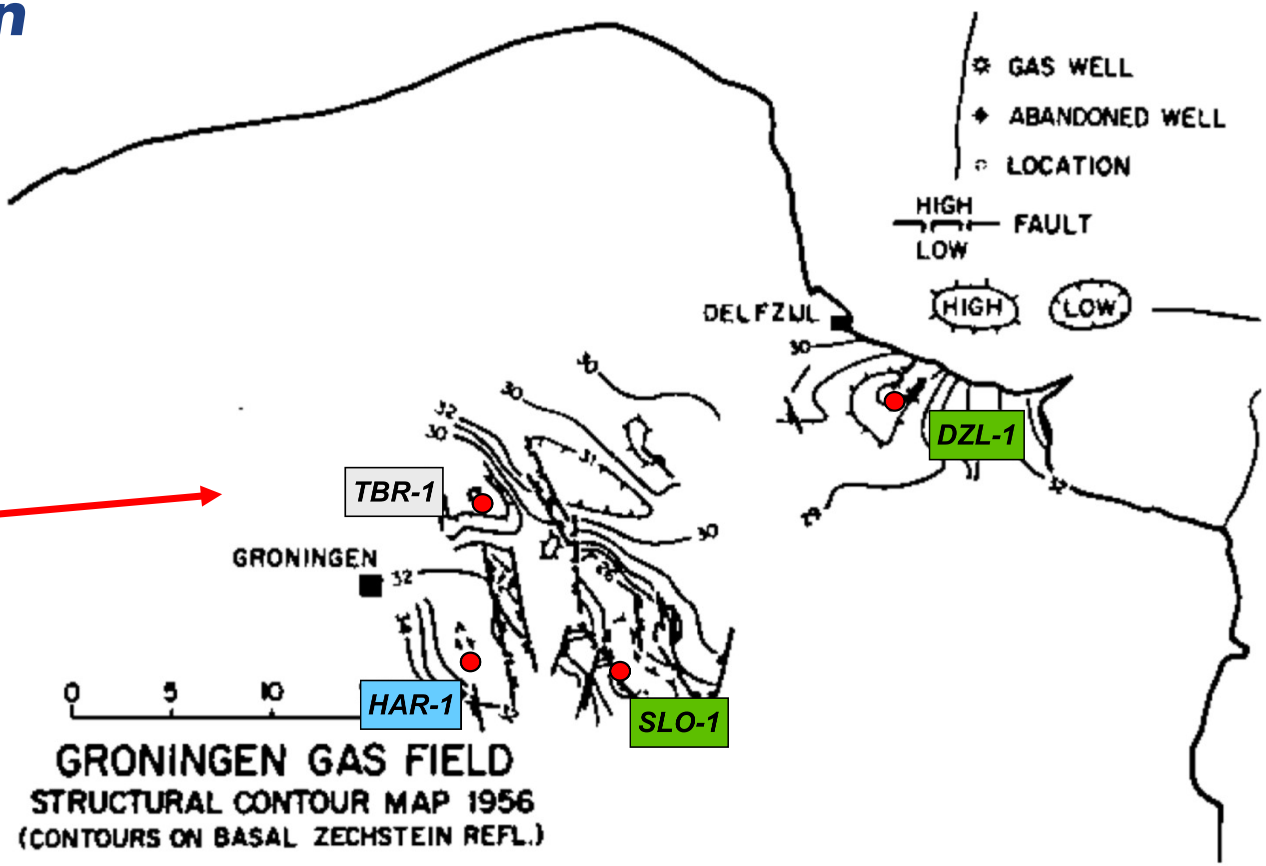

Fig. 3. — Carte en isobathes à la base du Zechstein du champ de Groningen (1956)

1950's exploration

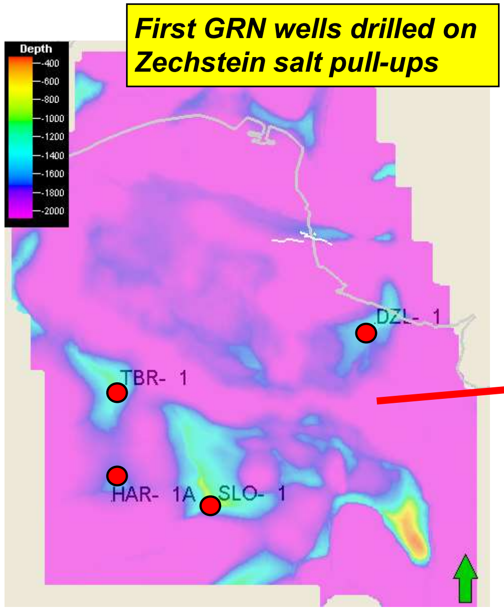

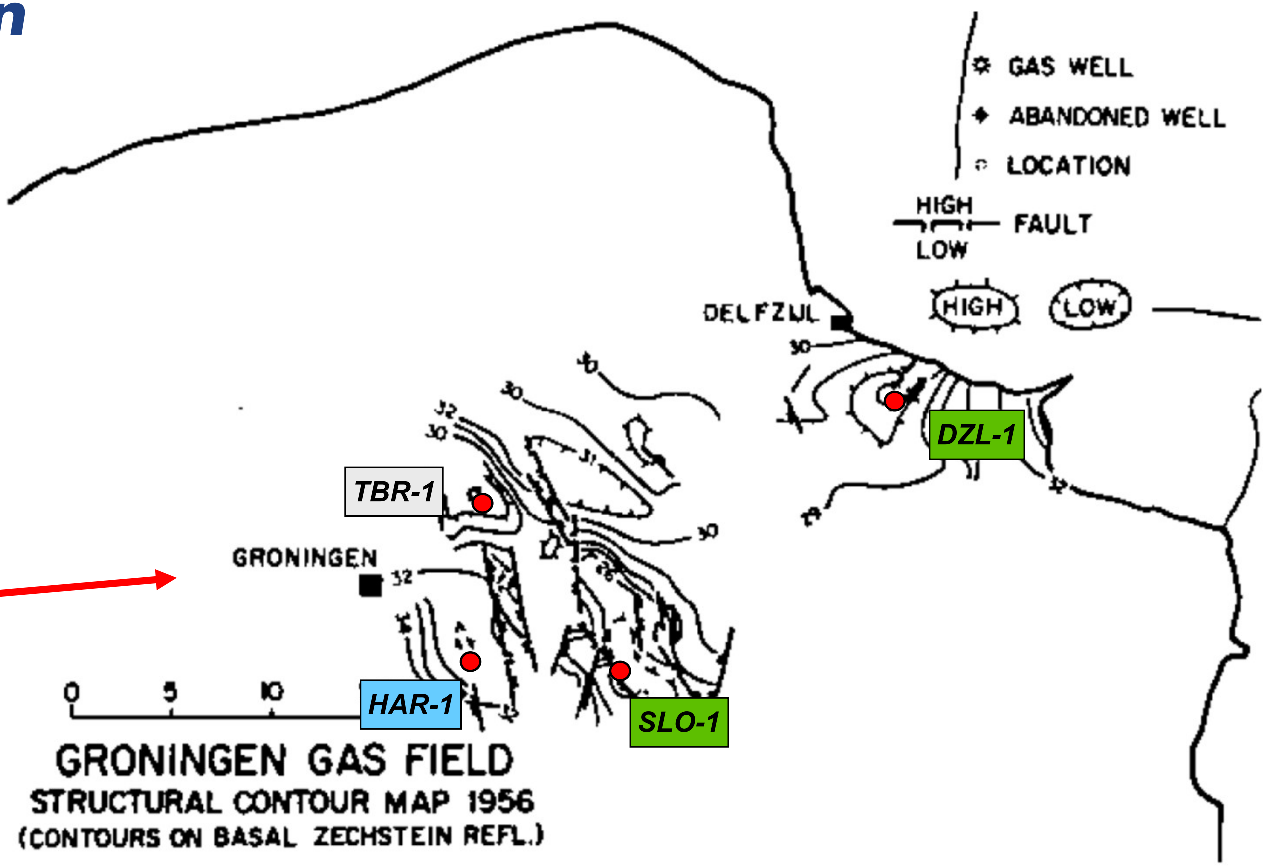

Fig. 3. — Carte en isobathes à la base du Zechstein du champ de Groningen (1956)

GIIP estimate August 3rd 1959 – 5 bcm

DISCOVERY WELL SLOCHTEREN–1

Notitie voor de heer Stheeman

Betreft: Reservoirinhoud van Slochteren

Bij een grondwatervlak dat voor de berekening is aangenomen op 2710 meter, een totale poreuze laagdikte van 25 meter, een gemiddeld connate water gehalte van 30%, een basis oppervlakte van 6,45 km2, een top oppervlakte van 2,25 km2 en een reservoirdruk van 357 at, bedraagt de reservoirinhoud van de Slochteren structuur 5 miljard m3 gas. Hierbij is de inhoud van de dolomieten, die niet te berekenen is, buiten beschouwing gelaten.

Oldenzaal, 3 augustus 1959
C.W.B.

thickness

area

GIIP

Contact (GDT)

water saturation

pressure

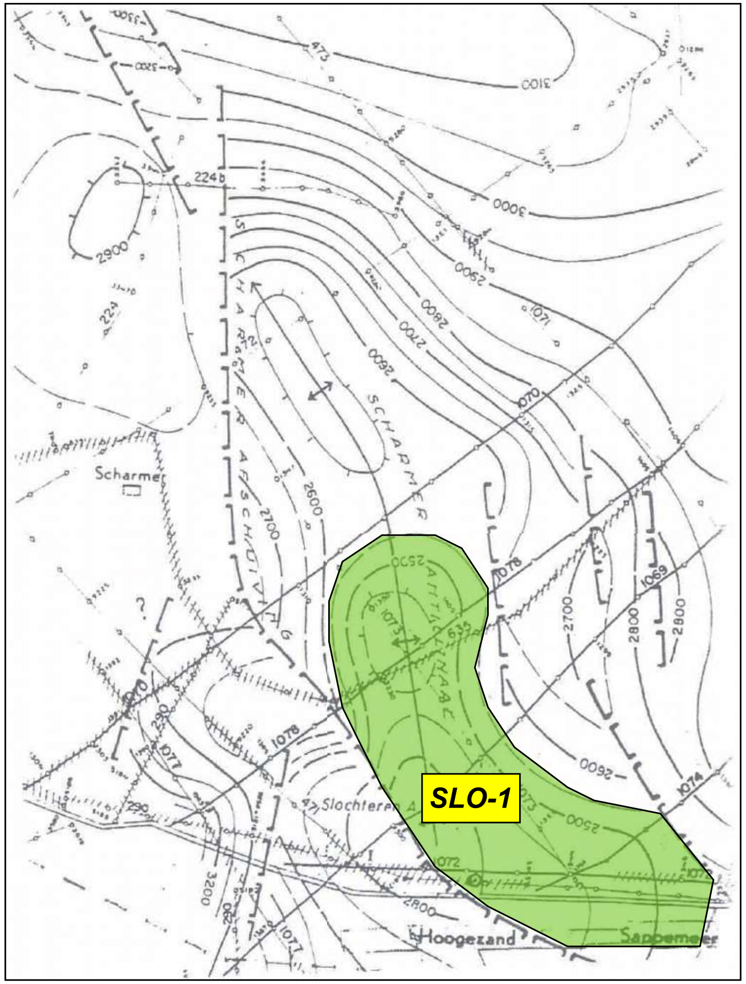

Early1960's: Appraisal prooves one single closure – 1080 bcm

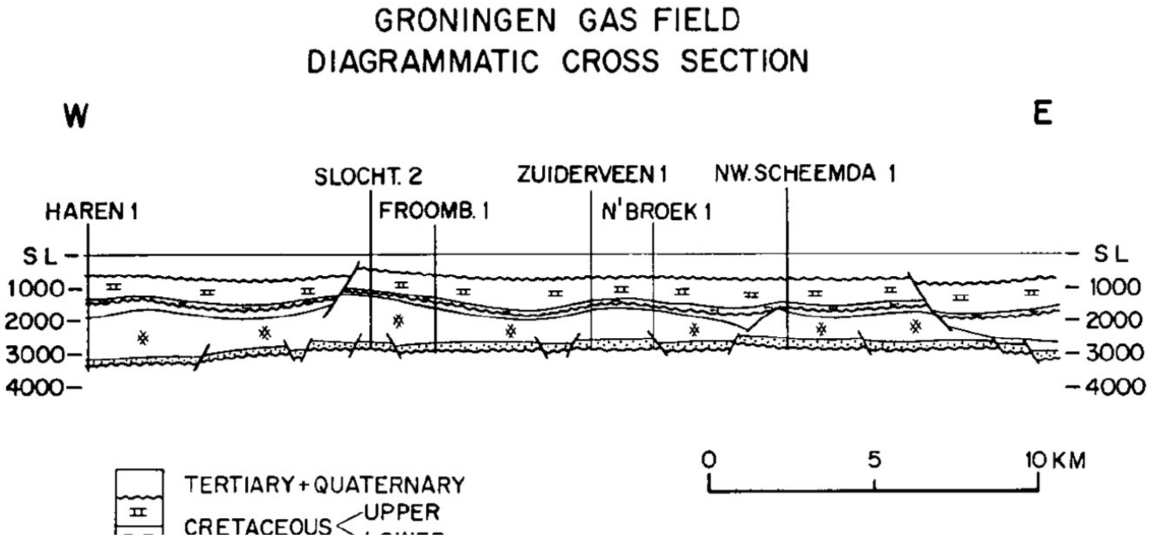

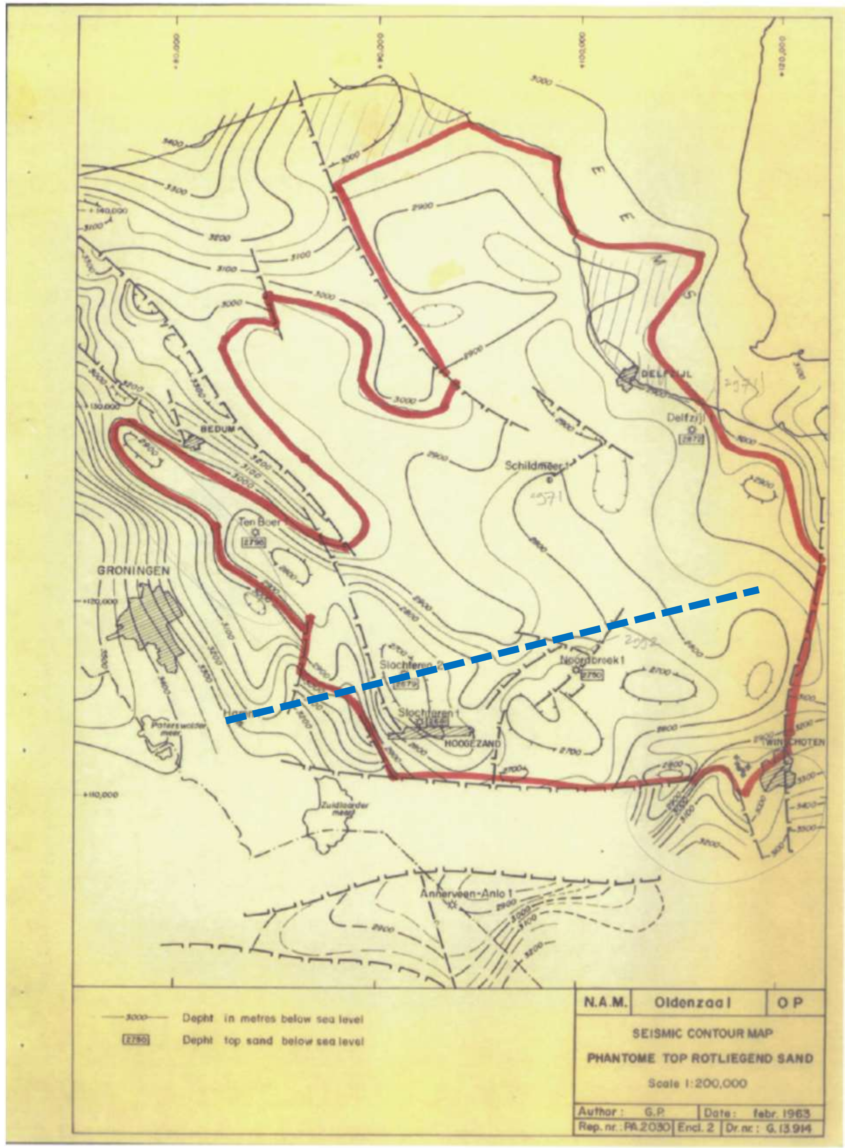

FIT4FUTURE

1966: Northern appraisal – 2480 bcm

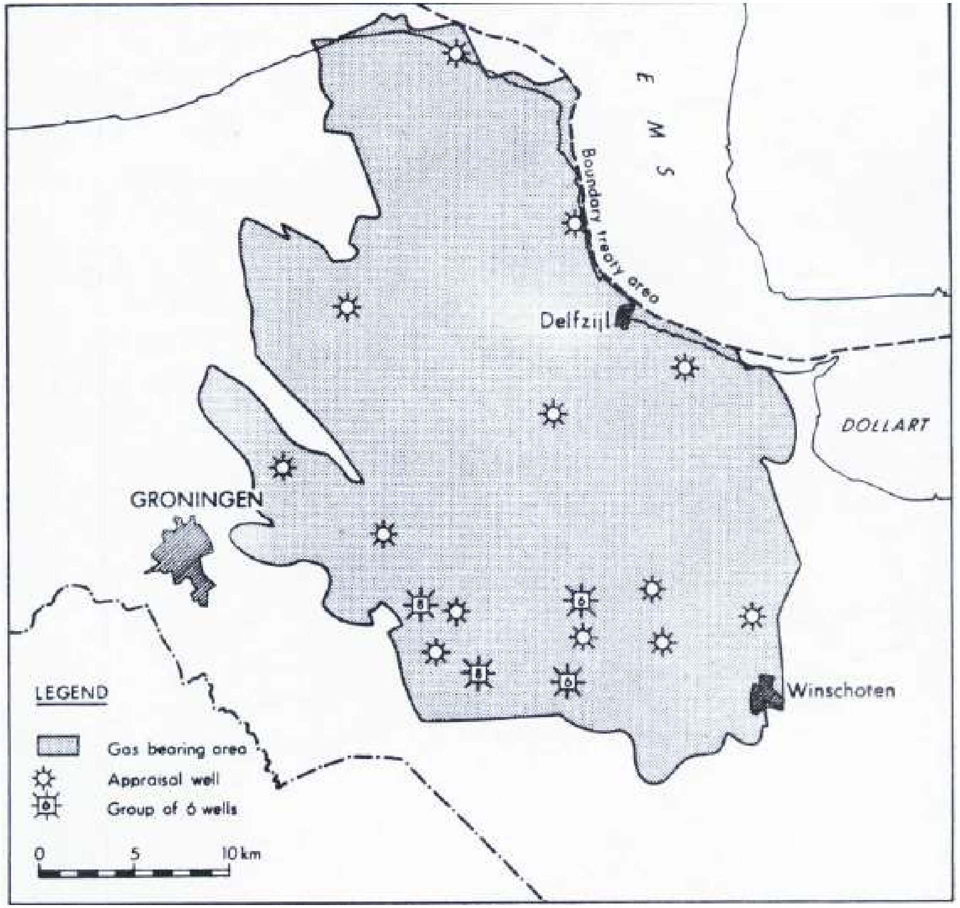

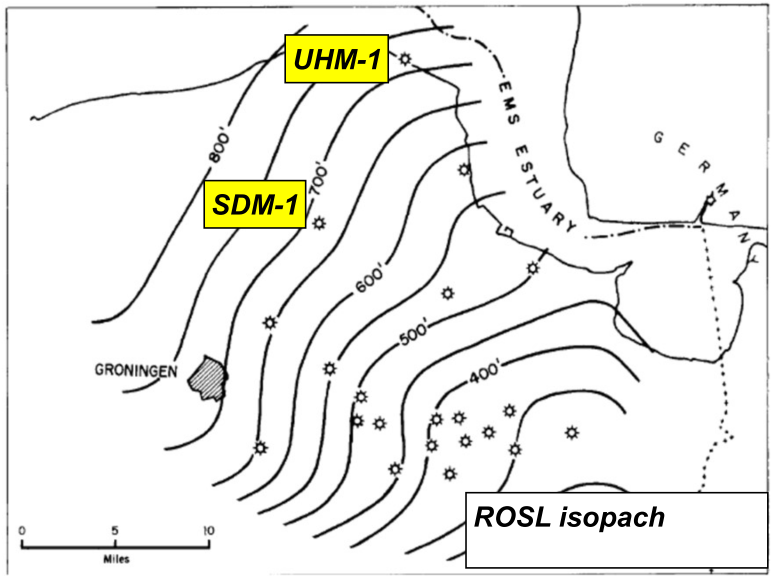

1969: Appraisal/development – 2730 bcm

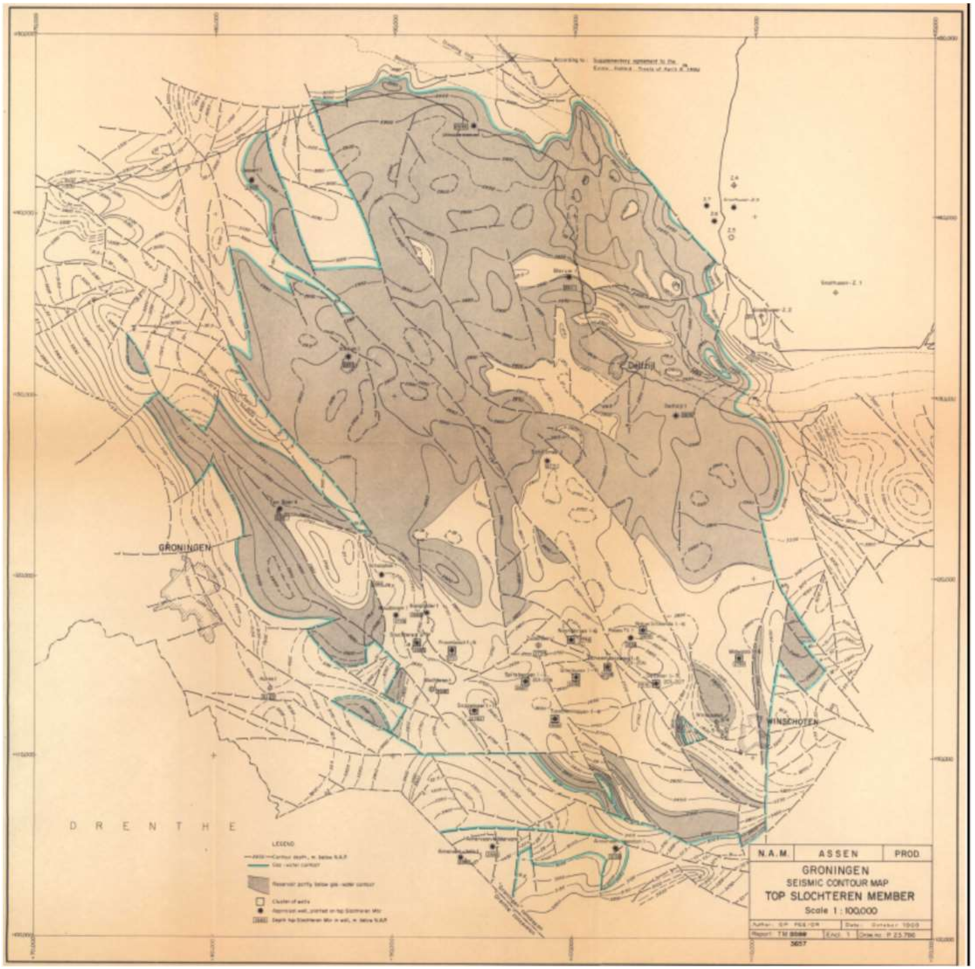

- Additional southern clusters (6)
- Appraisal wells (5)
- New structure USQ and Eems-Dollard area
- Seismic surveys in periphery (1100km)

1970's: Changing field development – 2809 bcm

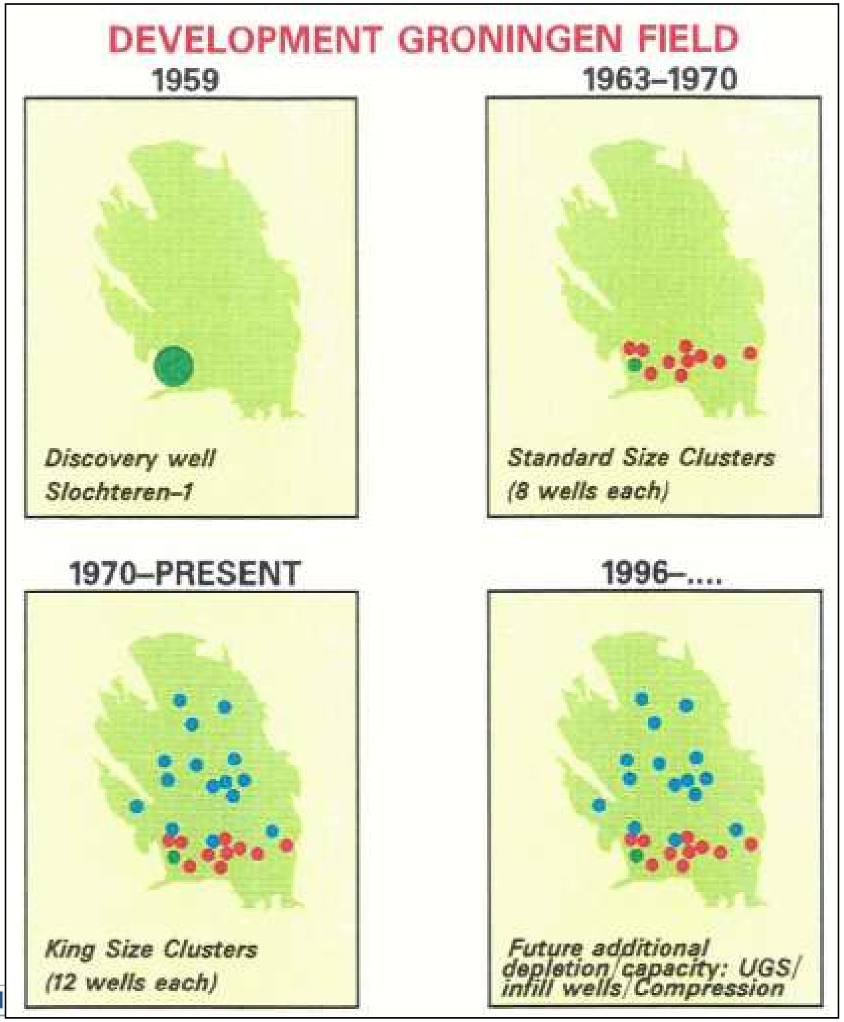

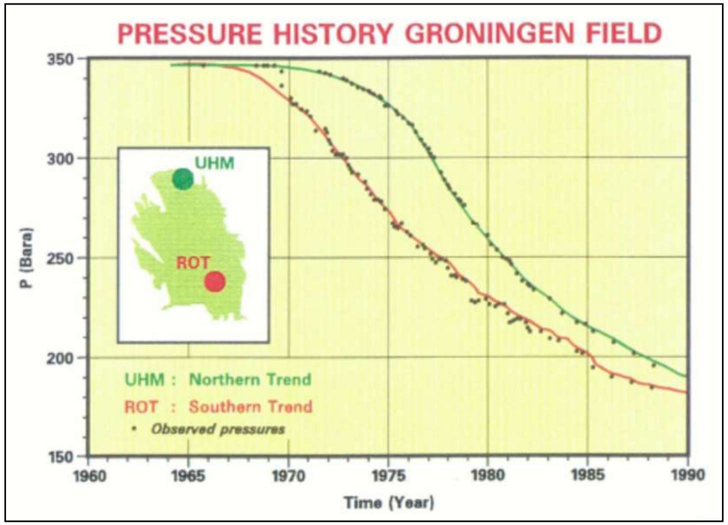

<u>Late 60's - early 70's</u>

- Pressure lag between North and South of the field
- Production preferentially from newly drilled northern and central king-size clusters

1980's: Continued appraisal – 2863 bcm

- Appraisal of peripheral areas
- New petrophysical approach
- Revised temperature distribution
- Acquisition of 3D seismic
- Depositional/facies model

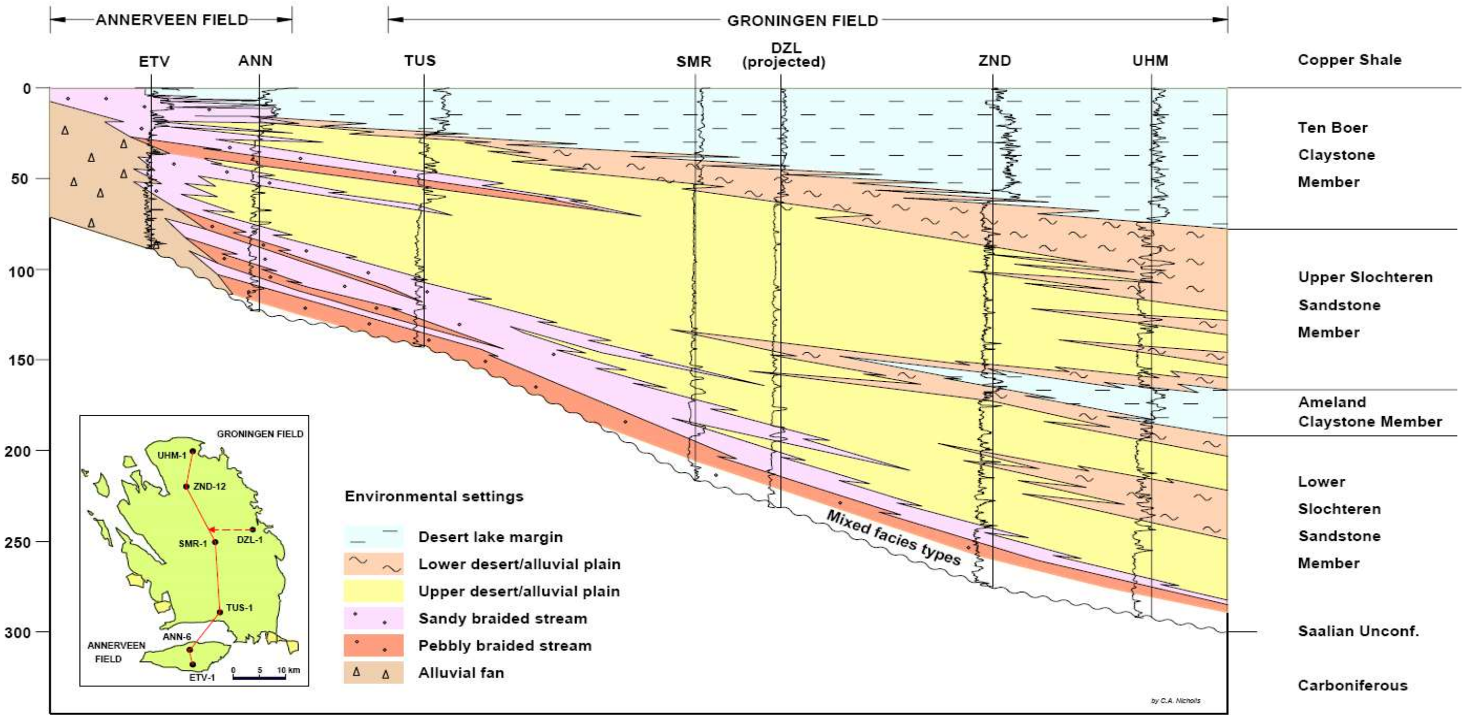

FIT4FUTURE

2000's: More technical developments – 2886 bcm

- Seismic inversion for improved property modelling
- Geochemistry and pressure monitoring
- SW Periphery development

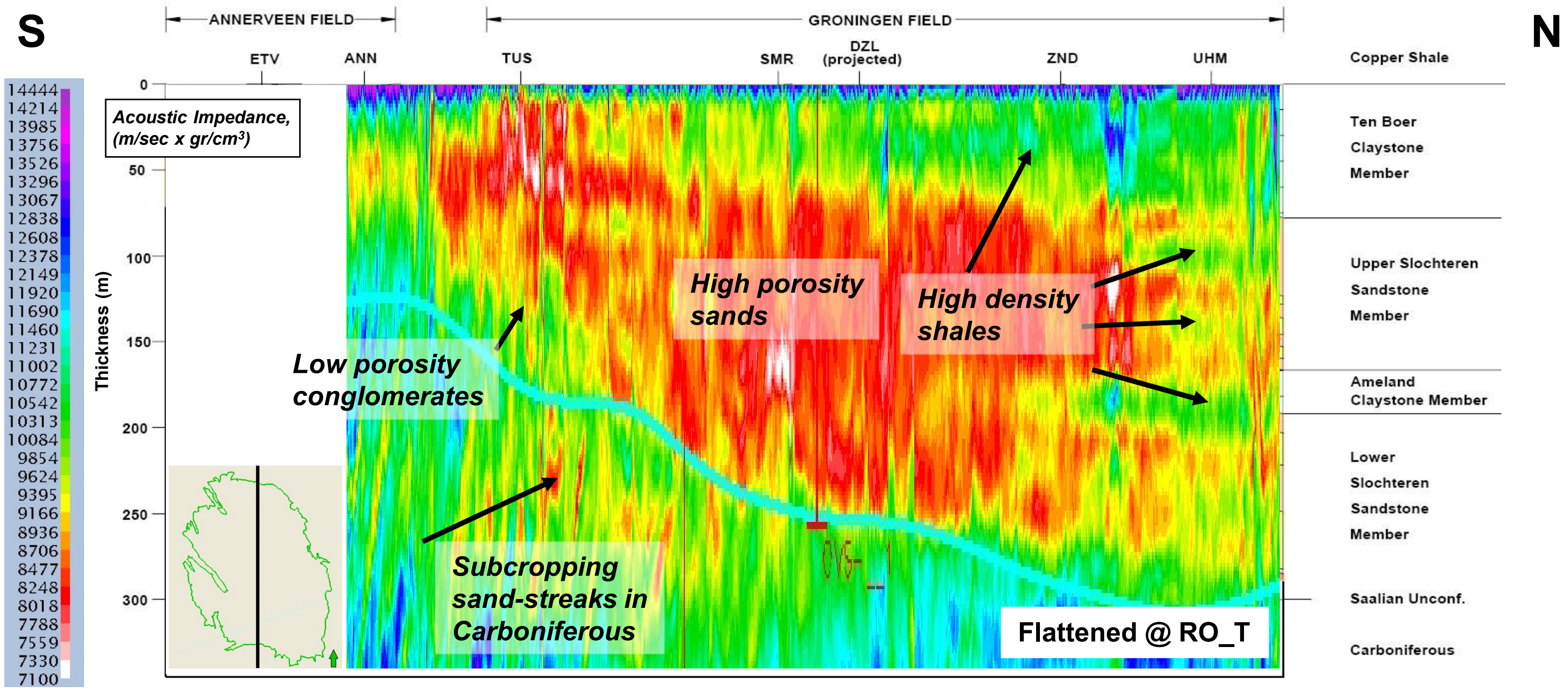

FIT4FUTURE

2012: High-resolution 3D models – 2917 bcm

- Advanced static modelling approaches – Petrel
- High-resolution 3D model grid
- Full well stock used for property modelling
- Improved structural model

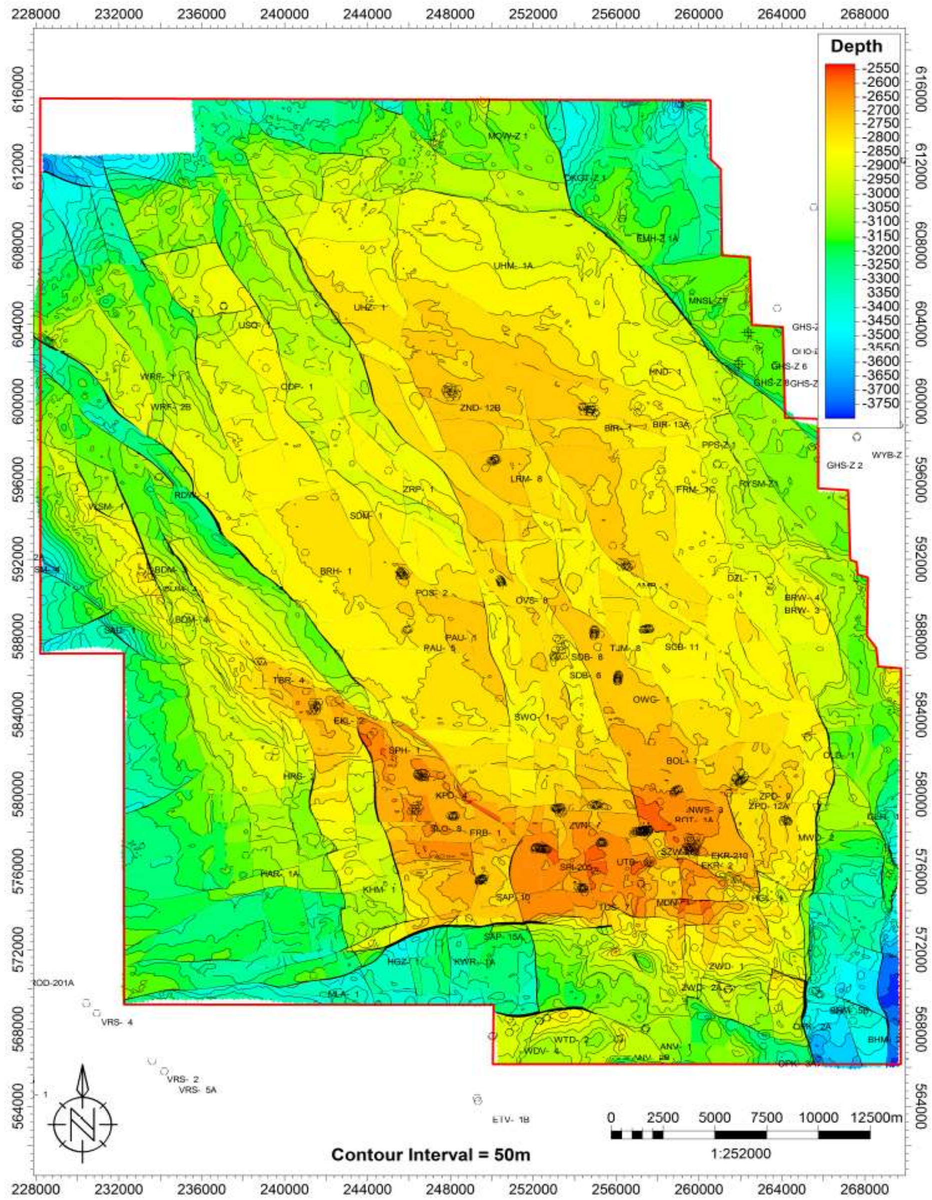

FIT4FUTURE

2018: More technical developments ~2890 bcm

- Extended model area to include lateral aquifers and Carboniferous layers
- Improved property modeling using inversion-derived porosity cube
- Extensive fine-tuning of modelling steps

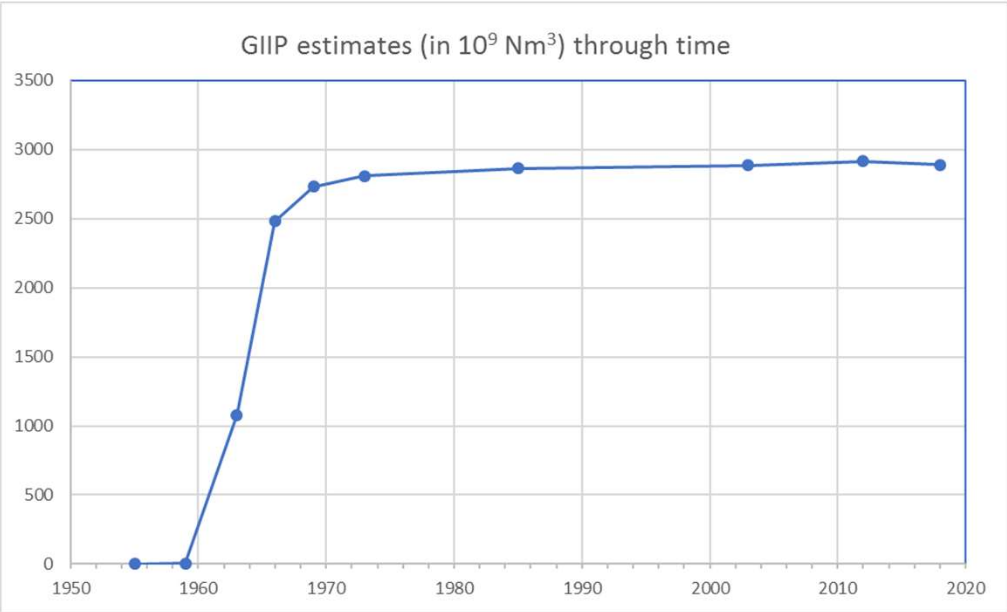

FIT4FUTURE

TECTONIC SETTING

Late Carboniferous Pangea Supercontinent

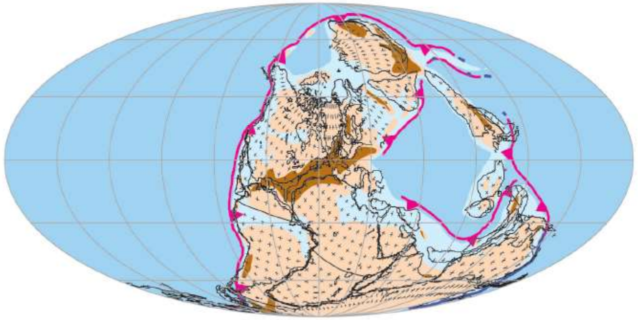

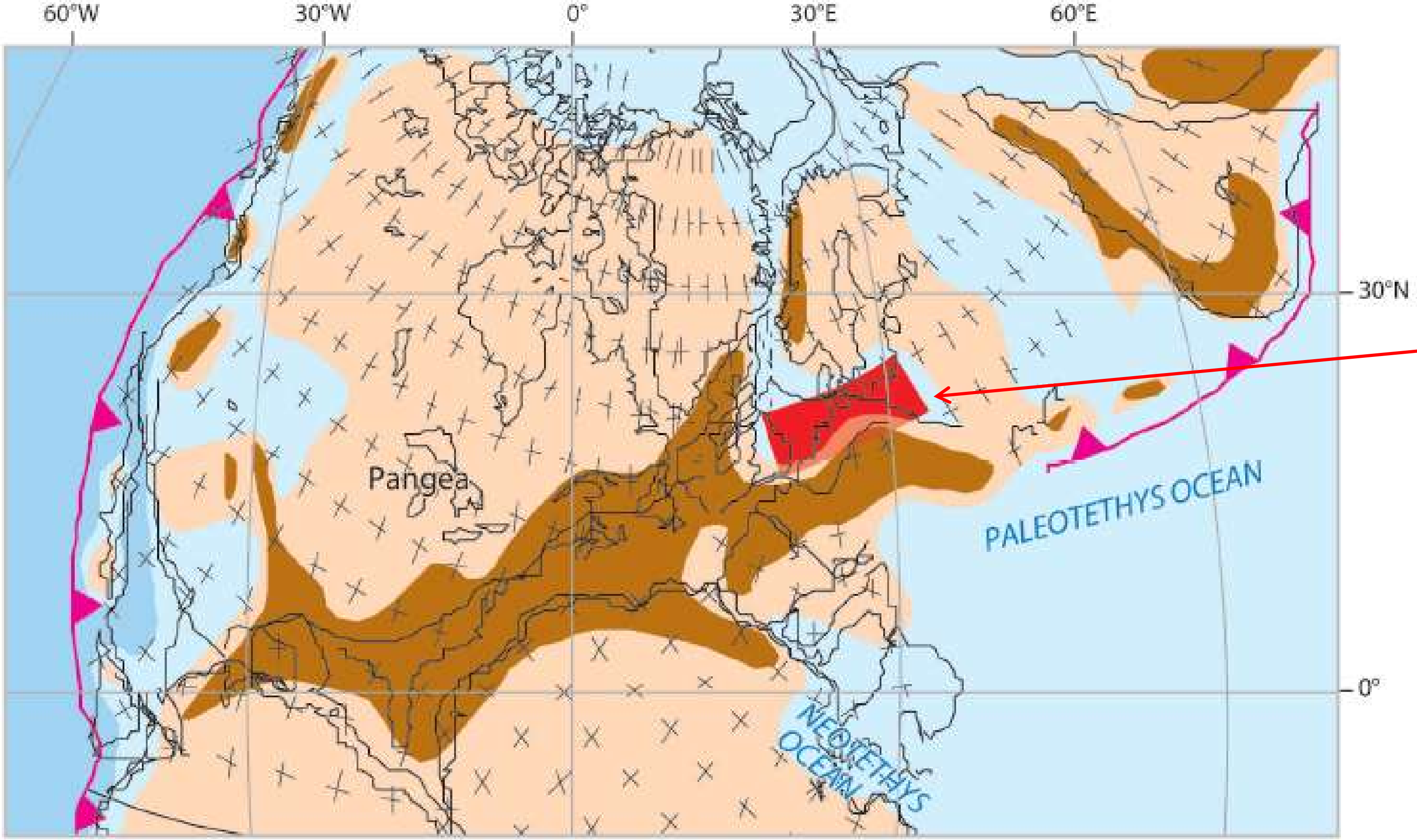

Southern Permian Basin

Rotliegend thickness map

Groningen area

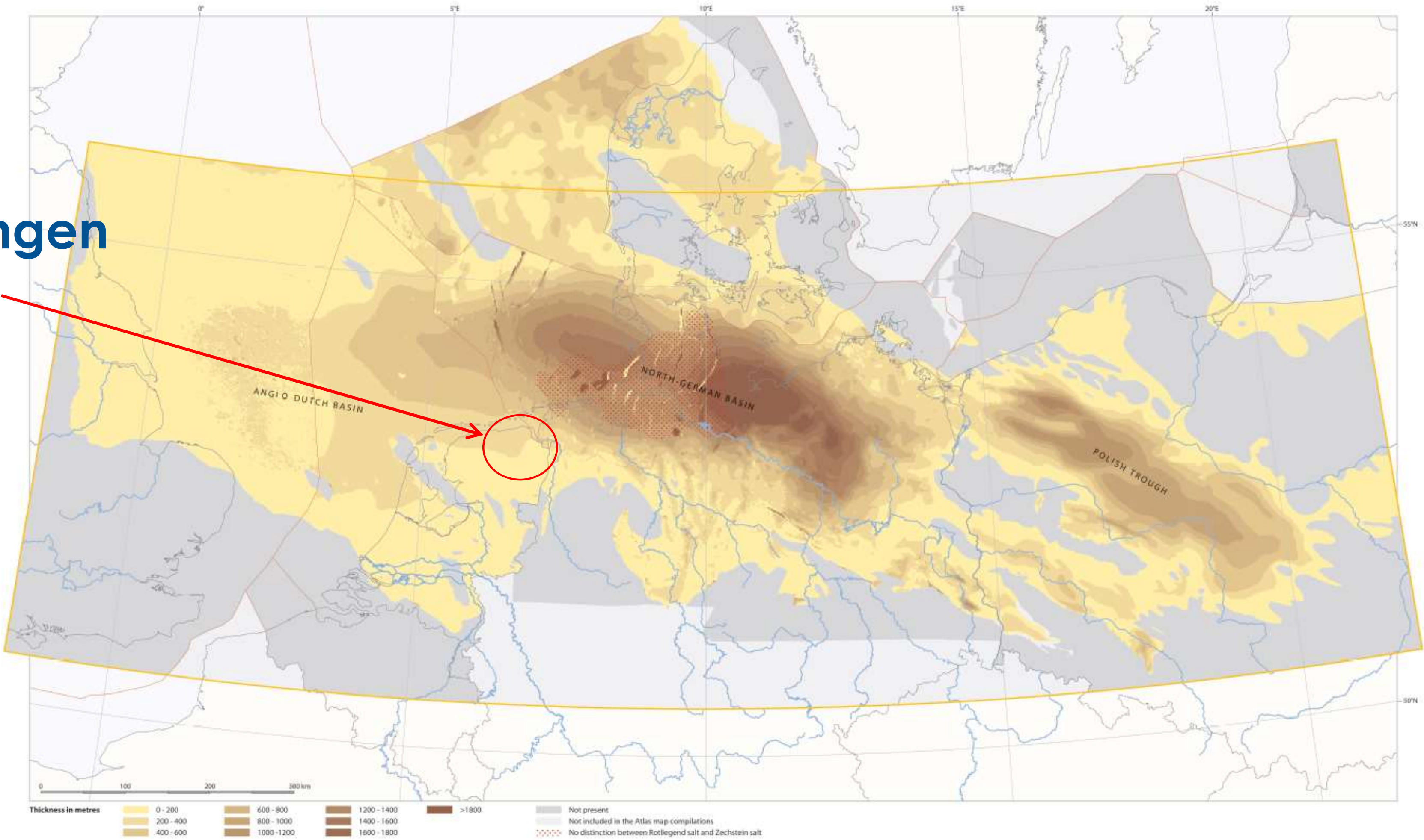

FIT4FUTURE

Schematic cross-section

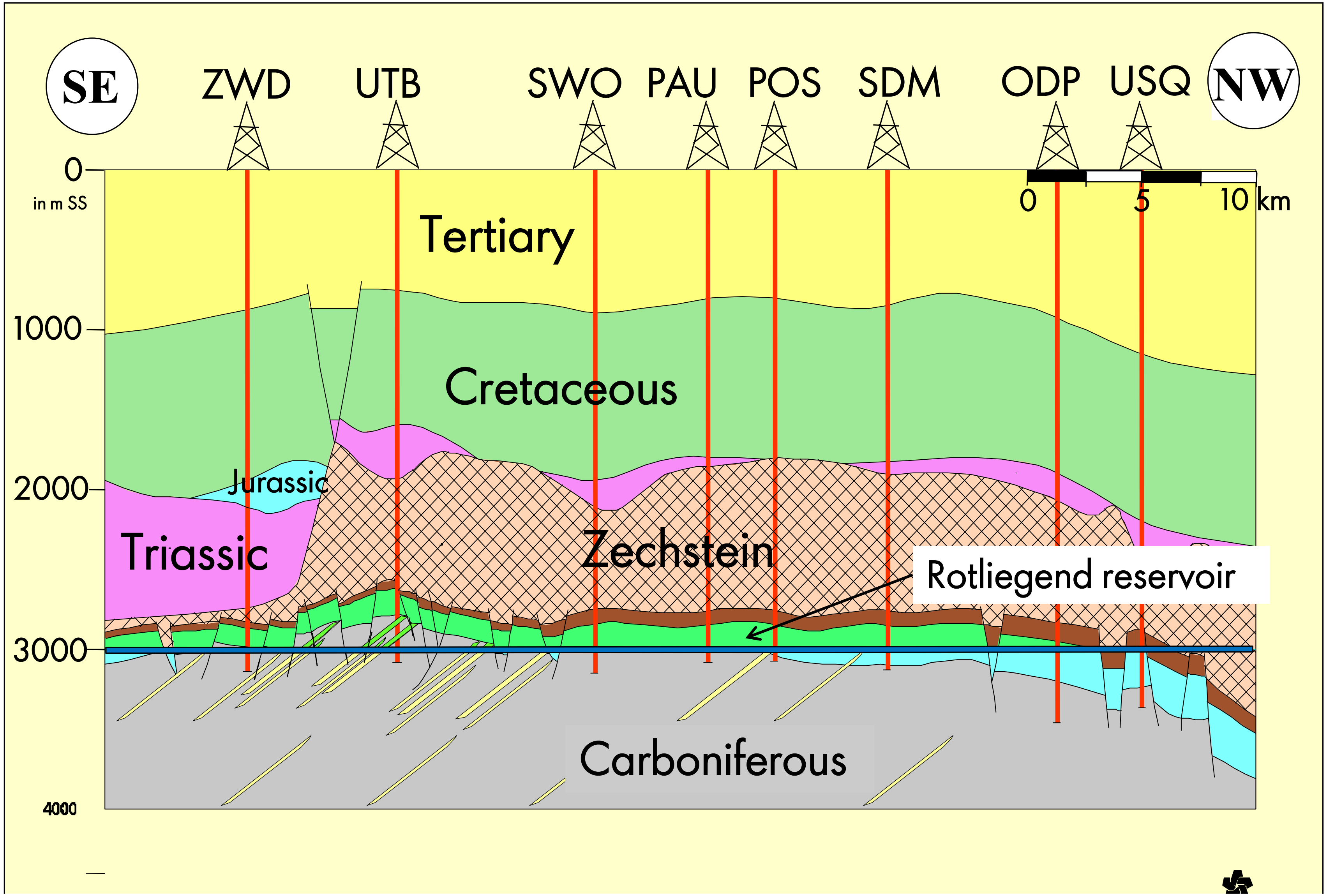

Main tectonic phases

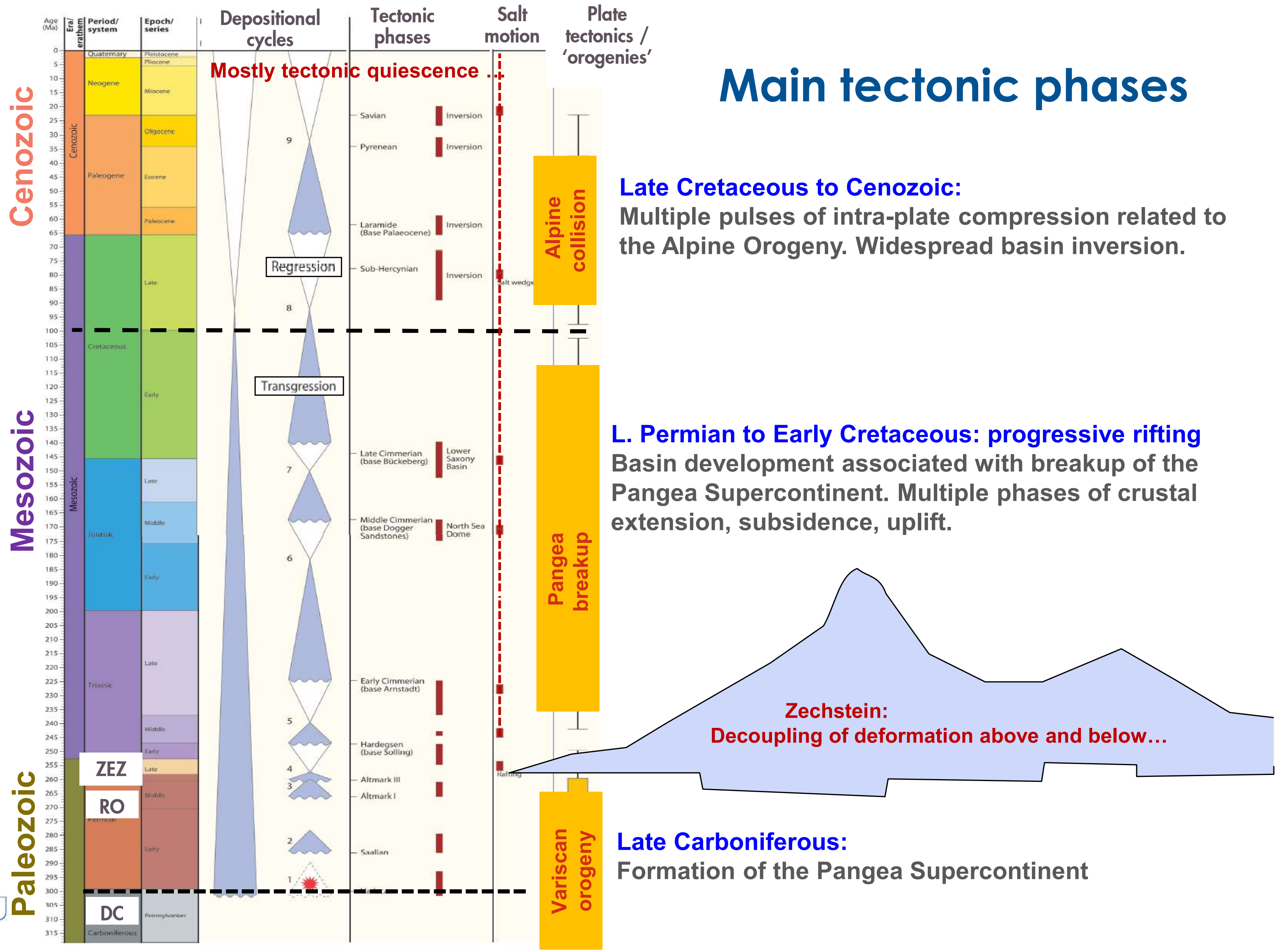

Late Cretaceous to Cenozoic:
Multiple pulses of intra-plate compression related to the Alpine Orogeny. Widespread basin inversion.

L. Permian to Early Cretaceous: progressive rifting
Basin development associated with breakup of the Pangea Supercontinent. Multiple phases of crustal extension, subsidence, uplift.

Late Carboniferous:
Formation of the Pangea Supercontinent

FIT4FUTURE

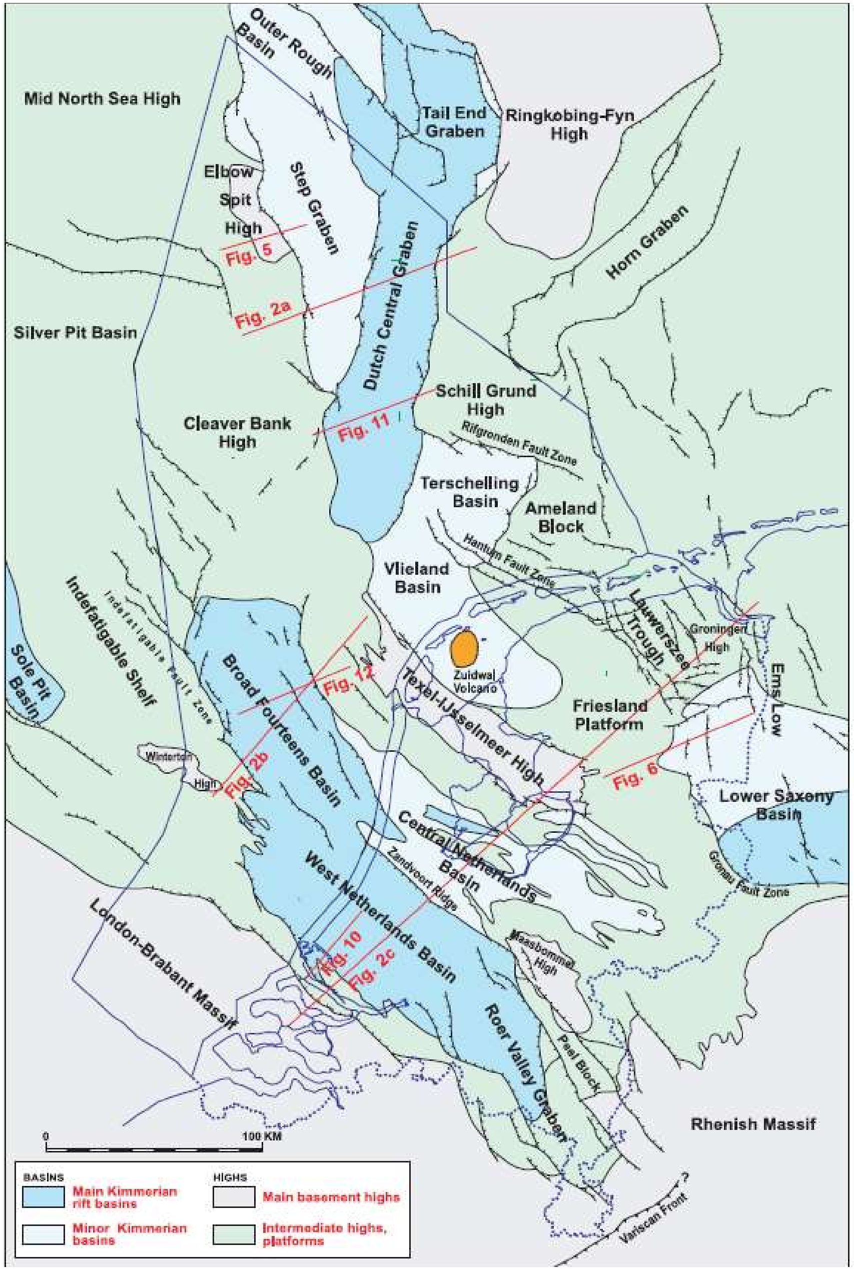

Main structural elements in the Netherlands

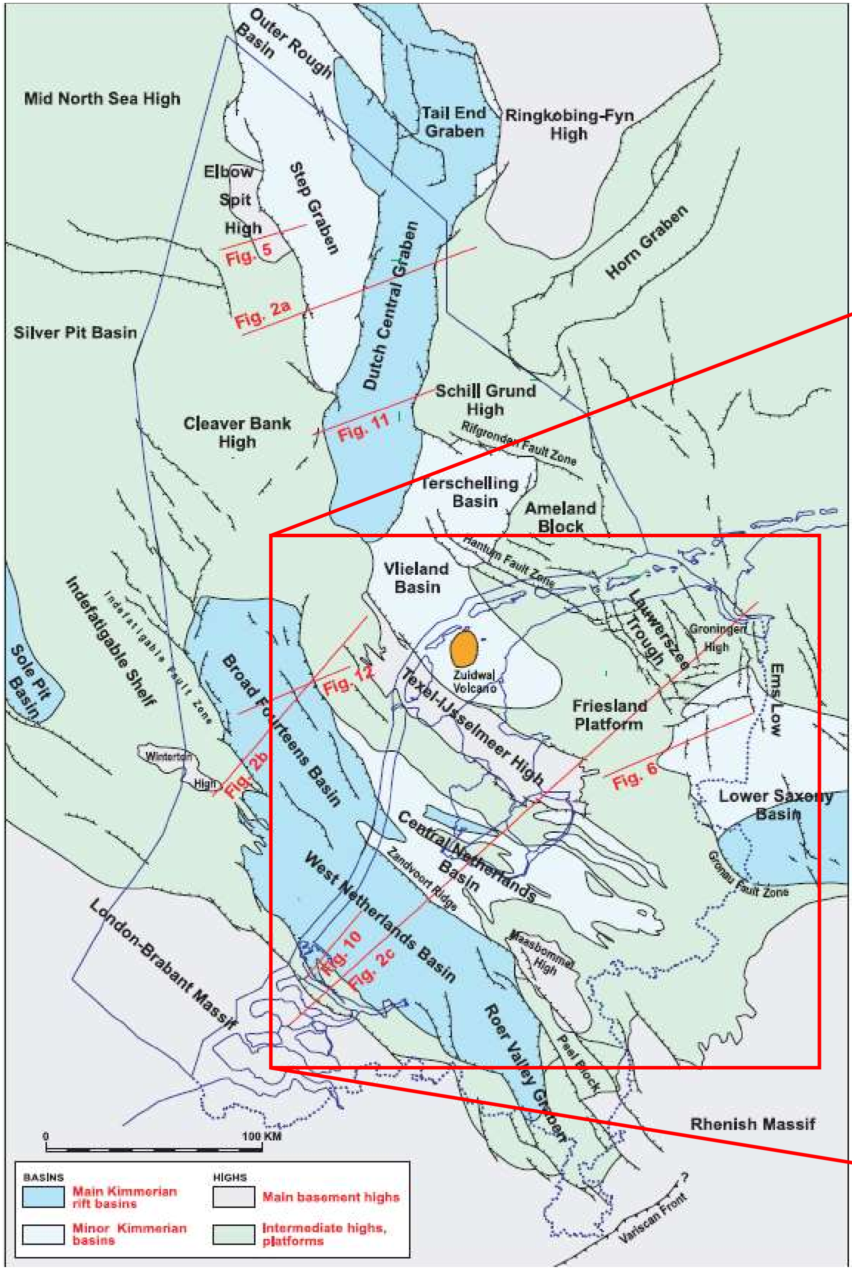

Main structural elements

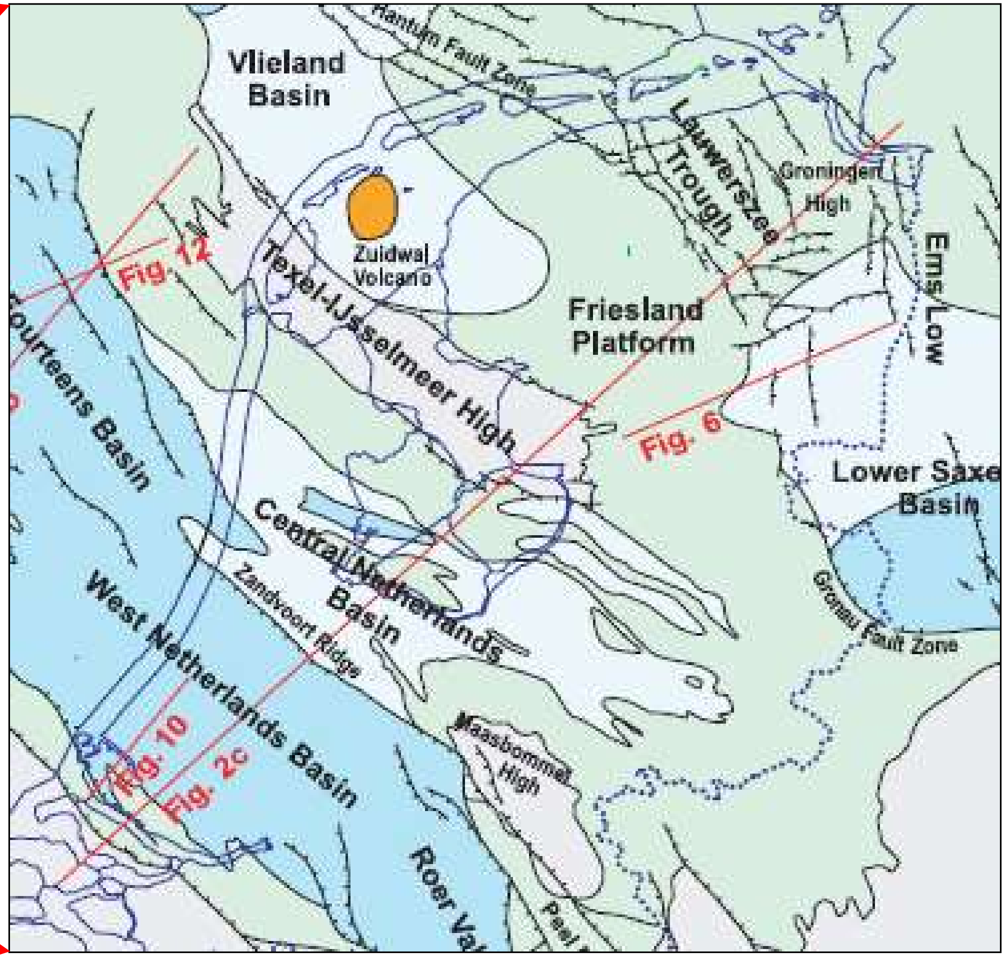

Regional geological overview

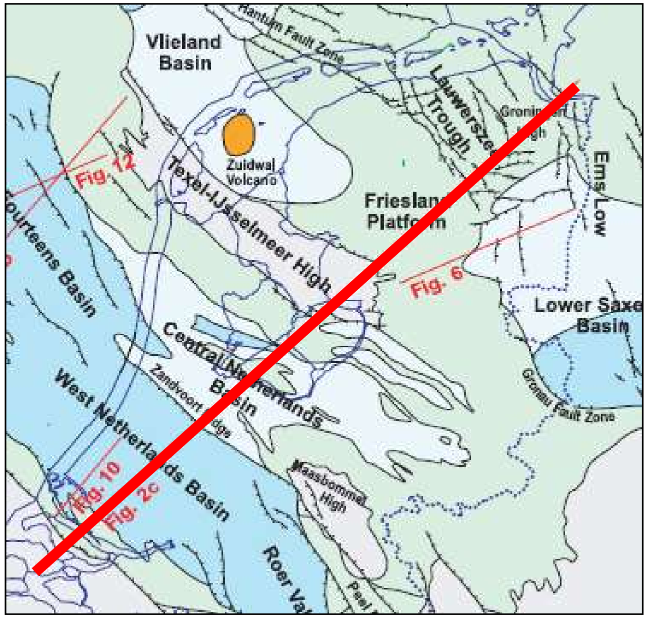

- Cenozoic
- Upper Cretaceous
- Lower Cretaceous
- Upper Jurassic
- Lower and Middle Jurassic
- Triassic
- Upper Permian (Zechstein)
- Middle and Upper Permian (Rotliegend)
- Carboniferous and older

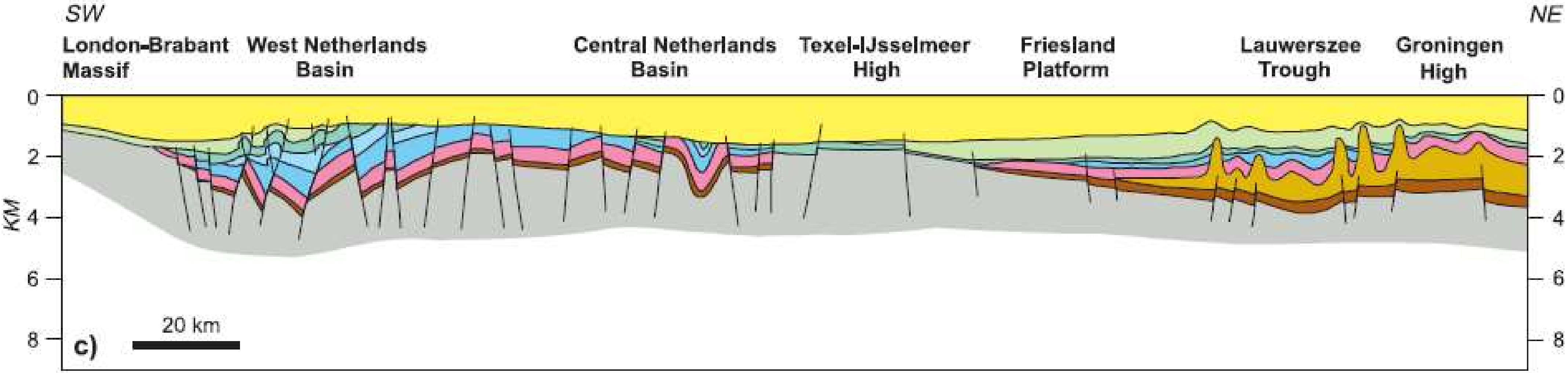

Regional Top_Rotliegend semblance map

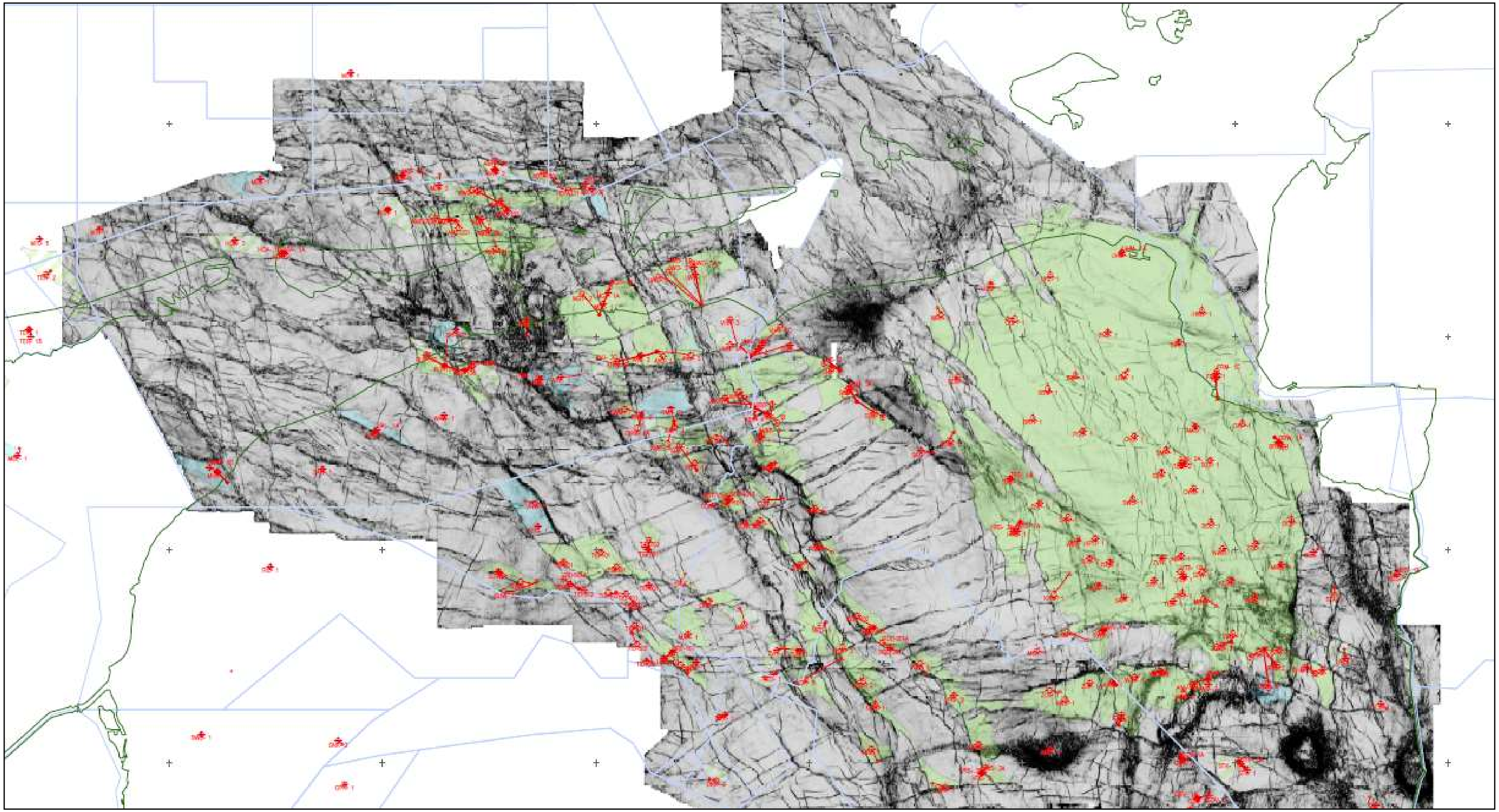

Top_Rotliegend structural map

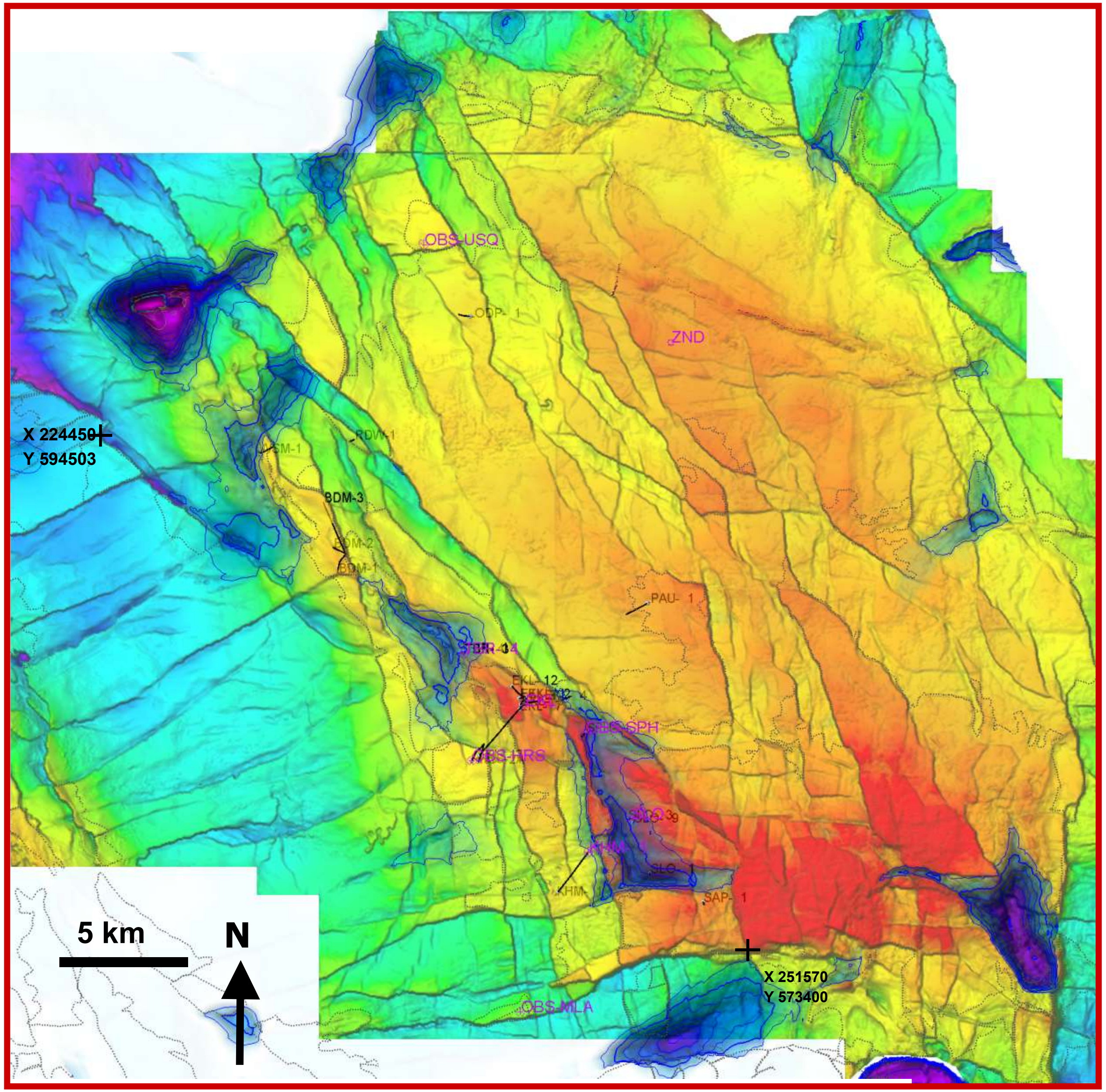

FIT4FUTURE

Top_Rotliegend structural map

Next slide

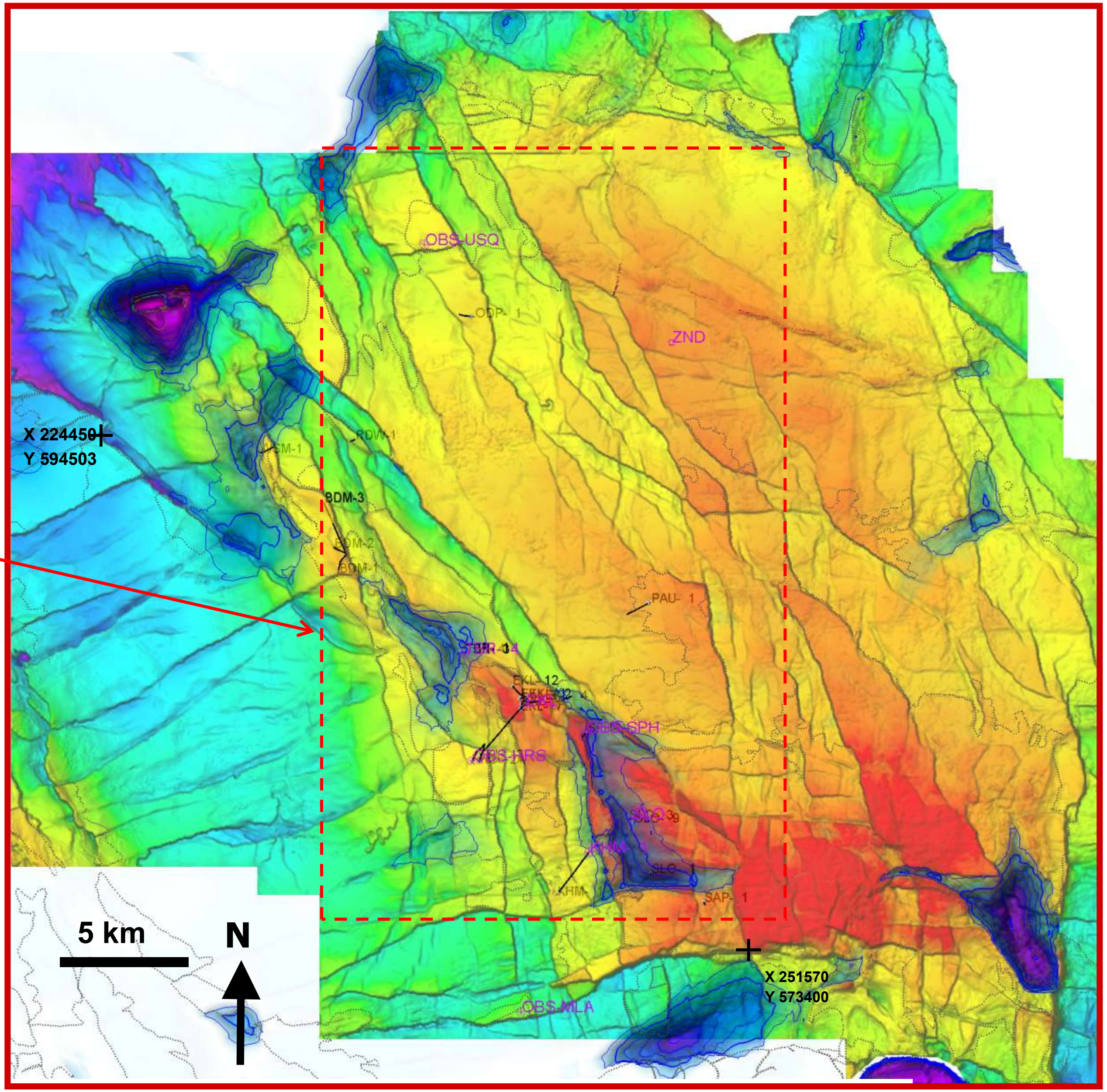

FIT4FUTURE

Detailed fault interpretation

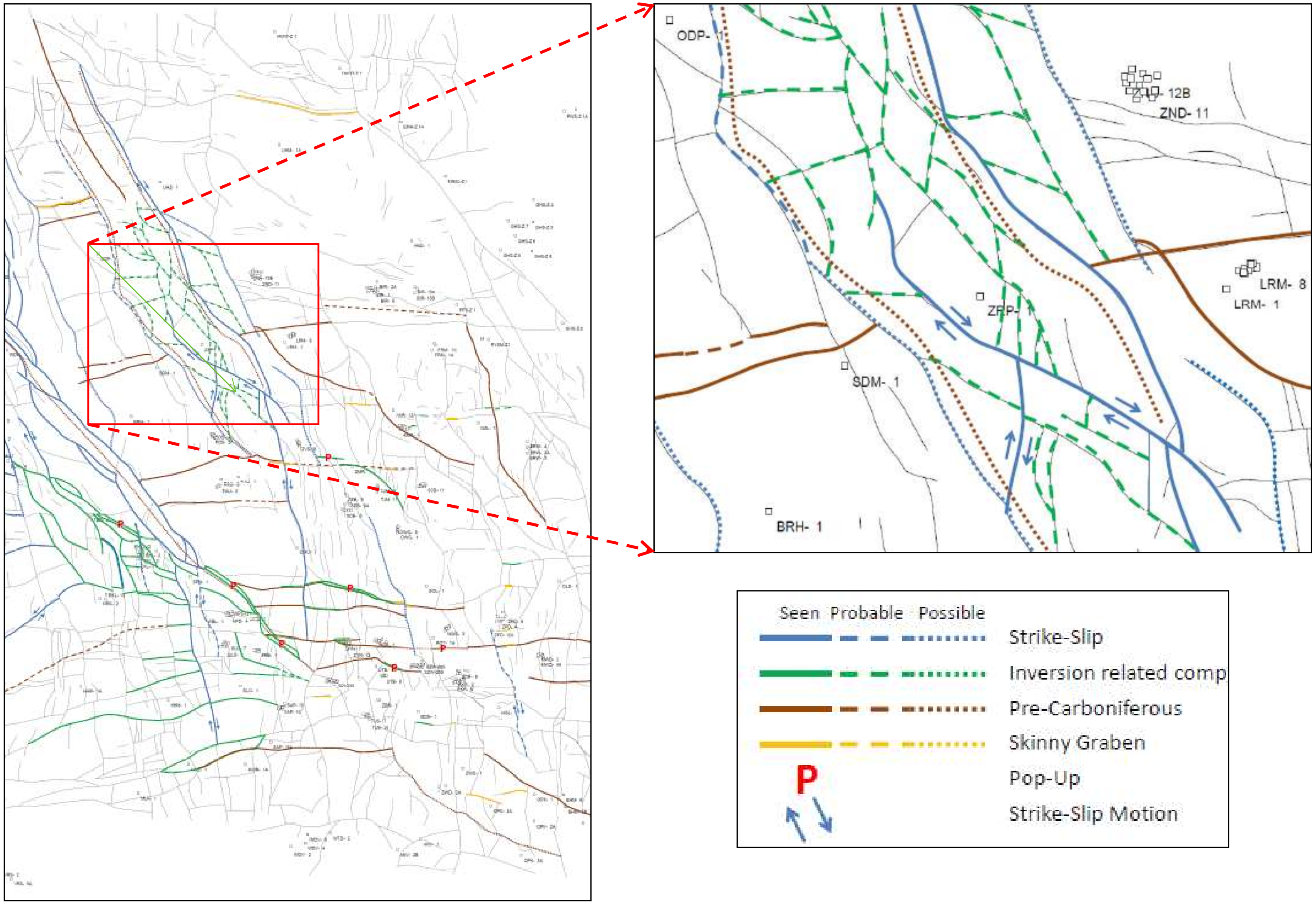

Underburden faulting

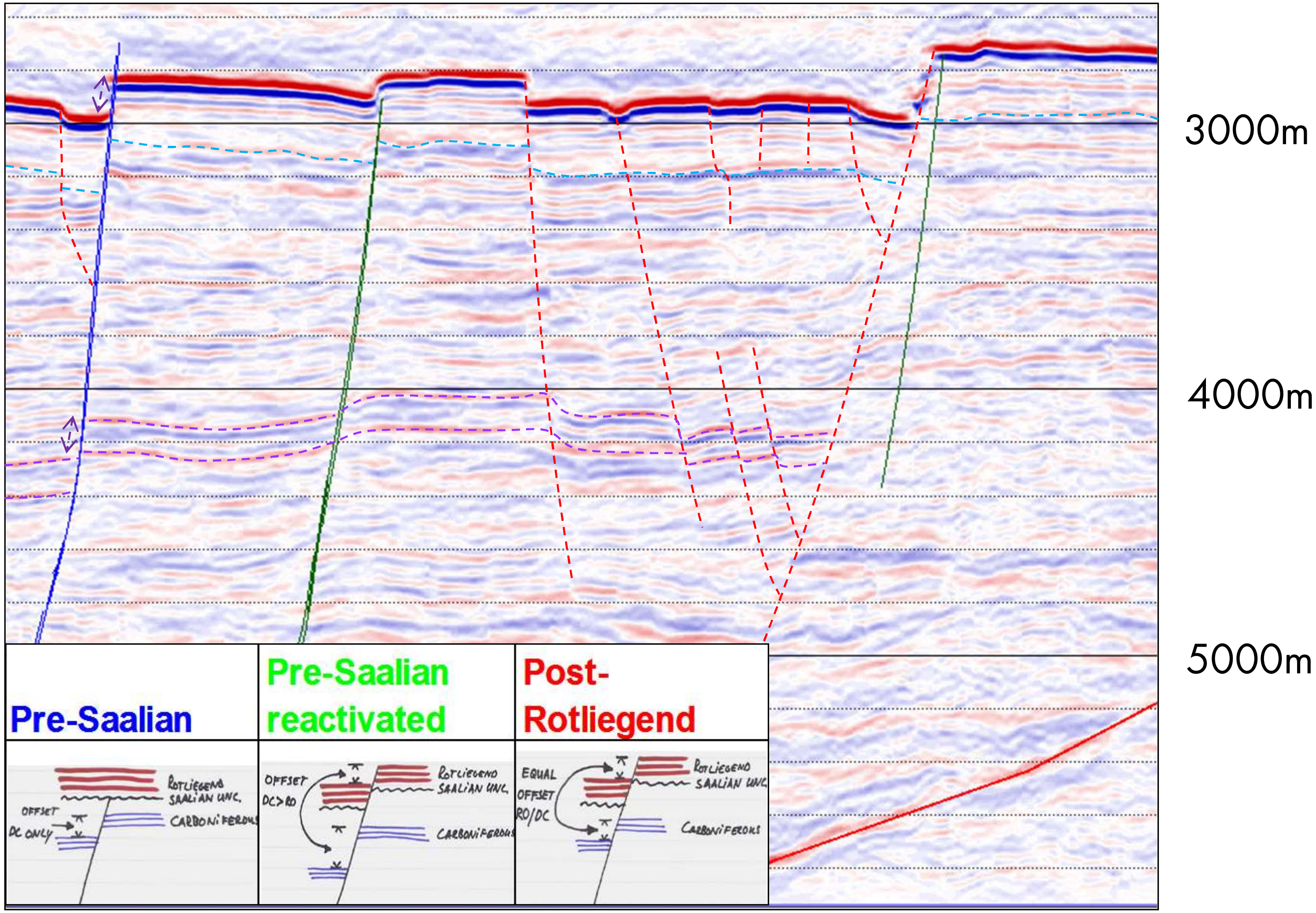

Groningen fault throw map

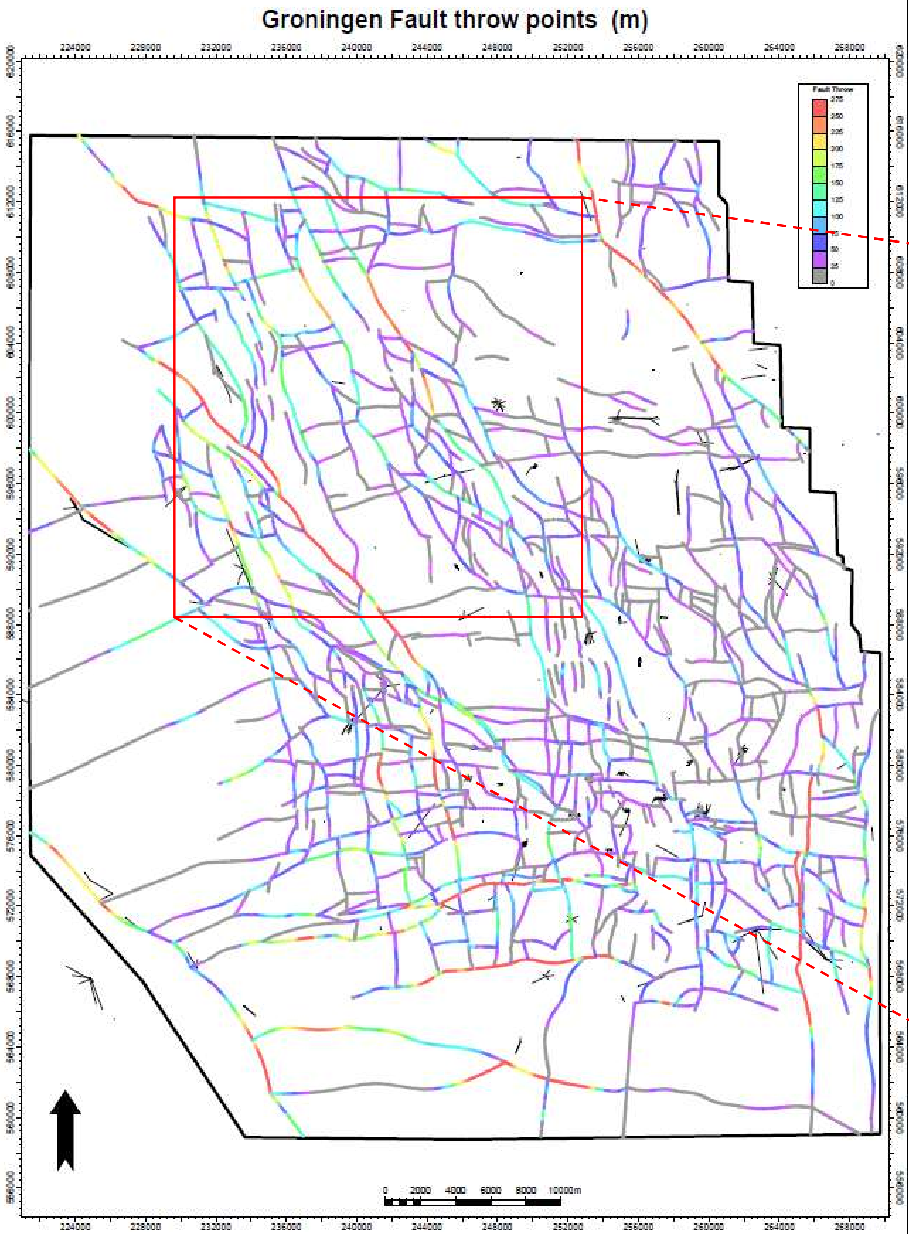

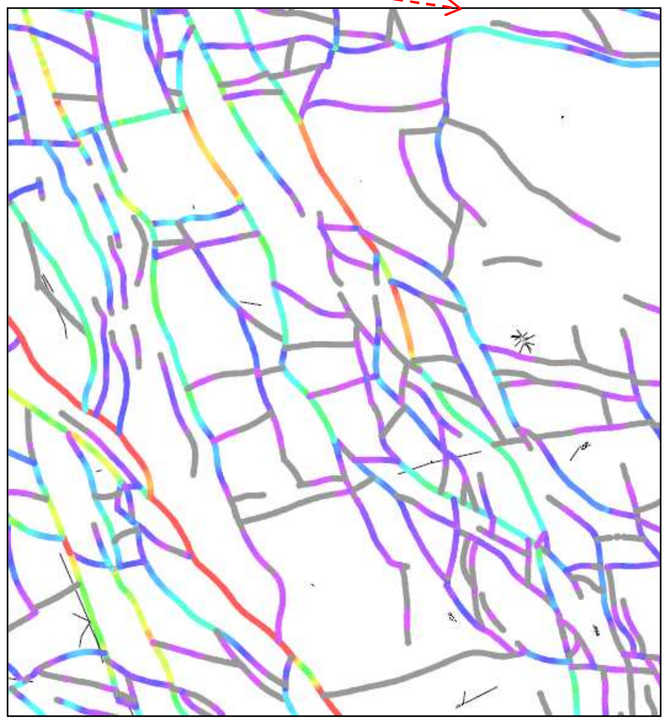

DEPOSITIONAL SETTING

Late Carboniferous Pangea Supercontinent

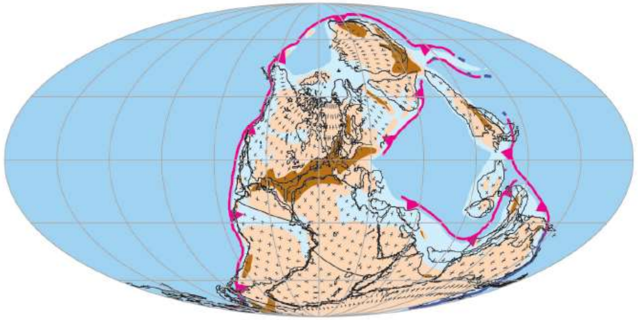

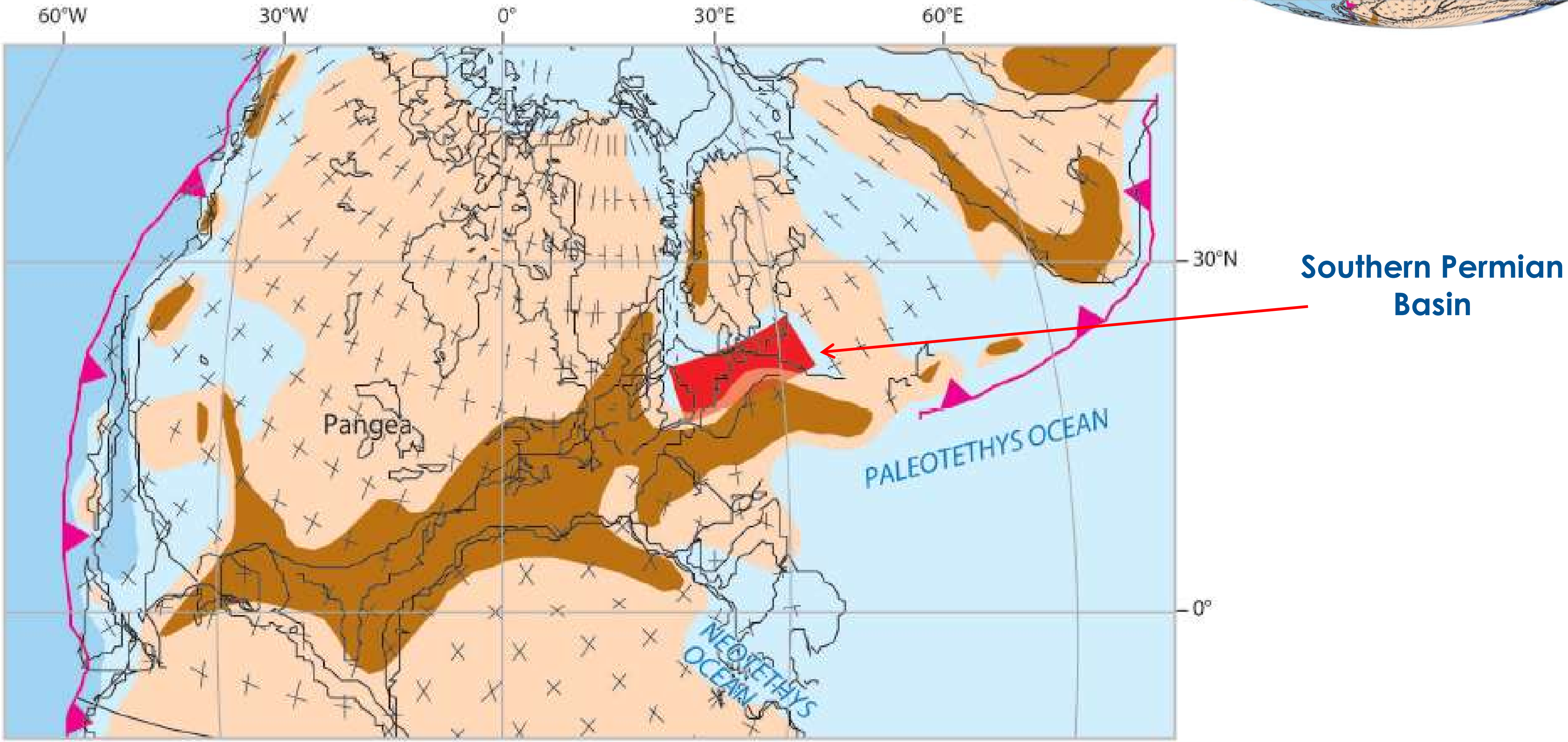

Rotliegend thickness map

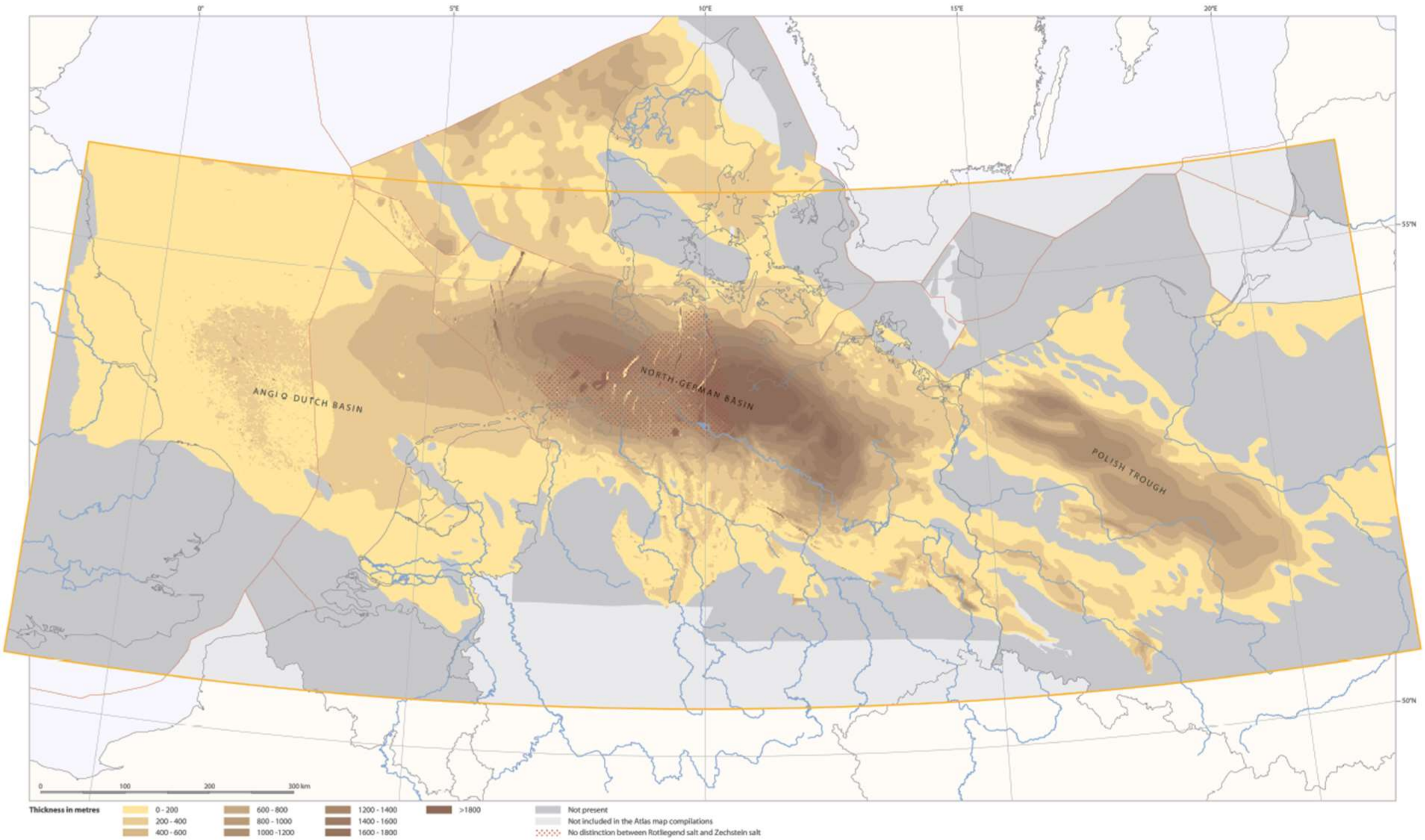

Depositional setting

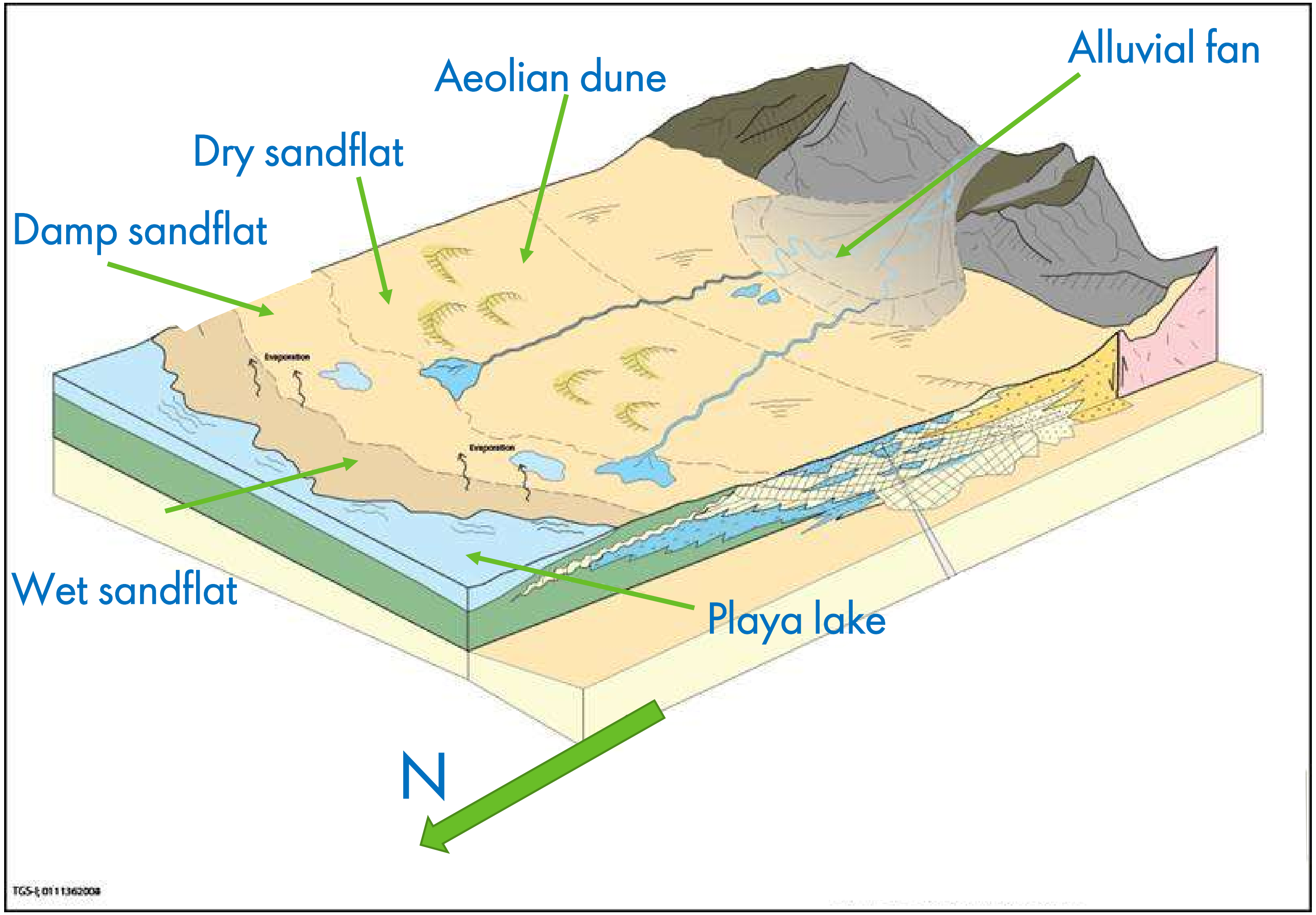

N-S section through Groningen field

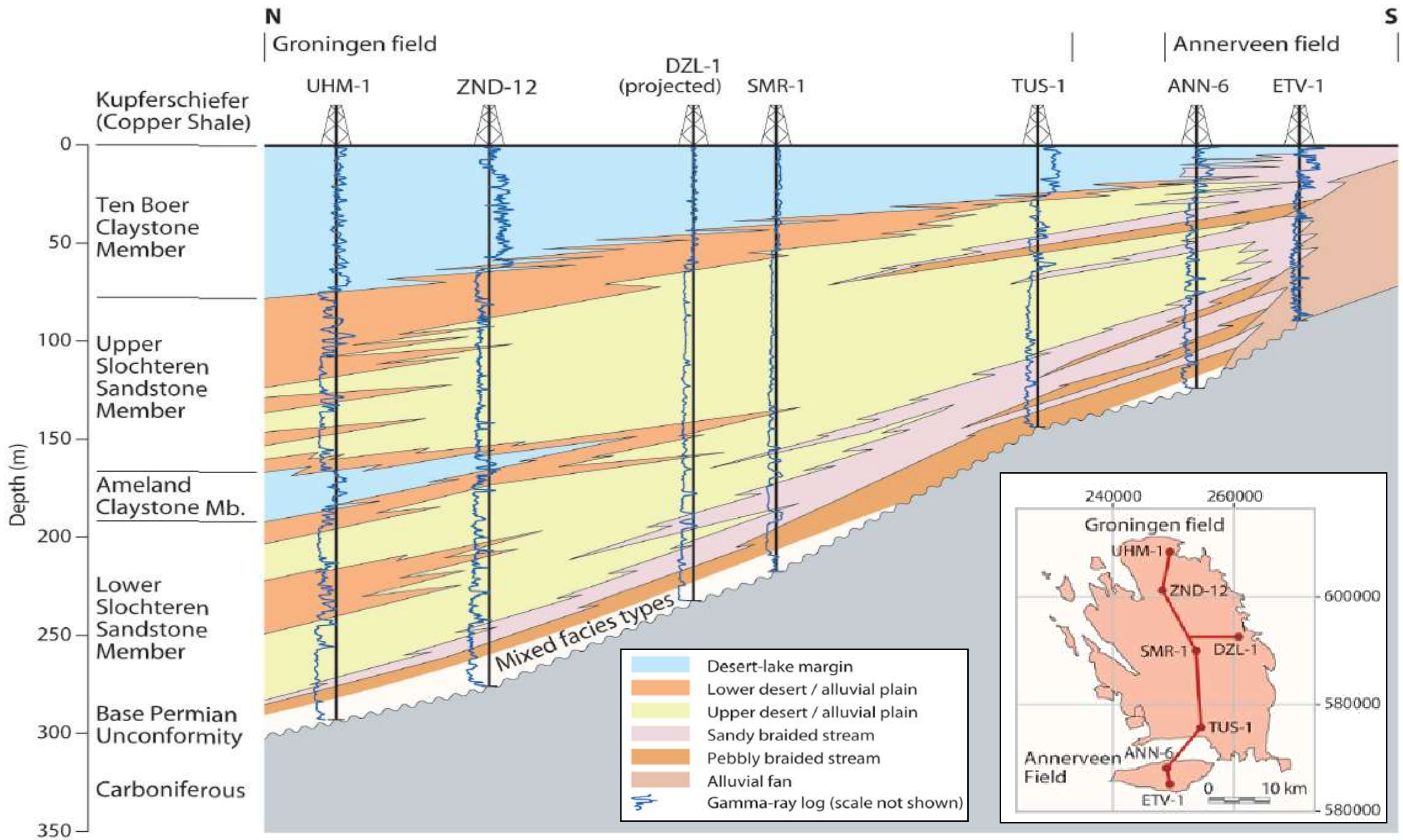

FIT4FUTURE

Recent analogue - Chott el Djerid area,

Dune and ephemeral fluvial facies

Dune and ephemeral fluvial facies

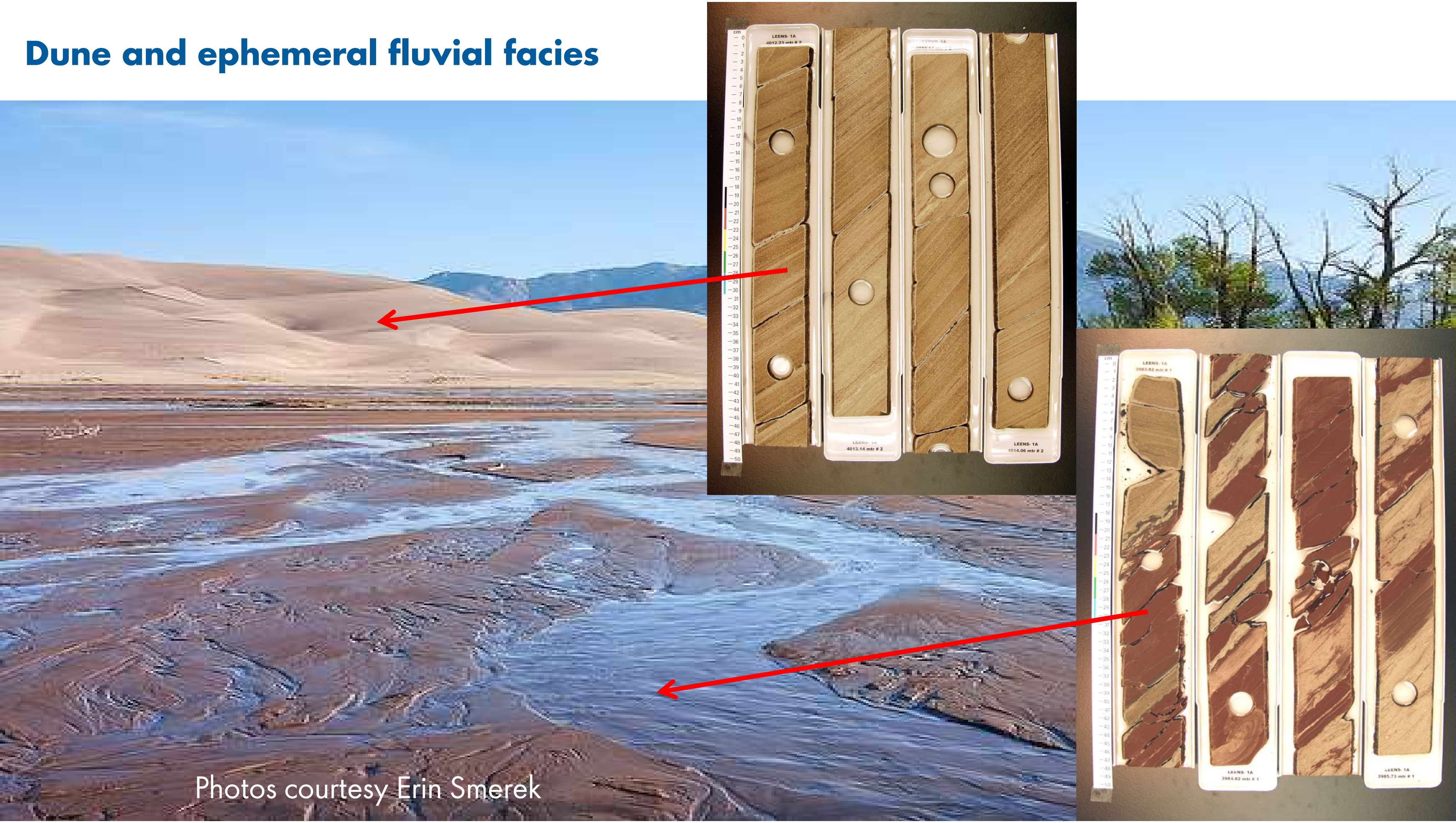

Photos courtesy Erin Smerek

Scales of observation

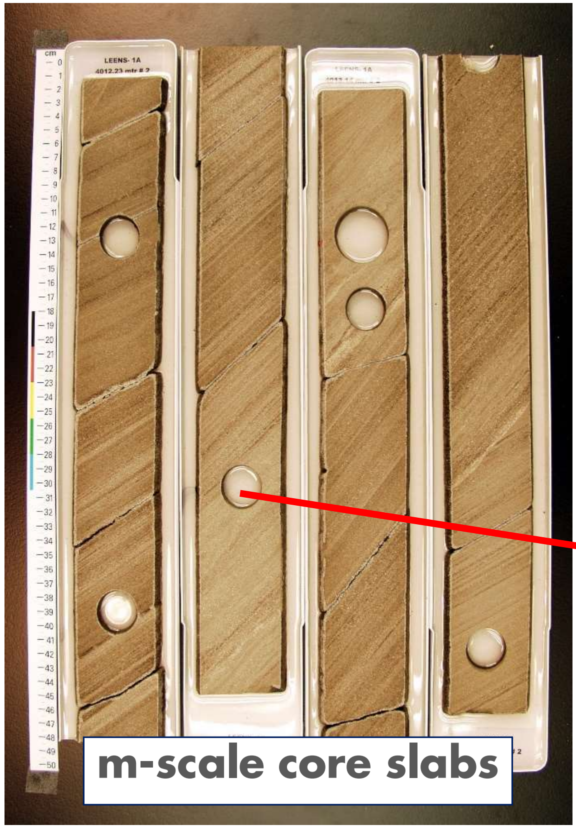

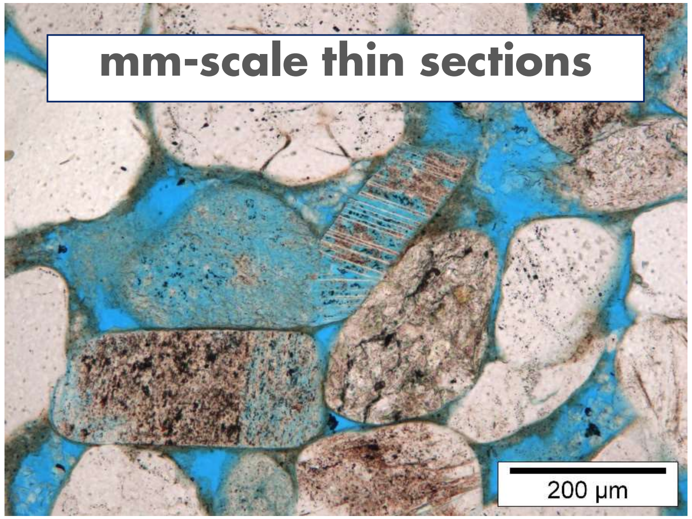

cm-scale
core plugs

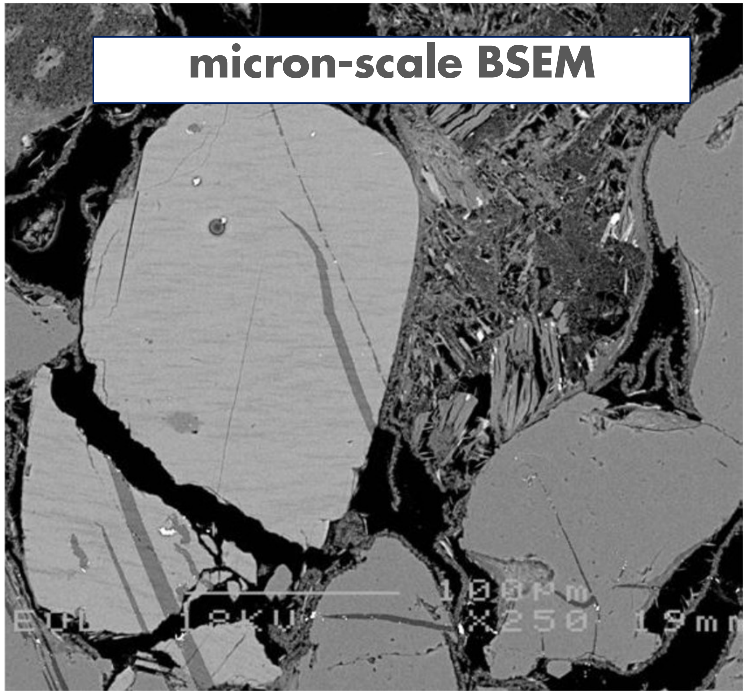

RESERVOIR MODEL

TOP_ROTLIEGEND SURFACE

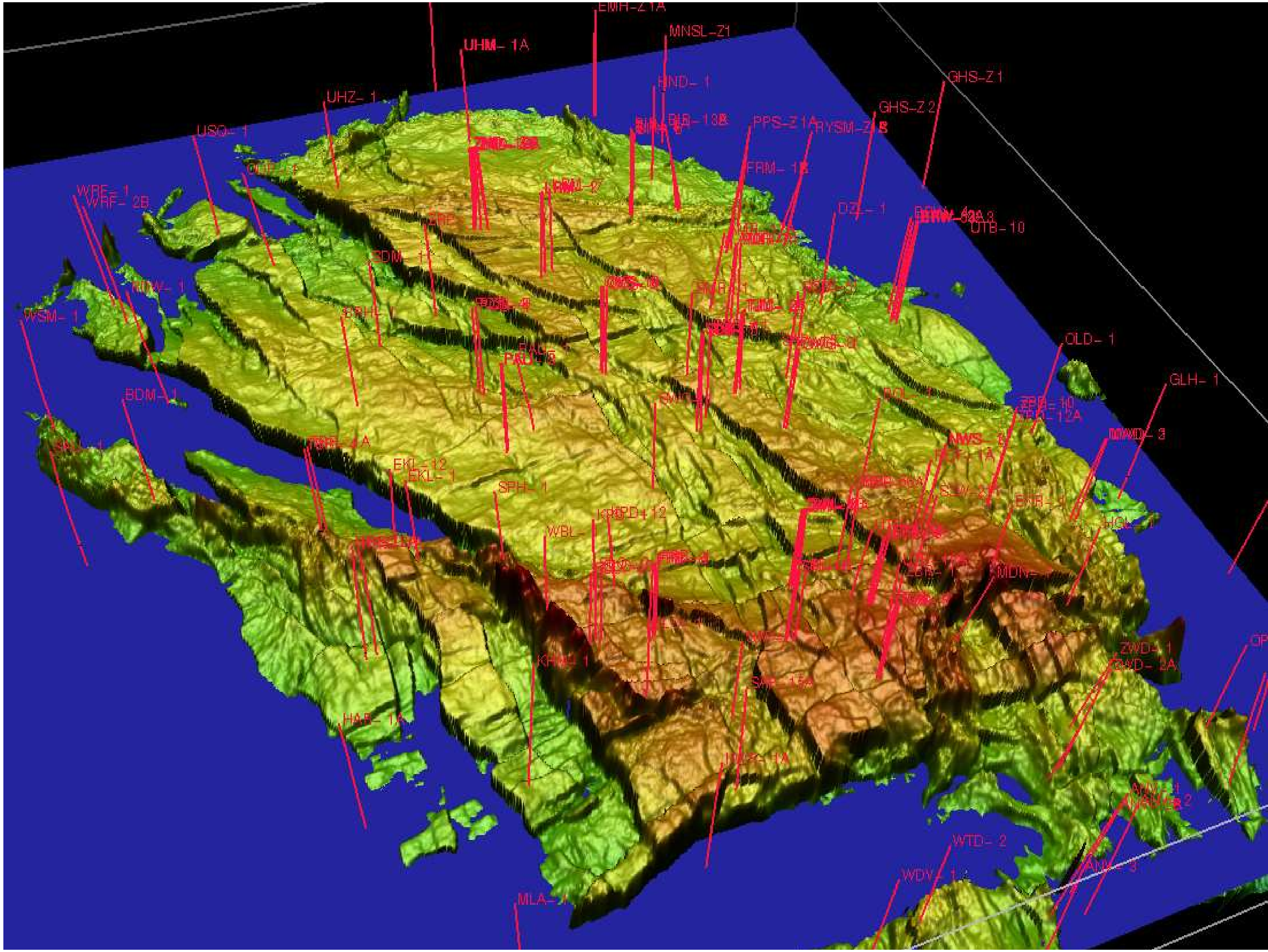

FIT4FUTURE

STRUCTURAL FRAMEWORK

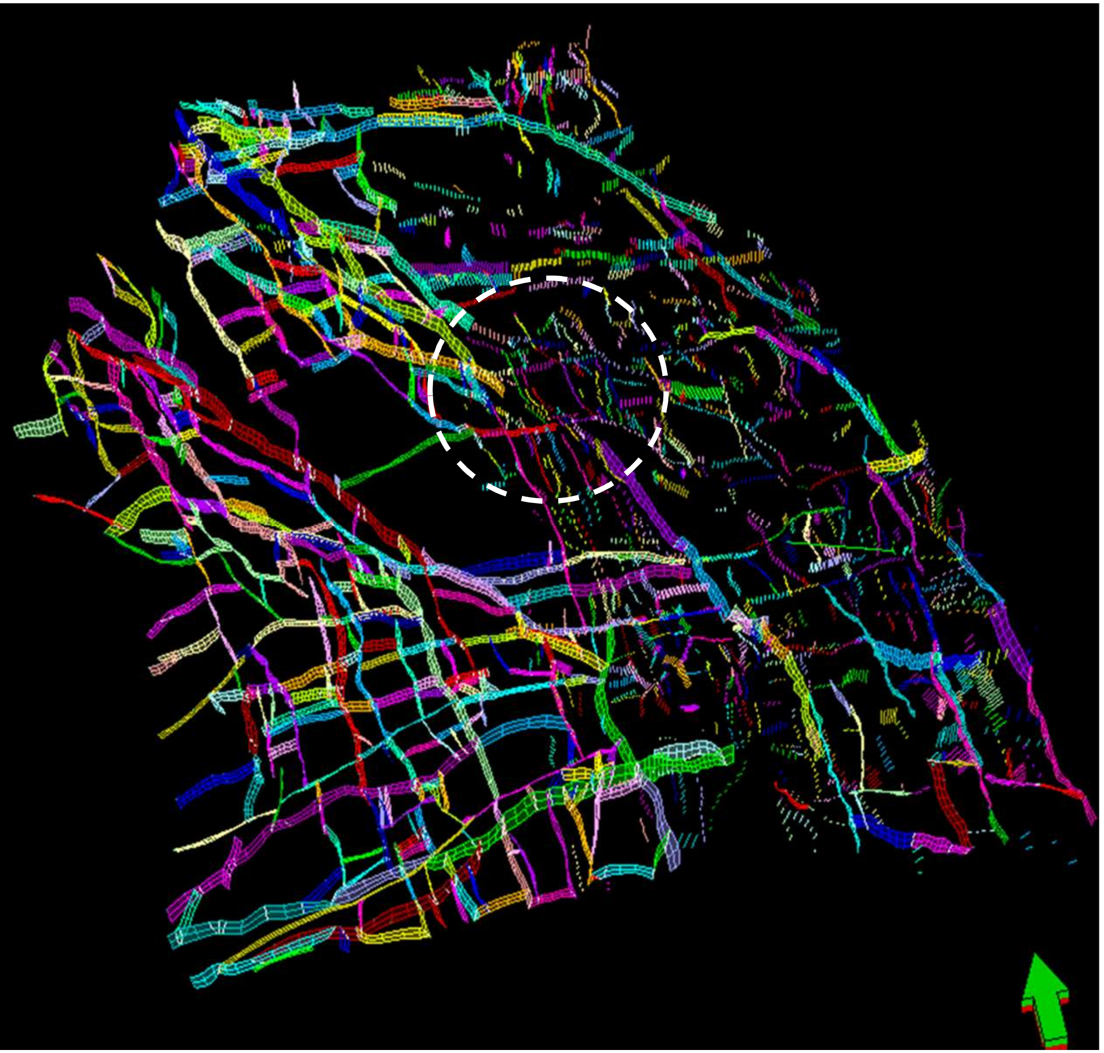

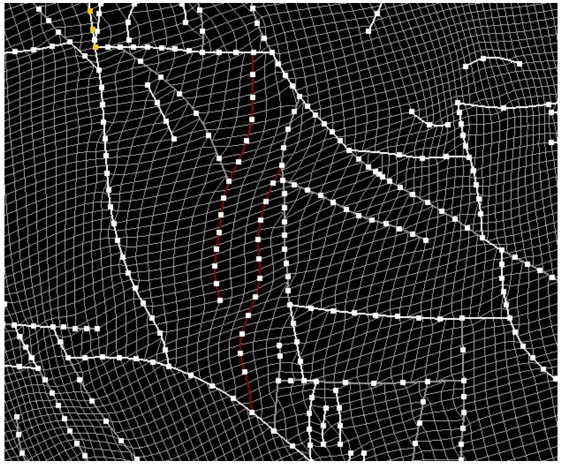

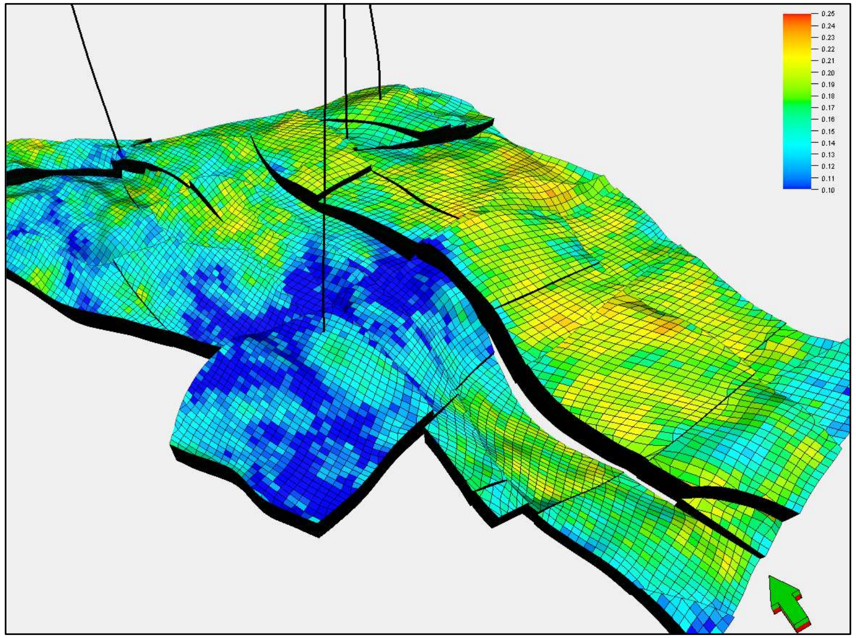

N-S section through saturation model

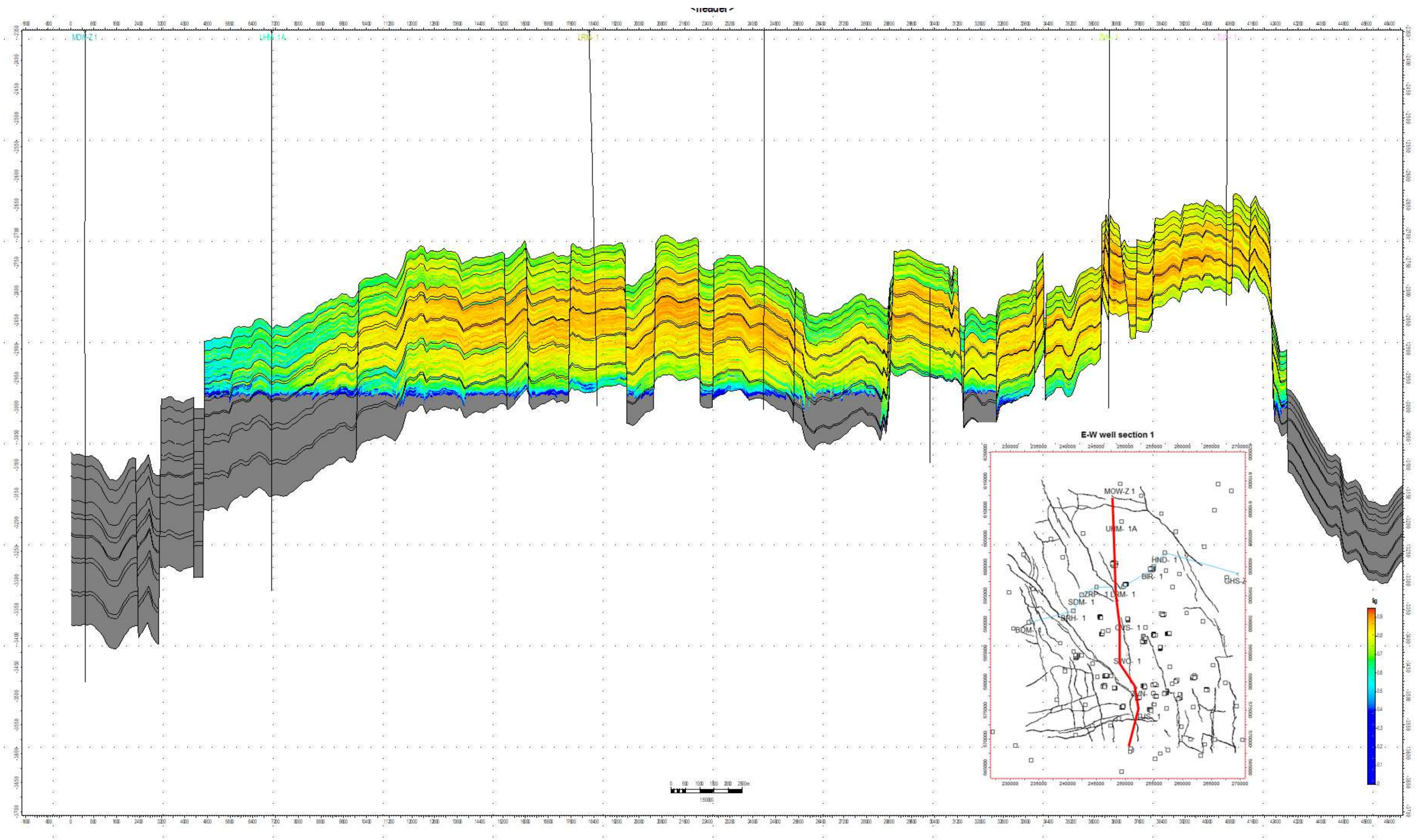

W-E section through saturation model

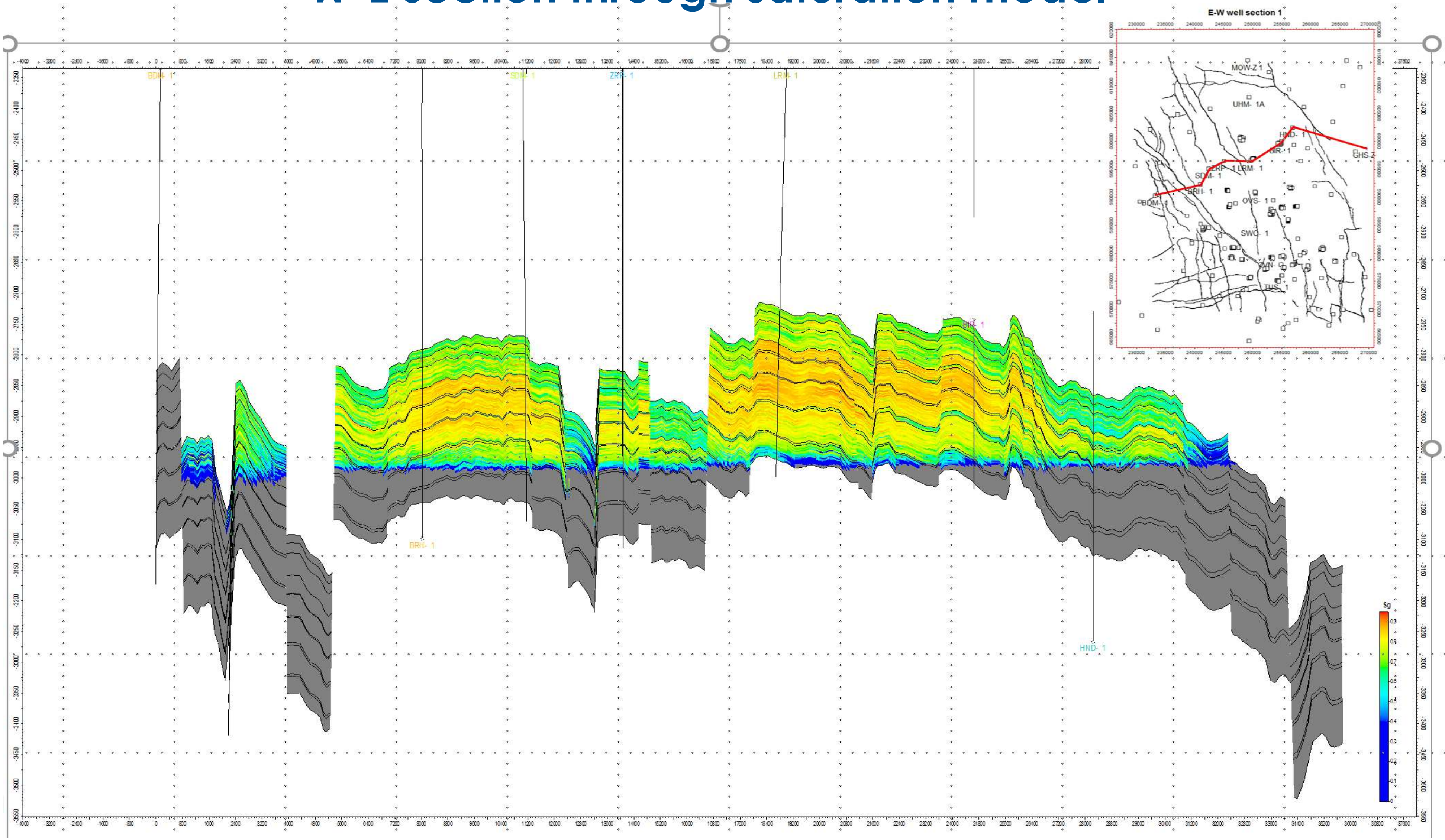

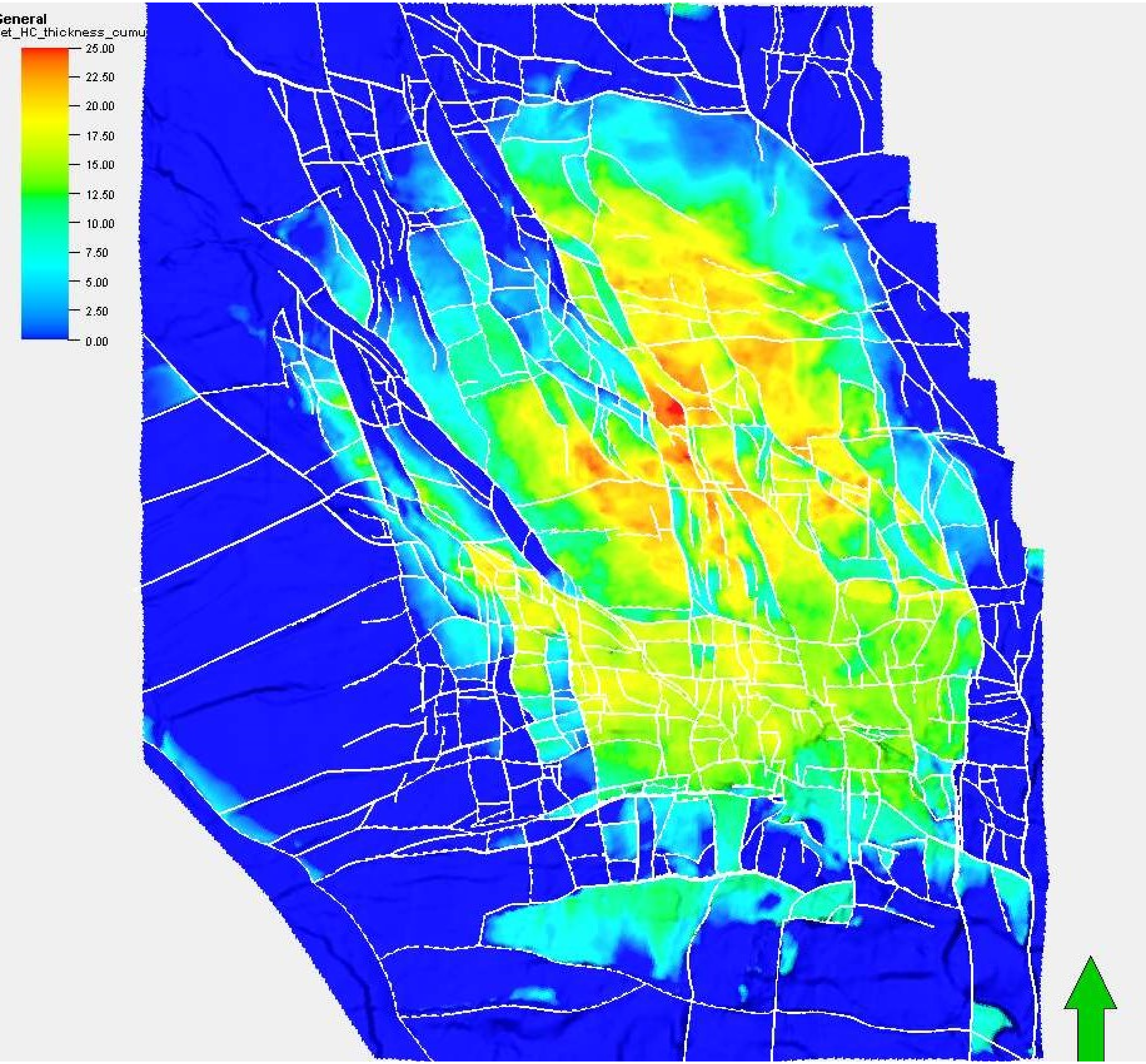

Property shown is net hydrocarbon thickness, calculated as:

POR * Sg * Thickness

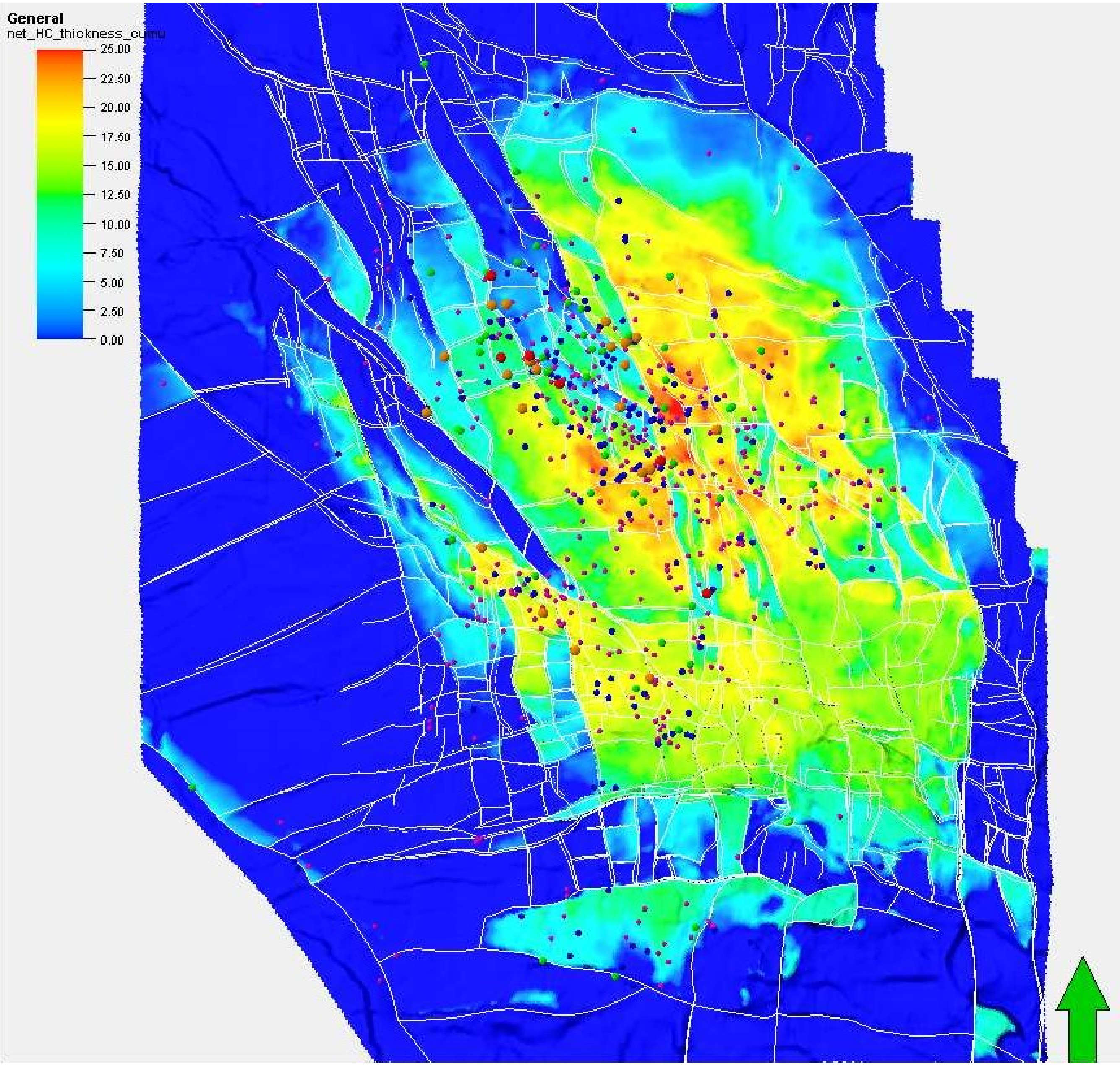

Property shown is net hydrocarbon thickness, calculated as:

POR * Sg * Thickness

Magnitude

- > 3
- 2.5 - 3
- 2 - 2.5
- 1.5 - 2
- 1 – 1.5

GAS PRODUCTION

Location of production clusters

Location of production clusters

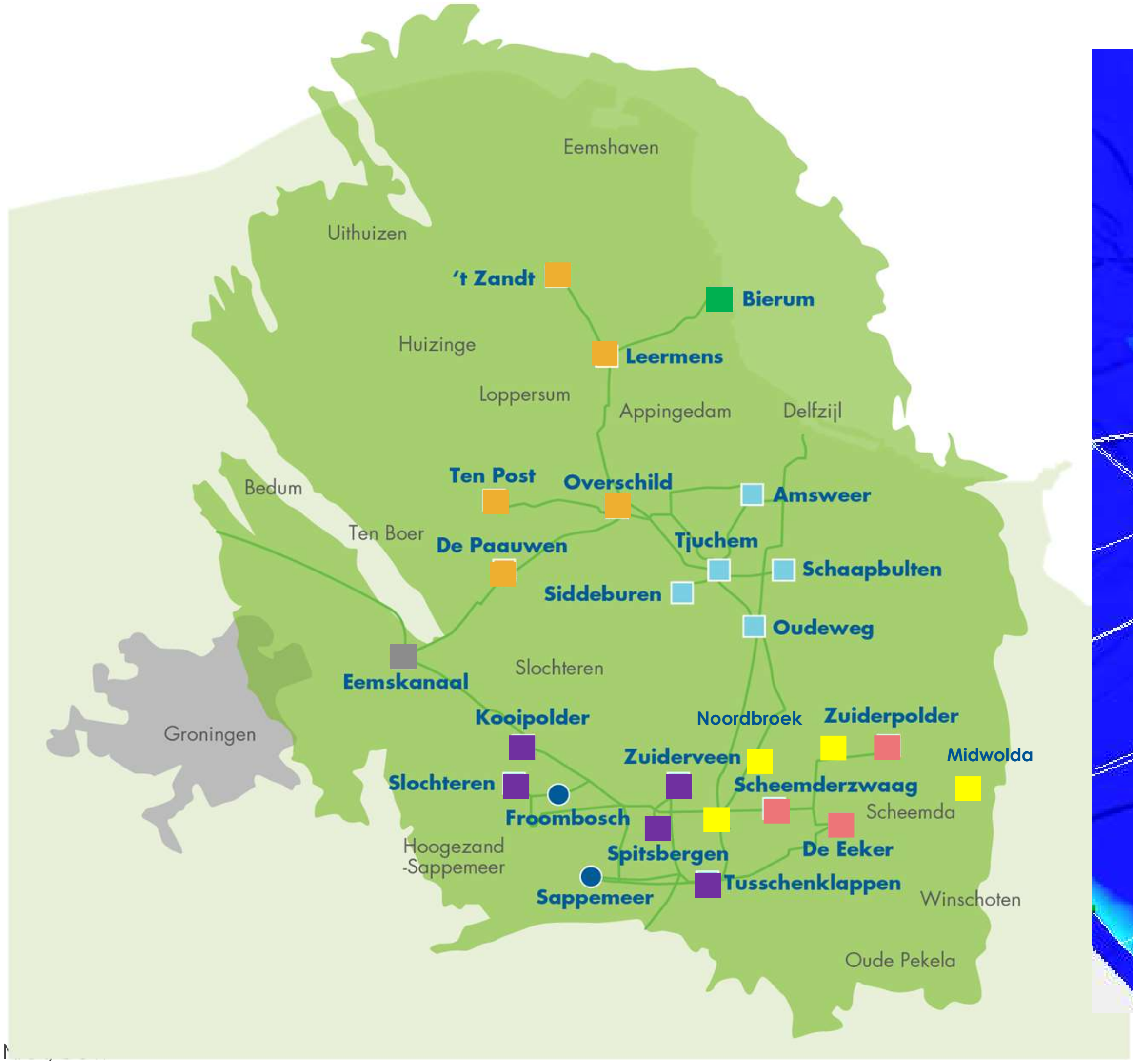

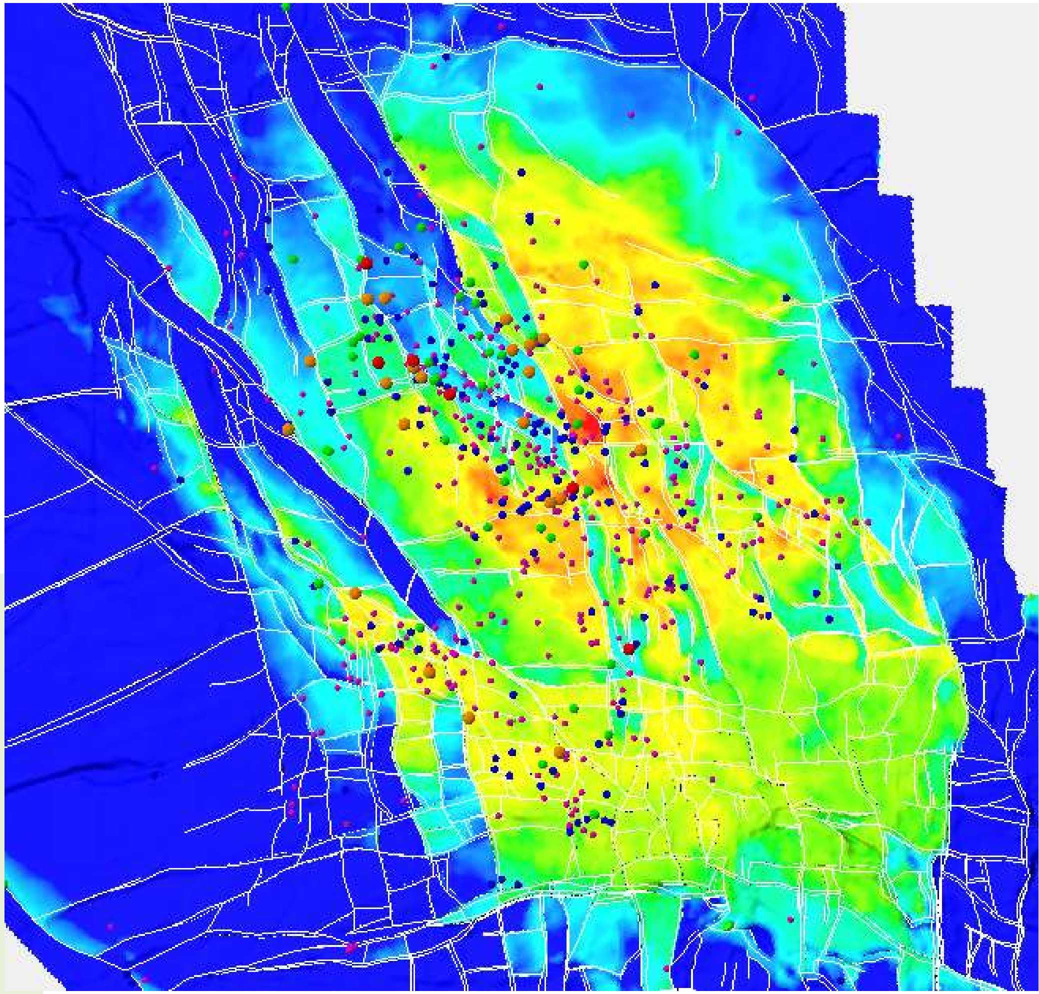

Cumulative production on January 1st 2022
2128.39 Bcm

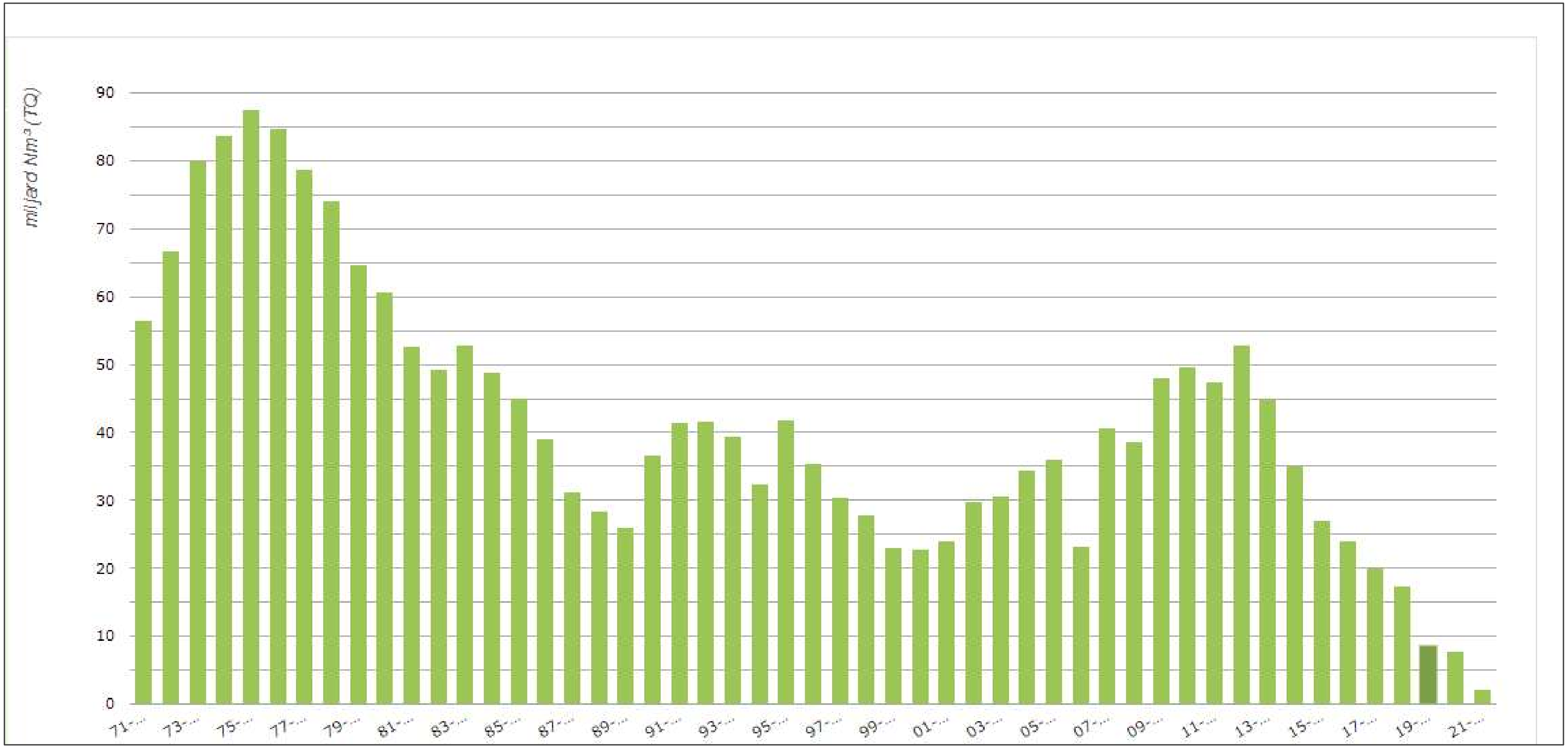

Groningen gas field
Production clusters
Loppersum
Bierum
Eemskanaal
Central East
Southeast
Southwest
Abandoned
Satellite locations
Eemshaven
Uithuizen
't Zandt
Bierum
Huizinge
Leermens
Loppersum
Appingedam
Delfzijl
Bedum
Ten Post
Overschild
Amsweer
Ten Boer
De Paauwen
Tjuchem
Schaapbulten
Siddeburen
Oudeweg
Eemskanaal
Slochteren
Groningen
Kooipolder
Zuiderpolder
Zuiderveen
Slochteren
Scheemderzwaag
Froombosch
Scheemda
Hoogezand
-Sappemeer
Spitsbergen
De Eeker
Tusschenklappen
Sappemeer
Winschoten
Oude Pekela

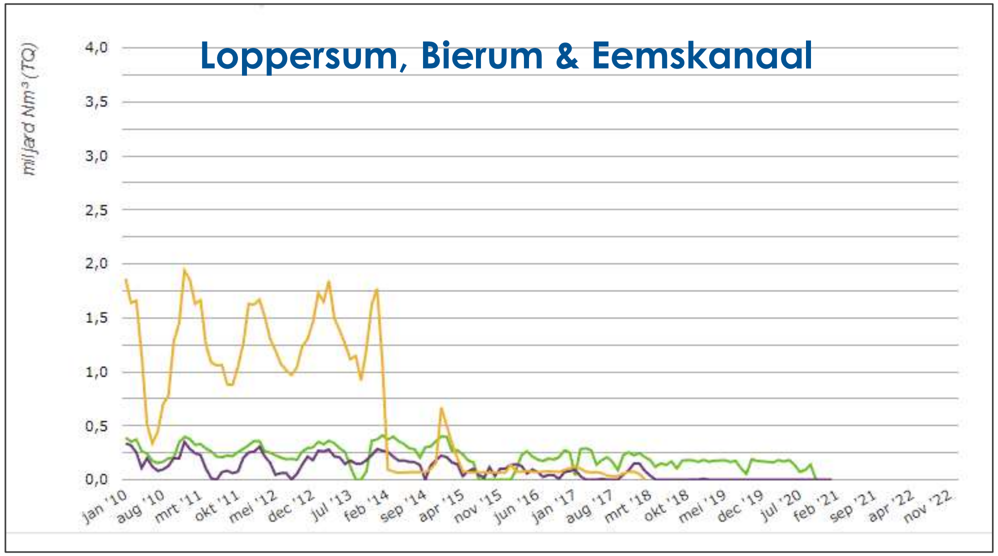

Loppersum, Bierum & Eemskanaal
miljard Nm³ (TQ)
4,0
3,5
3,0
2,5
2,0
1,5
1,0
0,5
0,0
jan '10
aug '10
mrt '11
okt '11
mei '12
dec '12
jul '13
feb '14
sep '14
apr '15
nov '15
jun '16
jan '17
aug '17
mrt '18
okt '18
mei '19
dec '19
jul '20
feb '21
sep '21
apr '22
nov '22


Groningen gas field
Production clusters
Loppersum
Bierum
Eemskanaal
Central East
Southeast
Southwest
Abandoned
Satellite locations
Eemshaven
Uithuizen
't Zandt
Bierum
Huizinge
Leermens
Loppersum
Appingedam
Delfzijl
Bedum
Ten Post
Overschild
Amsweer
Ten Boer
De Paauwen
Tjuchem
Schaapbulten
Siddeburen
Oudeweg
Eemskanaal
Slochteren
Groningen
Kooipolder
Zuiderpolder
Zuiderveen
Slochteren
Scheemderzwaag
Froombosch
Scheemda
Hoogezand -Sappemeer
Spitsbergen
De Eeker
Tusschenklappen
Sappemeer
Winschoten
Oude Pekela

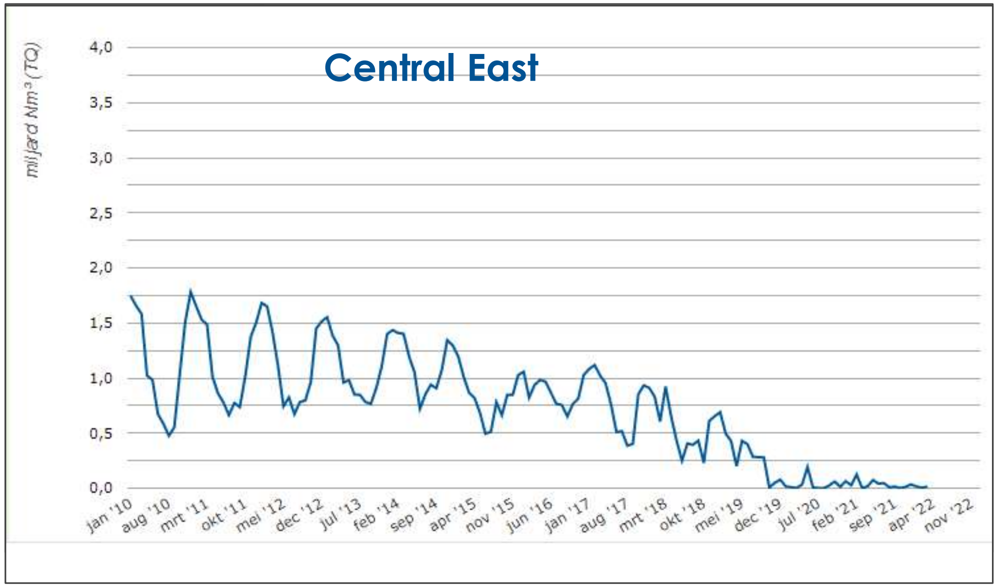
Central East
miljard Nm³ (TQ)
4,0
3,5
3,0
2,5
2,0
1,5
1,0
0,5
0,0
jan '10
aug '10
mrt '11
okt '11
mei '12
dec '12
jul '13
feb '14
sep '14
apr '15
nov '15
jun '16
jan '17
aug '17
mrt '18
okt '18
mei '19
dec '19
jul '20
feb '21
sep '21
apr '22
nov '22


Groningen gas field
Production clusters
Loppersum
Bierum
Eemskanaal
Central East
Southeast
Southwest
Abandoned
Satellite locations
Eemshaven
Uithuizen
't Zandt
Bierum
Huizinge
Leermens
Loppersum
Appingedam
Delfzijl
Bedum
Ten Post
Overschild
Amsweer
Ten Boer
De Paauwen
Tjuchem
Schaapbulten
Siddeburen
Oudeweg
Eemskanaal
Slochteren
Kooipolder
Zuiderpolder
Groningen
Zuiderveen
Slochteren
Scheemderzwaag
Froombosch
Scheemda
Hoogezand
-Sappemeer
Spitsbergen
De Eeker
Sappemeer
Tusschenklappen
Winschoten
Oude Pekela

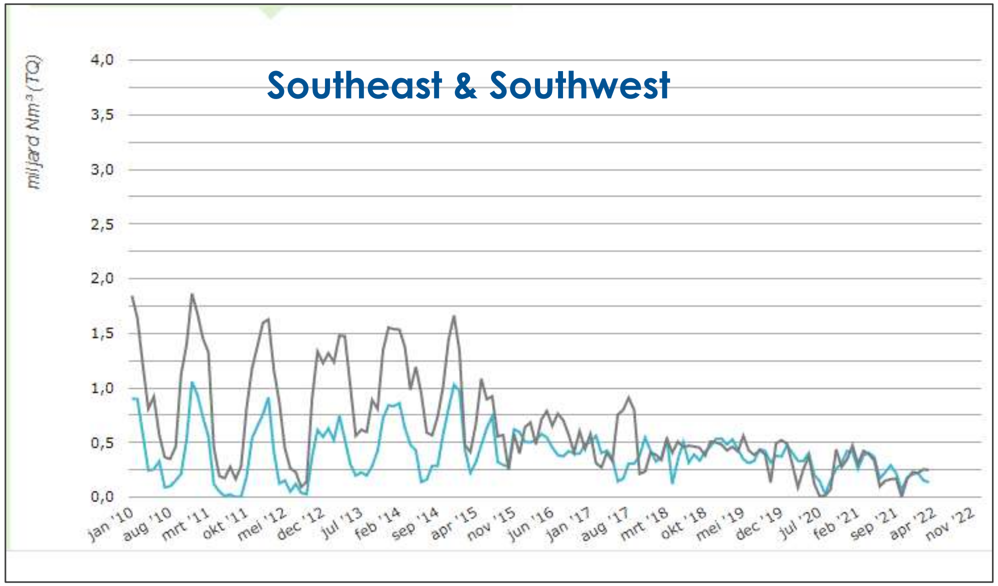
Southeast & Southwest
miljard Nm³ (TQ)
4,0
3,5
3,0
2,5
2,0
1,5
1,0
0,5
0,0
jan '10
aug '10
mrt '11
okt '11
mei '12
dec '12
jul '13
feb '14
sep '14
apr '15
nov '15
jun '16
jan '17
aug '17
mrt '18
okt '18
mei '19
dec '19
jul '20
feb '21
sep '21
apr '22
nov '22

ANNUAL GAS PRODUCTION

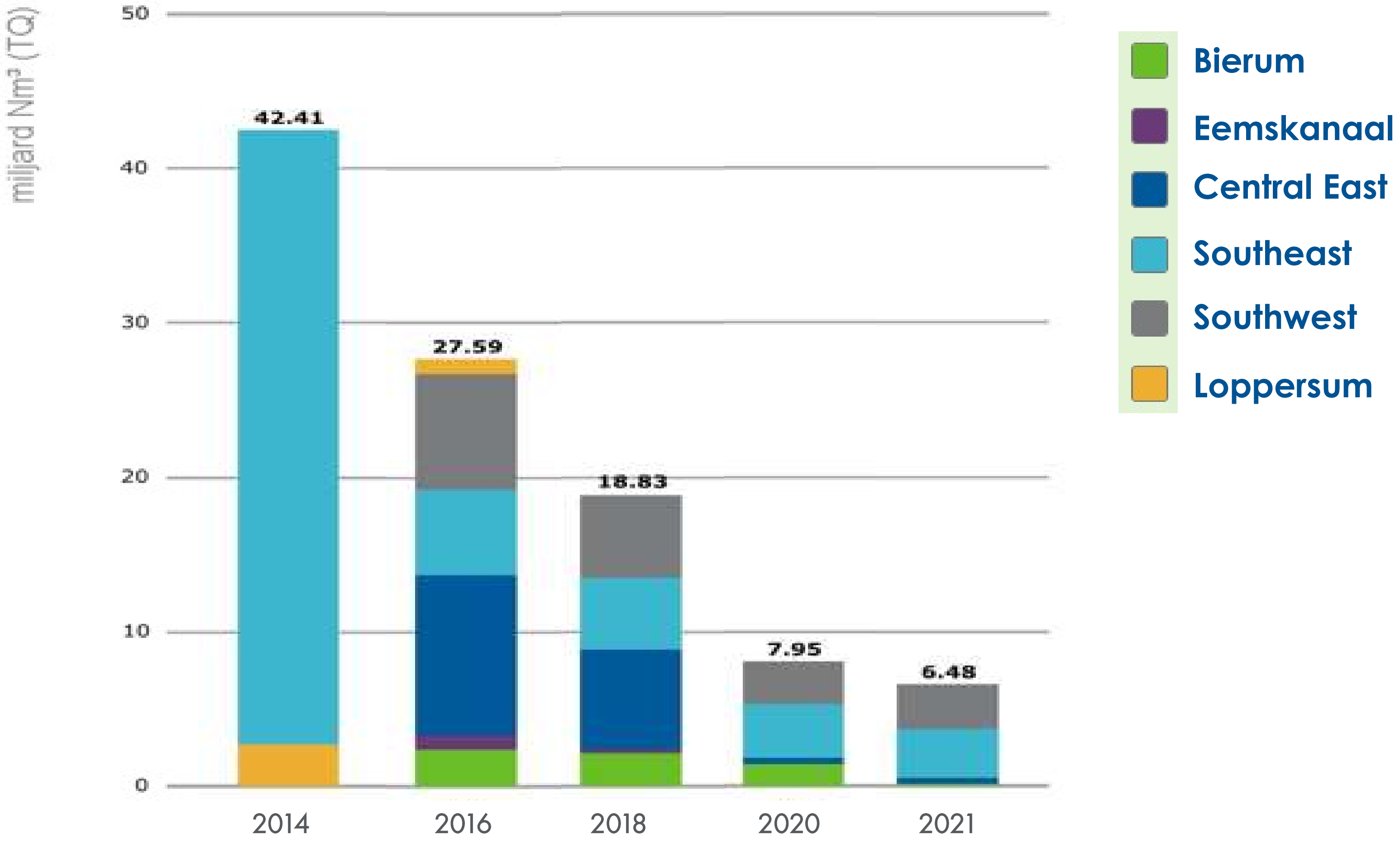

ONEgas

NAM


Groningen gas field
Production clusters
Loppersum
Bierum
Eemskanaal
Central East
Southeast
Southwest
Abandoned
Satellite locations
Eemshaven
Uithuizen
't Zandt
Bierum
Huizinge
Leermens
Loppersum
Appingedam
Delfzijl
Bedum
Ten Post
Overschild
Amsweer
Ten Boer
De Paauwen
Tjuchem
Schaapbulten
Siddeburen
Oudeweg
Eemskanaal
Slochteren
Groningen
Kooipolder
Zuiderpolder
Zuiderveen
Slochteren
Scheemderzwaag
Froombosch
Scheemda
Hoogezand
-Sappemeer
Spitsbergen
De Eeker
Tusschenklappen
Sappemeer
Winschoten
Oude Pekela

Overburden faulting and s

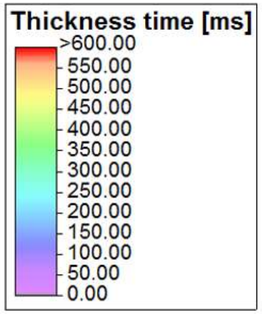

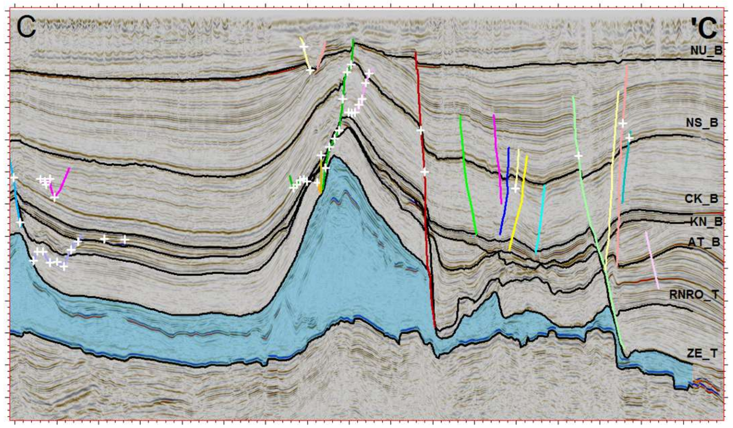

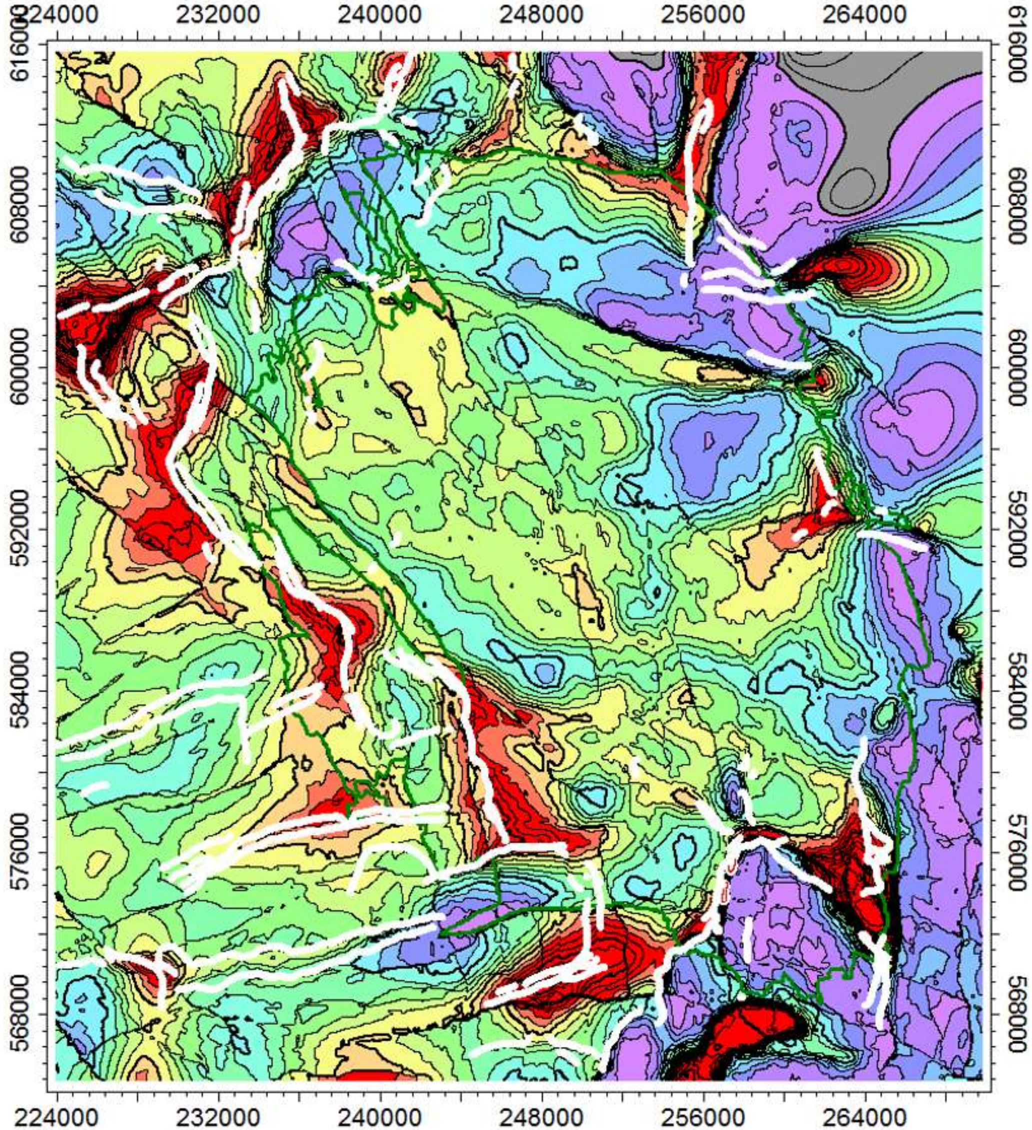

Overburden faults

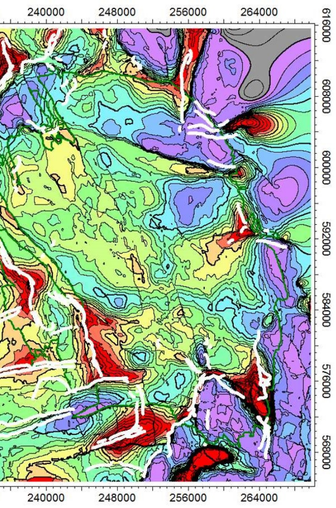

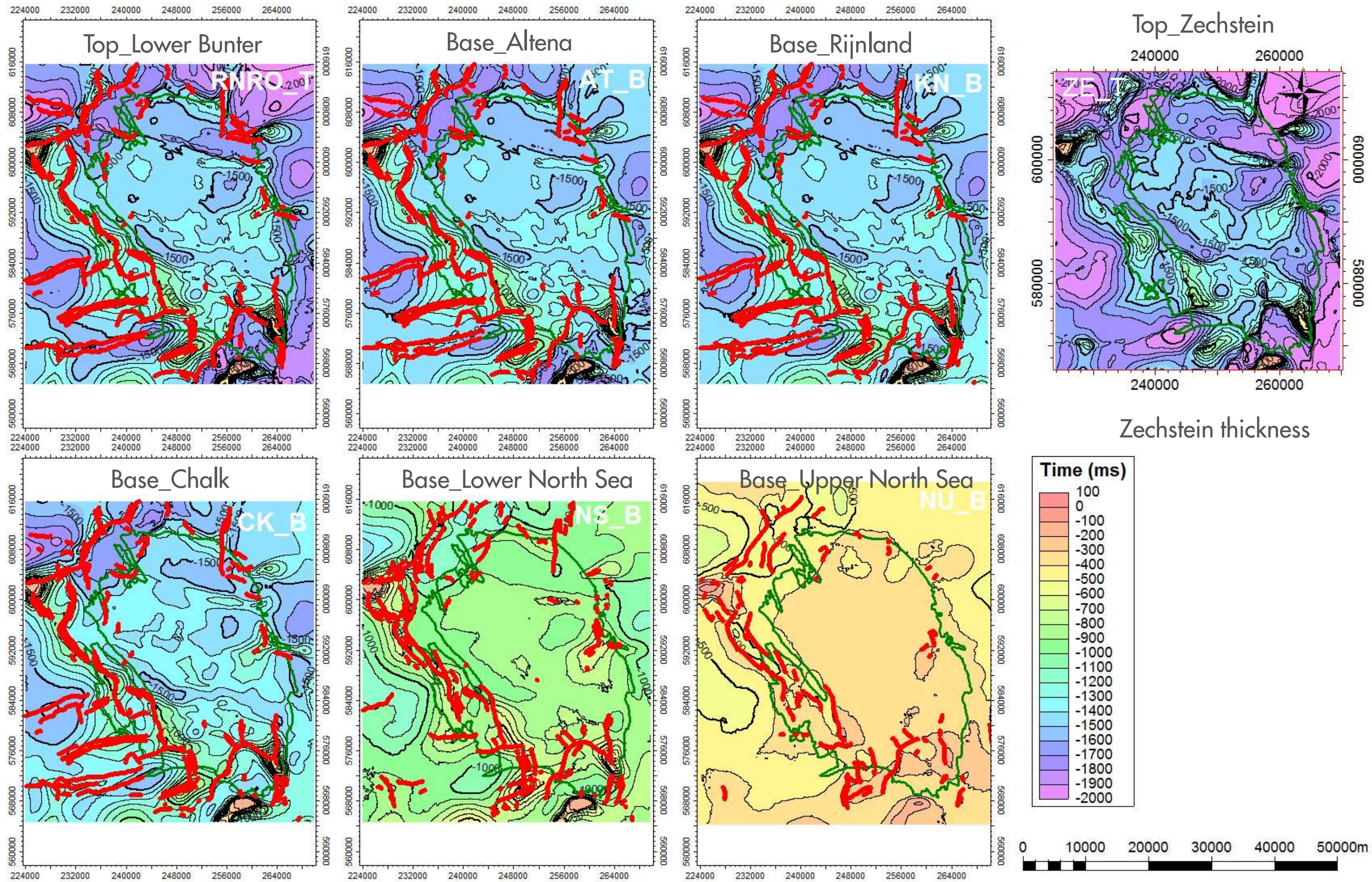

Seismically constrained porosity modelling

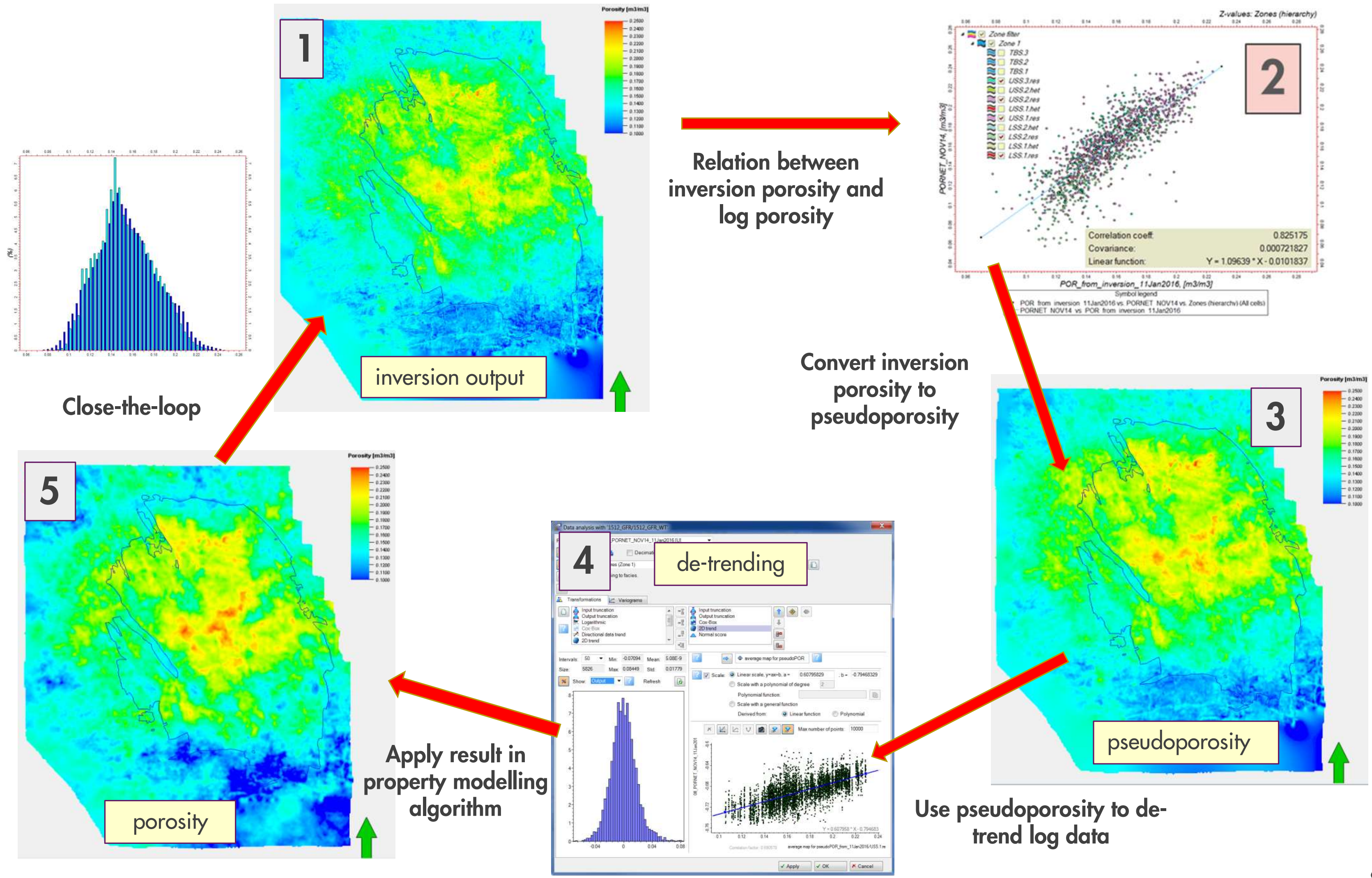

Number of recorded earthquakes in the Groningen field

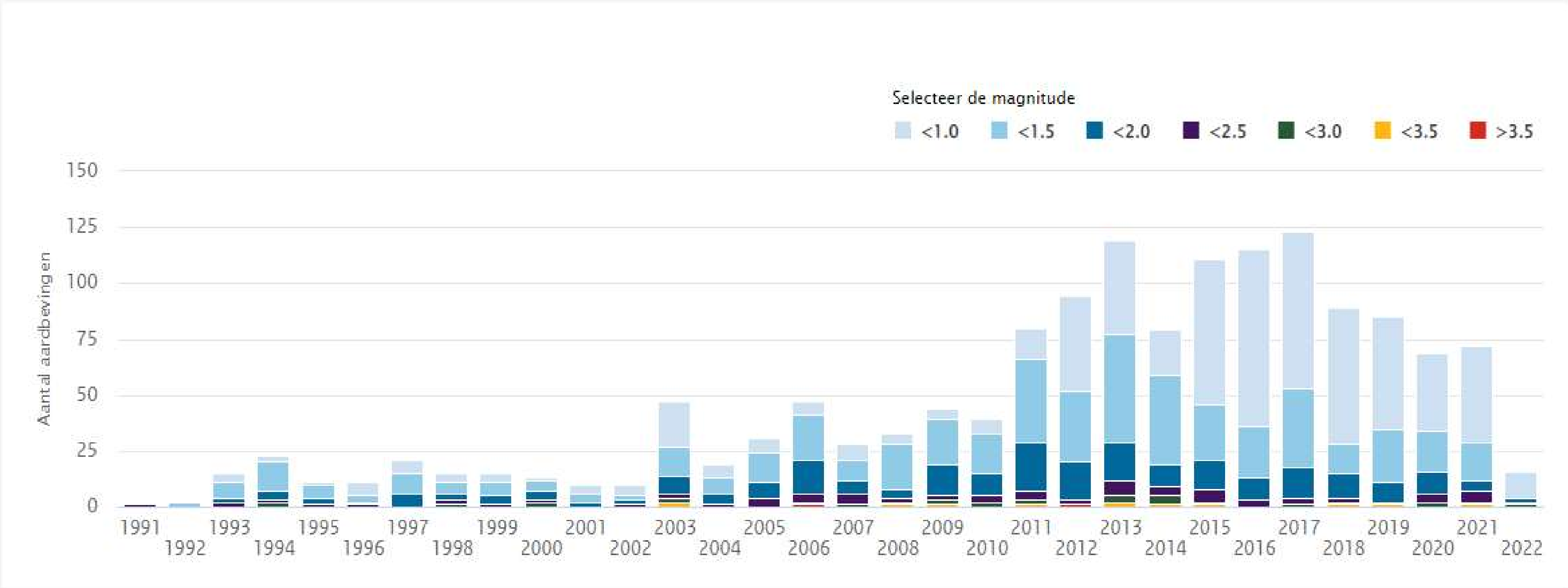

Bron: KNMI

Laatst bijgewerkt: 29-05-2022

NAM

Compaction and subsidence

Rob van Eijs, Onno van der Wal, Hermann Bähr, Gini Ketelaar,
Stijn Bierman, Ross Towe, Dirk Doornhof, Pepijn Kole

content

- Why subsidence is a major concern
- Subsidence and compaction measurements
- Subsidence history matching and forecasting

Compaction and subsidence

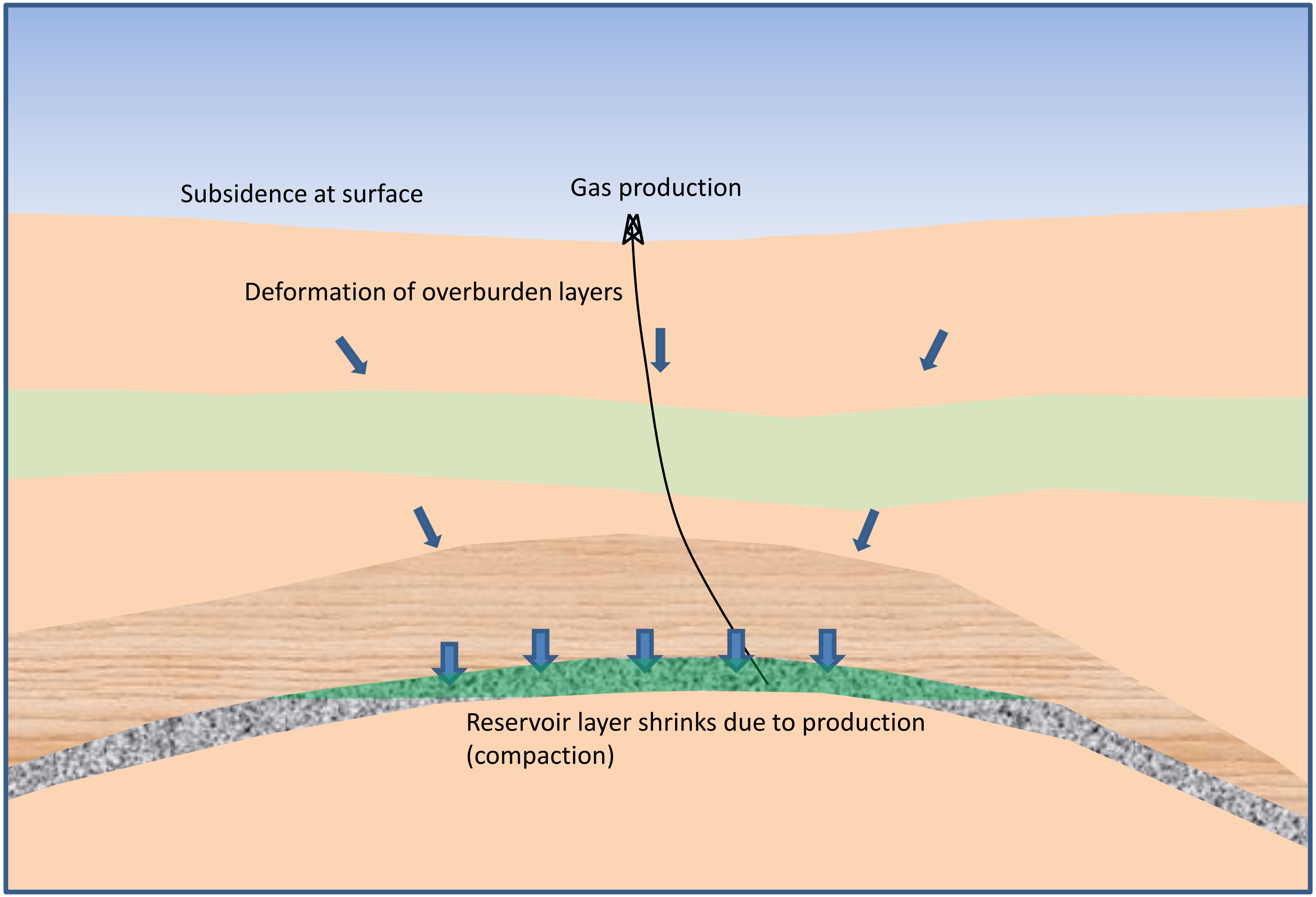

Why subsidence is a major issue

- Main Issue:
  - Parts of Groningen below sea level
  - Considered to be an issue already before start of production
- Subsidence mitigation:
  - 340 million Euro paid
  - 570 million foreseen

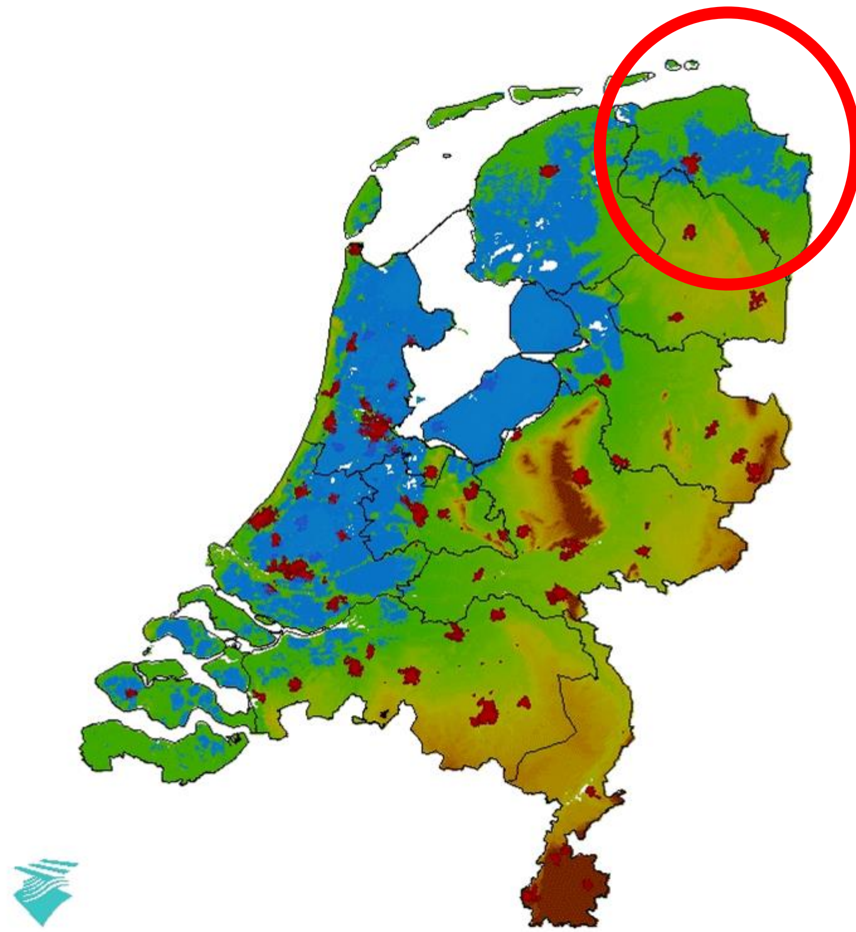

Bron: Actueel Hoogtebestand Nederland (AHN)

content

- Why subsidence is a major concern
- Subsidence and Compaction measurements
- Subsidence history matching and forecasting

Data to constrain compaction and subsidence in Groningen – **geodetic measurements**

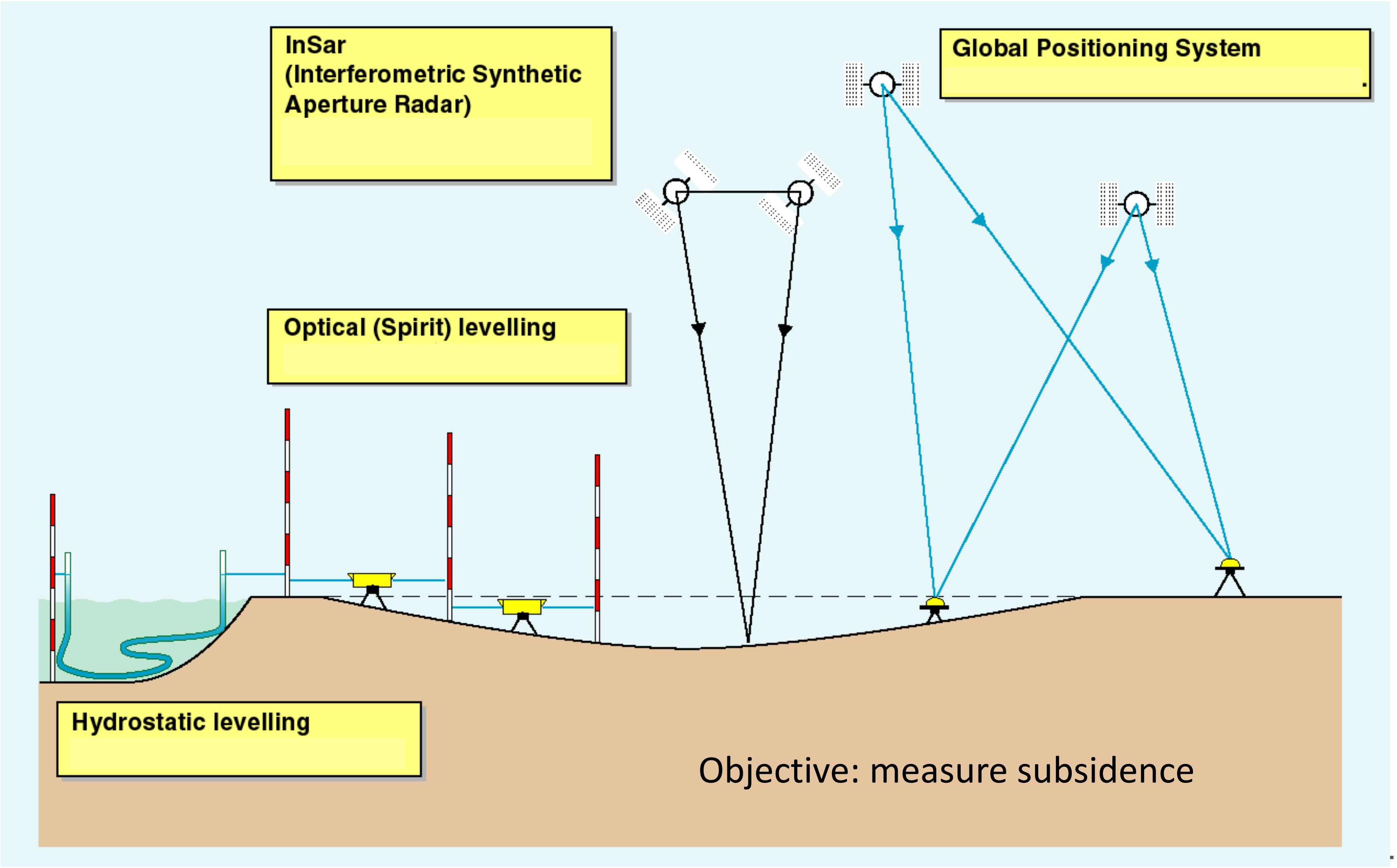

levelling network in the northern part of the Netherlands – data since 1964

Permanent GPS stations • Levelling benchmark

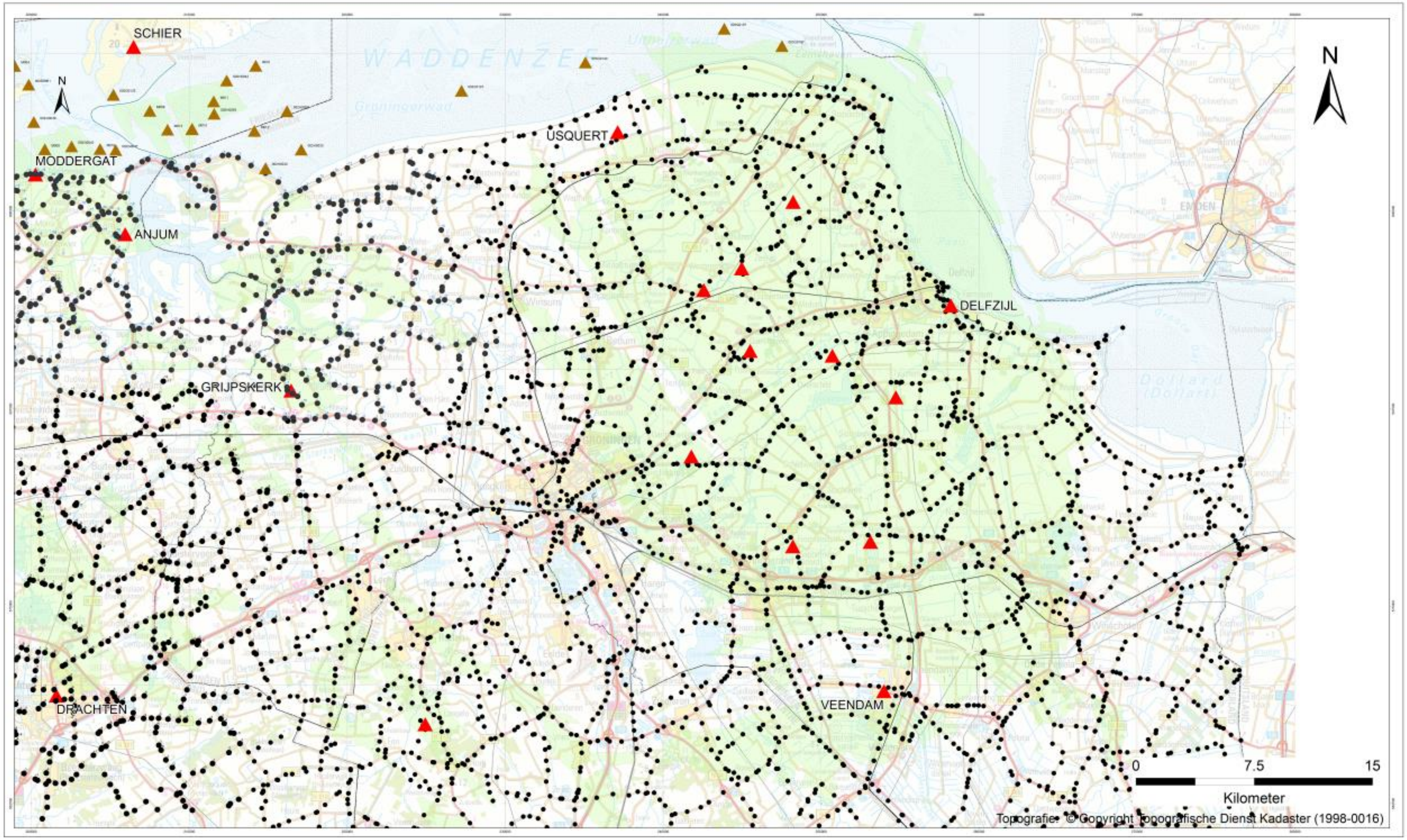

NAM

PS-InSAR scatterers data since 1993

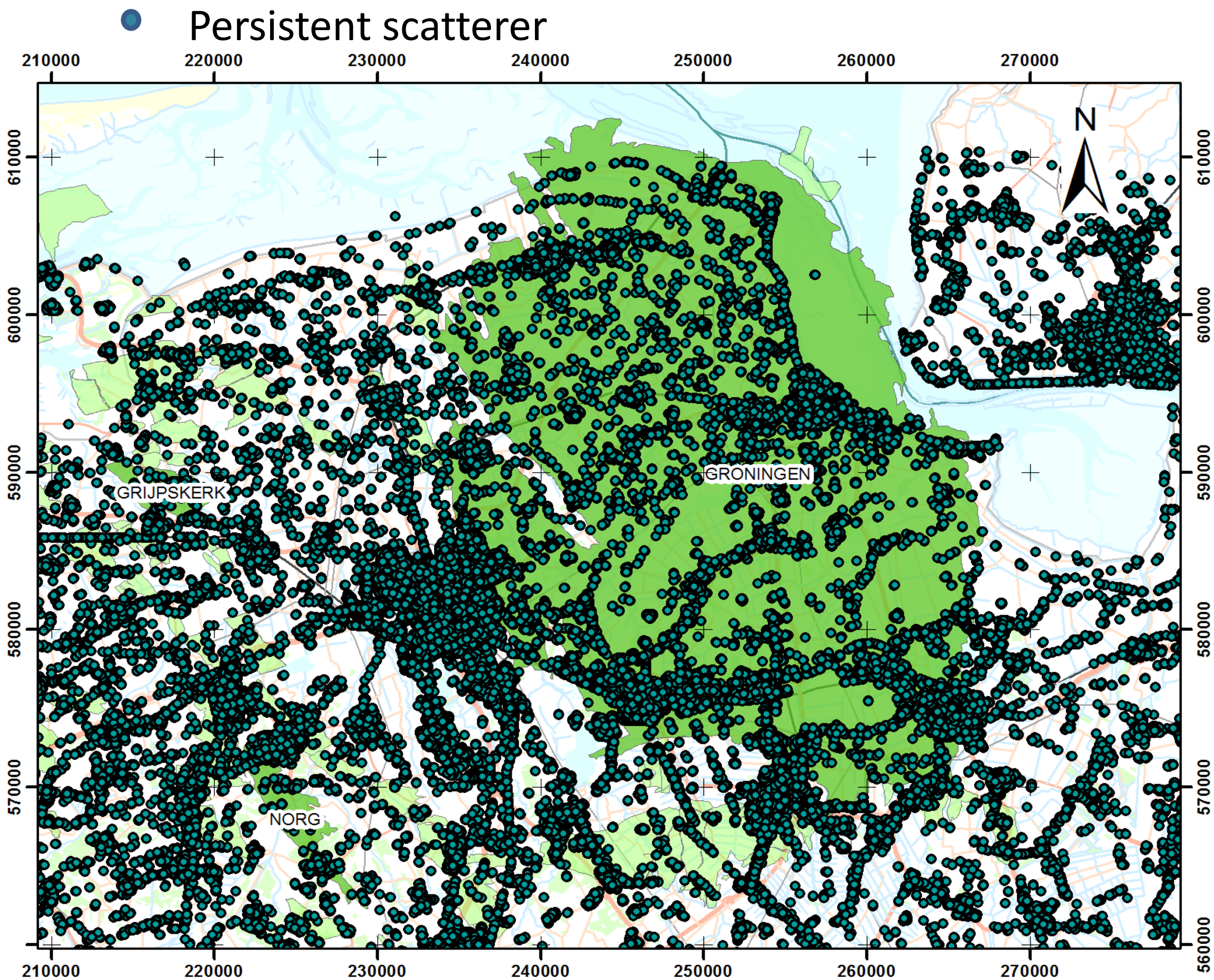

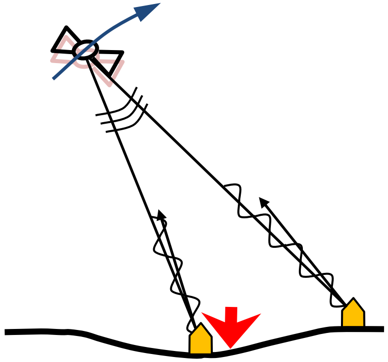

Integration of InSar and levelling

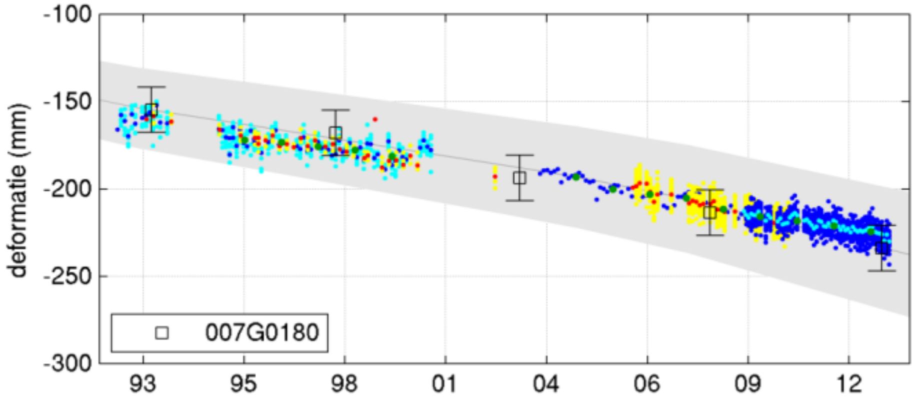

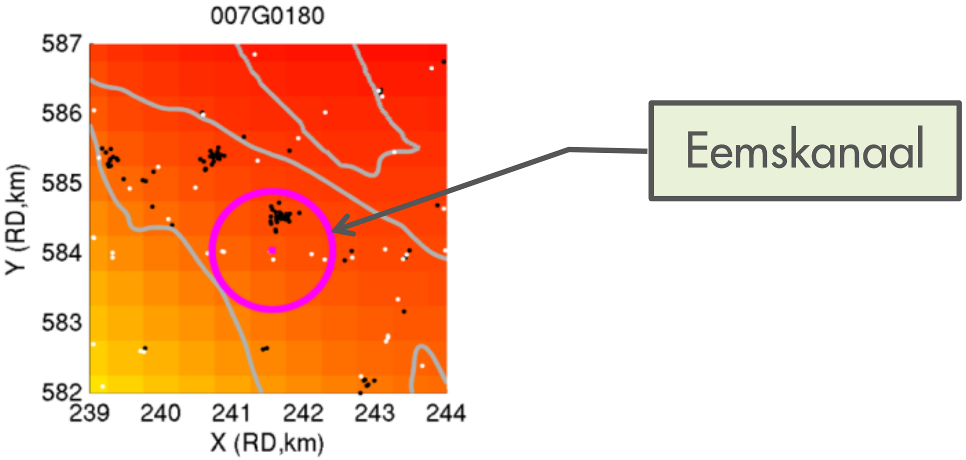

Continuous GNSS monitoring

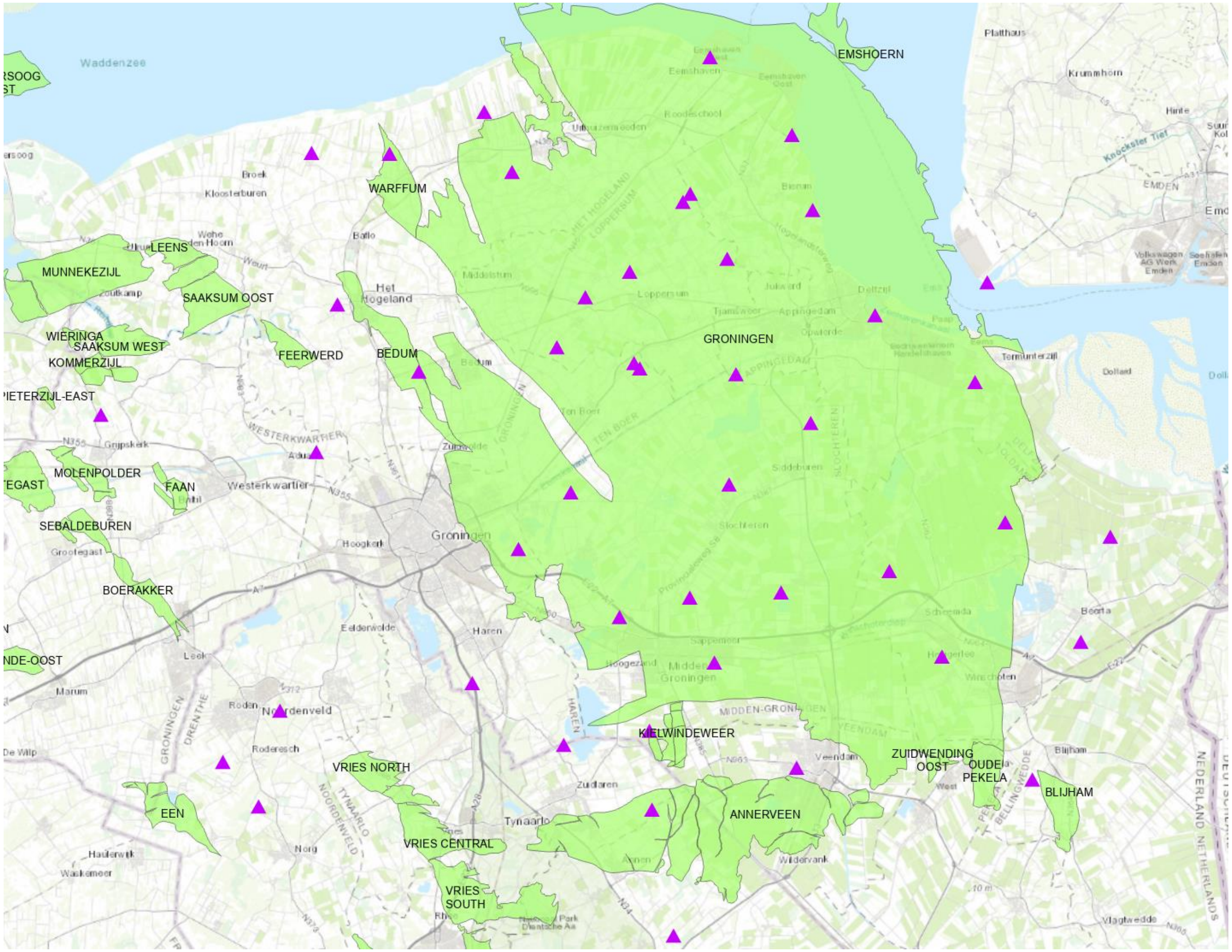

Data to constrain compaction and subsidence in Groningen – laboratory measurements

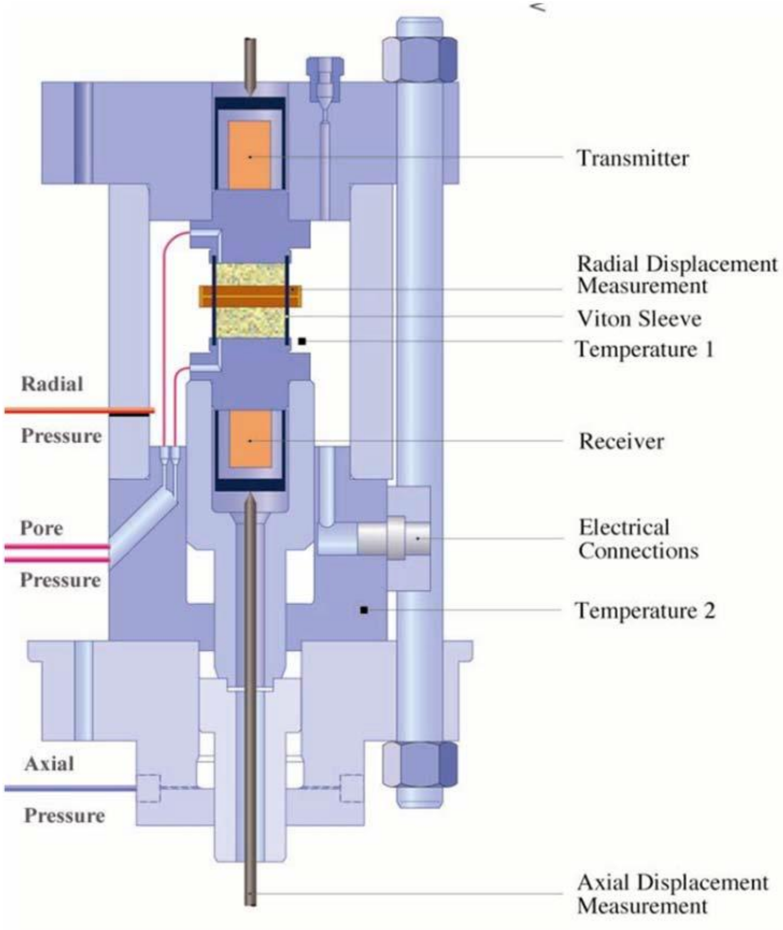

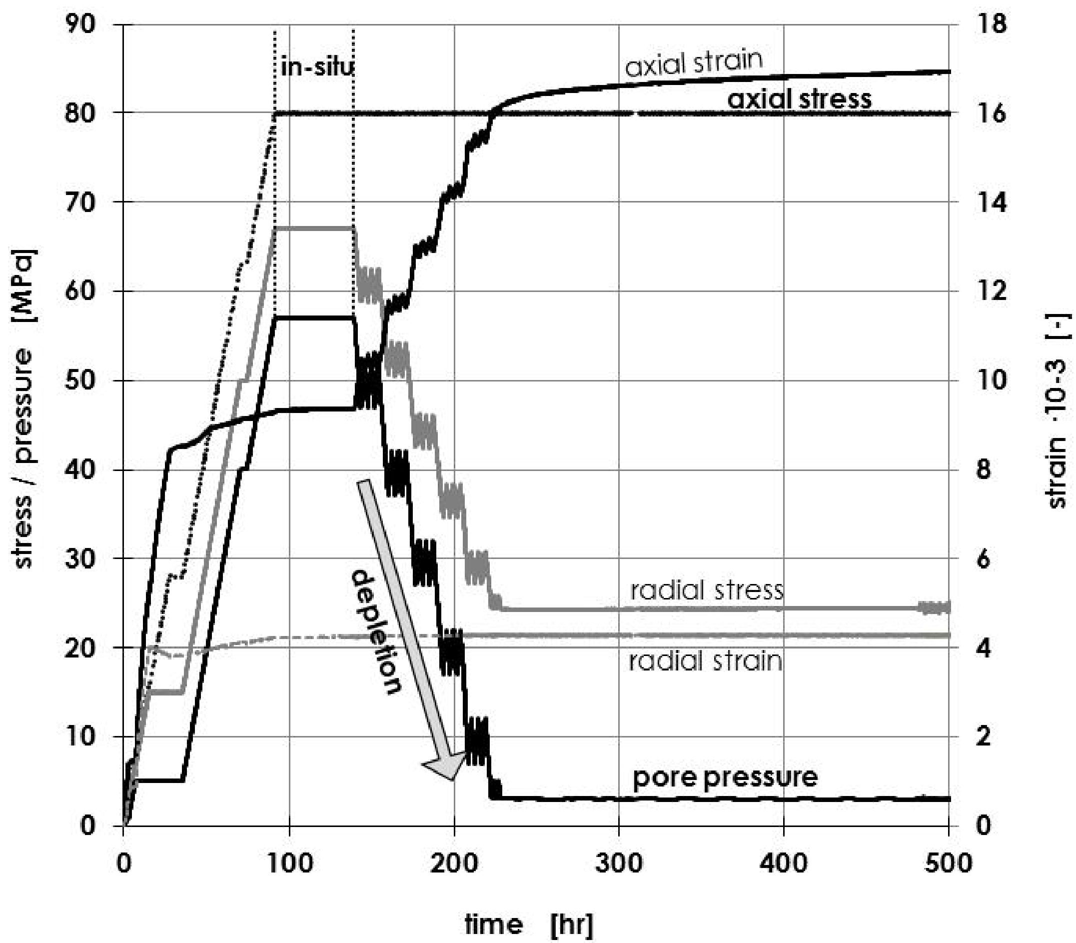

Hol et al. (2015)

Objective: measure compressibility (Cm) of the rock

Data to constrain compaction and subsidence in Groningen – **laboratory measurements**

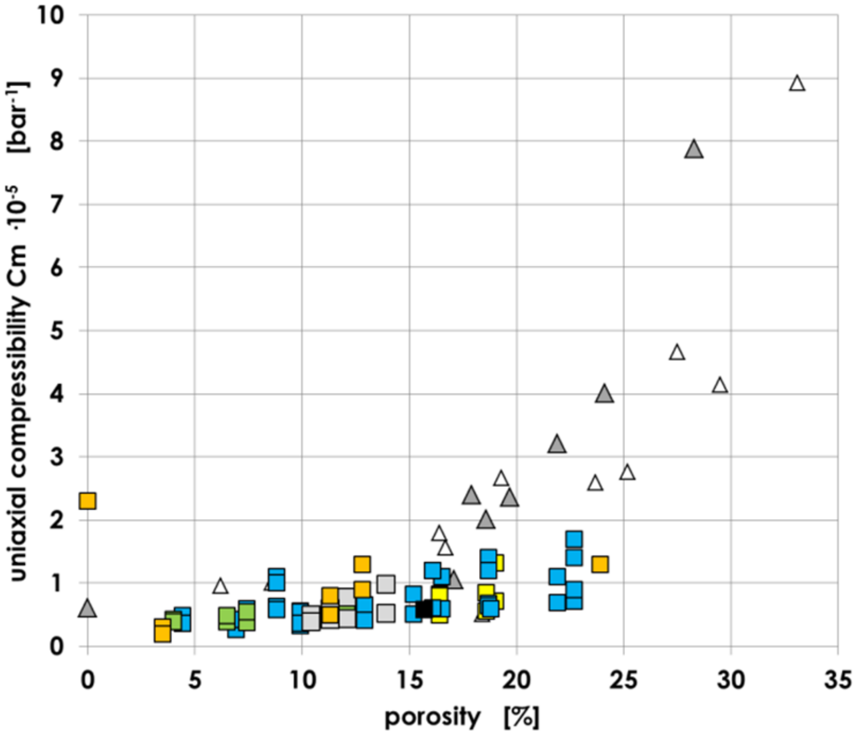

Pijnenburg et al. (2019) Inelastic Deformation of the Slochteren Sandstone: Stress-Strain Relations and Implications for Induced Seismicity in the Groningen Gas Field. JGR Solid Earth

Some observations:

- Cm increases with porosity
- Inelastic strain increases with porosity, typically 50% for a 20% porosity sample
- Time dependent behaviour: research objective in DEEP.nl

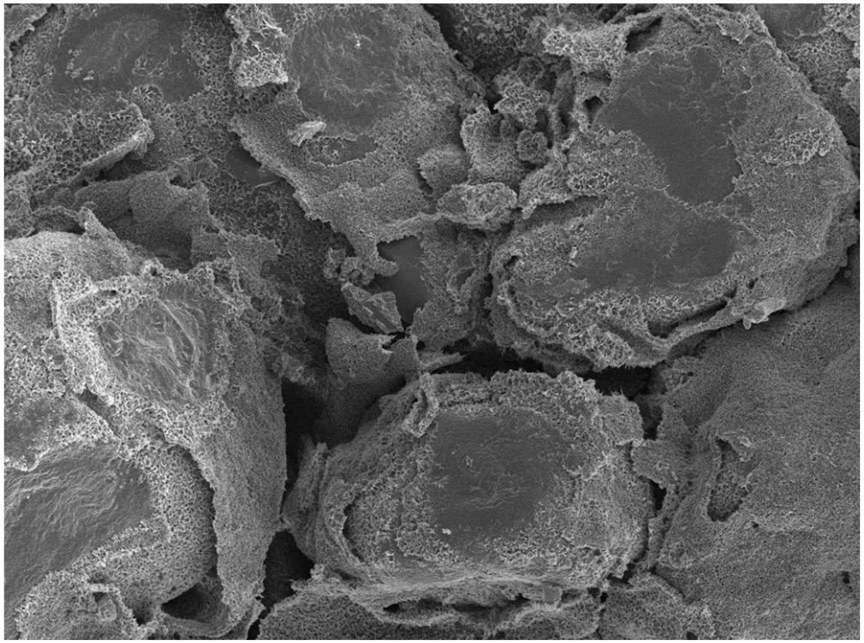

Data to constrain compaction and subsidence in Groningen – **laboratory measurements – MGT-3, Eemskanaal-12**

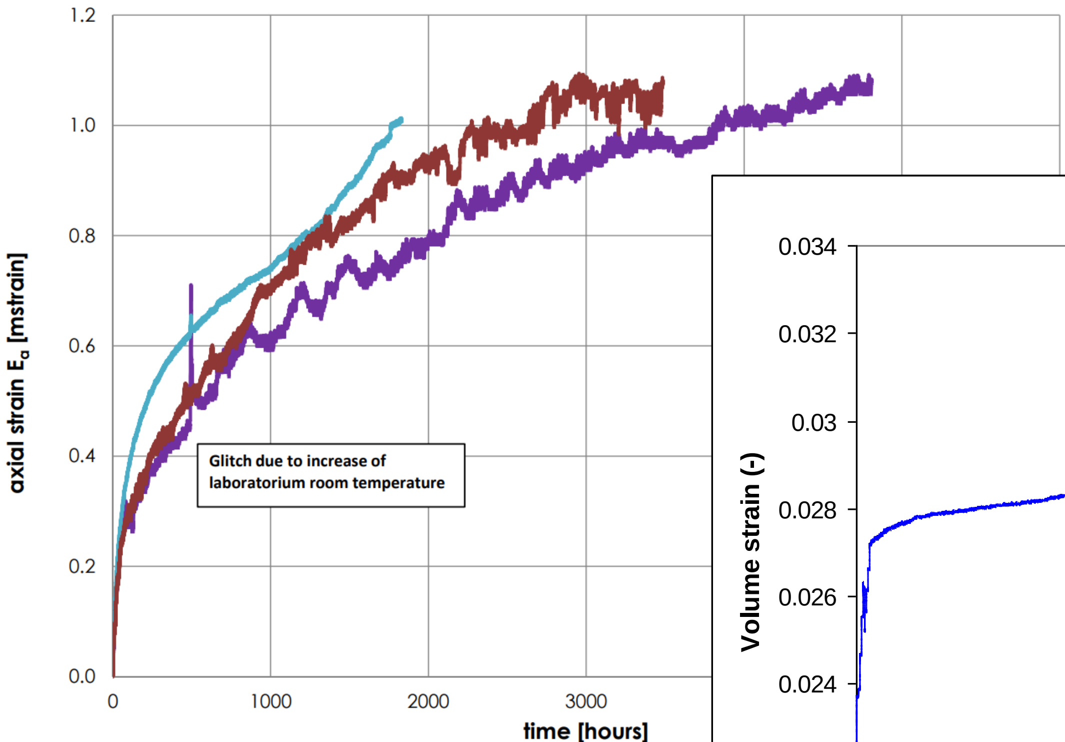

Eemskanaal-12

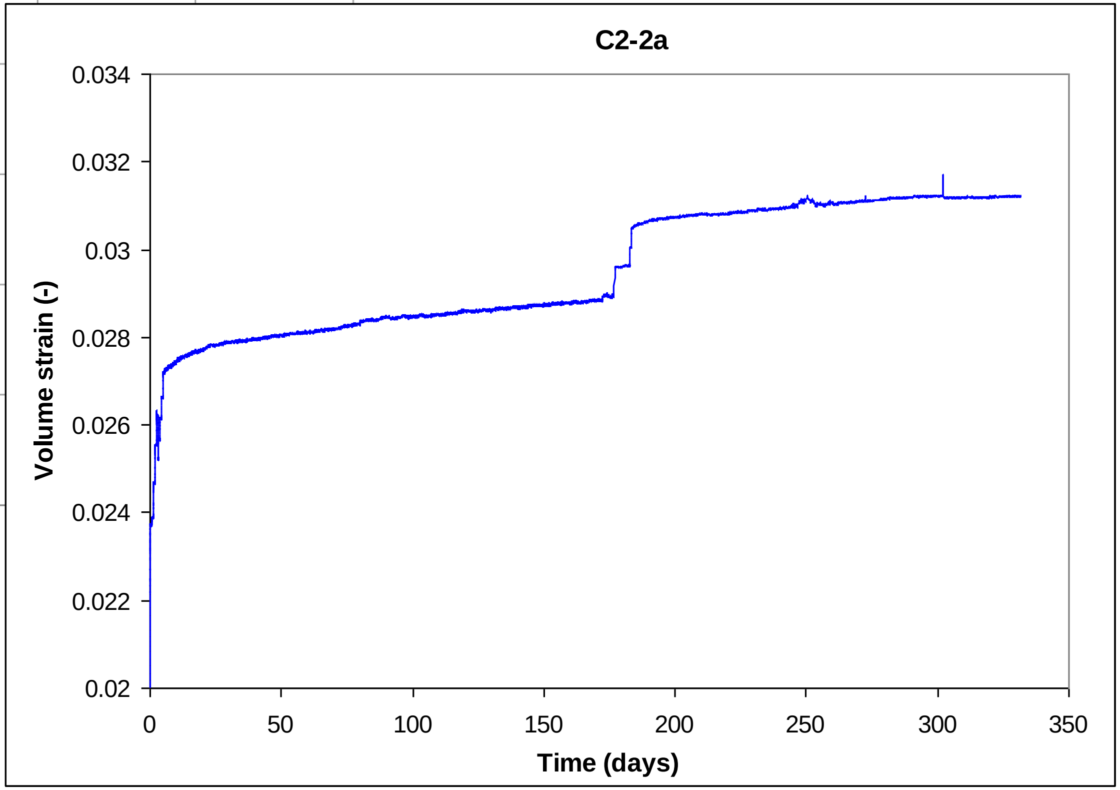

Data to constrain compaction and subsidence in Groningen – **In-situ compaction**

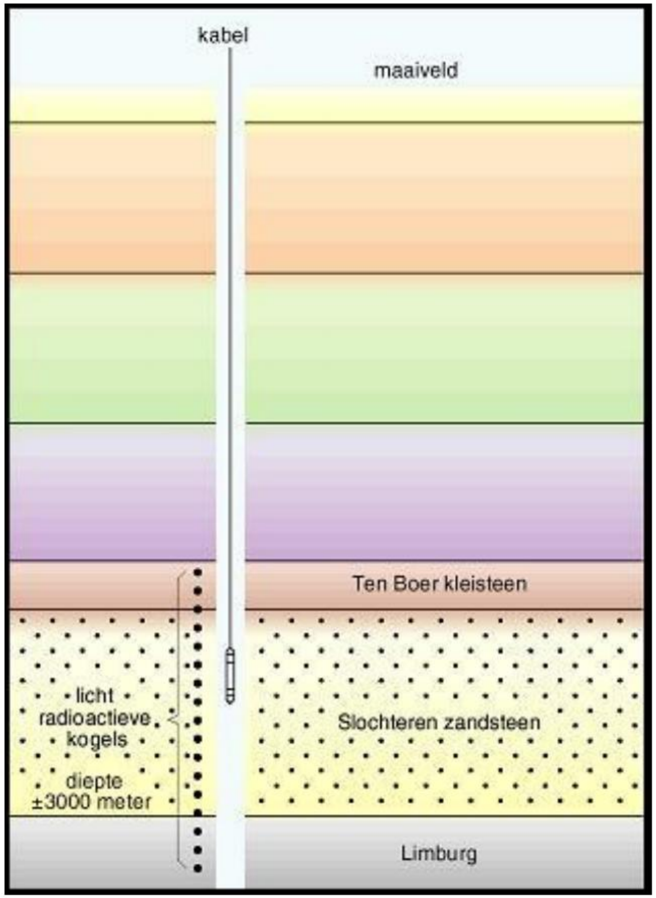

$$\Delta h = h_{ref} * \Delta P_p * C_m$$

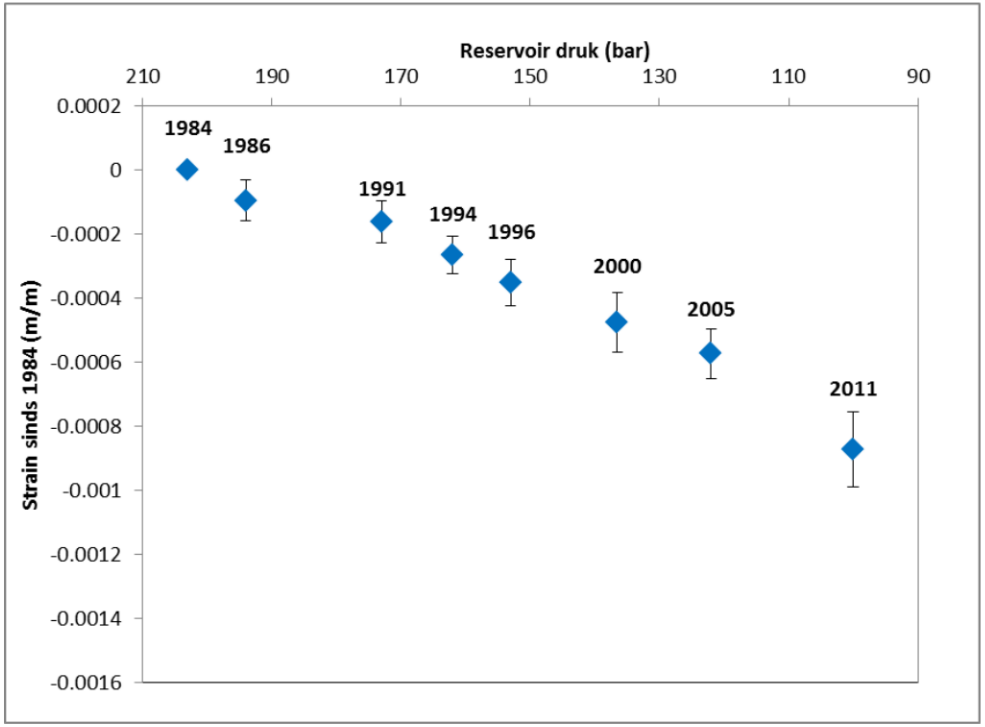

Objective: measure compaction in the field

Data to constrain compaction and subsidence in Groningen – In-situ compaction. **Distributed Strain Sensing Measurement ZRP-3**

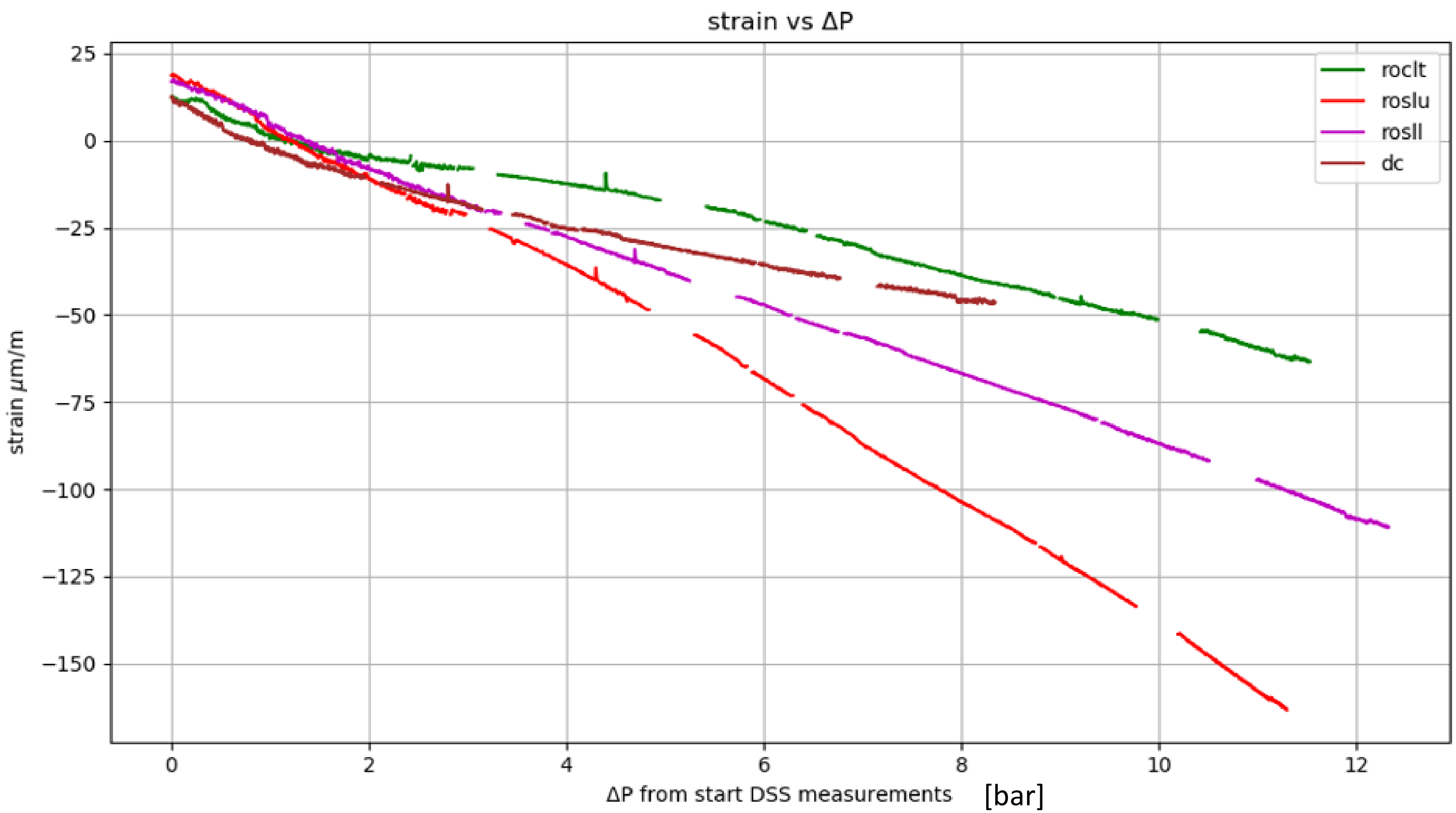

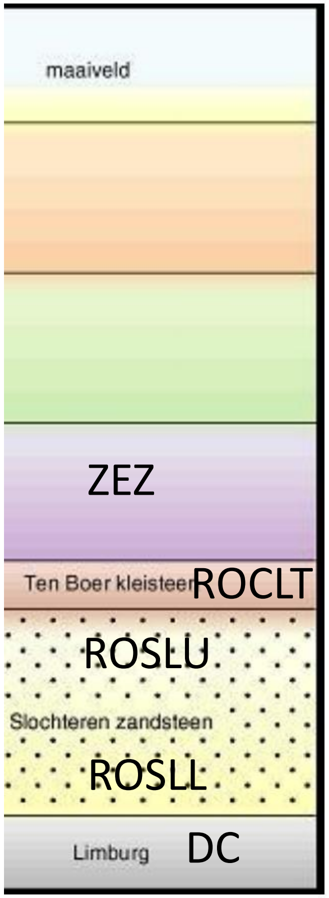

Objective: measure compaction in the field

content

- Why subsidence is a major concern
- Compaction and subsidence measurements
- Subsidence history matching and forecasting

Subsidence – prognosis

Only based on first lab results

- Cm from core
- Analytical equations to forward predict subsidence (Geertsma, 1973)

>1 meter

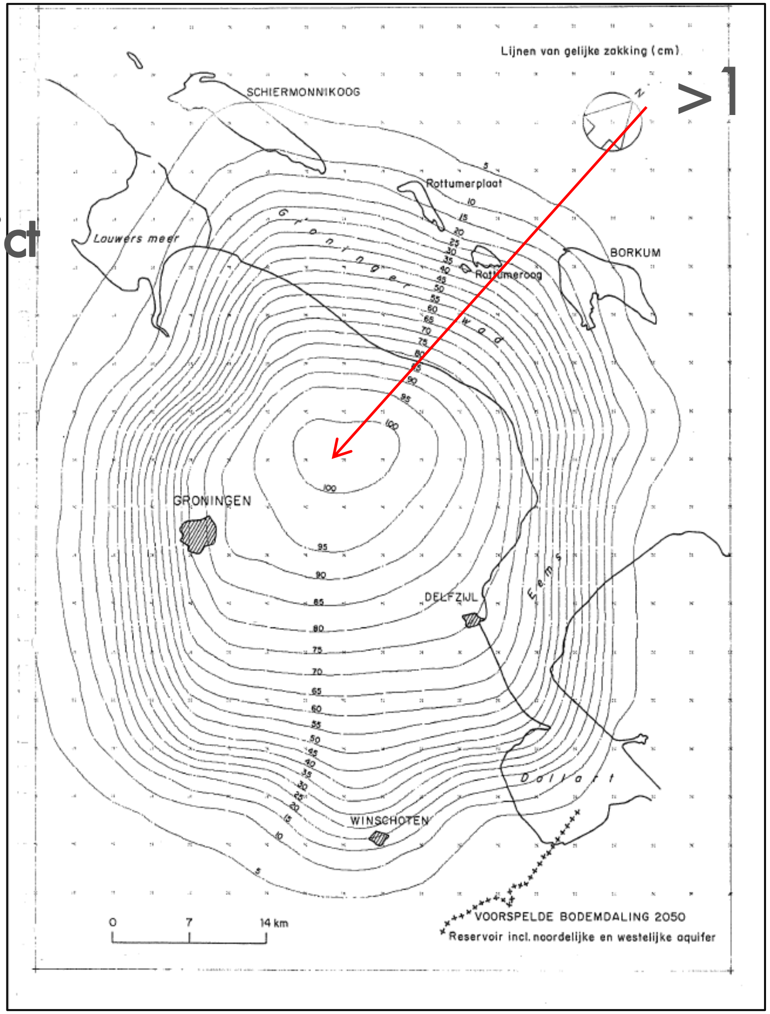

Subsidence – Maximum predicted subsidence at end of field life through time

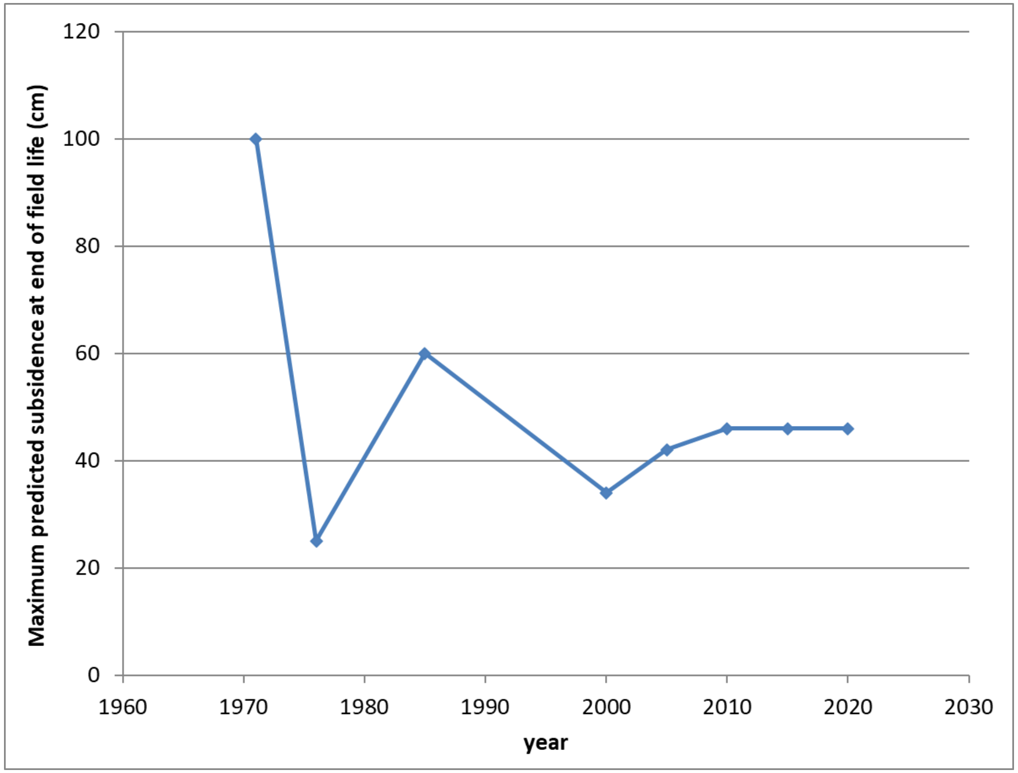

Convergence of predictions

- More geodetic available to constrain uncertainty
- Guidance from observations above other fields (Ameland)
- Analytical and numerical models

Forecasting subsidence – latest methodology (Shell, NAM) and results

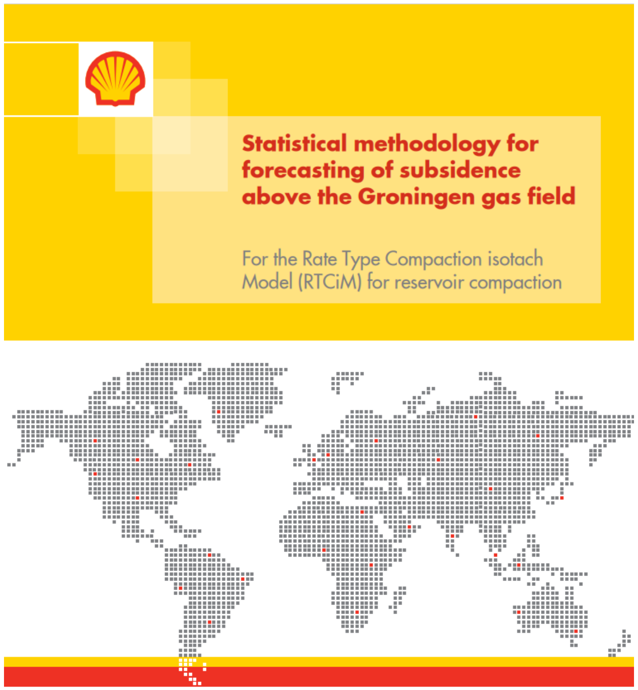

Unrestricted
SR.20.00973
September 2020

Link

+

Groningen long term subsidence forecast

NAM-report	EP202008201822, unrestricted
Version 0	Original version
Version 1	updated parameter values for model uncertainty
Version 2	Appendix B added describing the effect of multiple reservoir realisations on the model uncertainty

Link

Two reports: theory + application to Groningen field and aquifers

Objectives

- Use statistical technique to history match historical levelling data
  → Bayesian MCMC
- Investigate plausible depletion scenarios for lateral aquifers
  → Thousands of possible scenarios investigated
- Investigate Compressibility correlations
  → Correlation to Vp, porosity and uniform distribution
- Use a "versatile" compaction model
  → RTCiM Rate Type compaction model
- Forecast subsidence – including uncertainty - for Groningen field and aquifers
  → Forecasts up to 2080. Uncertainty based on variance covariance assessments for measurements and models

Definition of aquifer areas

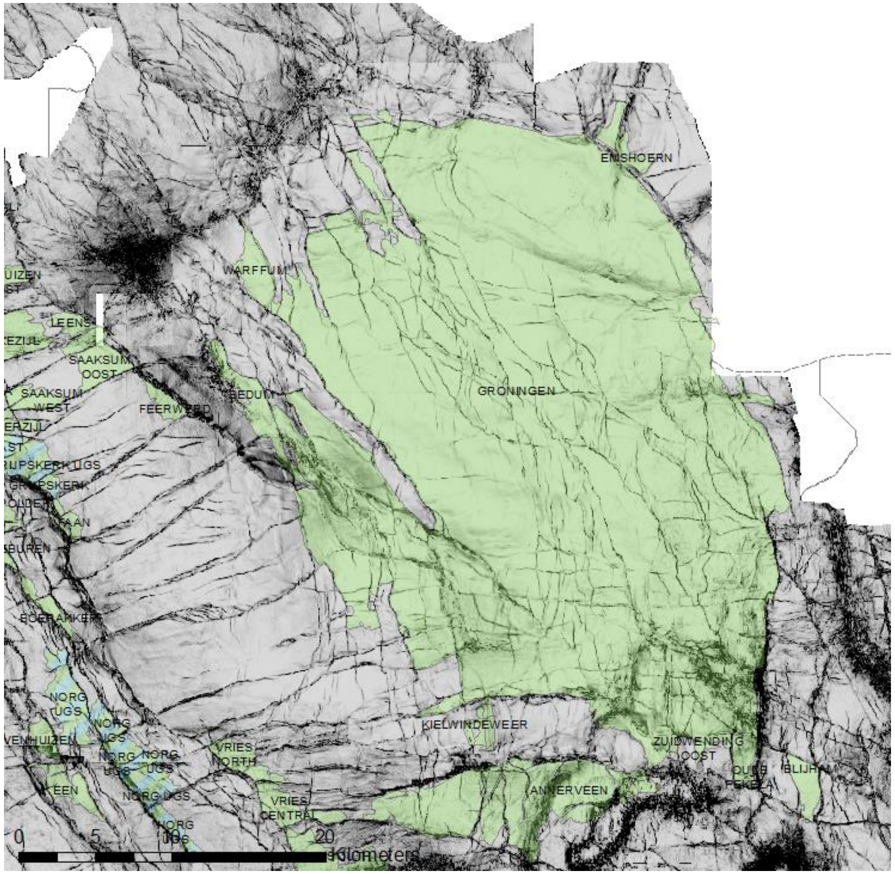

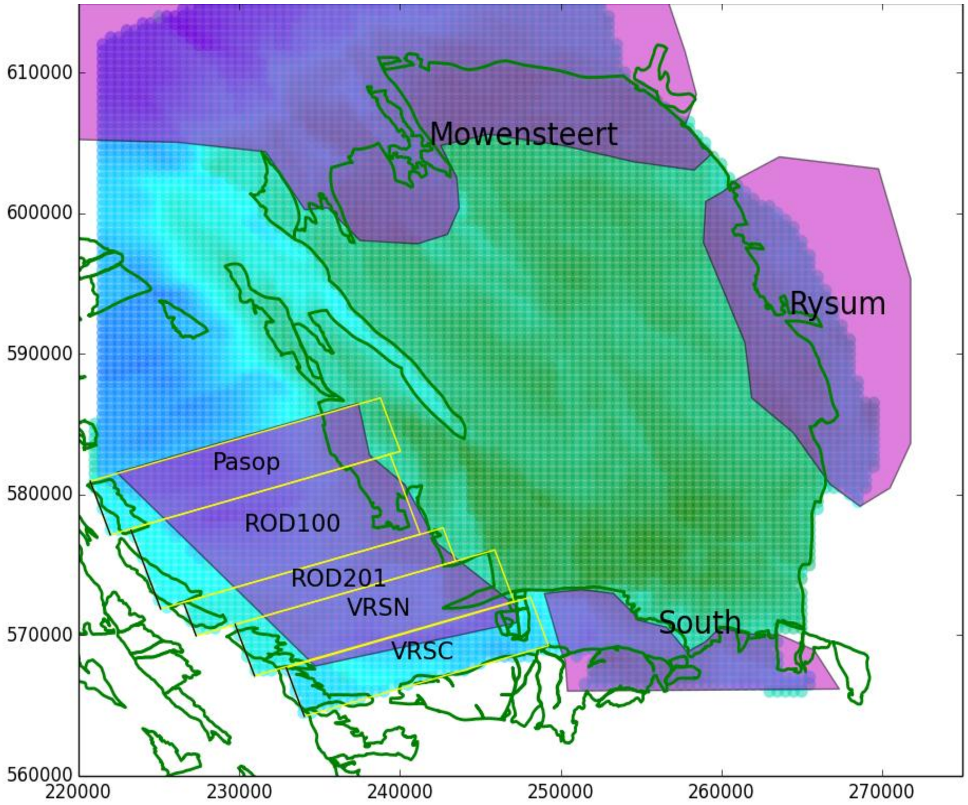

Semblance map

Purple aquifers

Pressure scenarios – prior uncertainty

Min low mid high max

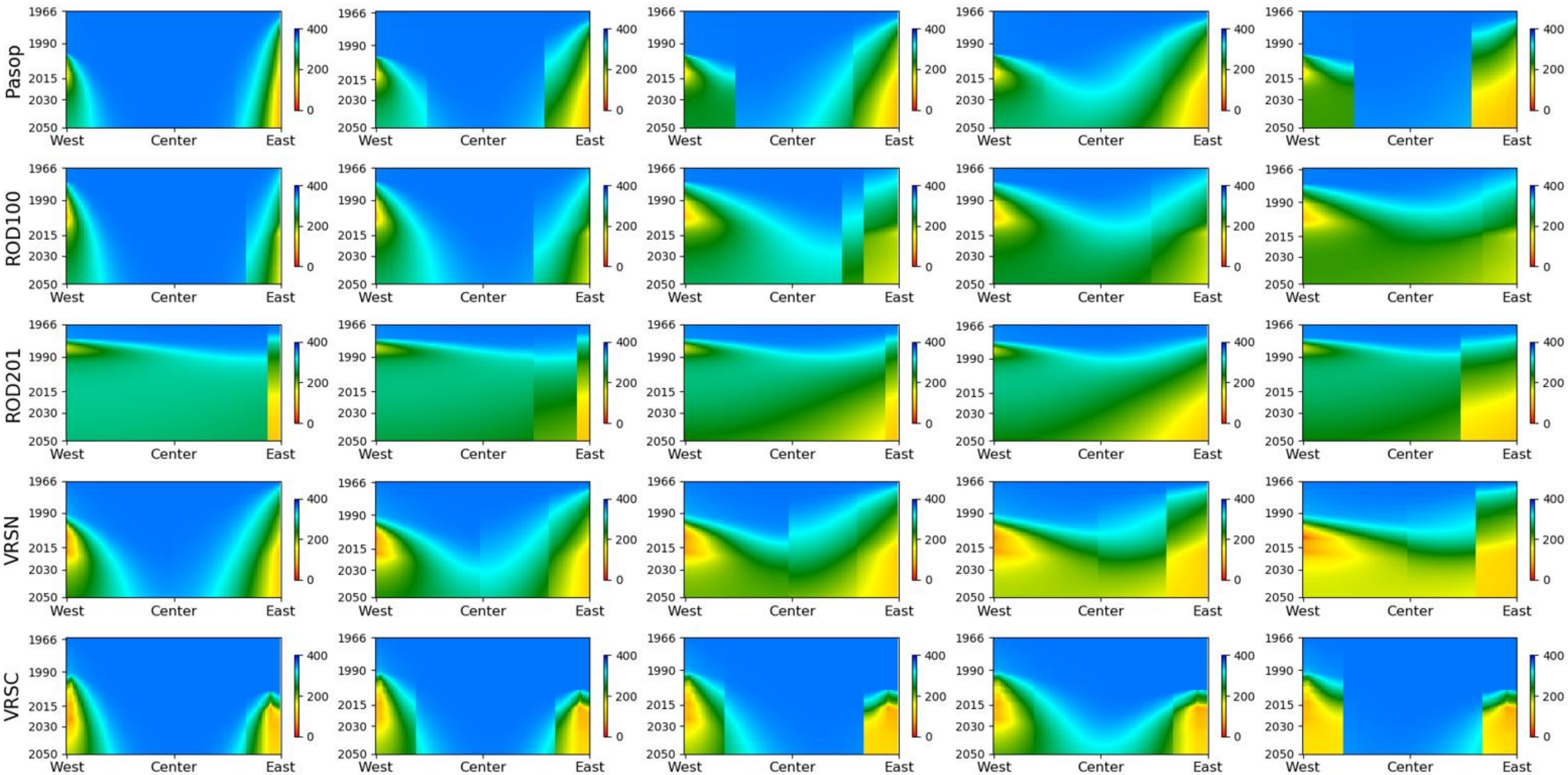

Compaction grids – prior uncertainty

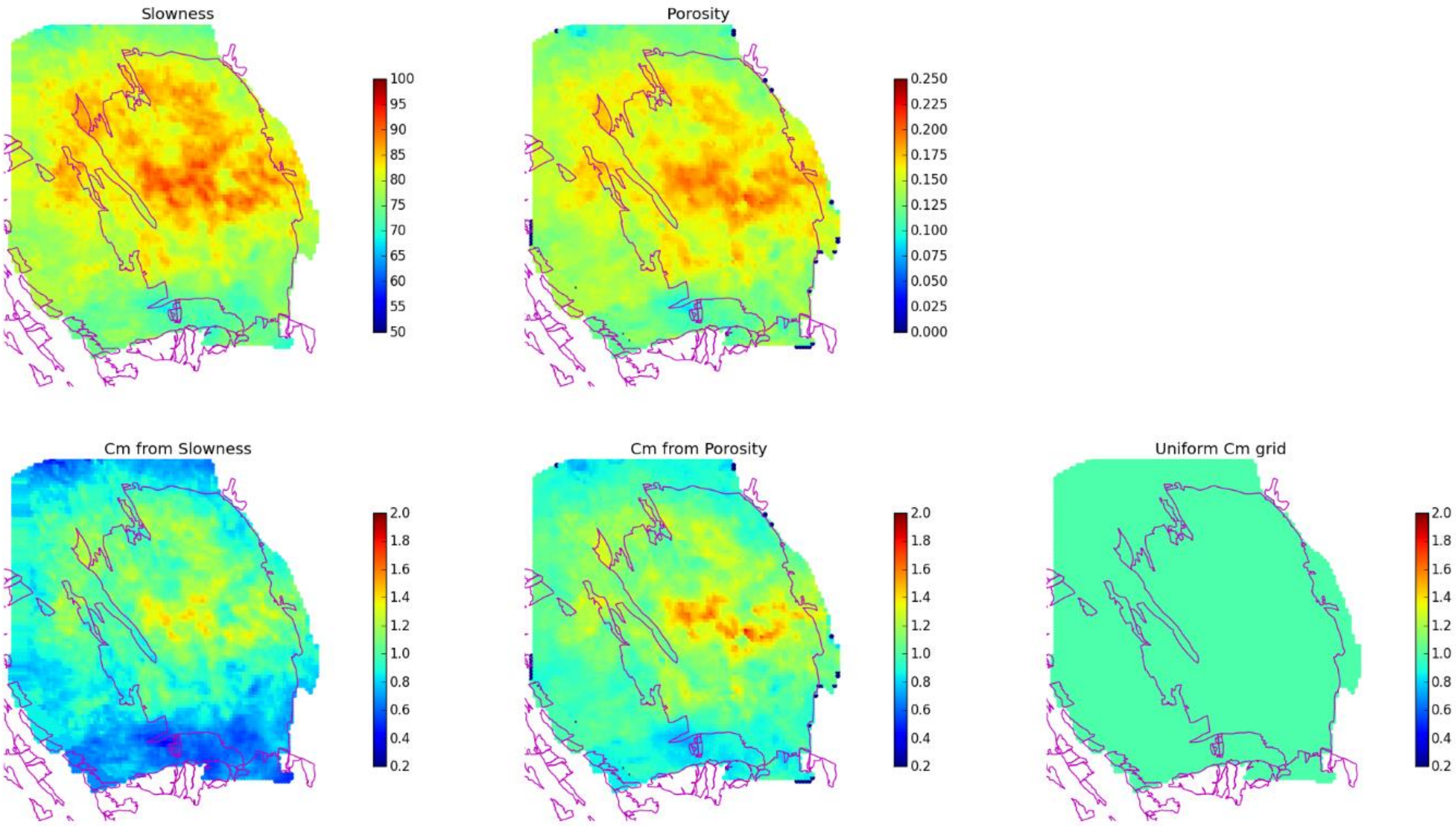

Levelling campaigns

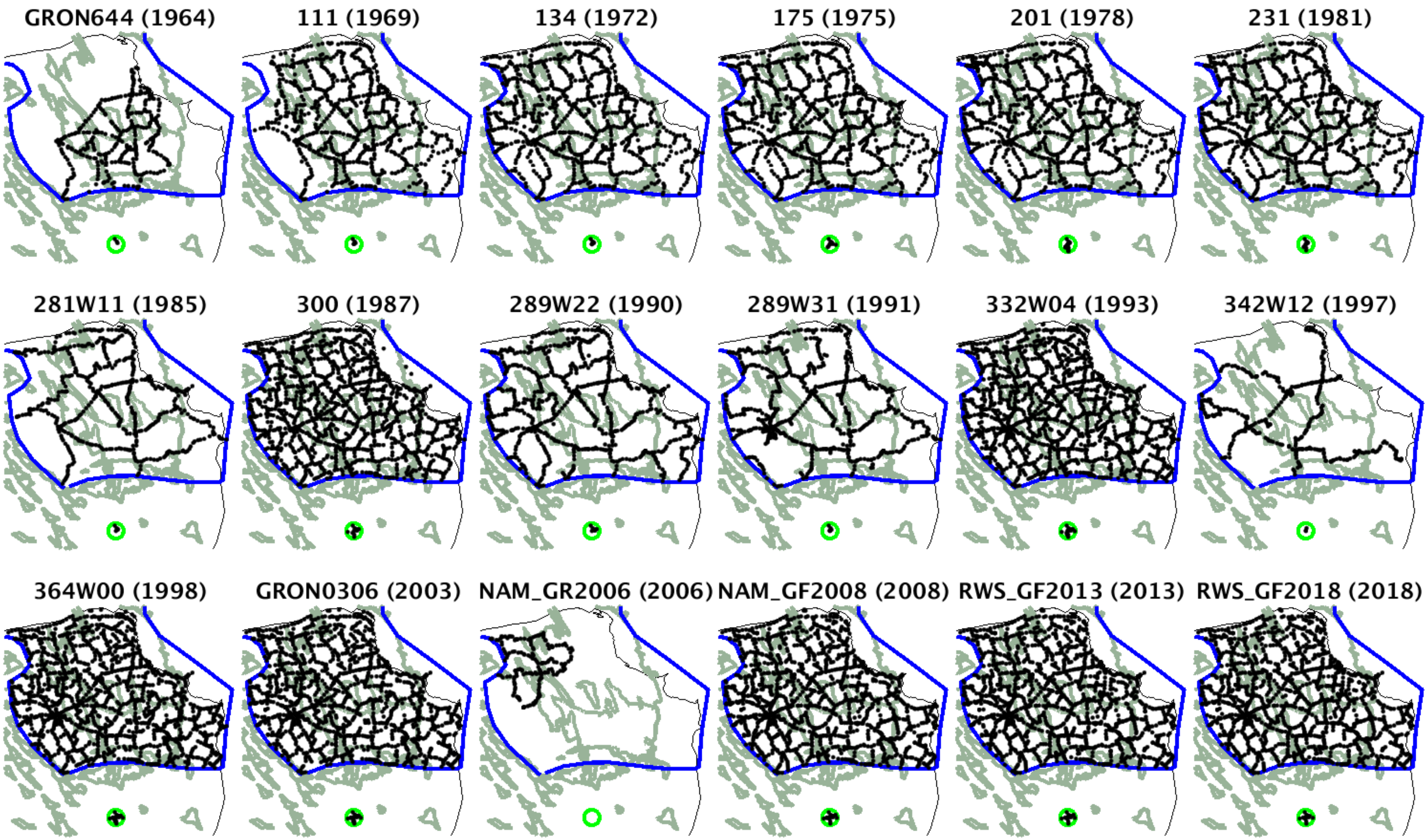

RTCiM

$$\varepsilon = \varepsilon_d + \varepsilon_s$$

$$\dot{\varepsilon}_s(t) = \left(\frac{\varepsilon(t) - \varepsilon_0}{\sigma'(t)} - C_{m_d}\right)\dot{\sigma}'_{ref}\left(\frac{\varepsilon(t) - \varepsilon_0}{\sigma'(t)\,.\,C_{m_{ref}}}\right)^{-1/b}$$

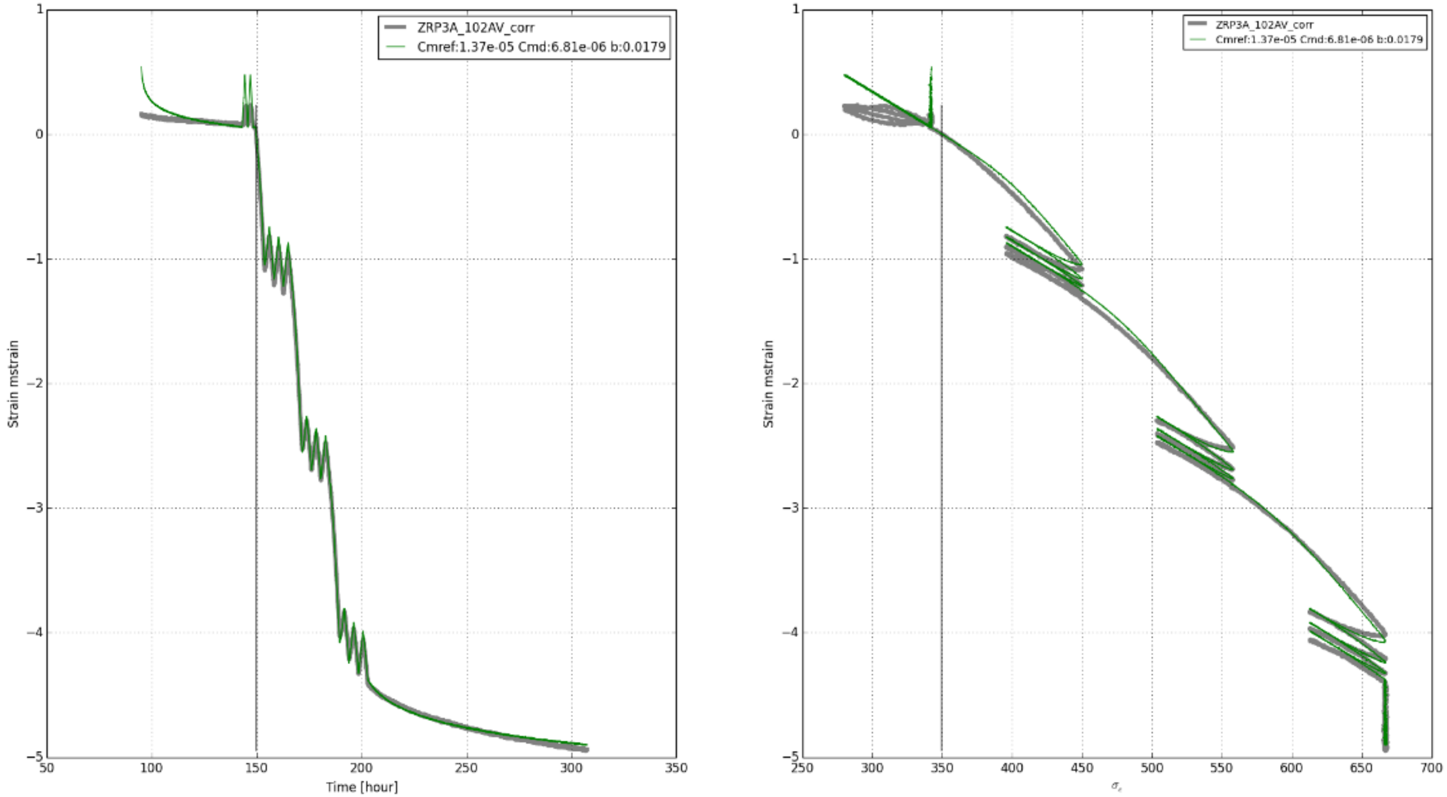

Model chain

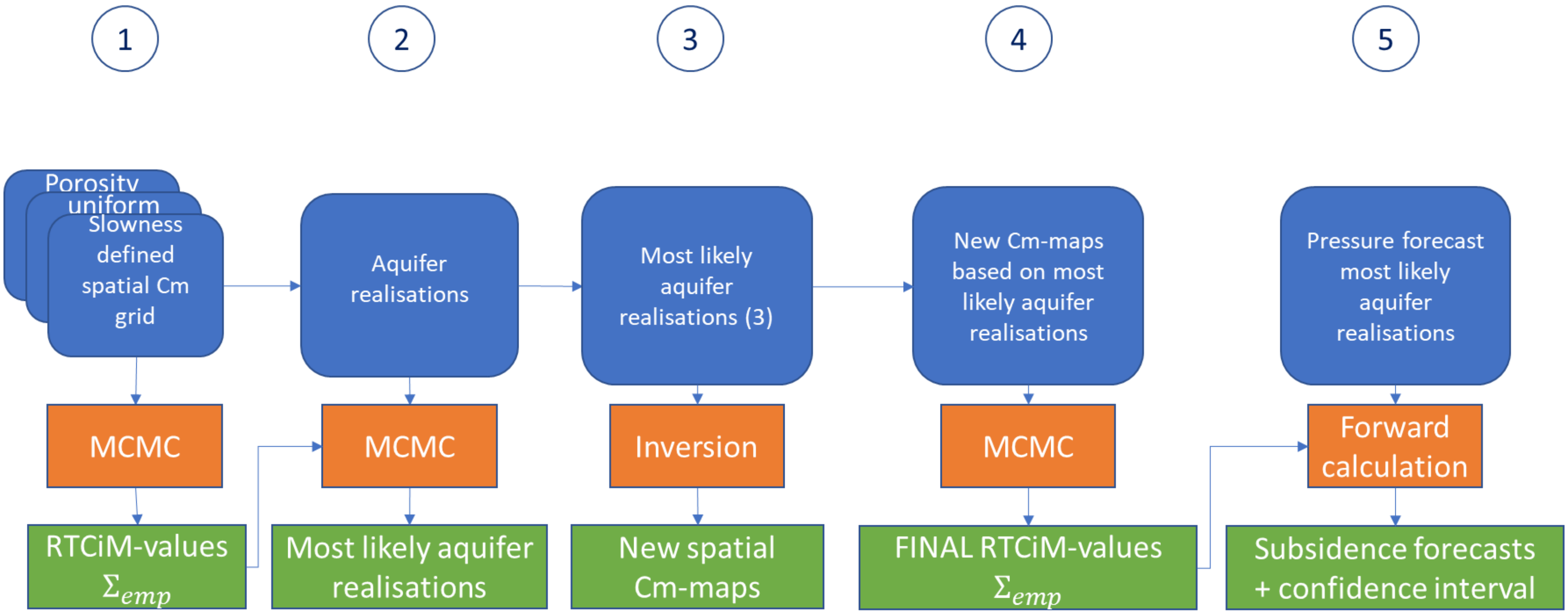
1
2
3
4
5
Porosity
uniform
Slowness defined spatial Cm grid
Aquifer realisations
Most likely aquifer realisations (3)
New Cm-maps based on most likely aquifer realisations
Pressure forecast most likely aquifer realisations
MCMC
MCMC
Inversion
MCMC
Forward calculation
RTCiM-values Σ_{emp}
Most likely aquifer realisations
New spatial Cm-maps
FINAL RTCiM-values Σ_{emp}
Subsidence forecasts + confidence interval

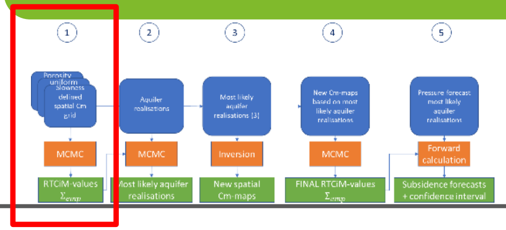

Step 1: initial parameter values and uncertainty

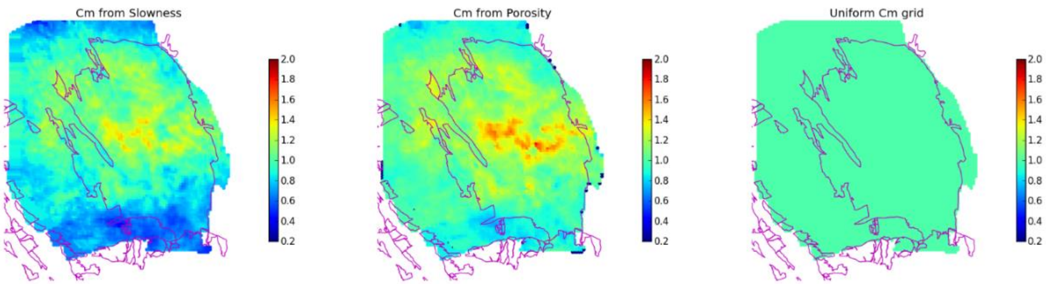

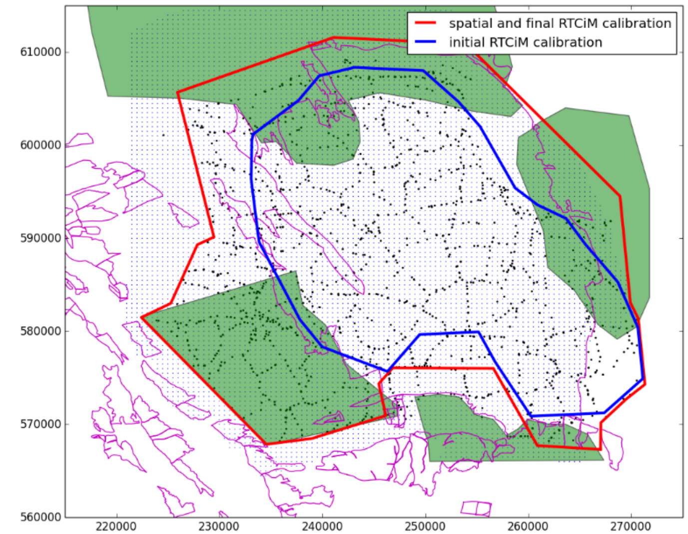

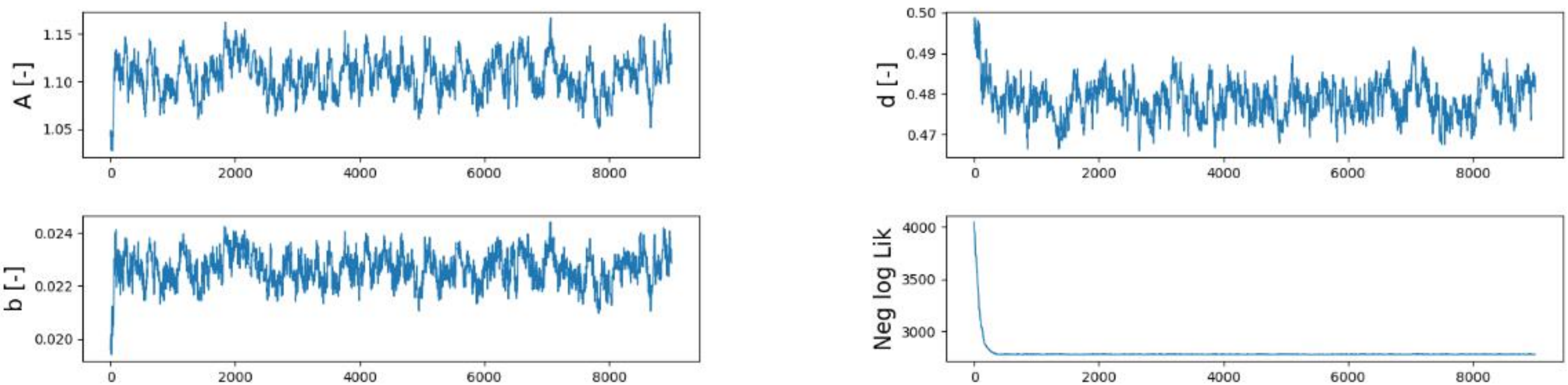

NAM

Step 2: aquifer scenarios

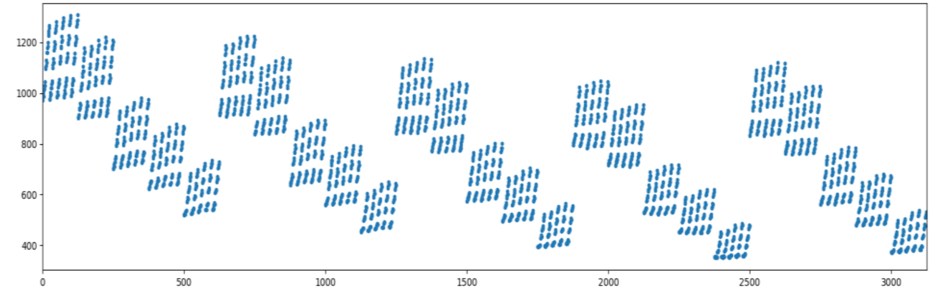

NLL

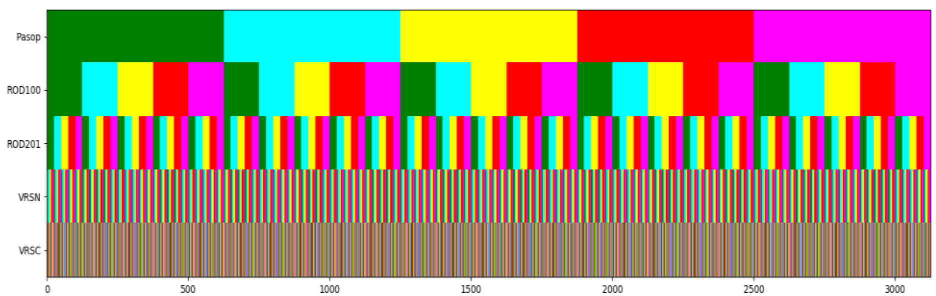

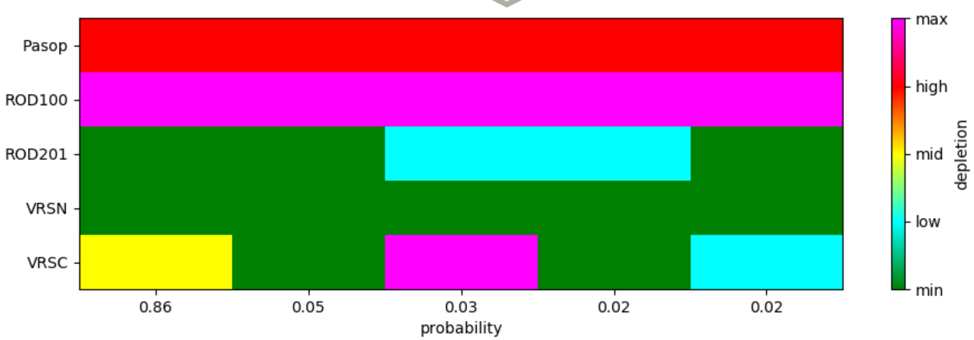

Depletion 2020

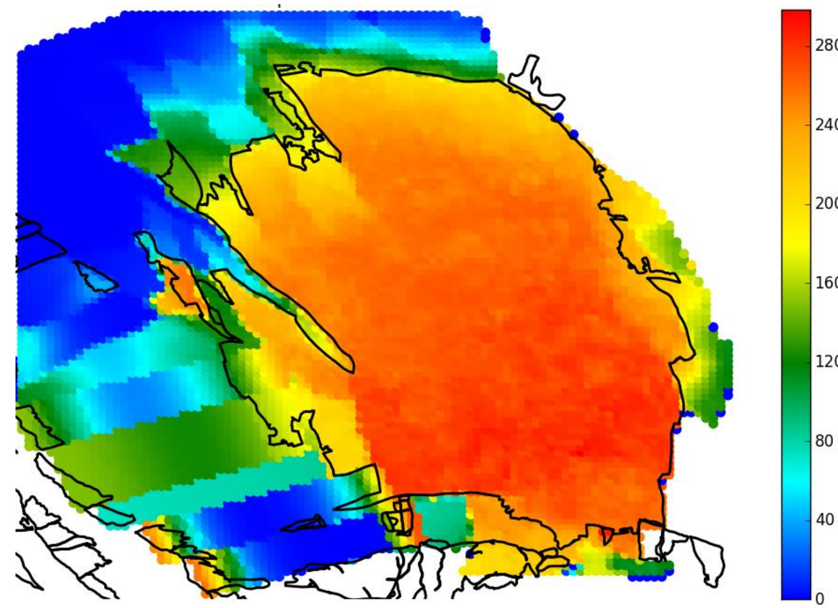

NAM

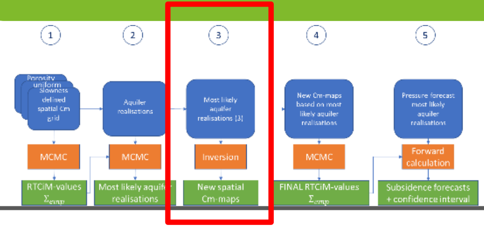

Step 3: inversion: improve spatial fit

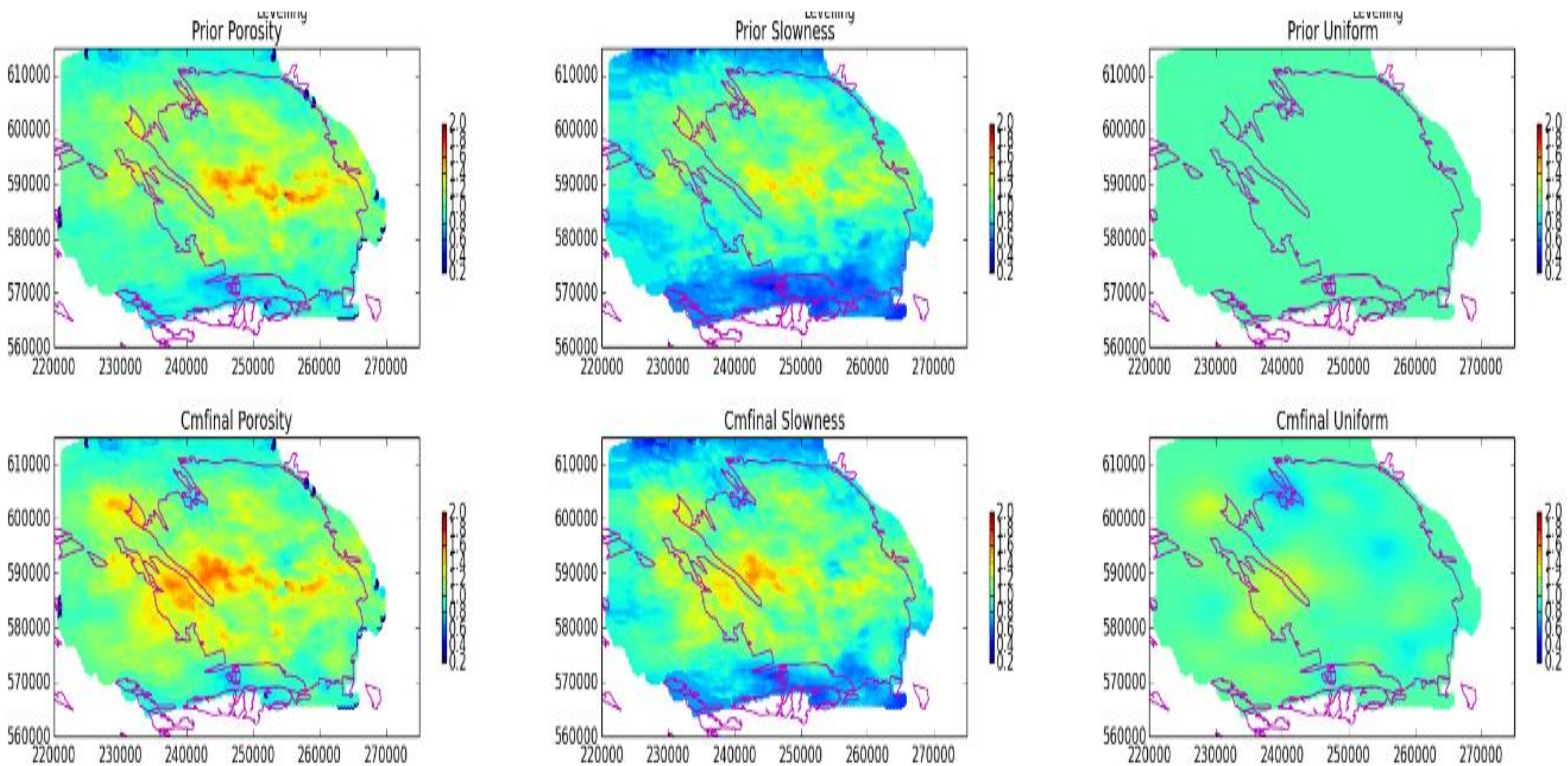

Use prior Cm grids and penalty multiplier to provide Apriori Cm maps using RMS and NLL values

NAM

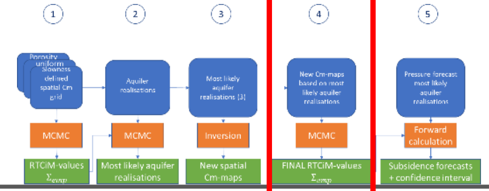

Step 4: improve temporal fit

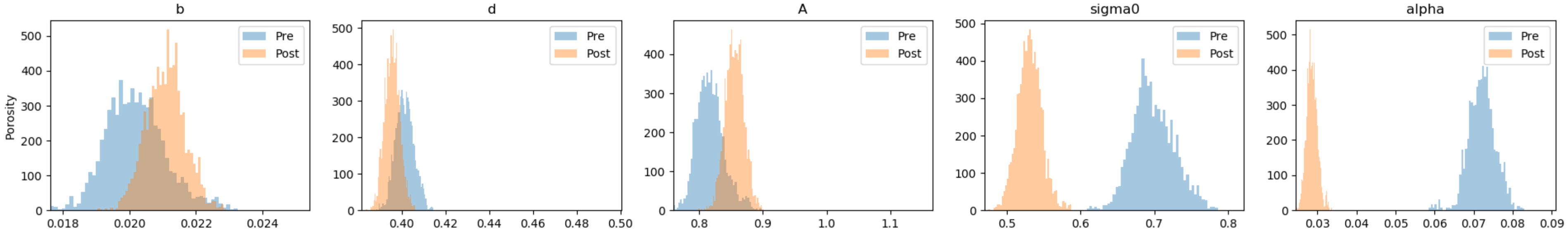

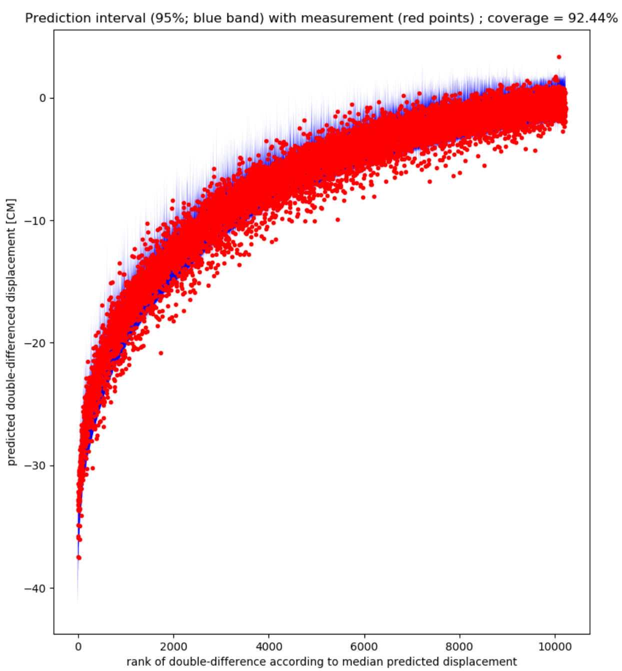

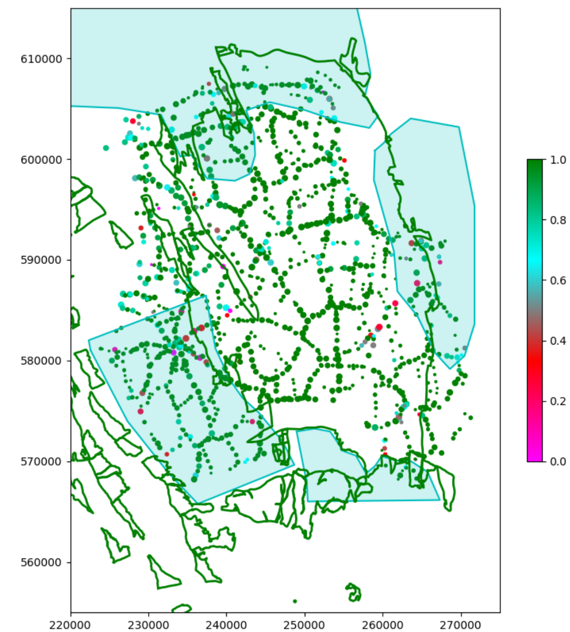

NAM

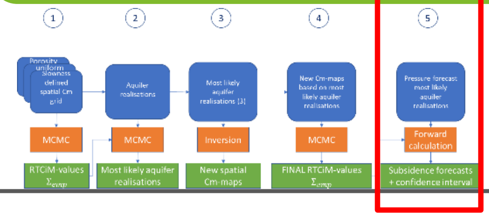

Step 5: forecasting: GNSS and InSAR validation

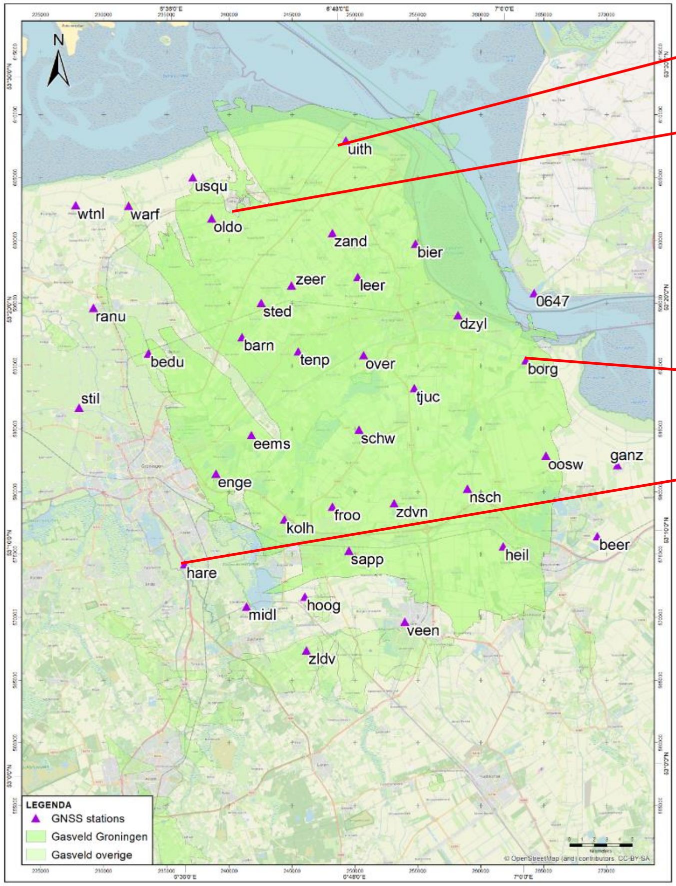

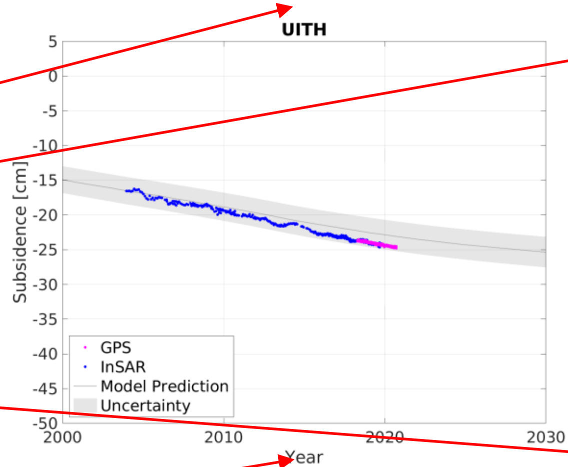

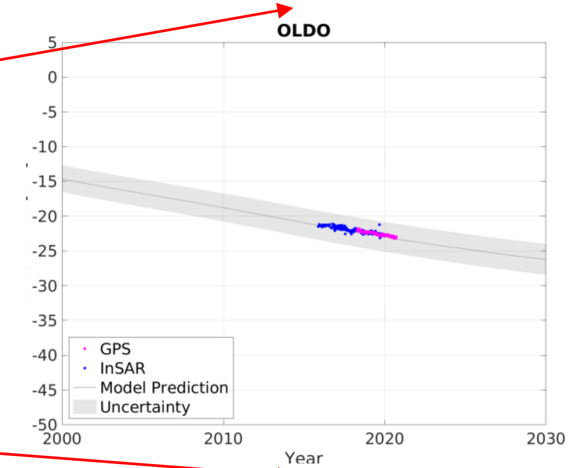

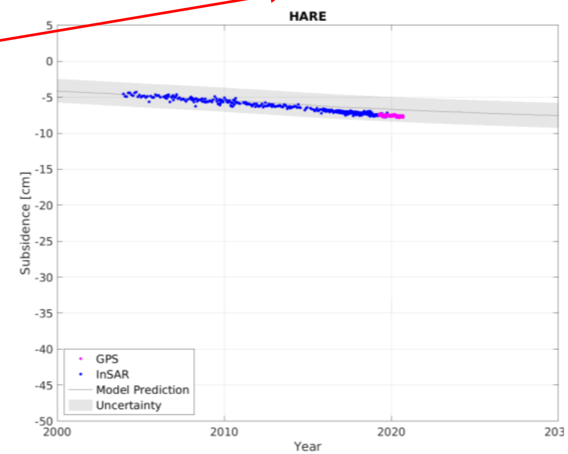

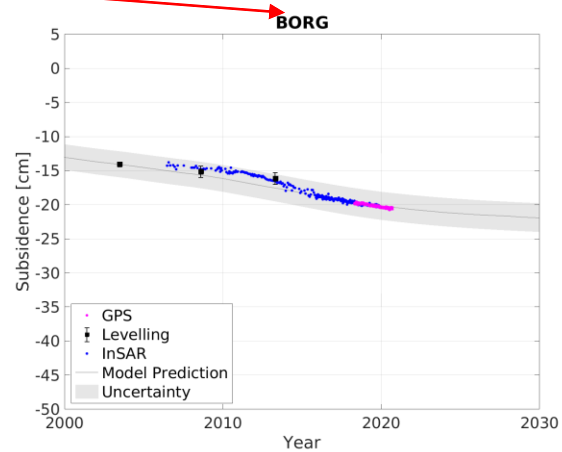

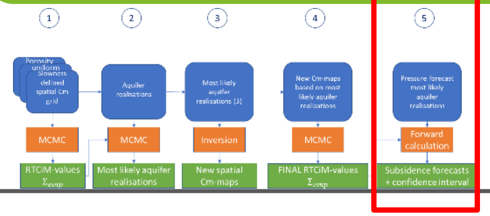

Step 5: forecasting: up to 2080

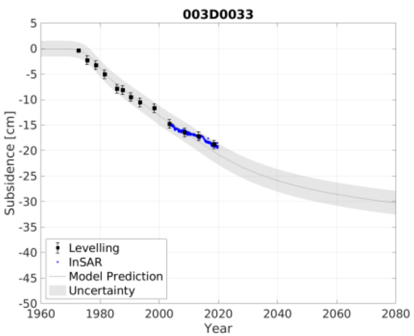

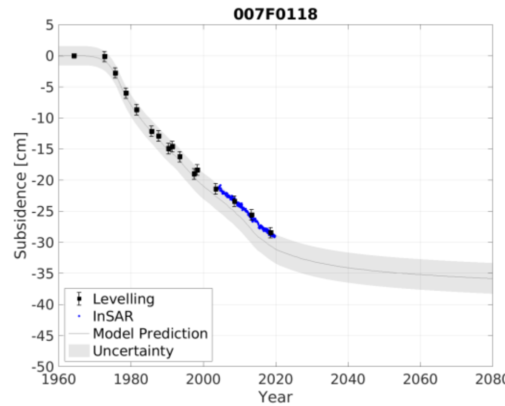

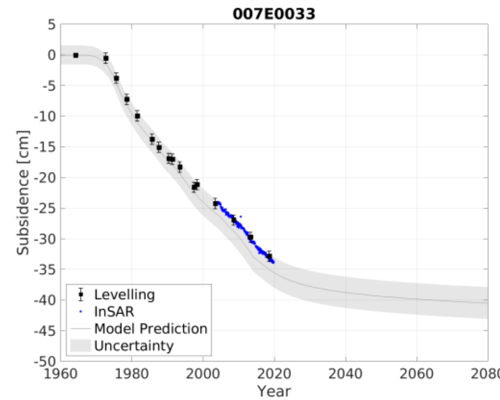

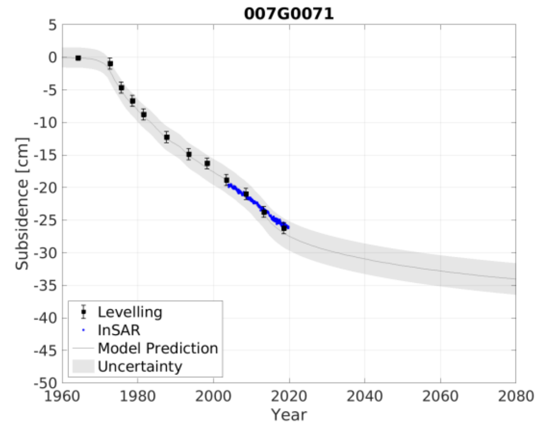

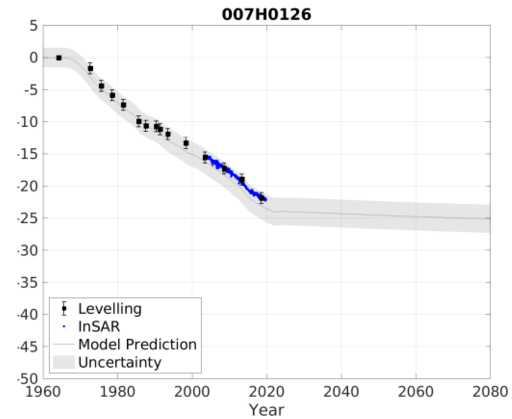

Conclusions

- Compaction behaviour of the Groningen cemented sandstone can best be described by a (visco)-elasto-plastic model. Based on lab studies and field observations
- measurements are matched by a Rate Type Compaction Model
- MCMC work flow was successfully applied to improve forecasting capabilities of subsidence, addressing multiple sources of uncertainty
- Improved understanding of likely depletion in lateral aquifers

Definition and Mmax for Tectonic Earthquakes in PSHA

Robert Youngs
Wood Environment & Infrastructure Solutions

Groningen Mmax II Workshop
June 13-17, 2022
South Amsterdam, The Netherlands

What is Mmax for a Seismic Source in PSHA

- A seismic source describes where earthquakes occur spatially
- The occurrence in time of earthquakes associated with the source is represented by
  - a probability distribution for occurrence (e.g., Poisson, Brownian Passage Time)
  - a probability distribution for earthquake magnitude (e.g., exponential, characteristic, maximum moment), often termed a frequency-magnitude distribution
- Mmax (m^u) is the upper limit on earthquakes that can occur associated with the seismic source, the upper truncation point of the frequency-magnitude distribution

Why is it Imposed

- Occurs “naturally” for seismic sources defined on basis of specific geologic structures through physical limits on the size of ruptures that can occur
  - For an individual fault, recurrence models such as characteristic (Youngs and Coppersmith (1985) or Maximum Moment (Wesnousky, 1986) impose limit through the size of the characteristic / maximum moment event
  - Systems of connected faults contain limit based on maximum size of the interconnected ruptures (e.g., Field et al., 2017)

Recurrence Models for Connected Fault Systems

Total long-term magnitude-frequency distribution for UCERF3 model (Field et. al., 2017)

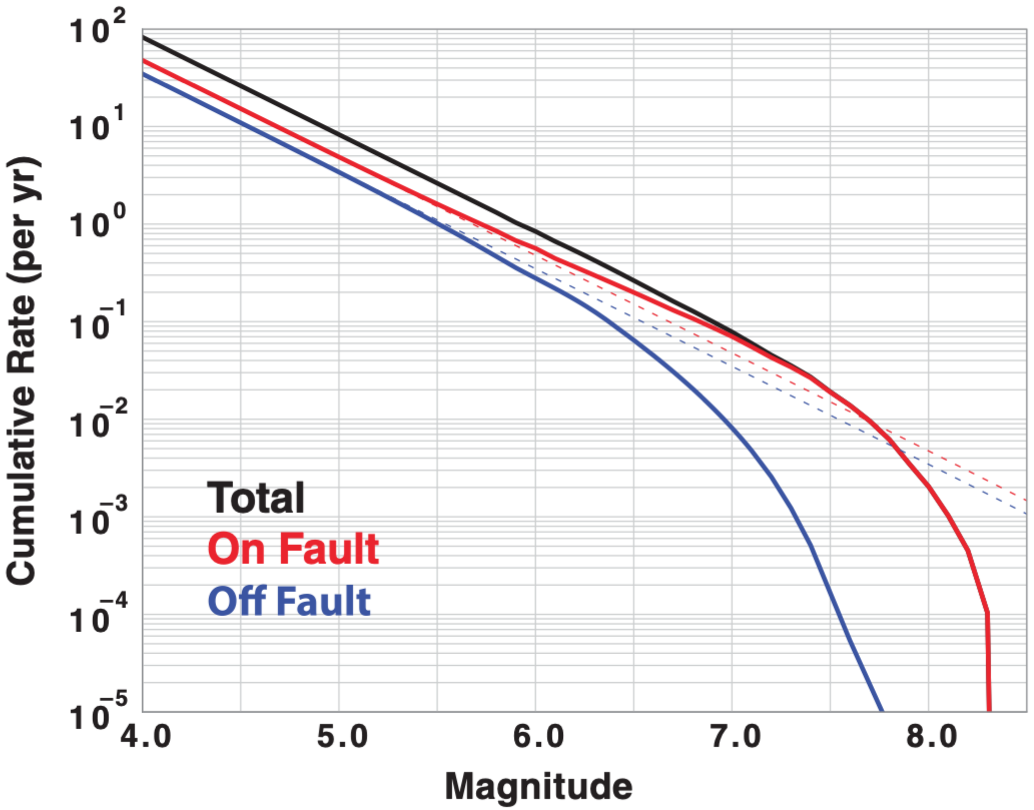

Modified characteristic model to accommodate potential linked ruptures (Wooddell et al., 2014)

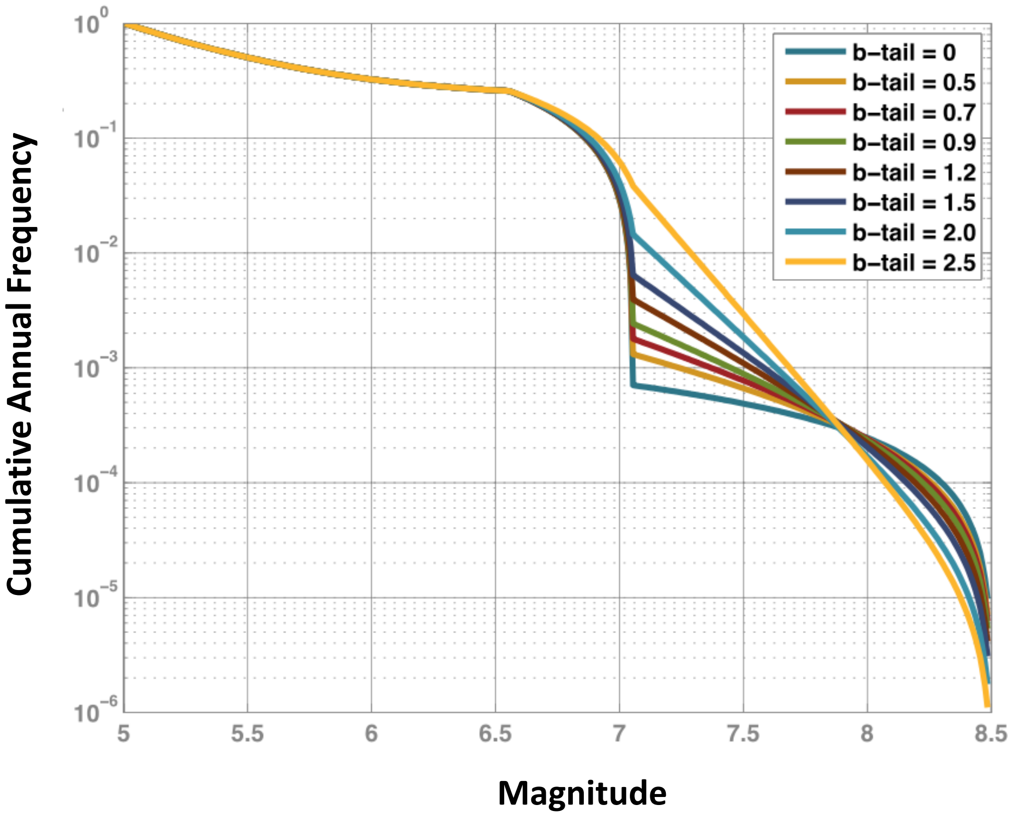

Why is it Imposed

- Imposed for zones or regions to produce a finite limit on the rate of seismic moment release (e.g., Knopoff and Kagan, 1977; Main, 1995)
- For unbounded G-R exponential magnitude-frequency distribution
  - Rate of decrease in frequency $\dot{N}(\boldsymbol{M}) \propto 10^{-b\boldsymbol{M}}$
  - Energy $\propto 10^{c\boldsymbol{M}}$ where *c* is factor in equation for moment $M_o(\boldsymbol{M}) = 10^{c\boldsymbol{M}+d}$
  - $\dot{E}(\boldsymbol{M}) \propto \dot{N}(M) \times M_o(\boldsymbol{M}) \propto 10^{(c-b)\boldsymbol{M}}$, therefore, as $\boldsymbol{M} \rightarrow \infty, \dot{E} \rightarrow 10^{(c-b)\infty}$
- Truncation at Mmax needed for exponential magnitude-frequency distribution as typically $c > b$, leading to infinite $\dot{E}$ at infinite $\boldsymbol{M}$
- ”Soft” Mmax for models such as gamma magnitude-frequency distribution (Kagan, 1993; Main et al., 1999) in which rate of decay in magnitude-frequency is greater than the rate of increase in seismic moment with magnitude

Mmax Assessments for Types of Seismic Sources Used in PSHA for Tectonic Events

- Geologic structure-specific (i.e., faults and fault zones)
  - Usually assessed using an estimate of maximum rupture dimension and empirical relationships between rupture dimensions and earthquake magnitude
- Seismic Source Zones
  1. Maximum observe plus an increment
  2. Maximum observed in analog regions
  3. Assessment of maximum rupture dimensions
  4. Seismicity and geodetics

Mmax Methods for Geological Feature-Specific Seismic Sources

Assess Maximum Dimensions for Rupture

- Maximum rupture length
  - Surface rupture length
  - Rupture length at depth
- Maximum length at depth X rupture width = maximum rupture area
- Maximum displacement
- Average displacement
- Rupture area x average displacement = seismic moment for maximum event

Relationships Between Rupture Dimensions and Magnitude

- Some of the better known for individual rupture parameters
  - Wells and Coppersmith (1994)
  - Stirling et al. (2013) (compilation)
  - Leonard (2014) (self-consistent scaling, ACR and SCR)
  - Somerville (2014) (CEUS area-moment)
  - Hanks and Bakun (2008, strike slip)
  - Anderson et al. (2017) (influence of slip rate)
  - Thingbaijam et al. (2017)
- Moment magnitude scale, **M**
  - Hanks and and Kanamori (1979) (given area, average slip, and crustal rigidity)

Addressing Statistical Variability in Empirical Relationships

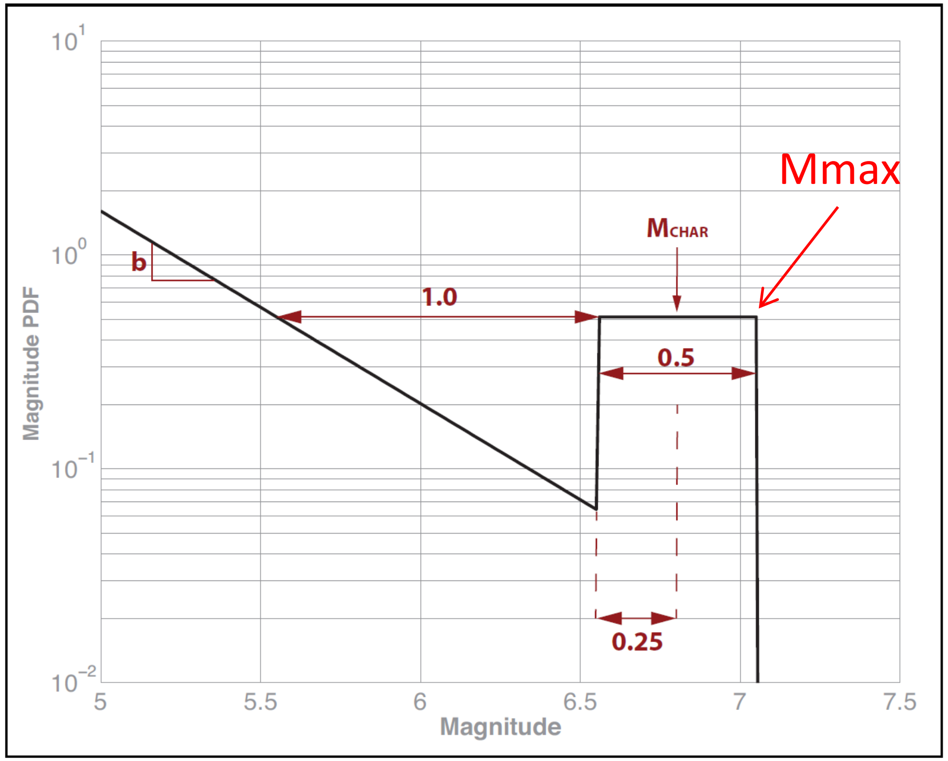

Figure 2. General form and parameters of the Youngs and Coppersmith (1985) MFD.

Youngs & Coppersmith, 1985

- Empirical relationships give expected **M** as a function of fault dimensions
- Statistical variability addressed by incorporating aleatory variability about this estimate in recurrence model
  - Uniform boxcar
  - Truncated normal

Epistemic Uncertainty in Mmax for Structure-Specific Sources

- Uncertainty in assessing maximum rupture dimensions (perhaps larger component of the two)
- Uncertainty in selection of appropriate empirical relationships

Mmax for Seismic Source Zones

1. Maximum observe plus an increment
2. Maximum observed in analog regions
3. Assessment of maximum rupture dimensions
4. Seismicity and geodetics

1. Maximum Observed Plus Δ

- Maximum possible should be at least as large as largest observed (within uncertainty in assessing magnitude of past earthquakes)
- Assessment of Δ
  - Scientific judgment – typically use a wide range (e.g., 0, 0.3, 0.6, in EPRI-SOG, 1988) with perhaps minimum value of Mmax
  - Statistical based on observed seismicity (e.g., Kijko and Sellevoli, 1989; Kijko, 2004)

Statistical Assessment of Δ

- From Kijko (2004)

$$m^u = E(M_{\max-obs}) + \int_{m_0}^{m^u} F_{m_{\max-obs}}(m)\,\mathrm{d}m$$

- Additive term provided in three forms
  - Based on truncated exponential model (Kijko and Sellevoli, 1989), the K-S estimator
  - Based on truncated exponential model with uncertain b-value (Kijko and Graham, 1998), the K-S-B estimator
  - Based on arbitrary magnitude distribution, Kijko et al. (2001), the N-P-G estimator

Statistical Estimates of Δ Require Large Samples

- Performance of K-S estimator as a function of sample size, N, and magnitude range of sample.
- Based on average value from 1000 simulated catalogs (Kijko, 2004)

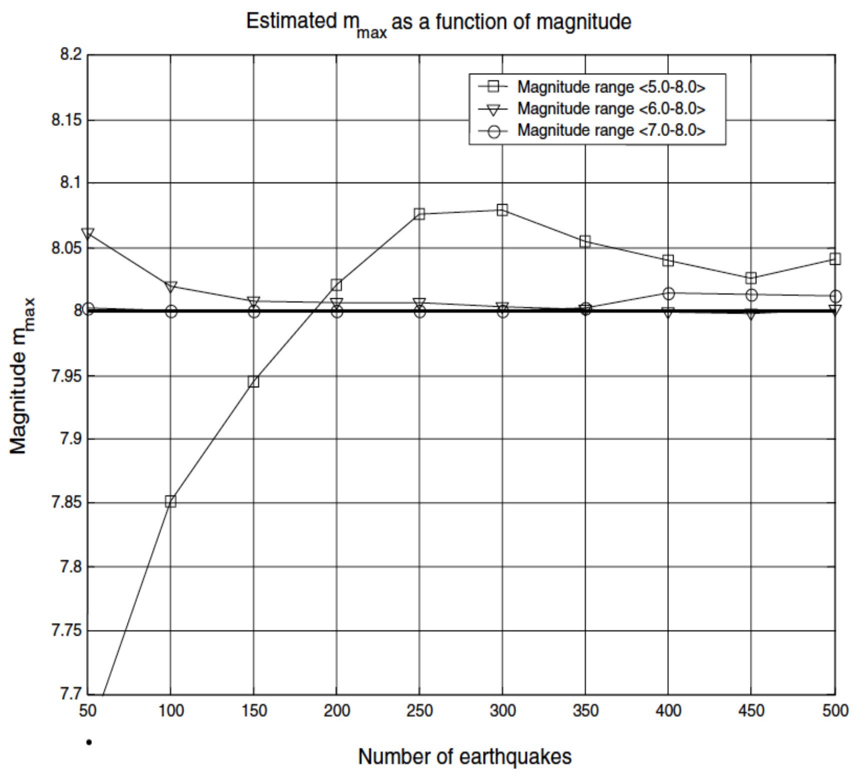

Uncertainty in Statistical Estimate of Mmax

- Variance in Mmax estimate is of the order of $\Delta^2 + \sigma^2(M_{max\text{-}obs})$ (e.g., Kijko, 2004)
- Confidence limits for Mmax are unbounded (Pisarenko, 1991; Kijko, 2004).
    - Asymtotically $P(m^u < \infty) = 1 - \alpha$ with α function of sample size
- Used as a basis for weighting method in combination with others (EPRI/DOE/NRC, 2012)

Fiducial distribution for Mmax (m^u)

$$P(m^u < z) = F(m^u) = 1 - F_{m_{max-obs}}(m_{max-obs} | z)$$

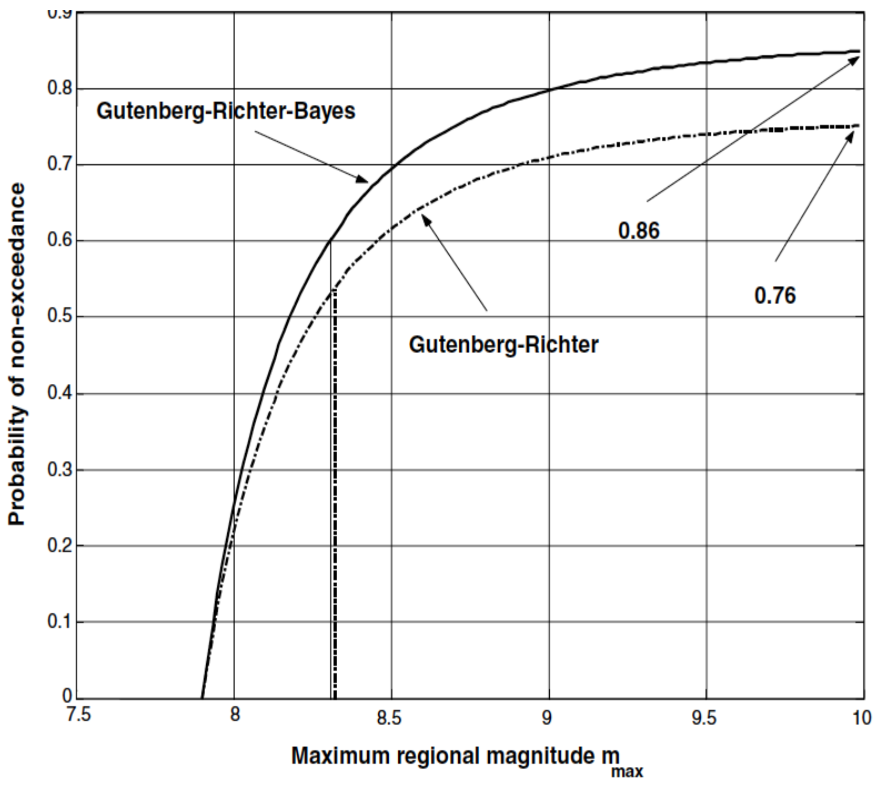

2. Maximum Observed in Analog Regions

- Define regions considered to be analogs for seismic source
- Assemble catalog of larger earthquakes that have occurred in the analog regions
- Use a representation of the distribution of earthquakes in this catalog for the assessing the distribution of Mmax

Example from Petersen et al. (2014) for CEUS (USGS Seismic Hazard Maps

- Analog regions – global stable continental regions (SCR) separated into extended margins and cratons
- Assembled catalog for each type of region (Wheeler, 2014a, 2014b)
- Using histogram of magnitudes in each catalog along with estimates of the $M_{max\text{-}obs}$ for past CEUS earthquakes, define epistemic uncertainty distribution for Mmax

Stable Continental Regions SCR: Analogues to CEUS for Assessing Mmax

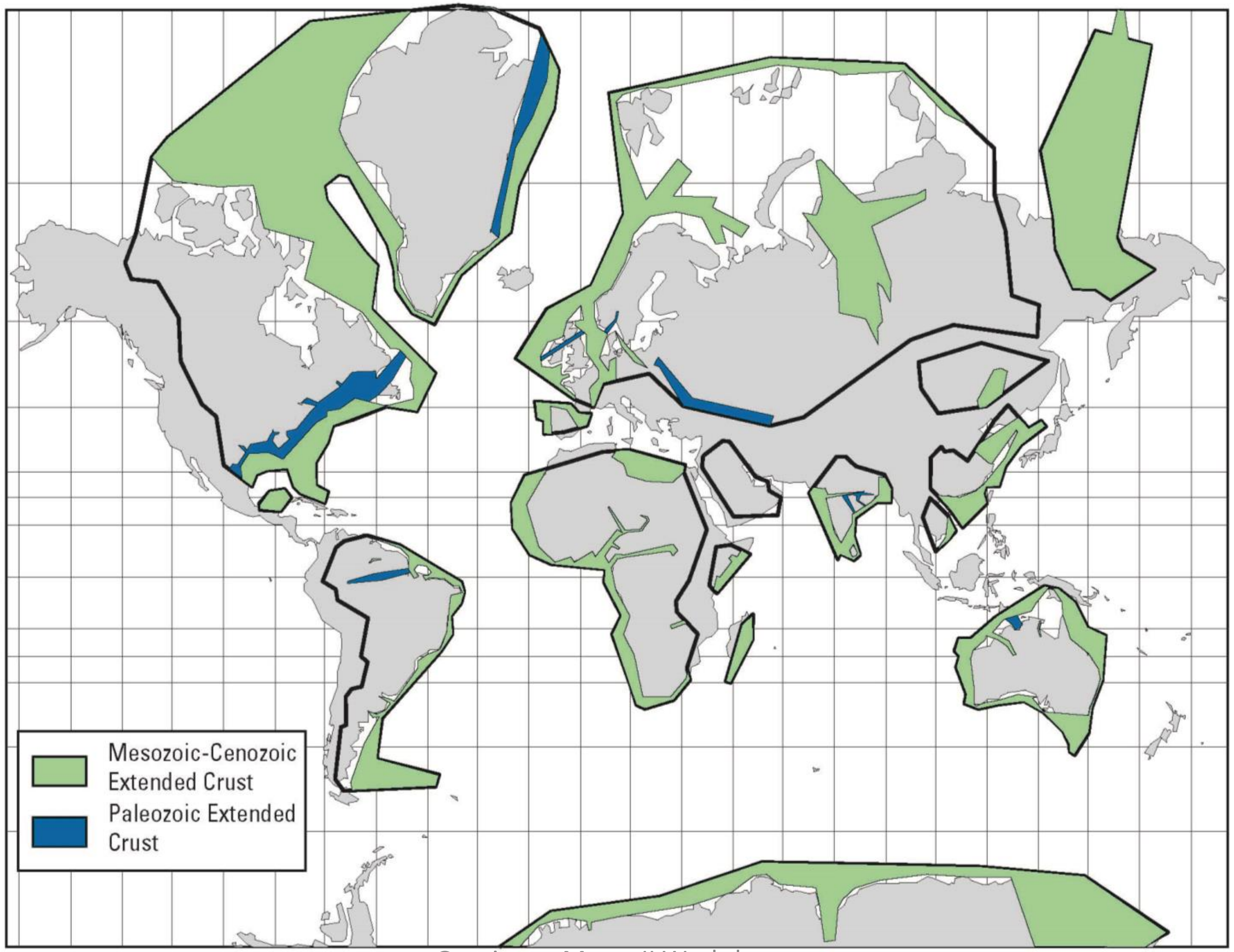

Wheeler (2009)

Petersen et al. (2014) SCR – Extended Margins

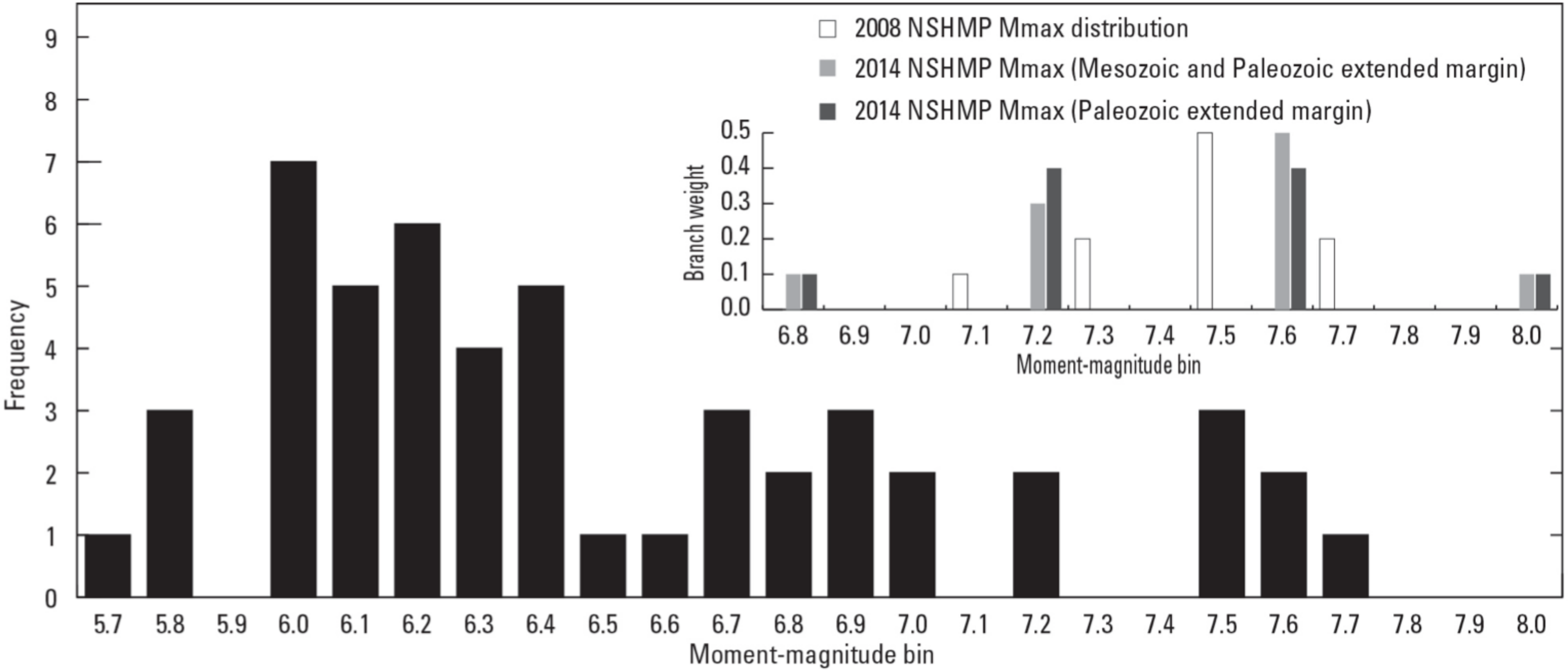

Figure 19. Distribution of large earthquake magnitudes (51 earthquakes) for extended margins in stable continental regions, worldwide. Mmax distributions used in the 2008 and 2014 updates shown in inset.

Petersen et al. (2014) SCR – Cratons

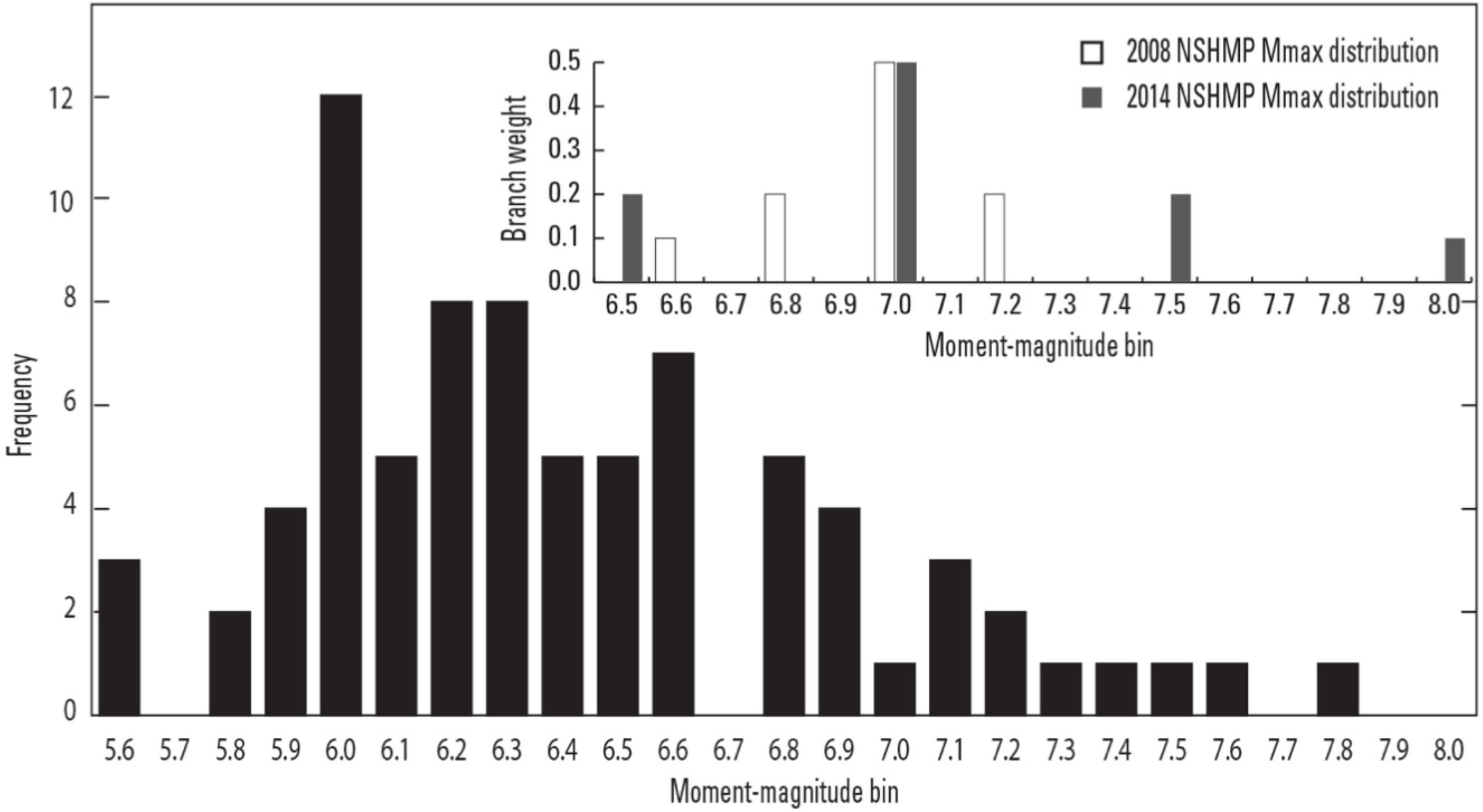

Figure 20. Distribution of large earthquake magnitudes (79 earthquakes) for cratons in stable continental regions, worldwide. Mmax distributions used in the 2008 and 2014 updates shown in the inset.

Johnston et al. (1994) Bayesian Approach to Assess distribution for m^u (Mmax)

- Subdivide SCR into domains on the basis of
  - Crustal type (extended or not extended)
  - Crustal age
  - State of stress
  - Orientation of structure with respect to stress (favorably or not favorably oriented)
- Using a catalog of SCR earthquakes, assess $m_{max\text{-}obs}$ for each super domain
- Use distribution of $m_{max\text{-}obs}$ adjusted for bias across super domains as a prior distribution for m^u
  - Used normal distributions for priors
- Update prior with likelihood function based on observed earthquake catalog in seismic source to produce posterior distribution for m^u (Mmax)

Example Application Using Johnston et al. (1994) Prior for Extended Crust

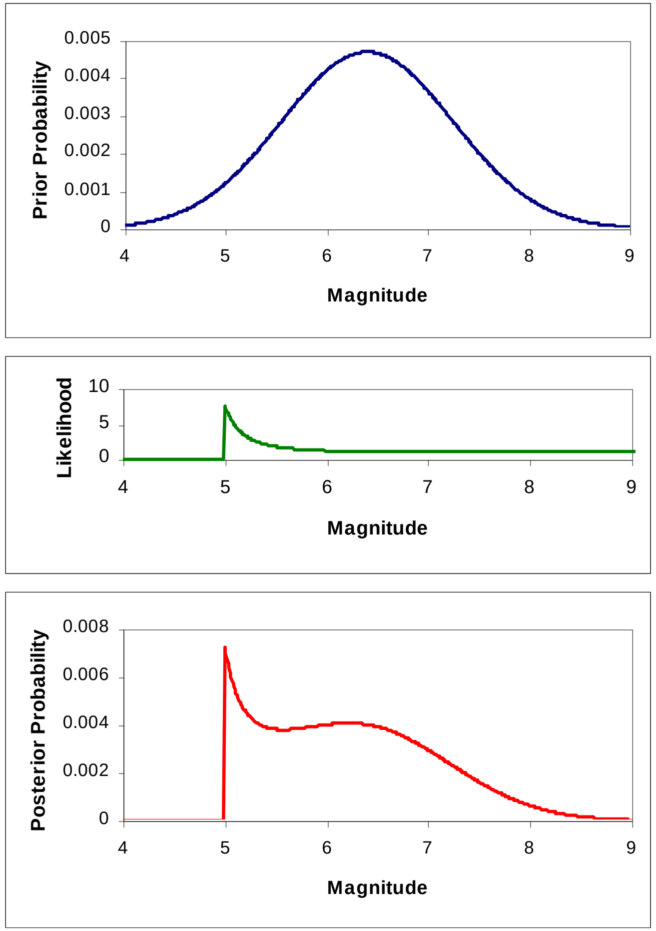

Extended crust

$\mu_{Mu} = 6.4$

$\sigma_{Mu} = 0.84$

5 events recorded between **M** 4.5 and **M** 5

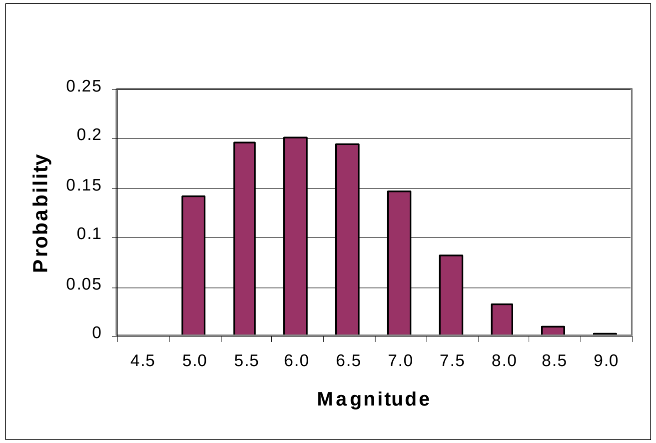

Likelihood Function for m^u (M_{max_obs})

- Assumption - earthquake size distribution in a source zone conforms to a truncated exponential distribution between m_0 and m^u
- Likelihood of m^u given observation of N earthquakes between m_0 and maximum observed, $m_{max\text{-}obs}$

$$L[m^u] = \begin{cases} 0 & \text{for } m^u < m_{\max-obs} \\ \left[1 - \exp\left\{-b\ln(10)(m^u - m_0)\right\}\right]^{-N} & \text{for } m^u \geq m_{\max-obs} \end{cases}$$

Example Likelihood Functions for Mmax given $m_{max\text{-}obs} = 6$

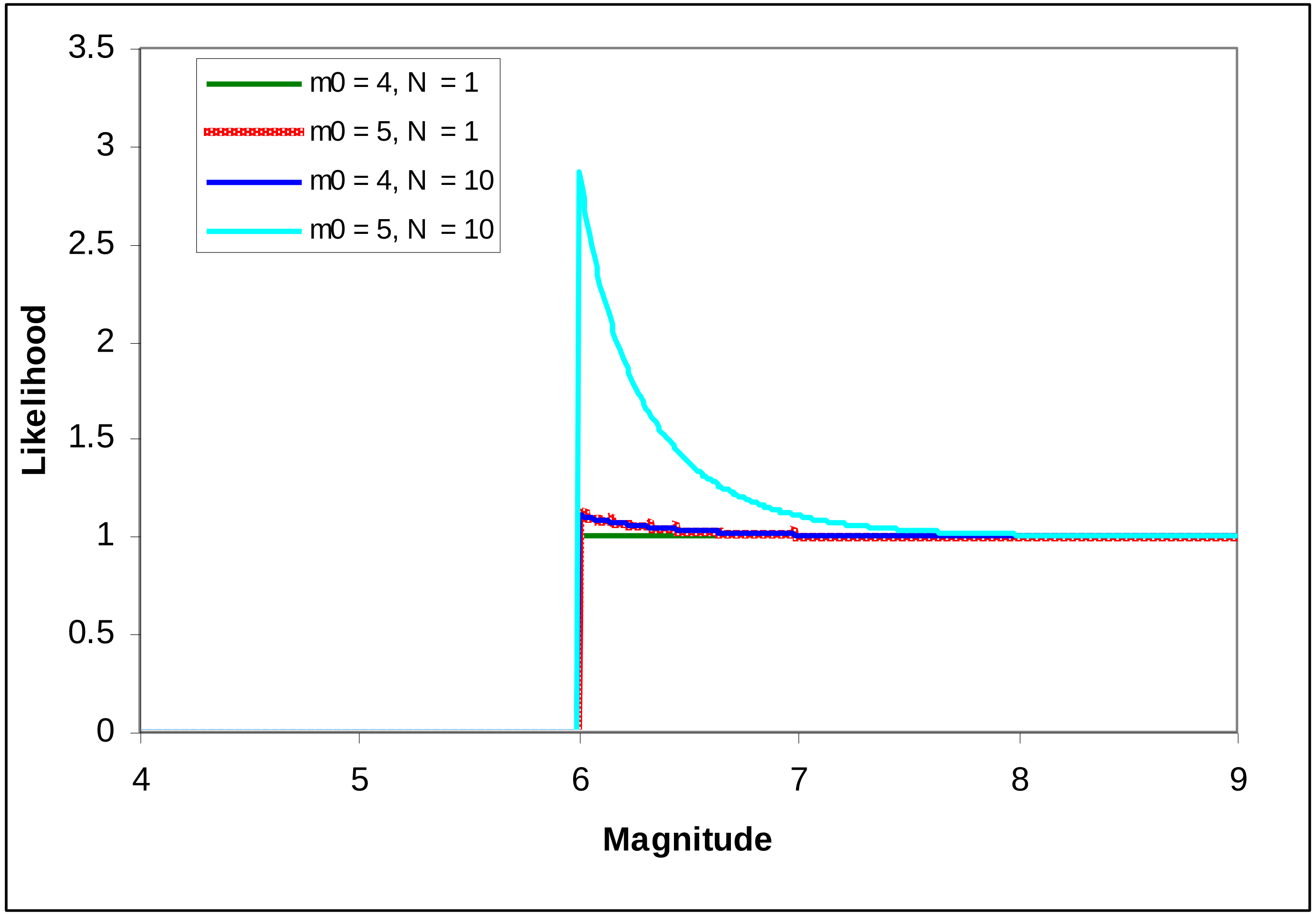

Results of Likelihood Function

- $m_{max\text{-}obs}$ is the most likely value of m^u
- Relative likelihood of values larger than $m_{max\text{-}obs}$ is a function of sample size *and* the difference $m_{max\text{-}obs} - m_0$
- Likelihood function integrates to infinity and cannot be used by itself to define a distribution for m^u (e.g., Zöller and Holschneider, 2016)
- Hence the need to combine likelihood with some form of prior distribution to produce a posterior distribution

Johnston et al. (1994) Bias Adjustment (1 of 3)

- "bias correction" from $m_{max\text{-}obs}$ to m^u based on distribution for $m_{max\text{-}obs}$ given m^u
- For a given value of m^u and N, estimate the median value of $m_{max\text{-}obs}$, $\hat{m}_{\max-obs}$

$$F[m_{\max-obs}] = \left[\frac{1-\exp(-b\ln(10)(m_{\max-obs}-m_0))}{1-\exp(-b\ln(10)(m^u-m_0))} \right]^N \quad \text{for } m_0 \le m_{\max-obs} \le m^u$$

- Use $m^u - \hat{m}_{\max-obs}$ to adjust from mean $m_{max\text{-}obs}$ to mean m^u

Bias Adjustment (2 of 3)

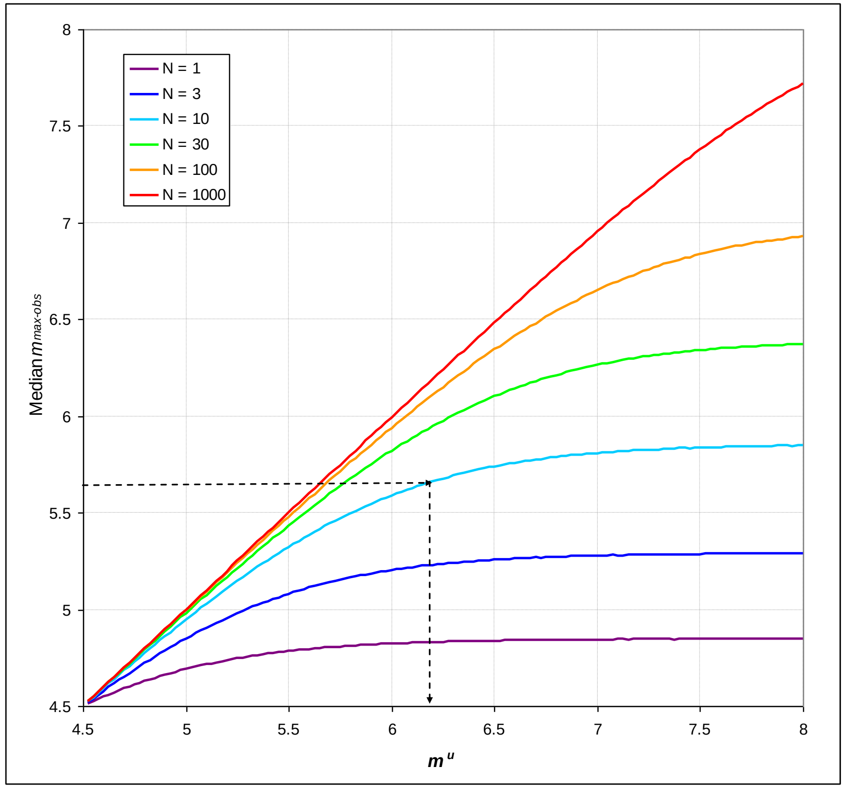

Example:

$m_{max\text{-}obs}$ = 5.7

$N(m \leq 4.5)$ = 10

m^u = 6.3 produces $\hat{m}_{\max - obs}$ = 5.7

Therefore, bias adjustment from a mean $m_{max\text{-}obs}$ of 5.7 is a mean m^u of 6.3

Bias Adjustment (3 of 3)

- Obtaining usable estimates of bias adjustment necessitated pooling "like" domains (trading space for time)
- "Super Domains" created by combining domains with the same characteristics
- Average of event counts in super domains used to adjust mean $m_{max\text{-}obs}$ to mean m^u (Mmax)

EPRI/DOE/NRC (2012) Update to Johnston et al. (1994) Mmax Priors

- Updated SCR earthquake catalog to using Schulte and Mooney (2005) and GMT catalog
- Reassessed significance of separation into extended and non-extended crust
  - Found that “significant” separation was between Mesozoic and younger extension (MESE) and combined older extension and non-extended (NMESE)
  - Significance of difference only marginal, included and alternate single prior for all SCR

Distributions of $M_{max\text{-}obs}$ in Super Domains

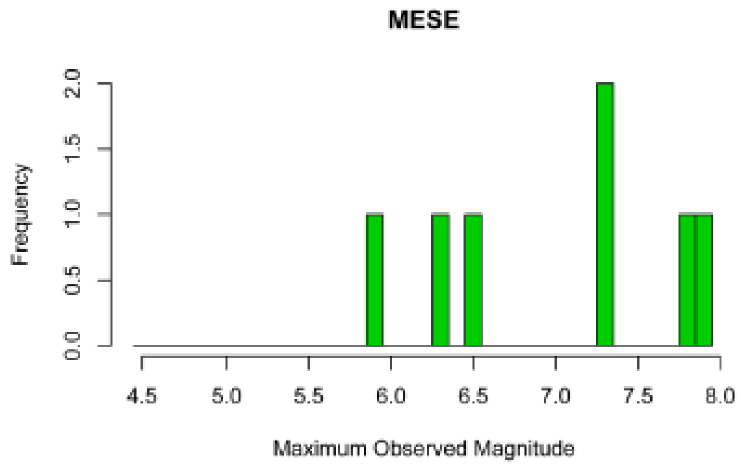

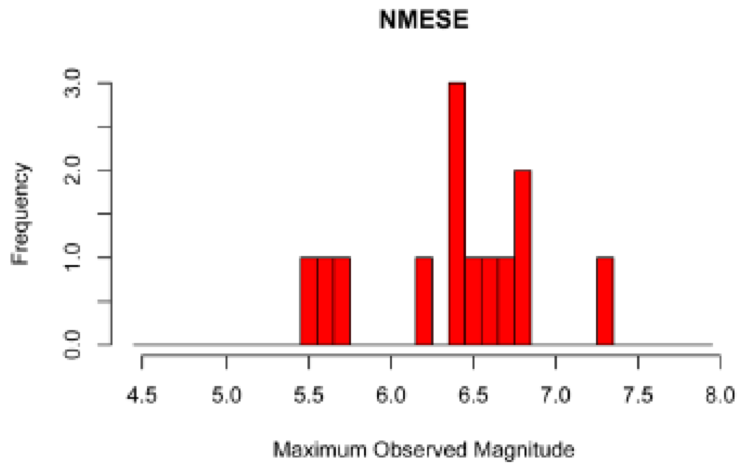

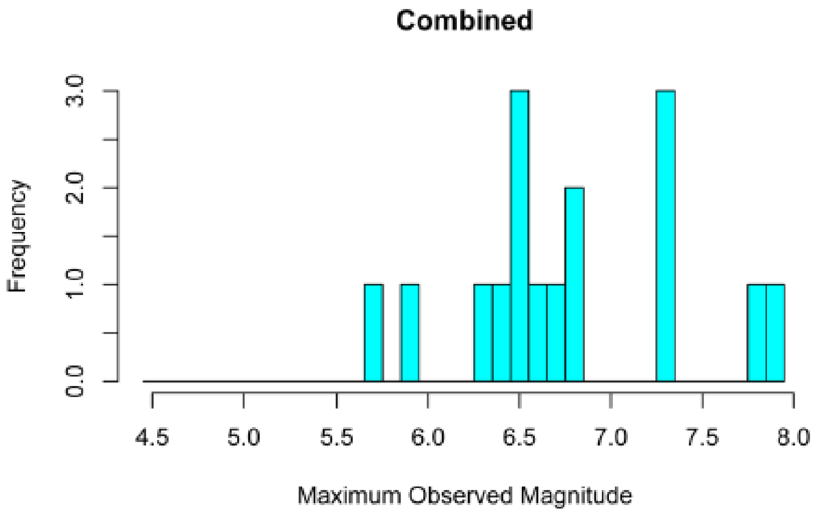

Bias Adjustments to Mean Mmax

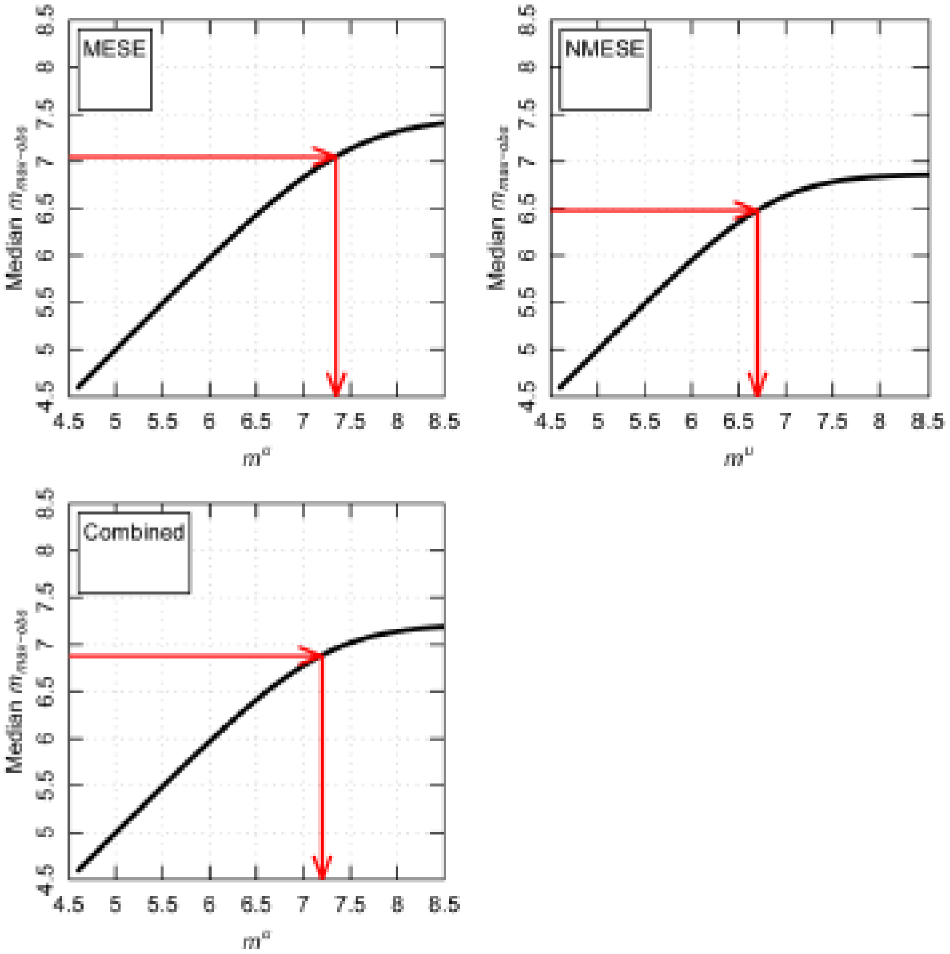

EPRI/DOE/NRC (2012) Updated Priors

Prior*	Mean Mmax	Sigma Mmax
Mesozoic and younger extended crust	7.35	0.75
Pre-Mesozoic extension and non-extended crust	6.70	0.61
Composite SCR crust	7.2	0.64

* Prior distributions limited to magnitude range **M** 5.5 to **M** 8.25

3. Use of Maximum Rupture Dimensions

- Parallels methods used for geologic feature-specific seismic sources
- Estimate the maximum dimensions of ruptures
  - Limits based on size of source
  - Limits based on size of geologic structures in source
- Use empirical relationships between magnitude and rupture dimensions

4. Seismicity and Geodetics Example

- Finite rate of moment release requires finite Mmax (e.g., Main, 1995) or at least a decay in the relative frequency of earthquakes that it greater than in increase in seismic moment with magnitude (e.g., Main and Burton, 1984)
- After fitting an appropriate magnitude distribution relationship (e.g., G-R) to the observed seismicity, the resulting recurrence relationship can be used to assess seismic moment rate as a function of Mmax
- Applying constrains on the seismic moment rate from geodetic data provides constrains on Mmax (e.g., Main et al., 1999).

Examples from Main et al. (1999) for the UK

Mmax estimates based on assessment of seismic moment rate based on either
  observed seismicity – dashed line
  estimated tectonic moment rate – solid line

(a) Truncated exponential

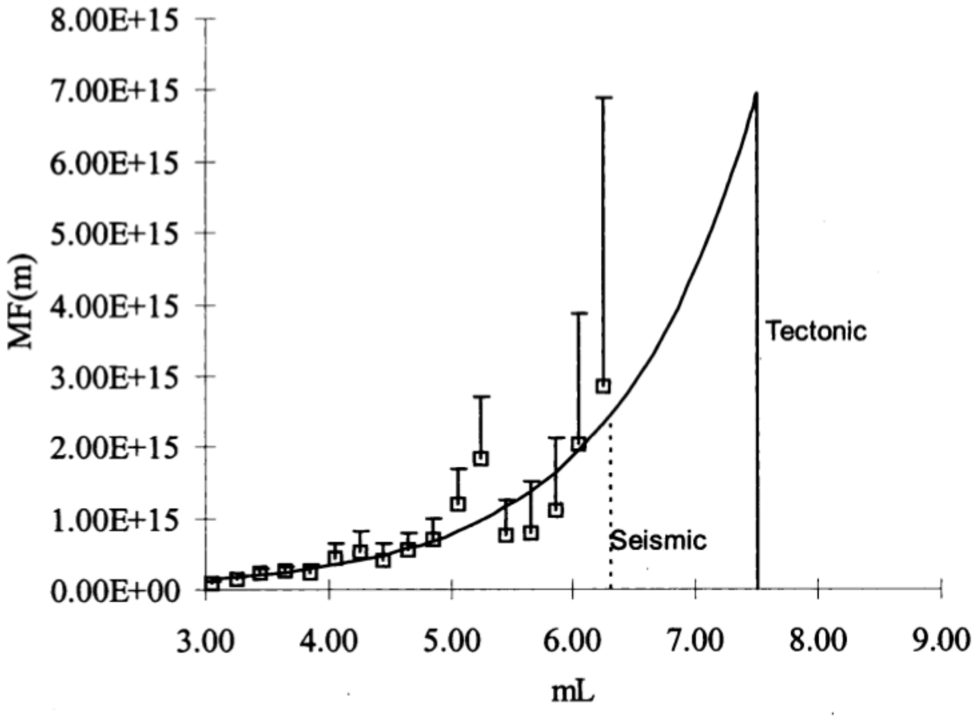

(b) gamma

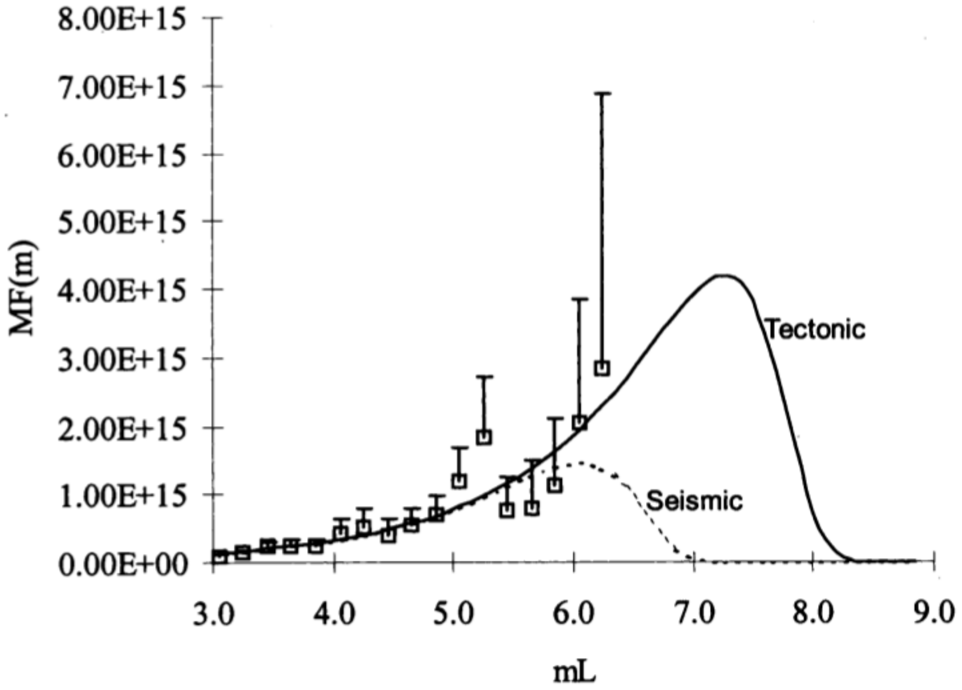

Recent Applications for SCR Regions Outside of Europe

- CEUS SSC – Bayesian (updated global priors) and Kijko (EPRI, USDOE, & USNRC, 2012)
- US seismic hazard model – Global Analogs (Petersen et al., 2014)
- Thyspunt site, South Africa – Bayesian (updated global priors) and Kijko (Bommer et al., 2015)
- Canada seismic hazard model (GSC) – Global Analogs (Adams et al., 2015)
- Australia – multiple expert elicitation (Griffin et al., 2018)

References

Adams, J., Halchuk, S., Allen, T., Rogers, G. (2015). Canada's 5th Generation seismic hazard model, as prepared for the 2015 National Building Code of Canada, 11th Canadian Conference on Earthquake Engineering, 21–24 July 2015, Victoria, Canada, Paper 93775, 11 pp.

Anderson, J.G., Biasi, G.P. and Wesnousky, S.G., 2017. Fault-Scaling Relationships Depend on the Average Fault-Slip Rate. Bulletin of the Seismological Society of America, 107(6), pp.2561-2577

Bommer, J. J., K.J. Coppersmith, R.T. Coppersmith, K.L. Hanson, A. Mangongolo, J. Neveling, E. M. Rathje, A. Rodriguez-Marek, F. Scherbaum, R. Shelembe, P. Stafford, and F. O. Strasser, 2015, A SSHAC Level 3 probabilistic seismic hazard analysis for a new-build nuclear site in South Africa, Earthquake Spectra, 31(2), 661-698.

Electric Power Research Institute (EPRI), U.S. Department of Energy, and U.S. Nuclear Regulatory Commission, 2012, Technical Report: Central and Eastern United States Seismic Source Characterization for Nuclear Facilities. NUREG-2115.

Electric Power Research Institute and Seismic Owners Group (EPRI-SOG), 1988, Seismic Hazard Methodology for the Central and Eastern United States: Technical Report No. NP-4726-A, volumes 1-10.

Field, E.H., et. al., 2017, A spatiotemporal clustering model for the third Uniform California Earthquake Rupture Forecast (UCERF3-ETAS): toward an operational earthquake forecast, Bulletin of the Seismological Society of America 107(3), 1049-1081.

Griffin, J., M. Gerstenberger, T. Allen, D. Clark, P. Cummins, R. Cuthbertson, V. Dimas, G. Gibson, H. Ghasemi, R. Hoult, N. Lam, M. Leonard, T. Mote, M. Quigley, P. Somerville, C. Sinadinovski, M. Stirling and S. Venkatesan, 2018, Expert elicitation of model parameters for the 2018 National Seismic Hazard Assessment, Geoscience Australia, Record 2018/28.

Hanks, T.C. and Bakun, W.H., 2008. M-log A observations for recent large earthquakes. Bulletin of the Seismological Society of America, 98(1), 490-494.

Hanks, T. C., and H. Kanamori, 1979, A moment magnitude scale, Journal of Geophysical Research, 84, 2348–2350.

Kagan, Y.Y., 1993, Statistics of characteristic earthquakes, Bulletin of the Seismological Society of America, 83(1), 7-24.

Johnston, A.C., Coppersmith, K.J., Kanter, L.R., and Cornell, C.A., 1994, The Earthquakes of Stable Continental Regions, Volume 1; Assessment of Large Earthquake Potential, Final Report Submitted to Electric Power Research Institute (EPRI). TR-102261-VI, v. 1.

Kijko, A., 2004, Estimation of the maximum earthquake magnitude, Mmax, Pure and Applied Geophysics 161, 1– 27.

Kijko, A., and Graham, G., 1998, Parametric-Historic’’ Procedure for probabilistic seismic hazard analysis. Part I: assessment of maximum regional magnitude mmax, Pure and Applied Geophysics, 152, 413–442.

References

Kijko, A., and Sellevoli, M.A., 1989, Estimation of earthquake hazard parameters from incomplete data files. Part I, utilization of extreme and complete catalogues with different threshold magnitudes, Bulletin of the Seismological Society of America, 79, 645–654.

Knopoff, L., and Y. Kagan, 1977, Analysis of the theory of extremes as applied to earthquake problems, J. Geophys. Res. 82, 5647-5657.

Leonard, M., 2014, Self-consistent earthquake fault-scaling relations: Update and extension to stable continental strike-slip faults, Bulletin of the Seismological Society of America 104, 2953–2965.

Main, I.G., 1995, Earthquakes as critical phenomena: implications for probabilistic seismic hazard analysis, Bulletin of the Seismological Society of America 85, 1299-1308.

Main, I.G. & Burton, P.W., 1984. Information theory and the earthquake frequency–magnitude distribution, Bull. seism. Soc. Am., 74, 1409–1426.

Main, I., Irving, D., Musson, R., and Reading, A., 1999, Constraints on the frequency-magnitude relation and maximum magnitudes in the UK from observed seismicity and glacio-isostatic recovery rates, Geophysics Journal International 137, 535-550

Petersen, M.D., Moschetti, M.P., Powers, P.M., Mueller, C.S., Haller, K.M., Frankel, A.D., Zeng, Yuehua, Rezaeian, Sanaz, Harmsen, S.C., Boyd, O.S., Field, Ned, Chen, Rui, Rukstales, K.S., Luco, Nico, Wheeler, R.L., Williams, R.A., and Olsen, A.H., 2014, Documentation for the 2014 update of the United States national seismic hazard maps: U.S. Geological Survey Open-File Report 2014–1091, 243 p., http://dx.doi.org/10.333/ofr20141091.

Pisarenko, V.F., 1991, Statistical Evaluation of Maximum Possible Magnitude, Izvestiya, Earth Physics 27, 757–763.

Schulte, S.M., and Mooney, W.D., 2005, An updated global earthquake catalog for stable continental regions—Reassessing the correlation with ancient rifts: Geophysical Journal International, 161, 707–721.

Somerville, P, 2014, Scaling Relations between seismic moment and rupture area of earthquakes in stable continental regions, PEER Report 2014/14, Pacific Earthquake Engineering Research Center, University of California, Berkeley, August.

Stirling, M., T. Goded, K. Berryman, and N. Litchfield, 2013, Selection of earthquake scaling relationships for seismic-hazard analysis, Bulletin of the Seismological Society of America, 103(6), 2993–3011, doi: 10.1785/0120130052

Thingbaijam, K.K.S., Martin Mai, P., and Goda, K., 2017, New Empirical Earthquake Source-Scaling Laws. Bulletin of the Seismological Society of America, 107(5), pp.2225-2246.

Wells, D.L., and Coppersmith, K.J., 1994, New empirical relationships among magnitude, rupture length, rupture width, rupture area, and surface displacement, Bulletin of the Seismological Society of America, 84 (4), p. 974-1002.

References

Wesnousky, S.G., 1986, Earthquakes, Quaternary faults, and seismic hazard in California: Journal of Geophysical Research, 91, 12,587-12,631.

Wesnousky, S.G., 2008, Displacement and geometrical characteristics of earthquake surface ruptures: Issues and implications for seismic-hazard analysis and the process of earthquake rupture, Bulletin of the Seismological Society of America, 98(4), pp.1609-1632.

Wheeler RL, 2009, Methods of Mmax estimation east of the rocky mountains. Open file report 2009-1018, USGS

Wheeler RL, 2011, Reassessment of stable continental regions. Seismological Research Letters, 82:141–143. doi:10.1785/ gssrl

Wheeler, R.L., 2014a, Earthquake catalog for estimation of maximum earthquake magnitude, Central and Eastern United States—Part A, Prehistoric earthquakes: U.S. Geological Survey Open-File Report 2014–1025–A, 26 p., *http://dx.doi.org/10.3133/ofr20141025A*.

Wheeler, R.L., 2014b, Earthquake catalog for estimation of maximum earthquake magnitude, Central and Eastern United States—Part B, Historical Earthquakes: U.S. Geological Survey Open-File Report 2014–1025–B, 30 p., http://dx.doi.org/10.3133/ofr20141025B.

Wooddell KE, NA Abrahamson, AL Acevedo-Cabrera, and RR Youngs. 2014. Hazard implementation of simplified seismic source characterization allowing for linked faults (abs), Seismological Research Letters, 85(2) 471.

Youngs, R.R., and Coppersmith, K.J., 1985, Implications of fault slip rates and earthquake recurrence models to probabilistic hazard estimates: Bulletin of the Seismological Society of America, v. 75, pp. 939-964.

Zöller, G., and M. Holschneider, 2016, The earthquake history in a fault zone tells us almost nothing about mmax, Seismological Research Letters, 87(1), 132-137.

Mmax values for (tectonic) seismic hazard and risk in Europe

(with a focus on the Netherlands)

Helen Crowley

Independent consultant (NAM)

European seismic hazard and risk models

- Released to the scientific community in December 2021, and to the media/public in April 2022.
- Referred to herein by their acronyms: ESHM20 and ESRM20
- The hazard model is an update to the ESHM13 model (output of the SHARE project)
- All data, models and results are openly released (CC-By license) and can be found starting here: www.efehr.org
- This is not a complete presentation of the European hazard or risk models, but focuses on some key elements that are of relevance to the definition of Mmax and its influence on the hazard and risk results (with a focus on low seismicity areas including the Netherlands).
- I led the development of ESRM20, but I was not a co-author of ESHM20, so I am presenting the information to the best of my knowledge (from consulting the technical report and through personal communication with Laureniu Danciu, lead author of ESHM20)

ESHM20 Inputs - Catalogues

Historical: EPICA (1000 – 1899) Instrumental: EMEC (1900 – 2014)

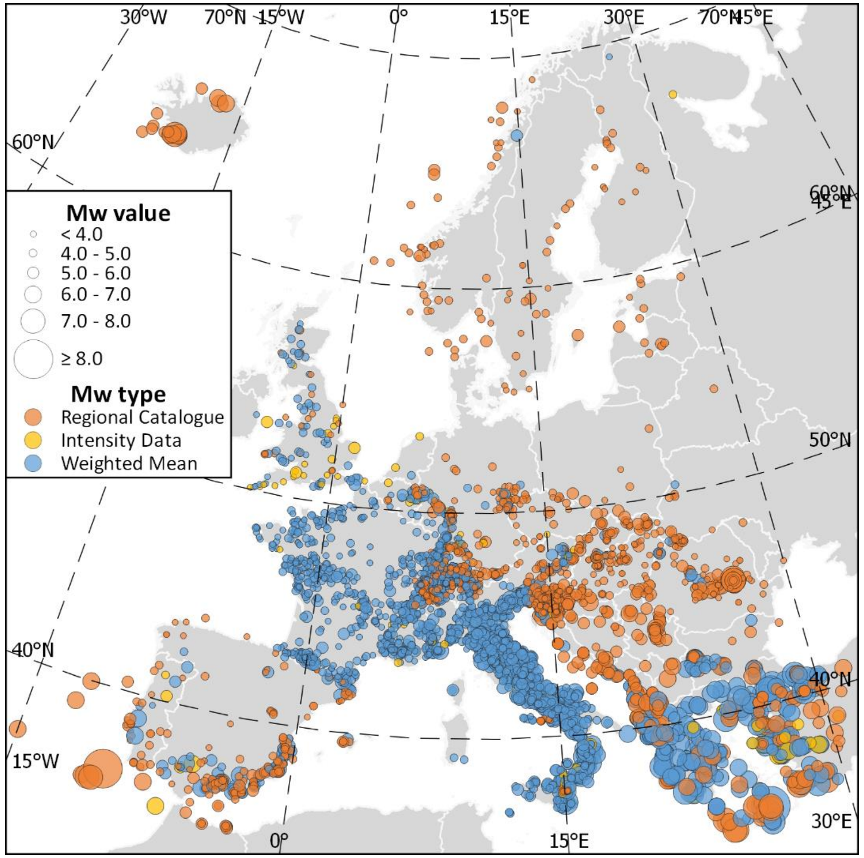

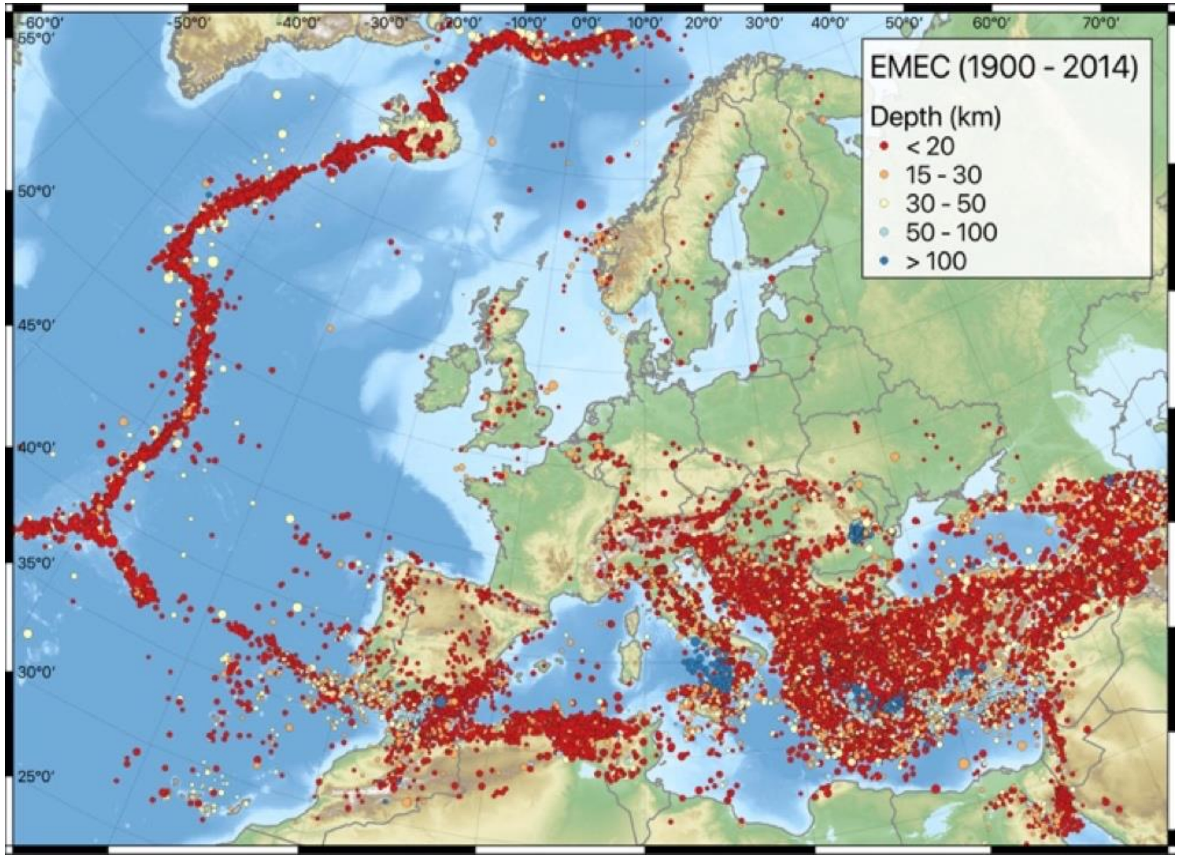

Danciu et al. (2021)

ESHM20 Inputs – Active faults

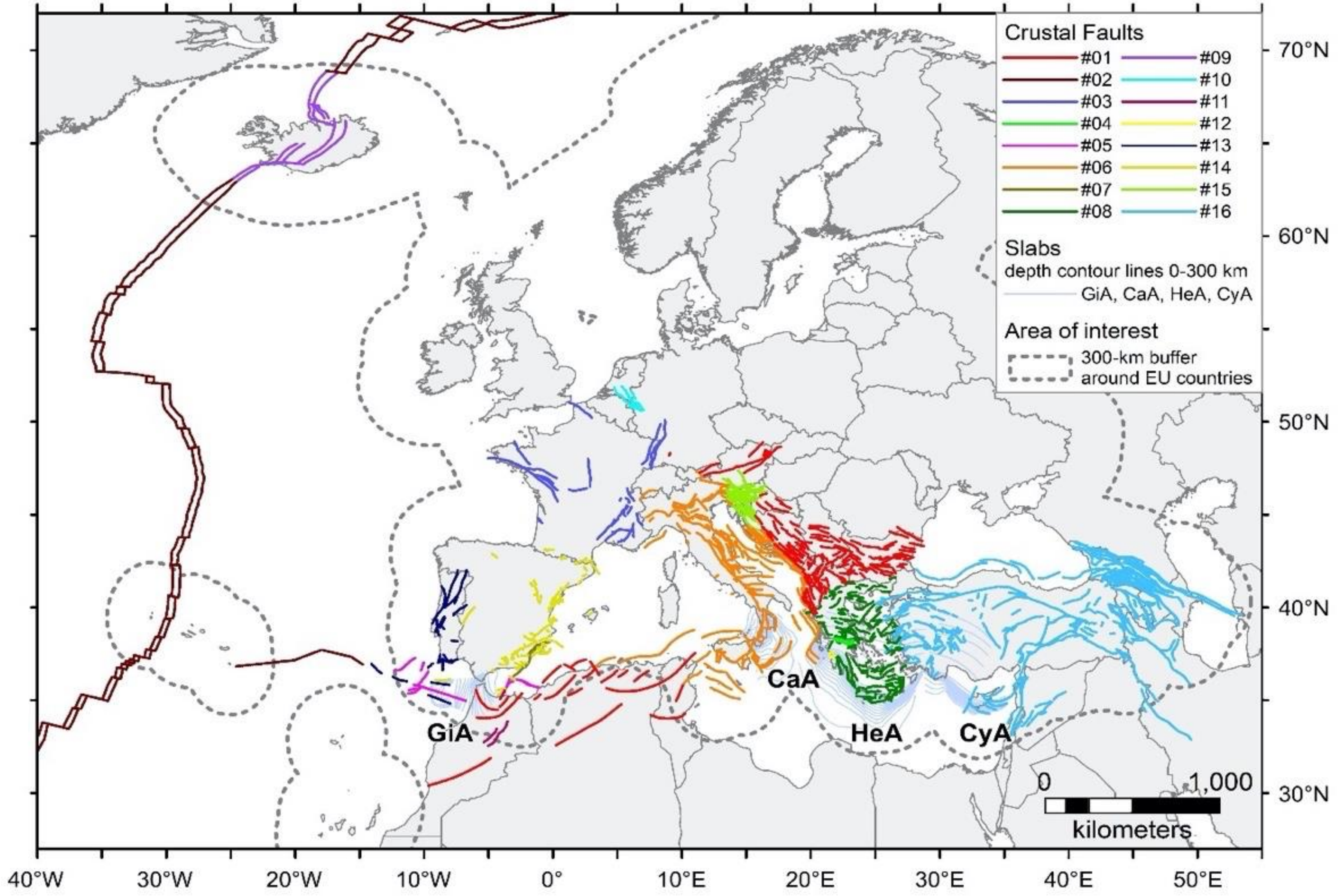

Danciu et al. (2021)

ESHM20 Inputs – Tectonic regionalisation

Geometry of the main plate boundaries (Bird, 2003).

Subdivisions of the plate interiors based on large-scale geologic maps and tectonic classifications (Asch, 2005; Johnston, 1994; Müller et al., 2008).

For the volcanoes - Global Volcanism Program (2013).

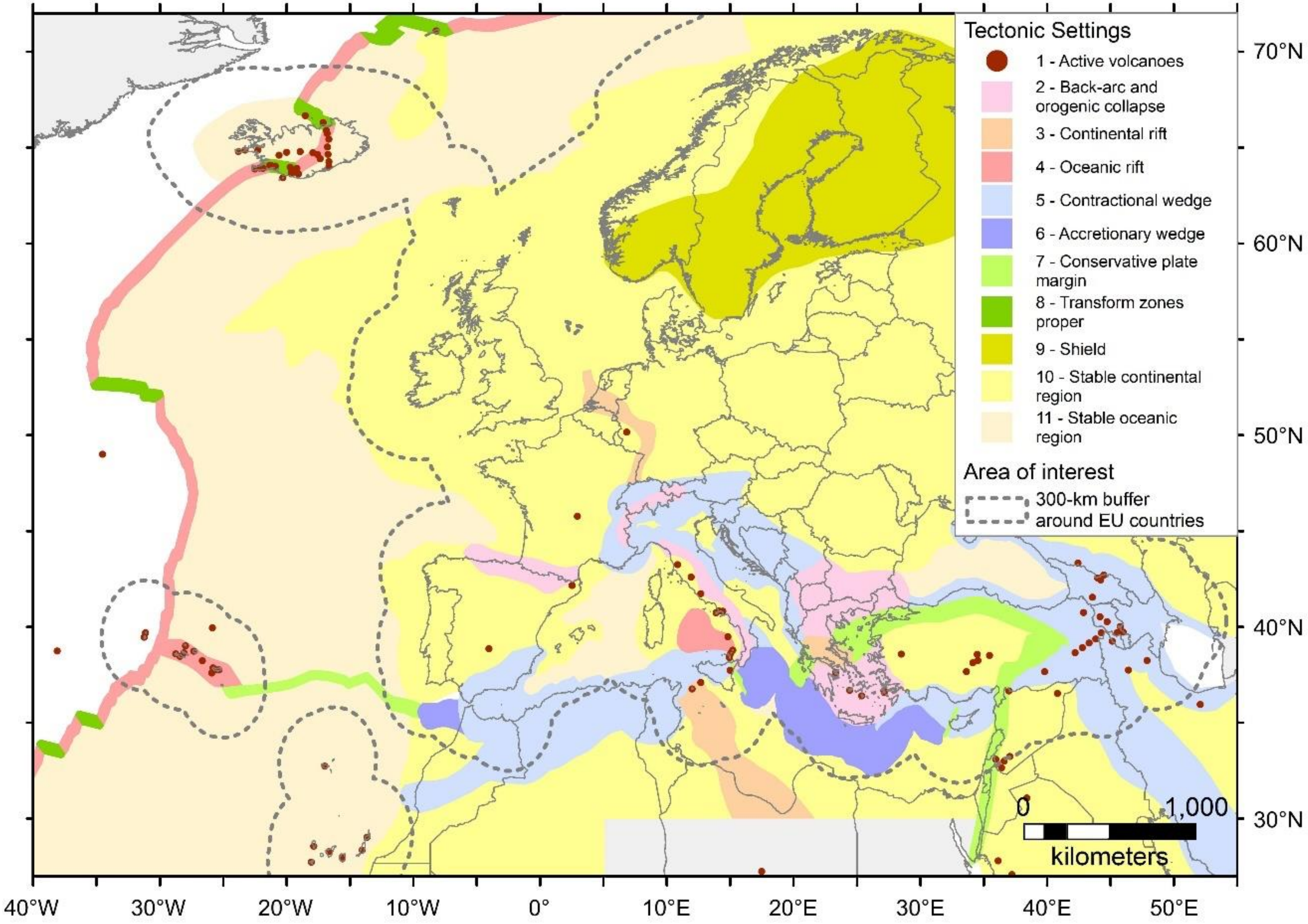

Danciu et al. (2021)

ESHM20 Inputs – super zones

- Super zones provide a spatial proxy to describe tectonic features, geological fault systems and seismicity patterns across Europe.
- Some parameters evaluated at the super zone level are then applied at the level of seismogenic sources.
- Super-zones cover large geographical regions, and there are three types in ESHM20:
  - completeness super zones (CSZ),
  - tectonic super zones (TECTO)
  - maximum magnitude super zones (MAXMAG).

Danciu et al. (2021)

ESHM20 Inputs – super zones

CSZ: Earthquake reporting rates are thought to be spatially homogeneous (used to define magnitude of completeness for different time windows)

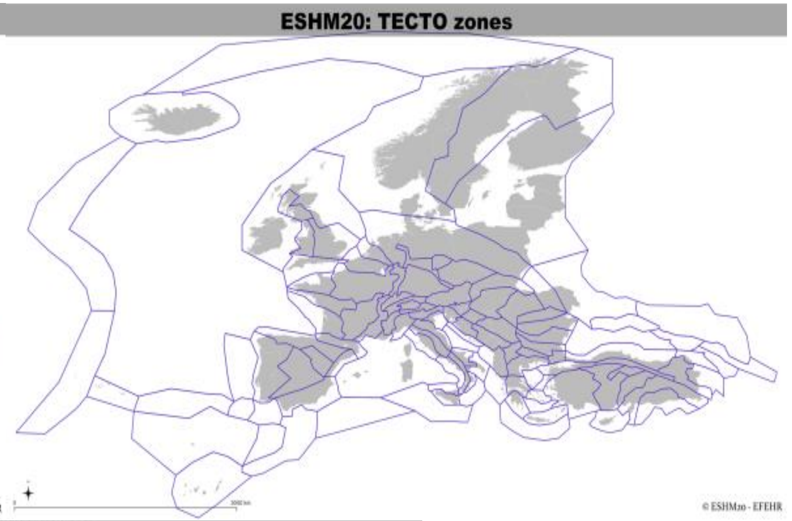

TECTO: Large scale tectonic zones (allows use of larger earthquake catalogue for incomplete zones for MFD)

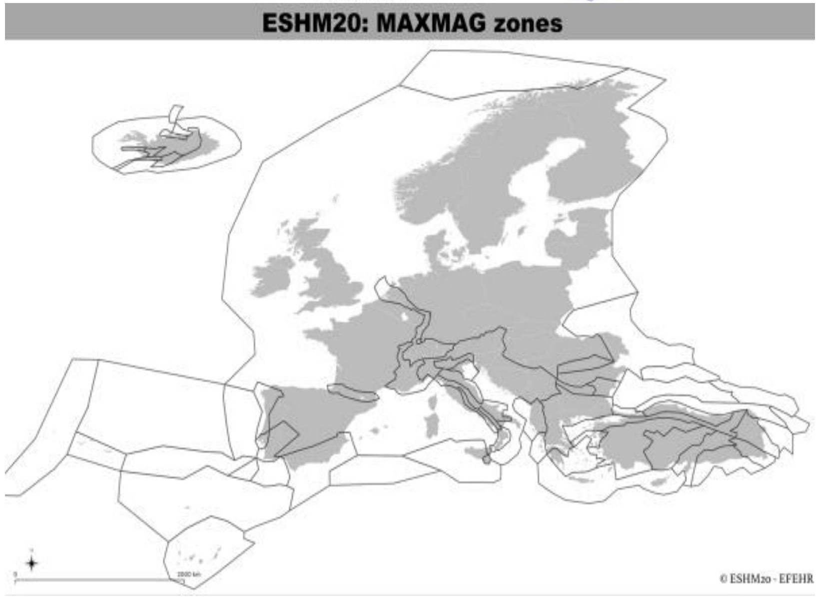

MAXMAG: Allows use of a larger earthquake catalogue for estimation of maximum magnitude

Danciu et al. (2021)

ESHM20 Seismogenic Source Logic Tree

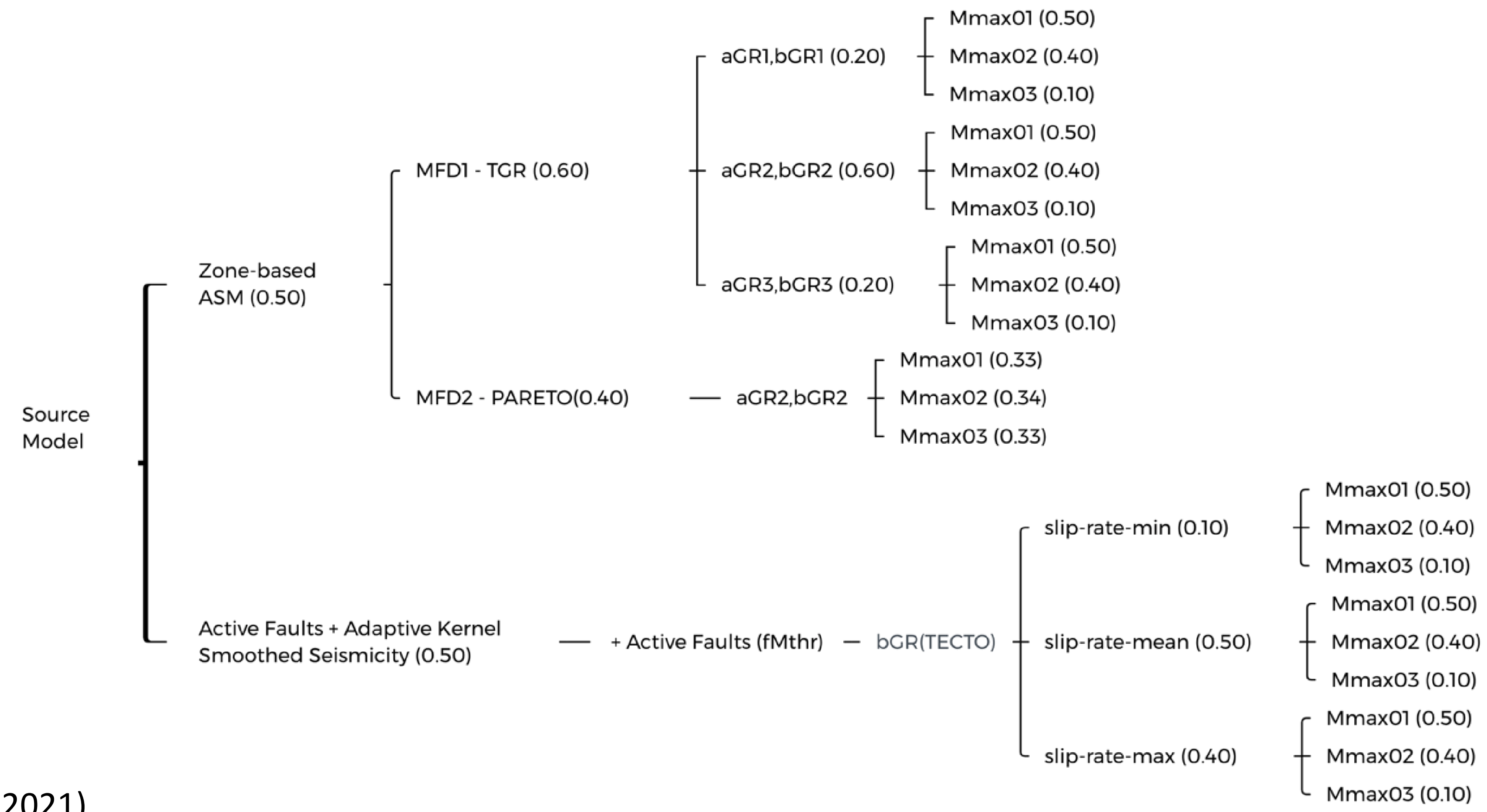

Danciu et al. (2021)

ESHM20 – Area source model (ASM)

- Area sources from national models were obtained and harmonized at the borders, guided by seismotectonic evidence, active faults, and major geologic/tectonic features, if available. If not, then the seismicity patterns are used: historical earthquake locations or recent clusters of seismicity.
- For each area source zone, based on declustered catalogue filtered for completeness, the magnitude-frequency distribution (MFD) is computed:

$$\mathrm{Log}_{10} N = a_{GR} – b_{GR} * Mw$$

where N is the cumulative number of earthquakes per year equal to or greater than a magnitude M

Danciu et al. (2021)

ESHM20 – Area source model (ASM)

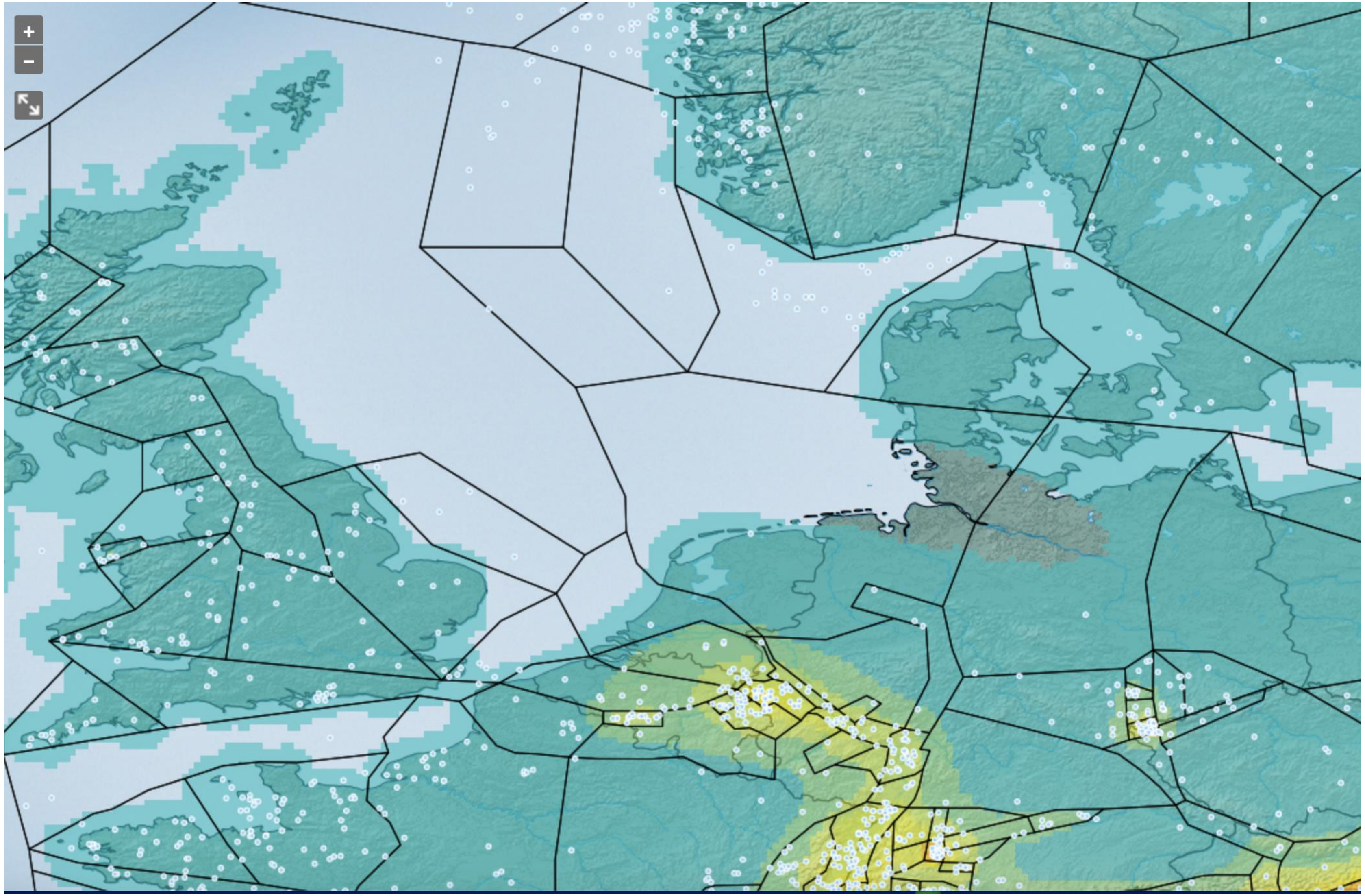

http://hazard.efehr.org

ESHM20 – Area source model (ASM)

Two representations of MFD:

- Double truncated Gutenberg-Richter MFD
- Tapered Pareto distribution (Kagan 1993)

"The Pareto has a faster decay of the rates towards the maximum magnitude. In many area sources without events above Mw 5, the rates obtained in the magnitude interval 5 to 6 from the GR model could be inflated. In these cases, the tapered Pareto distribution provides alternative estimates for the rates in the moderate to large magnitude range."

Danciu et al. (2021)

ESHM20 – Mmax (ASM)

- A constant activity rate is assumed when applying the maximum magnitude to the area sources (the MFDs converge towards the same N (M > 0)).

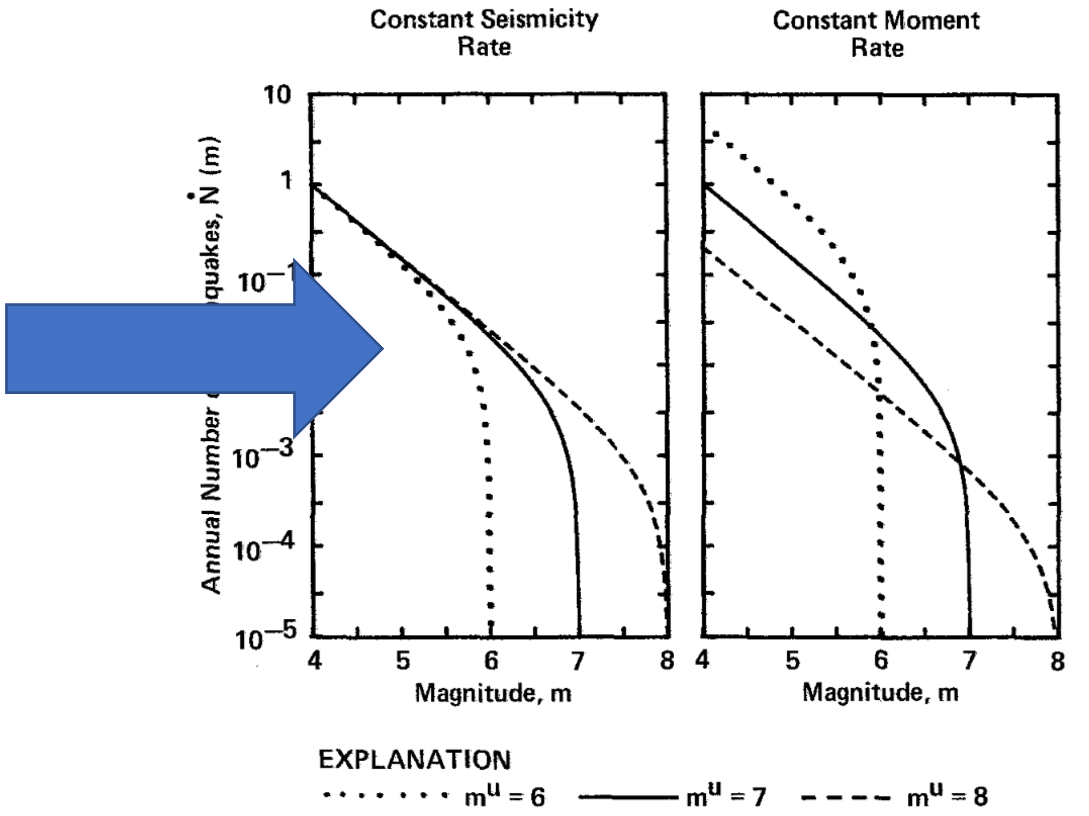

Youngs and Coppersmith (1985)

ESHM20 – Mmax (ASM)

- EPRI approach (Johnston et al., 1994) for stable continental regions
- *"In low-to-moderate seismicity regions a single distribution was assumed, in analogy with the global analog approach (Wheeler 2009, 2011): the magnitude of the largest observed earthquake, with proper consideration of its uncertainty, was taken as the lower value for the distribution of maximum magnitude ... whereas the other values were obtained by 0.2 increments*."

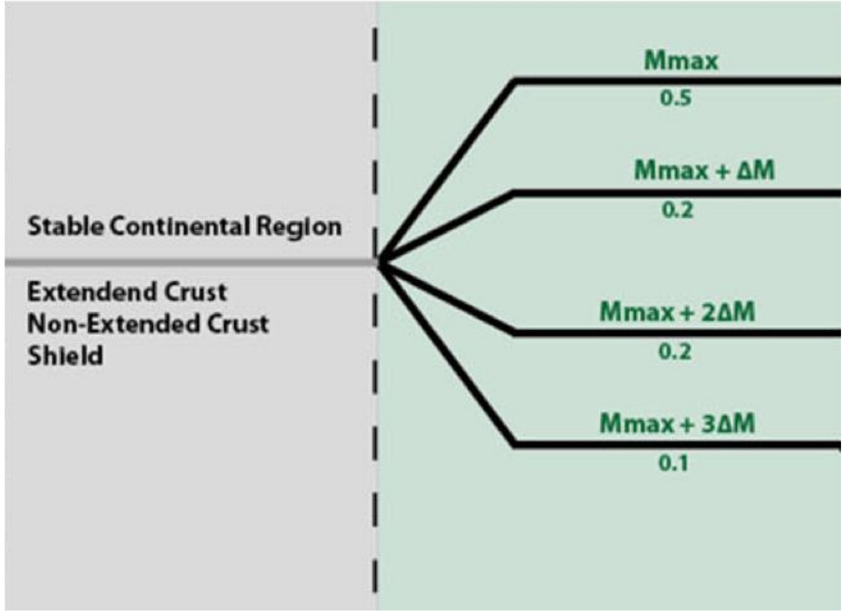

ESHM13 Mmax logic tree – this has been collapsed to 3 branches in ESHM20

Woessner et al. (2015)

ESHM20 – Mmax (ASM)

For the double truncated GR:

Branch	Weights	Assumptions (Low-moderate seismicity regions)
MmaxLow	0.50	Lower Value: Mmax observed, accounting for magnitude uncertainty of 0.3 (analog approach)
MmaxMid	0.40	Mid Value: MmaxLow plus a magnitude increment of (0.2+2*0.2)/2 = 0.3
MmaxUpper	0.10	Upper Value: MmaxLow plus a magnitude increment of 3*0.2 = 0.6

Danciu et al. (2021)

ESHM20 – Mmax (ASM)

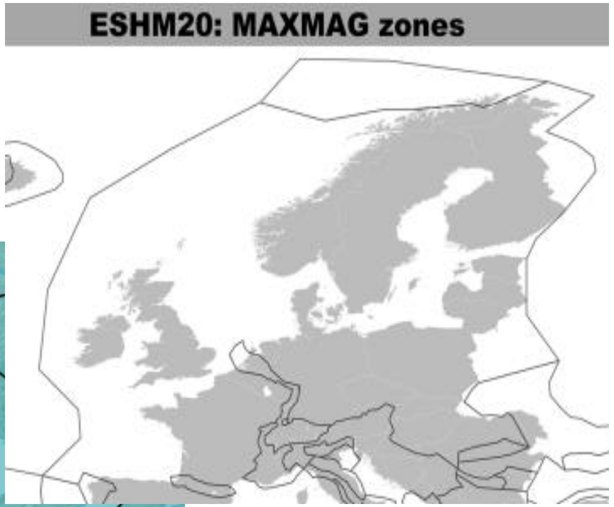

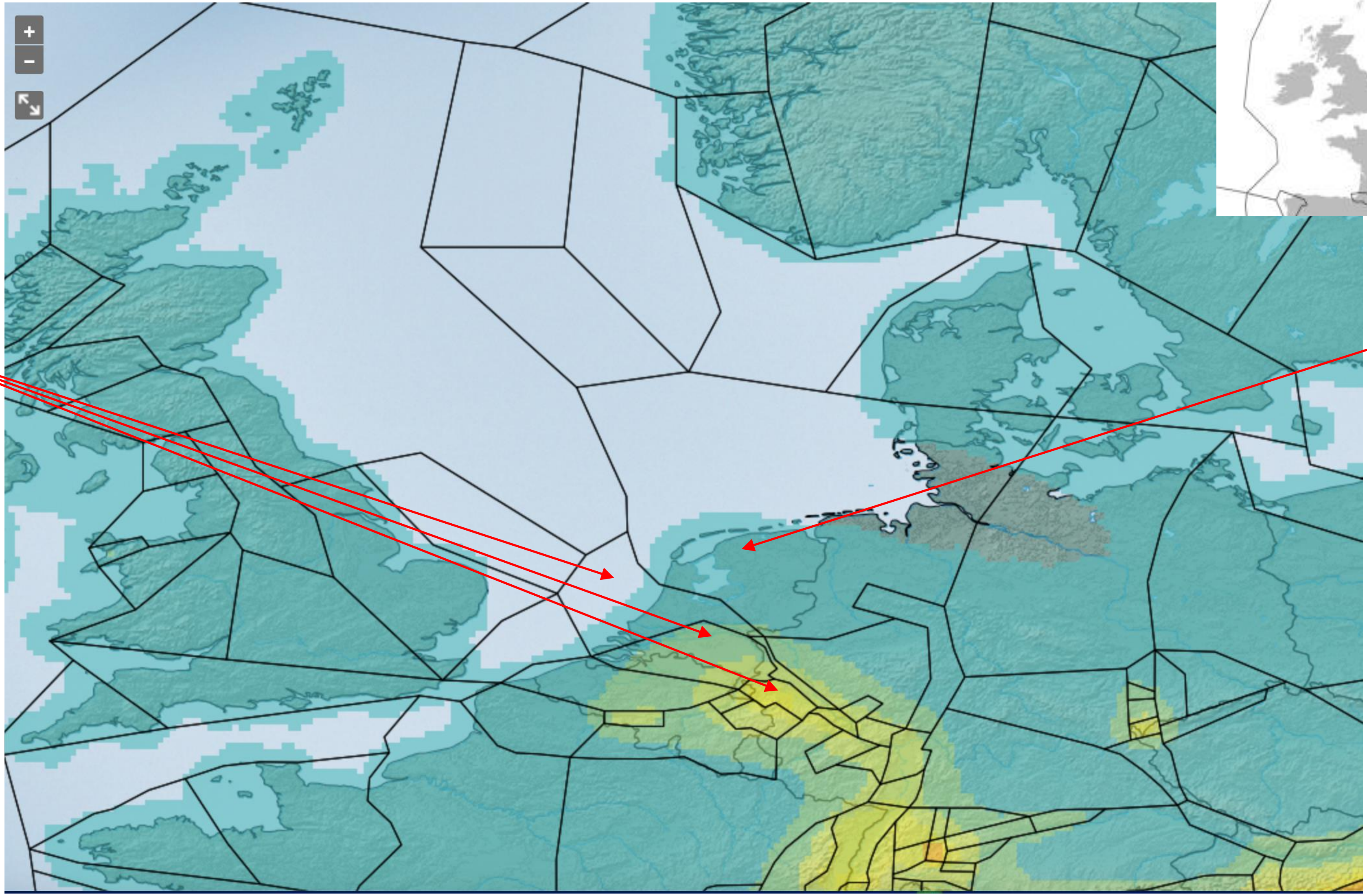

TruncGR Mmax
6.6 (0.5)
6.9 (0.4)
7.2 (0.1)

Seismogenic depth modelled from 7km to 13km with hypocentral depth at 12.3km

TruncGR Mmax
6.3 (0.5)
6.6 (0.4)
6.9 (0.1)

Seismogenic depth modelled from 3km to 25km with hypocentral depth at 12.3km

http://hazard.efehr.org

ESHM20 – Mmax (ASM)

- Tapered Pareto distribution requires corner magnitude which has been estimated as a function of the observed maximum magnitude.
- A default logic tree of M_{corner}=6.0, 6.2 and 6.4 (equal weights) is used for area sources with an observed maximum magnitude lower than 5.5.

Danciu et al. (2021)

ESHM20 – Mmax (ASM)

For these sources
Pareto M_{corner}
6.0 (0.33)
6.2 (0.34)
6.4 (0.33)

For M_{corner} = 6.0, *eff*M_{max} (at an annual rate of 10^{-4}) 5.4

For M_{corner} = 6.0, *eff*M_{max} 6.2

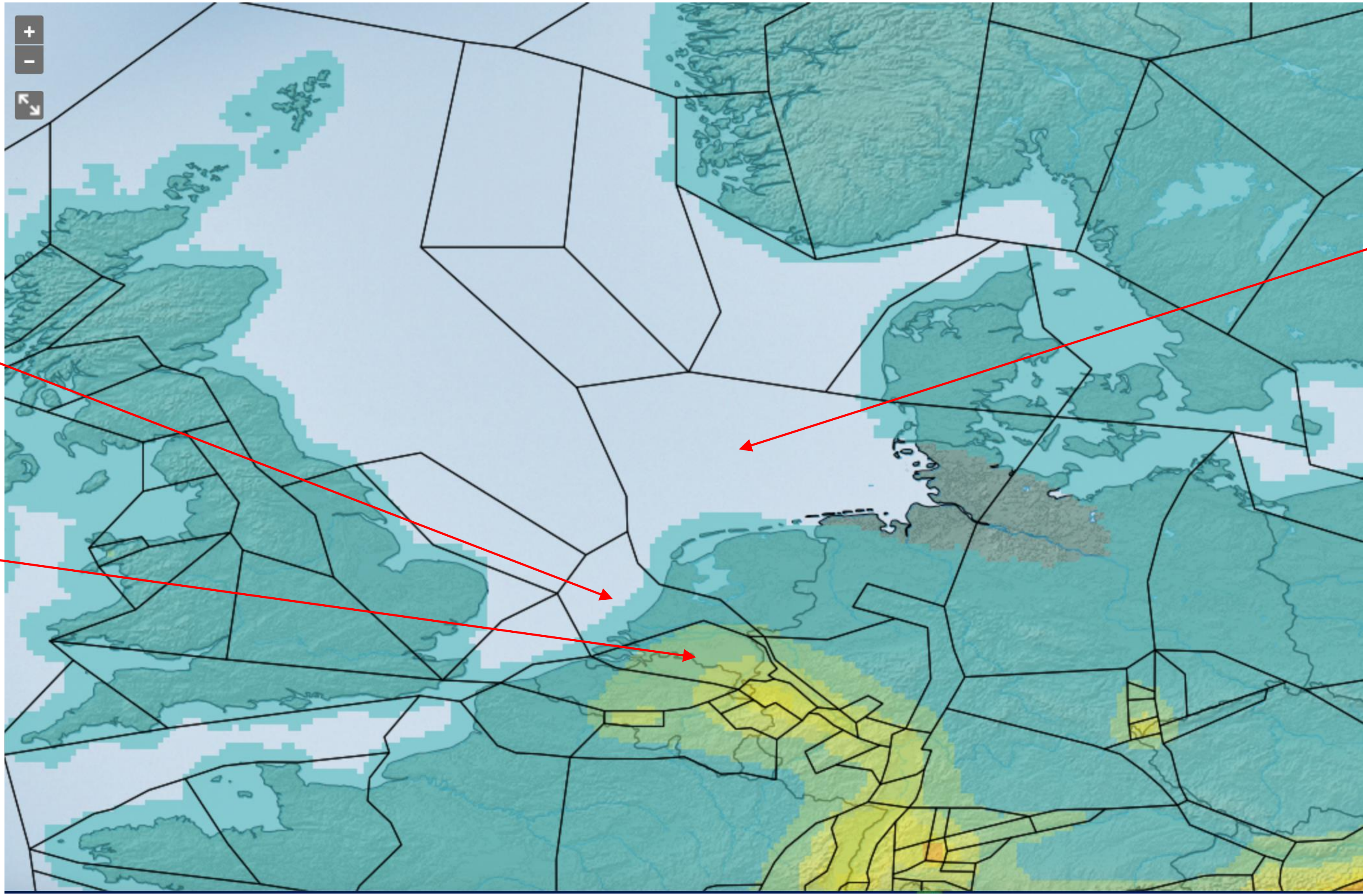

From M_{corner} = 6.0, *eff*M_{max} 5.2

http://hazard.efehr.org

ESHM20 – Active faults (+ seismicity) model

- Seismic productivity is divided into two categories: background seismicity and active faults; seismic productivity below a magnitude threshold (i.e. M5.9) is in the background, and seismic productivity above M-threshold is on active faults. Hence, active faults serve as a spatial proxy for moderate-to-large magnitude events
- Minimum set of basic fault parameters that define the seismogenic source model:
  - Geometry (Location: Lat, Lon, Depth; Size: Length, Width; Orientation: Strike, Dip)
  - Behavior (Rake and Slip Rate).
- Arbitrary area model of Anderson and Luco (1983), a truncated exponential magnitude-frequency distribution, is used to characterize the seismic activity of each entry of the active faults.

Danciu et al. (2021)

ESHM20 – Active faults (Mmax)

- A constant seismic moment rate is assumed when assigning maximum magnitude to active faults.

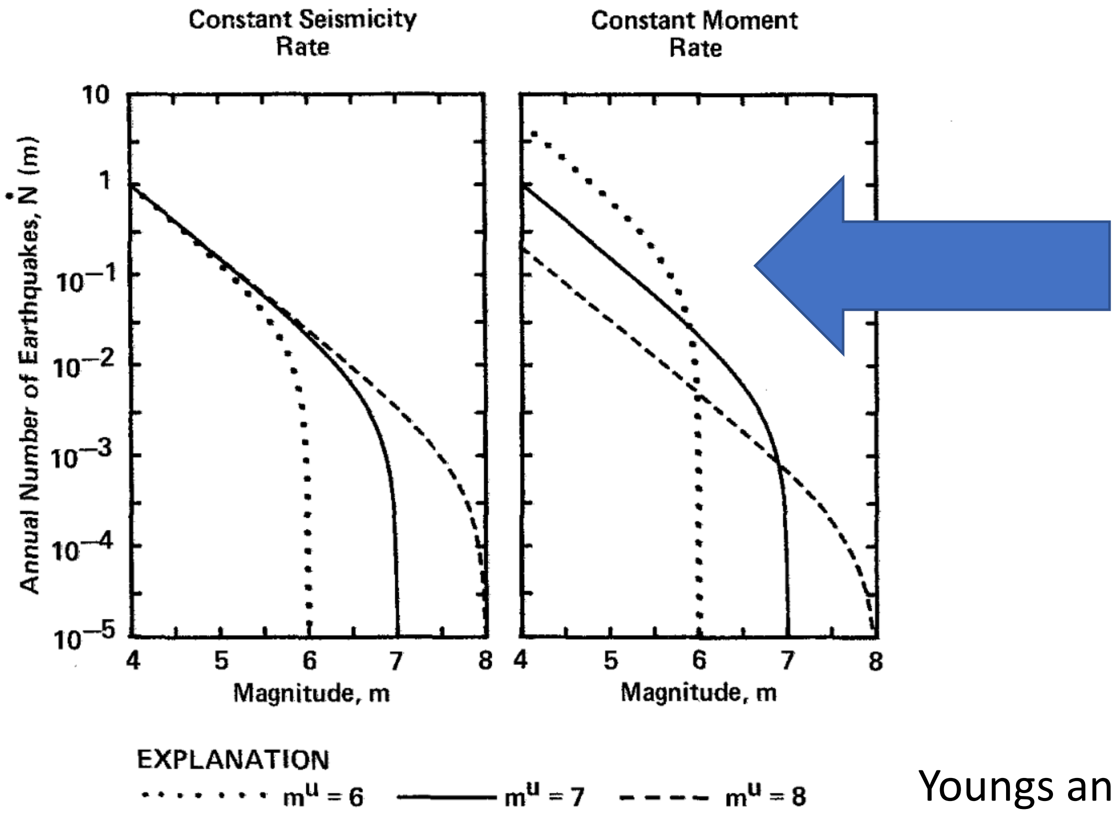

Youngs and Coppersmith (1985)

ESHM20 – Active faults (Mmax)

- The maximum magnitude of each fault source is obtained by use of fault scaling laws (FSL).
- The generalized functional form between rupture dimensions (L, W, A, D) and moment magnitude (Mw) is (X) = a + bME , where X is the rupture dimension under consideration and the coefficients a and b are empirically determined.
- The FSL developed by Leonard (2014) is used for crustal ruptures and by Allen and Hayes (2017) for subduction interface ruptures.

Danciu et al. (2021)

ESHM20 – Active faults (Mmax)

Branch	Weights	Assumptions
MmaxLow	0.50	Lower Value: Most likely value of the event on the fault, based on the average fault area and the resulting average maximum magnitude
MmaxMid	0.40	Mid Value: Highest value maximum magnitude on the fault, often coincides with the larger magnitude event on the fault buffers; measures the uncertainties of the fault geometry to maximum magnitude conversion;
MmaxUpper	0.10	Upper Value: Upper Maximum Magnitude to occur on a fault, with a proxy from the TECTO range, allowing the fault to capture larger magnitudes & ruptures

Table provided by Laurentiu Danciu

ESHM20 – Active faults (Mmax)

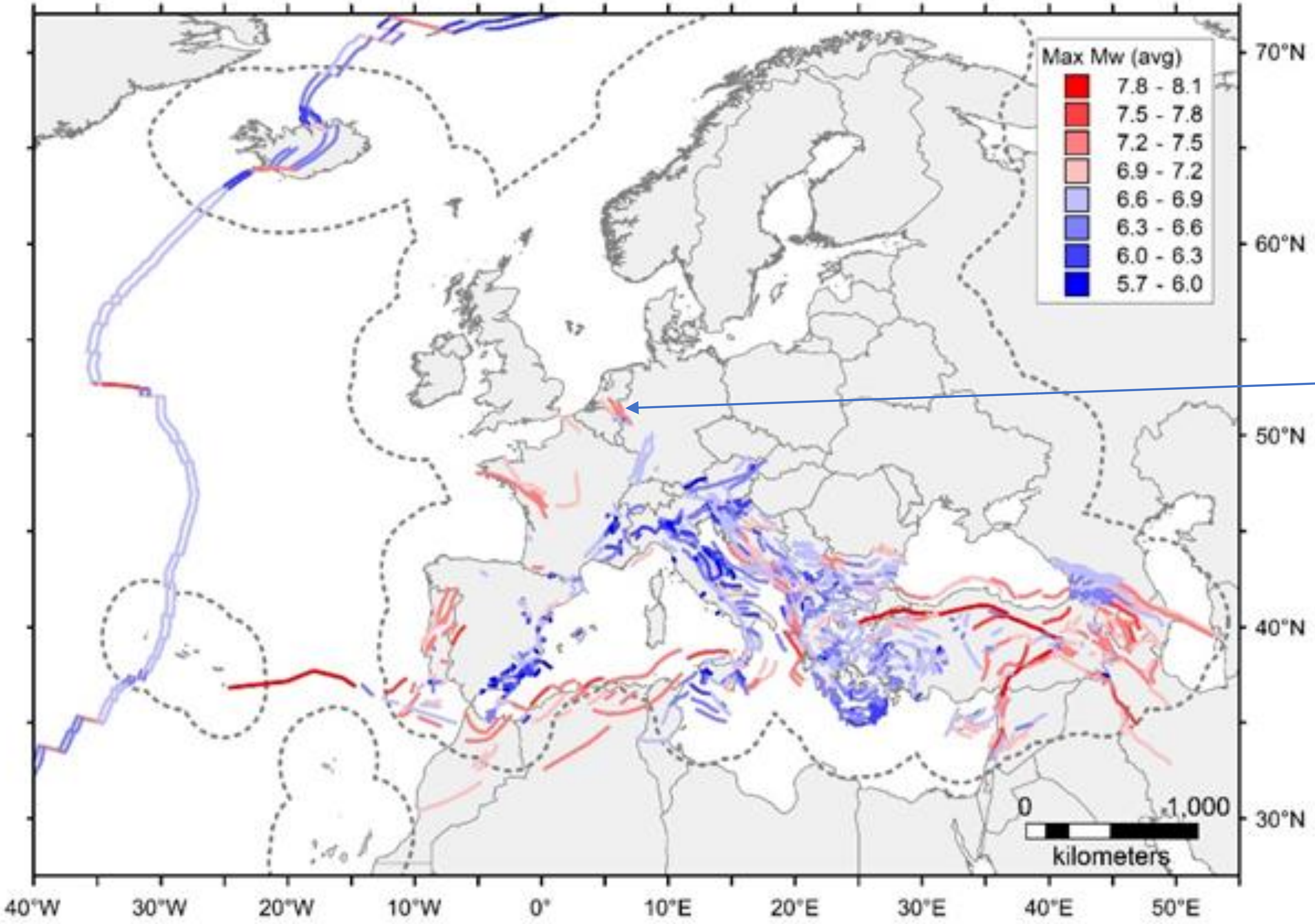

MmaxLow varies from 6.3 to 7.3 for the faults in the Lower Rhine Graben

Danciu et al. (2021)

Influence of Mmax on Hazard

Mmax
6.6
6.9
7.2

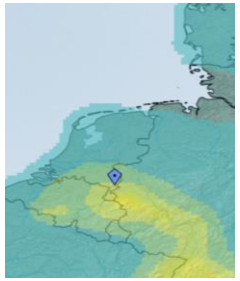

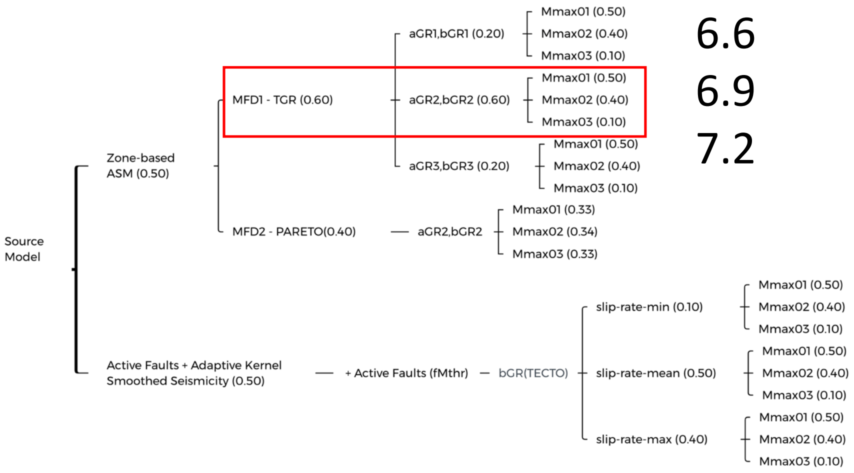

- Taking the double truncated GR area sources, and running the hazard for the three Mmax branches separately:

"Mmax …does not exert a very strong influence on hazard estimates except for long- period spectral accelerations and low annual exceedance frequencies" Julian's introductory slides

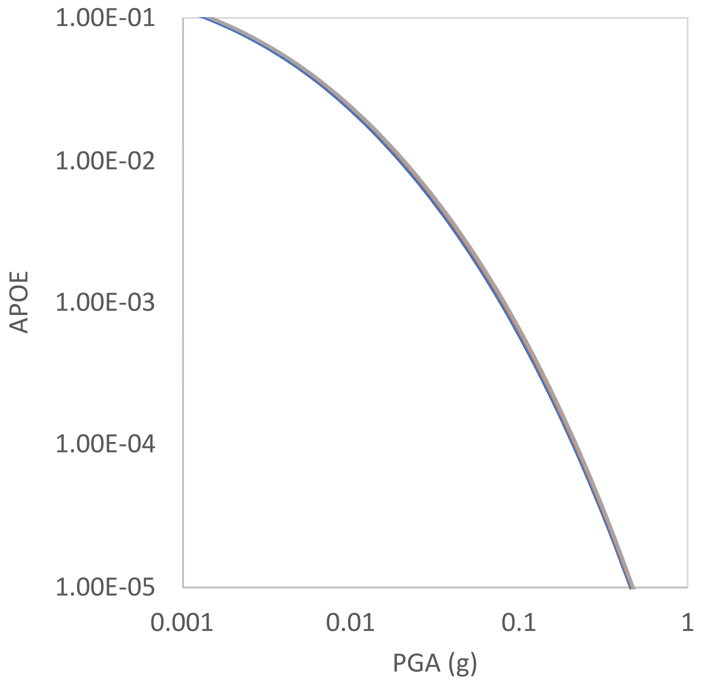

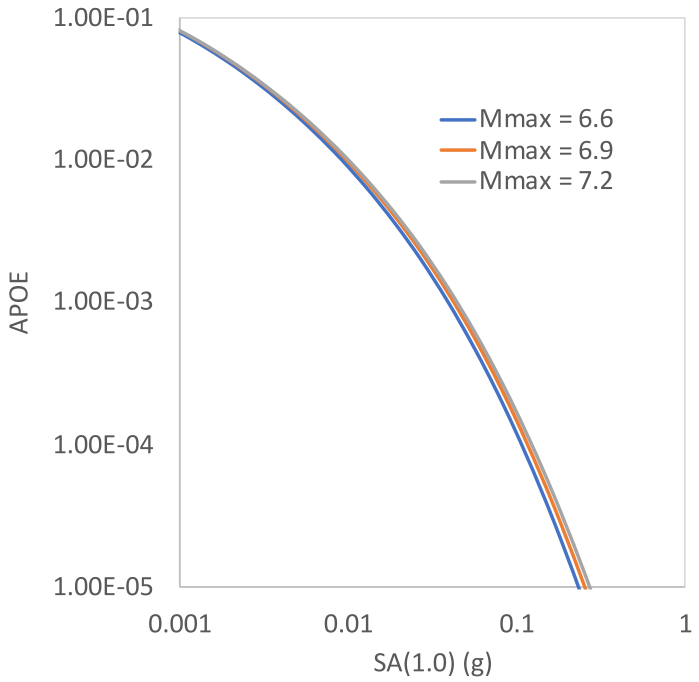

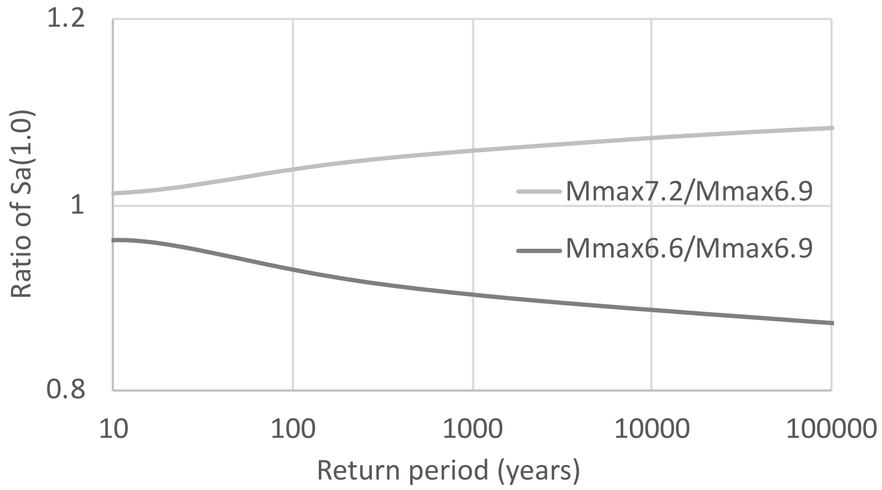

Influence of Mmax on Risk

- Risk calculations using the three Mmax GR area source branches for the municipality of Roermond:

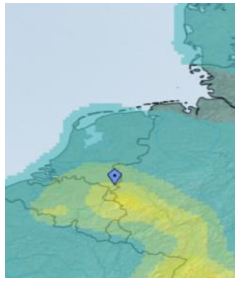

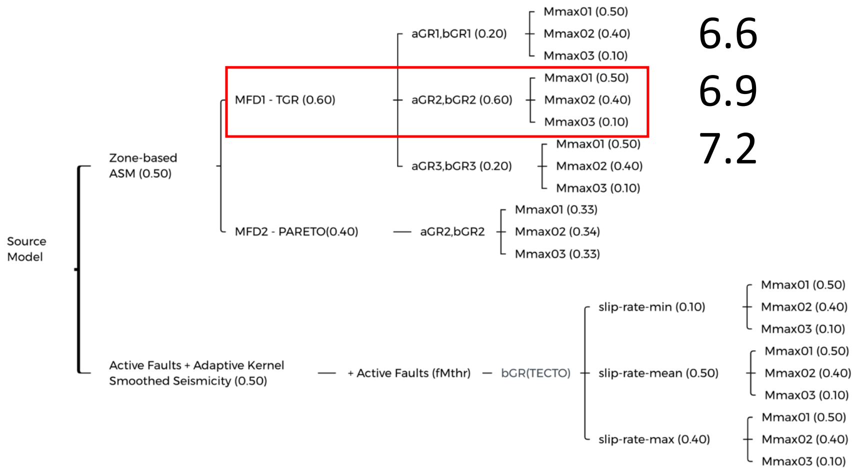

Mmax
6.6
6.9
7.2

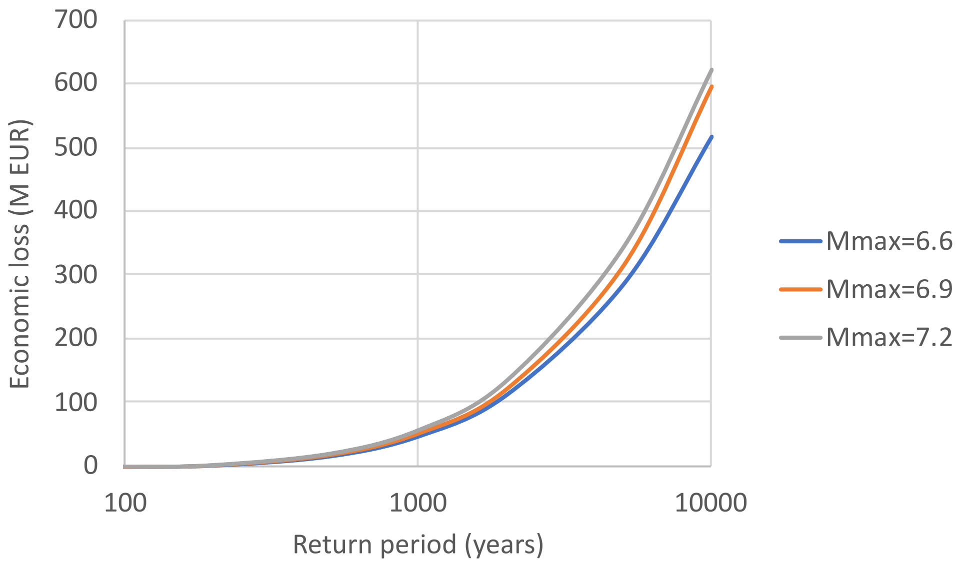

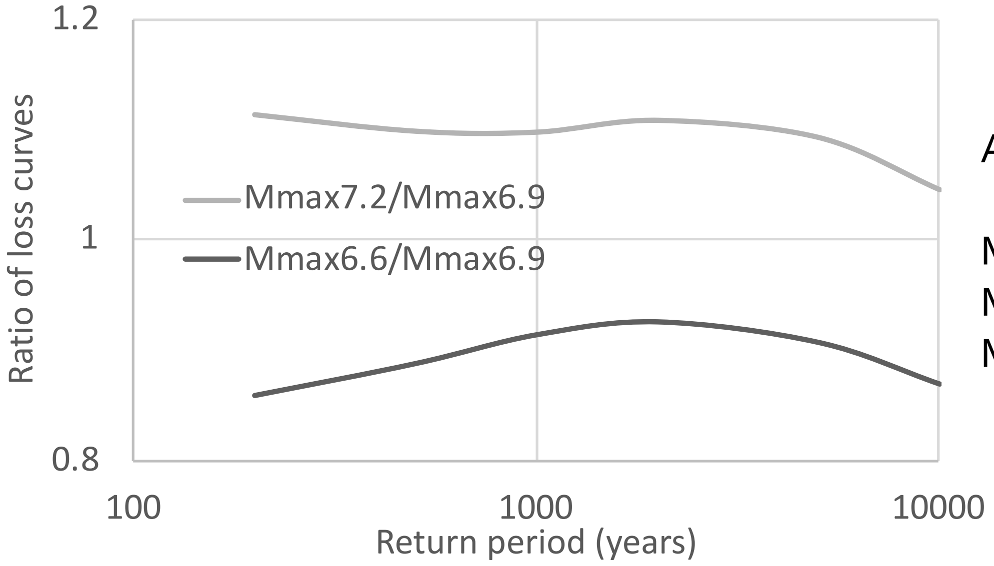

Average annual losses:

Mmax6.6 = 280k EUR
Mmax6.9 = 320k EUR
Mmax7.2 = 340k EUR

Note full correlation of logic tree branches assumed (all sources have same branch of Mmax) so impact might be overstated, though most contribution to loss is only from one or two sources.

References

- Danciu L., Nandan S., Reyes C., Basili R., Weatherill G., Beauval C., Rovida A., Vilanova S., Sesetyan K., Bard P-Y., Cotton F., Wiemer S., Giardini D. (2021) - The 2020 update of the European Seismic Hazard Model: Model Overview. EFEHR Technical Report 001, v1.0.0, https://doi.org/10.12686/a15
- Bird, P. (2003). An updated digital model of plate boundaries. Geochemistry, Geophysics, Geosystems, 4(3). https://doi.org/10.1029/2001GC000252
- Asch, K. (2005). The 1:5 Million International Geologial Map of Europe and Adjacent Areas - final version for the internet.- BGR, Hannover. Retrieved from https://www.bgr.bund.de/EN/Themen/Sammlungen- Grundlagen/GG_geol_Info/Karten/Europa/IGME5000/IGME_Project/IGME_Downloads.html
- Johnston, A. C. (1994). Seismotectonic interpretations and conclusions from the stable continental region seismicity database (The Earthquakes of Stable Continental Regions—v. 1 Assessment of Large Earthquake Potential, A. C. Johnston, K. J. Coppersmith, L. R. Kanter, and C. A. Cornell (Editors) No. Report TR102261V1). Palo Alto, California: Electric Power Research Institute.
- Müller, R. D., Sdrolias, M., Gaina, C., & Roest, W. R. (2008). Age, spreading rates, and spreading asymmetry of the world's ocean crust: Digital models of the World's Ocean crust. Geochemistry, Geophysics, Geosystems, 9(4), n/a-n/a. https://doi.org/10.1029/2007GC001743
- Global Volcanism Program. (2013). Volcanoes of the World, v. 4.3.4. Venzke, E (ed.). Smithsonian Institution. https://doi.org/10.5479/si.GVP.VOTW4-2013 [Data set]. Retrieved from https://volcano.si.edu/database/webservices.cfm
- Youngs RR, Coppersmith KJ, (1985) Implications of fault slip rates and earthquake recurrence models to probabilistic seismic hazard estimates. Bull Seismol Soc Am 75: 939–964.
- Anderson JG, Luco JE (1983) Consequences of slip rate constraints on earthquake occurrence relations. Bull Seismol Soc Am 73:471–496.
- Woessner J., Danciu L., Giardini D., Crowley H., Cotton F., Grunthal G., Valensise G., Arvidsson R., Basili R., Demircioglu M., Hiemar S., Meletti C., Musson R., Rovida A., Sesetyan K. and Stucchi M (2015) The 2013 European Seismic Hazard Model - Key Components and Results, Bulletin of Earthquake Engineering, Volume 13, Issue 12, pp 3553-3596.
- Kagan, Y.Y. (1993) Statistics of characteristic earthquakes, Bulletin of the Seismological Society of America, 83(1), 7-24.
- Johnston, A.C., Coppersmith, K.J., Kanter, L.R., and Cornell, C.A. (1994) The Earthquakes of Stable Continental Regions, Volume 1; Assessment of Large Earthquake Potential, Final Report Submitted to Electric Power Research Institute (EPRI). TR-102261-VI, v. 1.

Induced earthquakes related to gas production

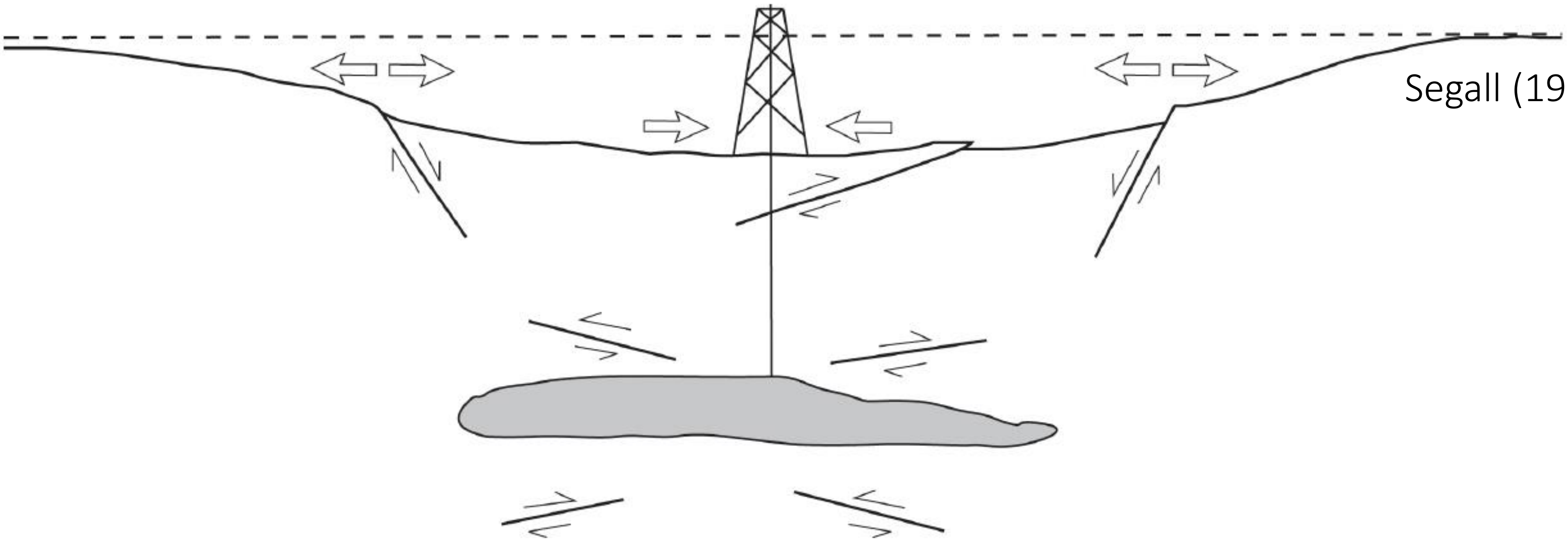

Segall (1989)

Groningen Mmax Workshop II
June 13th, 2022

SAN DIEGO STATE UNIVERSITY

Matthew Weingarten
Assistant Professor
Dept. of Geological Sciences

Introduction

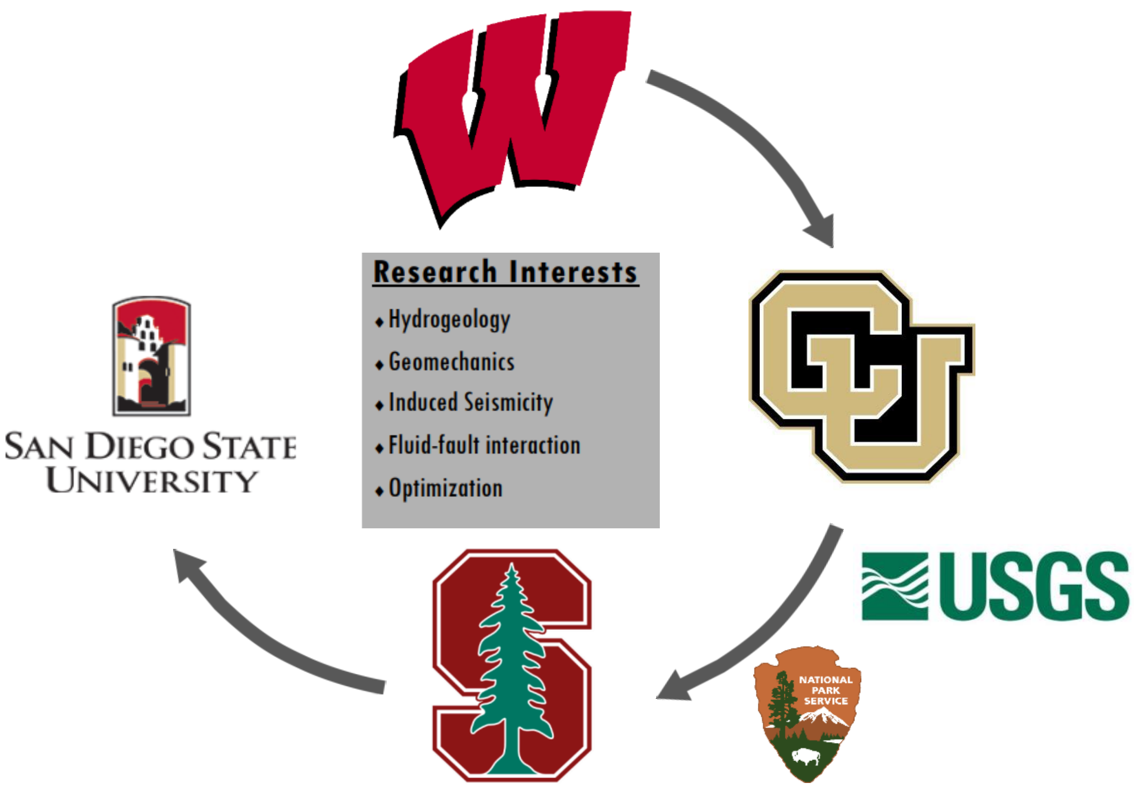

Introduction

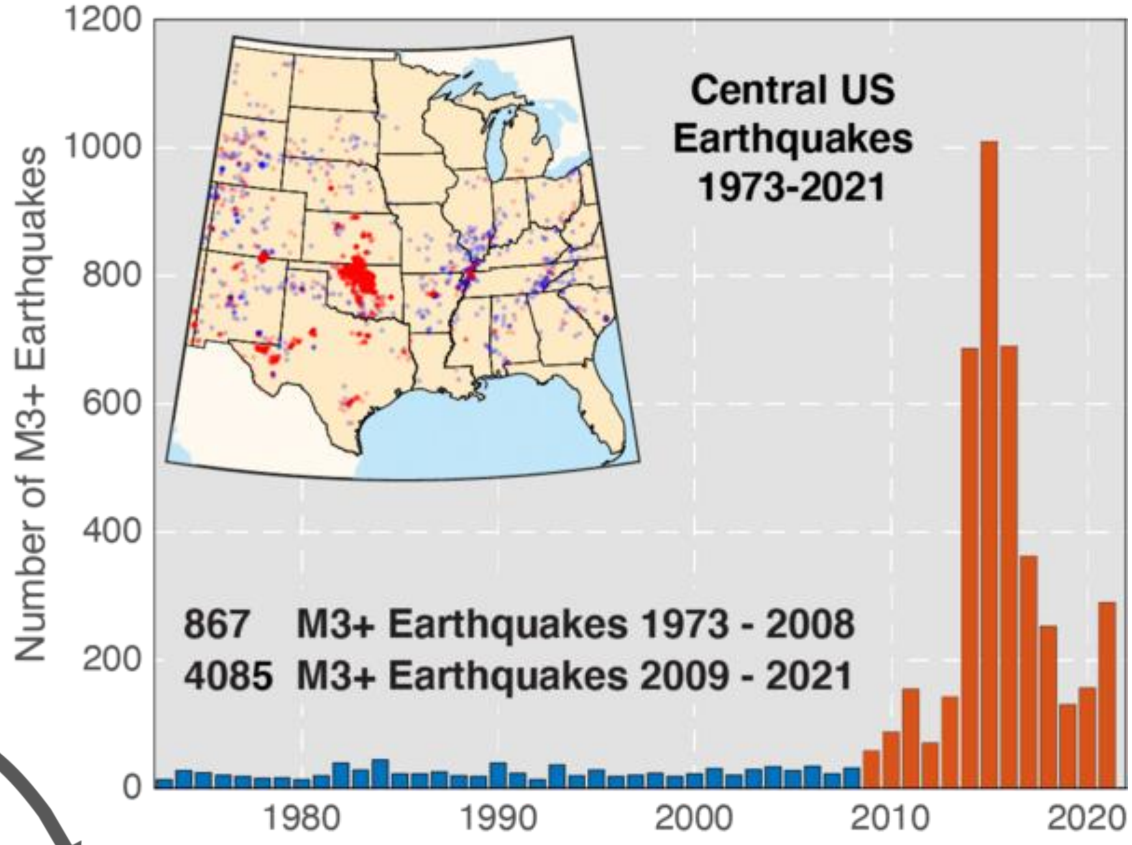

Research Interests

- Hydrogeology
- Geomechanics
- Induced Seismicity
- Fluid-fault interaction
- Optimization

San Diego State University

USGS

Gas Production Induced Seismicity
Two Cases Studies

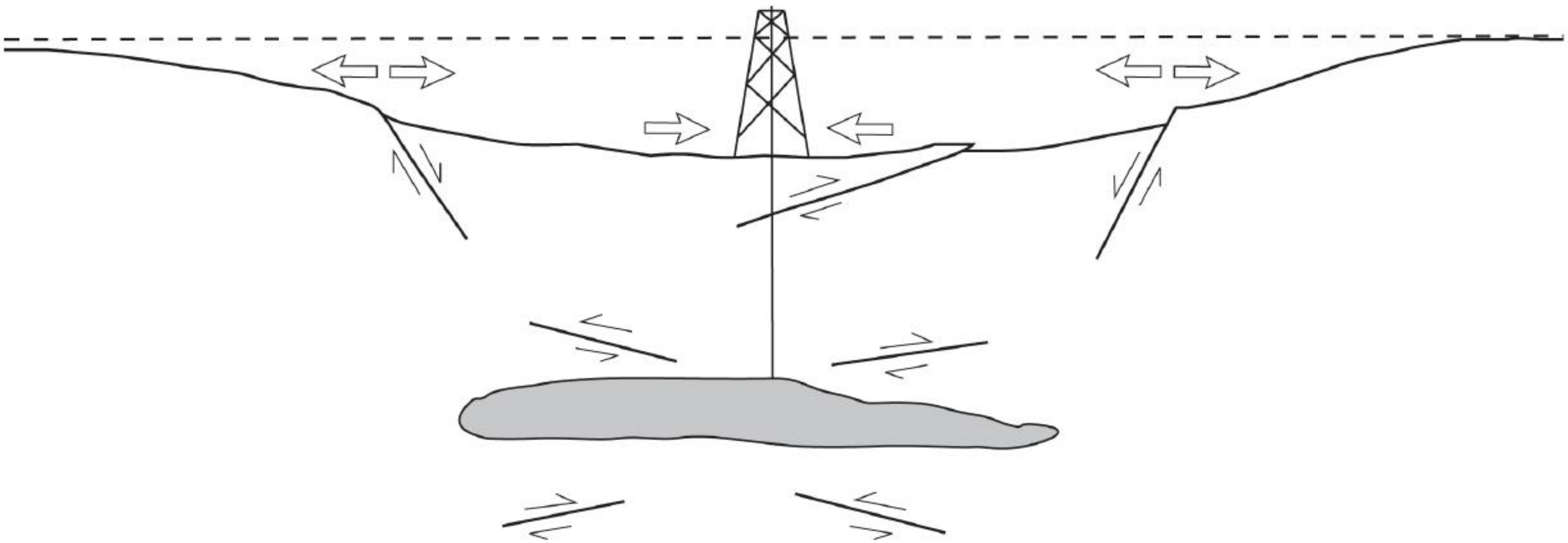

Gazli	**Lacq**
Uzbekistan	France
April 1976 M_s7.0	Sept. 1978 M_L4.2
May 1976 M_s7.3	April 2016 M_L4.0
March 1984 M_s7.0	
Adushkin et al. (2000)	Segall et al. (1994)

Gas Production Induced Seismicity
Mechanism: Poroelasticity

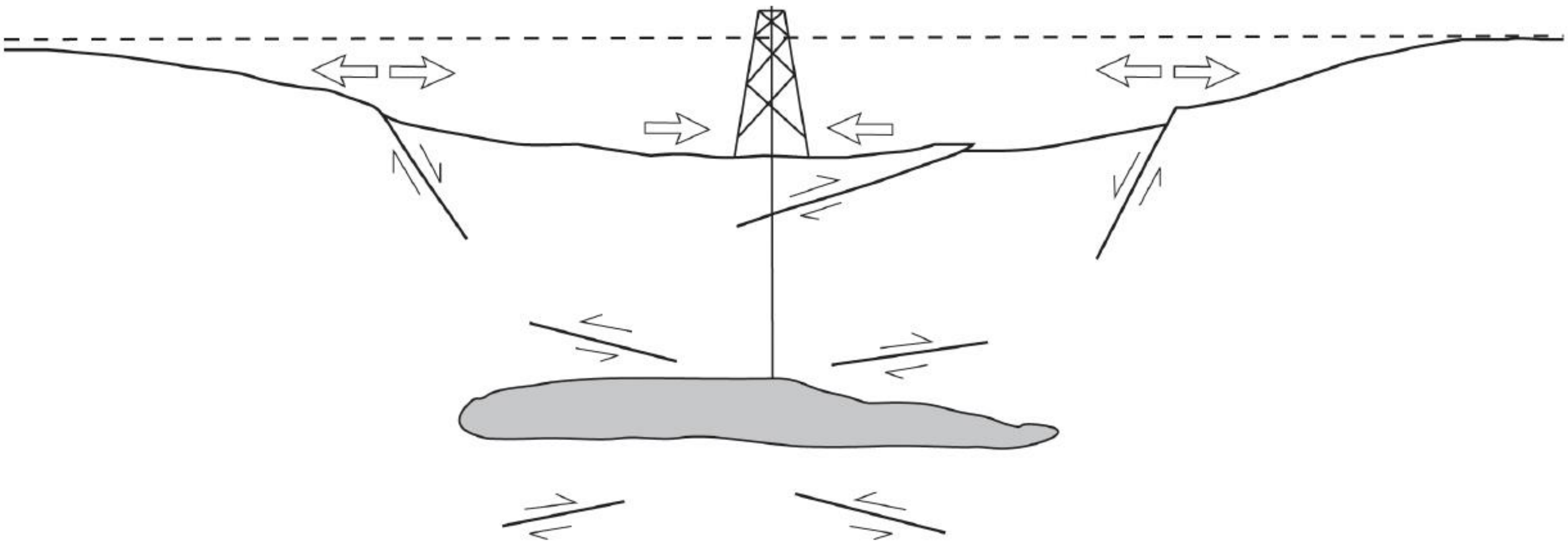

Fluid-to-solid coupling
a change in fluid pressure produces a stress change in porous material

Solid-to-fluid coupling
a change in applied stress produces a change in pore fluid pressure

Segall (1989)

Gas Production Induced Seismicity
Mechanism: Poroelasticity

(1) $$2G\varepsilon_{ij} = \sigma_{ij} - \frac{\nu}{(1+\nu)}\sigma_{kk}\delta_{ij} + \frac{3(\nu_u - \nu)}{B(1+\nu)(1+\nu_u)}p\delta_{ij}$$

(2) $$\Delta m = \frac{3\rho(\nu_u - \nu)}{2GB(1+\nu)(1+\nu_u)}\left(\sigma_{kk} + \frac{3}{B}p\right).$$

G: shear modulus
p: pore pressure
Δm: Δfluid mass content
ε_{ij}: strain
σ_{ij}: stress
ν: drained Poisson ratio
ν_u: undrained Poisson ratio
δ_{ij}: Kronecker Delta function
B: Skempton's coefficient

Equation 1 relates *strain* to stress and pore pressure

Equation 2 relates *changes in fluid mass content* to stress & pore pressure

Segall (1989)

Gas Production Induced Seismicity
Theoretical Example

Withdrawal of fluid from a rectangular region of thickness T and depth D surrounded by low permeability host rock

Calculated change in horizontal normal stress σ_{yy} (normalized)

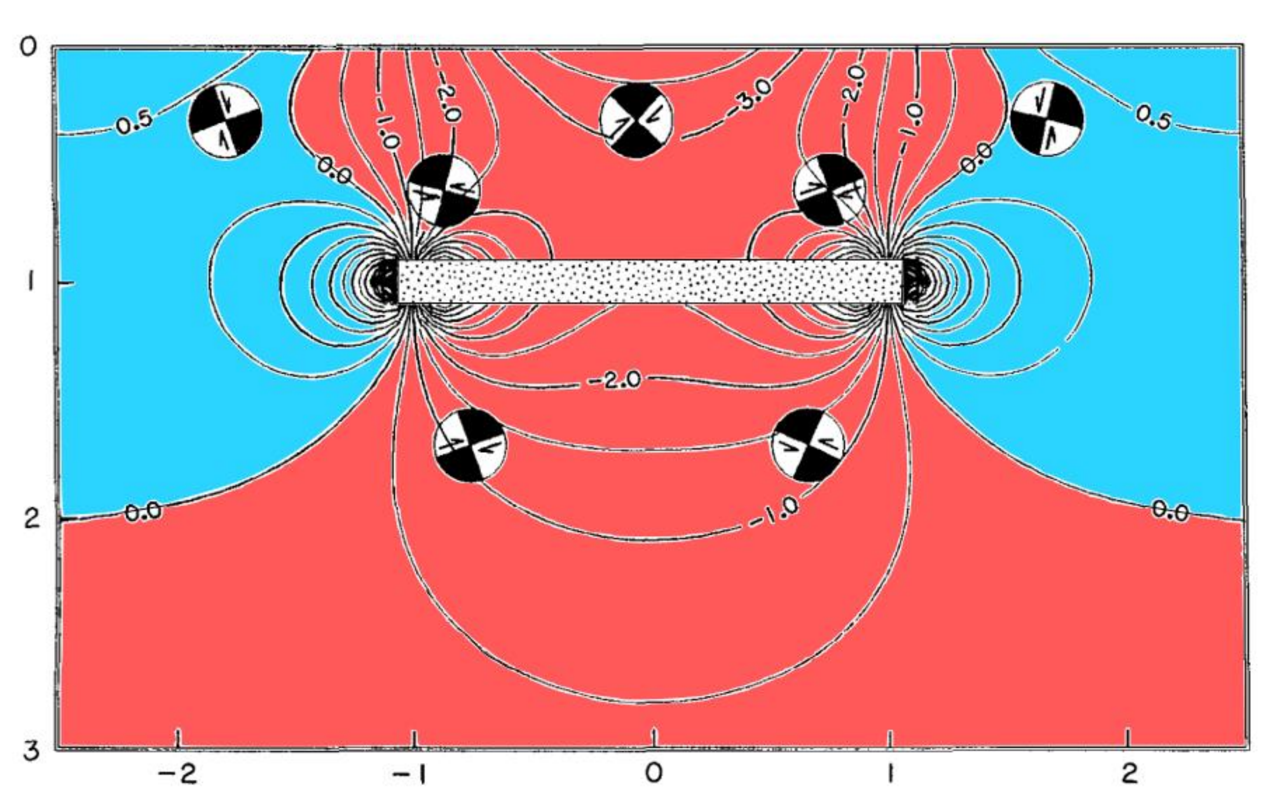

Red = compression
Blue = tension

Segall (1989)

Gas Production Induced Seismicity
Theoretical Example

Withdrawal of fluid from a rectangular region of thickness T and depth D surrounded by low permeability host rock

Calculated change in horizontal normal stress σ_{yy} (normalized)

Reverse faulting predicted above and below the reservoir

Normal faults predicted to slip on the reservoir flanks

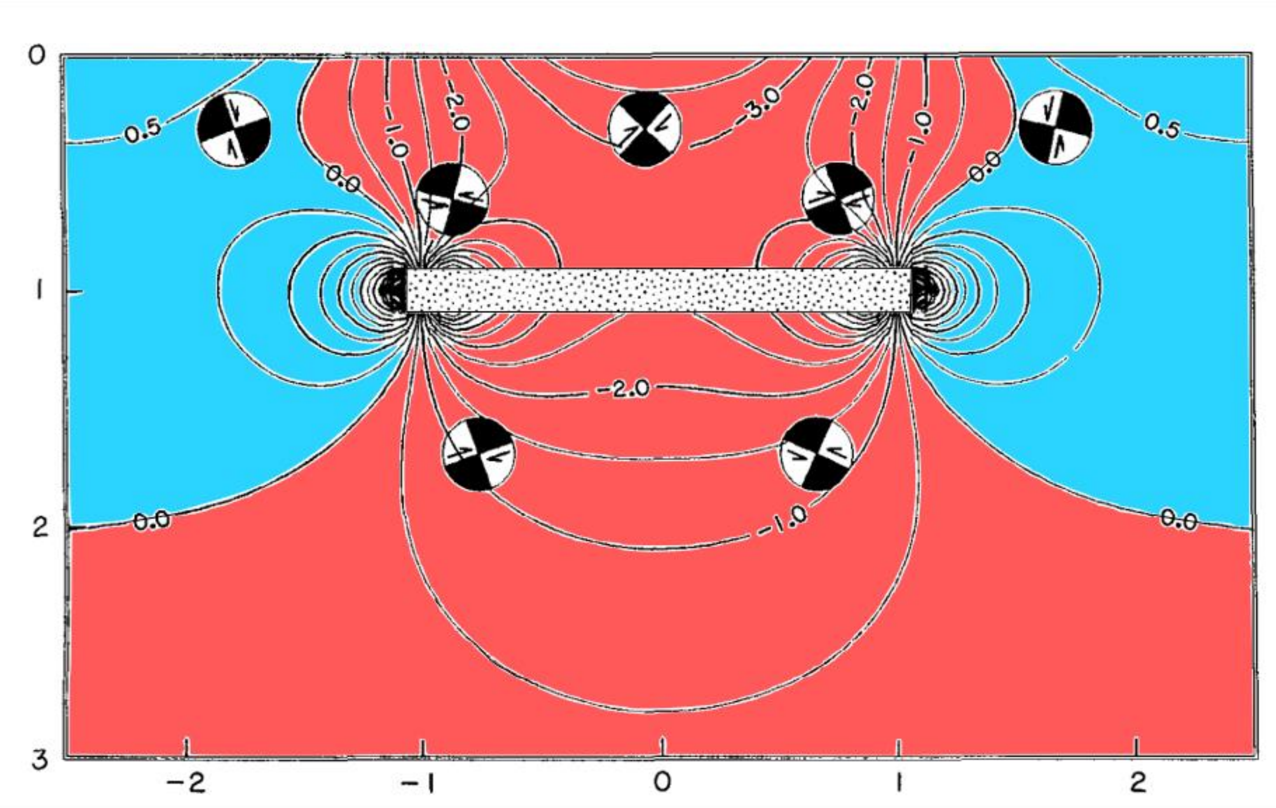

Red = compression
Blue = tension

Segall (1989)

Gas Production Induced Seismicity
Stress Change & Subsidence

Order of magnitude estimates of extraction-induced stress change:

$$\frac{stress\ change}{subsidence} \sim \frac{2\mu}{reservoir\ depth}$$

For μ = 10 GPa & D = 2 km

1 cm of subsidence yields a stress change of ~0.1 MPa

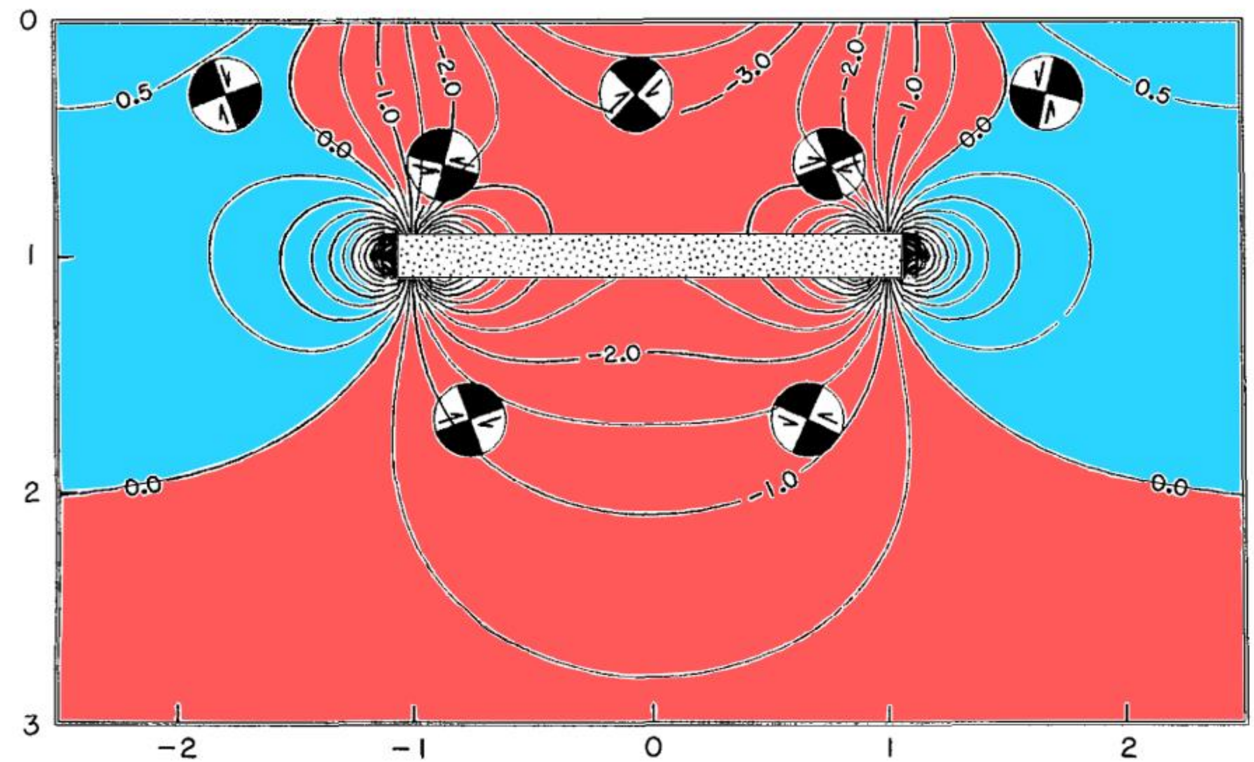

Red = compression
Blue = tension

Segall (1989)

Gas Production Induced Seismicity
Two Cases Studies

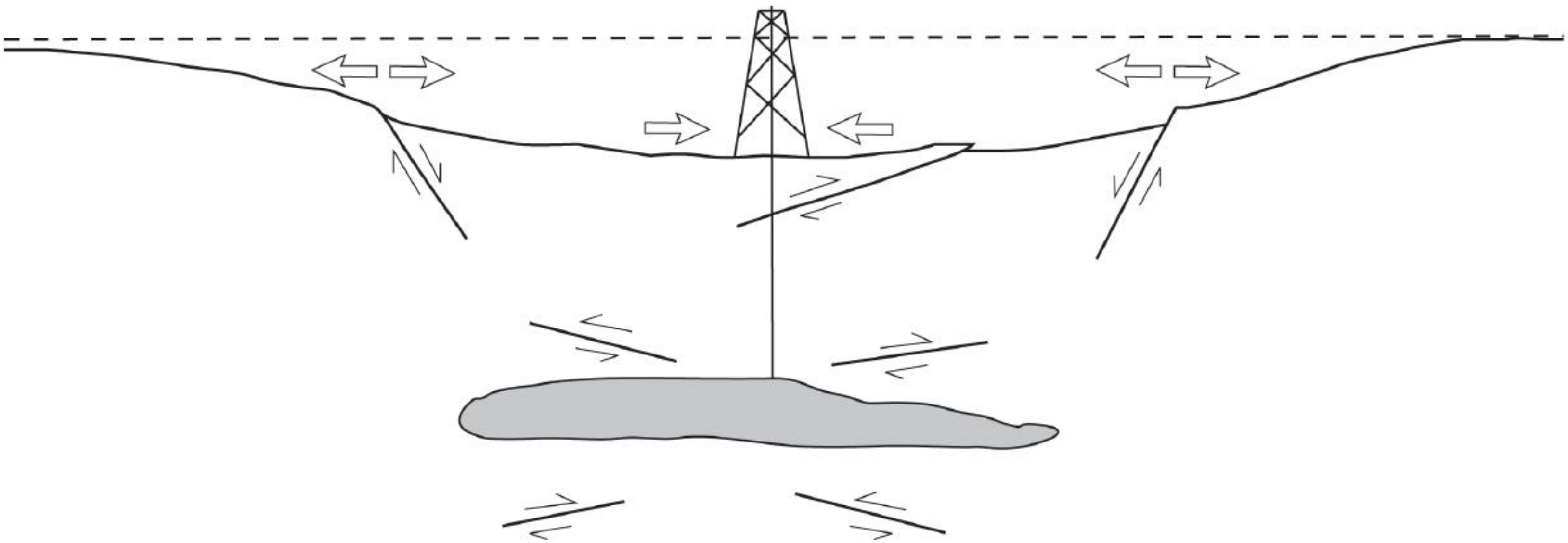

Gazli
Uzbekistan

April 1976 M_s7.0
May 1976 M_s7.3
March 1984 M_s7.0

Adushkin et al. (2000)

Lacq
France

Sept. 1978 M_L4.2
April 2016 M_L4.0

Grasso et al. (2020)

Gas production Induced Seismicity
Gazli Field, Uzbekistan

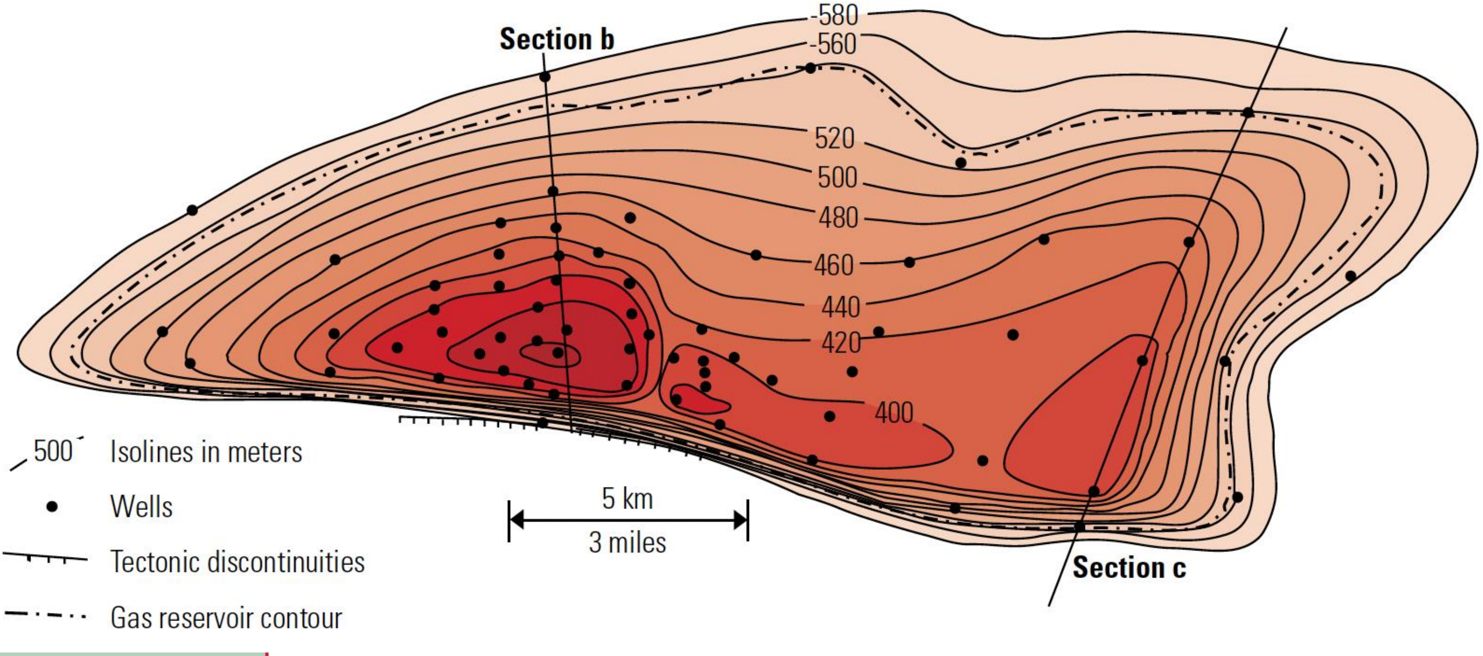

Asymmetric anticline with dimensions 38 km by 12 km

Discovered in 1956 -- gas production began in 1962

Formations of Jurassic-Neocene age overlying Paleozoic-aged sediments

Adushkin et al. (2000)

Gazli Field
Structural Background

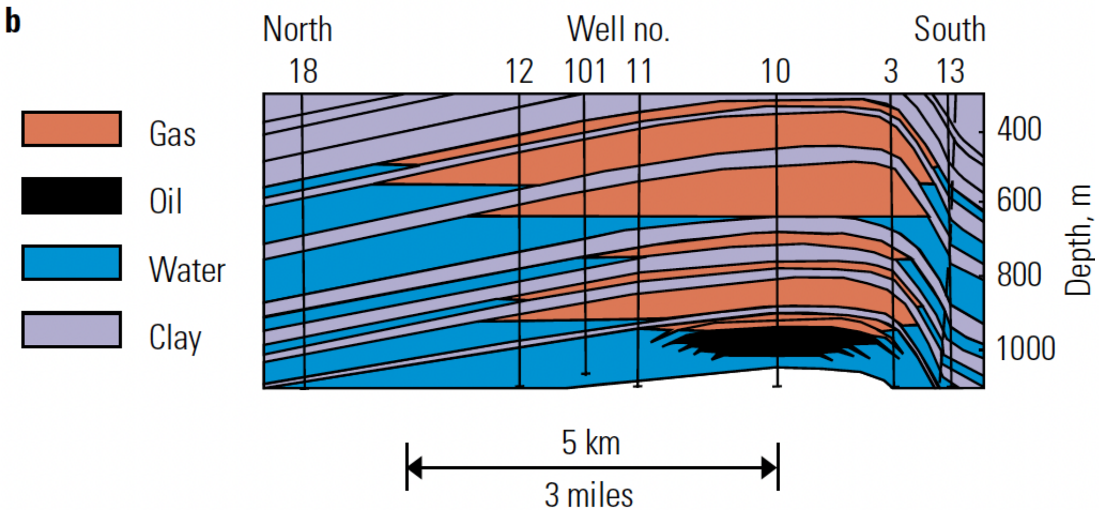

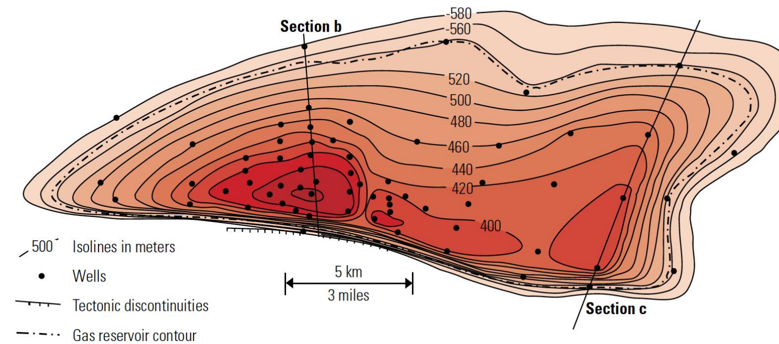

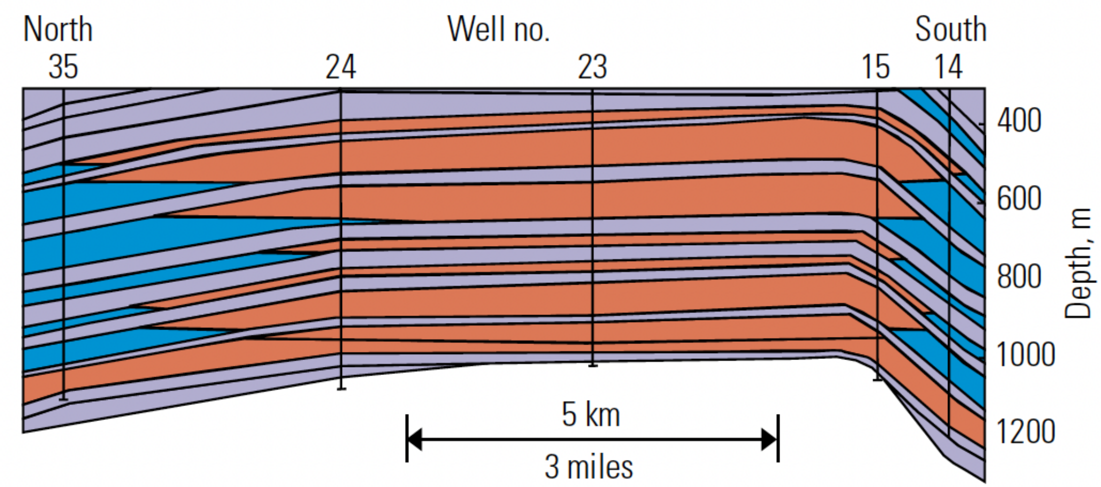

The field has 11 accumulations—10 gas and condensate, and one oil—all located in Cretaceous sediments

Porosity of the sandstone is high and averages 20 to 32%. Permeability of all but one producing horizons ranges from 675 to 1457 mD.

Adushkin et al. (2000)

Gazli Field

Gas Production & Water Injection (1962 – 1976)

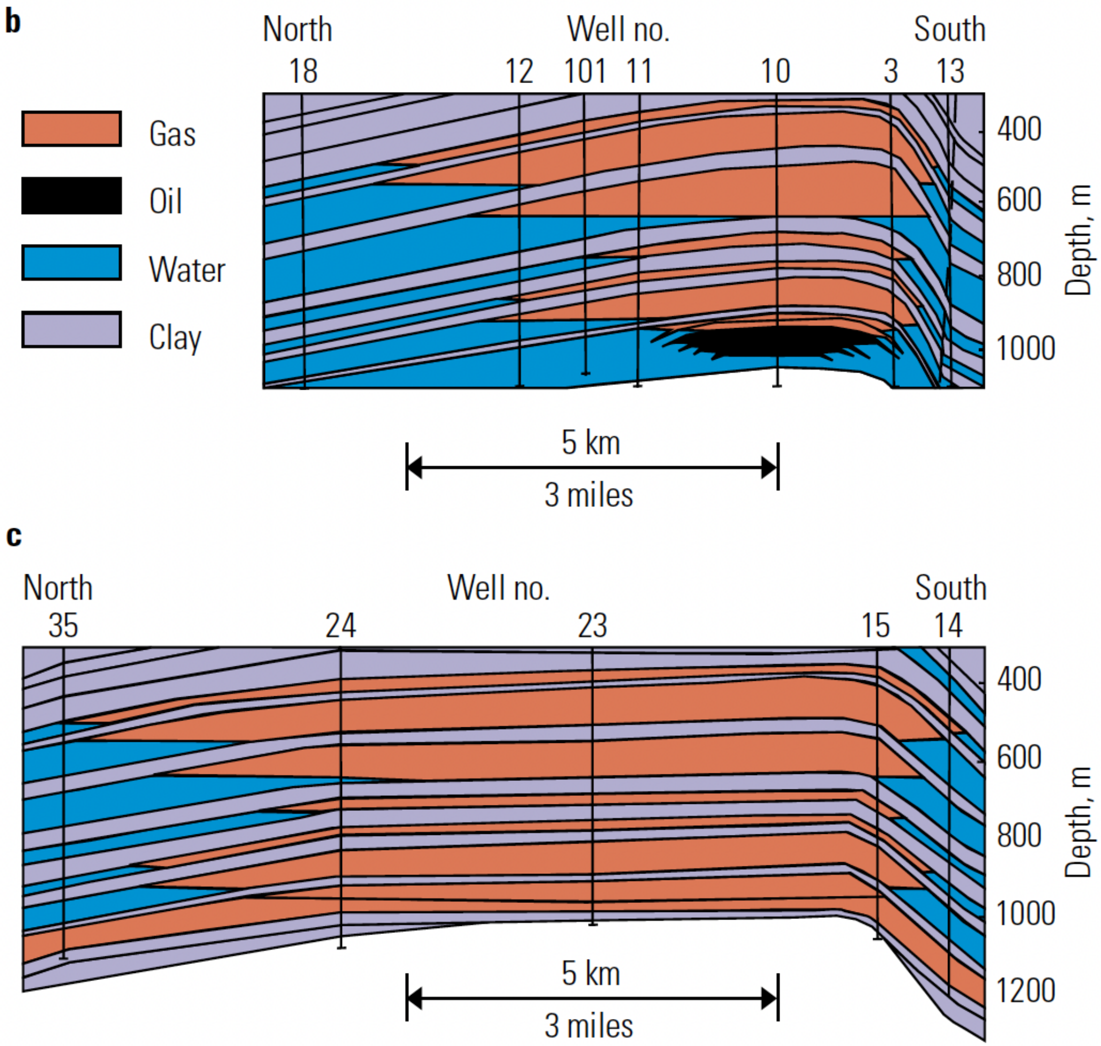

From 1966 – 1971, roughly *20 billion m^3/year* of gas were produced. Production peaked in 1971 and began to decline.

Initial reservoir pressure: ~7 MPa
1976 reservoir pressure: ~3 MPa
1985 reservoir pressure: ~1.5 MPa

Subsidence rates averaged 10.0 mm/yr in the period 1964 to 1968 and 19.2 mm/yr from 1968 to 1974 (total: ~15.5 cm)

Water Injection: from 1962-1976 roughly 600,000,000 m^3 of water was injected for pressure support

Simpson & Leith (1985) ; Adushkin et al. (2000)

Water Volumes
Major US Oil & Gas Basins

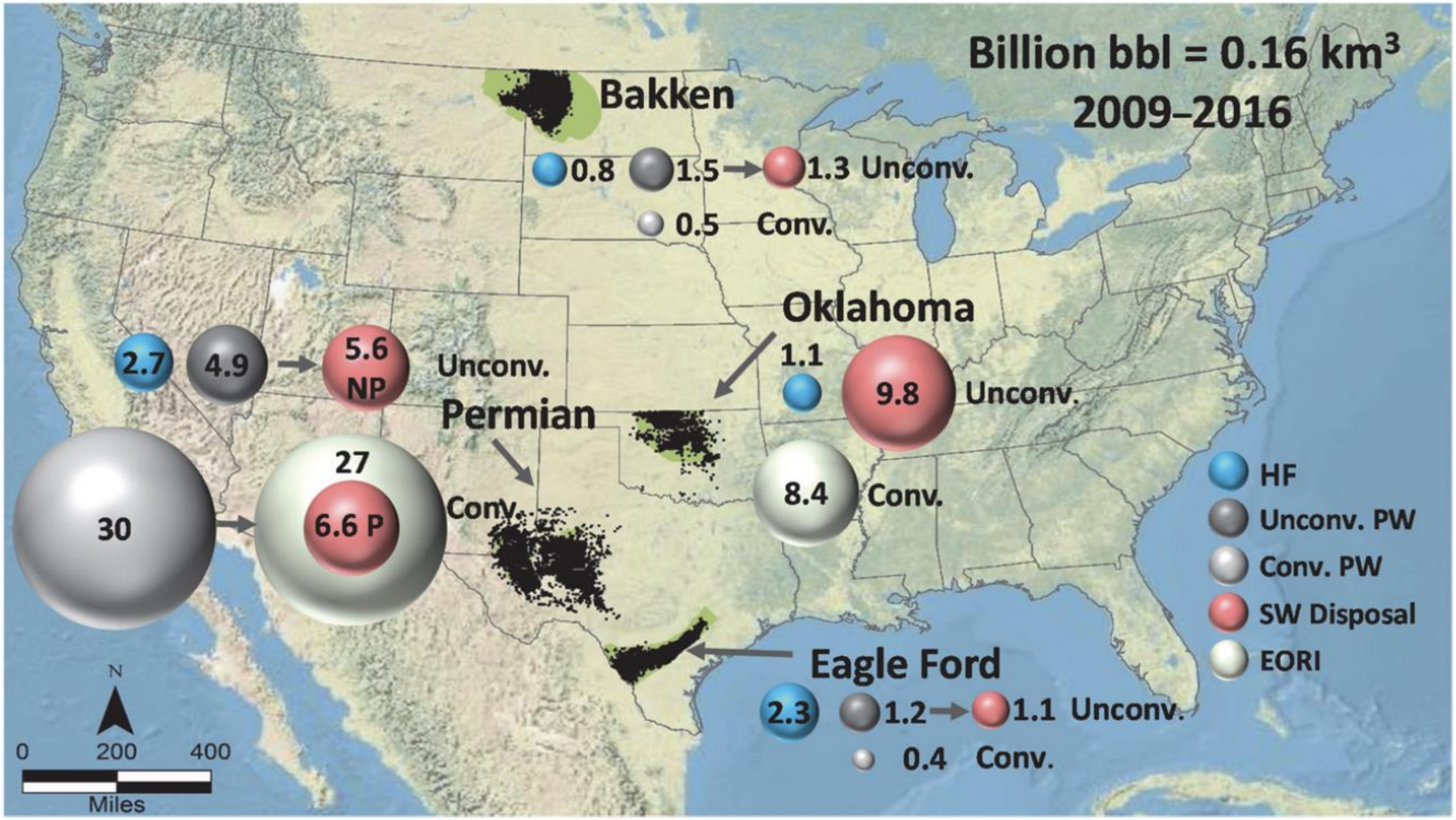

For context, Gazli water injection volume from 1962 – 1976 represents roughly ***one third*** of water injection volume in Oklahoma from 2009 – 2016 (across 800+ Arbuckle wells).

Gazli 1962 – 1976: ~3.8 billion barrels injected
Oklahoma 2009 – 2016: ~9.8 billion barrels injected

Scanlon, Weingarten et al. (2018)

Gazli Field
Major Seismic Events (1976 – 1984)

Bulletin of the Seismological Society of America, Vol. 75, No. 5, pp. 1465–1468, October 1985

THE 1976 AND 1984 GAZLI, USSR, EARTHQUAKES—WERE THEY INDUCED?

BY DAVID W. SIMPSON AND WILLIAM LEITH

On 19 March 1984, a magnitude $M_S = 7.0$ earthquake struck the desert town of Gazli in Soviet Uzbekistan (Figure 1, inset). This event was unusual in that it followed on the heels of two other events of the same magnitude that shook this gas-producing region in 1976 (Aptekman *et al.*, 1978; Kristy *et al.*, 1980; Hartzell, 1980). Prior to 1976, this region had been relatively aseismic. All three events resulted in extensive damage in the town of Gazli, which lies 50 km west of the ancient city of Bukhara. The 1984 earthquake, which was centered (like those before it) some 30 km to the north of Gazli (Figure 1), produced a maximum intensity of 8 ball* in Gazli. Although more than one hundred people were injured, only one death occurred. Pumping operations in the gas field, 15 km to the north, were apparently interrupted for only a few hours.

Simpson & Leith (1985)

Gazli Field
Major Seismic Events (1976 – 1984)

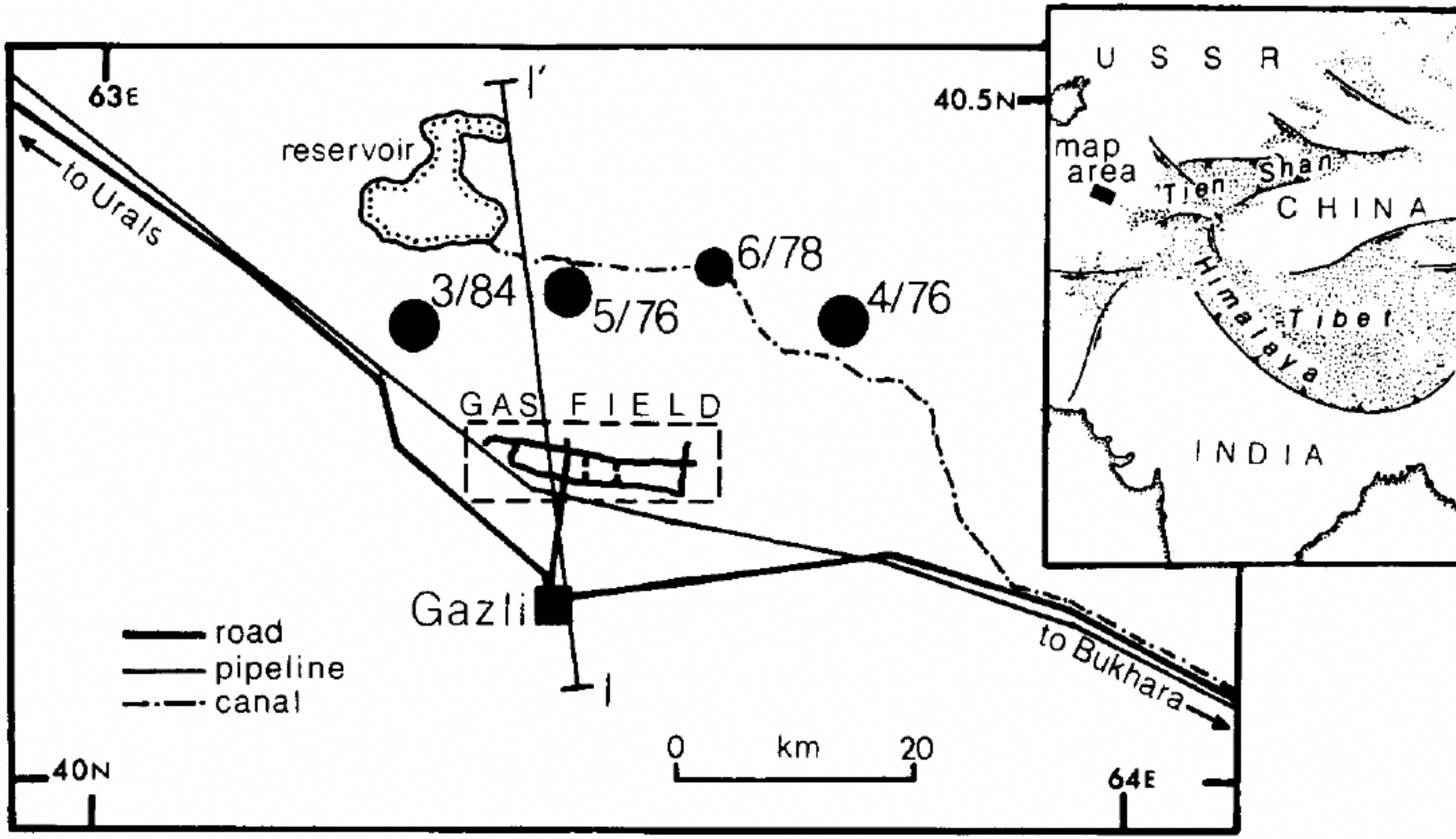

FIG. 1. Sketch map of the Gazli area, with the epicenters of the 1976 and 1984 earthquakes plotted. The line of the sketch cross-section of Figure 2 is indicated, *I-I′*.

Simpson & Leith (1985)

Gazli Field

Background Seismicity (1962-1976)

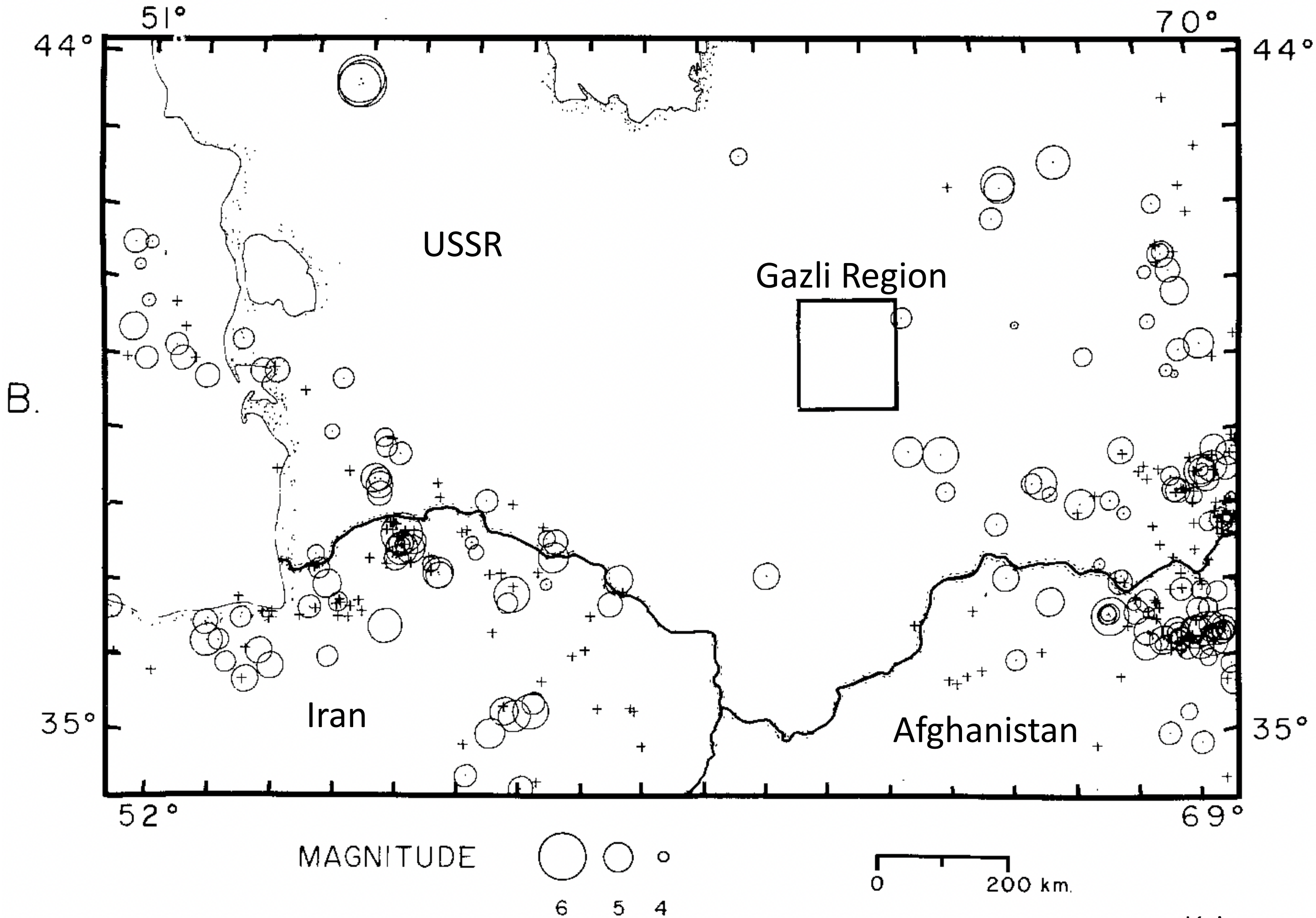

Kristy et al. (1980)

Gazli Field
Major Seismic Events (1976 – 1984)

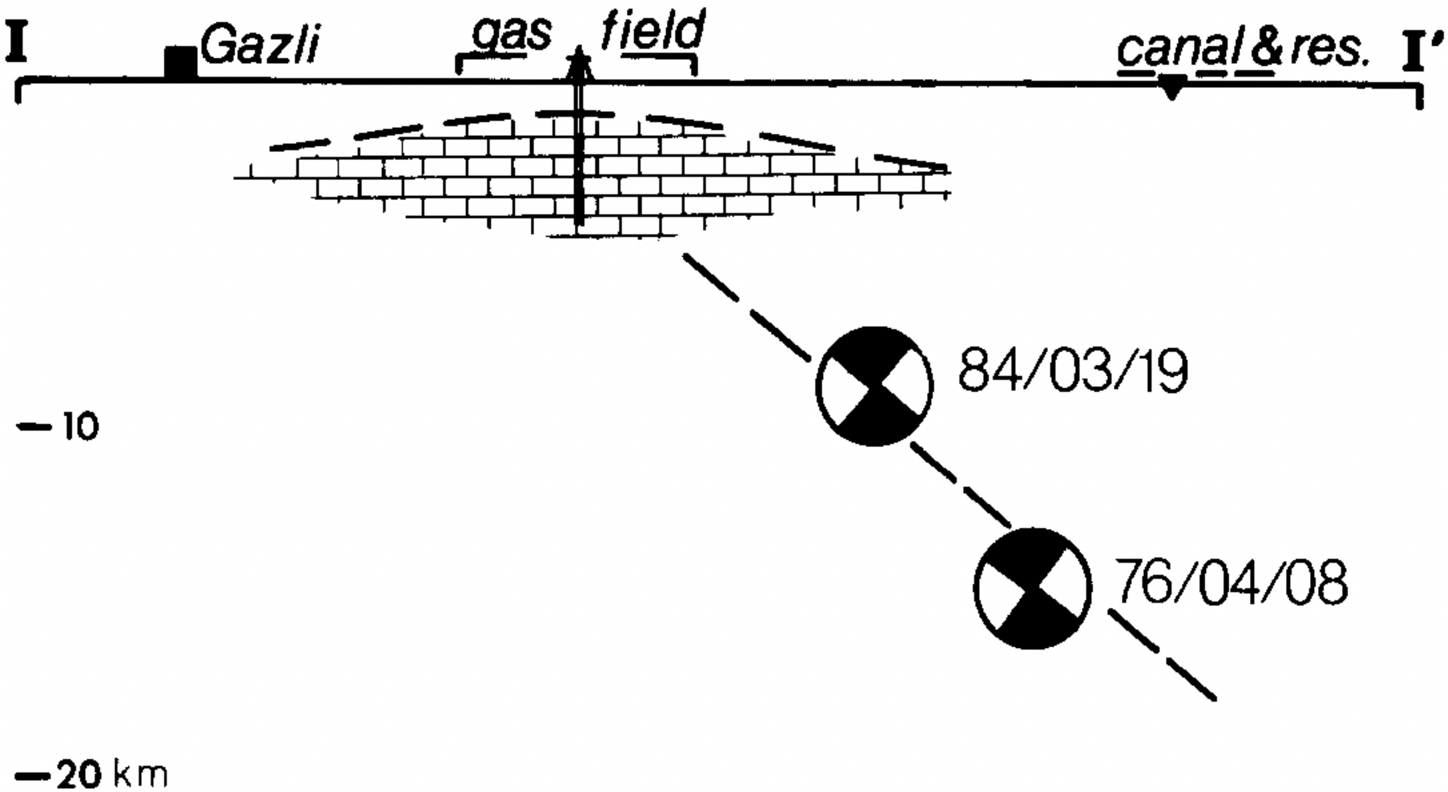

Simpson & Leith (1985)

Gazli Field
1976 & 1984 Surface Deformation

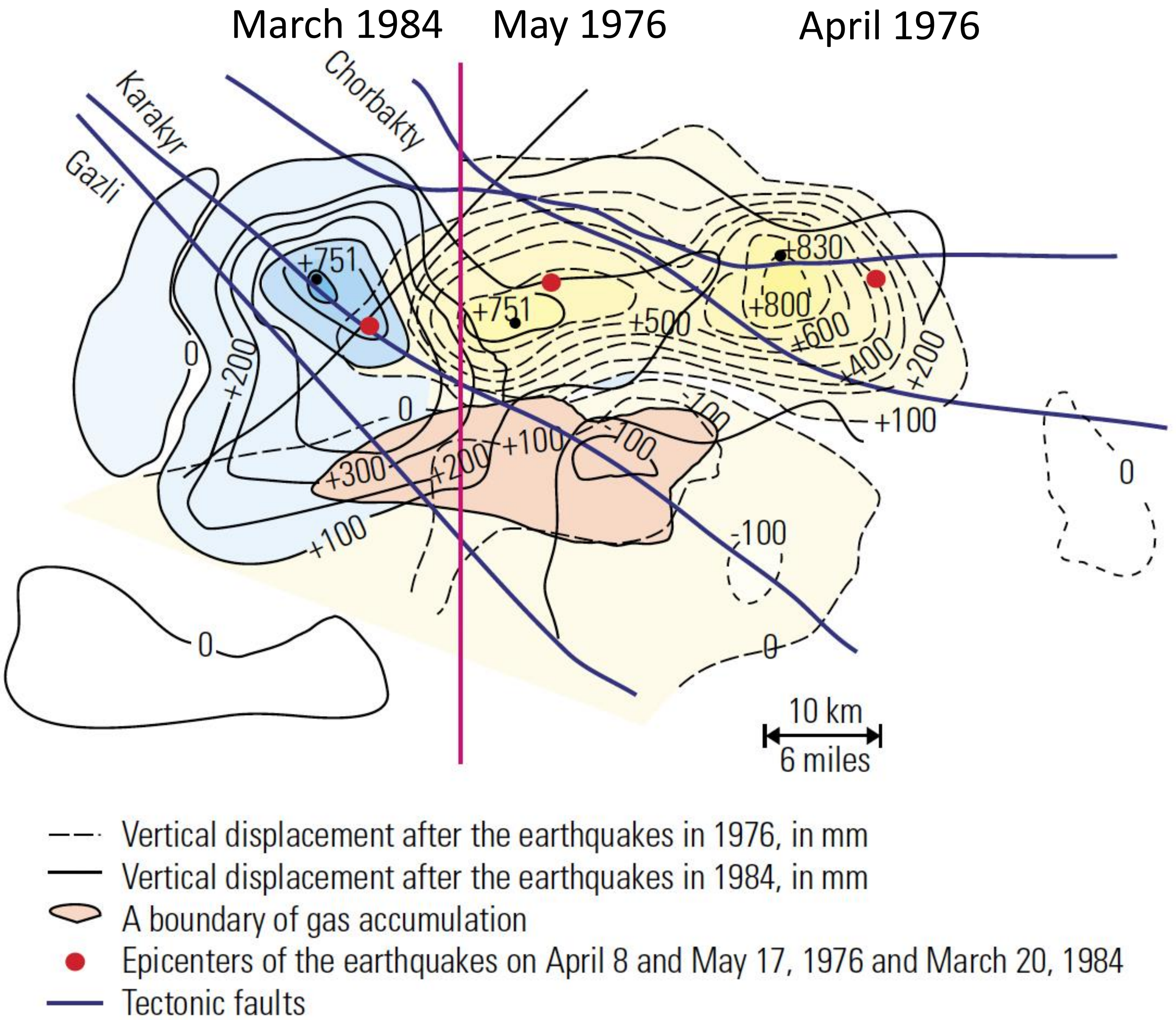

Adushkin et al. (2000)

Gazli Field
Evidence for Triggered Seismicity

1. Background quiescence prior to onset of gas production.

2. The occurrence of two M = 7.0 events followed by a third, 8 years later does not follow any typical foreshock-aftershock pattern. The entire sequence, however, has included a high level of aftershock activity.

3. Mass withdrawal has significantly modified effective stresses at depth.

4. Source modeling of the 1984 earthquake indicates that the rupture propagated downward which is uncommon for thrust mechanism events (Eyidogan et al., 1985).

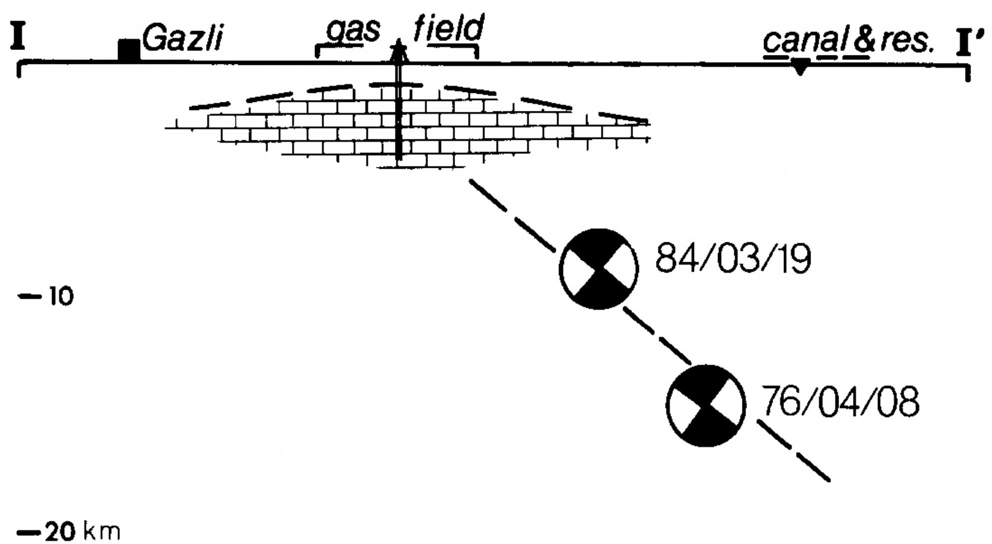

Simpson & Leith (1985); Grasso (1992)

Gazli Field
Transition to Gas Storage (1988 – 1993)

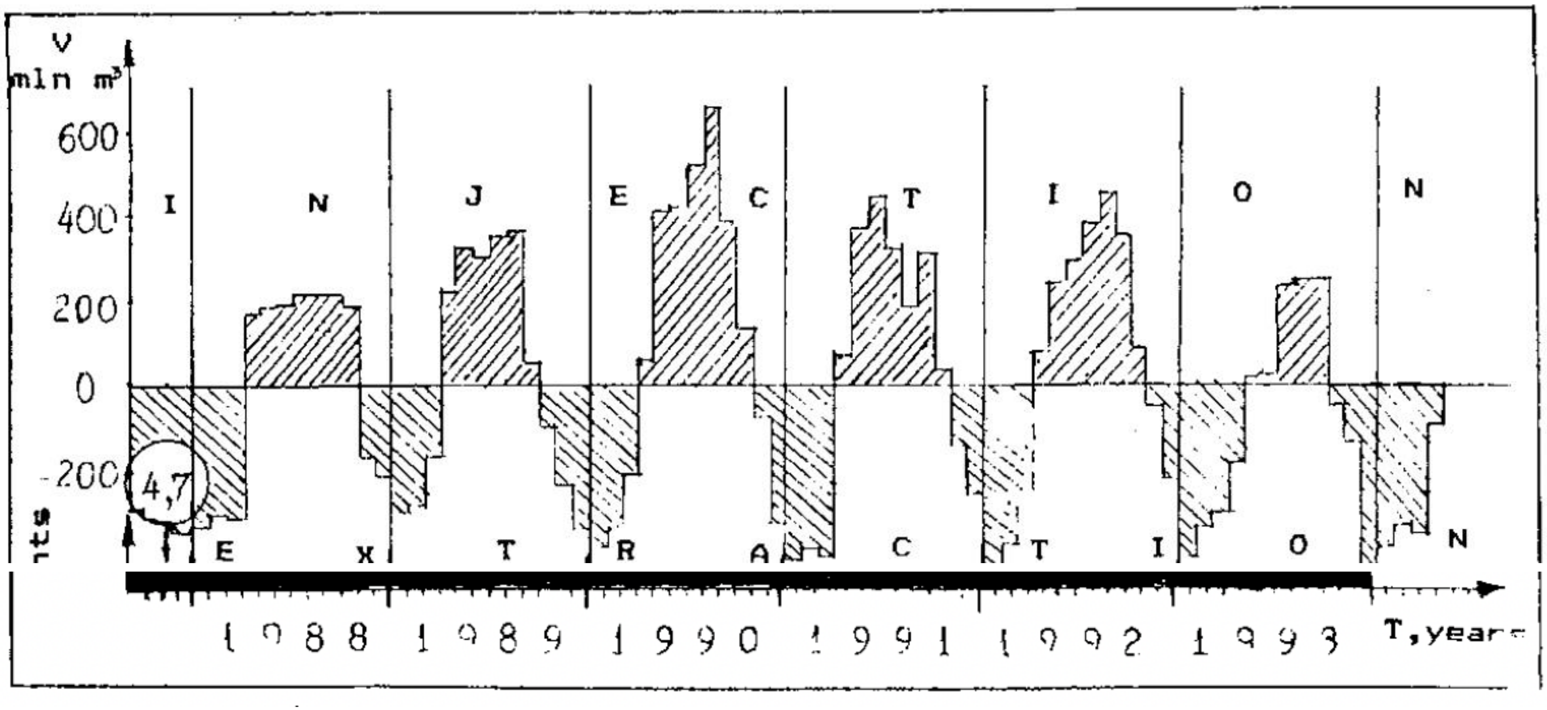

Plotnikova et al. (1996)

Gazli Field
Seismicity (1988 – 1993 deployment)

Deployment located hundreds of earthquakes in the vicinity of the gas field – many >**M**4.0 – with an **M**4.7 being the largest event

Plotnikova et al. (1996) found gas extraction was followed by a *decrease* in the earthquake frequency

Gas *injection* was associated with an increase of seismic event numbers by 40-60%

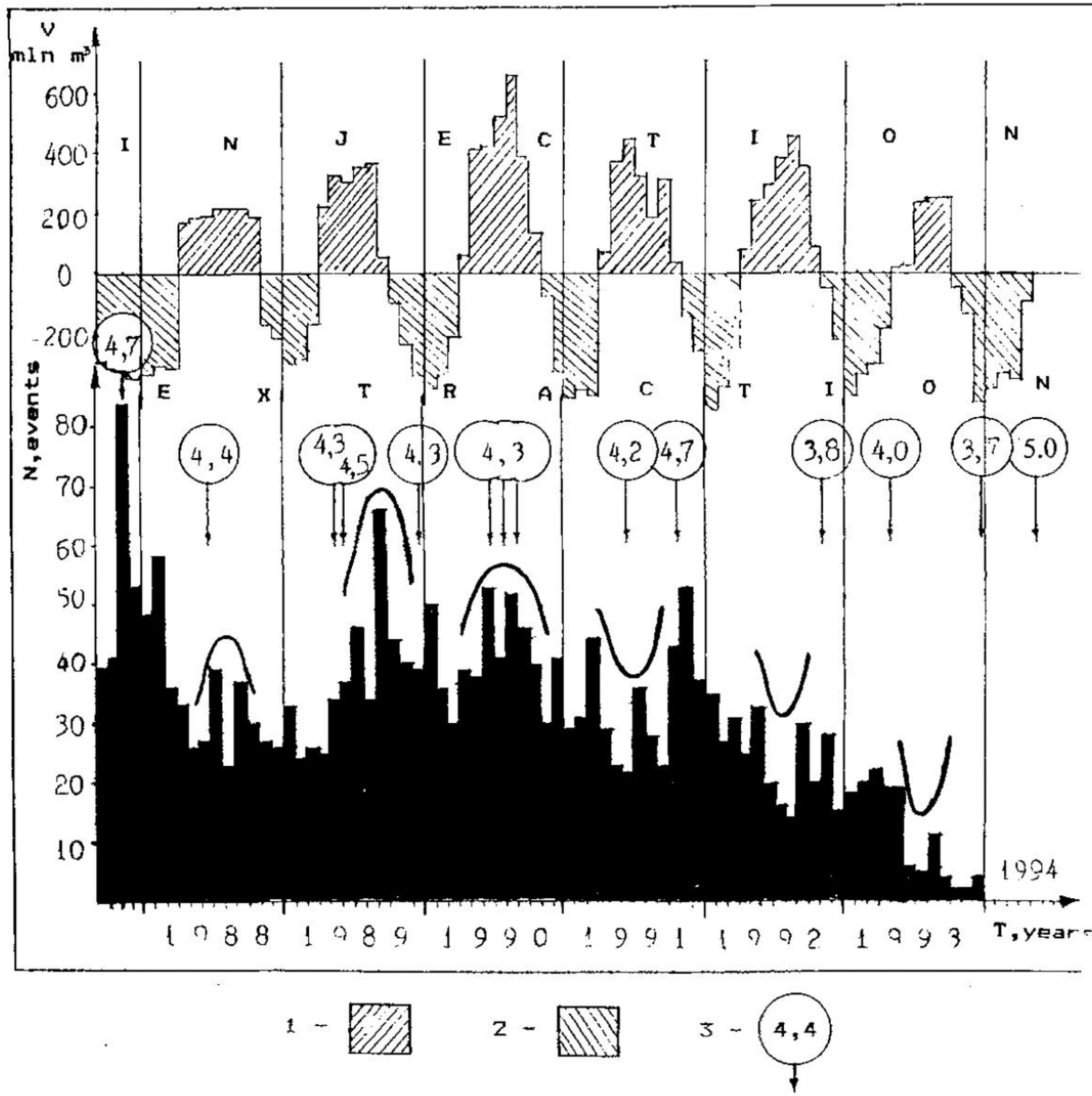

Plotnikova et al. (1996)

Gas Production Induced Seismicity
Two Cases Studies

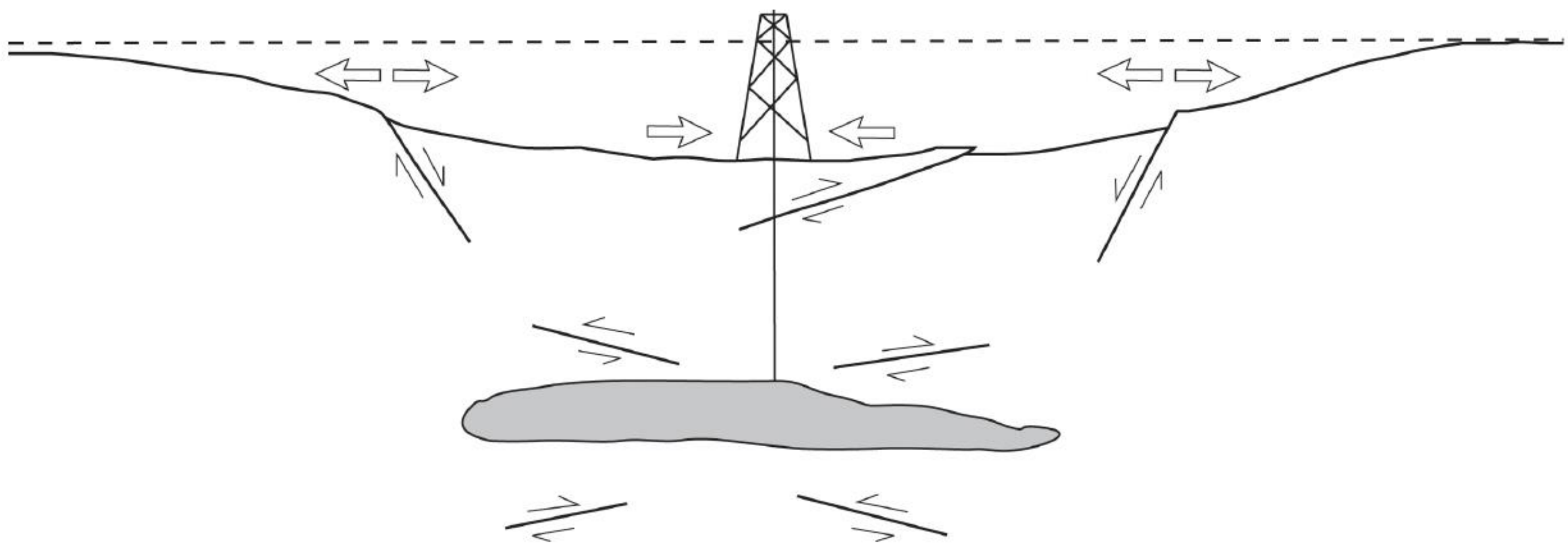

Gazli	**Lacq**
Uzbekistan	France
April 1976 M_s7.0	Sept. 1978 M_L4.2
May 1976 M_s7.3	April 2016 M_L4.0
March 1984 M_s7.0	
Adushkin et al. (2000)	Grasso et al. (2021)

Gas production Induced Seismicity
Lacq Oil & Gas Field

One of the best-documented cases of gas production related seismicity

Shallow oil reservoir (0.7 km)

Deep gas reservoir (3.2 – 5.5 km)

Quick facts:

(1) Oil production start date: 1950

(2) Gas production start date: 1957

(3) Shallow wastewater disposal: 1955

(4) Deep wastewater disposal: 1974

(5) Highly overpressured reservoir: +30 MPa above hydrostatic prior to pumping

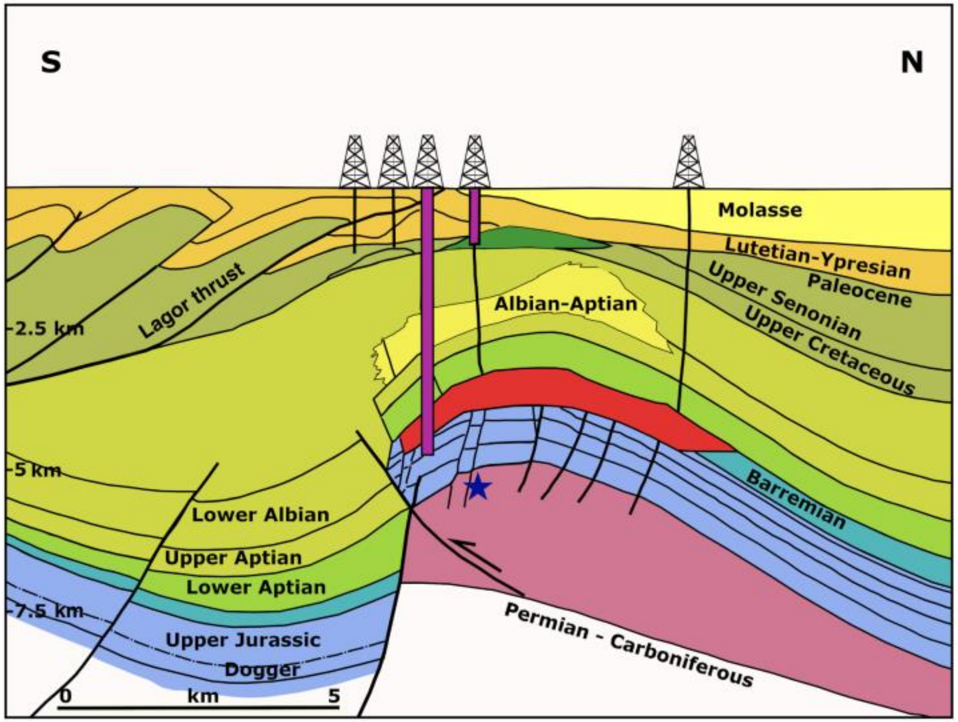

Grasso et al. (2021)

Gas production Induced Seismicity
Lacq Oil & Gas Field

Gas field produced 254 billion m^3 of gas from 1957 – 2012. Gas production reduced to a negligible value by 2012.

Cumulative water injection is ~24.4 million m^3 since 1974

Fractured limestone reservoir is highly permeable: 50 -10,000 mD

Large pressure depletion across the reservoir in excess of ~60 MPa

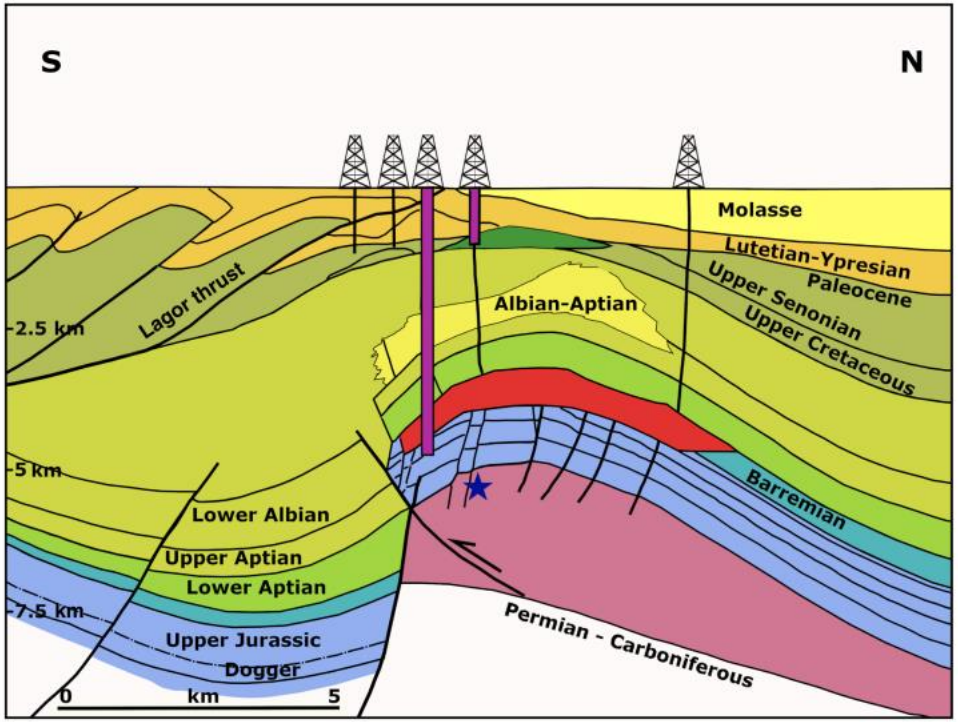

Grasso et al. (2021)

Lacq Oil & Gas Field
Regional Seismicity

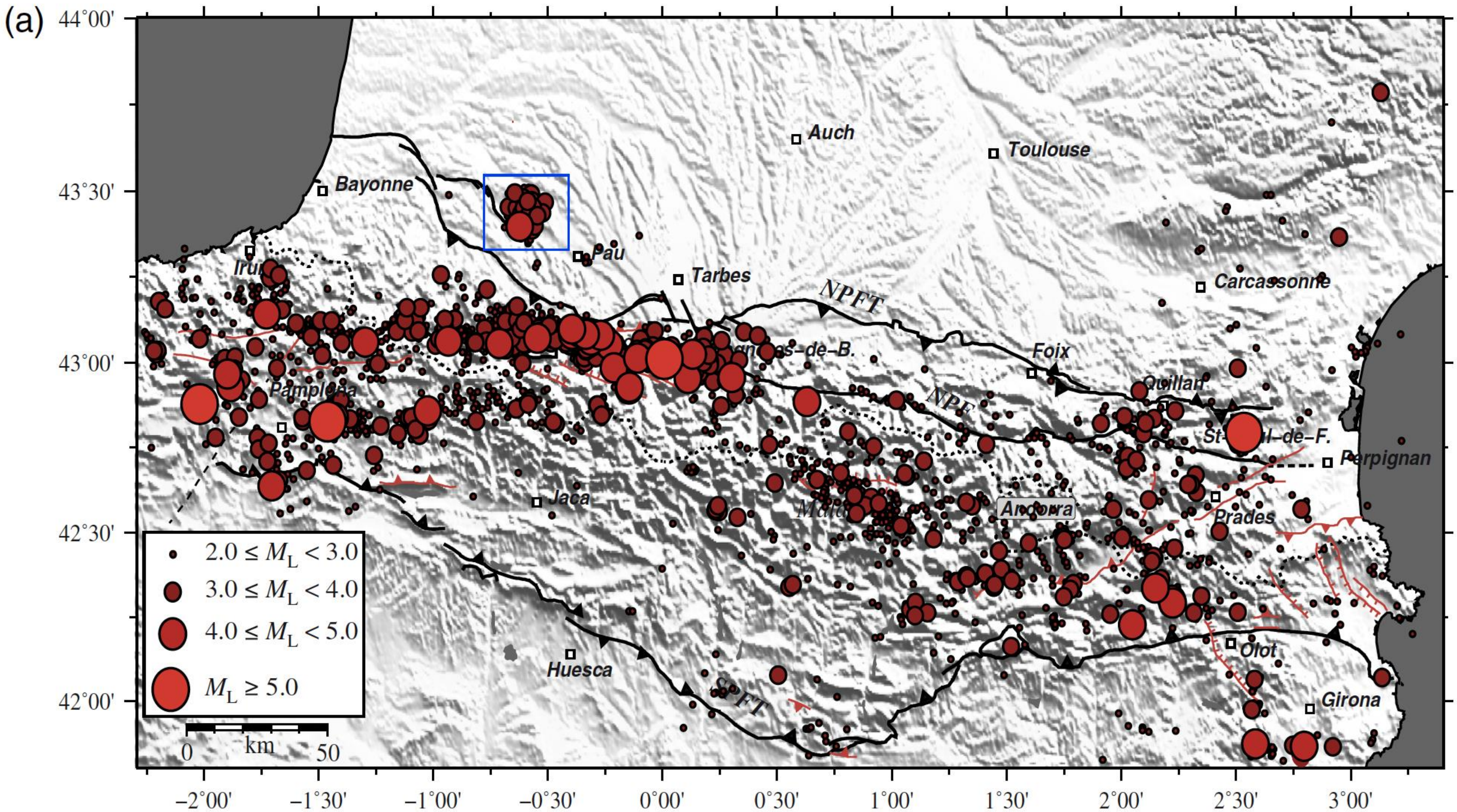

Grasso et al. (2021)

Lacq Gas Field
Spatial Distribution of Seismicity

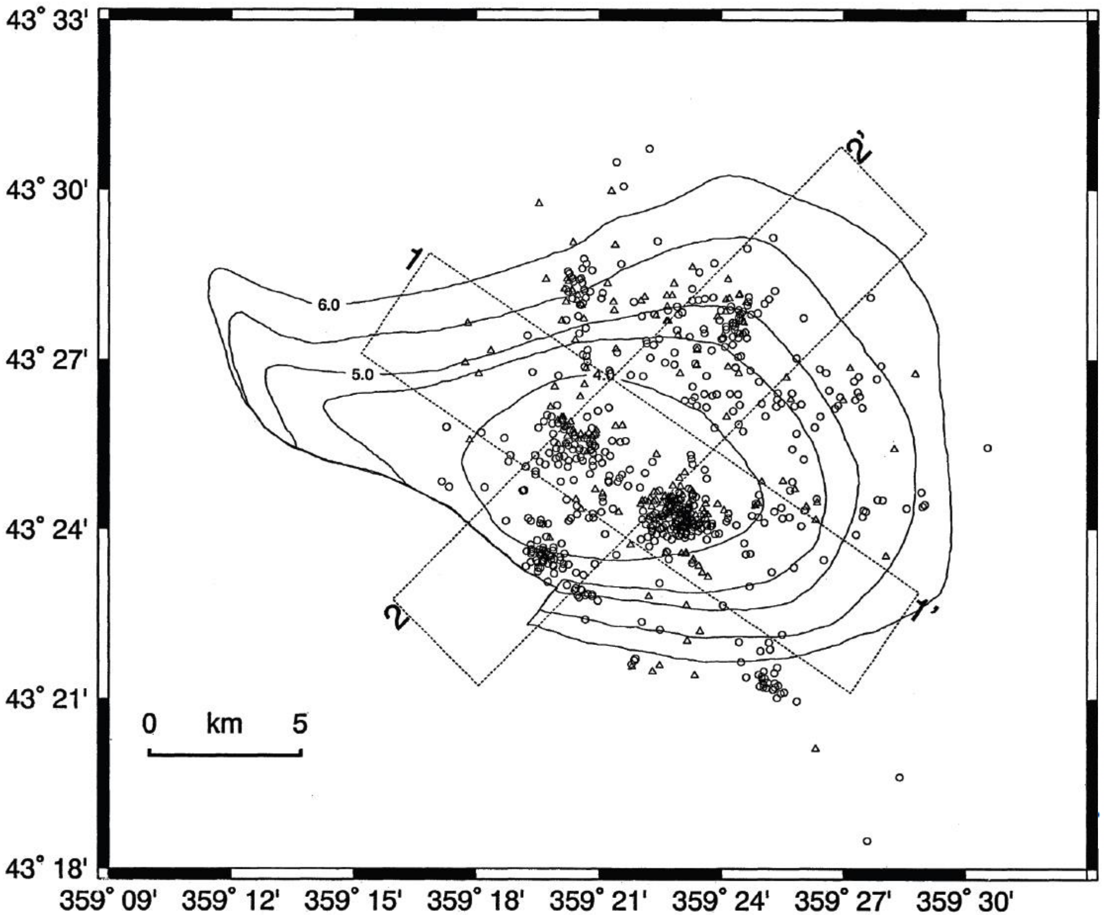

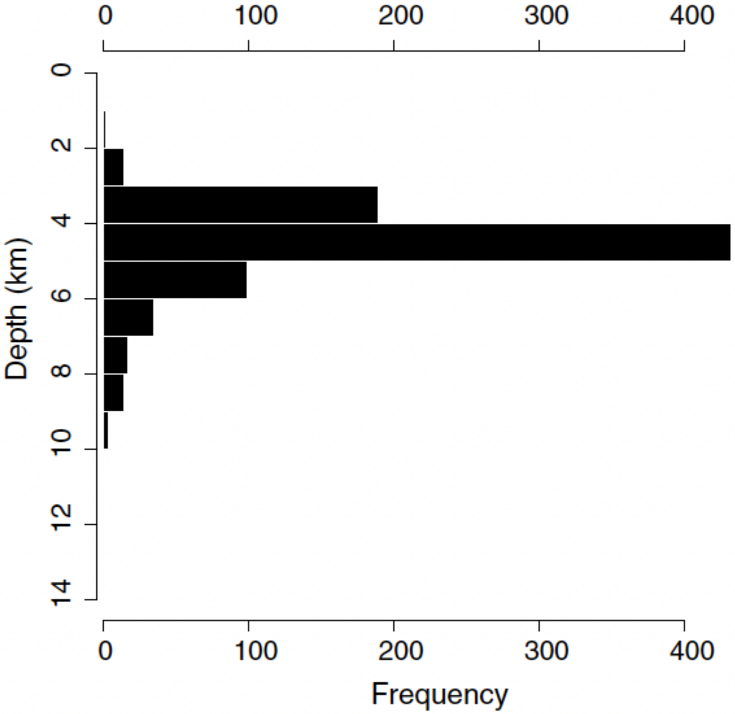

Segall, Grasso and Mossop (1994) Grasso et al. (2021)

Lacq Gas Field
Temporal Evolution of Seismicity

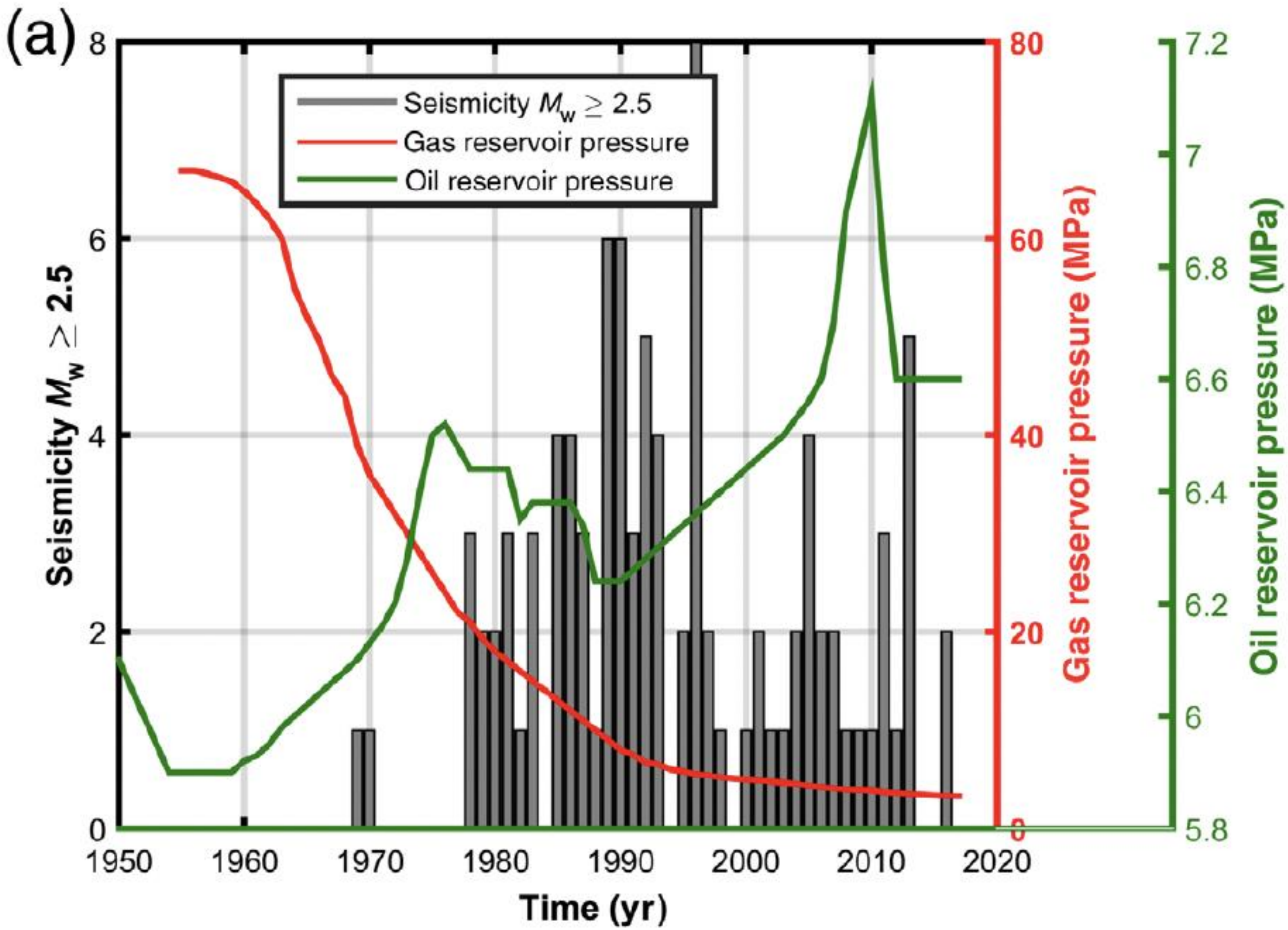

Grasso et al. (2021)

Lacq Gas Field
Subsidence

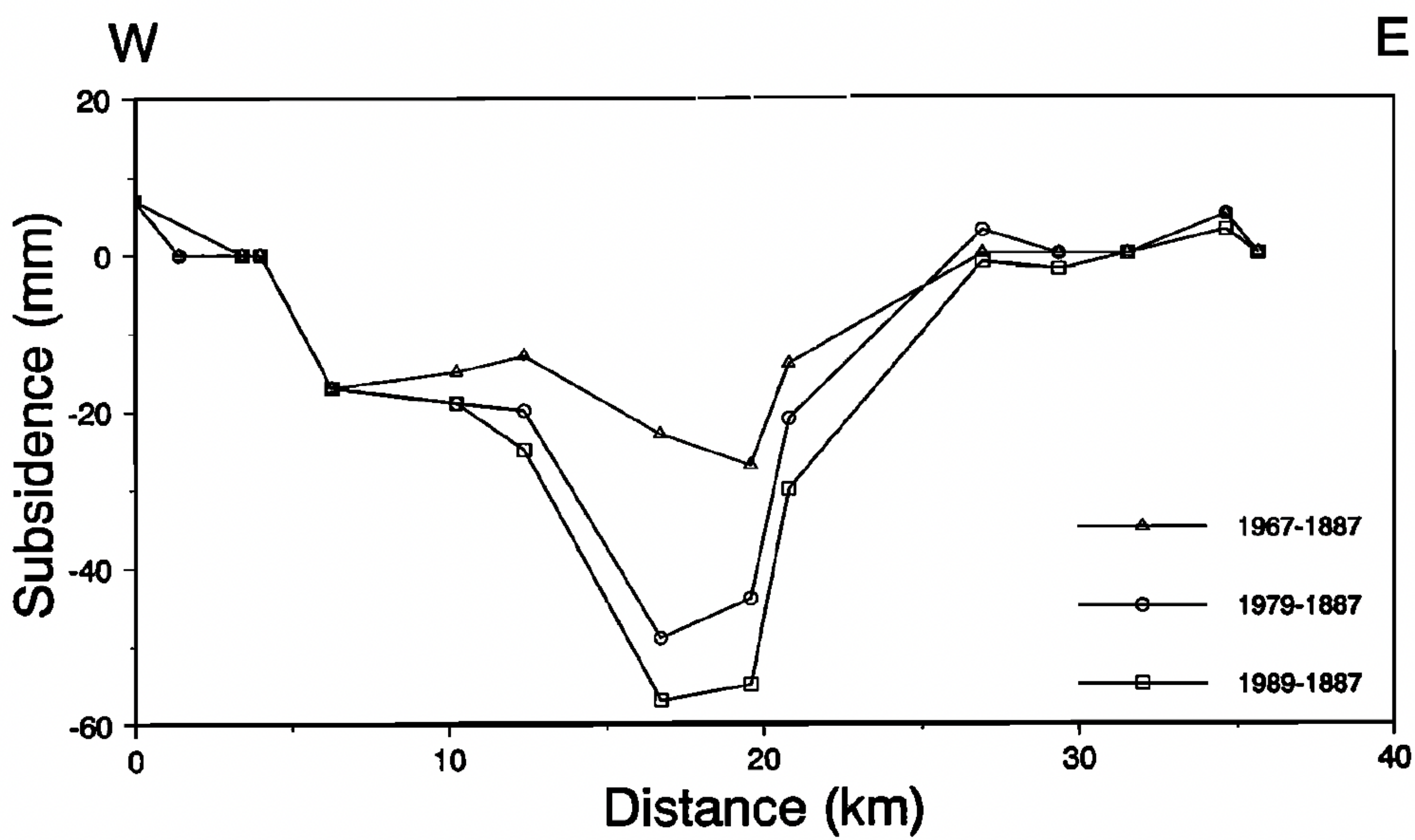

Segall, Grasso and Mossop (1994)

Lacq Gas Field
Subsidence

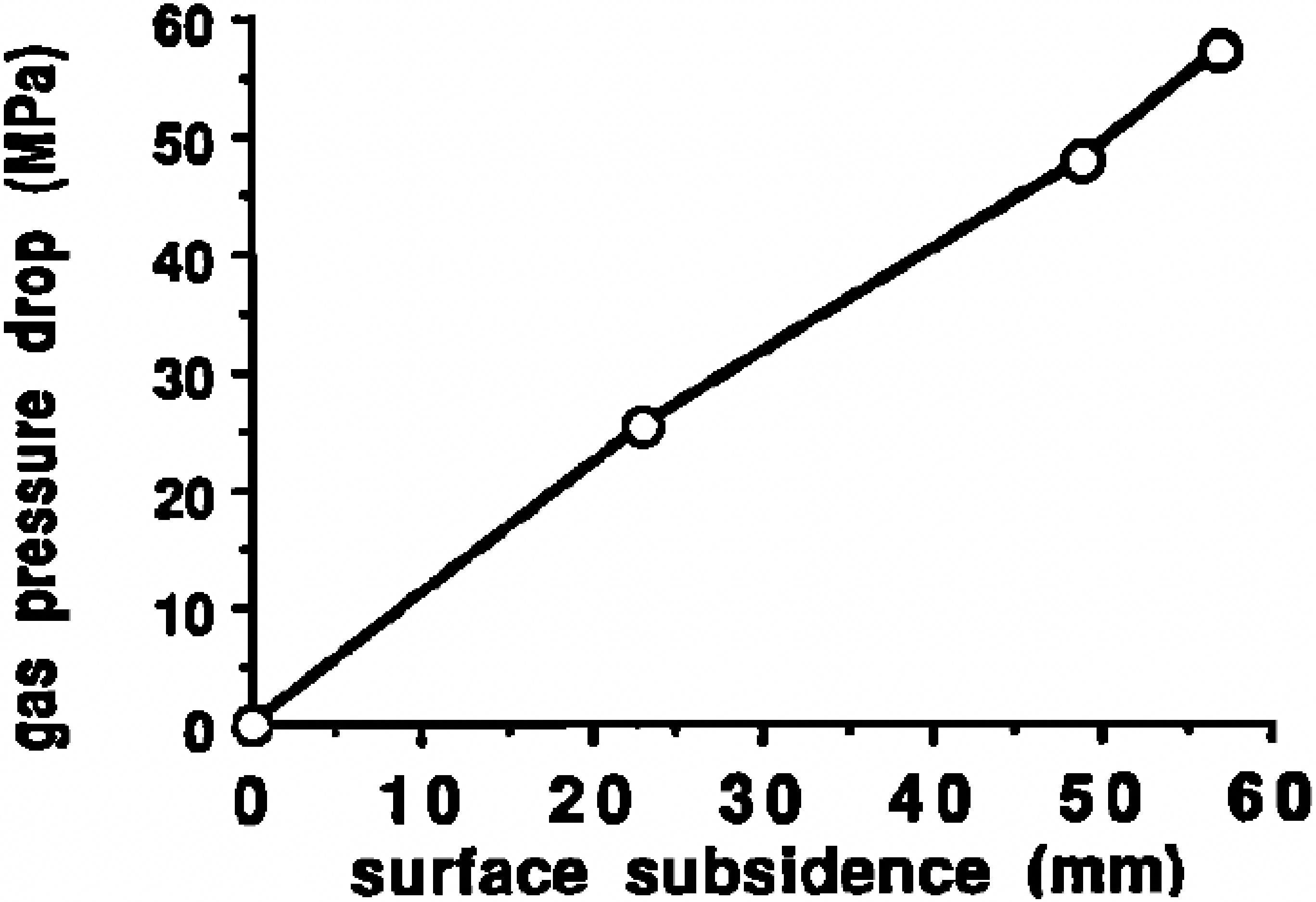

Segall, Grasso and Mossop (1994)

Lacq Gas Field
Poroelastic Modeling

Poroelastic stressing and induced seismicity near the Lacq gas field, southwestern France

Paul Segall

Department of Geophysics, Stanford University, Stanford, California

Jean-Robert Grasso

Laboratoire de Géophysique Interne et Tectonophysique, Observatoire de Grenoble, Grenoble France

Antony Mossop

Department of Geophysics, Stanford University, Stanford, California

Abstract. Hundreds of shallow, small to moderate earthquakes have occurred near the Lacq deep gas field in southwestern France since 1969. These earthquakes are clearly separated from tectonic seismicity occurring in the Pyrenees, 25 km to the southwest. The induced seismicity began when the reservoir pressure had declined by $\sim$ 30 MPa. Repeated leveling over the field shows localized subsidence reaching a maximum of 60 mm in 1989. Segall (1989) suggested that poroelastic stressing, associated with volumetric contraction of the reservoir rocks, is responsible for induced seismicity associated with fluid extraction. To test this model, we compare the observed subsidence and hypocentral distributions with the predicted displacement and stress fields. We find that the relationship between average reservoir pressure drop and subsidence is remarkably linear, lending support to the linear poroelastic model. Displacements and stresses are computed

Segall, Grasso and Mossop (1994)

Lacq Gas Field
Poroelastic Modeling

Table 1. Parameters Used in Calculations

Symbol	Quantity	Value
α	Biot Coefficient	0.25
ν	Poisson's Ratio	0.25
μ	Shear Modulus	2.3×10^4 MPa
Δp	Pressure Decline	60 MPa
T	Reservoir Thickness	250 m
d	Reservoir Depth	3.5 km
R	Reservoir Radius	7.0 km

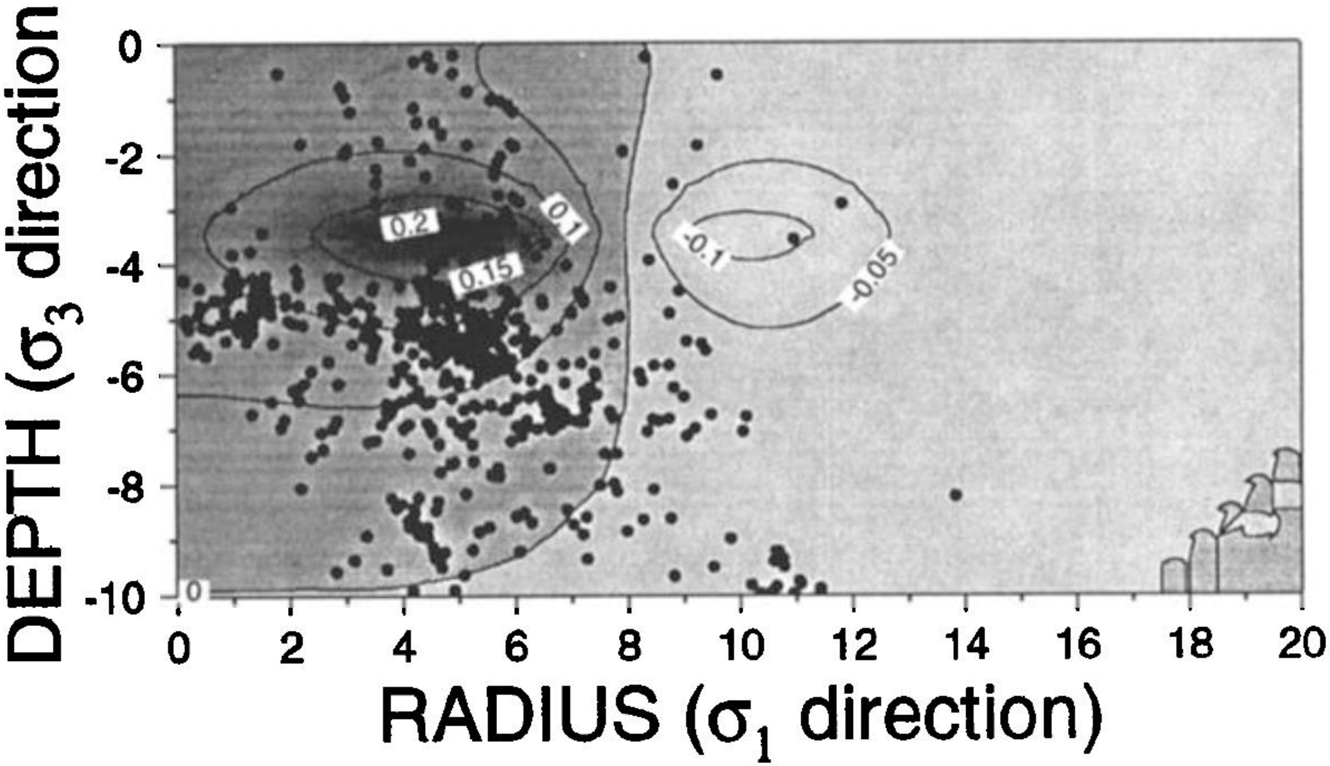

Segall, Grasso and Mossop (1994)

Lacq Gas Field
Poroelastic Modeling

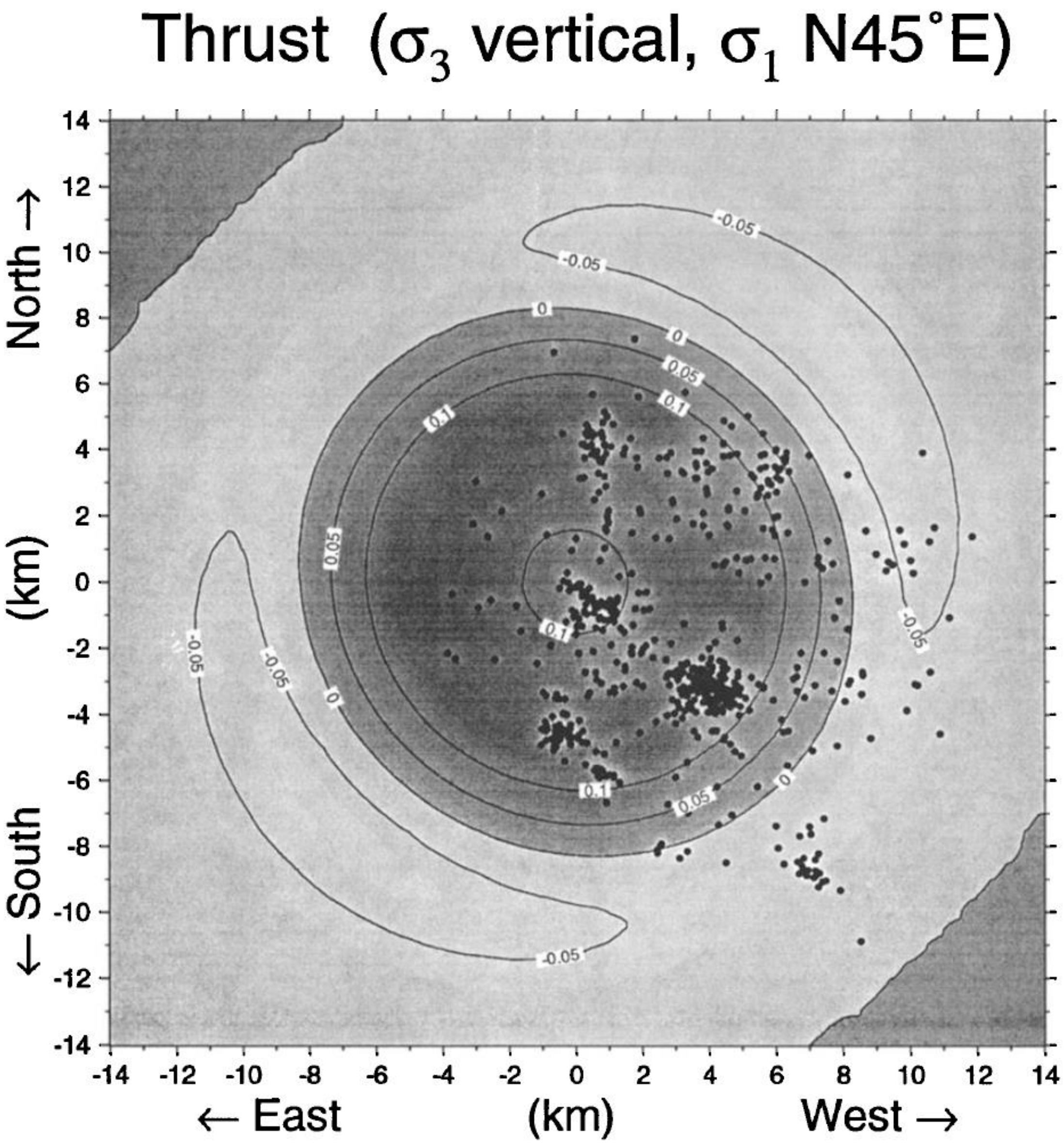

80% of the seismicity in the 1975–1993 period is located in areas where stress changes, as estimated from a reservoir depletion model, are positive

Stress changes are on the order of 0.1 – 0.2 MPa

Segall, Grasso and Mossop (1994)

Lacq Gas Field
Influence of Water Injection?

Did Wastewater Disposal Drive the Longest Seismic Swarm Triggered by Fluid Manipulations? Lacq, France, 1969–2016

Jean-Robert Grasso*[1], Daniel Amorese[2], and Abror Karimov[1]

ABSTRACT

The activation of tectonics and anthropogenic swarms in time and space and size remains challenging for seismologists. One remarkably long swarm is the Lacq swarm. It has been ongoing since 1969 and is located in a compound oil–gas field with a complex fluid manipulation history. Based on the overlap between the volumes where poroelastic model predicts stresses buildup and those where earthquakes occur, gas reservoir depletion was proposed to control the Lacq seismic swarm. The 2016 M_w 3.9, the largest event on the site, is located within a few kilometers downward the deep injection well. It questions the possible interactions between the 1955–2016 wastewater injections and the Lacq seismicity. Revisiting 60 yr of fluid manipulation history and seismicity indicates that the impacts of the wastewater injections on the Lacq seismicity were previously underevaluated. The main lines of evidence toward a wastewater injection cause are (1) cumulative injected volume enough in 1969 to trigger M_w 3 events, onset of Lacq seismicity; (2) 1976 injection below the gas reservoir occurs only a few years before the sharp increase in seismicity. It matches the onset of deep seismicity (below the gas reservoir, at the injection depth); (3) the (2007–2010) 2–3 folds increase in injection rate precedes 2013, 2016 top largest events; and (4) 75% of the 2013–2016 events cluster within 4–8 km depths, that is, close to and downward the 4.5 km deep injection well. As quantified by changepoint

Grasso et al. (2021)

Lacq Gas Field

Gas production & Water injection (1969-2016)

TABLE 1

Fluid Manipulation Phases, 1955–2016, Lacq Field

Lacq Fluid Manipulations (1955–2016)

Fluid Manipulation Phase	Extraction Operation (Depth, Type)	Injection Operation (Depth, Type)
Phase I (1955–1974)	3–5 km, Gas reservoir	0.7 km, Wastewater
Phase II (1974–2006)	3–5 km, Gas reservoir	4.5 km, Wastewater
Phase III (2006–2012)	3–5 km, Gas reservoir	0.7 and 4.5 km, Wastewater
Phase IV (2013–2016)	Negligible	4.5 km, Wastewater

1955 is the onset of the gas extraction.

Grasso et al. (2021)

Lacq Gas Field

Gas production & Water injection (1969-2016)

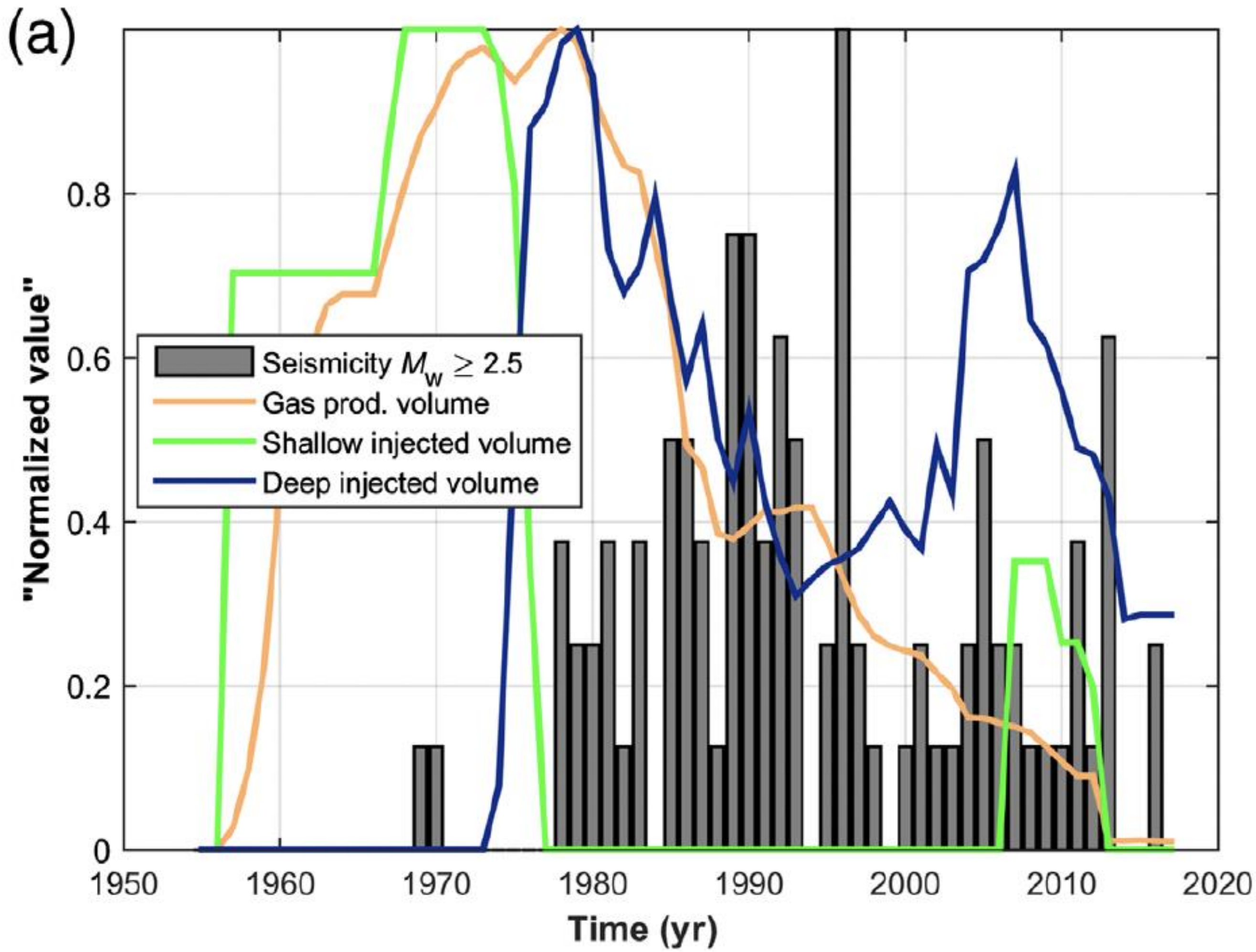

Grasso et al. (2021)

Induced earthquakes related to gas production

Reviewed two classic case studies of gas production induced earthquakes at Gazli, Uzbekistan and Lacq, France

Both fields were located relatively seismically quiescent regions prior to the onset of gas production

Both fields fit the established mechanism for gas extraction related events: poroelastic response to mass removal

One underappreciated aspect of both the Gazli and Lacq cases may be the combined effects of stresses induced by gas extraction and pressure increases from deep(er) water injection. Further modeling of the combined effect may be warranted.

Groningen M_{MAX} Workshop II, 13-17 June 2022
Infinity Building, South Amsterdam, The Netherlands

Evaluating Proposals of Human-Induced Earthquakes

Gillian R. Foulger
Durham University, U.K.

The team

- Leaders:
  - Prof. Gillian Foulger
  - Prof. Jon Gluyas
- Post-docs:
  - Dr. Miles Wilson
  - Dr. Max Wilkinson
  - Dr. Najwa Mhana
  - Dr. Timur Tezel

Earth-Science Reviews 178 (2018) 438–514

Contents lists available at ScienceDirect

Earth-Science Reviews

journal homepage: www.elsevier.com/locate/earscirev

Invited review

Global review of human-induced earthquakes

Gillian R. Foulger[a,*], Miles P. Wilson[a], Jon G. Gluyas[a], Bruce R. Julian[a], Richard J. Davies[b]

[a] Department of Earth Sciences, Durham University, Durham DH1 3LE, UK
[b] School of Civil Engineering and Geosciences, Newcastle University, Newcastle upon Tyne NE1 7RU, UK

ABSTRACT

The Human-induced Earthquake Database, *HiQuake*, is a comprehensive record of earthquake sequences postulated to be induced by anthropogenic activity. It contains over 700 cases spanning the period 1868–2016. Activities that have been proposed to induce earthquakes include the impoundment of water reservoirs, erecting tall buildings, coastal engineering, quarrying, extraction of groundwater, coal, minerals, gas, oil and geothermal fluids, excavation of tunnels, and adding material to the subsurface by allowing abandoned mines to flood and injecting fluid for waste disposal, enhanced oil recovery, hydrofracturing, gas storage and carbon sequestration. Nuclear explosions induce earthquakes but evidence for chemical explosions doing so is weak. Because it is currently impossible to determine with 100% certainty which earthquakes are induced and which not, *HiQuake* includes all earthquake sequences proposed on scientific grounds to have been human-induced regardless of credibility. Challenges to constructing *HiQuake* include under-reporting which is ~30% of M ~4 events, ~60% of M ~3 events and ~90% of M ~2 events. The amount of stress released in an induced earthquake is not necessarily the same as the anthropogenic stress added because pre-existing tectonic stress may also be released. Thus earthquakes disproportionately large compared with the associated industrial activity may be induced. Knowledge of the magnitude of the largest earthquake that might be induced by a project, M_{MAX}, is important for hazard reduction. Observed M_{MAX} correlates positively with the scale of associated industrial projects, fluid injection pressure and rate, and the yield of nuclear devices. It correlates negatively with calculated inducing stress change, likely because the latter correlates inversely with project scale. The largest earthquake reported to date to be induced by fluid injection is the 2016 M 5.8 Pawnee, Oklahoma earthquake, by water-reservoir impoundment the 2008 M ~8 Wenchuan, People's Republic of China, earthquake, and by mass removal the 1976 M 7.3 Gazli, Uzbekistan earthquake. The minimum amount of anthropogenic stress needed to induce an

HiQuake: www.inducedearthquakes.org

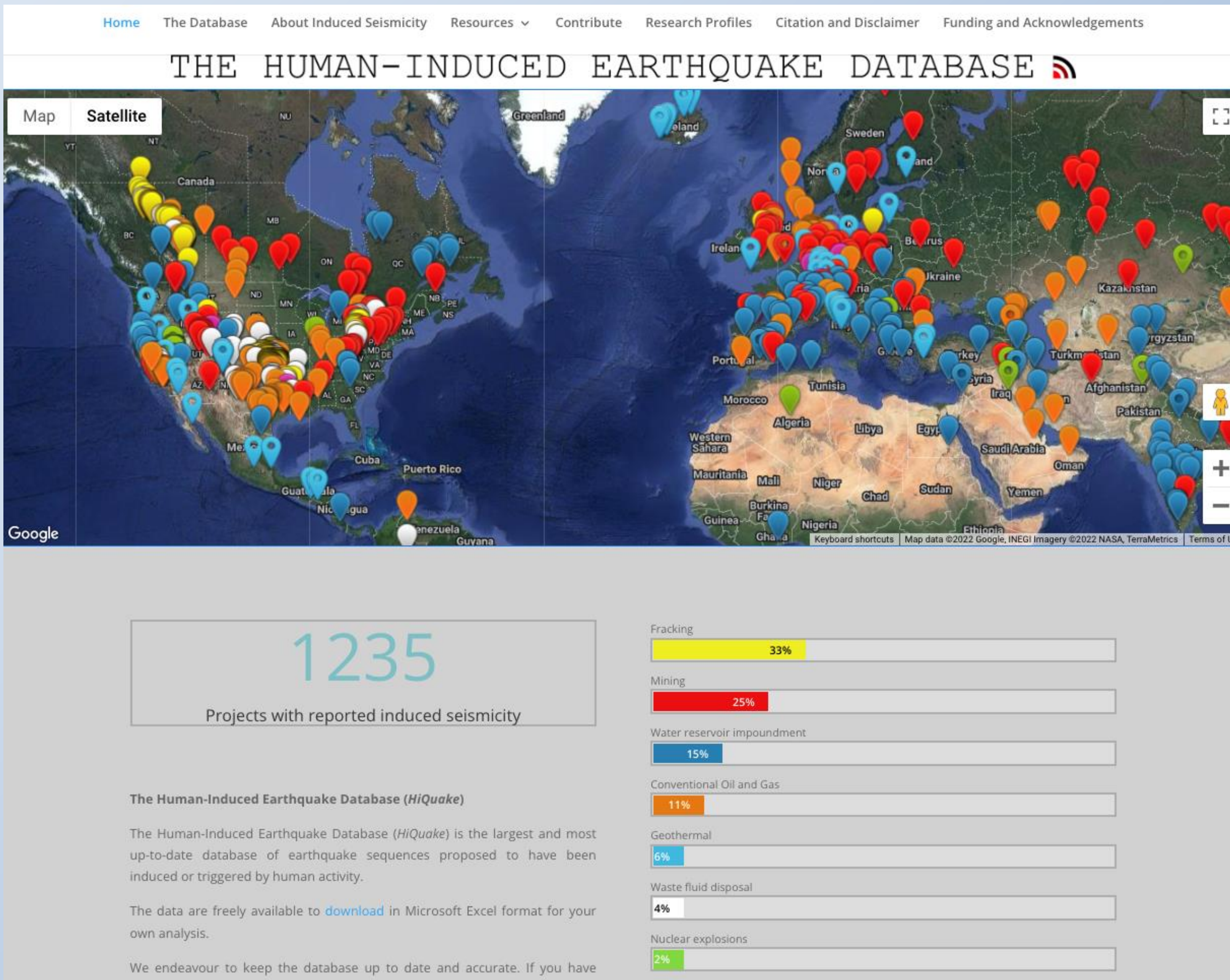

HiQuake: Website analytics

- Released: 26th January 2017
- Total number visits: 412,638
- No. multi-visit users: 3,560
- No. countries with at least one user: 184 (/195)

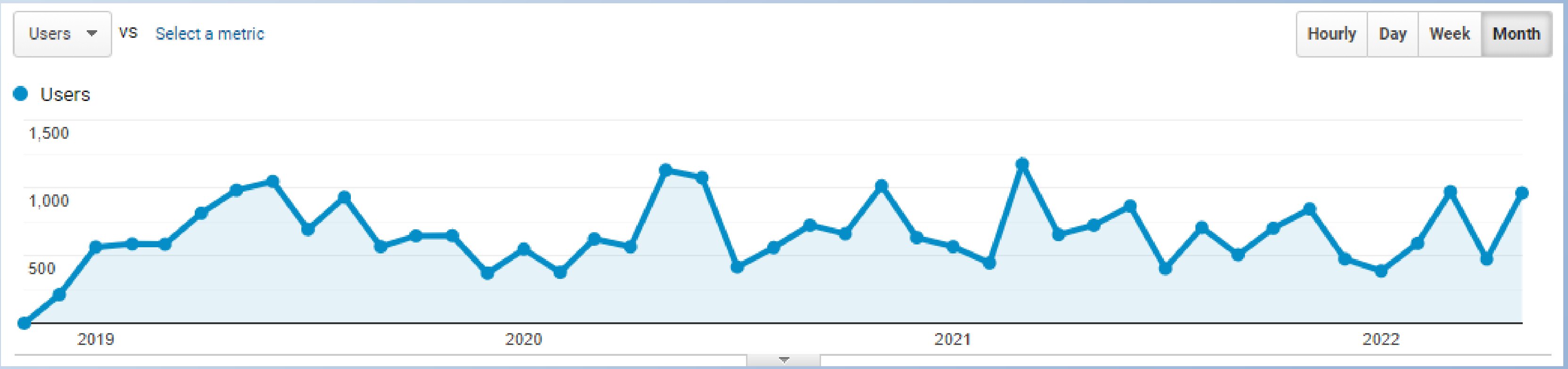

HiQuake: Website analytics

	Country	Users	% Users
1.	Australia	6,107	22.47%
2.	United States	4,321	15.90%
3.	India	2,770	10.19%
4.	South Africa	1,969	7.24%
5.	China	1,273	4.68%
6.	United Kingdom	1,076	3.96%
7.	South Korea	708	2.60%
8.	France	638	2.35%
9.	Japan	629	2.31%
10.	Italy		

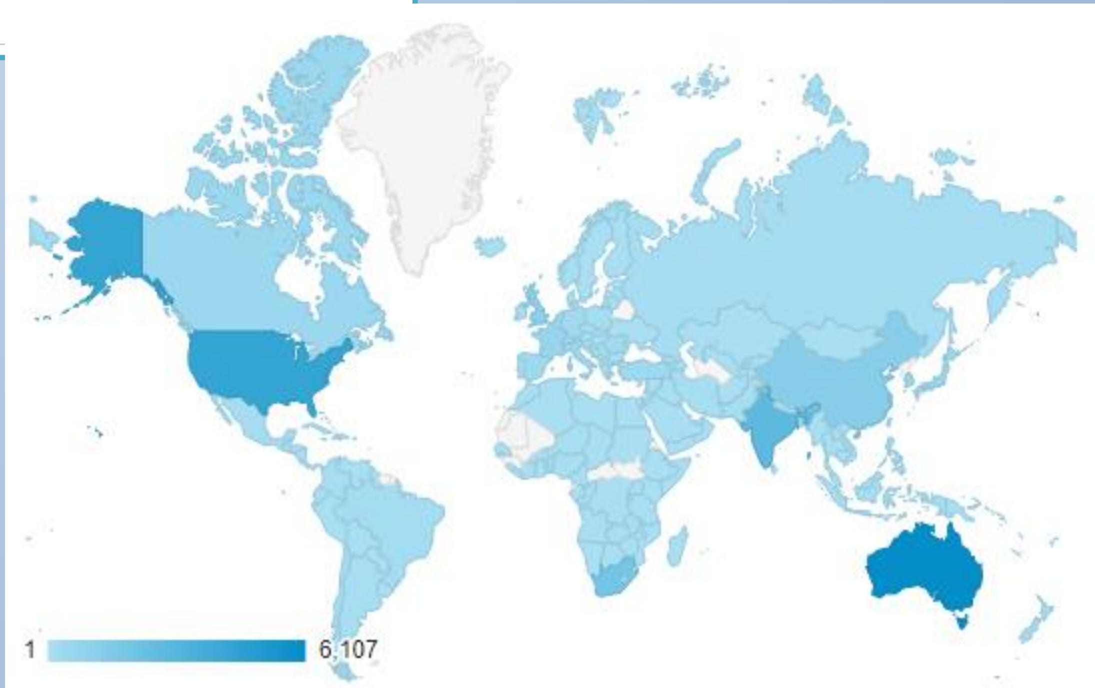

HiQuake: Paper citations

Foulger, G.R., Wilson, M.P., Gluyas, J.G., Julian, B.R., & Davies, R.J. (2018). Global review of human-induced earthquakes. *Earth-Sci. Rev.*, **178**, 438-514

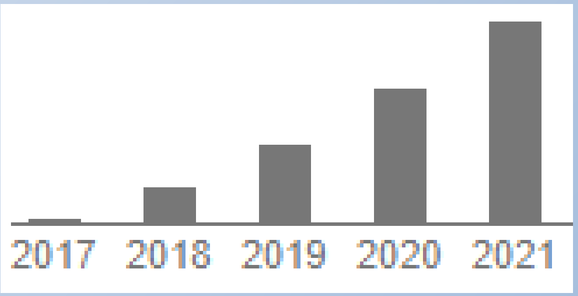

324 citations

Wilson, M.P., Foulger, G.R., Gluyas, J.G., Davies, R.J., & Julian, B.R. (2017). *HiQuake*: The human-induced earthquake database. *Seismol. Res. Lett.*, **88**, 1560-1565

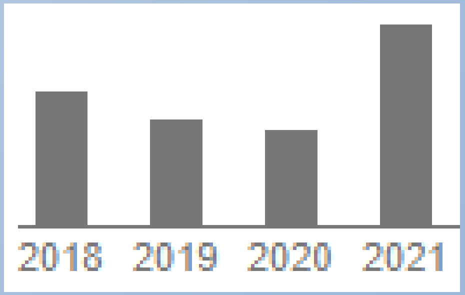

66 citations

Problems

- Starting problem: No way of knowing if a proposal of human-induction correct or not
  - Upfront decision: – include all proposals
  - Opinion on reliability user's responsibility
- Ending problem: Stakeholders wanted guidance on reliability of cases
  - But a non-verifiable post-dictive problem!
  - necessitated expert-opinion approach – will be bias and noise
  - We focused on reducing both bias and noise

How to assess the strength of cases?

- To reduce bias among expert opinions – use questionnaires
- History of questionnaires:
  - Davis & Frohlich [1993]
  - Davis et al. [1995]
  - Frohlich et al. [2016]
  - Verdon et al. [2019]

Example: Davis & Frohlich [1993]

Designed for fluid injection 7 questions $\geq$ 5 yes = probably induced 4 yes = ambiguous $\leq$ 3 yes = unlikely to be induced
1. Background seismicity: Are these events the first known earthquakes of this character in the region?
2. Temporal correlation: Is there a clear correlation between the time of injection and the times of seismic activity?
3a. Spatial correlation: Are epicenters near the wells?
3b. Spatial correlation: Do some earthquakes occur at depths comparable to the depth of injection?
3c. Local geology: If some earthquakes occur away from wells, are there known geologic structures that may channel fluid flow to the sites of the earthquakes?
4a. Injection practices: Are changes in fluid pressure sufficient to encourage seismic or aseismic failure at the bottom of the well?
4b. Injection practices: Are changes in fluid pressure sufficient to encourage seismic or aseismic failure at the hypocentral locations?

Example: Davis & Frohlich [199

Designed for fluid injection 7 questions ≥ 5 yes = probably in 4 yes = ambiguou ≤ 3 yes = unlikely to be in
1. Background seismicity: Are these events the first known ea region?
2. Temporal correlation: Is there a clear correlation between the seismic activity?
3a. Spatial correlation: Are epicenters near the wells?
3b. Spatial correlation: Do some earthquakes occur at depths compar the depth of injection?
3c. Local geology: If some earthquakes occur away from wells, are there known geologic structures that may channel fluid flow to the sites of the earthquakes?
4a. Injection practices: Are changes in fluid pressure sufficient to encourage seismic or aseismic failure at the bottom of the well?
4b. Injection practices: Are changes in fluid pressure sufficient to encourage seismic or aseismic failure at the hypocentral locations?

Problems:

- subjective
- narrow
- restricted
- …etc.

Structure of Project: Three Phases

Goal: Produce the best possible gradings for all the cases in *HiQuake*

1. Design & trial suite of questionnaire schemes
2. Develop a final, generic scheme – E-PIE
3. Apply to all 1235 cases in *HiQuake*

Phase 1: Design & trial suite of questionnaire schemes

Phase 1: Design & trial schemes

- Three questionnaire schemes developed:
  - "Strength of Case" (SoC; "quick") scheme – subjective
  - "Generic Verdon" (GV) scheme – hybrid
  - "Number of Evidence" (NoE) scheme – objective

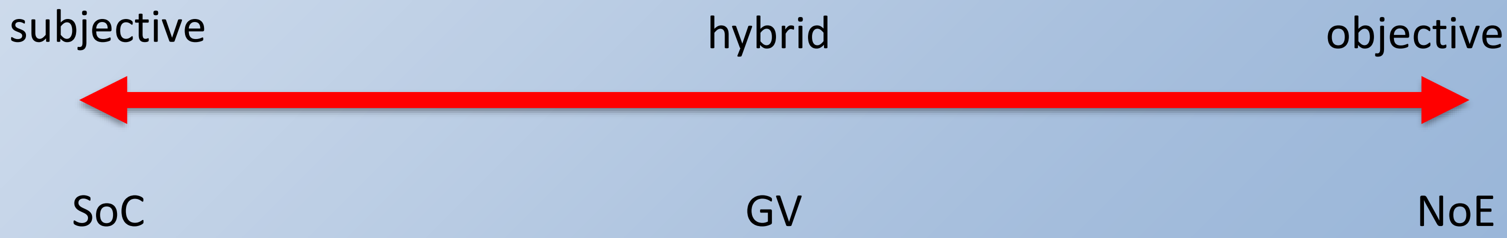

Strength of Case (SoC; “quick”) scheme

- Subjective

1	Case very weak/highly unlikely
2	Case weak/unlikely
3	Case moderate/plausible
4	Case strong/likely
5	Case very strong/highly likely

Generic Verdon (GV) scheme

- Hybrid, 7 questions

6. Is there a plausible mechanism to have caused the events?	
a. No significant pore-pressure increase or decrease occurred that can be linked in a plausible manner to the event hypocentral position	-5
b. Some pore-pressure or poroelastic stress change occurred (increase in pore-pressure or positive Coulomb Failure Stress [CFS]>0.1 MPa, or a decrease in pore pressure of > 1 MPa) that can be linked in a plausible manner to the event hypocentral position	+2
c. A large pore-pressure or poroelastic stress change occurred (increase in pore pressure or positive CFS >1 MPa, or a decrease in pore pressure of > 5 MPa) that can be linked in a plausible manner to the event hypocentral position	+5

6. Do the non-seismic data, e.g. pore-pressure changes, support the suggested induction process?	
a. The non-seismic data provide little or no support for the proposed induction process	−5
b. The non-seismic data support the proposed induction process to some extent	2
c. The non-seismic data support the proposed induction process strongly	5

Verdon JP, Baptie BJ, Bommer JJ (2019) An Improved Framework for Discriminating Seismicity Induced by Industrial Activities from Natural Earthquakes. *Seismol Res Lett* **90**: 1592-1611

Number of Evidence (NoE) scheme

- Objective

1. Background seismicity
2. Epicentral location
3. Hypocentral depth
4. Temporal correlations
5. Physical model
6. Stress: industrial
7. Swarm/aftershock activity
8. Stress
9. Earthquake magnitude
10. b-value
11. Total number of earthquakes
12. Focal mechanisms
13. Direct nucleation effects observed
14. Surface deformation

Results studied

- Applied to 55 large-M_{MAX} cases

- Two result types:
  - Dataset quality
  - Strength of evidence for human induction

- Between-analyst correlations
- Between-scheme correlations

Results between analyst: Generic Verdon

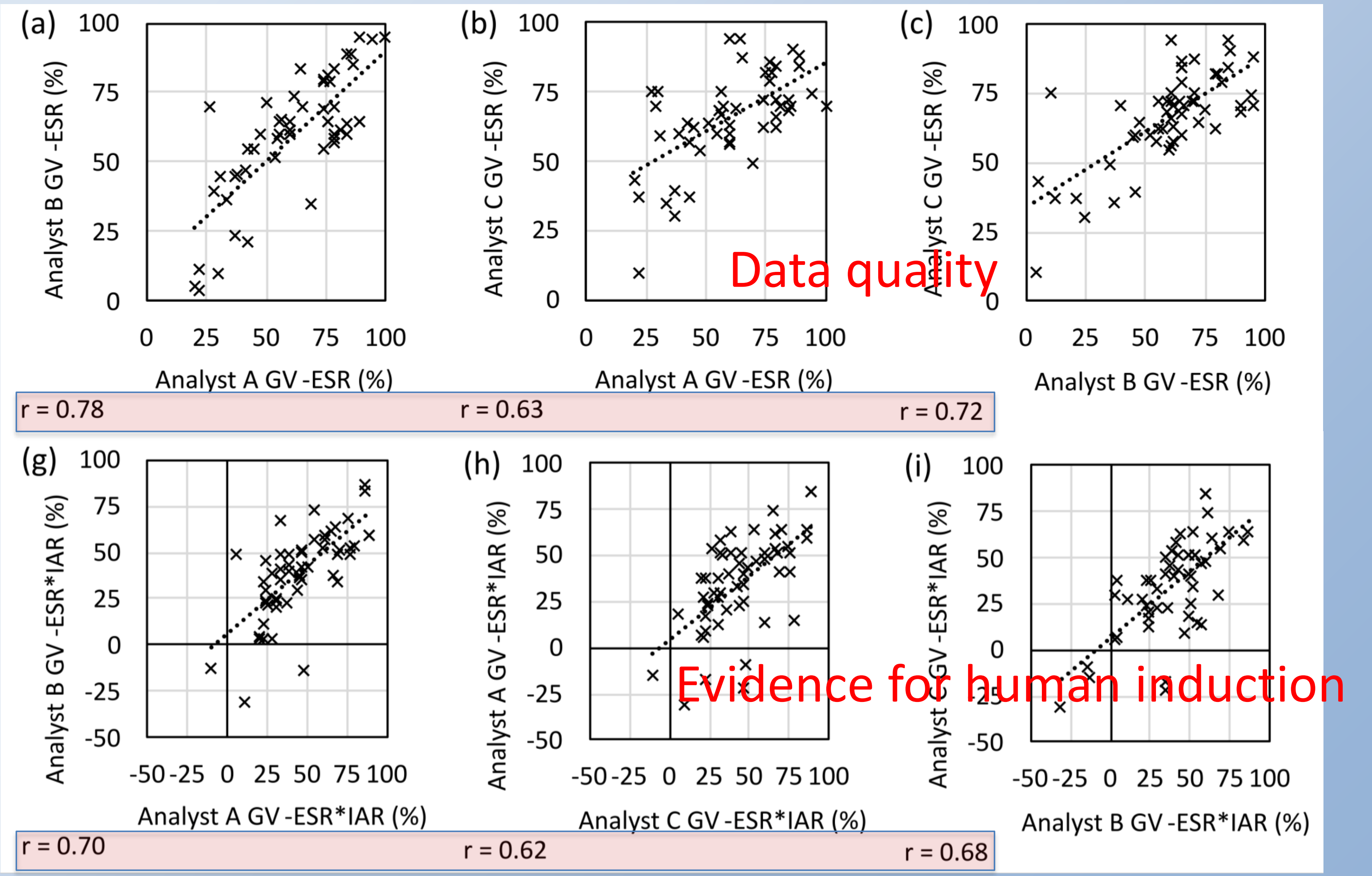

Results between schemes:
Generic Verdon *vs.* Strength of Case ("quick")

Evidence for human induction

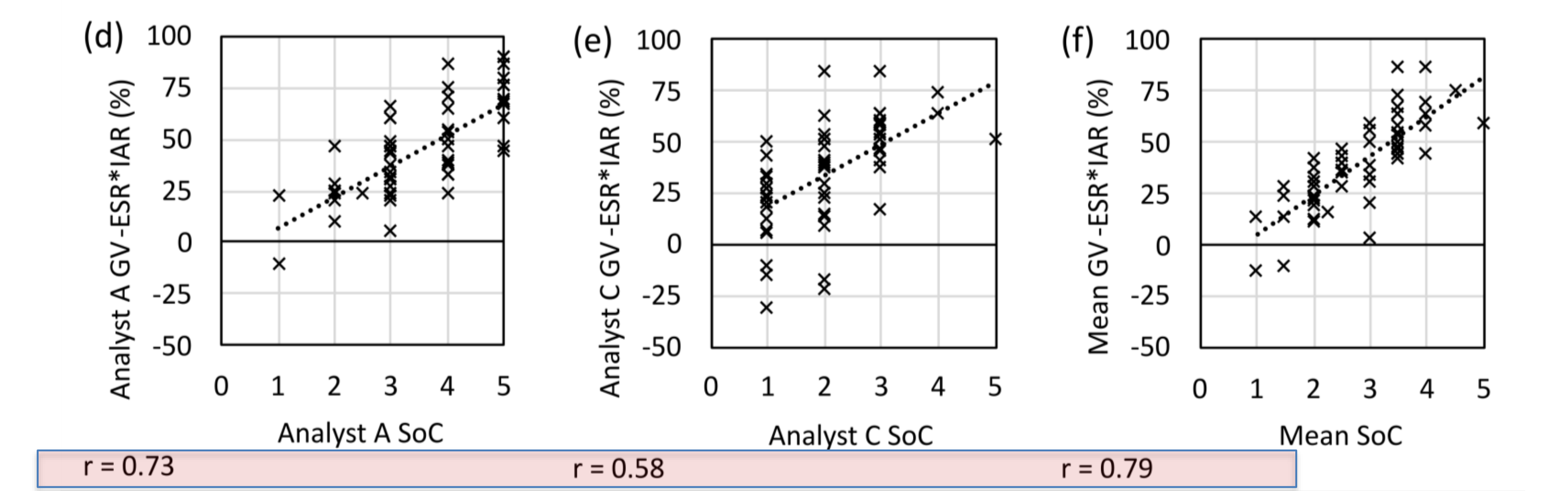

Results between schemes:
Generic Verdon *vs.* Strength of Case (“quick”)

Evidence for human induction

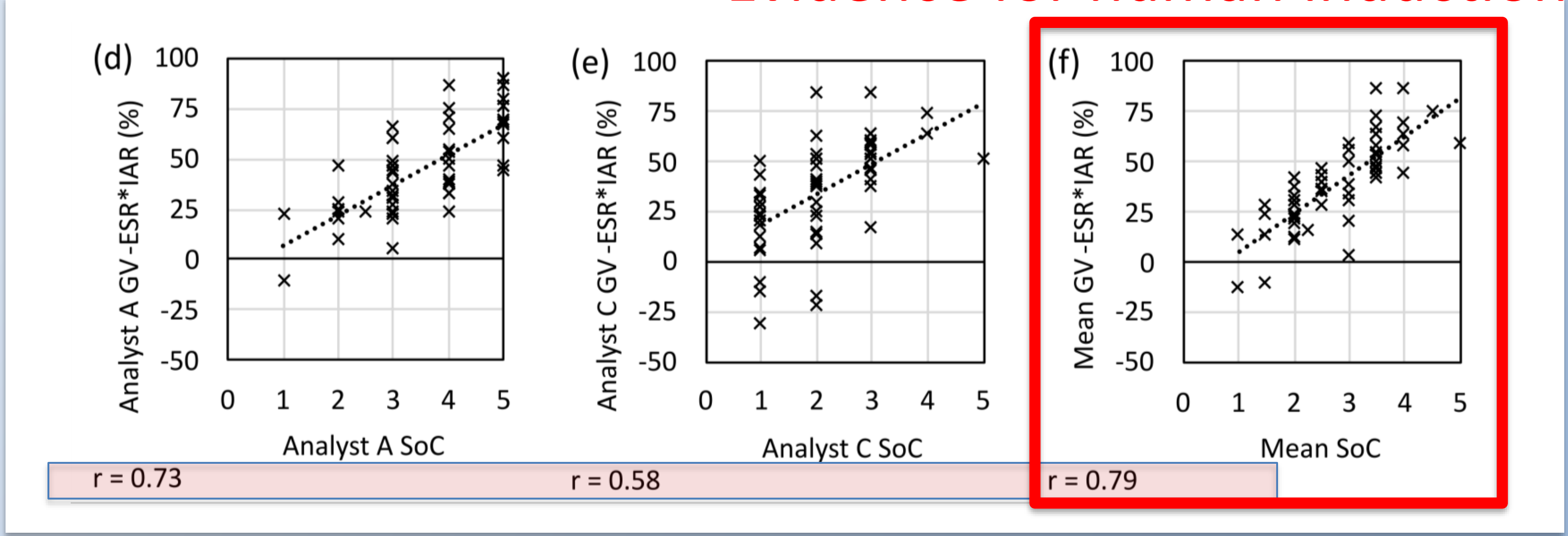

Evidence for human-induction *vs.* M_{MAX}

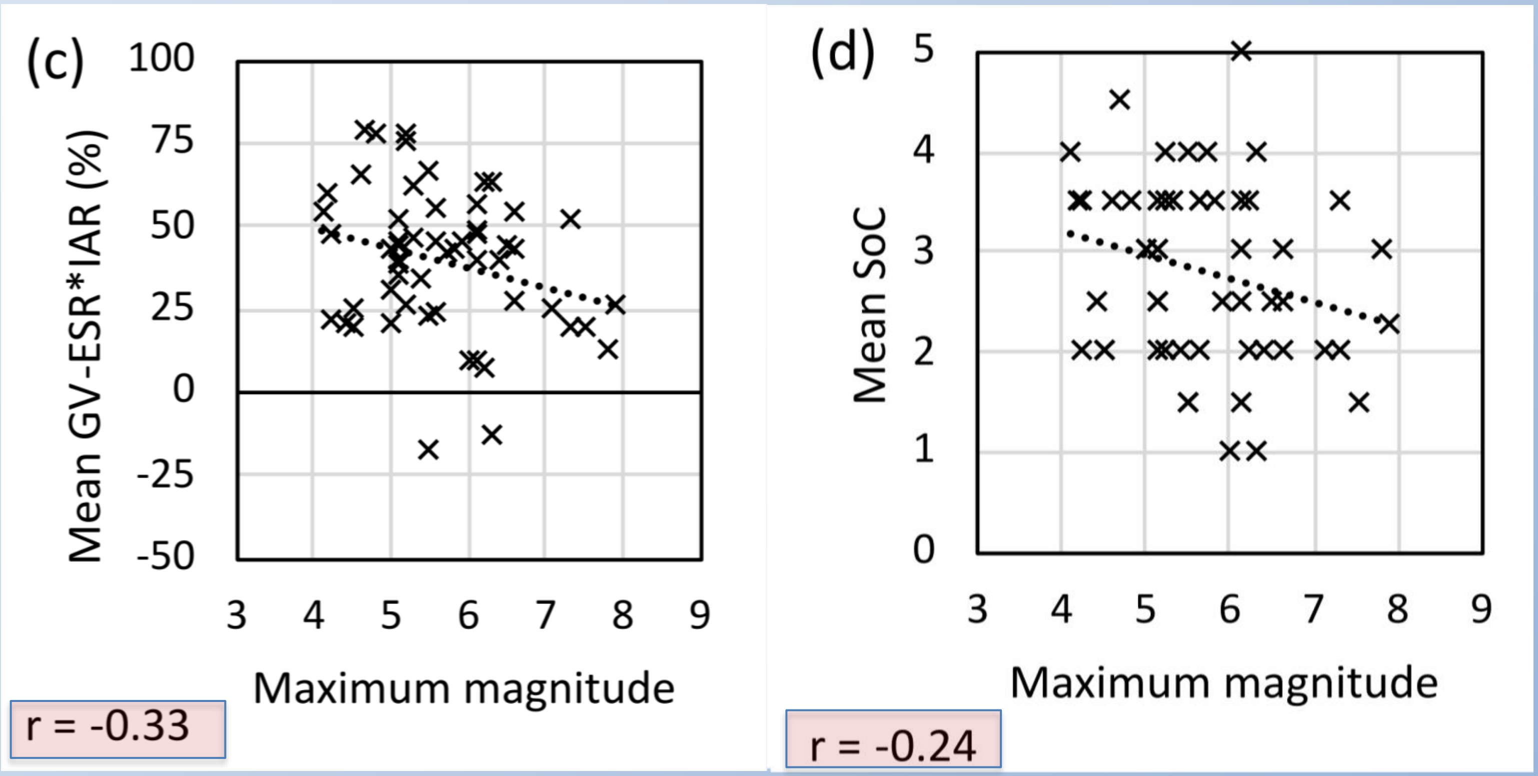

Application to “natural” earthquakes

Evidence for human induction

Case	Generic Verdon (%)	Strength of Case (%)	Number of Evidence (%)
Reykjanes Peninsula, Iceland	-17 -35	20 20	0 0
Coso geothermal field, California	-24 -29	20 20	0 0
Lombok, Italy (2018)	-52 -34	20 20	0 0
Tbilisi, Georgia (2002)	26 -34	20 20	0 0

Application to “natural” earthquakes

Evidence for human induction

Case	Generic Verdon (%)	Strength of Case (%)	Number of Evidence (%)
Reykjanes Peninsula, Iceland	-17 -35	20 20	0 0
Coso geothermal field, California	-24 -29	20 20	0 0
Lombok, Italy (2018)	-52 -34	20 20	0 0
Tbilisi, Georgia (2002)	26 -34	20 20	0 0

Phase 1: Conclusions

- Developed & trialed 3 schemes:
  - subjective SoC scheme
  - hybrid GV scheme
  - objective NoE scheme
- Between-analyst variation: correlation coeff's R ~ 0.8 to 0.4
- Mean SoC ("quick") results comparable to GV (R ~0.8)
- M_{MAX} correlates weakly negatively with evidence of induction
- GV scheme may recognize new human-induced earthquakes

Phase 2: Develop a final, generic scheme

E-PIE

(Evaluating Proposals of human-Induced Earthquakes)

Phase 2: E-PIE generic scheme

Orientation	
How plausible is the proposed induction mechanism? • Is it a well-established phenomenon? • Is it reported for multiple localities? **How wide, in space and time, is the range of likely environmental modulation?** • Only near-field, rapid response to operations likely • Up to medium-field, medium-term response to operations likely • Out to far-field, delayed response to operations likely	
Proposed-induced earthquakes (PIEs)	
1. PIEs–temporal: Did the PIE sequence onset before, during or after the industrial activity?	10
a. Insufficient information available	
b. The PIE sequence began before the onset of the industrial activity	Exit
c. The PIE sequence began while the industrial activity was minimal OR after its cessation	
d. The PIE sequence began while the industrial activity was substantial	
2. PIEs–epicenters: Is there spatial collocation between the PIEs and the likely area of environmental modulation by the industrial activity?	100
a. Insufficient information available	
b. The PIEs are outside the likely area of environmental modulation by the industrial activity	
c. The PIEs are peripheral to the likely area of environmental modulation by the industrial activity	
d. The PIEs are within the likely area of environmental modulation by the industrial activity	
3. PIEs–hypocenters: Is there spatial collocation between the PIEs and the likely volume of environmental modulation by the industrial activity?	100
a. Insufficient information available	
b. The PIEs are beneath the likely volume of environmental modulation by the industrial activity	
c. The PIEs are peripheral to the base of the likely volume of environmental modulation by the industrial activity	
d. The PIEs are within the likely volume of environmental modulation by the industrial activity	
4. PIEs–temporal: Is there temporal correlation between the PIEs and specific industrial events?	100
a. Insufficient information available	
b. There is little or no temporal correlation between the PIEs and specific industrial events	
c. There is weak temporal correlation between the PIEs and specific industrial events	
d. There is strong temporal correlation between the PIEs and specific industrial events	

Pre-industrial earthquakes	
5. Pre-industrial earthquakes–epicenters: Is there evidence for pre-industrial earthquakes at or near the site of the PIEs?	10
a. Insufficient information available	
b. Pre-industrial earthquakes occurred at or near the site of the PIEs	
c. Pre-industrial earthquakes occurred in the wider region around the site of the PIEs	
d. Pre-industrial earthquakes did not occur at or near the site of the PIEs or in the wider region around it	
6. Pre-industrial earthquakes–hypocenters: Is there evidence for pre-industrial earthquakes in the same volume as the PIEs?	10
a. Insufficient information available	
b. Pre-industrial earthquakes occurred at or near the site of the PIEs at similar or shallower depths	
c. Pre-industrial earthquakes occurred in the wider region around the site of the PIEs at similar or shallower depths	
d. Pre-industrial earthquakes did not occur at or near the site of the PIEs or in the wider region around it at similar or shallower depths	
Additional data	
7. Focal mechanisms: Are the focal mechanisms consistent with a natural and/or induced earthquake cause?	10
a. Insufficient information available	
b. The focal mechanisms ARE consistent with the regional stress and NOT consistent with the proposed induction mechanism	
c. The focal mechanisms ARE consistent with the regional stress and ARE consistent with the proposed induction mechanism OR The focal mechanisms are NOT consistent with the regional stress and NOT consistent with the proposed induction mechanism	
d. The focal mechanisms are NOT consistent with the regional stress and ARE consistent with the proposed induction mechanism	
8. Other–seismic data: Are there other seismic data to support a natural or induced cause, *e.g.*, swarm, foreshock-aftershock pattern, b-value, total number of earthquakes, stress release corresponding to the earthquake magnitude or seismicity?	10
a. Insufficient information available	
b. Other seismic data support a natural origin	
c. Other seismic data are equivocal	
d. Other seismic data support an induced origin	
9. Other–non-seismic data: Are there non-seismic data that support a natural or induced cause, *e.g.*, direct nucleation effects, precursory surface deformation?	10
a. Insufficient information available	
b. The non-seismic data support a natural origin	
c. The non-seismic data are equivocal	
d. The non-seismic data support an induced origin	

Phase 2: Develop a final, generic scheme

Orientation **How plausible is the proposed induction mechanism?** • Is it a well-established phenomenon? • Is it reported for multiple localities? **How wide, in space and time, is the range of likely environmental modulation?** • Only near-field, rapid response to operations likely • Up to medium-field, medium-term response to operations likely • Out to far-field, delayed response to operations likely	
Proposed-induced earthquakes (PIEs)	
1. PIEs–temporal: Did the PIE sequence onset before, during or after the industrial activity?	10
2. PIEs–epicenters: Is there spatial collocation between the PIEs and the likely area of environmental modulation by the industrial activity?	100
3. PIEs–hypocenters: Is there spatial collocation between the PIEs and the likely volume of environmental modulation by the industrial activity?	100
4. PIEs–temporal: Is there temporal correlation between the PIEs and specific industrial events?	100
Pre-industrial earthquakes	
5. Pre-industrial earthquakes–epicenters: Is there evidence for pre-industrial earthquakes at or near the site of the PIEs?	10
6. Pre-industrial earthquakes–hypocenters: Is there evidence for pre-industrial earthquakes in the same volume as the PIEs?	10
Additional data	
7. Focal mechanisms: Are the focal mechanisms consistent with a natural and/or induced earthquake cause?	10
8. Other–seismic data: Are there other seismic data to support a natural or induced cause, *e.g.*, swarm, foreshock-aftershock pattern, b-value, total number of earthquakes, stress release corresponding to the earthquake magnitude or seismicity?	10
9. Other–non-seismic data: Are there non-seismic data that support a natural or induced cause, *e.g.,* direct nucleation effects, precursory surface deformation?	10

Phase 2: Develop a final, generic scheme

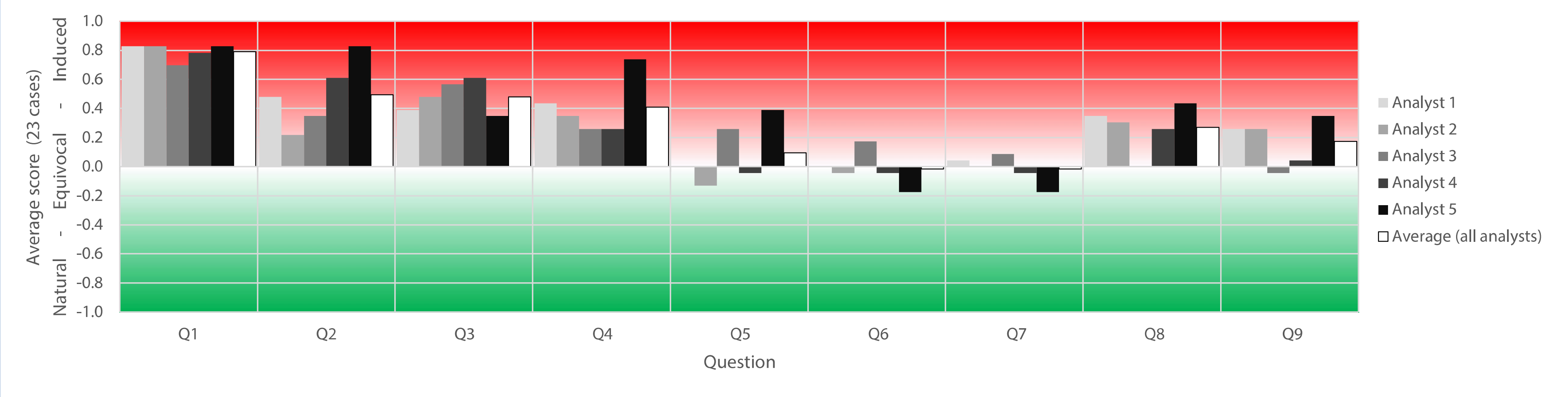

Score results

5 analysts, 9 questions, 23 cases

Phase 2: Logical implications

Question #	Answer b. (green)	Answer c. (yellow)	Answer d. (red)
1	Rn	Pe	Pe
2	Rn	Pe	Pe
3	Rn	Pe	Pe
4	Pe	Pe	Ri
5	Pe	Pe	Pe
6	Pe	Pe	Pe
7	Rn	Pe	Ri
8	Pe	Pe	Pe
9	Pe	Pe	Pe

Phase 2: E-PIE – Display of results

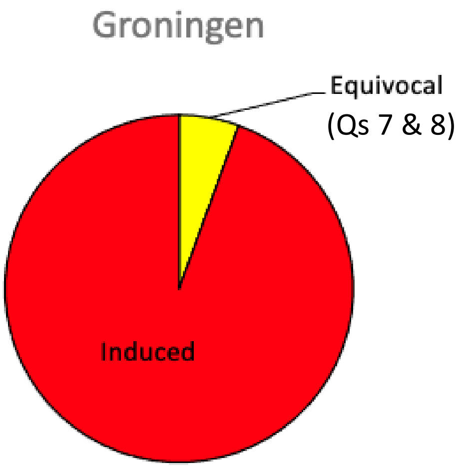

many authors

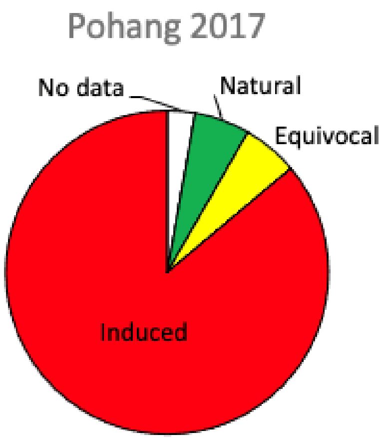

Grigoli et al. 2018
Kim et al. 2018
McGarr 2018

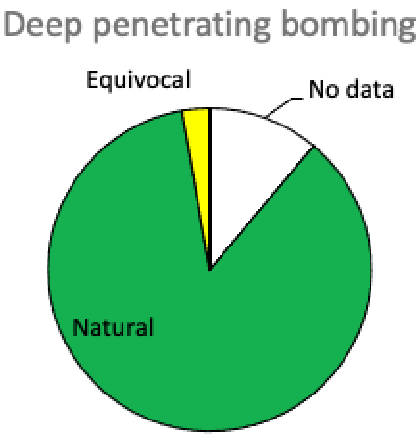

Balassanian 2005

Phase 2: E-PIE test on 23 cases

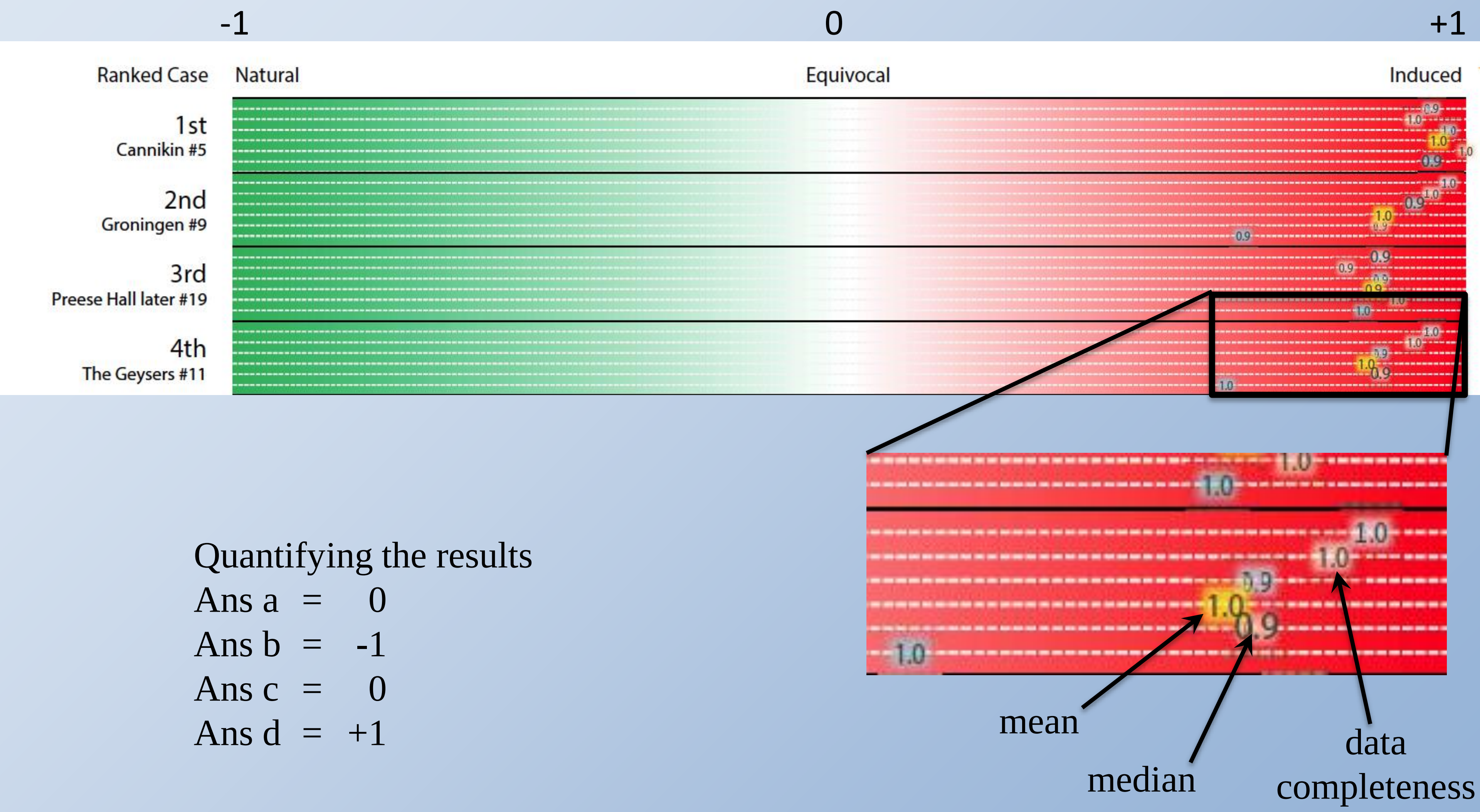

Quantifying the results

Ans a = 0

Ans b = -1

Ans c = 0

Ans d = +1

Phase 2: Test on 23 cases

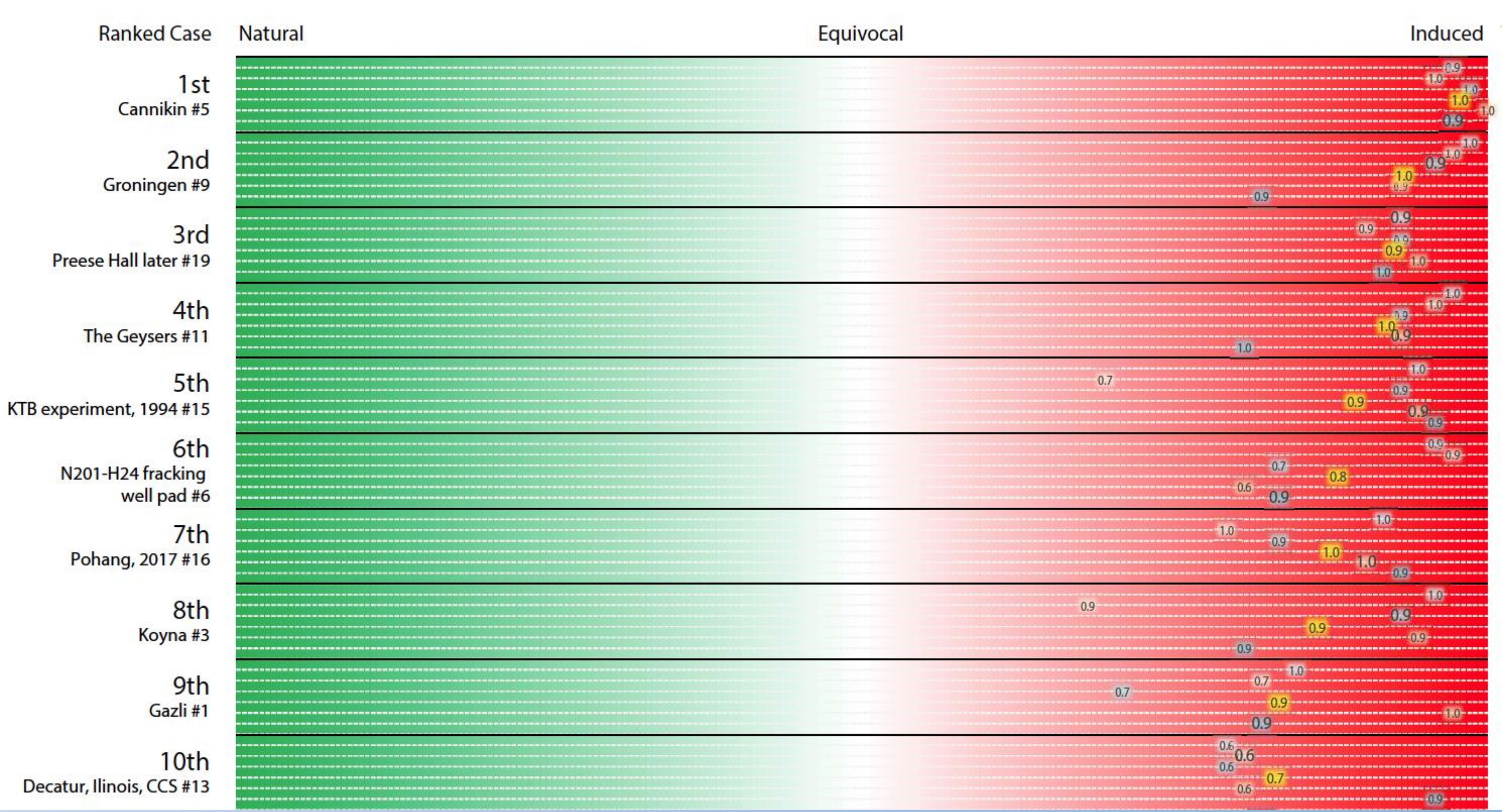

Phase 2: Test on 23 cases

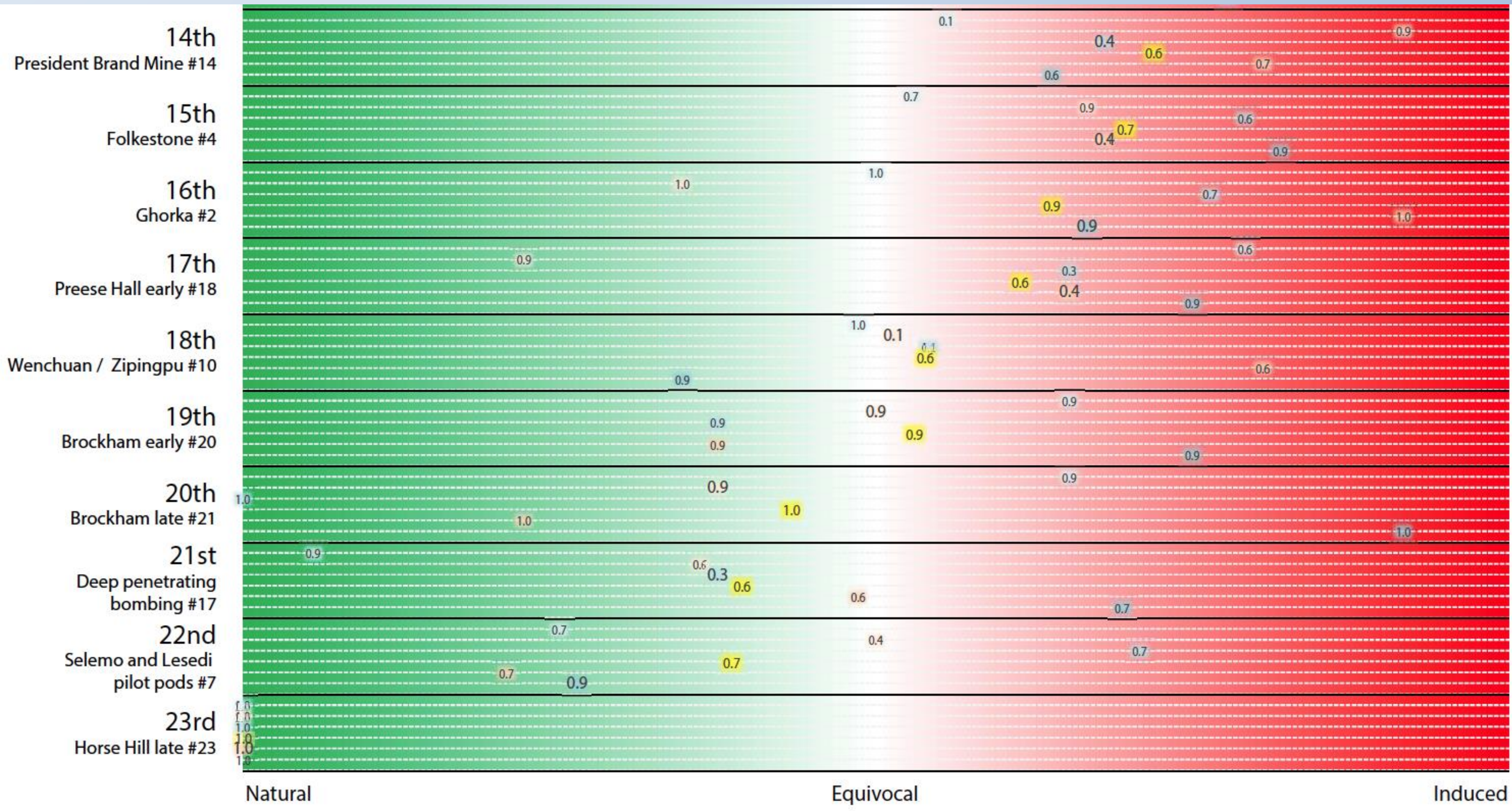

Phase 2: E-PIE test on 23 cases

Phase 2: Analyst scatter vs. case strength

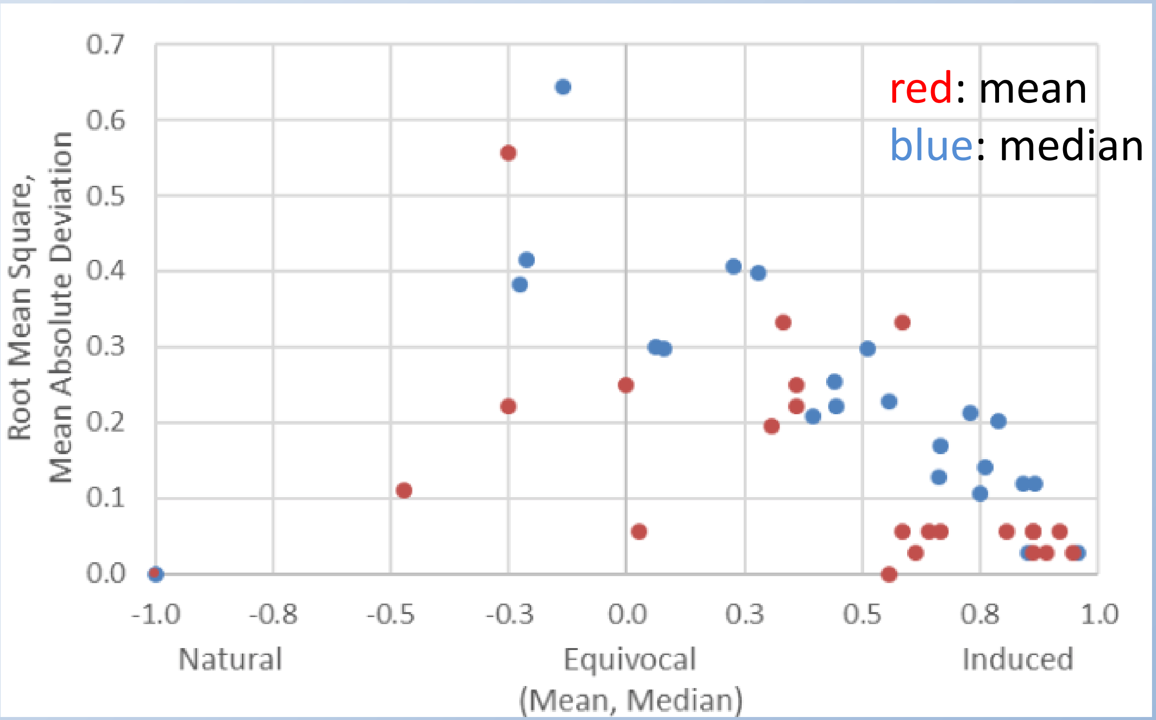

Phase 2: Analyst scatter as pie charts

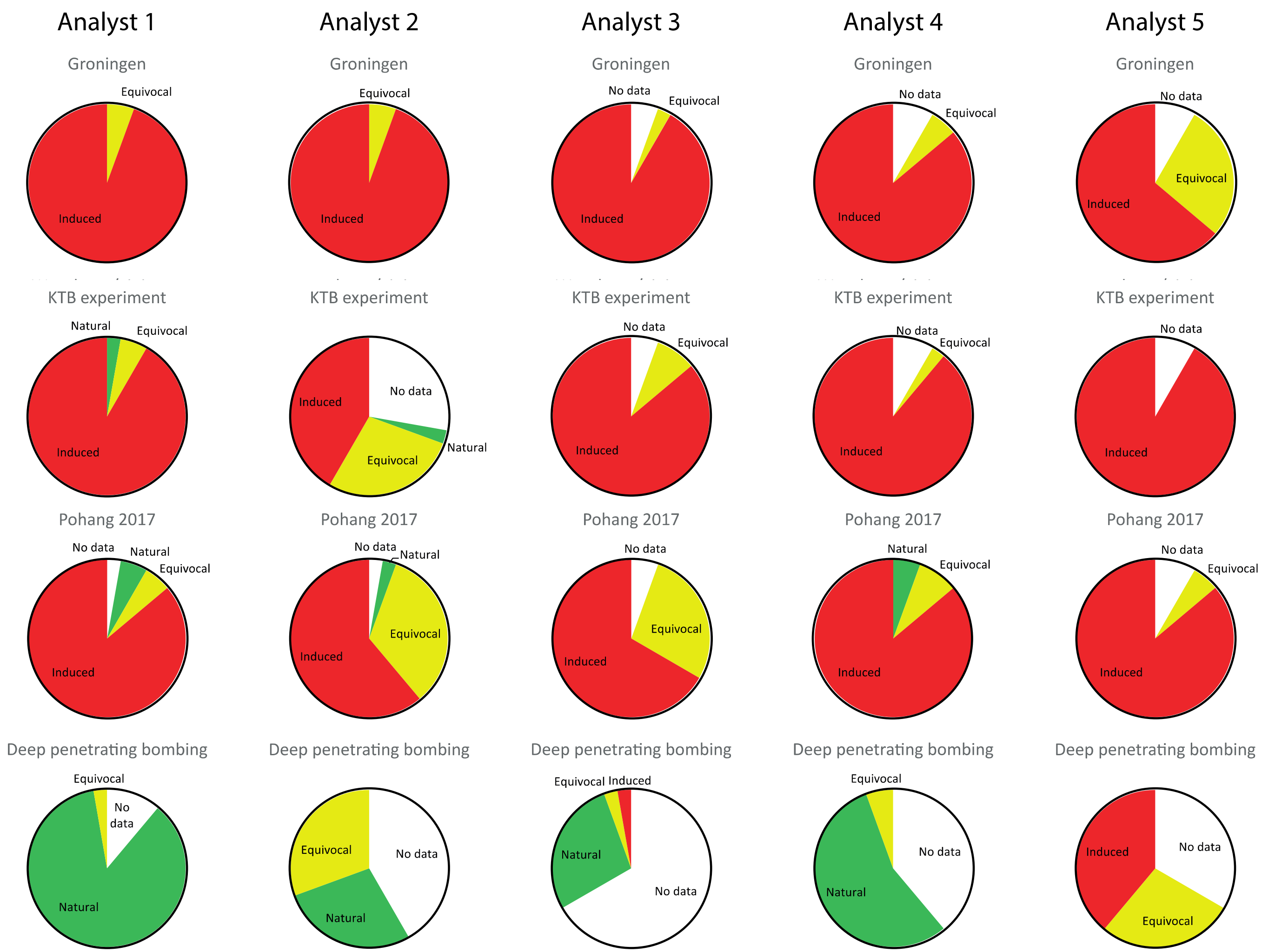

Phase 2: Compare E-PIE with Verdon et al. (2019)

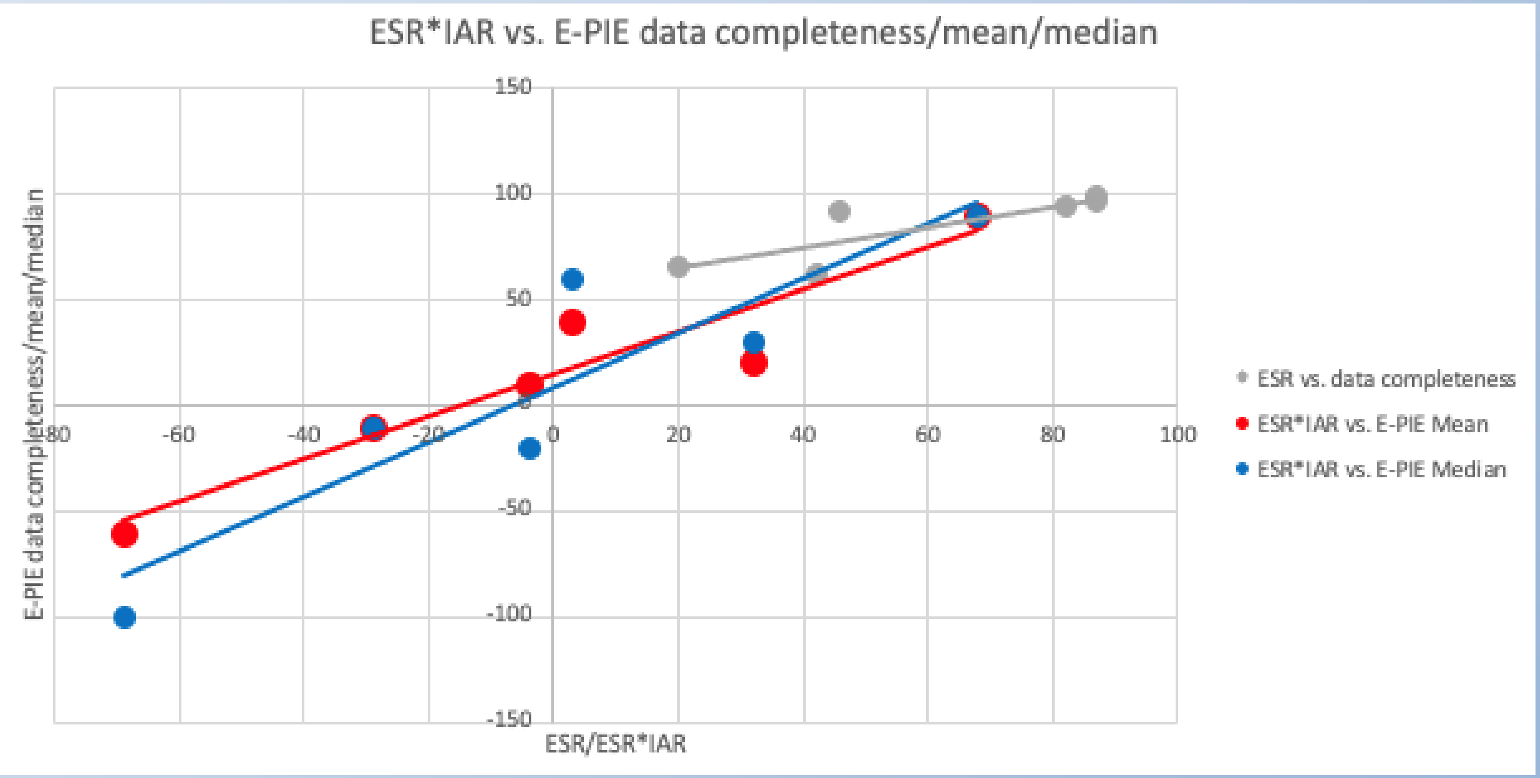

Phase 2: Conclusions

- E-PIE performs well on test cases
- E-PIE repeatability good for strong cases, poorer for weak cases
- E-PIE agrees well with Verdon et al. (2019) fluid-injection scheme

Phase 3: Grade all cases in *HiQuake*

Phase 3: Apply to all cases in *HiQuake*

Plan of work

1. Multiple analysts score all cases using SoC ("quick") scheme
2. Single analyst score all cases using E-PIE
3. Analyze & publish results
4. Publish paper(s)
5. Upload to www.inducedearthquakes.org

Phase 3: Apply to all cases in *HiQuake*

Plan of work

1. Multiple analysts score all cases using SoC ("quick") scheme – 100%
2. Single analyst score all cases using E-PIE – 15%
3. Analyze results – 30%
4. Publish paper(s)
5. Upload to www.inducedearthquakes.org – to discuss

Phase 3: Apply to all cases in *HiQuake*

SoC ("quick") score results (rounded averages)

			Case very weak/ highly unlikely	Case weak/ unlikely	Case moderate/ plausible	Case strong/ likely	Case very strong/ highly likely
Earthquake cause (main class)	**Number of cases**	**0**	**1**	**2**	**3**	**4**	**5**
CCS	3	0	0	0	0	1	2
Chemical explosion	1	0	1	0	0	0	0
Coal Bed Methane (CBM)	1	0	1	0	0	0	0
Construction	2	0	0	1	1	0	0
Conventional Oil and Gas	136	0	0	6	82	29	19
Deep penetrating bombs	4	0	4	0	0	0	0
Fracking	412	0	0	0	83	217	112
Geothermal	73	0	0	7	22	20	24
Groundwater extraction	8	0	0	0	5	3	0
Mining	303	0	3	72	101	53	74
Nuclear explosions	28	0	0	0	12	8	8
Oil and Gas	8	0	0	0	1	7	0
Oil and Gas/Waste fluid injection	4	0	0	0	4	0	0
Research	14	0	0	1	0	1	12
Waste fluid disposal	49	0	0	4	7	13	25
Water reservoir impoundment	189	0	2	23	82	52	30
Total	**1235**	**0**	**11**	**114**	**400**	**404**	**306**

Phase 3: Apply to all cases in *HiQuake*

SoC ("quick") score results (rounded averages)

Groningen

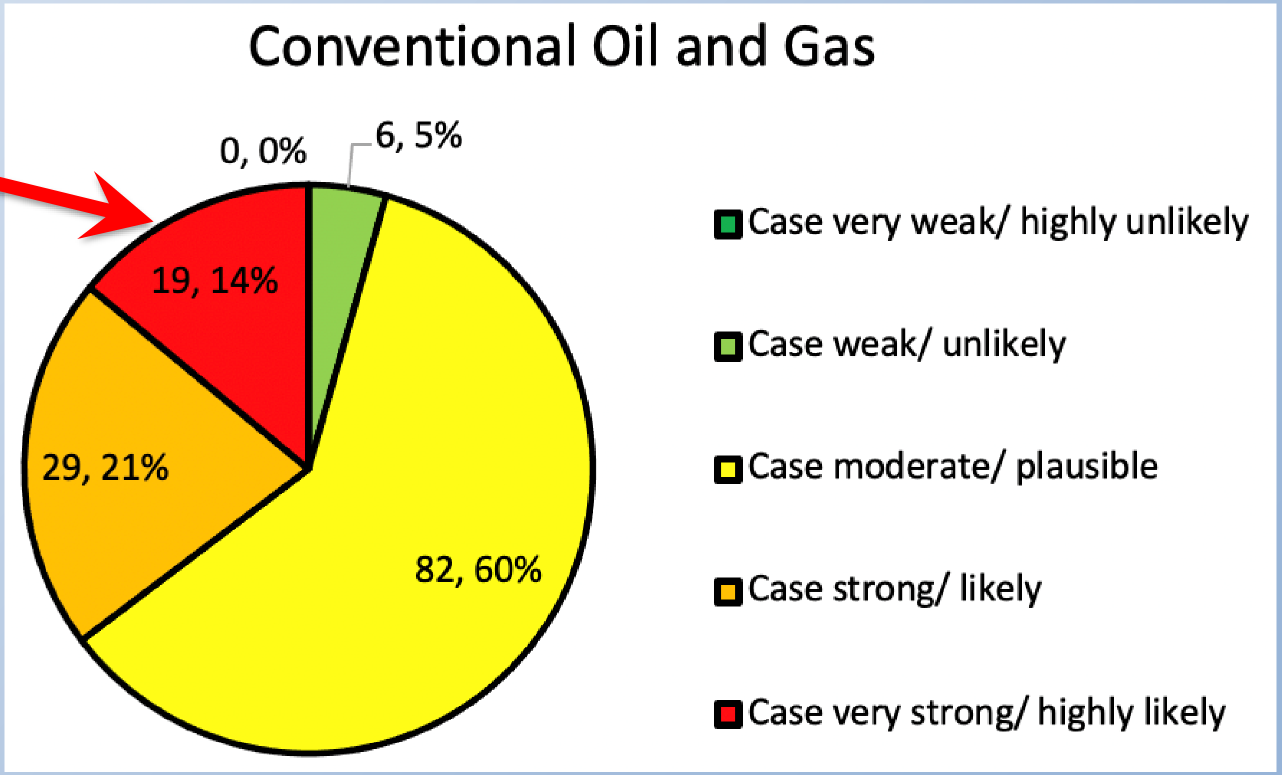

Example: Conventional Oil and Gas (total 136 cases, *e.g.*, Groningen)

Phase 3: Apply to all cases in *HiQuake*

SoC (“quick”) score results (rounded averages)

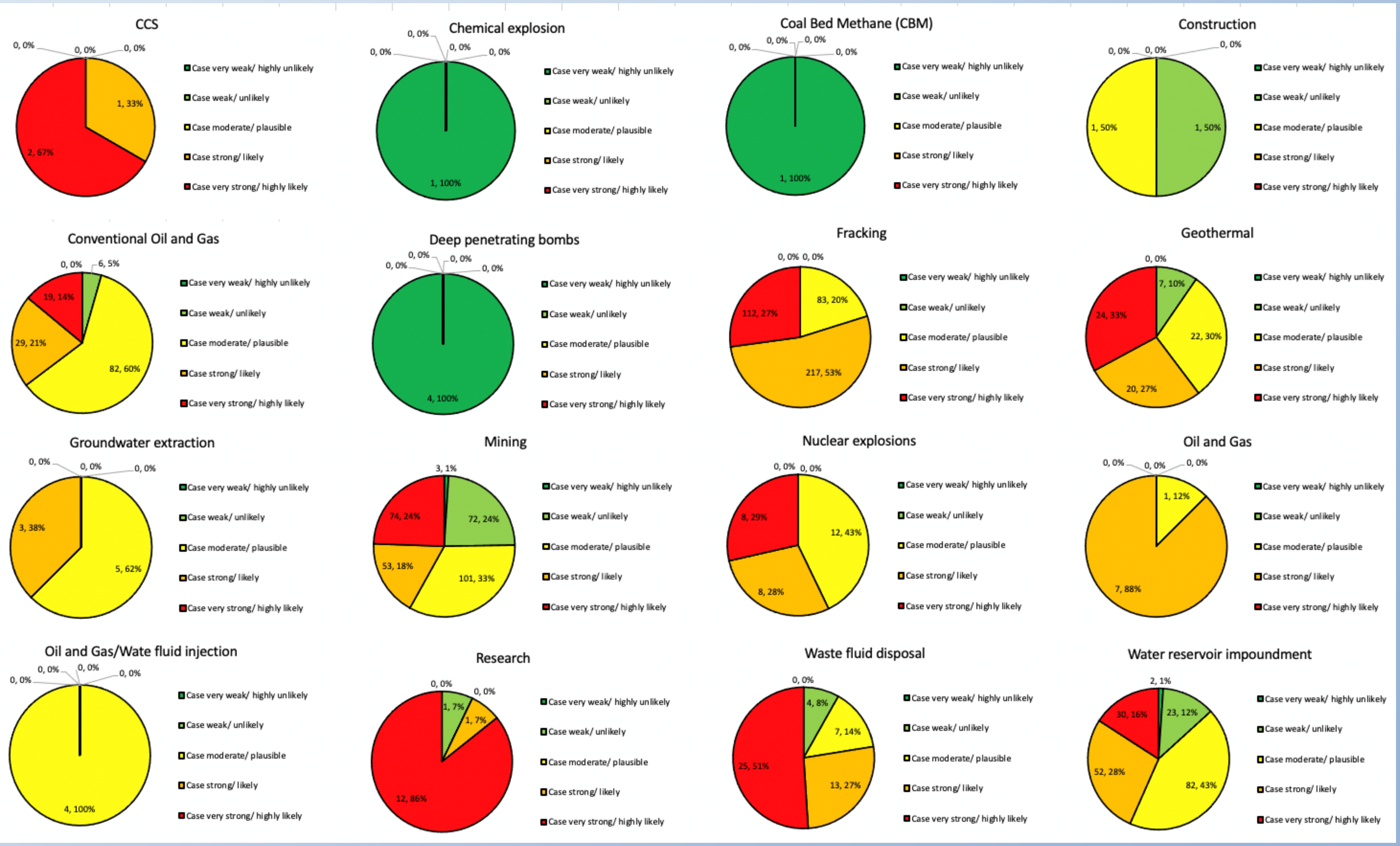

Phase 3: Apply to all cases in *HiQuake*

SoC (“quick”) score results (rounded averages)

Entire *HiQuake* database (total 1235 cases)

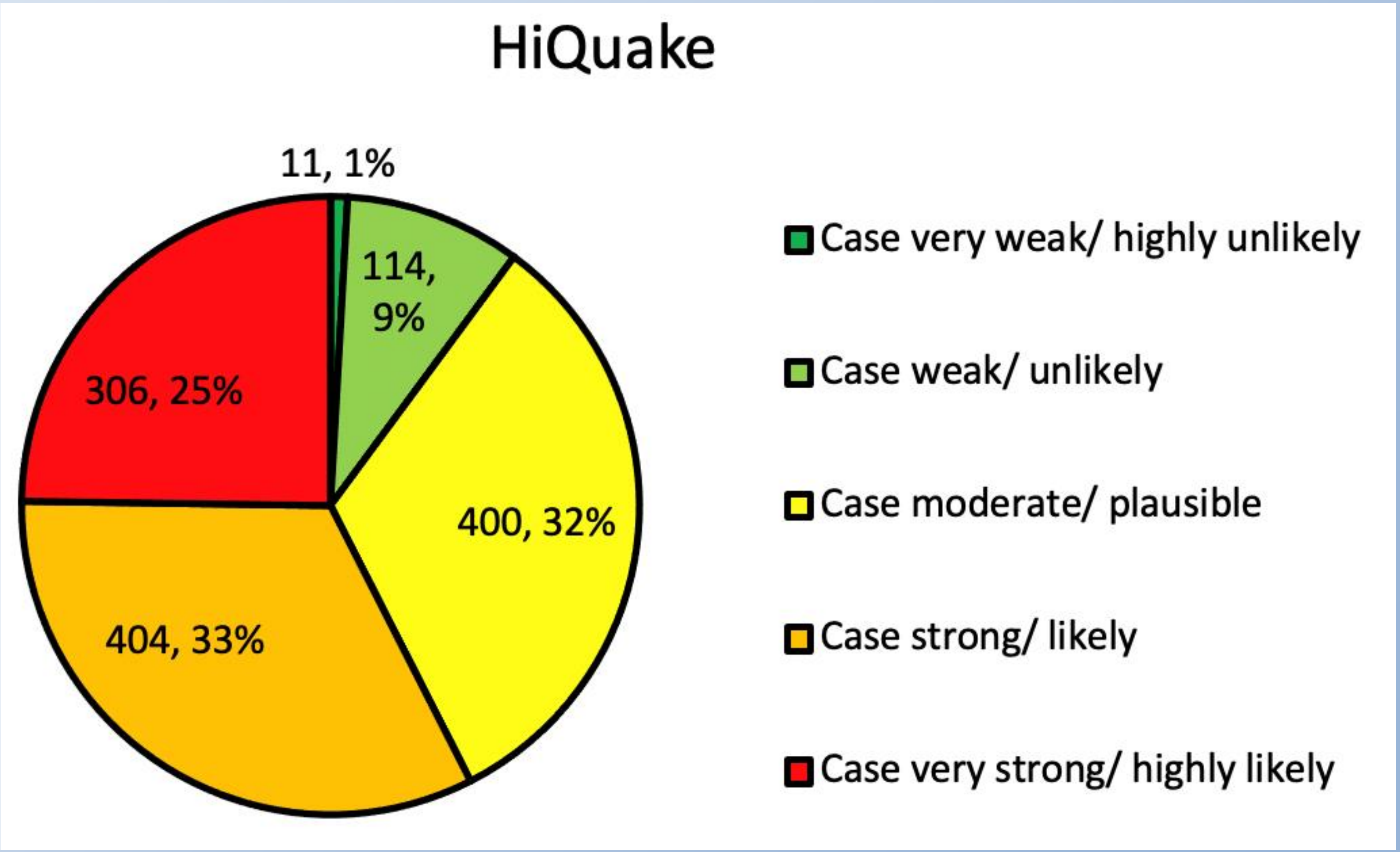

Phase 3: Apply to all cases in *HiQuake*

E-PIE results

Correlation of SoC (“quick”) & E-PIE – 23 cases

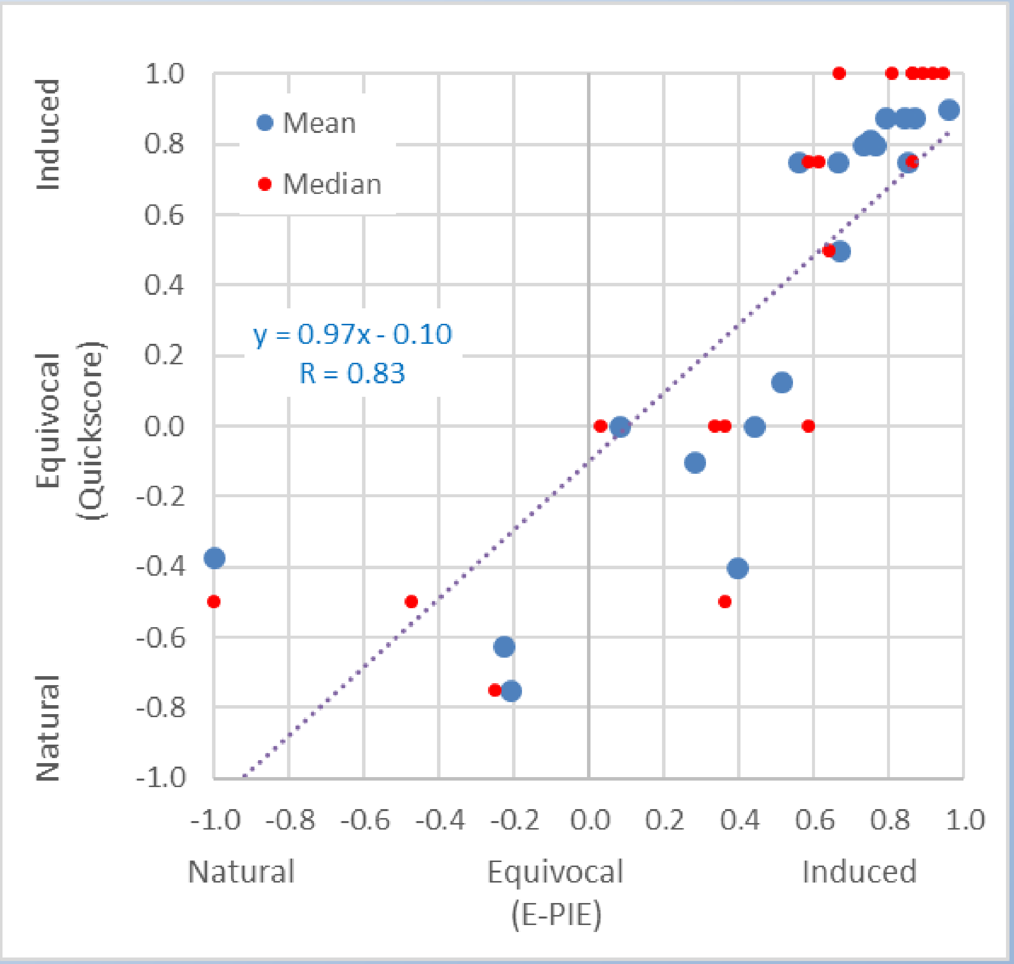

Phase 3: Apply to all cases in *HiQuake*

E-PIE results

158 cases

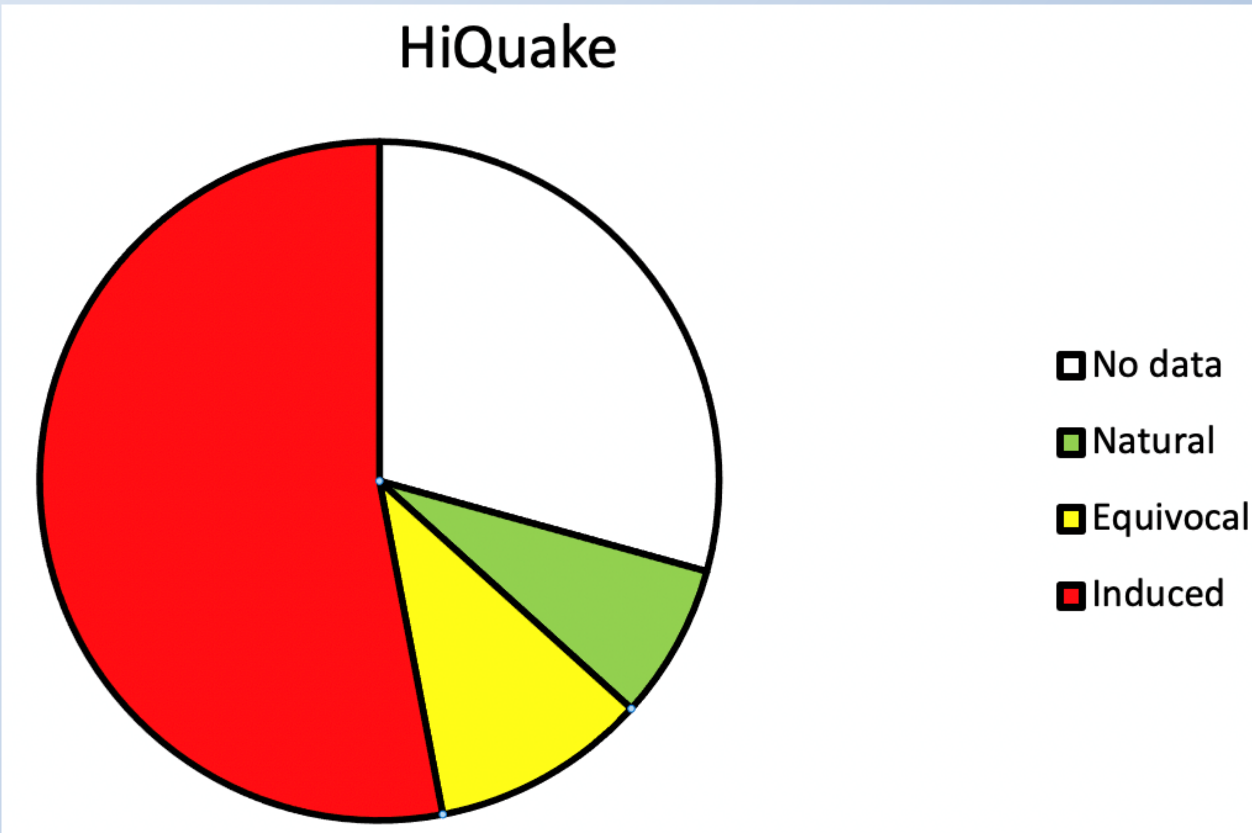

Entire *HiQuake* database (total 1235 cases)

"Quick"

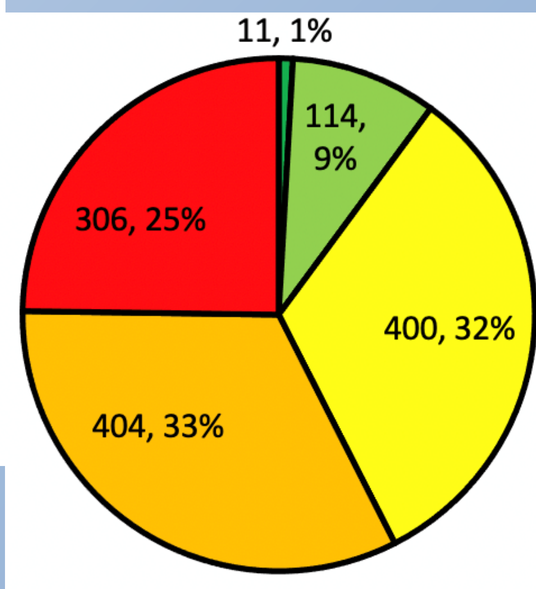

Phase 3: Conclusions

- Average SoC ("quick") scores complete for *HiQuake*
  - preliminary, noise reduced results
- Application of E-PIE in progress
  - will reduce bias
- Good correlation between mean "quick" & E-PIE
- Initial results suggest:
  - 50-60% strong evidence for human induction
  - 30-40% weak evidence for human induction
  - 10% natural

Deliverables to date

1. Submitted to Bulletin of the Seismological Society of America: *Human-Induced Earthquakes: The Performance of Questionnaire Schemes*
2. Submitted to Journal of Seismology: *Human-Induced Earthquakes: E-PIE – A Generic Tool for Evaluating Proposals of Induced Earthquakes*
3. *HiQuake* grading data to date

Ongoing work

Plan of work

1. Multiple analysts score all cases using SoC (Quick) scheme – 100%
2. Single analyst score all cases using E-PIE – 15%
3. Analyze results – 30%
4. Publish paper(s)
5. Upload to www.inducedearthquakes.org – to discuss

That's all folks

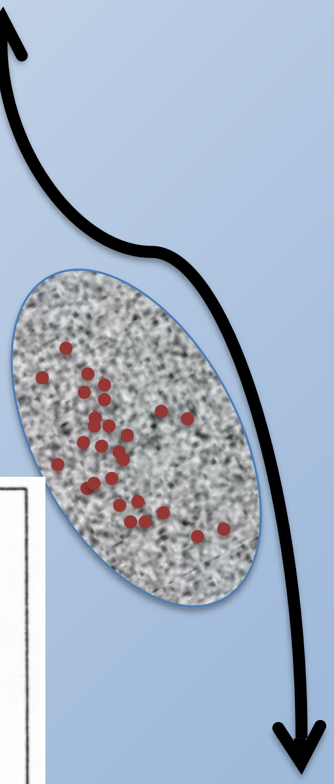

Workshop on Maximum Magnitude of earthquakes in Groningen

DAY 2

Tuesday 14th June: Groningen seismicity and fault ruptures

Start	End	Speaker	Presentation
8:30	9:15	Bernard Dost	History of seismic monitoring in the Groningen field
9:15	10:30	Steve Oates	Groningen earthquakes: focal depths and fault ruptures
10:30	11:00		*Coffee break*
11:00	11:45	Chris Spiers	Properties of Groningen reservoir and fault rocks
11:45	12:30	Rick Wentinck	Geomechanical model of fault rupture in the Groningen field
12:30	13:30		*Lunch*
13:30	14:45	Jean-P. Ampuero	Physics-based models of natural and induced seismicity
14:45	15:15		*Coffee break*
15:15	16:30	Mark Zoback	Crustal stresses and earthquake triggering
16:30	17:00	All	General discussion

Koninklijk Nederlands
Meteorologisch Instituut
Ministerie van Infrastructuur en Milieu

History of seismic monitoring in the Groningen gas field

Bernard Dost, Elmer Ruigrok, Jesper Spetzler, Gert-Jan van den Hazel, Jordi Domingo, Pauline Kruiver

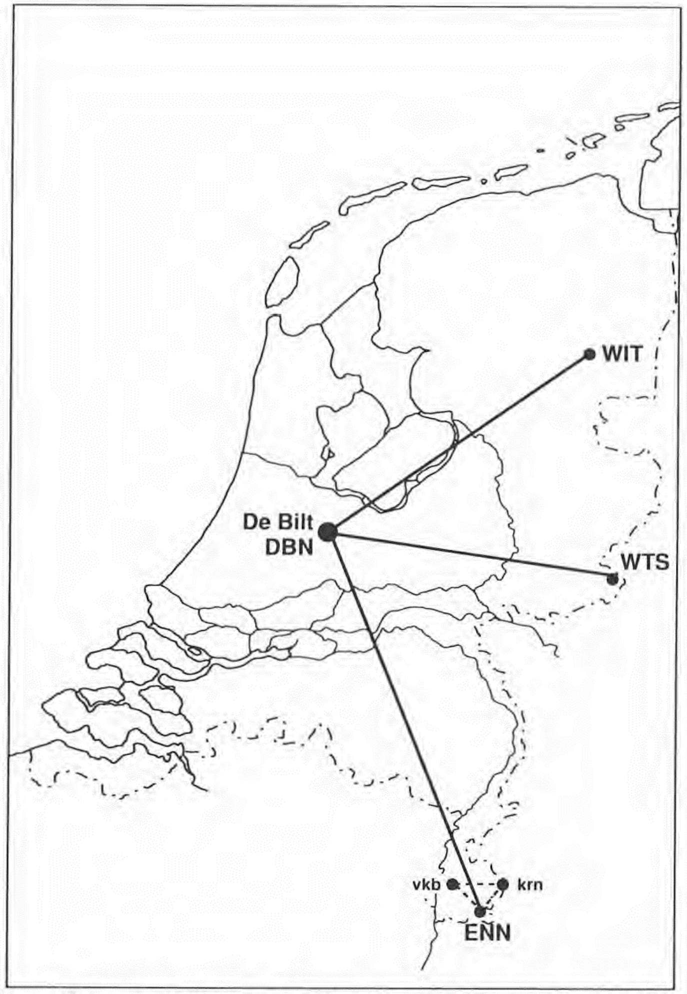

Fig. 1 Seismic stations in the Netherlands in operation in 1989

KNMI permanent network in 1989:

Natural seismicity was only observed in the SE of the Netherlands and no induced seismicity was observed until 1986

WIT:

Grenet, Z (1951-1979), Press-Ewing Z,N,E (1963-66), Wilmore-MK-II SP, Z (1966-93)

Streckeisen STS1 (1995-2013)

WTS: Wilmore MK-II SP, Z (1974-1993)
Streckeisen STS2 (2000-present)

ENN/HGN:

Willmore MK-II (Z) (1980-1993)
Streckeisen STS1 (1993-present)

DBN:

Galitzin (1914-1994), Press-Ewing (1966-198?),
Teledyne-Geotech SL210/220 (1976-1995),
Streckeisen STS-2 (1995-present)

Network development (1989-1995)

Assen network (temporary)

- Installed after the first induced events were recorded in 1986
- Operational 1989-1994 (orange circles)
- Instrumentation: Willmore MK III, Z (red triangles)

FSW experimental borehole

- Installed in 1991, 300m deep, 75m vertical sensor-spacing
- High noise environment, strong noise reduction with depth
- Most effective noise reduction at 75-150m depth

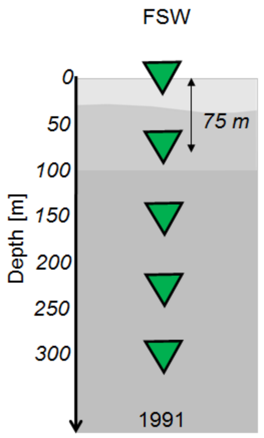

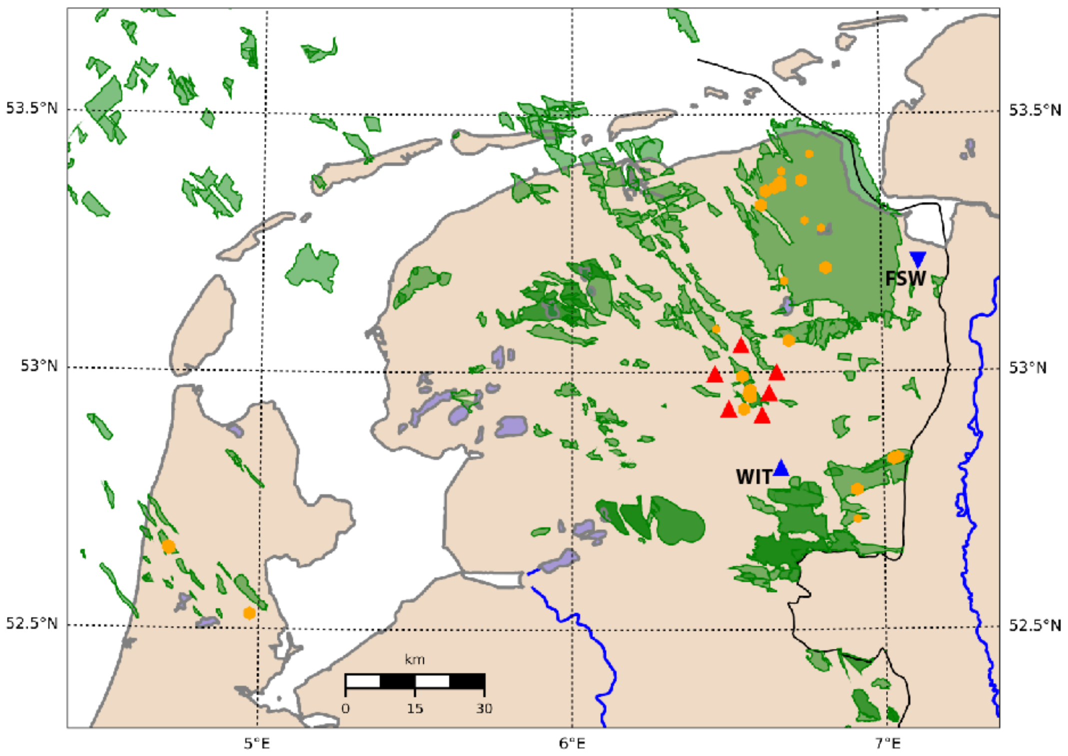

Station	Name	Open since	Closed at	Latitude	Longitude	Components
ZYN	Zeyen	1988-12-01	1994-06-01	53,053	6,544	HHZ
WSB	Westerbork	1988-12-01	1994-07-01	52,917	6,611	HHZ
RLD	Rolde	1989-02-01	1994-06-01	53,000	6,659	HHZ
LGV	Laaghalerveen	1989-09-01	1994-06-01	52,929	6,504	HHZ
BVS	Bovensmilde	1989-09-01	1995-01-01	52,997	6,460	HHZ
MWD	Marwijksoord	1989-09-01	1994-04-01	52,960	6,634	HHZ
WIT	Witteveen	1993-11-16	2013-12-01	52,814	6,670	HHZ

Assen network

- Recording of the 1992-07-22 M 2.6, Assen event
- Lowest trace: station WIT
- Only Z-component. In 1994 one of the stations (WSB) was upgraded to 3C recording
- Due to high surface noise, no triggers for small (M<2) Groningen events

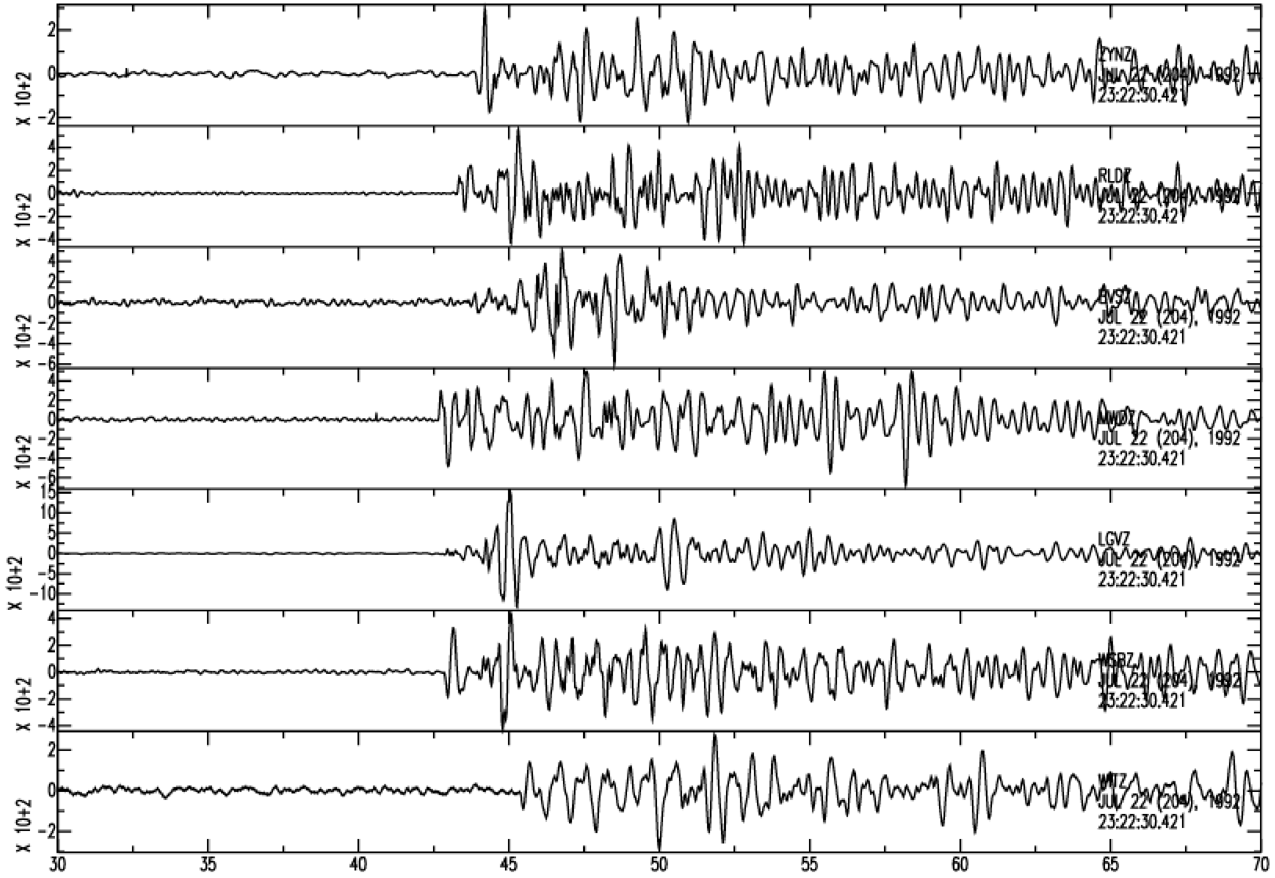

Network development (1995)

- Seismicity was mainly recorded around smaller gas fields
- Borehole network covering an area of app 100*50 km
- Borehole configuration: 200m depth, 50m vertical spacing
- ENM, WDB, ZLV, HWF, ENV, VLW, VBG were added in the NE (Groningen, Drenthe)
- WMH, OTL and PPB in the West (Noord-Holland)
- Average inter-station distance: 20 km
- Surface accelerometers were added at locations of felt events

Network expansion (2009-2010)

- Additional boreholes to cover smaller fields outside Groningen (NIW, SUH) and one in Groningen (SPY)
- Boreholes in Friesland (WYN, FDG, ZWE) for monitoring of deep salt mining

Plans were developed to intensify monitoring of the Groningen gas field and decrease inter-station distance (2008).

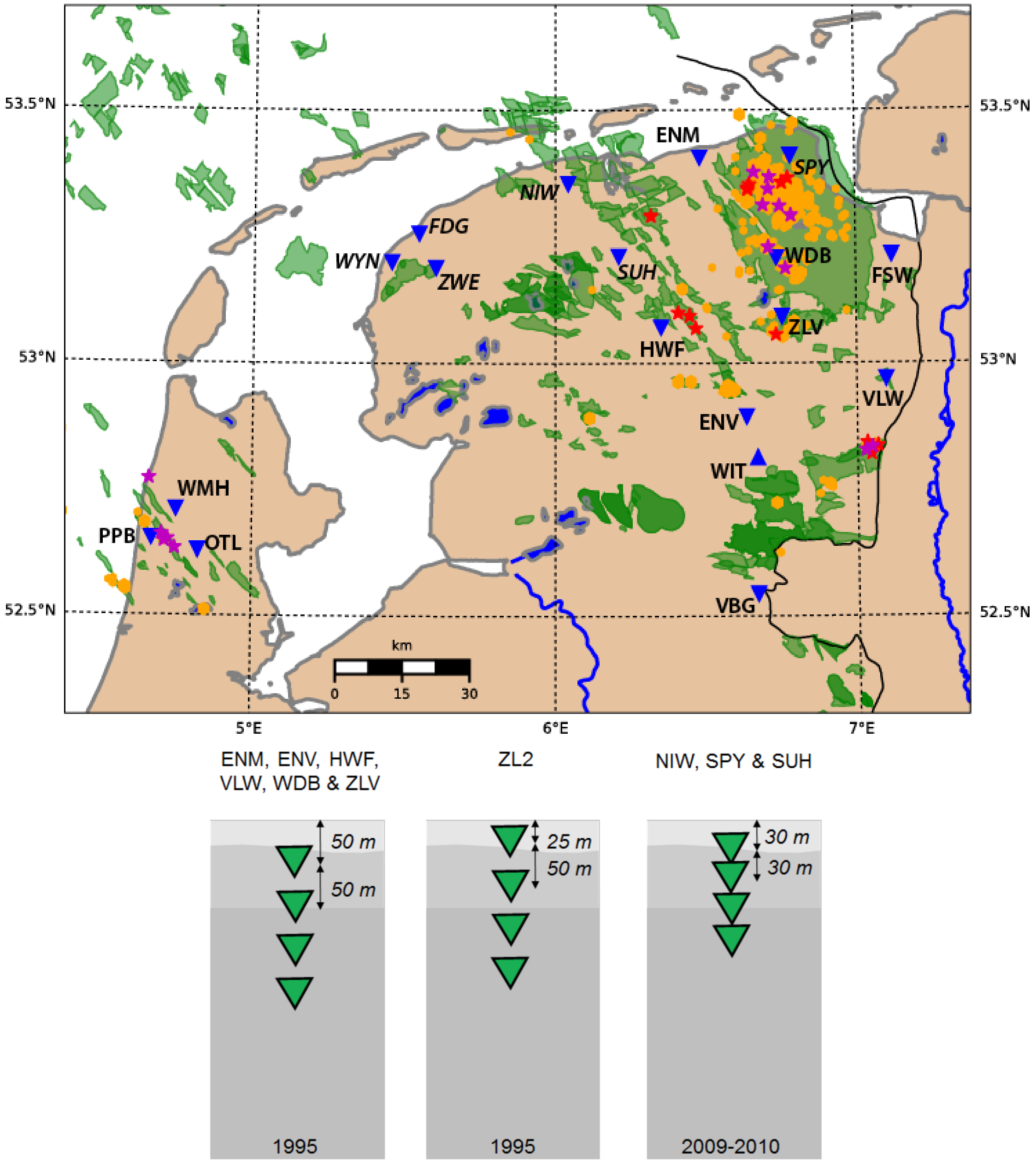

Network design

- Based on measured average noise levels in FSW at 225m depth, a magnitude treshold (Magnitude of Completeness, MoC) was calculated for the NL network
- Design criteria: Felt events have been reported for ML≥1.8, so a MoC= 1.5 was used as input
- In 2013 (Figure right) all gas fields showing seismicity are located within the MoC=1.5 contour
- The network was not designed to optimise location accuracy. Average inter-station distance ~20 km and average location uncertainty estimated at ~ 1 km for events within the network.

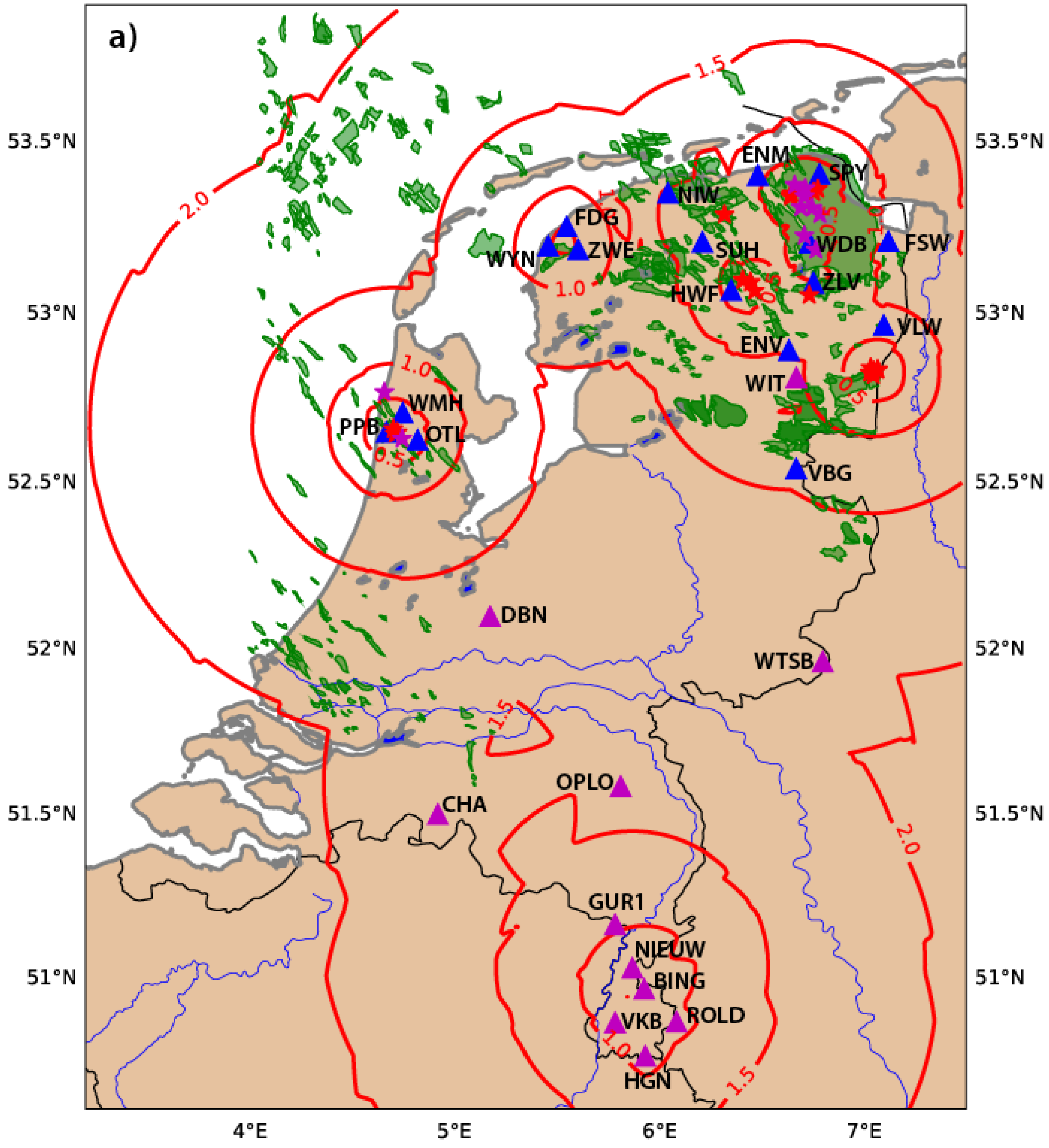

borehole geophone stations (blue triangle), surface seismic stations (magenta triangle), surface accelerometers (red stars)

Network update

- In 2014 the Groningen network was updated, reducing the average station distance in the field to ~5 km
- The new network allows a higher location accuracy and more detailed studies (e.g. effect of variations in shallow velocity structure, detailed source studies)
- The MoC in Groningen was lowered to ML~0.5
- Newly instrumented areas outside Groningen:

  Twente (T, wastewater injection), Norg and Grijpskerk (N & GK, both gas-storage), Zuid-Holland (ZH, geothermal operations)

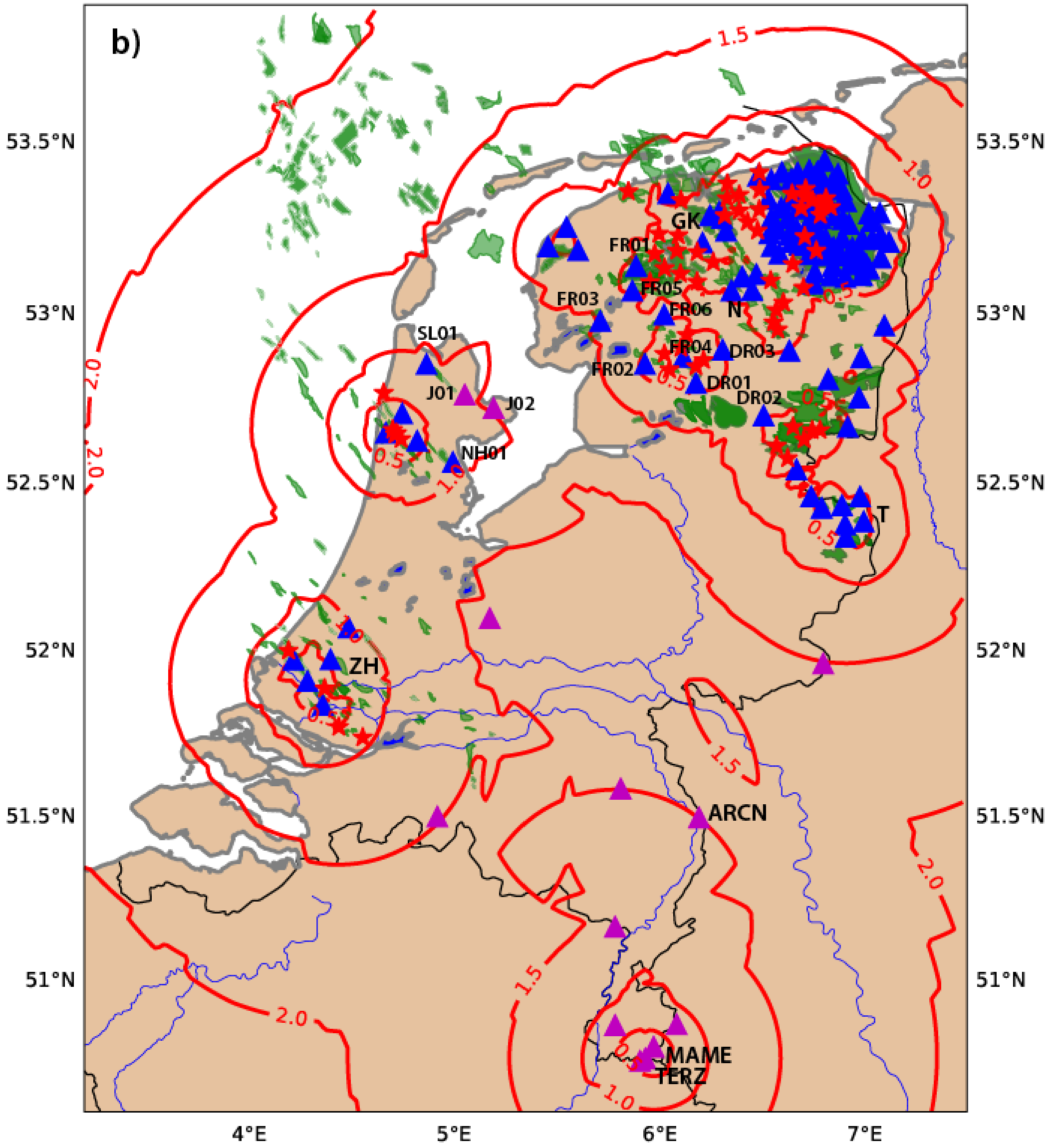

borehole geophone stations (blue triangle), surface seismic stations (magenta triangle), surface accelerometers (red stars)

Development of seismicity

- After 2000 production of the Groningen field increased and also seismicity increased.

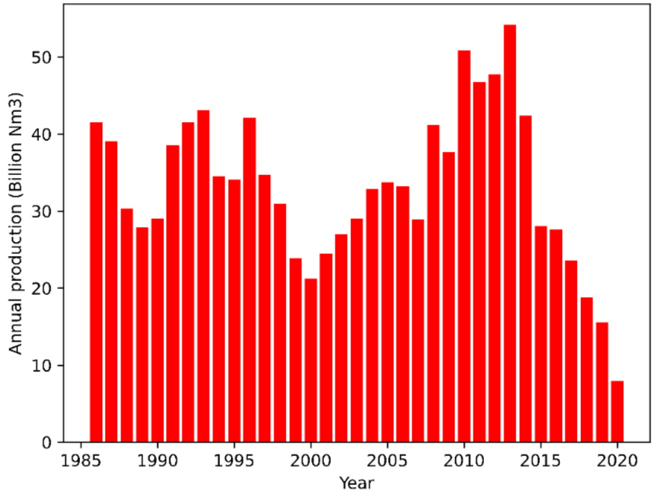

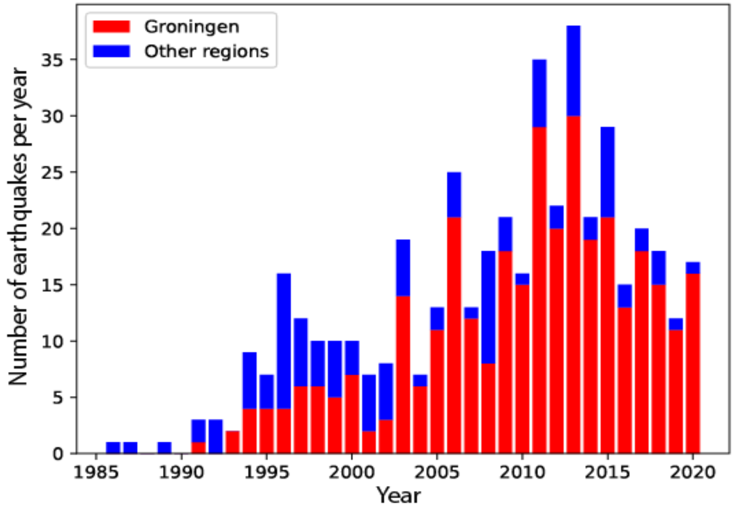

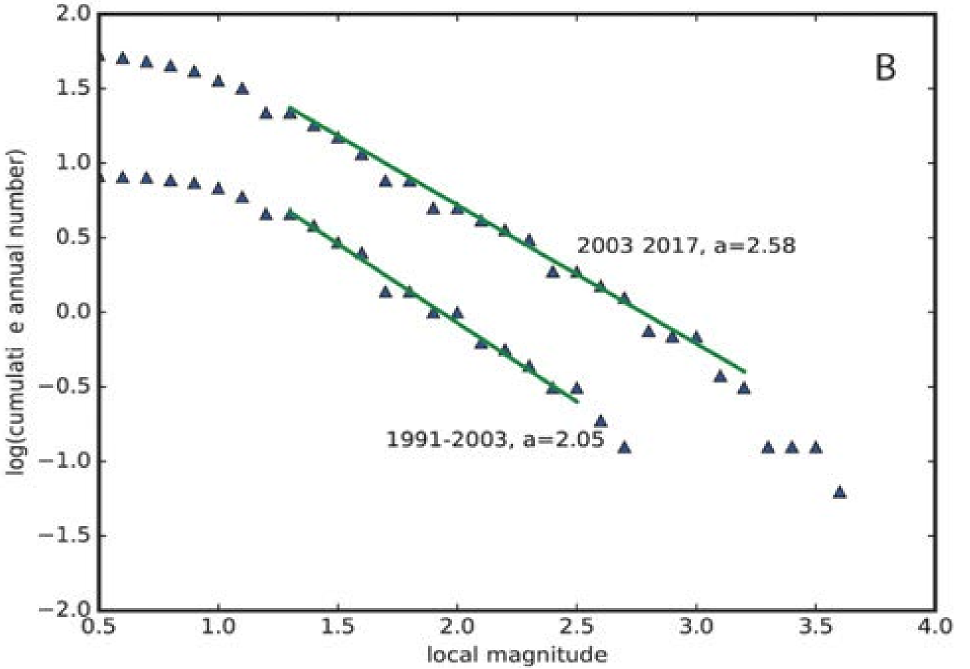

Temporal changes

- Over time the b-value remained constant, while the activity rate increased
- Magnitude of completeness, derived from FM curves, changed from ML 1.2 (2003-12) to ML 0.5 (2014-16)

Start date	End date	M_c	R	b
6 Apr 2003	23 Feb 2009	1.2	95.6	0.94 ± 0.03
19 Aug 2009	23 Aug 2012	1.2	81.5	1.06 ± 0.04
23 Aug 2012	21 Aug 2014	0.8	96.1	0.96 ± 0.04
24 Sep 2014	27 Sep 2016	0.5	98.2	0.85 ± 0.05

Spatial distribution of seismicity

- Top right (1986-2004): most activity at smaller fields
- Lower left (2004-2014): most activity at the Groningen gas field
- Lower right (2014-2022): increasing number of small events recorded in Groningen

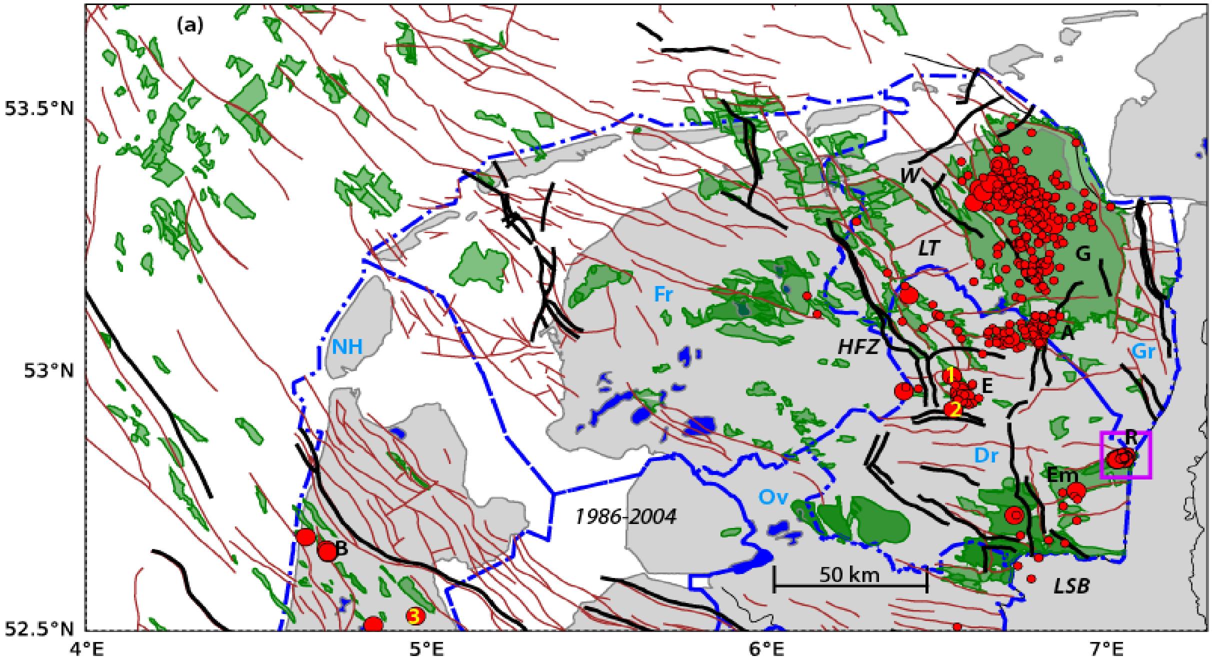

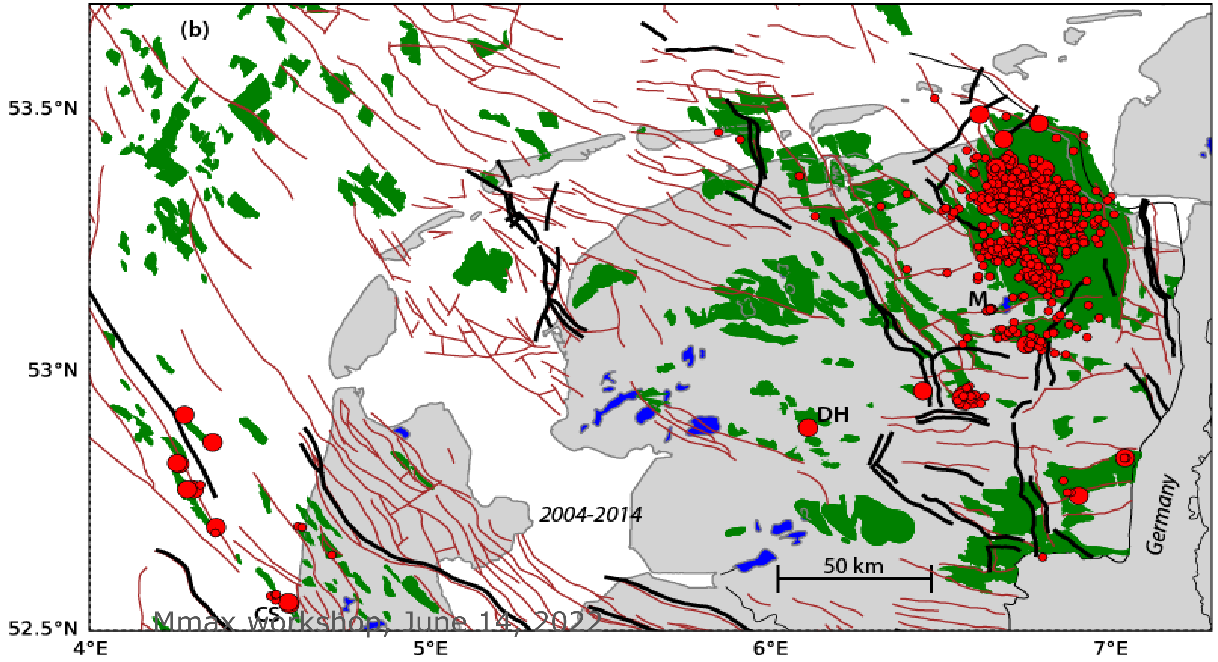

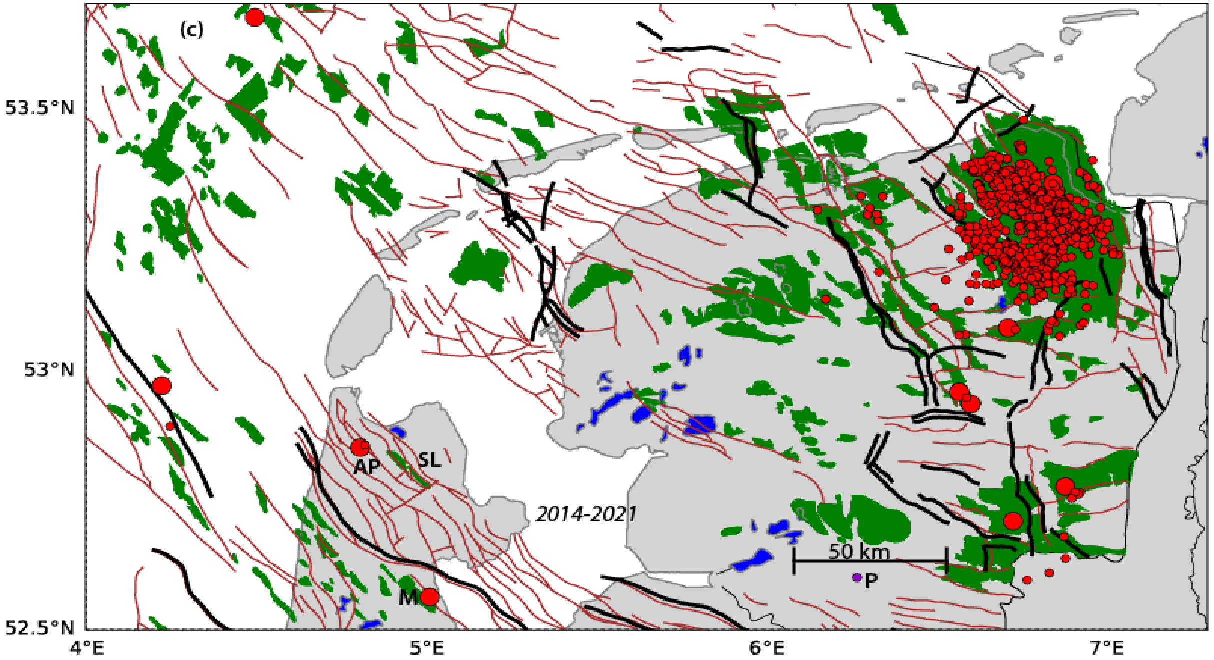

Groningen network

- G-network:
  Geophone string, 50m vertical sensor separation + surface accelerometer
- B-network:
  Update of existing accelerometer network installed in buildings
- Household network (TNO/NAM)
- 4 broad-band sensors co-located with G stations
- Deep boreholes at reservoir depth (ZRP, STDM)
- Other temporary surface stations (NARS)

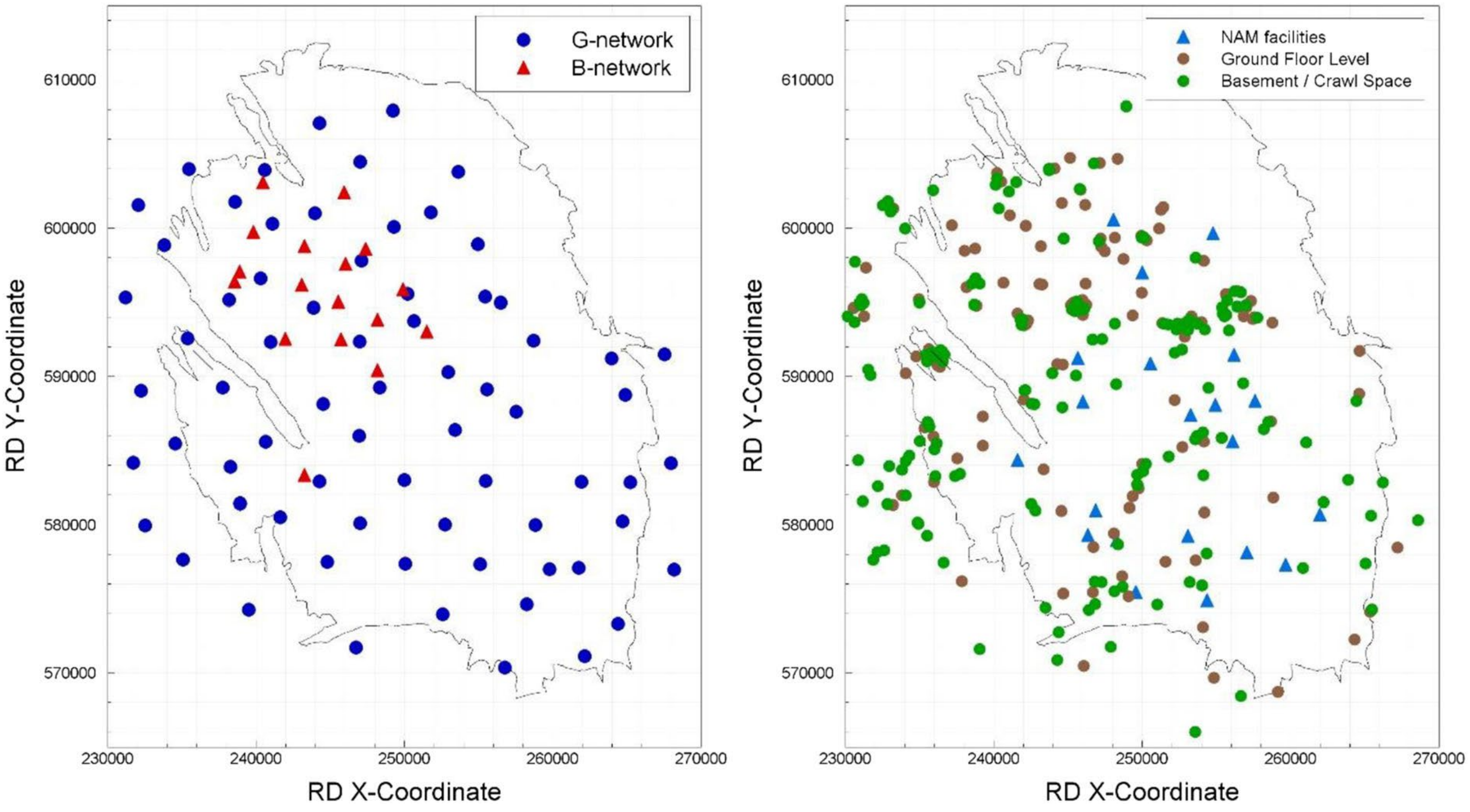

Ntinalexis et al., J. Seism. 2019

Instrumentation

G-station

B-station

Household network

Broadband stations at 100 m depth, co-located with G-stations

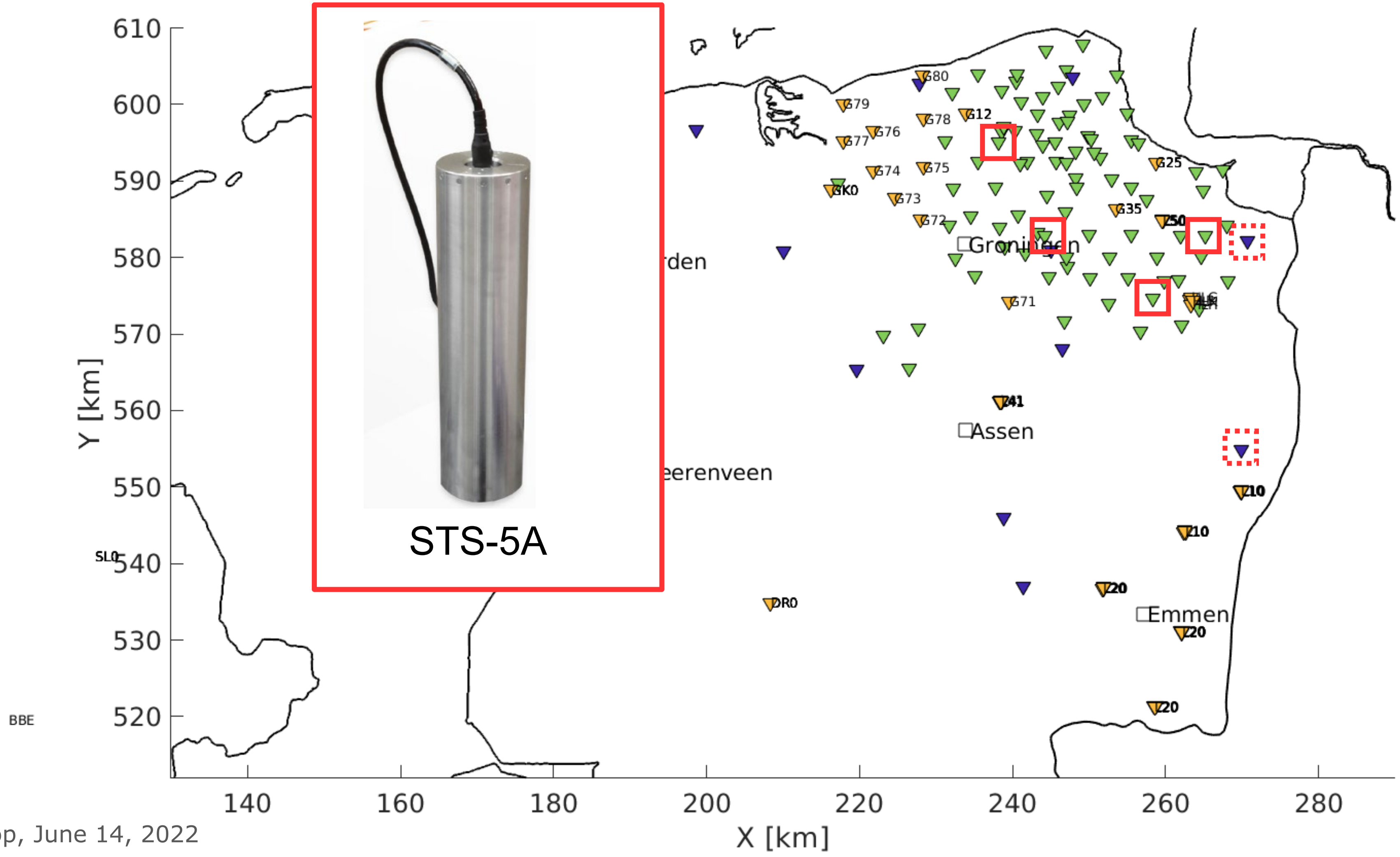

Seismic noise levels

Boreholes (top figure):

- Reduction of 20-30db between the surface sensor and sensors at depth

Comparison measured noise levels (lower figure)

- P90 rms velocities of the Z-component in the 5-40 Hz passband.
- The logarithmic mean over 122 geophones: -0.947 ± 0.328 (113 μm/s)
- The logarithmic mean over 60 accelerometers: 0.467 ± 0.315 (2931 μm/s)

On average a factor 25.9 difference in noise level

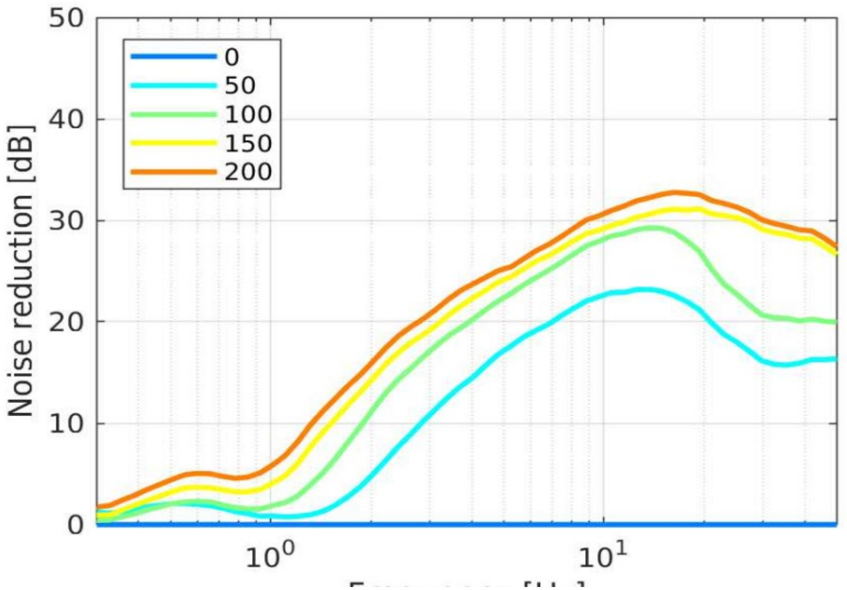

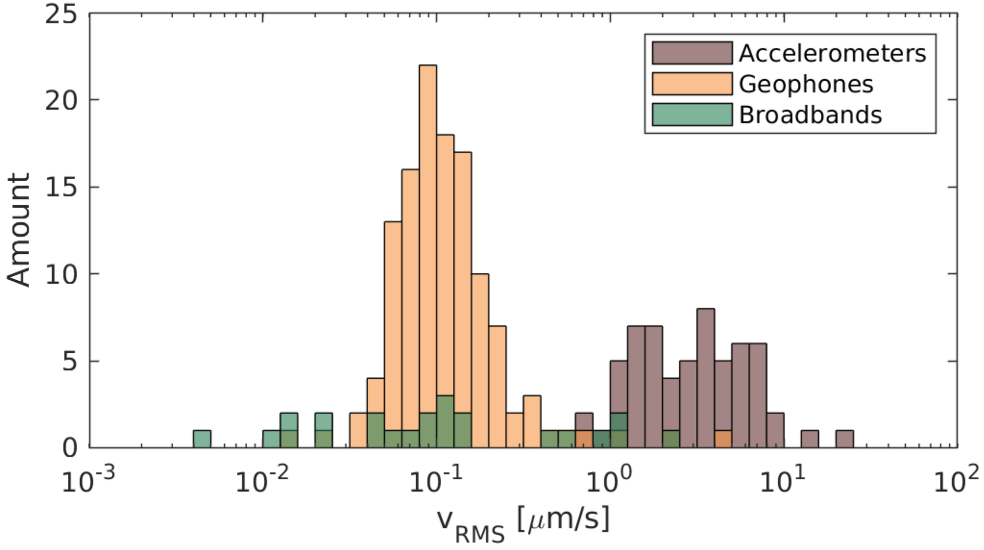

Sensor orientations

The orientations of the borehole sensors were unknown and are determined using

- Check-shots
- Explosions
- Cross-correlation with surface sensors

Both with known location and timing

- Teleseismic events

Essential information for e.g. source studies

- 70*5*3 = 1050 channels

The orientation of accelerometers in operation before 2014 were only recently checked in preparation of their publication on the KNMI Web portal

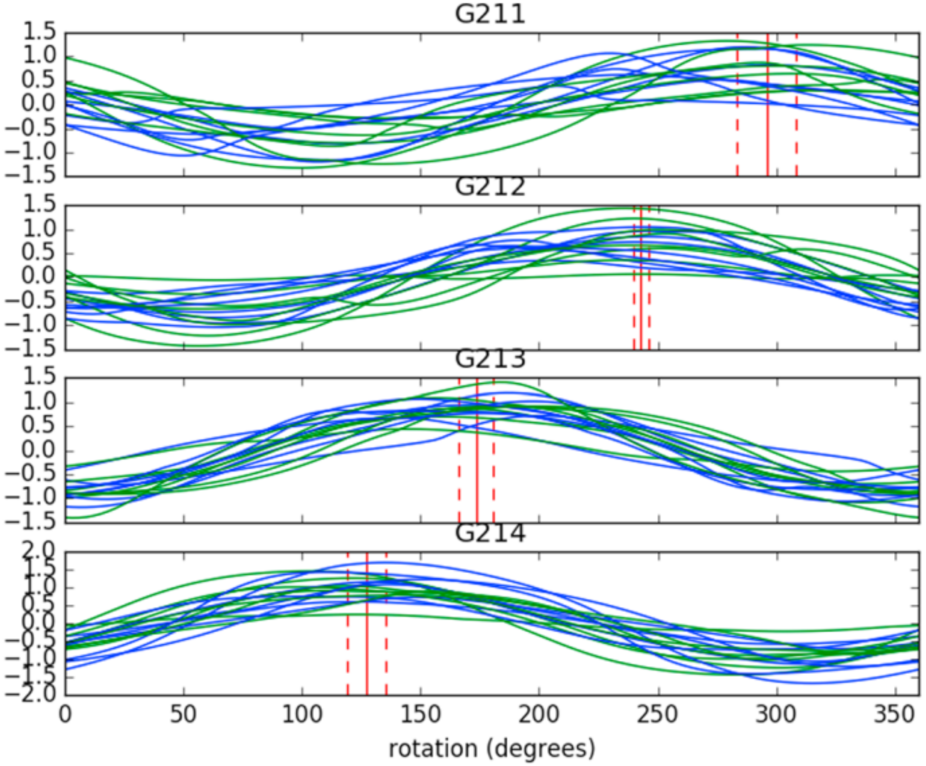

Max. cross-correlation coefficient with respect to the surface accelerometer as a function of the rotation of the geophone for different borehole levels (50,100, 150 and 200m depth).
Red lines: average rotation and ± 1 standard deviation
Hofman et al., 2017, JGR

Quality control

- Gain settings
  Recorded teleseismic events should show similar amplitudes over the network

Fiji quake PKP max Z-comp particle velocity

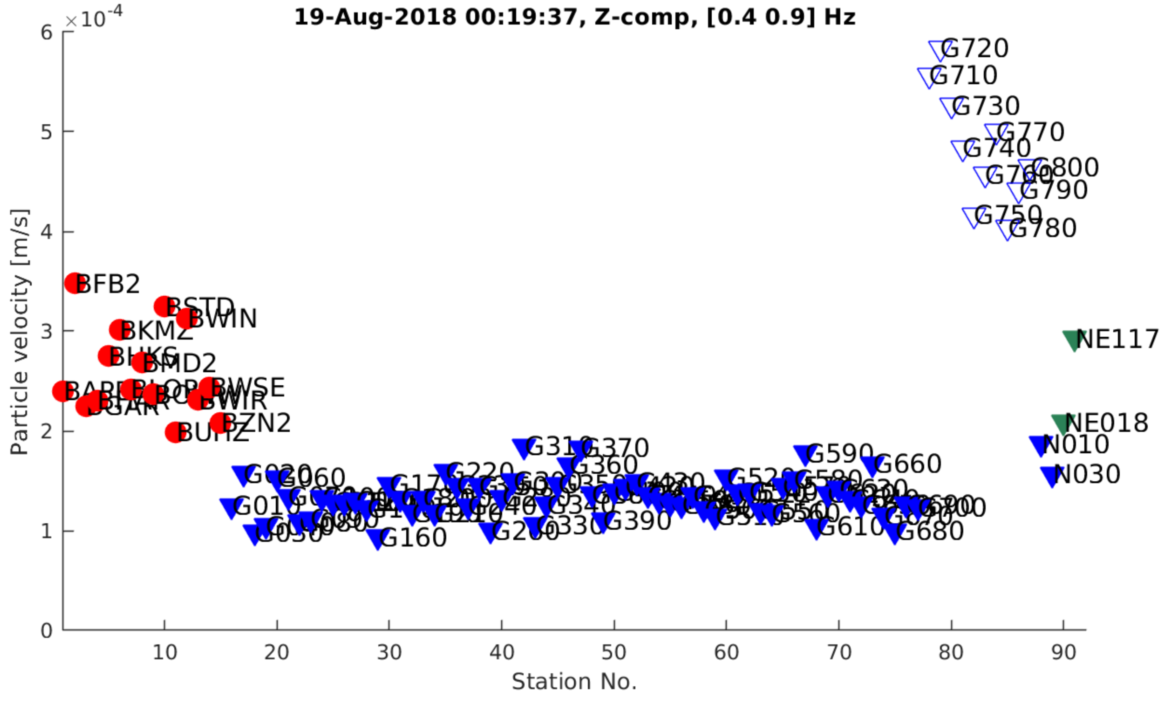

A difference in gain setting was found between the accelerometers of the B- and G-network and the later installed G710-800 accelerometers.

Data were not yet used in GMM development

It did influence Mw calculations, not the ML calculations (based on 200m borehole geophone signals)

Ntinalexis et al., J. Seism. 2019

Quality control

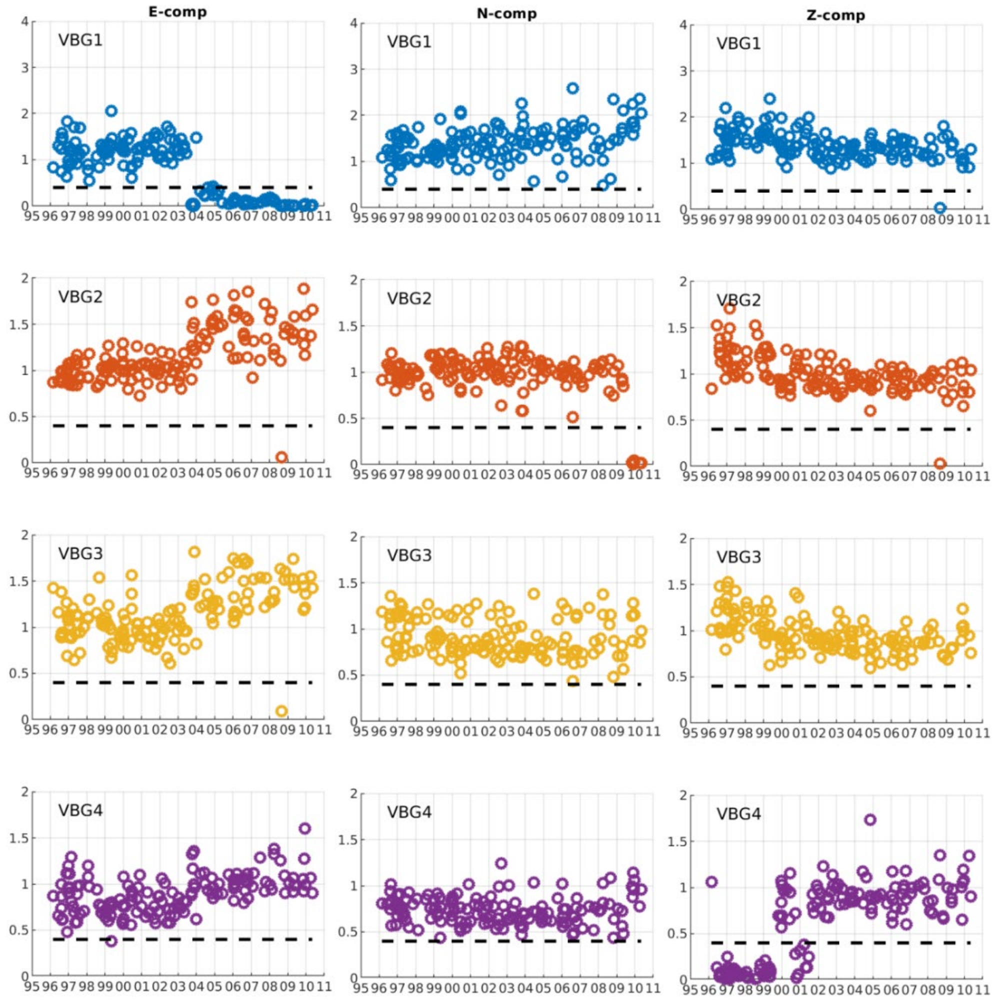

Triggered borehole data (1995-2011):

The maximum absolute amplitude value of individual borehole channels , normalized with respect to the average maximum absolute amplitude of this channel

Periods of degrading amplitudes can easily be identified.

KEM 11c: Quality assurance and publication of the KNMI 1995-2013 induced seismicity data, evaluation by NORSAR

Magnitude

Local magnitude (ML)

- Fast calculation (max hor. comp. WA simulated signal), based on 200m deep sensor data

Moment magnitude (**M**)

- No saturation, based on physics
- Calculated from earthquake spectra or through moment tensor inversion

Relation between M and ML required for hazard assessment

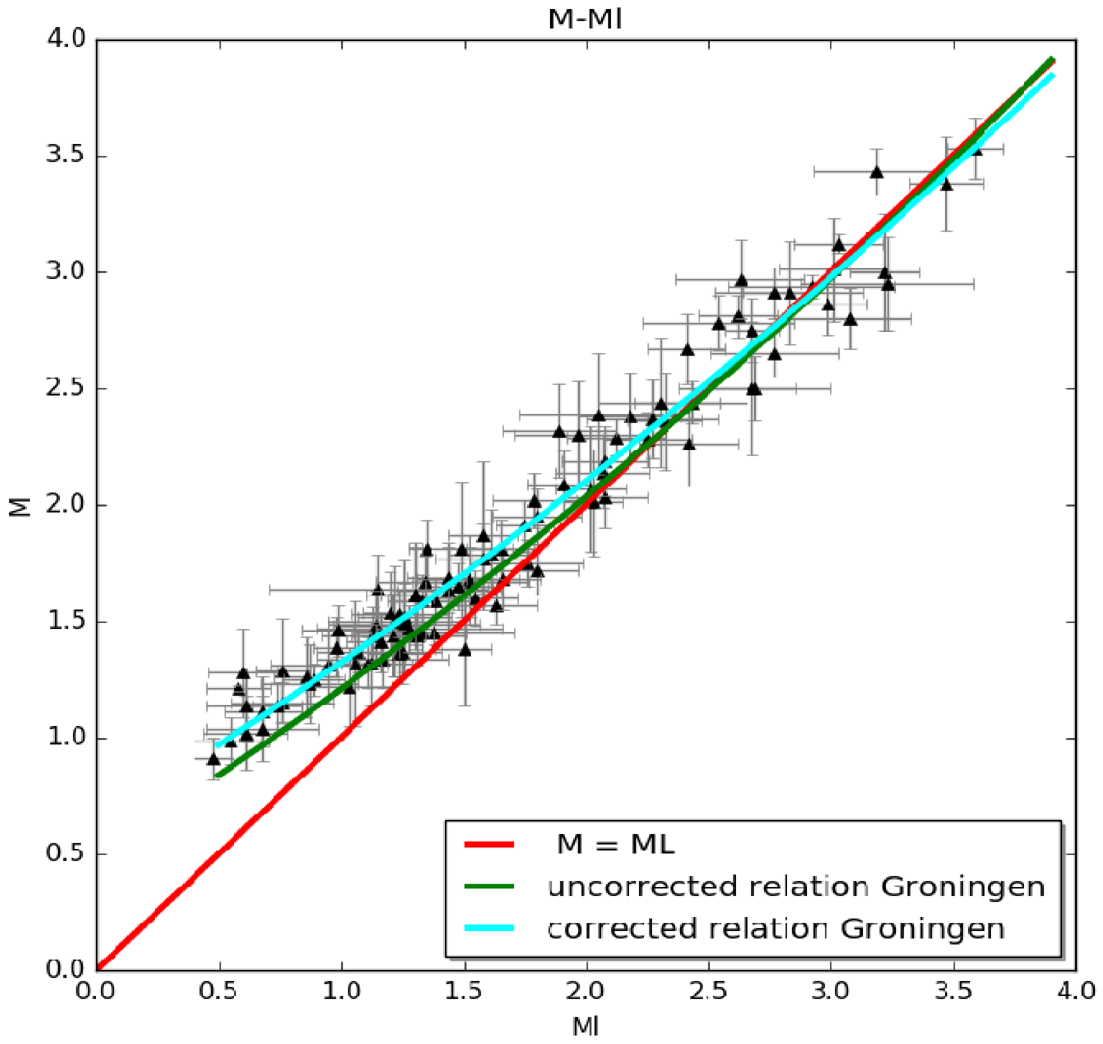

Dost et al., SRL, 2018, 2019

Earthquake location

- Accurate velocity model (NAM 3D)
- Rapid location using hypocenter software (uncertainty x,y,z ~0.5 km)
- Application of new location algorithms (e.g. EDT)
- Re-location using:
  - Modified EDT method (Spetzler & Dost, 2017, GJI)
  - Relative locations of clusters (Jagt et al., 2017, NJG)
  - Moment tensor inversion (Willacy et al., 2018, 2019; Kuehn et al., 2020; Dost et al. (2020))

3D velocity model for Groningen

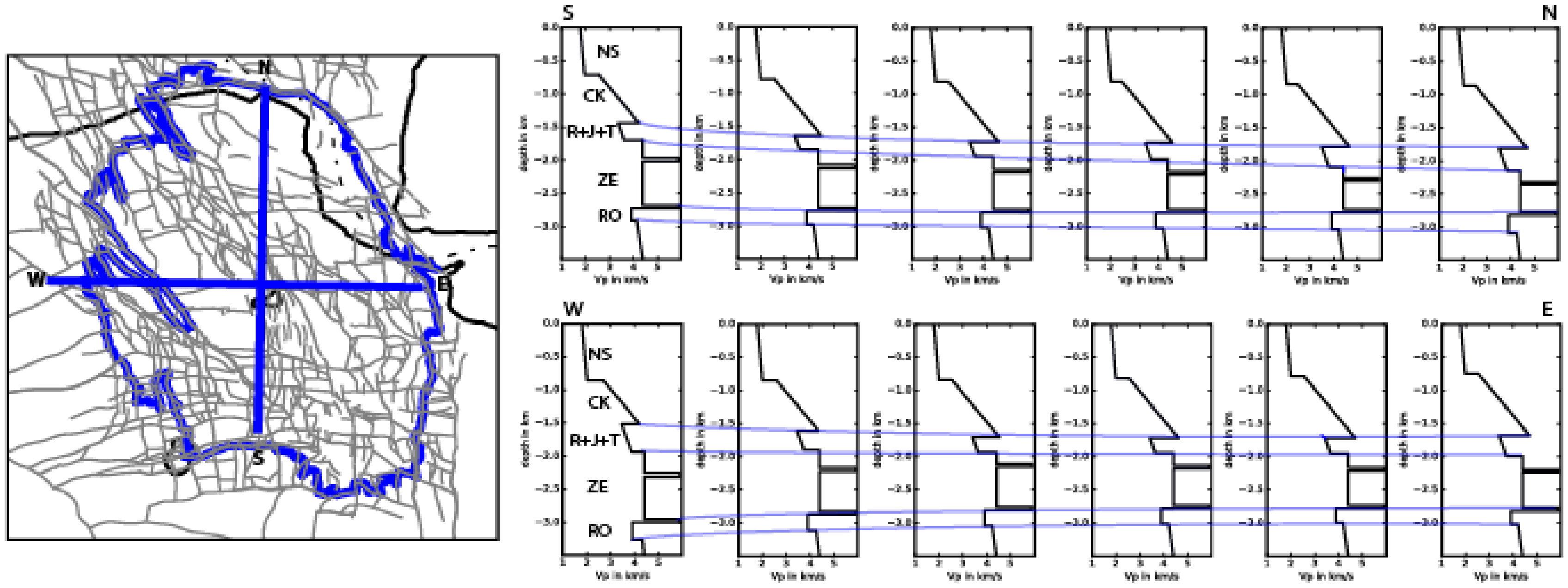

- EW and NS transects of P-velocity model through the Groningen field. Shown are averages in depth and velocity over a box with a 5 km radius.
- 3D model contains both P- and S-velocities (Romijn, 2017)
- S-N: Increase in the depth of the Chalk (CK) layer and a deepening of the top reservoir.
- W-E: a shallowing of the top reservoir

Hypocenter location

Old network:
Interstation distance ~20 km
Location accuracy 0.5-1 km

New network:
Interstation distance 4-5 km
Location accuracy 0.1-0.3 km

Vertical misfit function

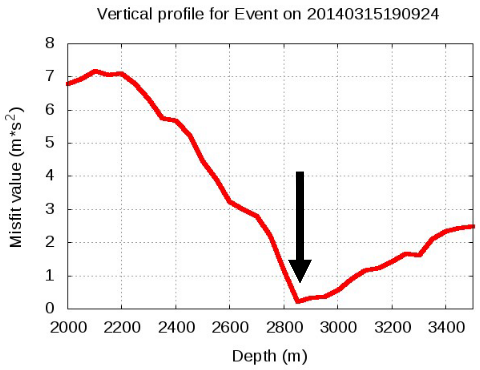

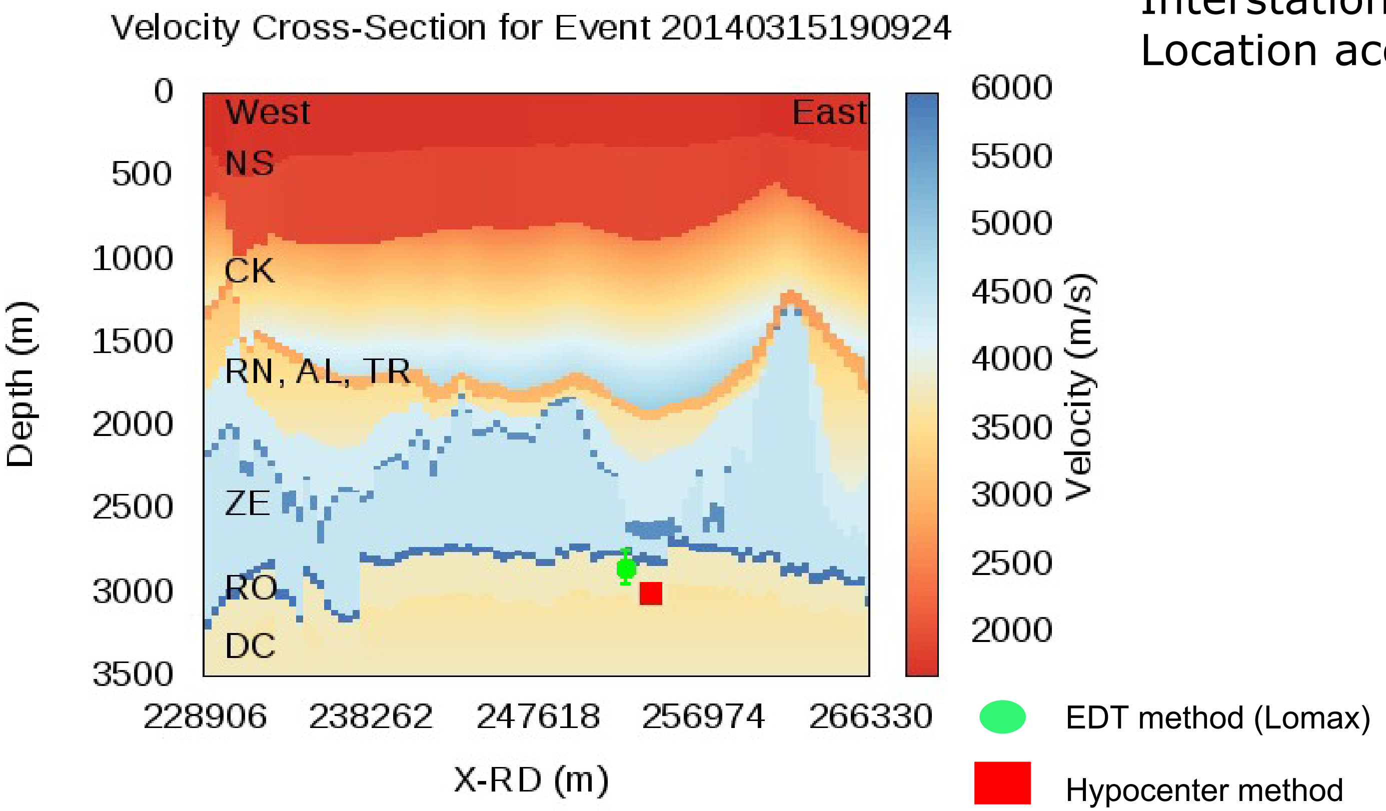

Analysis of deep boreholes (NAM, microseismicity) shows most events are confined to the reservoir e.g. Pickering (2015)

Spetzler & Dost, 2017, GJI

Hypocenter location

Improved resolution shows good correlation with existing faults

Addition of information on the earthquake mechanism will corroborate or falsify this apparent correlation

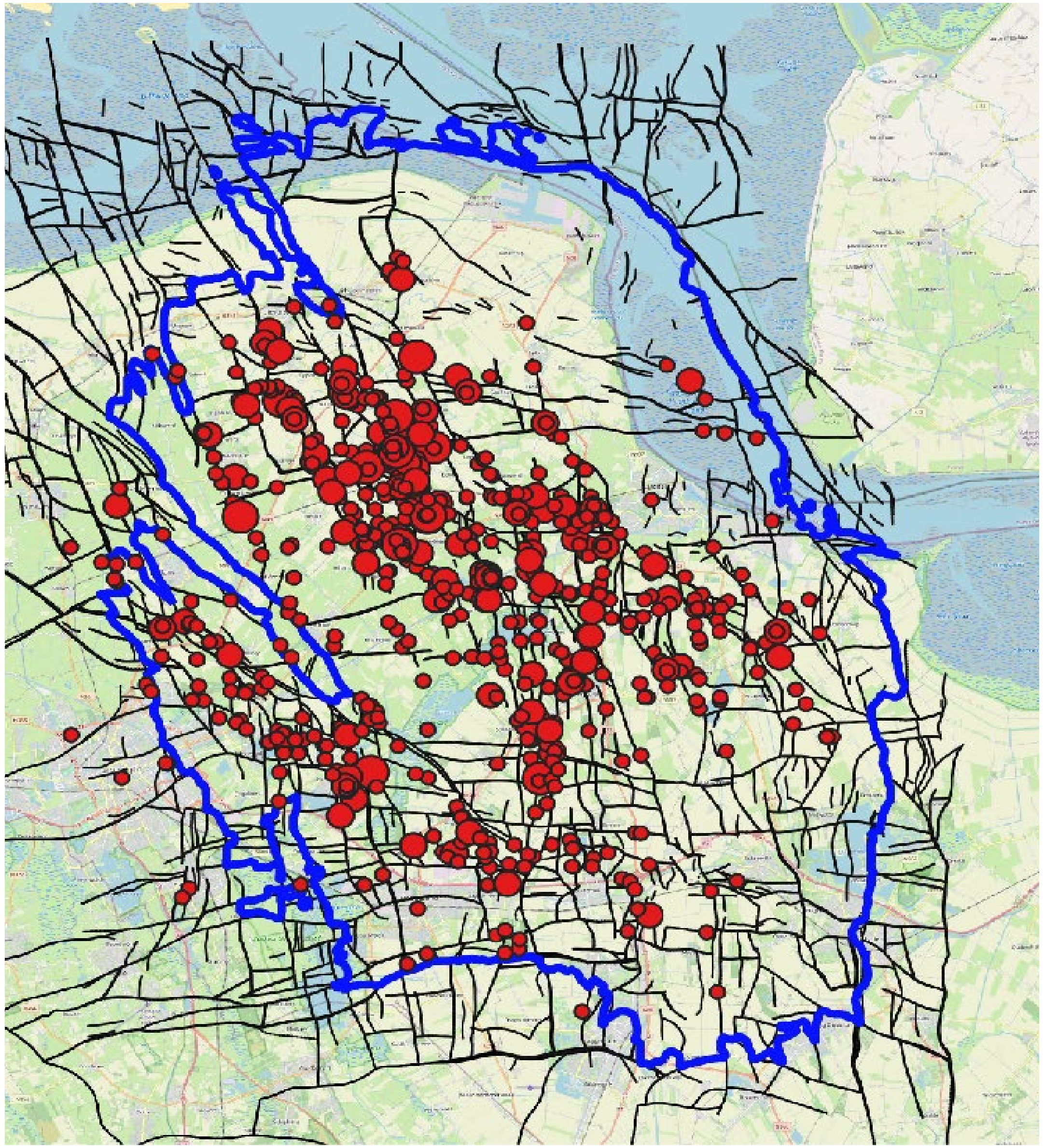

Moment tensor solutions for Groningen

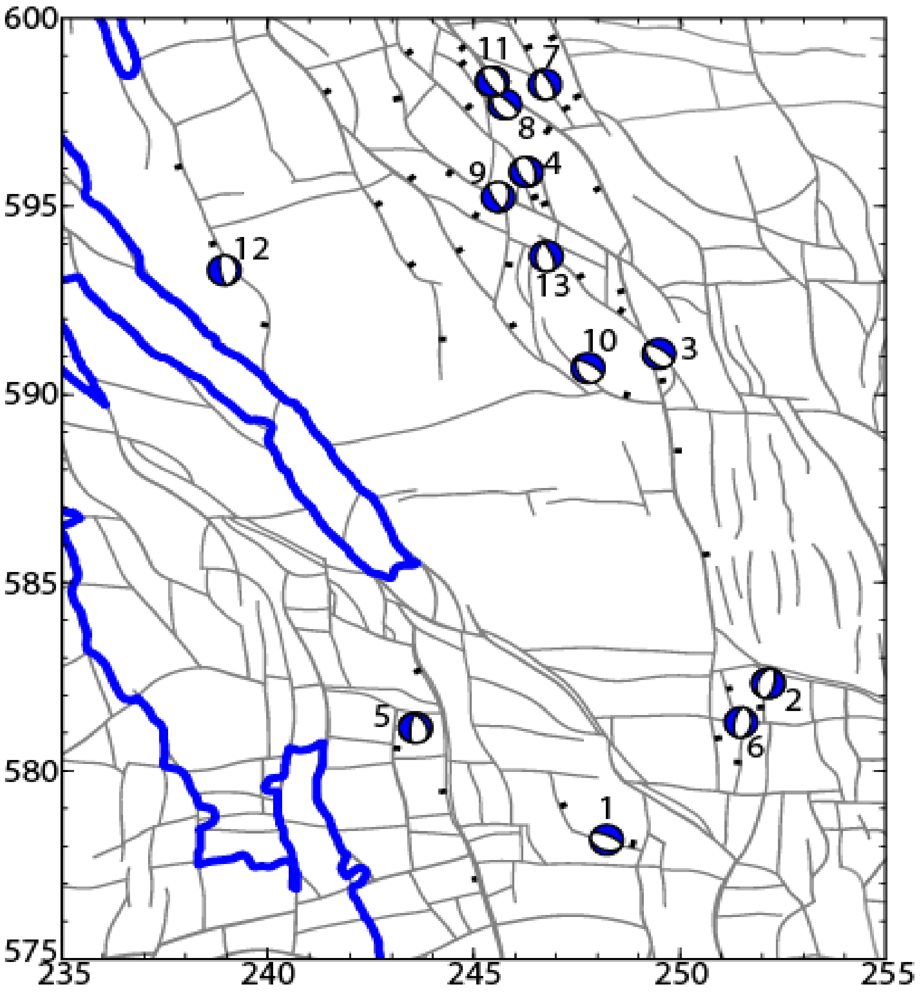

Dost et al., 2020, BSSA

- M ≥ 2.0, 2016-2019
- Method:
  - Full waveform probabilistic optimization method (Pyrocko/Grond)
- Results:
  - Normal faulting, dip 50-70º
  - Re-activated faults are identified
  - Locations from MT inversion are within 250m from re-location solutions using other inversion methods.
  - Double Couple (DC) solutions allow to distinguish between neighboring faults
  - A consistent negative isotropic component was found (up to 50%).

Re-activated faults

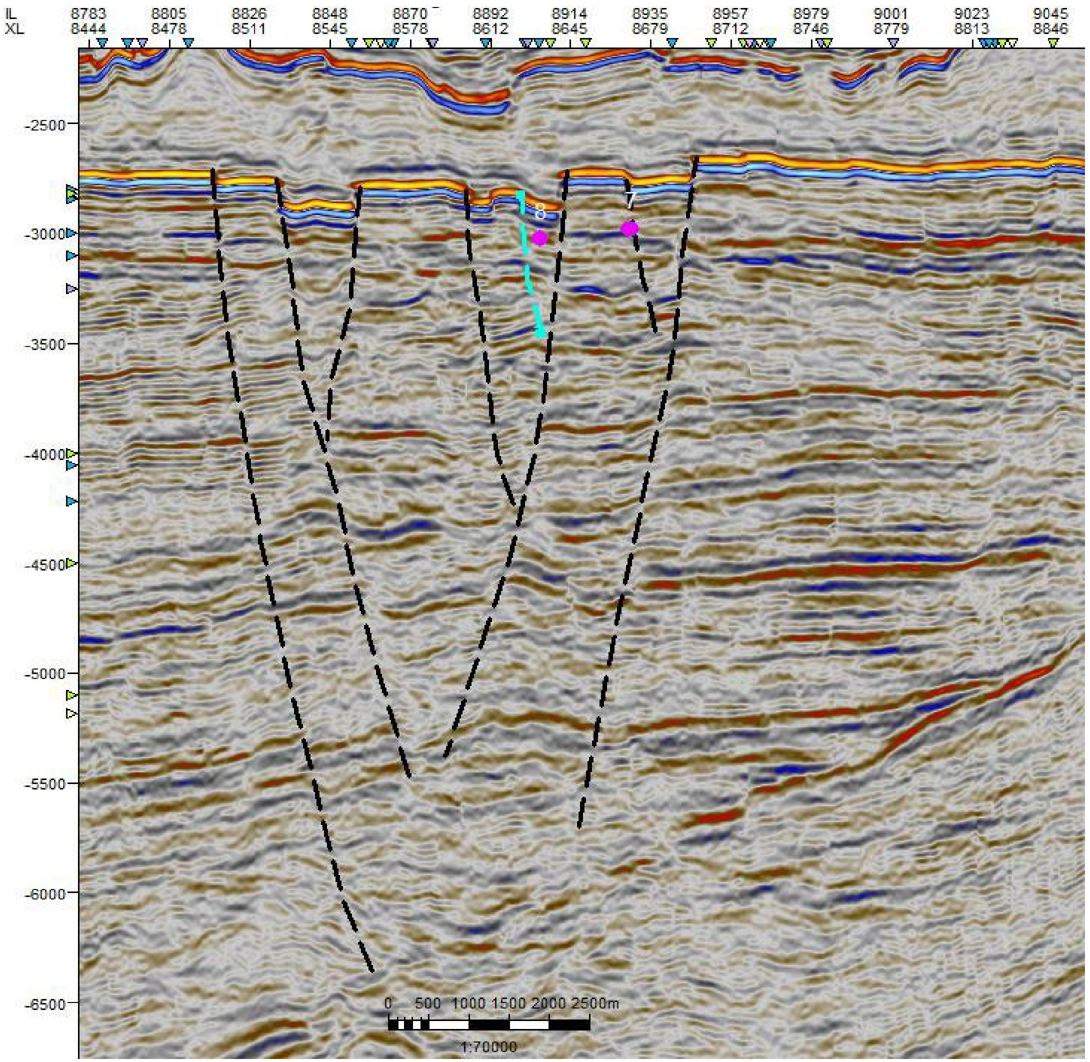

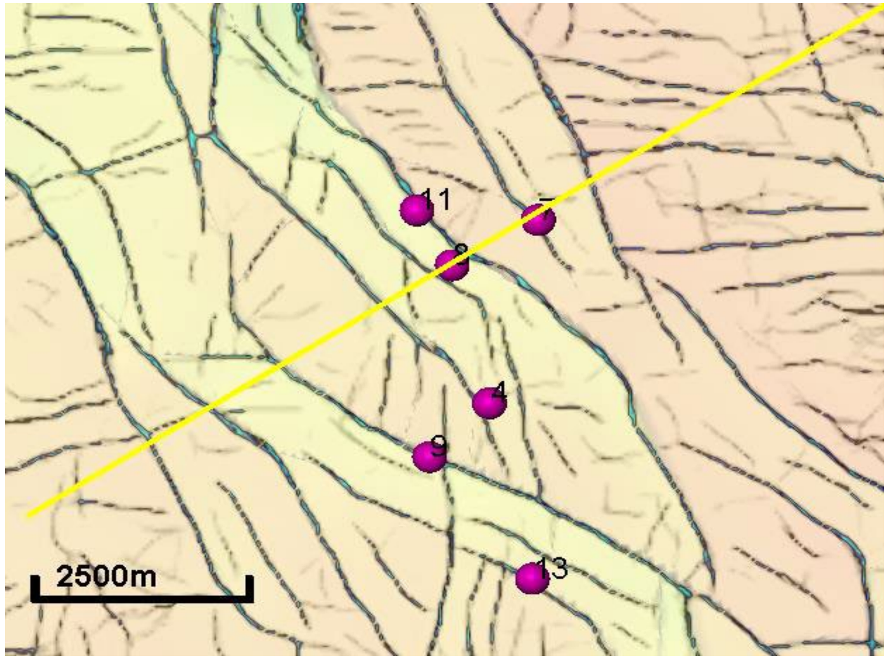

Interpretation:

- Re-interpretation of faults using ant-tracking show continuation in the Carboniferous
- Events occur mainly along faults with a small throw

Dost et al., 2020, BSSA

Data products

Open data policy: waveform data, event Catalog, shakemaps (M>2.0), comparison with GMM

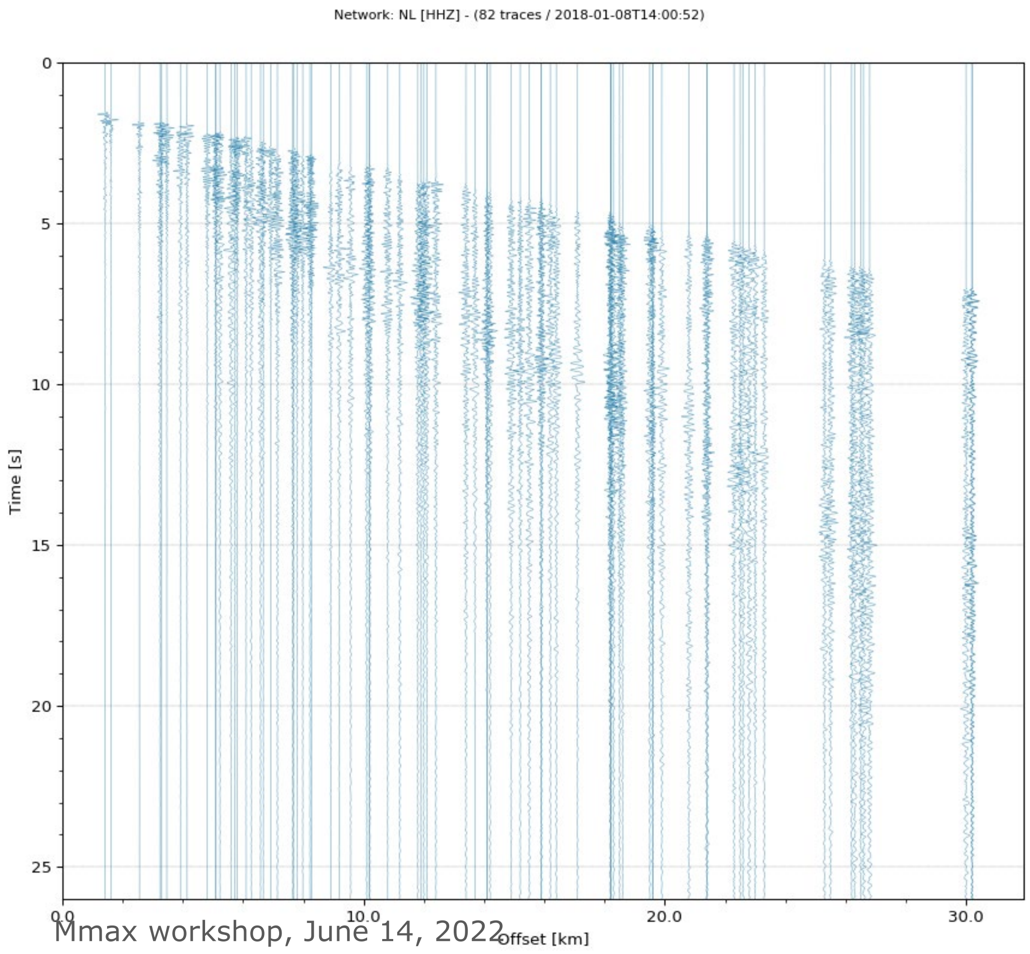

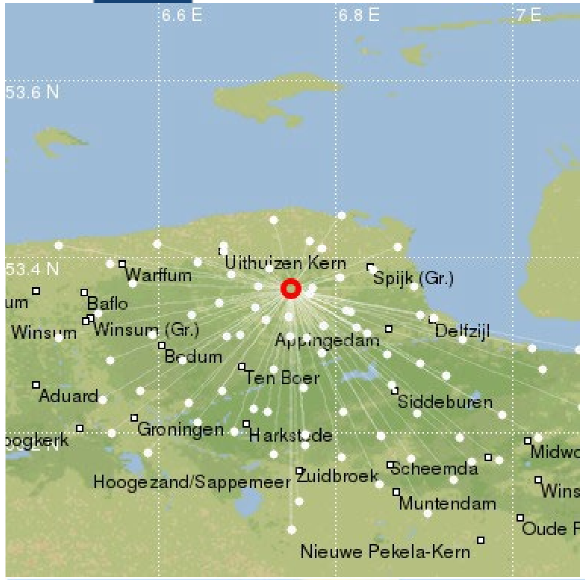

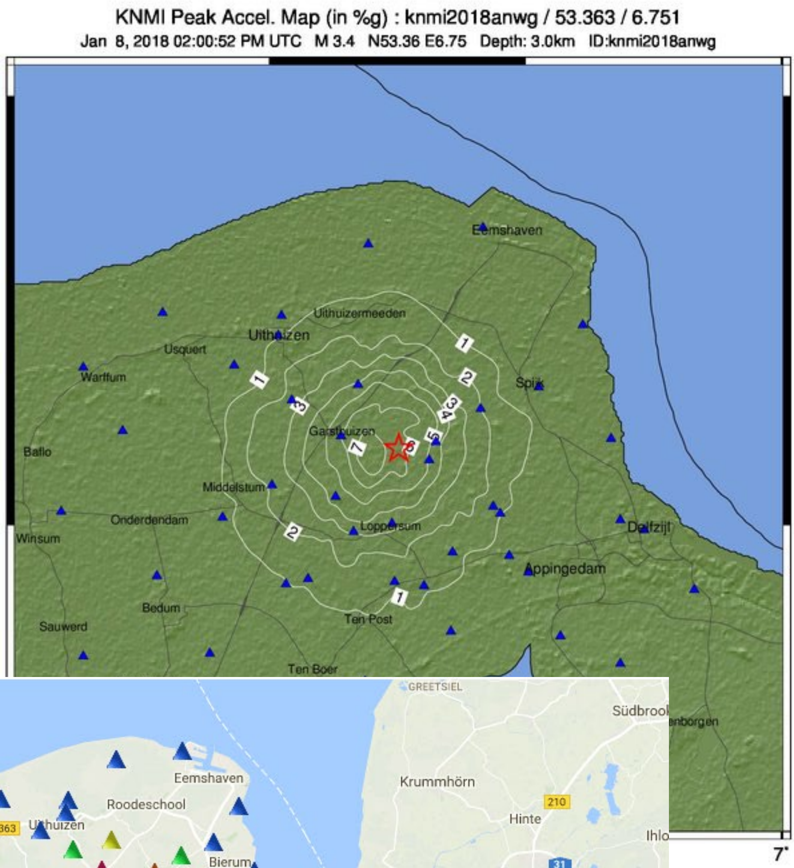

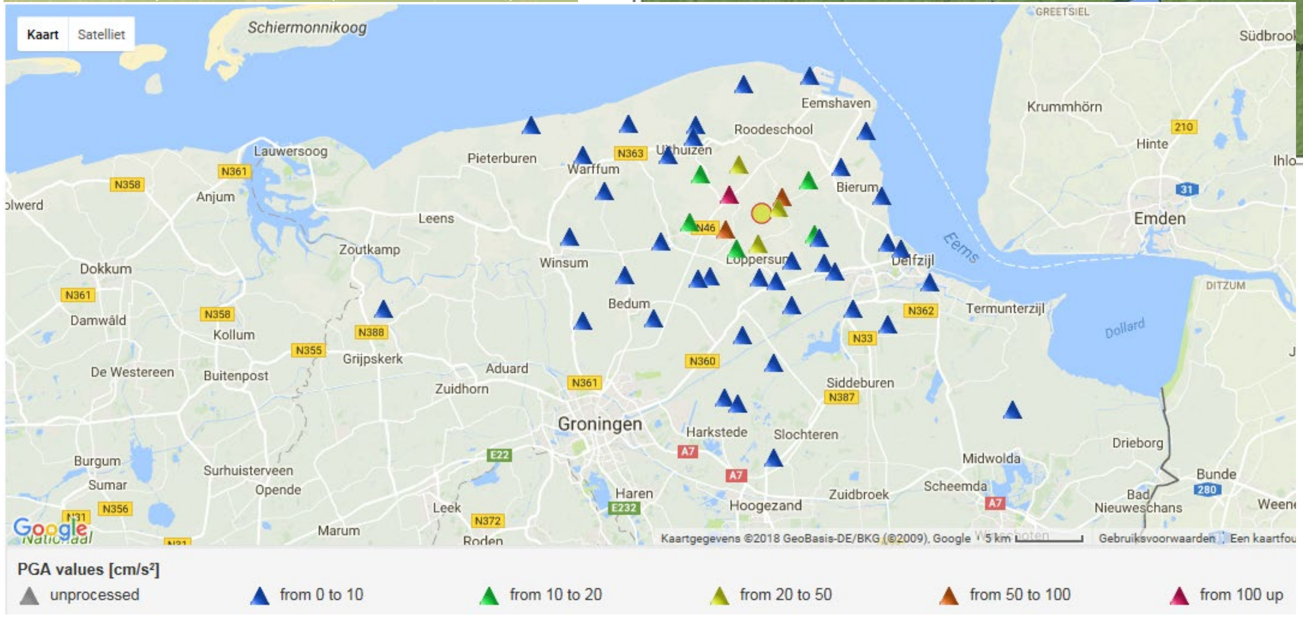

Conclusions

- Monitoring of the Groningen gas-field developed from a network capable to detect events (1995-2014) to a network capable to study e.g. the relation between seismicity and existing faults (>2014).
- Data are used in e.g. the development of Groningen GMMs.
- Dense borehole networks as the Groningen network require new ways of (automated) quality control.
- Most events occur within the reservoir, which was also seen in microseismicity studies using deep boreholes at reservoir level.
- Moment tensor inversion results show a good correspondence between seismicity and known faults in Groningen.
- All data and products are open available from http://rdsa.knmi.nl .

Groningen earthquakes: focal depths and fault ruptures

Steve Oates
Shell GSNL-PTD

With numerous contributions from Ewoud van Dedem, Sara Minisini, Jelena Tomic, Remco Romijn, Tom Piesold, Brian Zurek & Matt Pickering

Summary

- Background
  - Groningen subsurface velocity model
  - Overview of induced earthquakes
- Event depths
  - Initial difficulties
  - Deep downhole array results
  - Full waveform inversion results
- Empirical Green's Function analysis
  - EGF deconvolution
  - Simple kinematic models of rupture
  - Rupture propagation analysis
- Conclusions

Groningen subsurface summary

- SE-NW geological cross-section of the Netherlands running through the Groningen gas field.
- From: “Geological Atlas of the Subsurface of the Netherlands”, TNO, 2004

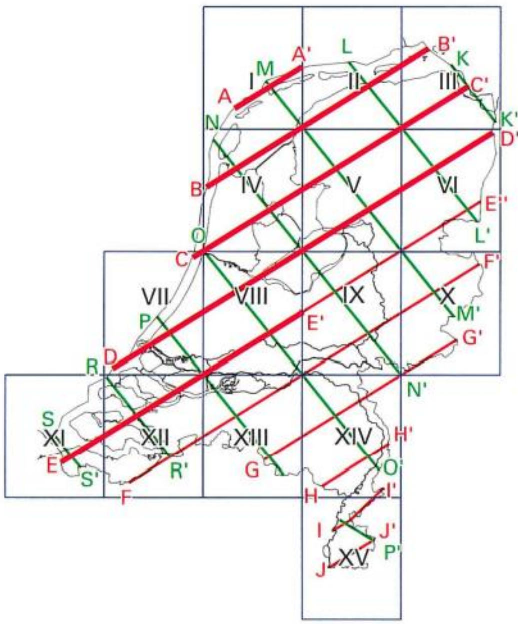

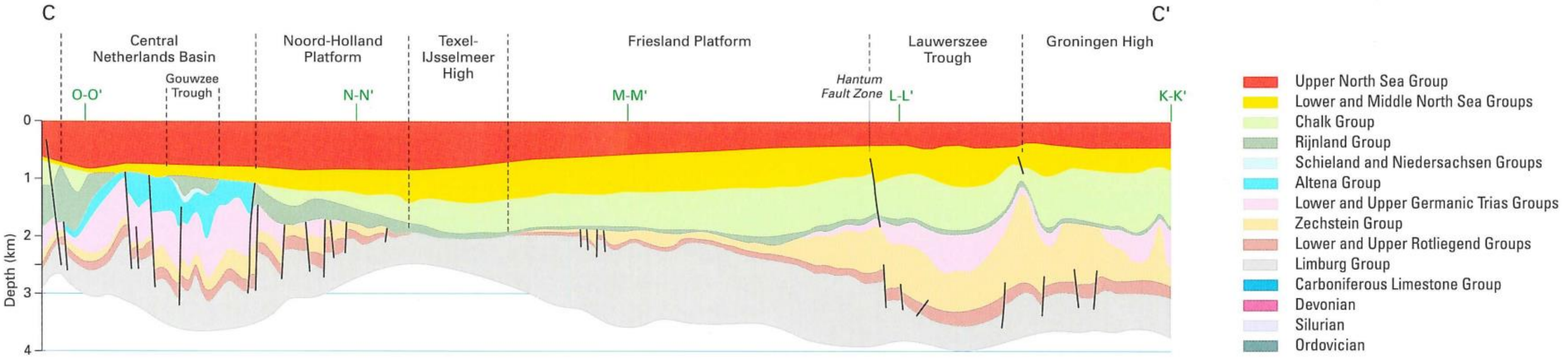

Groningen seismicity overview

- Earthquake locations from the KNMI database (red dots); the shallow borehole array locations (green diamonds); deep borehole arrays in SDM-1 and ZRP-1.
- Willacy et al Leading Edge 2020.

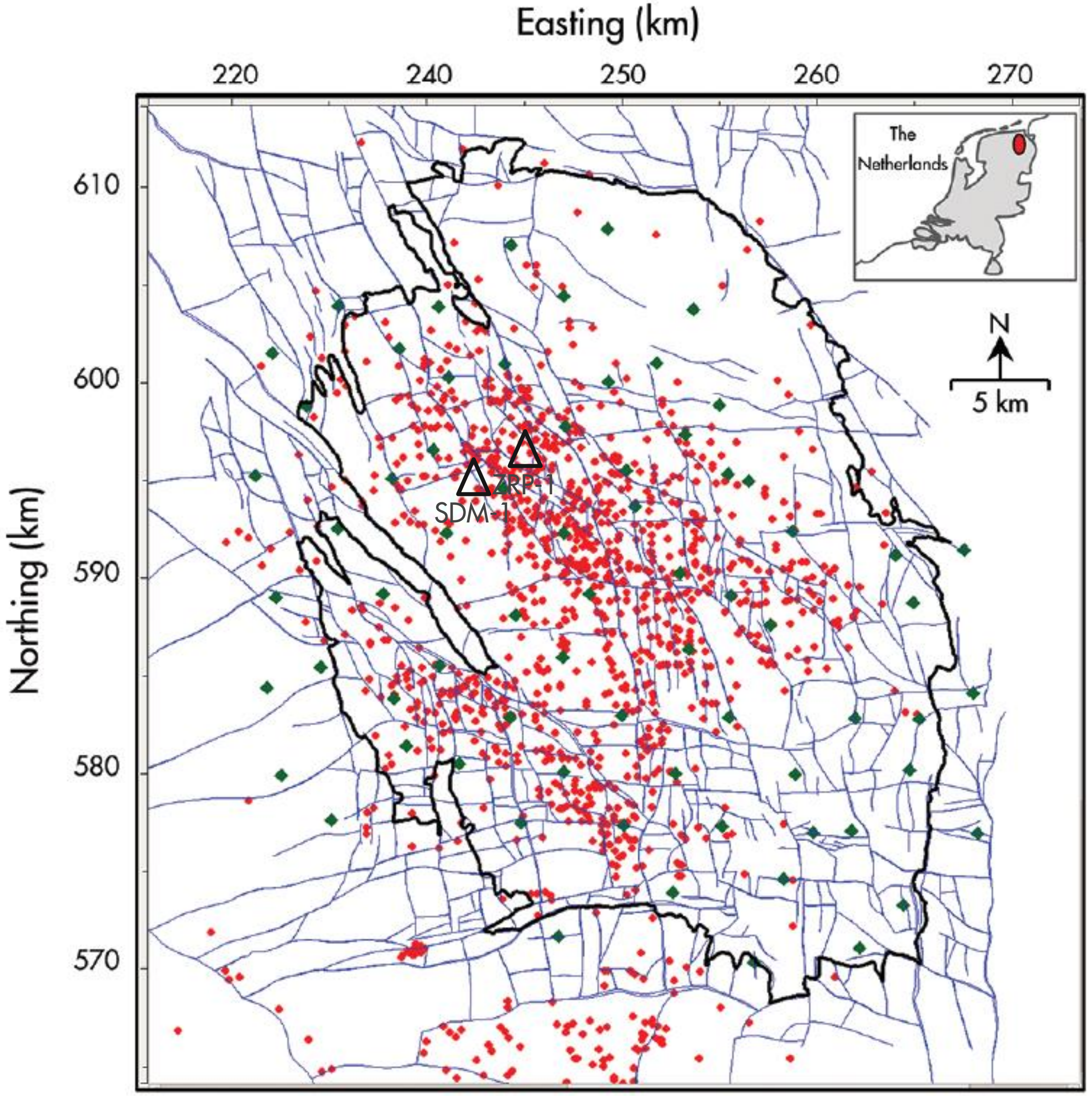

Groningen velocity model around ZRP-1

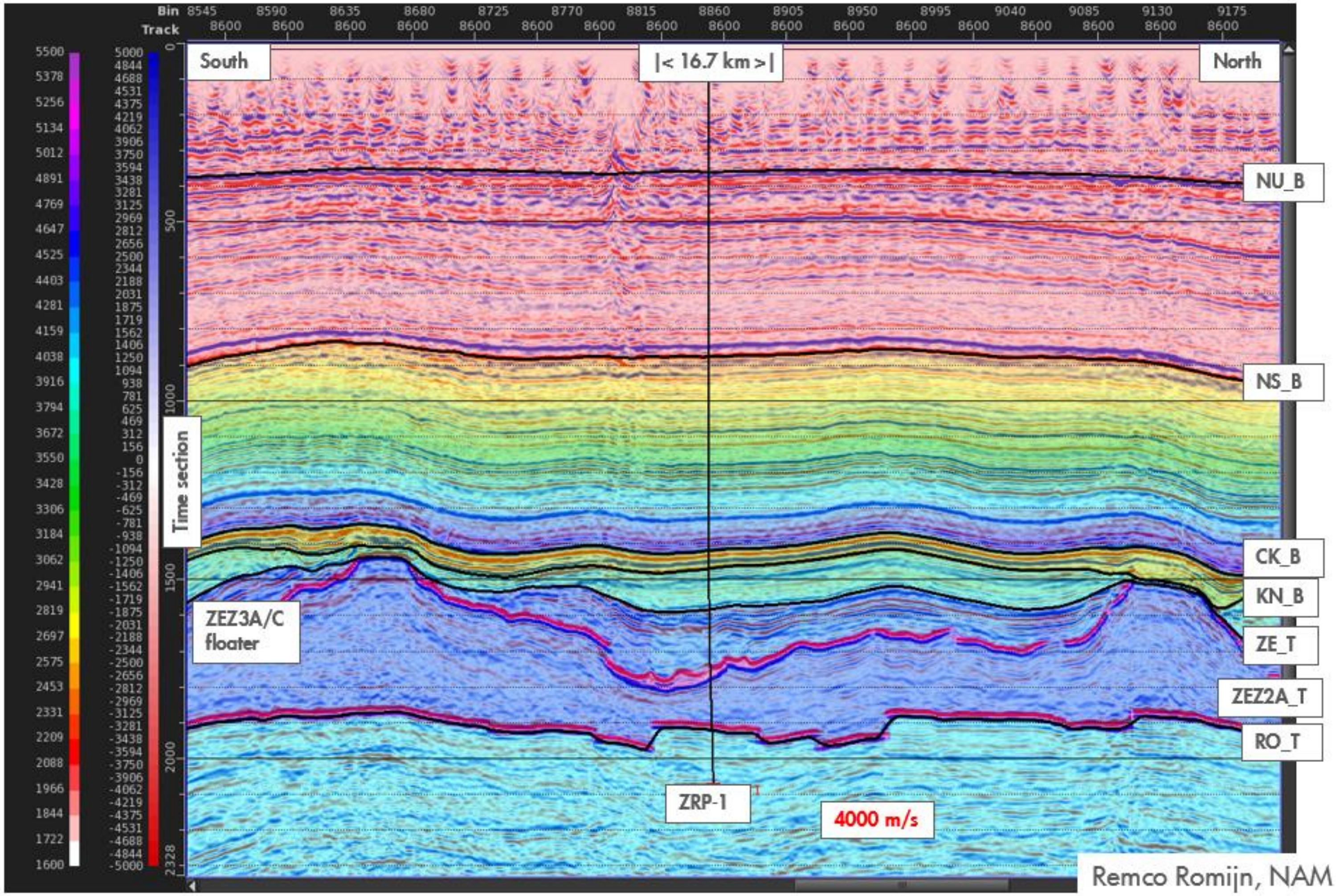

Finite difference modelling – DC source in reservoir

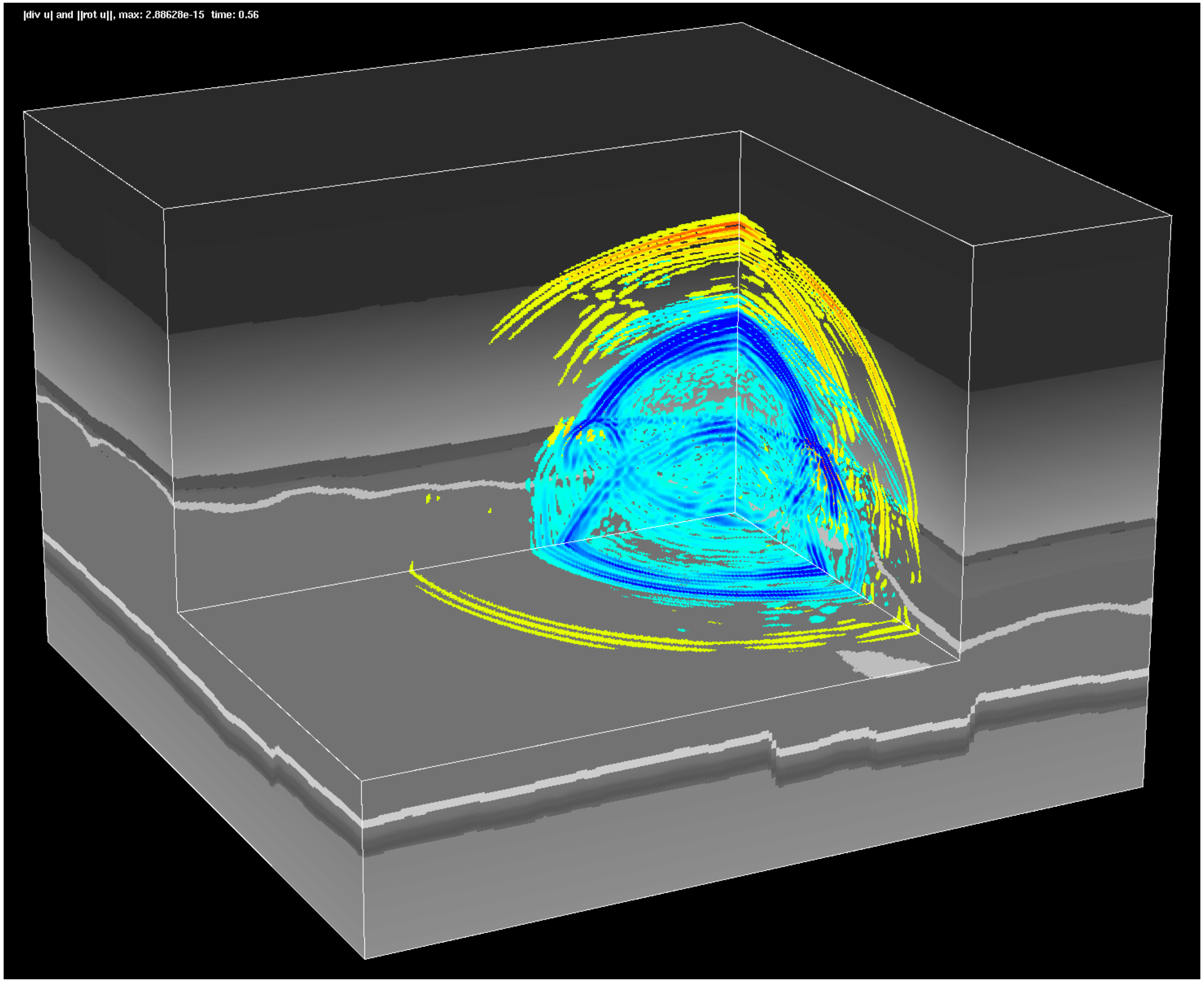

Finite difference modelling – DC source in reservoir

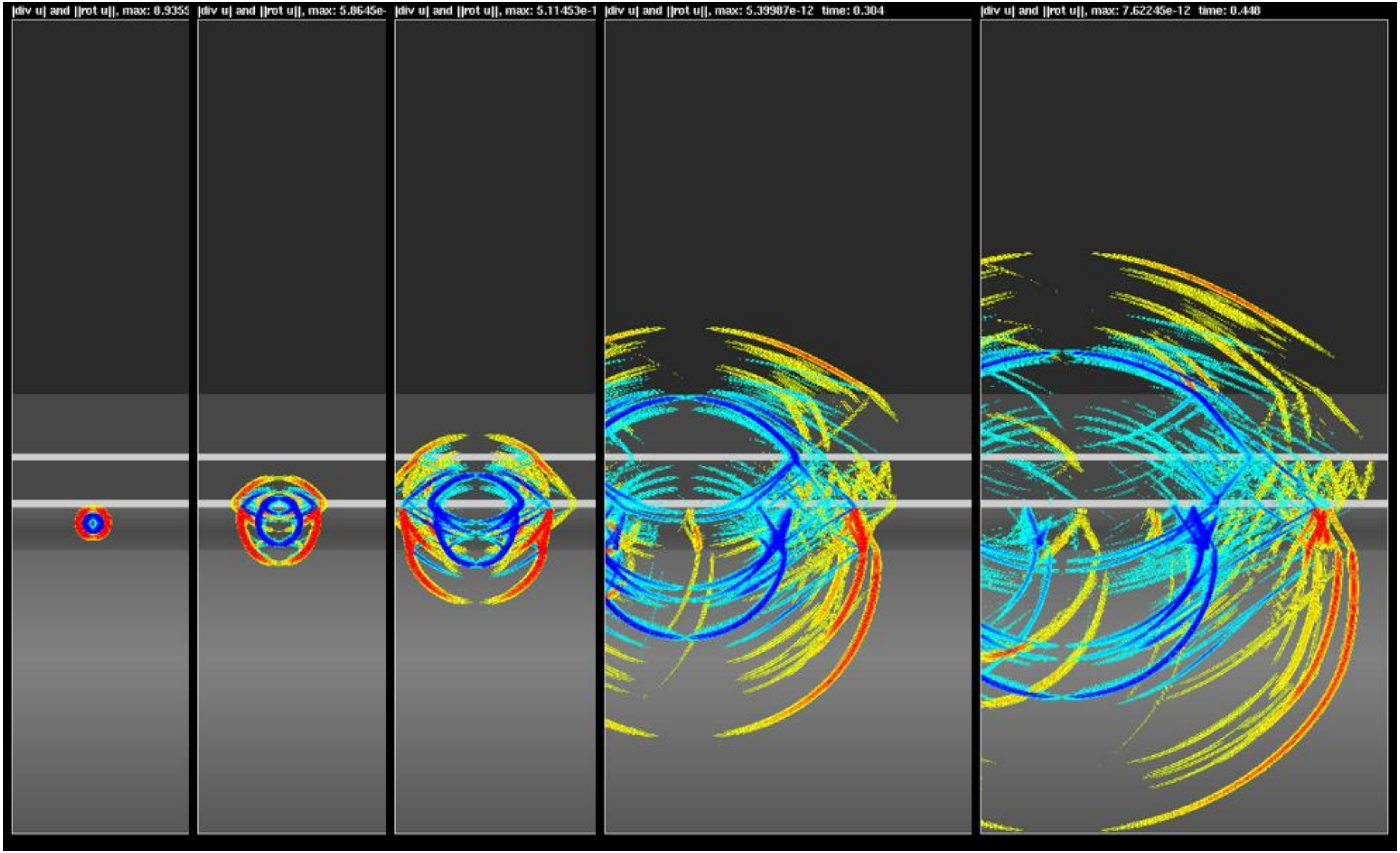

Groningen event depths

- KNMI’s location workflow calculates epicentral location and assumes events in the reservoir at depths of approximately 3km – motivated by sparseness of original near surface array, difficulty to reliably pick S arrivals and need for a robust automated workflow.
- A number of discussions in the public domain following the 2012 Huizinge earthquake, focused attention on the need to verify the event depths.
- NAM installed in-well geophone arrays in Stedum-1 and Zeerijp-1 with the main objective of constraining event depths – are events in the reservoir, above the reservoir or below it?

Deployment of deep arrays Stedum and Zeerijp

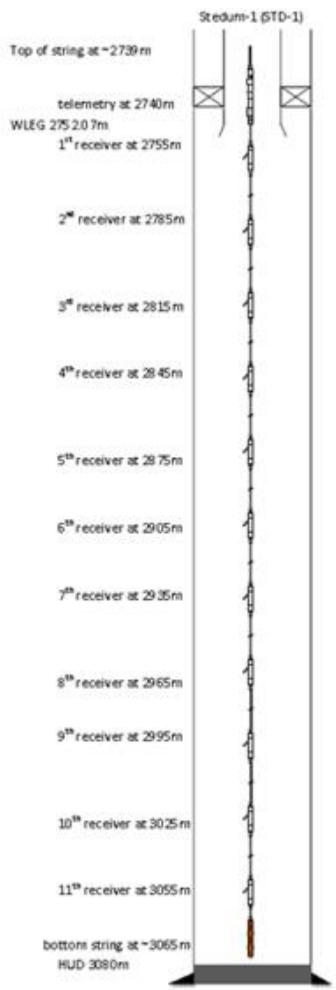

Stedum-1: geometry as planned

Stedum-1: deployment 8th Oct 2013

Groningen event depths – initial difficulties

- Initial event locations obtained by Magnitude (Baker-Hughes) placed the detected events deep in the basement.
- KNMI observed that many events fell on the same sloping trajectory in a depth-offset plot leading to the realization that the picked first arrivals were head waves but the inversion code was treating these as direct arrivals resulting in incorrect locations.
- Resolving this led to events locating in and around the reservoir... (next slide)

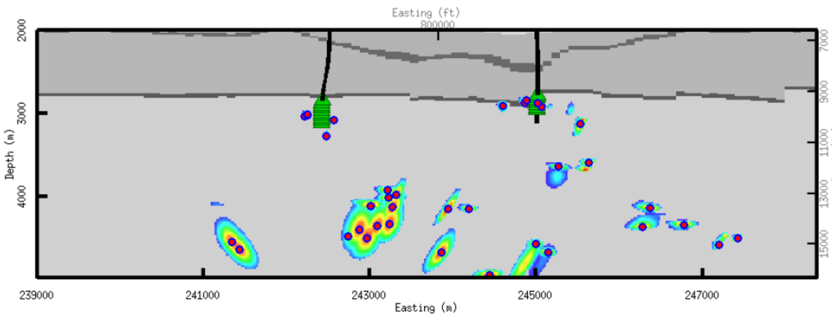

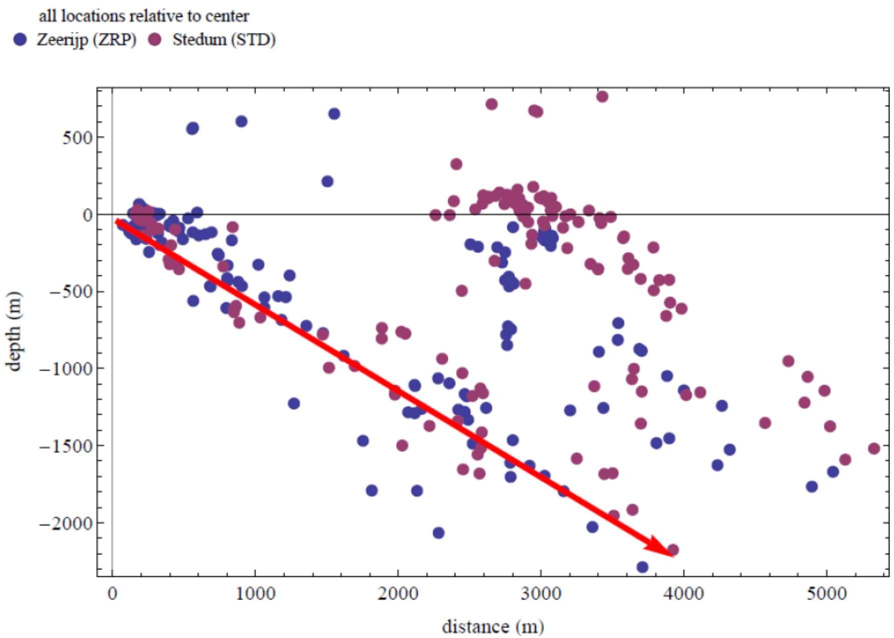

Dirk Kraaijpoel, KNMI

Magnitude deep array locations to Jan 20th 2015

- Event locations from Magnitude using revised data processing workflow.

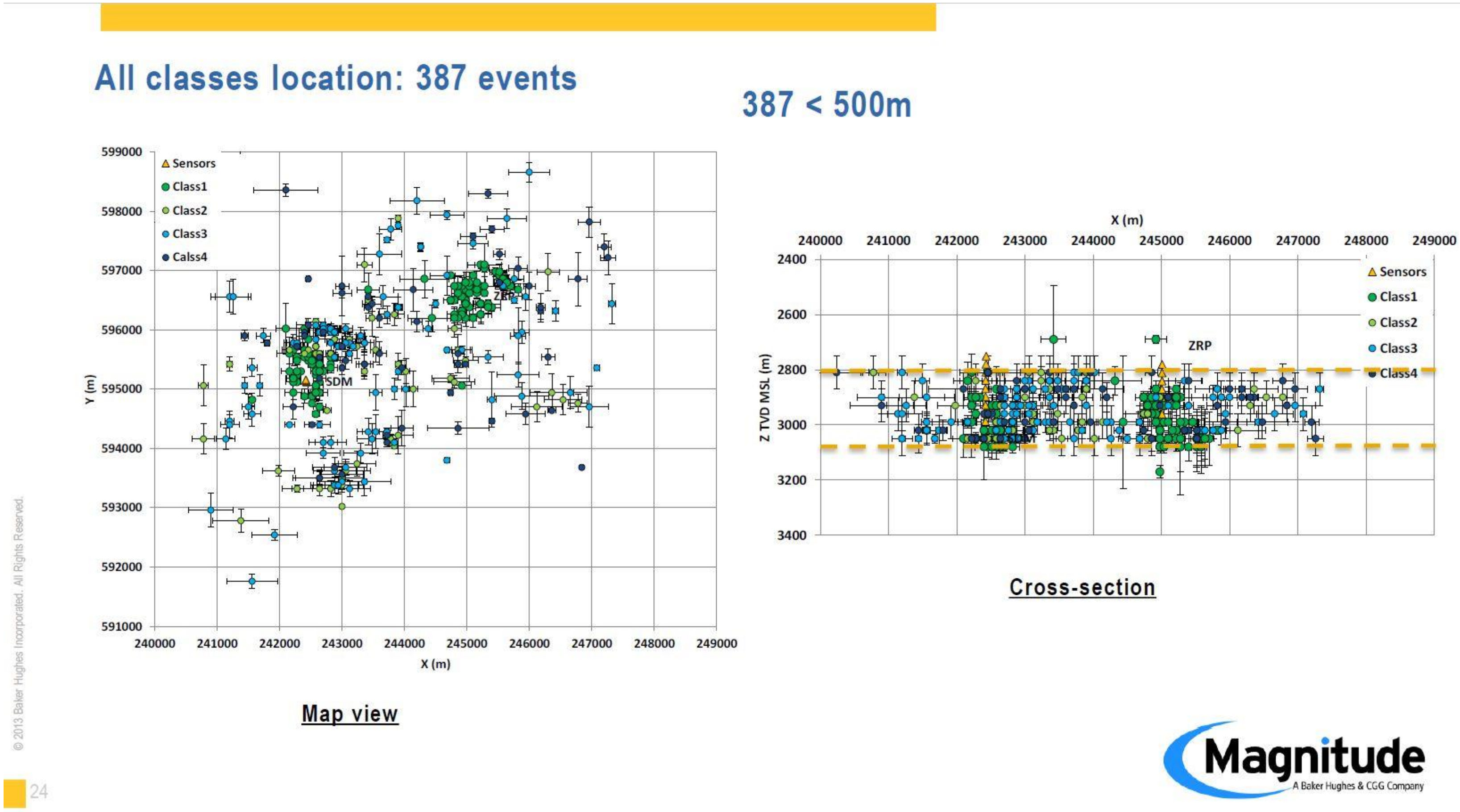

Full Waveform Inversion results

- Typical FWI objective function example.
- Objective function displayed is one minus the normalized cross-correlation coefficient between observed and synthetic data.
- Objective function strongly localized in reservoir interval.
- Willacy et al Leading Edge 2020.

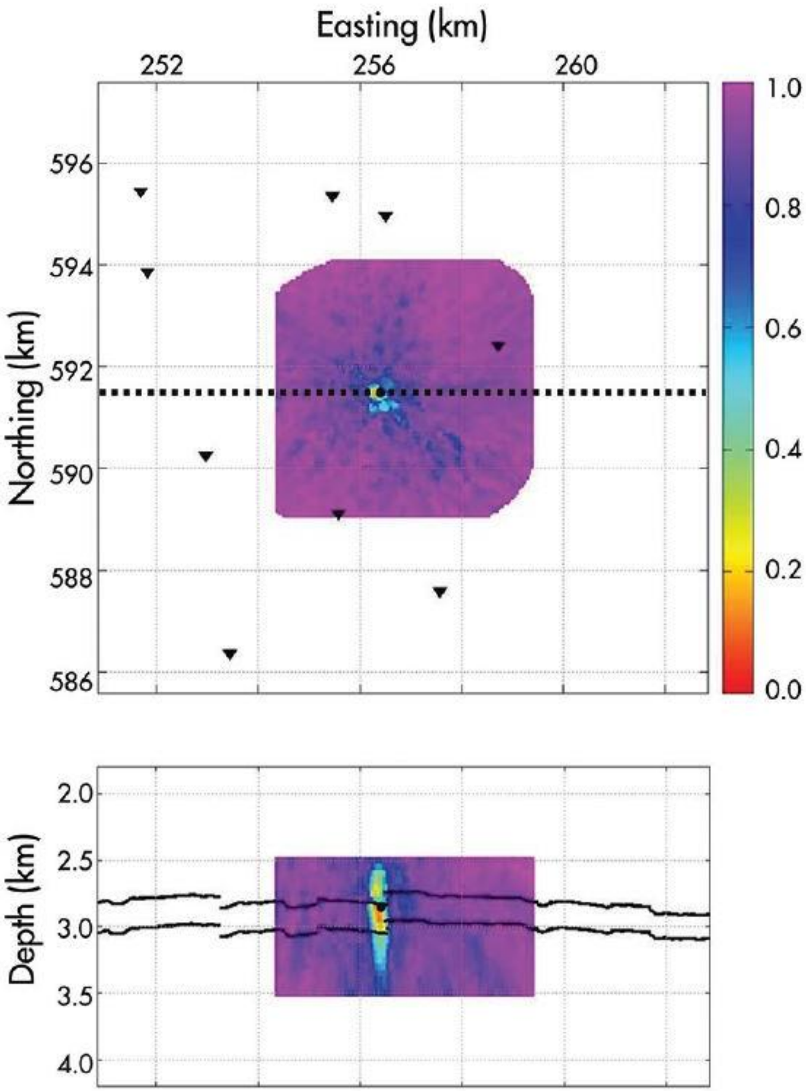

Full Waveform Inversion results

- WE and NS profiles showing top and base reservoir interfaces and FWI event locations projected onto the sections.
- Magenta locations from deep downhole array; blue and red from near-surface array (manual and automatic FWI workflows).
- Willacy et al Leading Edge 2020. See also Willacy et al Leading Edge 2018.

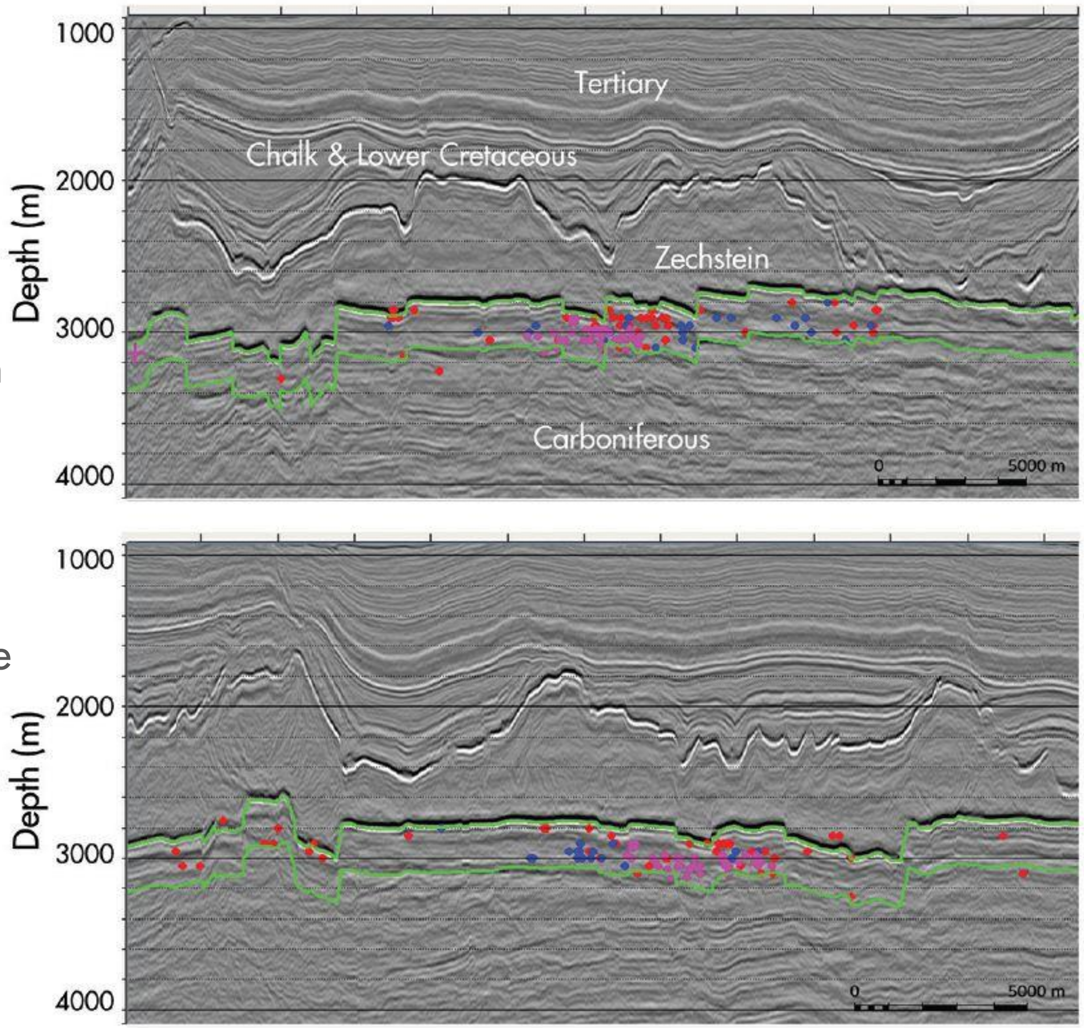

Groningen events in the reservoir?

- Groningen velocity structure (Rotliegend acts as a waveguide) leads to complex seismograms (multiple arrivals, mode conversions, trapped waves etc…) on deep downhole array and near-surface network data.
- Waveform complexity makes event location challenging – model-driven arrival picking needed.
- NAM-Magnitude workflow based on interpretive arrival picking locates events in and around the reservoir.
- FWI results support this – FWI objective function strongly localised in reservoir interval.

Summary

- Background
  - Groningen subsurface velocity model
  - Overview of induced earthquakes
- Event depths
  - Initial difficulties
  - Deep downhole array results
  - Full waveform inversion results
- Empirical Green's Function analysis
  - EGF deconvolution
  - Simple kinematic models of rupture
  - Rupture propagation analysis
- Conclusions

EGFs in a nutshell – example 17123/18002 (M=1.7/3.4)

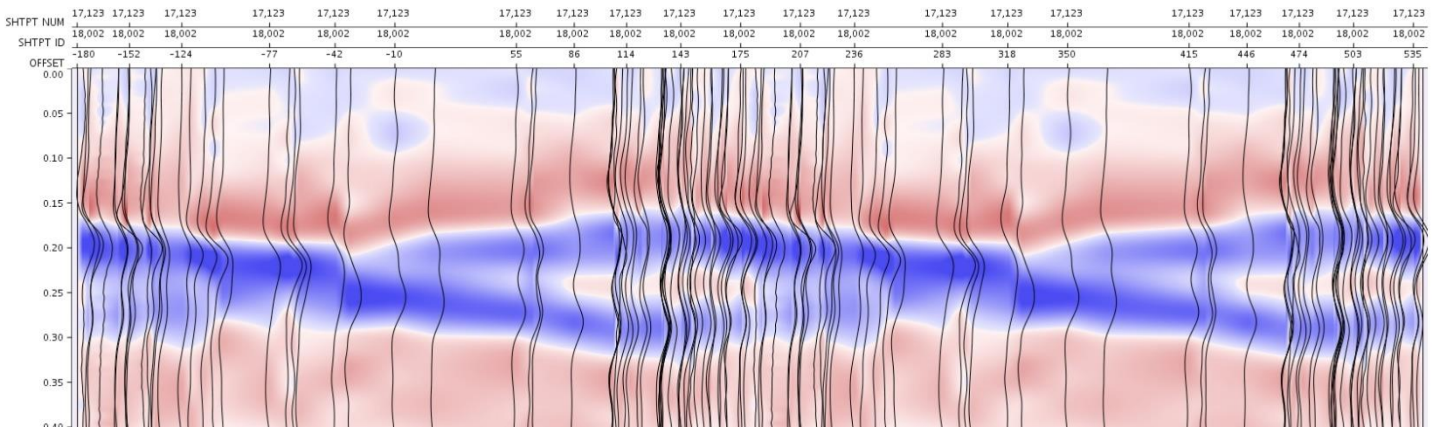

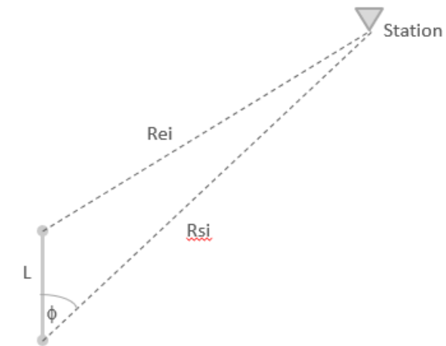

- EGF event pairs identified by high wave-form similarity
- Collocated larger 'parent' event and smaller 'child' event.
- Deconvolution of parent seismogram by child removes common propagation effects, leaving relative source time function (RSTF) – can be seen as an expression of the propagating rupture.
- Duration of RSTF = picked time between zero crossings.
- Duration as a function of source-station azimuth fits simple model of rupture propagation dominated by a starting and stopping phase.
- Simple expression for Doppler broadening can be inverted for rupture propagation strike, length and velocity.
- Interpretation also supported by synthetic seismic models.

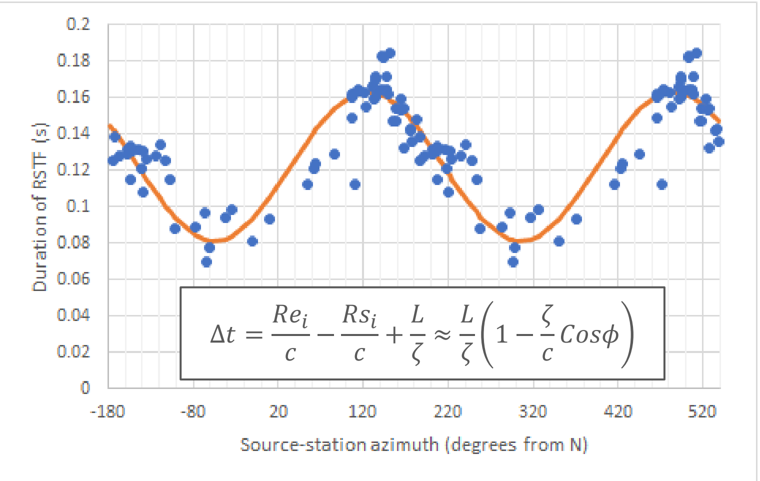

Cluster FWI results – van Dedem et al EAGE 2018

Full waveform results for events from 2015 to 2018

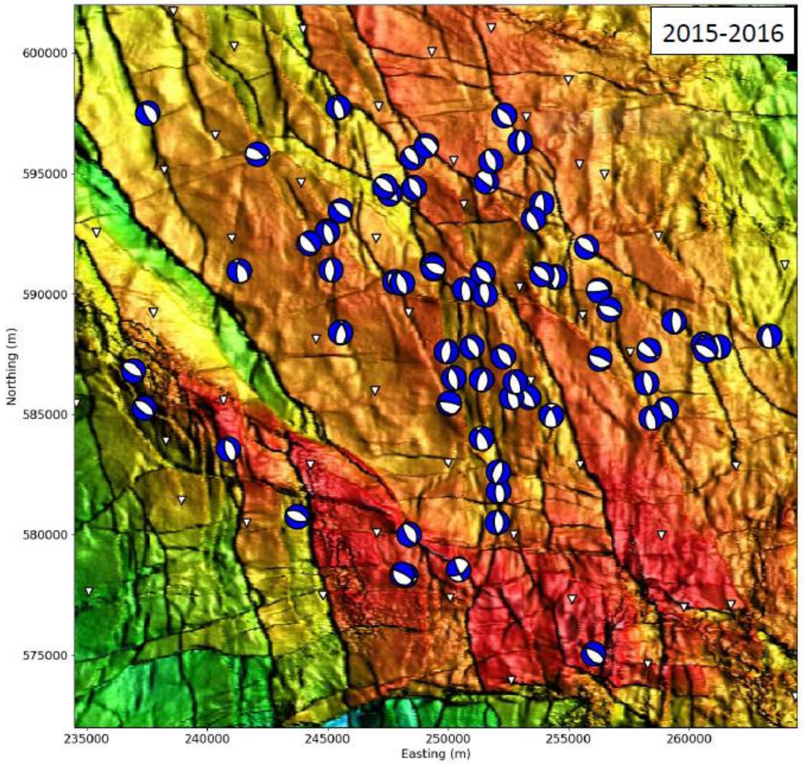

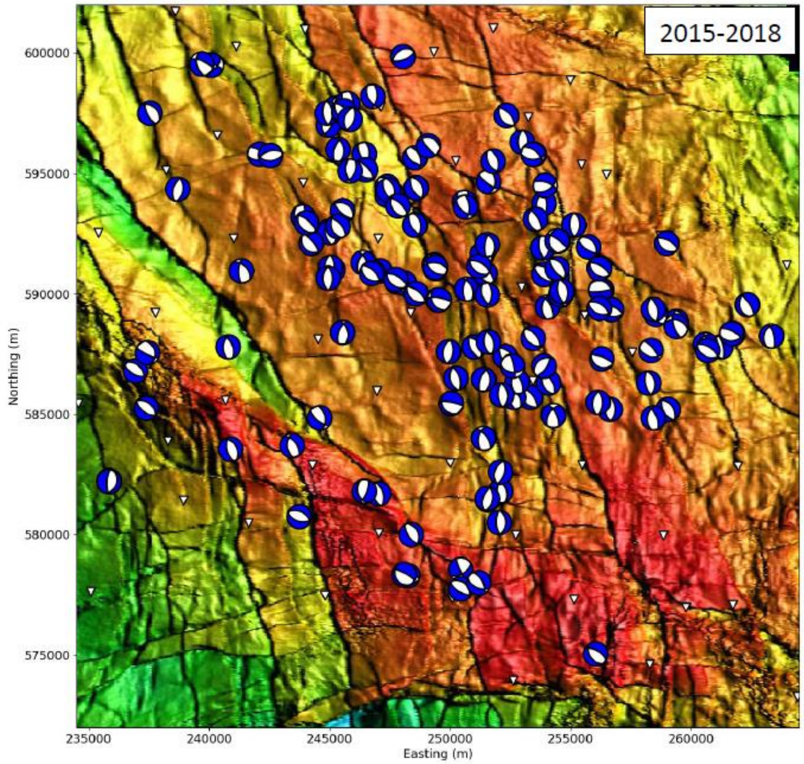

Note: all events are located within the reservoir section

Cluster FWI results – van Dedem et al EAGE 2018

Full waveform results of identified event clusters

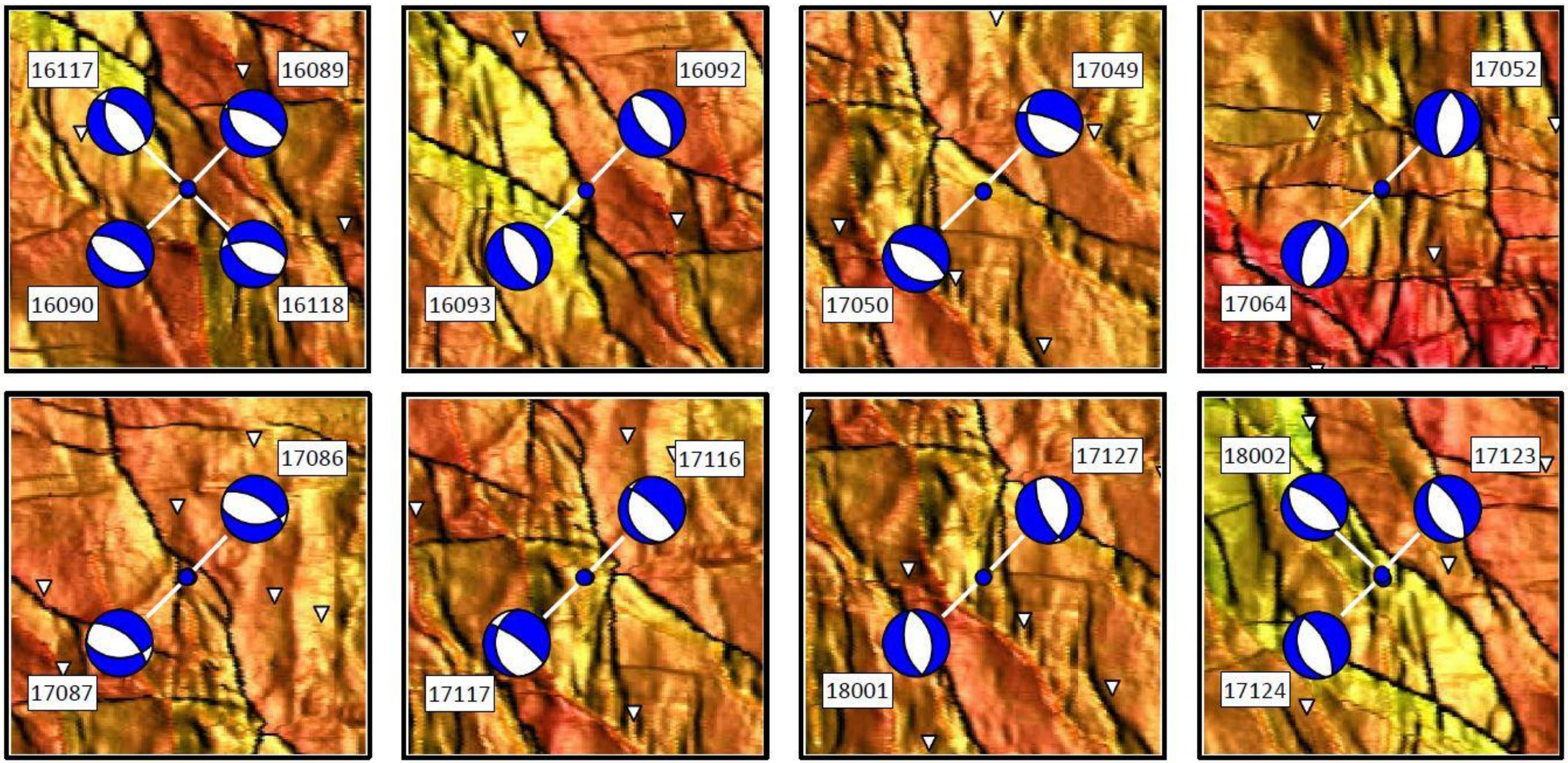

KNMI catalogue – foreshock-aftershock sequences

- Statistical evidence of temporal and spatial clustering seen calibration of the ETAS aftershock component of the Groningen seismological models – in the region of 20% of the located Groningen earthquakes should be regarded as aftershocks.
- Example: observation of aftershock sequence on downhole array following M = 3, 13th February 2014.
- Looking at catalogue as a whole:
  - N/day for following 5 and 7 events plotted with event magnitude if M≥2.2
  - Shows in many cases coincidence of large events with bursts of seismicity – foreshock-aftershock sequences.

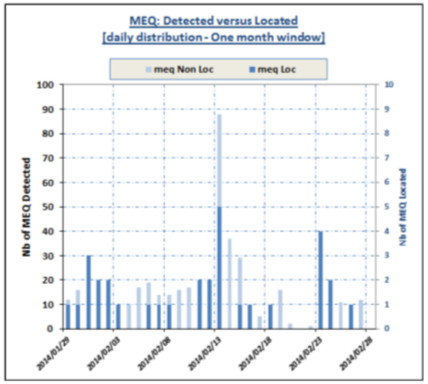

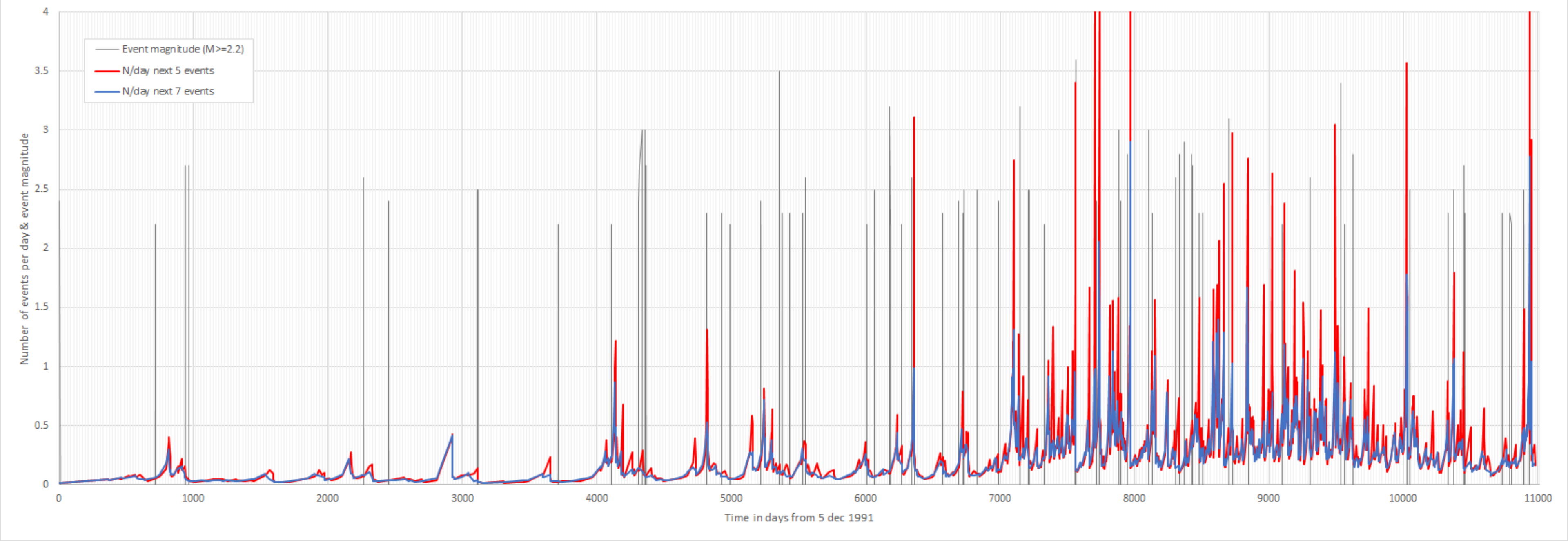

EGFs background – Li et al & Savage

Deconvolve seismograms from a pair of nearby events to give relative source time function (eg. Li et al 1995):

$U_l(t) = S_l(t) * P(t) * R(t) * I(t)\ ;\ U_g(t) = S_g(t) * P(t) * R(t) * I(t)$

$U_l(t) * (U_g(t))^{-1} = S_l(t) * (S_g(t))^{-1} = S_r(t) \approx S_l(t)$

The relative source time function only equals the source time function of the larger event if the source time function of the smaller event is a delta function:

$U_l(t) * (U_g * S_g^{-1})^{-1} \approx S_l(t)$

We use deconvolution implemented as a spectral division with additive noise:

$$\widetilde{U}_l(\omega)D(\omega) = \frac{\widetilde{U}_g(\omega)\widetilde{U}_l(\omega)}{\widetilde{U}_g^2(\omega) + N.\max(\widetilde{U}_g^2(\omega))}$$ (Berkhout 1977)

Directional variation of pulse width and amplitude is usually analysed for rupture direction by applying the theory in Savage's paper for source directivity effects:

$T(\psi) = T(1 - (\zeta/c)\cos(\psi));\ A(\psi) = A/(1 - (\zeta/c)\cos(\psi))$.

EGF duration – simple kinematic rupture models

Summary of model expressions for duration in which starting- and stopping-phases dominate.

Unilateral rupture propagation:

$$\Delta t \approx \frac{L}{\zeta}\left(1 - \frac{\zeta}{c} Cos\phi\right) + w_t$$

Bilateral rupture propagation:

$$\Delta t \approx \frac{L}{\zeta}\left(1 + \frac{\zeta}{c} |Cos\phi|\right) + w_t$$

Both events (unilateral) propagating ruptures, $N \gg 1$:

$$\Delta t \approx \frac{(L + l)}{\zeta}\left(1 - \frac{\zeta}{c} Cos\phi\right) + w_t$$

Δt is independent of source-source offset.

w_t is a remaining wavelet width.

Azimuthal variation gives clean estimate of length and strike.

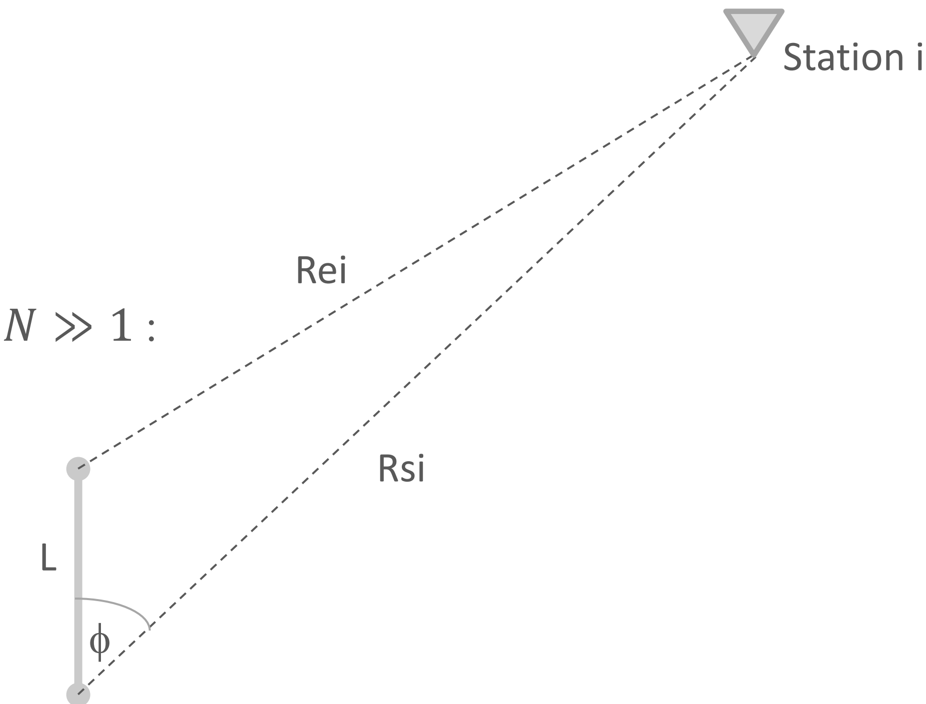

EGF – data processing workflow

- EGF event pairs – Identified by high wave-form similarity (XCORR) $\rightarrow$ idented SIPMAP files.

- Trace identing – Calculate ϕ, the azimuth from N, from source and station coordinates.
- Blanking – Traces are blanked outside a wide window to exclude the direct P arrivals.
- Deconvolution – A spectral division algorithm with additive noise (SIPMAP/NOFDEC).
- Trace scaling – Long gate AGC to balance amplitudes after deconvolution.
- Stack – For each station offset/azimuth, sum RSTF of all levels and components.
- Trace reject – Where S/N is low, discard source-station offsets greater than 20km.
- Duplicate traces – Copy traces to $\phi = 2\pi + \phi$ to clearly show azimuthal periodicity.
- SEGY output – DSCOUT/SEGY using standard SEGY headers.

- Trace plotting – Plot traces (using INTViewer) sorted on azimuth, in the range $[-\pi, 3\pi]$.
- Arrival picking – Pick duration as time between initial and final zero crossings of RSTF.
- Model inversion – Invert for Doppler model parameters by fitting sinusoid with Excel Solver.

Example input event pair data

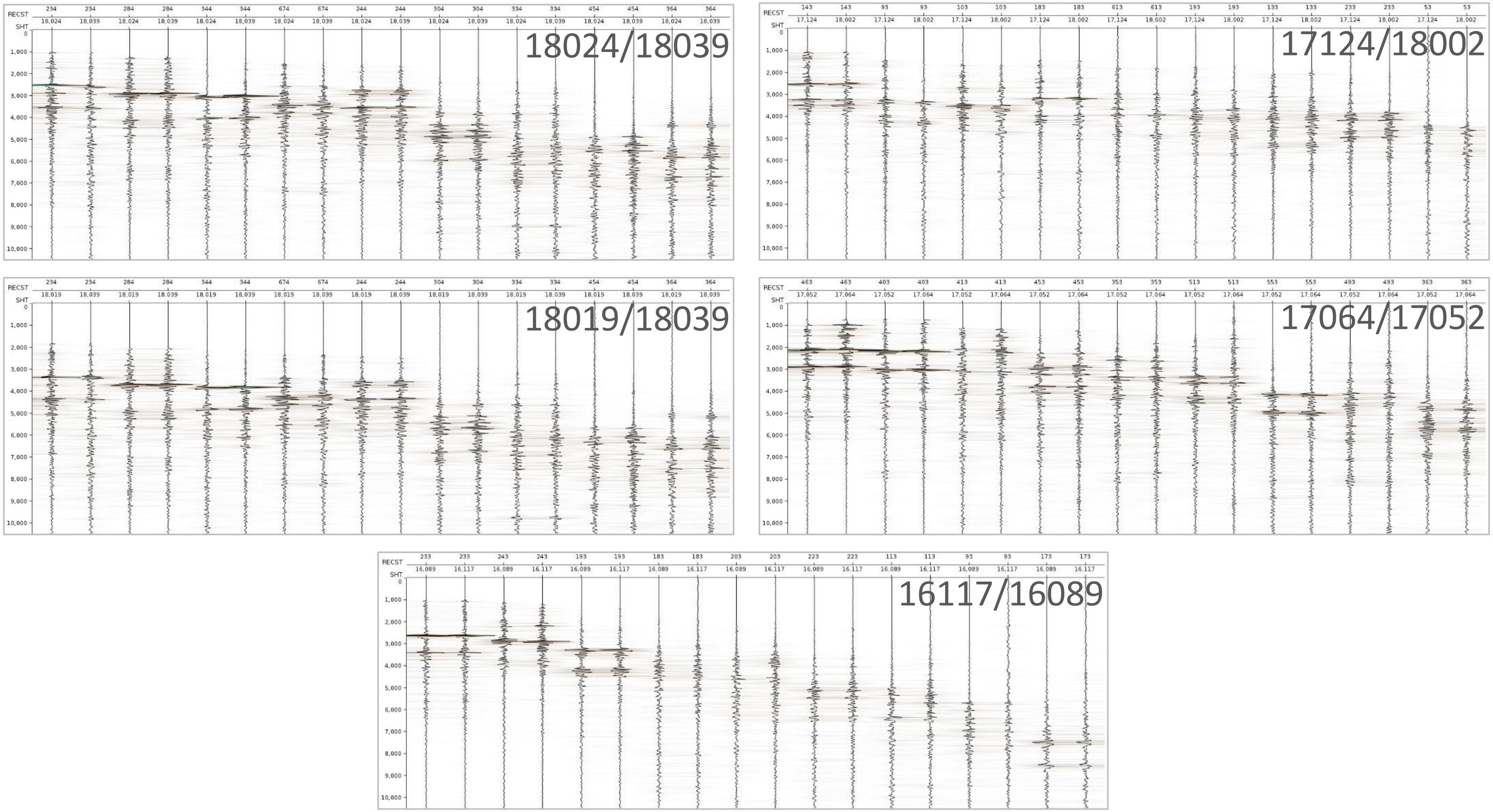

Selection of highly correlated trace pairs with long gate AGC (E component, depth 150m, short epicentral distances).

EGF RSTF – events 18024/18039 (M=1.6/1.8)

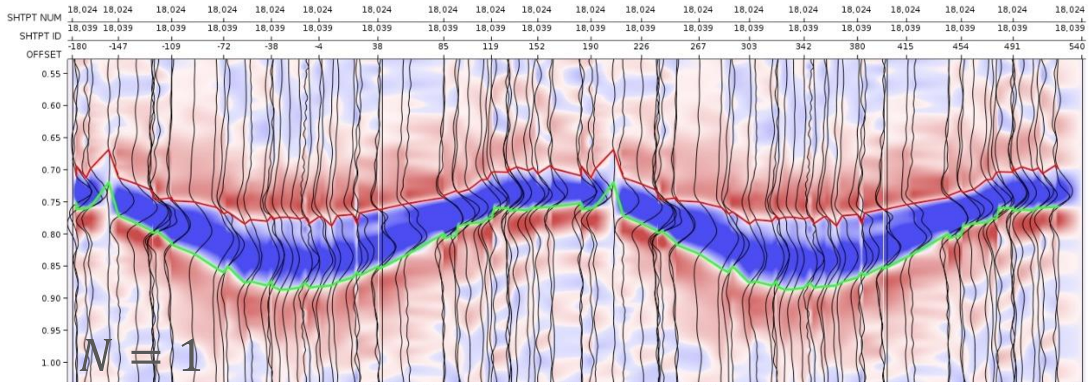

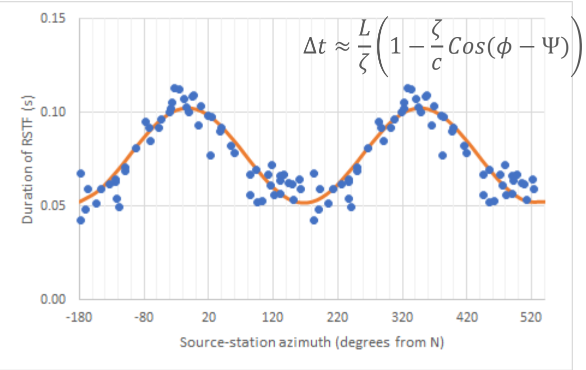

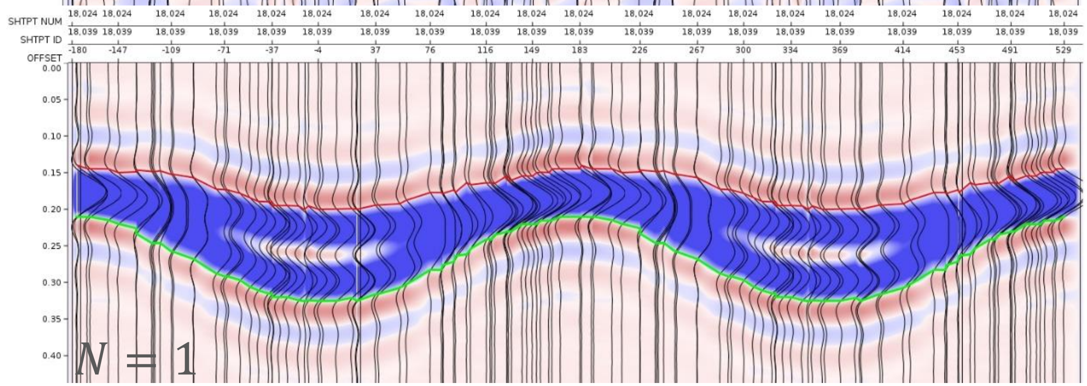

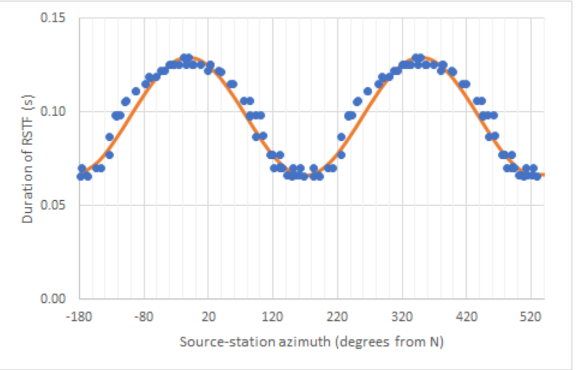

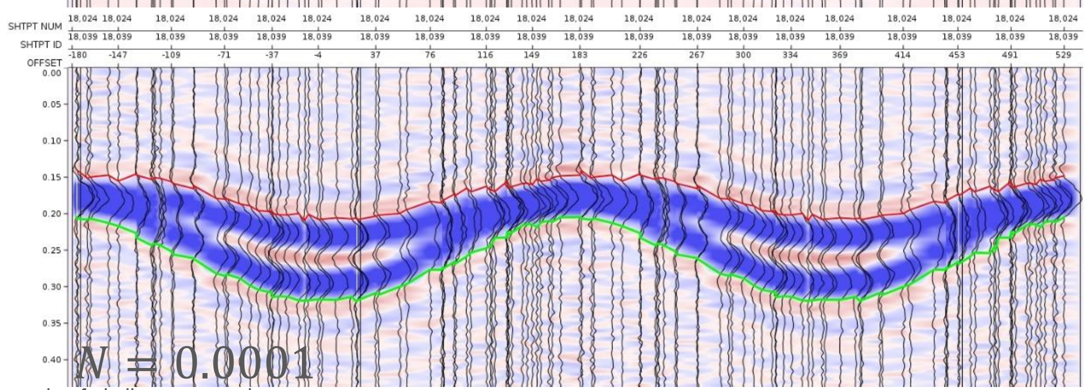

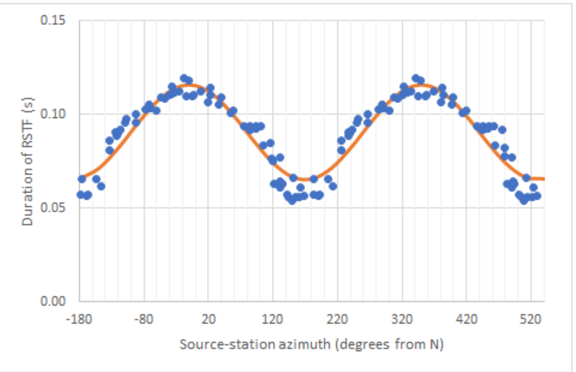

EGF RSTF – events 17124/18002 (M=0.4/3.4)

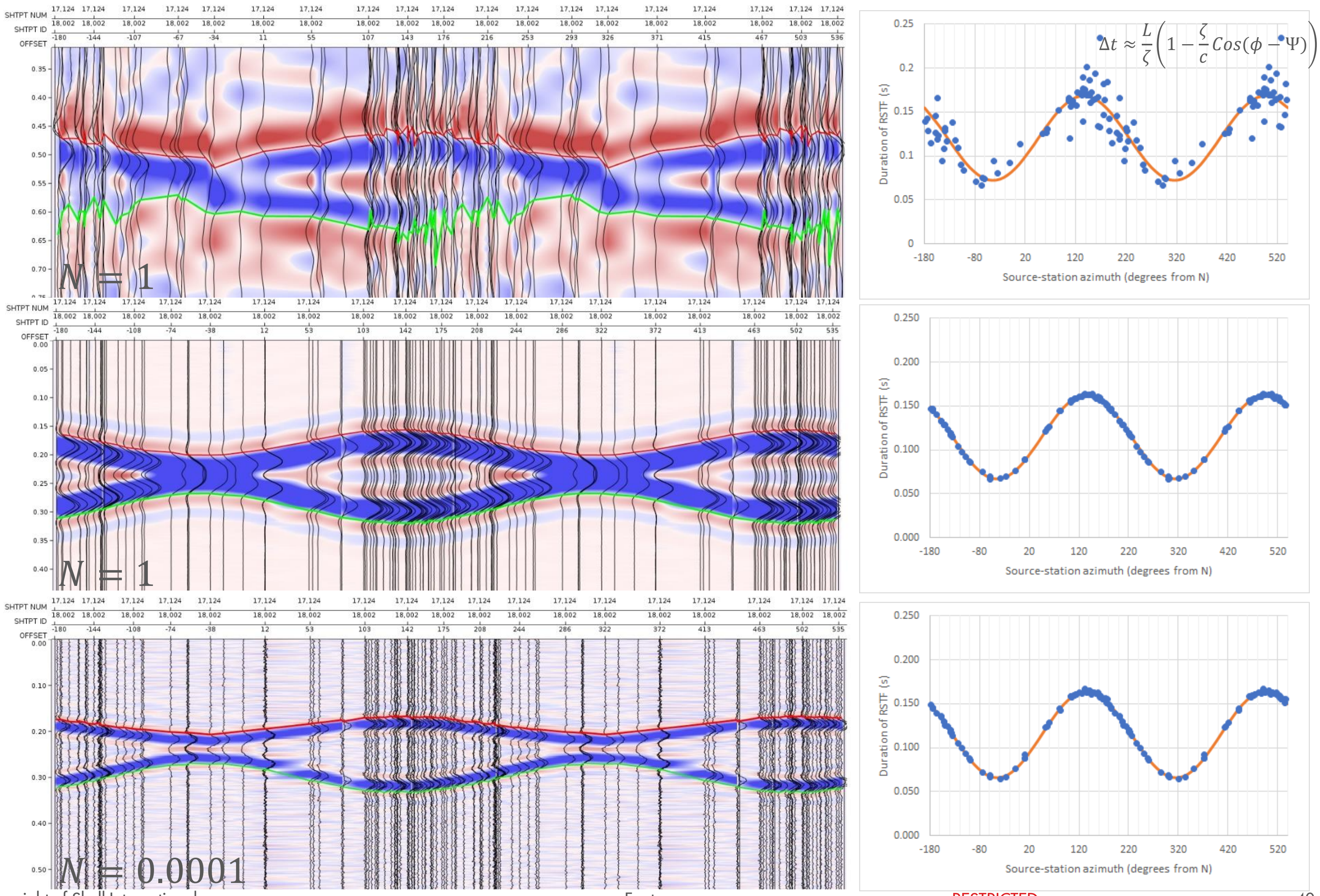

EGF RSTF – events 17064/17052 (M=0.7/2.6)

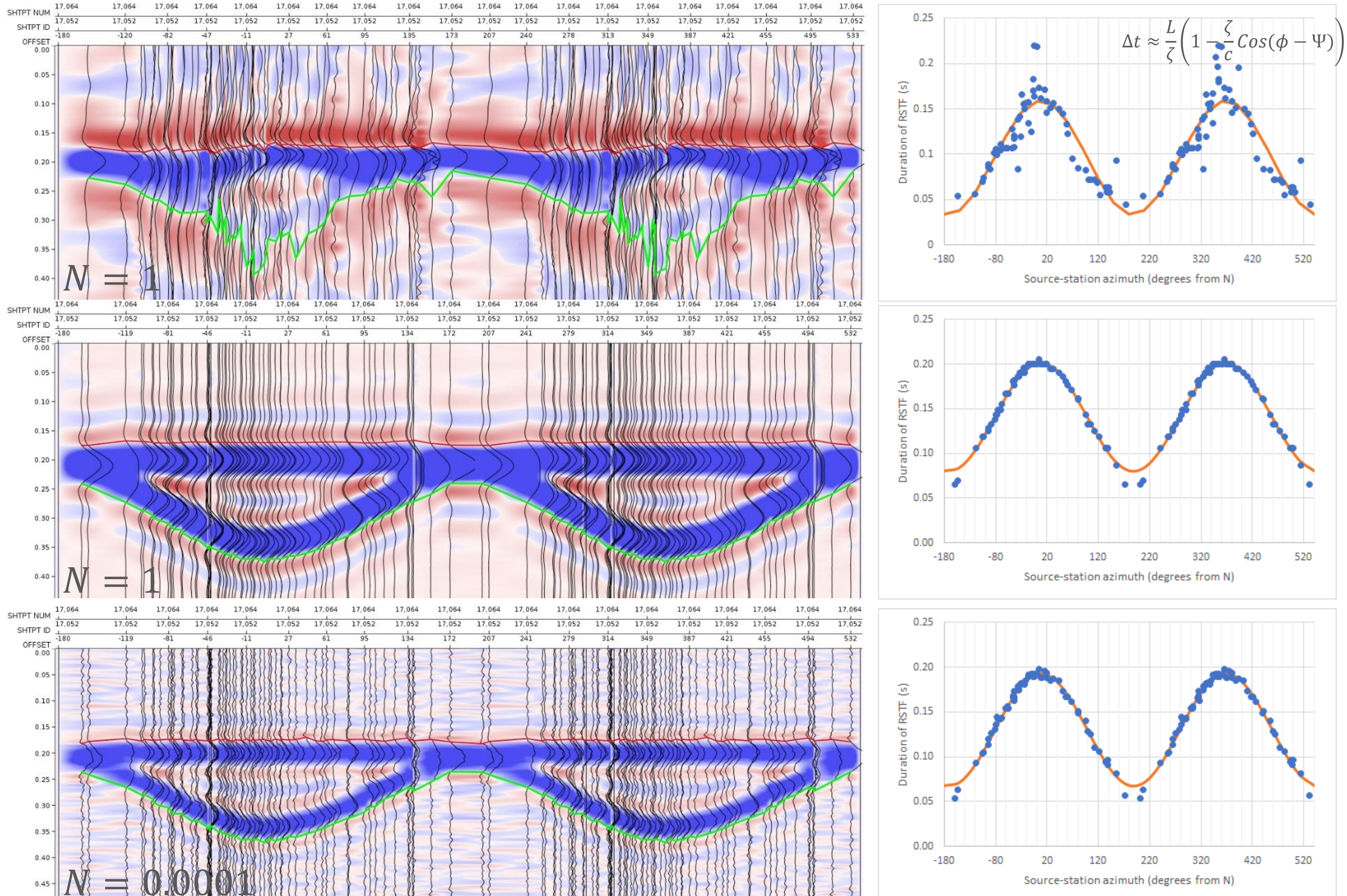

EGF RSTF – events 16117/16089 (M=1.0/1.9)

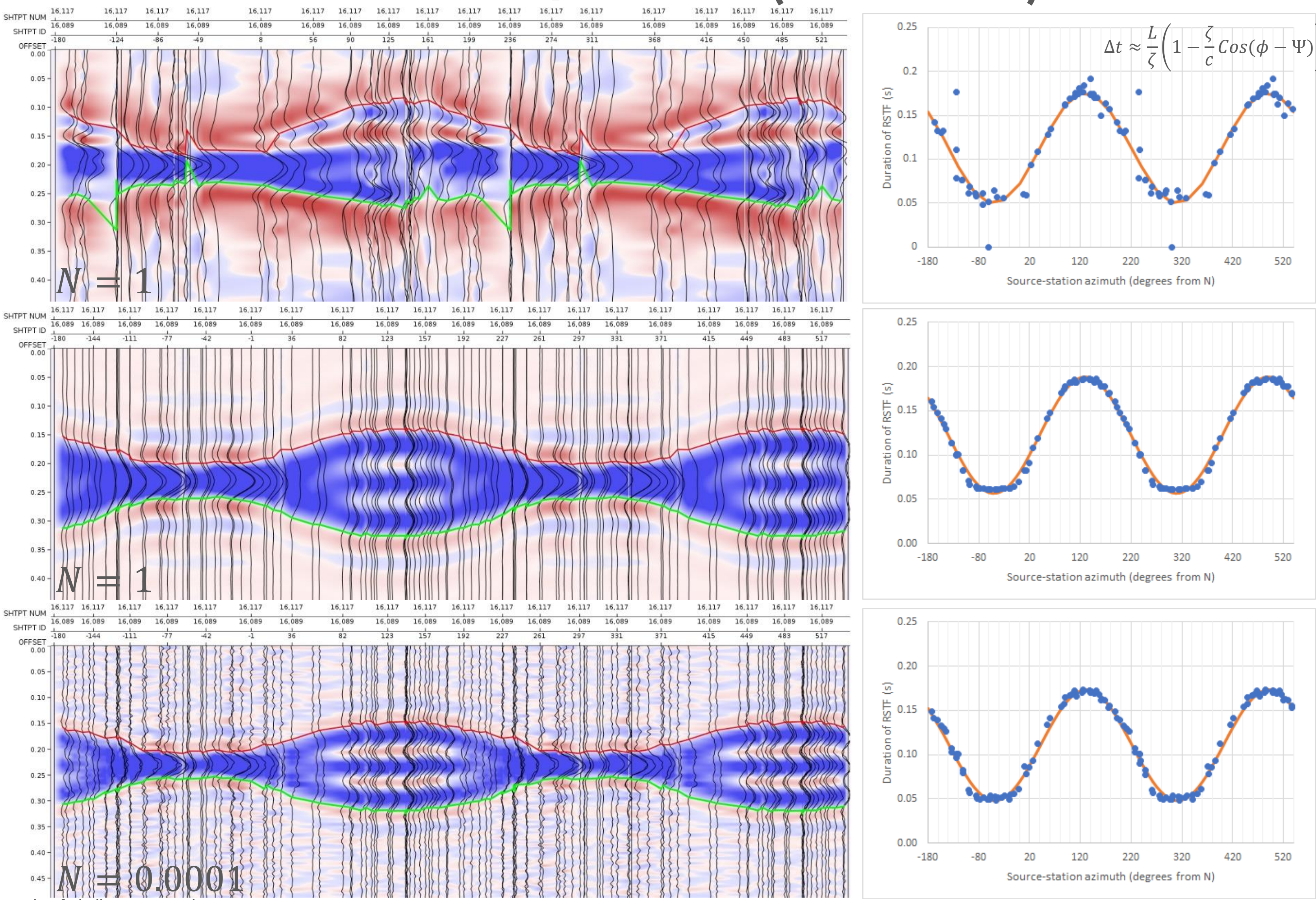

EGF rupture directions v. mapped faults

- Very good consistency with underlying fault map. Quality metric based on L1-norm applied to residuals: $\xi = 1 - \Sigma/\Sigma_0$
- Displaying best 10 event pairs with $\xi \geq 0.5$
- Where FWI focal mechanisms are available, the strike of the slip vector aligns with the rupture propagation vector and the fault trace

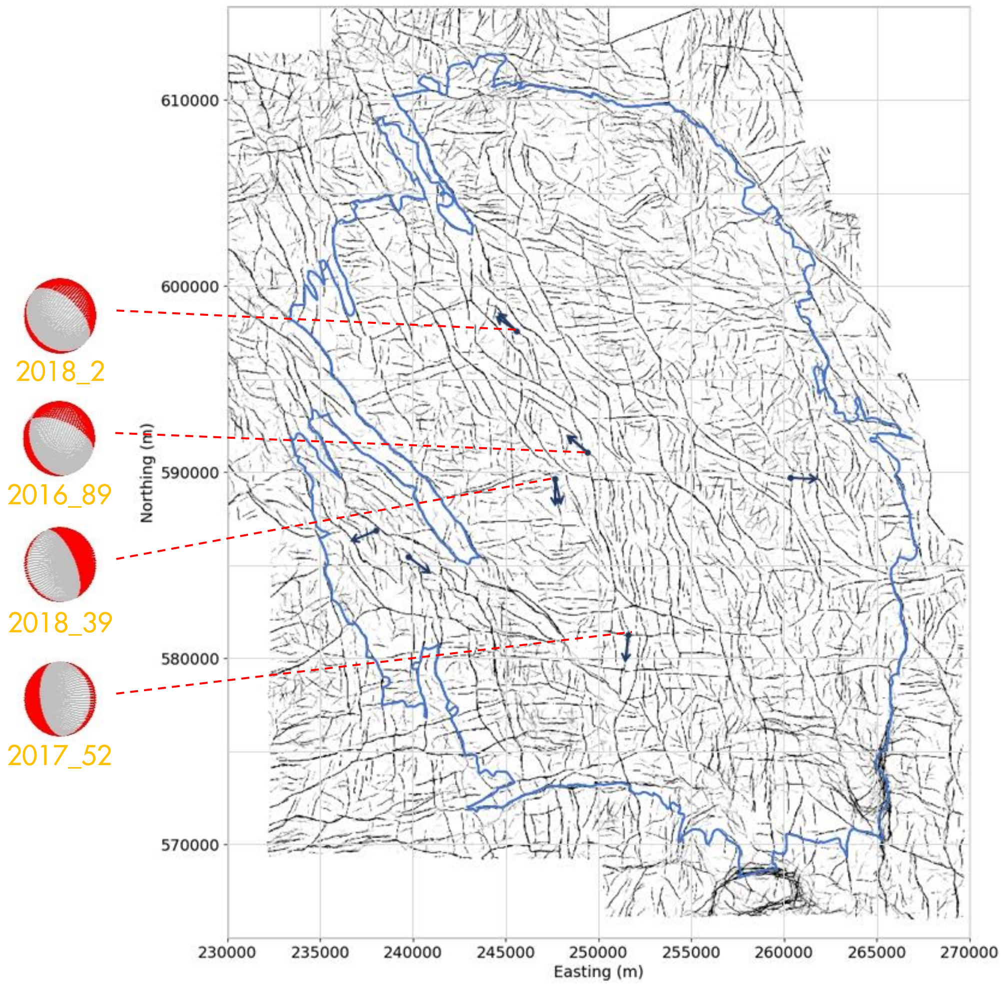

EGF rupture directions v. mapped faults

- Correlation with underlying fault map reduces as we admit lower quality event pairs.
- Displaying best 22 event pairs with $\xi \geq 0.25$
- For the event pairs with $0.50 \geq \xi \geq 0.25$ (the beach balls shown here), there is more variability in the alignment of the strike of the slip vector with the rupture propagation vector and the fault trace.

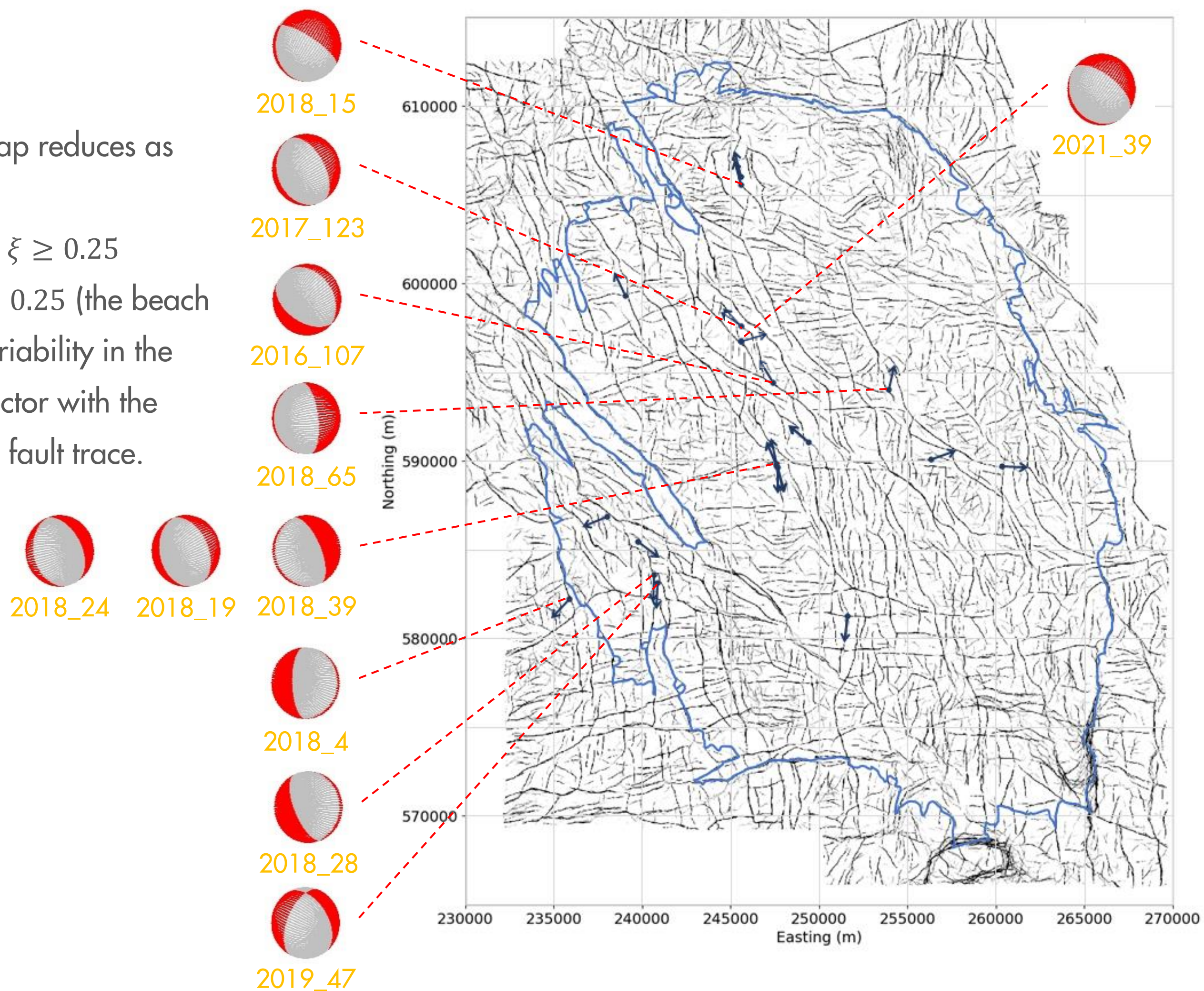

EGF rupture directions v. mapped faults

- Even for lowest quality event pairs still see many correlations with underlying fault map.
- Displaying all 31 remaining events with $0.25 \geq \xi \geq 0$

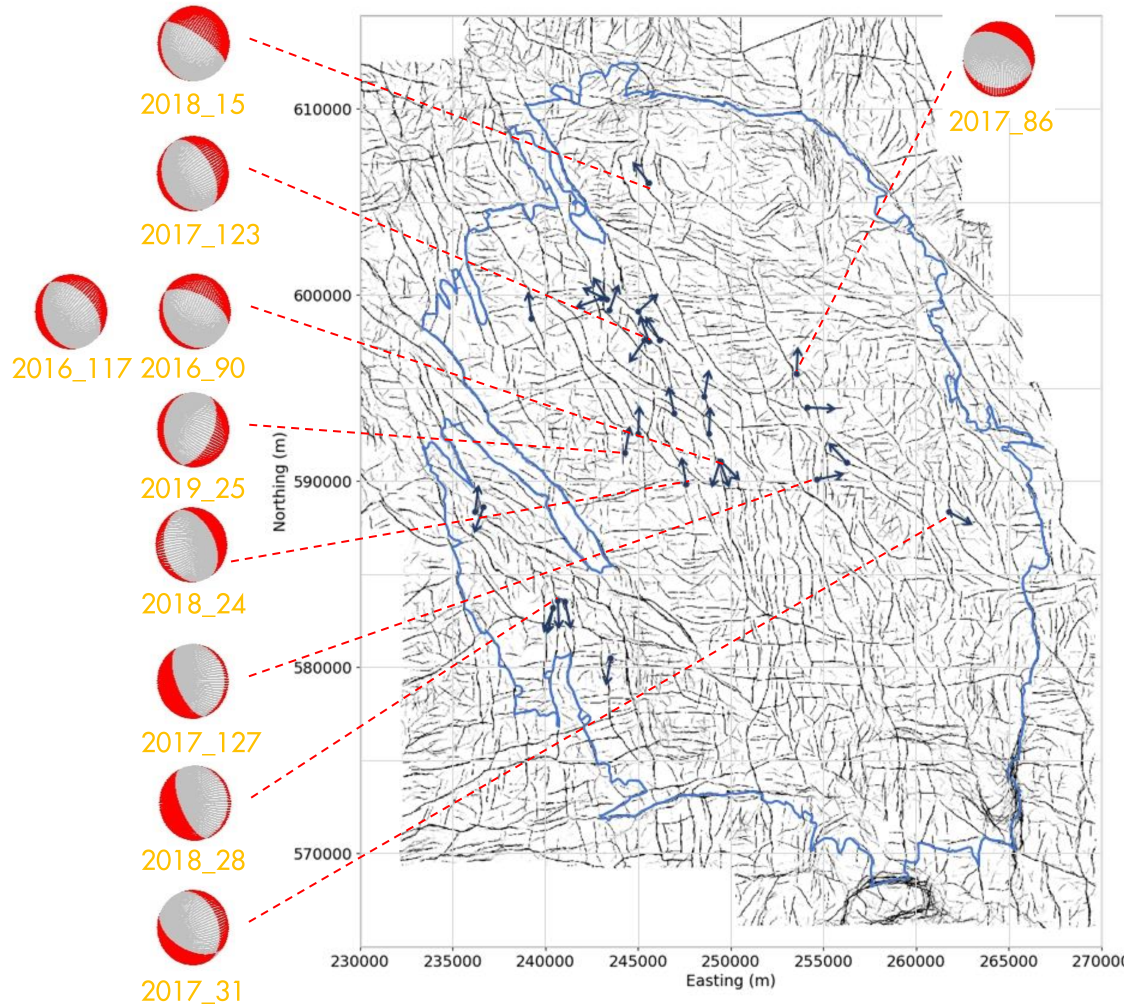

EGF rupture directions v. mapped faults

- Even for lowest quality event pairs still see many correlations with underlying fault map.
- Displaying all 31 remaining events with $0.25 \geq \xi \geq 0$

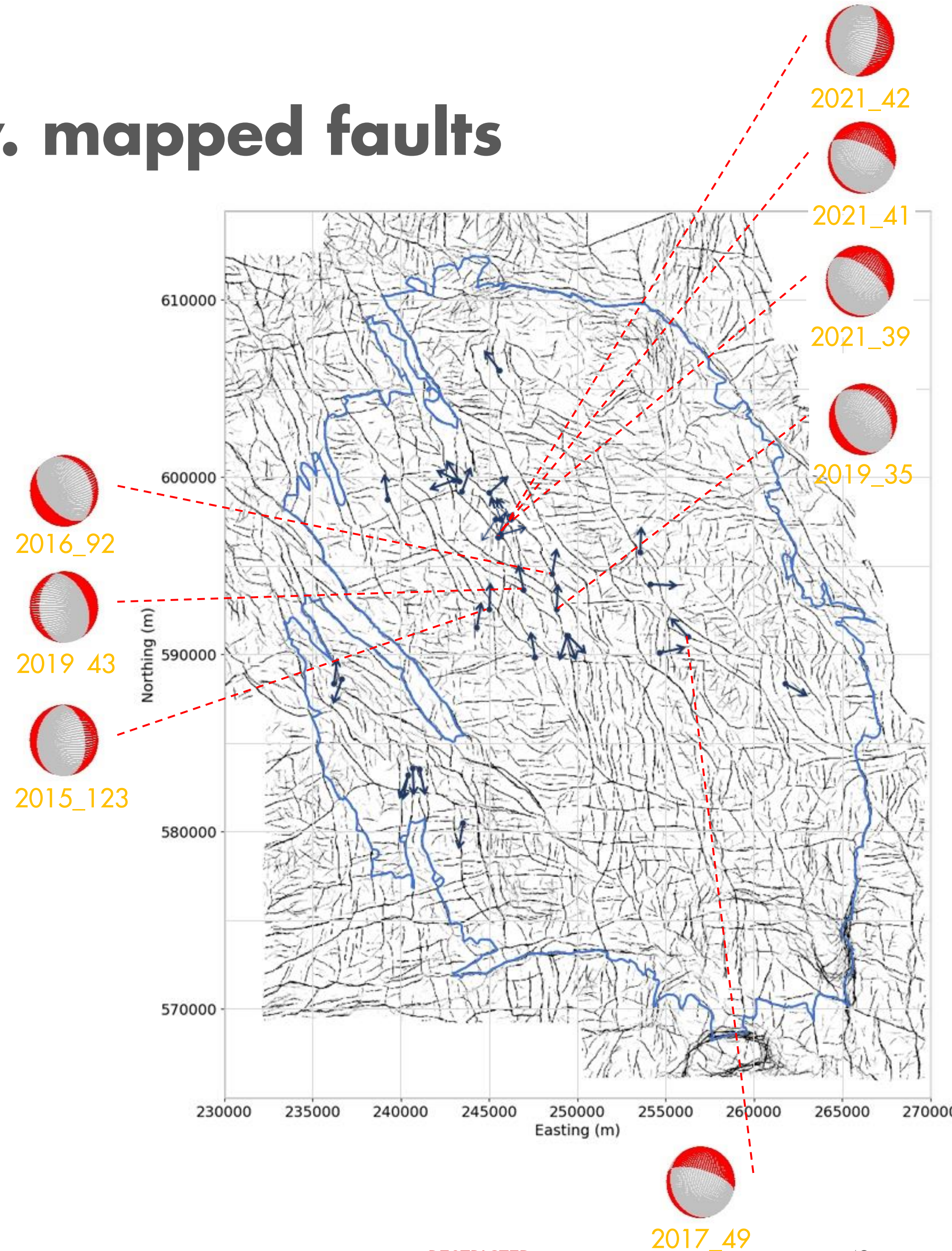

EBN and NAM fault maps

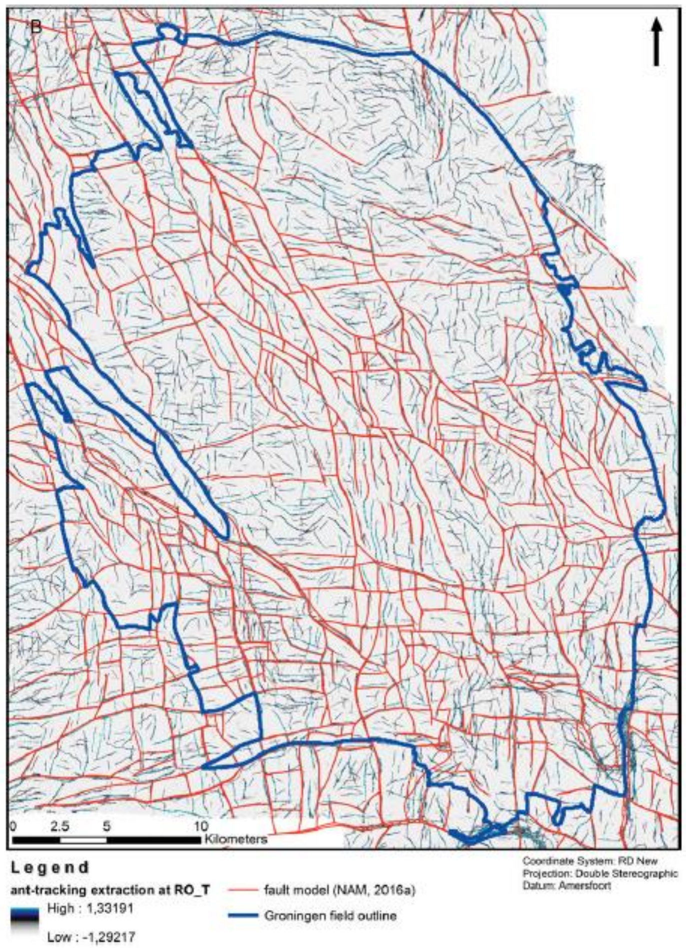

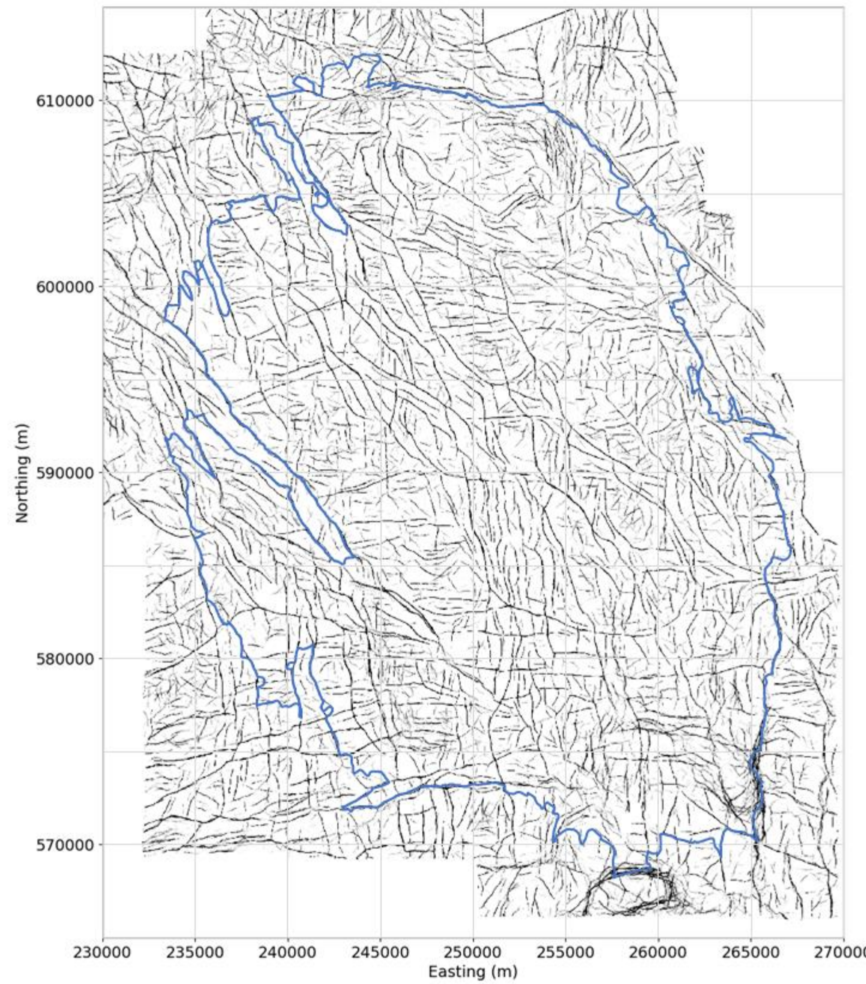

- Additional details of EBN map required to explain some of the rupture vector directions observed.

Estimation of slip velocity

Beresnev (2002) showed that maximum slip velocity is the source attribute which can be inferred from the corner frequency. As follows for a Brune source model:

$$v_{max} = \frac{2\pi f_c U}{e} = \frac{2\pi f_c M_0}{e\mu A}$$

Here we are interested in finite ruptures for which we should not assume the Brune model to be valid. The average slip divided by the duration should however give an estimate for a lower bound on the average slip velocity:

$$\bar{v} \geq U/\Delta t$$

We generally don't know the slip displacement but believe we know the stress drop! With stress drop and slip displacement approximately related by the shear modulus:

$$\mu \approx L_D \Delta\sigma/U \rightarrow \bar{v} \geq L_D \Delta\sigma/\ \mu\Delta t$$

EGF results – summary of attributes of all events

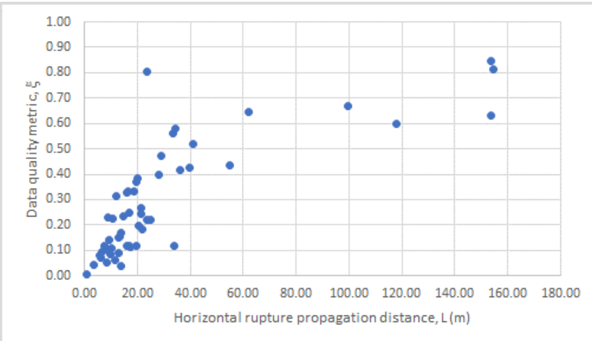

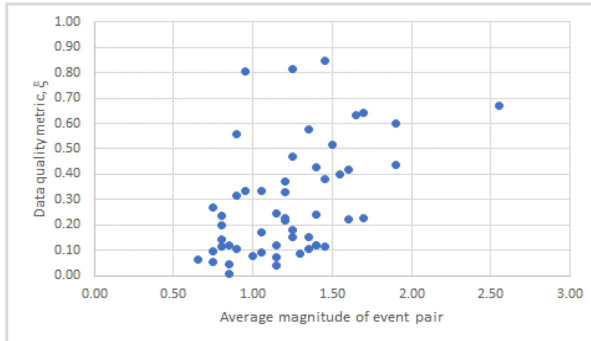

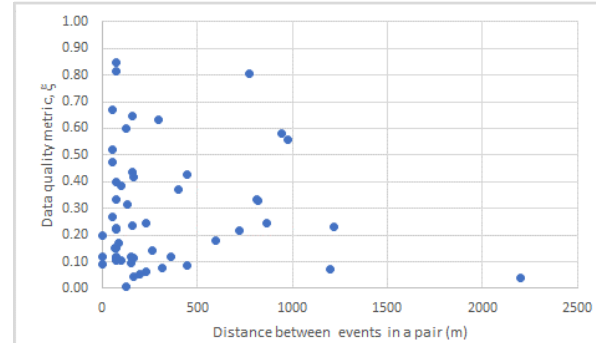

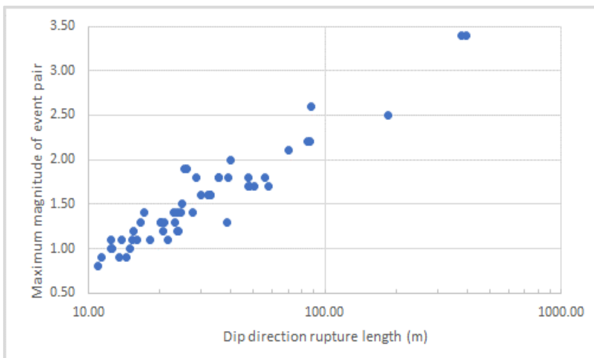

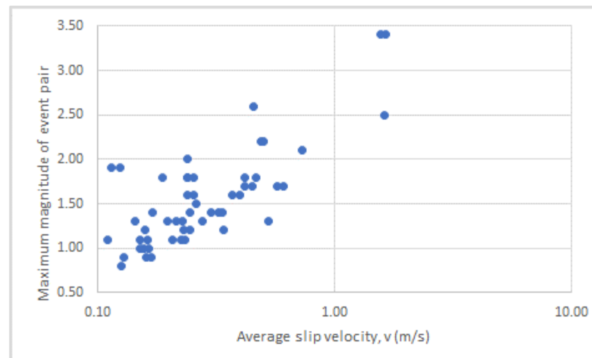

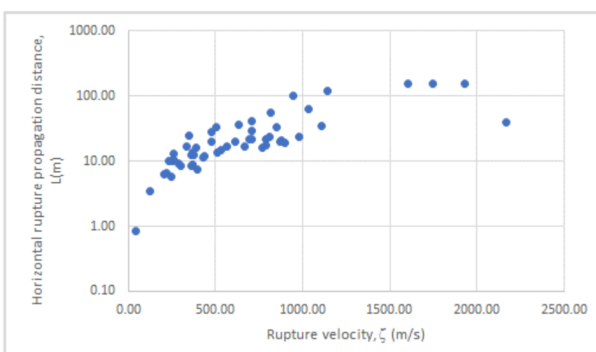

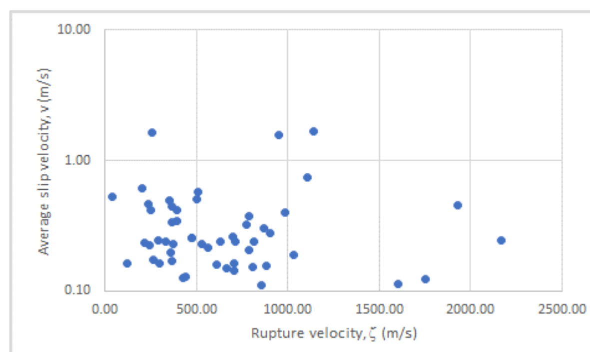

Findings & Conclusions from EGF analysis

- See clear evidence of rupture propagation.
- Extracted rupture directions agree very well with EBN fault map for best quality event pairs.
- RSTF durations are consistent with unilateral propagation between dominant starting- and stopping-phases.
- Estimated dip direction rupture size can be contained within reservoir for all but one event.
- Estimates of slip velocities (of the order of 0.1 to 1 m/s) and rupture velocities (up to about 0.9 of the shear velocity) are consistent with other published studies.
- Processing simple synthetics recovers input parameter values provided use low additive noise.

So. Where's the catch?

- Rupture propagation lengths obtained from Doppler broadening fit look rather small for the larger magnitude events.
- And why is rupture propagation always seen to be unilateral? Do ruptures really run between junctions as suggested by King and Nabelek?
- Iminishi and Takeo's model suggests we may be seeing only the high frequency stopping phases radiated by the rupture front where it is tangent to the boundary.
- This could explain our observations…
- …but break the link between rupture length and observed propagation distance.
- To ***estimate*** dip direction rupture extent we need to assume a representative stress drop either explicitly as here or implicitly as in Leonard's Mo-L-W-D correlations.

Overall Conclusions

- Arrival time inversion and Full Waveform Inversion (FWI) workflows applied to deep downhole array data and near surface network data show event hypocentres in and around reservoir.
- EGF analysis shows clear evidence of rupture propagation and, for all but the largest event analysed, estimated dip direction rupture size can be contained within the reservoir.
- FWI locations generally show alignment of focal mechanism with top Rotliegend faults.
- For the highest quality EGF data, the azimuth of the horizontal component of the rupture vector aligns with the fault trace and focal mechanism.

EGF duration – unilateral rupture propagation

Consider a source model in which a starting phase and stopping phase dominate:

$$Re_i = \left\{L^2 + Rs_i^{\,2} - 2LRs_i Cos\phi\right\}^{1/2}$$

$$if\ Rs_i \gg L, Re_i \approx Rs_i\{1 - 2LCos\phi/Rs_i\}^{1/2} \approx Rs_i - LCos\phi$$

$$S_l(t) = W(t) * \left[\delta\left(t - \frac{Rs_i}{c}\right) + \delta\left(t - \frac{L}{\zeta} - \frac{Re_i}{c}\right)\right]$$

$$S_g(t) = W(t) * \left[\delta\left(t - \frac{Rs_i}{c}\right)\right]$$

$$S_l(t) * S_g^{-1}(t) = \delta(t) + \delta\left(t + \frac{Rs_i}{c} - \frac{L}{\zeta} - \frac{Re_i}{c}\right)$$

$$\Delta t \approx \frac{Re_i}{c} - \frac{Rs_i}{c} + \frac{L}{\zeta} \approx \frac{L}{\zeta}\left(1 - \frac{\zeta}{c}Cos\phi\right)$$

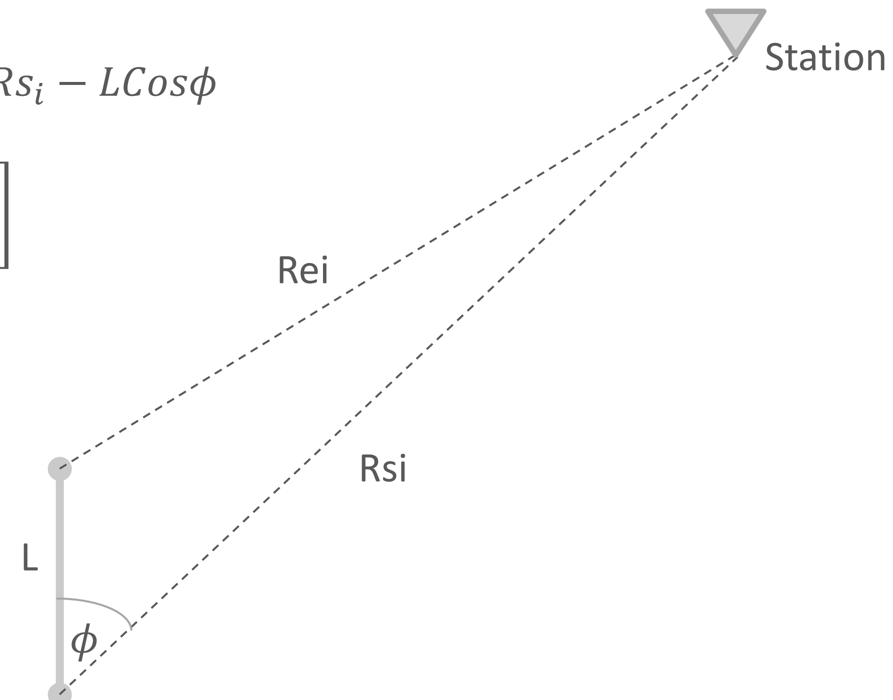

Groningen Mmax Workshop II
Amsterdam, 13-17 June 2022

Properties of Groningen reservoir and fault rocks

Chris Spiers

Emeritus Professor,
HPT Laboratory, Faculty of Geosciences, Utrecht University
+
many colleagues and students

Two NAM-funded projects at UU (2015-2021):

1) Compaction of the Slochteren sandstone

2) Fault strength and stability

Aim = understand + quantify controlling physical processes under in-situ conditions

Universiteit Utrecht

Experimental approach – HPT Lab

- Multiple triaxial testing rigs
- Direct shear rigs
- Ring shear testing rigs
- HT compaction cells
- Adsorption / dilatometry
- Permeametry
- Impedance spectroscopy
- True crustal HPT+Chemical conditions


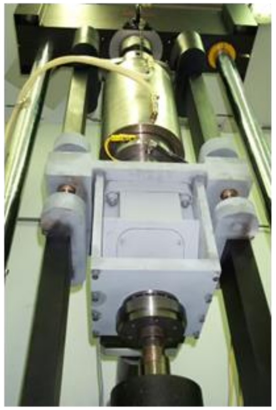





Universiteit Utrecht

What processes control reservoir compaction?

Thanks to: Ronald Pijnenburg, Bart Verberne, Hadi Mehranpour, Jeroen van Stappen, Suzanne Hangx

1. Poro-elastic deformation - yes
2. Permanent compaction – plasticity / creep ???

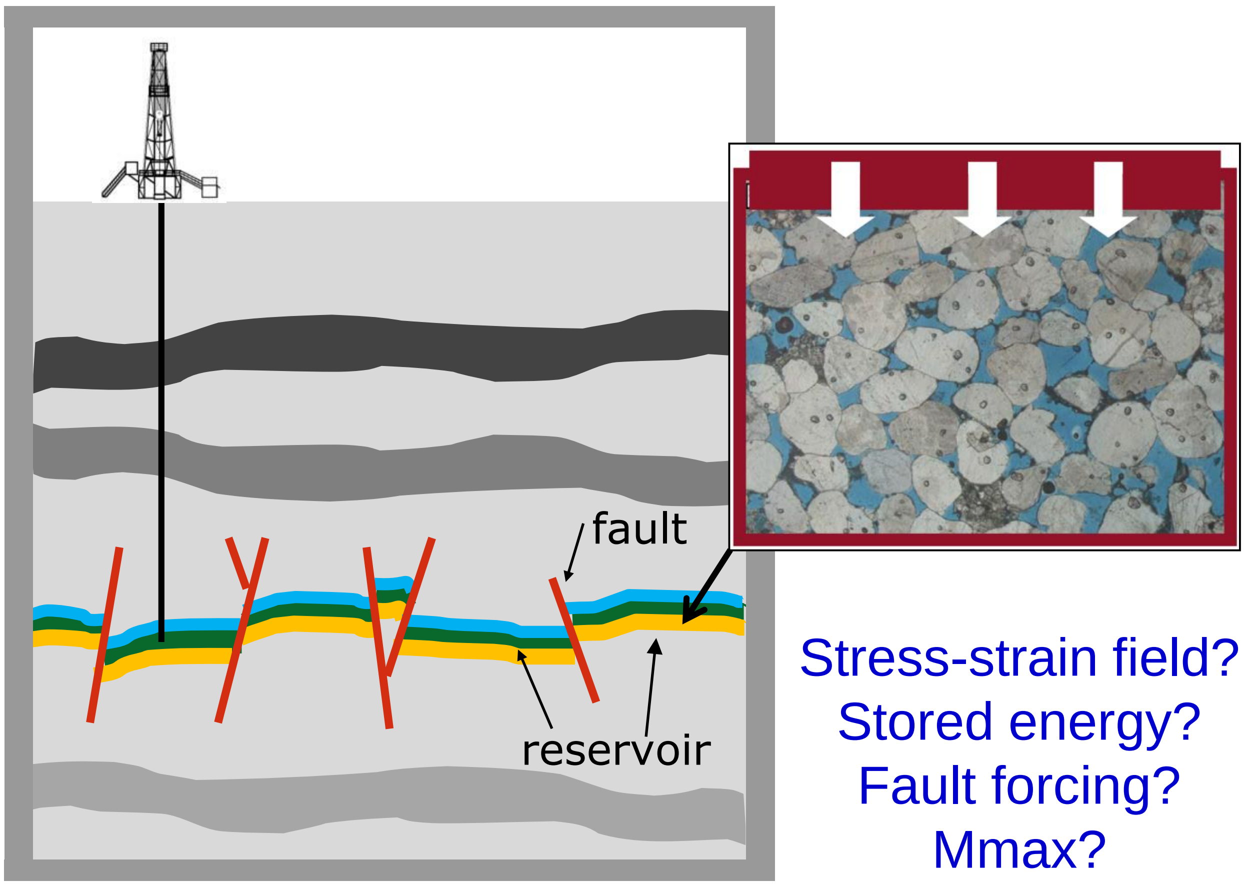

$$\sigma_e = \sigma - P_f$$

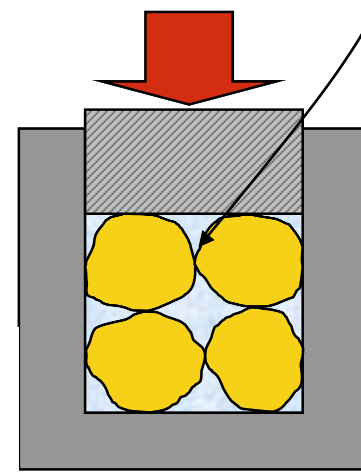

Stress-strain field?
Stored energy?
Fault forcing?
Mmax?

What processes control reservoir compaction?

Step 1: Samples for experiments and analysis

Cores from Stedum en Zeerijp (nov 2015, thanks to NAM)

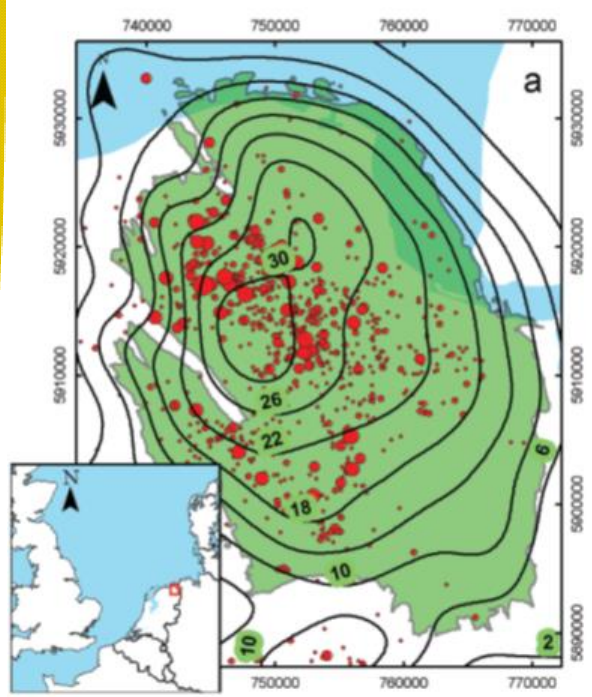

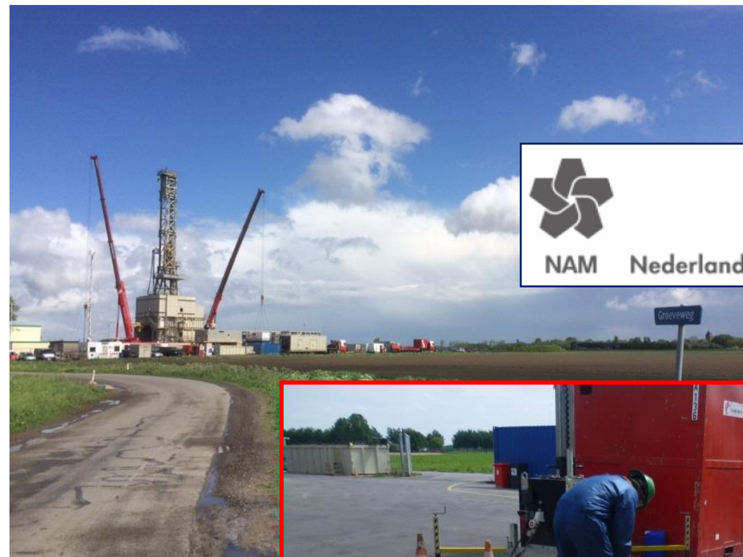

NAM Nederlandse Aardolie Maatschappij B.V.

Universiteit Utrecht

Universiteit Utrecht

Conventional triaxial compression experiments

Triaxial pressure vessel

Slochteren sandstone (reservoir)
SDM-1 Well
ZRP-3a (drilled in 2015)
courtesy of NAM

Compression/relaxation tests

Hydrostatic stress-cycling
(increase P_c at constant P_p)

Axial stress-cycling
(at constant P_c and P_p)

- Porosity = 12 – 26%
- $\dot{\varepsilon} \sim 10^{-5}\ s^{-1}$
- $T = 100\,^{\circ}C$, $P_c \leq 40$MPa
- Pore fluid ≈ 4M saline brine
- $P_e = P_c - P_p$ = 1 to 40 MPa

Pijnenburg et al (JGR 2018, 2019a,b)

Universiteit Utrecht

Stress-cycling tests (ZRP-3a samples)

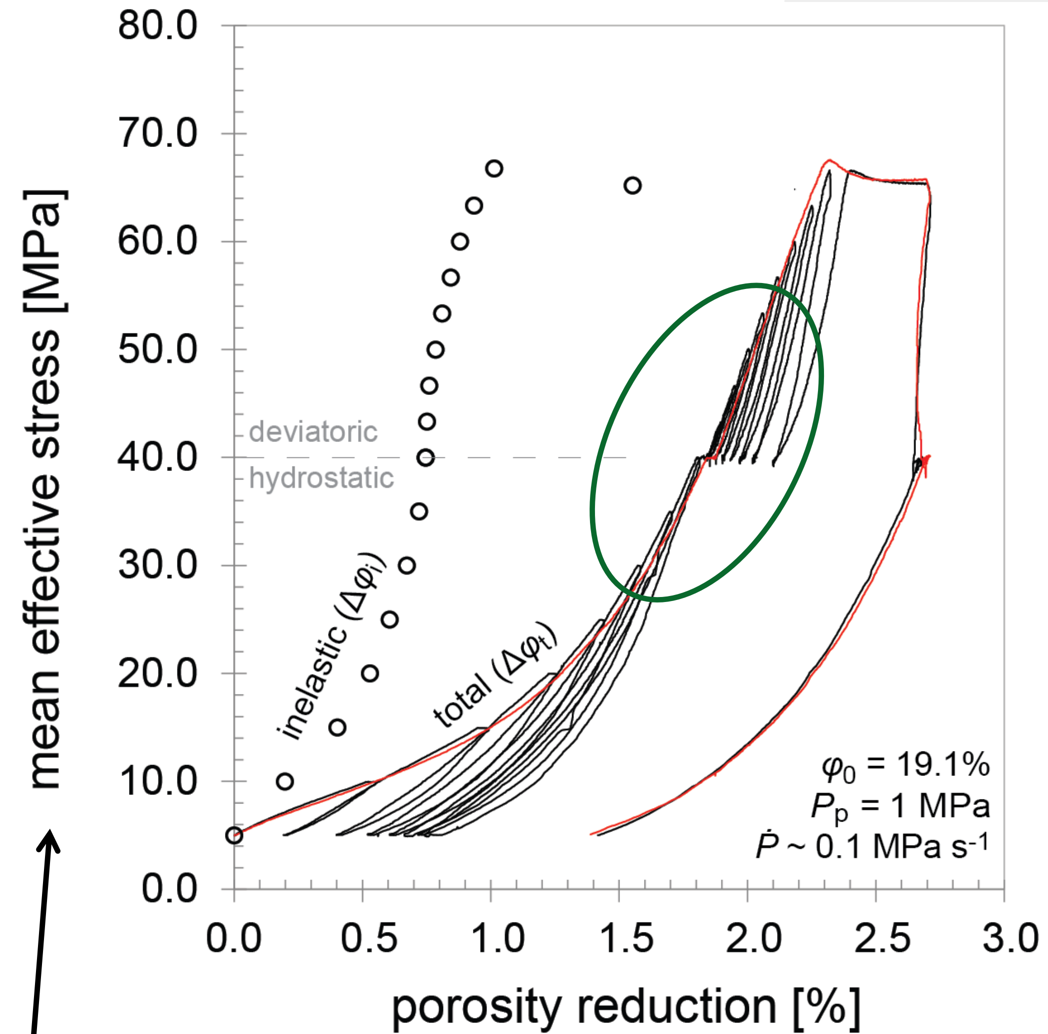

$(\sigma_1 + 2\sigma_3)$ /3 – pore pressure

- **load-cycled = monotonically loaded behaviour**
- **Inelastic/plastic deformation = 30-60% of total** (cf. Hol et al., 2018; Van Eijs et al)
- **→ 30-60% of mechanical work is dissipated**

'Sister samples' ZRP-3a

Pijnenburg, Verberne, Hangx and Spiers (JGR 2019a)

Universiteit Utrecht

Fit to plasticity model: Modified Cam-clay

Porosity 13% 21% 26%

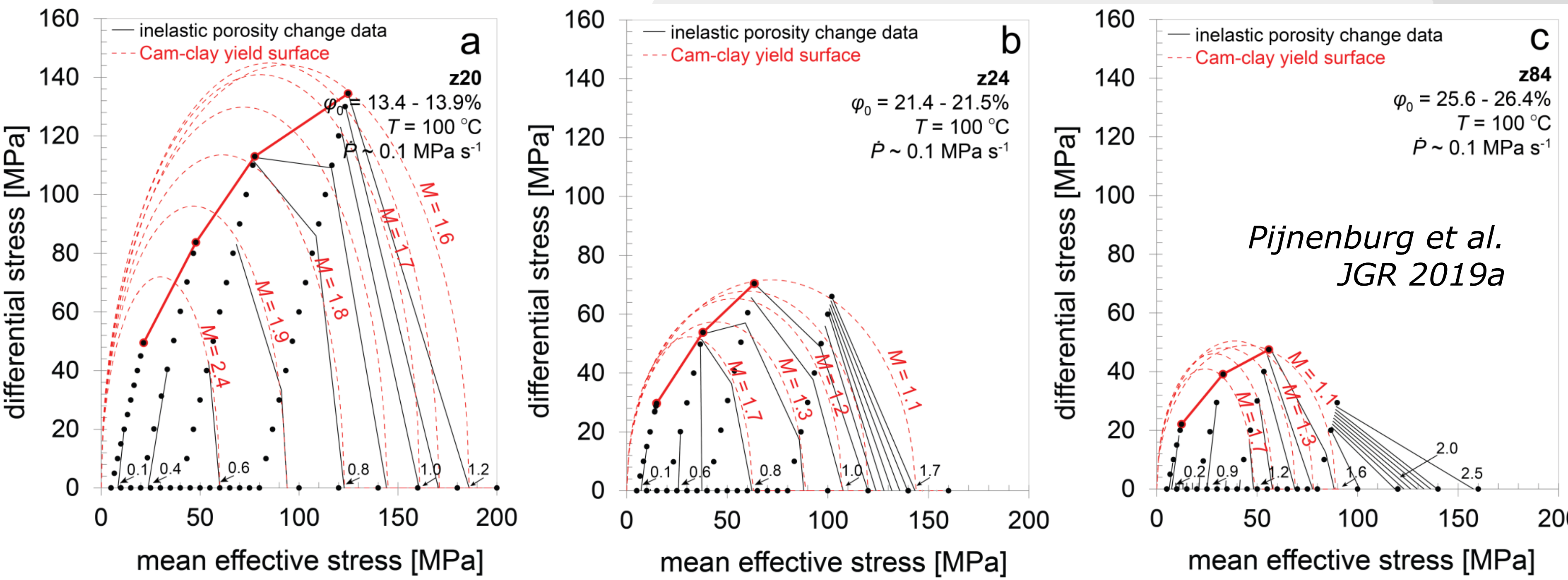

- Fair fit of Cam-clay model to data (***M*** decreases with porosity esp > 20%)
- **Add to (non)linear elastic law >>> compaction model**

- Experiments show rate-sensitivity (10-20% more inel. ε at $\dot{\varepsilon}$ ~ 10^{-9} s^{-1})

≈ Rate Type Compaction Model (Van Eijs et al 2019)

Predicted *in-situ* stress evolution for 1-D compaction

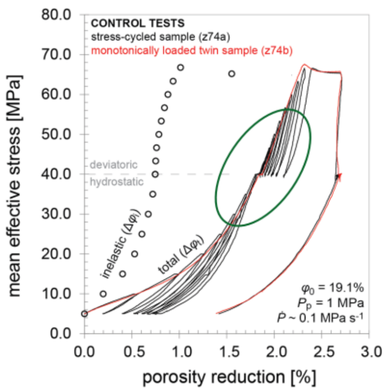

assumed elastic

E_a = 5 GPa; v_a = 0.2
E_a = 8 GPa; v_a = 0.2
E_a = 14 GPa; v_a = 0.2

true elastic

E = 12 GPa; v = 0.2
E = 15 GPa; v = 0.2
E = 17 GPa; v = 0.1

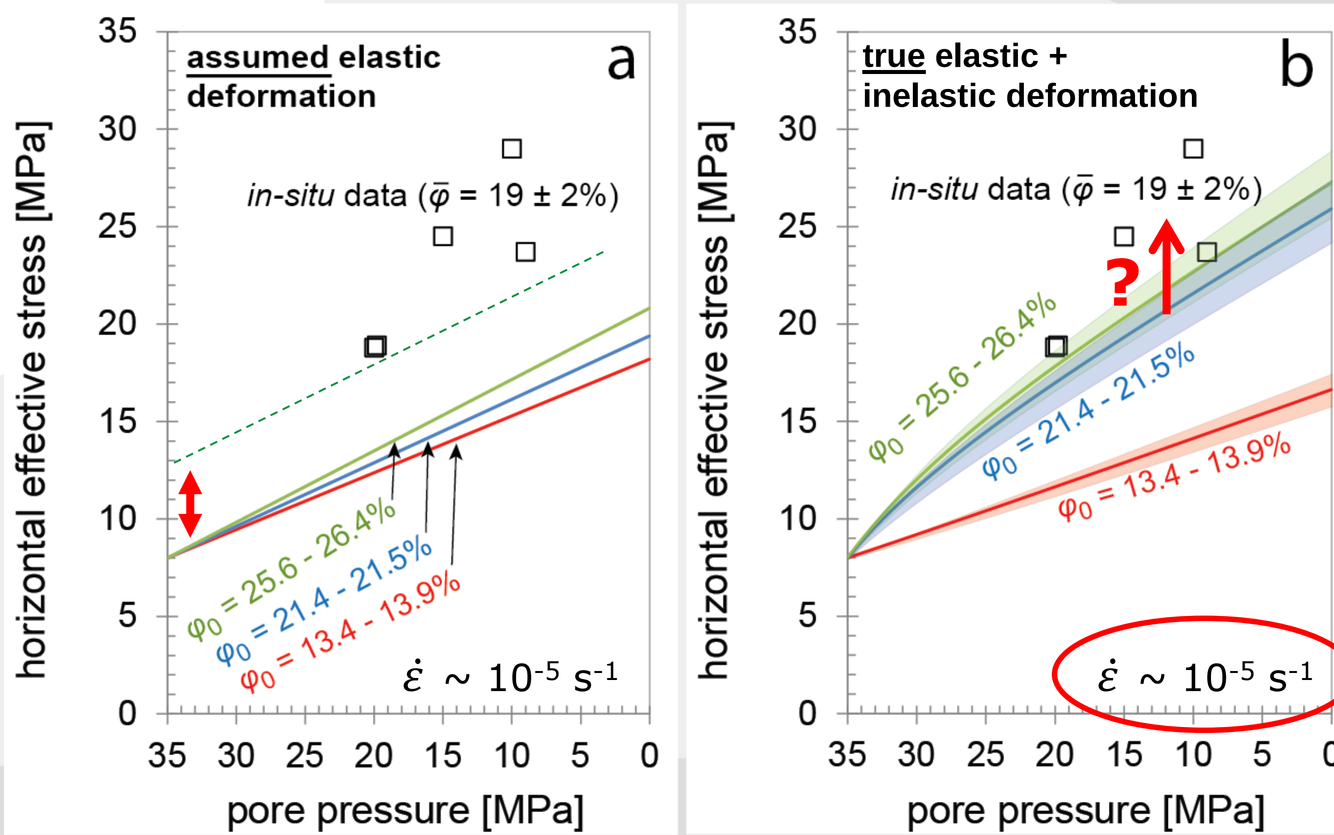

- **Including inelastic effect improves predictions of in-situ stress evolution**
  (at least in parts of the field where averaged porosity is high; $\varphi \approx 19 \pm 2\%$)

Pijnenburg et al. JGR 2019a

Universiteit Utrecht

Model comparison to 1-D depletion experiments

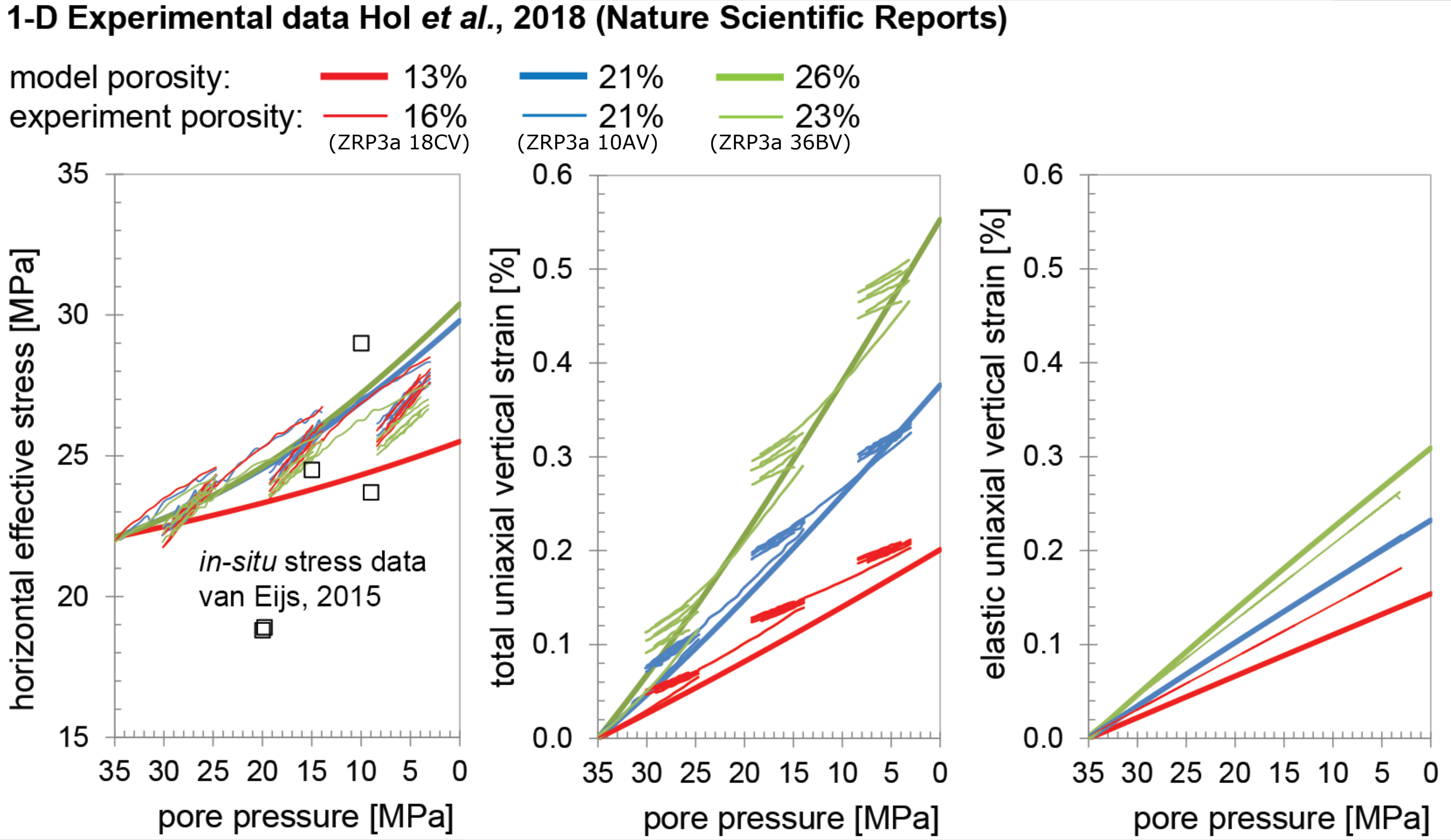

Impact on M-max + rupture simulations

Universiteit Utrecht

1) 50% plastic strain → 50% less energy → reduces M_w by only 0.2

Depletion-induced stress (criticality)

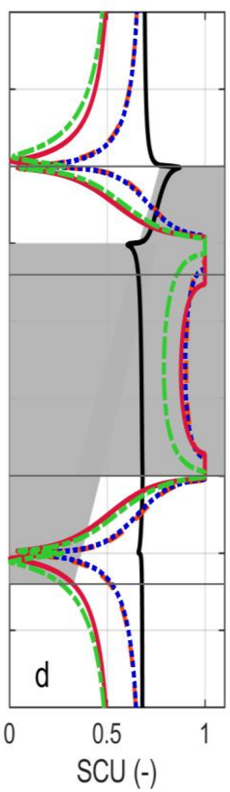

Φ=26.4%

Dynamic rupture ($\mu_s = 0.6$, $\mu_s = 0.45$, $D_c = 0.01$ m)

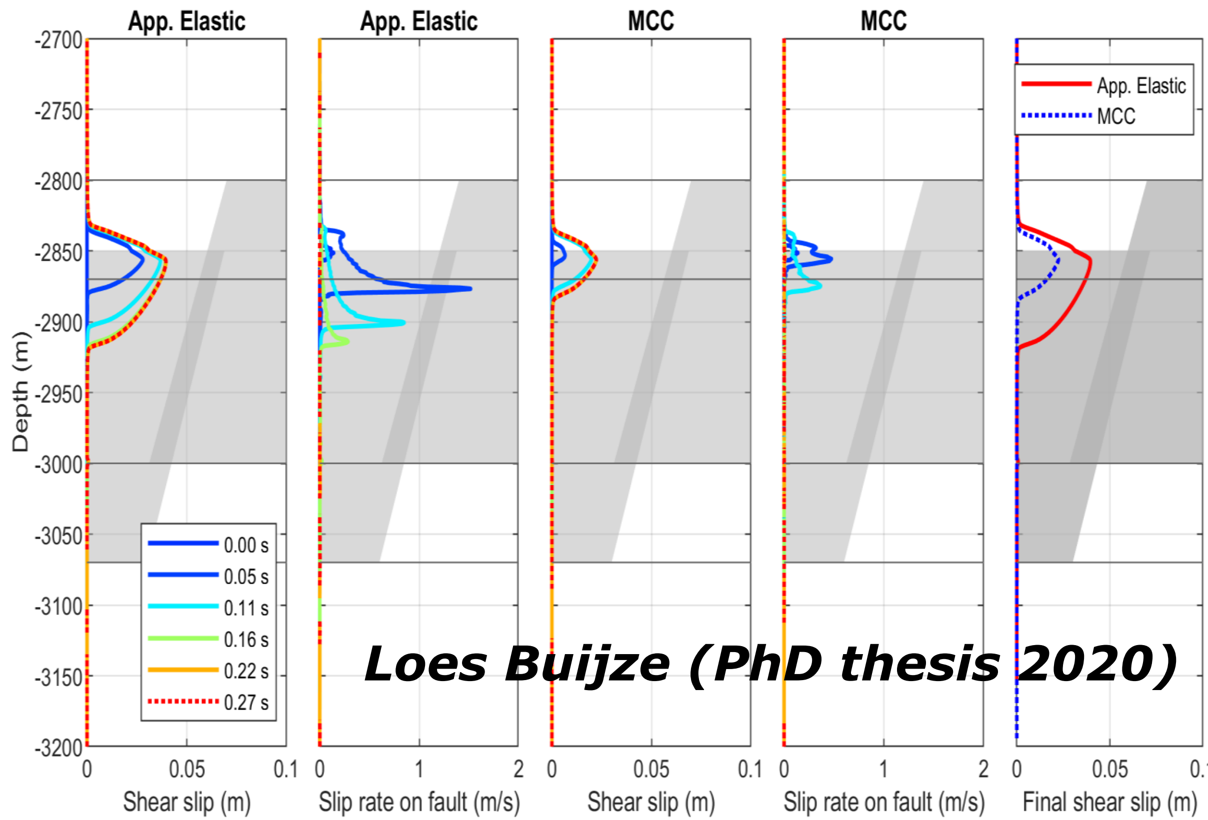

Loes Buijze (PhD thesis 2020)

2) M-CamClay elastoplasticity causes less slip (+ smaller rupture size, depending on stress)

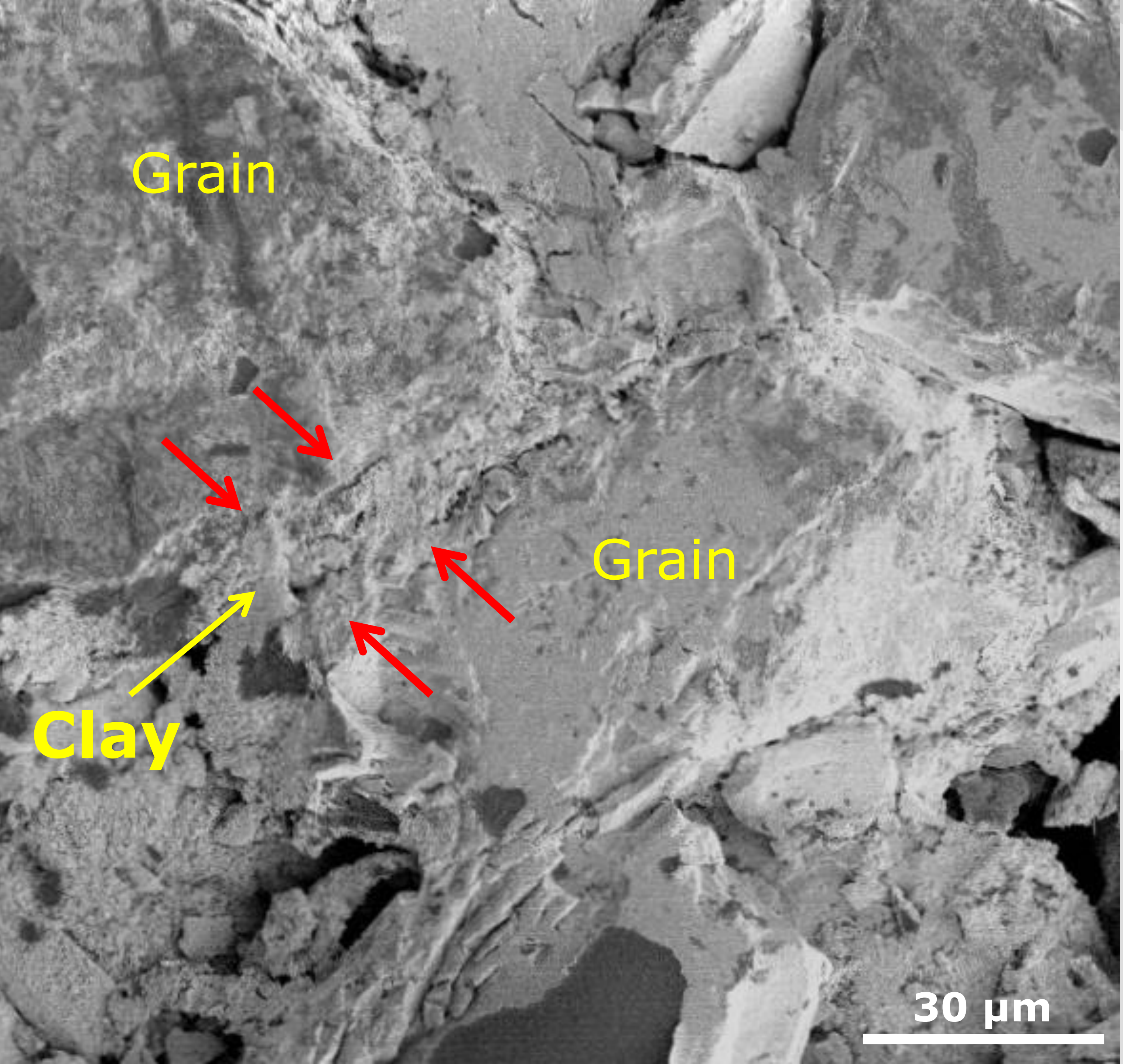

Pijnenburg et al. JGR 2019b

See also Pijnenburg & Spiers, RMRE 2020

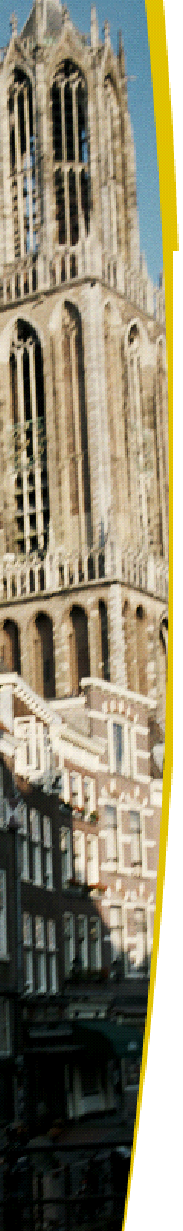

Fault strength and stability

Luuk Hunfeld, Jianye Chen, Yuntao Ji, Loes Buijze, Dawin Baden, Andre Niemeijer

Static fault strength and failure

- Mohr-Coulomb or Byerlee failure

$$\tau = S_0 + \mu(\sigma_n - P_f)$$

- Re-activation by change in stress-state

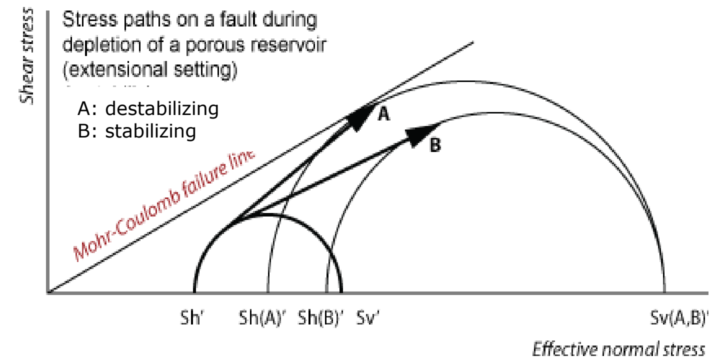

Failure plus slip-weakening

- Simplified post failure behavior (slip weakening)
- Stress drop, stress transfer, magnitudes

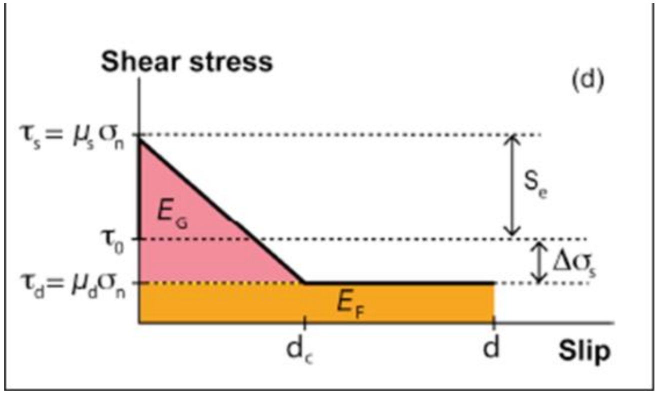

Rate-and-state dependent friction (Dieterich/Ruina)

- Coefficient of friction is function of velocity + time/slip
- Reproduce many aspects of natural seismic cycles
- Aseismic/seismic slip, stress drop, coseismic slip, postseismic creep…

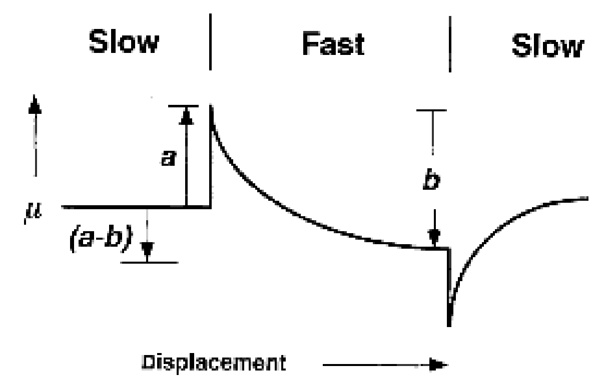

Friction and failure behavior of Groningen faults

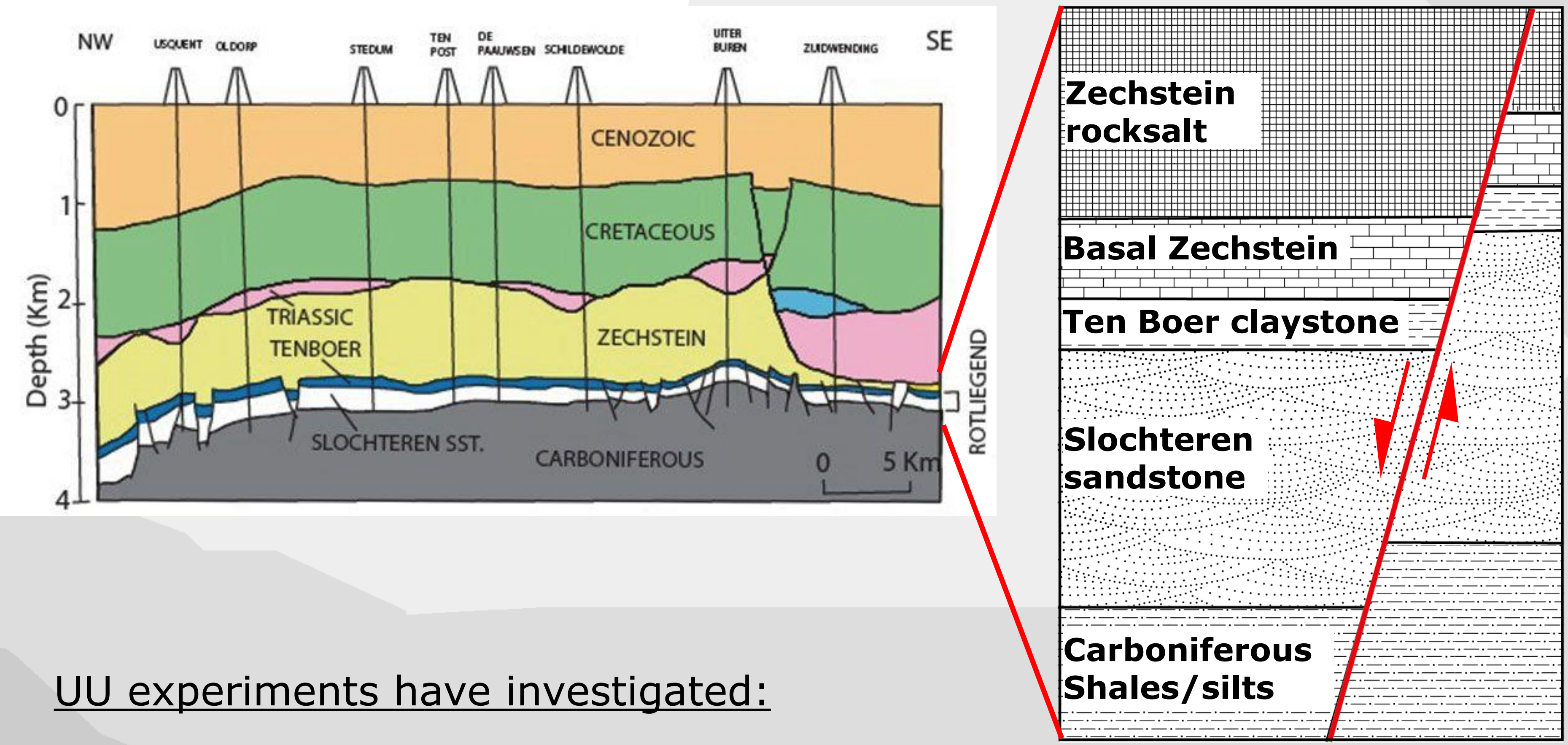

UU experiments have investigated:

- Low-velocity / RSF friction (EQ nucleation)
- Dynamic friction and slip-weakening (simulated seismic slip)
- (Scale effects)

Exposed equivalents of Groningen faults (?)

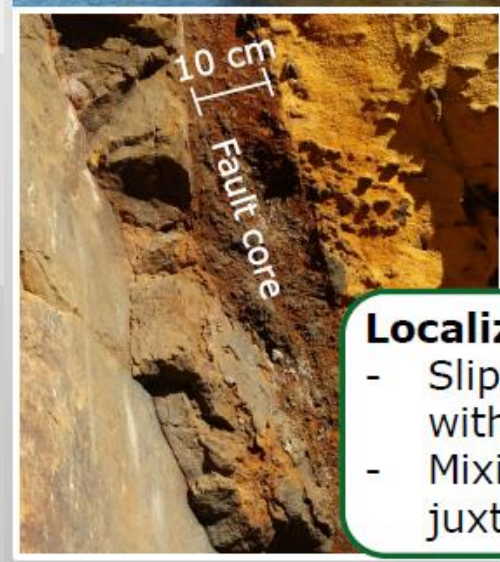

Localized deformation

- Slip localized on mm-cm wide zones filled with fine-grained gouge material
- Mixing of gouge materials in faults juxtaposing different lithologies

Utrecht University

Velocity-stepping friction (RSF) experiments: Low velocities

- Simulated fault gouges
- Direct shear
- True reservoir P-T conditions
- In-situ pore fluid (brine/gas)
- Slip velocities 0.1-10 µm/s

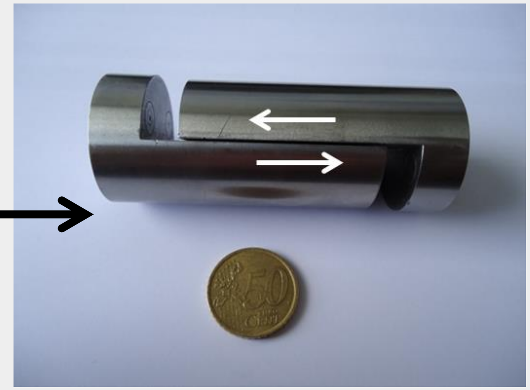

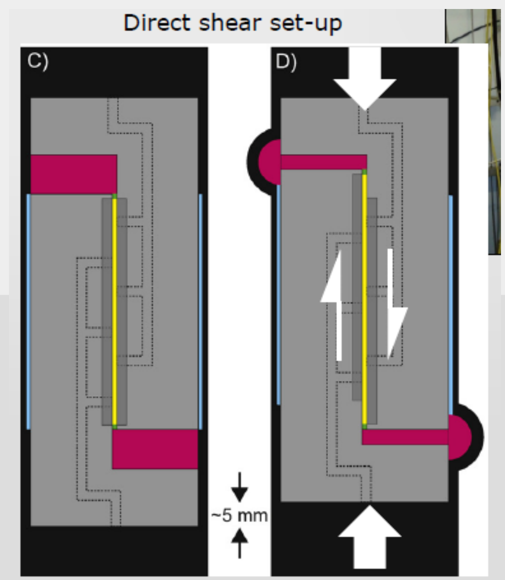

After Samuelson & Spiers (2012)

Triaxial apparatus

Low-V friction behaviour (RSF)

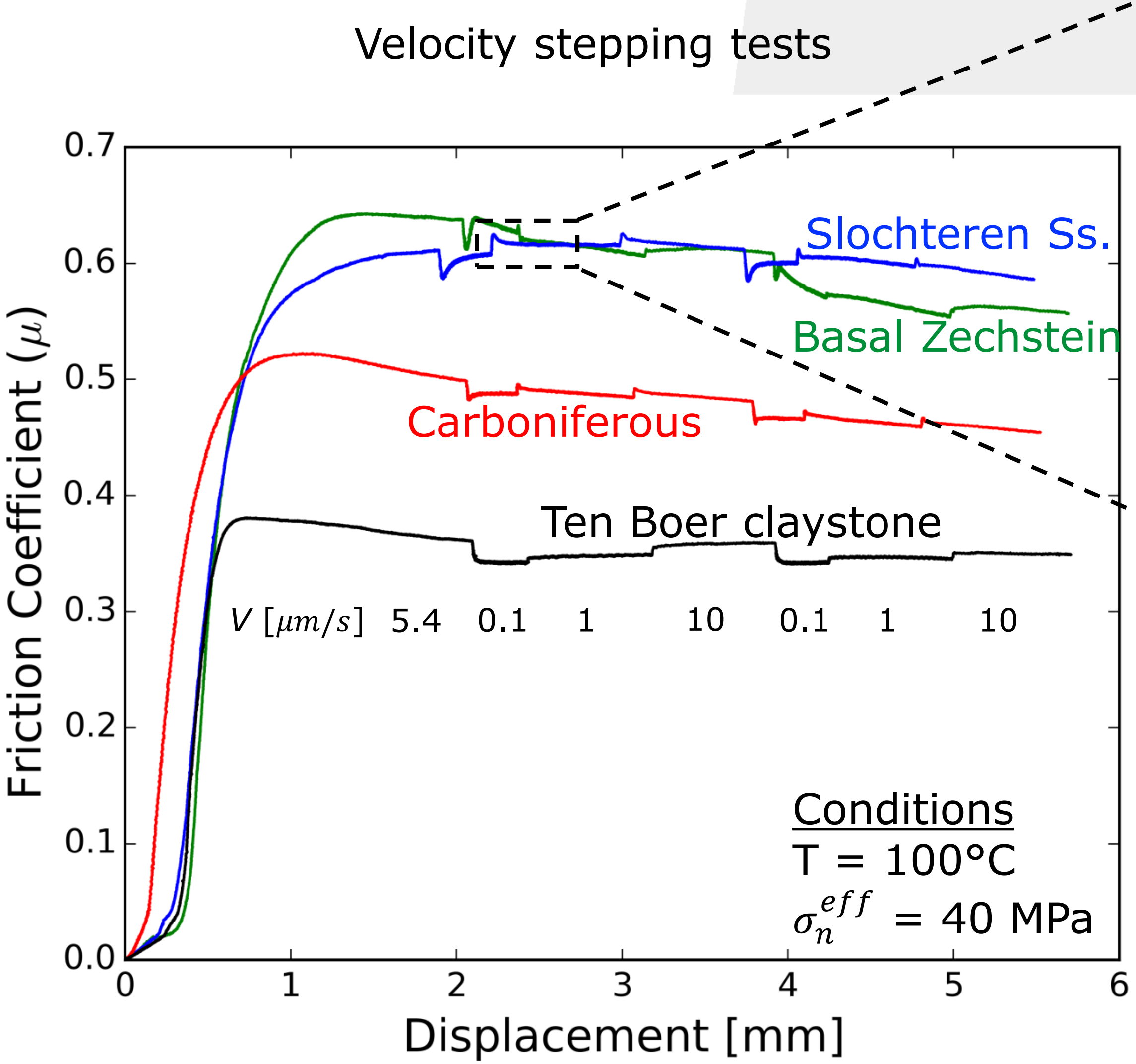

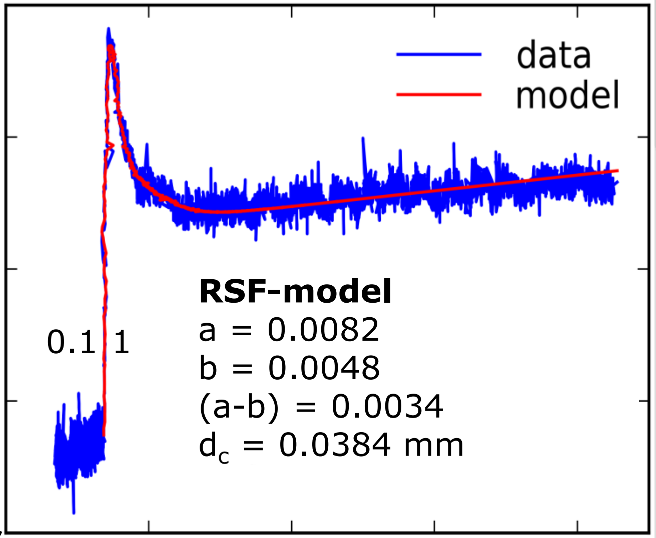

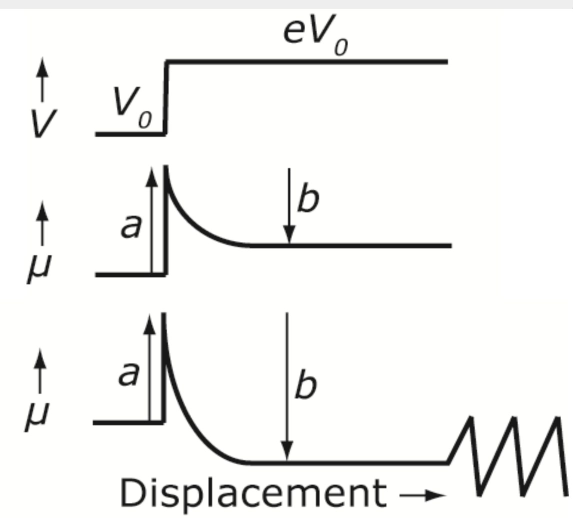

(a-b)>0 V-strengthening
(a-b)<0 V-weakening
(unstable)

Hunfeld et al. (2017) *JGR: Solid Earth*

Utrecht University

Full RSF data set

Mechanical stratigraphy (strength & rate-dependence)

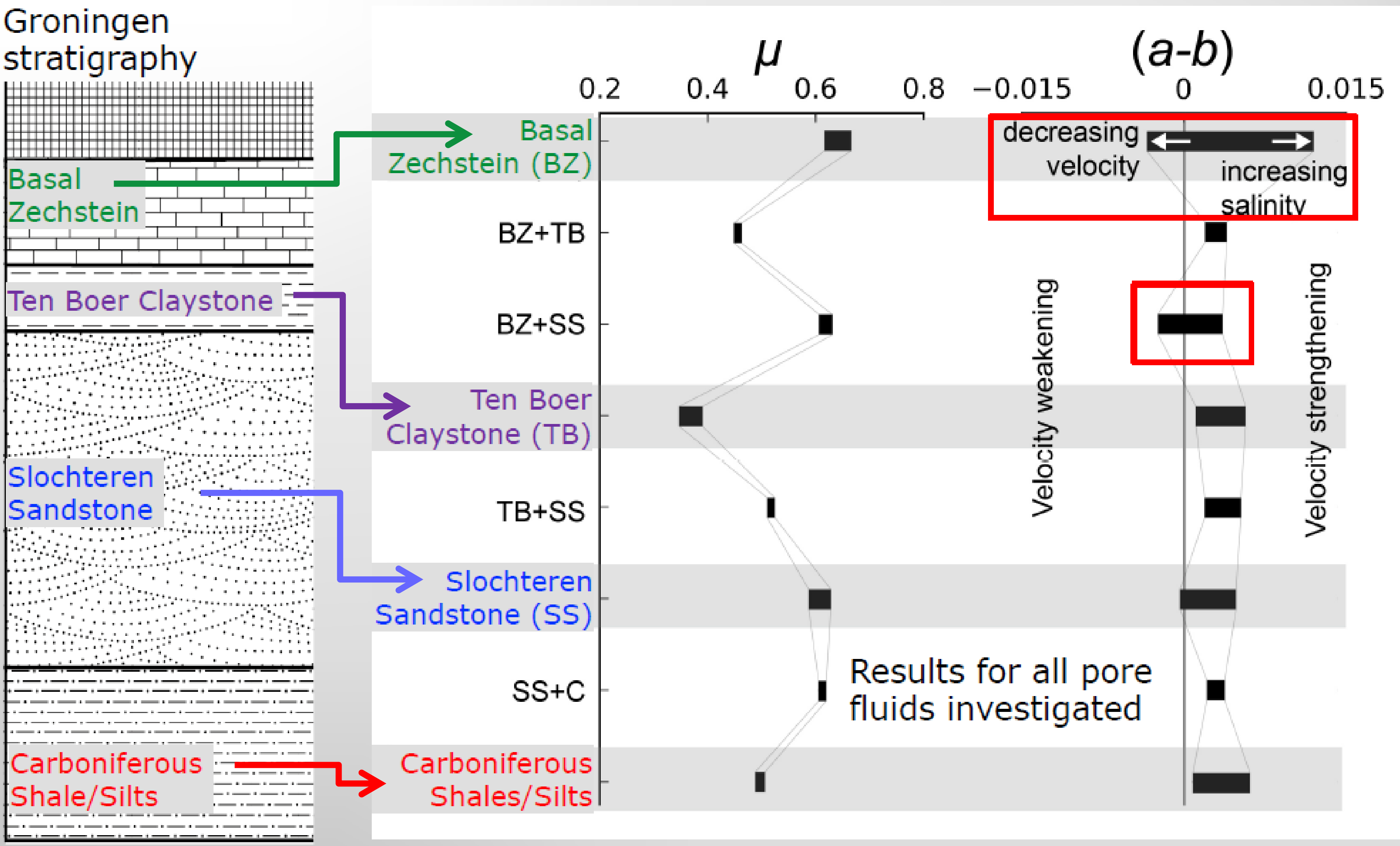

Hunfeld et al. (2017, 2019) *JGR: Solid Earth*

Utrecht University

Healing and reactivation experiments

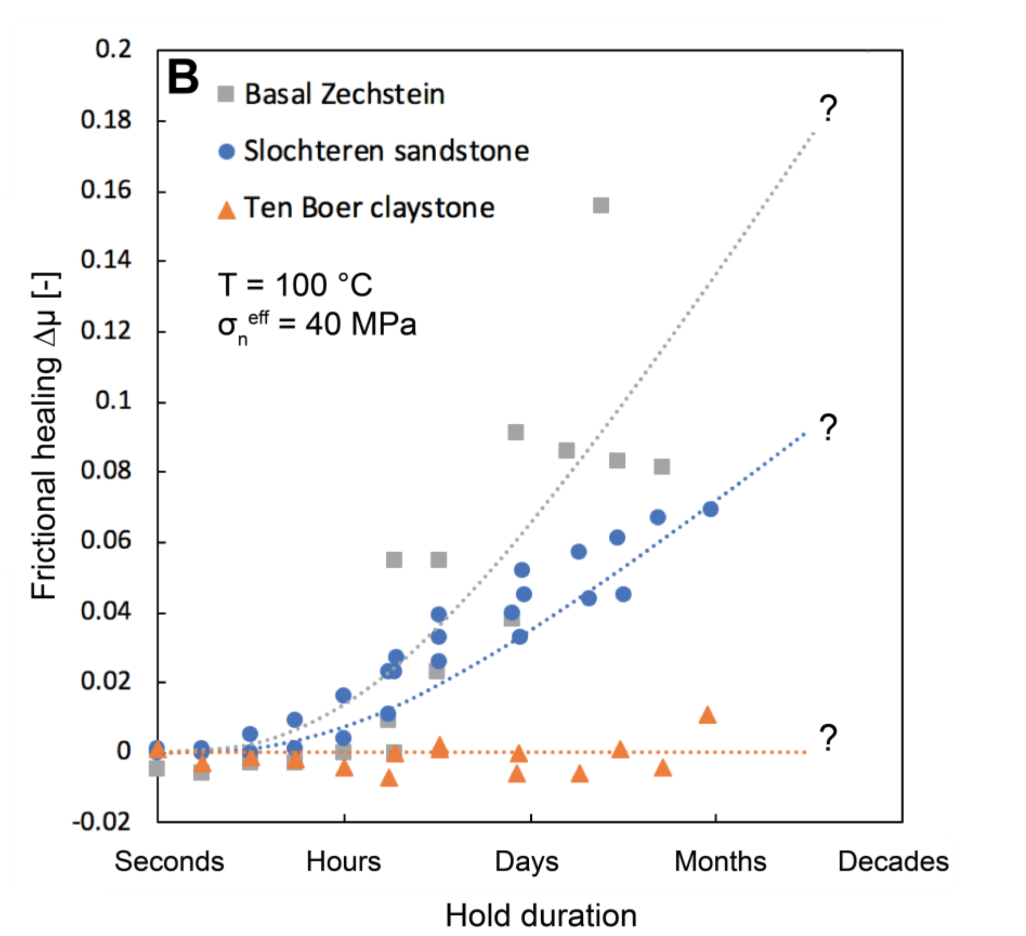

- Slide-Hold-Slide tests under in-situ conditions
- Major healing + stress drop in Basal Zechstein + Slochteren Sst gouges

  Compaction/Cementation
- None in Ten Boer or Carboniferous

Hunfeld et al. (JGR, 2020)

Utrecht University

Dynamic weakening experiments at seismic slip rates

<u>HV Weakening mechanisms :</u>

- Melt lubrication
- Flash heating
- Carbonate decomposition
- Nanopowder lubrication
- Silica-gel lubrication
- Thermal pressurization, devolatization & fluidization

<u>Difficulties:</u>

- Large displacements (m)
- Low normal stress
- Often dry

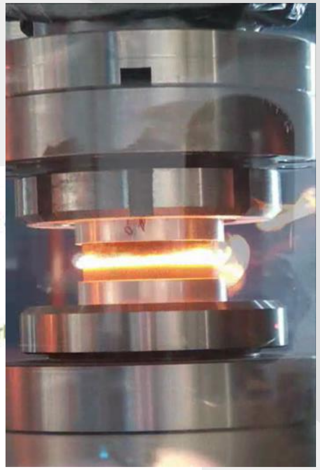

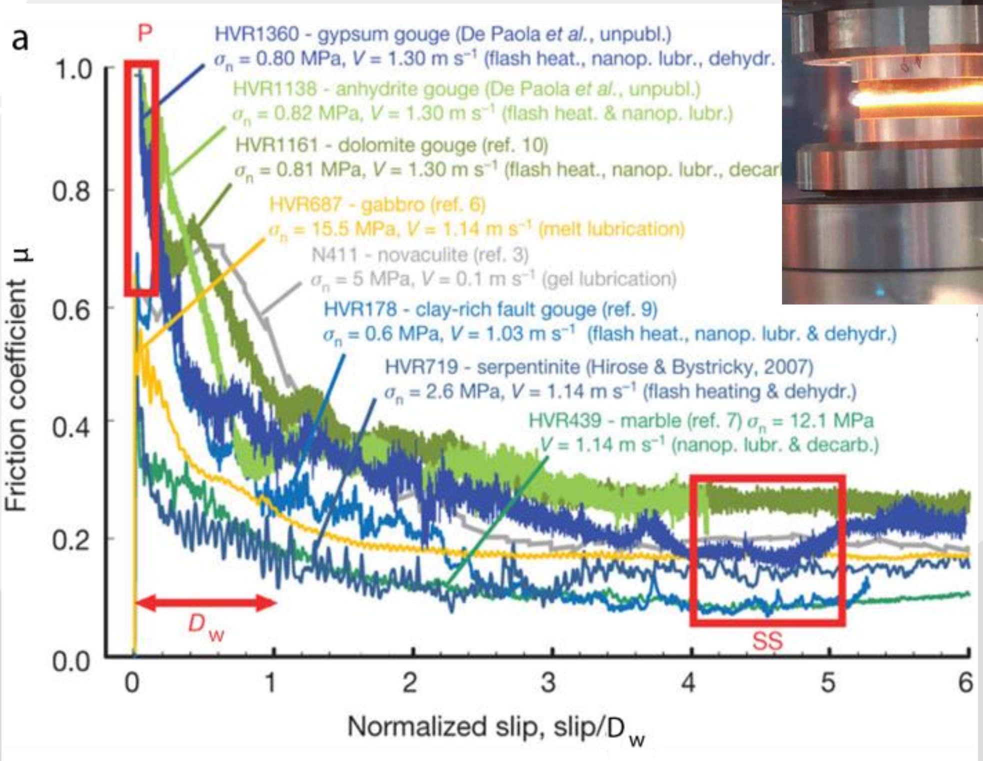

Di Toro et al., *Nature* (2011)

Do these effects occur in induced events ??
(small displacements, high normal stress, wet)

Utrecht University

Low-to-High Velocity Rotary Shear Apparatus

China Earthquake Administration, Beijing

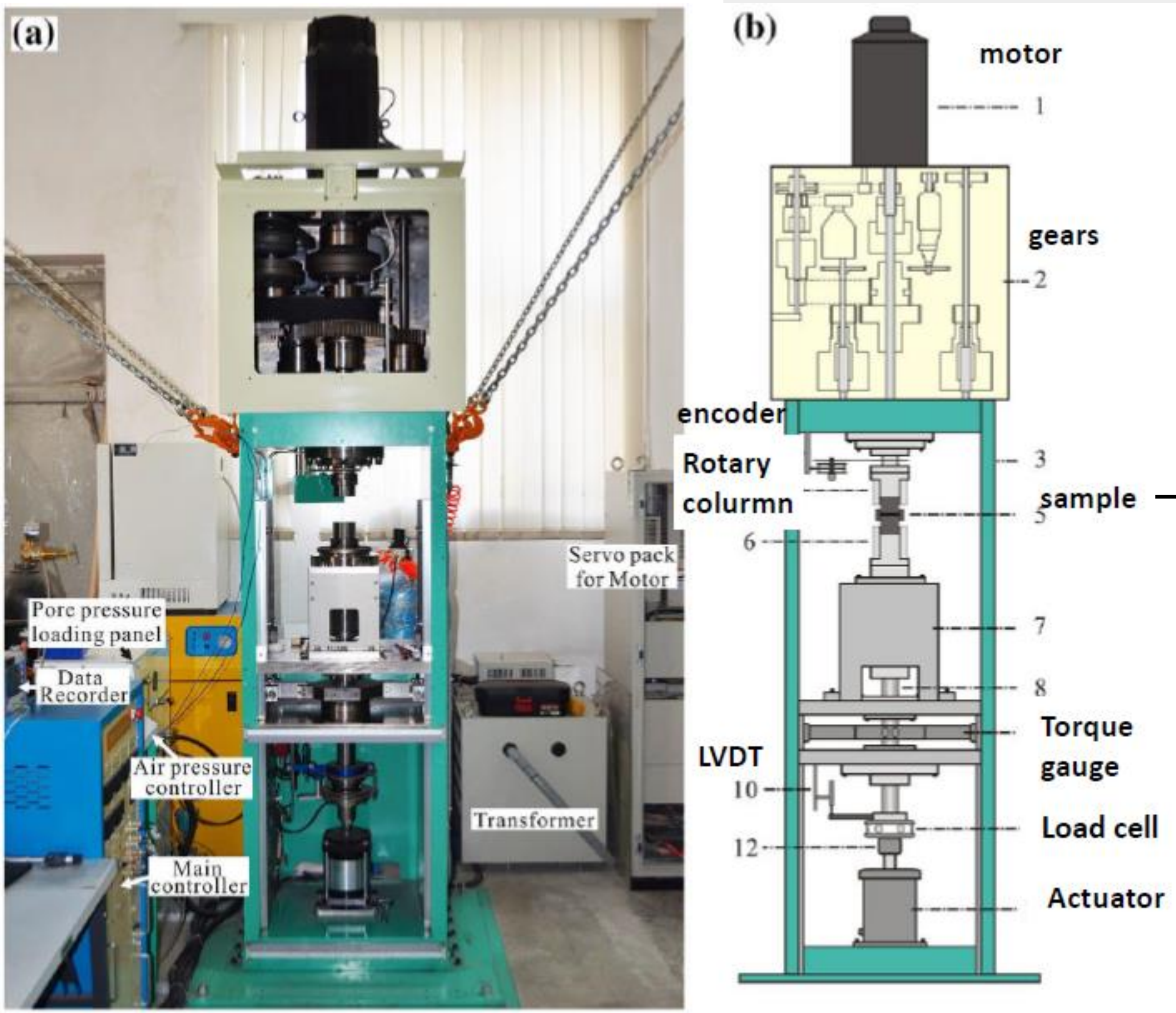

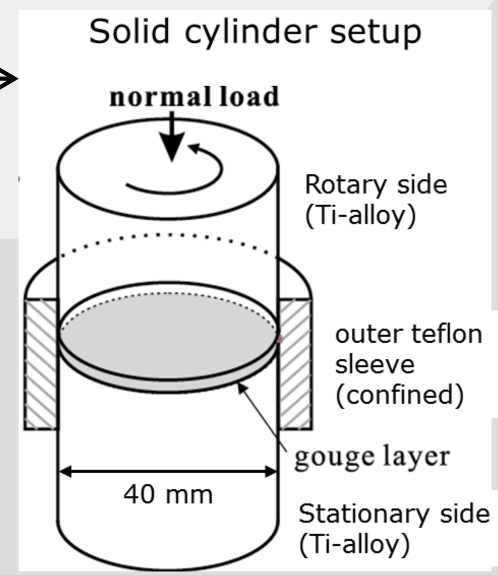

Utrecht University

Simulated seismic slip experiments (M3-4)

China Earthquake Administration, Beijing

Seismic slip pulse:

- 10 -20 cm total slip
- Peak velocity = 1 to 1.5 m/s
- Up to 10 MPa normal stress (solid cylinder)
- Up to 20 MPa normal stress (ring setup)
- Fluid-saturated gouge (1 atm)

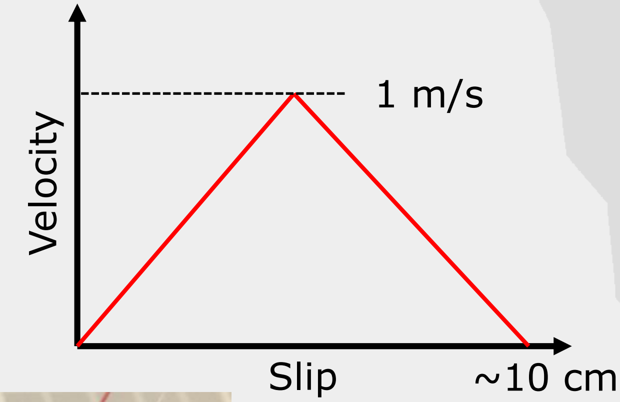

Solid cylinder setup

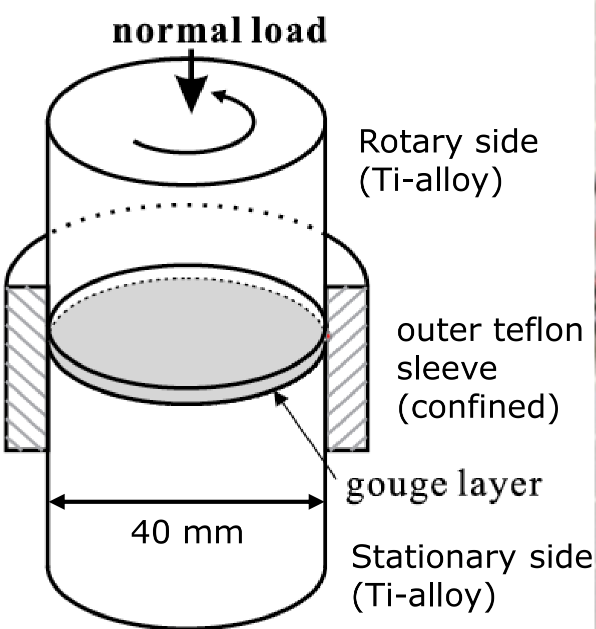

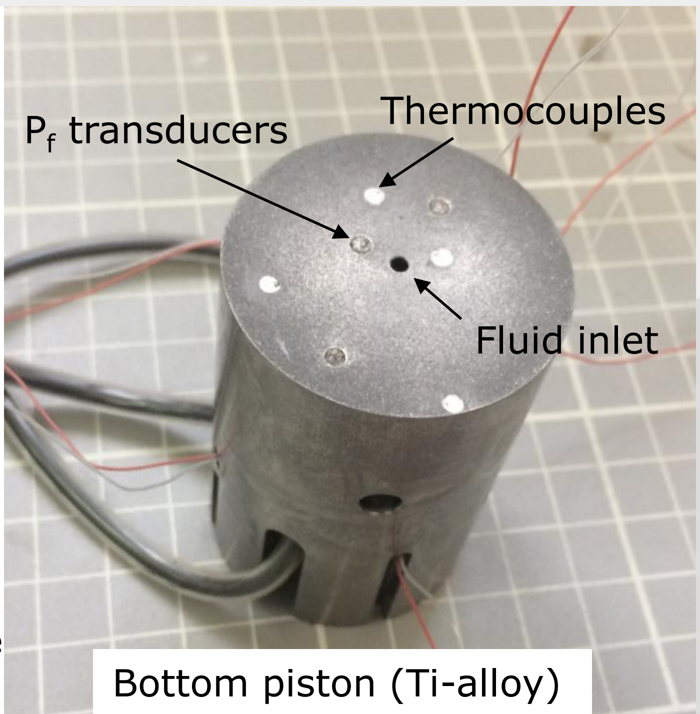

Bottom piston (Ti-alloy)

Hunfeld, Chen et al. (GRL 2021)

Simulated seismic slip experiments – solid cylinder

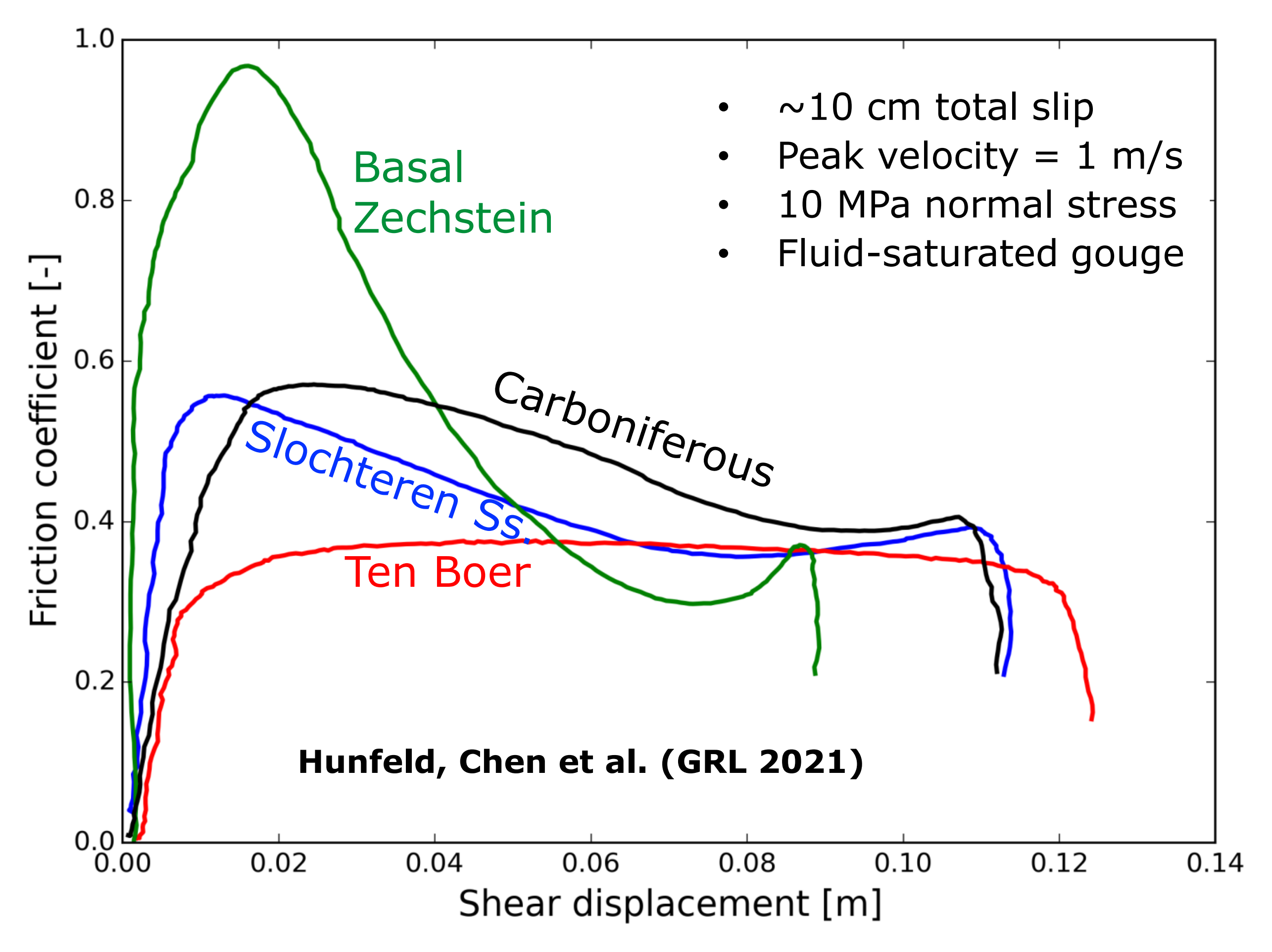

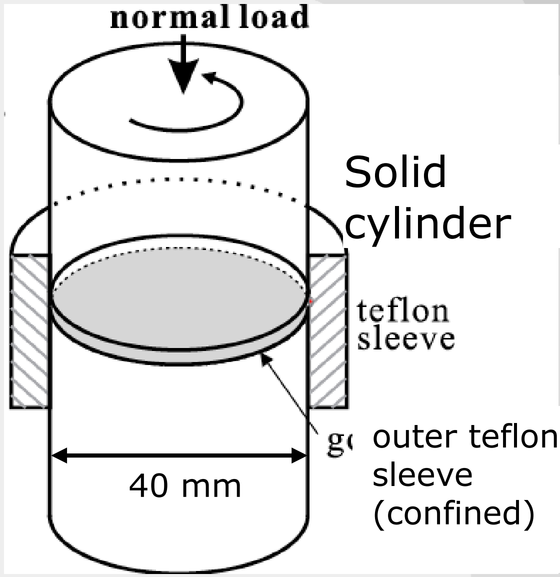

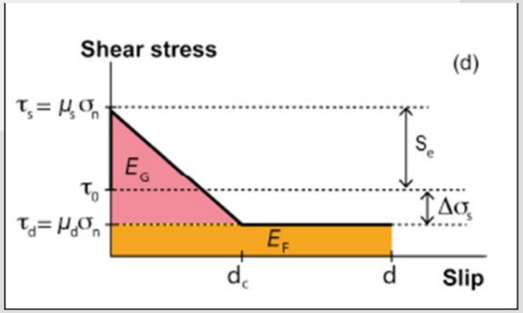

- Dynamic weakening in all Groningen gouges except Ten Boer.
  - Residual friction 0.3<μ<0.4
  - Slip weakening similar to model assumptions

Utrecht University

Simulated seismic slip experiments – ring

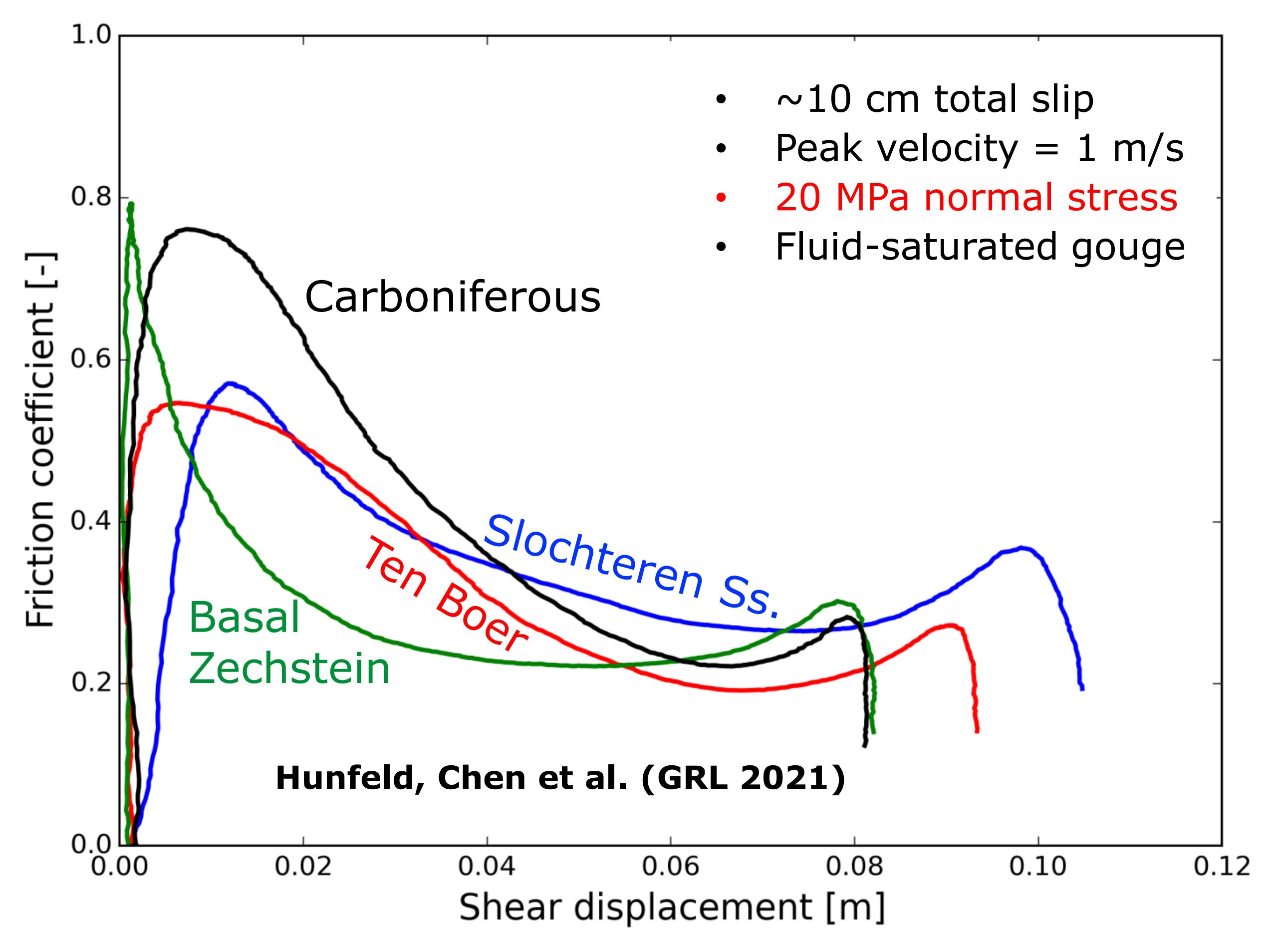

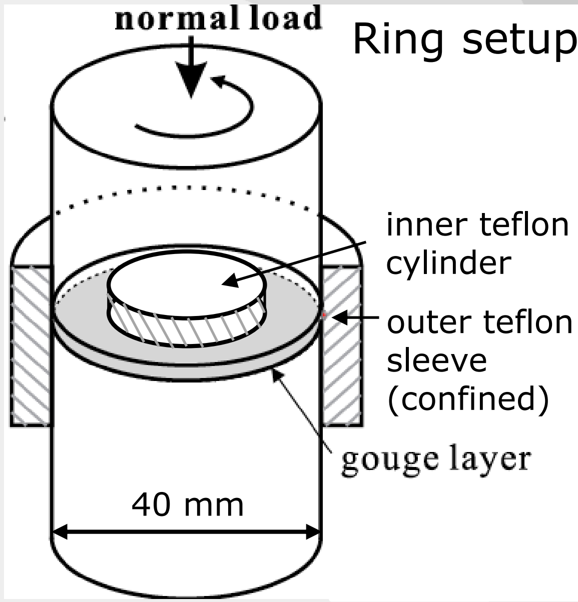

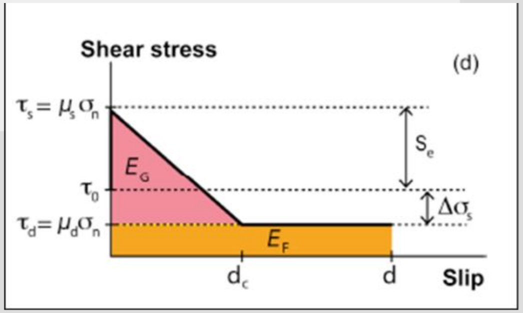

- Dynamic weakening in all formations (strongest/fastest in Basal Zechstein)
- Residual friction 0.2<μ<0.3
- High peak friction in clay-bearing gouges (TB & C) due to **machine effects?**

New approach – HV pressure vessel CEA

(Chen et al., submitted)

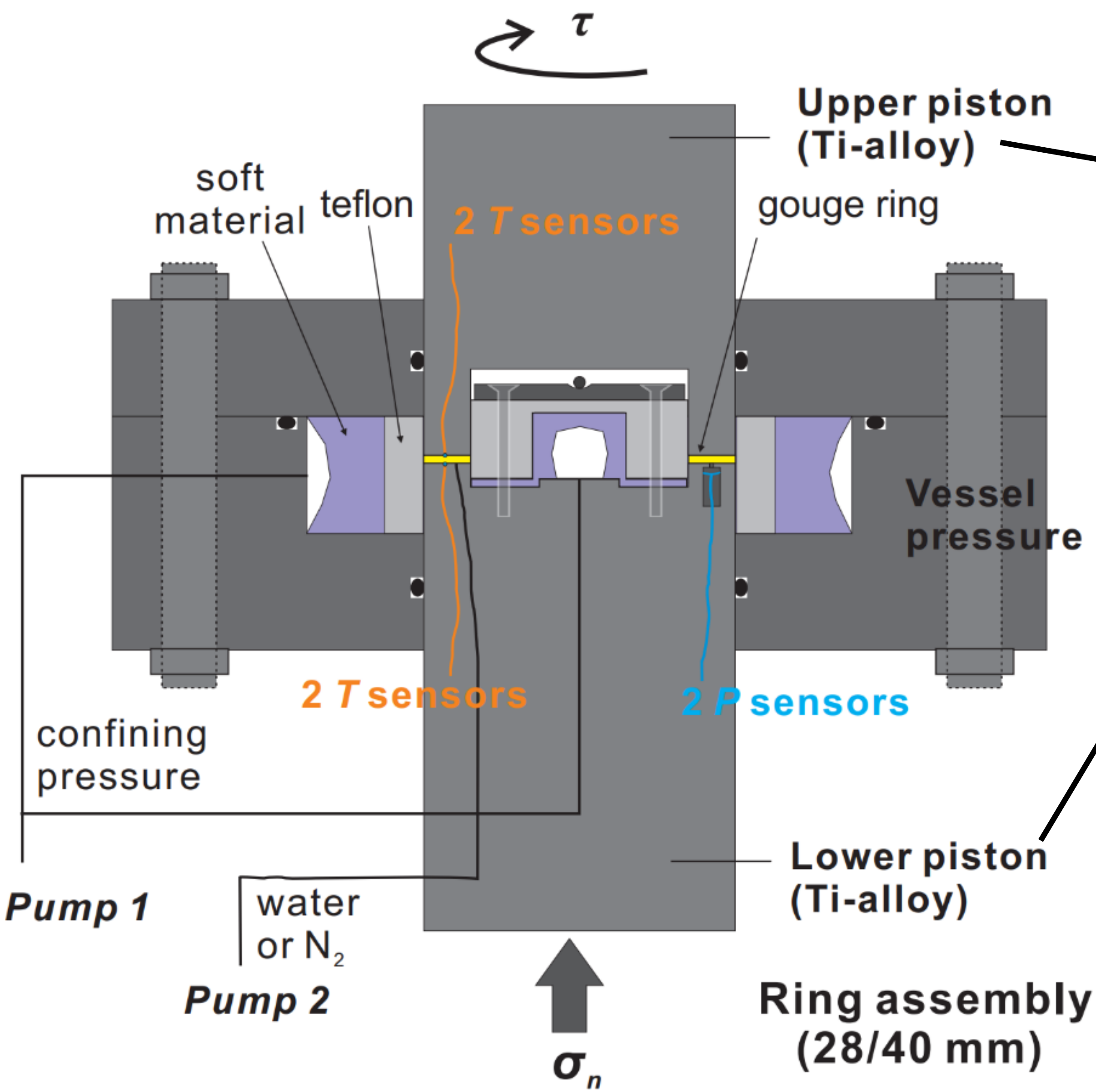

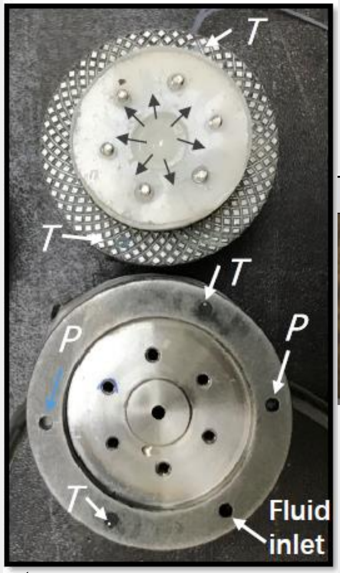

No extrusion

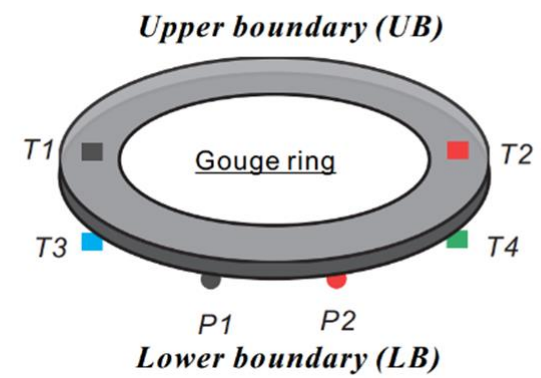

Utrecht University

Experimental conditions

(Chen et al., submitted)

- Initially room T
- ~15 cm total slip (Pre-slip 1.6 mm/s for 0.4 m)
- Peak velocity = ~1.6 m/s, Pulse duration ≈ 0.3 s
- Improved confining conditions (no extrusion)
- **Up to 31 MPa effective normal stress**
- Controlled fluid pressure (dry, < 0.5 MPa, **up to 5MPa**)
- Better Temperature and Pore fluid pressure measurements

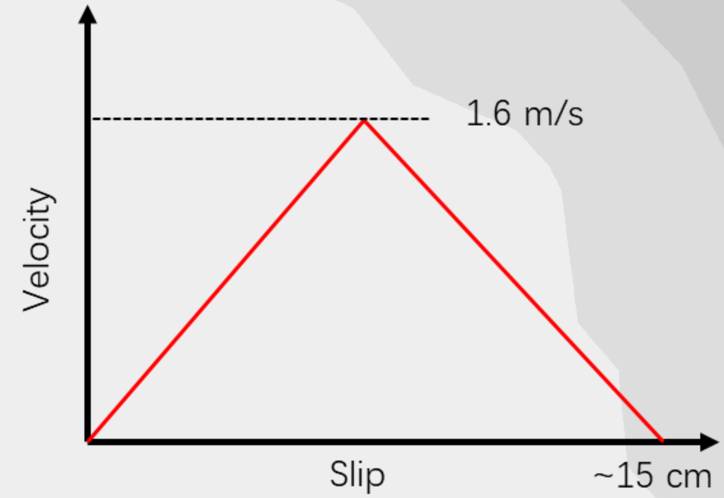

Gouge Materials

Basal Zechstein (13 runs)
Carboniferous shale (14 runs)
Sandstone (19 runs)
Grain size (<125/50 µm)

Experiments

Series I:
σ_n vary from 5 to 31 MPa

Series II:
σ_n~10 MPa (dry, different Pf)

Typical results – HV slip pulse

Utrecht University

Blow-up of coseismic phase

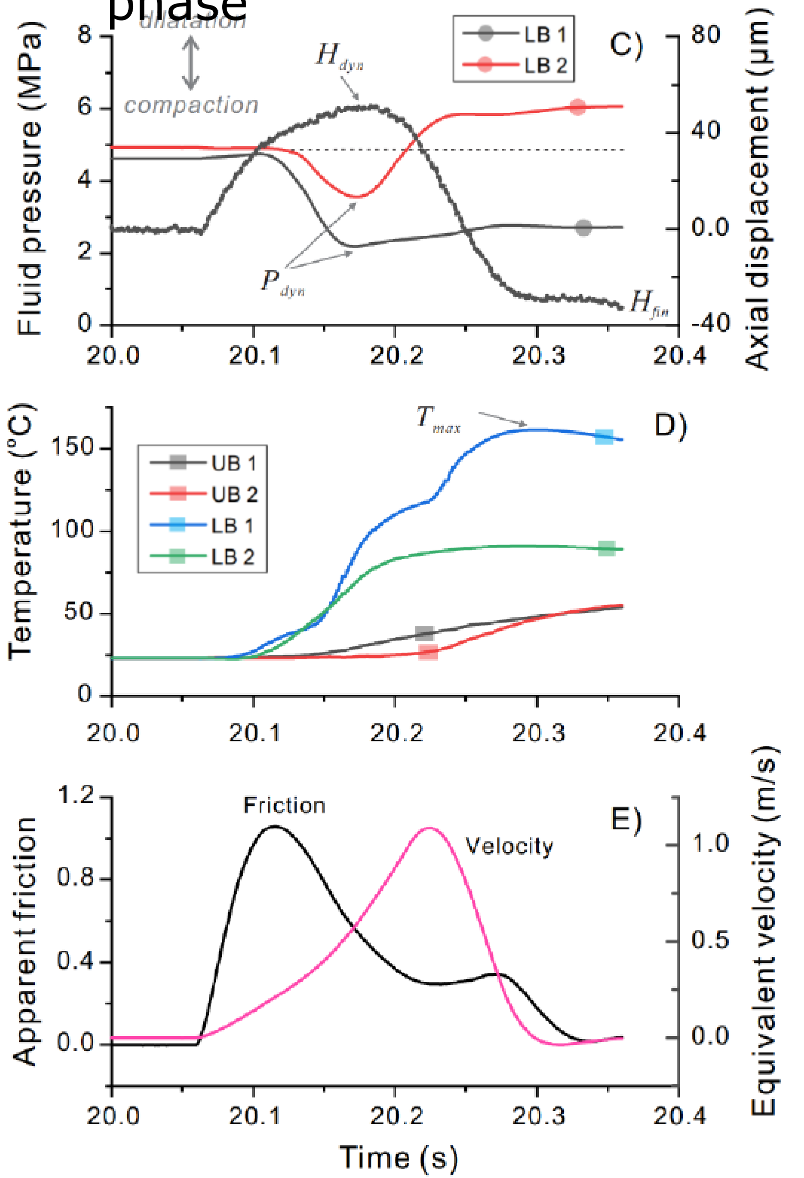

B. Zechstein Gouge

$P_f \approx 5$ MPa

$\sigma_n^e = 15.5$ MPa

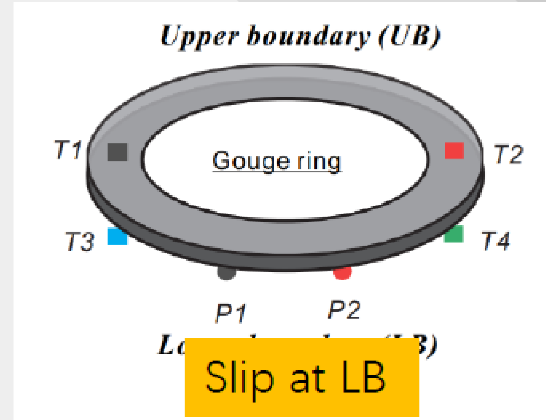

Slip at LB

Key observations

- Gouge dilates as slip is initiated (H)
- Pf at lower (slip) surface drops then increases
- T increases at slip surface (< 200 ℃)
- Weakening starts at 0.3 m/s
- Min dynamic friction attained at ~ Vmax

(Chen et al., submitted)

All mechanical data - HV slip pulse

Utrecht University

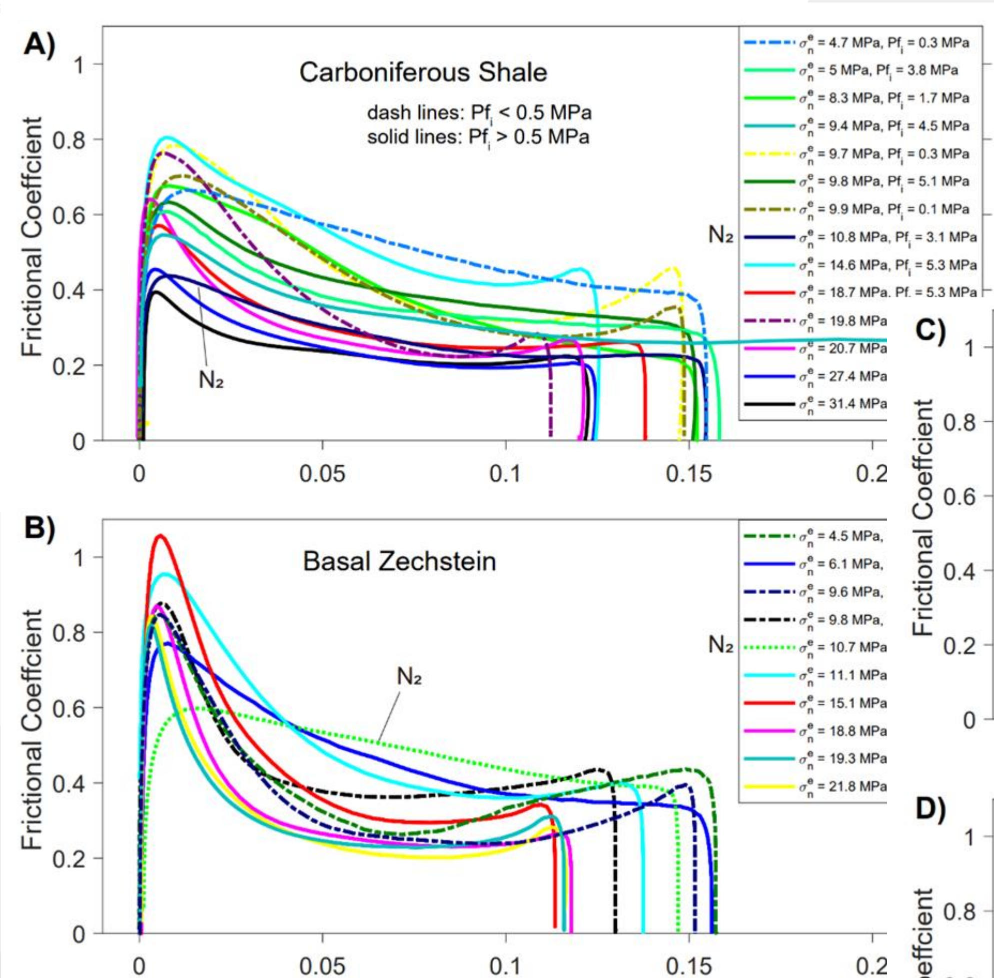

Key observations

- Wet samples weaken markedly
- Dry (N2 saturated) much less

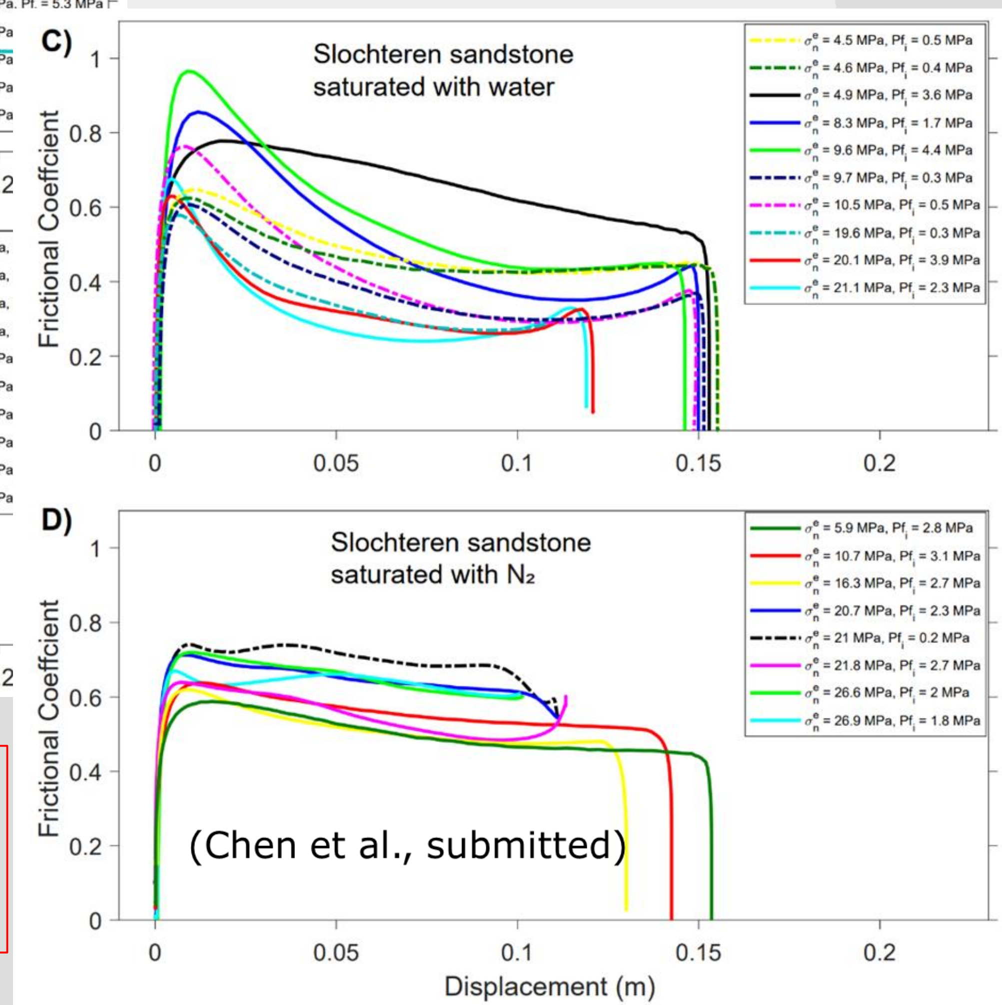

All samples saturated with pressurized water …

…except where indicated with N_2

Quantifying dynamic slip weakening

High P_f data only

Parameter Set I

- Peak friction (μ_{pk})
- Min dynamic friction (μ_d)
- Dw & Gc

following Mizoguchi et al. (2007)

$$\mu_a = \mu_{ss} + (\mu_{pk} - \mu_{ss})e^{(\ln 0.05.d/D_w)}$$

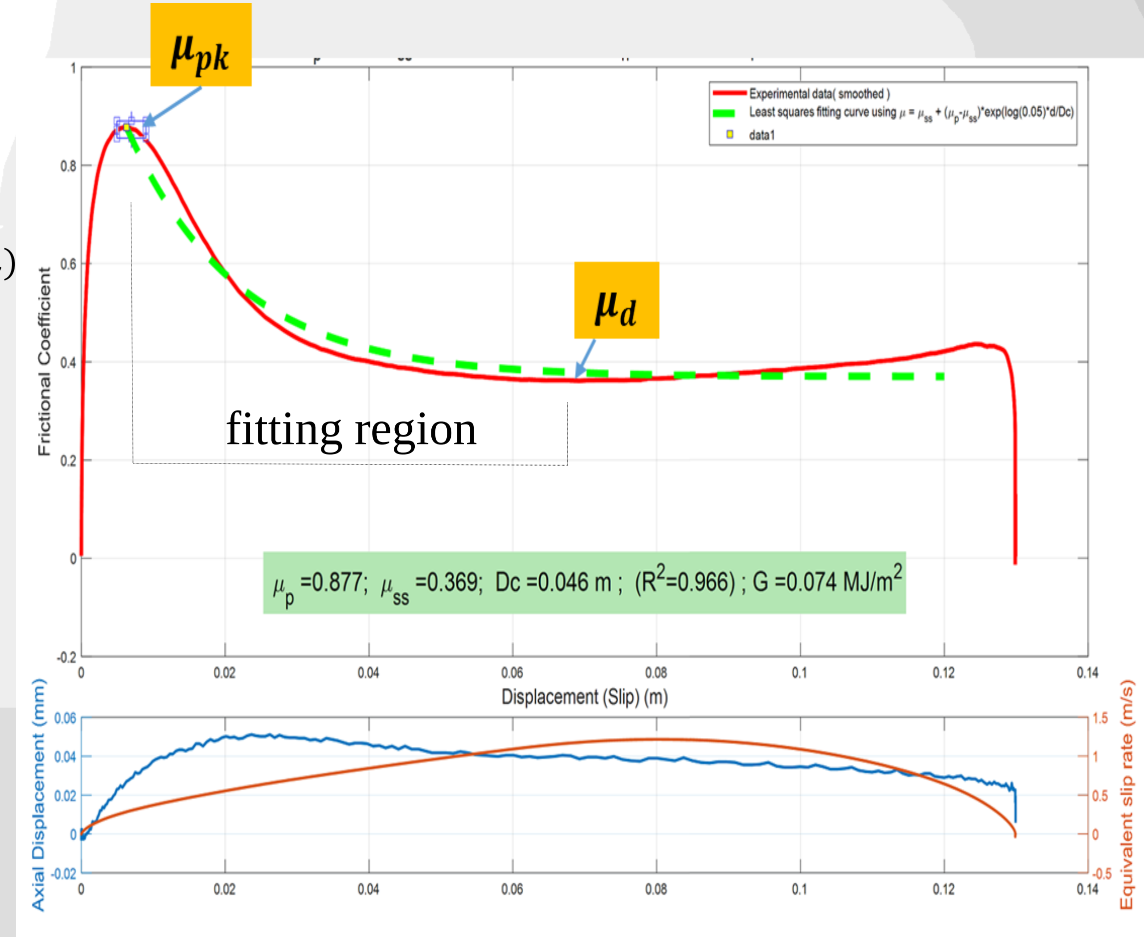

Parameter Set II

- Peak stress (τ_{pk})
- Stress drop ($\Delta\tau$)
- Weakening rate (W)

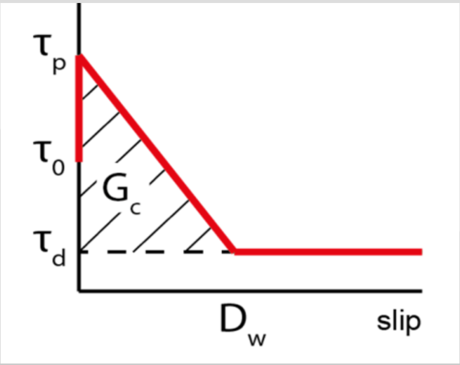

(Chen et al., submitted)

Utrecht University

Quantifying dynamic slip weakening

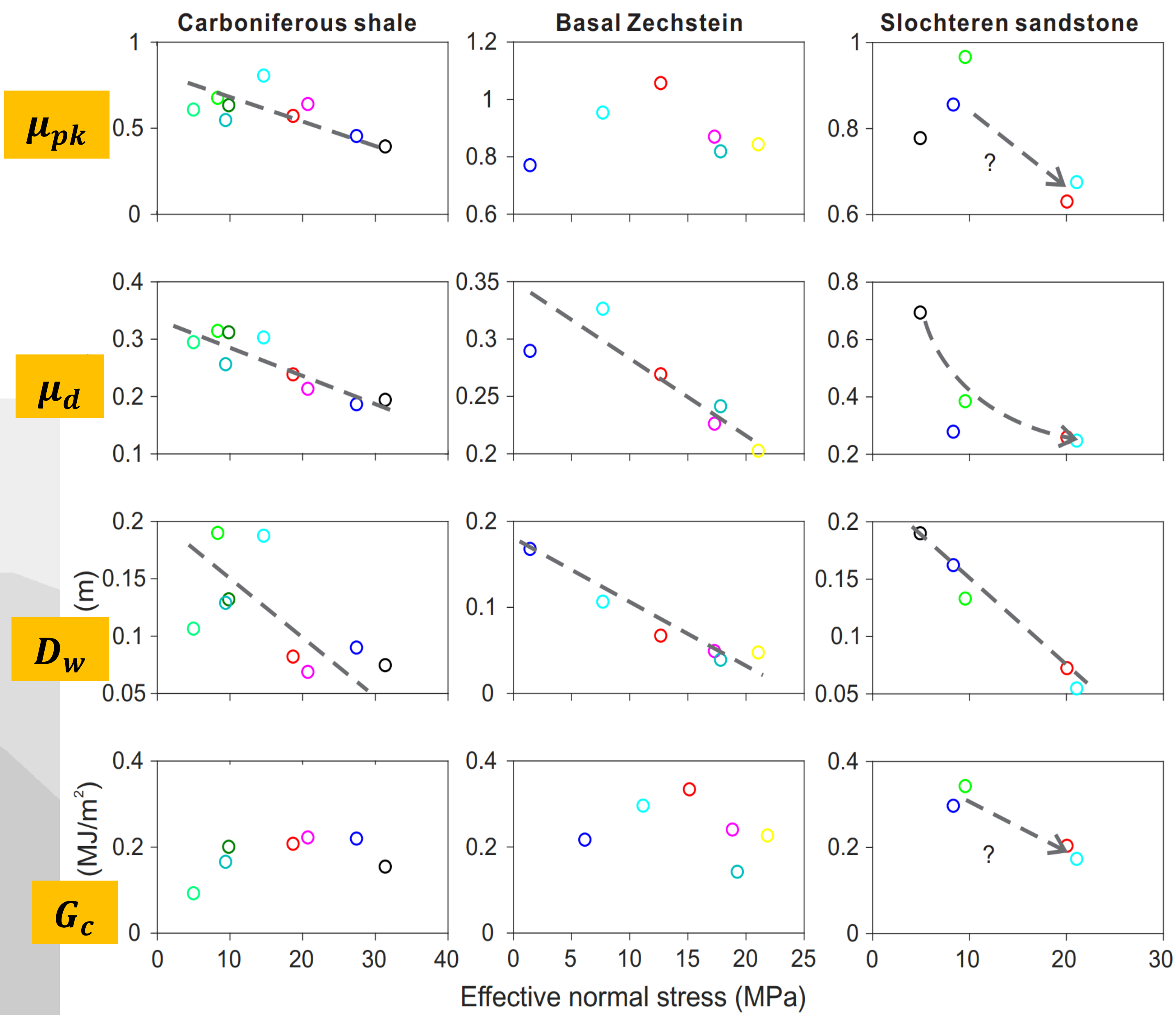

Parameter Set I

>>>>>

Loes Buijze
J-P Ampuero

(Chen et al., submitted)

Utrecht University

Quantifying dynamic slip weakening

Parameter Set II

$\Delta\tau$ (MPa)

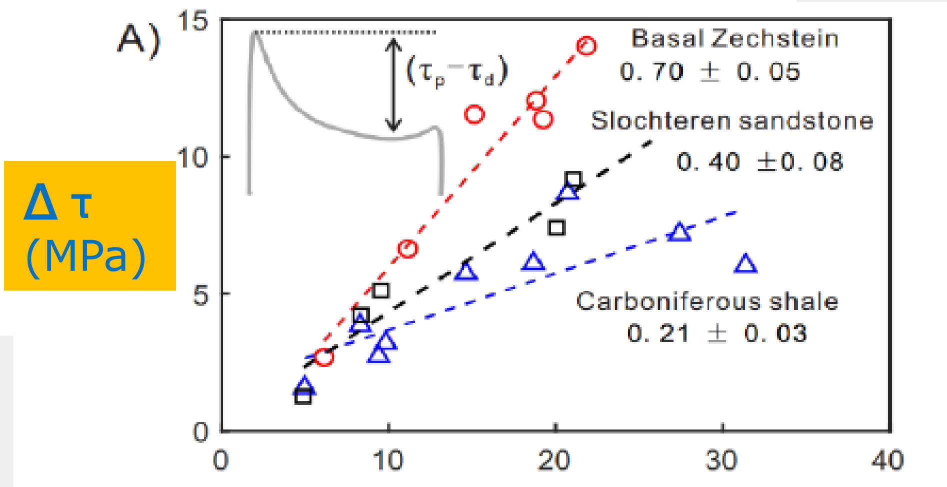

W_{max} (MPa /mm)

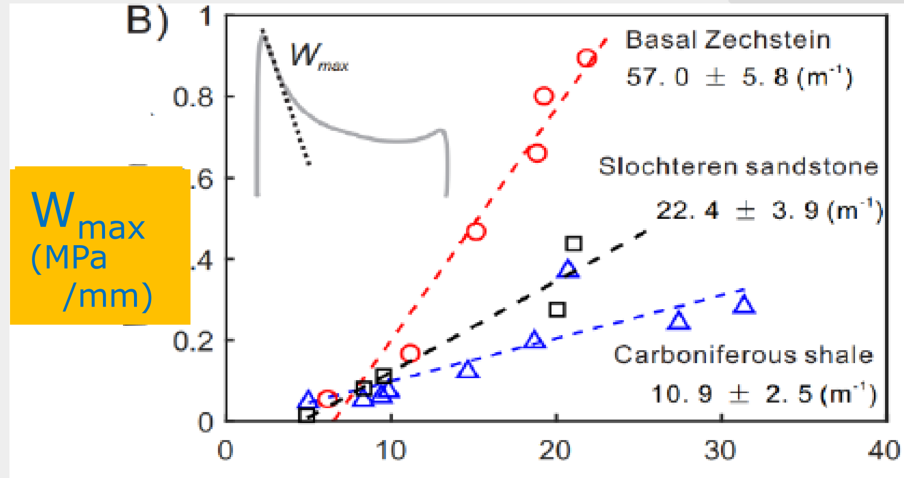

W_{ave} (MPa /mm)

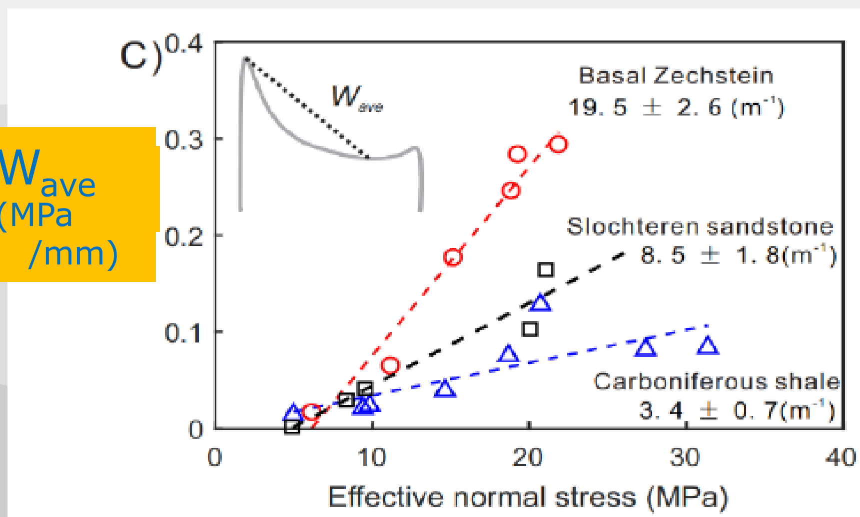

Lowest values in Carboniferous Shales/Siltstones

(Chen et al., submitted)

Utrecht University

What is the slip weakening mechanism?

Weakening mechanisms	**Evidence against**	
Flash heating	cf. dry experiment	(no)
Compaction-caused pressurization	dilatation was observed	(no)
Thermal pressurization	Pf decrease was observed	(no)
Phase transition	high Pf_i	(unlikely)

Clues

- Normal stress insensitive
- Weakening when V > 0.2 m/s
- Re-strengthening as V decreases
- Weakening when T is low

While

- Water must be involved

Flash heating

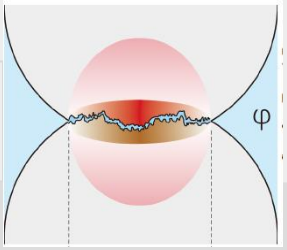

Flash pressurization

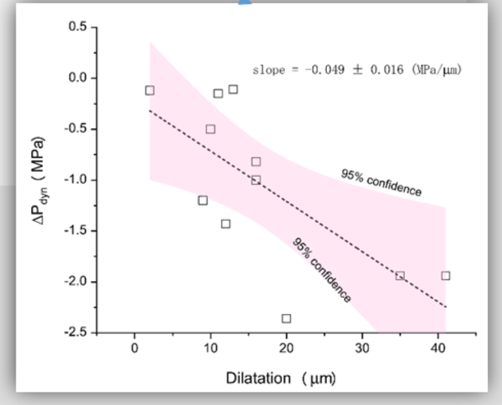

(Chen et al., submitted)

Latest HV slip pulse data vs depth

- From the perspective of frictional stability, Basal Zechstein is most likely to nucleate seismogenic slip

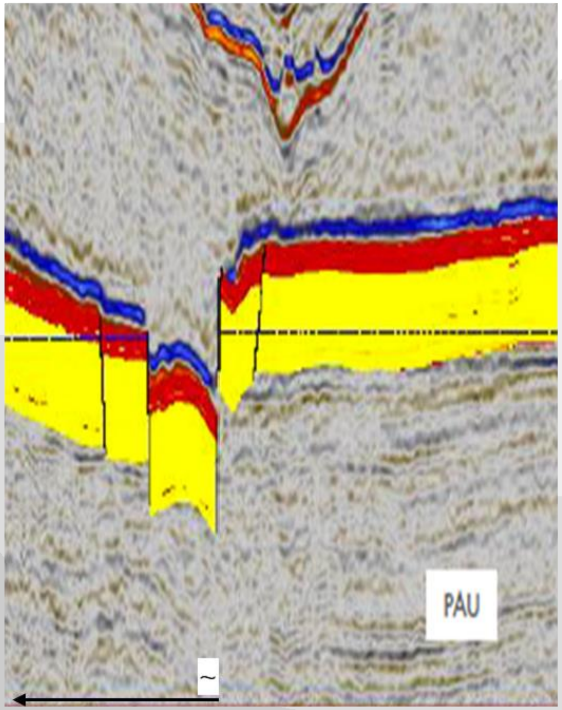

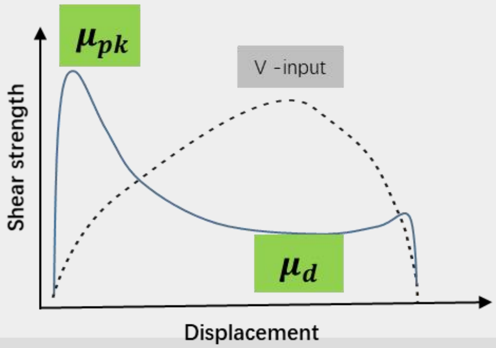

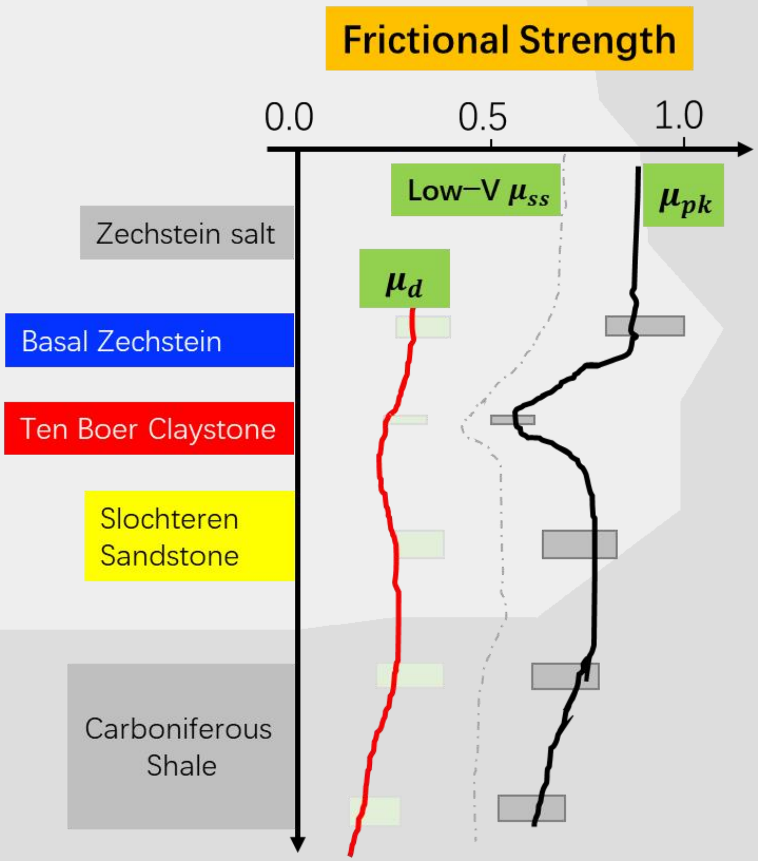

(Chen et al., submitted)

Utrecht University

Latest HV slip pulse data vs depth

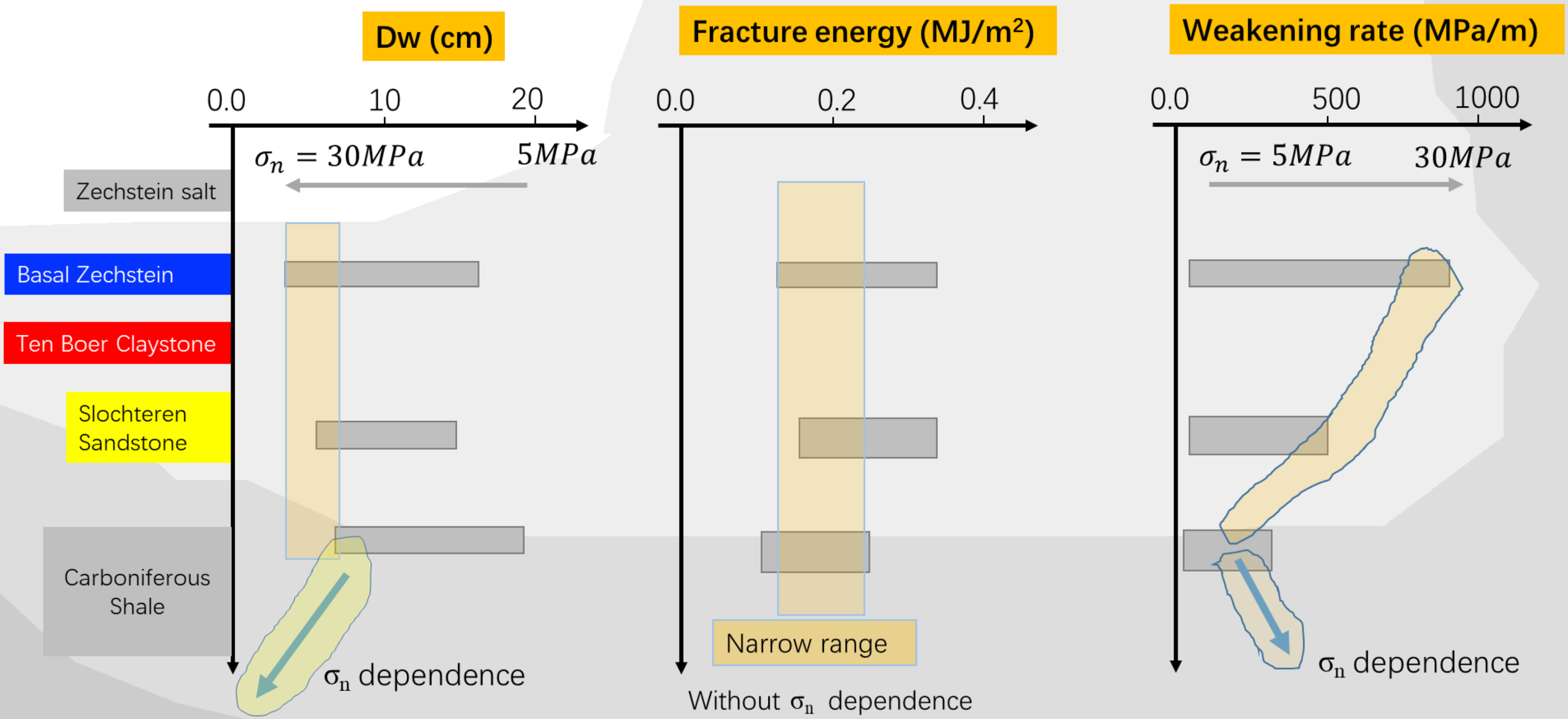

(Chen et al., submitted)

Utrecht University

Conclusions

- Reservoir behaviour
  - Deformation is 30-60% plastic/dissipative (more at field loading rates)
  - Stored E for seismic release lower than expected – minor impact on M(max)
  - E-P Constitutive model - low strength at high porosity (> 20%)
    improves predictions of stress evolution (?)
    otherwise minor impact vs linear elastic assumption

- Fault behaviour under in-situ conditions
  - Basal Zechstein / Slochteren: strong + healing and instability prone
  - Ten Boer + Carboniferous: weaker, no healing
  - RSF behaviour characterized
  - Dynamic slip weakening characterised vs normal stress (flash pressurization?)
  - Carboniferous >>> lowest slip weakening rate, normal stress effects

- Impact of results on rupture / event modelling
  - Impact of sandstone plasticity – Loes Buijze
  - Dynamic slip weakening data - similar to model assumptions (e.g. Wentink)
    - applied by Pablo Ampuero, Loes Buijze

Thanks for your attention !!

References UU Work

Buijze, L., van den Bogert, P. A. J.,Wassing, B. B. T., & Orlic, B. (2019). Nucleation and arrest of dynamic rupture induced by reservoir depletion. *Journal of Geophysical Research: Solid Earth*, *124*, 3620–3645. https://doi.org/10.1029/2018JB016941

Chen, J., Hunfeld, L. B., Niemeijer, A. R., & Spiers, C. J. (submitted).. Fault weakening during short seismic slip pulse experiments: Implications for induced earthquakes in the Groningen gas field.

Hunfeld, L. B., Niemeijer, A. R., & Spiers, C. J. (2017). Frictional properties of simulated fault gouges from the seis- mogenic Groningen gas field under in situ *P–T* chemical conditions. *Journal of Geophysical Research: Solid Earth*, *122*. https://doi.org/10.1002/2017JB014876

Hunfeld, L. B., Chen, J., Niemeijer, A. R., & Spiers, C. J. (2019). Temperature and gas/brine content affect seismogenic potential of simulated fault gouges derived from Groningen gas field caprock. *Geochemistry, Geophysics, Geosystems*, *20*, 2827–2847. https://doi.org/10.1029/2019GC008221

Hunfeld, L. B., Chen, J., Hol, S., Niemeijer, A. R., & Spiers, C. J. (2020). Healing behavior of simulated fault gouges from the Groningen gas field and implications for induced fault reactivation. *Journal of Geophysical Research: Solid Earth*, *125*, e2019JB018790. https://doi.org/10.1029/2019JB018790

Hunfeld, L. B., Chen, J., Niemeijer, A. R., Ma, S., & Spiers, C. J. (2021). Seismic slip-pulse experiments simulate induced earthquake rupture in the Groningen gas field. *Geophysical Research Letters*, *48*, e2021GL092417. https://doi.org/10.1029/2021GL092417

Pijnenburg, R. P. J., Verberne, B. A., Hangx, S. J. T., & Spiers, C. J. (2018). Deformation behavior of sandstones from the seismogenic Groningen gas field: Role of inelastic versus elastic mechanisms. *Journal of Geophysical Research: Solid Earth*, *123*. https://doi.org/10.1029/2018JB015673

Pijnenburg, R. P. J., Verberne, B. A., Hangx, S. J. T., & Spiers, C. J. (2019). Inelastic deformation of the Slochteren sandstone: Stress-strain relations and implications for induced seismicity in the Groningen gas field. *Journal of Geophysical Research: Solid Earth*, *124*. https://doi.org/10.1029/2019JB017366

Pijnenburg, R. P. J., Verberne, B. A., Hangx, S. J. T., & Spiers, C. J. (2019). Intergranular clay films control inelastic deformation in the Groningen gas reservoir: Evidence from split-cylinder deformation tests. *Journal of Geophysical Research: Solid Earth*, *124*. https://doi.org/10.1029/2019JB018702

Pijnenburg, R. P. J. & Spiers, C. J. (2020). Microphysics of Inelastic Deformation in Reservoir Sandstones from the Seismogenic Center of the Groningen Gas Field. Rock Mechanics and Rock Engineering, *53*, 5301–5328 .https://doi.org/10.1007/s00603-020-02215-y

Spiers, C. J., Hangx, S. J. T., & Niemeijer, A. R. (2017). New approaches in experimental research on rock and fault behaviour in the Groningen gas field. *Netherlands Journal of Geosciences*, *96*(05), s55–s69. https://doi.org/10.1017/njg.2017.32

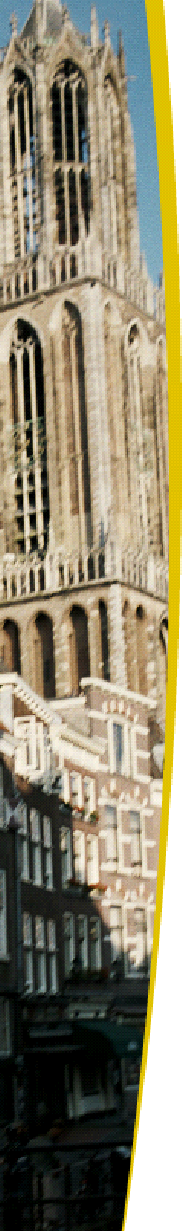

Virtual visit to UU HPT Lab and NAM Research Programme on Groningen ?

View these YouTube films – just released by NAM:

Full collection of NAM films (Jan van Elk & Dirk Doornhof 2020):

https://www.youtube.com/channel/UCt3ZLGyqqvwJTlwsUANWo7g

UU HPT Lab:

1) https://www.youtube.com/watch?v=9p_uMjbsdns
2) https://www.youtube.com/watch?v=mDfn2QUh--Y
3) https://www.youtube.com/watch?v=5U_otubQAyg

Universiteit Utrecht

NAM Nederlandse Aardolie Maatschappij B.V.

Universiteit Utrecht

Identifying the inelastic mechanisms:
Sequential deformation + imaging + particle velocimetry

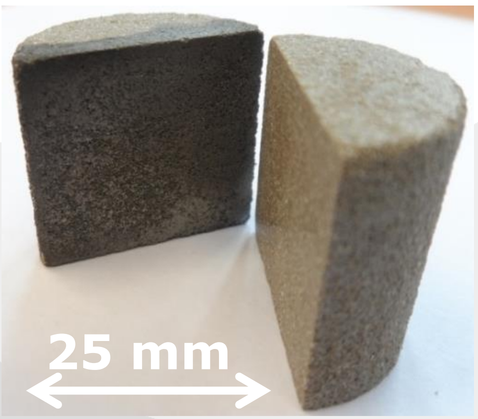

ZRP-3a Slocht. ss.
φ = 20%
$P_c - P_p$ = 40 MPa
T = 100° C
$\dot{\varepsilon}$ = 10^{-5} s^{-1}

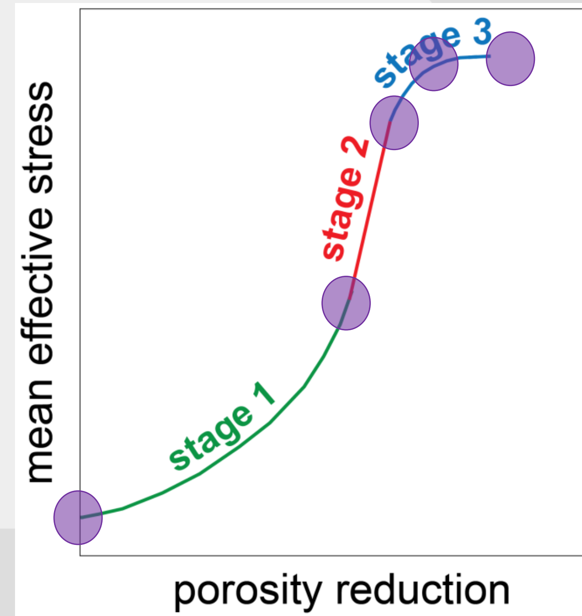

- 4 experiments
- Imaging after each experiment

Pijnenburg, Verberne, Hangx and Spiers (JGR 2019b)

Universiteit Utrecht

Identifying the inelastic mechanisms – core data:

–

No significant difference in reservoir crack densities in 2015 versus 1965– Stage 3 deformation not reached!!!

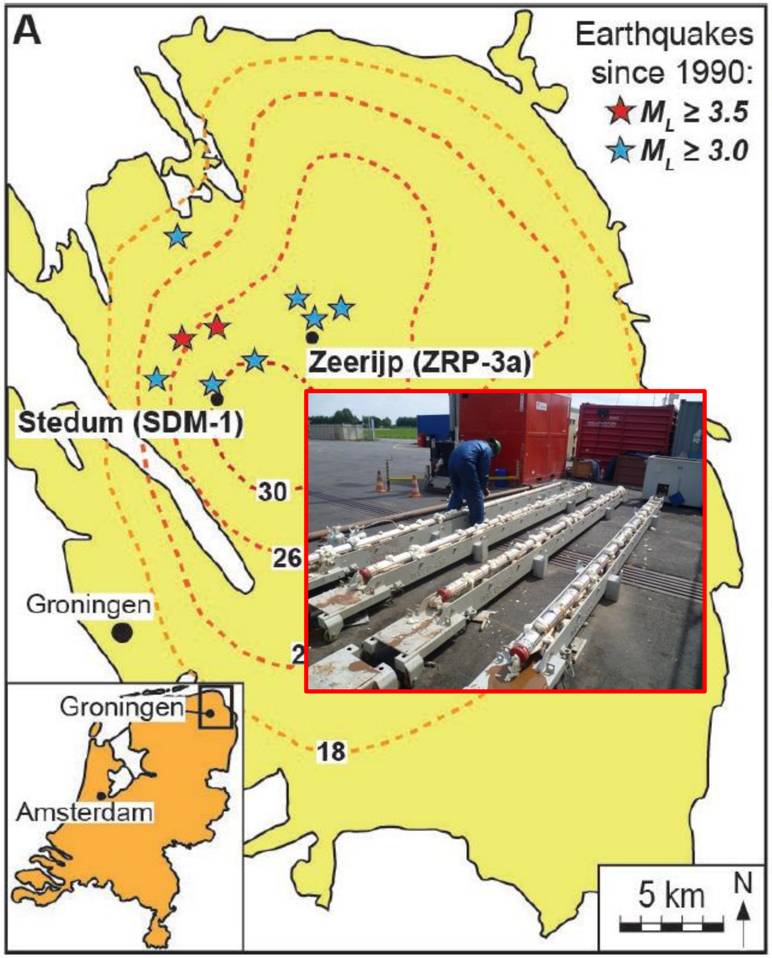

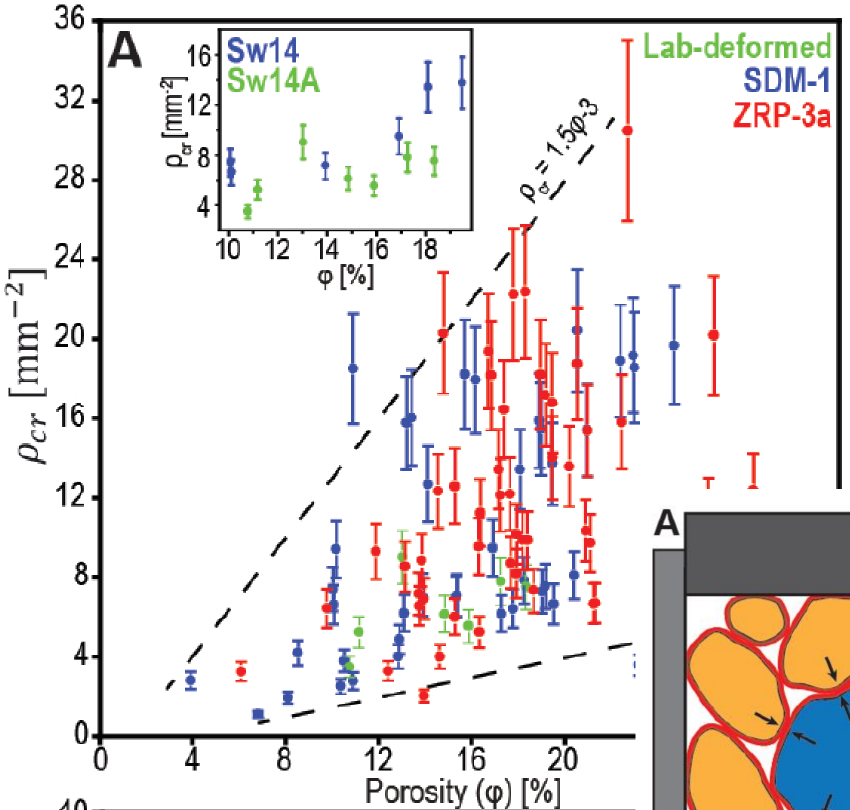

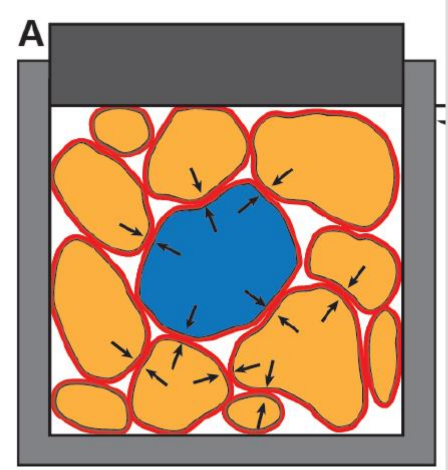

Verberne, Pijnenburg Hangx and Spiers (submitted Geology)

Universiteit Utrecht

Similar results in 1-D Compaction (Shell)

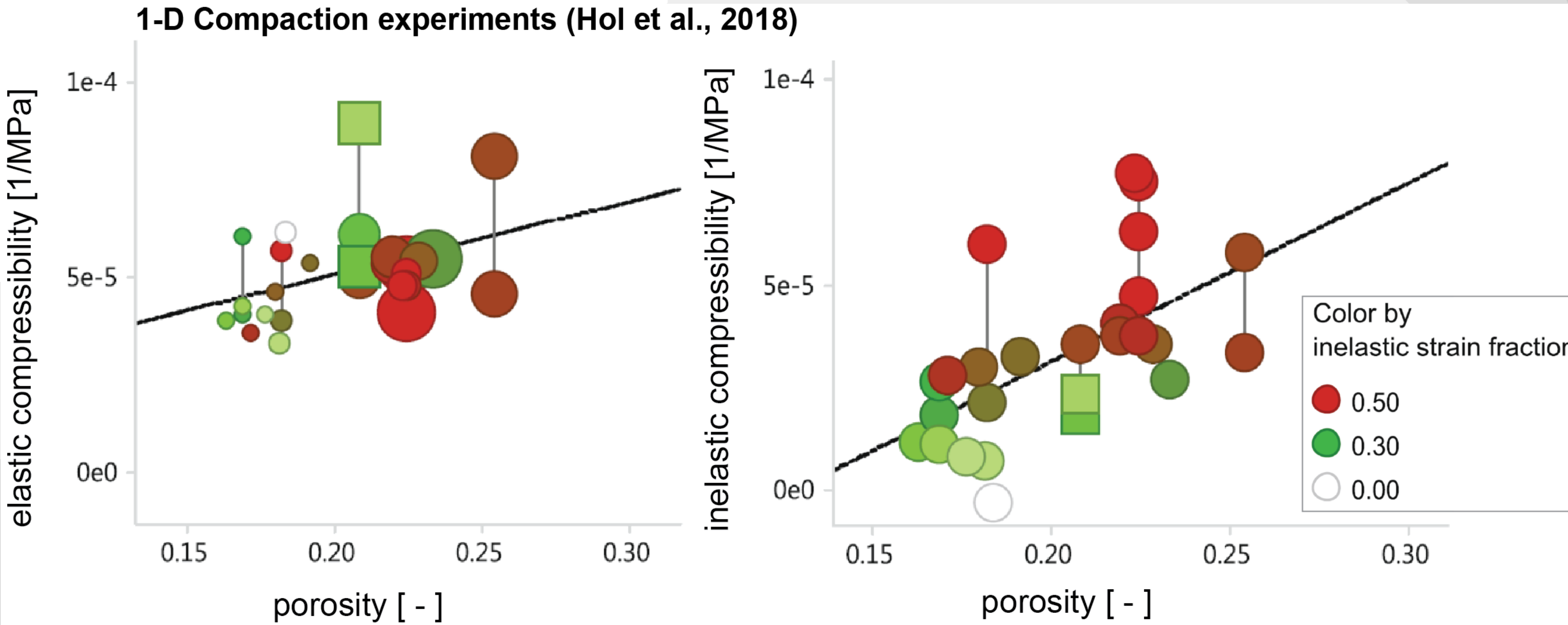

- 20-60% of total strain is inelastic in 1-D (uniaxial strain) compaction experiments (Hol et al., 2018)
- **Significant dissipation!**

Are lab friction experiments not too small?

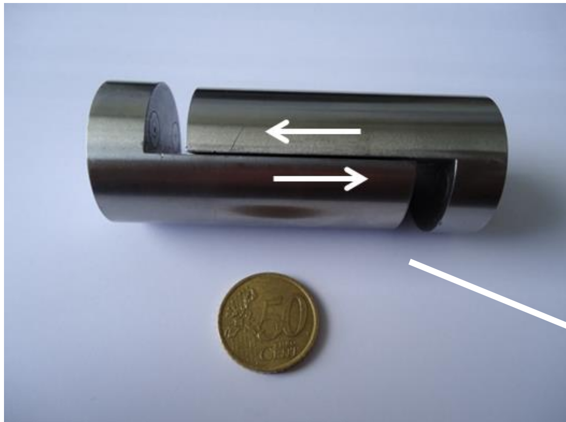

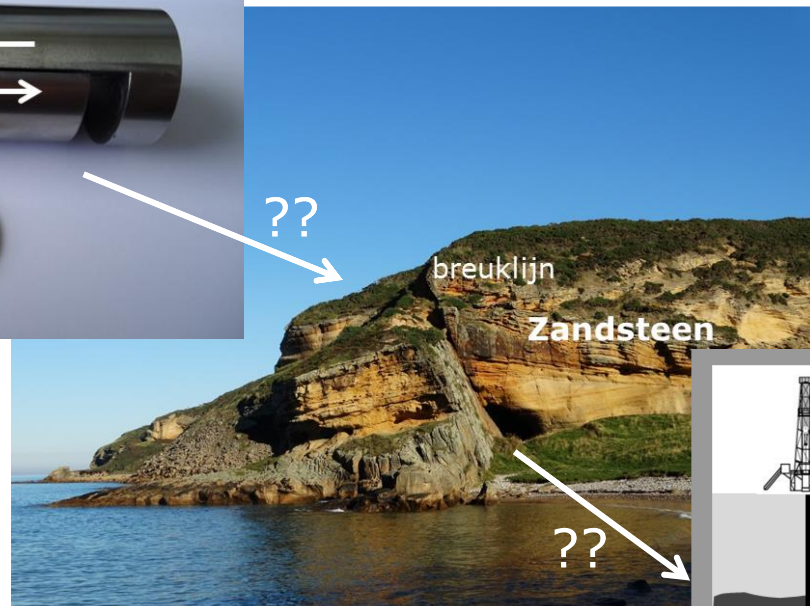

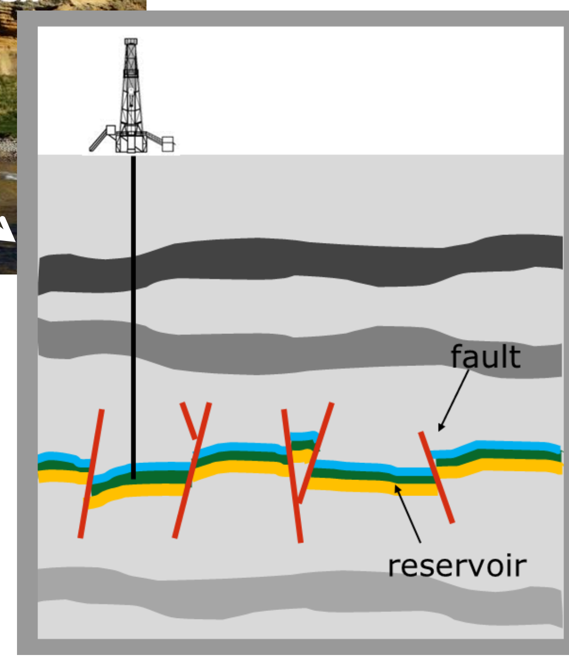

To model field scale behaviour
we must know fault properties
at least at the mesh scale - 1 m scale!

Universiteit Utrecht

...and so to Japan

Large scale earthquake simulator

National Inst for Earth Sciences Research and Disaster Resilience

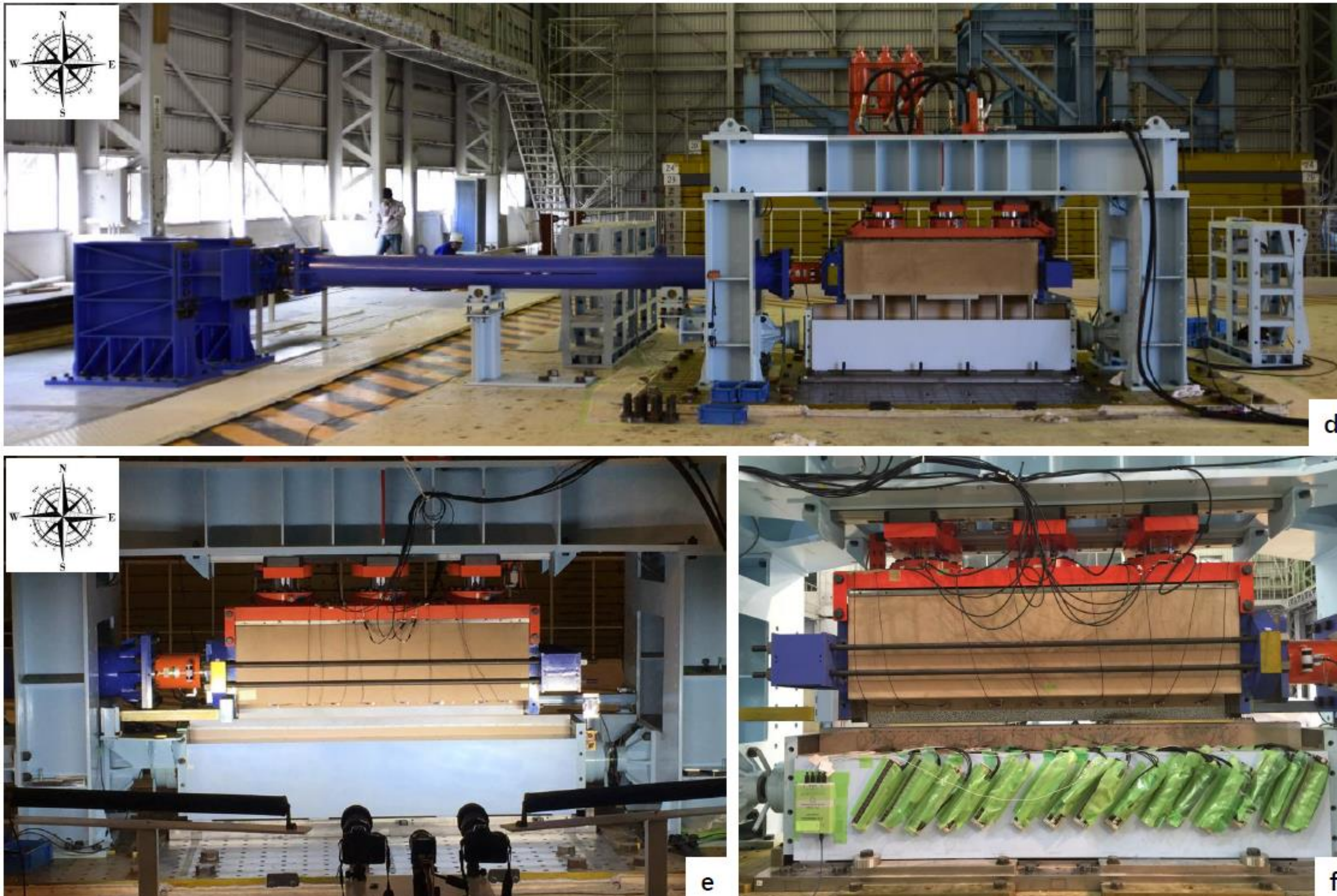

Fault strength evolution: initial/static to dynamic

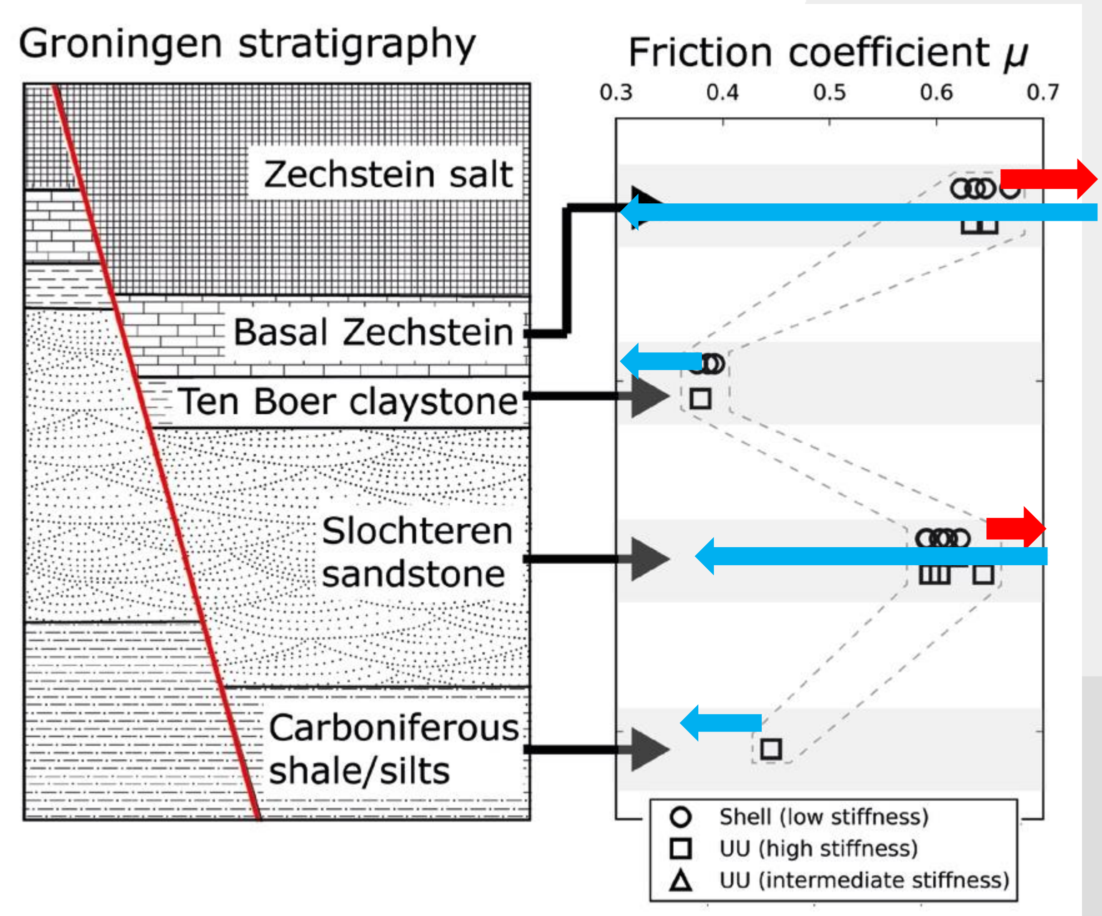

Hunfeld et al. (GRL, 2021)

Basal Zechstein / Slochteren Sst show

- V-weakening RSF behaviour
- Most healing / high strength
- Largest dynamic strength drop
- Highest seismogenic potential?

Rupture arrest and runaway into the Carboniferous underburden

Mmax workshop organized by NAM - Amsterdam - June 2022

Rick Wentinck

in collaboration with Marloes Kortekaas, EBN

Content

- Faults in the Carboniferous underburden
- Analytical model for rupture arrest on flat fault planes
- Dynamic rupture simulations of rupture arrest on faults with jogs and steps

Faults in the Carboniferous

- The opening of the North Atlantic about 140 Ma ago led to transtensional/wrench faulting of pre-existing faults.
  Large flower structures of faults in NW-SE direction were formed.

- Currently, there is a normal stress regime with a modest horizontal field stress anisotropy from N-S tectonic compression.

- Discontinuities in major E-W faults and mild pop-up blocks suggest that parts of the major NW-SE faults may function as 'step-overs' for the tectonic compression.
  If so, the NW-SE faults could have been partly reactivated in the last millions of years.

- Intact Carboniferous shale has a cohesion strength > 10 MPa but the clay-rich rock heals very slowly relative to the sandstone after reactivation[1].
  So, if reactivated, parts of the faults in the Carboniferous may have a relatively low cohesion strength.

1) L. Hunfeld, PhD thesis Univ. Utrecht, (2020).

Rotliegend fault pattern and top of the Lower Carboniferous

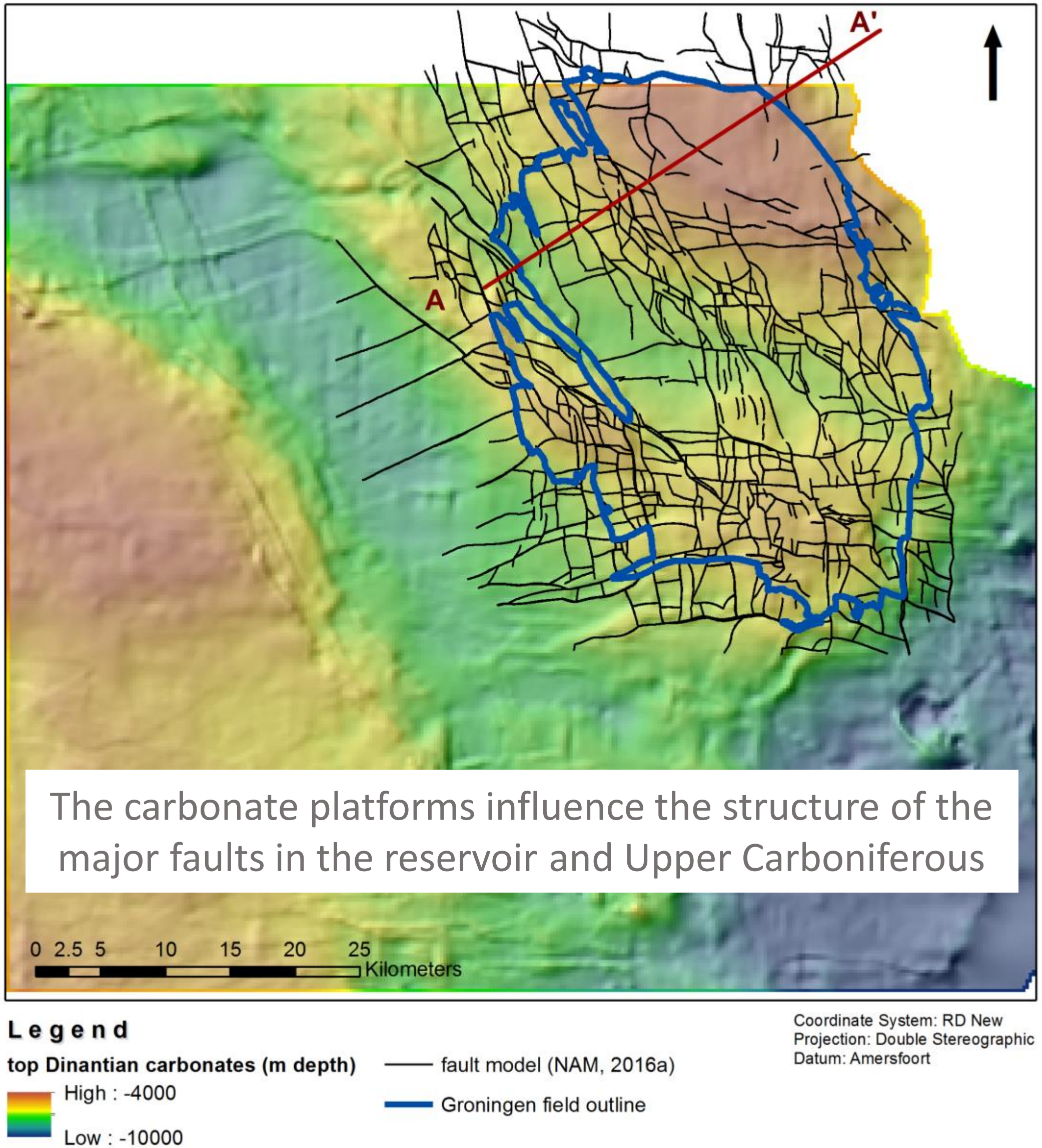

The carbonate platforms influence the structure of the major faults in the reservoir and Upper Carboniferous

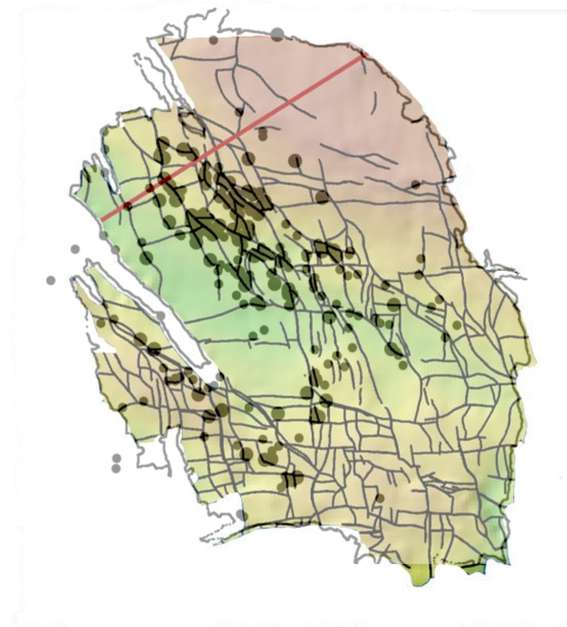

black dots: $M_L \geq 1.5$ tremors

Deep seated faults along seismic cross-section A-A'

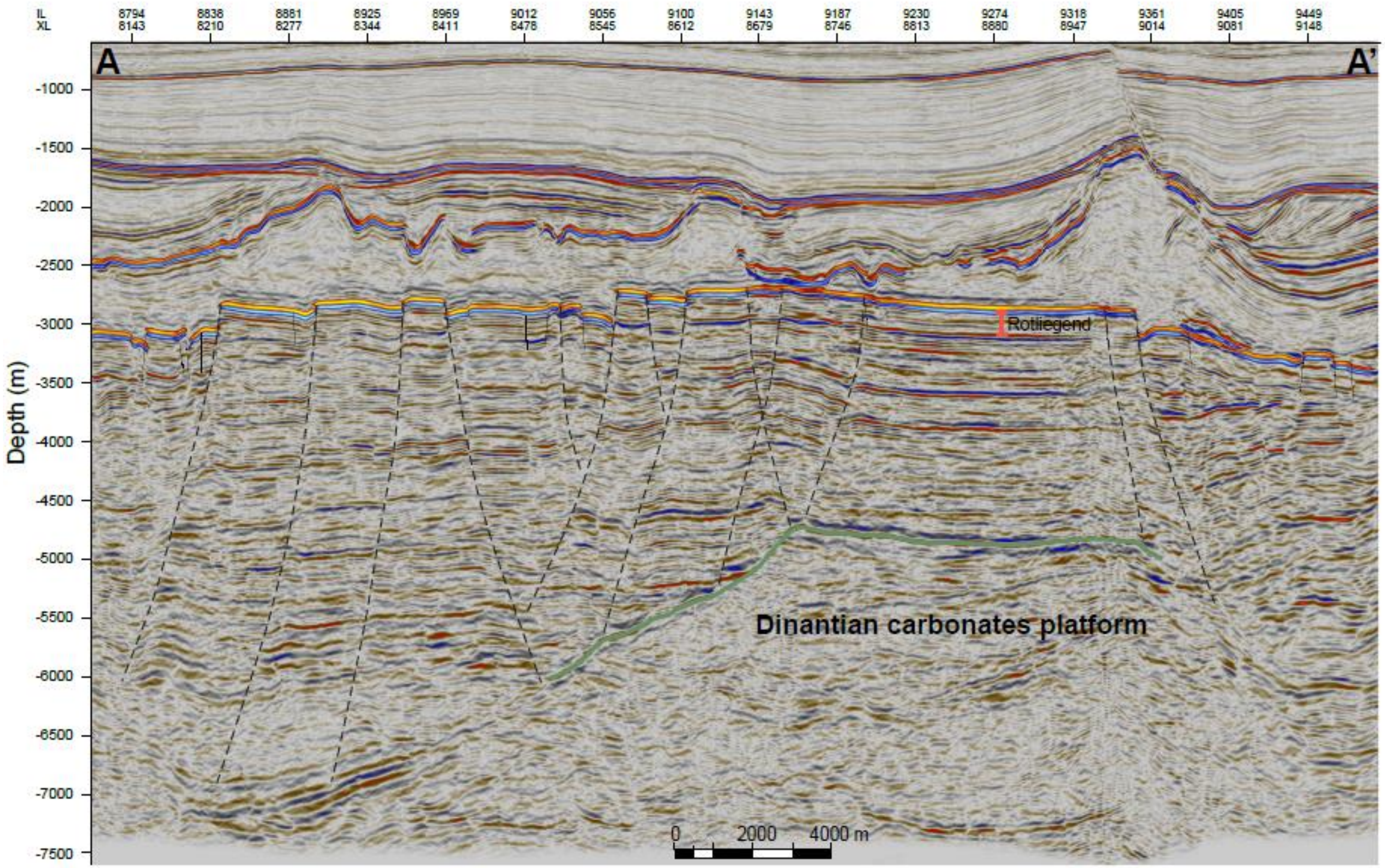

Analytical model for rupture arrest and runaway

Originates from Galis et al. 2015 - 2019:

- The reservoir is considered as a region of perturbed stress on a large fault plane deeply penetrating into the Carboniferous.
- Outside the reservoir, the fault is loaded by the field stress.
- The rupture starting in the reservoir is seen as a potential nucleation of a much larger rupture in the rest of the fault plane outside the reservoir.
- Arrest and runaway conditions follow from an energy balance at the fracture tip and much depends on fault dip, fault strike azimuth and cohesion strength in the fault zone.
- The model is mostly applicable for faults with no or little throw relative to the reservoir thickness.

Minimal radius of a circular rupture for runaway

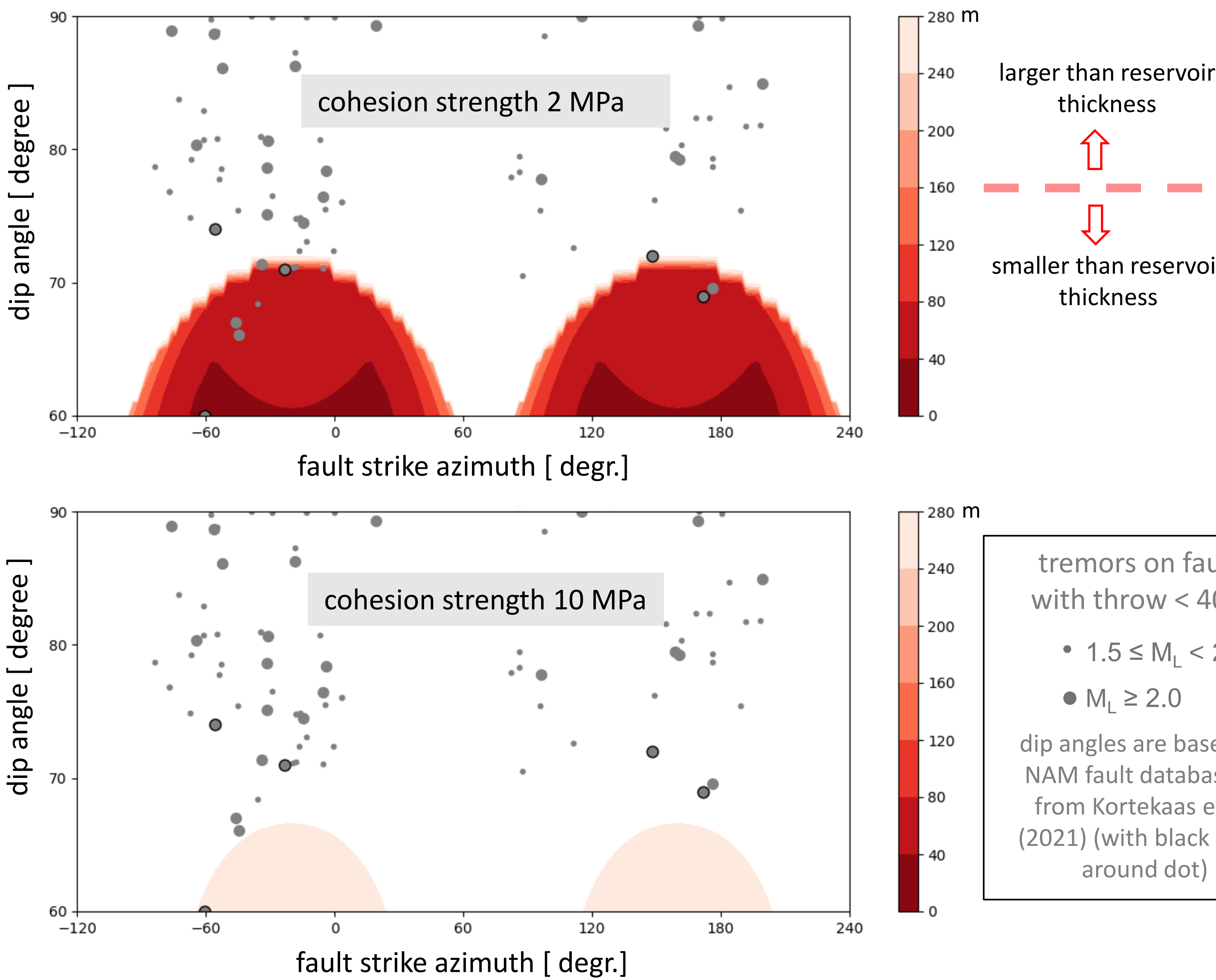

tremors on faults with throw < 40 m

- $1.5 \leq M_L < 2.0$
- $M_L \geq 2.0$

dip angles are based on NAM fault database or from Kortekaas et al. (2021) (with black circle around dot)

Dip angle uncertainty

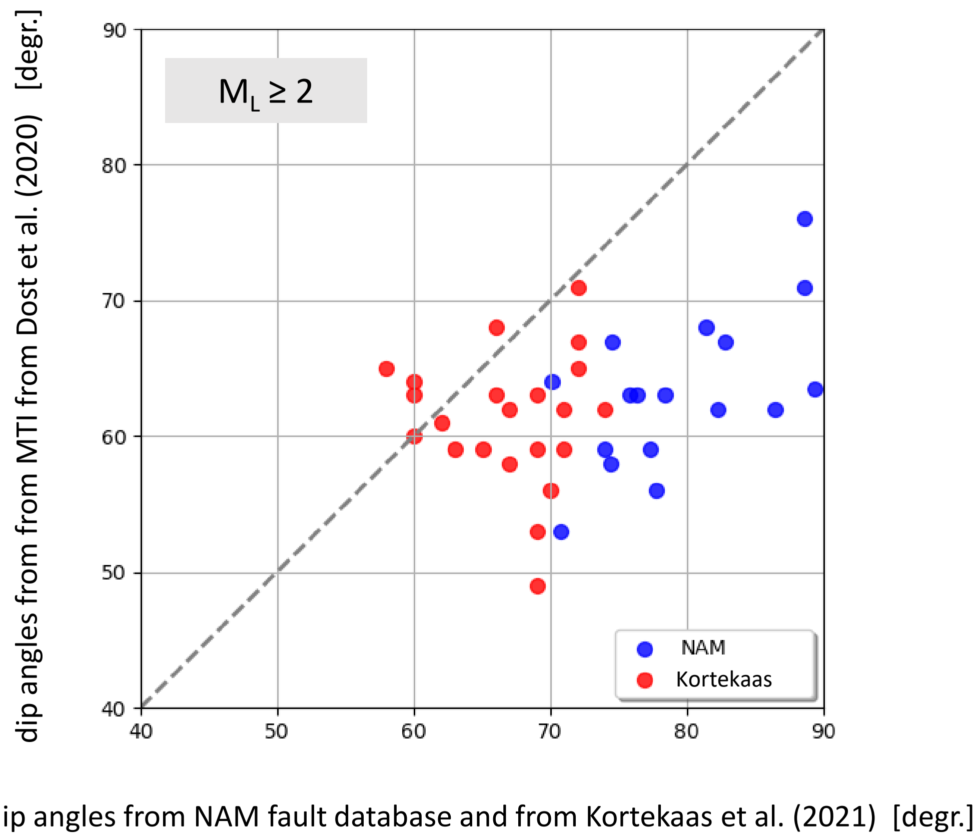

Analytical model - main results

- Ruptures from M > 2 tremors with a low dip angle have potential to penetrate into the Carboniferous if the fault zone has a low cohesion strength.

- This holds even more for ruptures elongated along fault strike.

But

- Real faults are not flat but have jogs, steps and kinks.

Jogs and steps

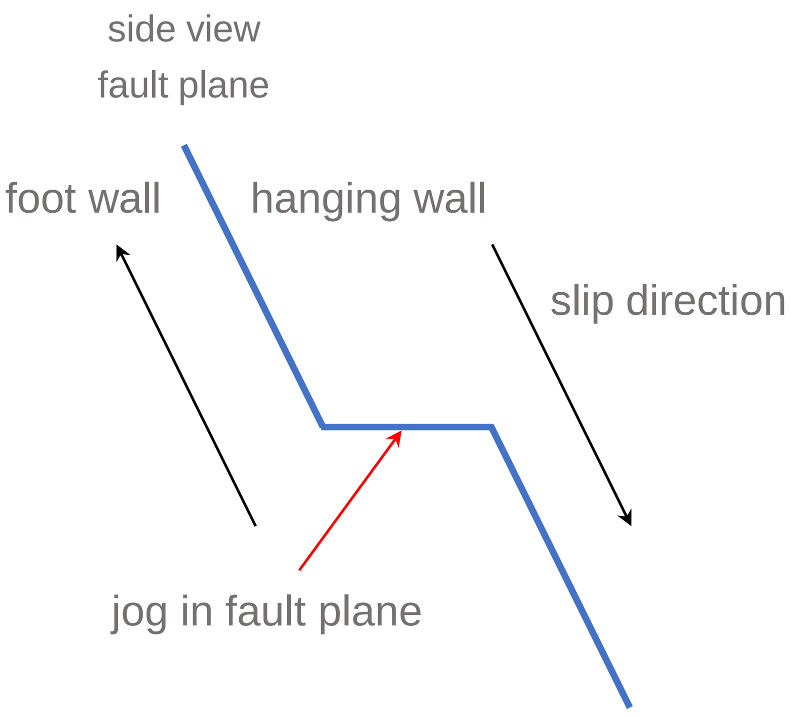

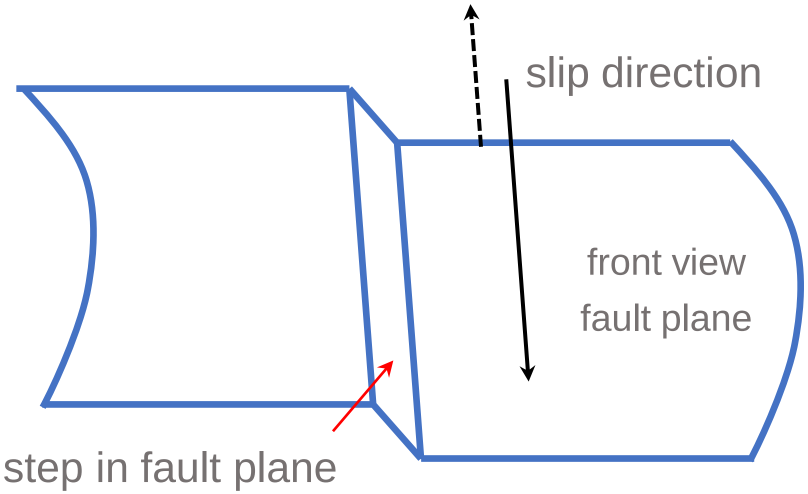

Central region of the Groningen field

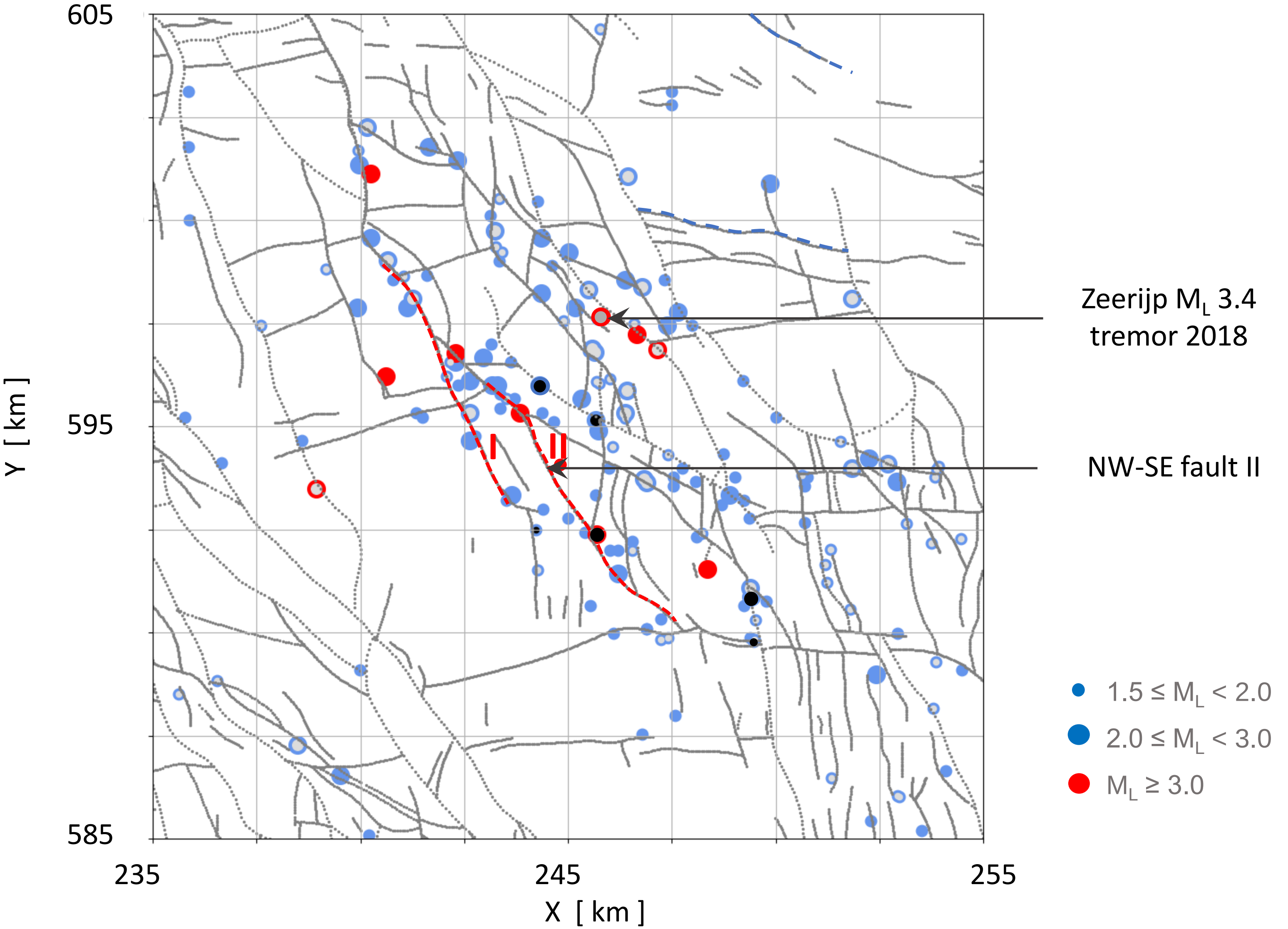

Indications for jogs - fault on Zeerijp M_L 3.4 tremor 2018

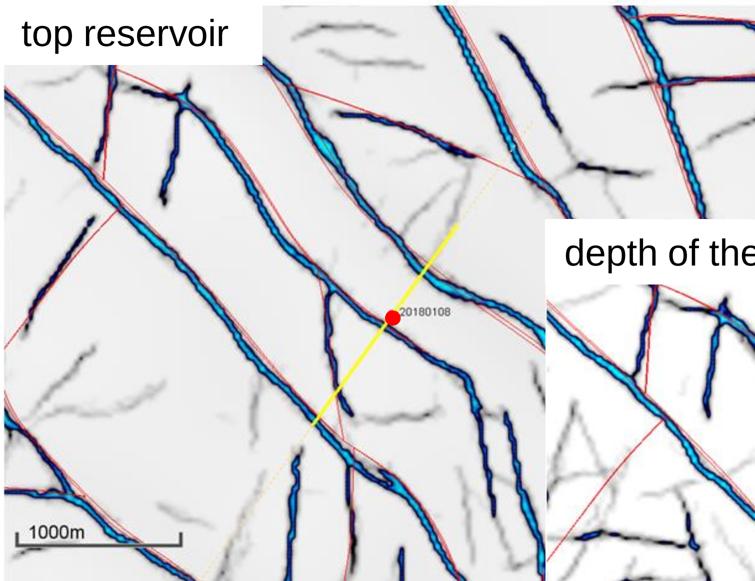

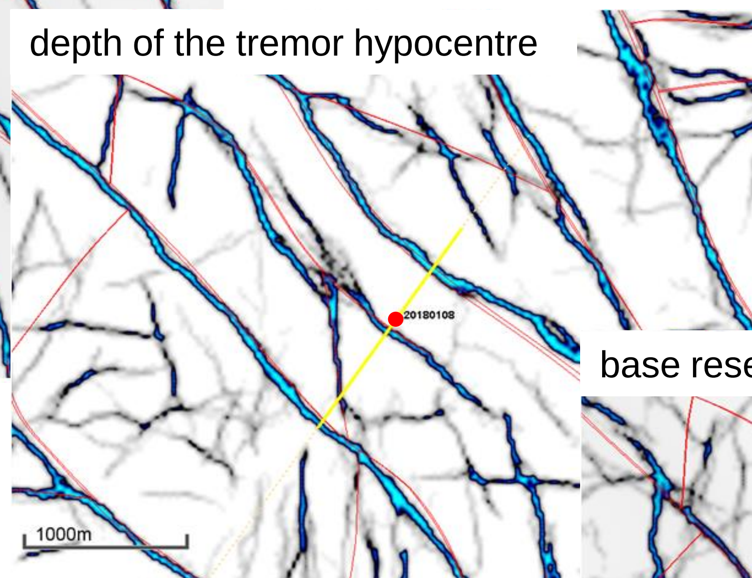

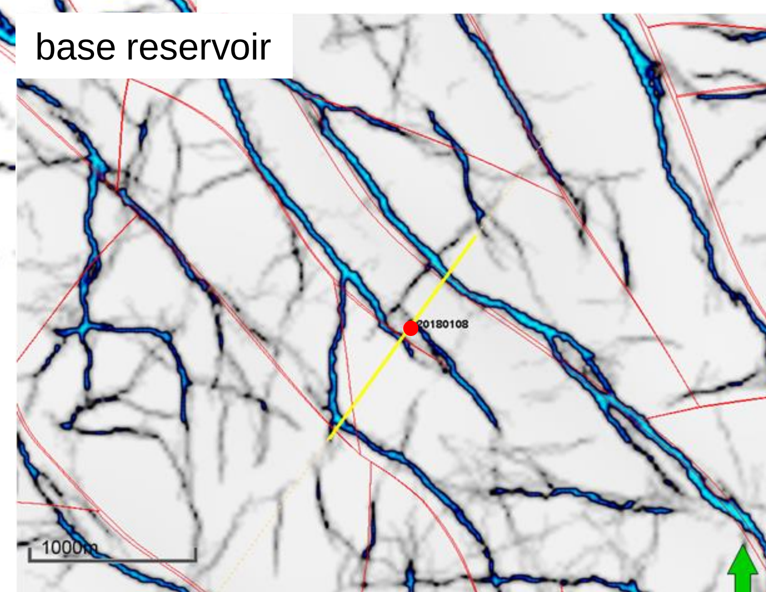

Marloes Kortekaas, EBN, The Netherlands, (2018).

Detailed geometry of fault II from the seismic attribute Ant-tracking

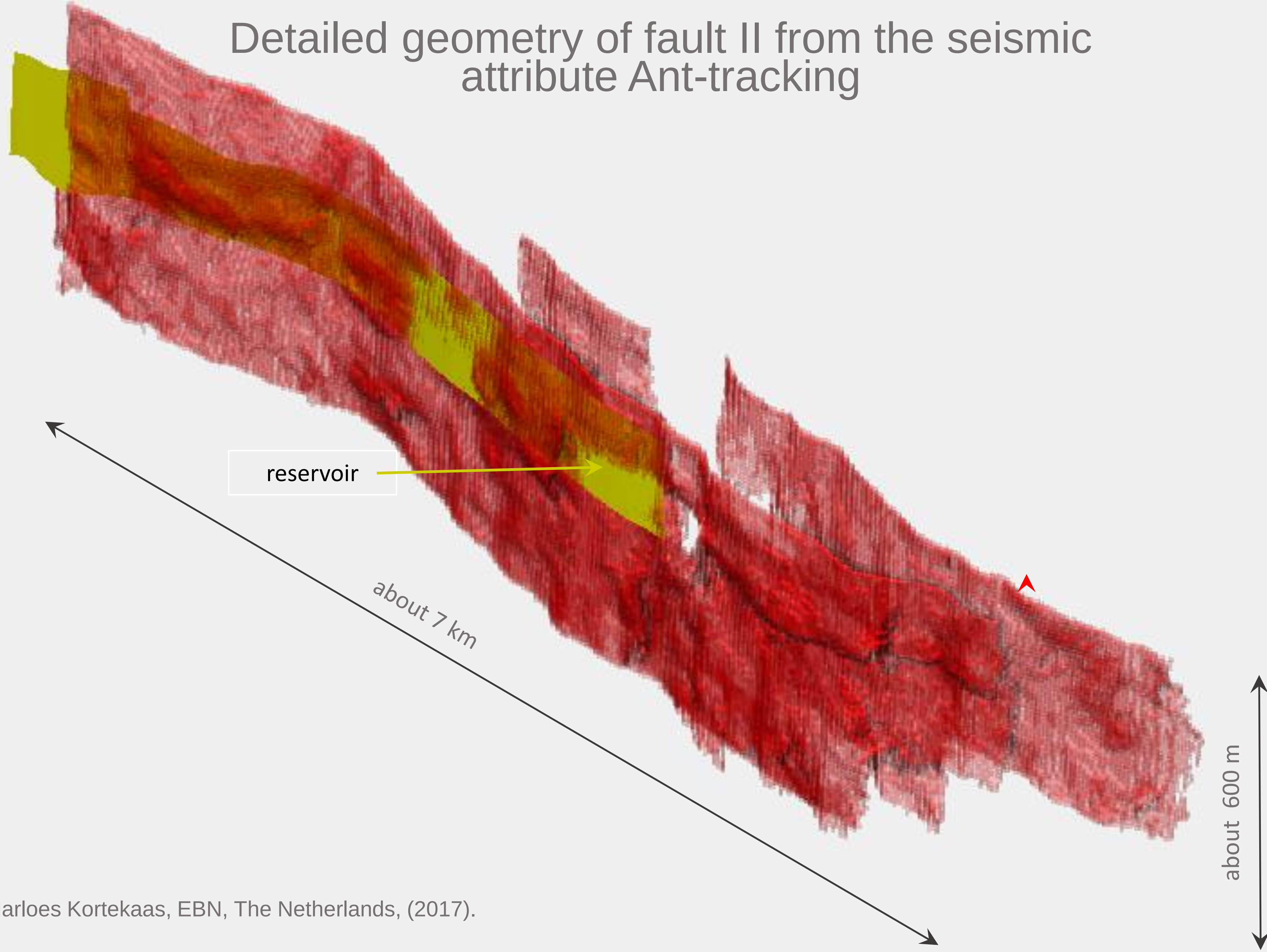

Marloes Kortekaas, EBN, The Netherlands, (2017).

Indications for jogs - fault II

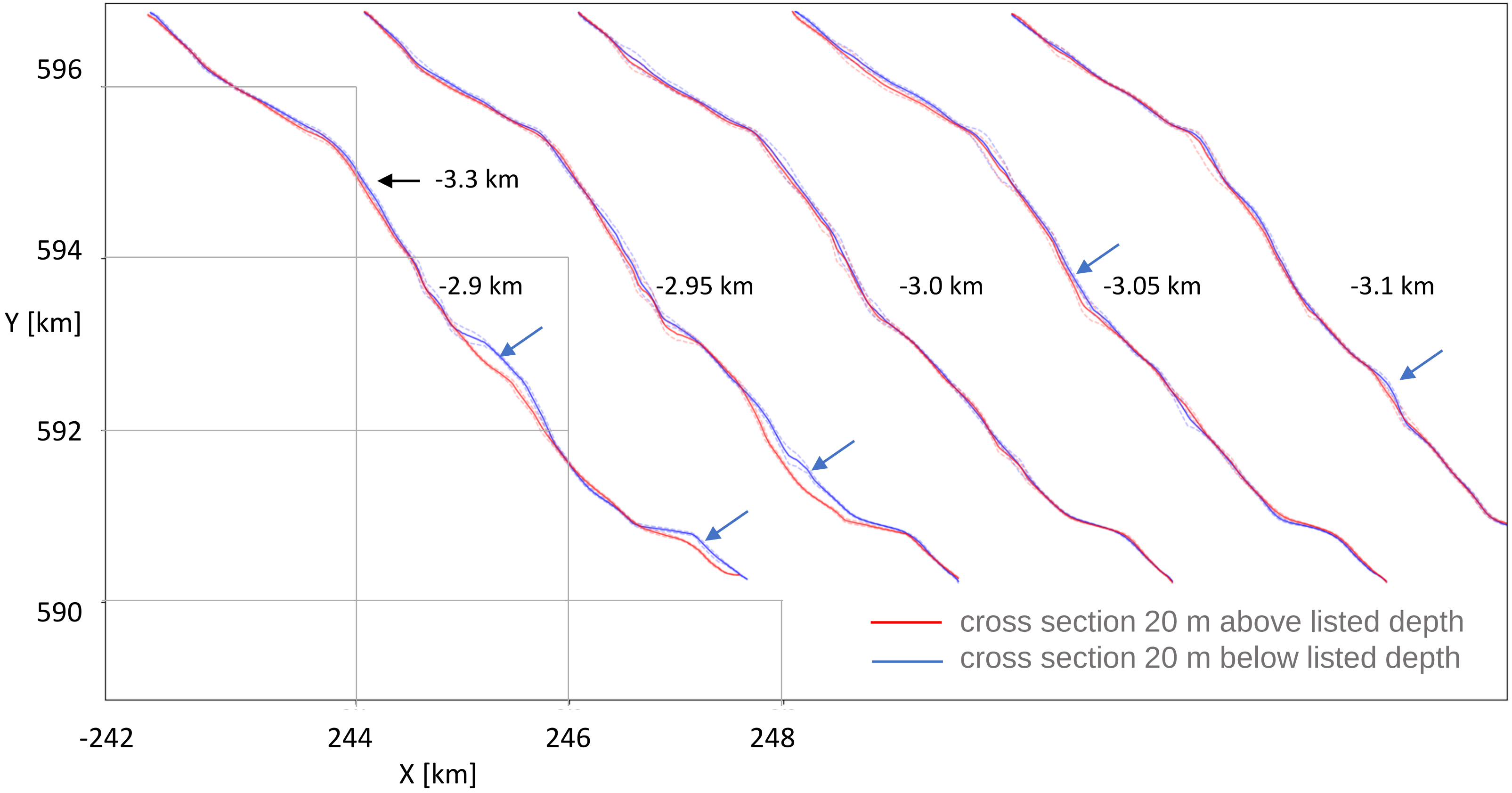

Dynamic rupture simulations with jogs, steps and kinks

The simulations include also:

- Non-uniform formations.
  The porosity in the reservoir considerably varies over depth with a lateral continuity over tenths to hundreds of meters.
  The elastic moduli, the cohesion strength and peak resistance for fault slip strongly vary with porosity and herewith thus with depth.

- Constitutive model for fault slip that includes the cohesion strength in the fault zone and a smooth transition from elastic to non-elastic deformation.
- Pressure diffusion into Zechstein and Carboniferous.
- Horizontal field stress anisotropy.

Reservoir sandstone properties

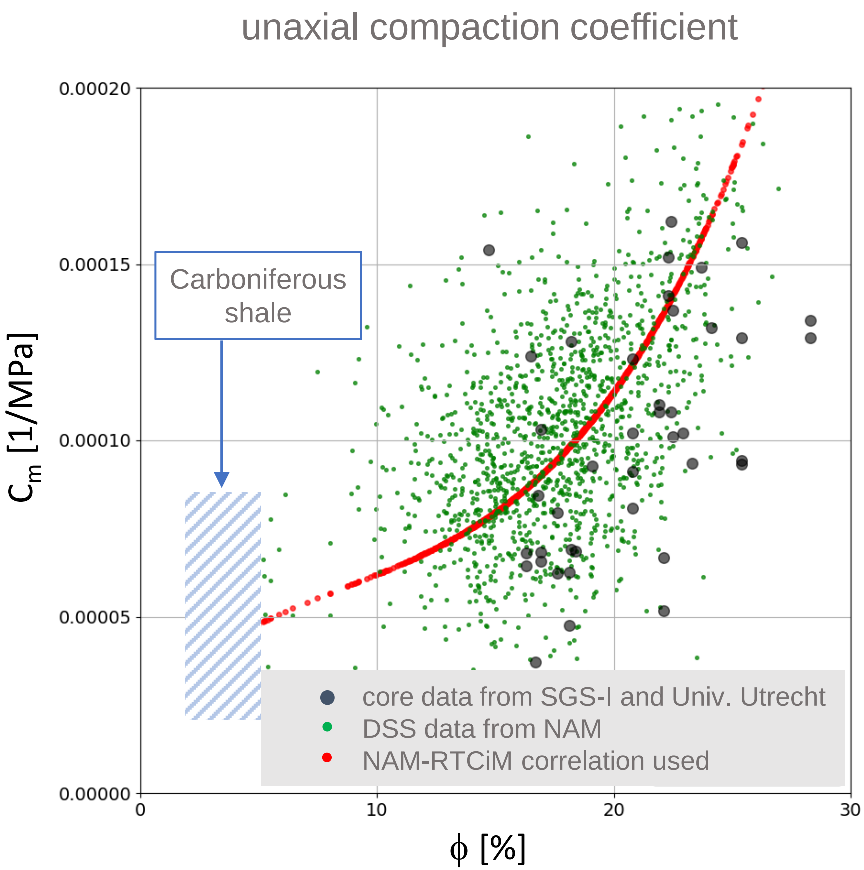

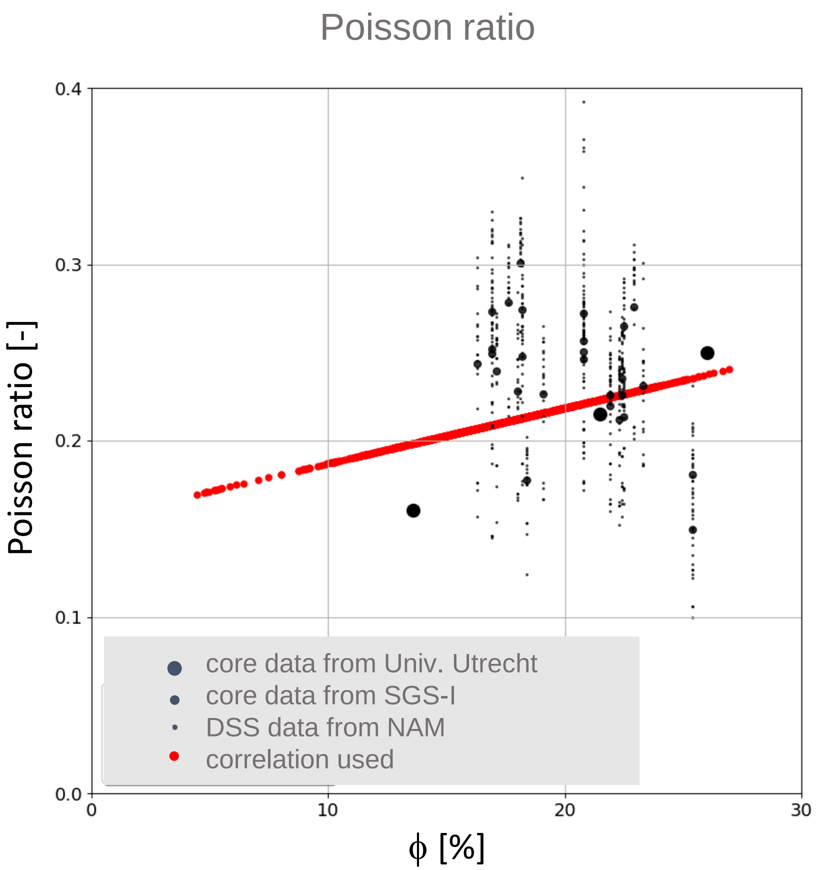

DSS: distributed strain sensing optical fibre cable in ZRP-3a well from P. Kole et al., NAM, (2020).

Reservoir sandstone properties

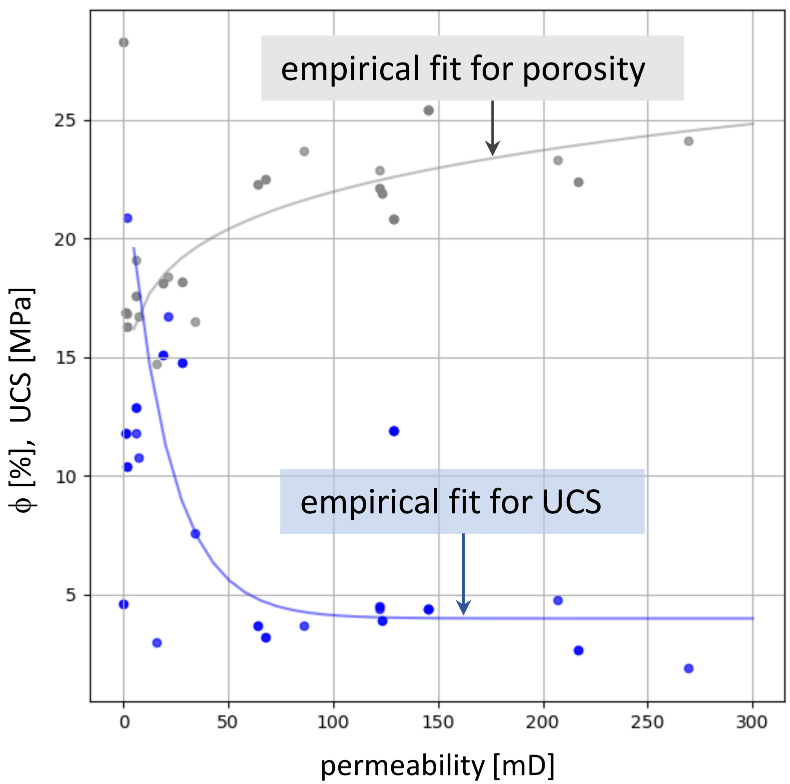

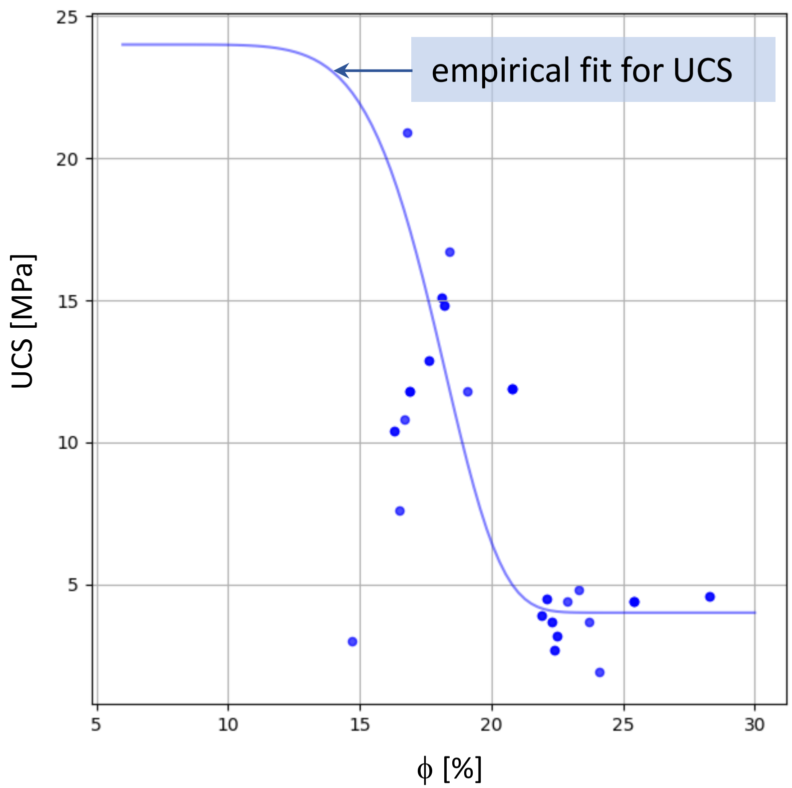

Unconfined compressive strength (UCS) from a scratch test on ZRP-3a well cores from S. Hol et al. SGS-I,(2018).
UCS of intact Carboniferous shale 50 - 100 MPa from A. van der Linden et al., SGS-I, (2020).

Cohesion strength $S_0 \sim 0.5$ x UCS.

Constitutive model for slip resistance in fault zone

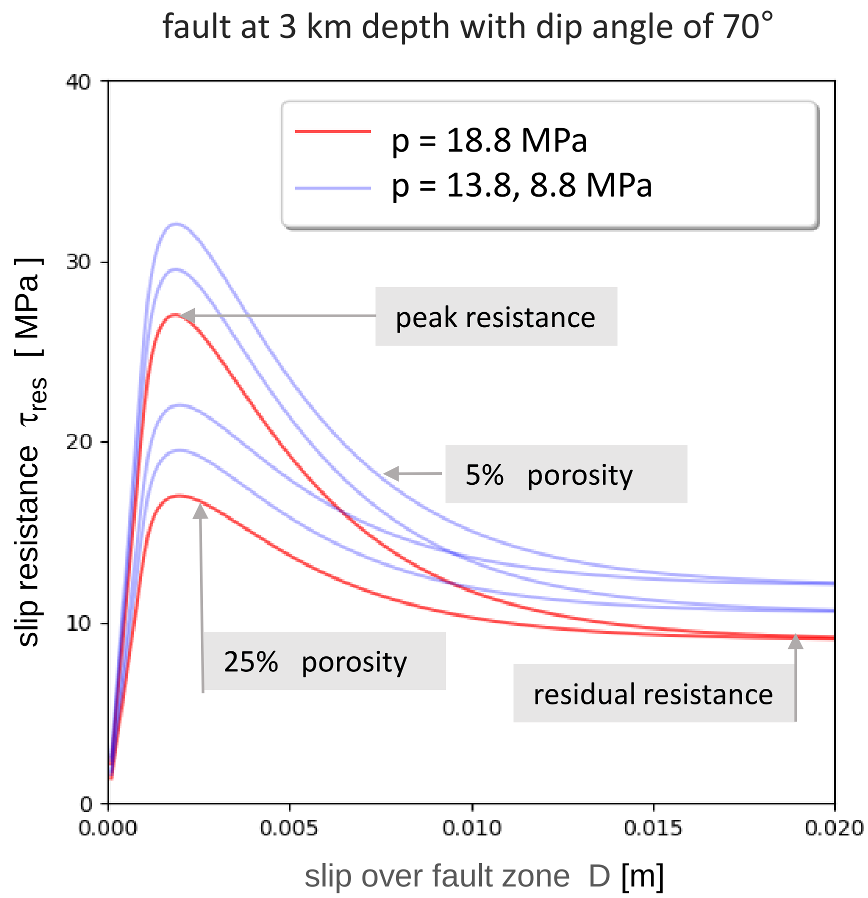

From Ohnaka, (2013).

Porosity over depth - central region

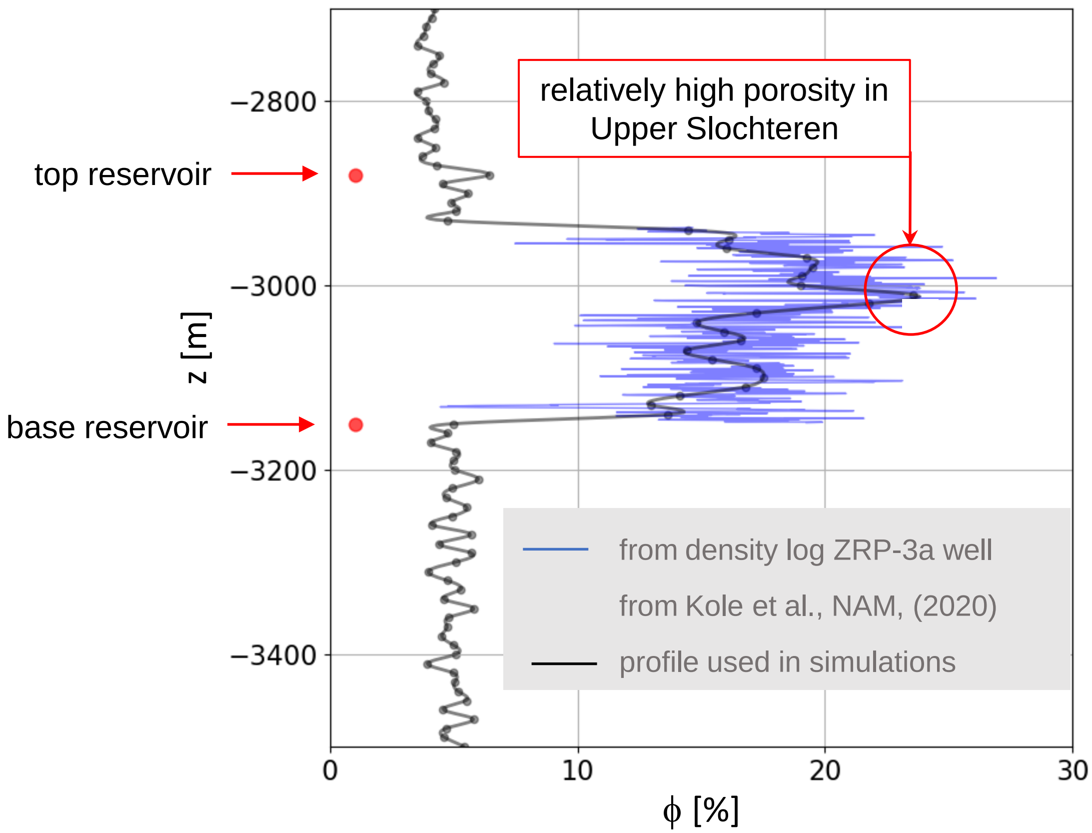

2D simulations - slip resistance and loading

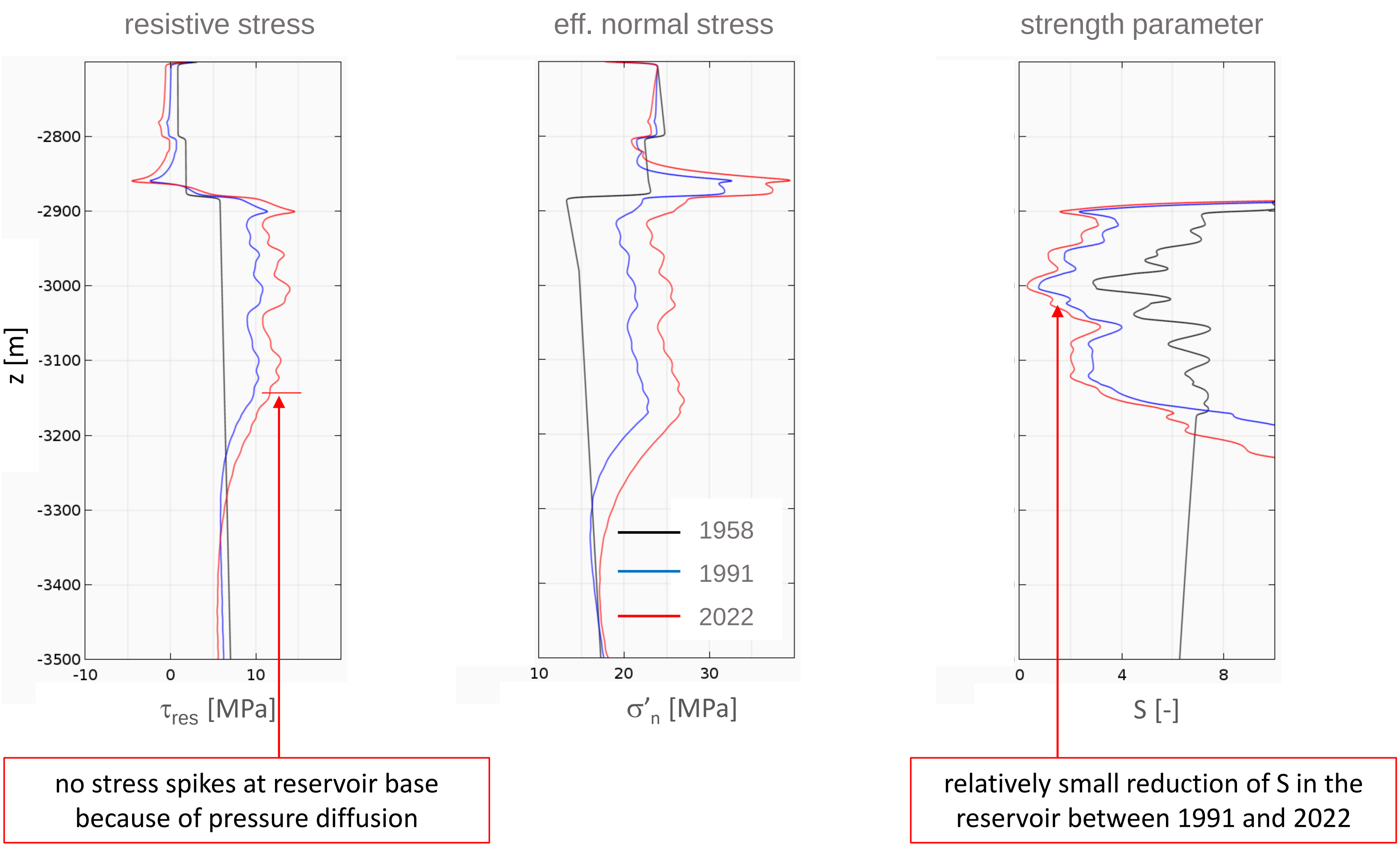

2D simulations - arrest by jogs

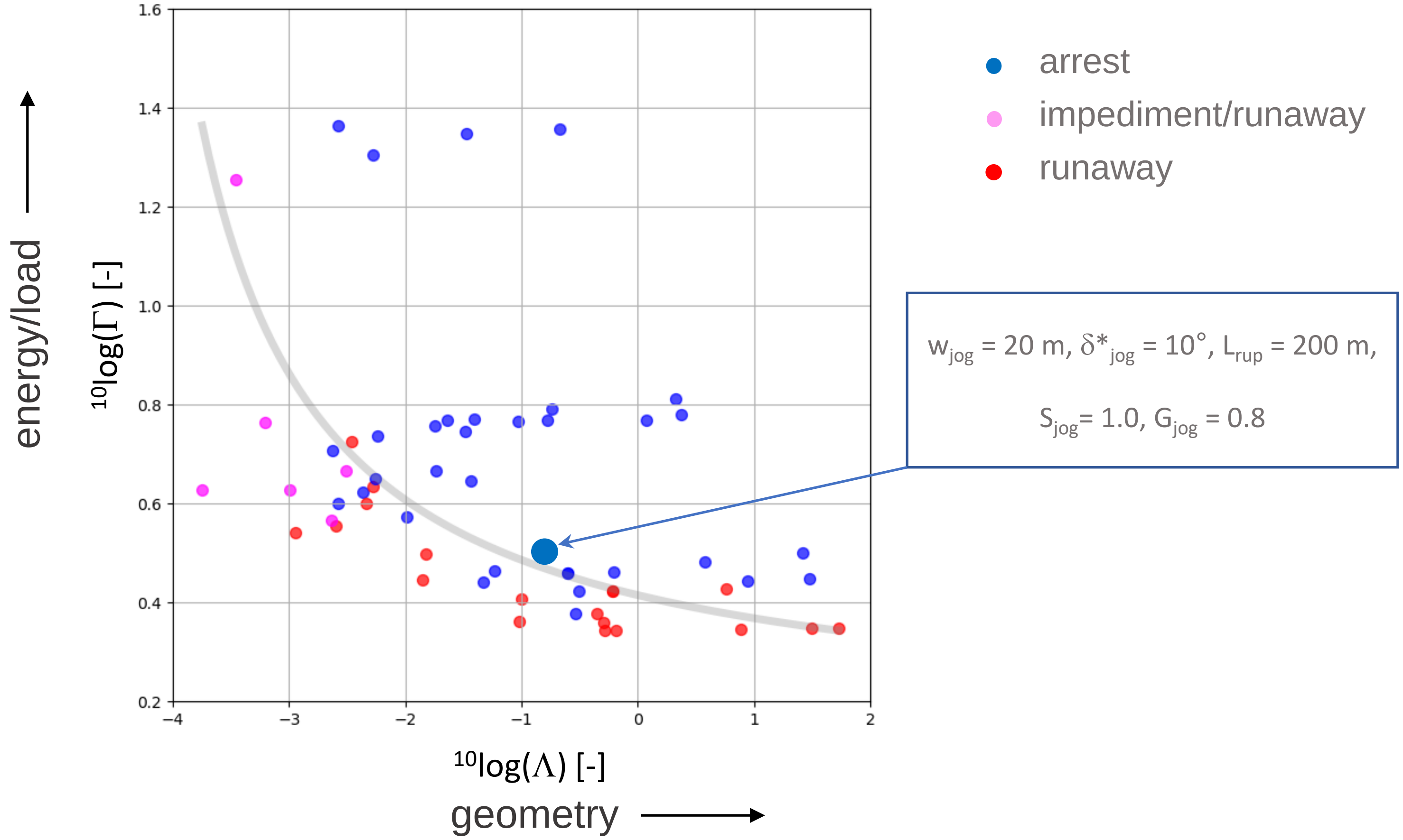

energy/load: $\Gamma = (S_{\text{jog}} + 1)^2 G_{\text{jog}}$ with $G_{\text{jog}} = \Delta G_{c,\text{jog}} / \bar{G}_{c,\text{jog}}$.

geometry: $\Lambda = w_{\text{jog}} / (T_{\text{jog}}^2 L^{**})$ with $T_{\text{jog}} = \tan(\delta^*_{\text{jog}})$ and $L^{**} = L_{\text{rup}}$

2D dynamic rupture simulations - results

- ❑ Rather smooth stress profile at the base of the reservoir.

- ❑ Modest change in the strength parameter S between 1991 and 2022 relative to the period before 1991.

- ❑ Relatively small jogs along fault dip stop ruptures propagating in dip direction.

But

- ❑ What about rupture arrest along fault strike?

3D simulations - step in fault plane

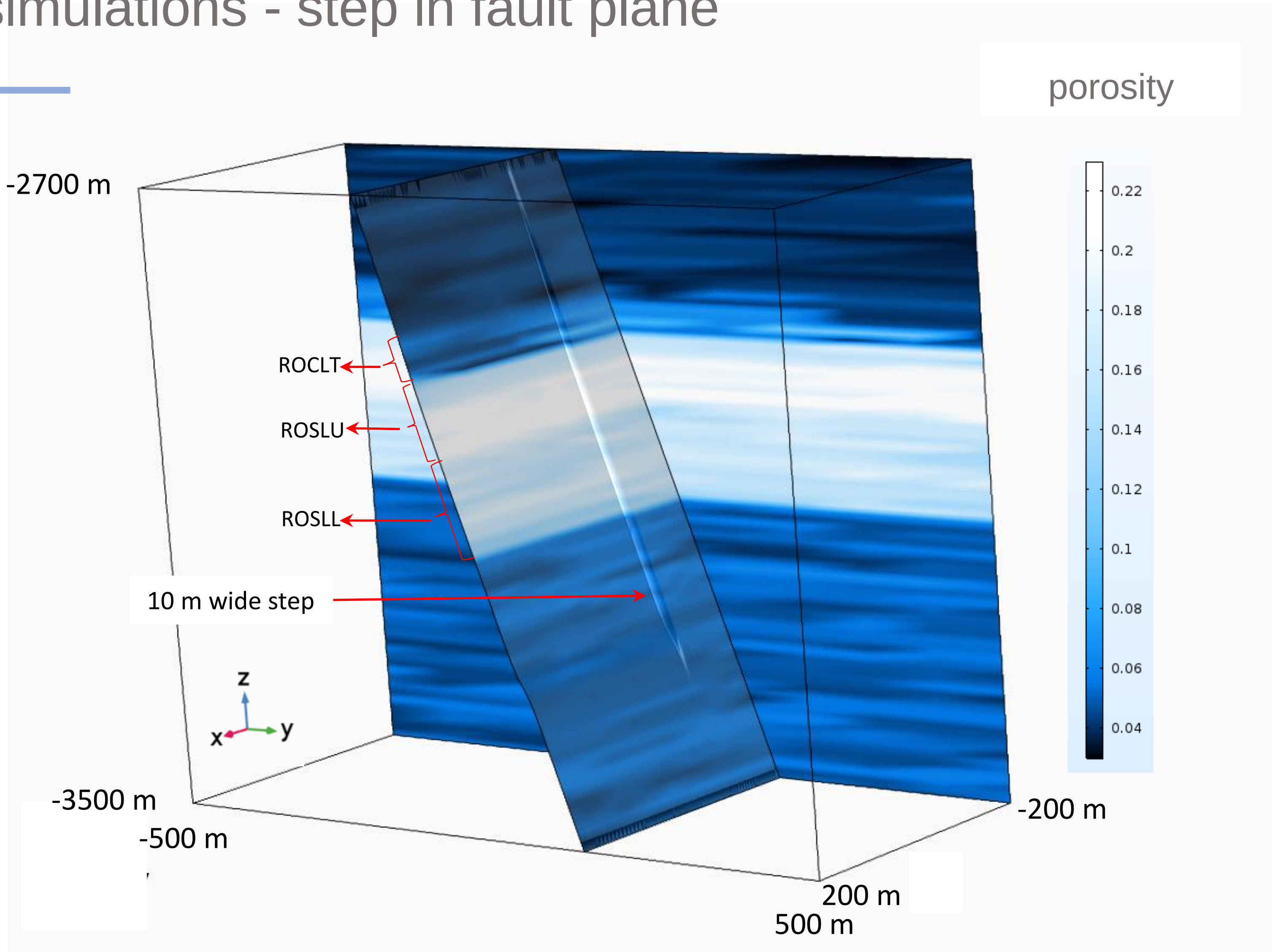

3D simulations - step in fault plane

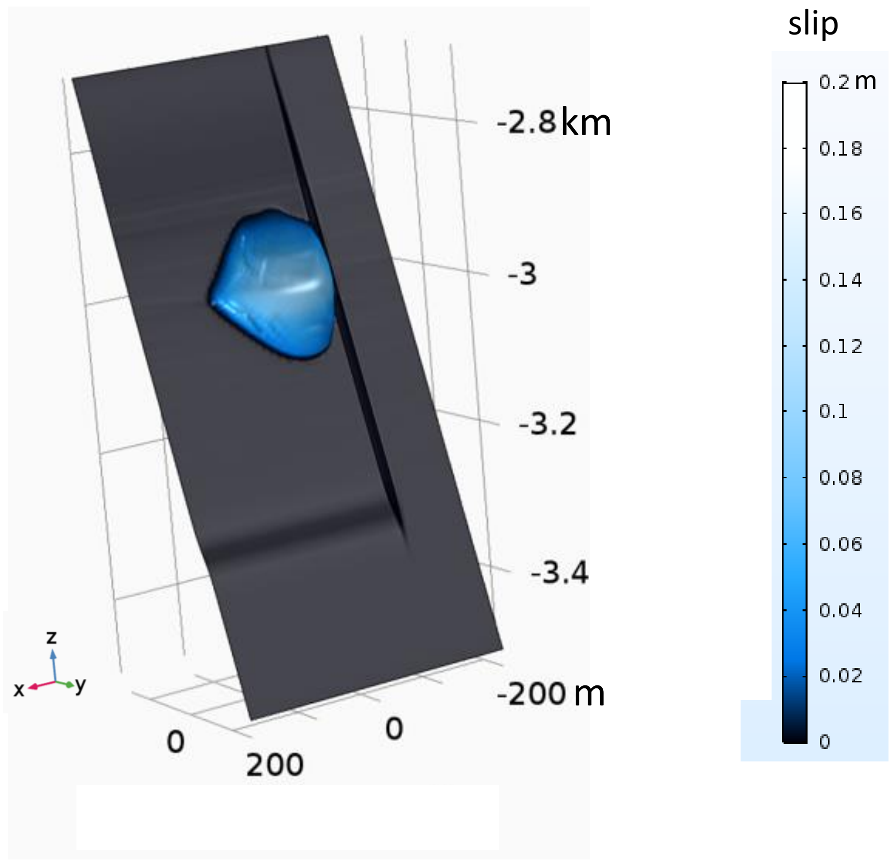

3D simulations - step in fault plane

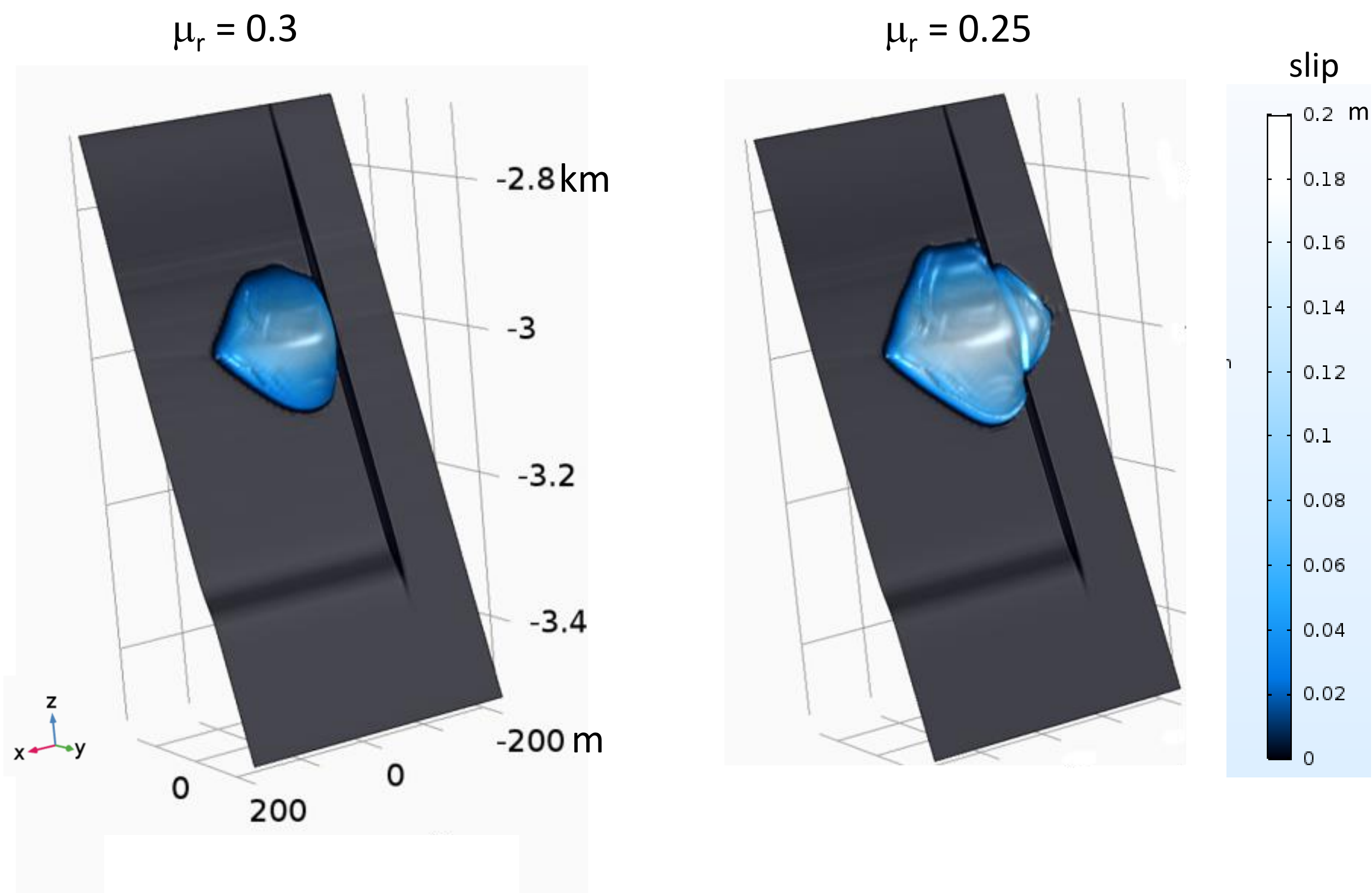

3D simulations - two kinks and end of jog

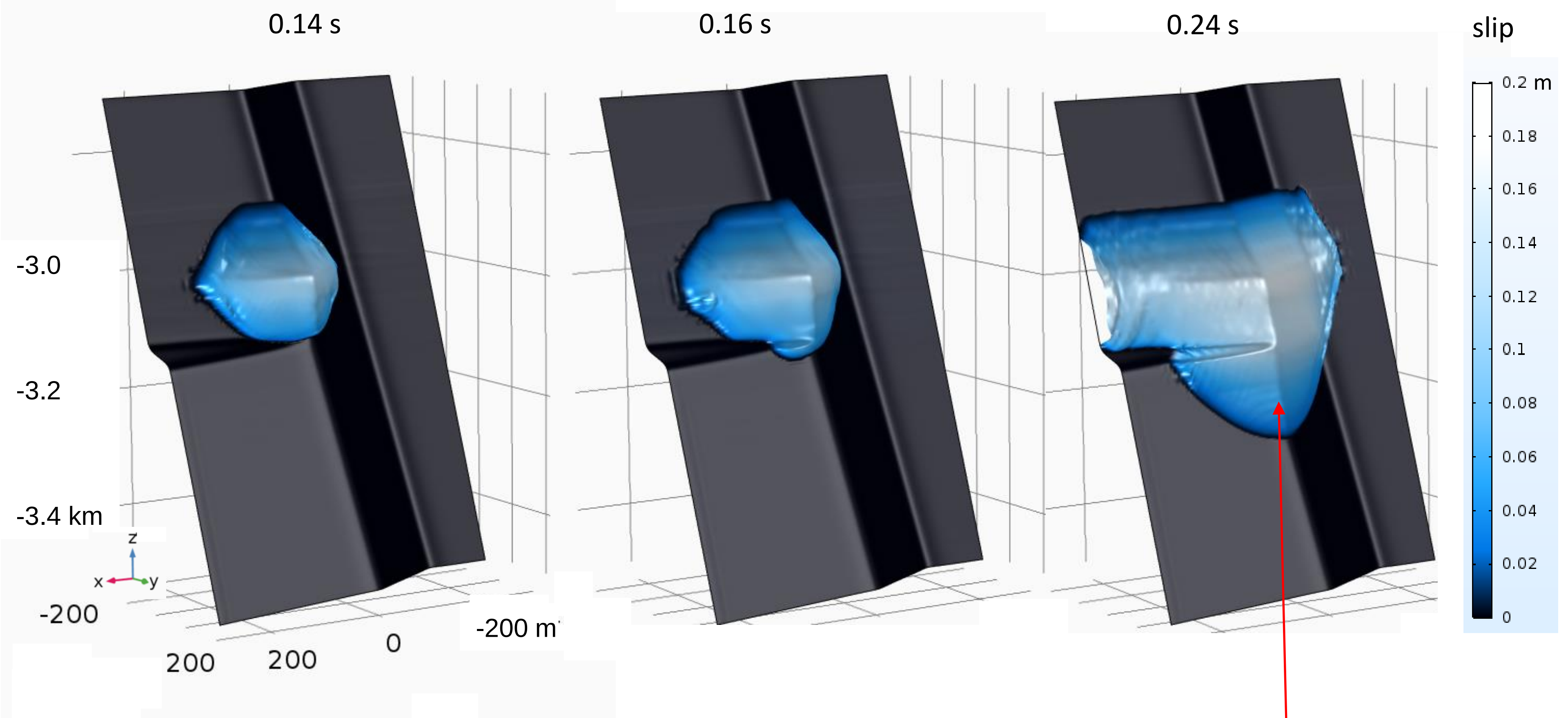

Rupture passes kinks, circumvents the end of a jog and penetrates into Carboniferous

Simulations - summary

- Jogs and steps of tenths of meters can arrest ruptures rather than kinks or plausible lateral variations in porosity.

- Passing these barriers is easier for more critically loaded faults.

- Jogs in the fault plane are effective barriers.
  But, of limited lateral extent, they may be only local barriers.

- Steps locally reduce the load on the fault and can stop ruptures. They are less effective than jogs.

Summary

- The analytical model indicates:

  Ruptures of $M_L \geq 2.0$ tremors had potential to penetrate into the Carboniferous if the cohesion strength in the fault zone in this formation would be low due to tectonic motions and poor healing.

- The simulations indicate:

  Jogs and steps of tenths of meters are effective to arrest ruptures rather than kinks or plausible lateral variations in porosity.

  A plausible explanation for uni-directional ruptures along fault strike are rupture barriers in the form of steps.

So far there are no indications that ruptures have propagated substantially into the Carboniferous. Plausible reasons for this are a sufficient cohesion strength in the fault zone in this formation and/or jogs and steps.

Simulations - other constraints/uncertainties considered

- ❑ Stress drop and rupture velocity.
- ❑ Rake angle.
- ❑ Nucleation conditions.

Main oscillation time of ground motions

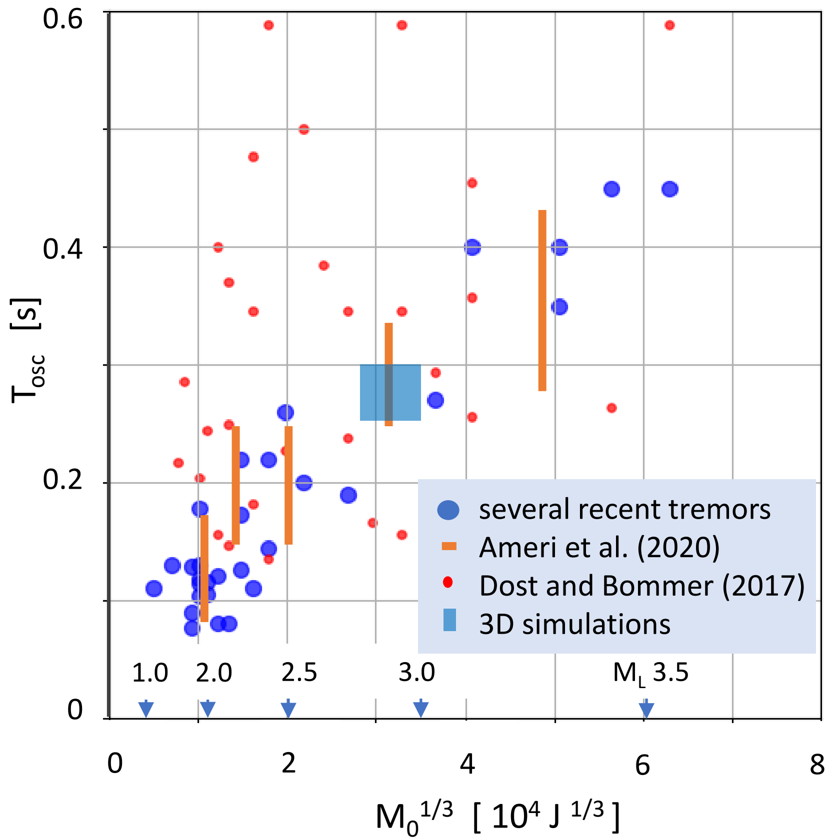

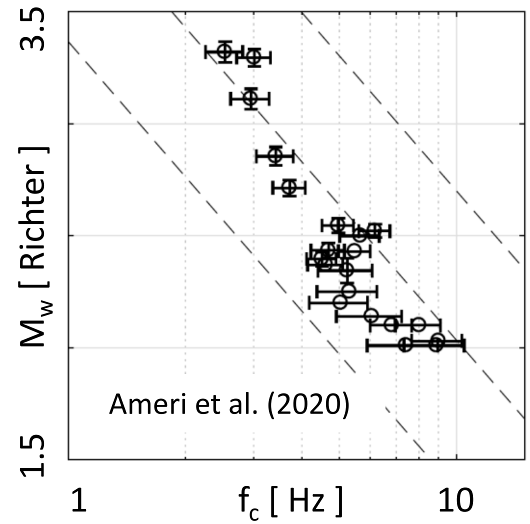

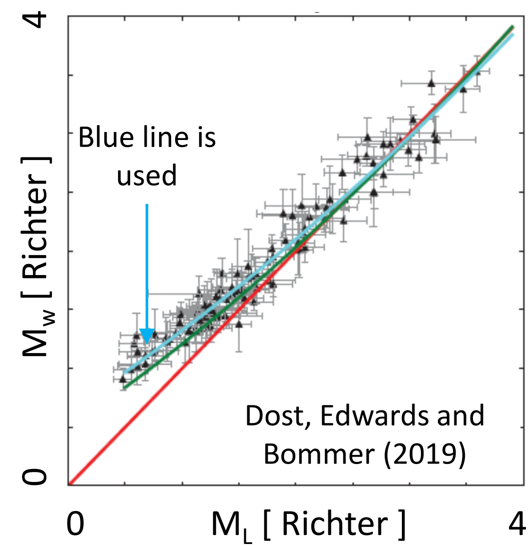

Blue dots from recent tremors derived from direct wave motions recorded by geophones < 6 km distance from epicenters. Uncertainty in T_{osc} ± 20 - 30%.

Derived stress drop

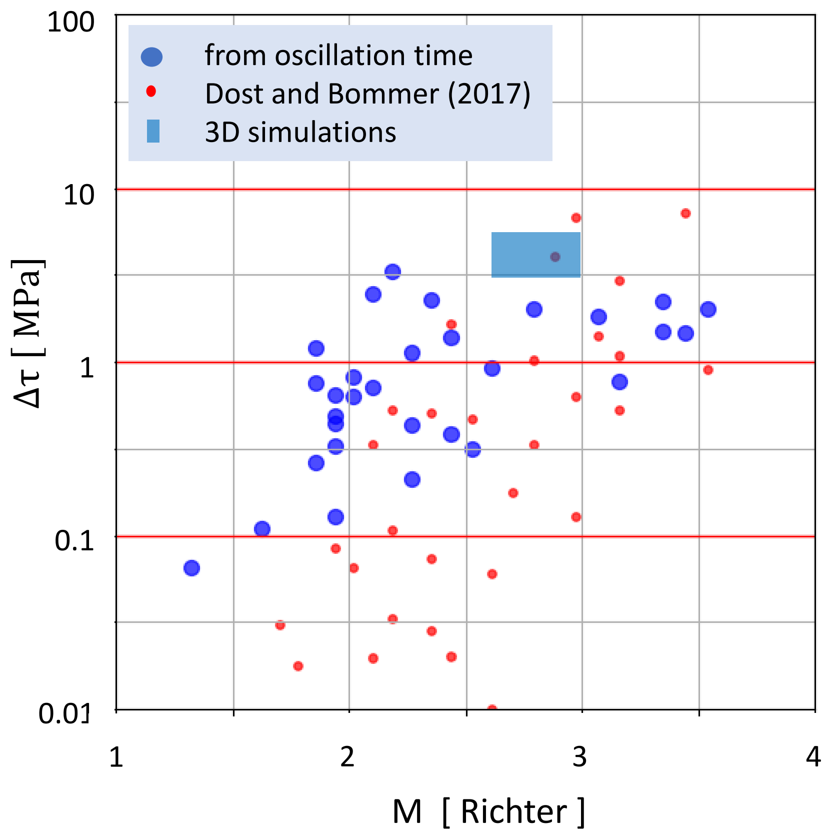

Stress drop based on Brune's source model and a rupture velocity of 2.3 km/s, equal to the average shear velocity in the reservoir.

3D simulations - more or less confined rupture

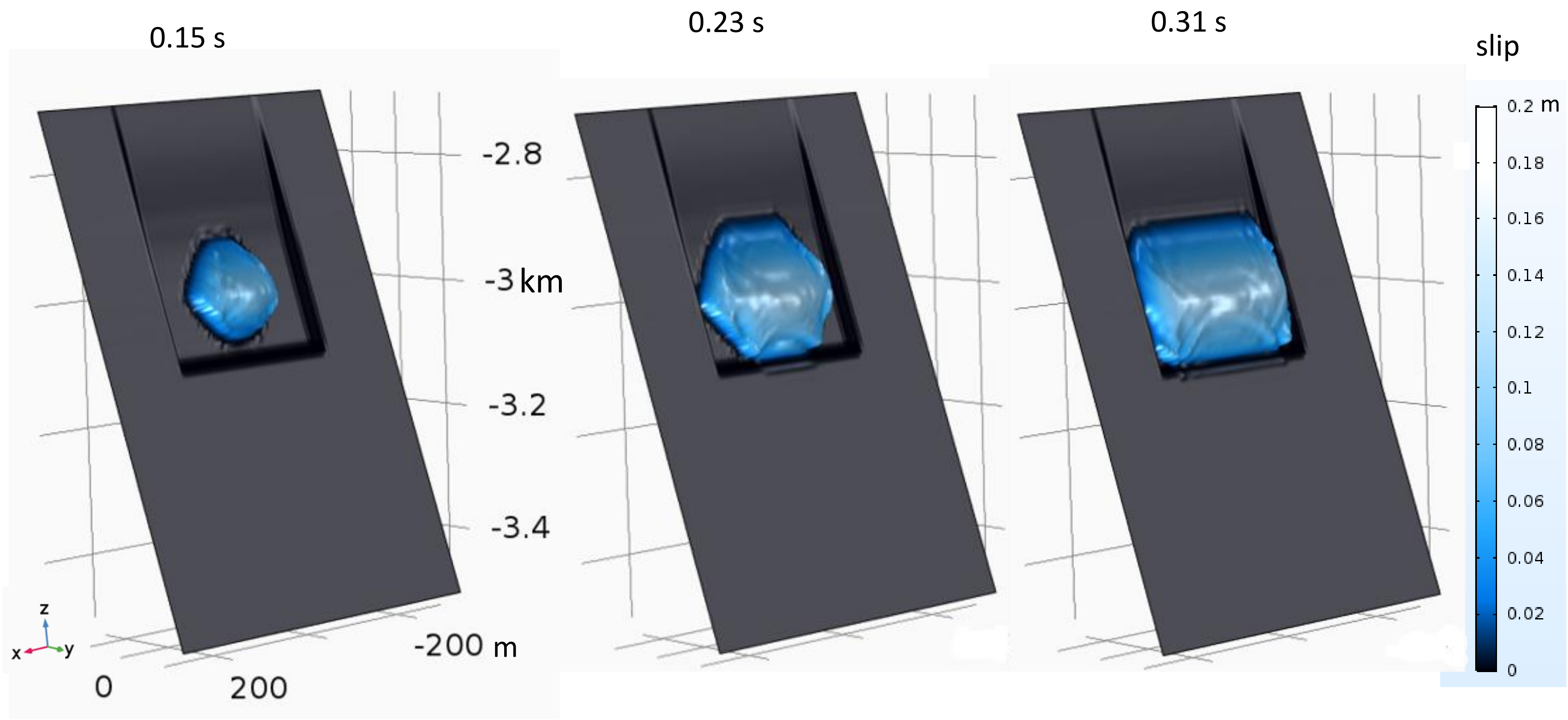

Stress drop increased by reducing the high-velocity residual friction coefficient from $\mu_r = 0.3$ to 0.2.

Figure shows results for $\mu_r = 0.3$. For lower μ_r values, ruptures pass these steps.

3D simulations - effect of stress drop

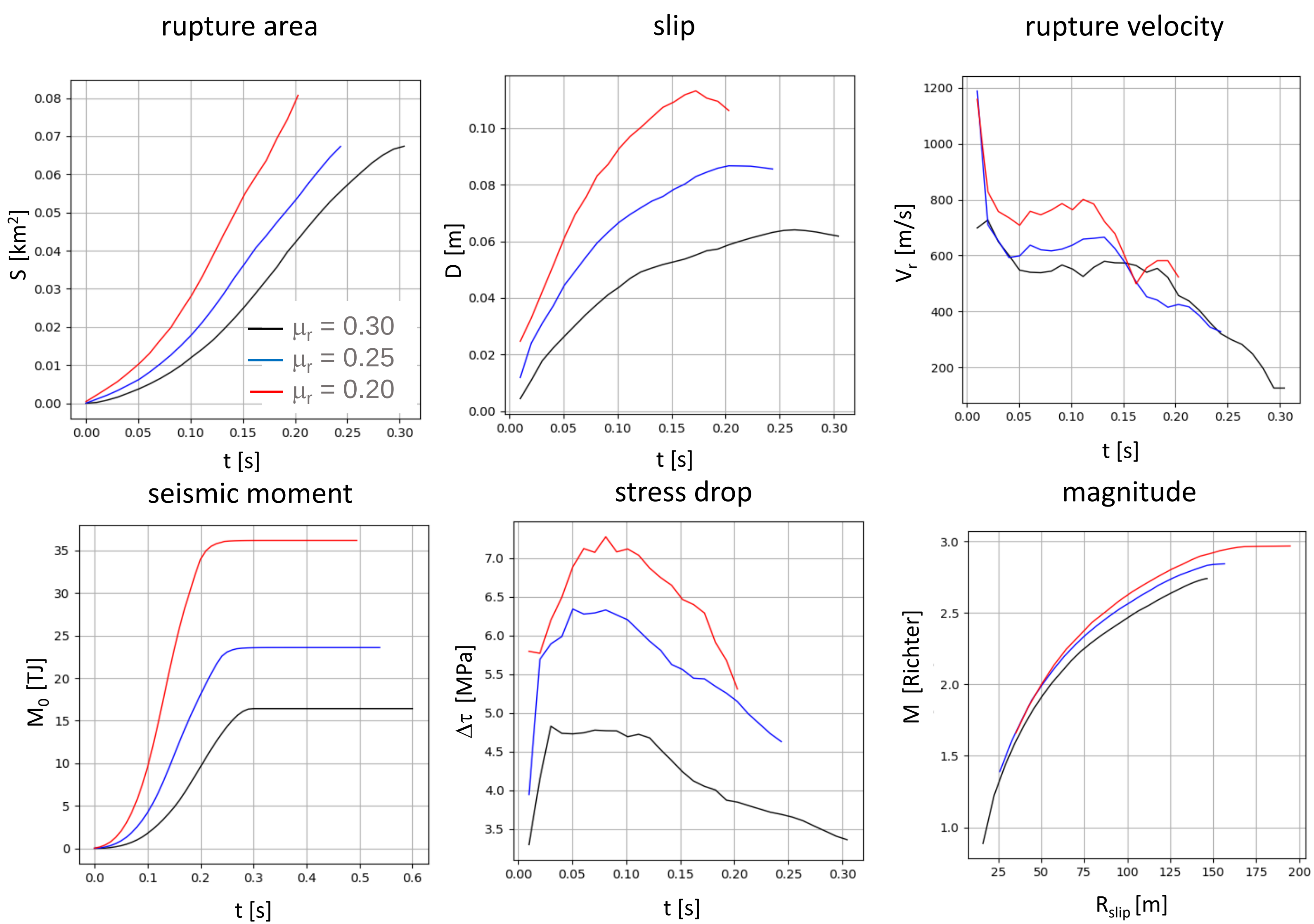

Rake angle

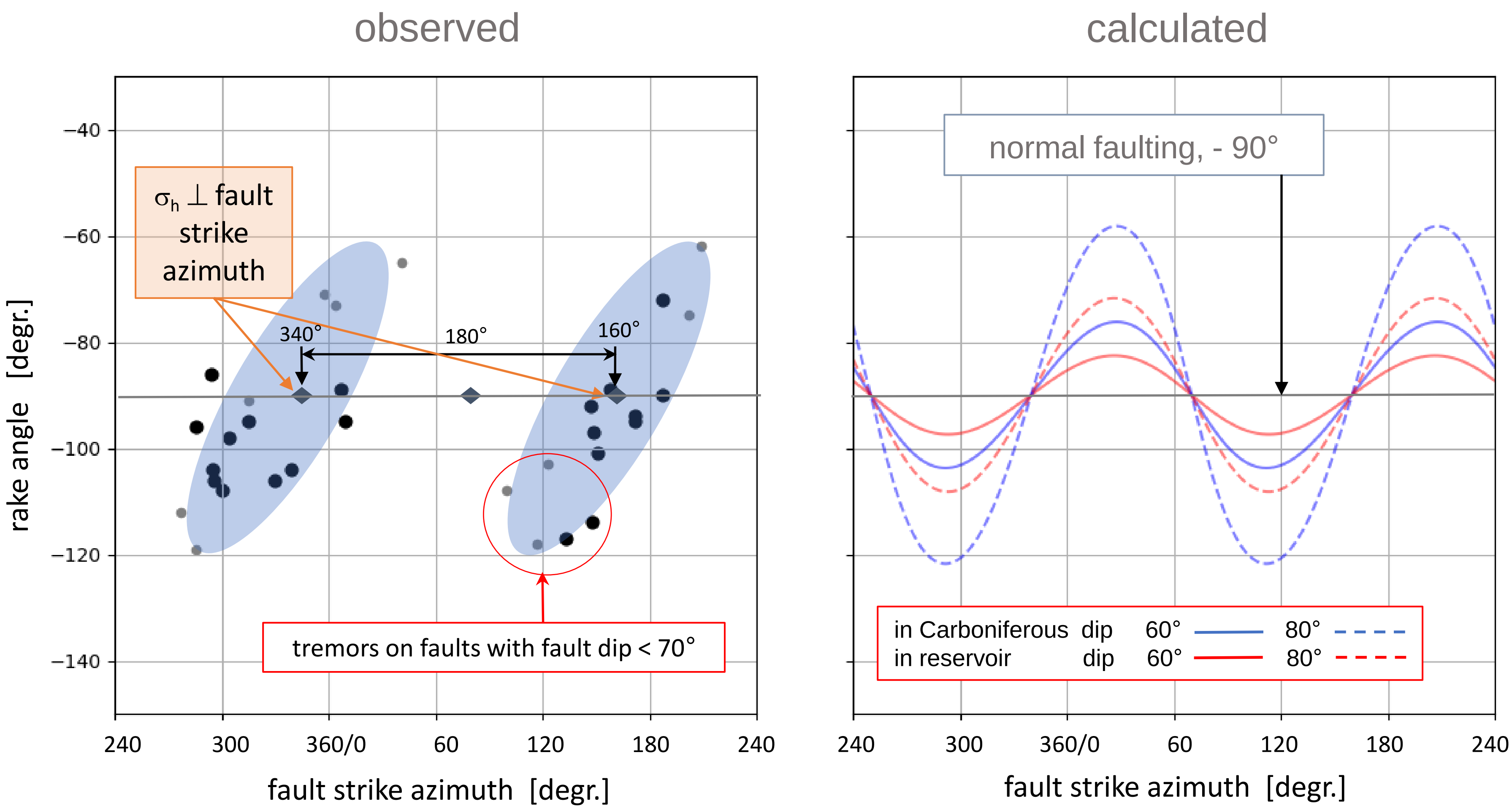

Simulations agree with calculations. Errors in observed rake angles ± 10°

So far, no explanation for rake angles strongly deviating from normal for large tremors with low dip angles.

Nucleation of tremors

In addition to fault geometry, the nucleation of a tremor in a simulation quite depends on

- ❑ horizontal field stress.
- ❑ peak resistance or cohesion strength of the sandstone.
- ❑ breakdown slip distance.

Tremors over time and nearest fault properties - no trends

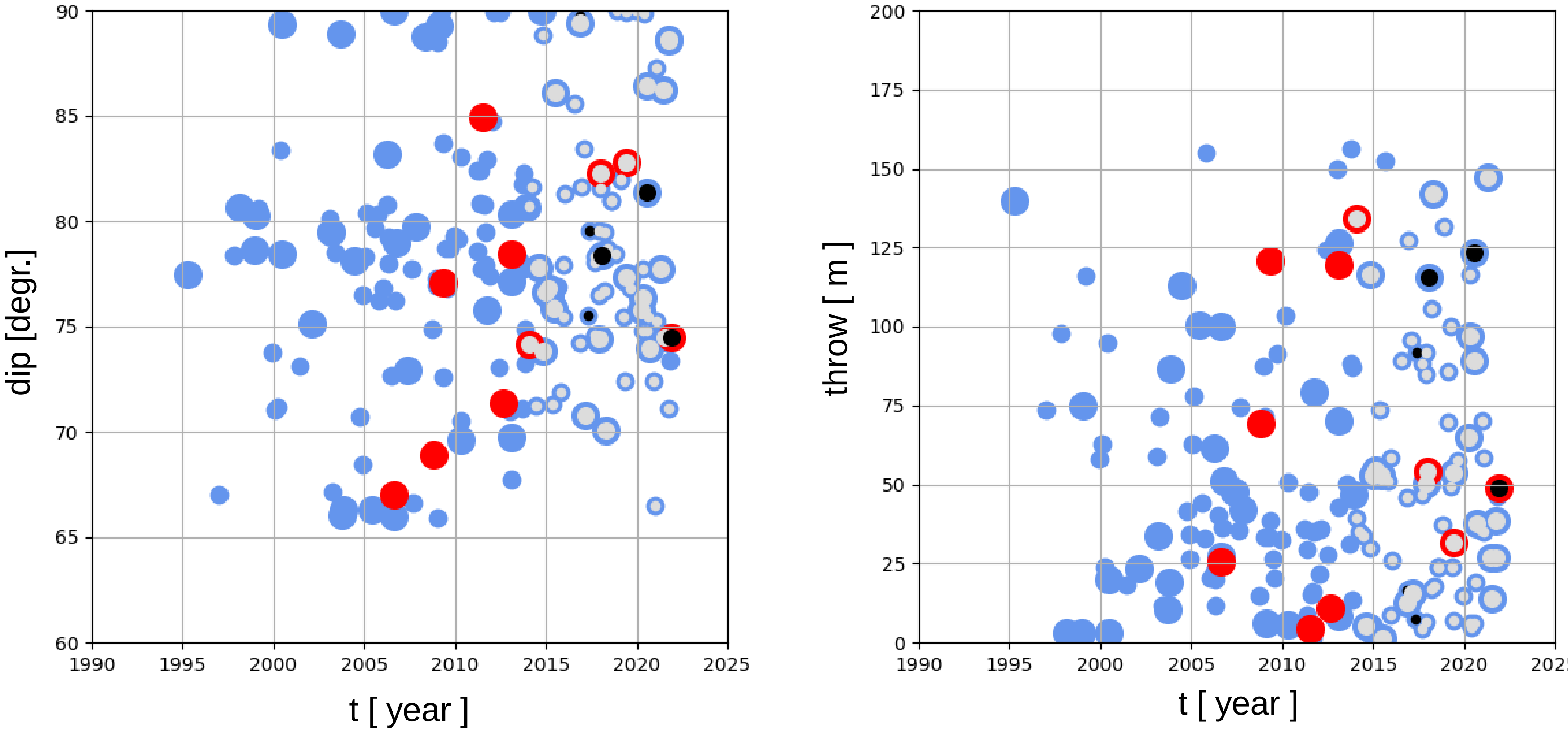

- $1.5 \leq M_L < 2.0$
- $2.0 \leq M_L < 3.0$
- $M_L \geq 3.0$

Grey filling: accurate epicenter location from Spetzler (2017,2021), Willacy et al. (2018), Dost et al., (2020} and Smith et al. (2020).
Black filling: accurate epicenter location and rake angle strongly deviating from normal faulting.

Mmax II Workshop, Amsterdam, June 14 2022

Physics-based models of natural and induced earthquakes

Pablo Ampuero, Huihui Weng (UCA/IRD Géoazur)

Loes Buijze (TNO)

GeoAZUR TERRE - OCÉAN - ESPACE

UNIVERSITÉ CÔTE D'AZUR

IRD Institut de Recherche pour le Développement FRANCE

Physics-based estimates of induced Mmax in the Groningen gas field, The Netherlands

J.P. Ampuero & H. Weng (Geoazur), L. Buijze (TNO) - Funded by NAM (2021/2022)

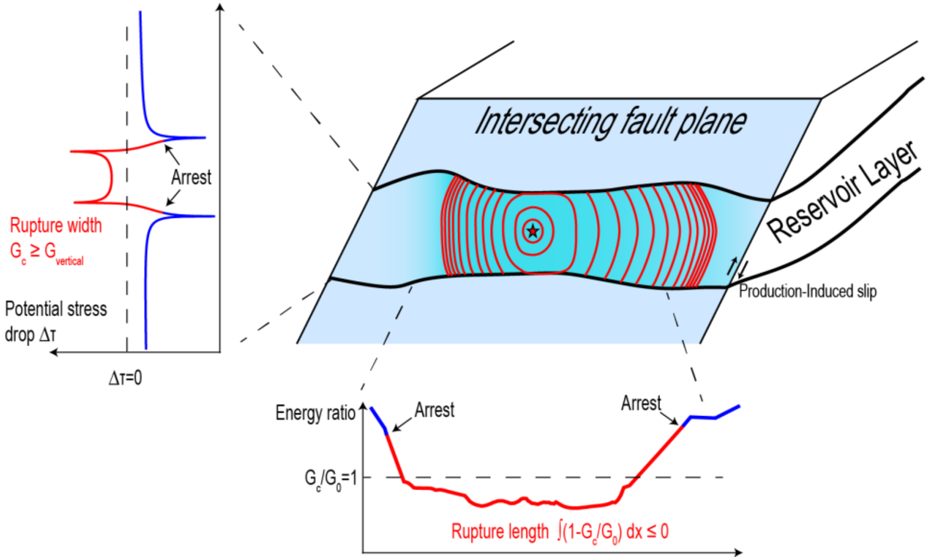

Efficient dynamic rupture modeling includes:

- Combined along-dip 2D LEFM and along-strike 2.5D LEFM
- Fault friction constrained by lab and seismological observations
- Groningen fault network geometry
- Models of fault stress induced by reservoir depletion

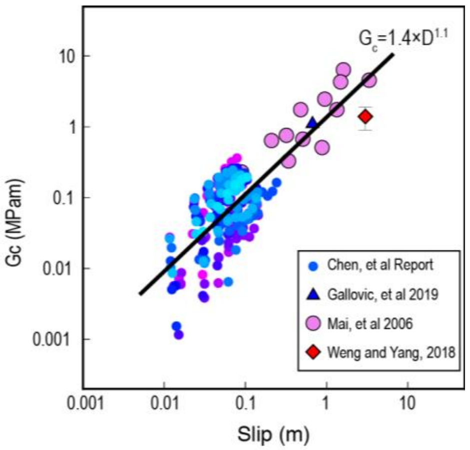

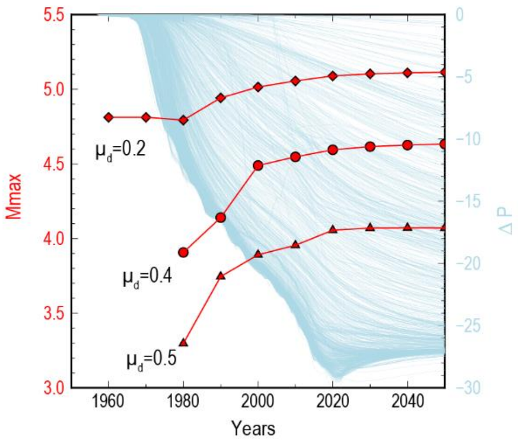

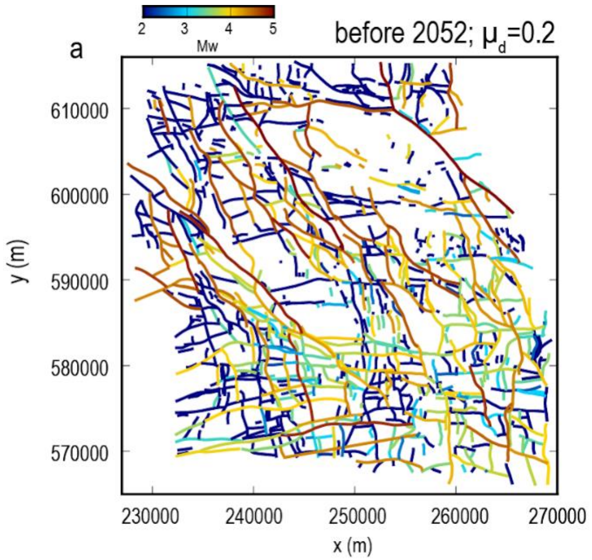

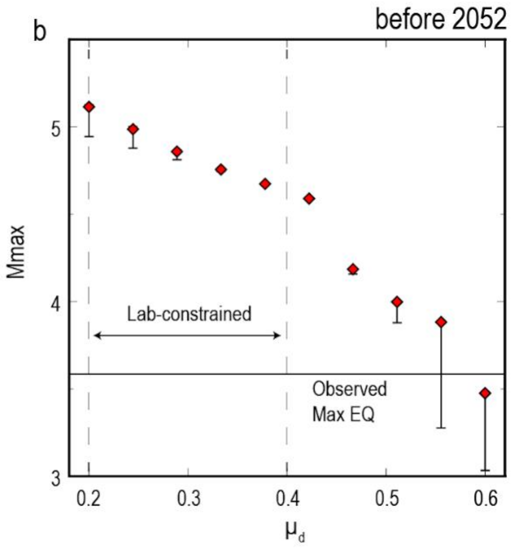

Why physics-based modeling of Mmax?

To complement empirical methods
in situations where data is insufficient.

But risky: garbage in, garbage out.

Challenges in earthquake mechanics

Deep process observed from the Earth's surface
Seismological observation hampered by scattering and attenuation

Laboratory experiments do not reproduce all conditions at depth
Diversity of coupled physical processes involved
Complex non-linear system
Modeling needs multi-physics, multi-scale approaches

Opportunities in earthquake mechanics

More earthquakes

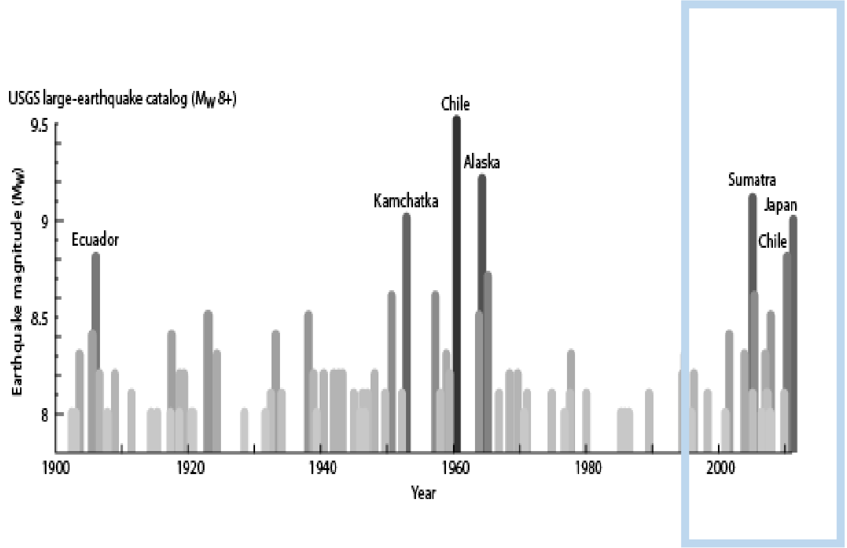

More data

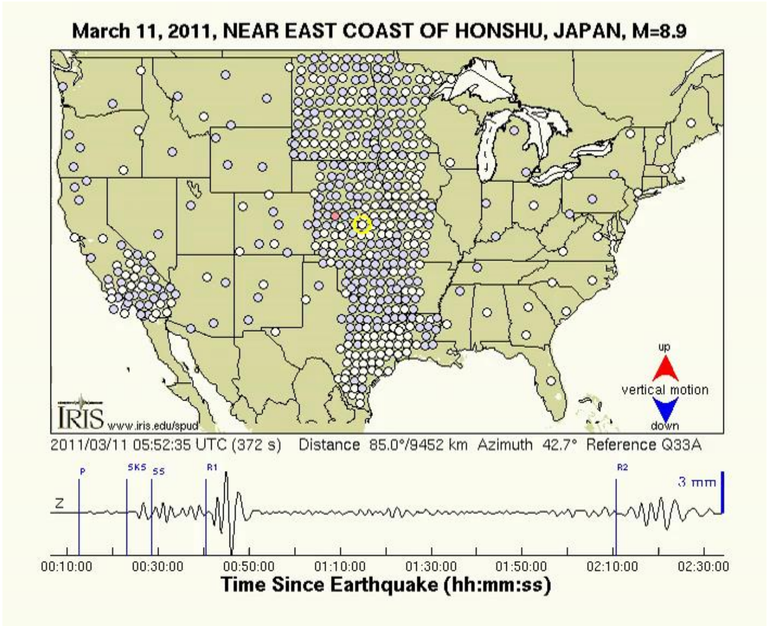

More computer power

+ More lab experiments

Dynamic rupture modeling on complex fault systems

Network of faults activated by the event

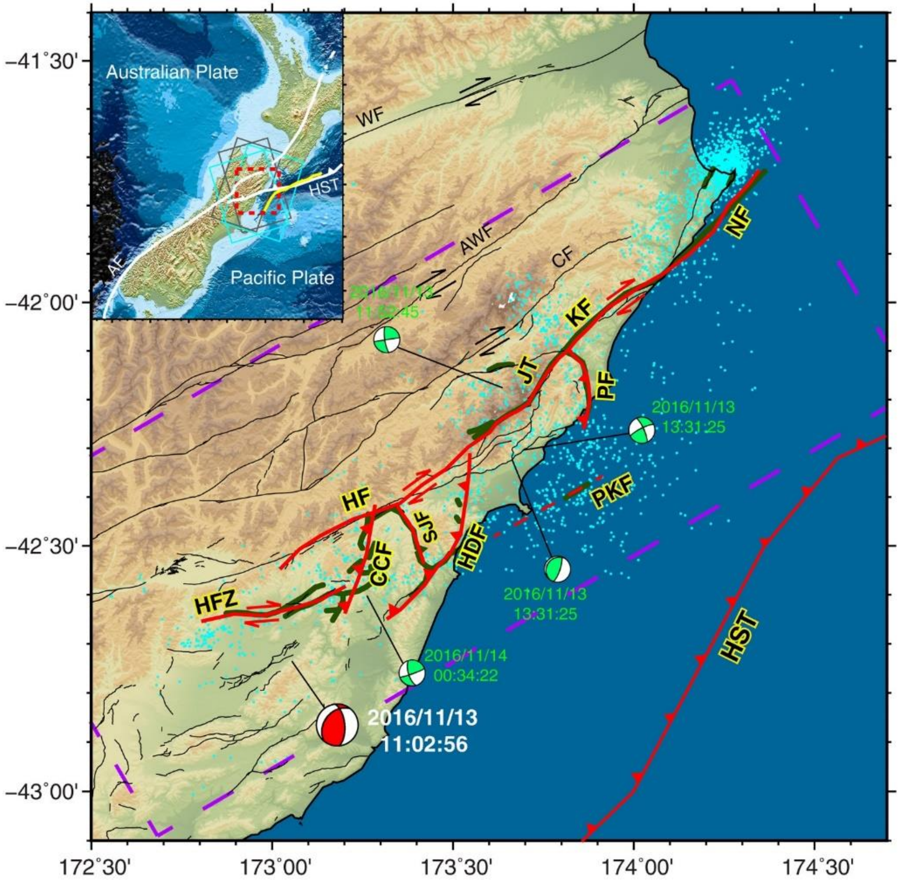

Slip rate evolution in our preferred dynamic rupture model

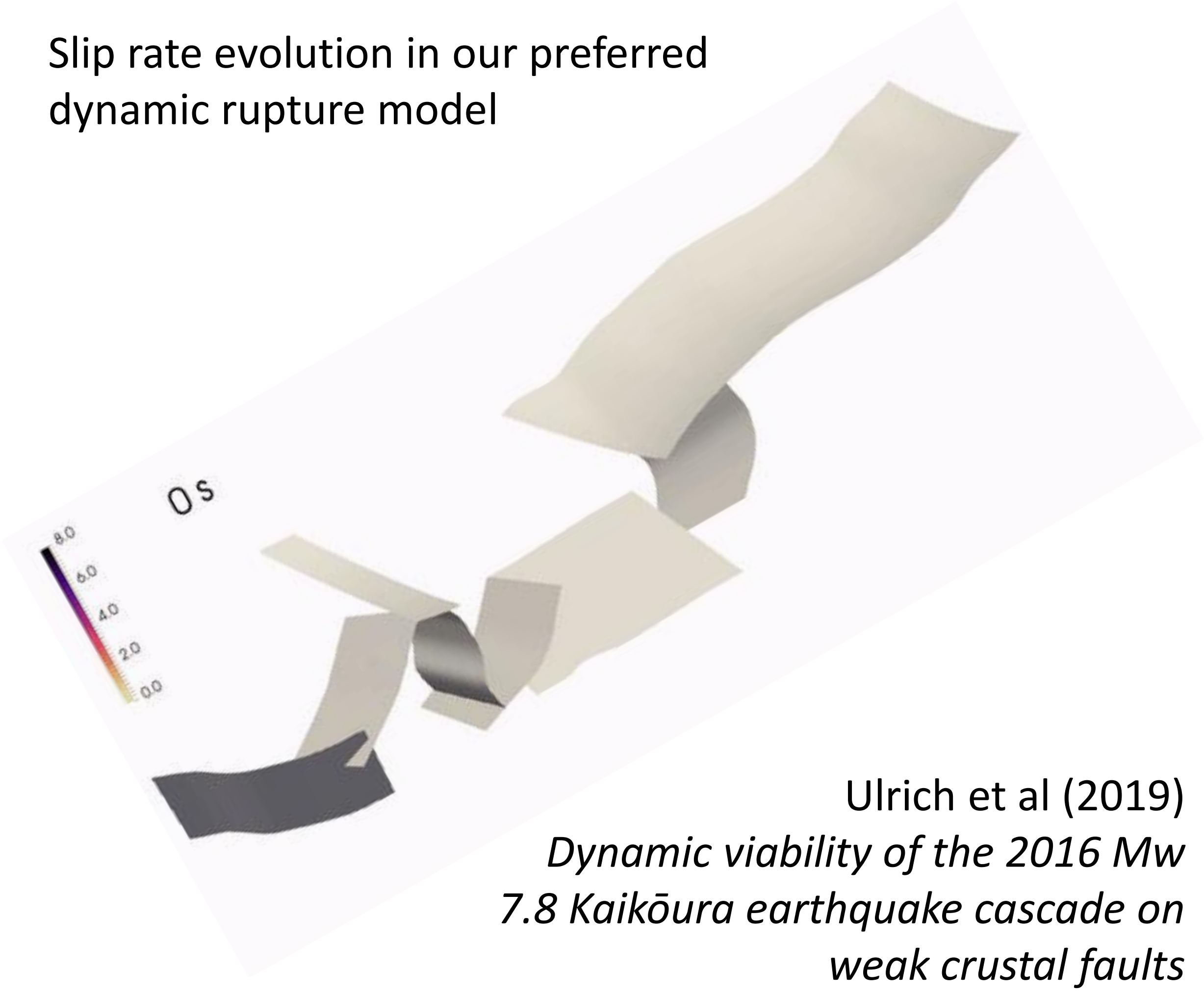

Ulrich et al (2019)
Dynamic viability of the 2016 Mw 7.8 Kaikōura earthquake cascade on weak crustal faults

Groningen fault model

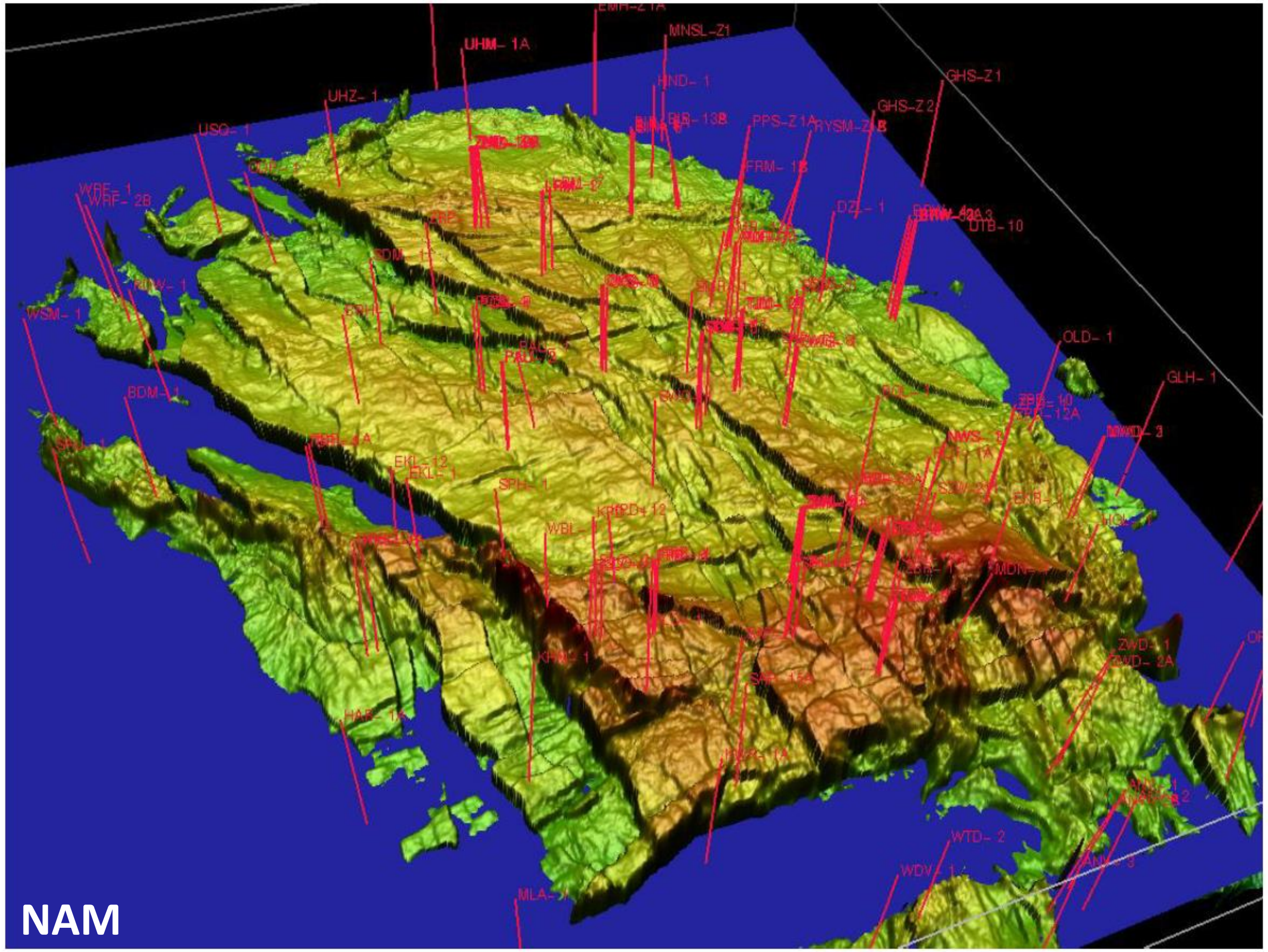

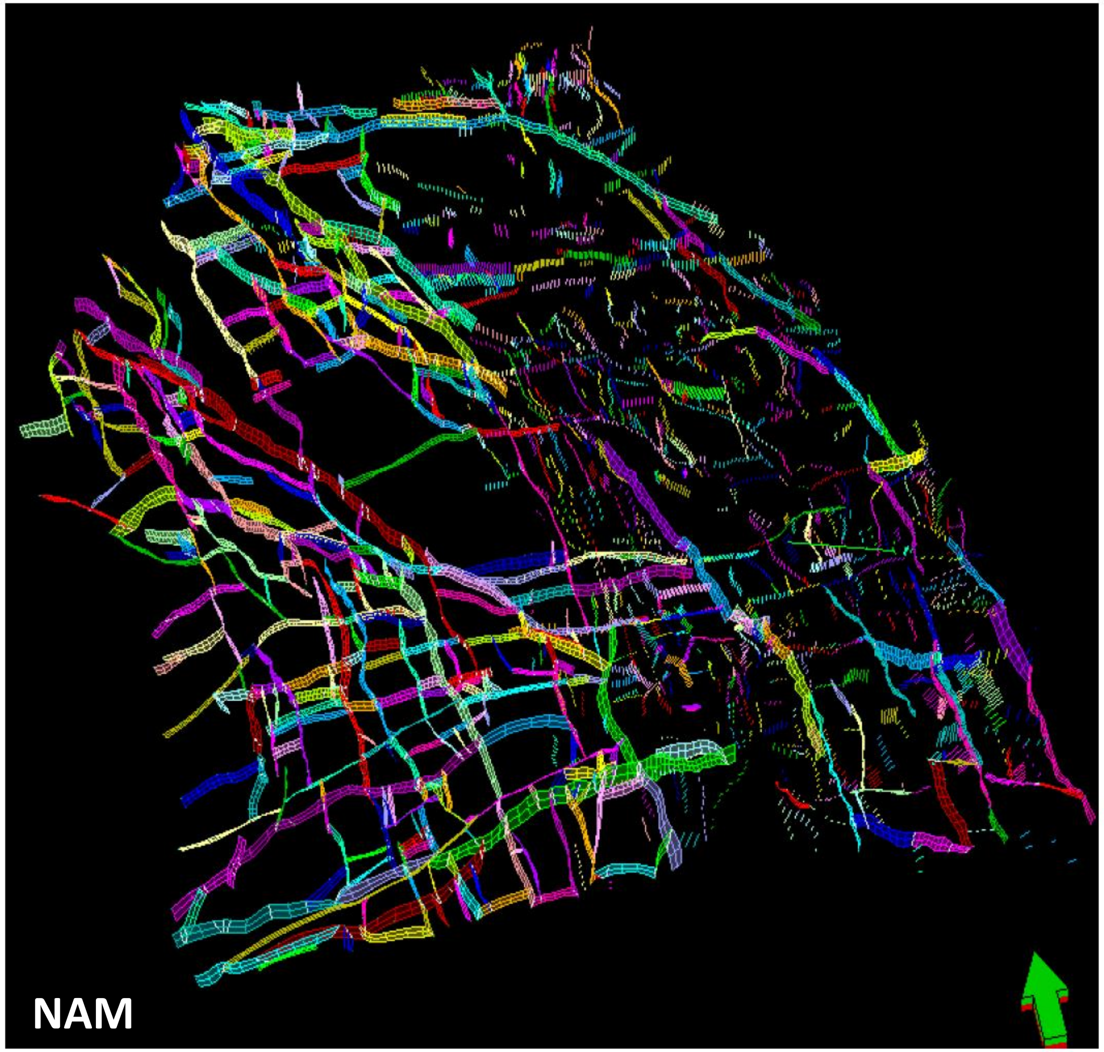

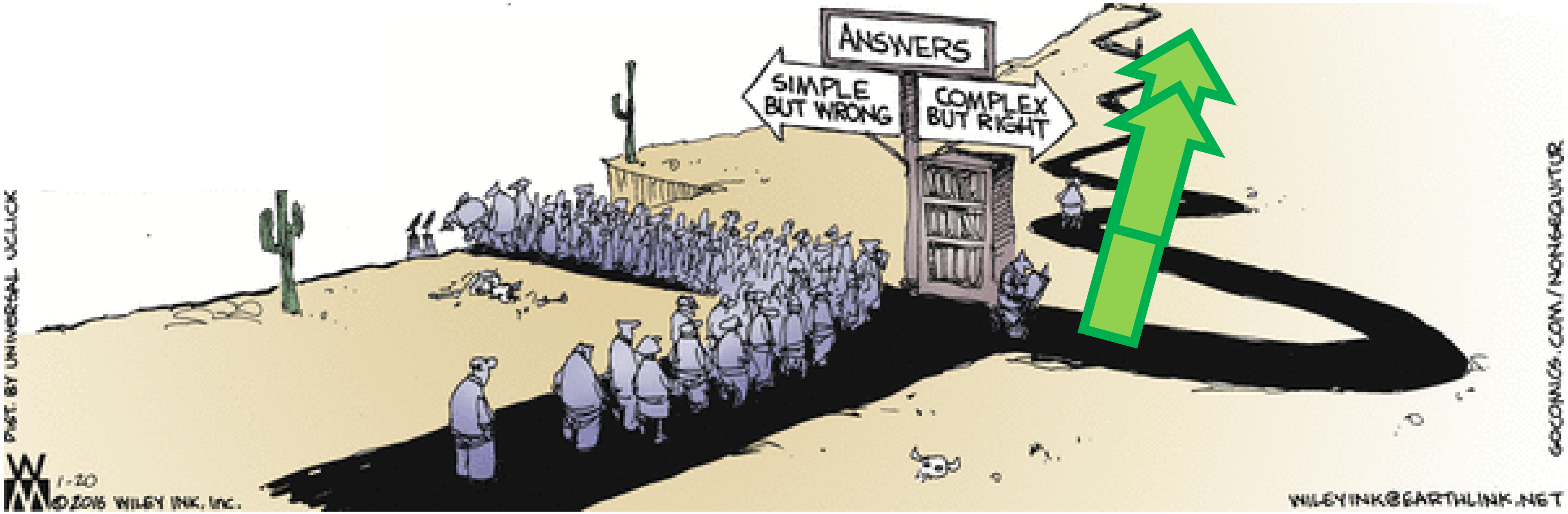
ANSWERS
SIMPLE BUT WRONG
COMPLEX BUT RIGHT
DIST. BY UNIVERSAL UCLICK
1-20
©2016 WILEY INK, INC.
GOCOMICS.COM/NONSEQUITUR
WILEYINK@EARTHLINK.NET

Overview

- Fracture mechanics of rupture **arrest**
- Rupture dynamics of very long ruptures
- Application to Groningen Mmax

SCIENCE ADVANCES | RESEARCH ARTICLE 2017

GEOPHYSICS

Induced seismicity provides insight into why earthquake ruptures stop

Martin Galis,[1*†] Jean Paul Ampuero,[2] P. Martin Mai,[1] Frédéric Cappa[3,4]

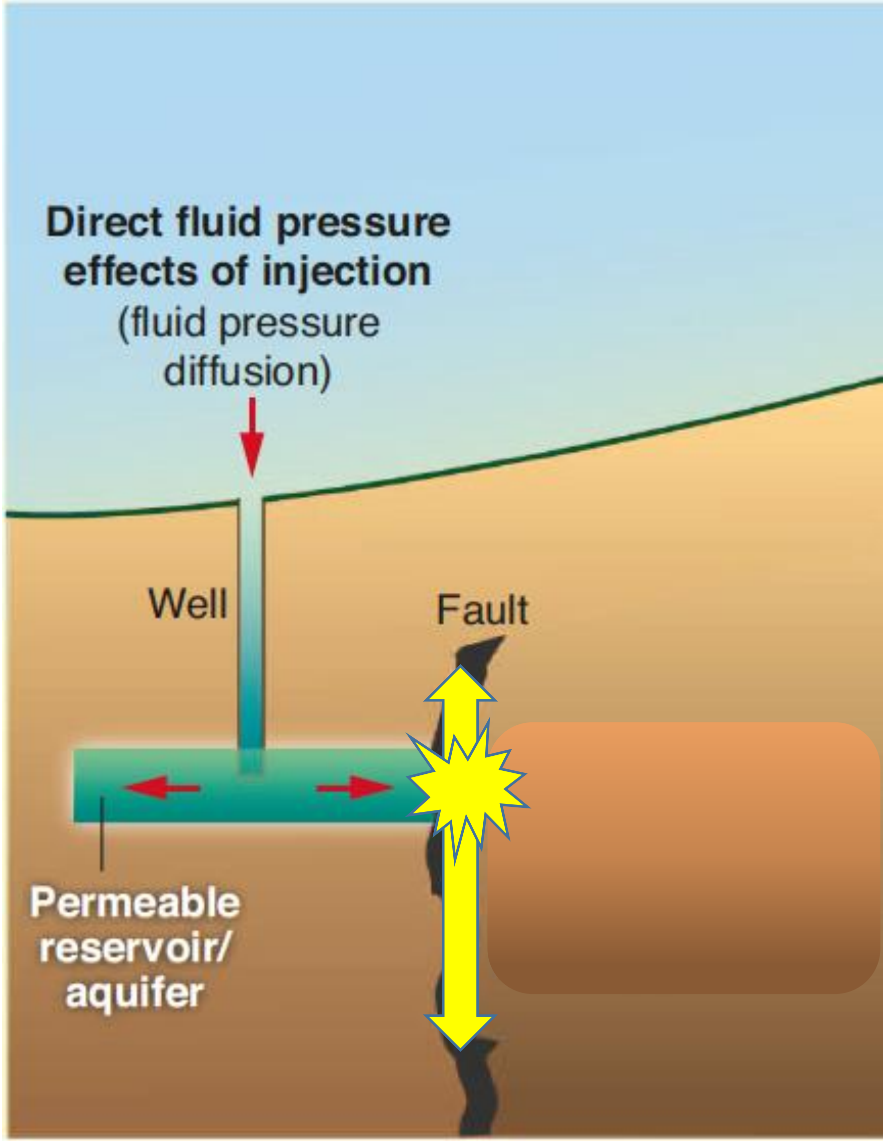

A rupture triggered by injection can propagate beyond the pressurized zone if the fault has enough pre-stress.

Size of earthquakes induced by fluid injection

A simplified problem:

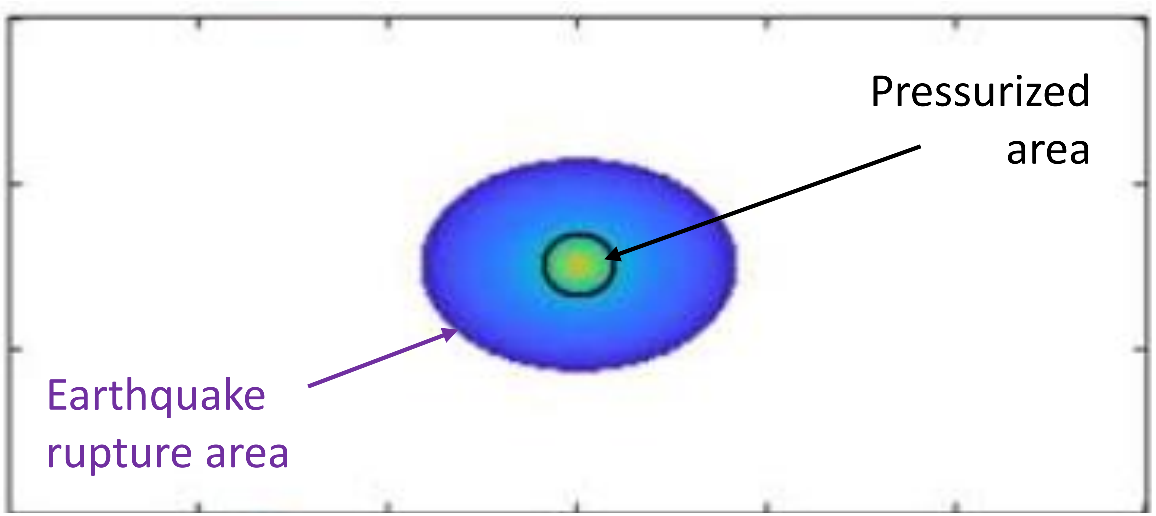

Linear slip-weakening friction

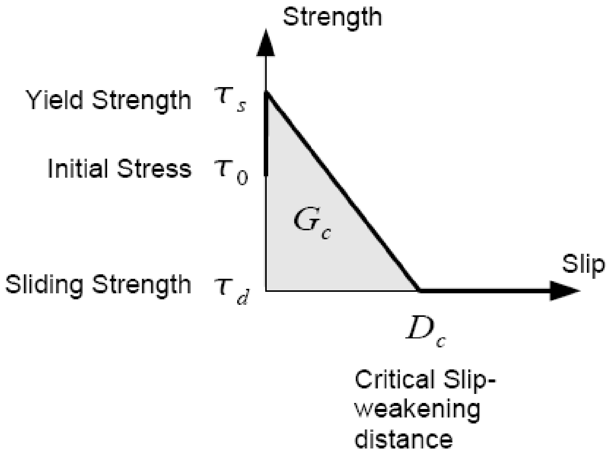

How far from the pressurized region can an induced rupture grow?

Size of earthquakes induced by fluid injection

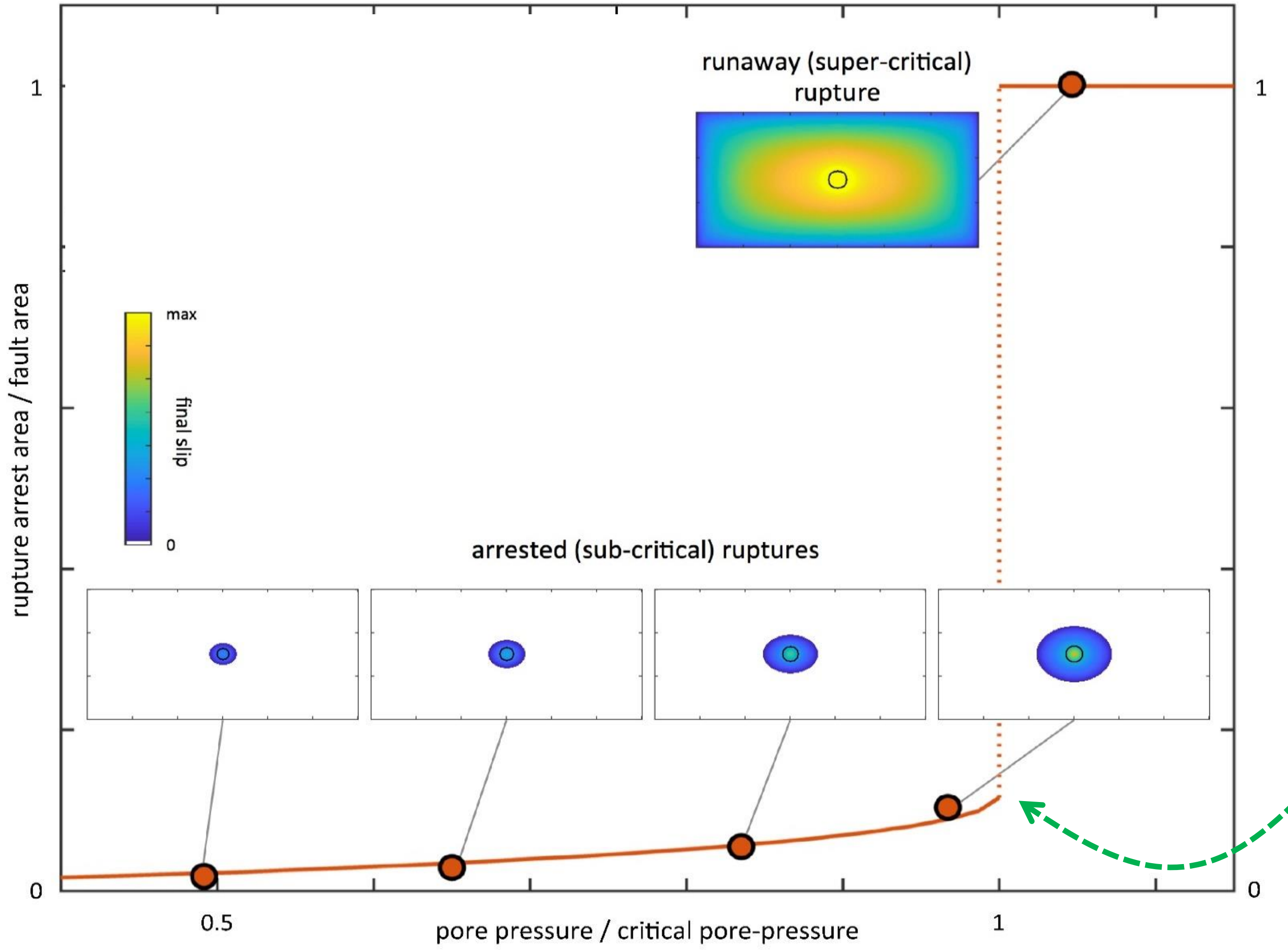

Largest arrested rupture → $M_{max-arr}$

(Galis et al 2017)

Fracture mechanics:
the crack-tip equation of motion

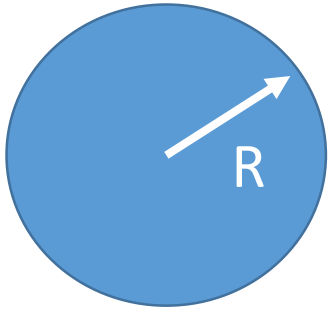

(1989)

Balance between fracture energy and energy release rate

$$G_c = G$$

For circular crack-like ruptures with rupture speed $\dot{R}(t)$:

$$G_c = g(\dot{R}) \frac{\Delta\tau^2 R}{2\mu} \rightarrow G_0$$

Ordinary Differential Equation $\dot{R} = f(R, \ldots)$

Solve → $R(t)$

Rupture arrest if $G_c \leq G_0$

Rupture arrest criterion in fracture mechanics theory

Static stress concentration at rupture tip:

$$\sigma \sim \frac{K_0}{\sqrt{r}}$$

where Ko =static stress intensity factor

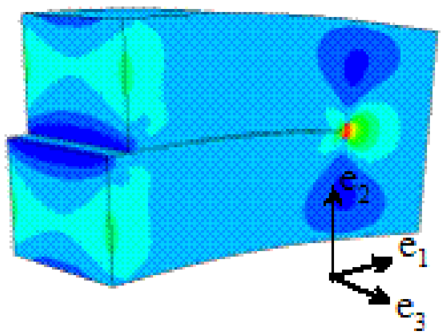

Static energy release rate

$$G_0 = K_0^2/2\mu$$

Rupture grows dynamically if Ko>Kc
Rupture stops if Ko=Kc

Arrest criterion $G_0 = G_c$ equivalent to:

$$K_0 = K_c = \sqrt{2\mu G_c}$$

Ko depends on stress drop $\Delta\tau$
Ko can be computed for any spatial distribution of $\Delta\tau$:

$$K_0(R) = \frac{2}{\sqrt{\pi R}} \int_0^R \frac{\Delta\tau(r)}{\sqrt{R^2 - r^2}}\, r dr$$

Rupture arrest predicted by fracture mechanics theory

Stress drop
= background
+ concentration

$$\Delta\tau = \tau_0 - \mu_d \sigma_0 + \mu_d P$$

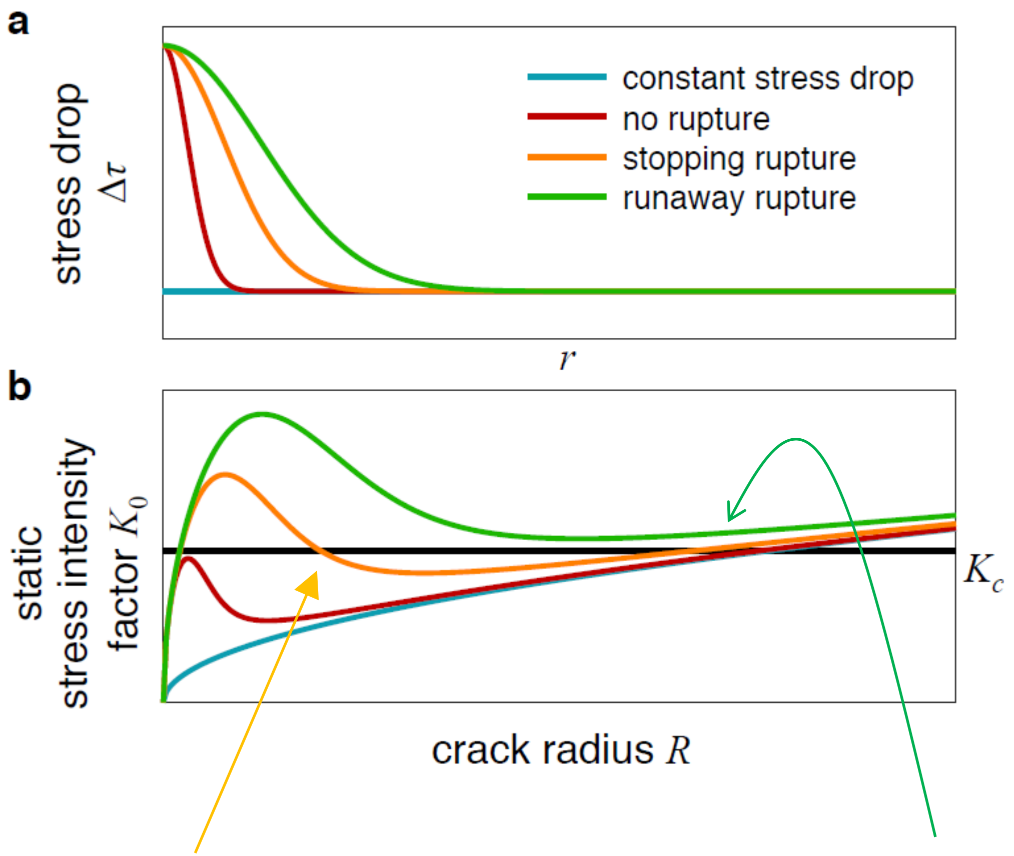

Rupture stops where $K_0 = K_c$

Rupture runs away because $K_0 = K_c$ is never met

Special case:
concentrated stress is a single force F

$$\Delta\tau(r) \doteq \Delta\tau_0 + F \cdot \delta(r)/(2\pi r)$$

$$F = \mu_d \cdot \Delta p \cdot A_p$$

$$K_0(R) = \frac{F}{(\pi R)^{3/2}} + 2\,\Delta\tau_0 \sqrt{\frac{R}{\pi}}$$

Rupture arrest in dynamic earthquake models is well predicted by fracture mechanics

Rupture nucleated at a highly stressed patch

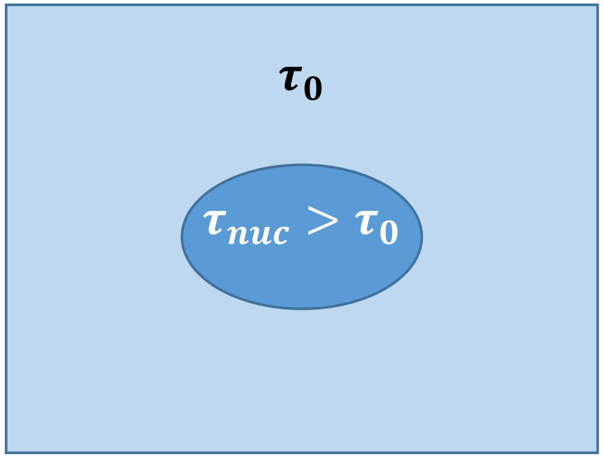

Will it stop?

How does final rupture size depend on nucleation size and overstress?

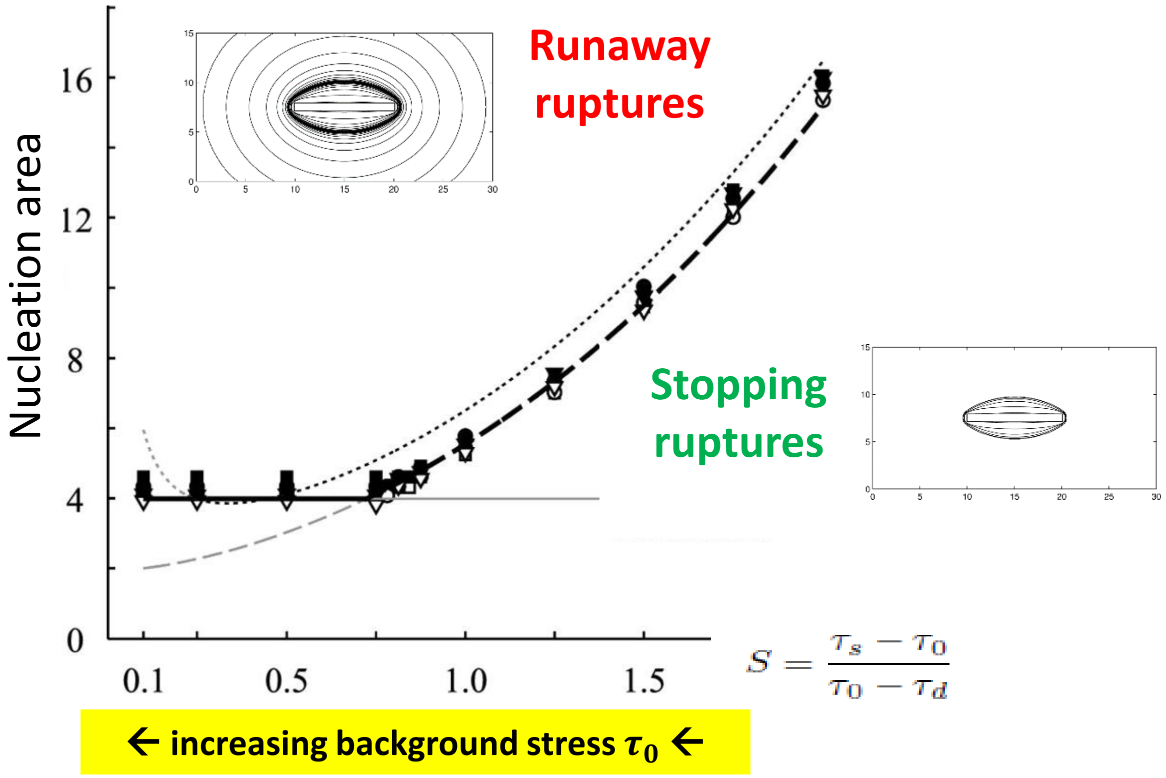

Galis et al (2014)

Rupture arrest in dynamic earthquake models is well predicted by fracture mechanics

Rupture nucleated at a highly stressed patch

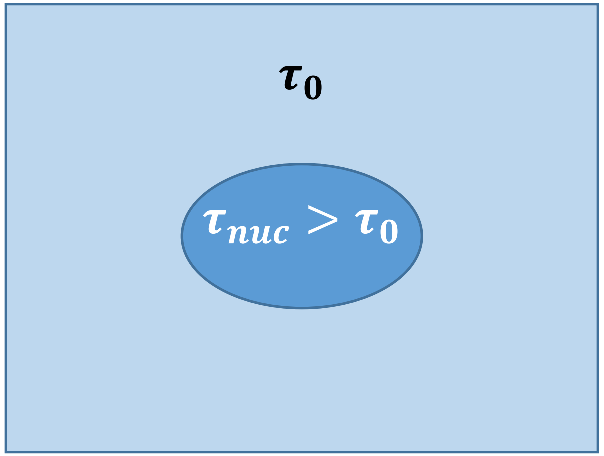

Will it stop?

How does final rupture size depend on nucleation size and overstress?

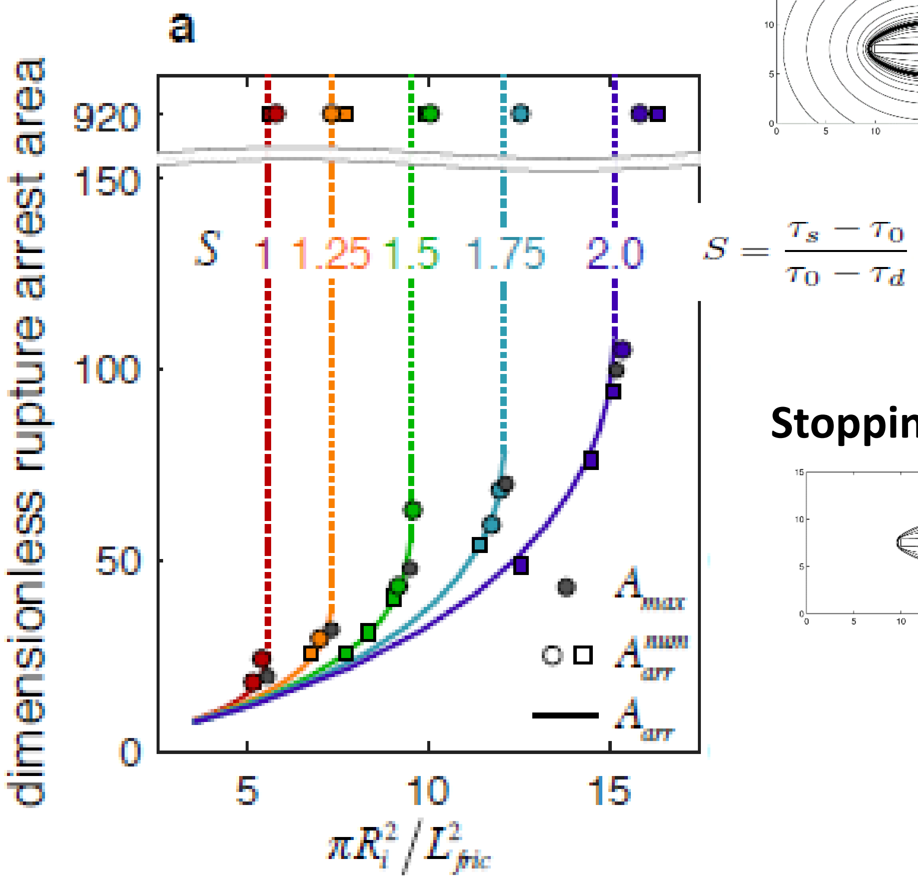

Nucleation area

Runaway ruptures

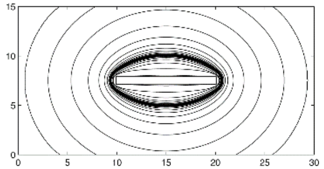

Stopping ruptures

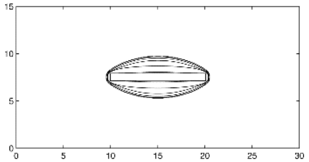

Size of earthquakes induced by fluid injection

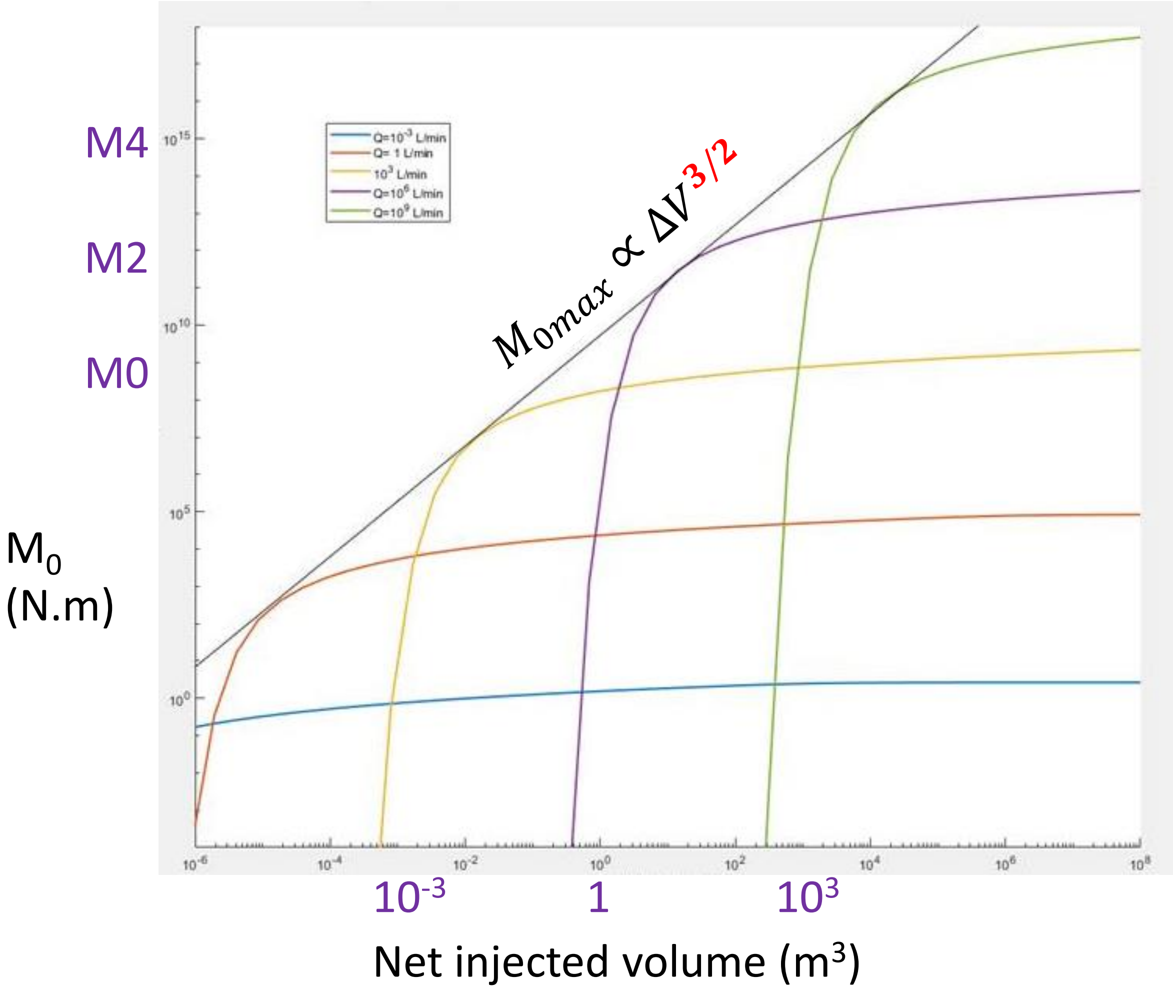

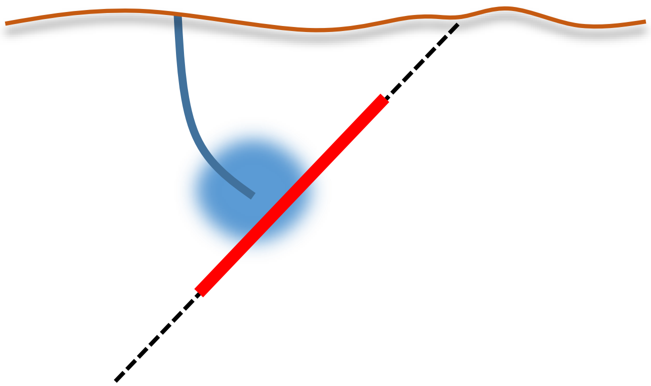

Injection at steady rate + isotropic diffusion
→ size of self-arrested ruptures
from fracture mechanics

Fault at given distance from injection point
Each curve: a different injection rate

Envelope: the largest self-arrested rupture

Fracture mechanics: $M_{0max} \propto \Delta V^{3/2}$

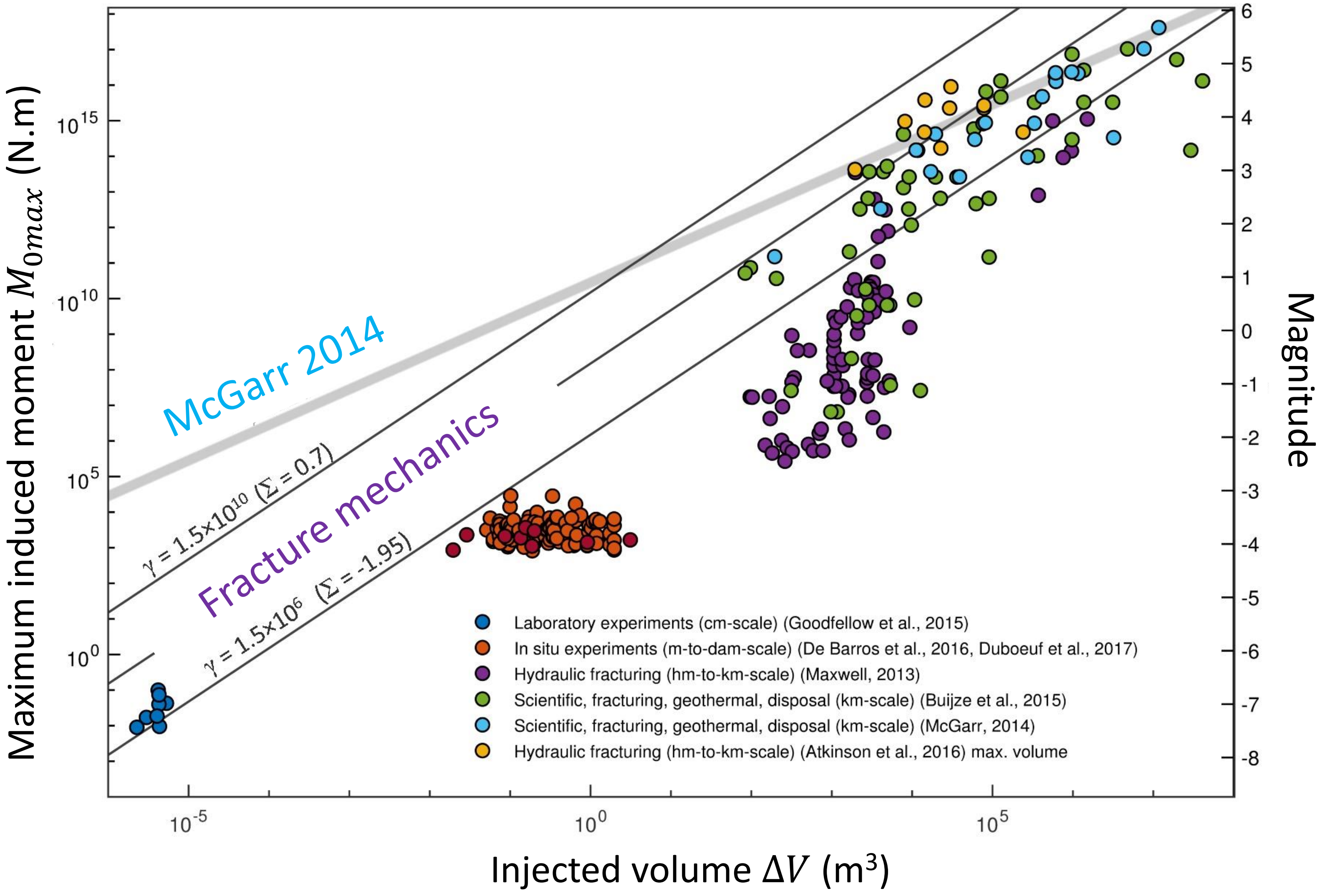

Galis et al (2017)

Application:
Controlling fluid-induced seismicity during a 6.1-km-deep geothermal stimulation in Helsinki, Finland

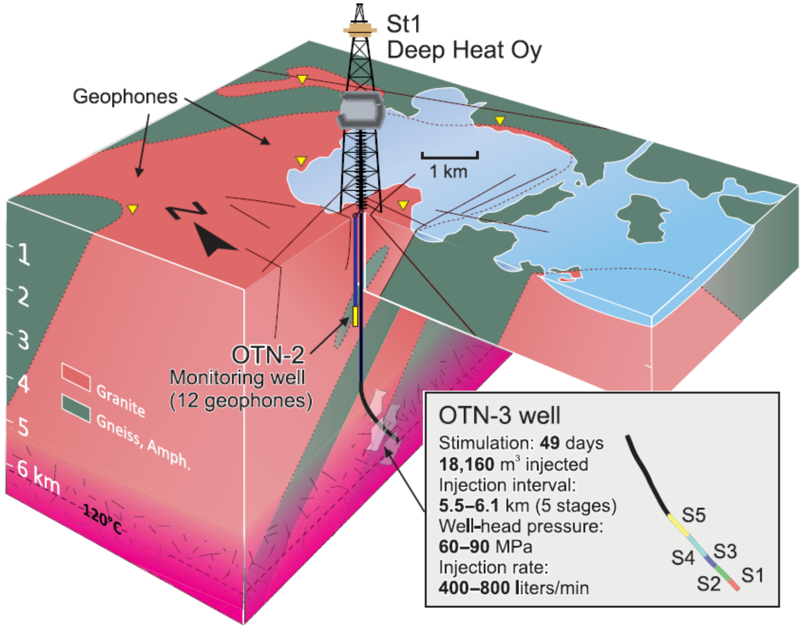

(Kwiatek et al, 2019)

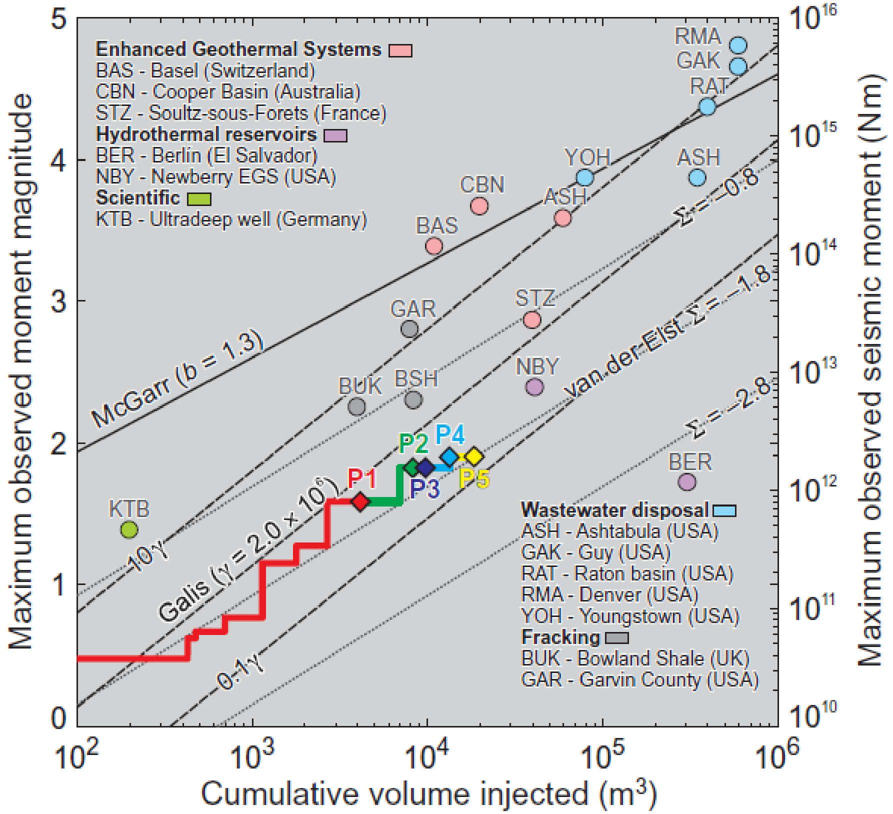

Fig. 5. Temporal evolution of maximum observed seismic moment versus cumulative volume of injected fluid at each phase (P1 to P5). Colored circles are from various injection projects (*8*, *19*, *20*). Maximum magnitude estimates using different models are shown with solid, dashed, and dotted lines (*8*, *10*, *15*). The γ and *b* parameter values used in (*8*, *10*) were calculated after the stimulation, assuming geomechanical and seismic parameters from this study, and plotted for comparison with the observed evolution of seismic moment (see Materials and Methods).

Laboratory quakes nucleated by a localized load

Rubinstein, Cohen and Fineberg (2007)

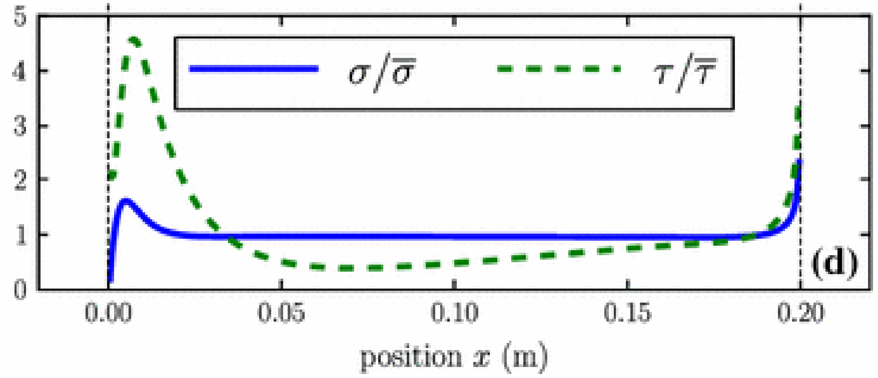

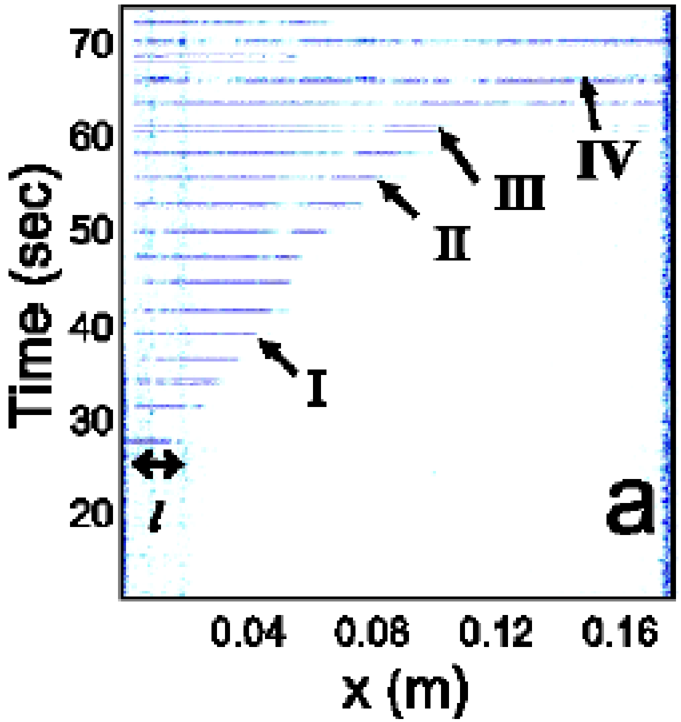

Rupture length

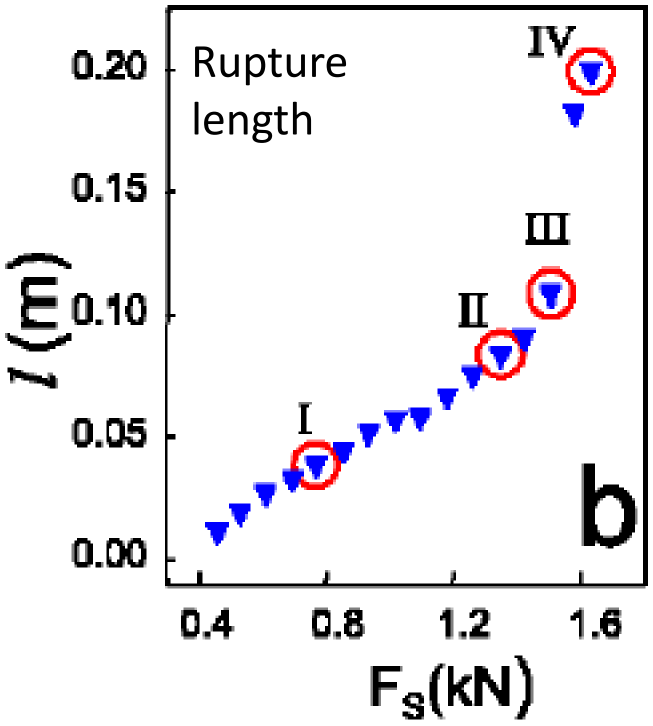

Loading force

Size of laboratory quakes predicted by fracture mechanics

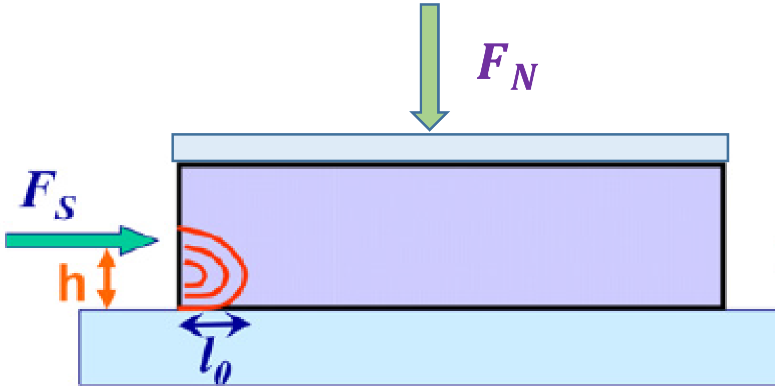

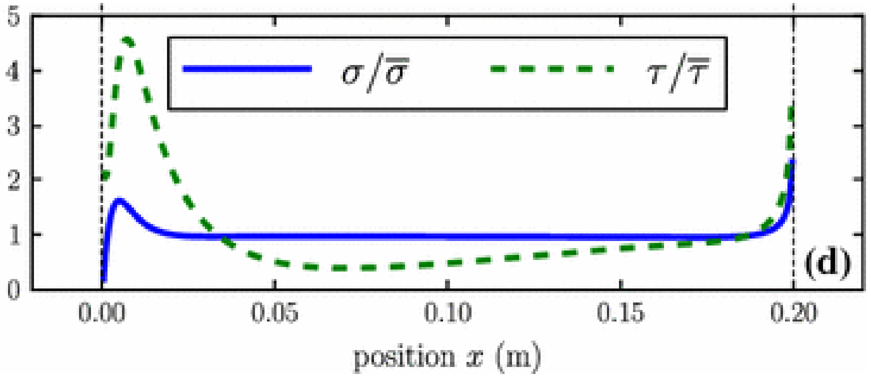

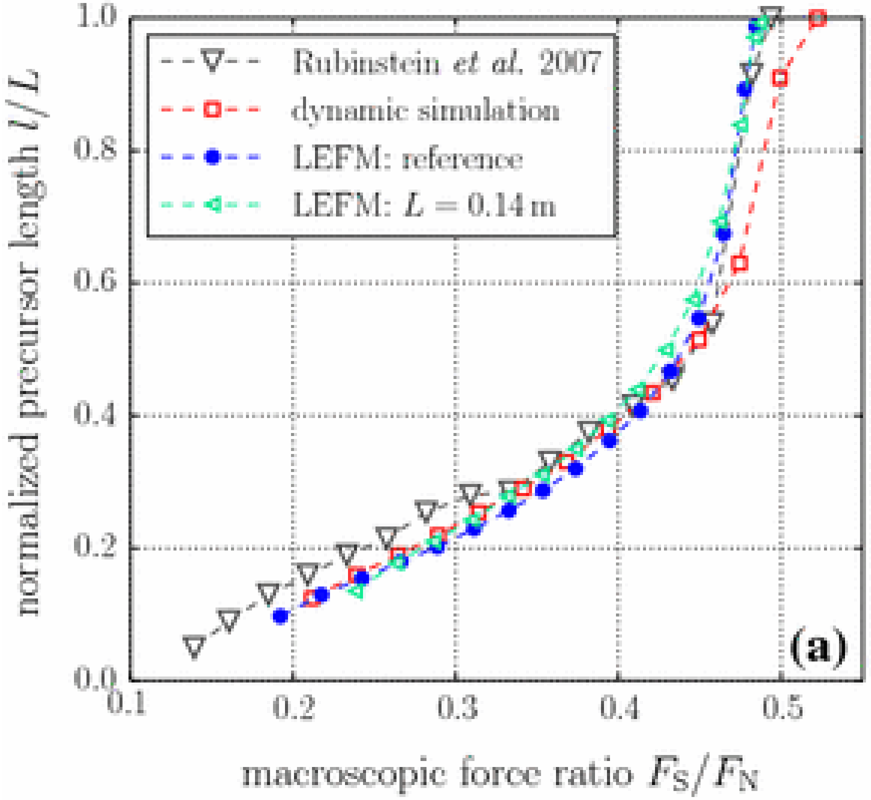

Kammer et al (Tribology Letters, 2015)

Faults driven by localized loads

Fault loaded by deep creep

Stress concentration

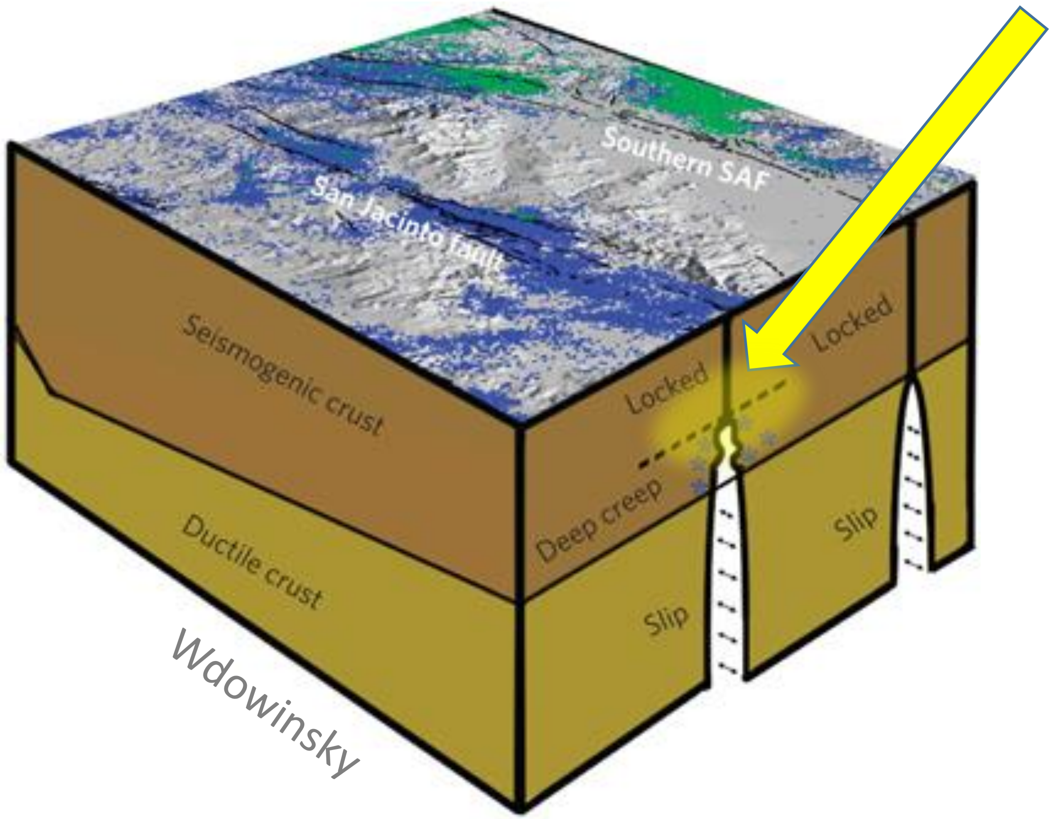

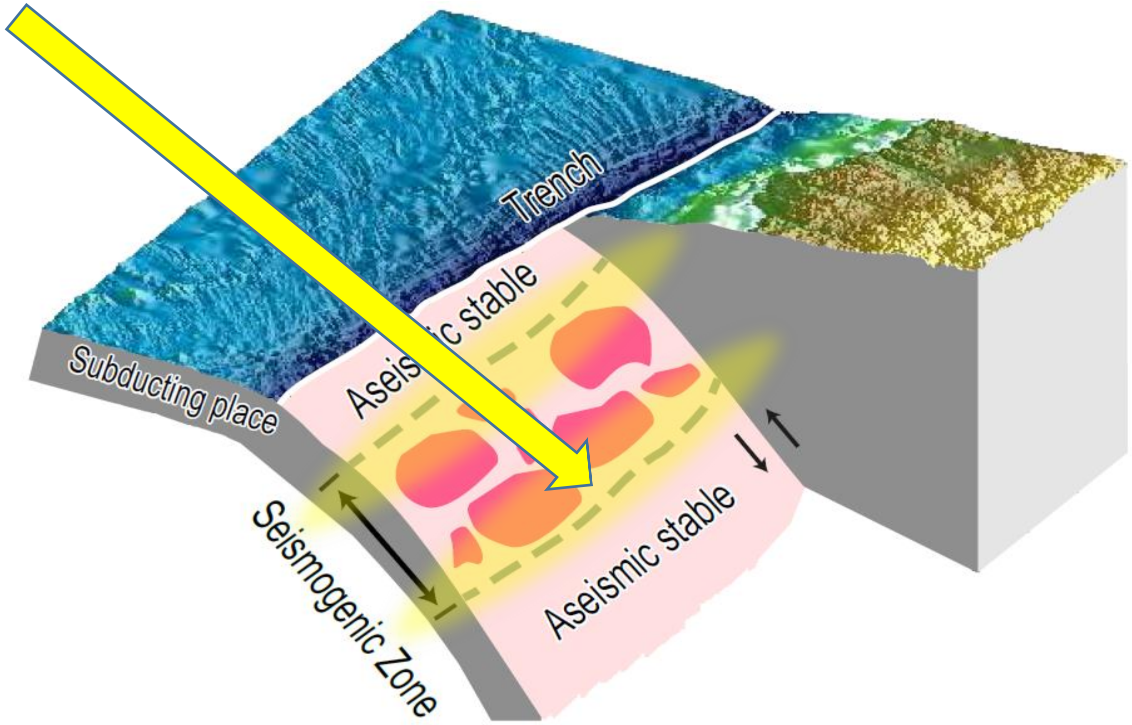

2014 Iquique earthquake foreshock swarms

IPOC stations
Regional catalog by CSN Chile
Seismic coupling by Metois et al (2013)

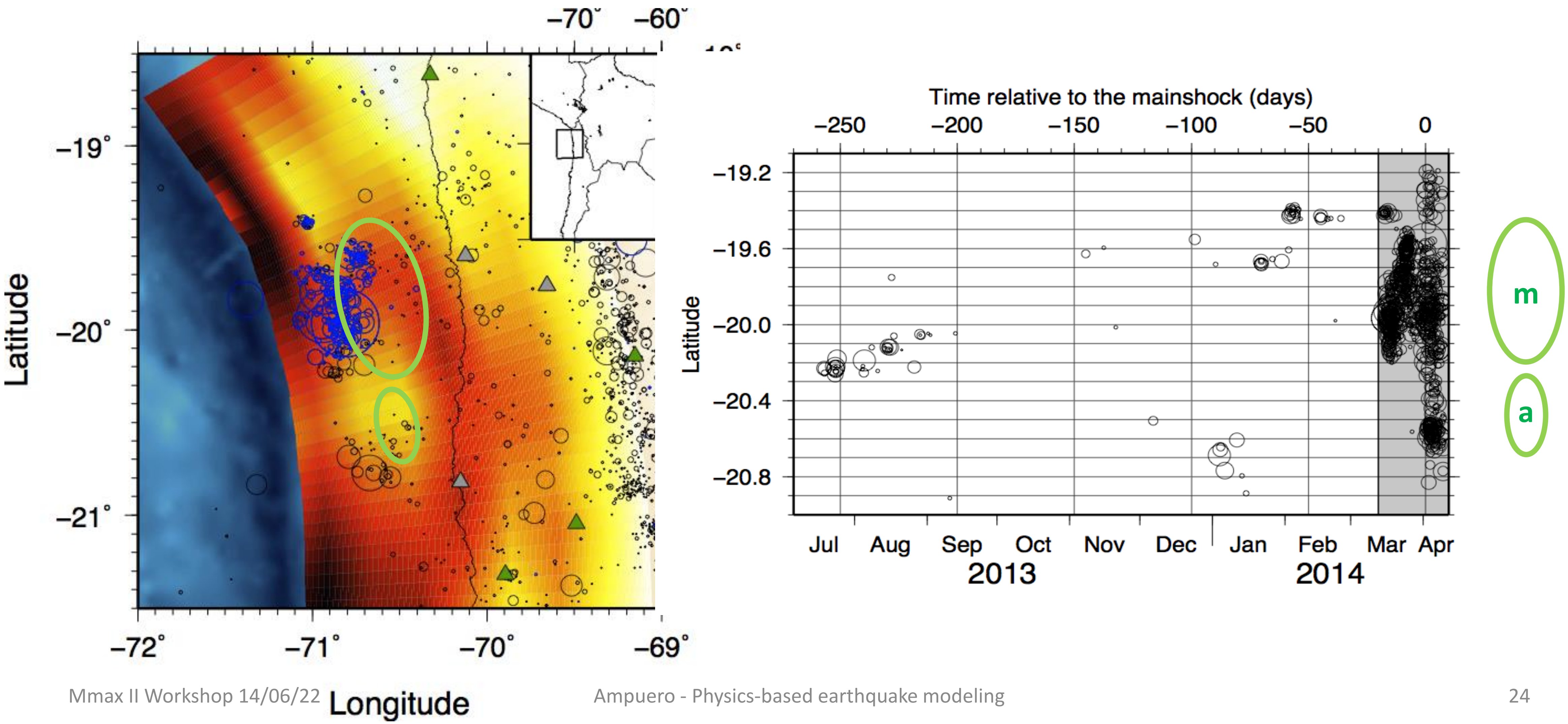

Rupture shape of micro-earthquakes on the San Andreas fault

Rupture aspect ratio ≈ 1.4
(Rubin, 2002)

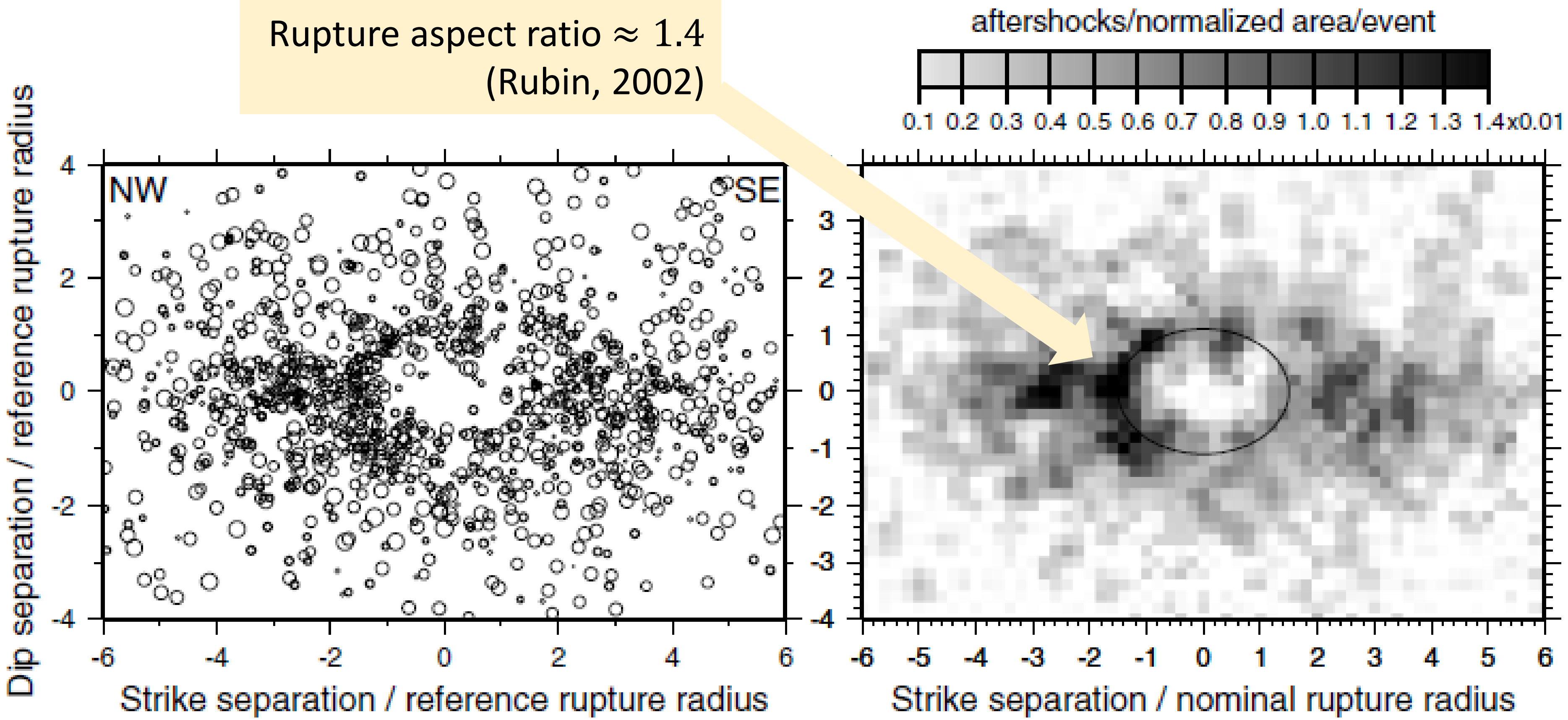

Fracture mechanics predicts aspect ratio $= 1/(1-\nu) \approx 1.4$
where ν is Poisson's ratio

A unique field experiment:
inducing and monitoring slip on a natural fault by fluid injection

In Geoazur SEISMES: Frédéric Cappa, Louis De Barros

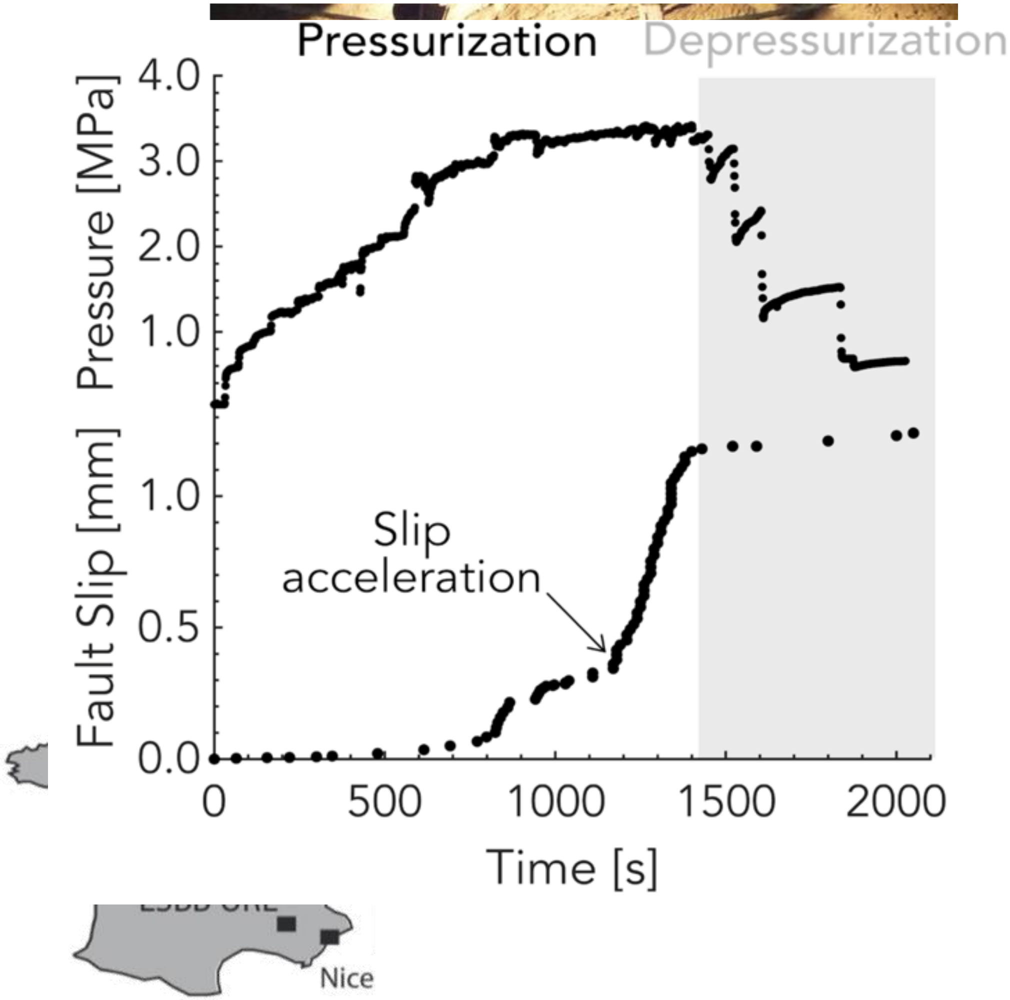

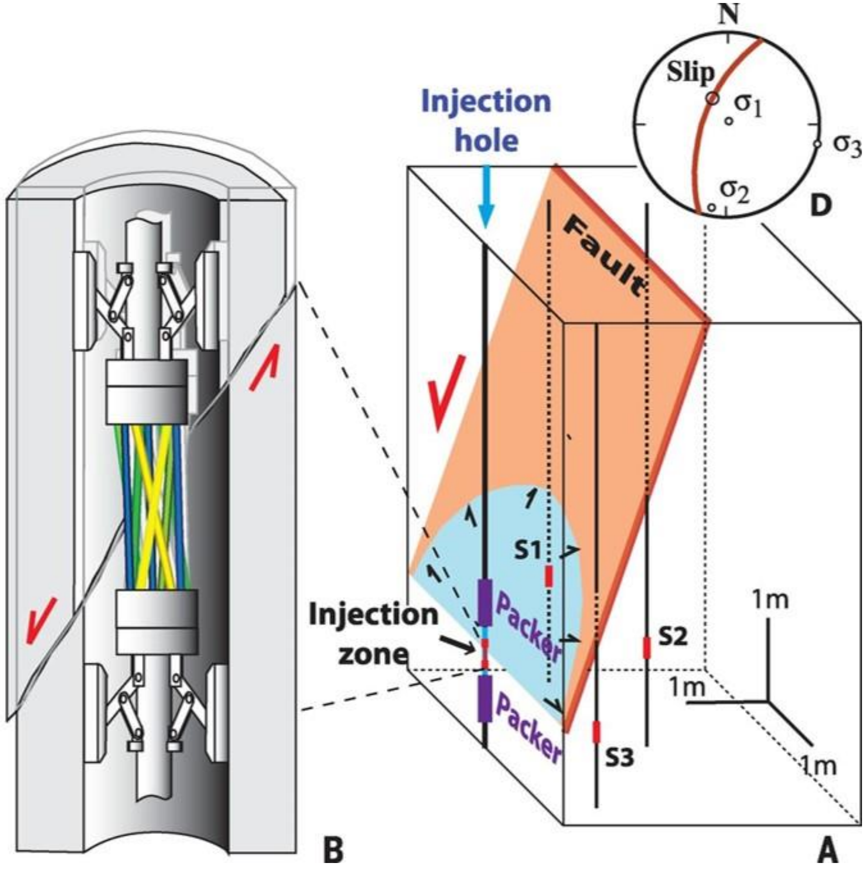

Guglielmi et al (Science, 2015)

LEFM prediction of aseismic slip front and seismic rupture arrest

Predicted nucleation length in the pressurized zone

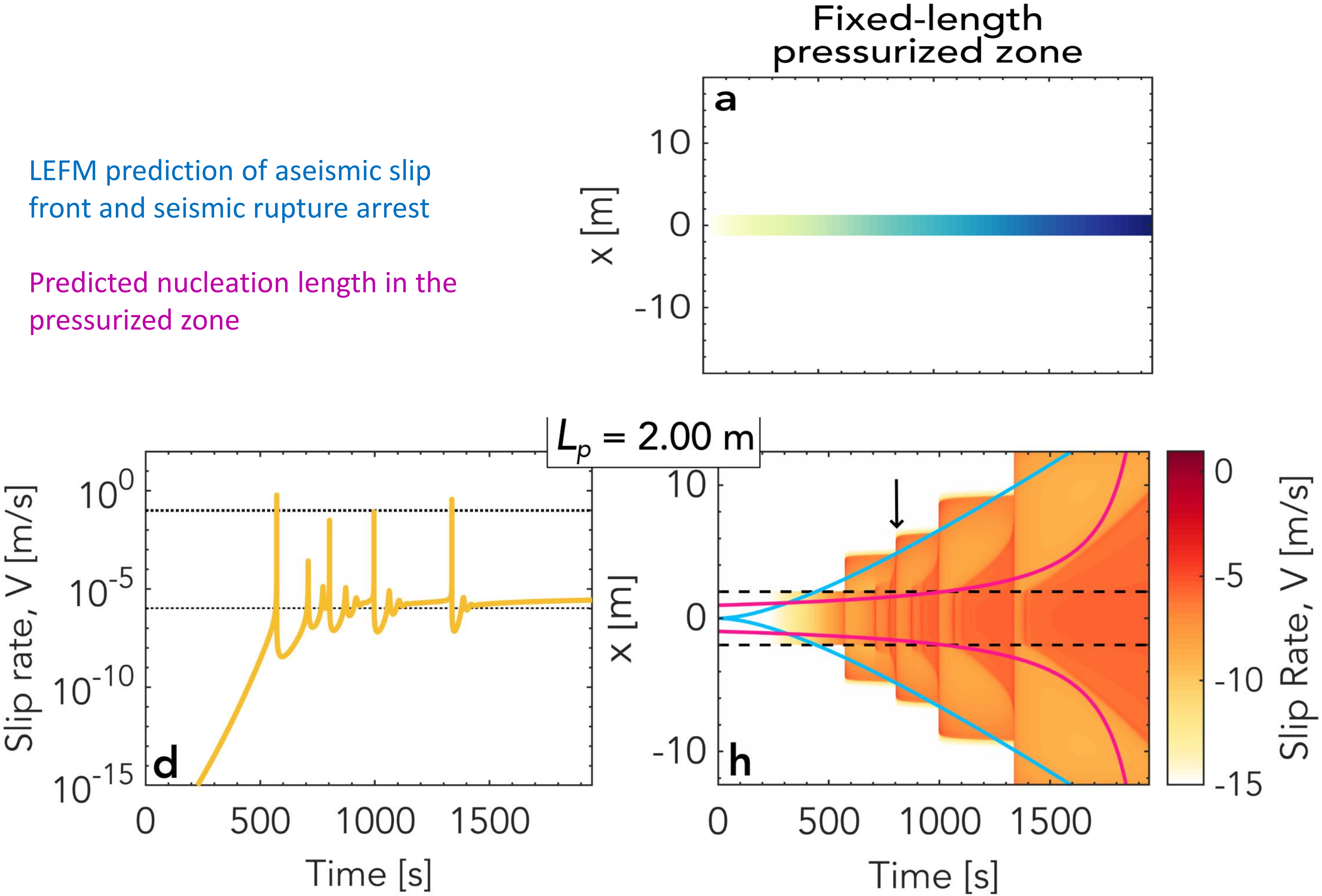

Depth-confined ruptures

Buijze et al (2019)

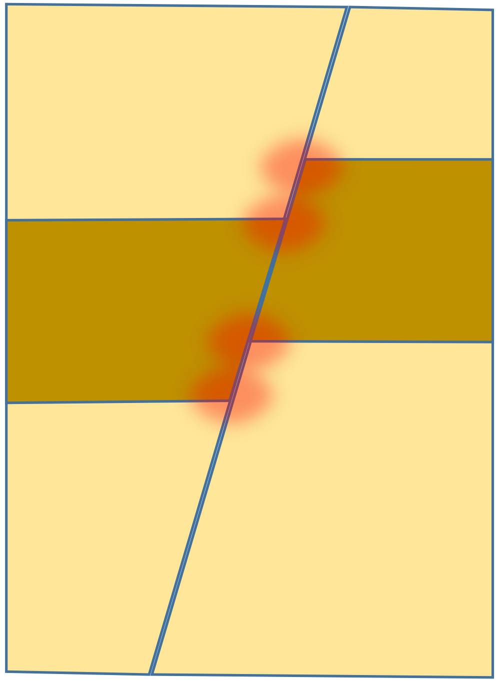

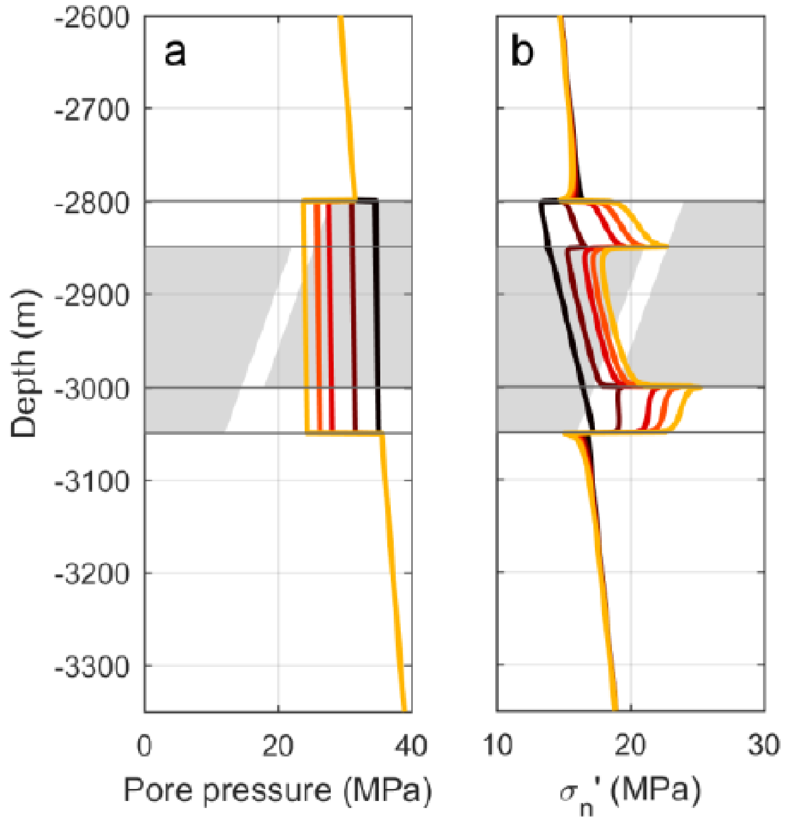

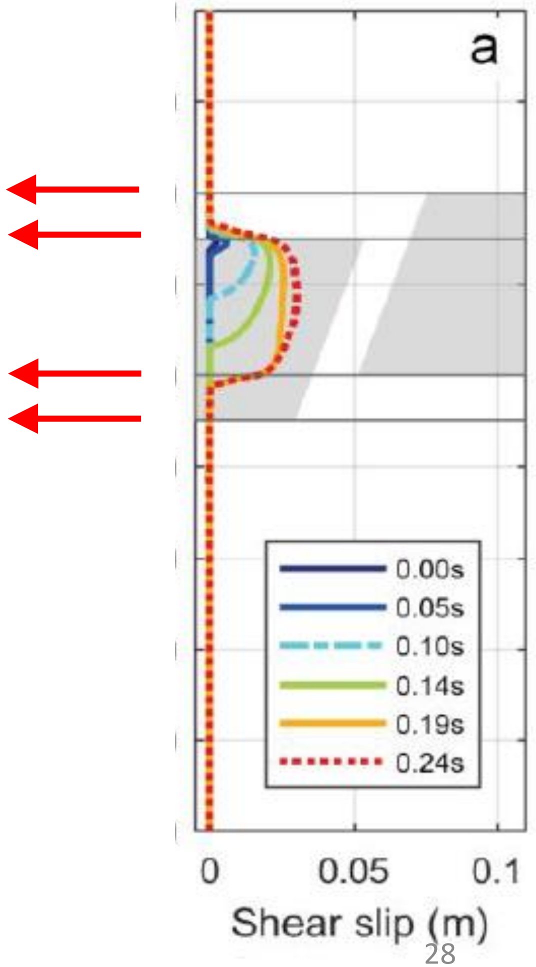

Depth-confined ruptures

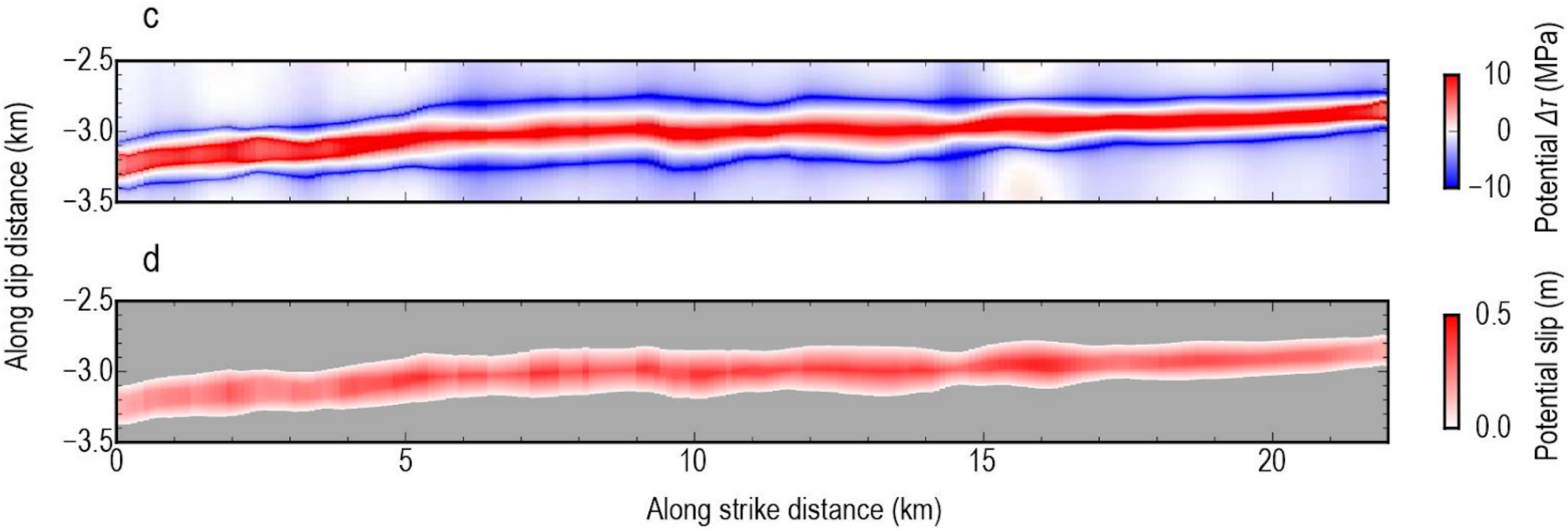

Overview

- Fracture mechanics of rupture arrest
- Rupture dynamics of very long ruptures
- Application to Groningen Mmax

JGR Solid Earth

RESEARCH ARTICLE
10.1029/2019JB017684

The Dynamics of Elongated Earthquake Ruptures

Huihui Weng[1] and Jean-Paul Ampuero[1,2]

Earthquakes triggered by elongated overstressed regions

Galis et al (GJI 2019)

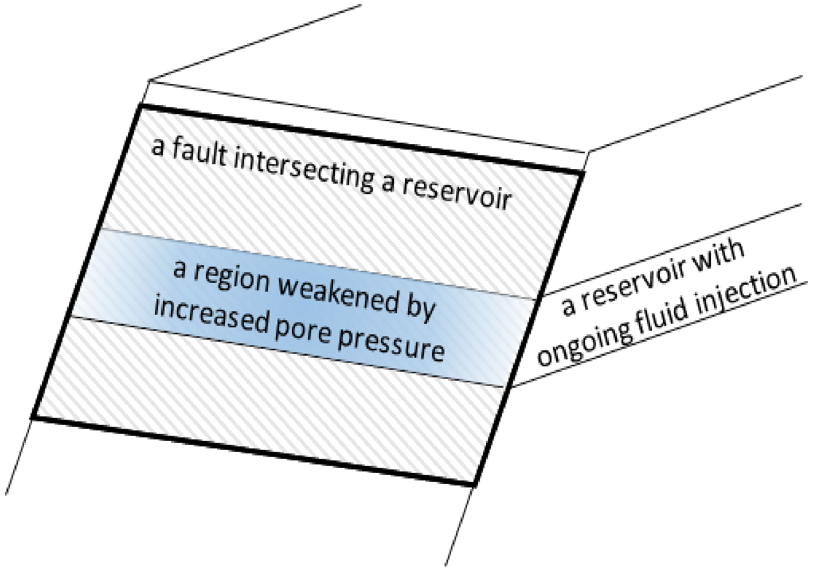

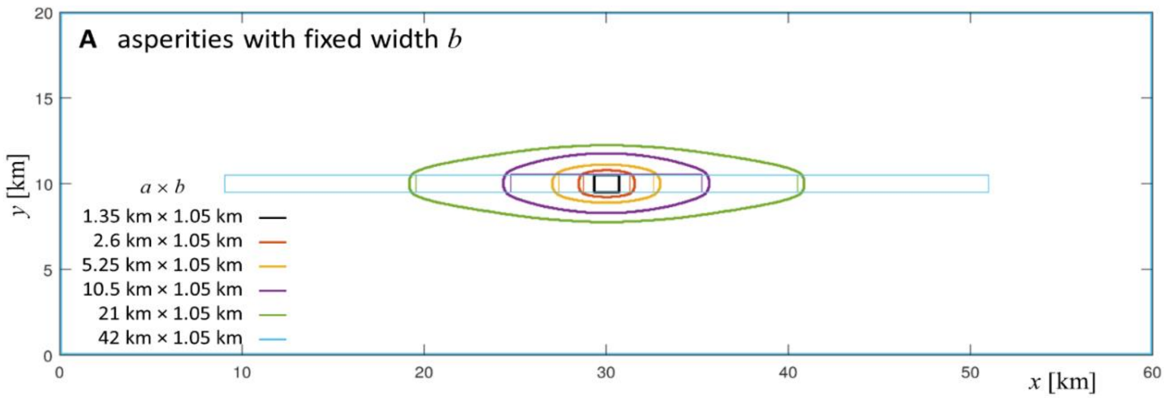

Faults driven by localized loads

Fault loaded by deep creep

Stress concentration

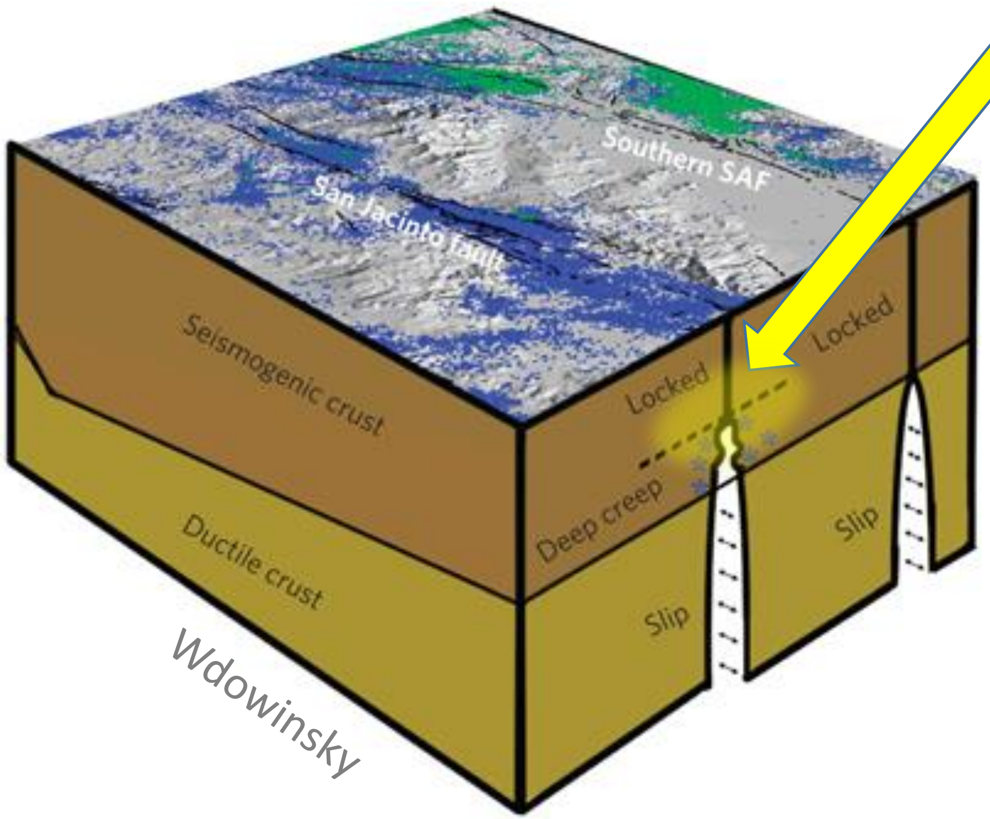

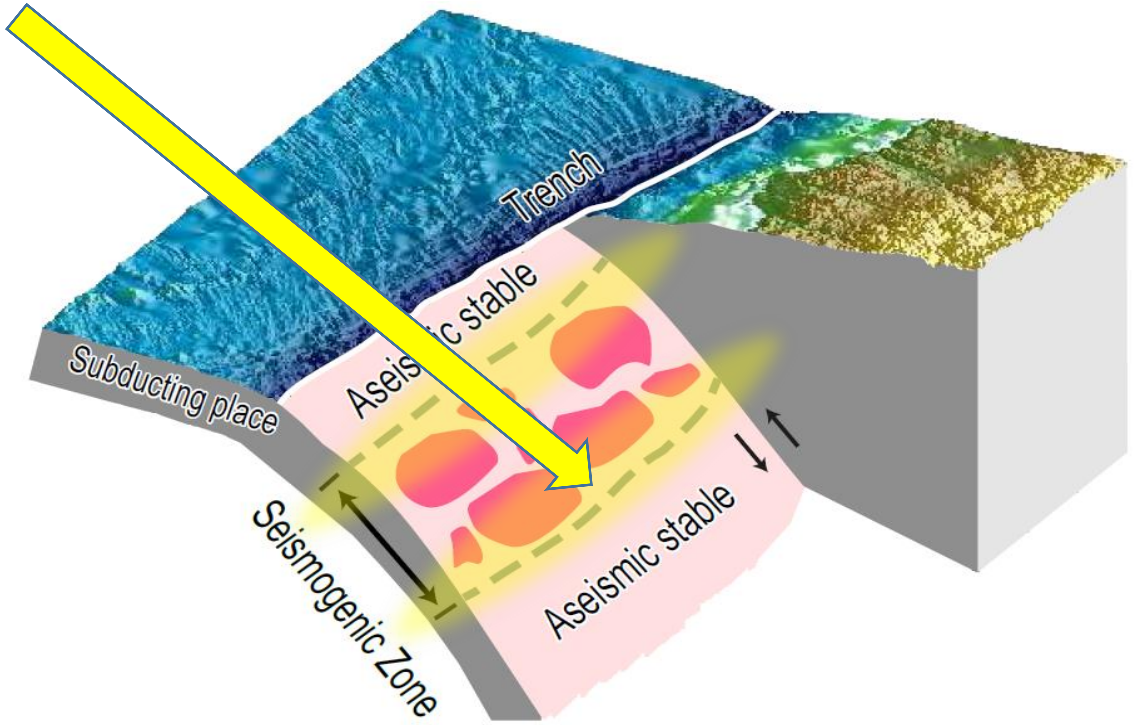

Earthquakes triggered by elongated overstressed regions

Galis et al (GJI 2019)

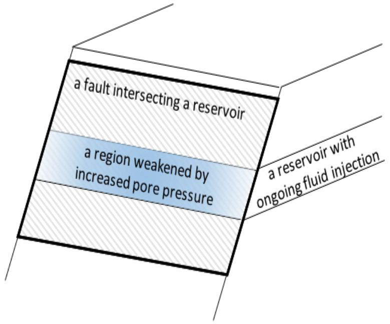

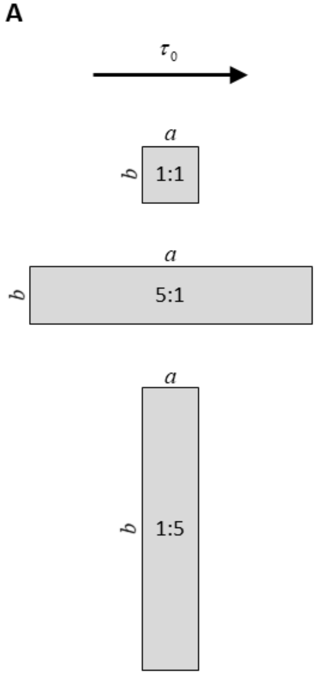

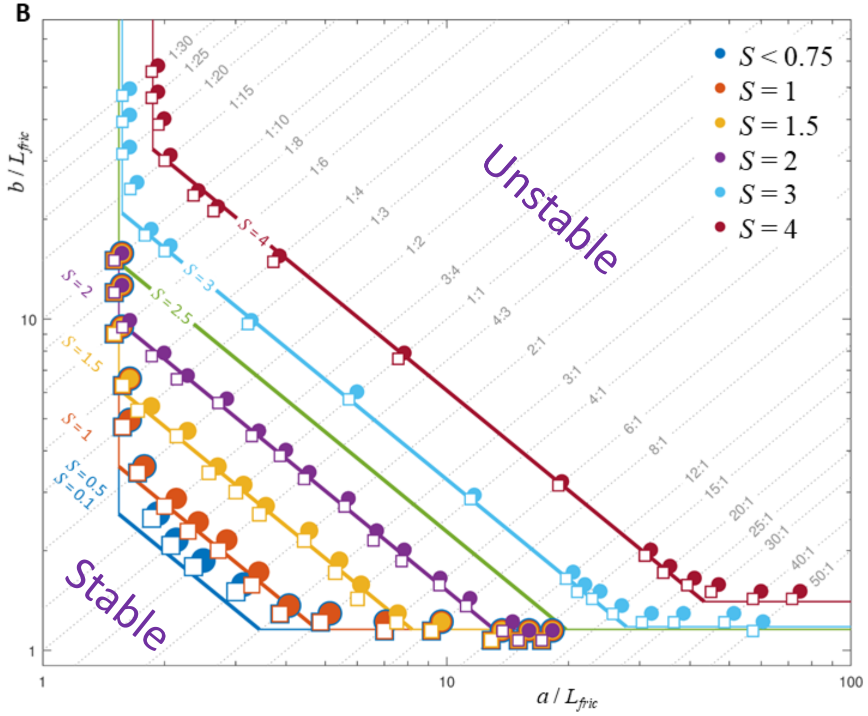

$$S = \frac{\tau_s - \tau_0}{\tau_0 - \tau_d}$$

Elongated earthquake ruptures

2004 Mw 6 Parkfield

Ma et al (2008)

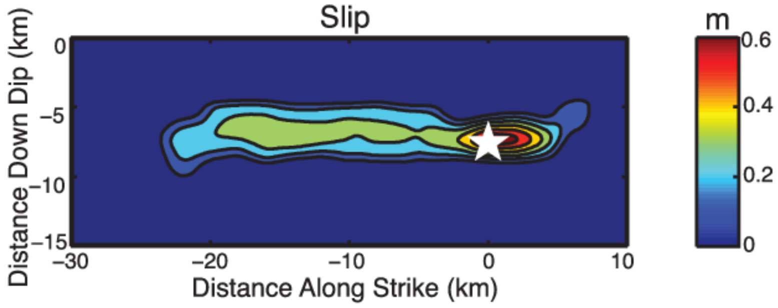

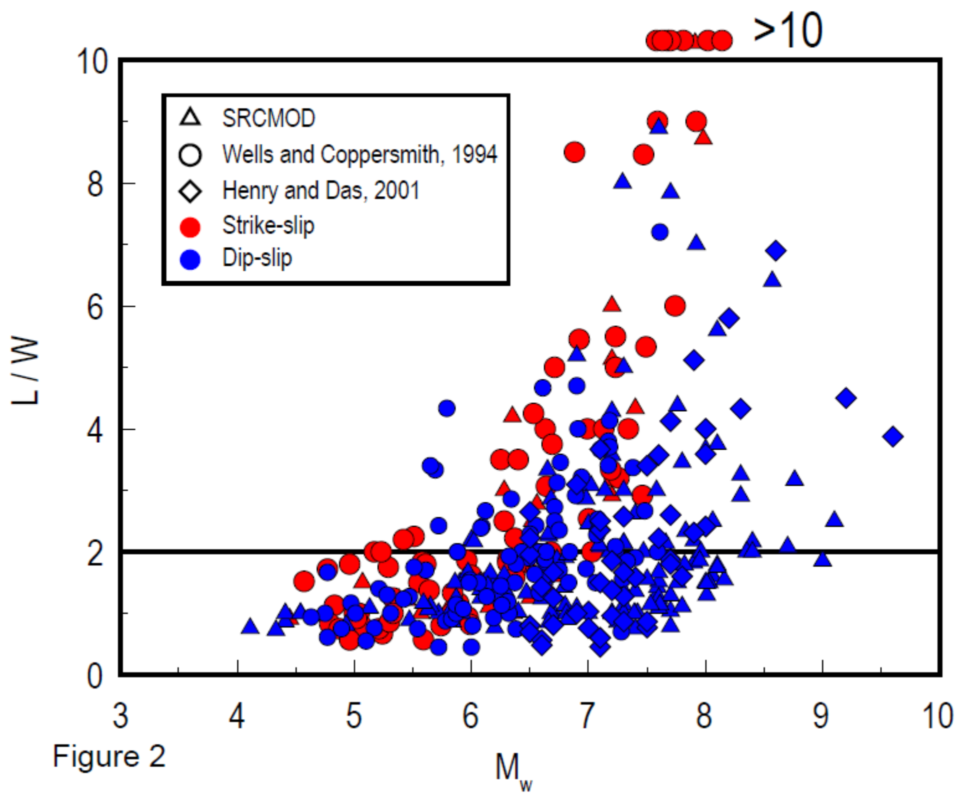

Figure 2

2004 Mw 9.3 Sumatra

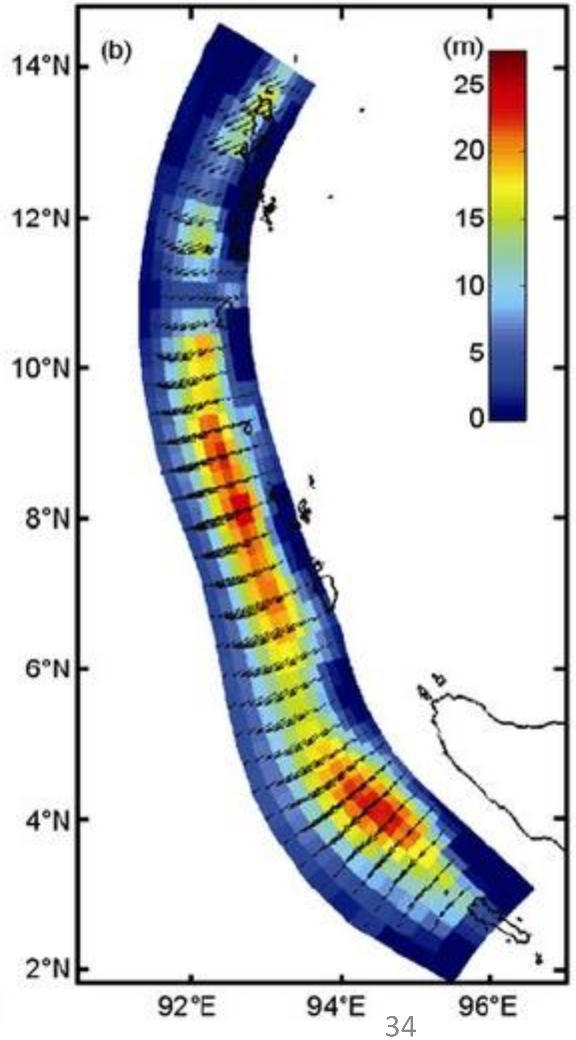

Pulses on long faults with finite seismogenic depth

Weng and Ampuero (2019, 2020)

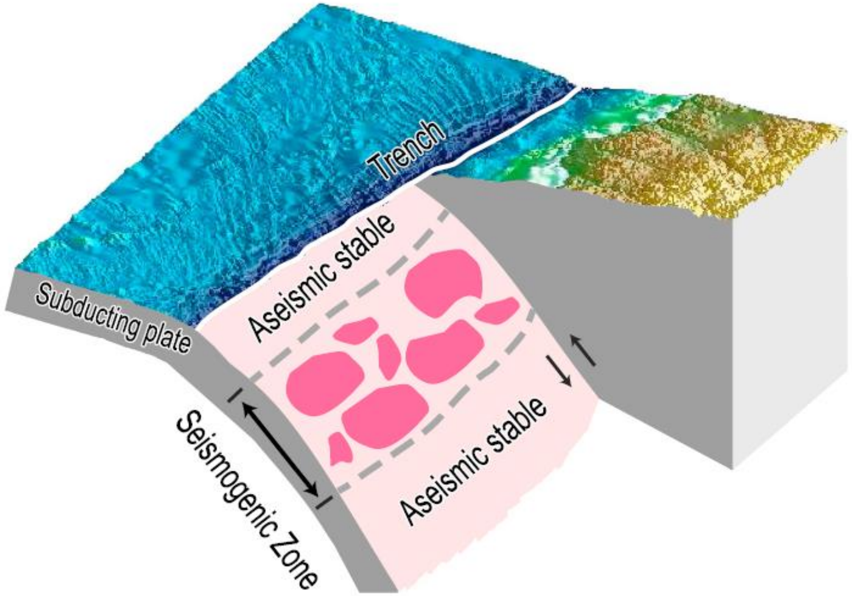

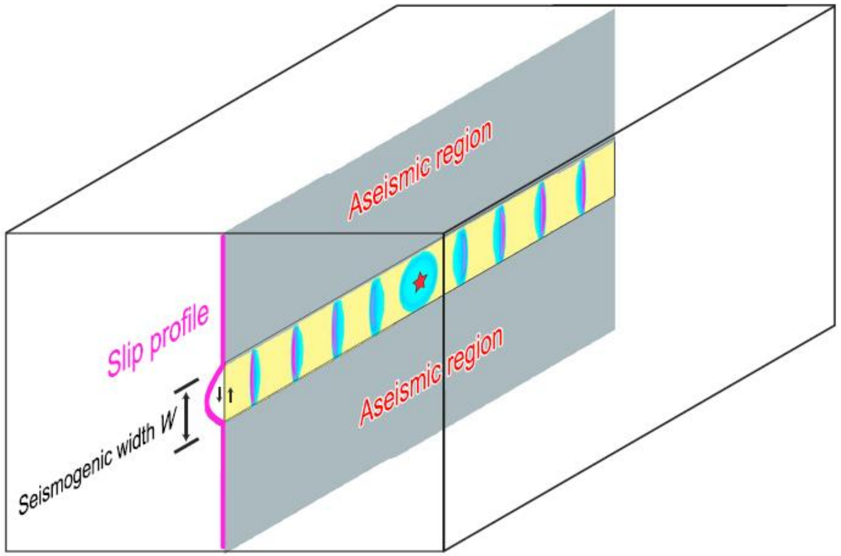

Note: pulse size < W
G depends on $\Delta\tau(x)$ near the rupture front, within a distance <W

Pulses on faults with finite seismogenic depth

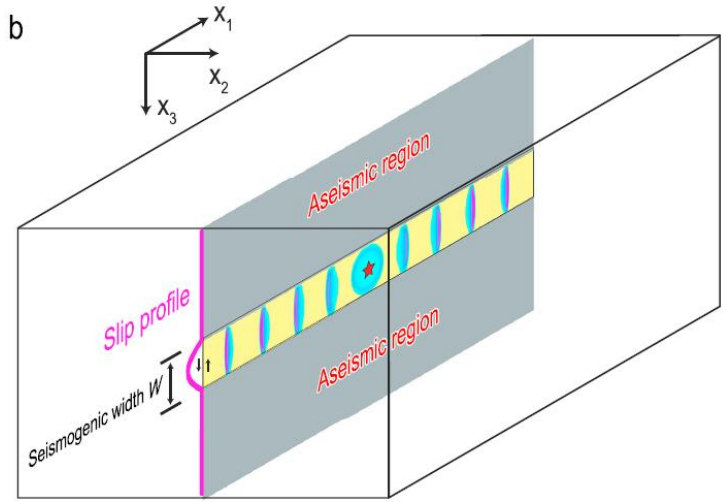

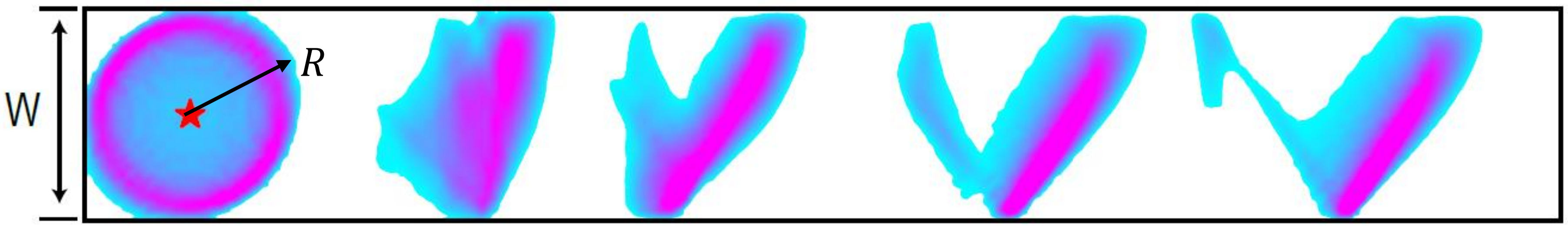

$K \propto \sqrt{R}$
$G \propto R$

$K \propto \sqrt{W}$
$G \propto W$

A crack-tip equation of motion for large earthquakes

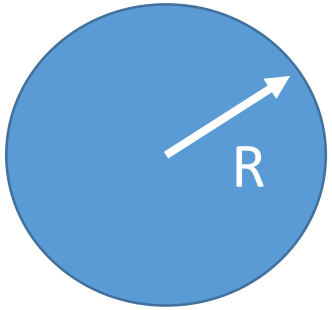

For circular ruptures:

$$G_c = g(\dot{R})\,\frac{\Delta\tau^2 R}{2\mu}$$

(Freund 1989)

For long ruptures **with finite width W**?

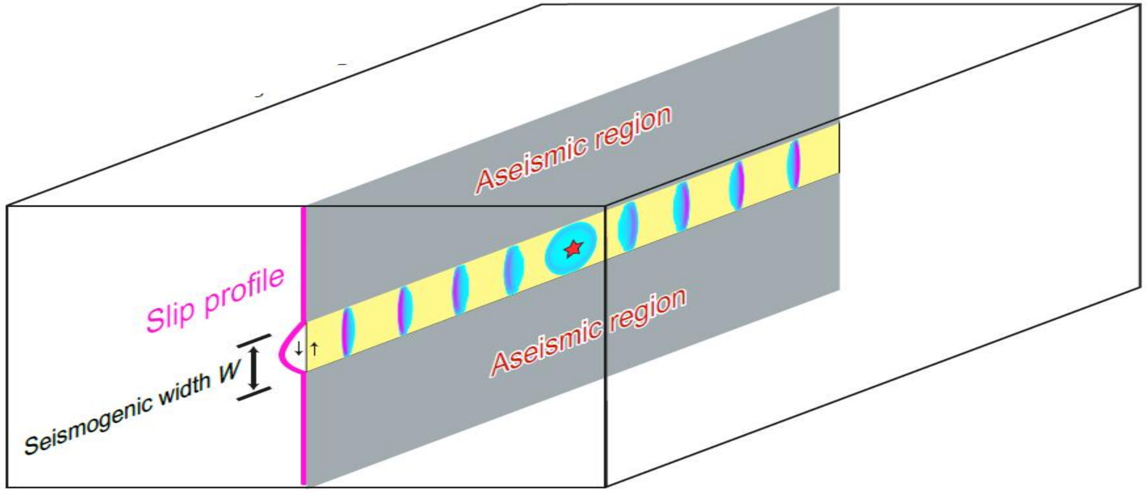

JGR Solid Earth

RESEARCH ARTICLE

10.1029/2019JB017684

The Dynamics of Elongated Earthquake Ruptures

Huihui Weng[1] and Jean-Paul Ampuero[1,2]

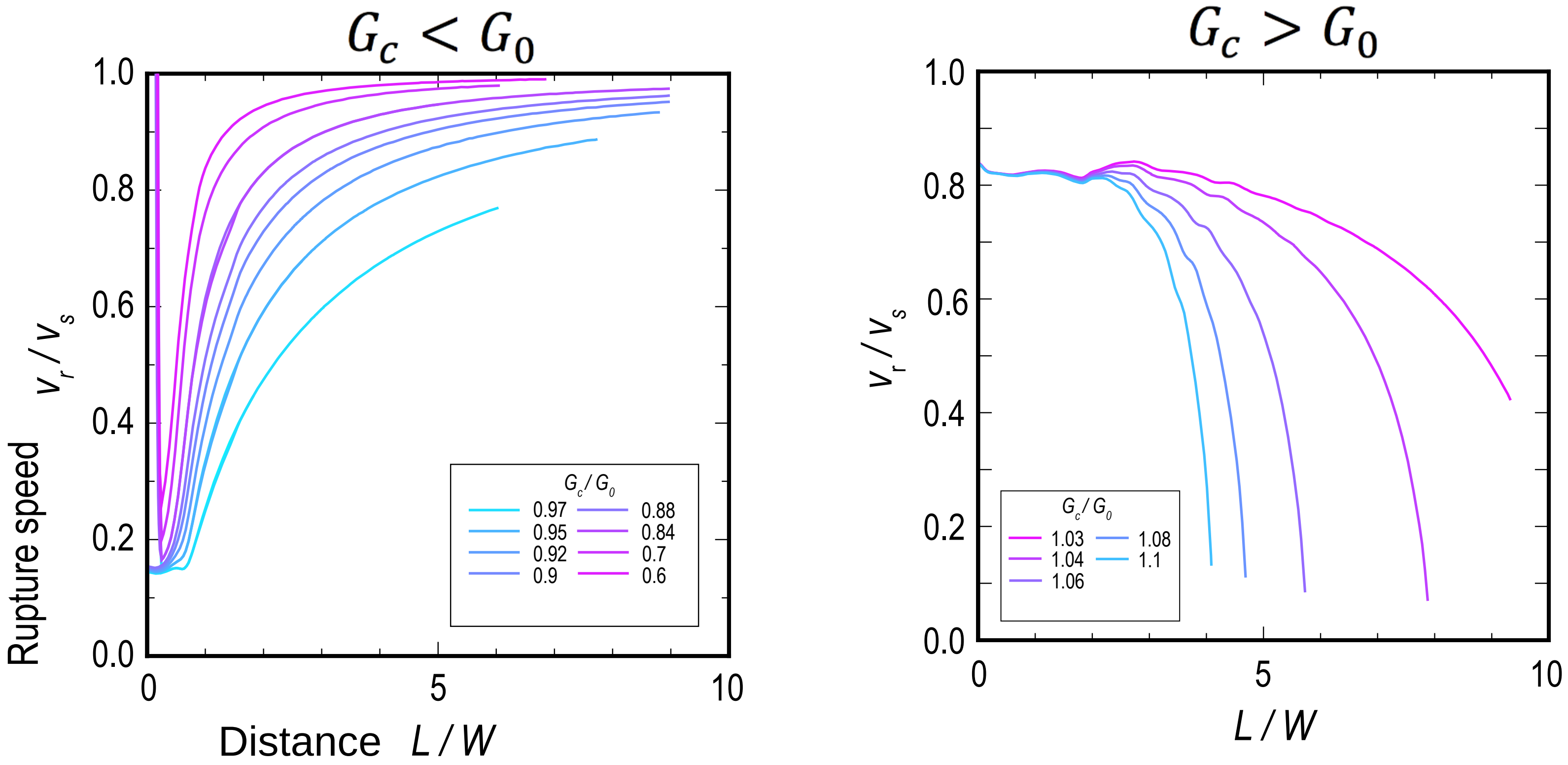

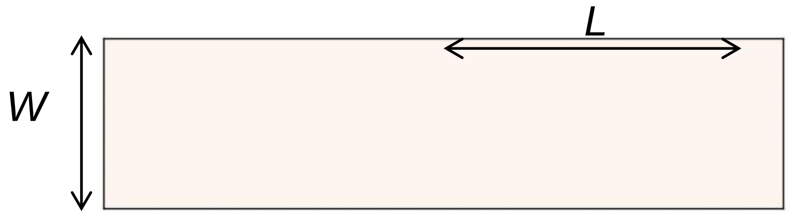

JGR Solid Earth

RESEARCH ARTICLE
10.1029/2019JB017684

The Dynamics of Elongated Earthquake Ruptures

Huihui Weng[1] and Jean-Paul Ampuero[1,2]

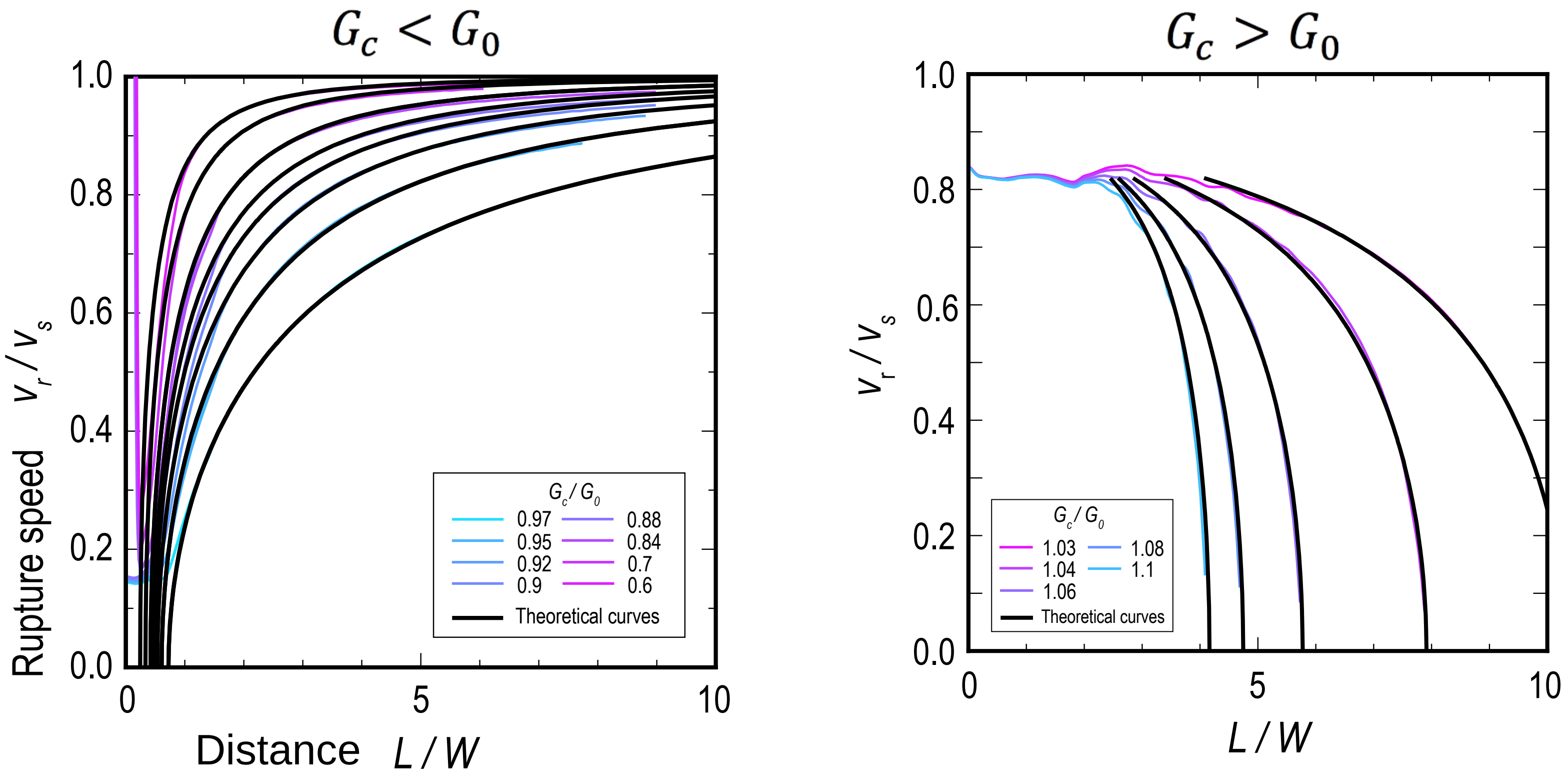

$$1 - G_c/G_0 = \mathcal{M}(v_r) \cdot \dot{v}_r$$

"Force" = "Mass" × Acceleration

Implications for rupture arrest

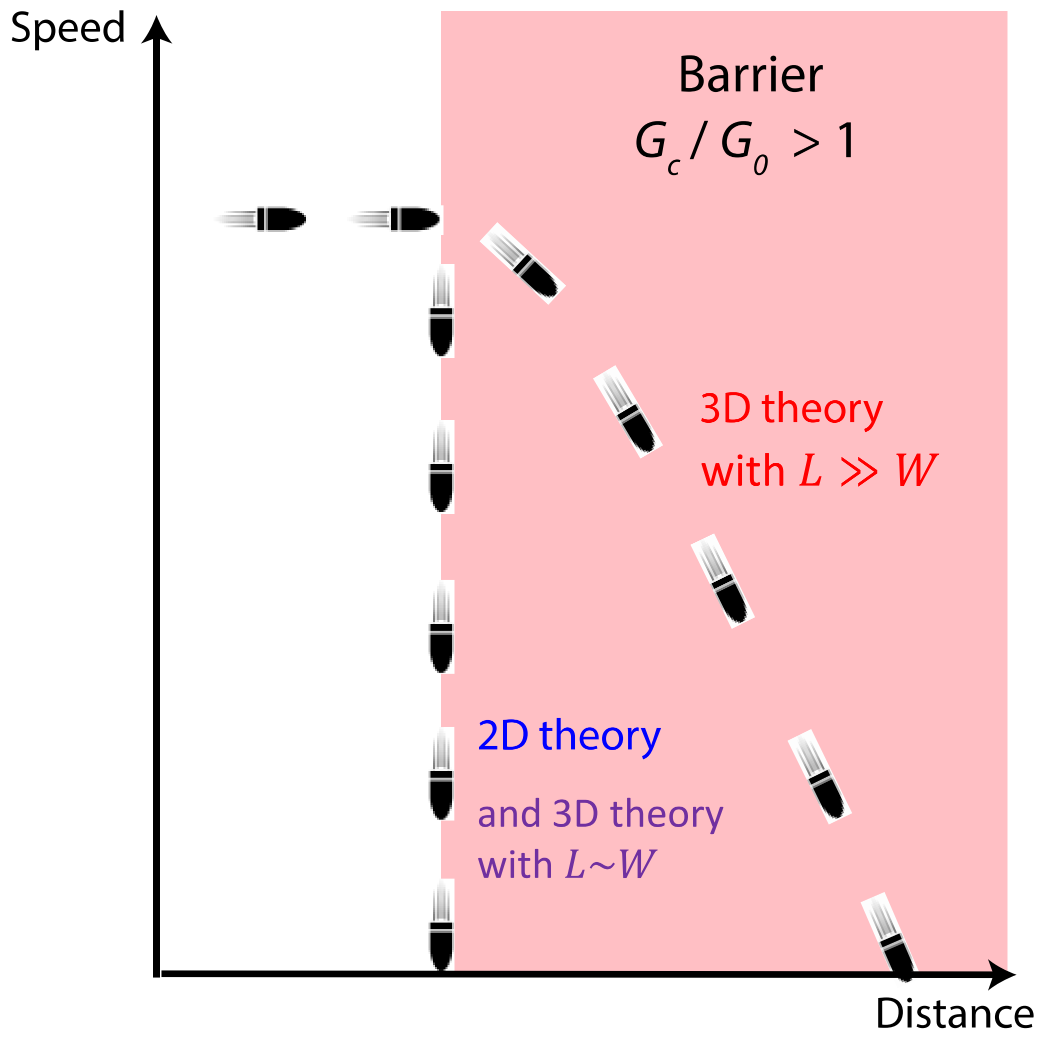

Determine earthquake size

Rupture potential

$$\Phi(L) = \int_0^L \mathcal{F}(G_c/G_0 \quad)dL$$

Rupture arrest condition

$$\Phi(L_1) = \Phi(L_2)$$

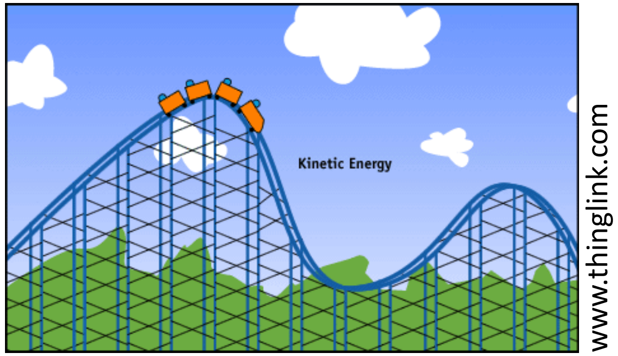

Analogy: gravity potential

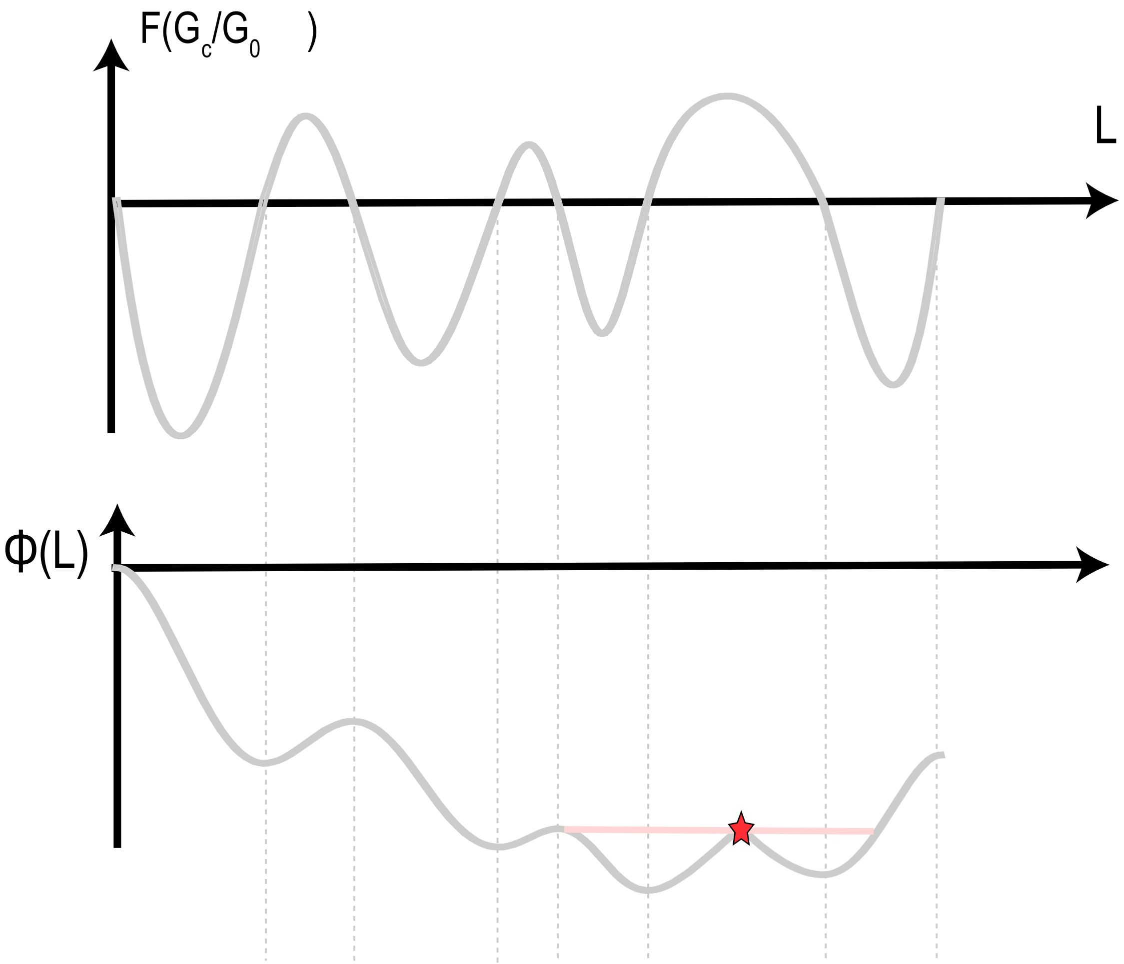

Determine earthquake size

Rupture potential

$$\Phi(L) = \int_0^L \mathcal{F}(G_c/G_0 \quad)dL$$

$$\Phi(L_1) = \Phi(L_2)$$

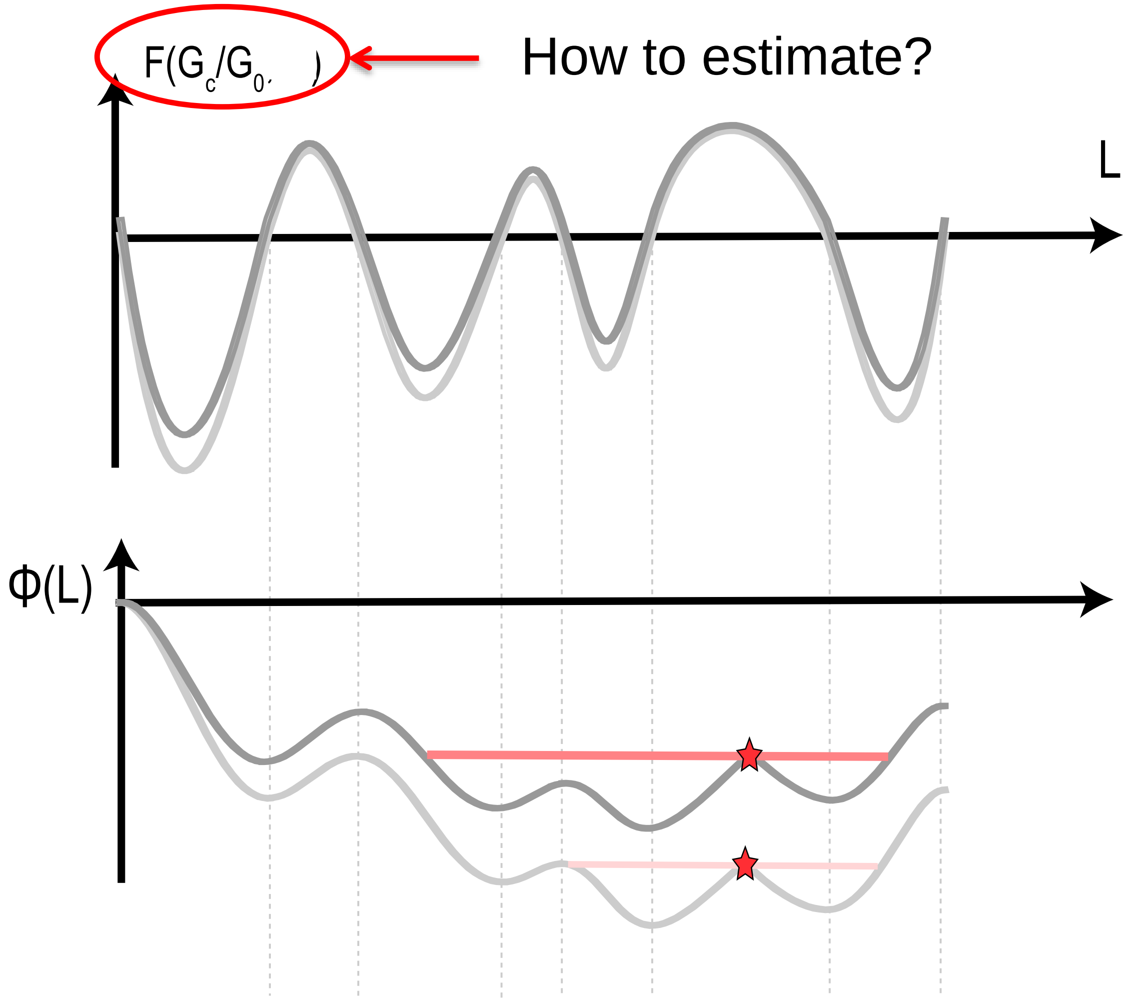

Arrest of long ruptures

Weng and Ampuero (2019)

Rupture length/width

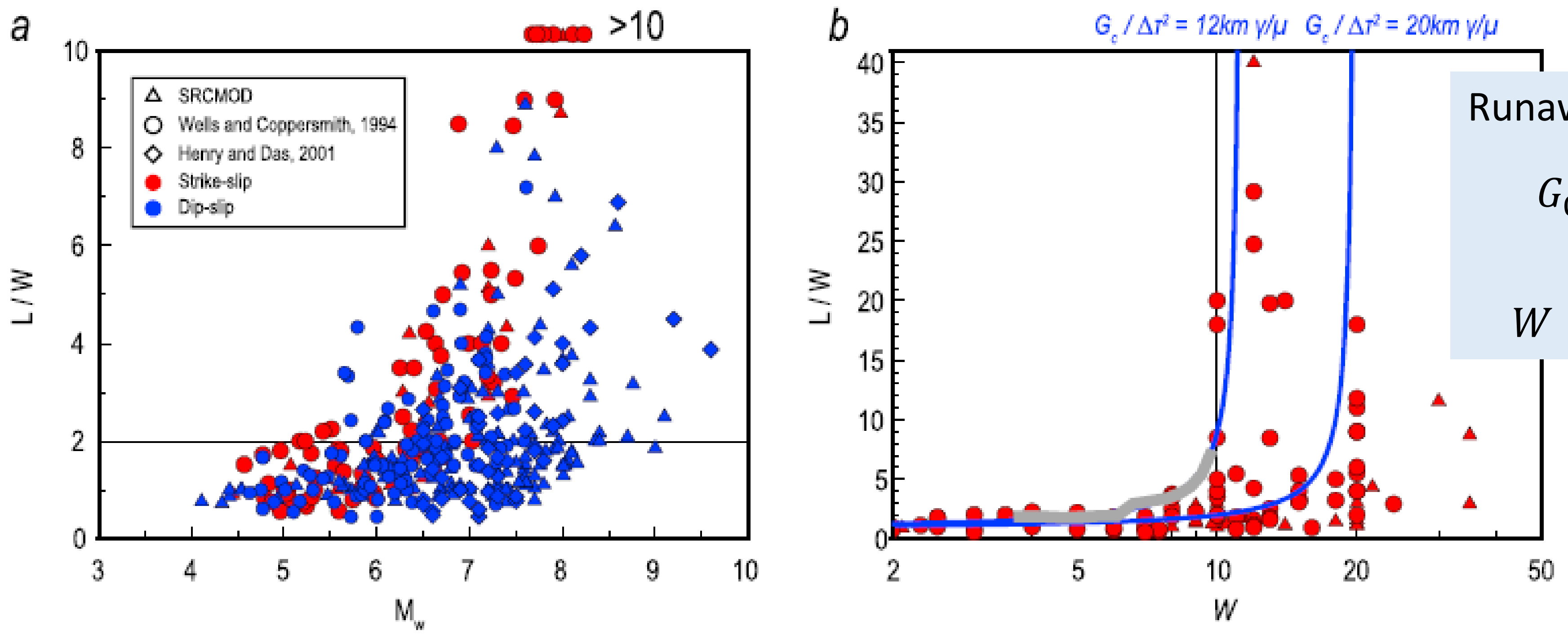

Earthquake magnitude

Rupture width

Runaway condition:

$$G_0 = \frac{\gamma \Delta\tau^2 W}{\mu} > G_c$$

$$W > W_c = \mu G_c / \gamma \Delta\tau^2$$

Constraints on energy release rate G_0

$$G_0 = \frac{\Delta\tau^2 W}{\pi\mu}$$

$$\Delta\tau = \frac{C\mu D}{W}$$

$$G_0 \sim \frac{\mu}{W} D^2$$

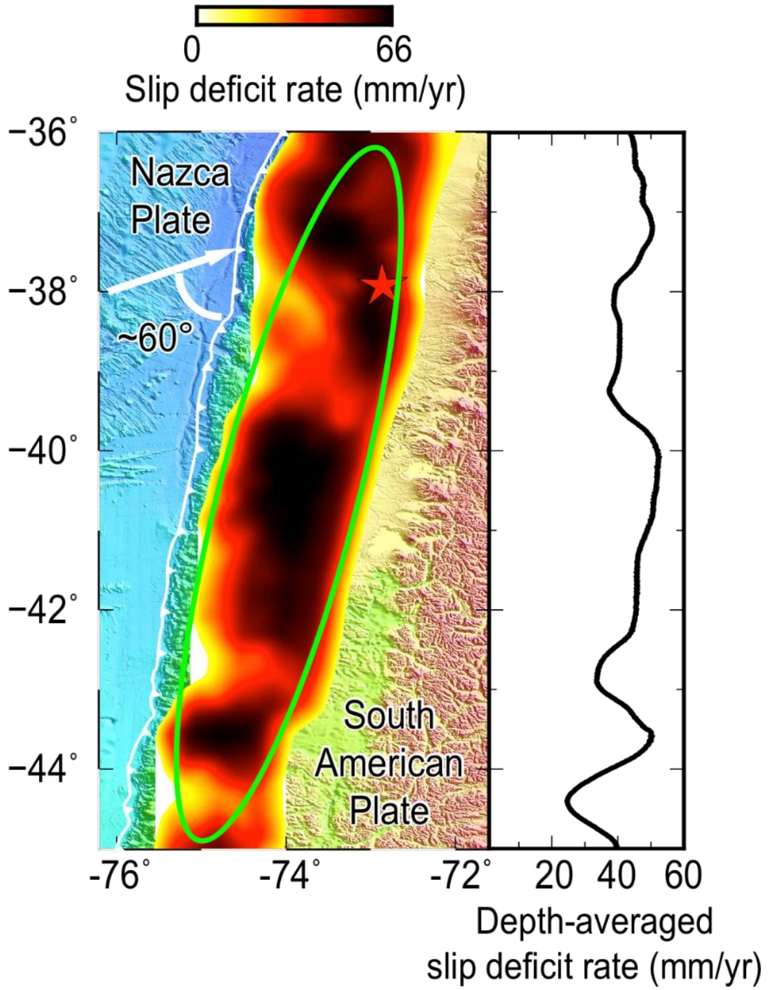

Constraints on fracture energy G_c

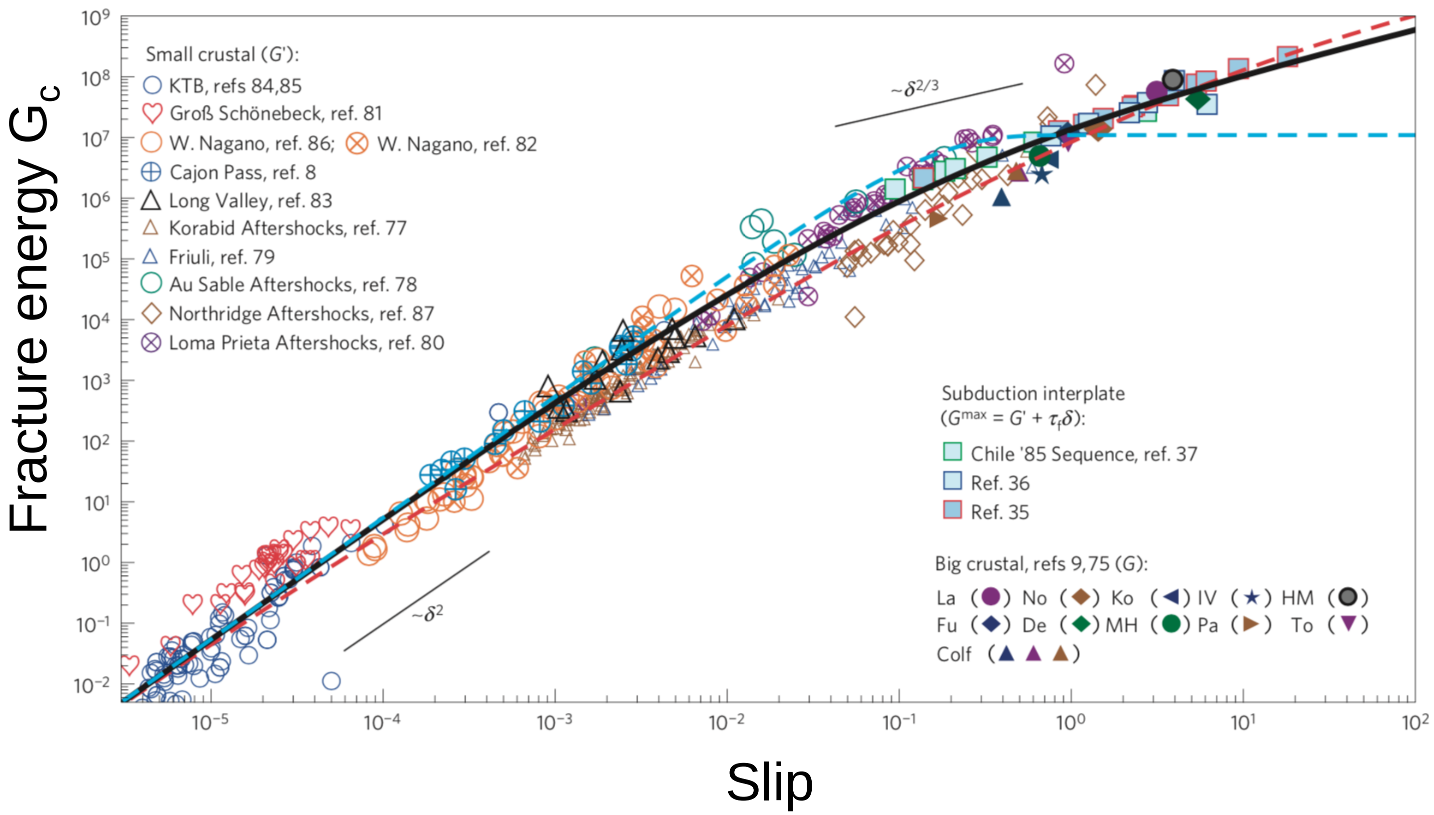

$$G_c \sim D^{0.7}$$

Viesca and Garagash, 2015

Physical constraints on earthquake size

Runaway rupture if $G_0 > G_c$

$$\left.\begin{matrix} G_c \sim D^{0.7} \\ G_0 \sim D^2 \end{matrix}\right\}$$ Runaway if $D > D^{run}$

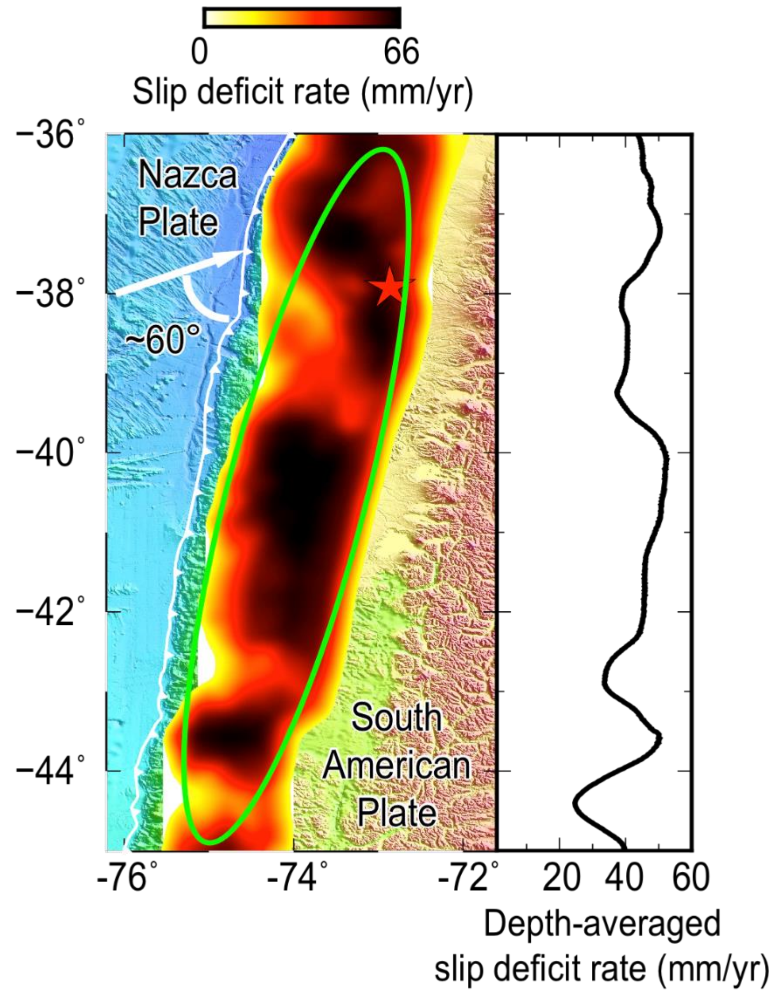

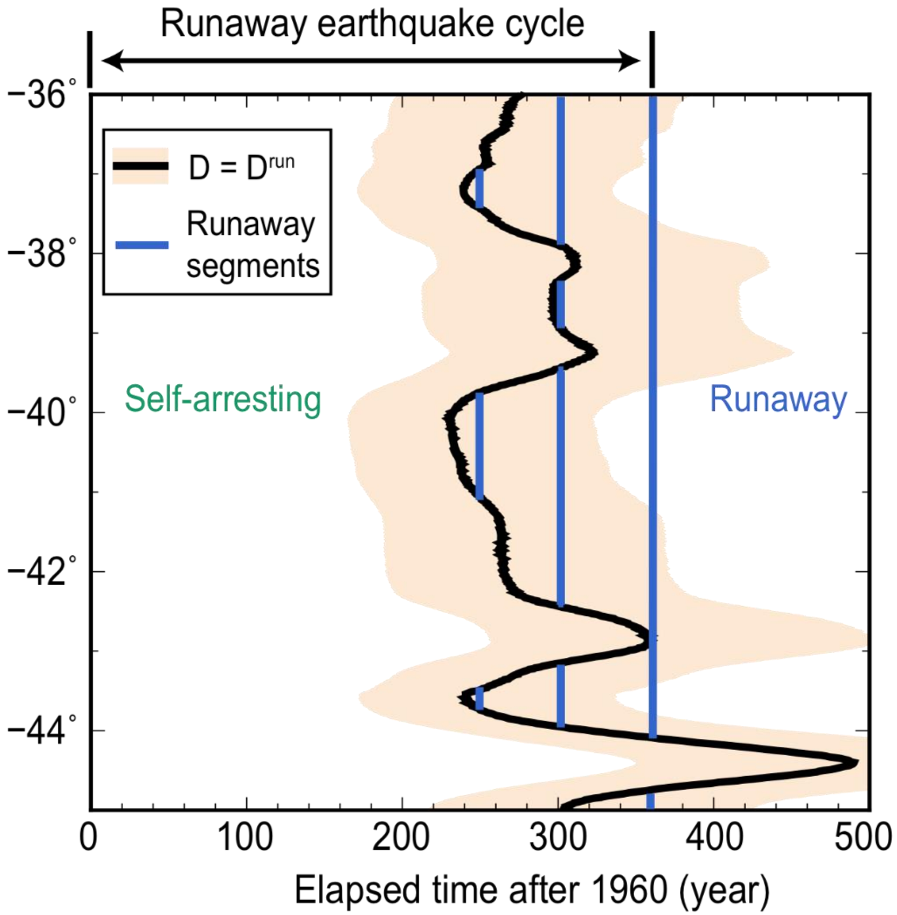

Connecting models of natural and induced earthquakes

Natural and induced seismicity share some common features
Opportunities to understand rupture processes at a fundamental level

Classical fracture mechanics provides useful insights on rupture initiation and arrest
New fracture mechanics theory can advance understanding of large earthquakes

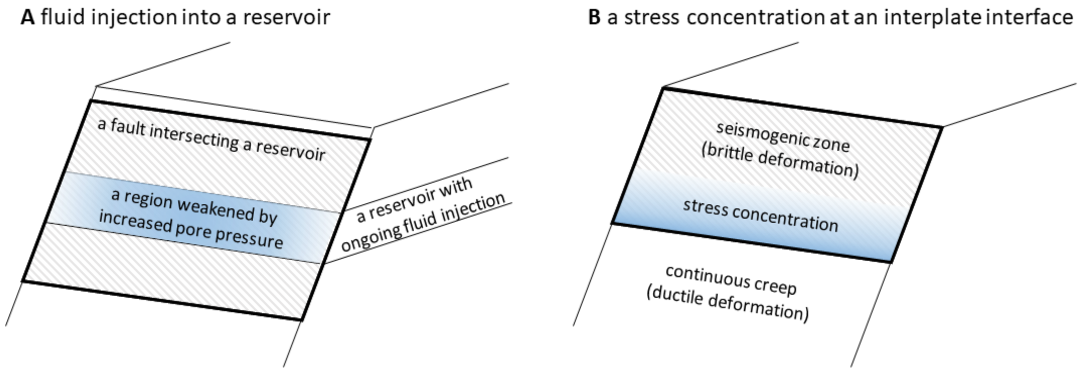

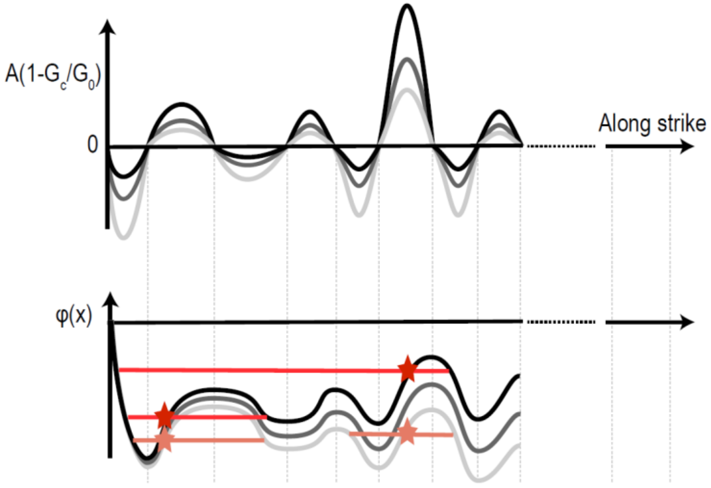

Overview

- Fracture mechanics of rupture arrest
- Rupture dynamics of very long ruptures
- Application to Groningen Mmax

Connecting theory, simulations,
and observations of natural and induced earthquakes

Application to Groningen Mmax

Galis et al (2017, 2019)

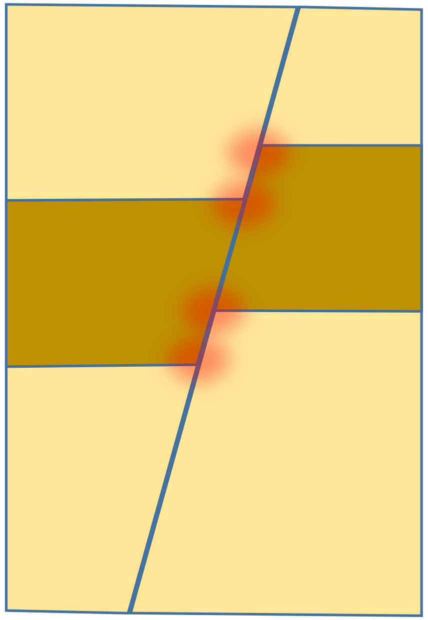

2D

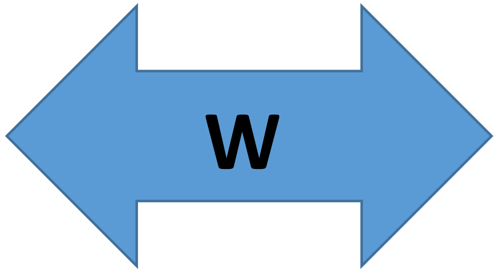

2.5D

Weng and Ampuero (2019, 2020)

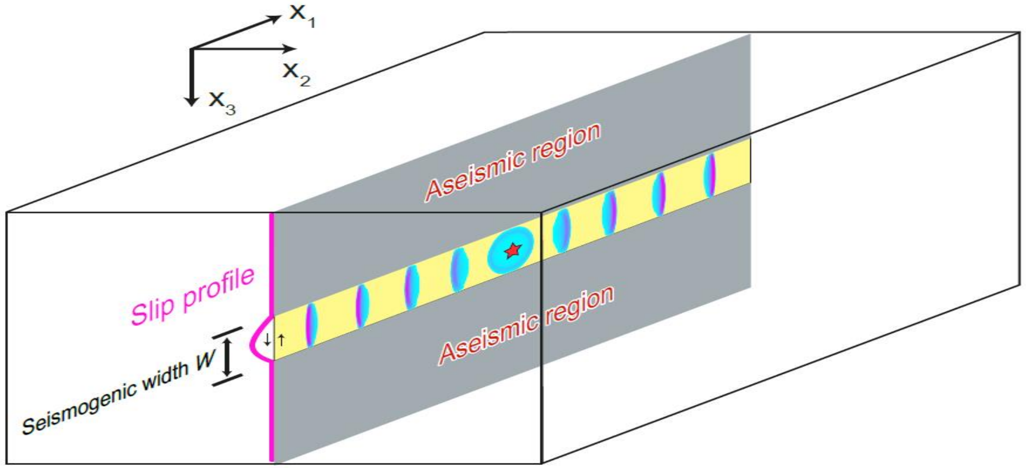

3D

Rupture arrest, Mmax

Needs:
Map of faults and offsets
Map of reservoir thickness
Stressing rates due to compaction
Material strength: Gc vs D relation

Application to Groningen Mmax

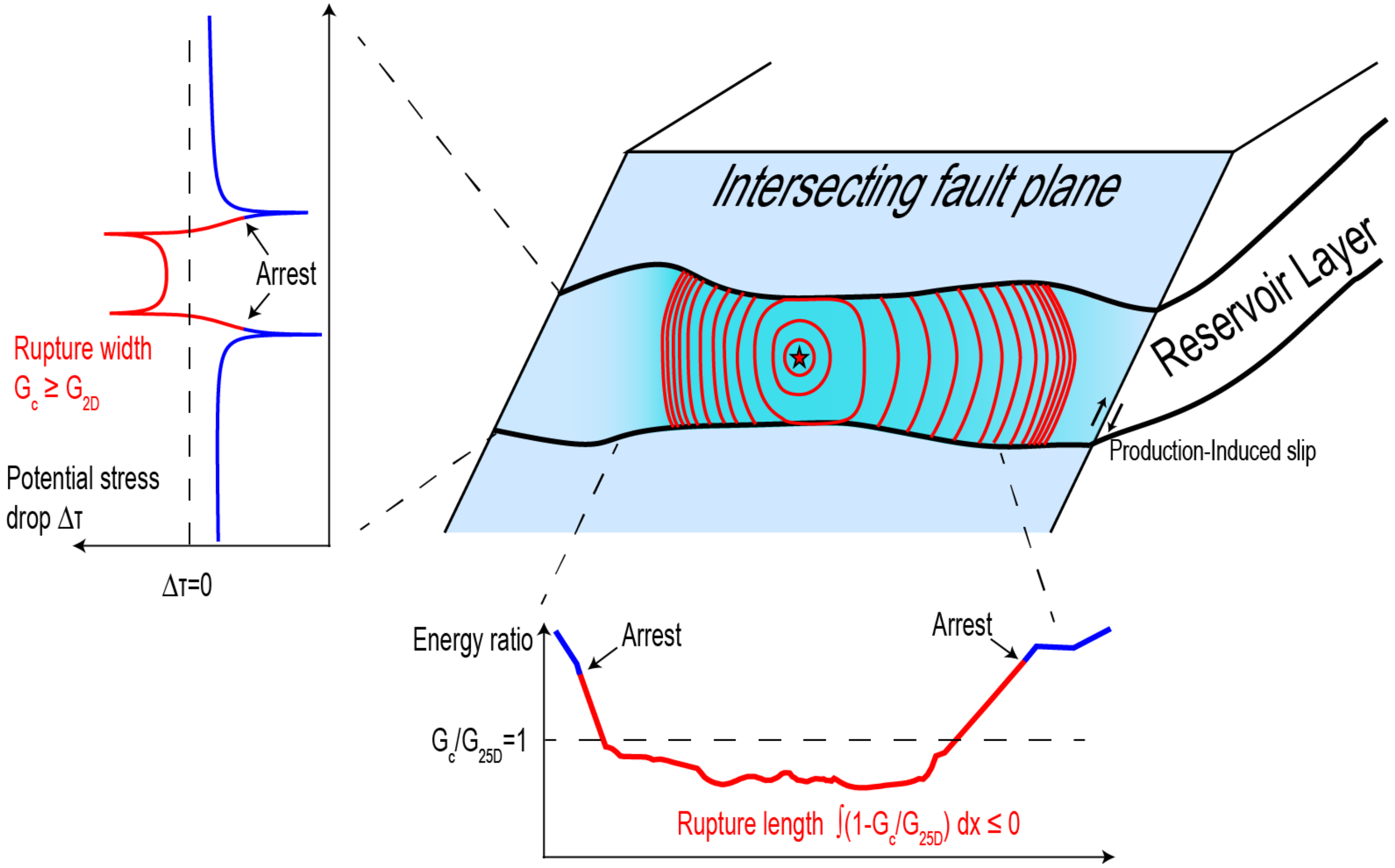

Application to Groningen Mmax

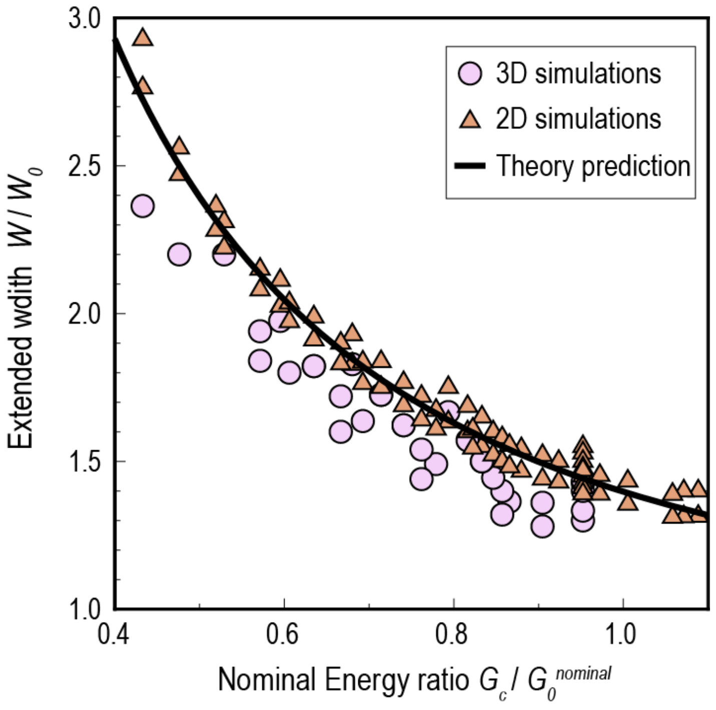

With 3D theory extended to:

1. Depth-dependent stress and Gc
2. Laterally variable W
3. Non-prescribed W

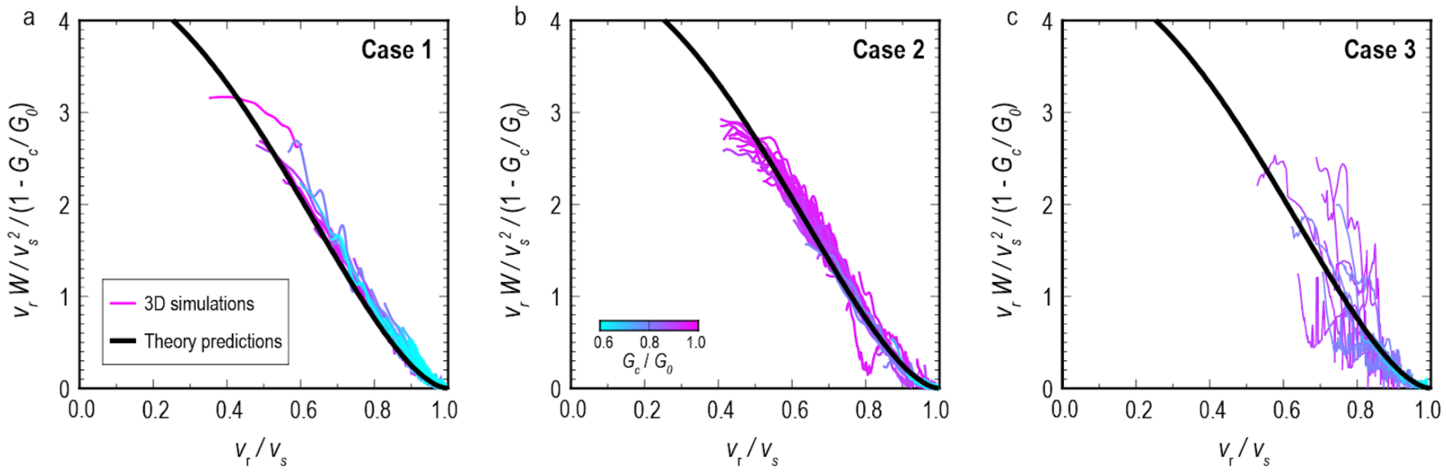

Application to Groningen Mmax

Scaling of fracture energy vs slip
constrained by lab experiment and earthquake observations

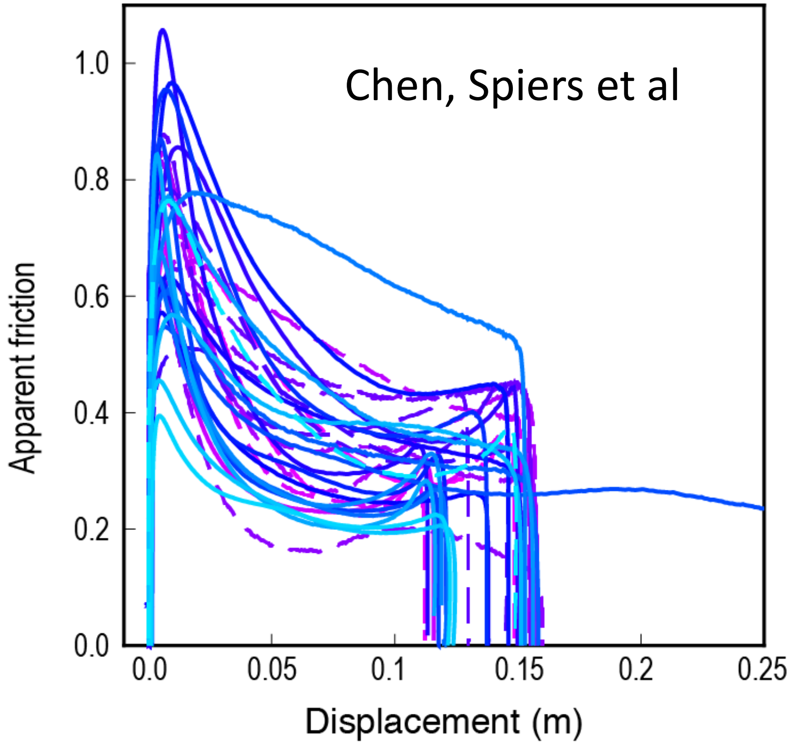

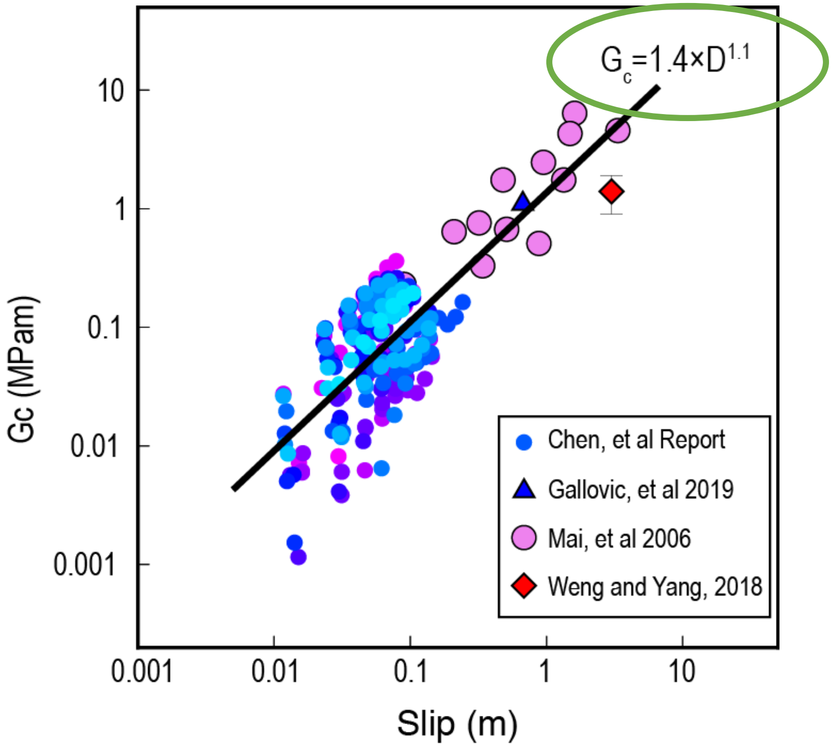

Scaling steeper than linear prevents runaway down-dip

Application to Groningen Mmax

Example evolution of
Mmax on one fault

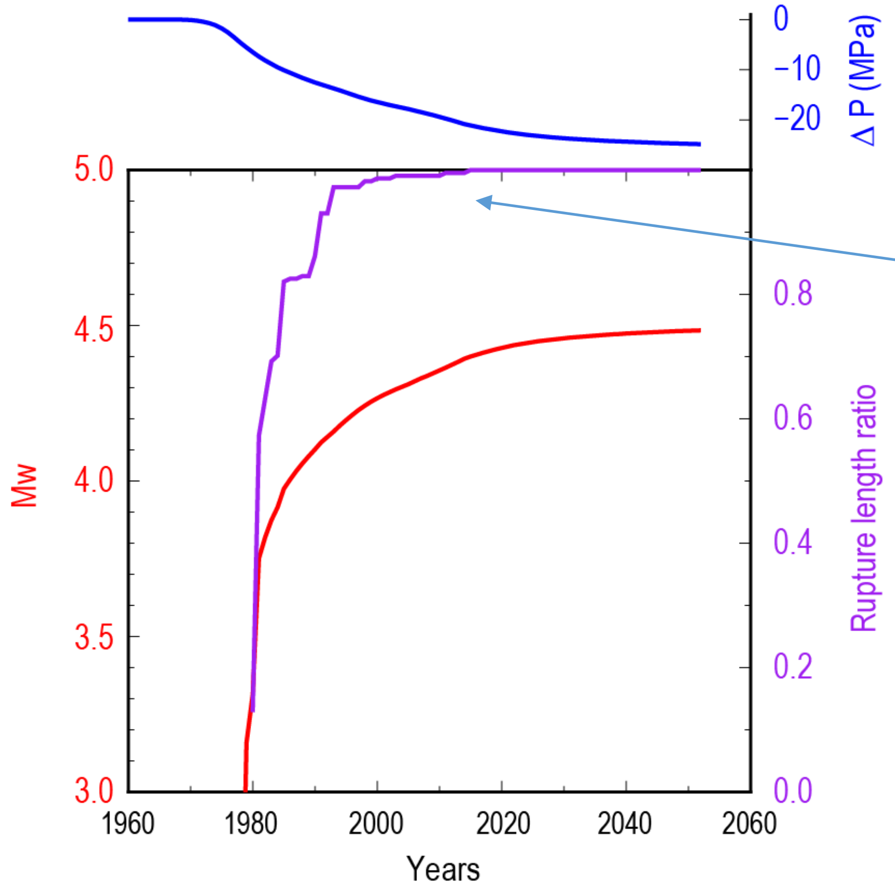

Onset of
full fault length rupture

Application to Groningen Mmax

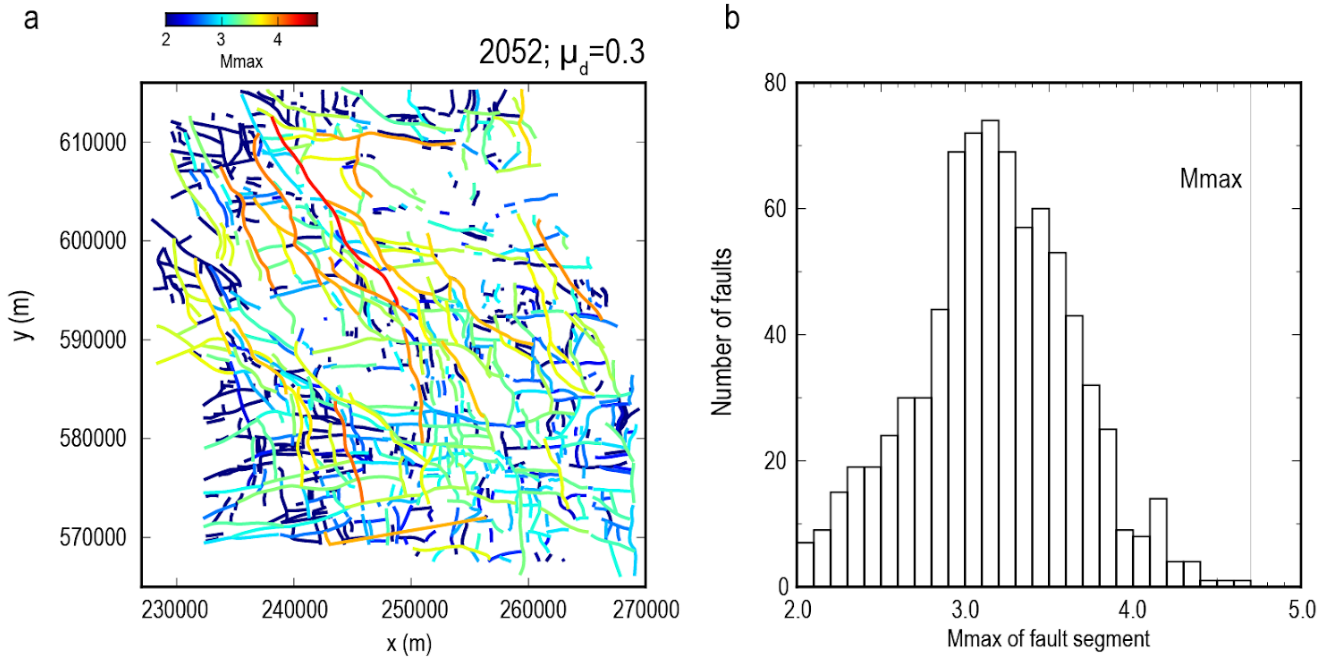

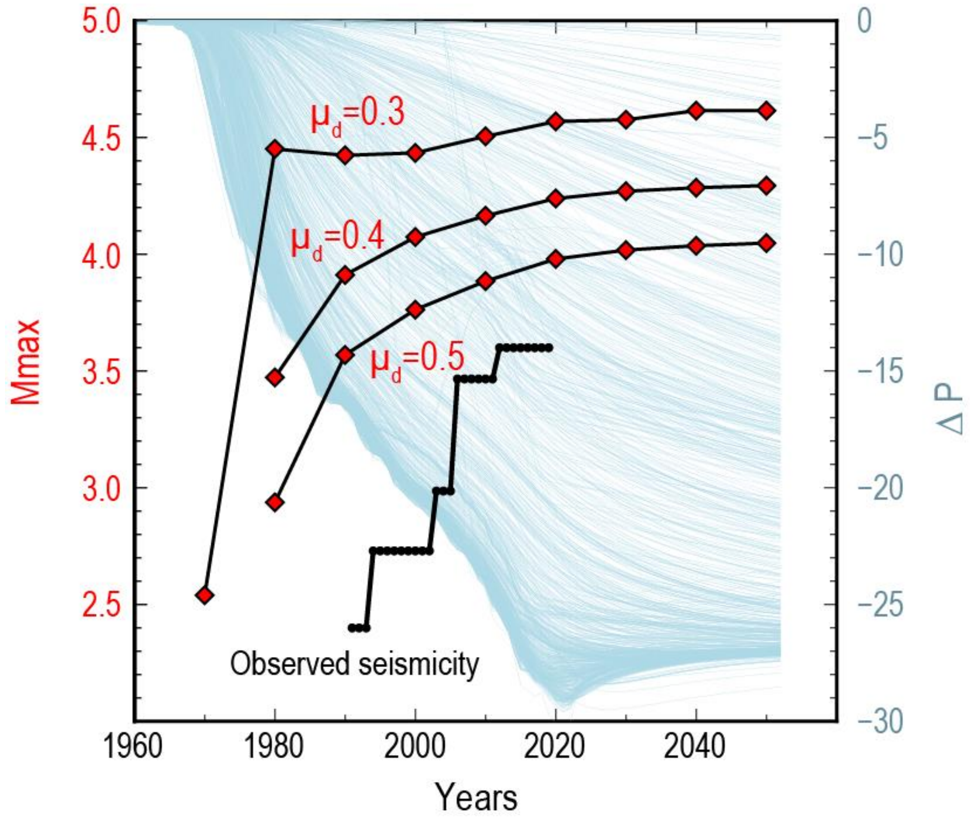

Computational efficiency of the model enables reservoir-scale application and sensitivity analyses

Crustal Stress and Earthquake Triggering

Mark D. Zoback

Benjamin M. Page Professor of Geophysics, *Emeritus*

Stanford | Stanford Center for Induced and Triggered Seismicity

School of Earth, Energy & Environmental Sciences

Stanford | NATURAL GAS INITIATIVE

School of Earth, Energy & Environmental Sciences and Precourt Institute for Energy

LELAND STANFORD JUNIOR UNIVERSITY
DIE LUFT DER FREIHEIT WEHT
1891

Groningen Mmax Workshop

June 13-15, 2022

Three Topics

1. Relevant Learnings From Injection Induced Seismicity

2. Poroelastic Stress Paths and Earthquakes Induced by Depletion

3. Mmax and the Potential for Faulting in the Carboniferous

Motivation – Can We Quantify Barriers to Fault Propagation That Would Limit Mmax?

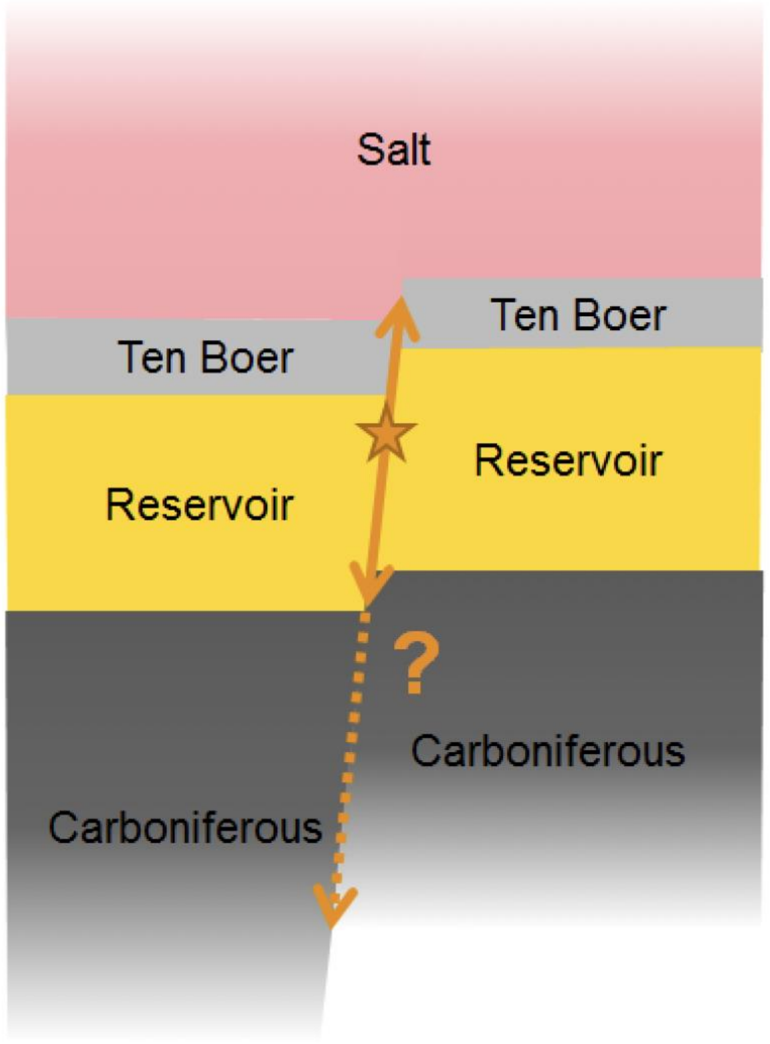

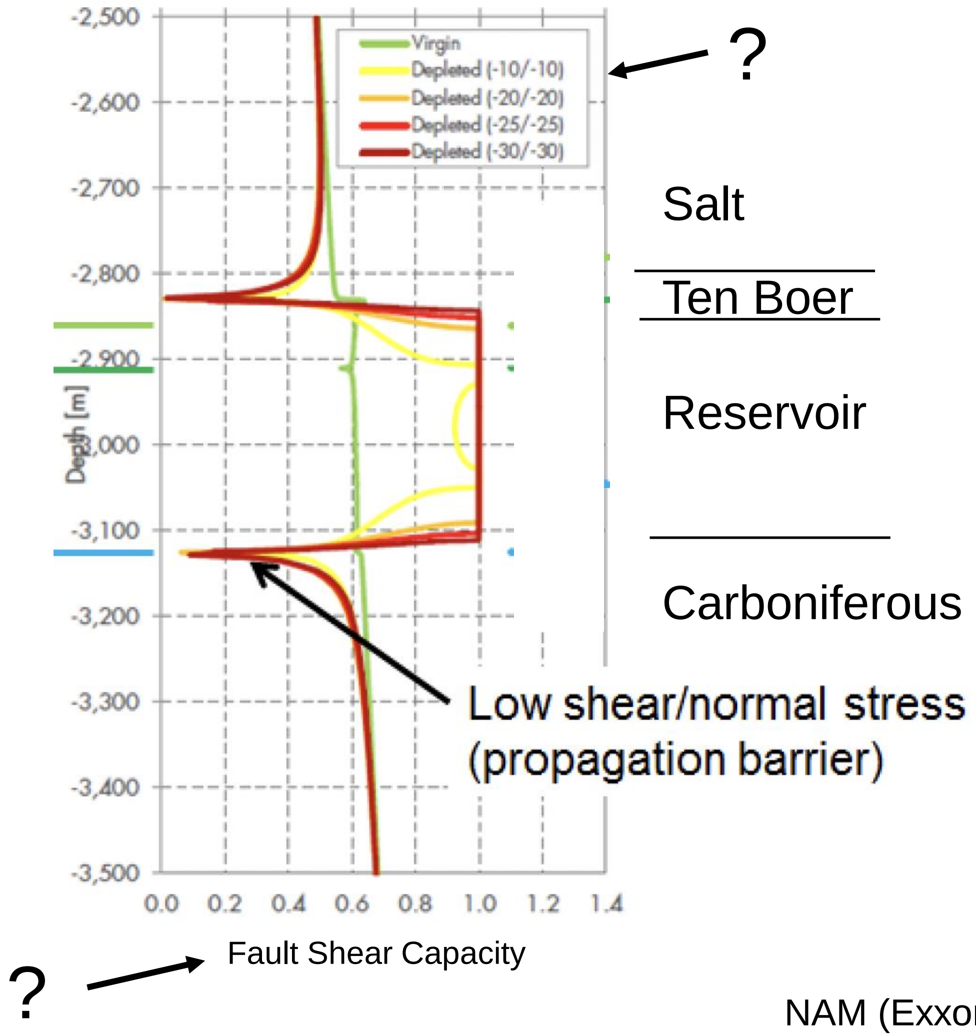

NAM (ExxonMobil Mmax) 2016

Barriers to Fault Propagation are Lithologically Controlled, Quantitatively Estimated and Can Help Understand Mmax

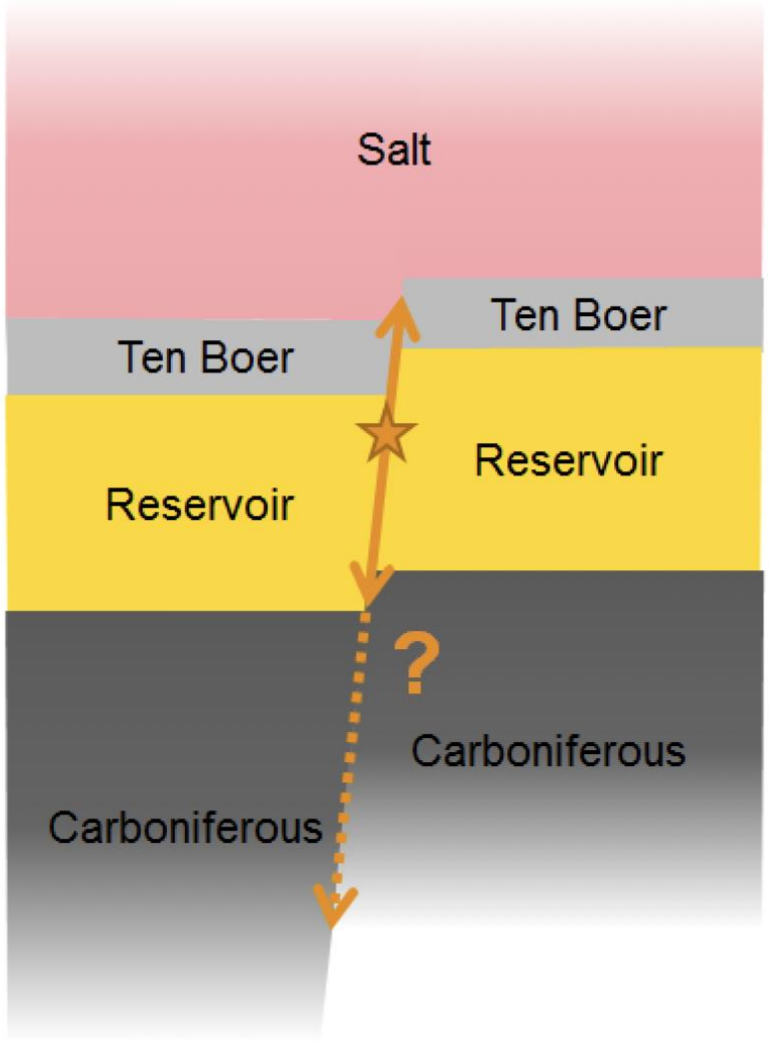

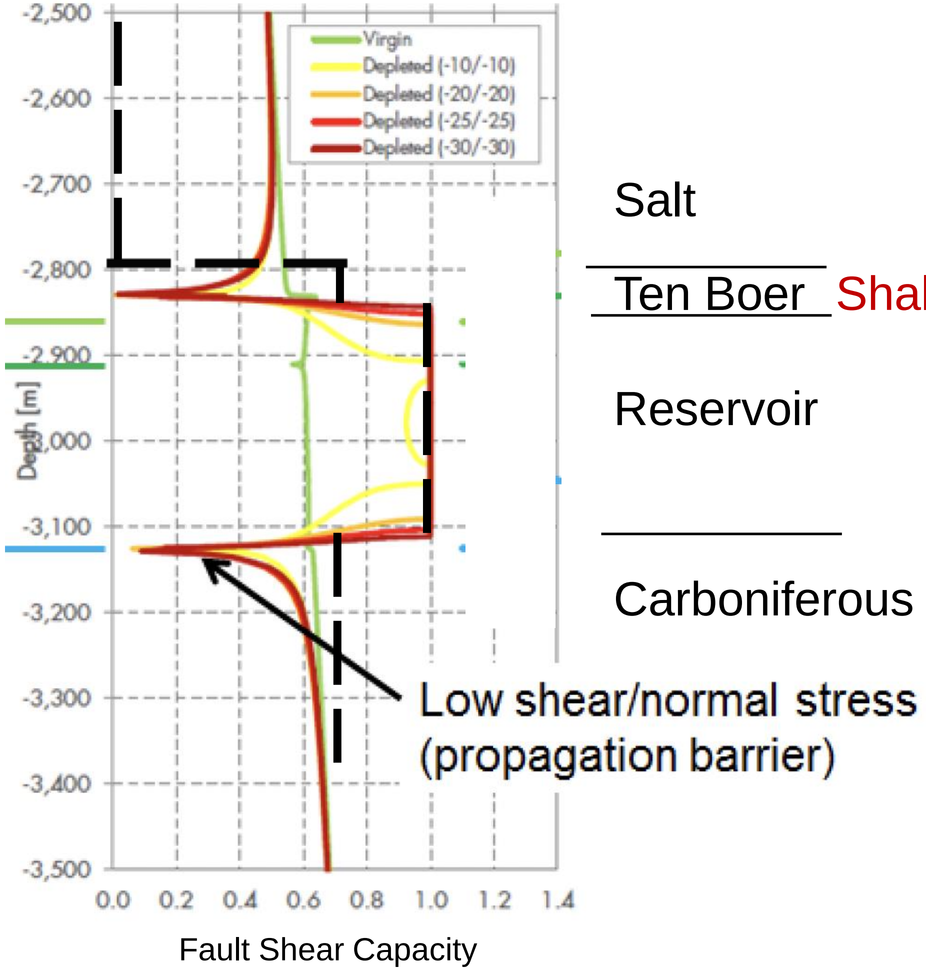

Salt

Ten Boer Shale

Reservoir

Carboniferous Shale

NAM (ExxonMobil Mmax) 2016

Three Topics*

1. Relevant Learnings From Injection Induced Seismicity

2. Poroelastic Stress Paths and Earthquakes Induced by Depletion

3. Mmax and the Potential for Faulting in the Carboniferous

**From the perspective of field (and lab) data interpreted in the context of basic geomechanical principles.*

Three Topics

1. Relevant Learnings From Injection Induced Seismicity
   - Applicability of Coulomb Faulting Theory
   - It is Commonly Observed that Sedimentary Rocks (As Well As Crystalline Basement) are in Frictional Equilibrium
   - Stress Magnitudes Vary Markedly with Lithology in
   - Sedimentary Sequences

1. Poroelastic Stress Paths and Earthquakes Induced by Depletion

3. Mmax and the Potential for Faulting in the Carboniferous

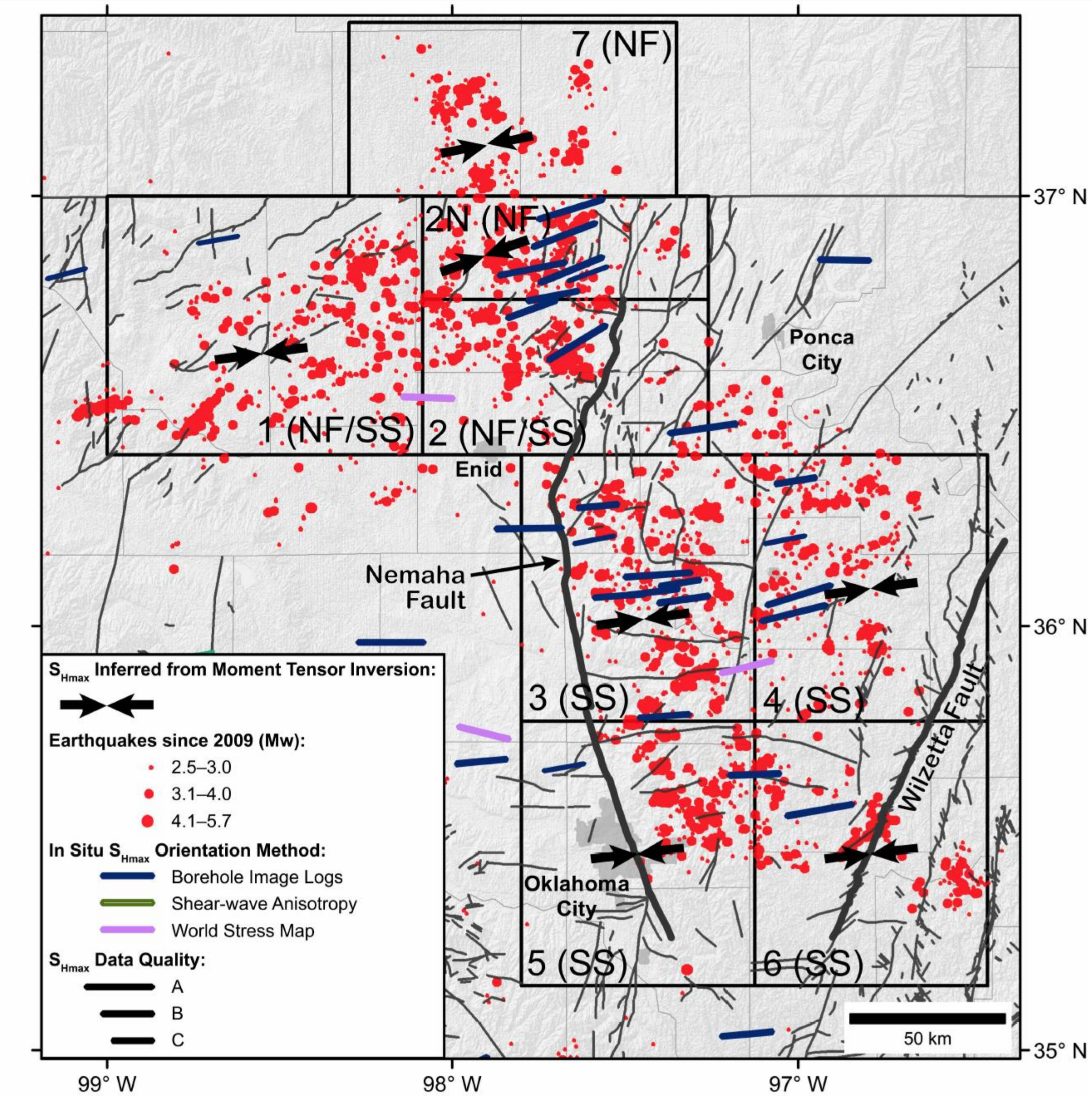

Alt and Zoback (BSSA, 2017)

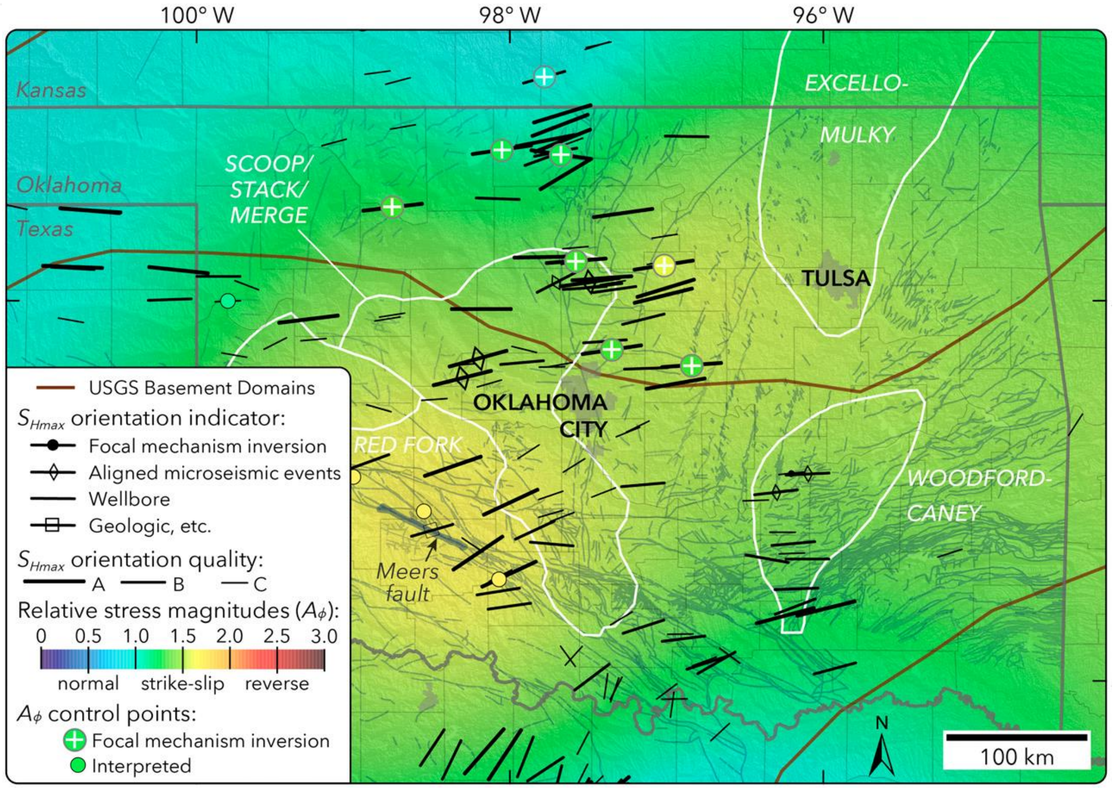

Lund Snee and Zoback (AAPG Bull., 2022)

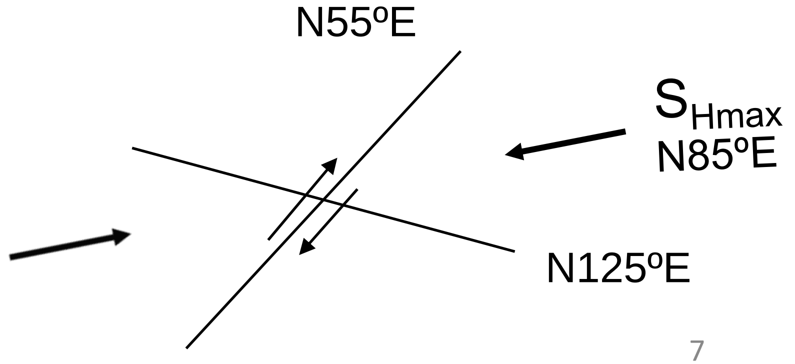

Basement Fault Activation Before Larger Earthquakes in Oklahoma and Kansas

Yongsoo Park*, Greg Beroza and Bill Ellsworth

In Review – *The Seismic Record*

**Poster Presentation by Yongsoo Park, in Session 7, Wednesday Afternoon*

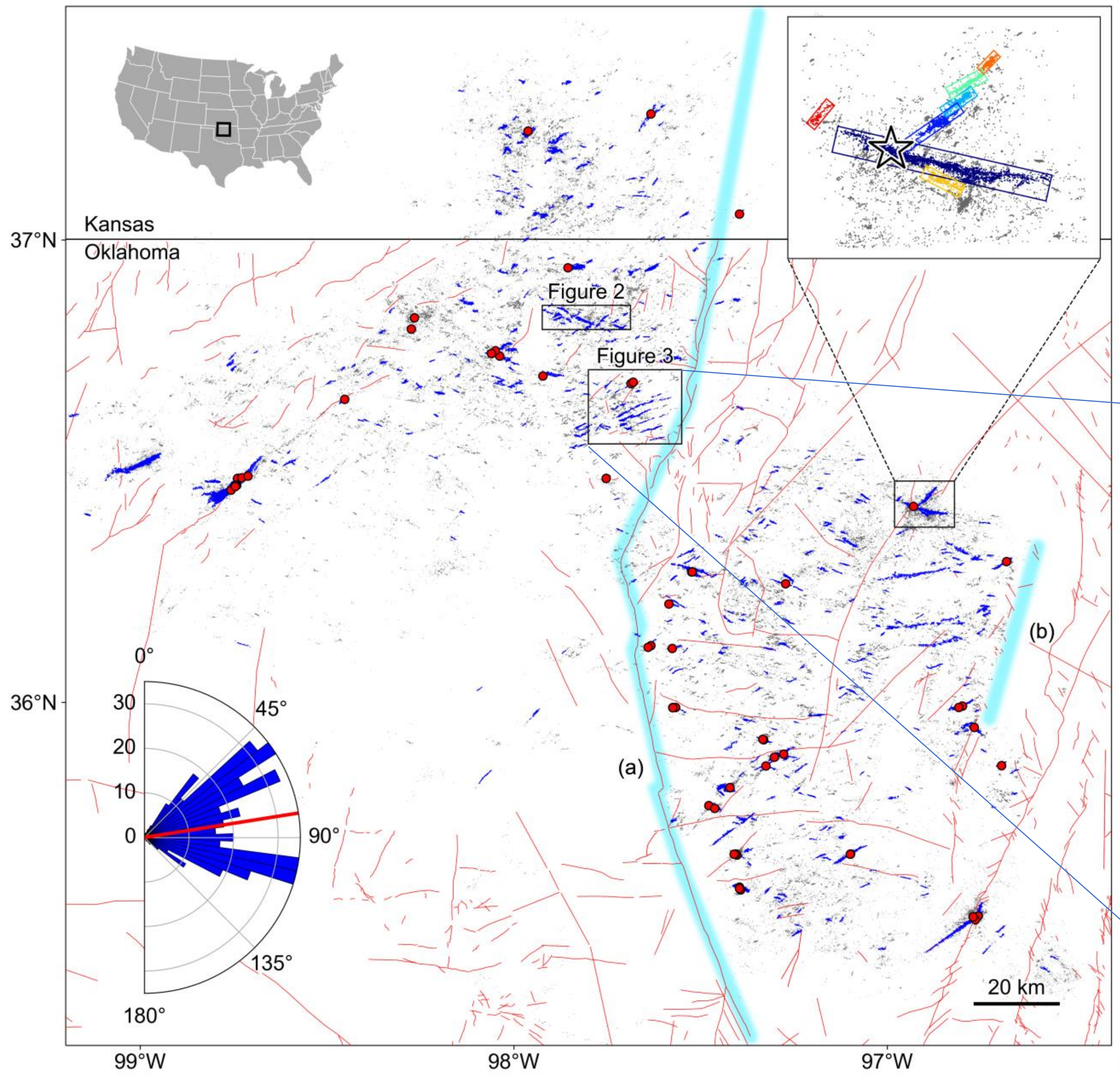

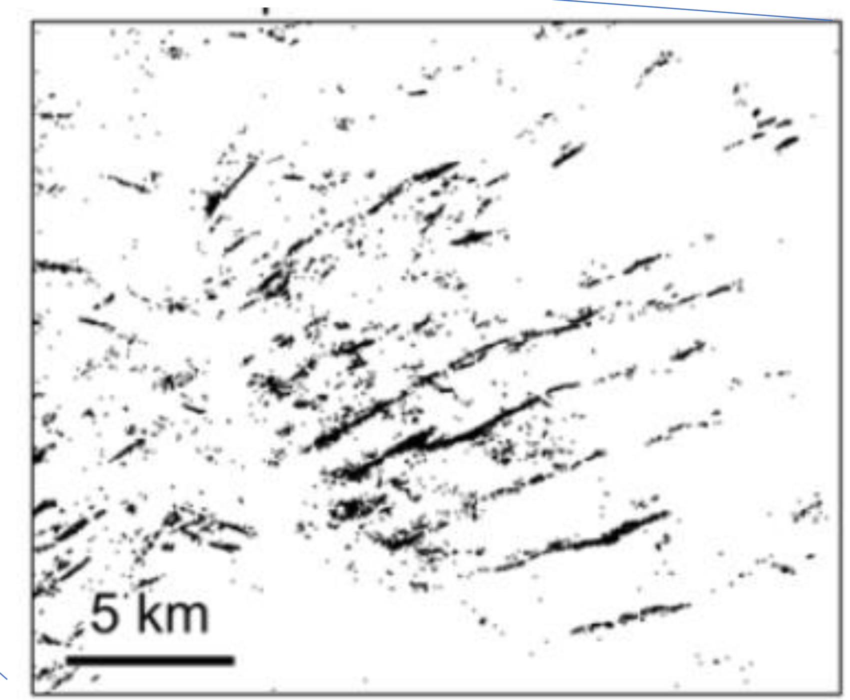

13,231 Earthquakes

In Retrospect, Every Well Constrained Focal Plane Mechanism Has One Plane Consistent With Prediction of Coulomb Faulting Theory

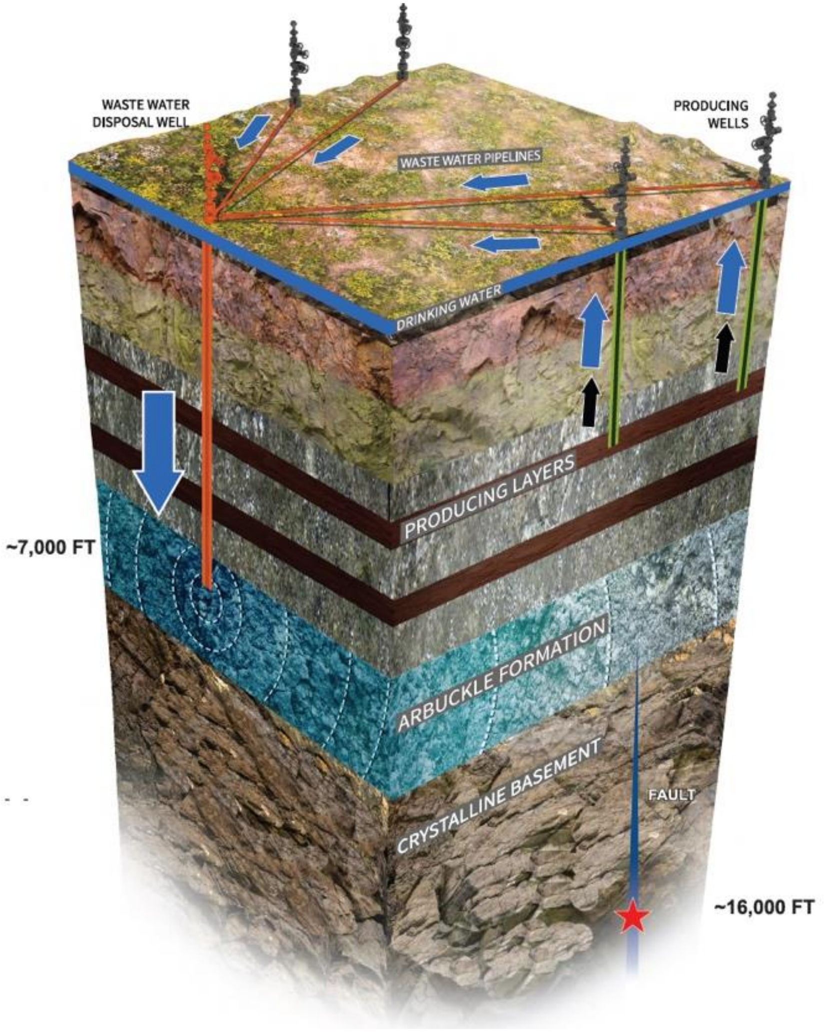

~ 1 MPa (145 psi) Pressure Change in Arbuckle

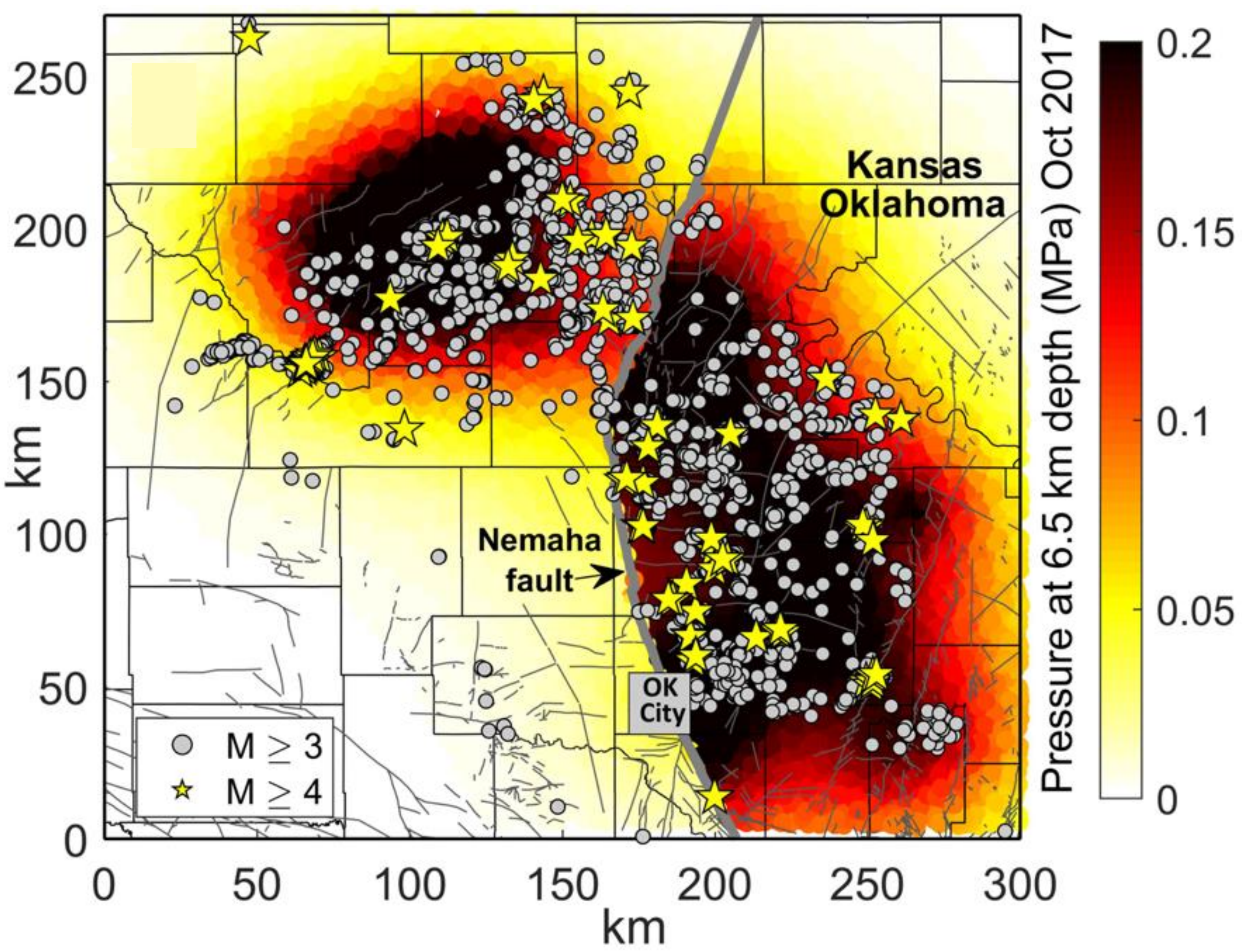

Langenbruch, Weingarten and Zoback (2018)

Anderson Faulting Theory Revisited

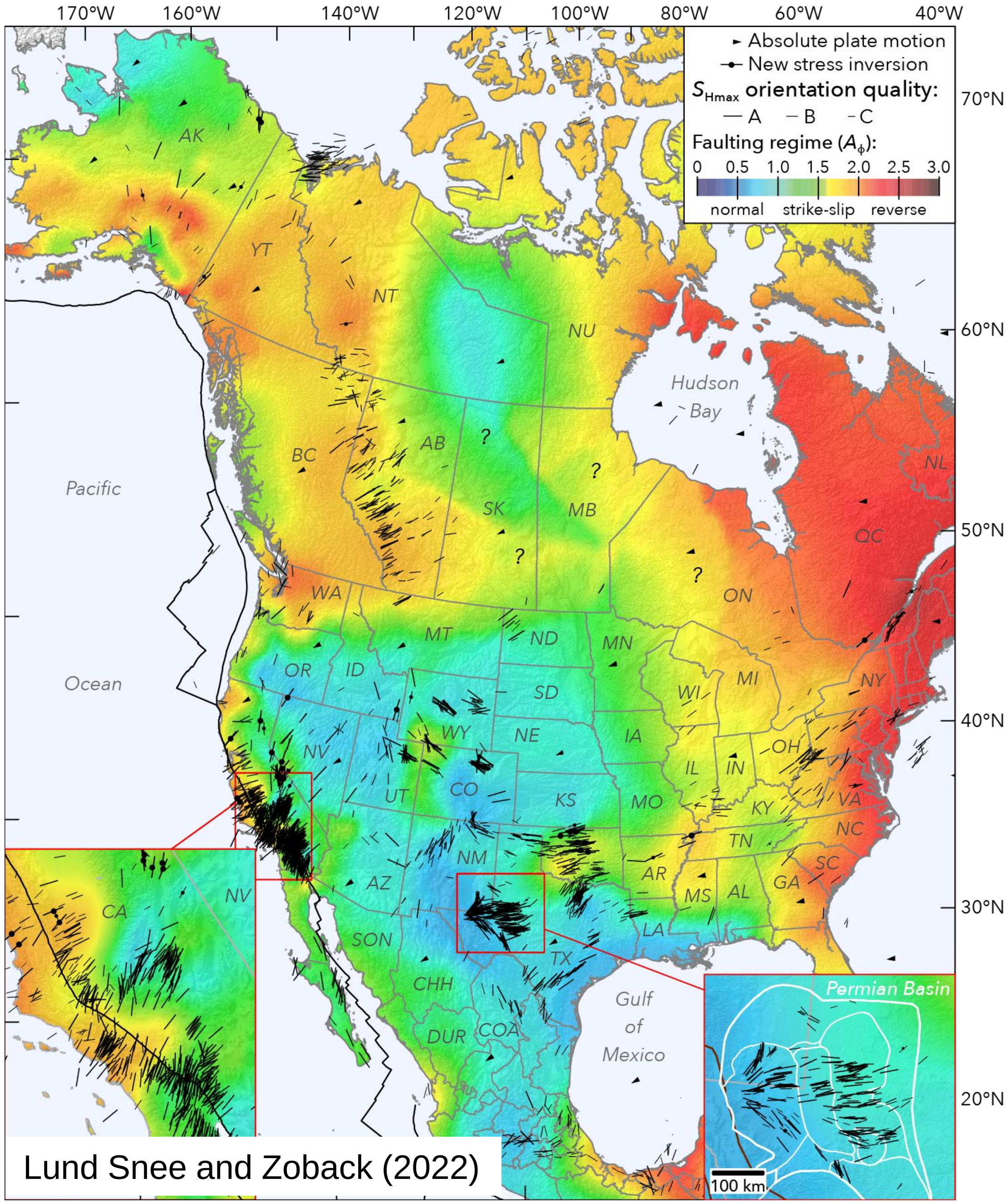

Lund Snee and Zoback (2022)

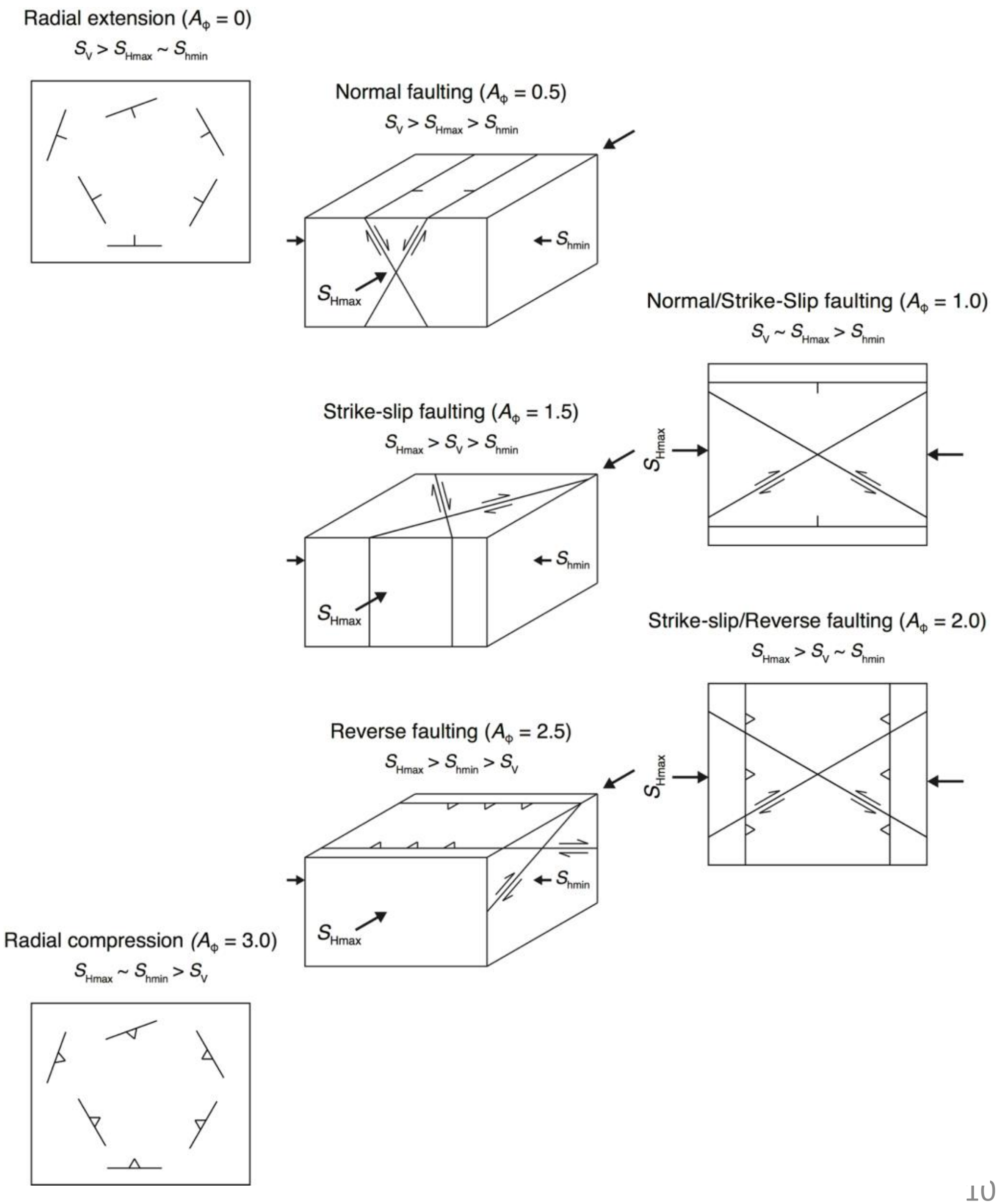

Permian Basin

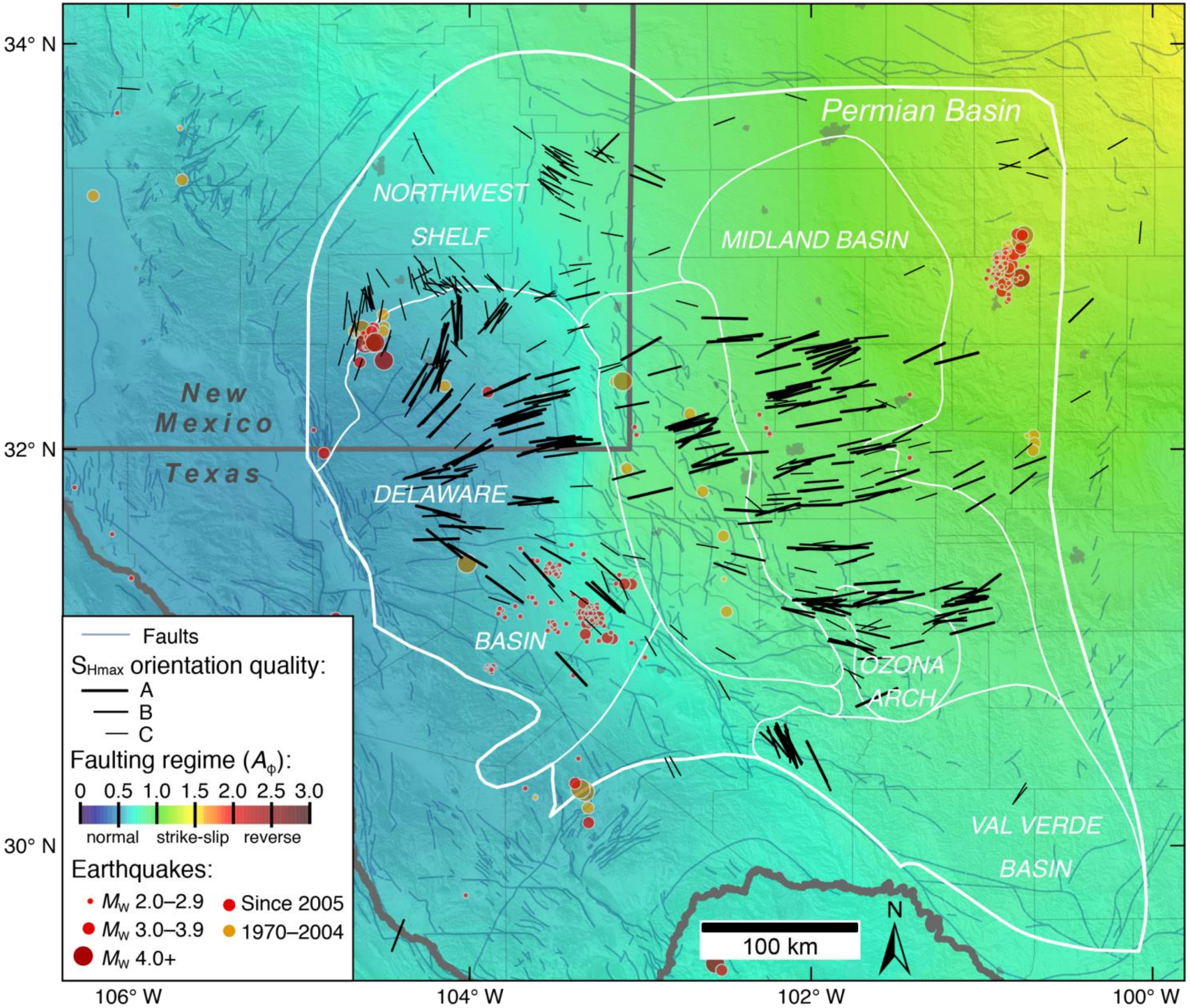

Lund Snee and Zoback (2017)

The Same is True for Shallow Earthquakes in the Delaware Basin In a Spatially Varying Stress Field

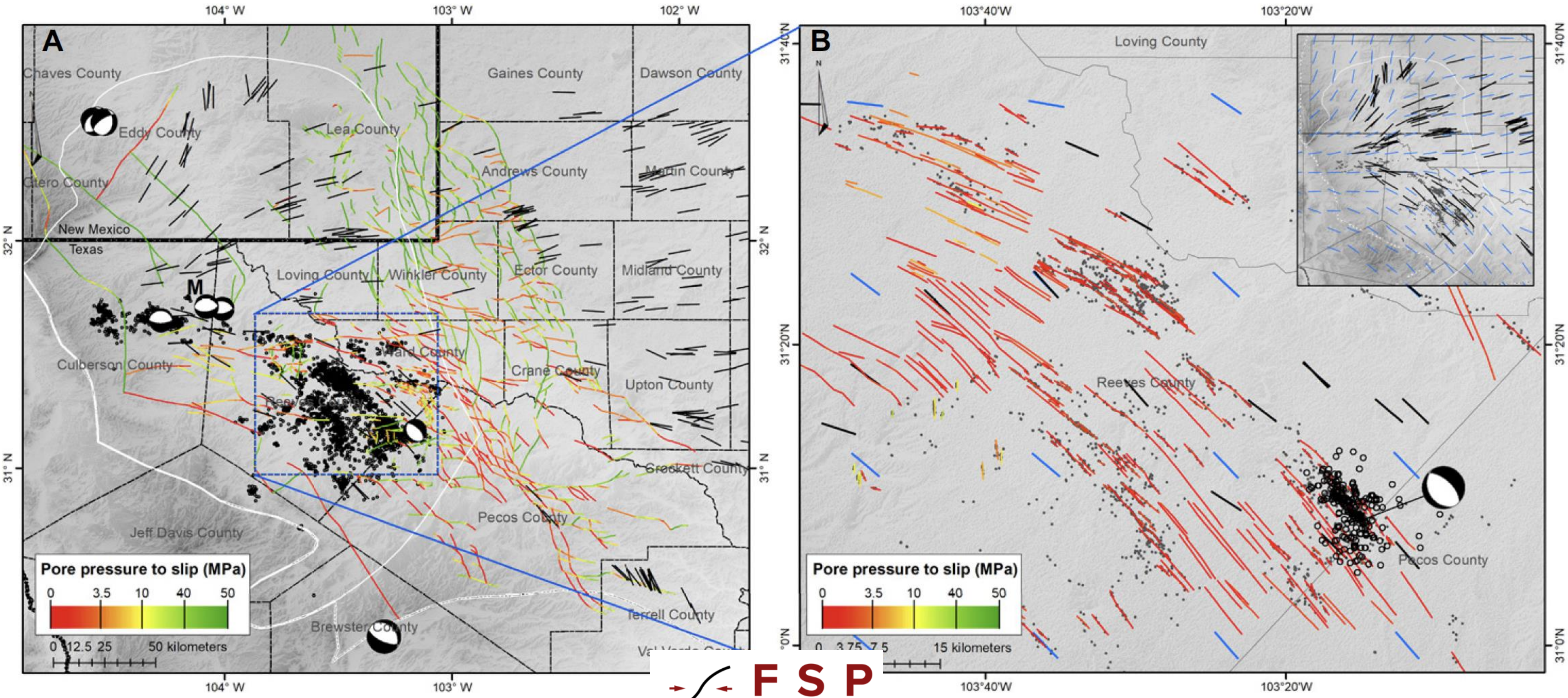

Dvory and Zoback (2021) from Lund Snee and Zoback (2022)

Three Topics

1. Relevant Learnings From Injection Induced Seismicity
   - Applicability of Coulomb Faulting Theory
   - It is Commonly Observed that Sedimentary Rocks (As Well As Crystalline Basement) are in Frictional Equilibrium
   - Stress Magnitudes Vary Markedly with Lithology in Sedimentary Sequences

1. Poroelastic Stress Paths and Earthquakes Induced by Depletion

3. Mmax and the Potential for Faulting in the Carboniferous

Basement Earthquakes in Oklahoma were Triggered by Very Small Pore Pressure Changes

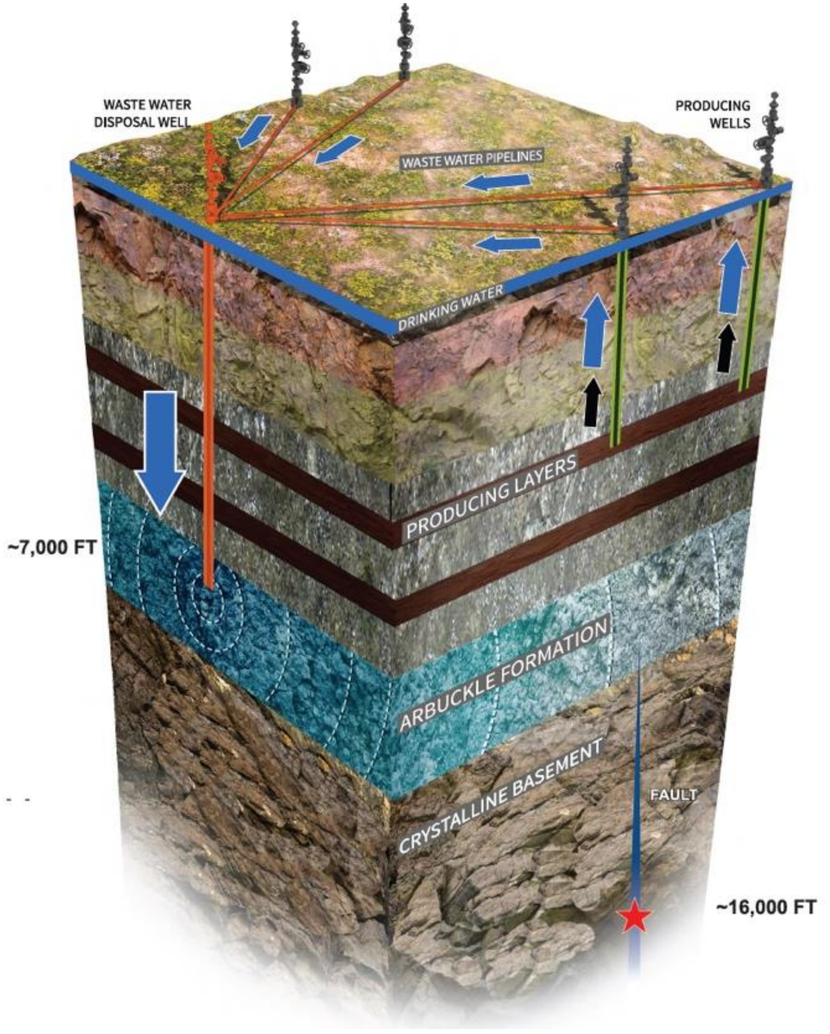

~ 1 MPa (145 psi) Pressure Change in Arbuckle

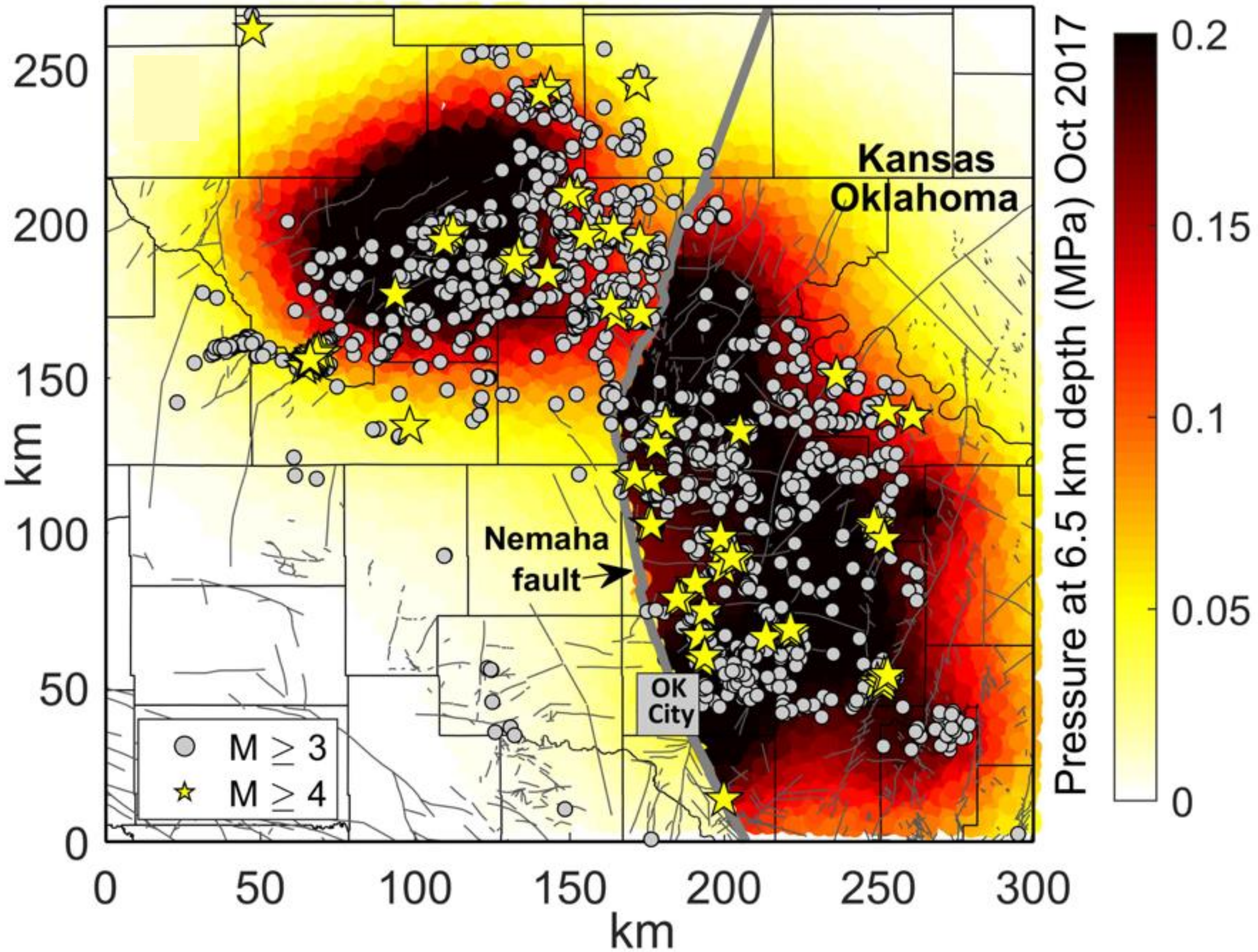

Langenbruch, Weingarten and Zoback (2018)

Basement Earthquakes in Oklahoma were Triggered by Very Small Pore Pressure Changes

~ 1 MPa (145 psi) Pressure Change in the Arbuckle, Ellenberger and Mt. Simon (Decatur, Ill.)

All cases of injection into a basal aquifer triggering slip in crystalline basement at with small pore pressure changes.

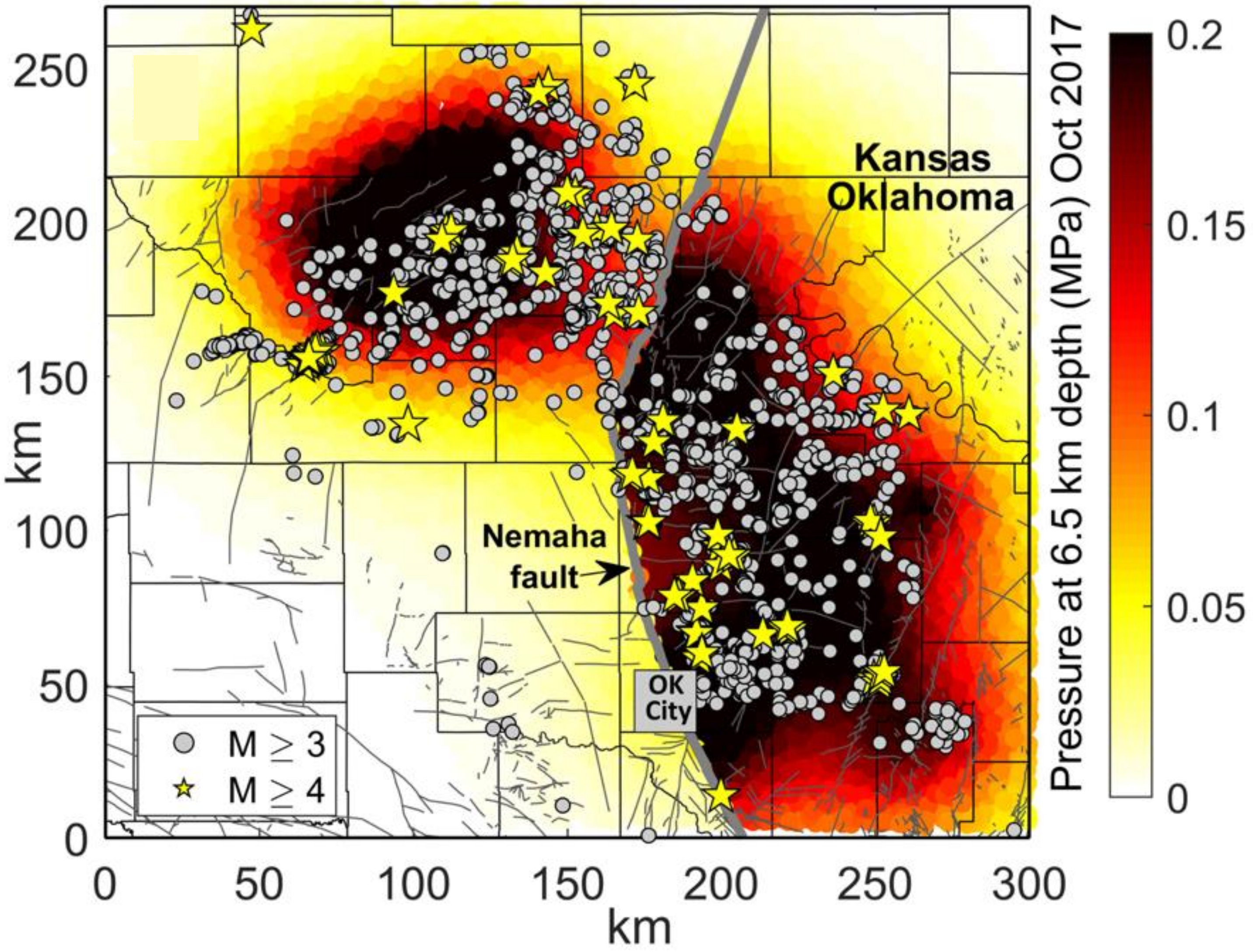

Langenbruch, Weingarten and Zoback (2018)

Shallow Normal Faulting in the Delaware Mountain Group

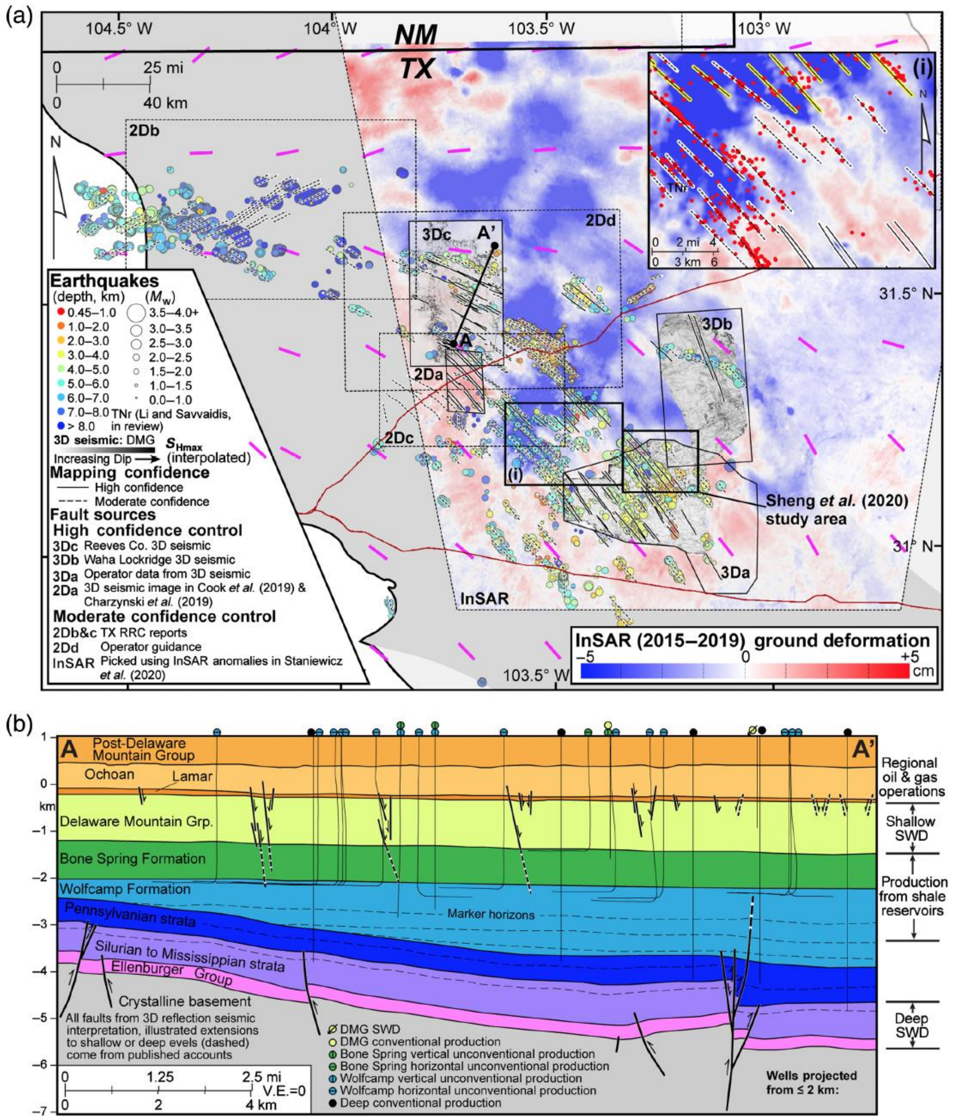

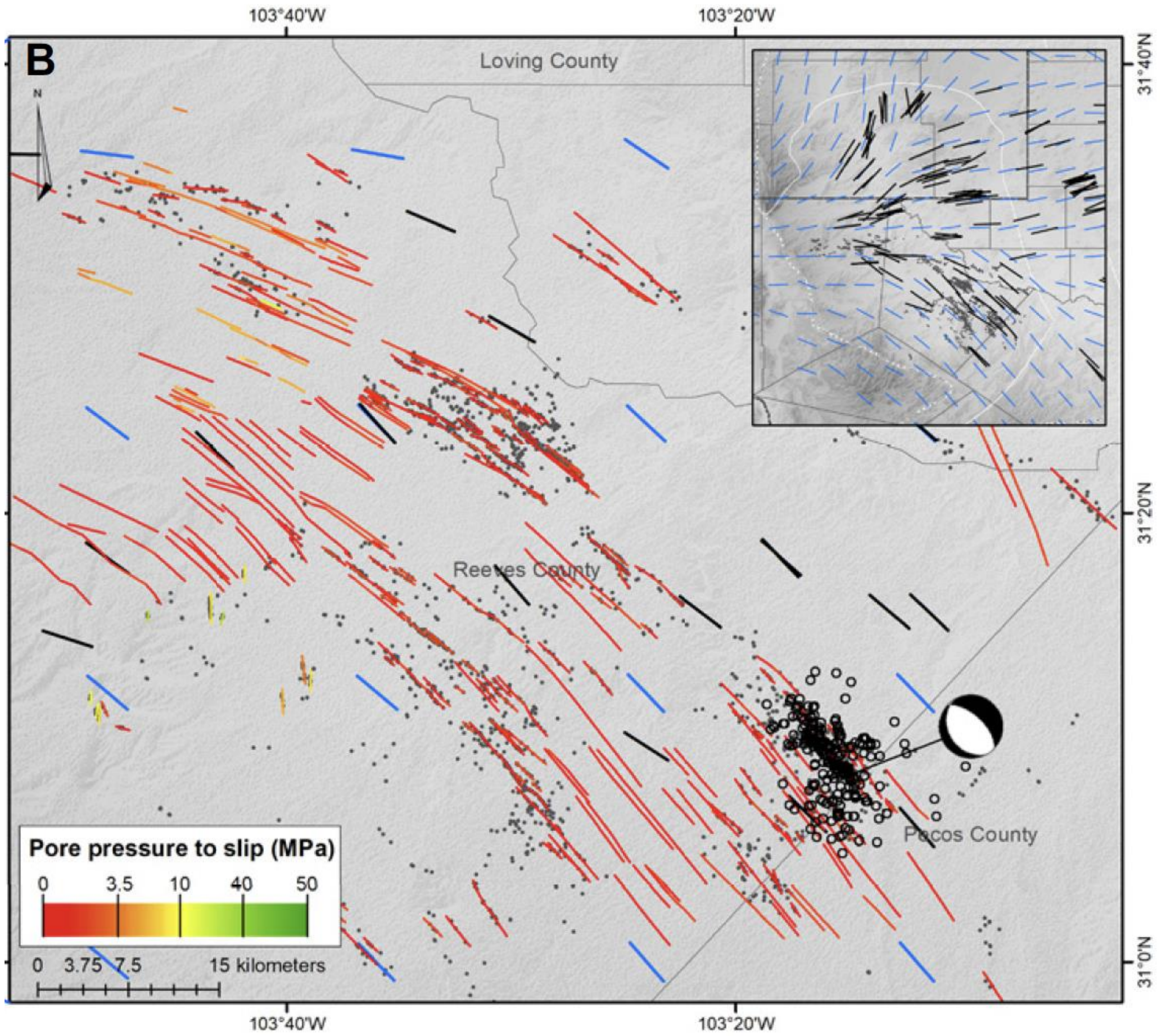

Hennings et al. (2021)

Assessing Whether Optimally-Oriented Normal Faults are Potentially Active is Straightforward

Easy

Often Easy

$$\frac{S_v - P_p}{S_{hmin} - P_p} = [(\mu^2 + 1)^{1/2} + \mu]^2$$

Easily Measured
With Mini-fracs or DFITs

Coulomb Criterion

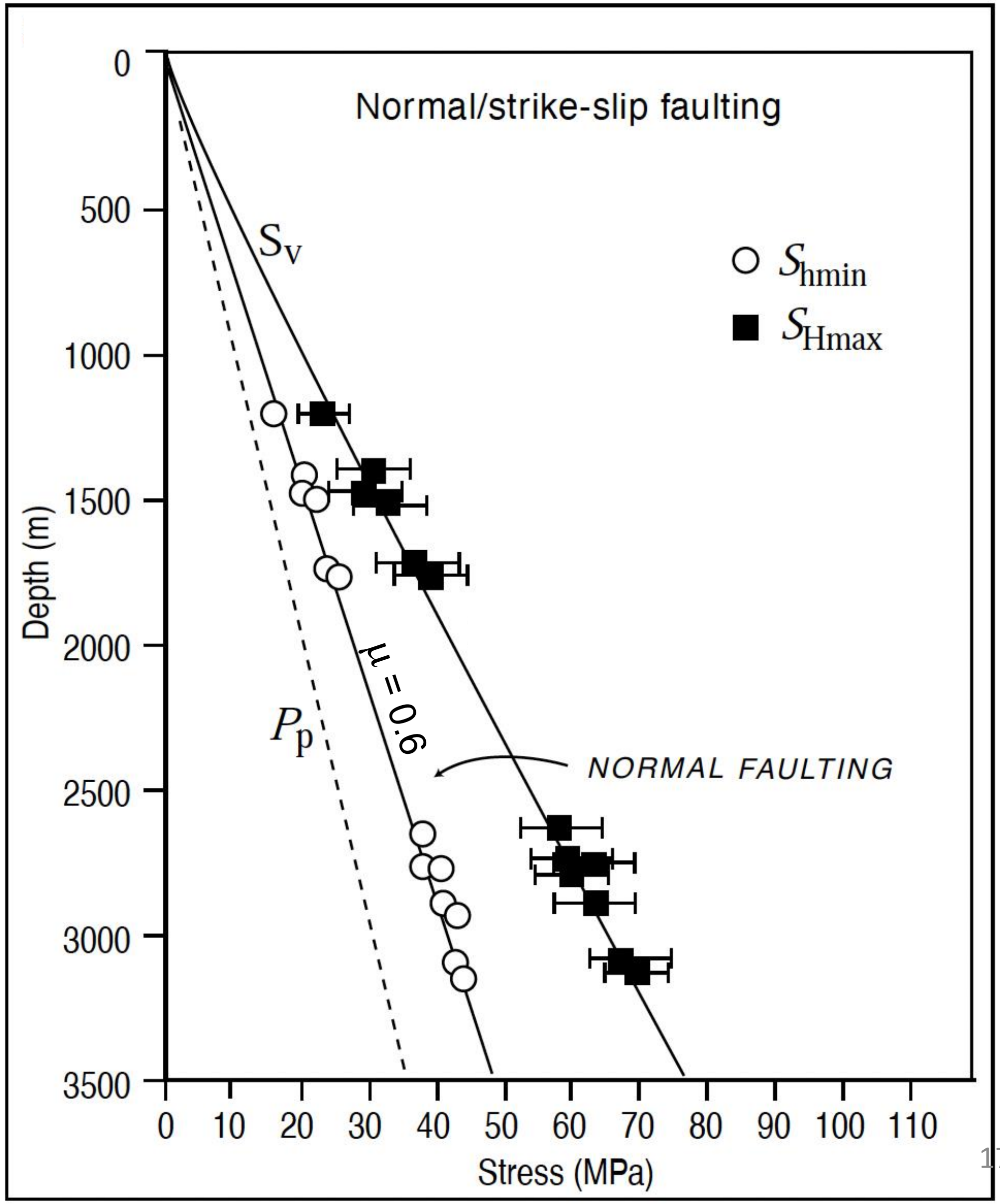

Shallow Normal Faulting in the Delaware Mountain Group

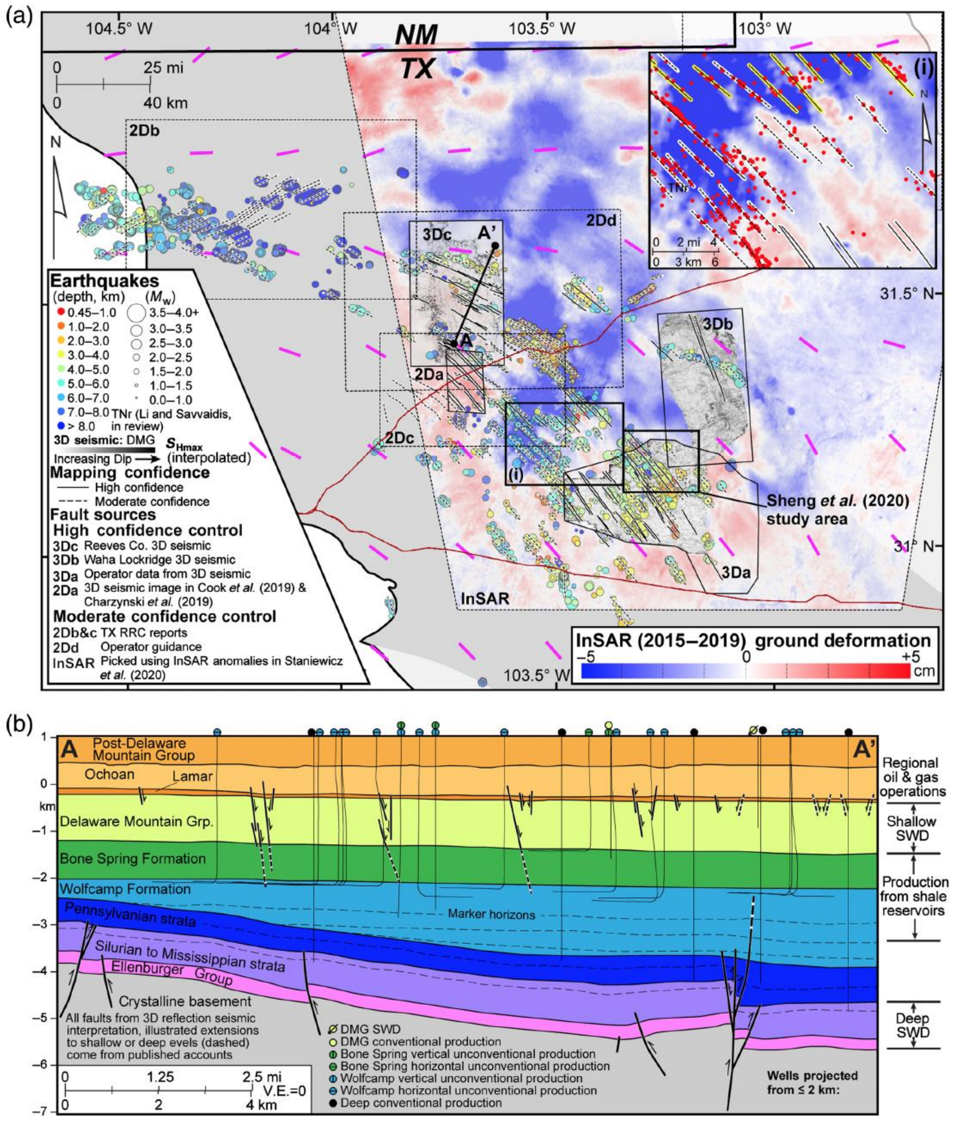

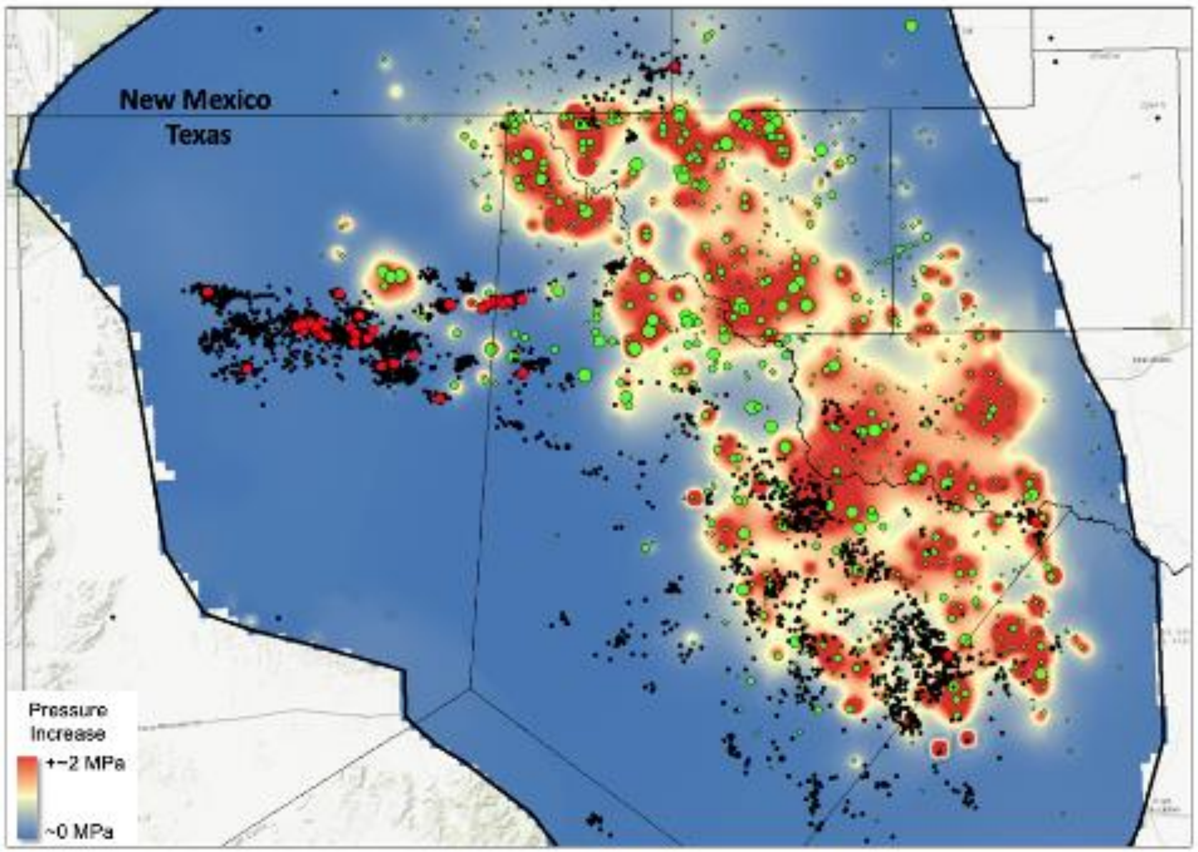

Ge et al. (2022)

Hennings et al. (2021)

Shallow Normal Faulting in the Delaware Mountain Group

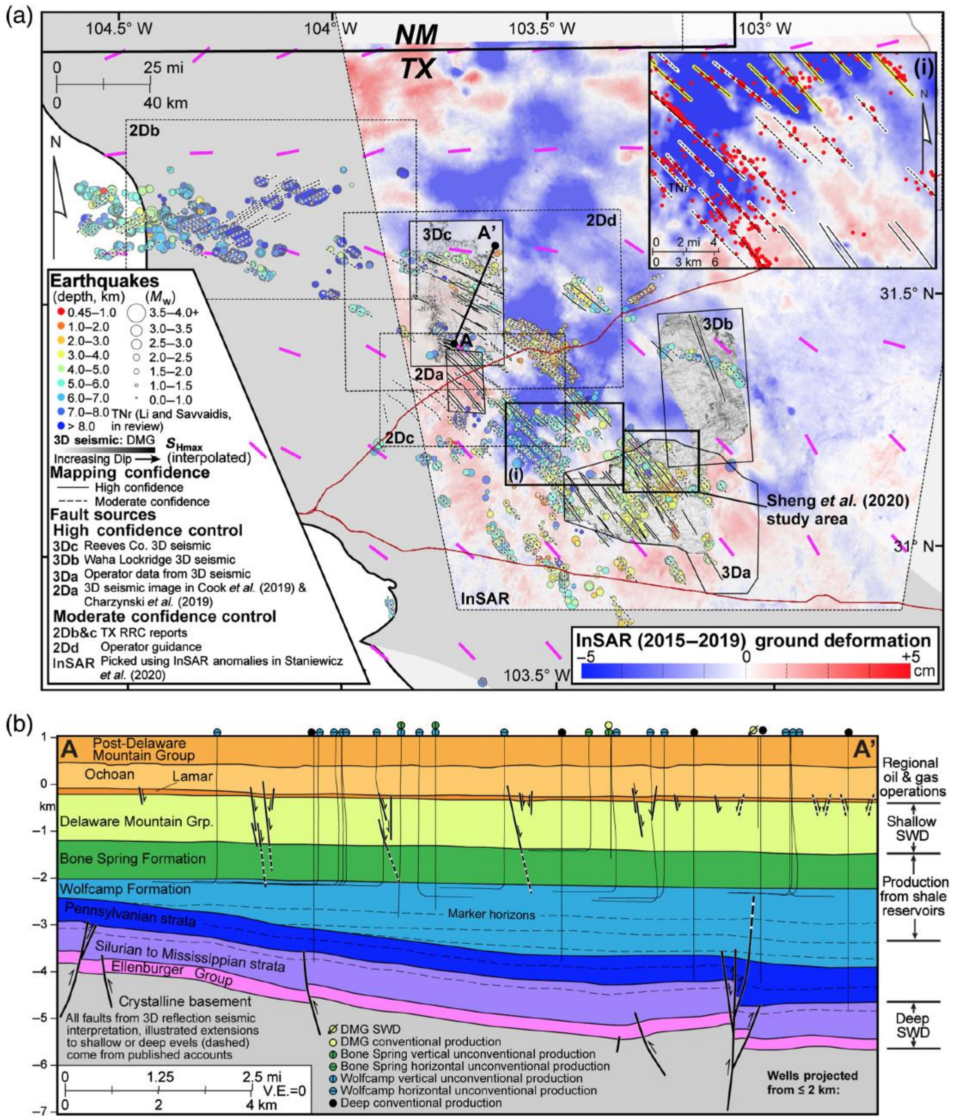

Hennings et al. (2021)

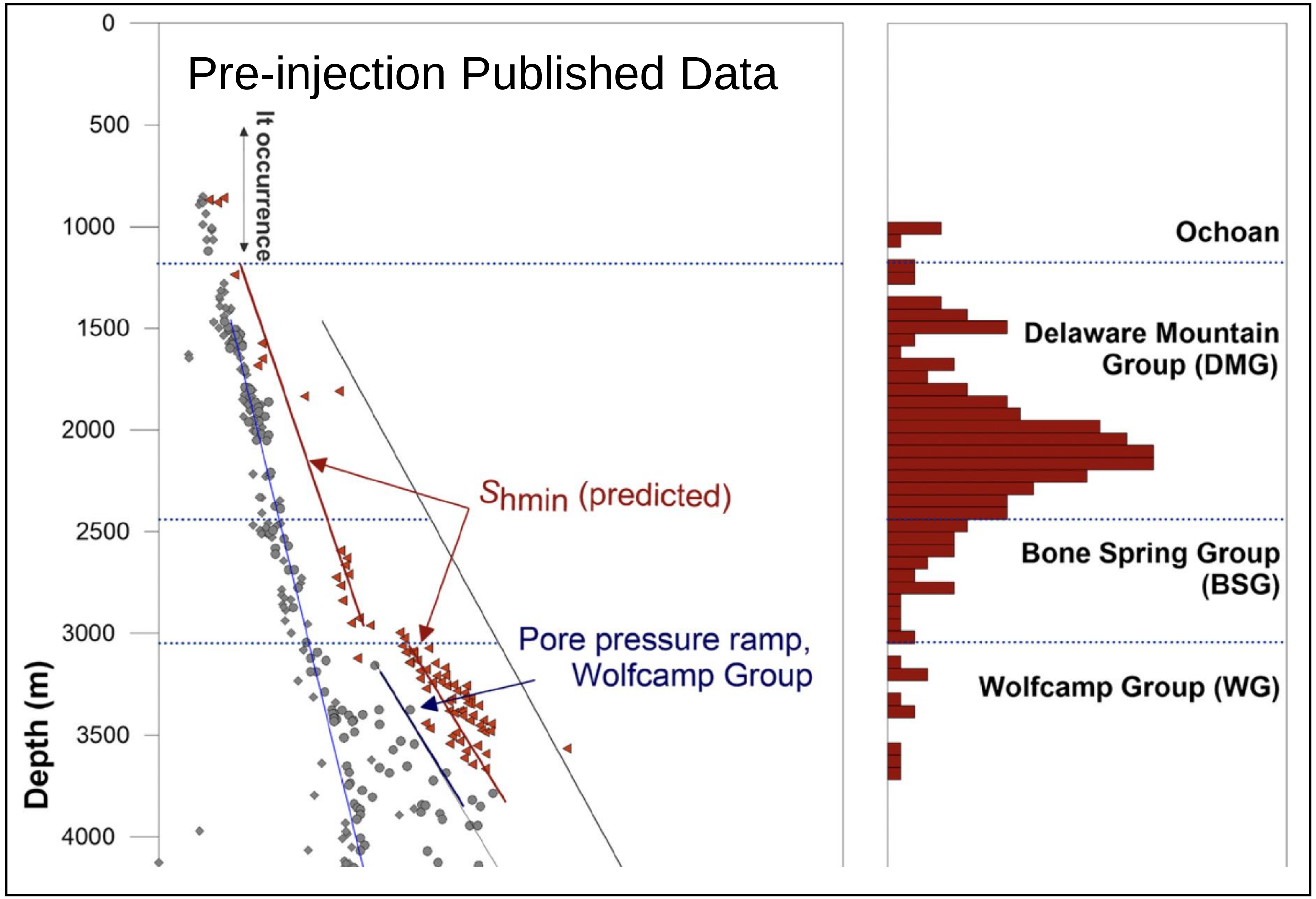

Dvory and Zoback (2021)

Optimally-Oriented Normal Faults are Present in Groningen

$$\frac{S_v - P_p}{S_{hmin} - P_p} = [(\mu^2 + 1)^{1/2} + \mu]^2$$

Coulomb Criterion

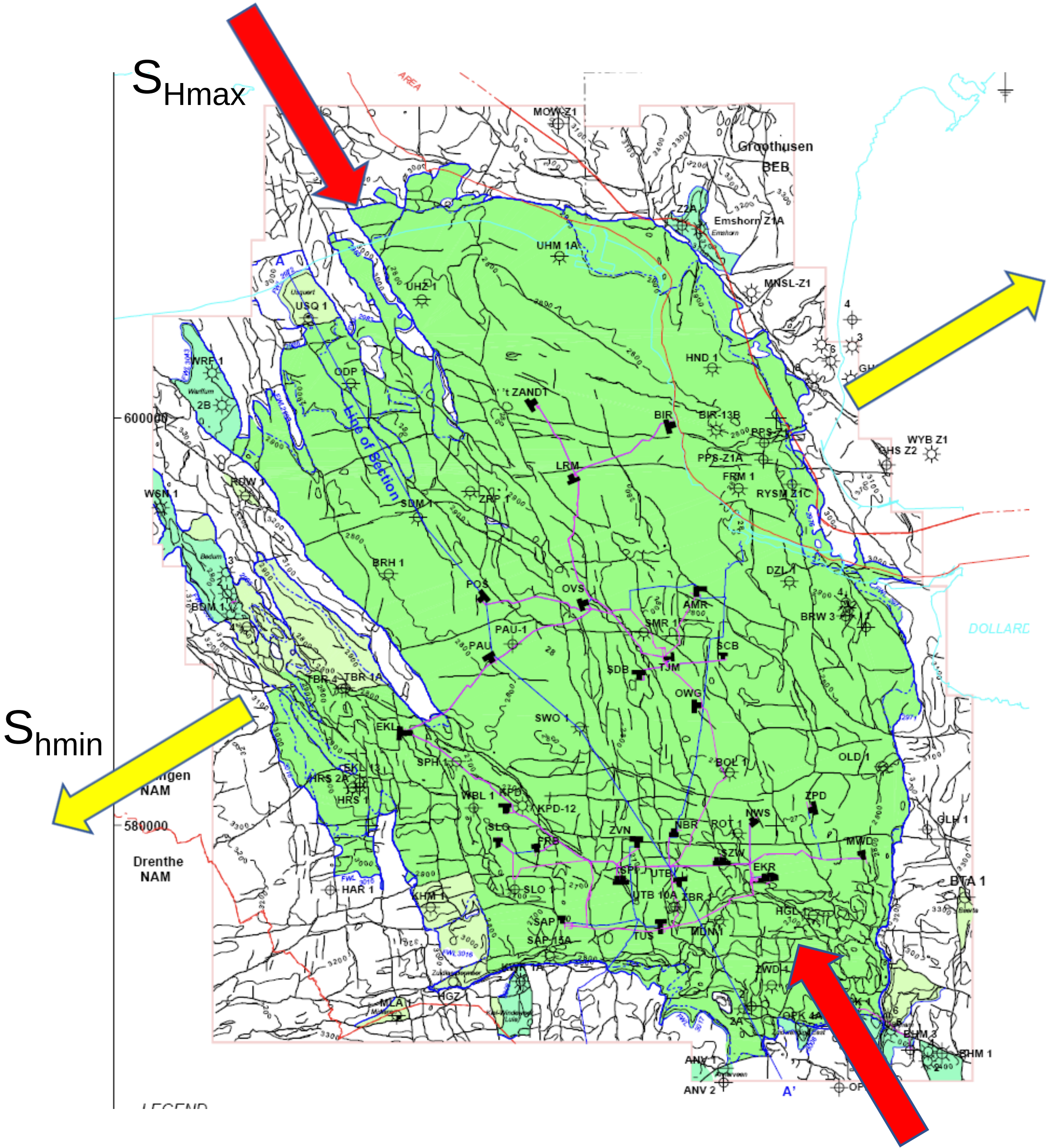

Three Topics

1. Relevant Learnings From Injection Induced Seismicity
    - Applicability of Coulomb Faulting Theory
    - It is Commonly Observed that Sedimentary Rocks (As Well As Crystalline Basement) are in Frictional Equilibrium
    - Stress Magnitudes Vary Markedly with Lithology in Sedimentary Sequences

1. Poroelastic Stress Paths and Earthquakes Induced by Depletion

3. Mmax and the Potential for Faulting in the Carboniferous

Detailed Measurements of the Variation of S_{hmin} With Depth In the Midland Basin

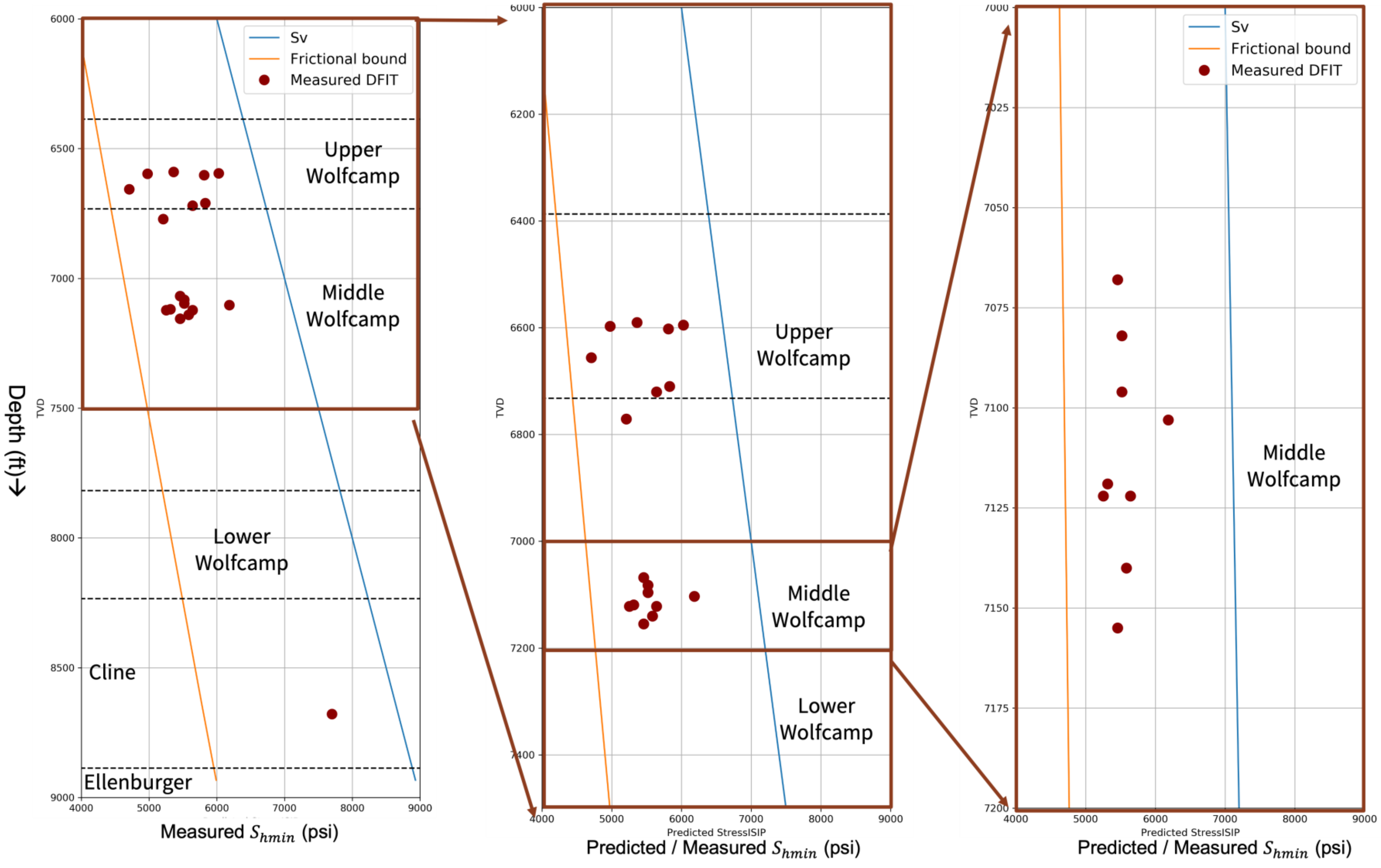

Singh and Zoback (*Geophysics*, 2022)

HFTS 1 –Measured Stress Magnitudes

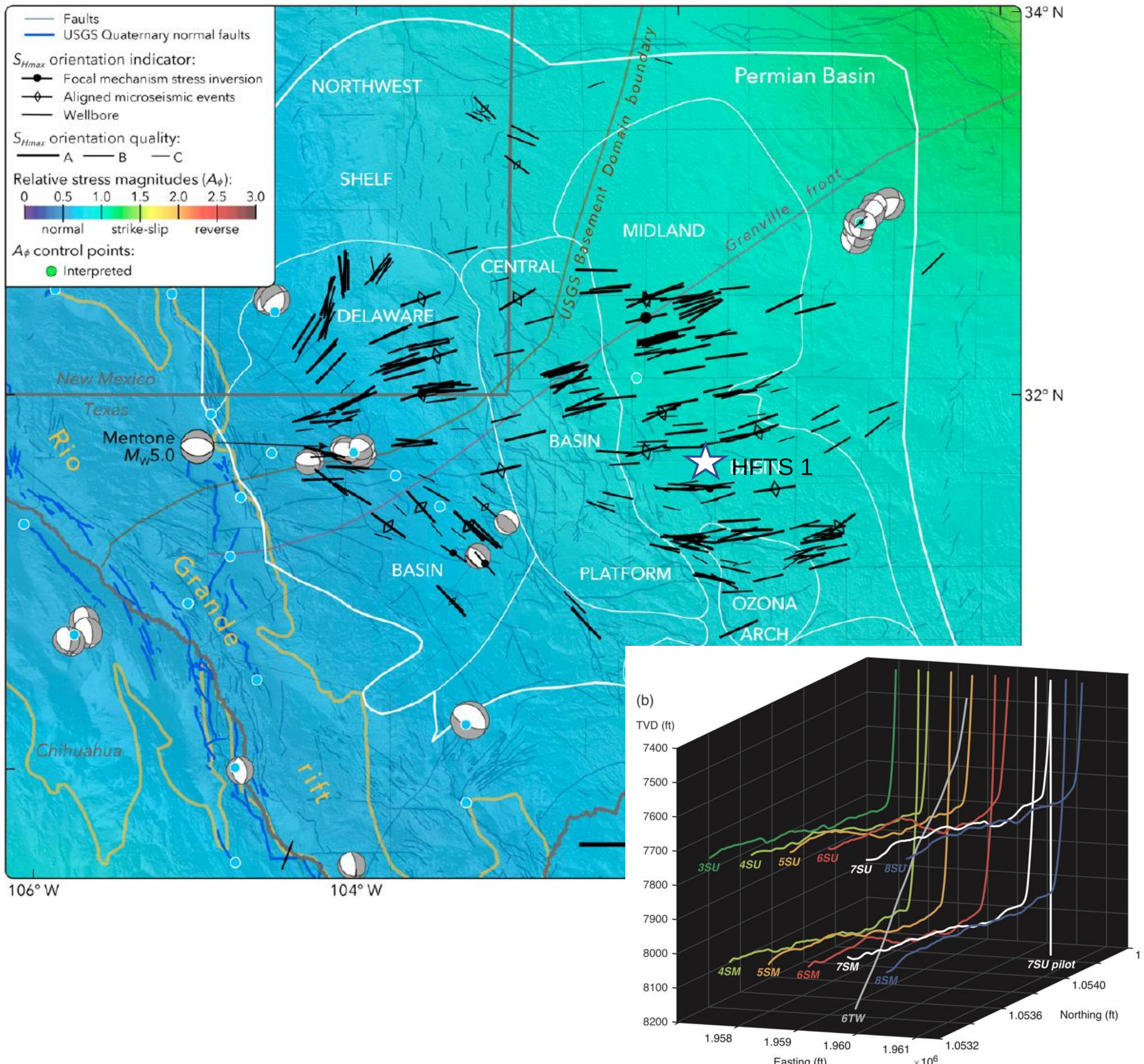

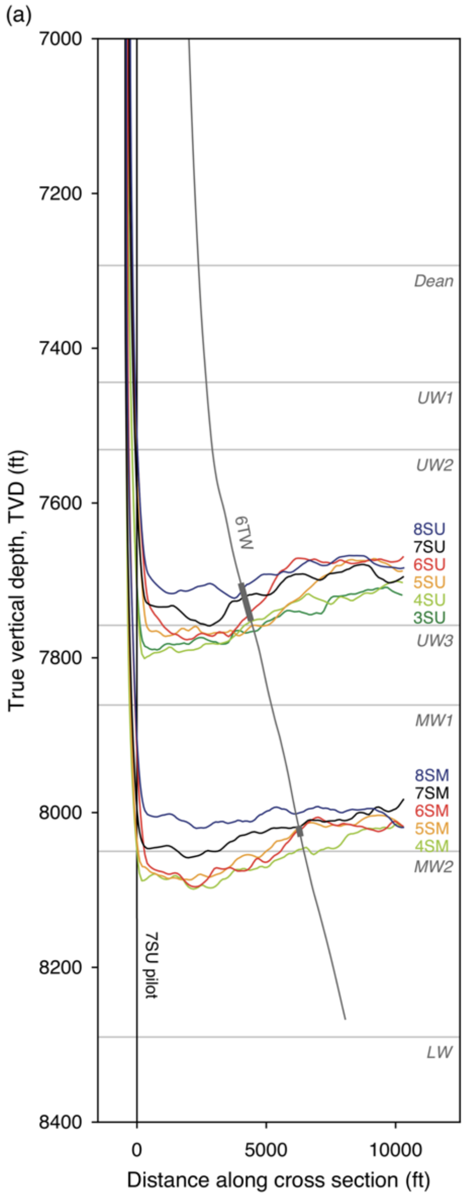

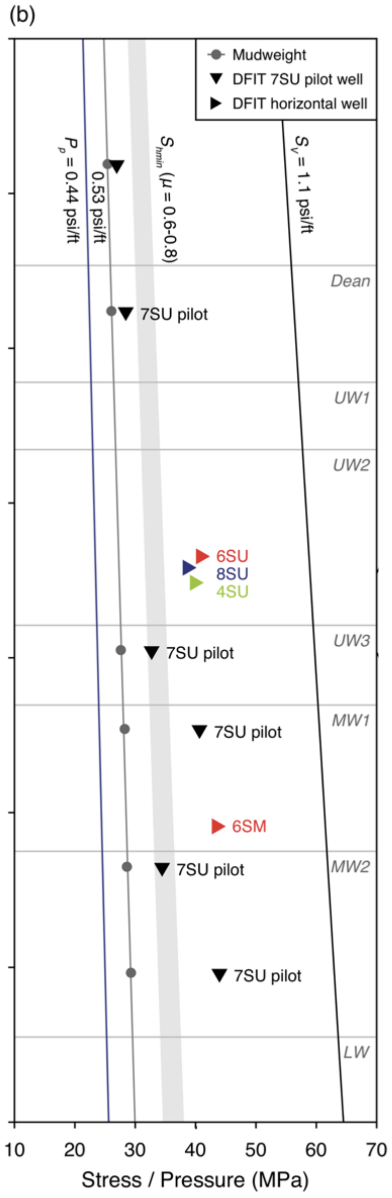

Kohli and Zoback (*Energies*, 2021)

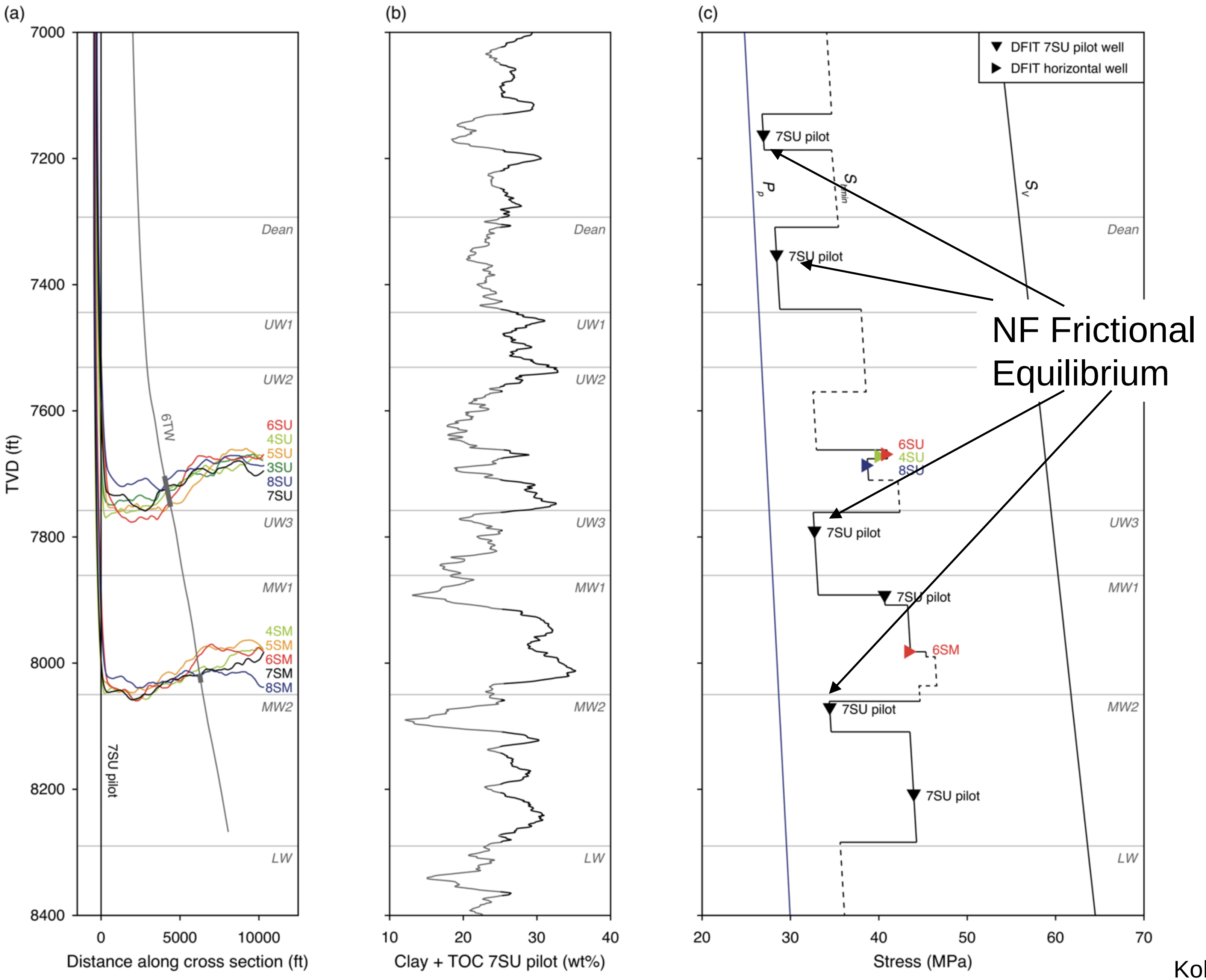

Kohli and Zoback (*Energies*, 2021)

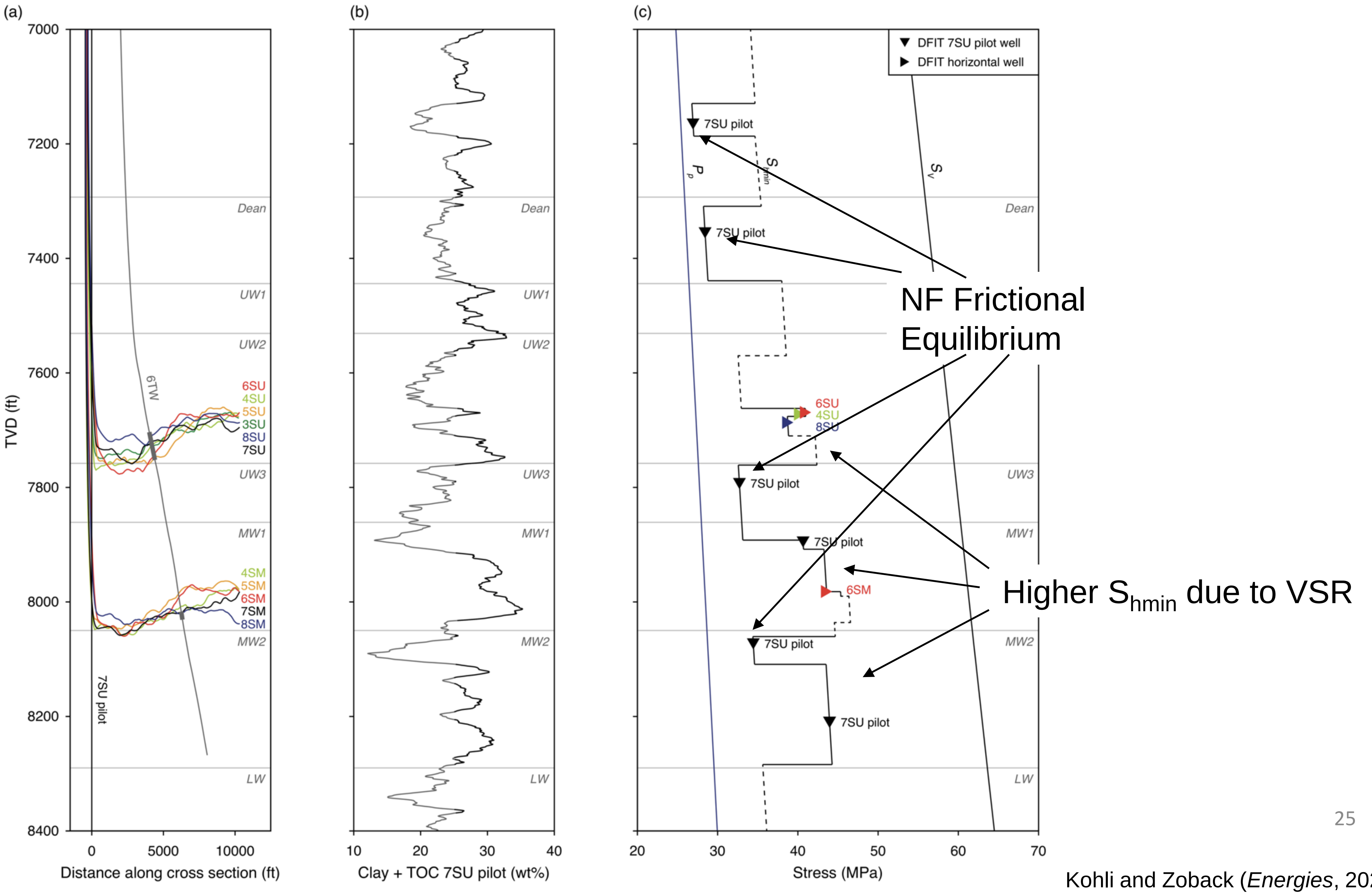

Kohli and Zoback (*Energies*, 2021)

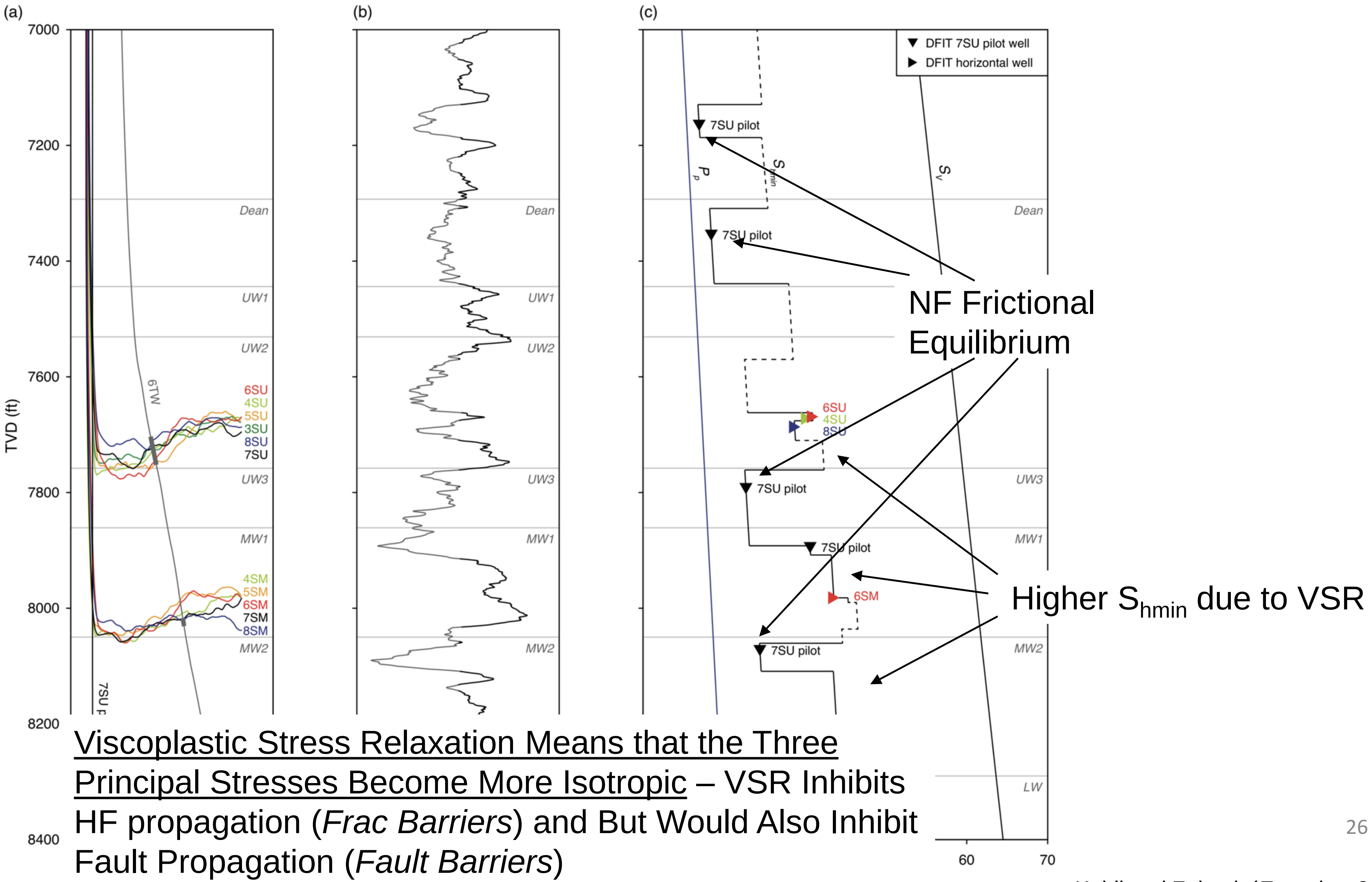

Viscoplastic Stress Relaxation Means that the Three Principal Stresses Become More Isotropic – VSR Inhibits HF propagation (*Frac Barriers*) and But Would Also Inhibit Fault Propagation (*Fault Barriers*)

Kohli and Zoback (*Energies*, 2021)

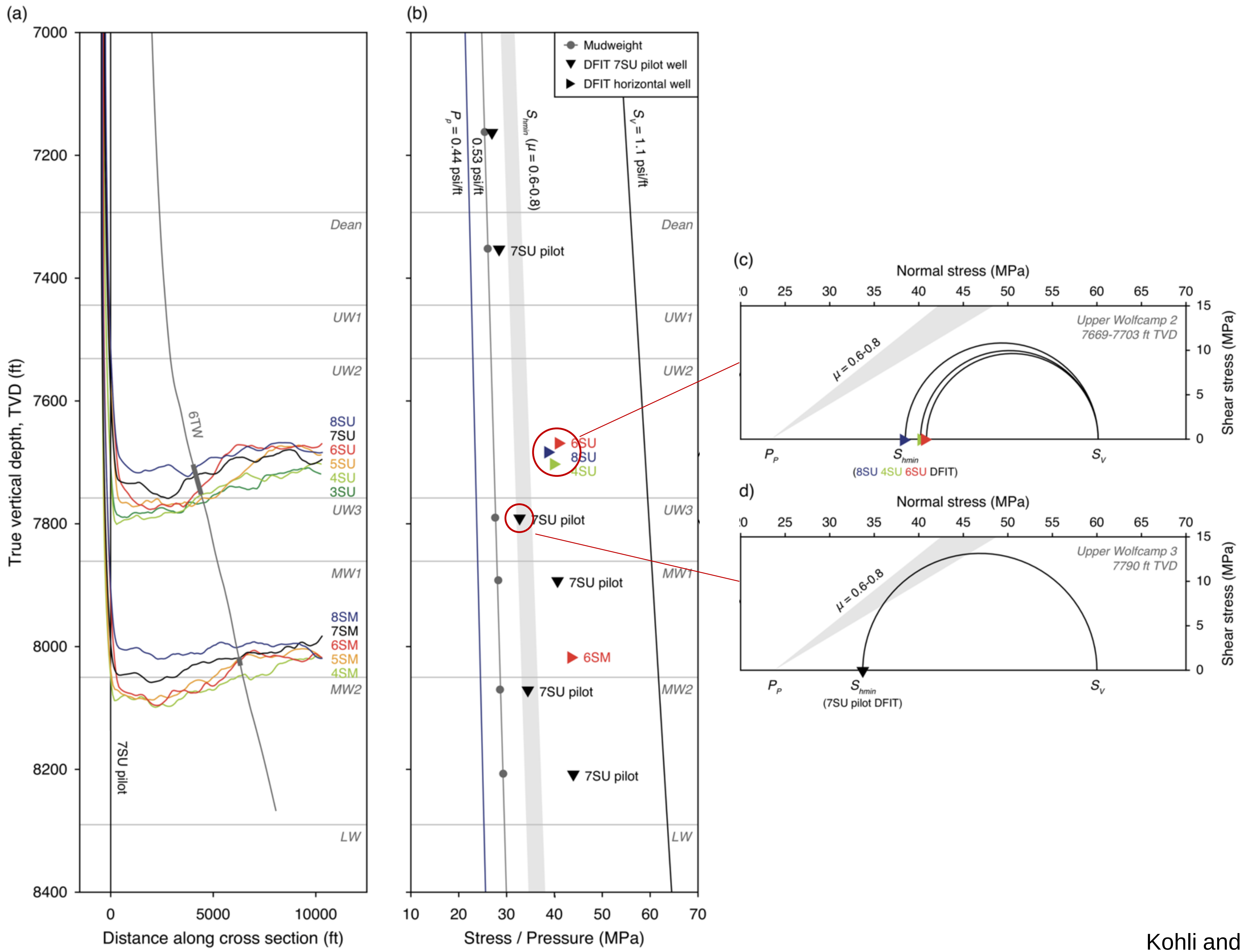

Kohli and Zoback (*Energies*, 2021)

In Normal Faulting Areas, High S_{hmin} Frac Barriers (due to VSR) May Also be Fault Propagation Barriers

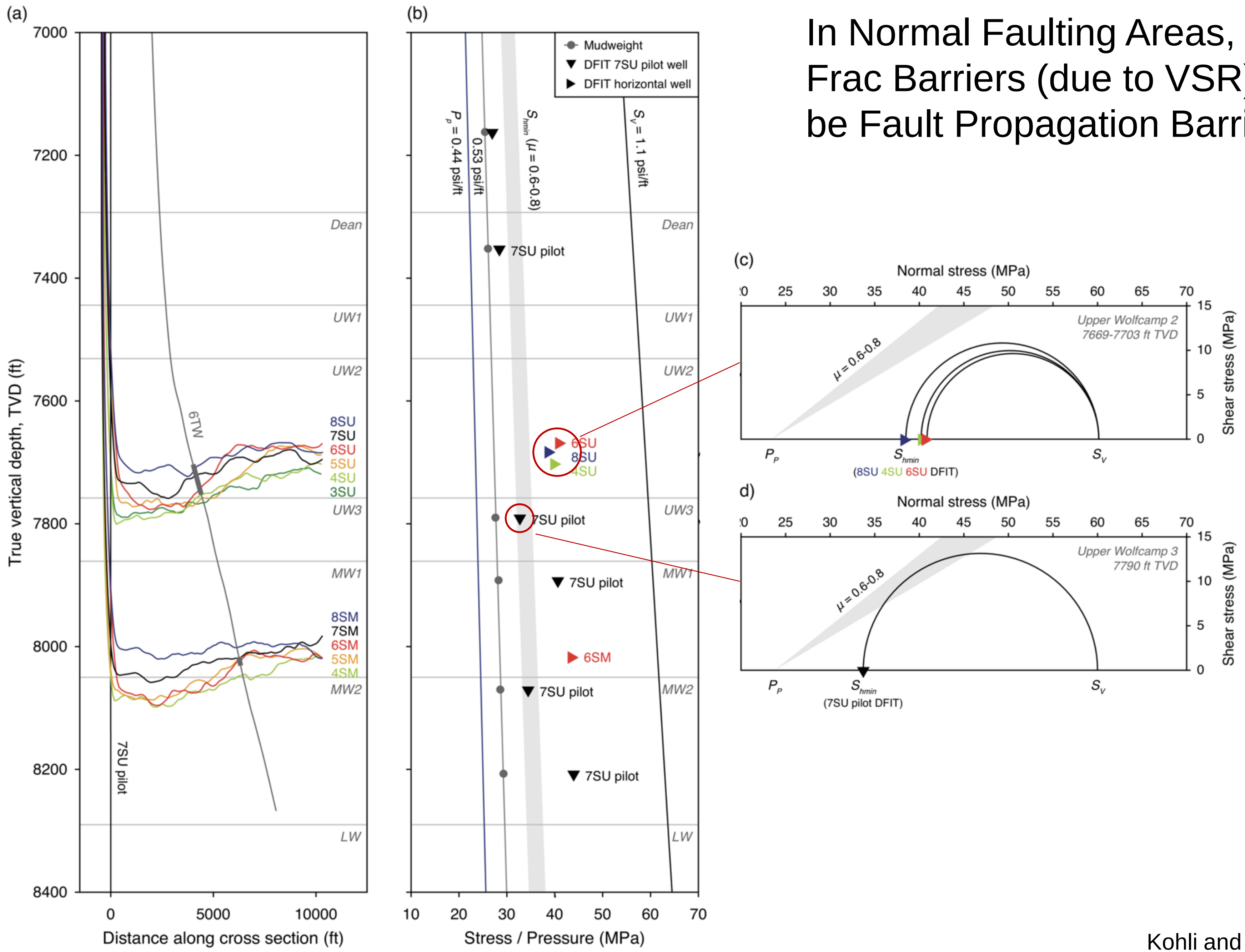

Kohli and Zoback (*Energies*, 2021)

Stress Relaxation Results in a More Isotropic Stress Field

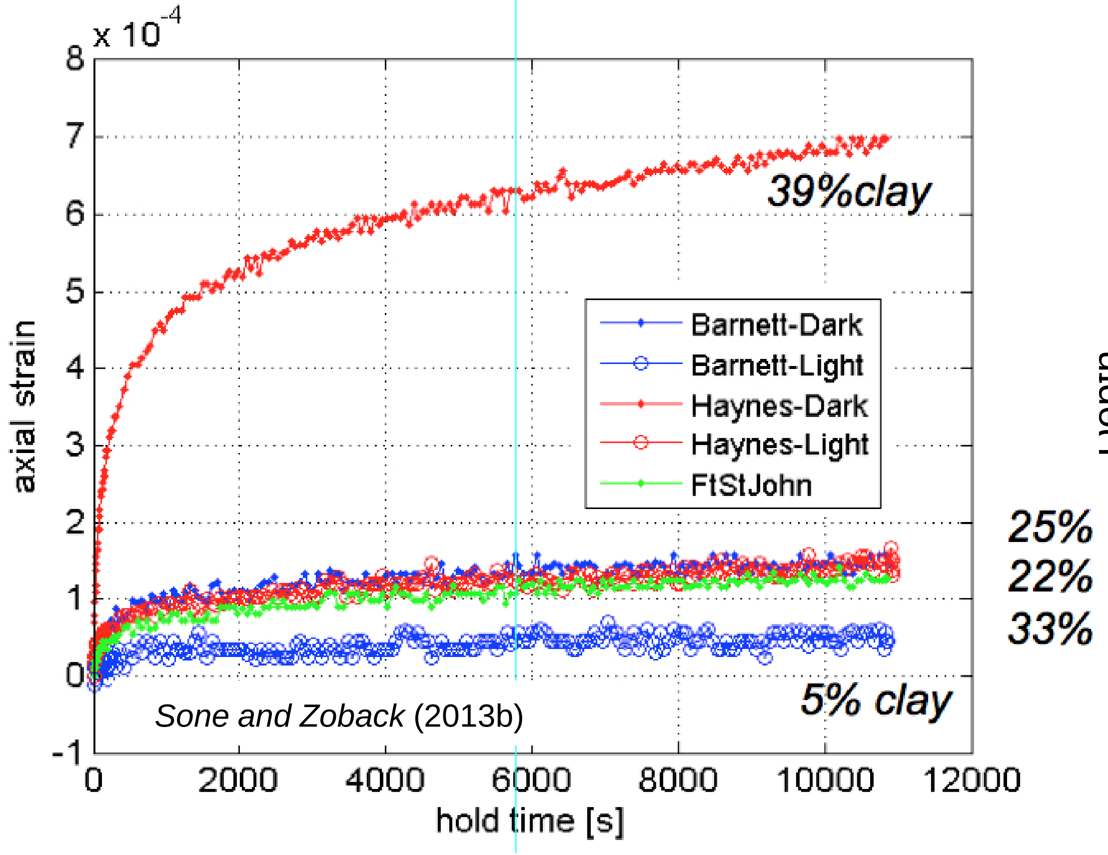

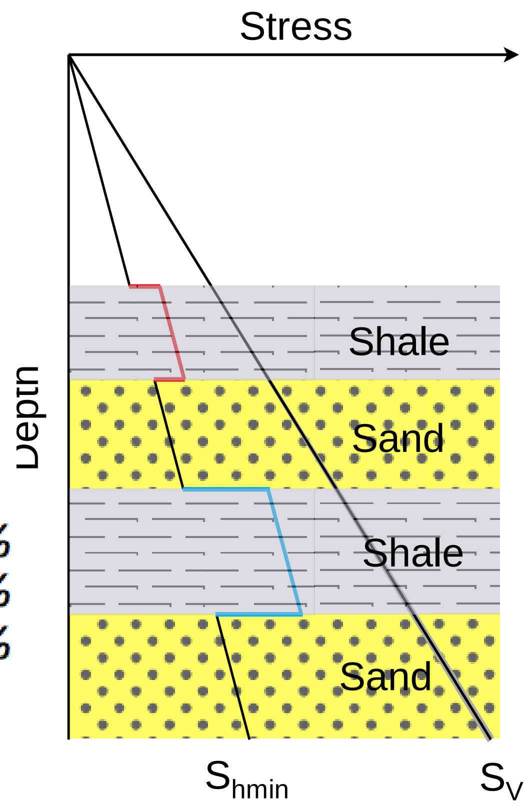

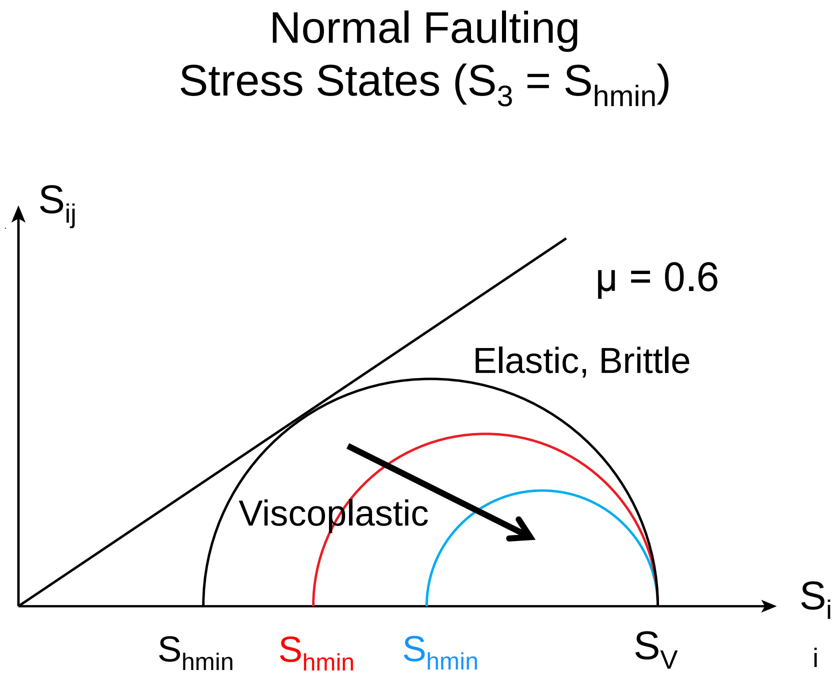

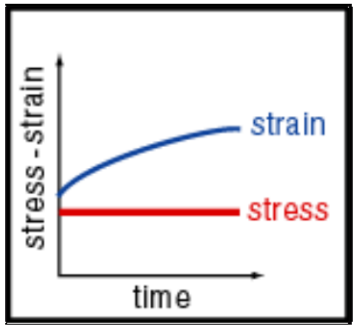

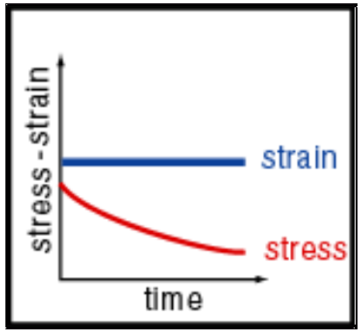

Complete Stress Relaxation in Shales and Mud Stones

Multi-Well Experiment (MWX)

- Western Colorado – Piceance Basin (1981-1988)
    - Tight gas reservoirs (k = 1-10 μD)
    - 3 vertical wells spaced hundreds of feet apart
- Normal faulting ($S_v > S_{Hmax} > S_{hmin}$)
- Hydrocarbon generation in active zone
    - P_p exceeds hydrostatic (overpressure)
    - Fracture gradient in sands increases with P_p
- Fracture gradient in shales very close to S_v (1.1 psi/ft)
    - Essentially total stress relaxation (high ductility)
    - Shale units likely act as frac barriers

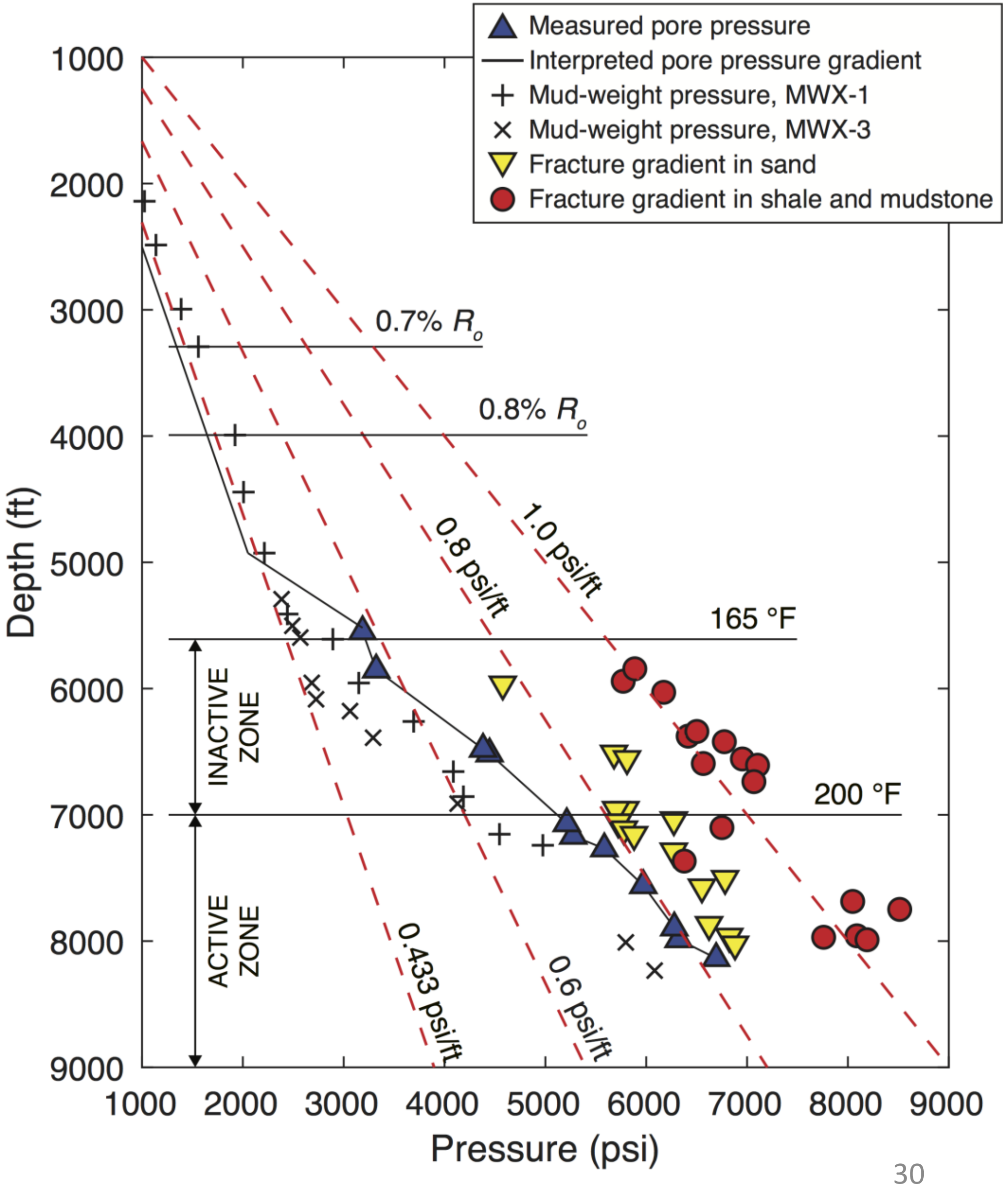

Long Term Creep Experiments - Creep Constitutive Law

Short term experiments (3 hr) suggest logarithmic behavior

$$e_{creep}(t) = A\log(t)$$

Longer term experiments better fit by a power law

$$\boxed{e_{creep}(t) = Bt^n}$$

Power law describes both elastic and creep response

$$J(t) = \frac{e}{s} = Bt^n$$

$$\log J(t) = \log B + n\log t$$

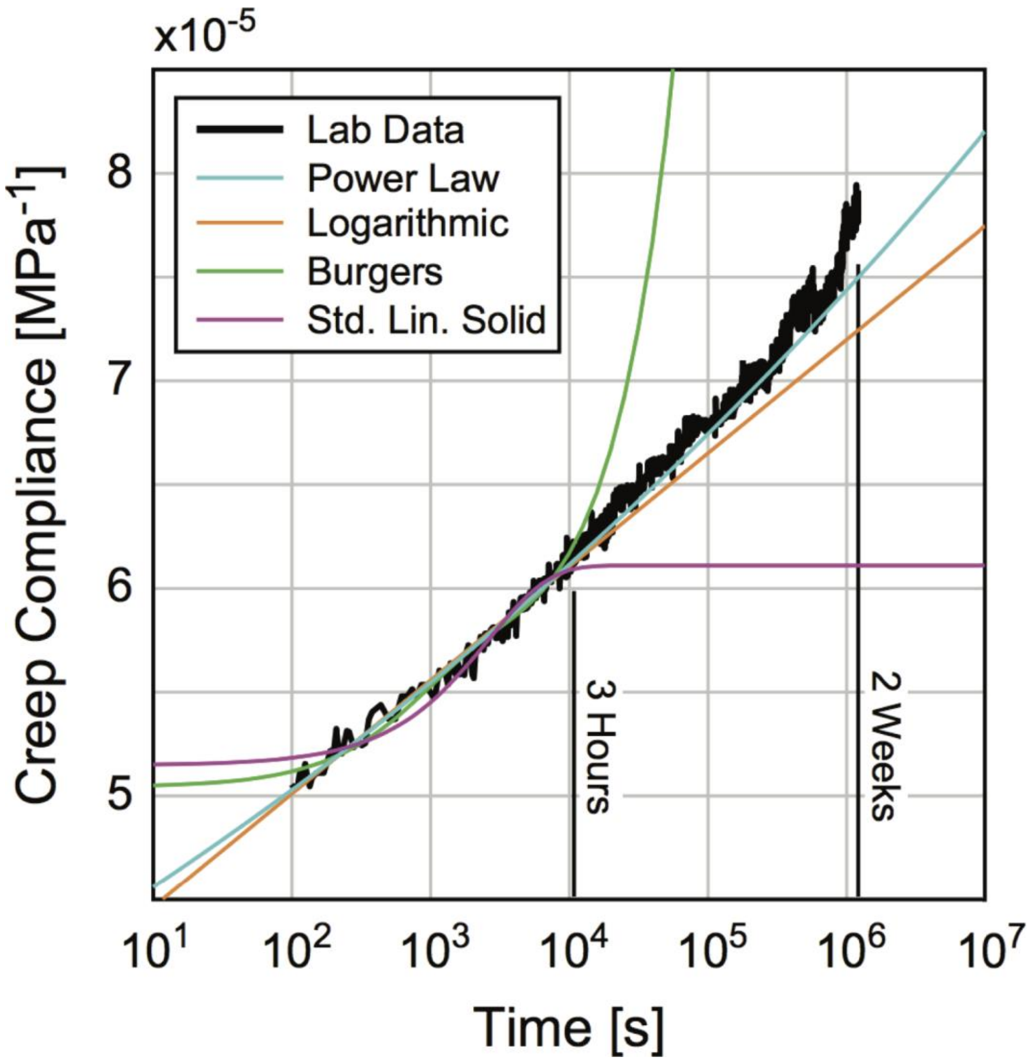

Viscoelastic Power Law

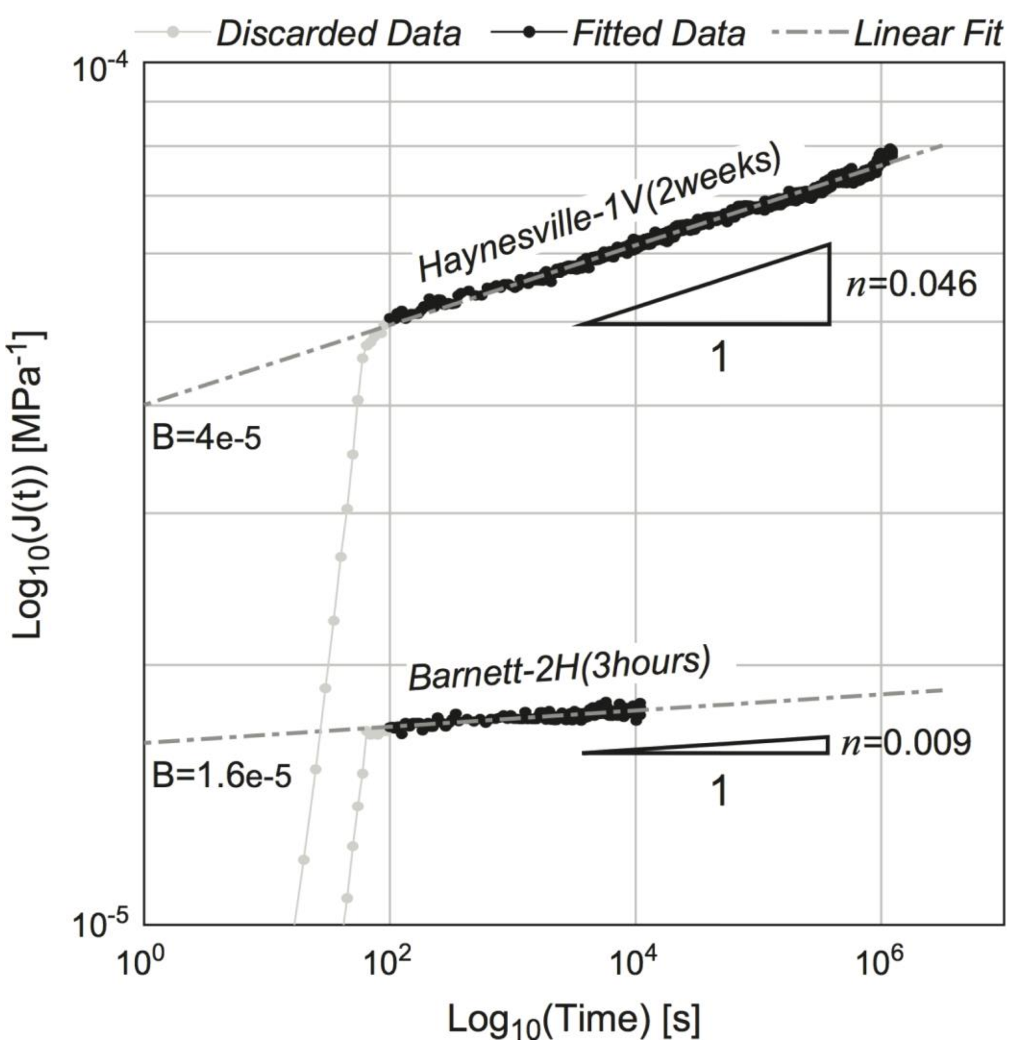

- In log-log space, creep strain is linear with time
- Separate elastic (grey) and creep (black) responses
- Model parameters have simple interpretations
  - *B* describes the elastic compliance
  - B^{-1} correlates with Young's modulus
  - *n* describes the time-dependent response
- Power law model equivalent to Kelvin model in series

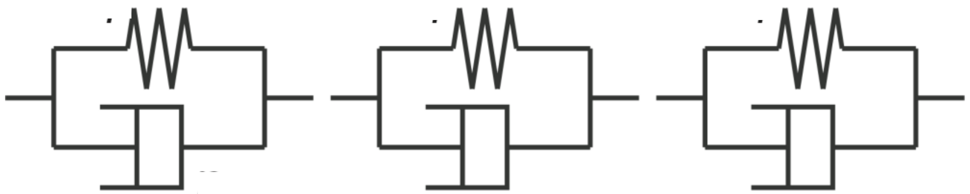

How Do We Implement The VSR Concept in Practice?

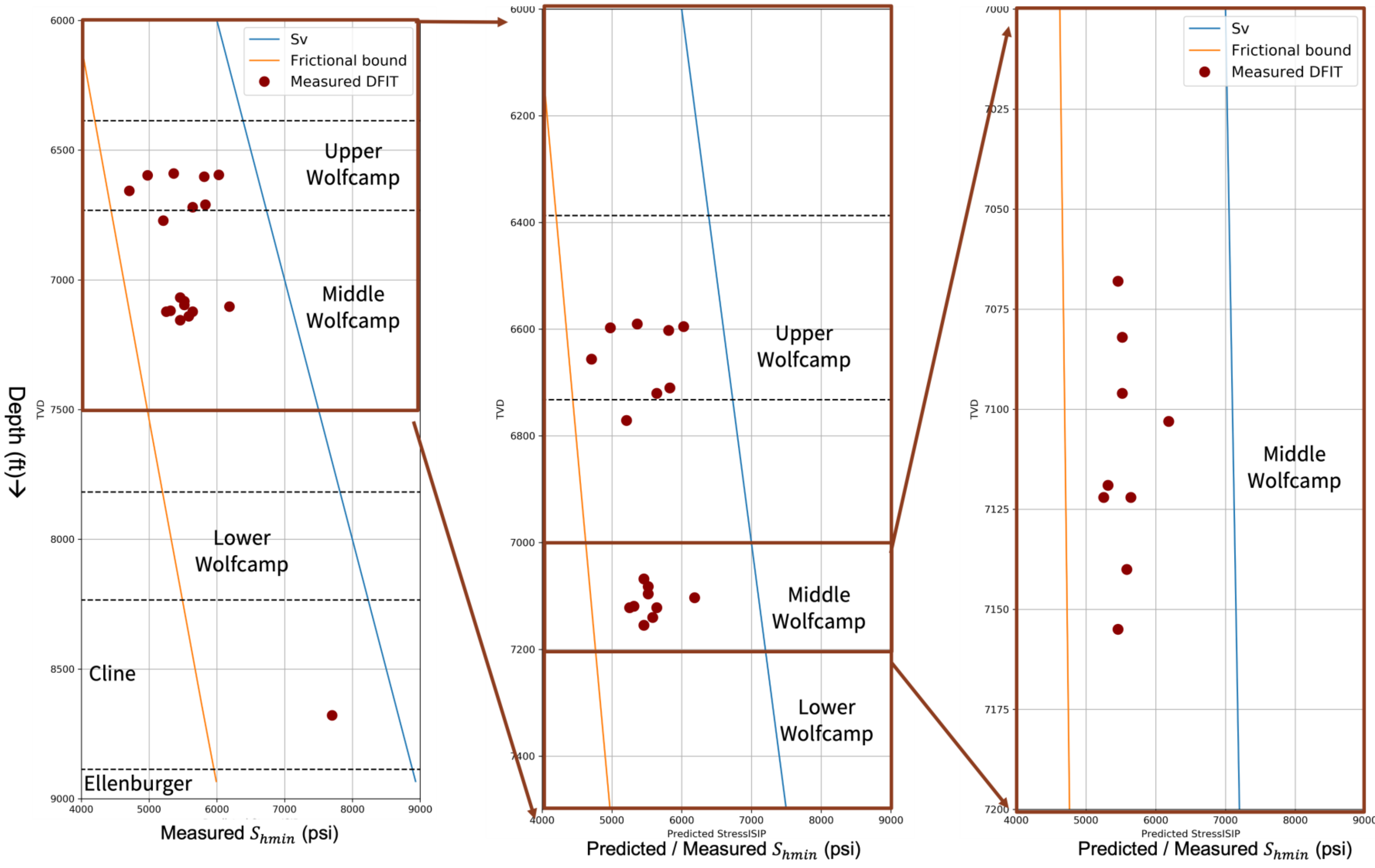

Singh and Zoback (*Geophysics*, 2022)

Predicting Variations of the Least Principal Stress With Geophysical Logs and a Few S_{hmin} Measurements

$$S_1 - S_3 = \epsilon_0 E_{horz} \frac{t^{-n}}{1-n}$$

$$\kappa(S_v - S_{hmin}) = \epsilon_0 \frac{t^{-n}}{1-n} E_{horz}$$

$$S_v - S_{hmin} = \epsilon_0 \frac{t^{-n}}{\kappa(1-n)} E_{horz}$$

$$S_v - S_{hmin} = n^*_{\epsilon t} E_{horz}$$

$$n^*_{\epsilon t} = f(v_{clay}, v_{calcite}, v_{quartz}, GR, \rho, \Omega, \phi)$$

Singh and Zoback (*Geophysics*, 2022)

S_{hmin} Profile is Computed by Fitting $n^*_{\epsilon t}$ as a Function of Well Logs

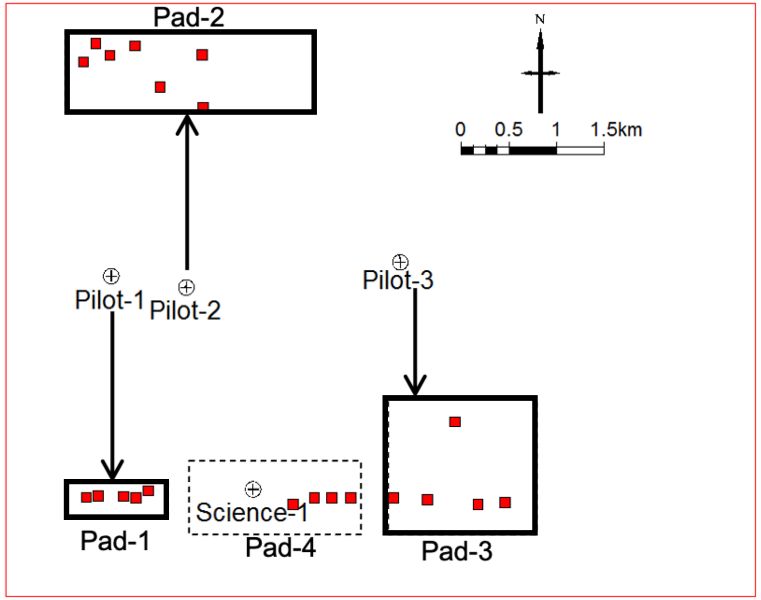

Step 1: **Fit**

Fit $n^*_{\epsilon t} = f(v_{clay}, v_{calcite}, v_{quartz}, GR, \rho, \Omega, \phi)$

Minimize:

$$RSS_{\mathrm{linear}} = \sum_{i=1}^{n}\left(y_i - \beta_0 - \sum_{j=1}^{p}\beta_j x_{ij}\right)^2$$

$$RSS_{lasso} = \sum_{i=1}^{n}\left(y_i - \beta_0 - \sum_{j=1}^{p}\beta_j x_{ij}\right)^2 + \lambda\sum_{j=1}^{p}|\beta_j|$$

$$RSS_{ridge} = \sum_{i=1}^{n}\left(y_i - \beta_0 - \sum_{j=1}^{p}\beta_j x_{ij}\right)^2 + \lambda\sum_{j=1}^{p}\beta_j^2$$

Step 2: **Predict**

Predict $n^*_{\epsilon t}$ as a function of depth (z) and calculate:

$$S_{hmin}(z) = S_V(z) - n^*_{\epsilon t}(z)E_{horz}(z)$$

Step 3: **Use geological constraints**

Use S_V and frictional bounds to constrain the stress profile

Singh and Zoback (*Geophysics*, 2022)

VSR Predicts 17 S_{hmin} Measurements ($R^2 \approx 0.9$)

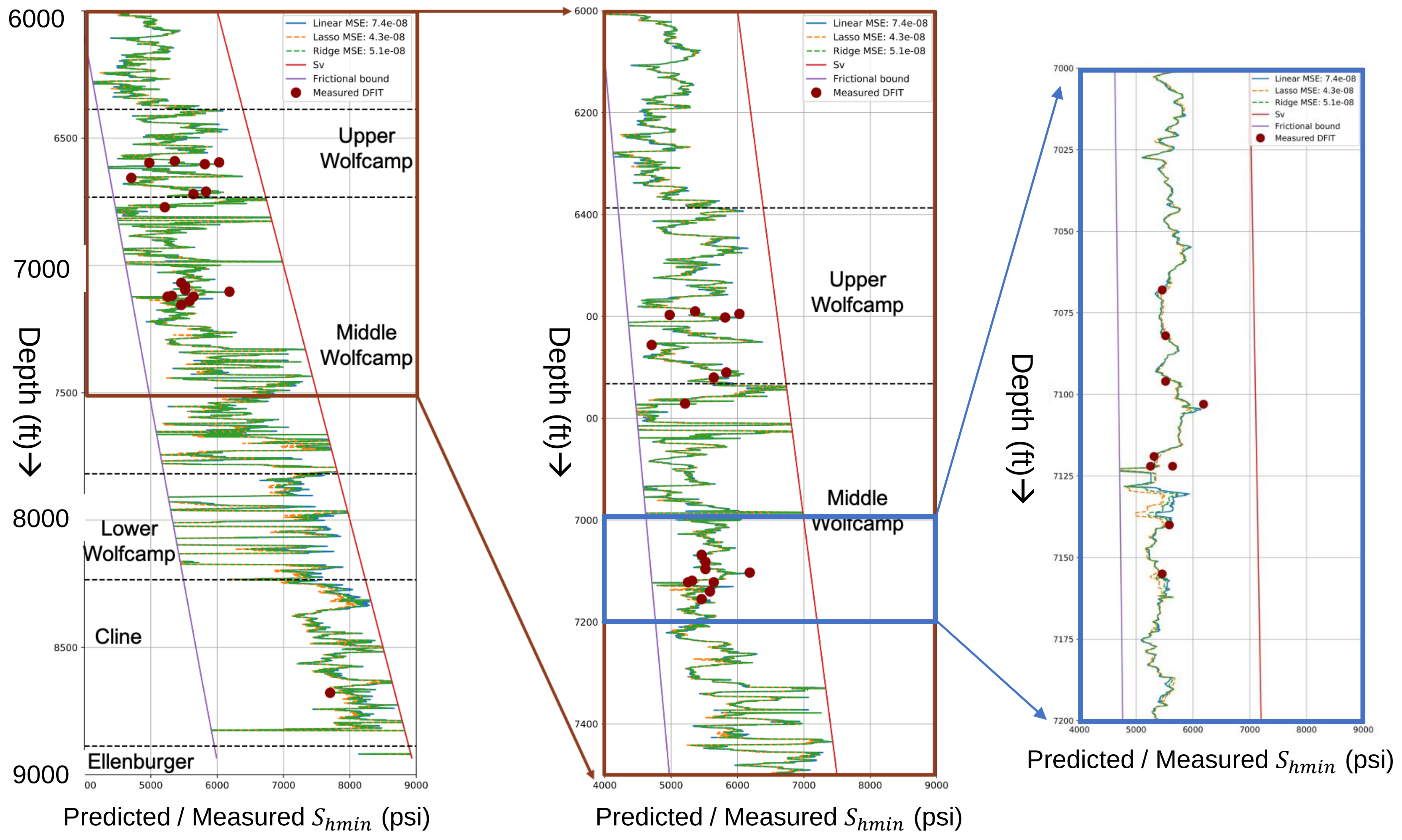

(Singh and Zoback, *Geophysics*, 2022)

Barriers to Fault Propagation are Lithologically Controlled, Quantitatively Estimated and Can Help Understand Mmax

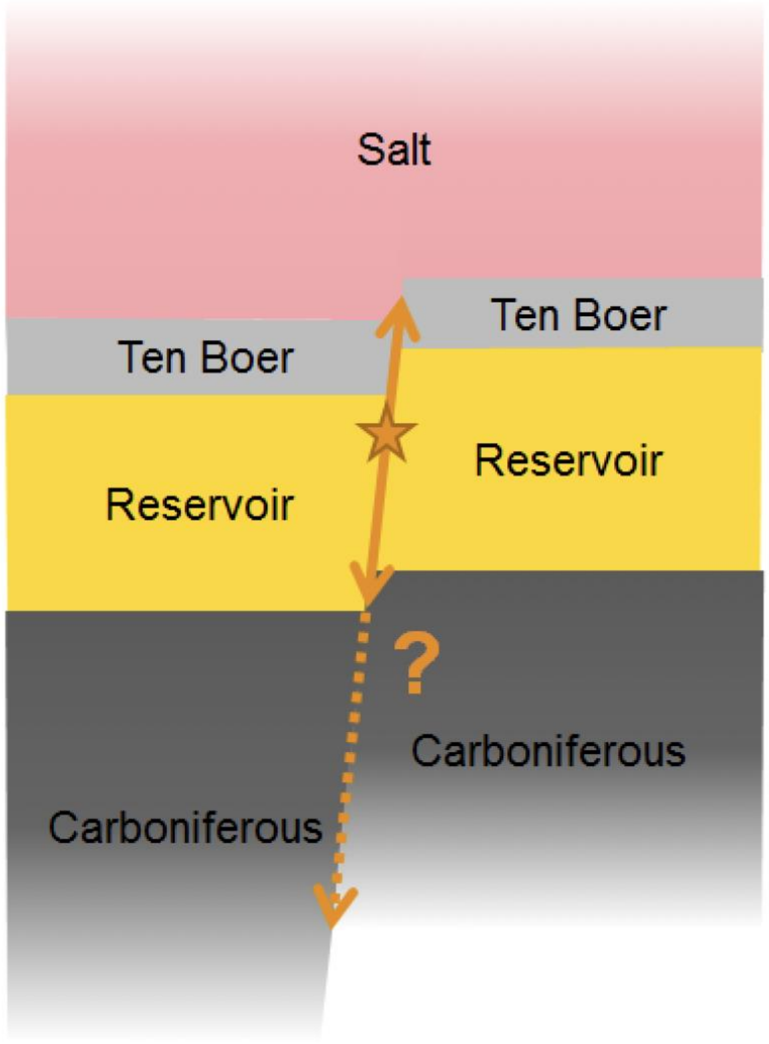

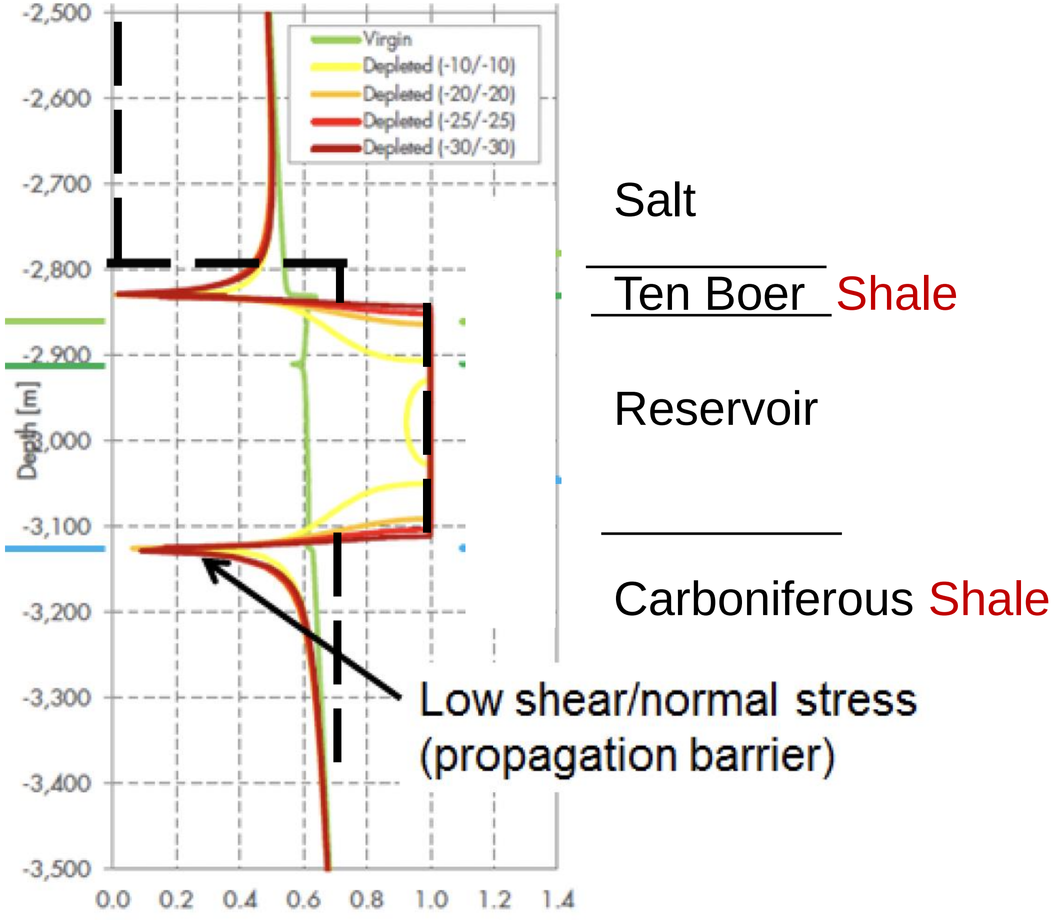

Fault Shear Capacity

NAM (ExxonMobil Mmax) 2016

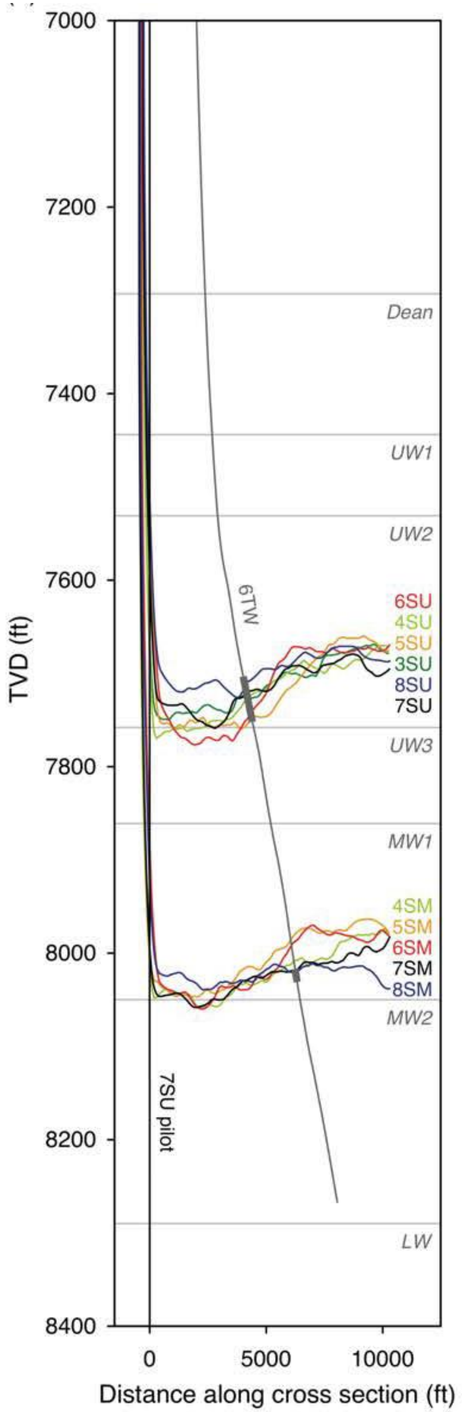

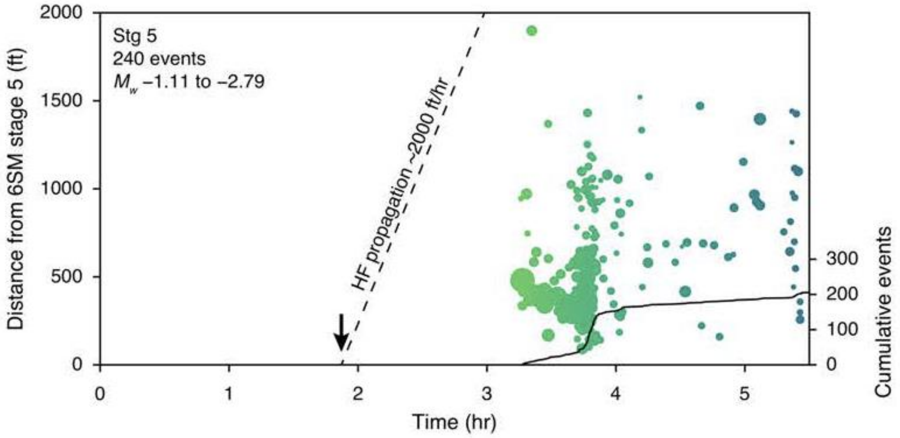

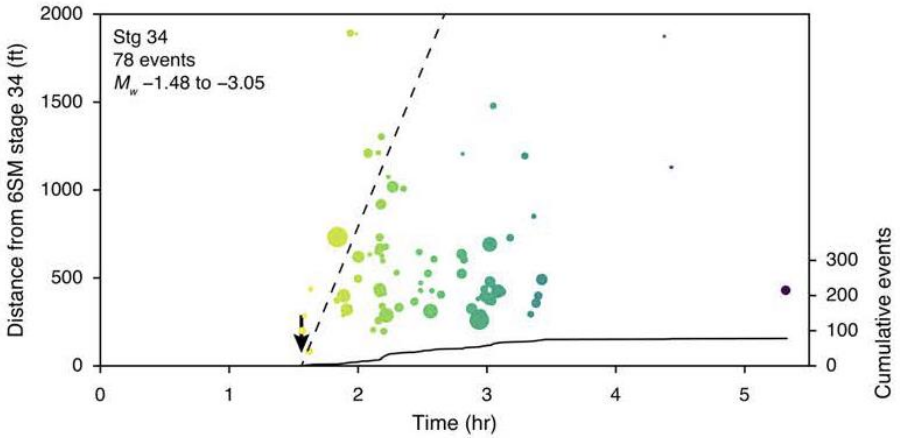

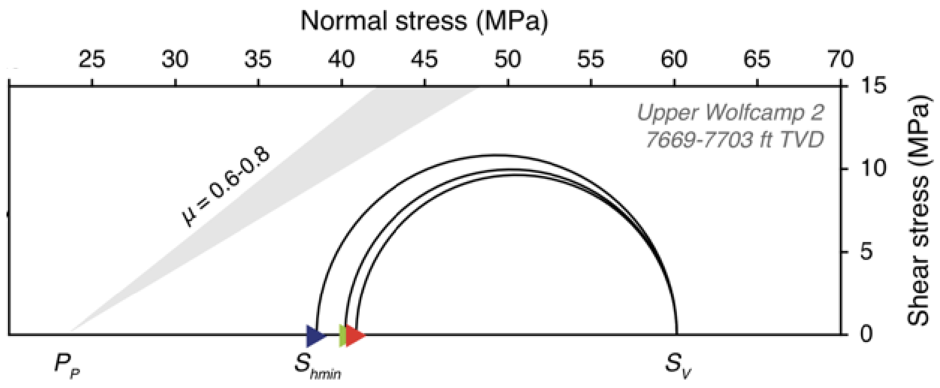

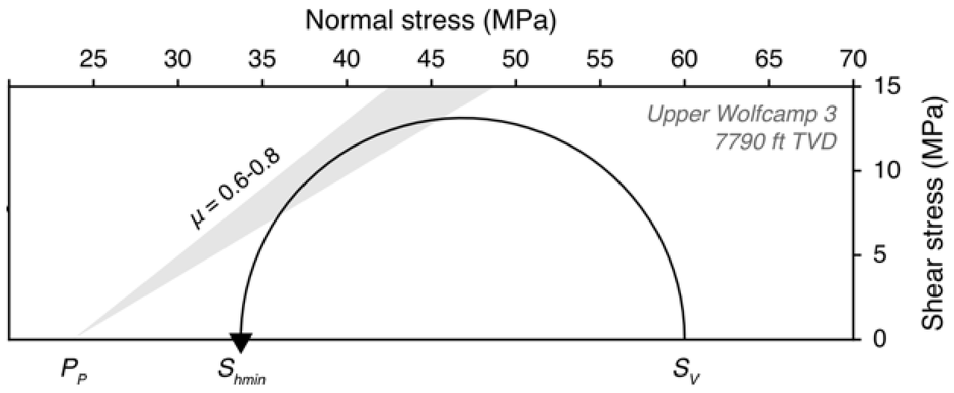

Kohli and Zoback (*Energies*, 2021)

Microseismic Triggering Pressure

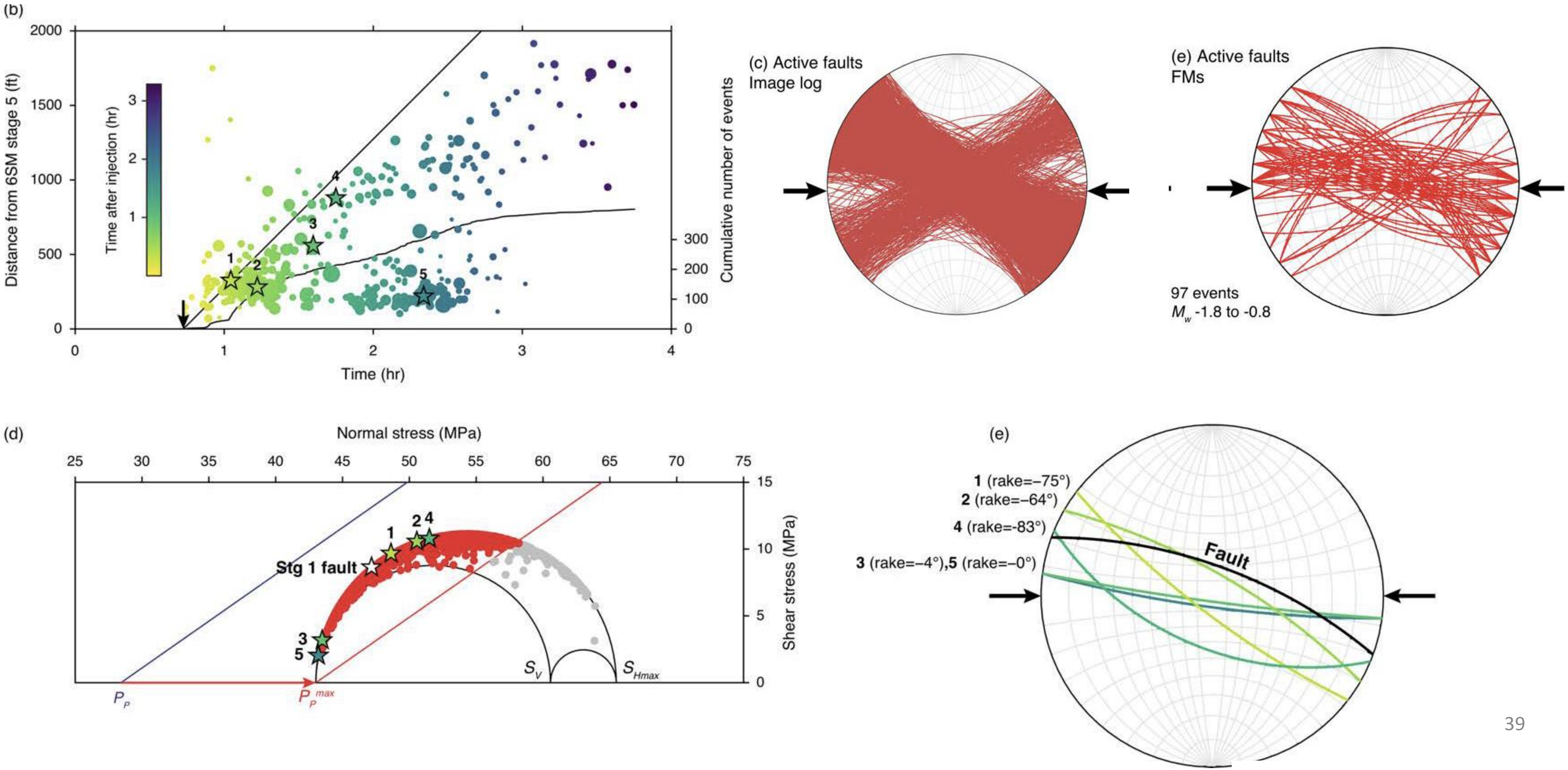

Kohli and Zoback (*Energies*, 2021)

Microseismic b-Values are High and Highly Variable

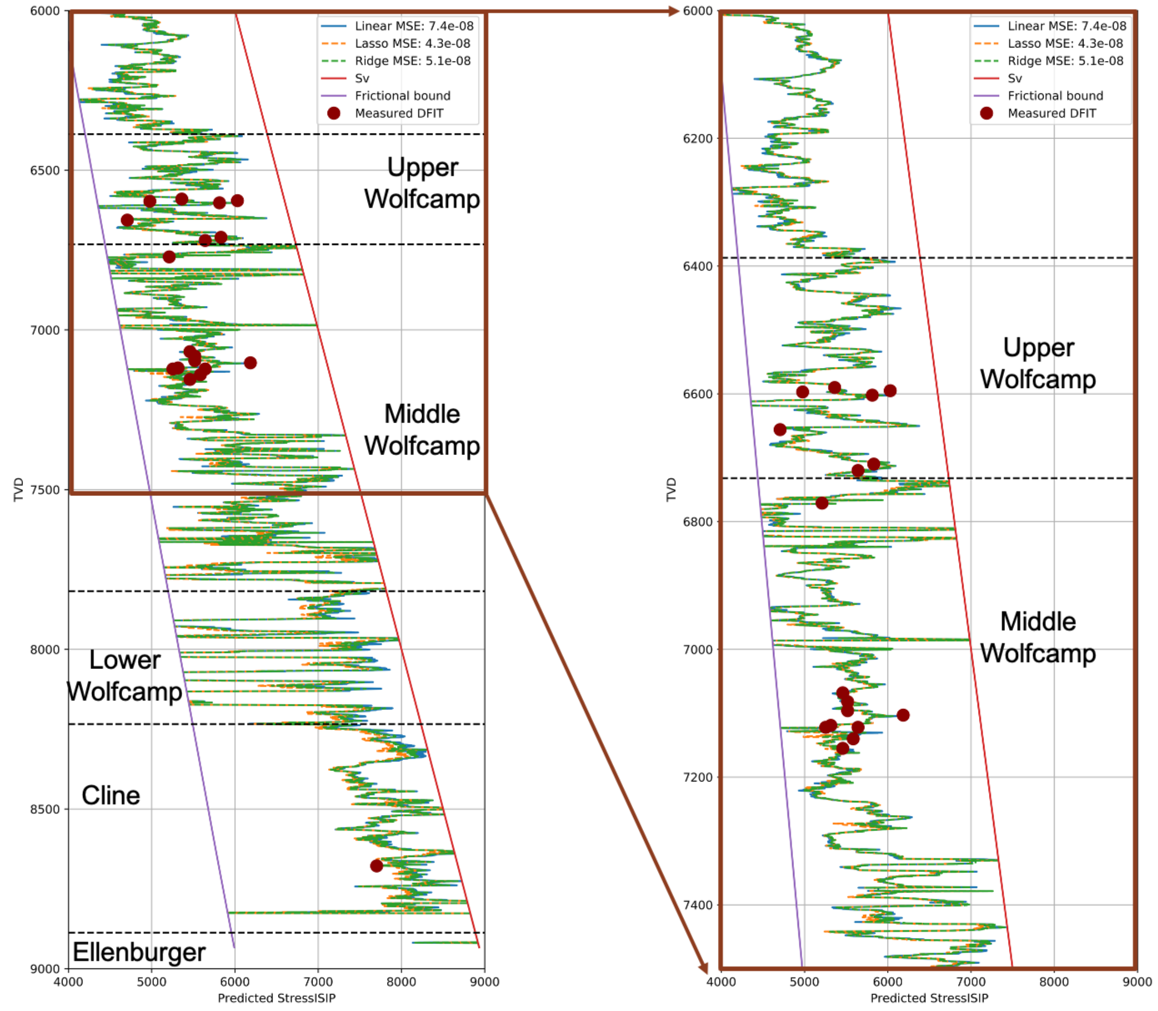

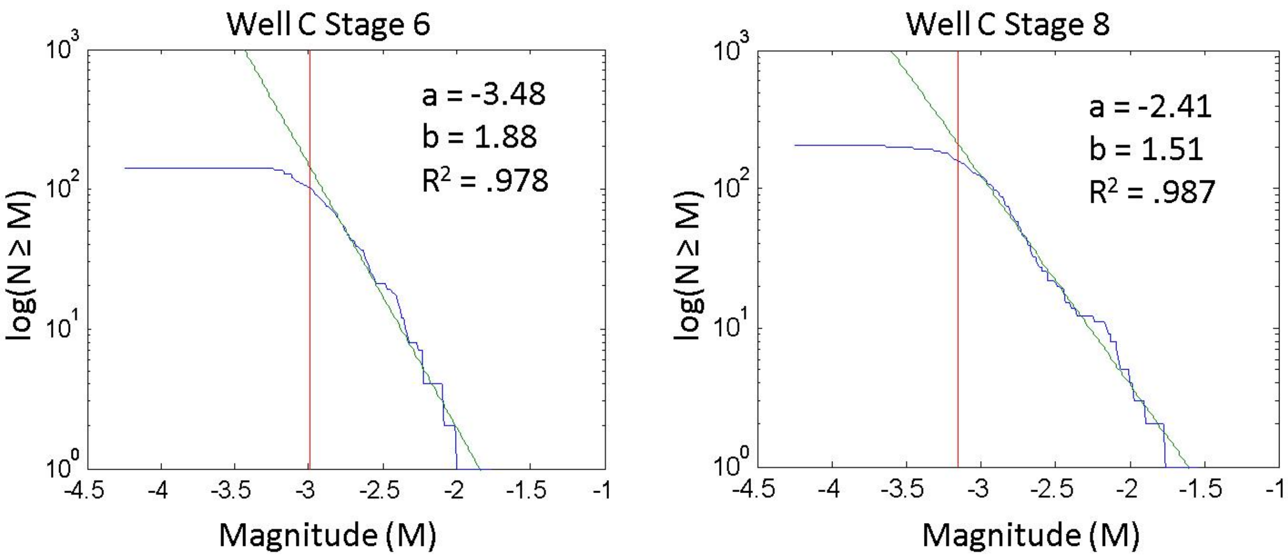

- Stages Exhibit Classic Log-Linear Scaling
- b-Values are Always Greater Than 1, and Variable Between Stages
- Greater Proportion of Small Events to "Large" Events

Three Topics

1. Relevant Learnings From Injection Induced Seismicity

2. Poroelastic Stress Paths and Earthquakes Induced by Depletion
   - Poroelastic Stress Paths for Beginners
     - Linear Elastic, ΔP is Homogeneous
   - Observations from Several Conventional Reservoirs
     - Linear Elastic, ΔP Homogeneous
   - Anomalously Steep Stress Paths Can Trigger Normal Faulting
   - What We Know About Groningen?

3. Mmax and the Potential for Faulting in the Carboniferous

Three Topics

1. Relevant Learnings From Injection Induced Seismicity

2. Poroelastic Stress Paths and Earthquakes Induced by Depletion
    - Poroelastic Stress Paths for Beginners
        - Linear Elastic, ΔP is Homogeneous
    - Observations from Several Conventional Reservoirs
        - Linear Elastic, ΔP Homogeneous
    - Anomalously Steep Stress Paths Can Trigger Normal Faulting
    - What We Know About Groningen?

3. Mmax and the Potential for Faulting in the Carboniferous

Stress Path Within a Homogeneous Poroelastic Depleting Reservoir

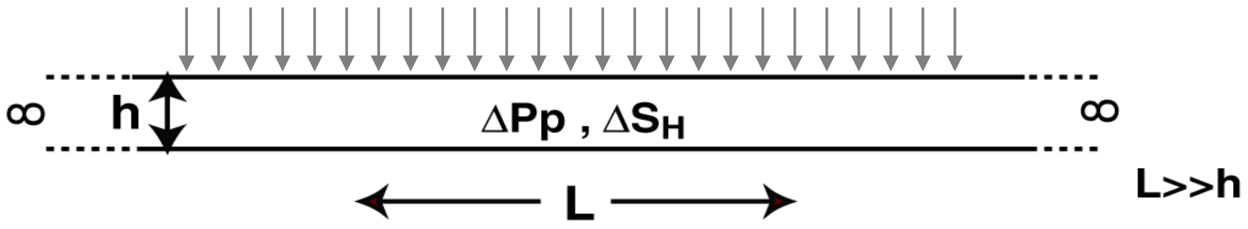

Using instantaneous application of force and pressure with no lateral strain:

$$S_{Hor} = \left(\frac{\nu}{1-\nu}\right)(S_v) + \alpha P\left(1 - \frac{\nu}{1-\nu}\right) \qquad \alpha = 1 - \frac{K_b}{K_g}$$

Take the derivative of both sides and simplify

$$\Delta S_{Hor} = \alpha \frac{(1-2\nu)}{(1-\nu)} \Delta P_p$$

$$A = \frac{\Delta S_{Hor}}{\Delta P_P}$$

Stress Path

if $\nu = 0.25, \alpha = 1$ $\qquad \Delta S_{Hor} = \frac{2}{3}\Delta Pp$

Quantifying Biot Coefficient in Unconventional Formations

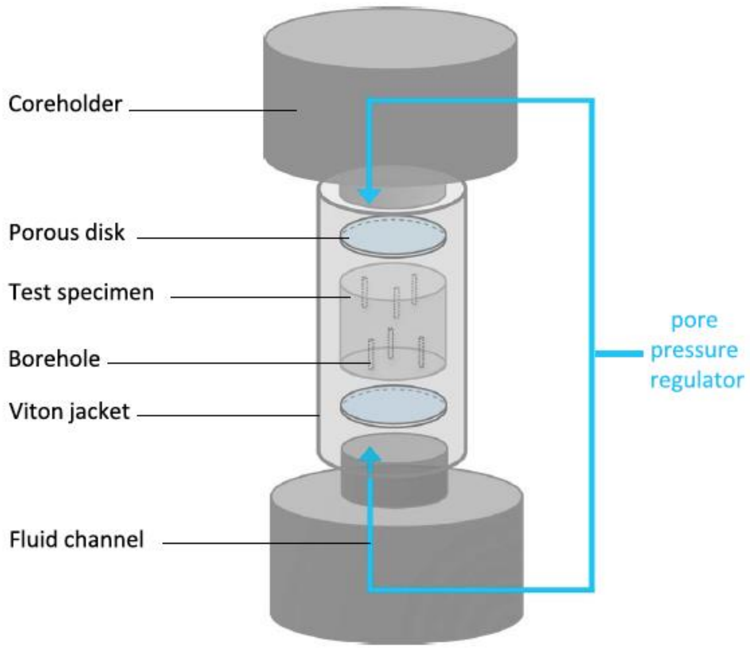

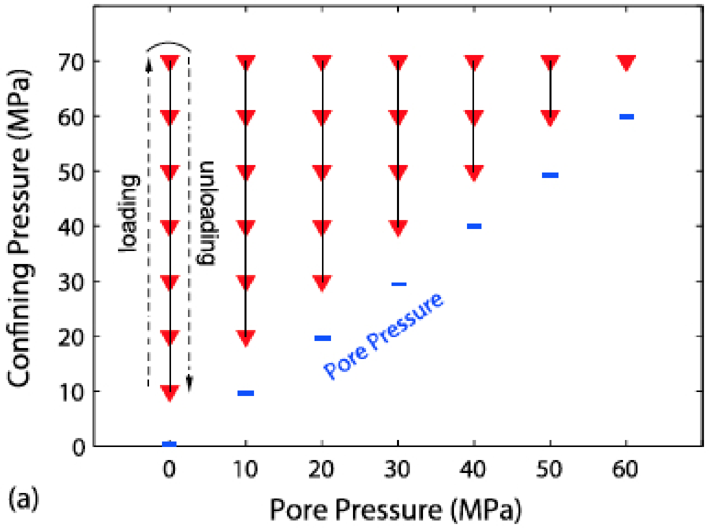

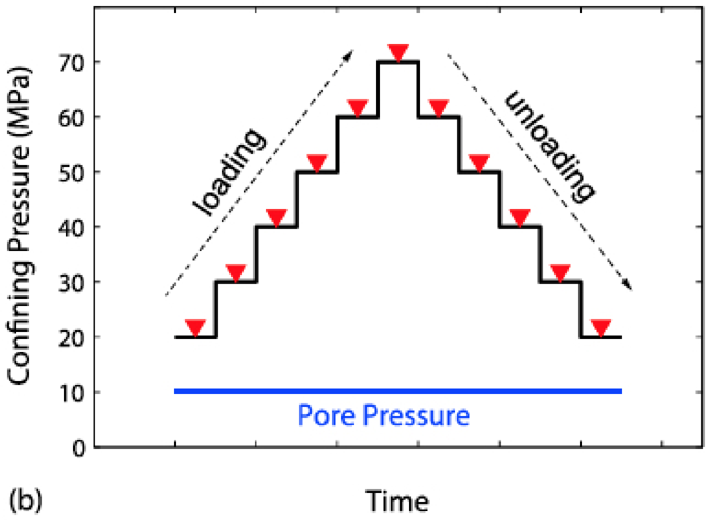

$$\alpha = 1 - \frac{K_{bulk}}{K_{grain}} = 1 - \frac{(\partial \sigma / \partial \varepsilon_v \mid P_p)}{(\partial P_p / \partial \varepsilon_v \mid \sigma)}$$

K_{bulk} = Drained bulk modulus of rock (Readily measured)

K_{grain} = Bulk modulus of solid grains (Difficult to estimate)

$\alpha \rightarrow 0$; Solid rock frame with no pores ($\Phi \rightarrow 0$). No pore pressure influence

$\alpha \rightarrow 1$; Very compliant porous solid ($K_{bulk} \rightarrow 0$). Maximum pore pressure influence

Laboratory Measurements of the Biot Coefficient

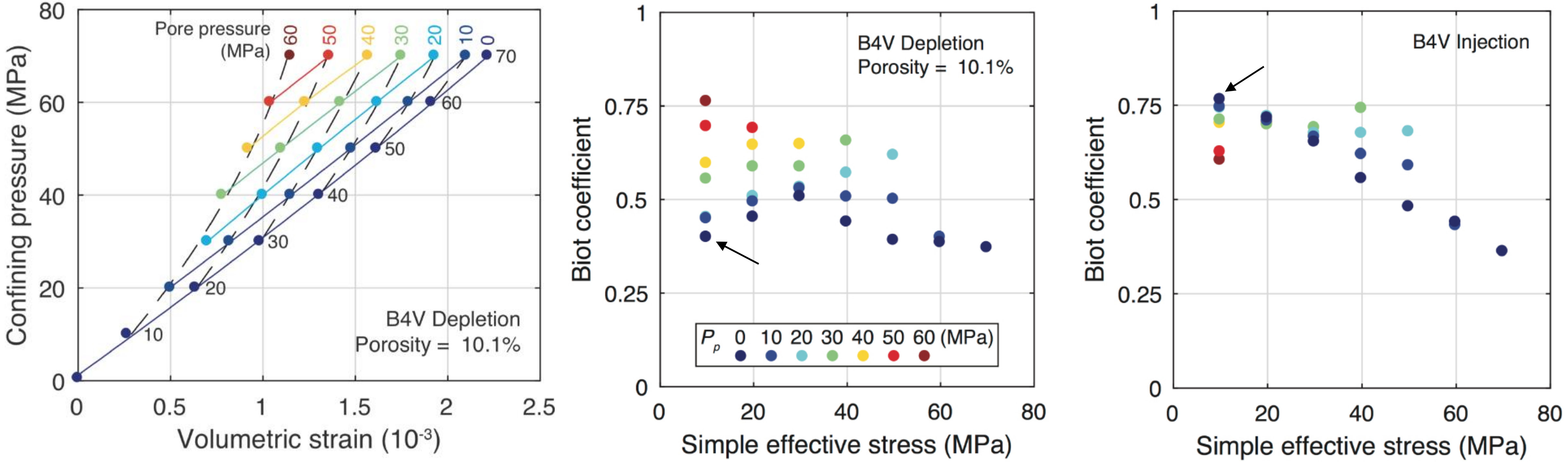

Cores from the Bakken Formation

Ma and Zoback JGR (2017)

Observed Stress Paths

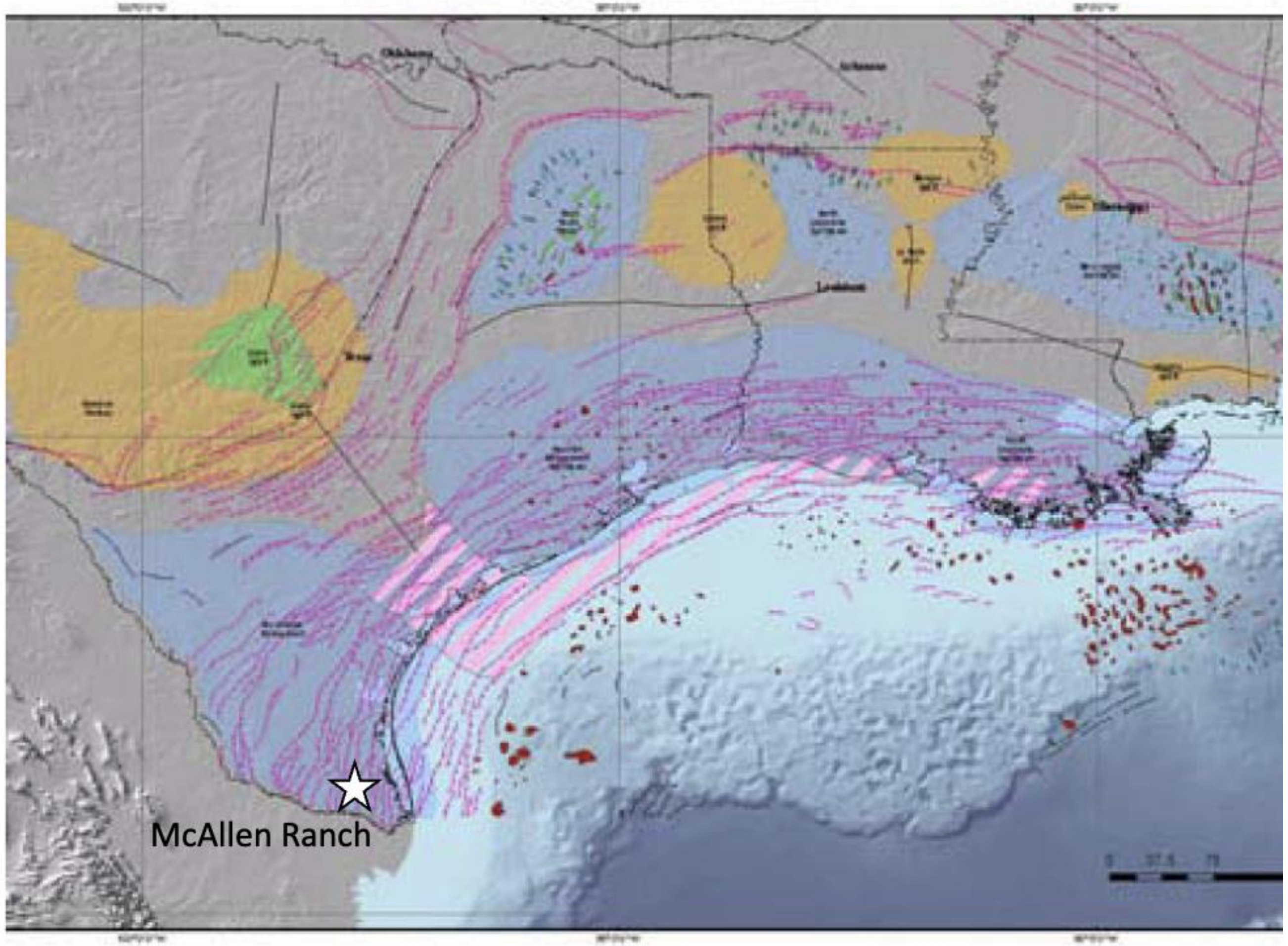

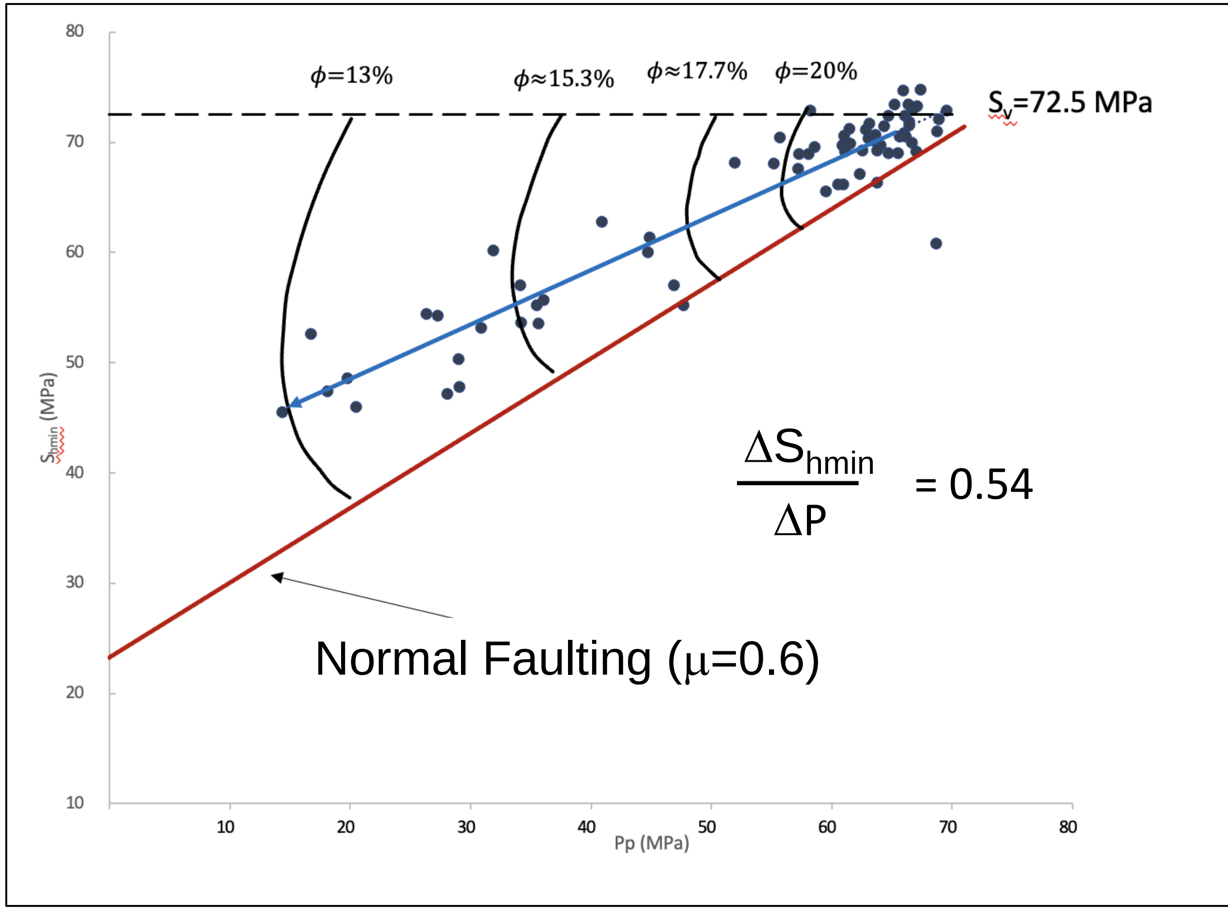

Vicksburg Formation
(McAllen Ranch, onshore GOM Texas)

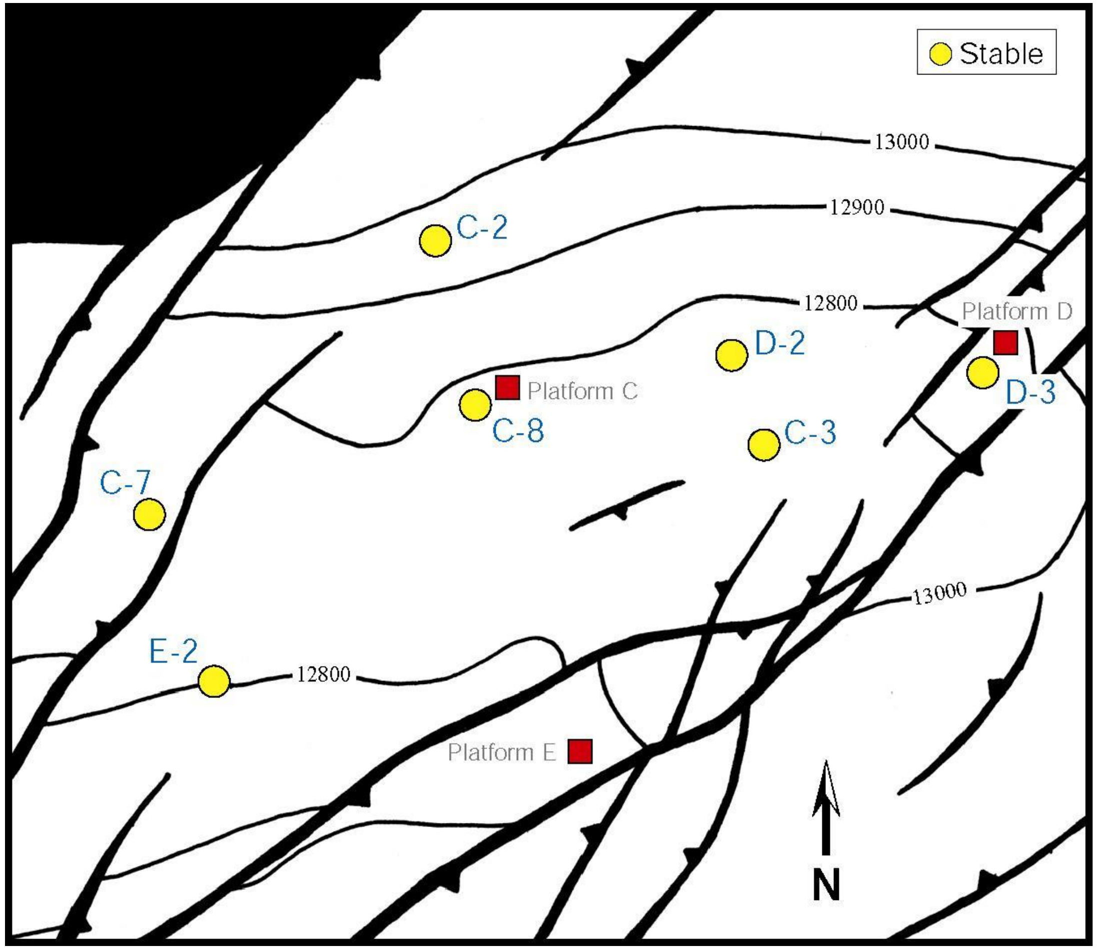
Stable
13000
12900
12800
C-2
Platform D
D-2
Platform C
D-3
C-8
C-3
C-7
13000
E-2
12800
Platform E
N

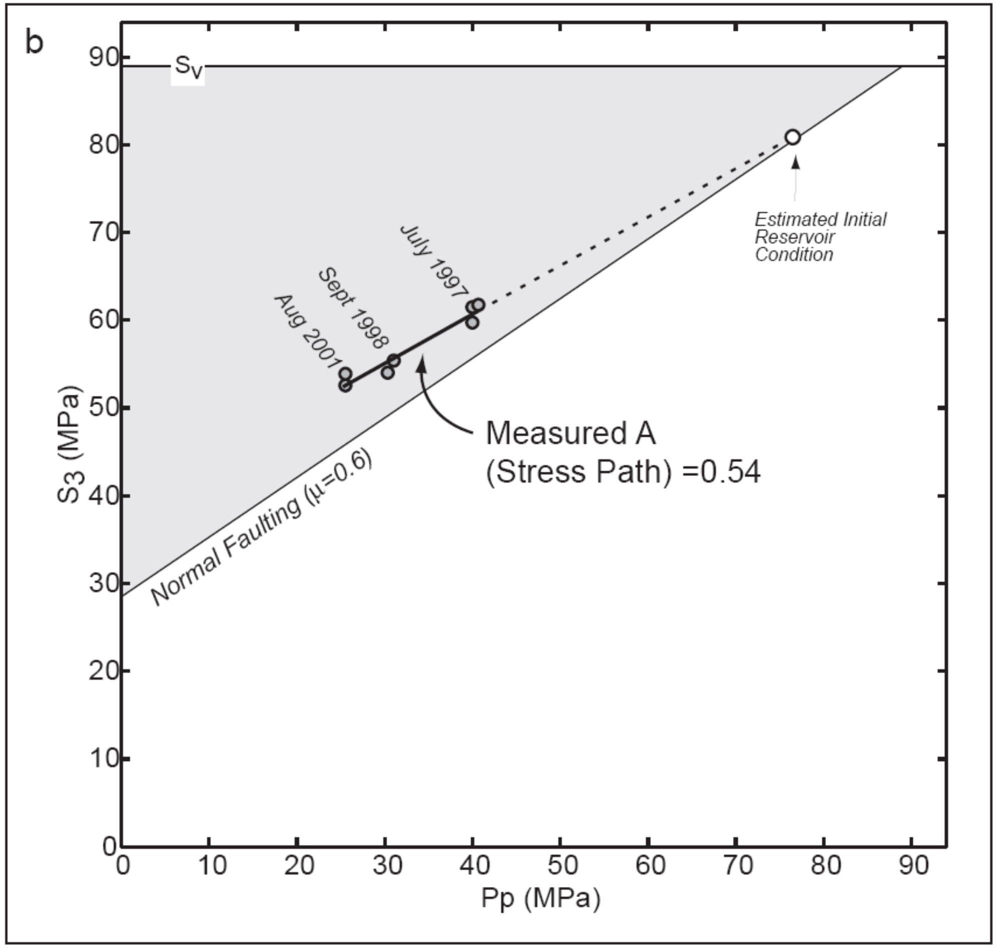
b
Sv
Estimated Initial Reservoir Condition
July 1997
Sept 1998
Aug 2001
Measured A
(Stress Path) =0.54
Normal Faulting (μ=0.6)
S3 (MPa)
Pp (MPa)

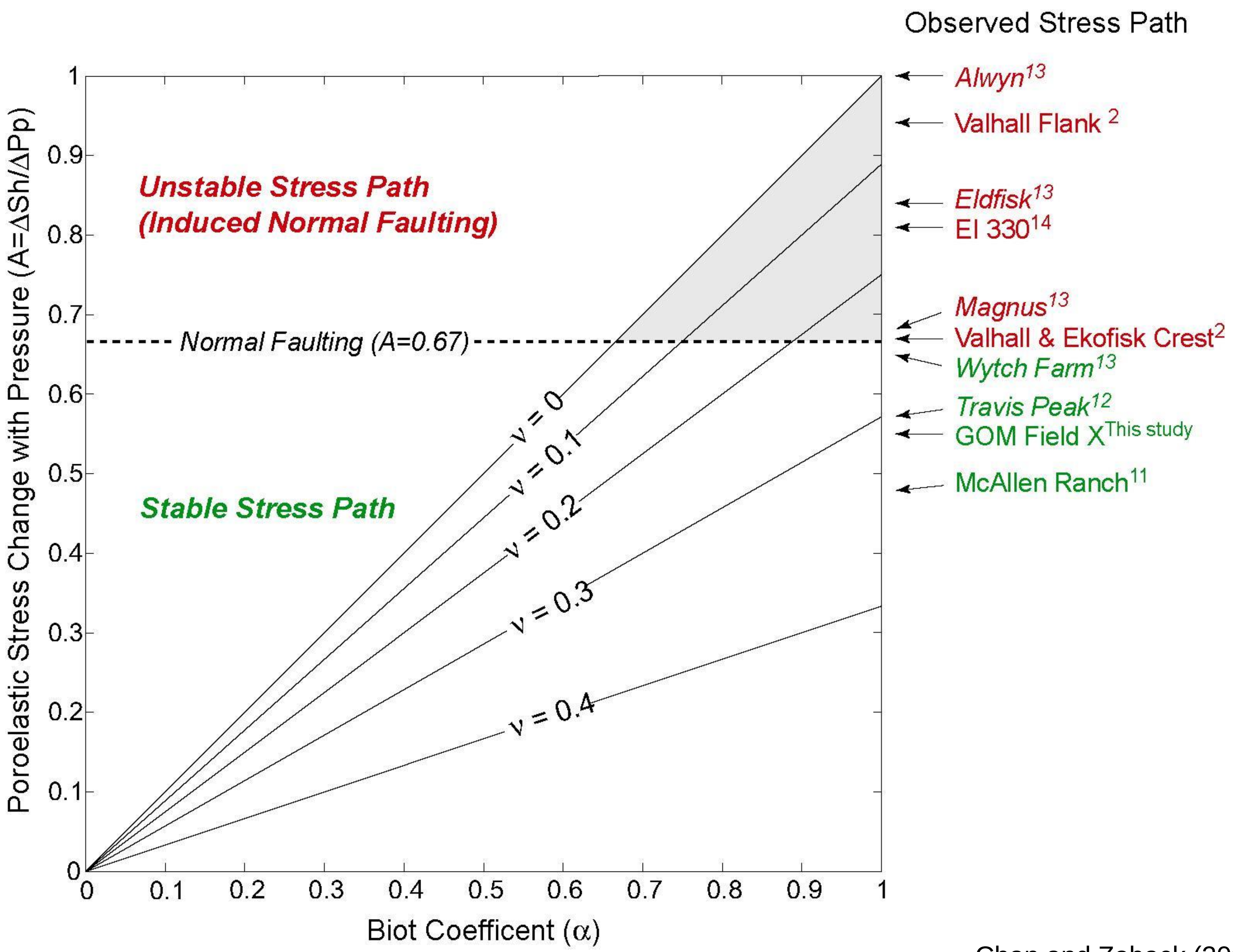

Chan and Zoback (2002)

No Earthquakes are Not Being Triggered Where There Has Been Past Production

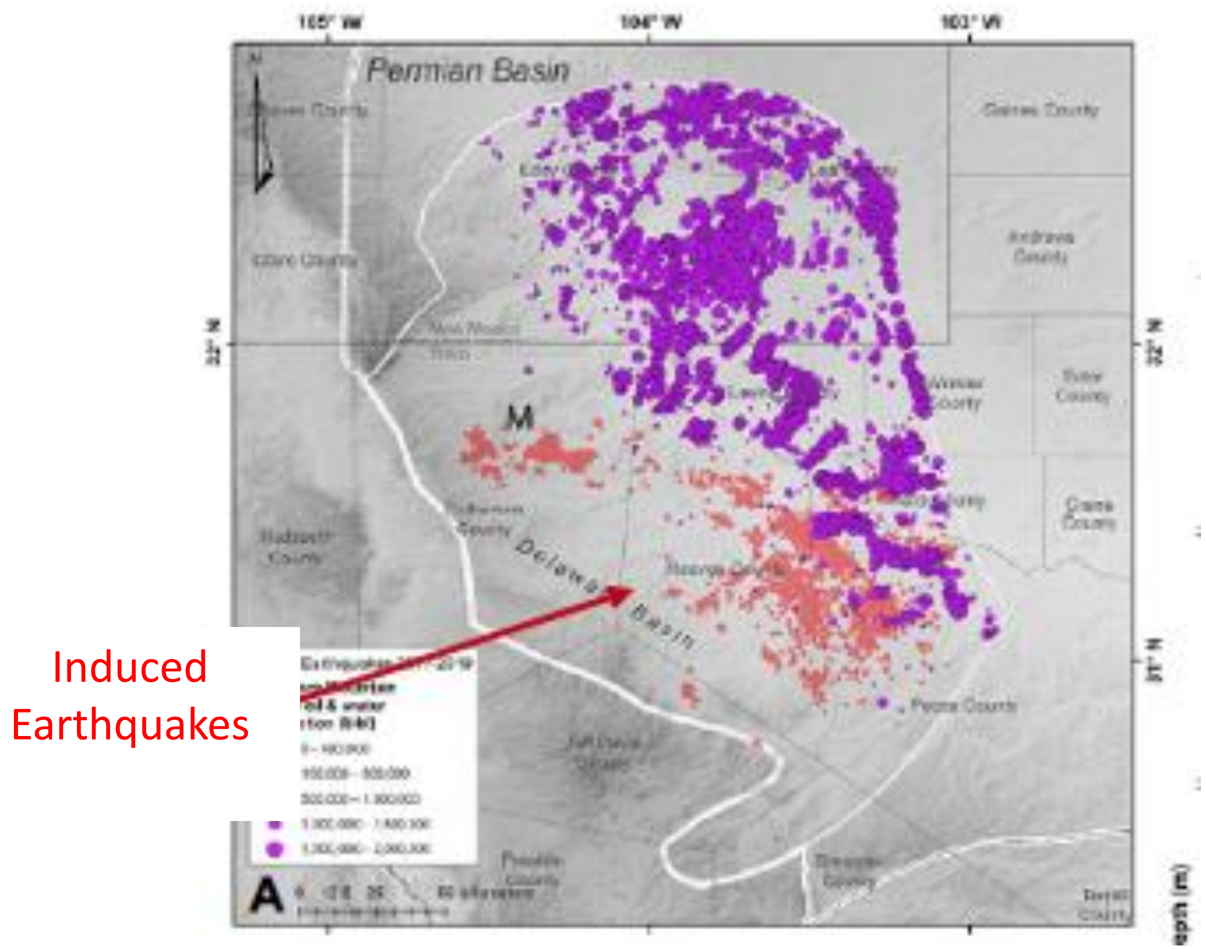

Delaware Mountain Group Production

Poroelastic Stress Path Associated with Depletion Makes Normal Faults More Stable

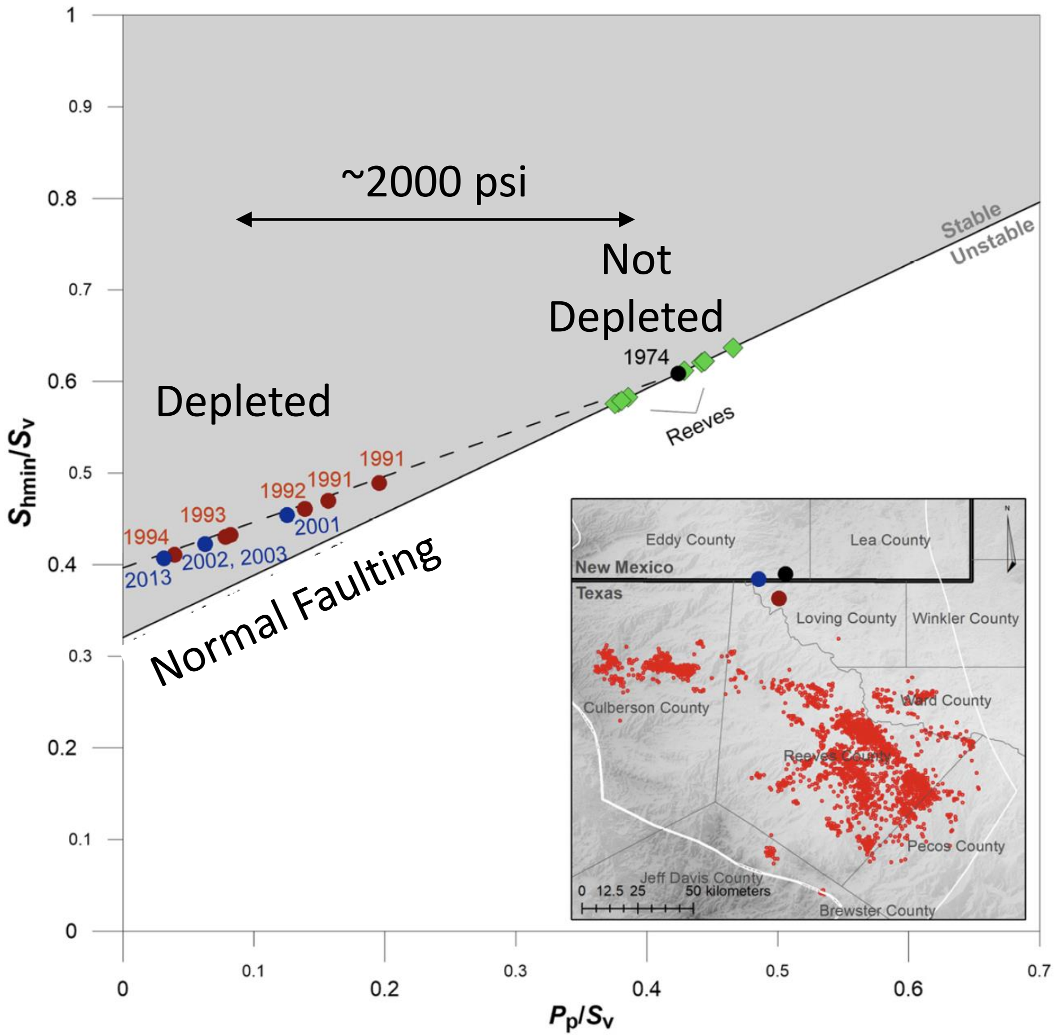

Field X GOM

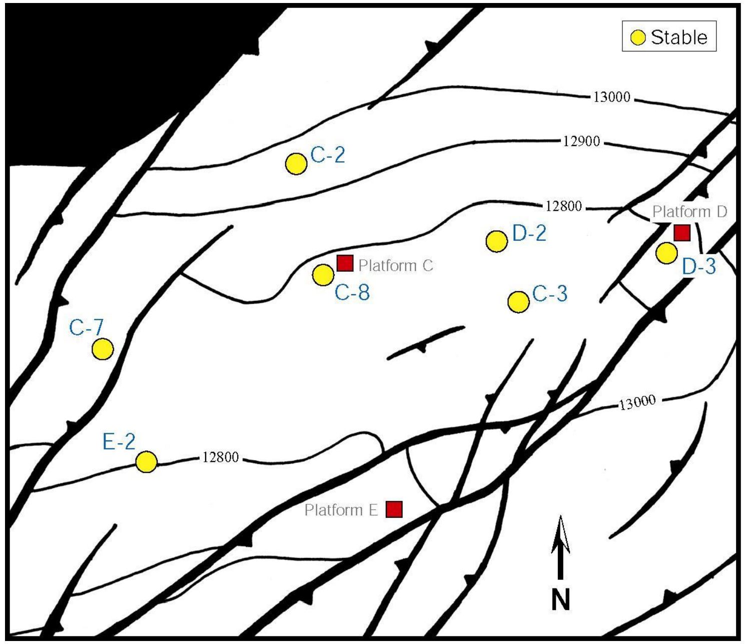

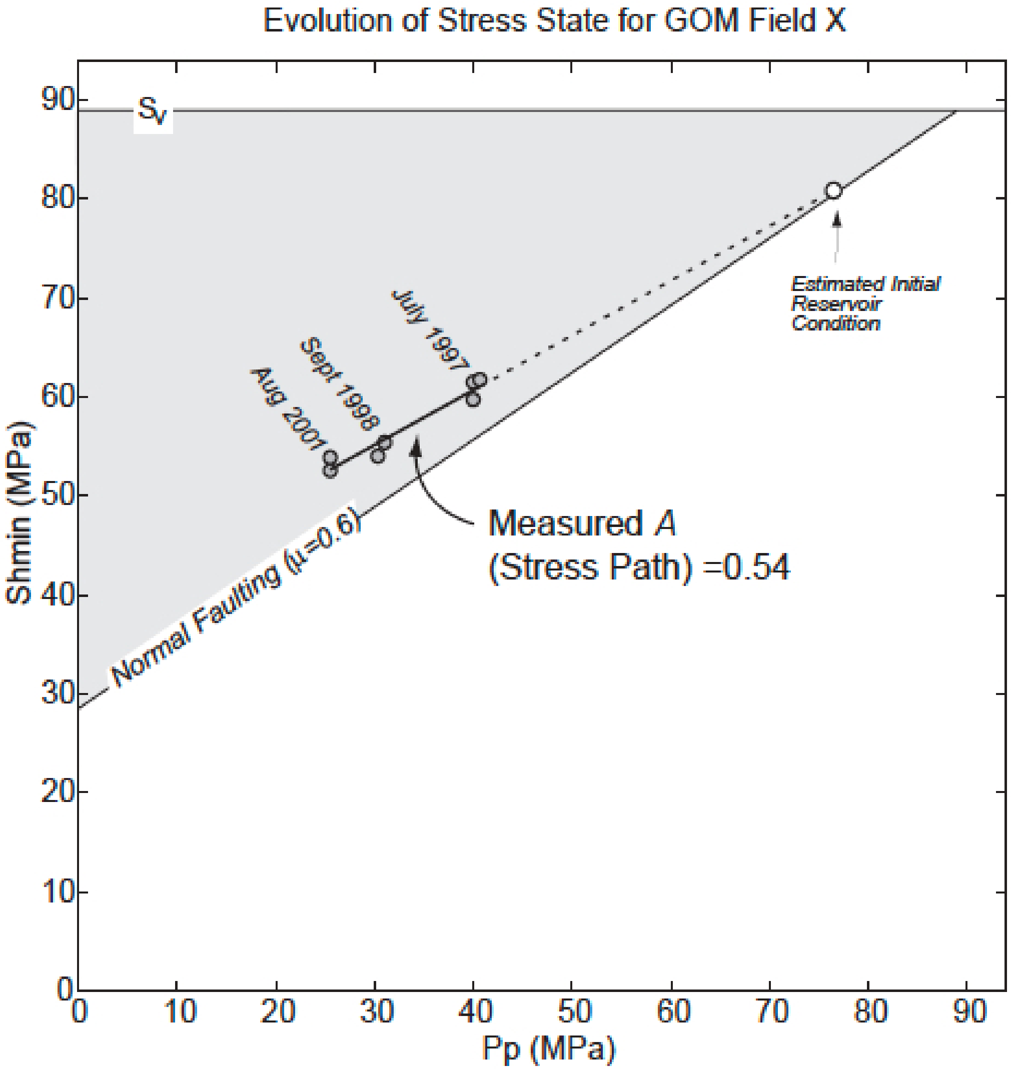

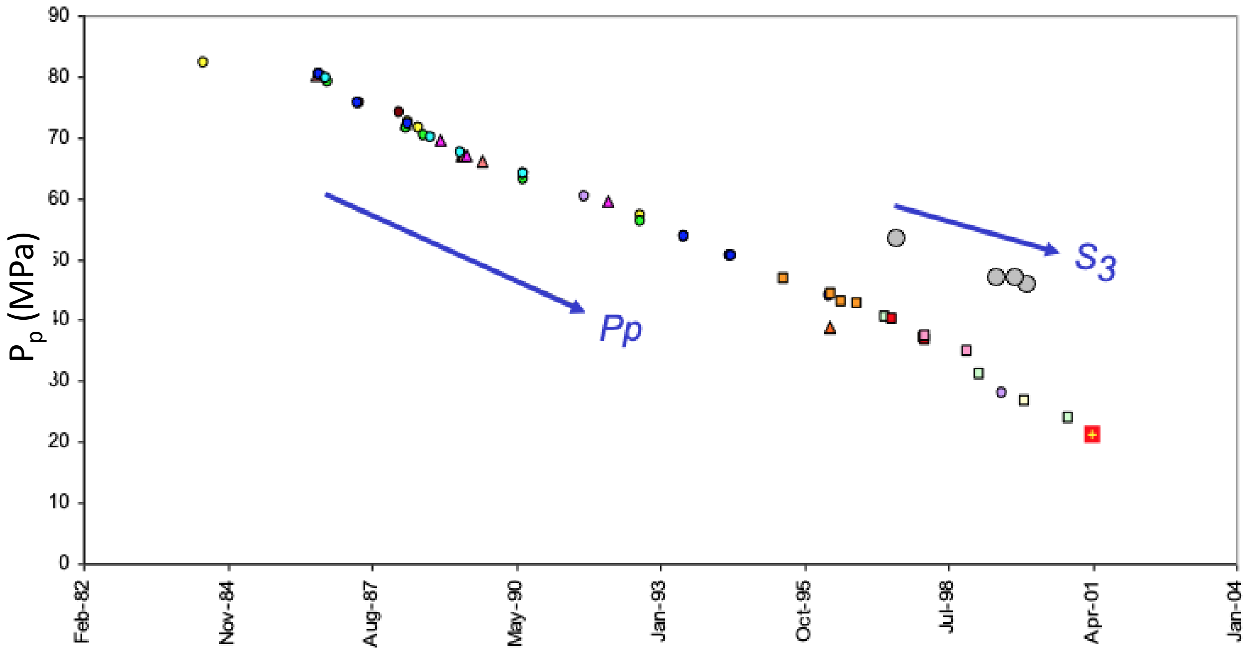

Zoback (2007)

Depletion-Induced Earthquakes Within Valhall Reservoir

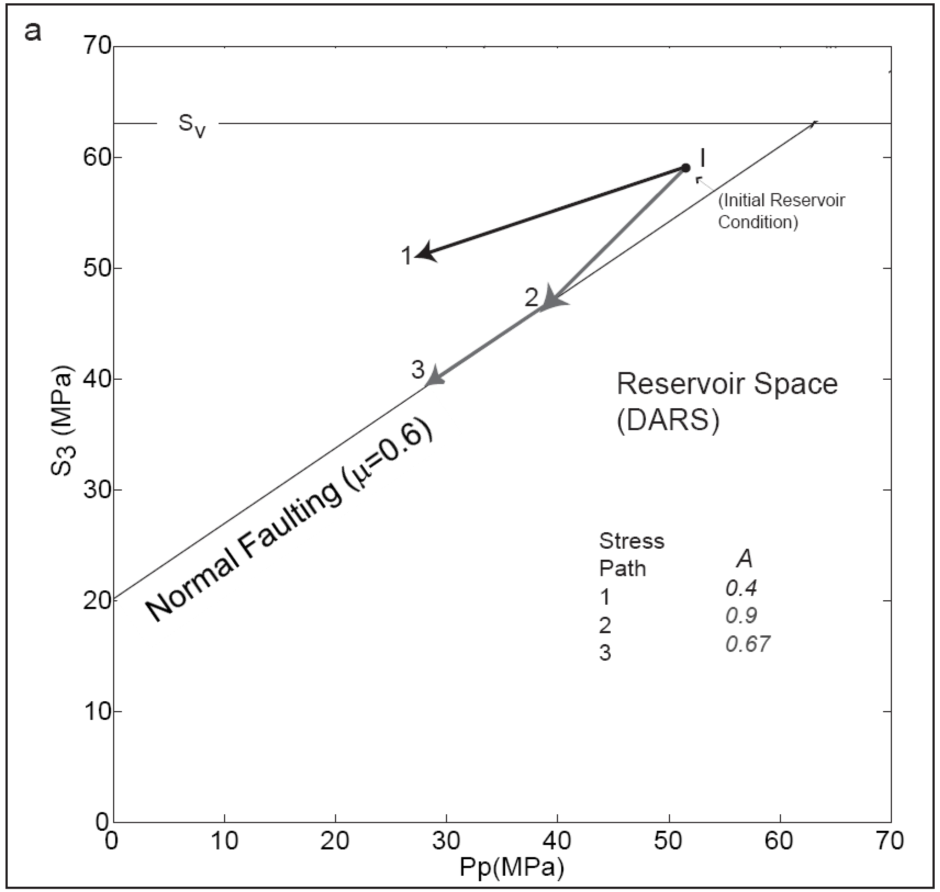

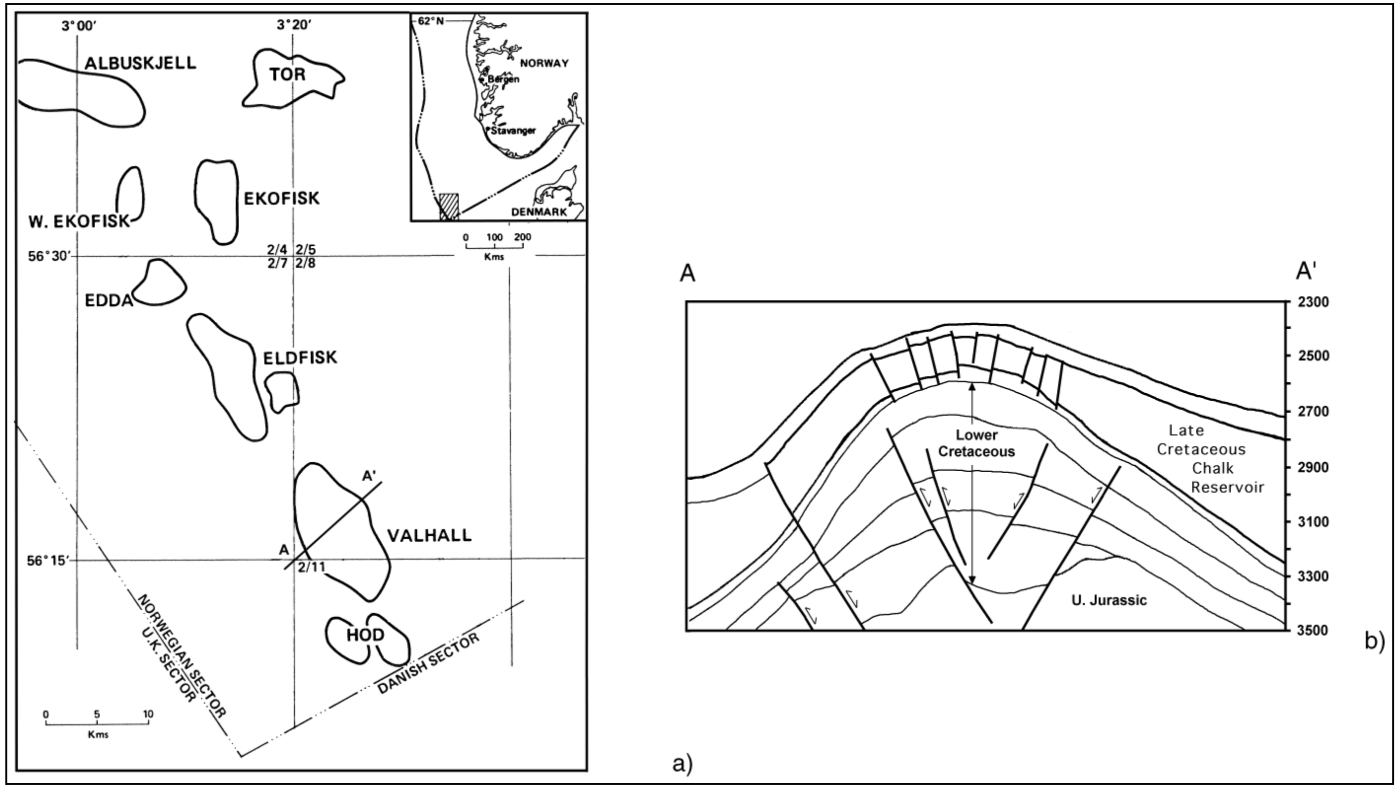

Zoback and Zinke (2002)

Depletion-Induced Earthquakes Within Reservoir

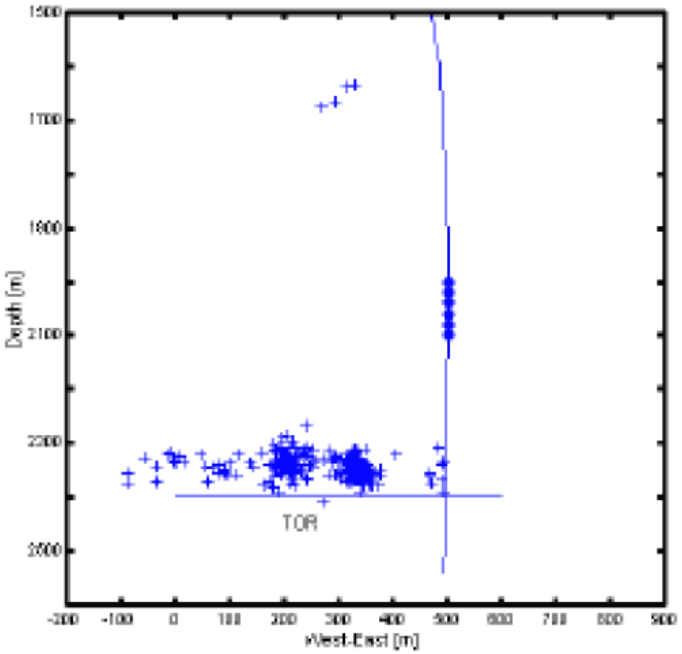

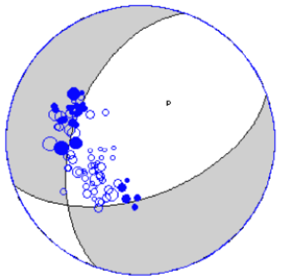

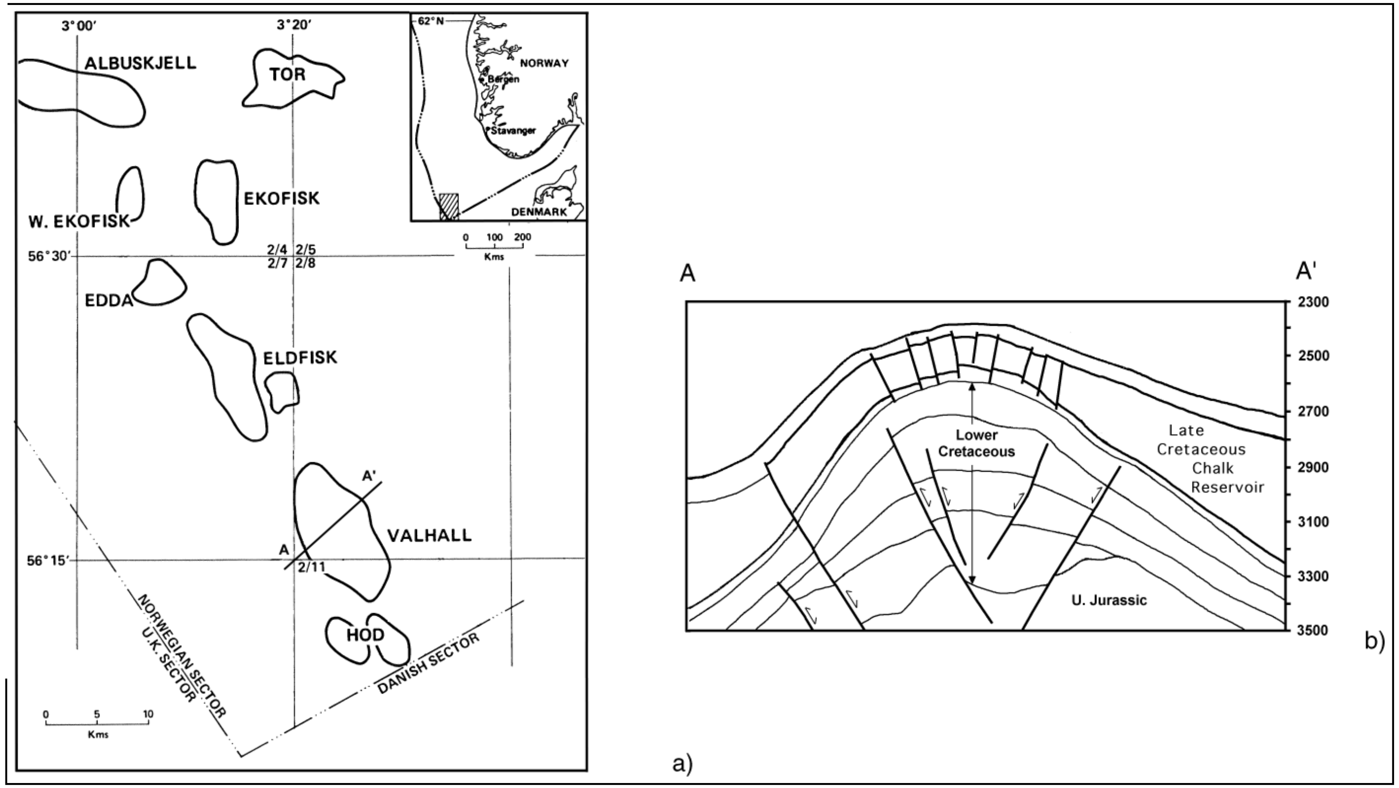

Zoback and Zinke (2002)

Depletion-Induced Earthquakes Within Reservoir

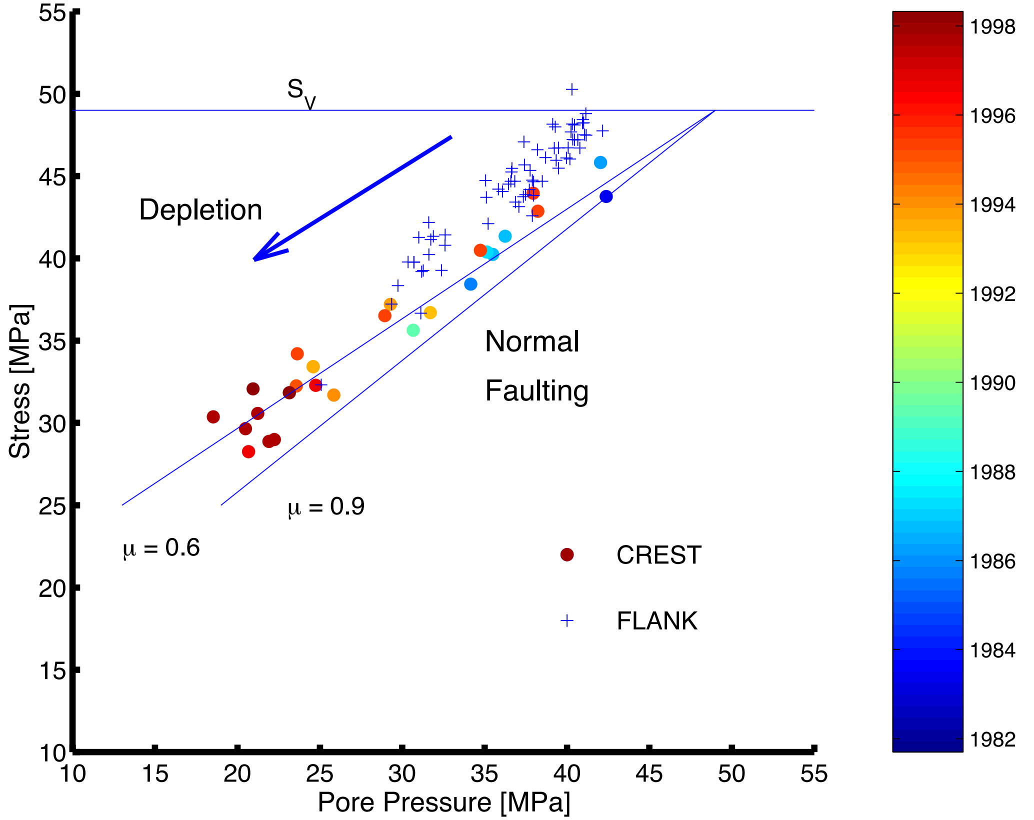

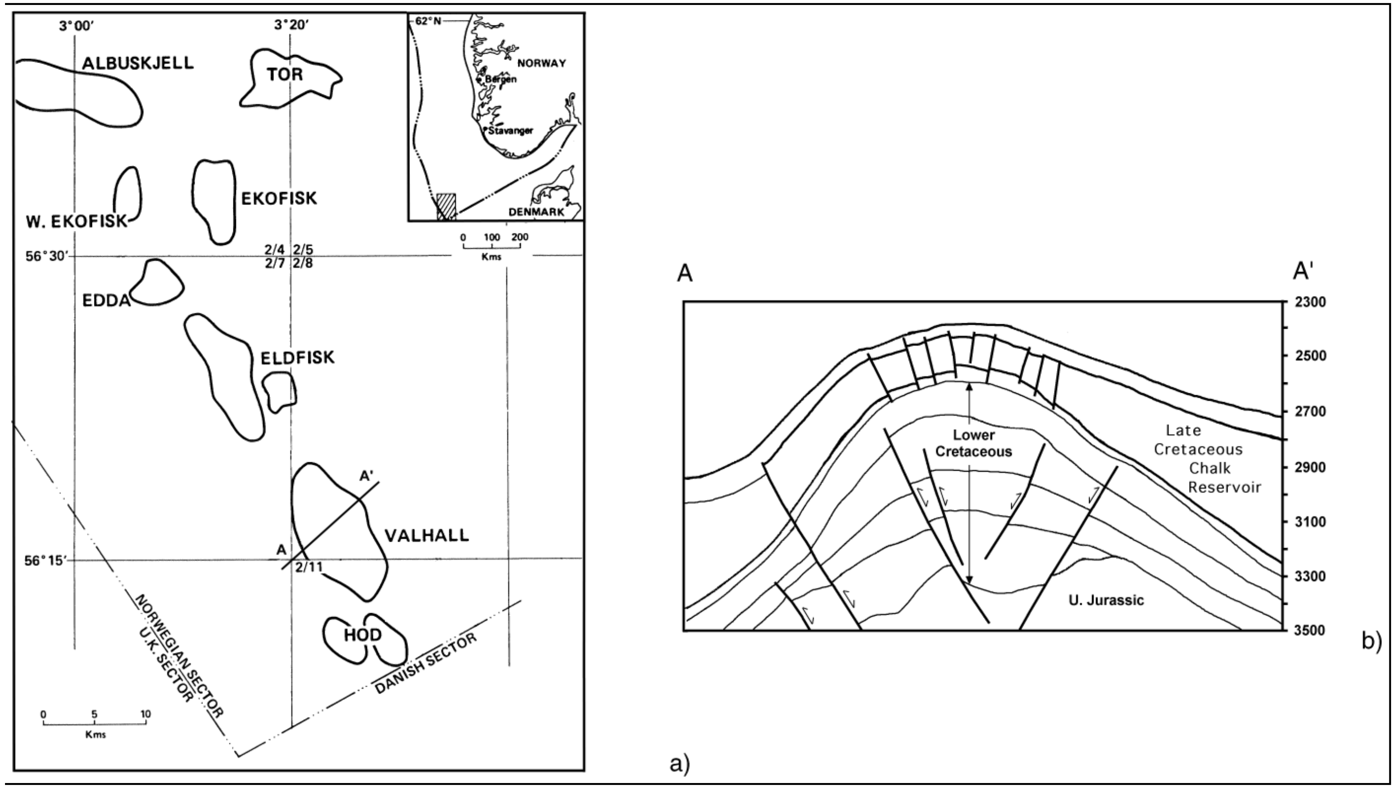

Zoback and Zinke (2002)

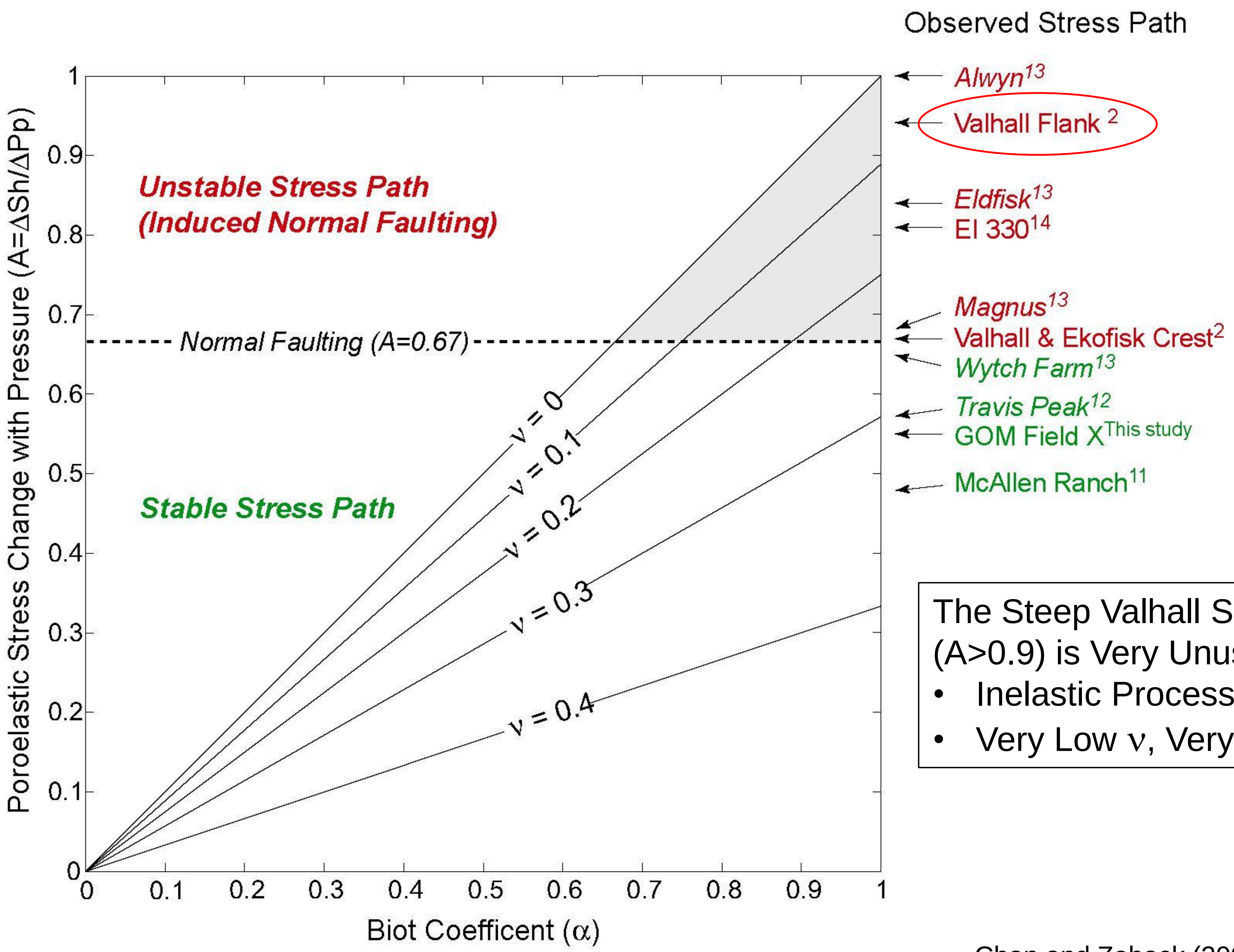

The Steep Valhall Stress Path (A>0.9) is Very Unusual

- Inelastic Processes?
- Very Low ν, Very High α ?

Chan and Zoback (2002)

Three Topics

1. Relevant Learnings From Injection Induced Seismicity

2. Poroelastic Stress Paths and Earthquakes Induced by Depletion

3. Mmax and the Potential for Faulting in the Carboniferous
   - Initial Pore Pressure and Stress State in Groningen
   - Does Reservoir Depletion Increase, or Decrease, the Likelihood of Triggered Slip in the Carboniferous?
   - What Does this Imply for Mmax?

Initial Stress State and Stress Path (A) In Groningen?

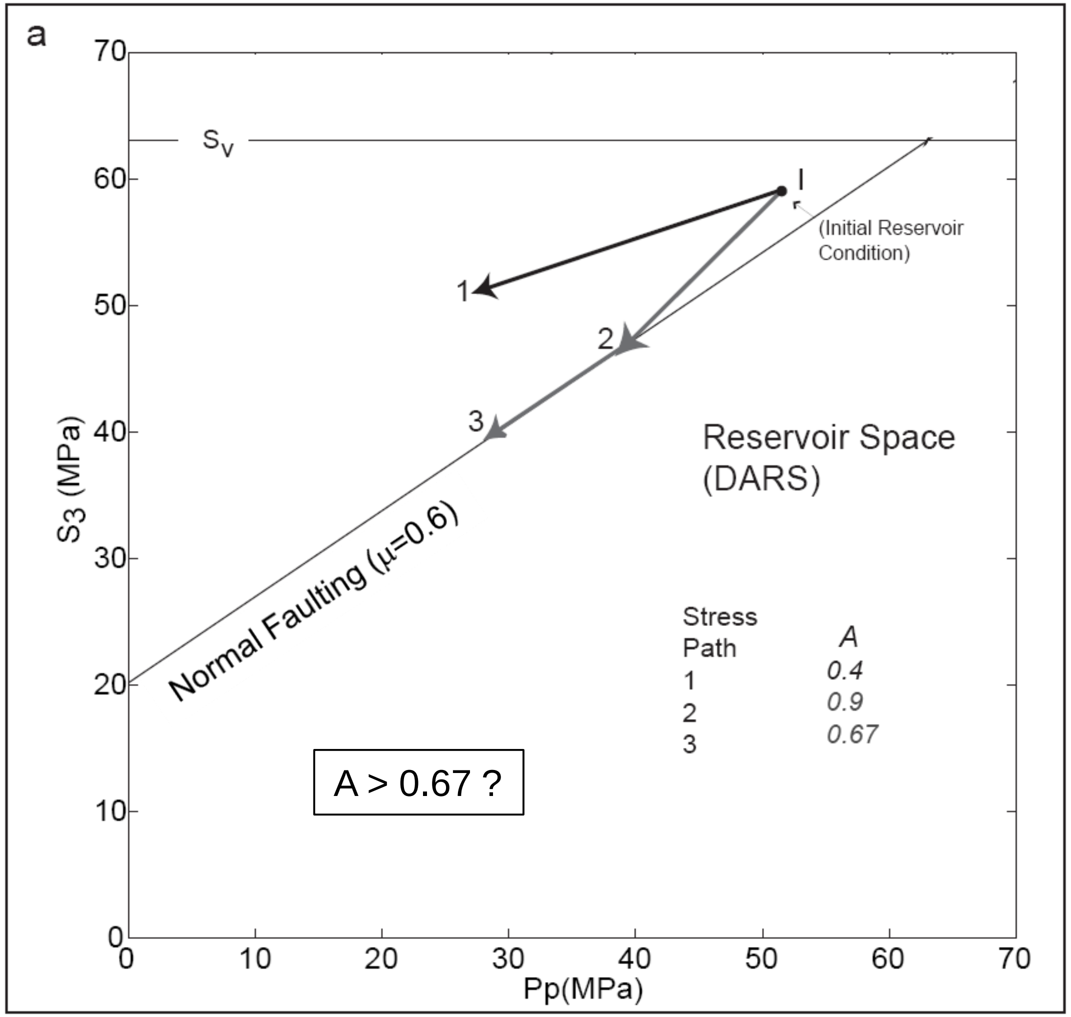

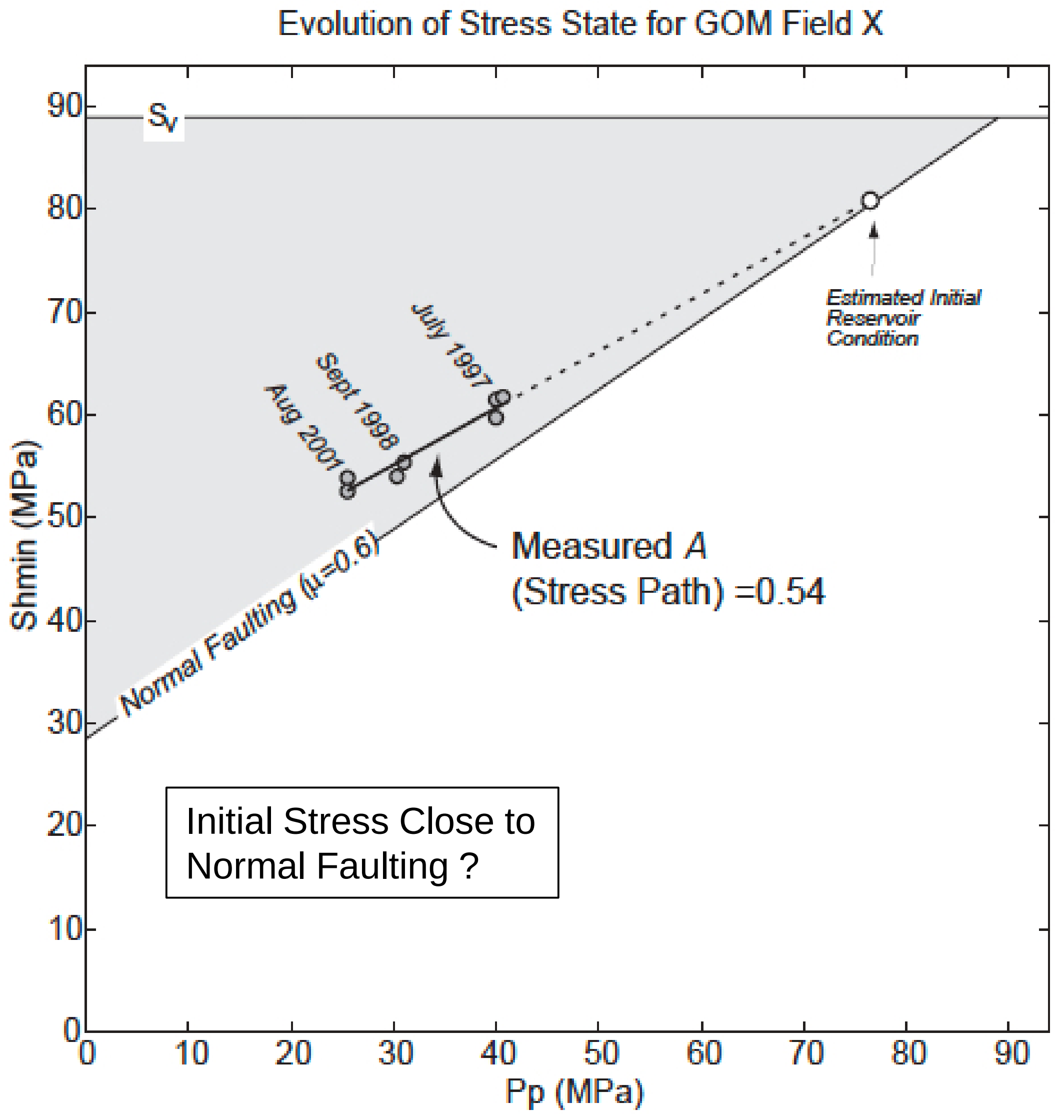

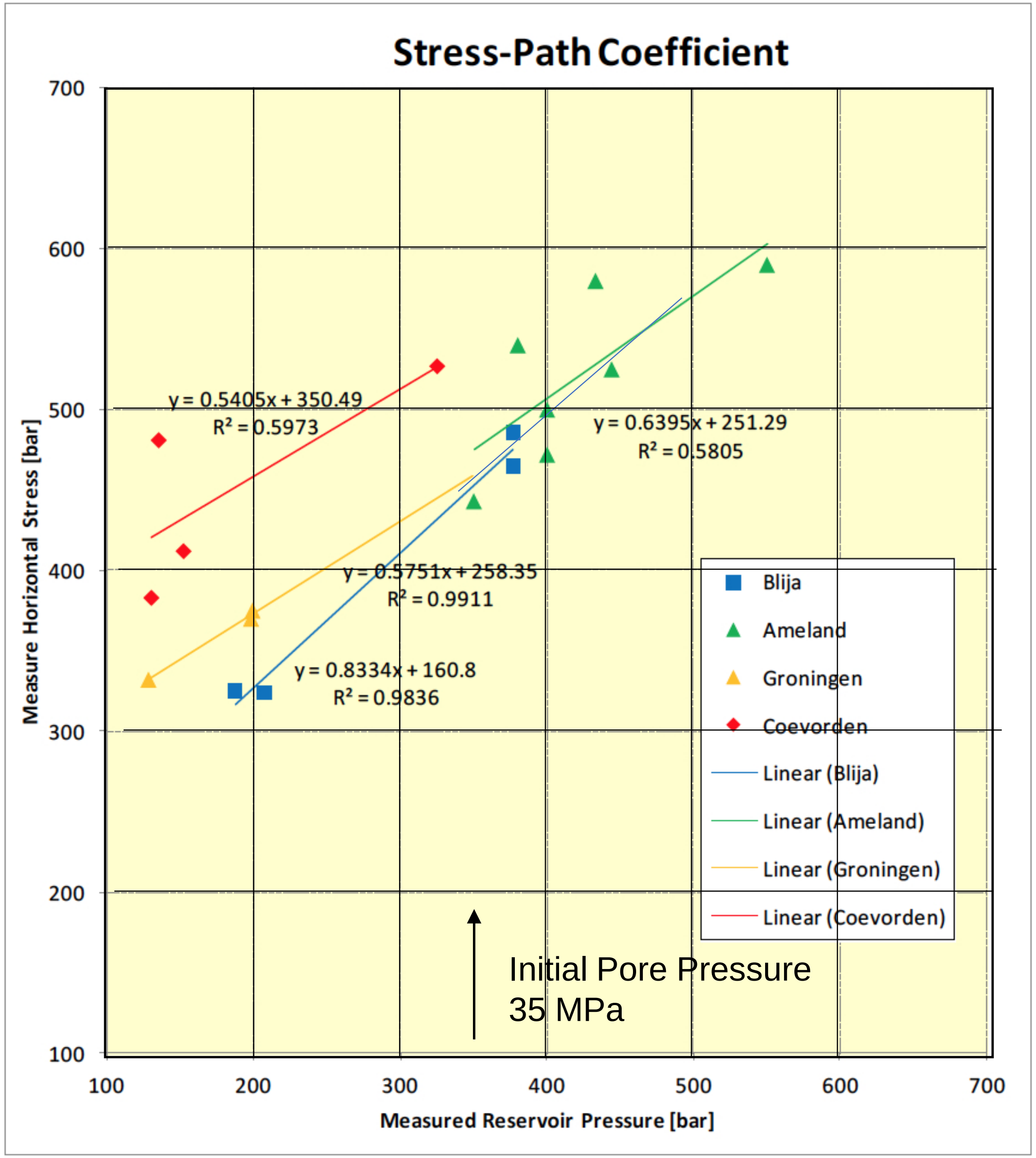

NAM, Technical Addendum to the Winningsplan Groningen (2013)

Groningen - 1

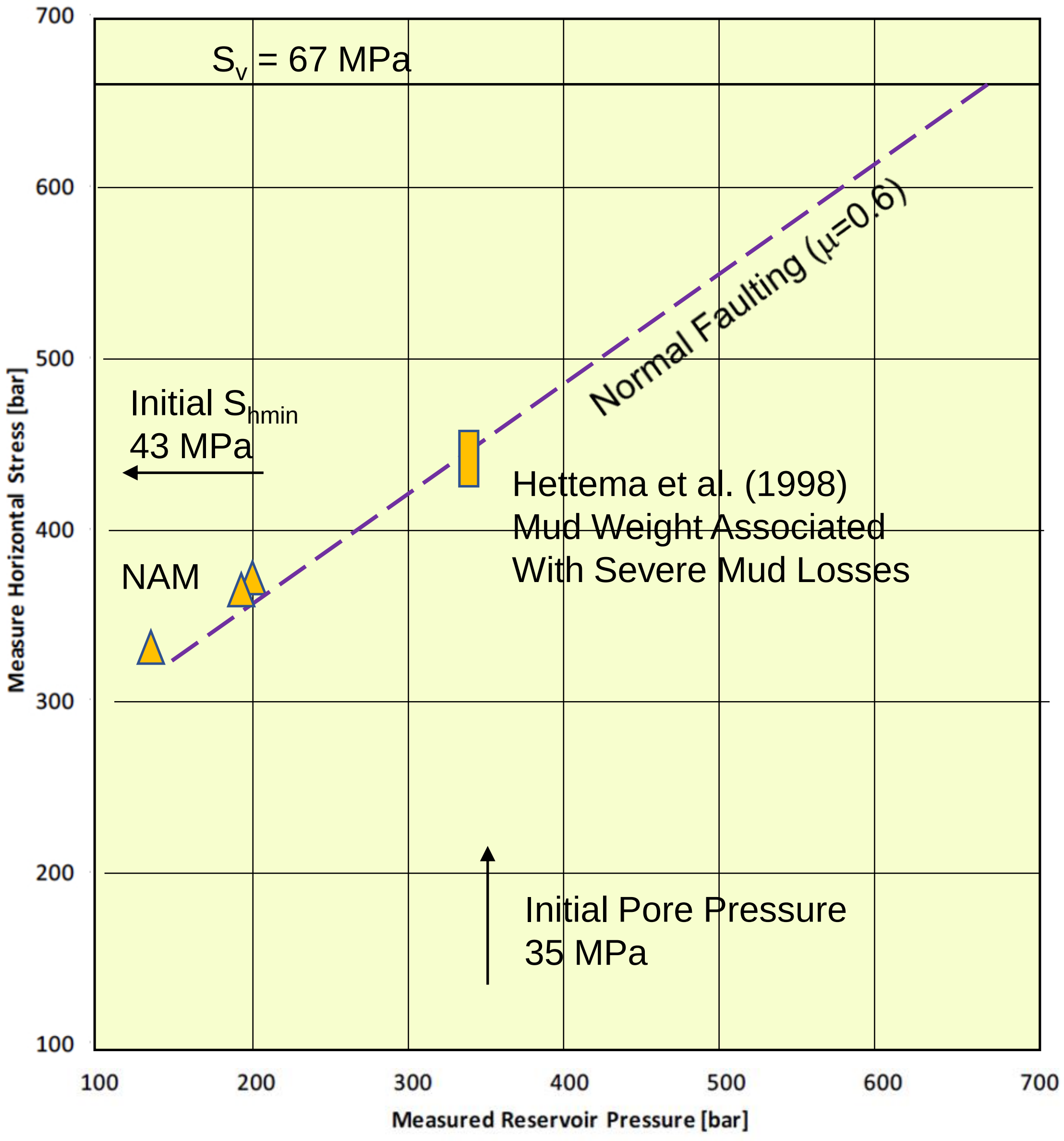

S_v = 67 MPa
Normal Faulting (μ=0.6)
Initial S_{hmin}
43 MPa
Hettema et al. (1998)
Mud Weight Associated
With Severe Mud Losses
NAM
Initial Pore Pressure
35 MPa
Measure Horizontal Stress [bar]
Measured Reservoir Pressure [bar]
100
200
300
400
500
600
700

Groningen - 2

Suppose you hypothesize that S_{hmin} was not in frictional equilibrium prior to production? In other words, S_{hmin} was closer to S_V?

$\Delta S/\Delta P > 1$, which is not physically reasonable.

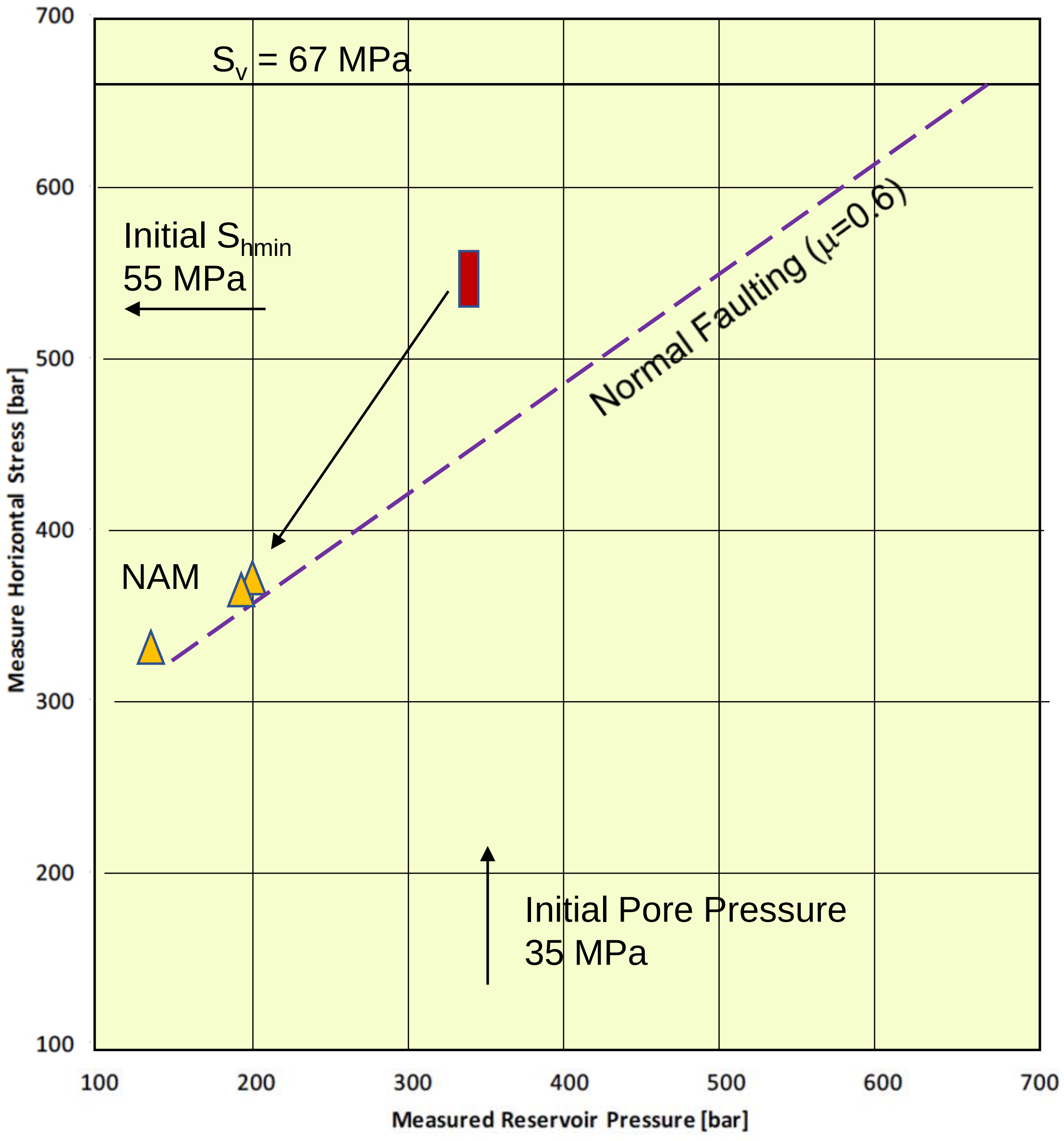

How Does Reservoir Depletion Affect Stress in Shales Above and Below the Reservoir?

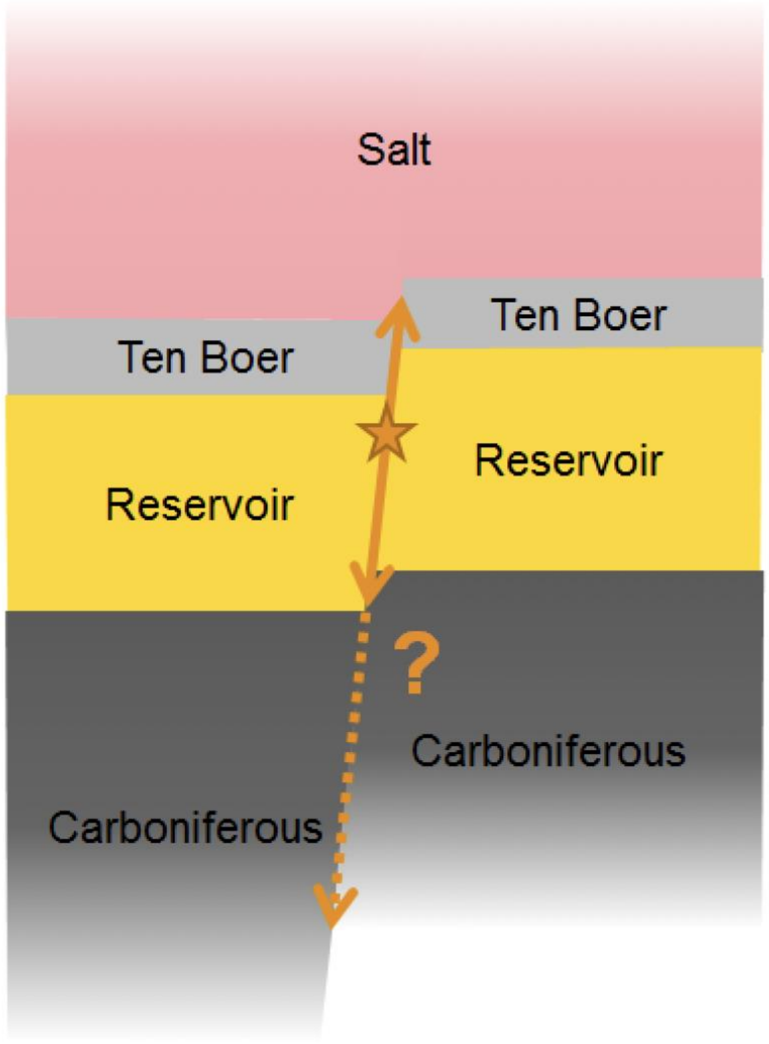

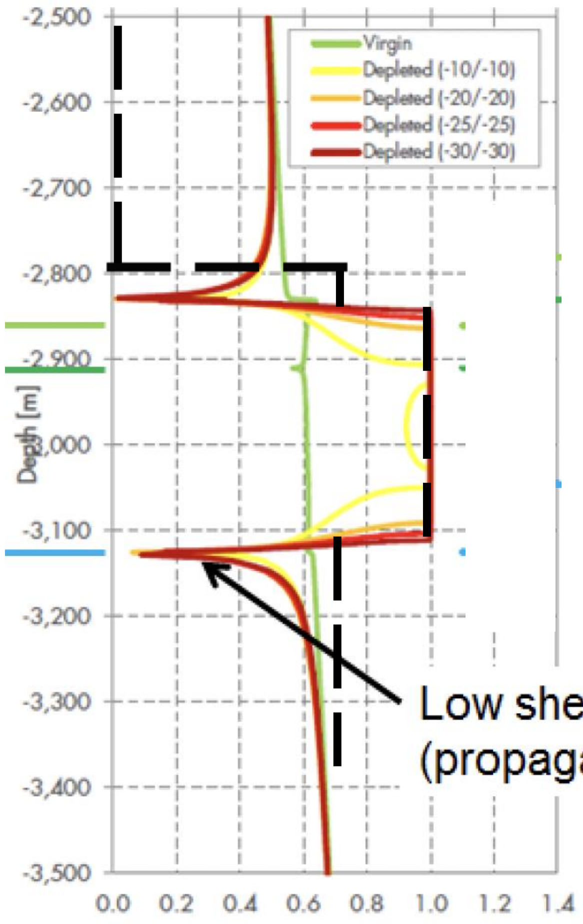

Salt

Ten Boer Shale

Reservoir

Carboniferous Shale

Low shear/normal stress
(propagation barrier)

NAM (ExxonMobil Mmax) 2016

Compaction and Subsidence in Coastal Louisiana

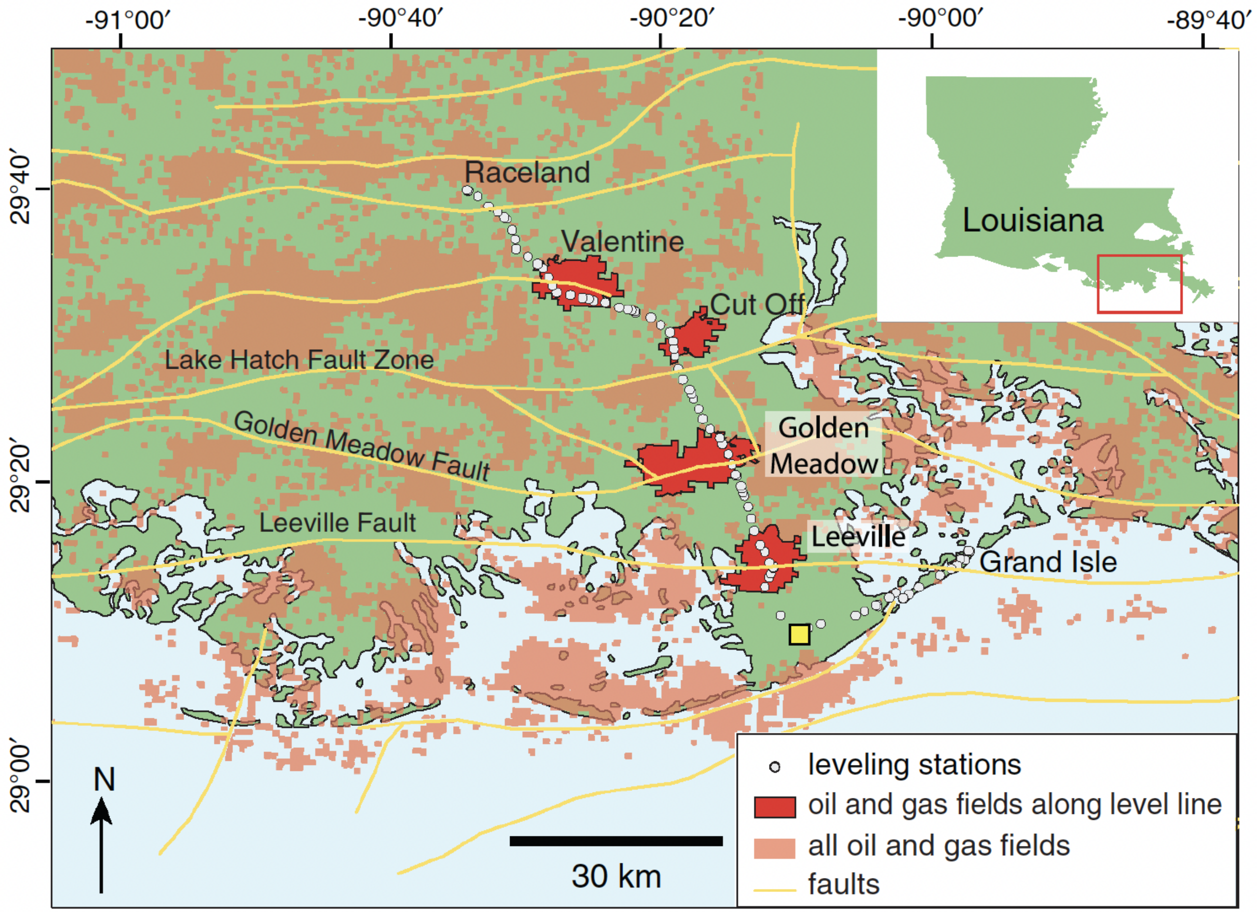

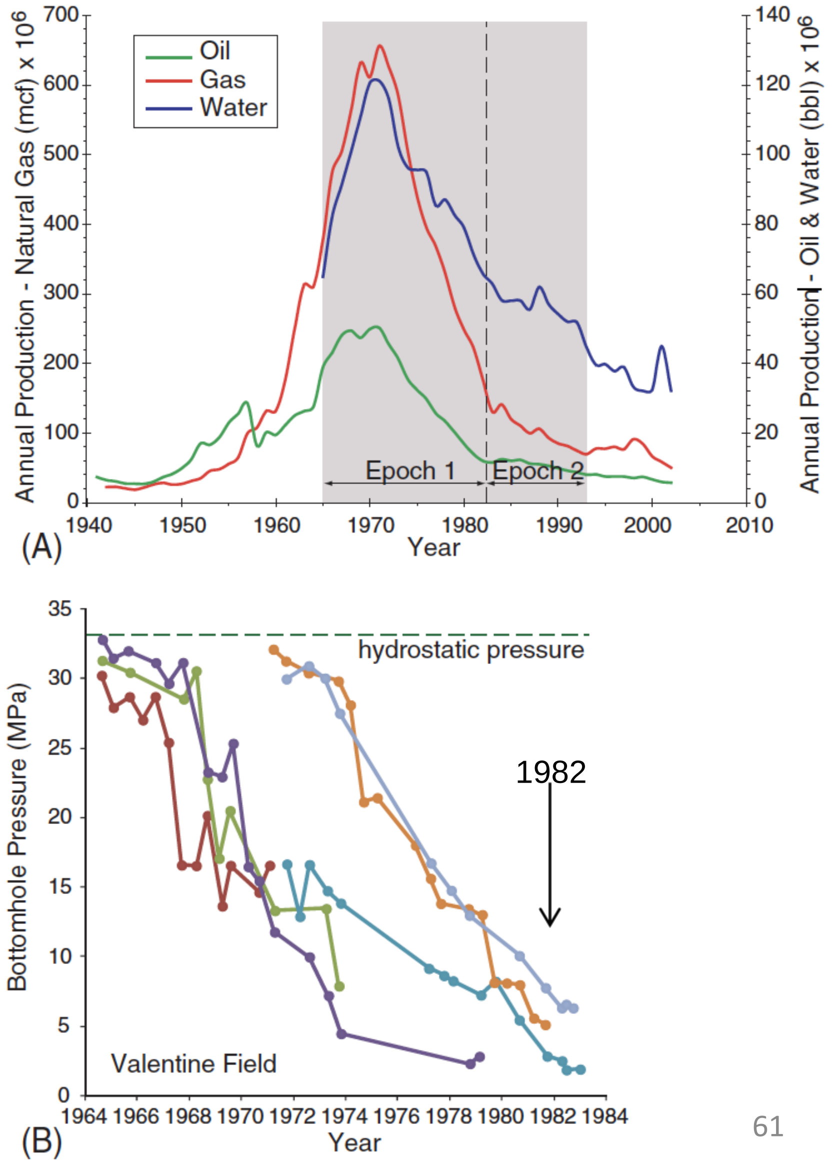

Chang, Mallman and Zoback (2014)

Most Compaction and Subsidence Occurs After Production Stopped

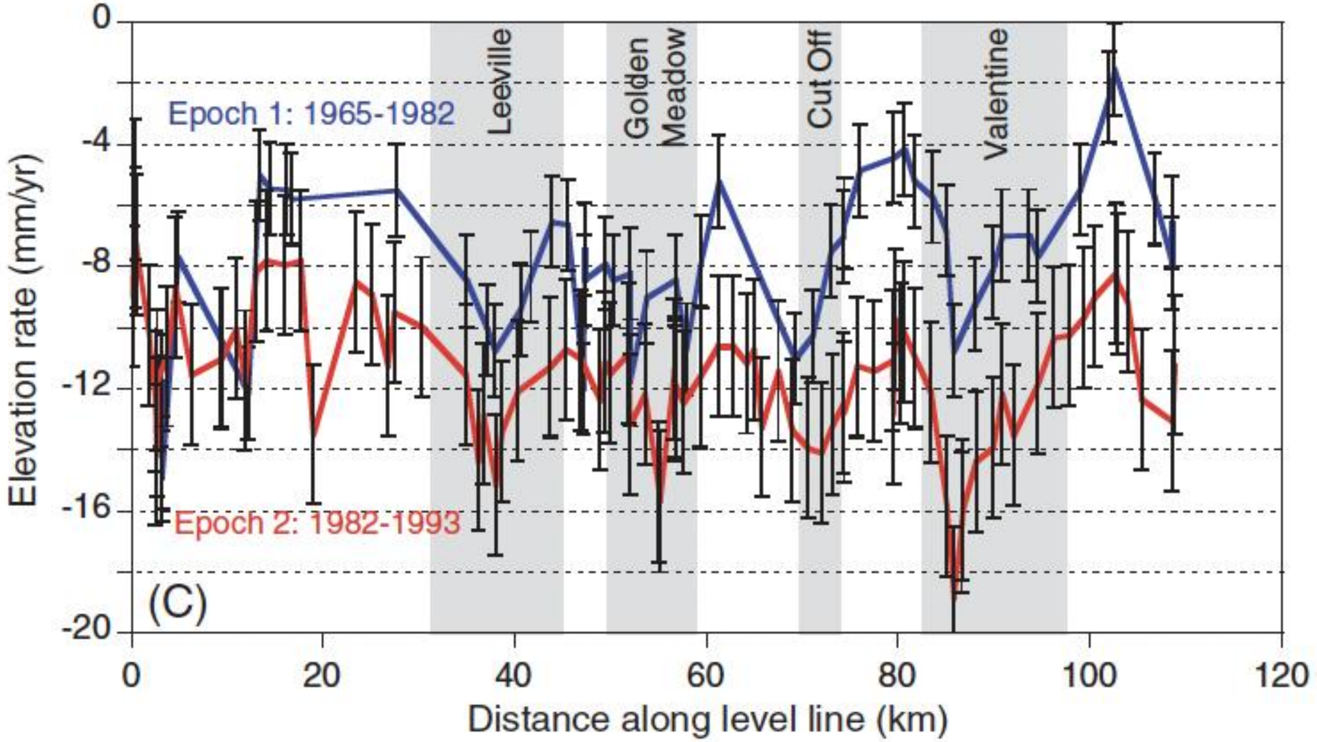

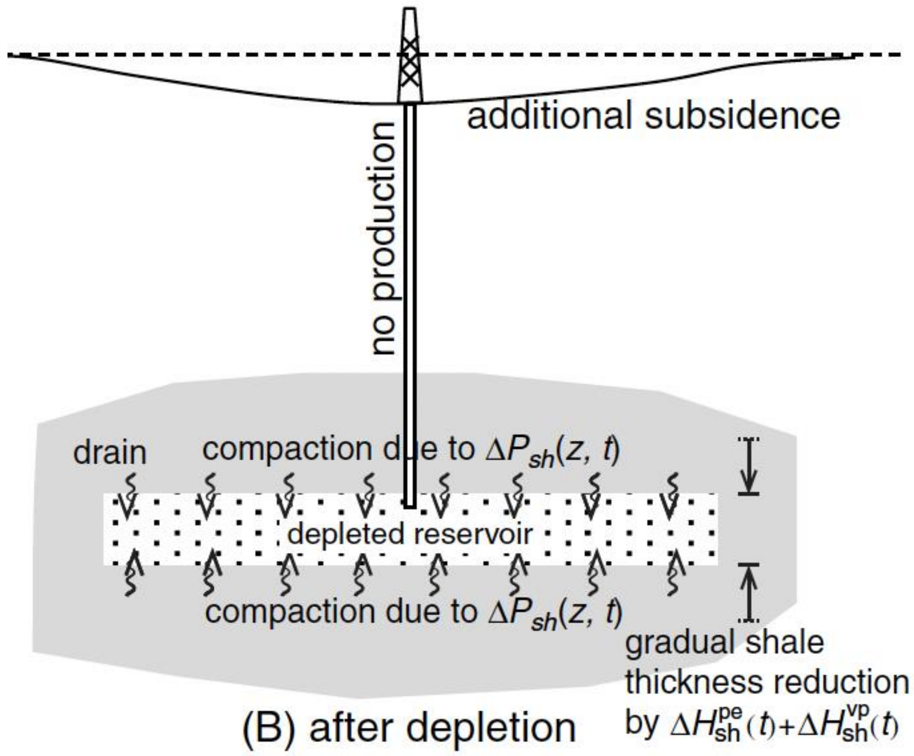

Time-Dependent Drainage from Shales Into Depleted Reservoir

Chang, Mallman and Zoback (2014)

Time Dependent Drainage from Shales Into Depleted Reservoir

$$\Delta H(t) = \Delta H_{\mathrm{res}} + \Delta H_{\mathrm{sh}}^{\mathrm{pe}}(t) + \Delta H_{\mathrm{sh}}^{\mathrm{vp}}(t)$$

$$\Delta H_{\mathrm{sh}}^{\mathrm{pe}}(t) = 2\int_0^\infty C_m \Delta P_{\mathrm{sh}}(z,t)dz = 4\sqrt{\frac{\alpha t}{\pi}} C_m \Delta P_{\mathrm{res}}$$

$$\Delta H_{\mathrm{sh}}^{\mathrm{vp}}(t) = 2\int_0^\infty \varepsilon_{\mathrm{vp}}(z,t)dz$$

Shale Permeability 10^{-19} m^2 (0.1 microdarcies)

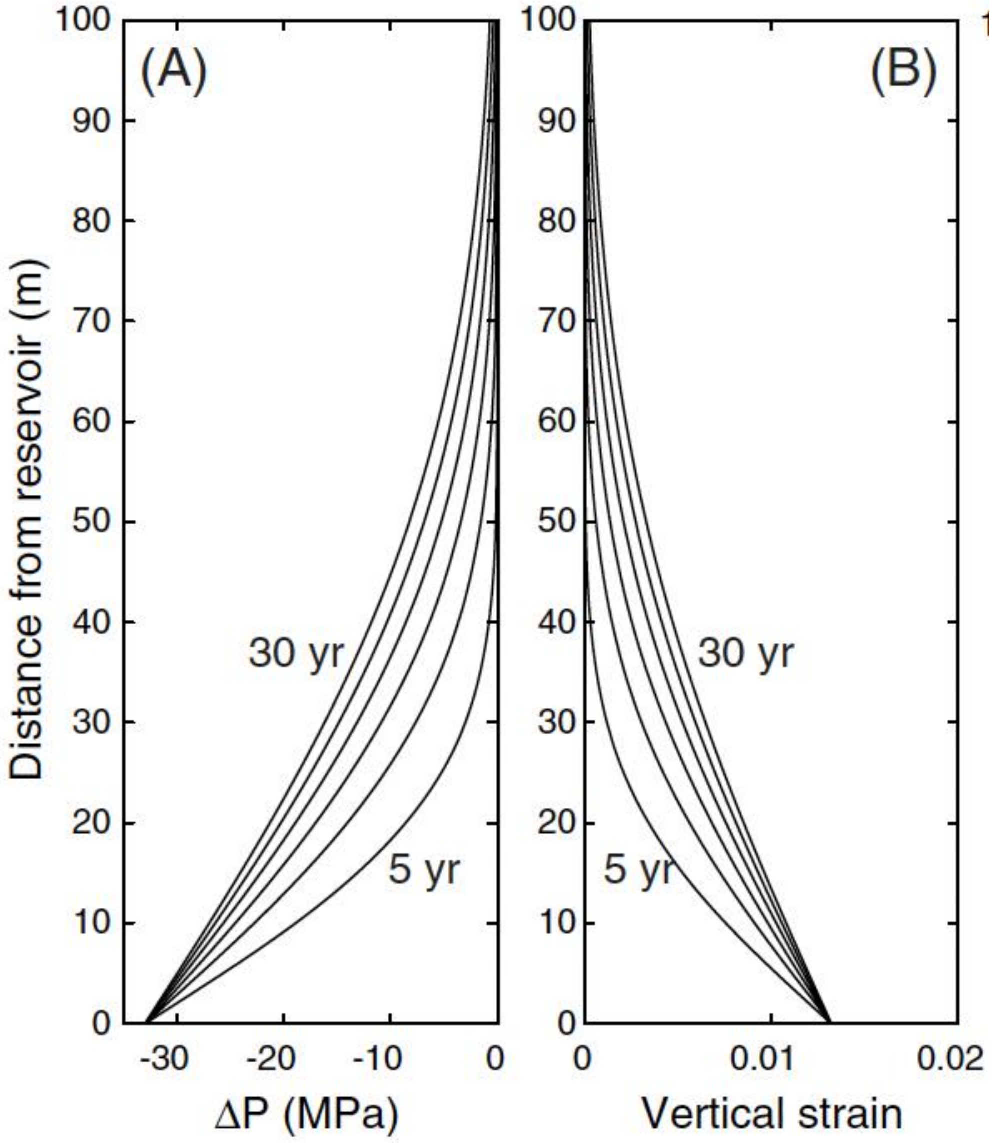

Chang, Mallman and Zoback (2014)

Carboniferous Shale?

1) Assume S_{hmin} is higher in the shale than in the reservoir.

2) Assume a “normal” stress path (A ~ 0.5) in the shale

3) Pressure depletion in the shale increases the barriers to vertical fault propagation

4) Rupture into the Carboniferous becomes less likely with time due to depletion

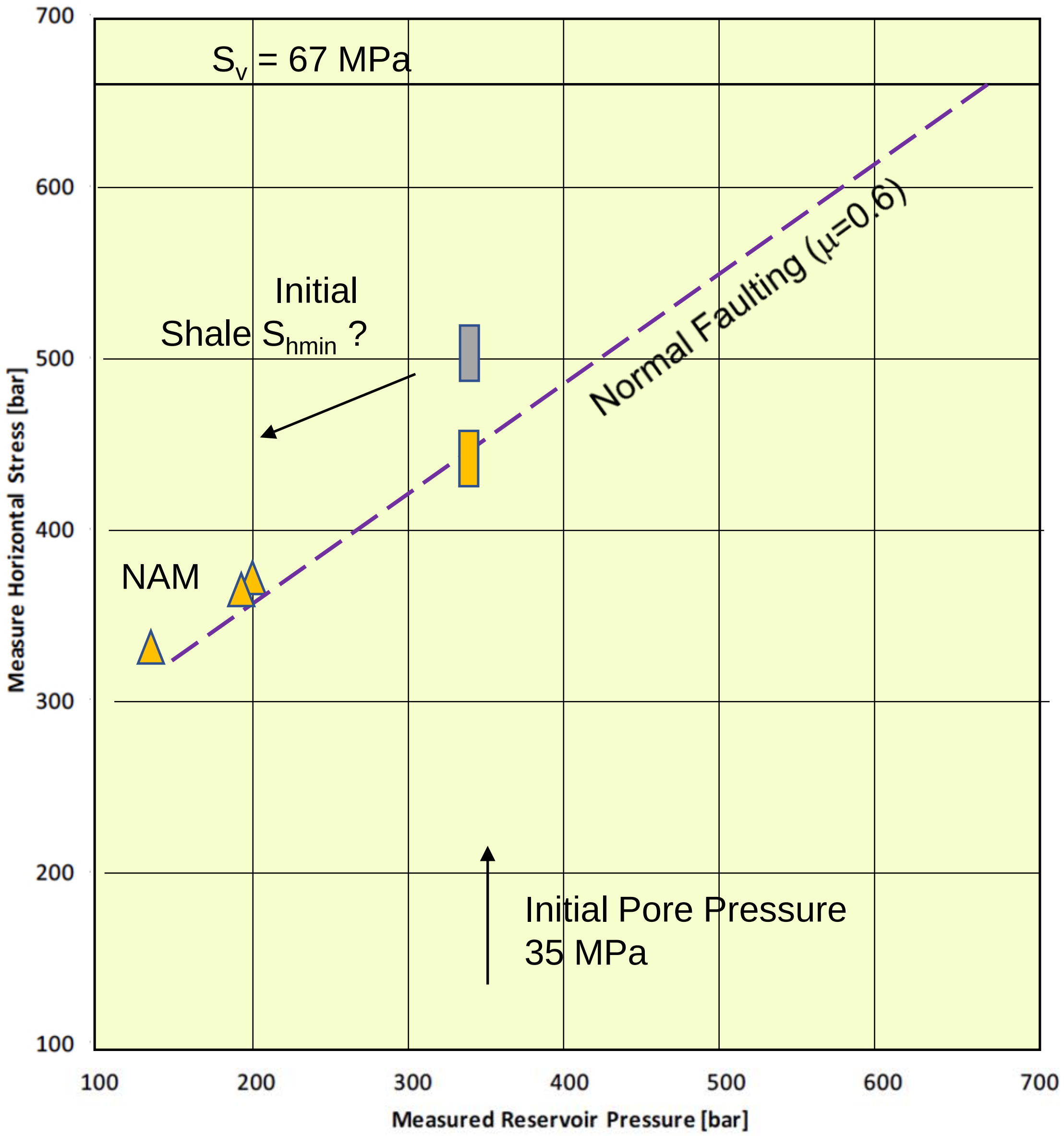

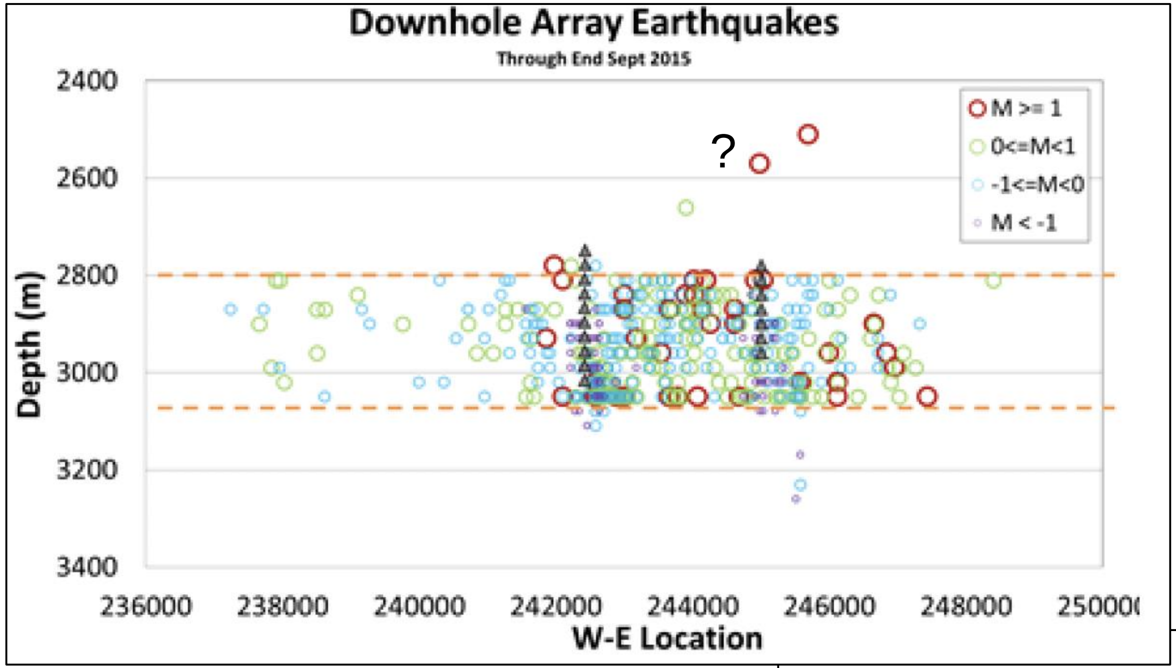

Implications of Groningen

- Earthquakes are Confined to the Reservoir
  - As predicted if there are fault barriers above and below
- The Probability of Rupture Propagation Outside the Reservoir is Very Low
  - In my opinion, much lower than 20%

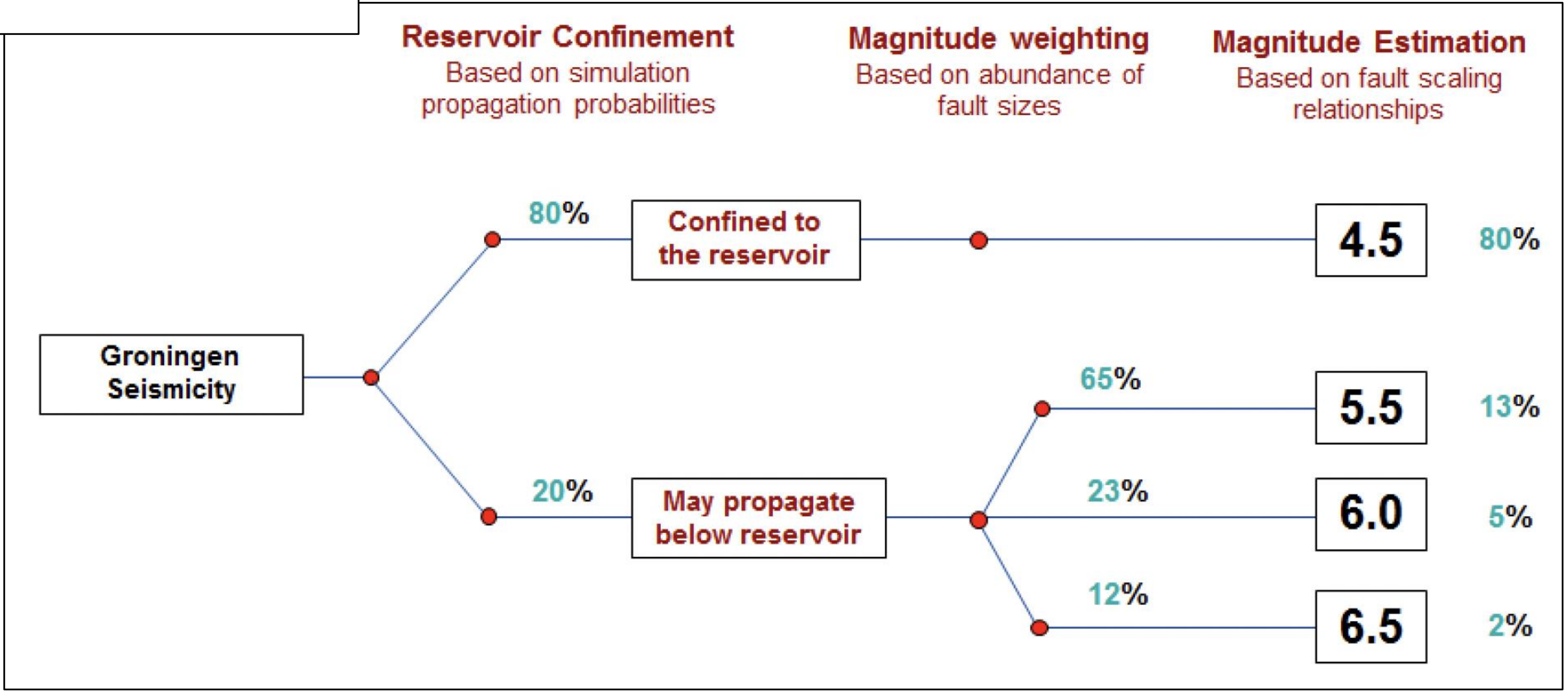

NAM (ExxonMobil Mmax) 2016

Workshop on Maximum Magnitude of earthquakes in Groningen

DAY 3

Wednesday 15th June: Groningen event-size distribution & Statistical estimates of Mmax

Start	End	Speaker	Presentation
8:30	9:30	Stephen Bourne	Groningen seismological model and earthquake recurrence
9:30	10:15	Laura Gulia	Re-assessment of earthquake distribution for Groningen
10:15	10:45		*Coffee break*
10:45	11:30	Jean-Ph. Avouac	Recurrence model for Groningen earthquakes
11:30	12:15	Zak Varty	Recurrence model for Groningen earthquakes
12:15	13:15		*Lunch*
13:15	14:00	A Muntendam-Bos	Groningen induced event-size distribution
14:00	14:45	Sander Osinga	Taper from recurrence relationship to Mmax
14:45	15:15		*Coffee break*
15:15	16:30	Gert Zöller	Proponent assessment for Mmax in the Groningen field
16:30	17:15	Nepomuk Boitz	Proponent assessment for Mmax in the Groningen field
17:15	18:00	All	General discussion

Summary of the Groningen seismological model

Statistical-mechanics, Bayesian inference, and seismicity forecasts for Probabilistic Seismic Hazard & Risk analysis

Seismological model: Version 6

Stephen Bourne, Steve Oates
Shell Global Solutions International

M_{max} Workshop II Meeting
Amsterdam, 15th June, 2022

Outline

Seismological models for Groningen seismicity

- Part 1: Event occurrence model
- Part 2: Event magnitude model

Groningen induced seismicity emerges over decades

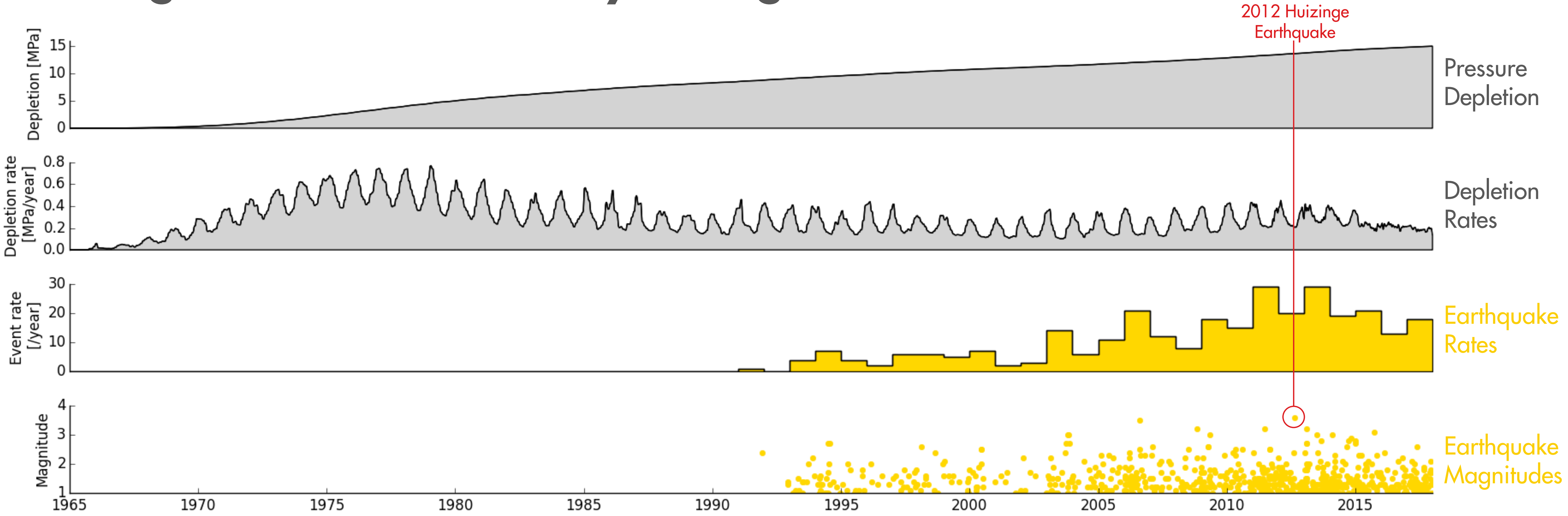

Induced seismicity increases slowly

- Earthquake rates *slowly* increased with time
- Earthquake magnitudes *slowly* increased with time

Induced seismicity follows induced stress

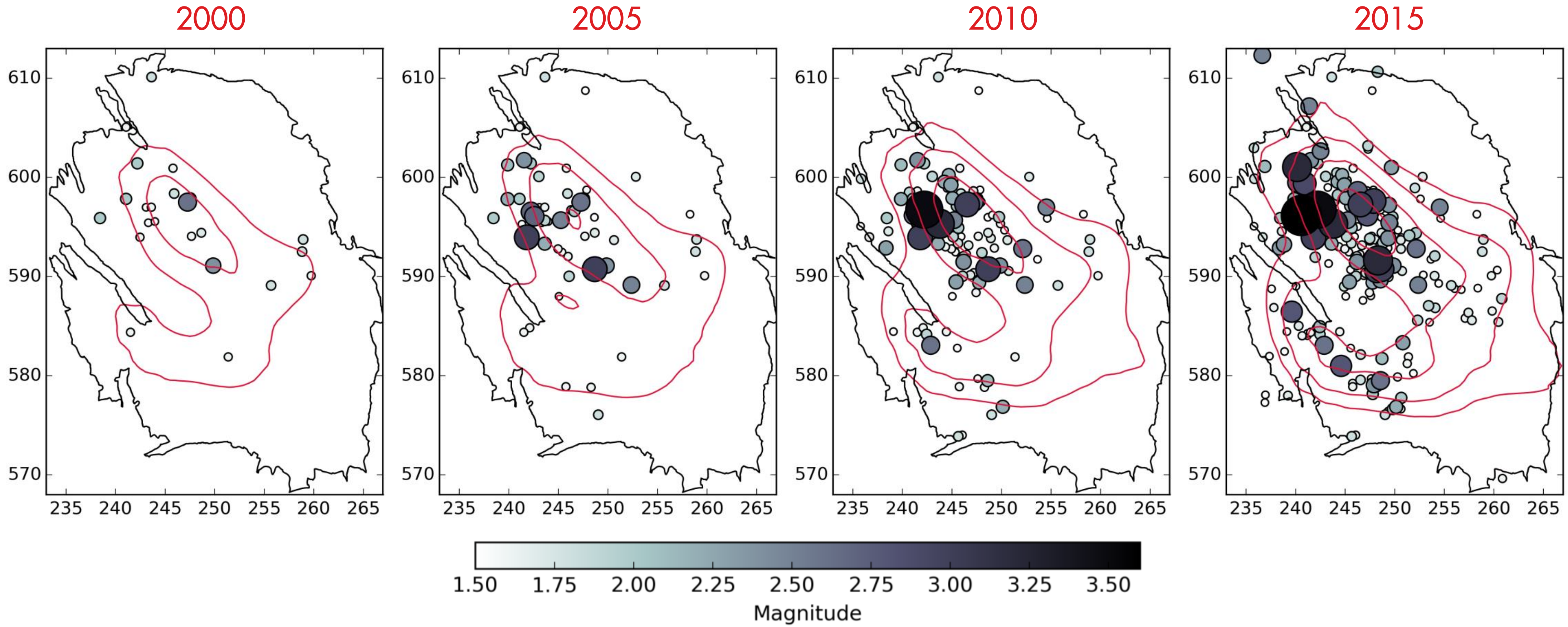

- Smoothed incremental Coulomb stress contours: 0.25, 0.30, 0.35, 0.40 MPa
- Earthquake rates and magnitudes appear to increase with incremental Coulomb stress

Induced seismicity *mostly* follows induced stress

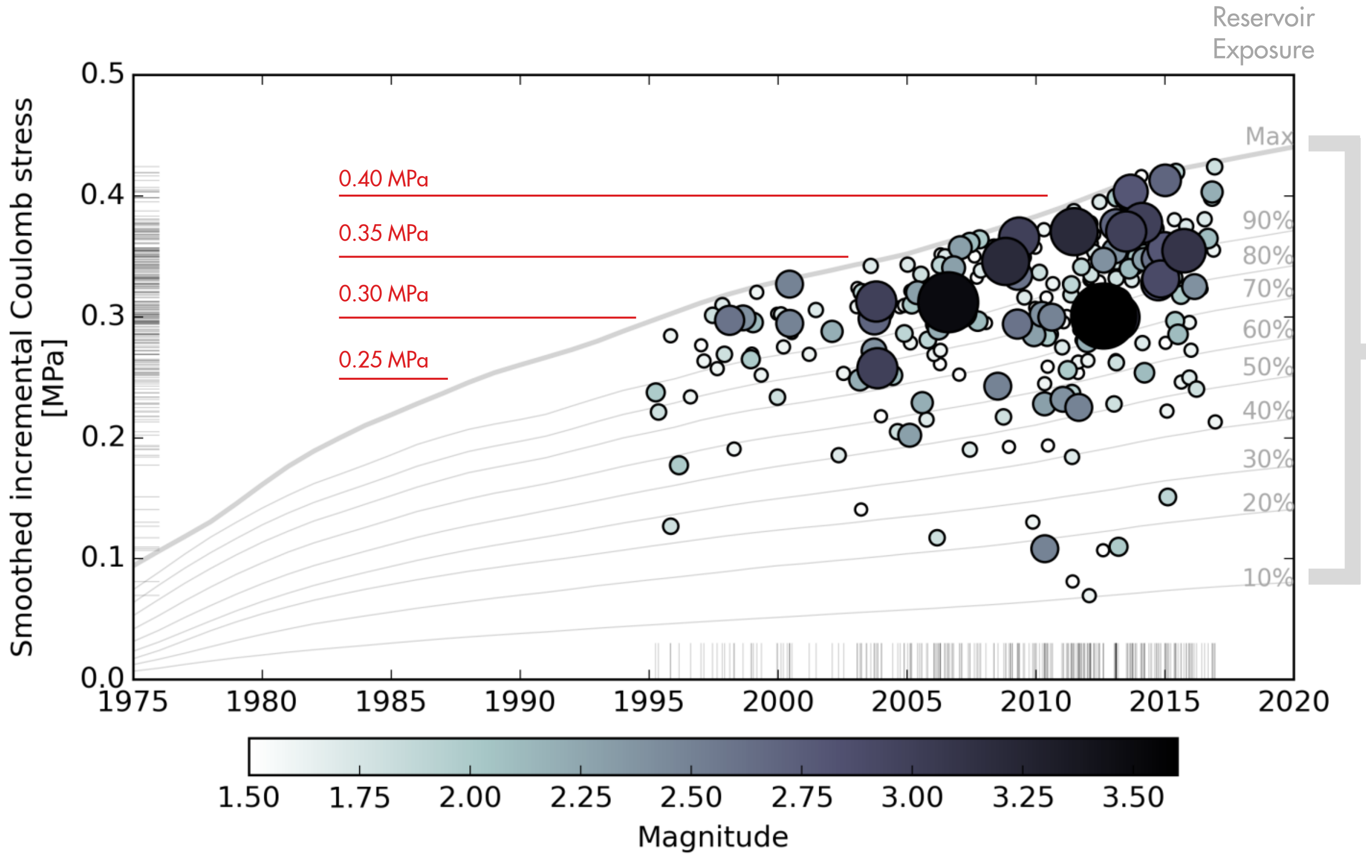

- Significant variability of induced stress at the time and location of induced earthquakes
- Earthquakes more likely at higher stresses
- Larger magnitudes more likely at higher stresses

An exponential rise of induced seismicity with induced stress

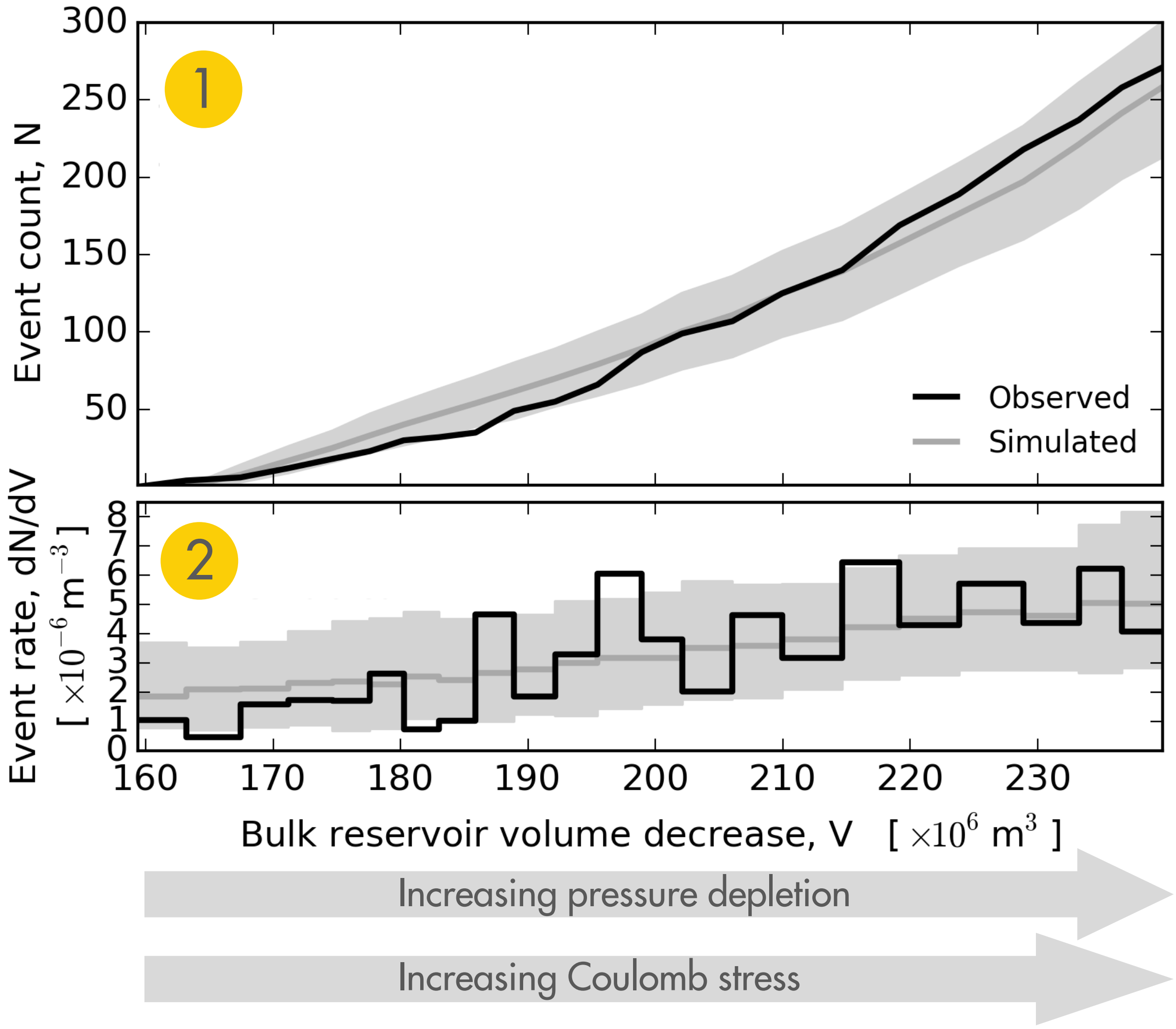

Observations

1. Numbers increase exponential-like with cumulative production
2. Numbers per unit gas production increases steadily

Interpretation

- Fault reactivations increase exponentially with increasing stress
- Fault strength is a highly-variable & disordered system
- Statistical trends emerge from large disordered systems

Poro-Elastic Thin-Sheet Deformations

Model

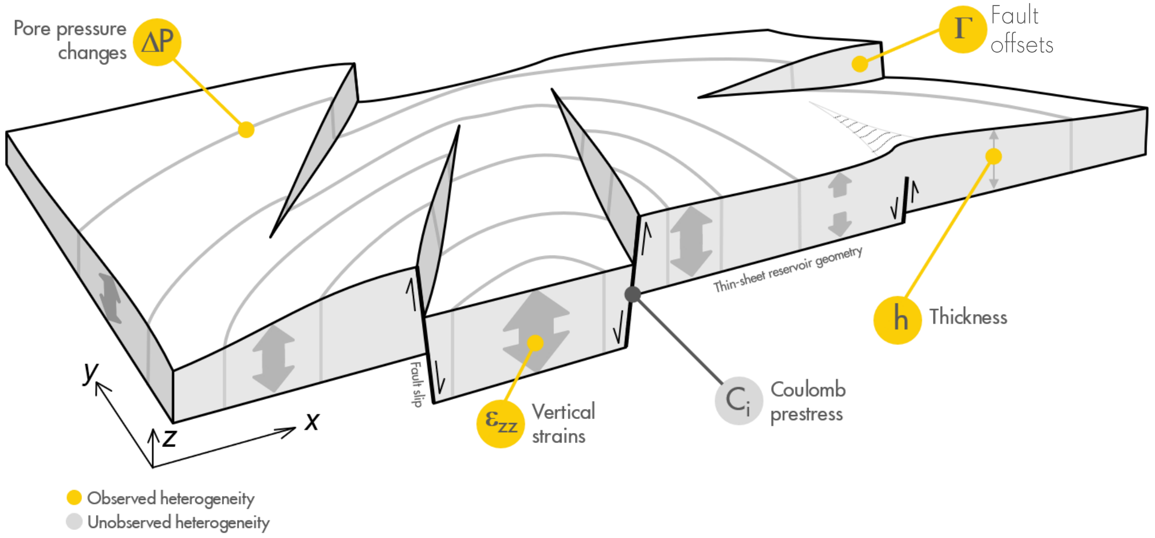

Assumptions

1. Pore pressure changes are consistent with dynamic model
2. Thin-sheet reservoir geometry means $\varepsilon_{zz} >> \varepsilon_{xx}, \varepsilon_{yy}$
3. Small induced deformations follow linear poro-elasticity
4. Stress re-distribution due to induced fault slip is negligible

Theory

1. Uniaxial displacement strains:

$$\bar{\epsilon}_{ij}(\mathbf{x}) = \begin{pmatrix} 0 & 0 & \bar{\epsilon}_{xz} \\ 0 & 0 & \bar{\epsilon}_{yz} \\ \bar{\epsilon}_{xz} & \bar{\epsilon}_{yz} & \bar{\epsilon}_{zz} \end{pmatrix} \qquad \begin{aligned} \bar{\epsilon}_{xz}(\mathbf{x}) &= -\frac{1}{2}\bar{\epsilon}_{zz}\partial_x z_o + \frac{1}{4}h\partial_x\bar{\epsilon}_{zz}, \\ \bar{\epsilon}_{yz}(\mathbf{x}) &= -\frac{1}{2}\bar{\epsilon}_{zz}\partial_y z_o + \frac{1}{4}h\partial_y\bar{\epsilon}_{zz}, \end{aligned}$$

2. Induced effective stresses:

$$\Delta\bar{\sigma}'_{ij}(\mathbf{x}) = 3K\left(\frac{1-2\nu}{1+\nu}\right)\begin{pmatrix} \frac{\nu}{1-2\nu}\bar{\epsilon}_{zz} & 0 & \bar{\epsilon}_{xz} \\ 0 & \frac{\nu}{1-2\nu}\bar{\epsilon}_{zz} & \bar{\epsilon}_{yz} \\ \bar{\epsilon}_{xz} & \bar{\epsilon}_{yz} & \frac{1-\nu}{1-2\nu}\bar{\epsilon}_{zz} \end{pmatrix}$$

3. Poro-elastic coupling:

$$\bar{\epsilon}_{zz} = \frac{1}{3K}\left(\frac{1+\nu}{1-\nu}\right)\alpha\Delta\bar{P}$$

4. Elastic heterogeneity:

$$\alpha(\mathbf{x}) = \frac{1}{1+H_r(\mathbf{x})/H_s} \qquad H_r = \Delta\bar{P}/\bar{\epsilon}_{zz} \qquad H_s = 3K_s(1-\nu)/(1+\nu)$$

5. Coulomb stresses:

$$C_m = \tau_m + \mu(\sigma_m + P)$$

$$C_m = \sqrt{(\tau_m^p + \gamma\alpha\Delta P)^2 + (\gamma\alpha\Gamma\Delta P)^2} + \mu\left(\sigma_m^p + P^p + (1-\gamma\alpha)\Delta P\right), \qquad \begin{aligned} \Gamma &= \tfrac{1}{2}\nabla(z_o) \\ \gamma &= (1-2\nu)/2(1-\nu) \end{aligned}$$

Source: Bourne, S. J., & Oates, S. J. (2017). Extreme threshold failures within a heterogeneous elastic thin sheet and the spatial-temporal development of induced seismicity within the Groningen gas field. Journal of Geophysical Research: Solid Earth, 122, 10,299–10,320. https://doi.org/10.1002/2017JB014356

Extreme Threshold Coulomb Stress Failure Probabilities

Model

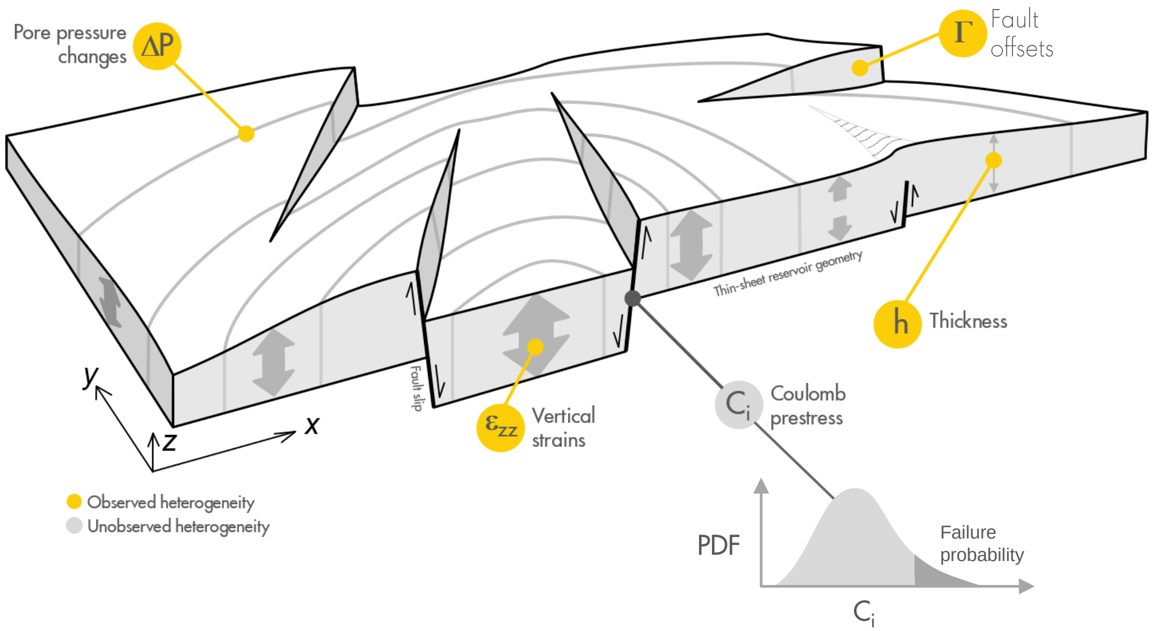

Assumptions

1. Frictional stability consistent with Coulomb stress failure criterion
2. Unobserved heterogeneities behave like stochastic prestress disorder
3. Induced failures initiate in the upper tail of the prestress distribution
4. Pore pressure changes due to induced fault slip are negligible

Theory

1. Extreme Threshold Failure Probabilities:

$$\Pr(F|C_i > C_t) = \begin{cases} \left(1 - \zeta \frac{C_t + \Delta C}{\bar{\sigma}}\right)^{-1/\zeta} & \text{if } \zeta \neq 0, \\ \exp\left(\frac{C_t + \Delta C}{\bar{\sigma}}\right) & \text{if } \zeta = 0, \end{cases}$$

2. Poisson Point Process: Intensity and Expected counts

$$\lambda = \rho \frac{\partial \Pr(F)}{\partial t}, \quad \Lambda(t_1, t_2) = \int_V \int_{t_1}^{t_2} \lambda \mathrm{d}V \mathrm{d}t$$

3. Likelihood Function:

$$\ell = \sum_{i=1}^{n} \log \lambda(\mathbf{x}_i, t_i) - \Lambda(t_1, t_2)$$

4. Bayesian Inference:
   Sample joint posterior probability distribution of model parameters given pore pressure model and observed earthquake times and epicenters

5. Aftershocks:
   Extends likelihood function to include Epidemic Type Aftershock Sequences

Source: Bourne, S. J., & Oates, S. J. (2017). Extreme threshold failures within a heterogeneous elastic thin sheet and the spatial-temporal development of induced seismicity within the Groningen gas field. Journal of Geophysical Research: Solid Earth, 122, 10,299–10,320. https://doi.org/10.1002/2017JB014356

Fault Reactivation is an Extreme Threshold Failure process

Not a Mean Value Failure process

Failure Probability

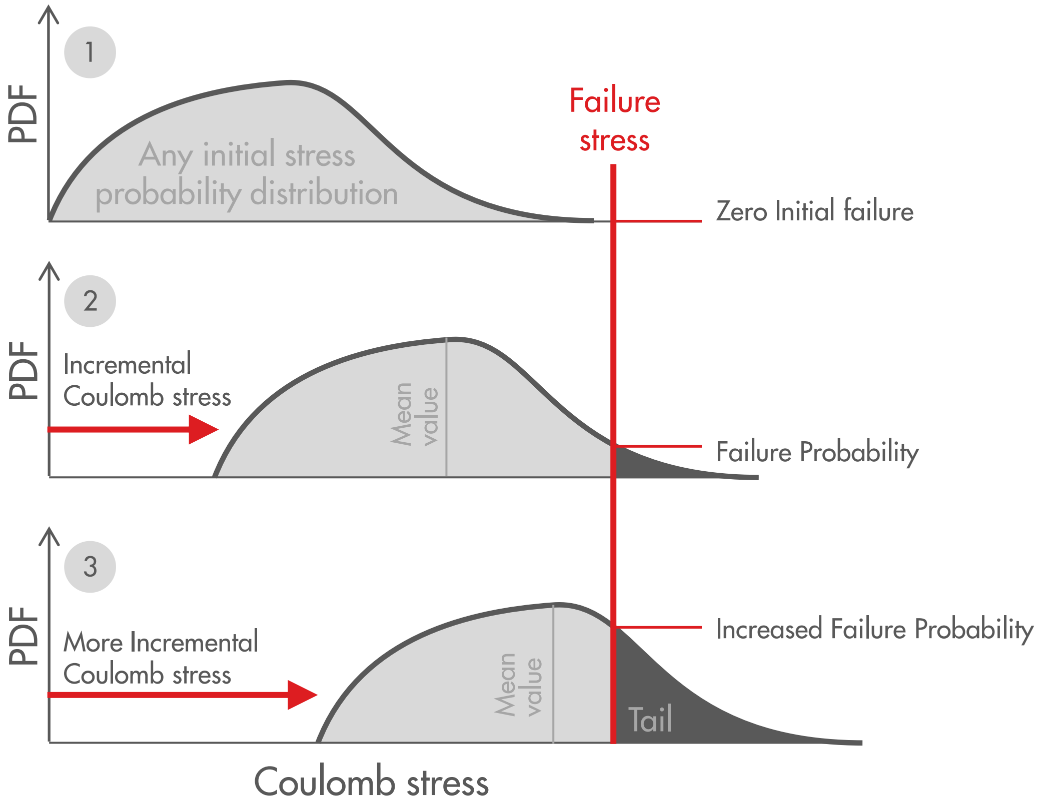

Extreme Threshold Theory

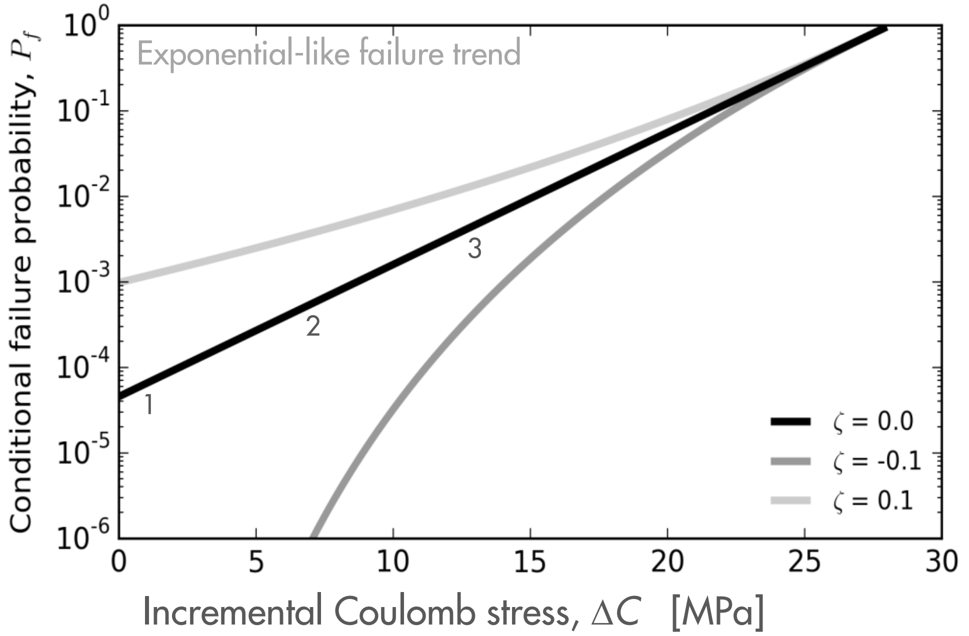

- Tail of the initial stress distribution fails first
- All probability tails follow Extreme Threshold Theory
- Mean value failure criteria are systematically optimistic

Bourne & Oates, 2017 (http://dx.doi.org/10.1002/2017JB014356)

Bourne et al., 2018 (http://dx.doi.org/10.1093/gji/ggy084)

Seismological model as a probability network of physical processes

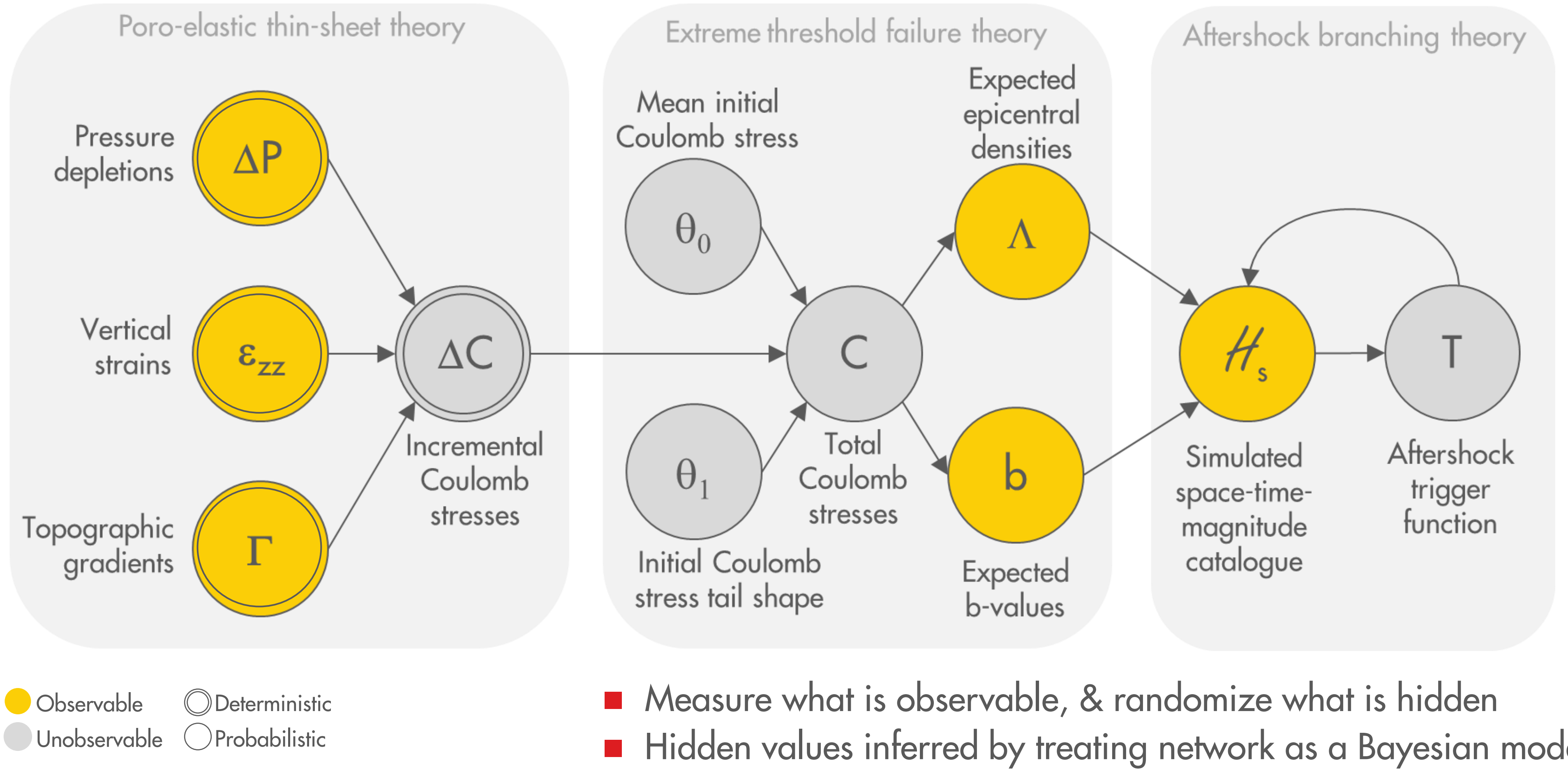

- Measure what is observable, & randomize what is hidden
- Hidden values inferred by treating network as a Bayesian model
- Yields ensemble of history-matched models

Model criticism
Event rate residuals

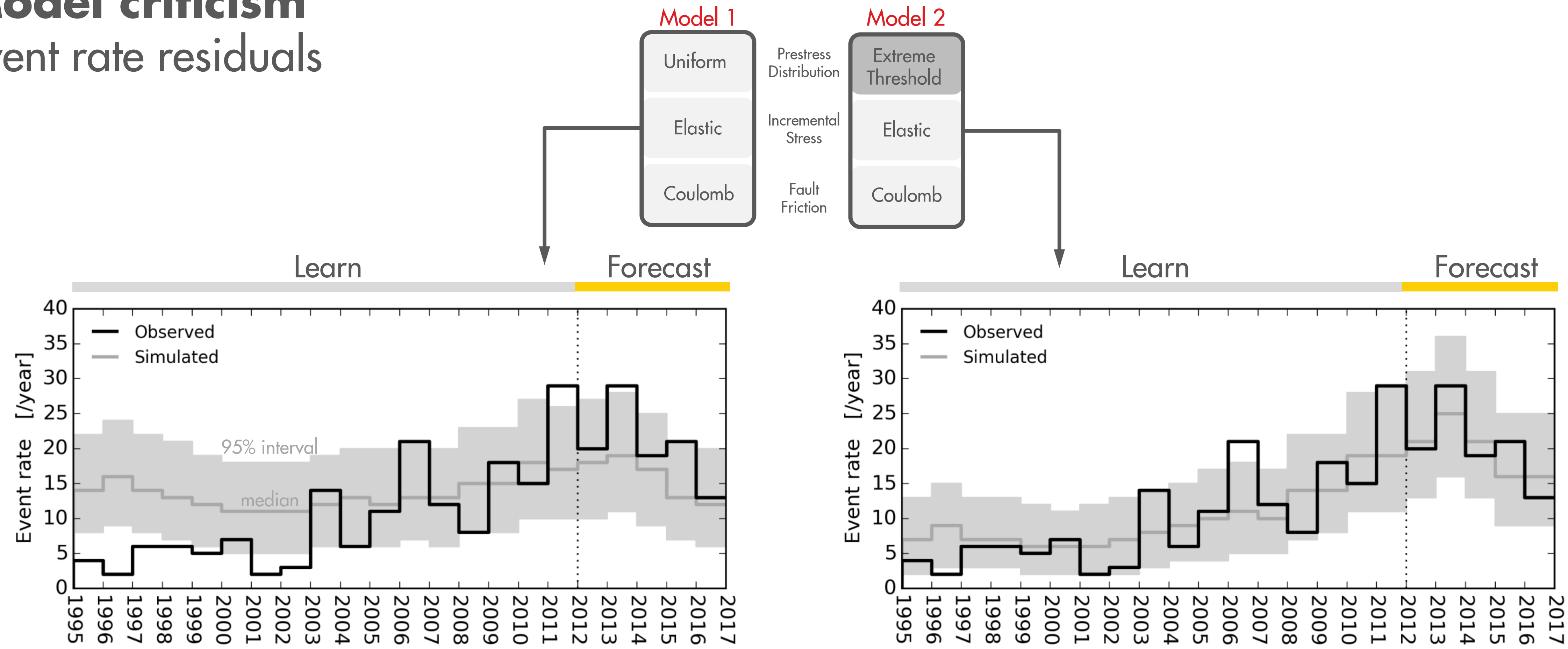

- **Model 1:** Uniform Prestress Distribution insufficient to describe increasing event rates from1995 to 2012
- **Model 2:** Exponential Extreme Threshold Failure trend improves performance over the learning and forecast periods

Model criticism

Epicentral density residuals

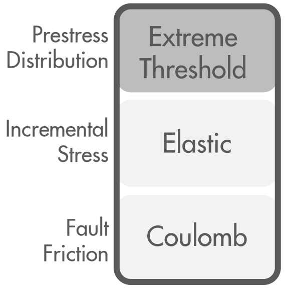

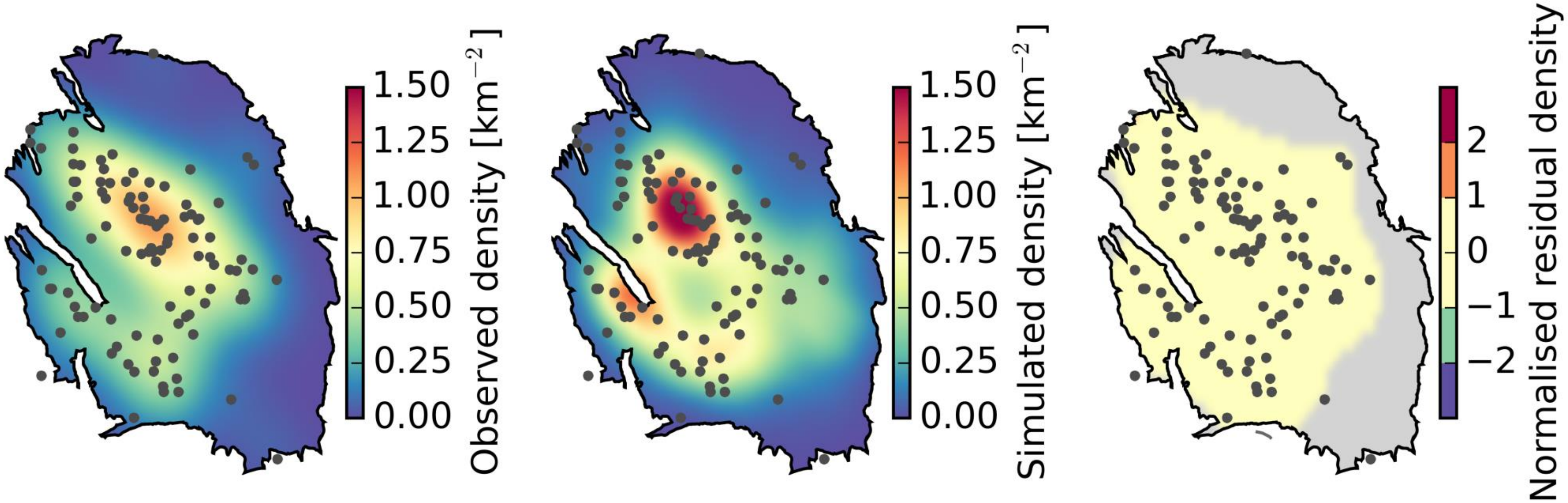

- Learning period: 1995 to 2012
- Forecast period: 2012 to 2017
- Extreme Threshold Failure model forecasts observed spatial density within stochastic variability

Expected epicentral density maps given history matched models

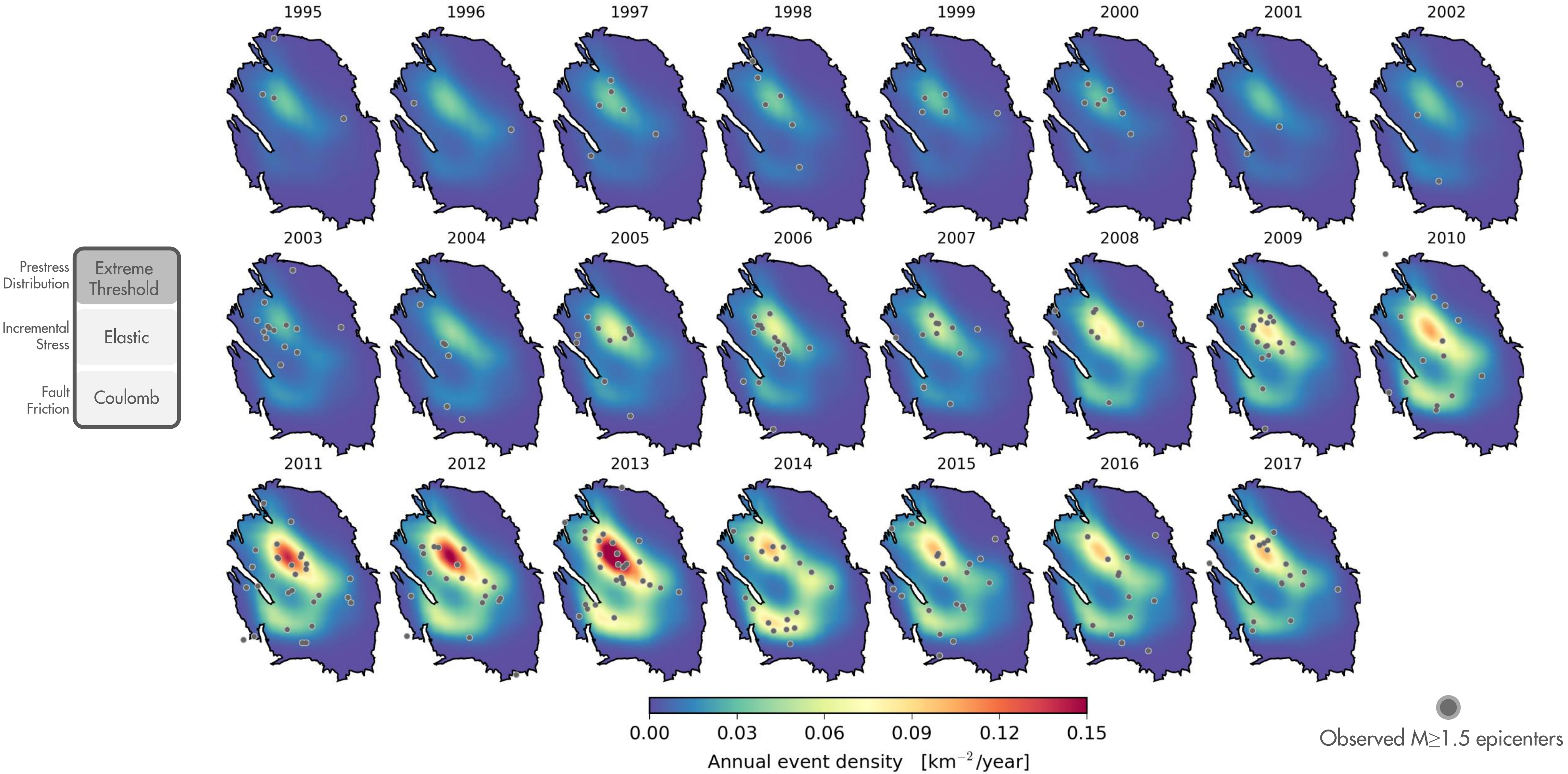

Epidemic Type Aftershock Sequence Model

After Ogata (2011)

Intensity function

$$\lambda = \lambda_p + \sum_{j=1}^{i-1} f(t_i - t_j, \mathbf{x}_i - \mathbf{x}_j | m_j)$$

Aftershock triggering function

$$f = Kg(t)h(r)e^{a(M-M_0)}$$

Temporal & spatial probability density functions

$$g(t) = \frac{(p-1)}{c}\left(\frac{t}{c}+1\right)^{-p}$$

$$h(r) = \frac{(q-1)}{\pi d}\left(\frac{r^2}{d}+1\right)^{-q}$$

Aftershock productivity

$$Ke^{a(M-M_0)}$$

Posterior distribution of ETAS parameters

Joint maximum likelihood estimates obtained for compaction-induced events and aftershocks

- 7 parameters: β_0, β_1, K, a, p, d, q; subject to the constraint c = 3 days

Uncertainties quantified by relative likelihoods

- No aftershocks (K = 0) may be confidently rejected
- Trade-off between compaction-induced event escalation (β_1) and aftershocks (K)
- Little constraint yet on aftershock productivity scaling with magnitude (0 < a < 2)

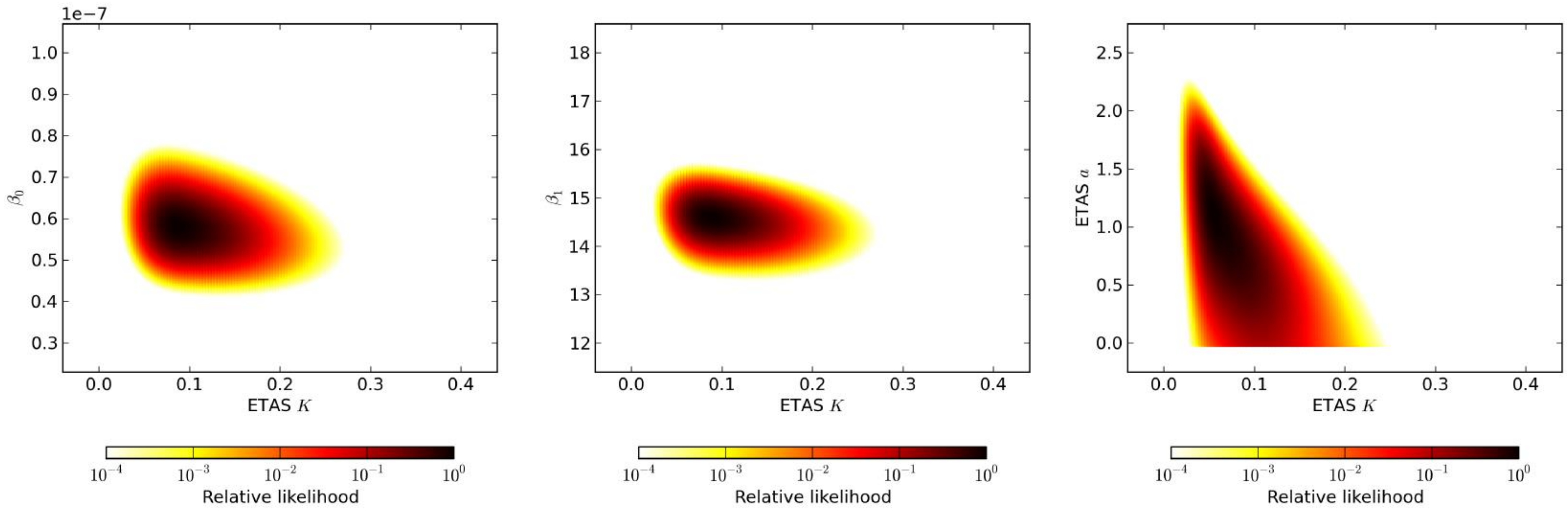

Posterior distribution of ETAS parameters

- Sparse data causes significant null space in estimates for *c*, *p*, *d*, *q*
- Earthquake simulations use Monte Carlo sampling of parameter values

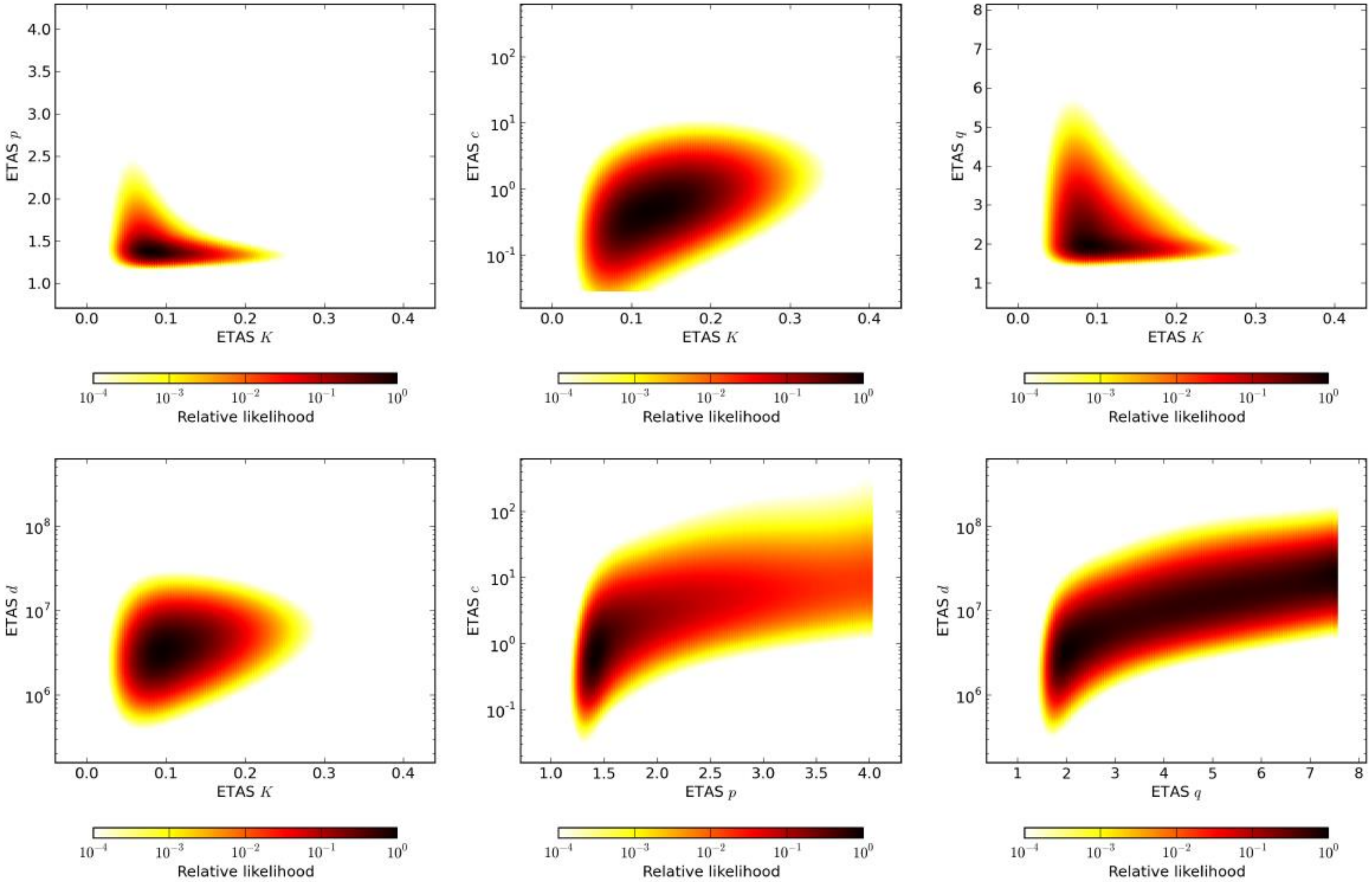

Simulated aftershocks match observed aftershocks

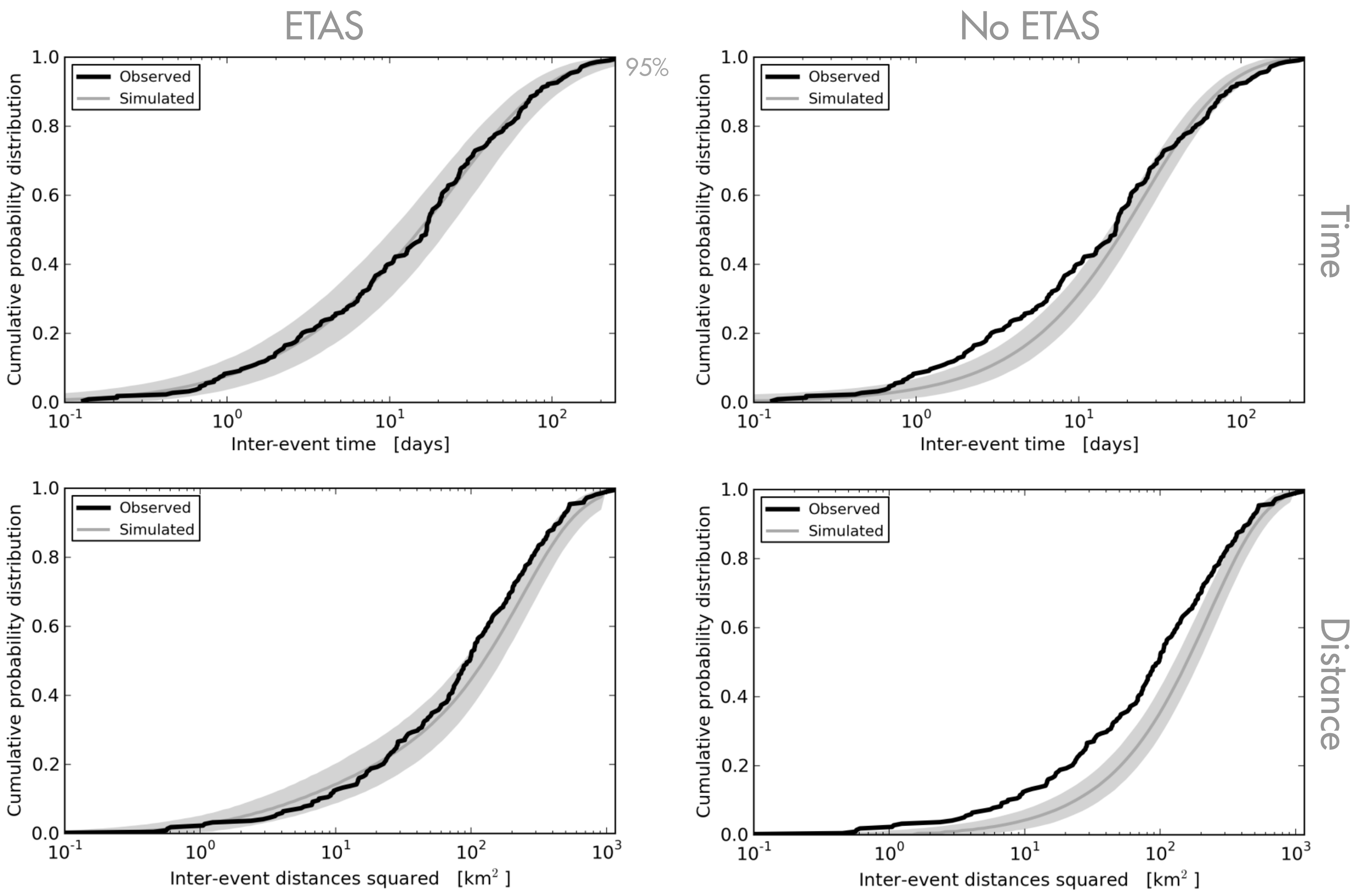

Out-of-sample forecast performance analysis

- Performance metric: Likelihood of observed events given the model
- Learning period: 1995-2013
- Evaluation period: 2013-2018

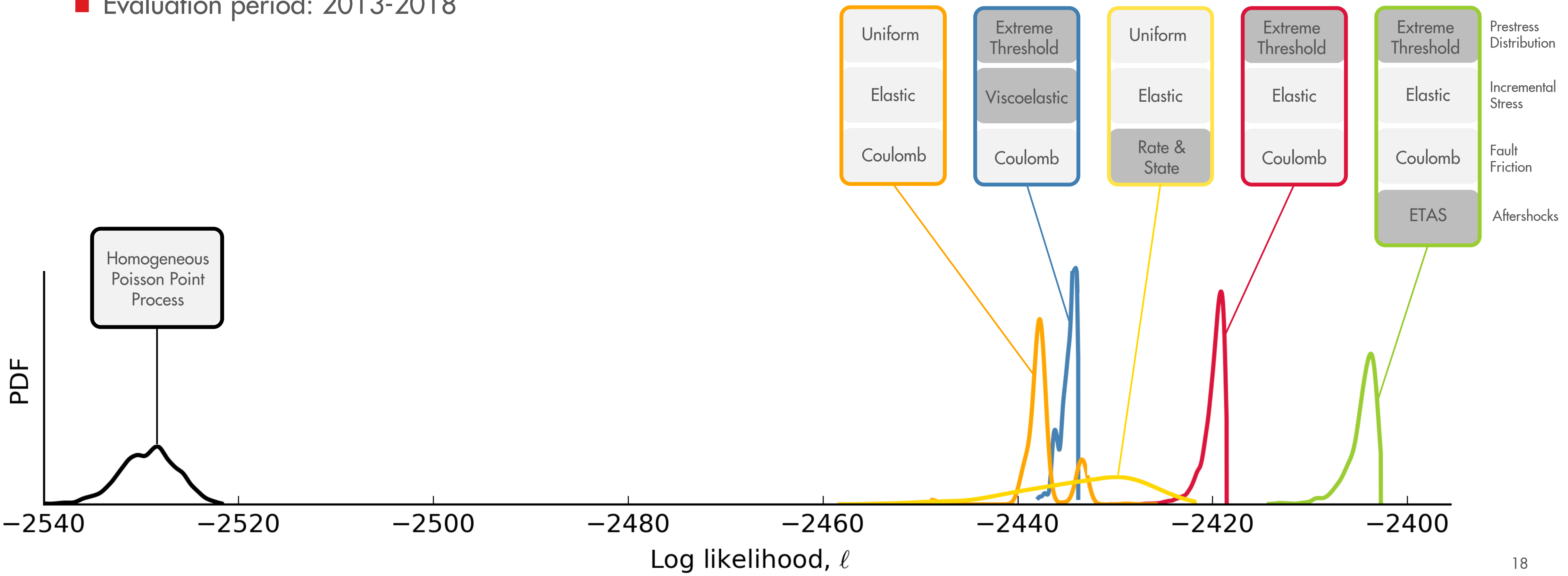

Summary

- Established a minimum physics-based theory based on statistical geomechanics for Groningen
- Pore-elastic thin-sheet theory
  - Computes smoothed incremental Coulomb stress according to resolvable geometric and elastic heterogeneities
- Extreme thresholds failure theory
  - Computes induced seismicity rates according to incremental Coulomb stress and the extremes of initial Coulomb stress
  - Computes the frequency-magnitude distribution and its dependence on incremental Coulomb stress
- Bayesian inference for hidden variables
  - Ensemble of realizations for each seismological model
  - Family of alternative seismological models represent different types of reservoir heterogeneity
- Model performance
  - Out-of-sample forecast testing provides objective performance ranking of alternative models
  - Analysis of residuals characterizes sources of poor model performance

Outline

Frequency-magnitude models for induced seismicity

- Model designs based on statistical mechanics
- Model inference based on Bayesian methods
- Model performance based on forecast performance
- Summary of outcomes

The observed magnitude distribution is stress-sensitive

Kolmogorov-Smirnov Threshold Analysis

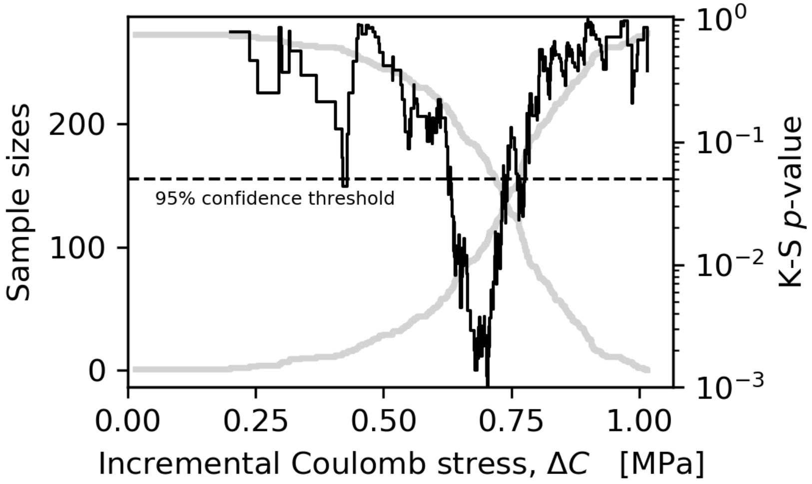

Optimal threshold

Earthquake Magnitudes Rise with Increasing Stress

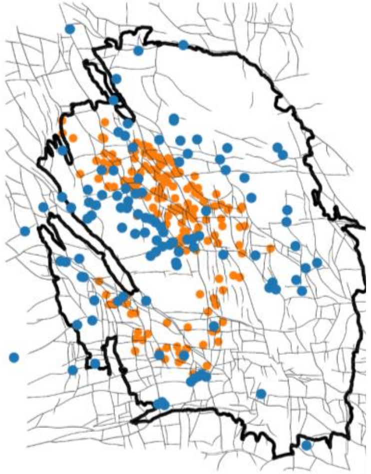

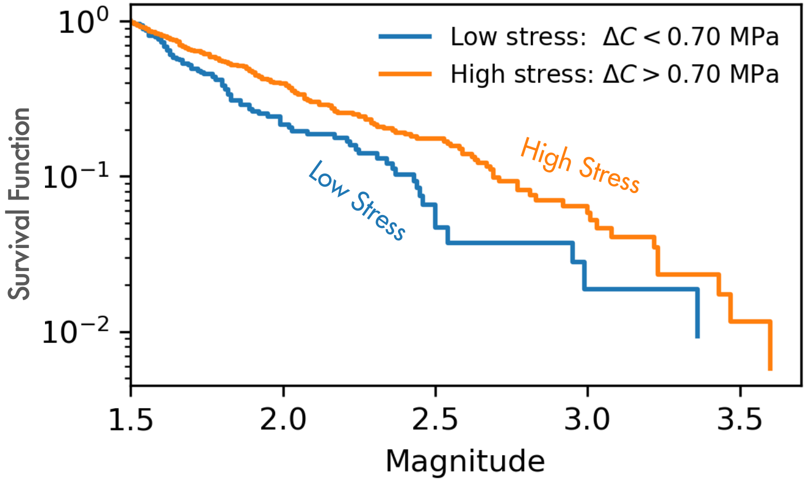

Two Competing Theories

1 Slope changes?

Stress-dependent power-law?

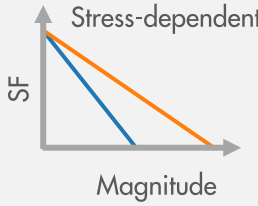

2 End-taper changes?

Stress-dependent tapered power-law?

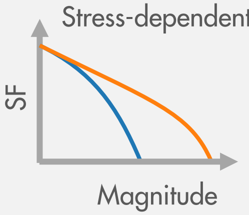

Statistical mechanics of disordered fault re-activation

Stochastic disorder leads to failures sizes with a Tapered Power-Law Distribution

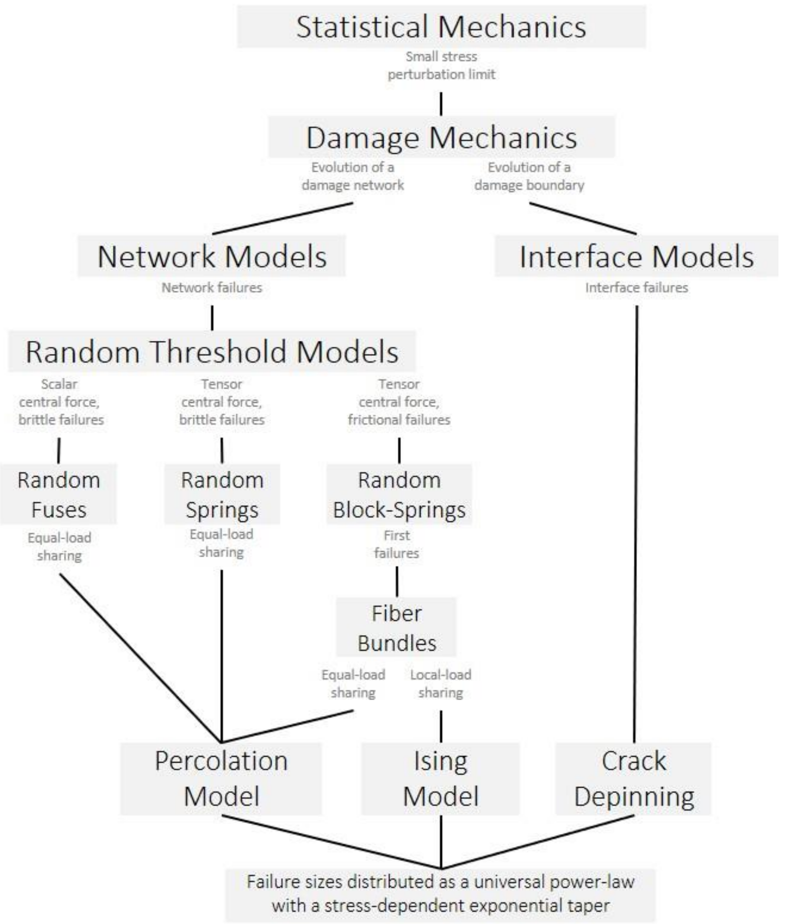

One result

Seismic Moment Distribution: Power-law with an Exponential Taper

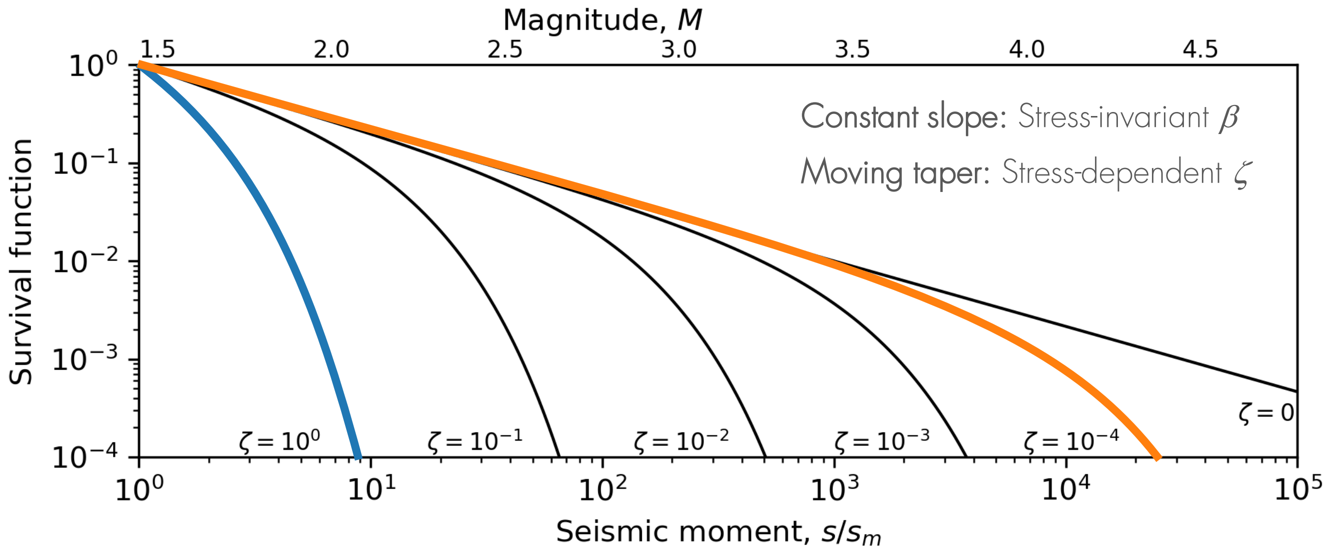

- Power-law with exponential taper: $P(> s \mid > s_m) = \left(\frac{s}{s_m}\right)^{-\beta} e^{-\zeta\left(\frac{s}{s_m}-1\right)}$
- Critical-point stress dependent taper: $\zeta = \theta_0(\theta_1 - \Delta C)^{\theta_2}$
- β-value defines the stress-invariant slope of the distribution
- ζ-value defines the stress-dependent exponential taper
- ζ-value exhibits critical point scaling

And also:
Within information theory, using the concept of maximum entropy to find the least informative probability distribution subject to observational constraints on the mean magnitude and mean total seismic moment rate (Main & Burton, 1984)

Bourne & Oates, 2020 (https://doi.org/10.1029/2020JB020013)

Does Groningen exhibit stress-dependent *b*-values or ζ-values?

MLE *b*-values appear to decrease with stress

MLE ζ-values appear to decrease with stress

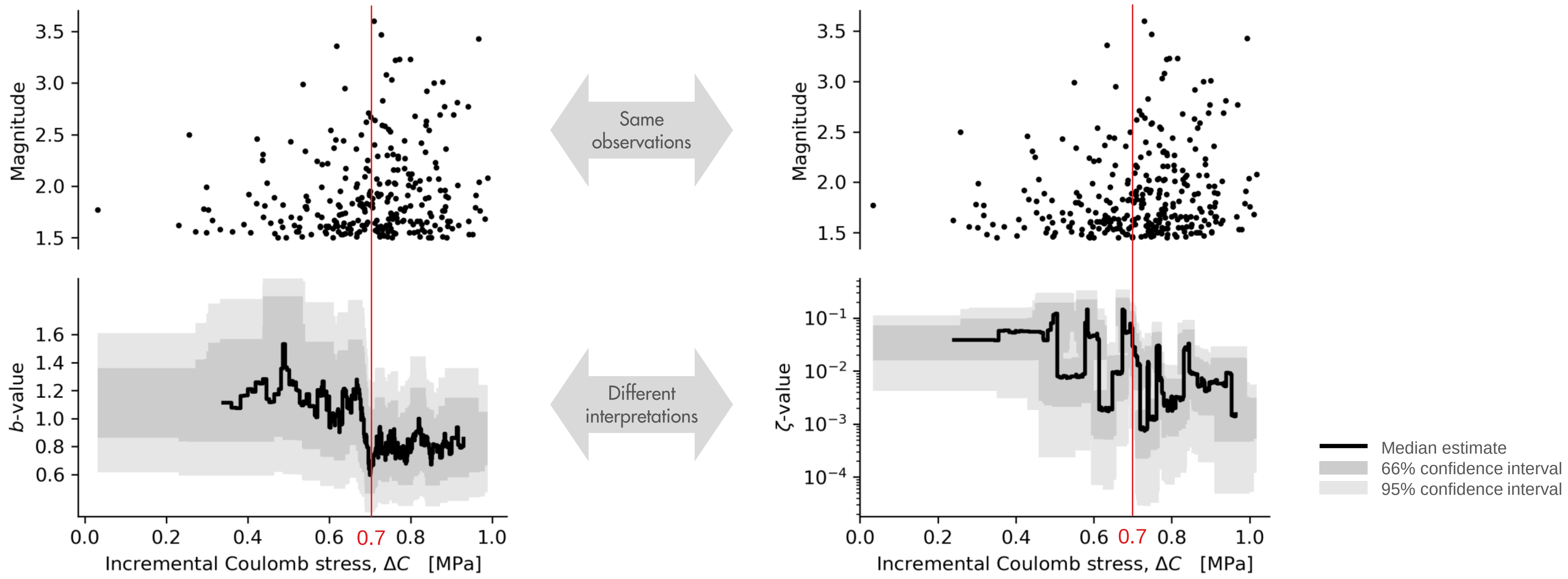

Significant evidence for stress-dependence of the exponential taper

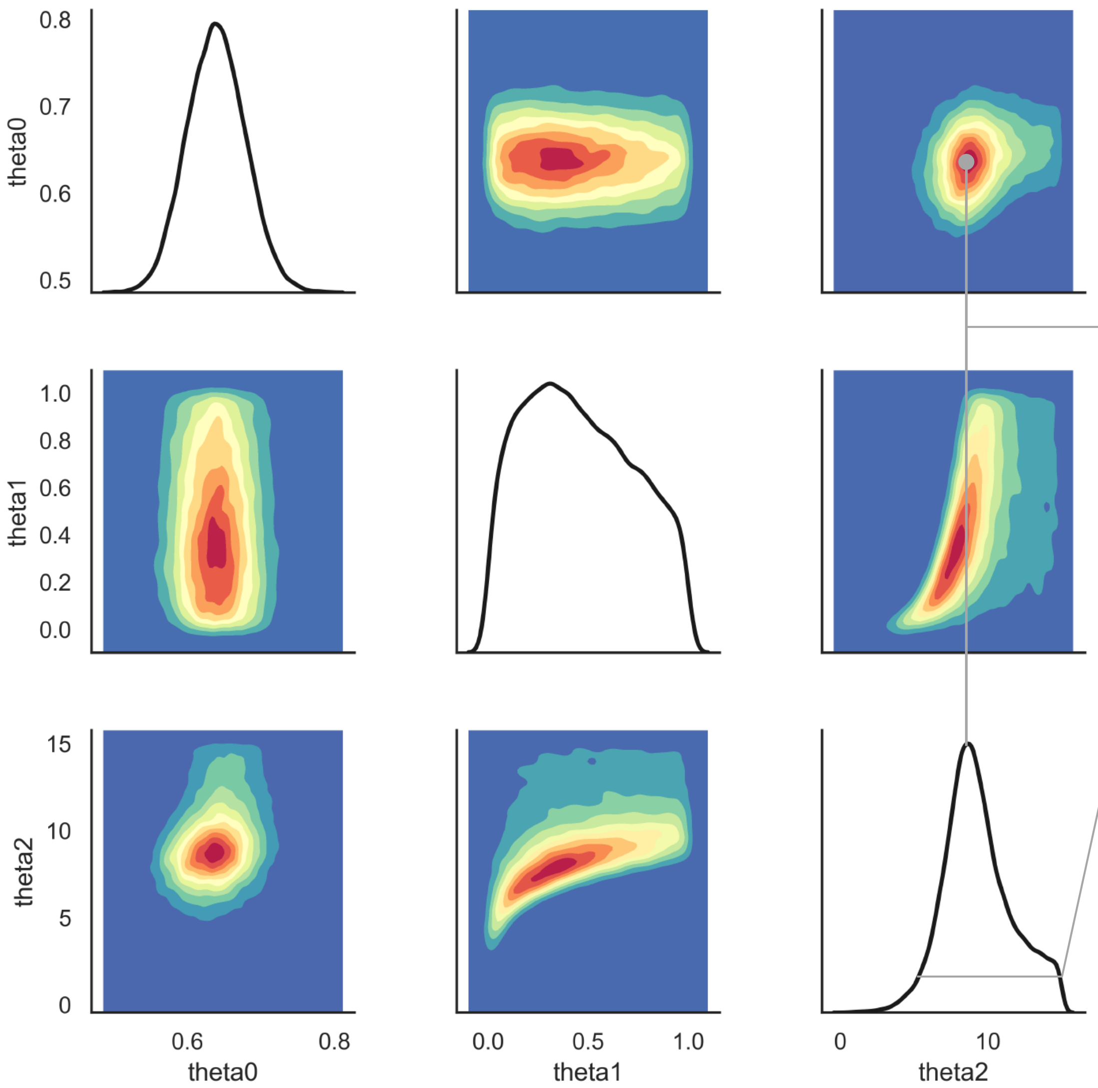

Stress-dependent ζ means θ_2 is not zero

MAP $\theta_2 = 9.33$

95% confidence = 5.7 to 14.8

$$P(\geq s | s \geq s_m) = \left(\frac{s}{s_m}\right)^{-\beta} e^{-\zeta(\frac{s}{s_m}-1)}$$

Moment distribution | Power-law | Exponential taper

$$\beta_i = \theta_0,$$
$$\zeta_i = \theta_1 e^{-\theta_2 \Delta C_i}$$

ζ stress sensitivity

Posterior distribution of stress-dependent magnitude distributions

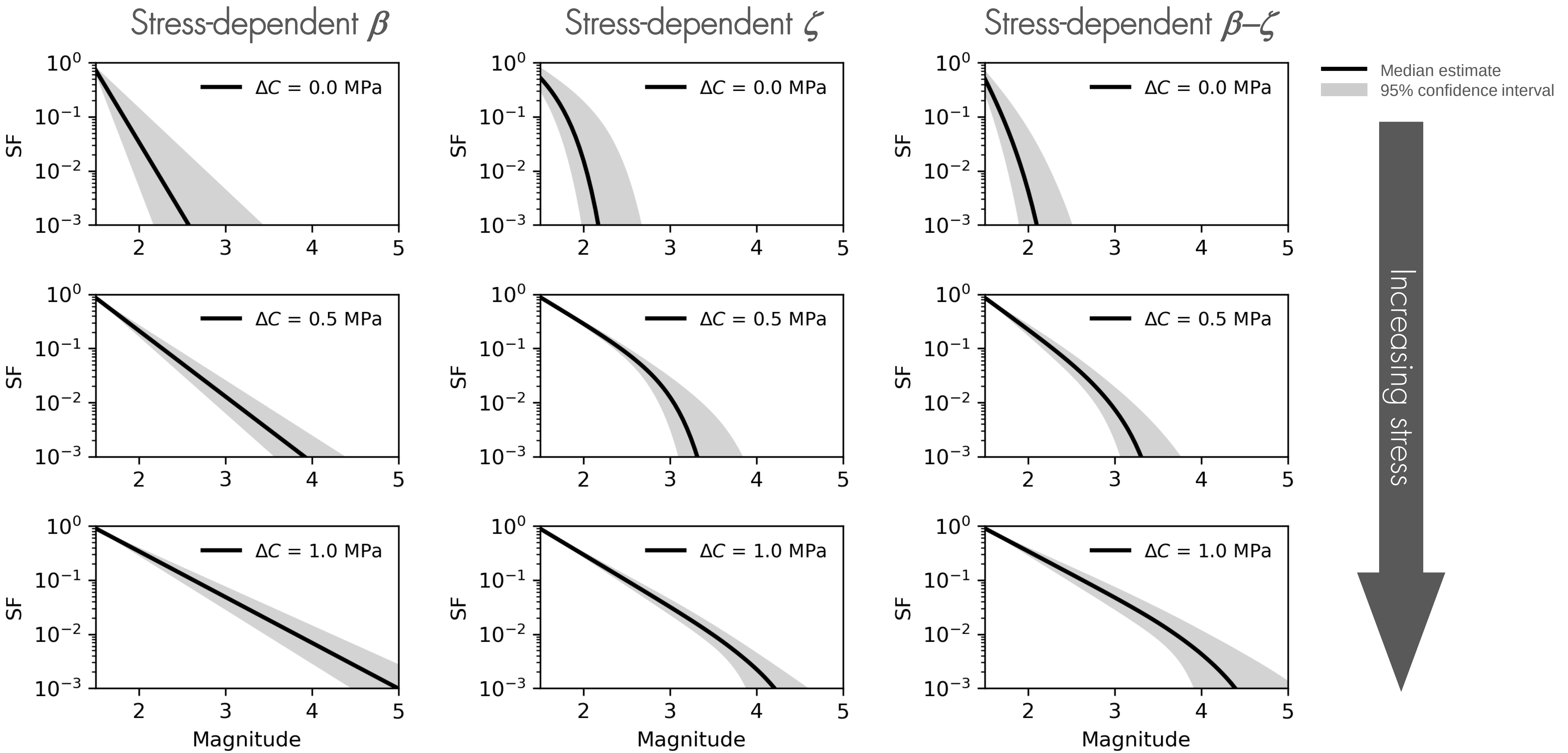

Maximum magnitude and total seismic moment time series

Stress-invariant model performance

Maximum magnitudes

Total seismic moment

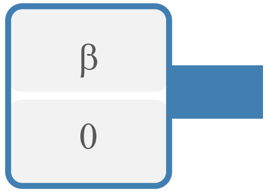

M$_1$

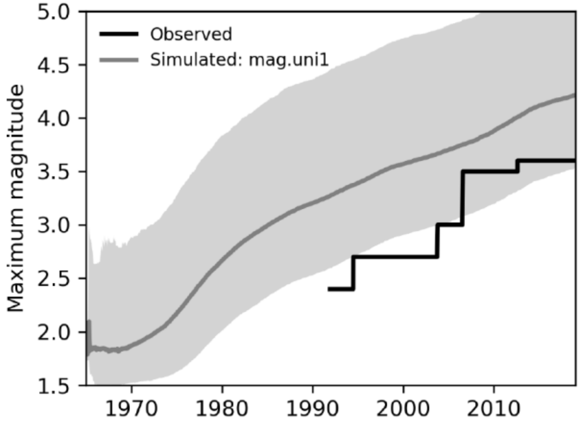

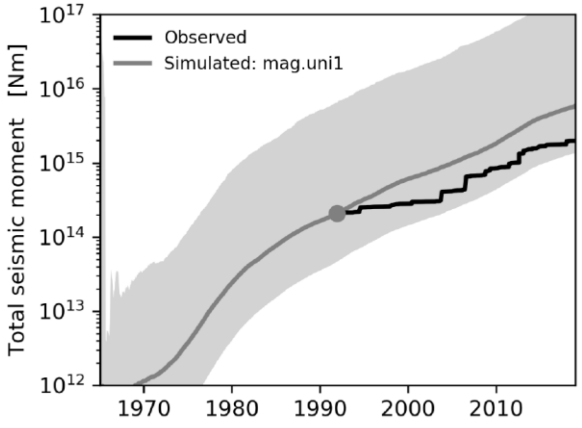

Power-law model

- Systematically and significantly over-states maximum magnitudes
- Systematically over-states seismic moment rate

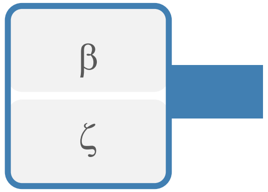

M$_3$

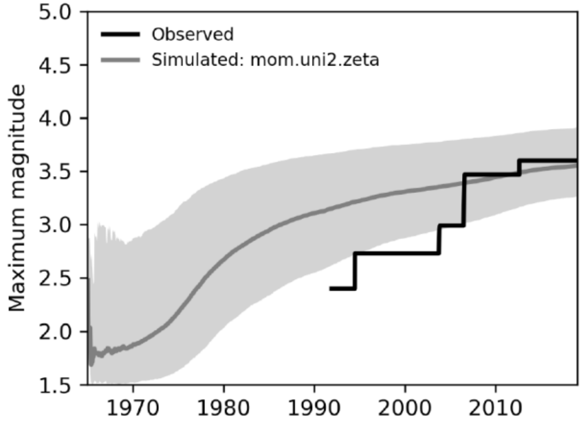

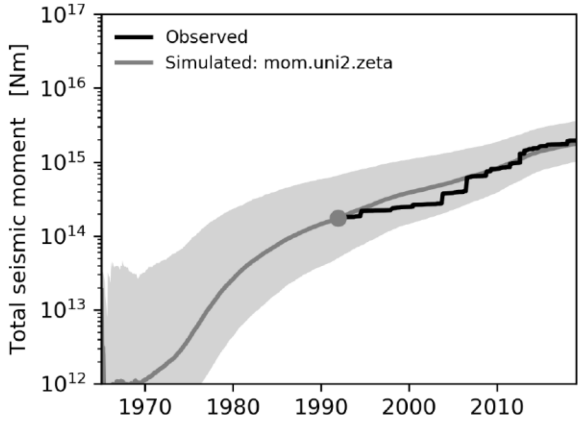

Tapered power-law model

- Significantly over-states early maximum magnitudes
- Matches moment rate with appropriate precise

Maximum magnitude and total seismic moment time series

Stress-dependent model performance

Maximum magnitudes | Total seismic moment

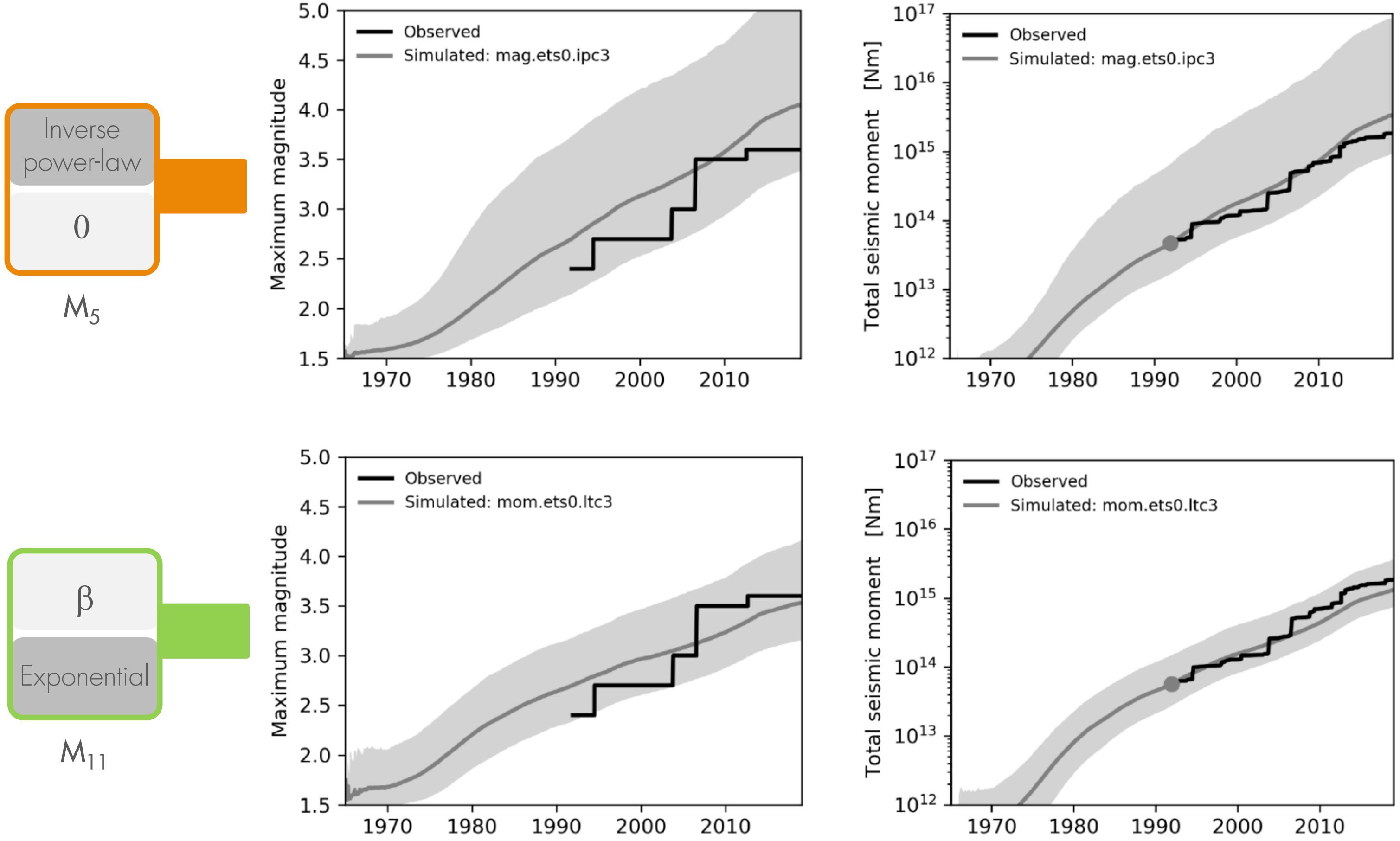

Stress-dependent β model

- Systematically over-states maximum magnitudes
- Matches seismic moment rate but upper bound over-stated

Stress-dependent ζ model

- Matches maximum magnitudes within 95% prediction interval
- Matches moment rate with appropriate precision

Ranking models according to the probability of better performance

Model class		M_i	P_{ij}, Probability of M_i out-performing M_j							
			M_1	M_2	M_3	M_5	M_7	M_{10}	M_{11}	M_{13}
Stress invariant	uni1	M_1	0.500	0.400	0.370	0.283	0.091	0.343	0.060	0.060
	uni1.zeta	M_2	0.600	0.500	0.580	0.374	0.192	0.424	0.110	0.080
	uni2.zeta	M_3	0.630	0.420	0.500	0.364	0.162	0.394	0.110	0.120
Stress-dependent β	ets0.ipc3	M_5	0.717	0.626	0.636	0.500	0.273	0.576	0.152	0.111
	ets0.htc3	M_7	0.909	0.808	0.838	0.727	0.500	0.727	0.253	0.192
Stress-dependent ζ	ets0.cps3	M_{10}	0.657	0.576	0.606	0.424	0.273	0.500	0.141	0.121
	ets0.ltc3	M_{11}	0.940	0.890	0.890	0.848	0.747	0.859	0.500	0.400
Stress-dependent β-ζ	ets0.b3.z2	M_{13}	0.940	0.920	0.880	0.889	0.808	0.879	0.600	0.500

M_j

Stress-dependent taper models yield lower magnitude exceedance rates

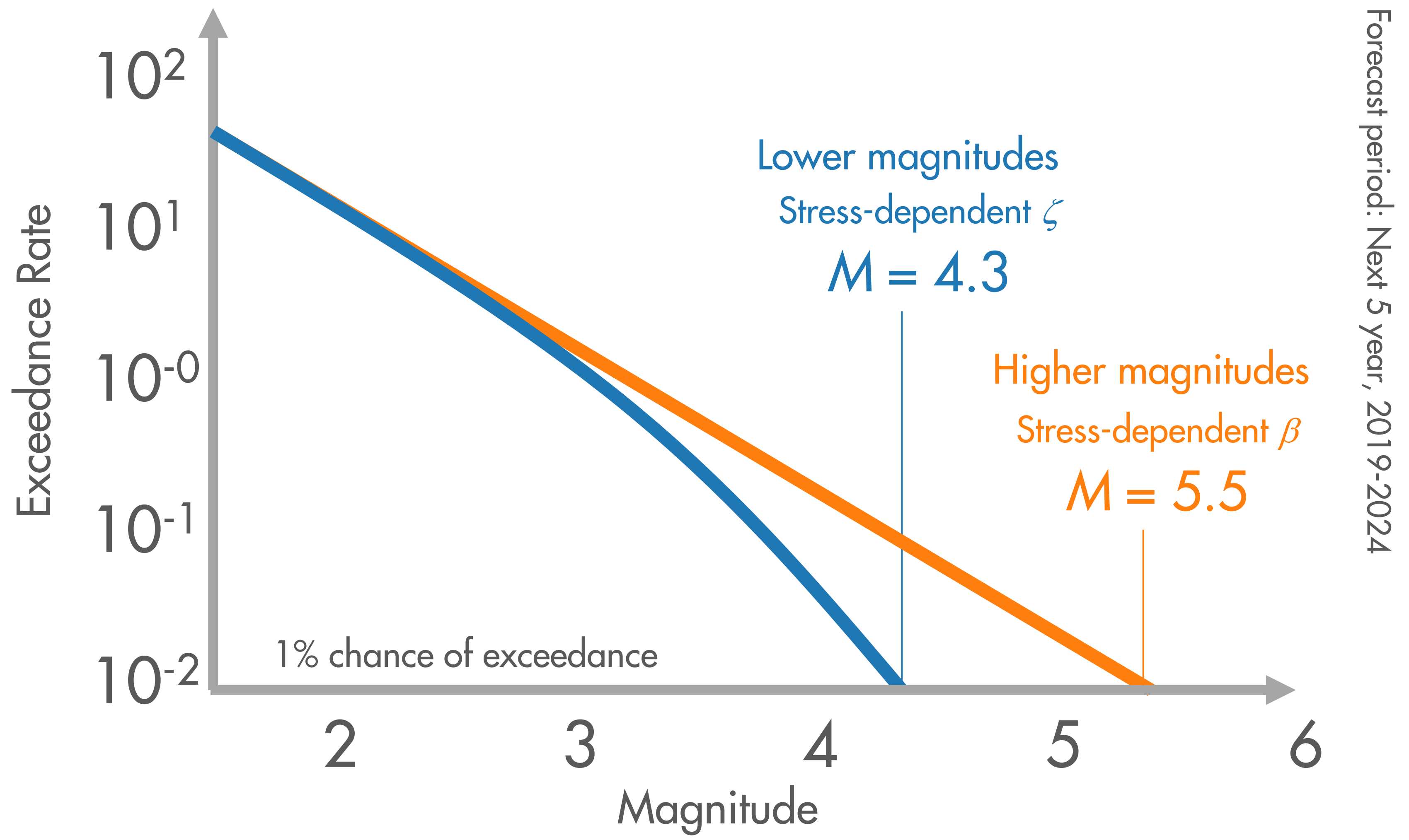

Summary

- Frictional failures within a mechanically disordered fault system is a stochastic process
- Statistical mechanics models exhibit magnitude distributions with stress-dependent tapers
- Bayesian inference allows Groningen data-driven ranking of many physics-based models
  - Worst models: Stress-invariant magnitude distributions
  - Better models: Stress-dependent power-law distributions with no tapering
  - Best models: Stress-dependent tapered power-law distributions
- A tapered power-law significantly reduces the probably of future large earthquakes

Re-assessing the earthquake-size distribution for the Groningen gas field

Laura Gulia

University of Bologna, Department of Physics and Astronomy, Bologna

1st day of the Workshop, van Thienen-Visser

- Dutch government decided to stop gas production in 2023
- Keep monitoring the seismicity in the field in the next years: what may we expect?

I'll try to answer in terms of b-value

The history of the b-value in the field in last 30 years and its possible evolution

- a brief overview on b-value
- state of the art for the Groningen gas field
- from theory to observations: what we expect to see in the field
- implication for PSHA

What b-value is?

$$\log_{10}N = a - b\,M$$

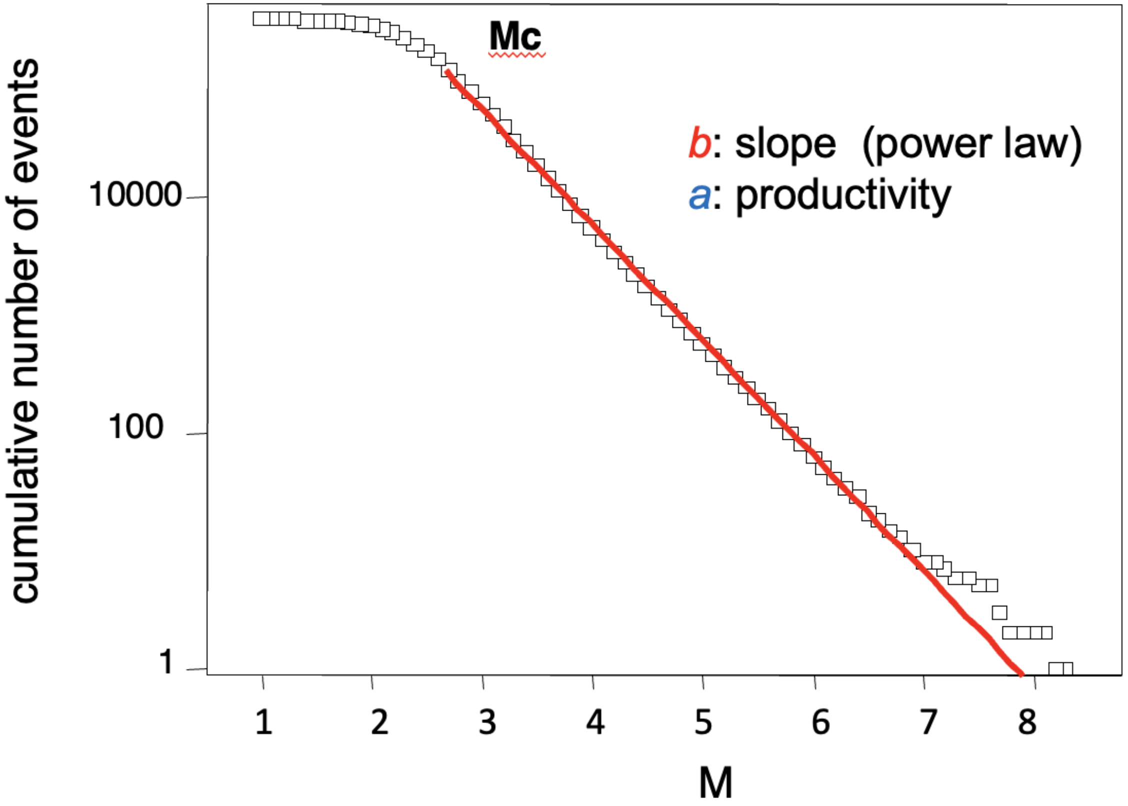

At a global scale **b-value** is **about** 1

but…is b-value steady and equal to 1?

No! b-value varies depending on…

a brief overview on b-value

…style-of-faulting

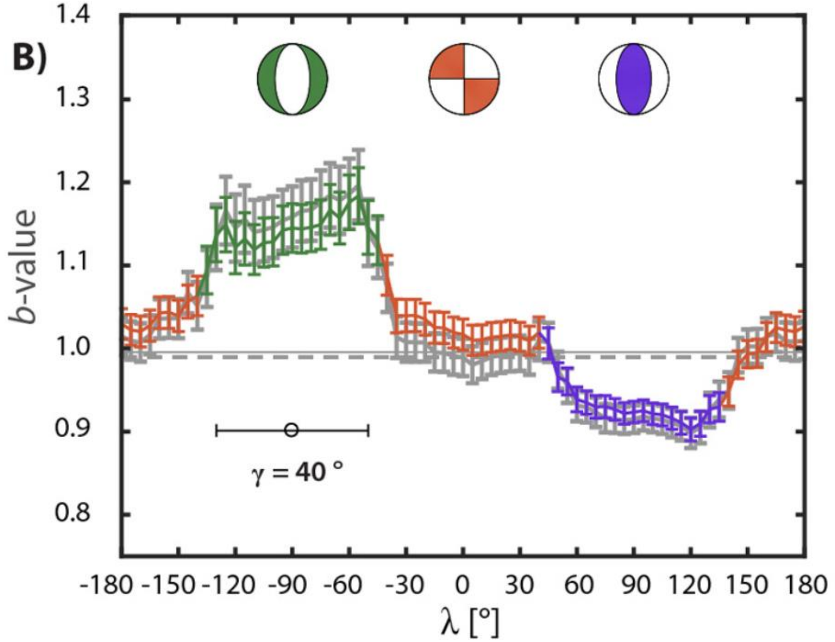

Schorlemmer et al., 2005, Nature

Petruccelli et al., 2019, EPSL

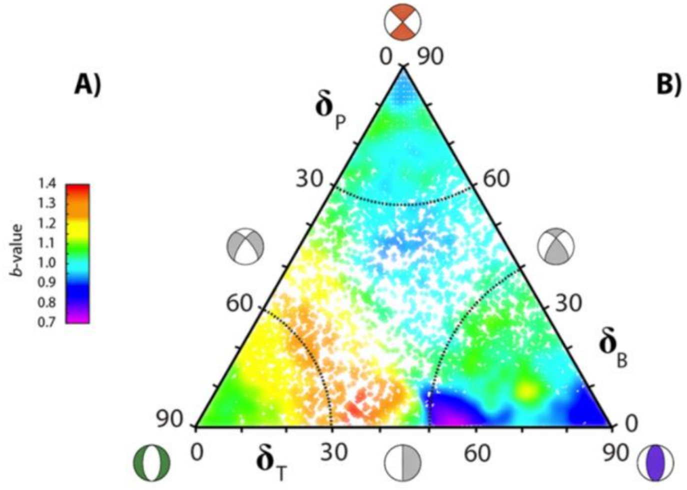

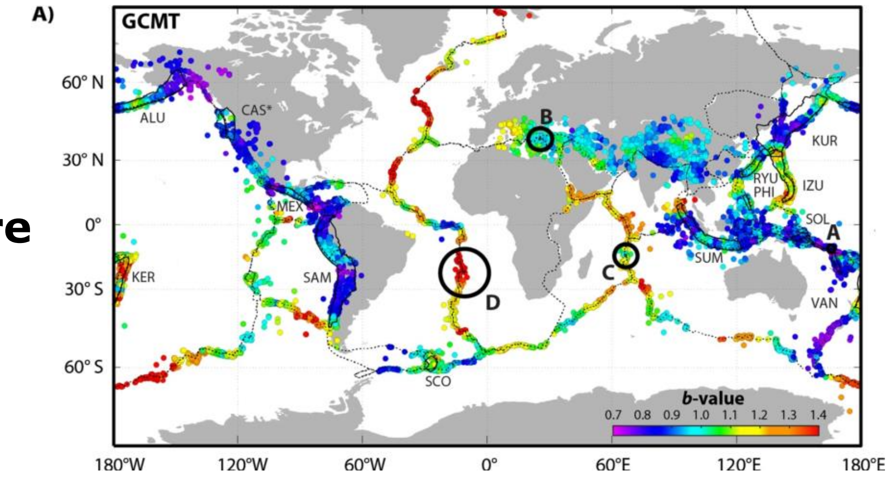

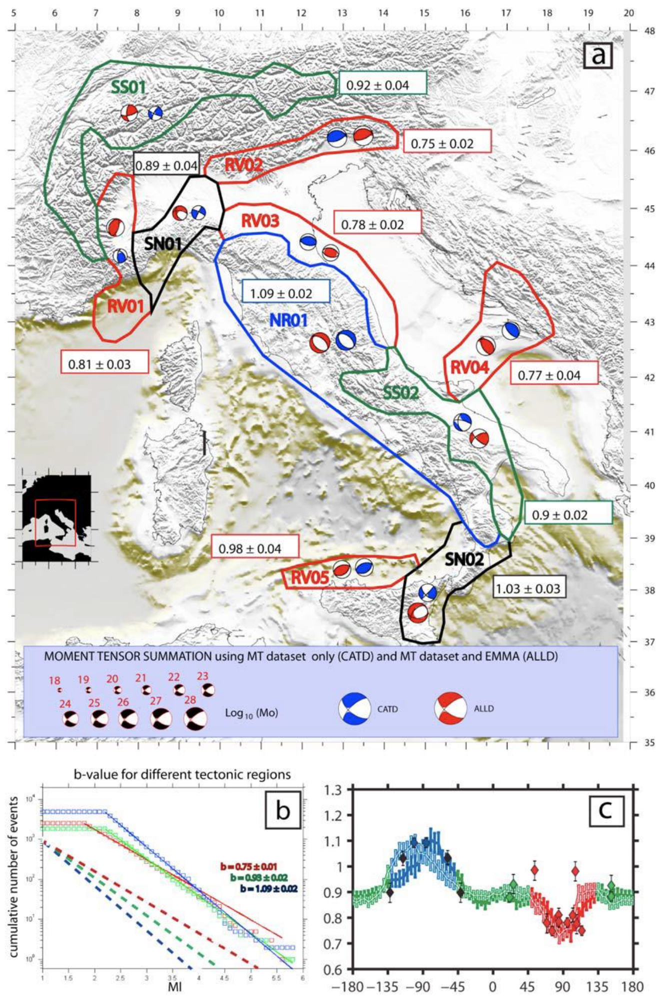

Gulia and Wiemer, 2010, GRL

…depth

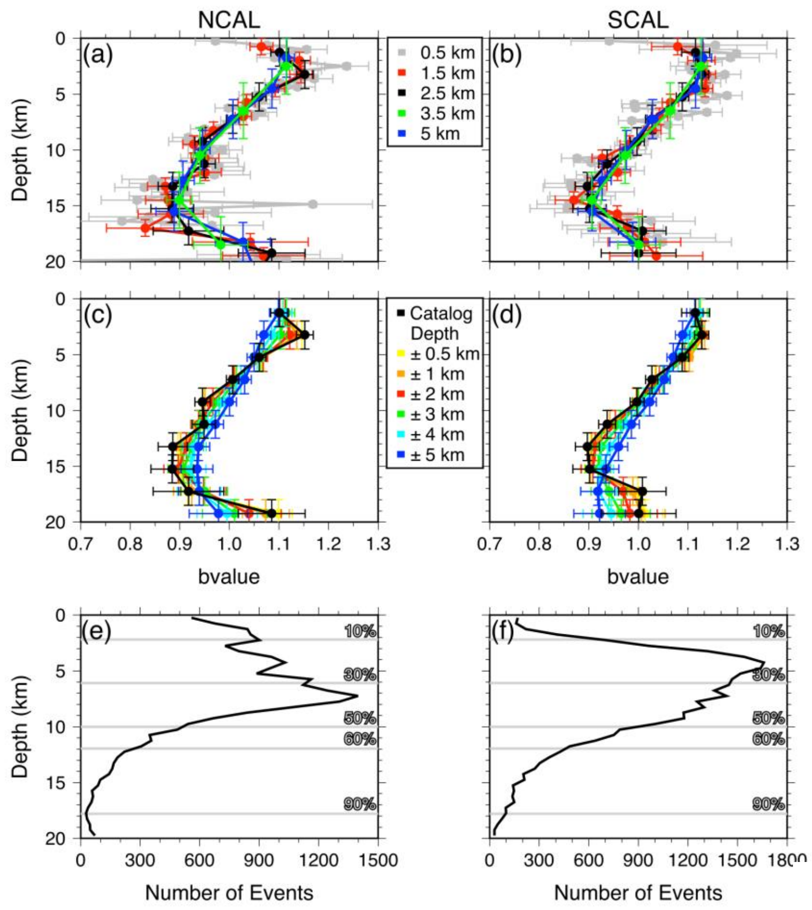

Petruccelli et al., 2019, EPSL

Simultaneous depen
on both style-of-faulti
depth

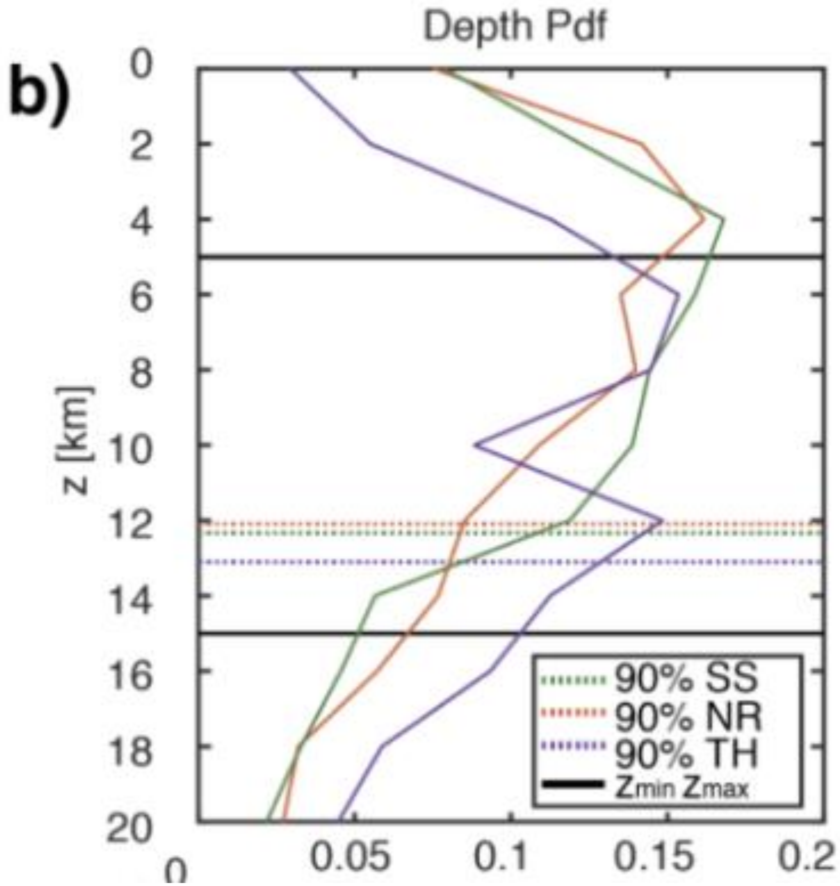

Spada et al., 2013, GRL

a brief overview on b-value

...space

Asperities ← Lower b-value

and

creeping parts ← Higher b-value

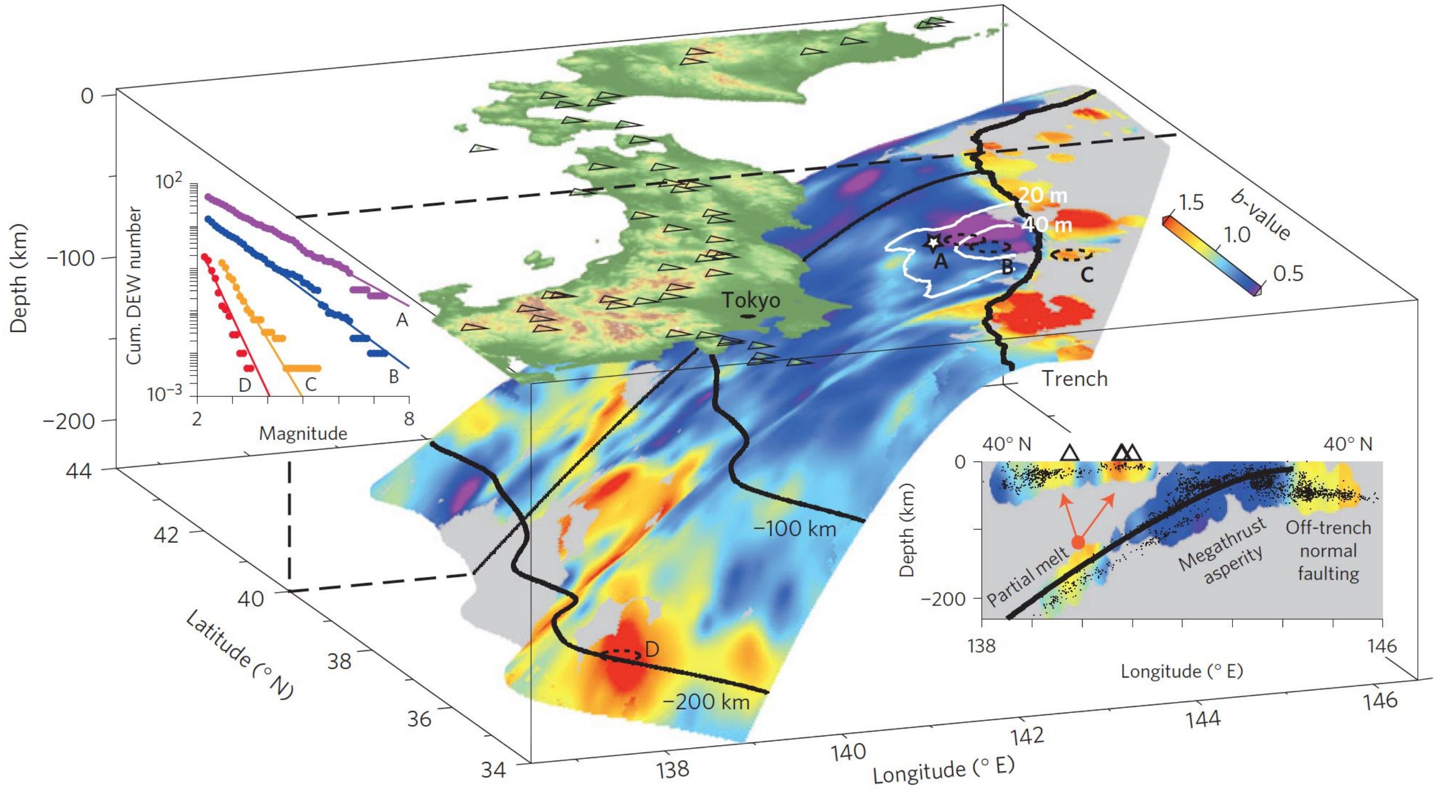

Tormann et al., 2015, Nature Geosci.

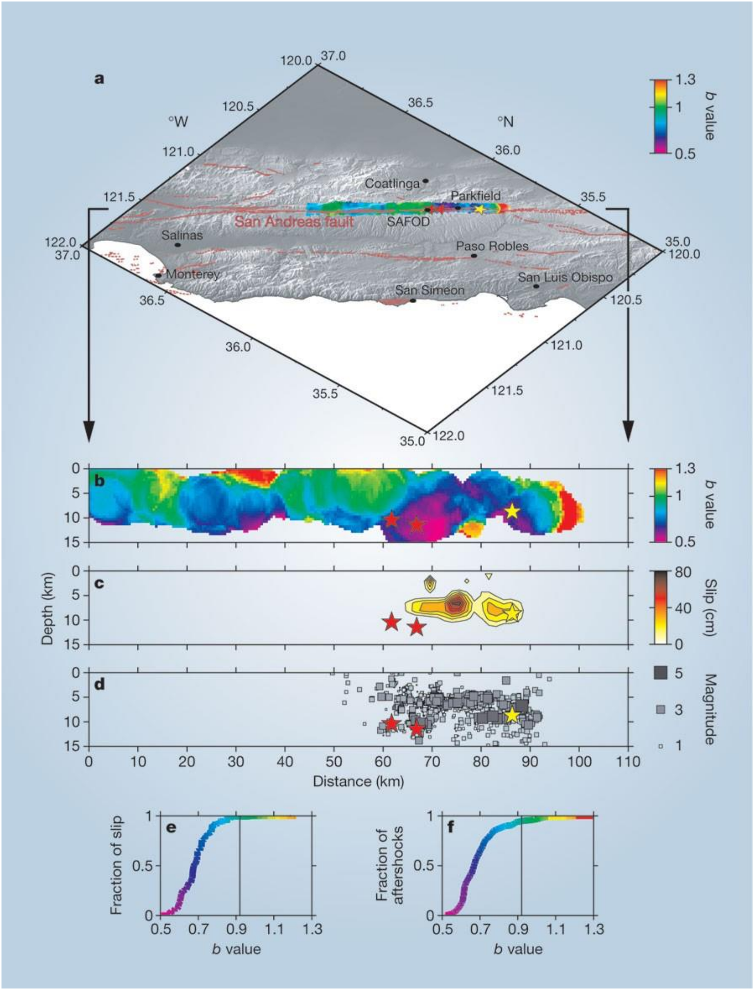

Schorlemmer and Wiemer, 2005, Nature

…and time!

Gulia et al., 2016, GRL modified

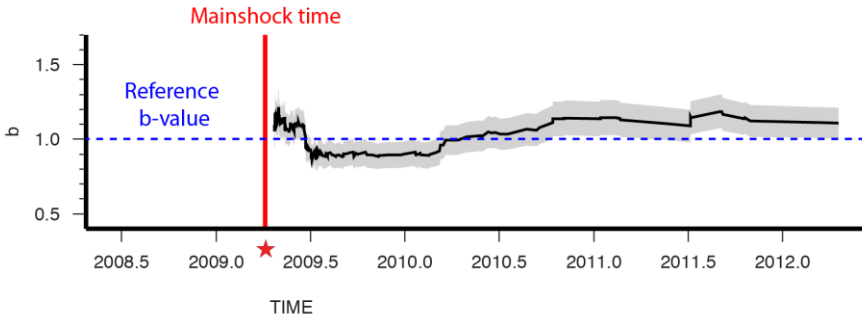

Tormann et al., 2015, Nature Geosci.

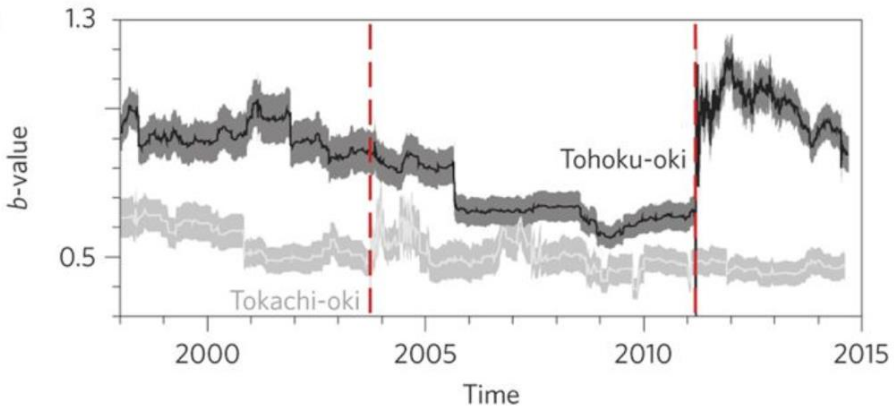

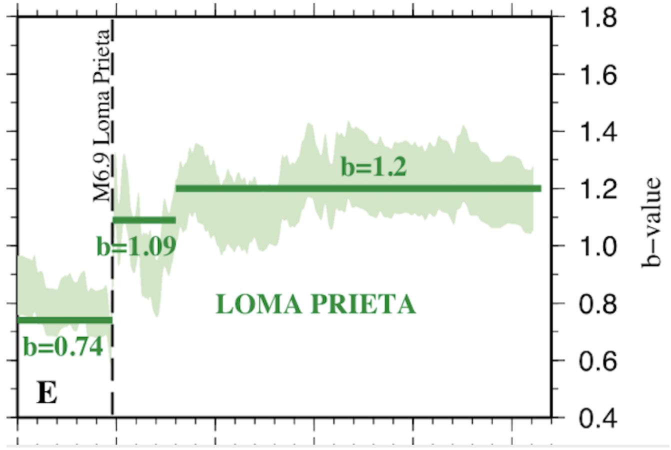

Tormann et al., 2012, GRL

The time variability is confirmed by laboratory experiments
(AE; e.g., Scholz, 1968; Amitrano, 2003; Goebel et al., 2013; Rivière et al., 2018)

Observations in natural contexts

lab experiments

a systematic b-value **decrease** as failure approaches

Why is b-value so important? And What does low and high b-value mean?

lab experiments
(Goebel et al., 2013, GRL)

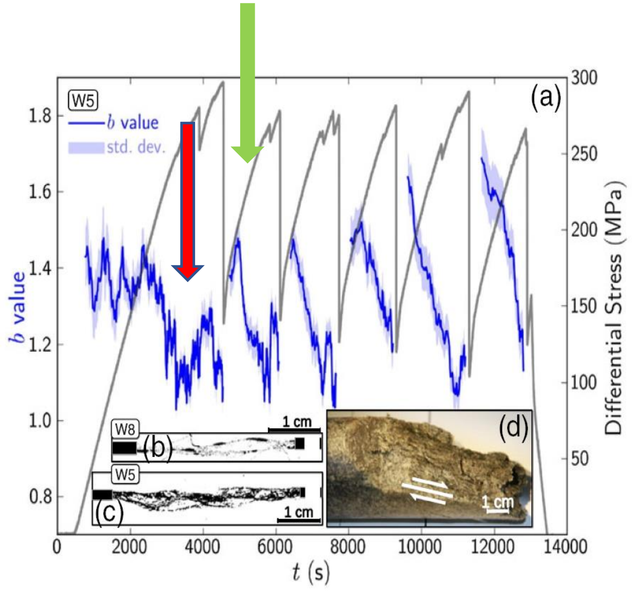

Observations in natural context
(Tormann et al., 2015, Nature Geosci.)

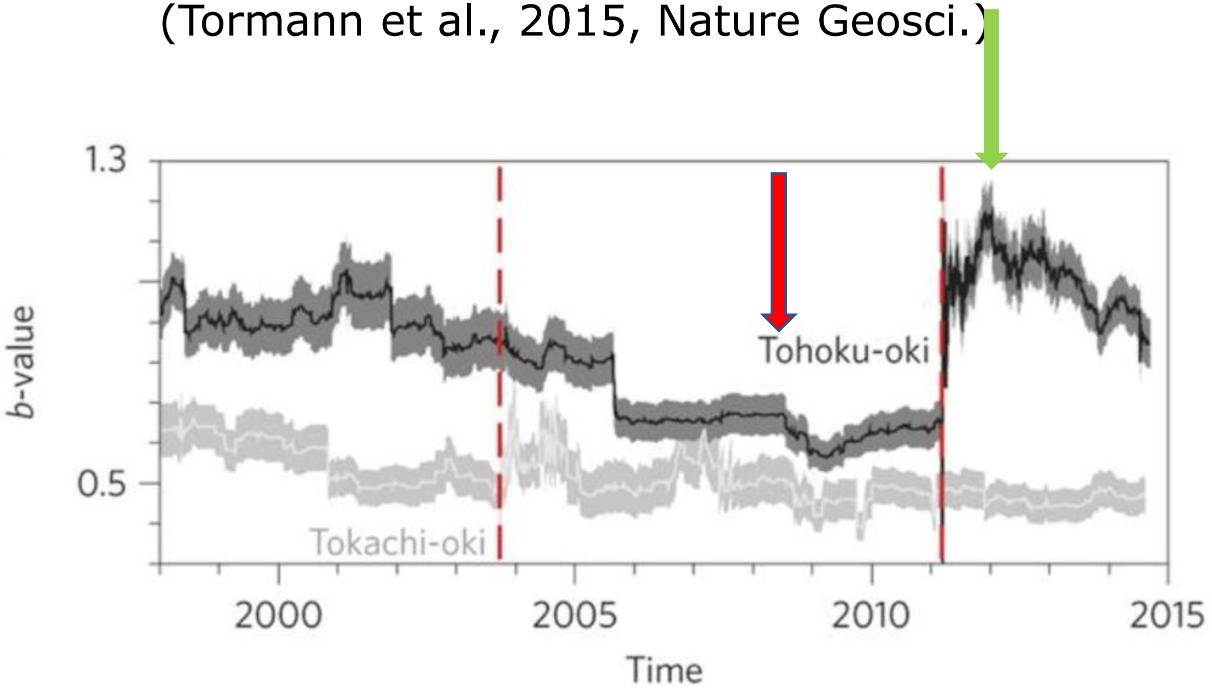

- b-value decrease → gradual loading
- b-value increase → stress-release (mainshock)

Why is b-value so important? Small changes in b-value have a high impact on rates of the largest events

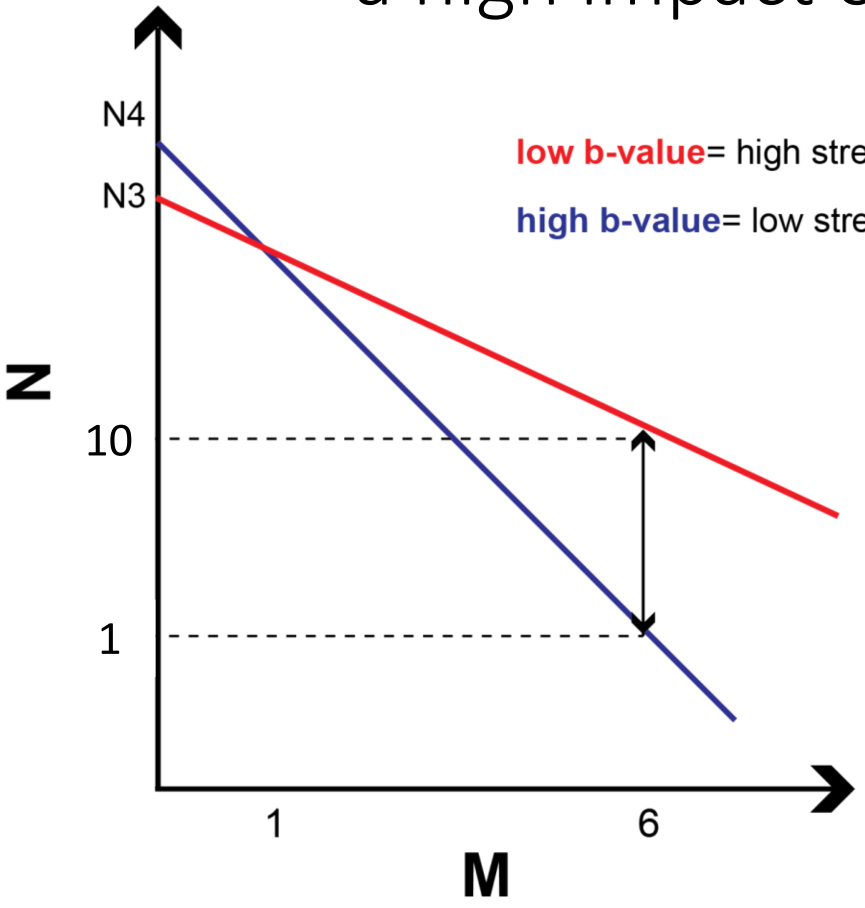

$$Tr = \frac{\Delta T}{10^{a-bM}}$$

$$Pr = \frac{1}{Tr}$$

Wiemer and Wyss, 1997, JGR

Pr of a M6+ is 10 times higher!!!

Is b-value decreasing and increasing SYSTEMATIC?
Can we extrapolate a general behaviour in faults?

We selected 58 well-monitored sequences from California, Japan, Alaska and Canada and for could calculate the time-series for 31

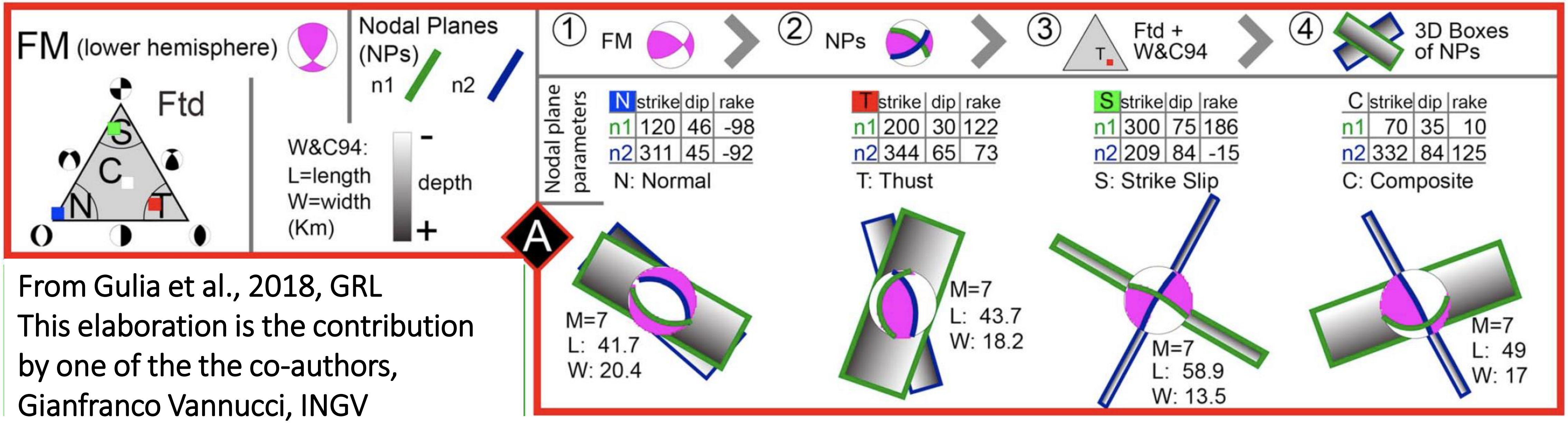

From Gulia et al., 2018, GRL
This elaboration is the contribution by one of the the co-authors, Gianfranco Vannucci, INGV

fault plane

Focal Mechanism
+
Wells&Coppersmith, 1994, BSSA

Sequence: events strictly related to the fault! Each single fault has an own b-value

Is b-value decreasing and increasing SYSTEMATIC?

Example, step-by-step
A single time-series - Parkfield, 2004, M6

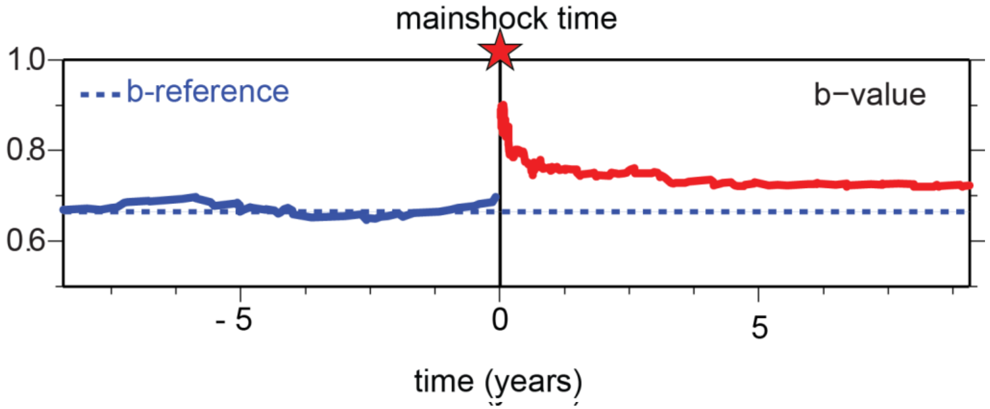

4.
Time-series
of all
the events
following
the
mainshock

The Parkfield time-series - difference in percentage respect to the reference value -

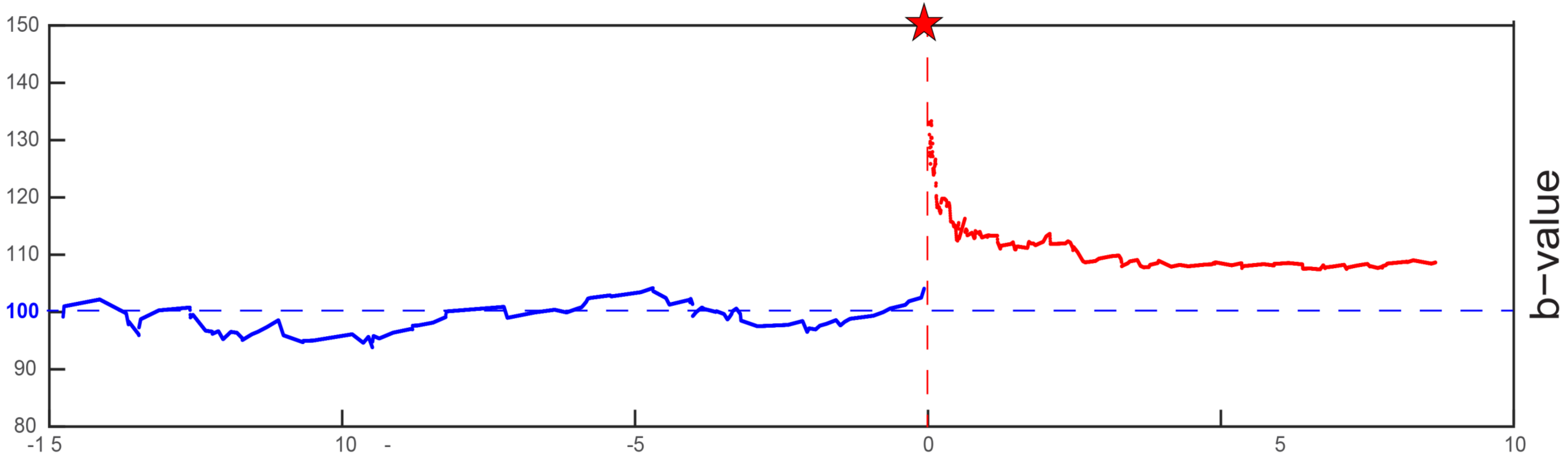

Stacking of the b-value 31 time-series

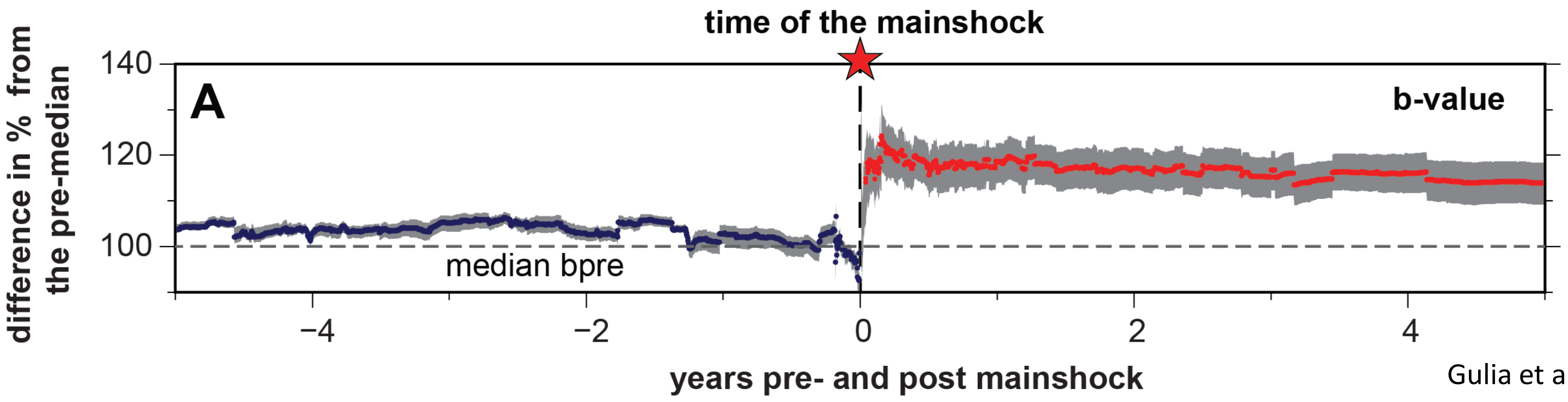

Gulia et al., 2018, GRL

b-value decreasing and increasing is SYSTEMATIC!!!

b-value in doughnuts around the fault plane

b-value changes are only near fault

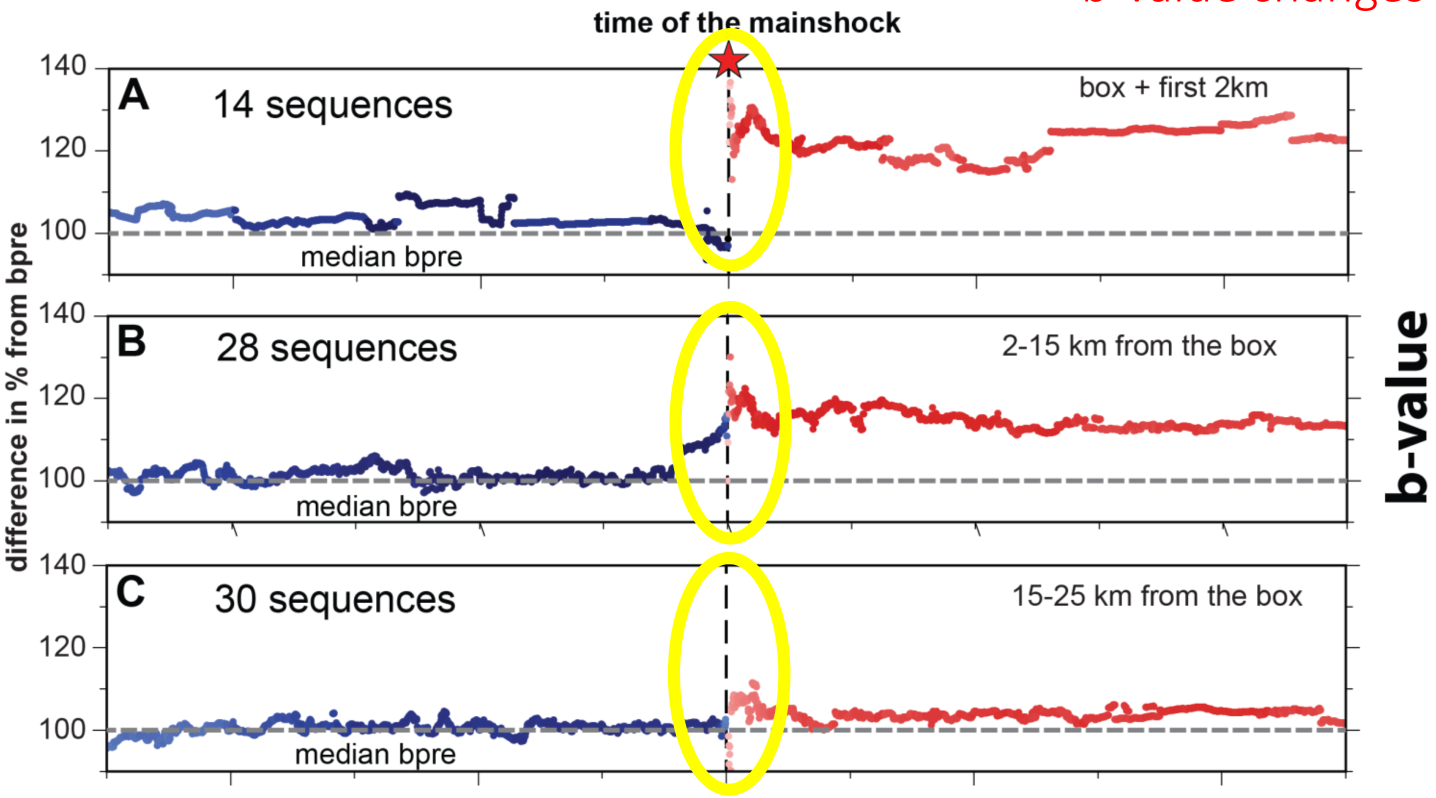

Gulia et al., 2018, GRL

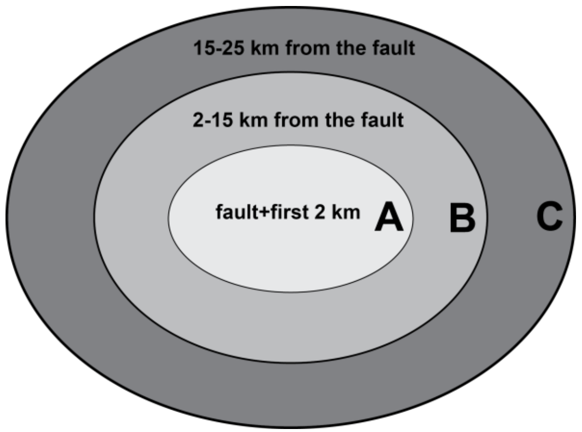

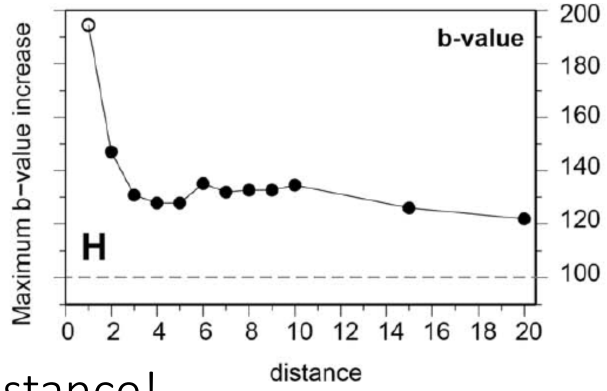

dependence with distance!

The importance of time-series

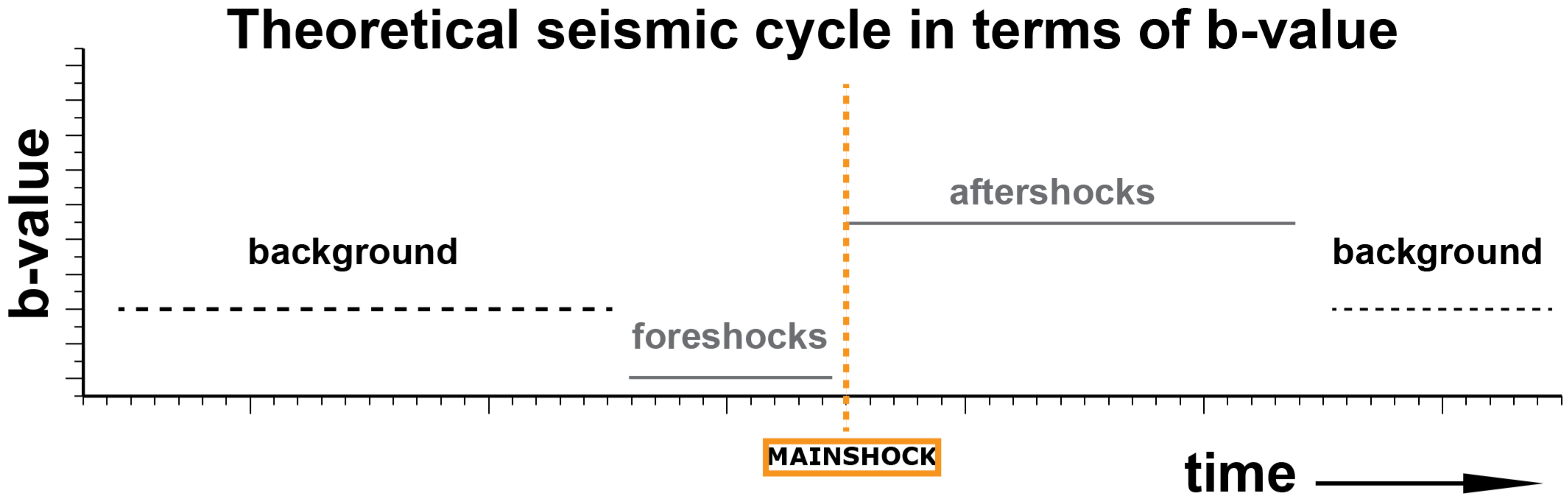

Hypothesis: b-value monitoring can tell us where we are in the seismic cycle, in real-time *(e.g. Foreshock Traffic Light System, Gulia and Wiemer, 2019, Nature)*

b-value

- varies depending on style-of-faulting, depth, time, space;
- is a proxy of the state of stress (loading / stress-release)
- can distinguish between asperities and creeping parts (by mapping)
- time variations occur near the fault plane (→ space)
- time variations are systematic (→ seismic cycle)

State of the art for the Groningen gas field (b-value)

Selection of significative figures from past studies

state of the art

b-value time-variations for the entire catalog (*no space*)

Netherlands Journal of Geosciences — Geologie en Mijnbouw |96 – 5 | s271–s278 | 2017 doi:10.1017/njg.2017.29

The effect of imposed production measures on gas extraction induced seismic risk

Annemarie G. Muntendam-Bos*, Johannes P.A. Roest & Hans A. de Waal

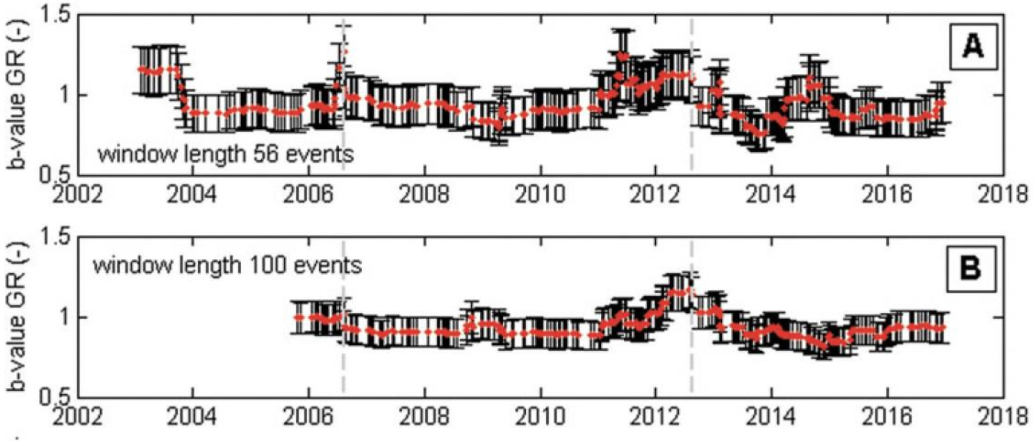

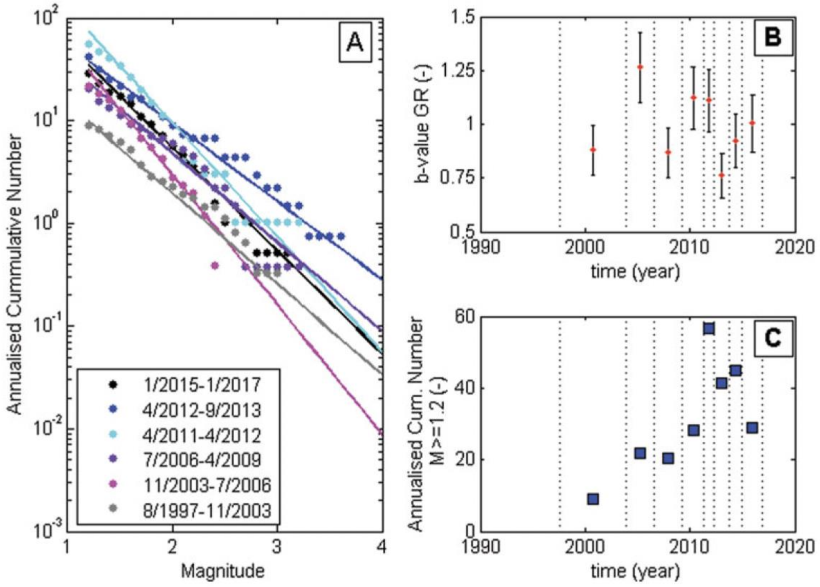

time window. We find quite some variation of the *b*-value for the Groningen field seismic history. Remarkably, the field-wide *b*-value seems to increase significantly prior to the two largest seismic events in the field: $M = 3.5$ in August 2006 and $M = 3.6$

actually be more likely. This implies that for short-term earthquake prediction of hydrocarbon-production-induced seismicity these types of analysis could be misleading. However, further investigation of regional changes of the *b*-value and activity rate is necessary to exclude the fact that our observations are driven by increases in seismicity in a different part of the gas field.

observations

and indeed, if we slpit the catalog in 2 parts (N and S)…

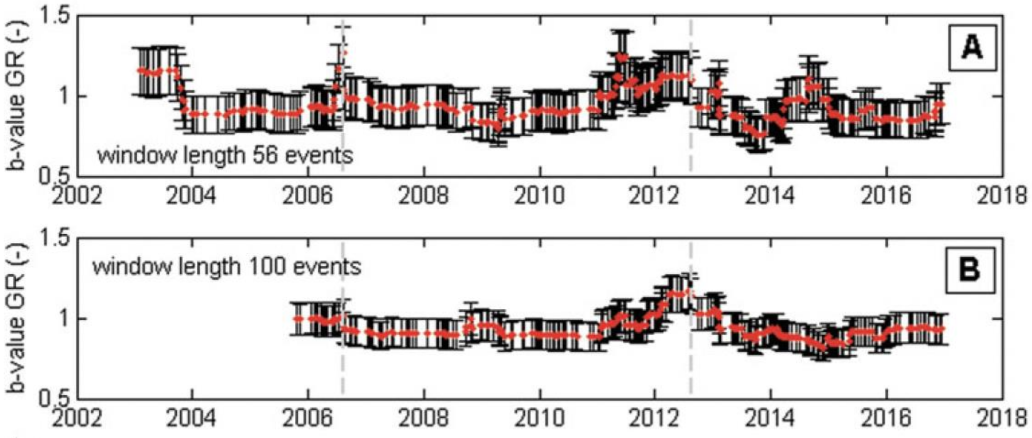

Muntendam-Bos et al., 2017, NJG

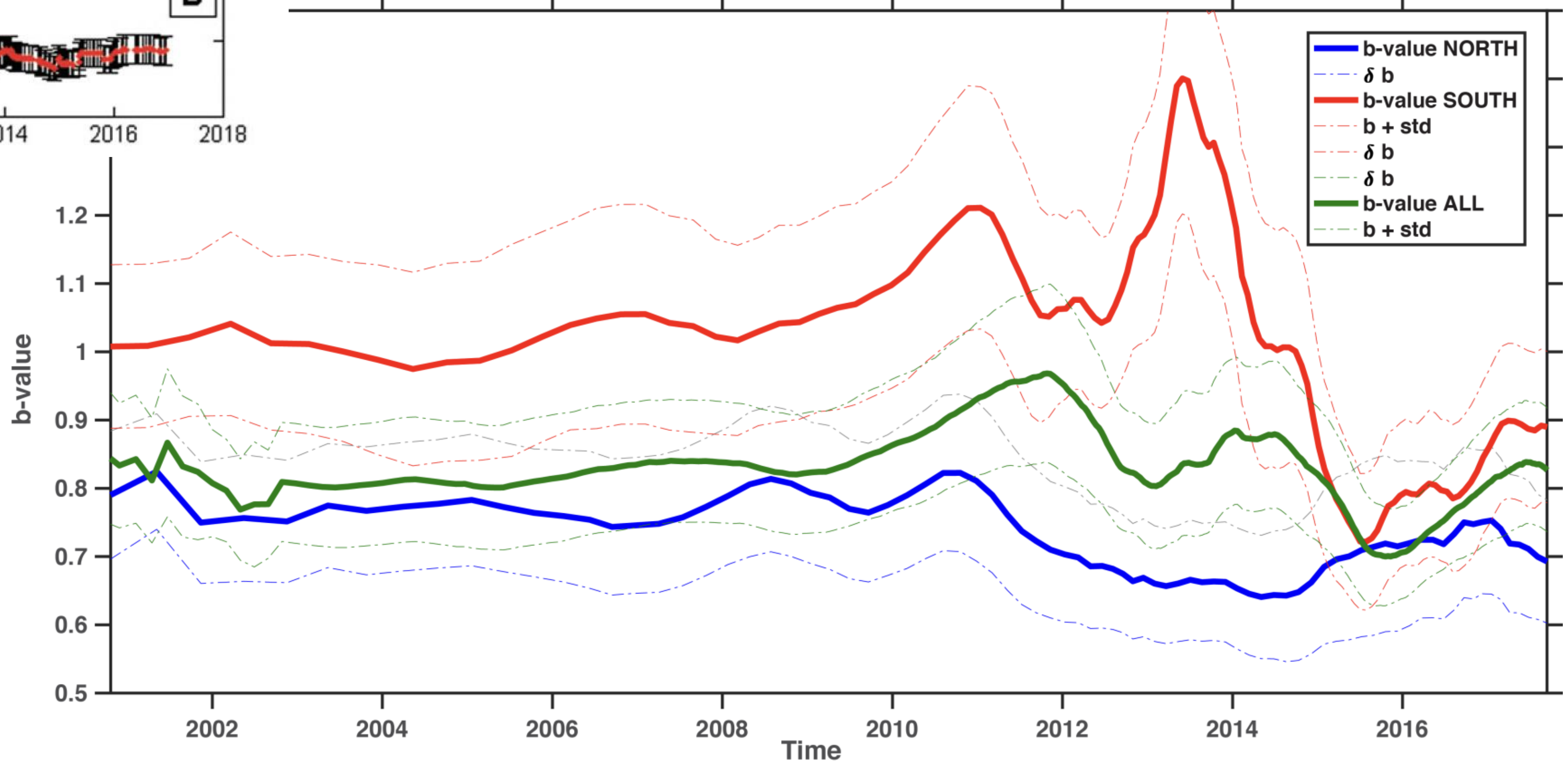

Gulia and Wiemer, 2019, poster

state of the art

b-value space-variations at 2 sites

2014

Restricted Draft Report SR.15.BinnedParetoMLE

Maximum Likelihood Estimates of *b*-Value for Induced Seismicity in the Groningen Field

by

C. K. Harris & S.J. Bourne (GSNL-PTI/RC)

The main conclusions of this study are the following:

1. The value of b_{MLE} for the entire Groningen catalogue (1st January 1995 – 31st December 2014) is consistent with the commonly accepted value $b = 1$.
2. While a subdivision of the catalogue into four subsets of equal numbers of events suggests more variability in the maximum likelihood estimator for the subsets than would be expected if the *b*-value of the underlying process were constant, a closer examination, involving further subdivisions of the catalogue, and the use of 95% confidence intervals obtained using simulated data, does not show any systematic dependence of *b* value on event rate.
3. Focusing on regions of 5 km radius centered on Loppersum and Ten Boer, we find that, while the b_{MLE} for Ten Boer is consistent with $b = 1$, the b_{MLE} for Loppersum is significantly lower, to the extent that we can be 99.9% confident that the *b* value of the underlying process is less than 1.
4. The temporal sequence of events for each of the regions around Loppersum and Ten Boer is split into two equal sub-catalogues and the value of b_{MLE} determined for each sub-catalogue. For both the Loppersum and Ten Boer regions, the two values of b_{MLE} were found to be consistent with an underlying *b* that is unchanging in time.

No time variations in the 2 sites till 2014

state of the art

b-value and compaction

AGU PUBLICATIONS

JGR

Journal of Geophysical Research: Solid Earth

RESEARCH ARTICLE

10.1002/2014JB011663

Key Points:
- Fluid extraction induced seismicity conforms to reservoir compaction
- Fraction of seismic to reservoir strain

A seismological model for earthquakes induced by fluid extraction from a subsurface reservoir

S. J. Bourne[1], S. J. Oates[1], J. van Elk[2], and D. Doornhof[2]

[1]Shell Global Solutions International B.V., Rijswijk, Netherlands, [2]Nederlandse Aardolie Maatschappij (NAM) B.V., Assen, Netherlands

2014

Figure 14. Maximum likelihood *b*-value estimates for subsets of the $M \geq 1.5$ between 1995 and 2012 binned according to reservoir compaction. Bin sizes were selected to ensure every bin contains 50 events. Vertical black bars denote the 67% confidence interval for the maximum likelihood estimate, and horizontal grey lines denote the bin sizes.

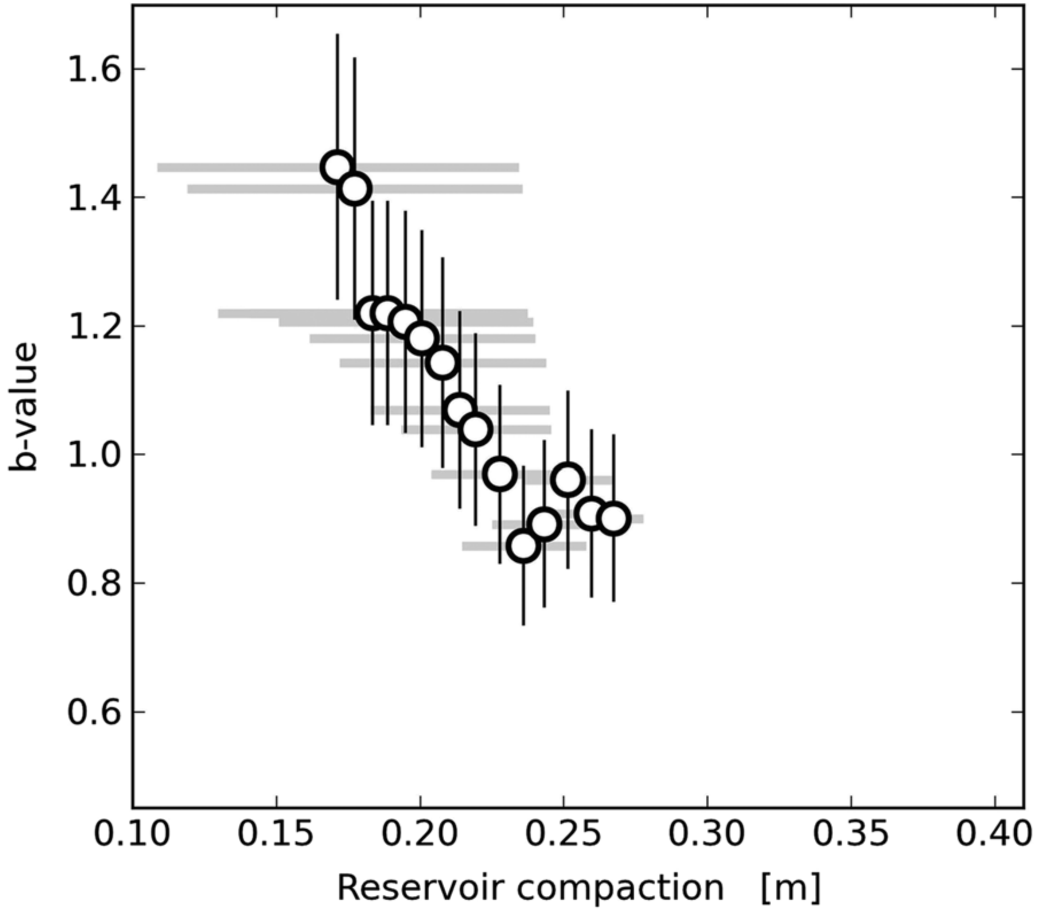

Estimates of the *b* value appear to depend on reservoir compaction. Each event was labeled according to the reservoir compaction at the event's origin time and epicenter. Based on these labels, subsets of events were selected within a range of compaction values. To avoid the possibility of bias from variable sample sizes, the range of compaction was adjusted to ensure each subset contained exactly 50 events. The

state of the art

4 zones with different b-values

2015

KNMI report | 1
PSHA Groningen, 2015 update

Probabilistic Seismic Hazard Analysis for Induced Earthquakes in Groningen;
Update 2015

Bernard Dost and Jesper Spetzler
KNMI, October 2015

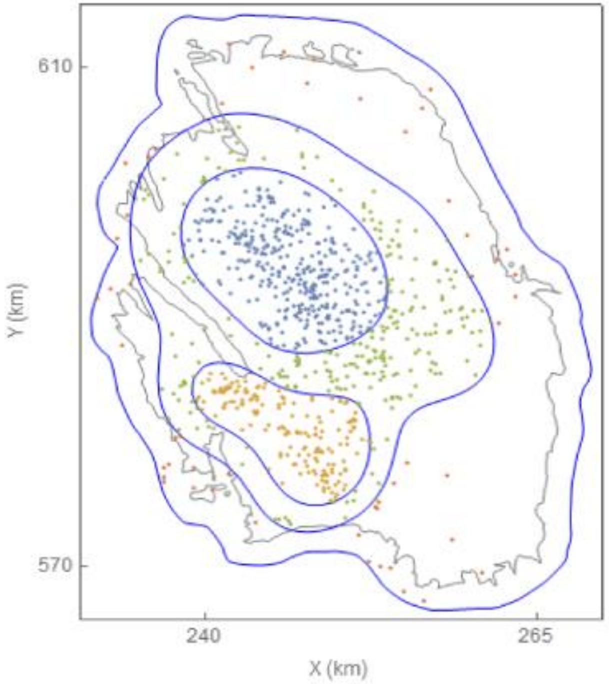

In the previous hazard map, the b-value was calculated for the complete earthquake catalog for Groningen (b= 1.0 ± 0.2) and assumed b=1 in the analysis. In the meantime spatial and temporal variations have been observed, see Harris and Bourne (2015) for a detailed explanation. Based on this observation, we have decided to estimate the b-value for each zone separately for the given calibration period. However, if the number of events in a zone is too small, annual rate < 5, an average value of b= 1.0 is selected. In this study, the range of b-value is limited to values between 0.8 and 1.0 to reduce the effect of random errors.

3 zones with different b-values

2017

KNMI report | 1
PSHA Groningen, 2017 update

Probabilistic Seismic Hazard Analysis for Induced Earthquakes in Groningen, Update June 2017

Jesper Spetzler and Bernard Dost
KNMI, de Bilt

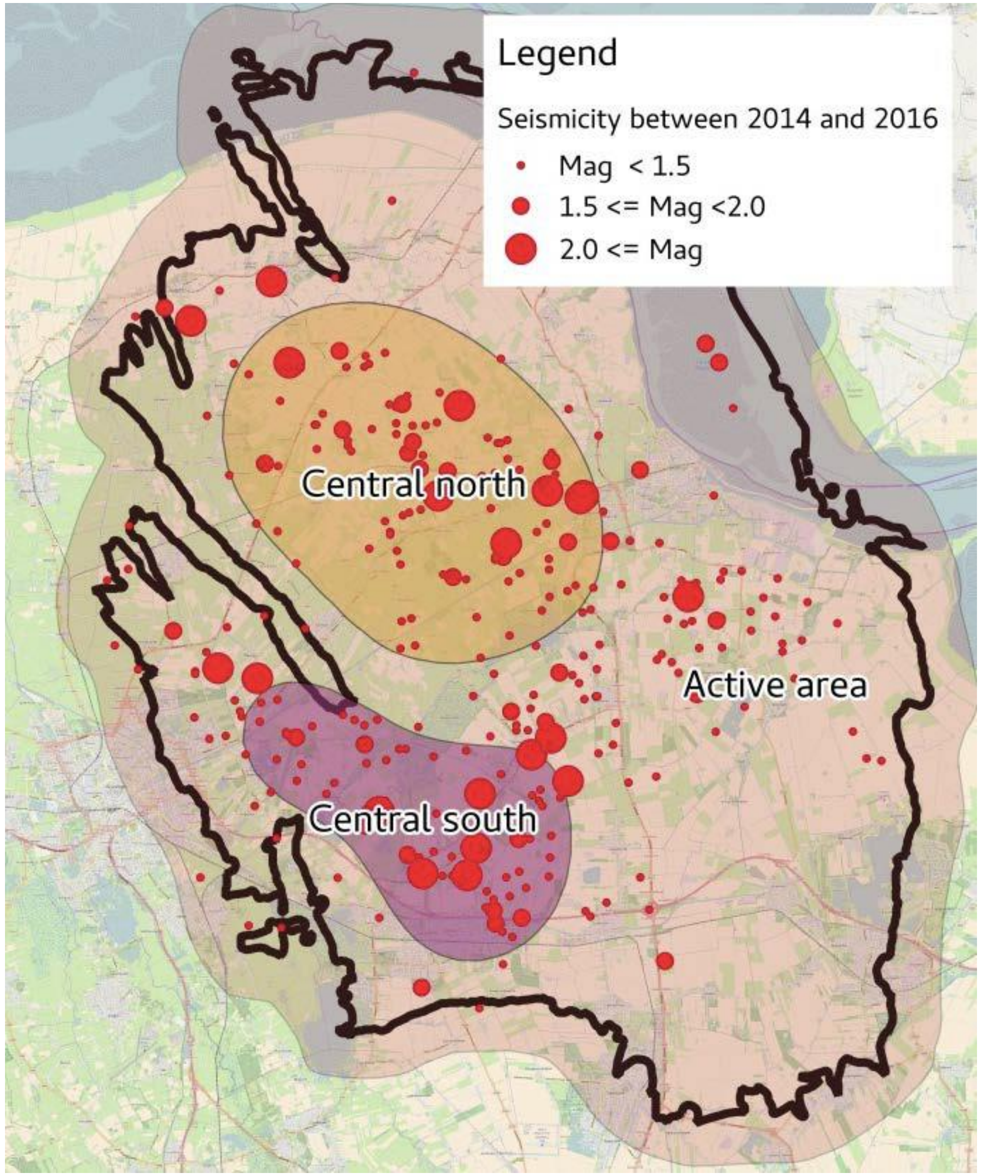

Conclusions from literature

- space-time b-value variations in the field
- corralation between b-value and compaction
- different b-value for different zones

From theory to observations: what we expect to see in the field

observations

1487 events from 5 Dec 1991 to 22 May 2022 with different Mc levels

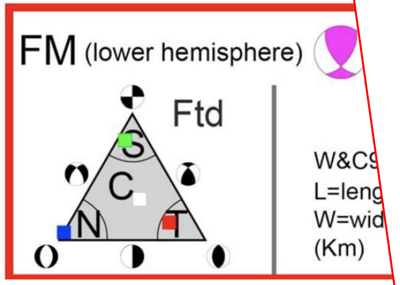

Selecting
<u>*significative*</u>
time-intervals
can help!

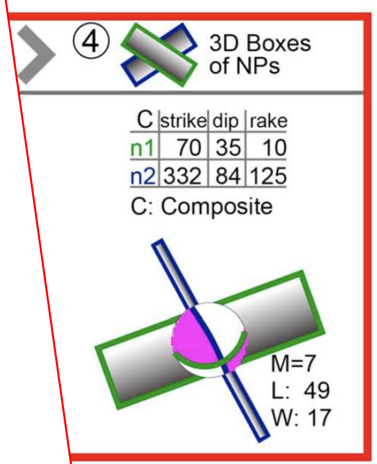

Not enough events for the ideal sampling

How ... we extract e time-space b-value signals with so a limited dataset?

observations

Field history – essential steps

Which are the significative time-intervals?

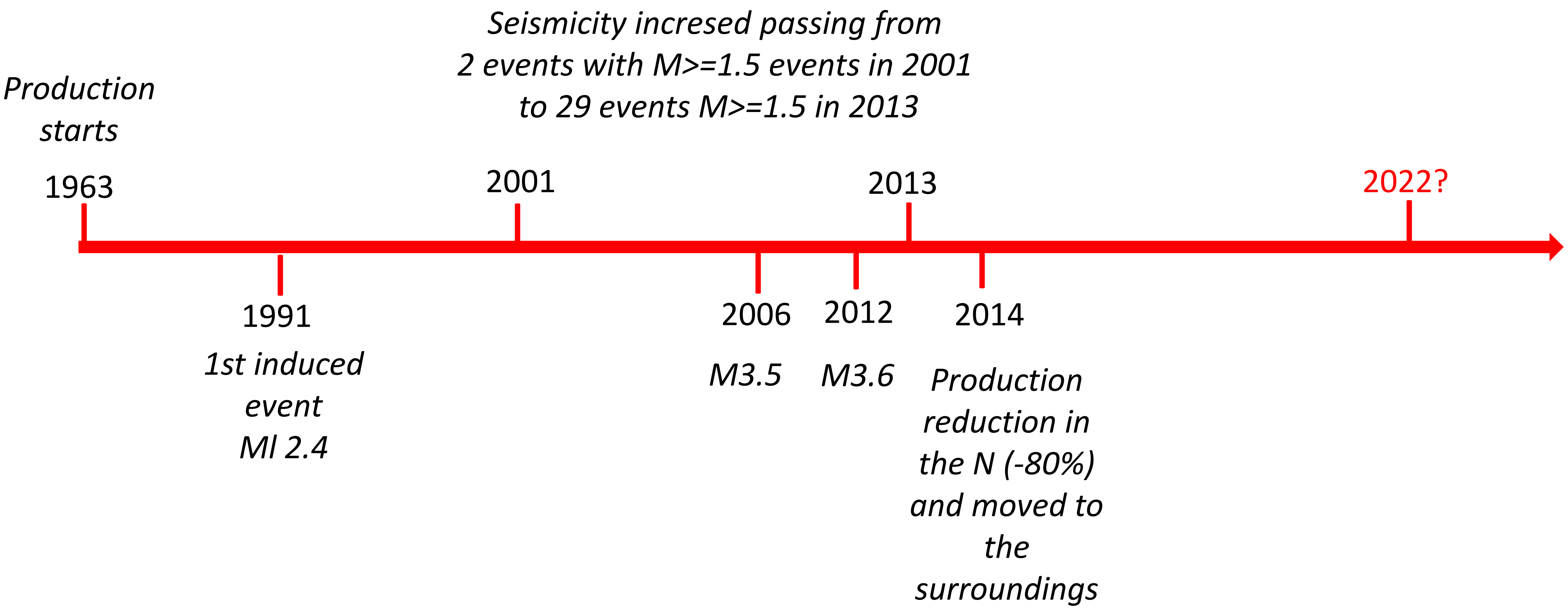

Theory

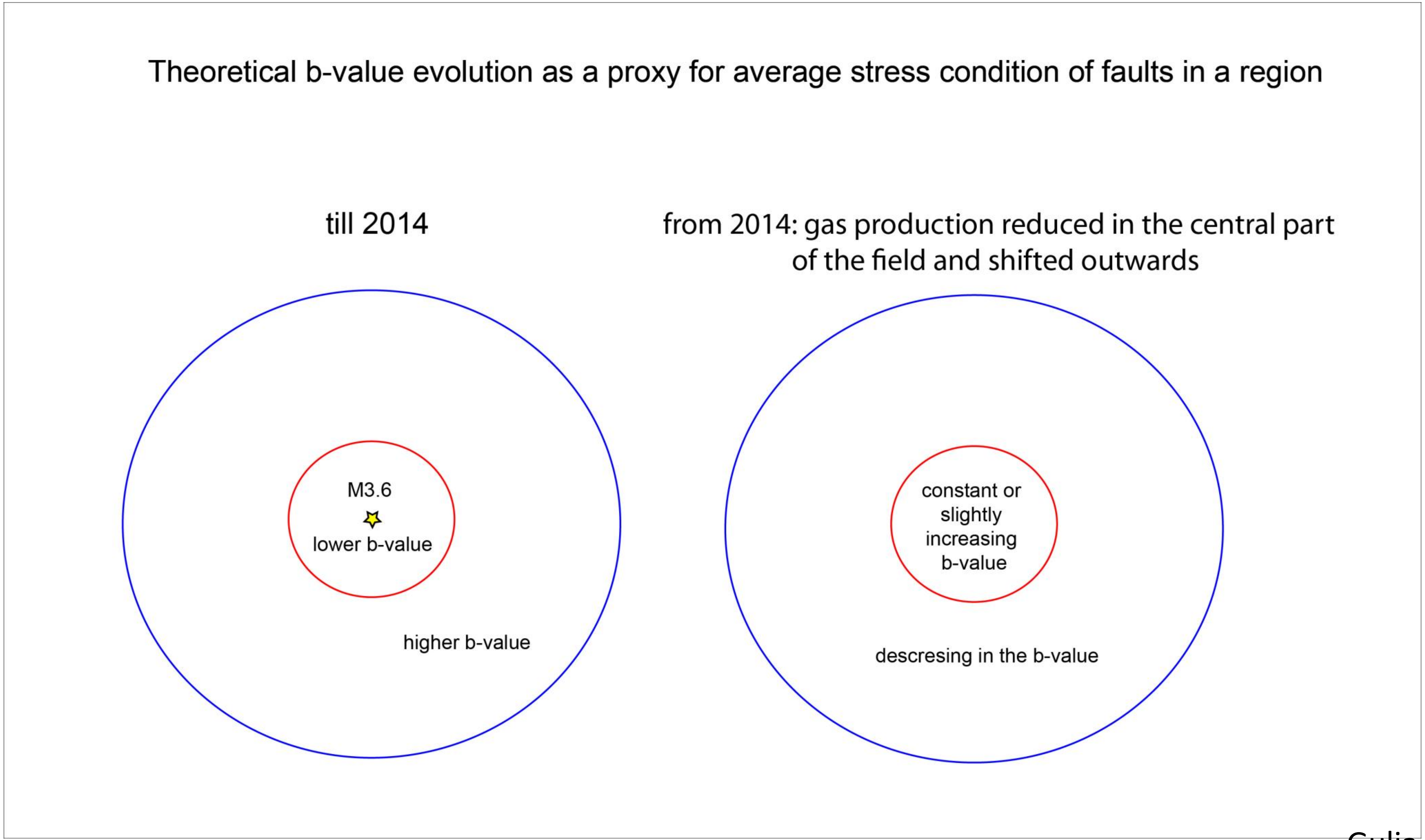

Gulia, in prep.

Expectations from theory

1991- 2014	2014- 22 May 2022
b-value increasing with the distance from M3.6 epicenter	constant or slighlty increasing b-value (*i.e still low b-value*) in the vicinity of the M3.6 and a decreasing b-value in the surroundings

→ a more homogeneous b-value in the entire field

What do we observe in the Groningen field?

observations

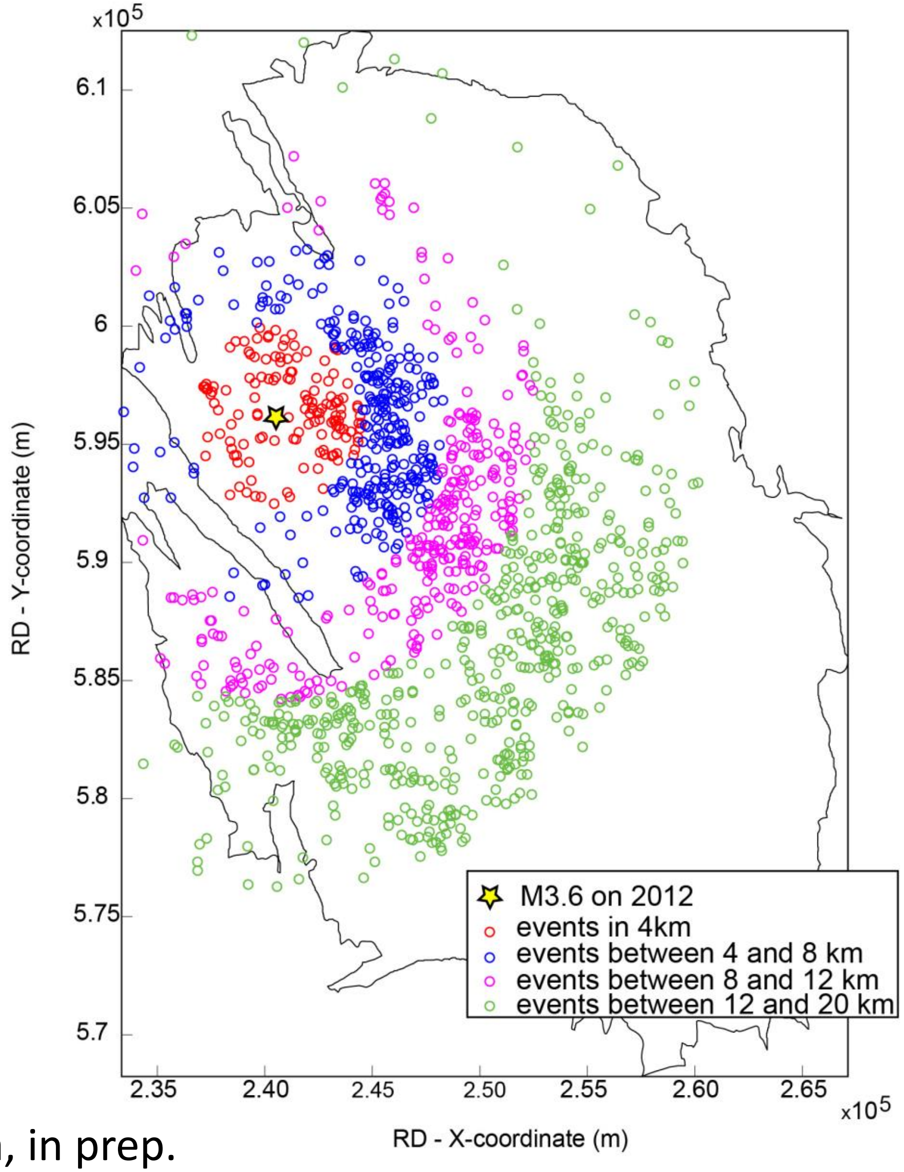

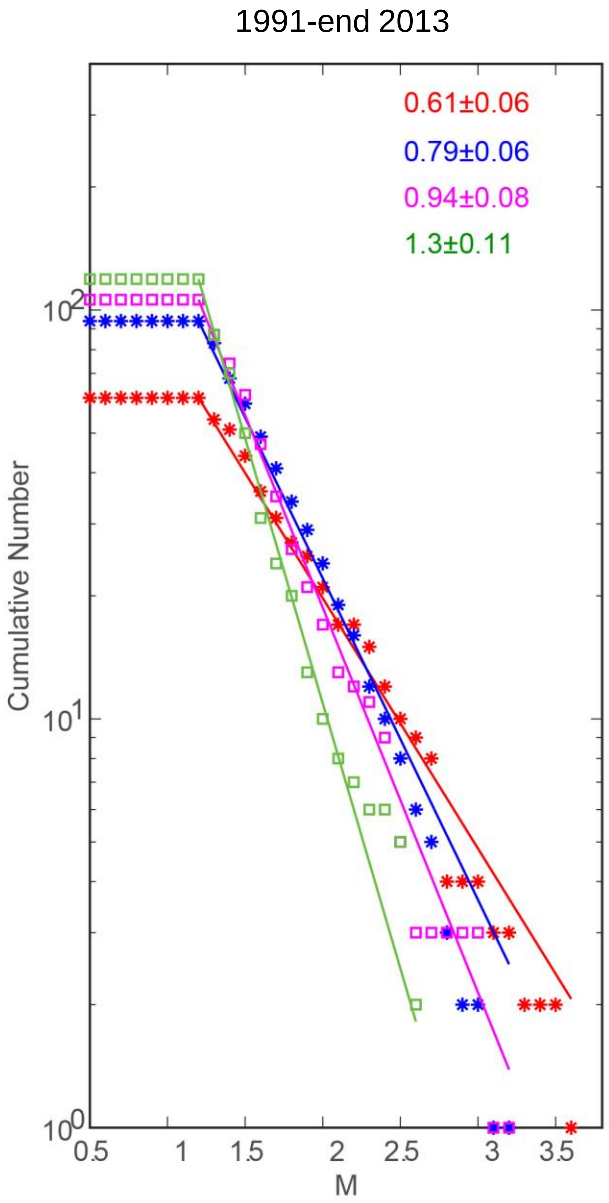

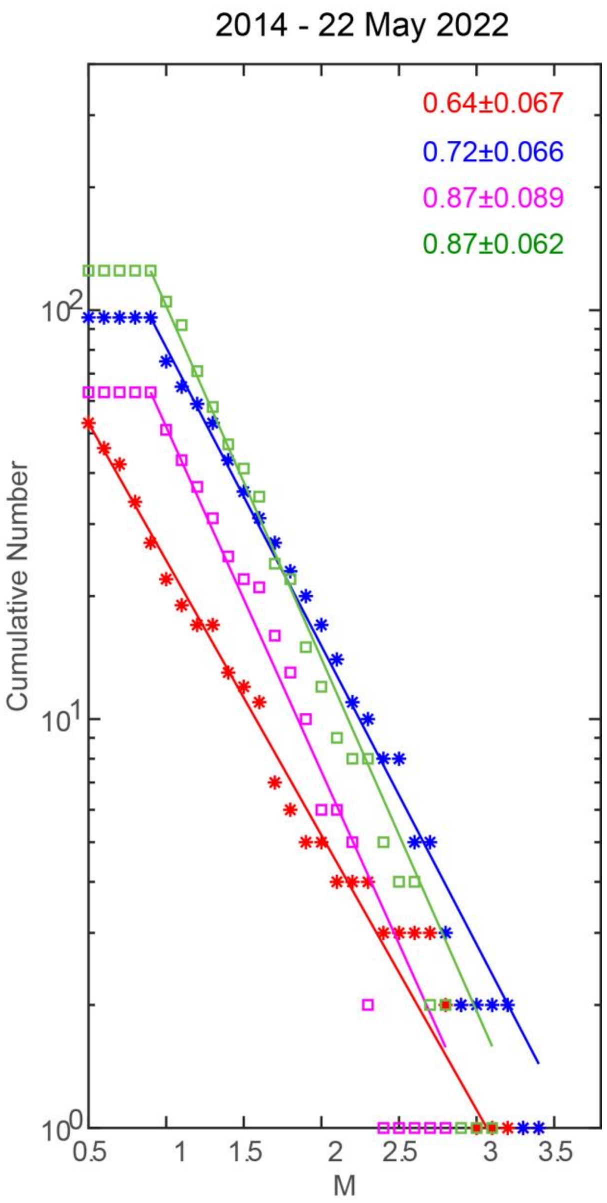

Gulia, in prep.

observations

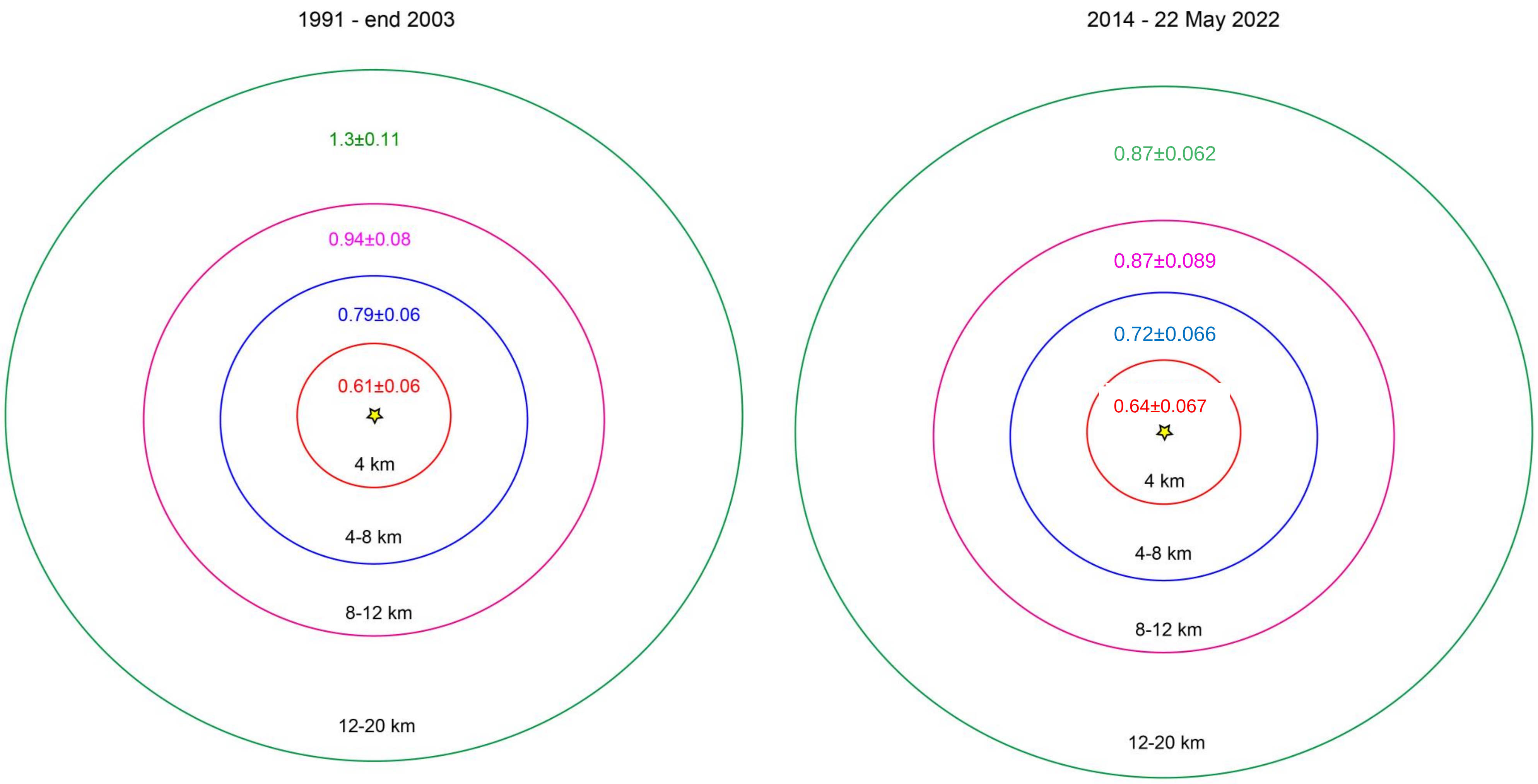

Gulia, in prep.

observations

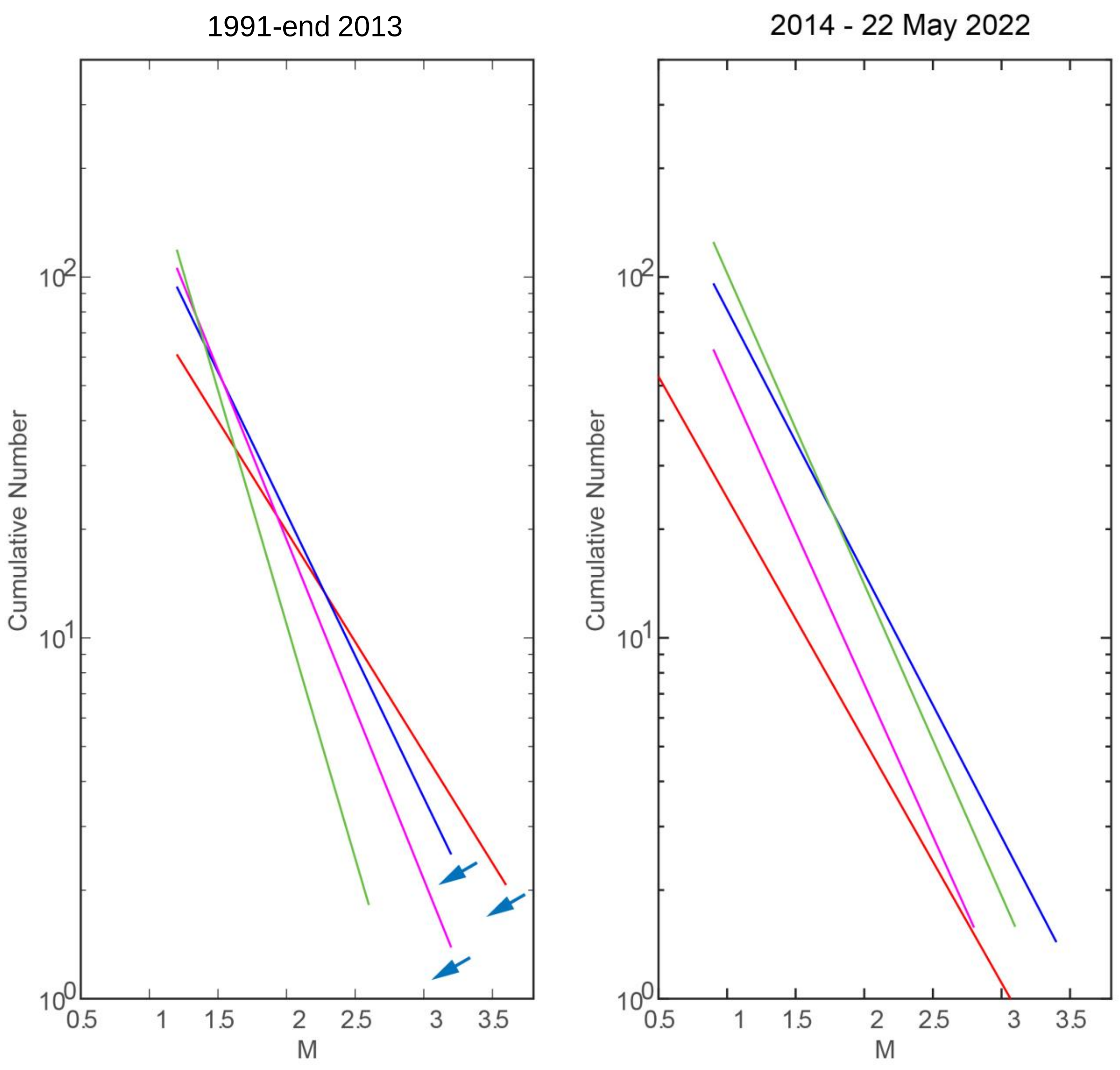

Gulia, in prep.

observations

The same trend can be highlighted by mapping b-value

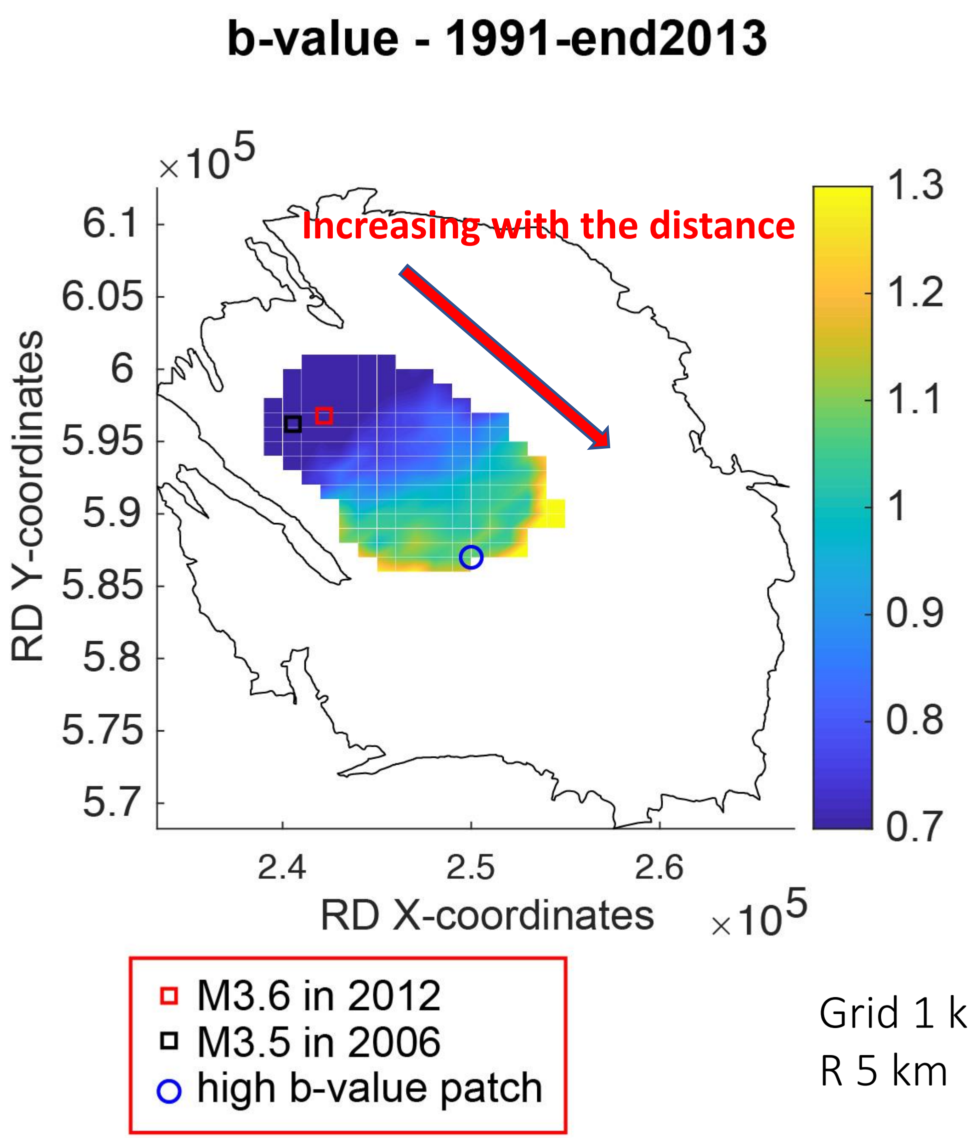

Grid 1 km
R 5 km

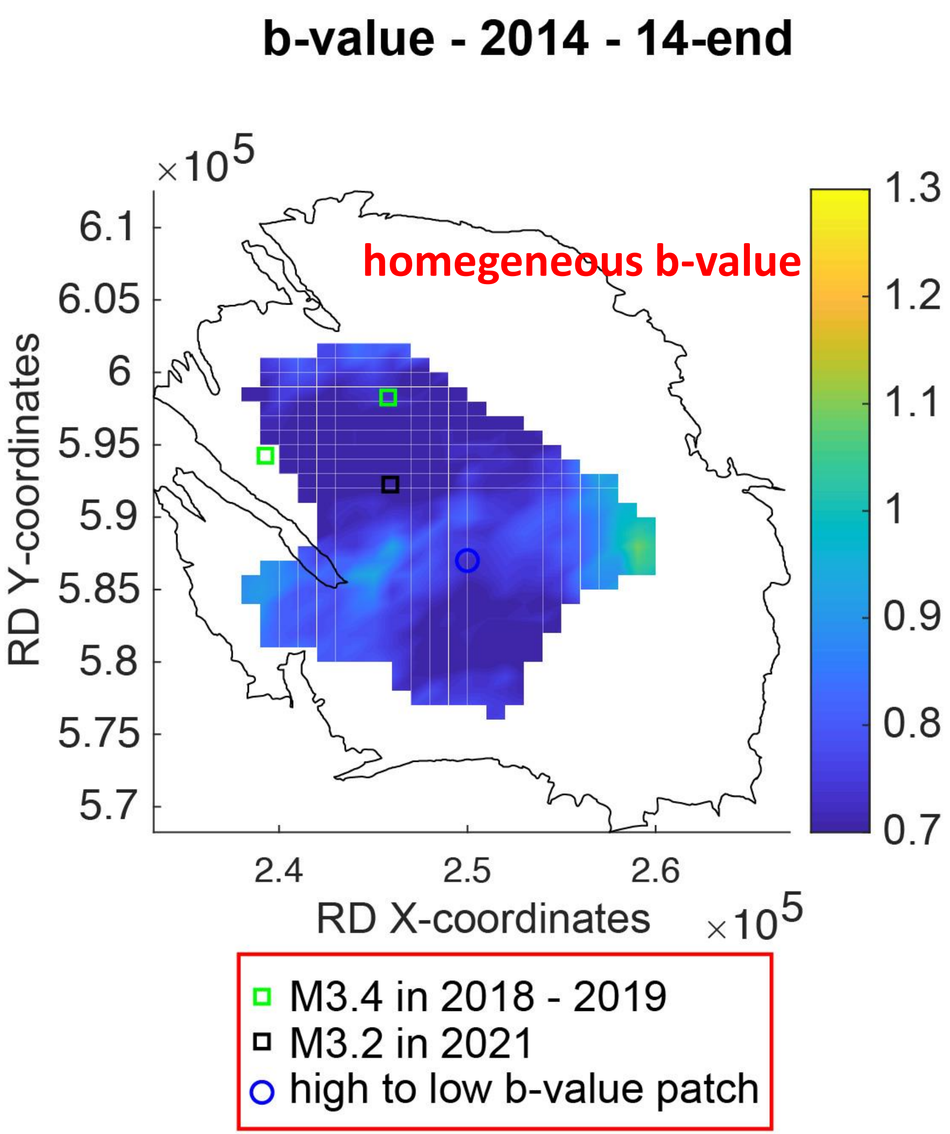

Gulia, in prep.

observations

Due to the time-varying Mc, I repeat the same maps by **b-positive** estimator (van der Elst, 2021, JGR)

ADVANCING EARTH AND SPACE SCIENCE

JGR Solid Earth

RESEARCH ARTICLE
10.1029/2020JB021027

Key Points:

- The distribution of magnitude differences is identical to the distribution of magnitudes, but with no reference to a minimum magnitude
- The positive subset of the differences between successive earthquakes is minimally biased by changing catalog completeness
- Unbiased statistics confirm subtle differences in *b*-value between foreshock and aftershocks in several recent sequences

B-Positive: A Robust Estimator of Aftershock Magnitude Distribution in Transiently Incomplete Catalogs

Nicholas J. van der Elst[1]

[1]U.S. Geological Survey, Earthquake Science Center, Pasadena, CA, USA

Abstract The earthquake magnitude-frequency distribution is characterized by the *b*-value, which describes the relative frequency of large versus small earthquakes. It has been suggested that changes in *b*-value after an earthquake can be used to discriminate whether that earthquake is part of a foreshock sequence or a more typical mainshock-aftershock sequence, with a decrease in *b*-value heralding a larger earthquake to come. However, the measurement of *b*-value during an active aftershock sequence is strongly biased by short-term incompleteness of the earthquake catalog and by data-windowing, and these biases have the same direction as the proposed signal. Here I develop a new estimator of the *b*-value that

a new estimator for the b-value, called "**b-positive**", not affected by detection problems

van der Elst, 2021, JGR

observations

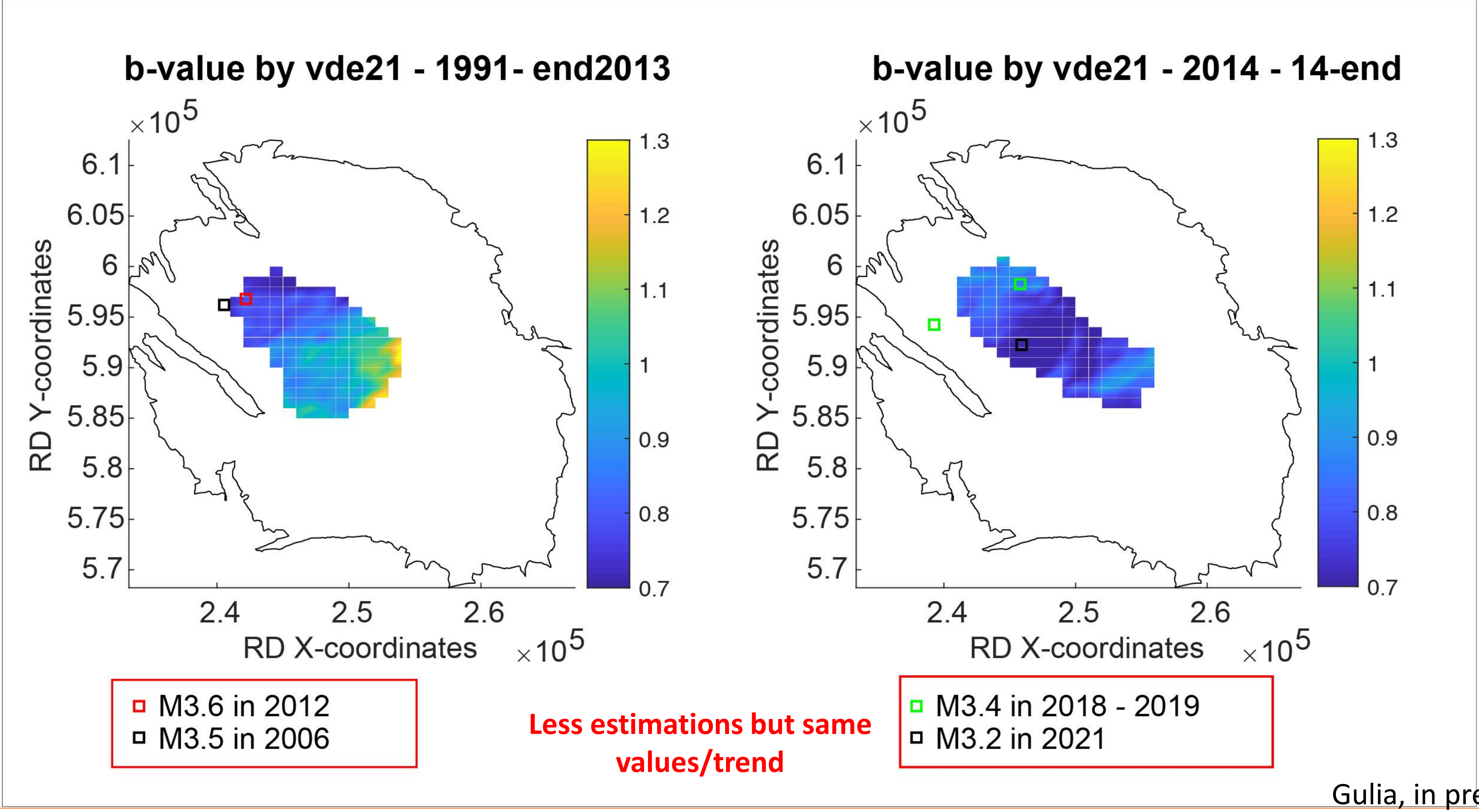

Less estimations but same values/trend

Gulia, in prep.

observations

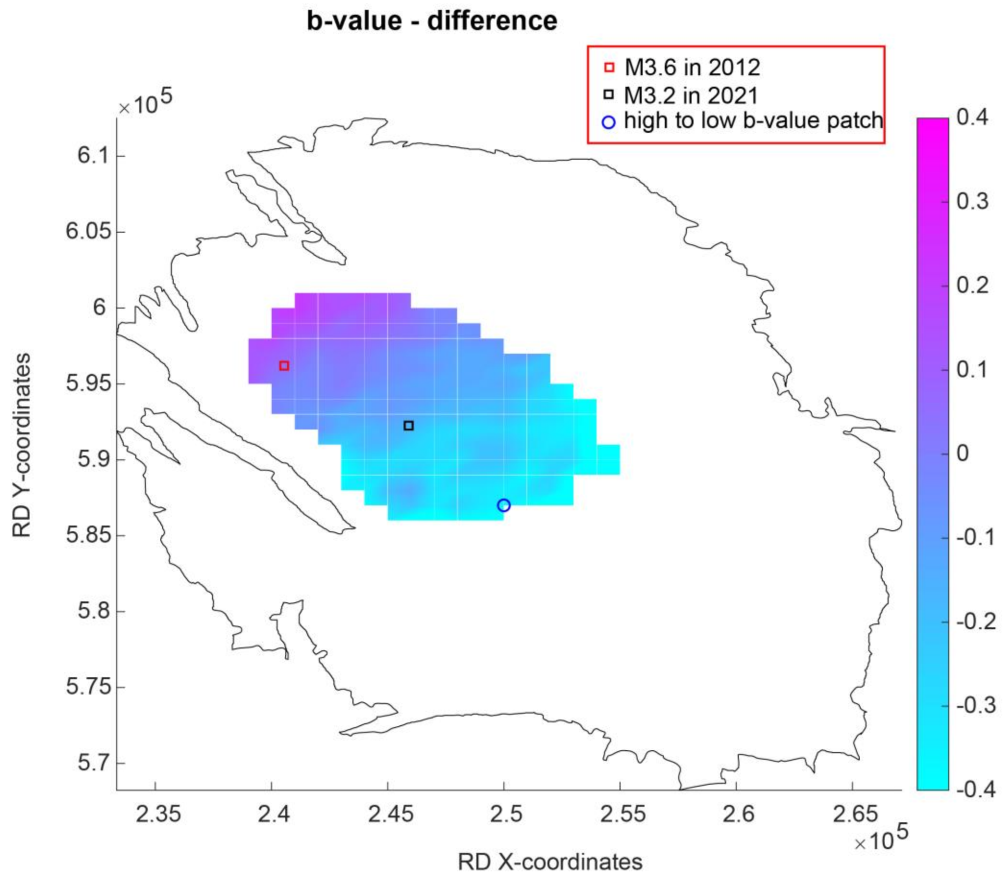

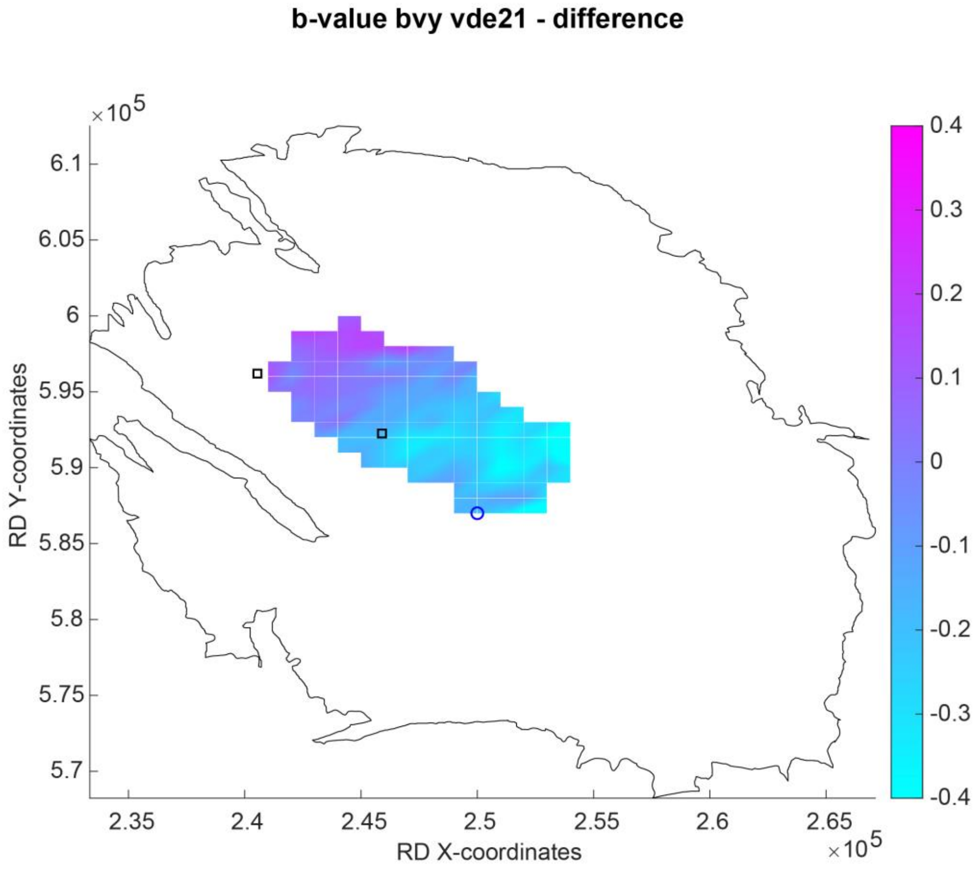

Gulia, in prep.

observations

FMDs in time for 3 different volumes

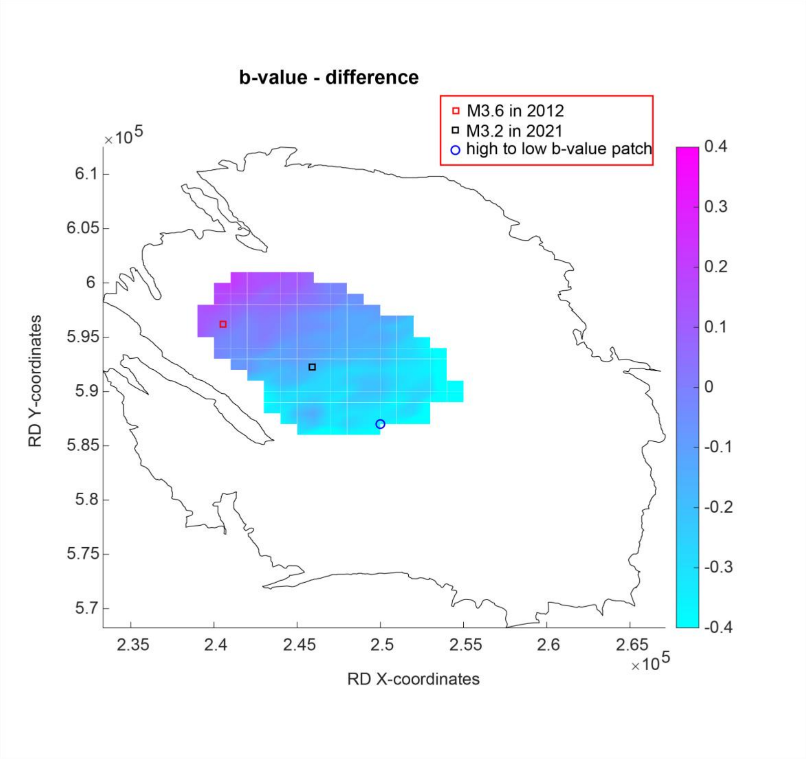

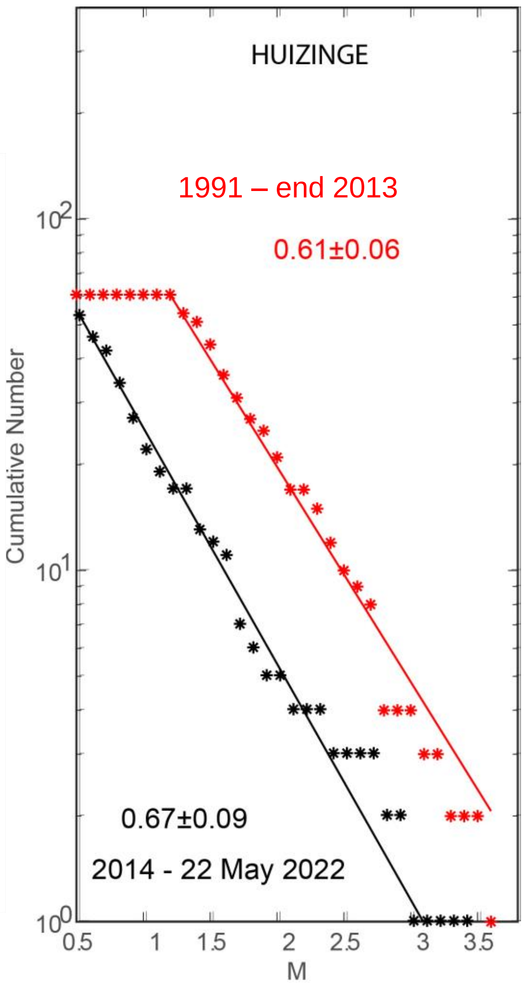

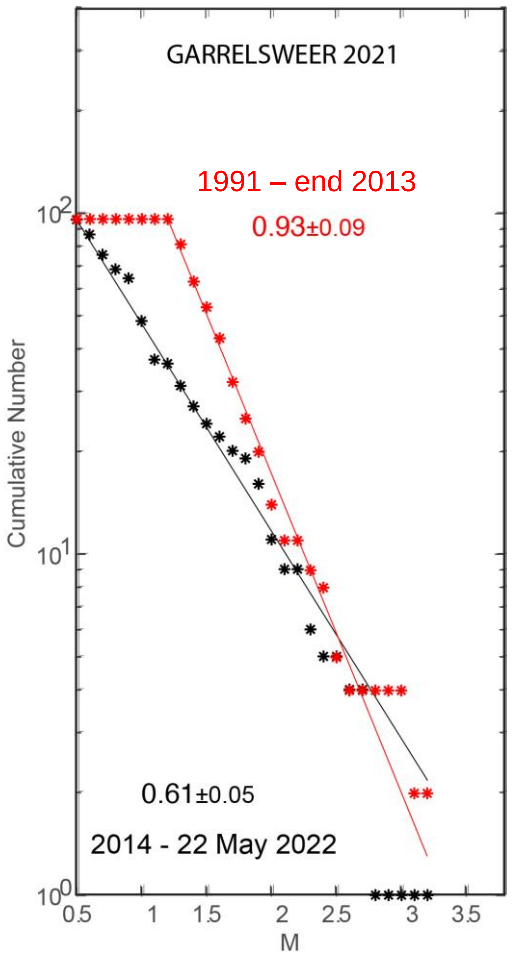

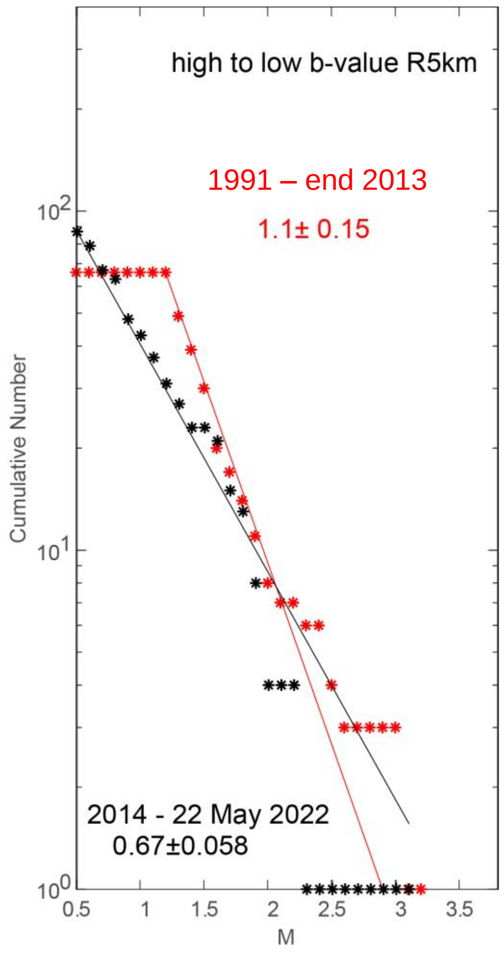

Gulia, in prep.

observations

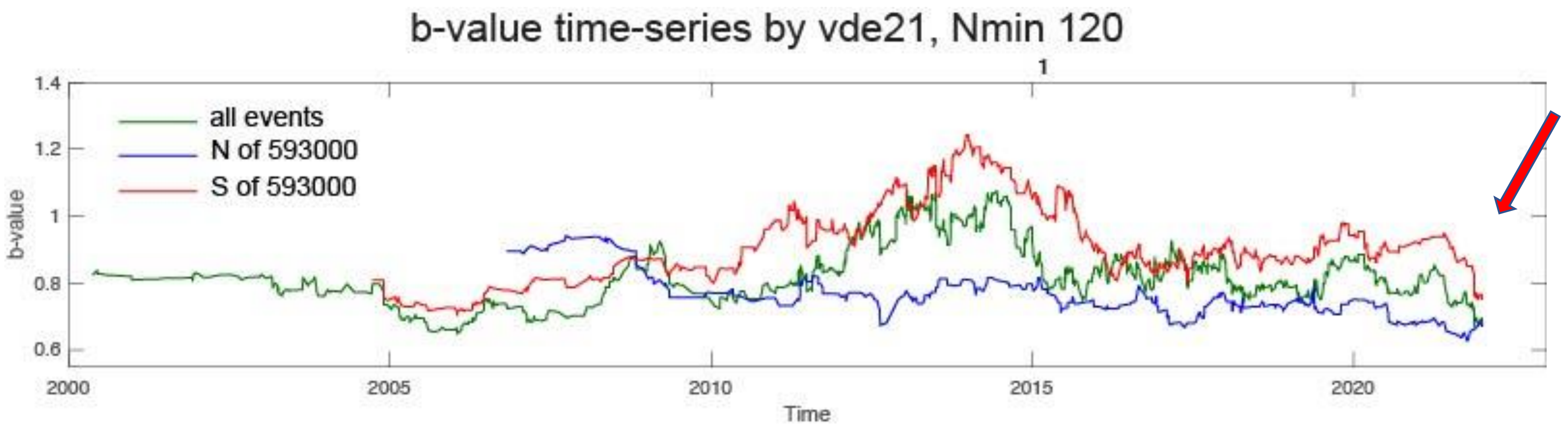

THEORY

a more homogeneous b-value in the entire field

Gulia, in prep.

observations

b-value and compaction

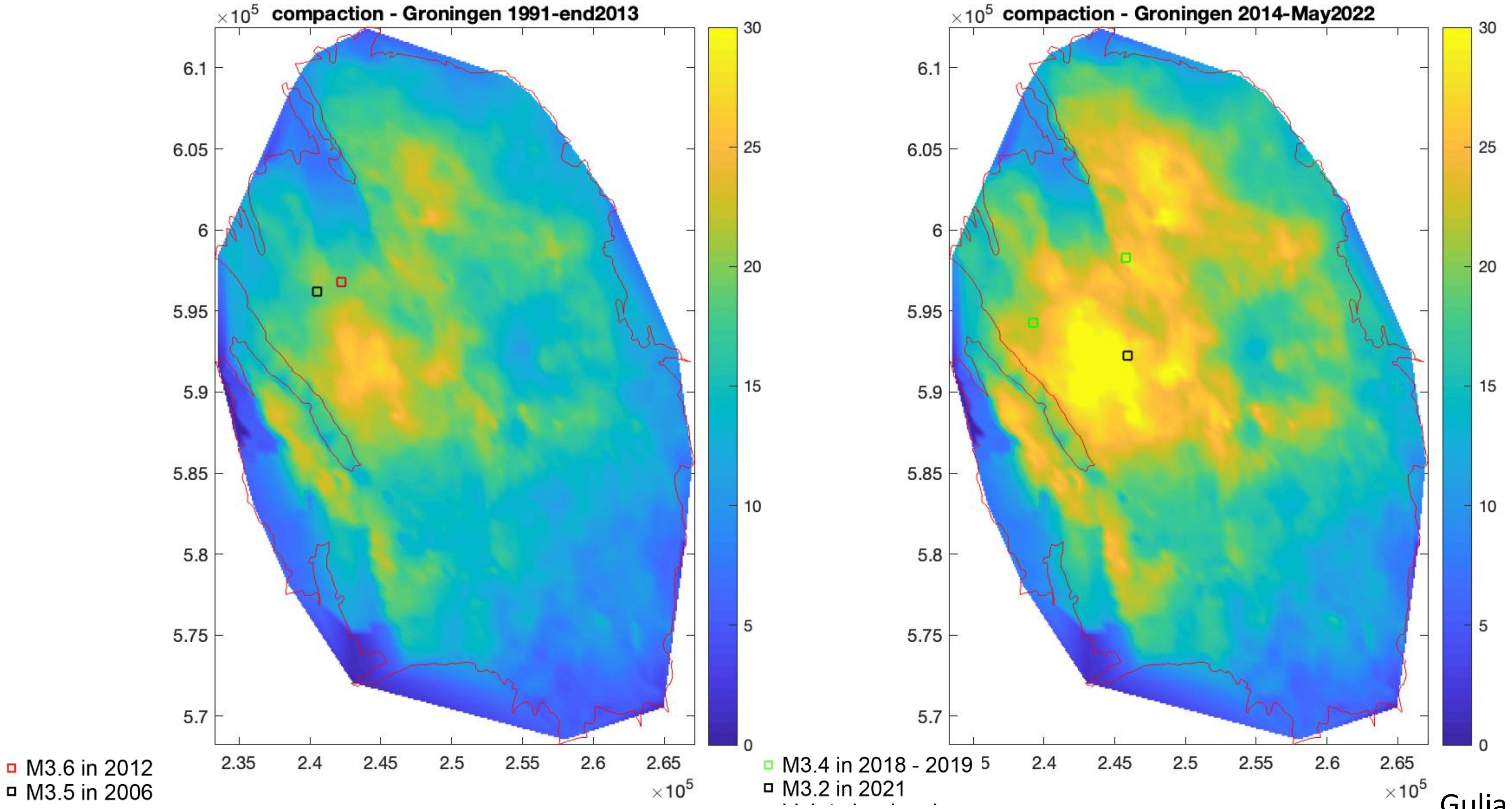

Gulia, in prep.

observations

b-value and compaction

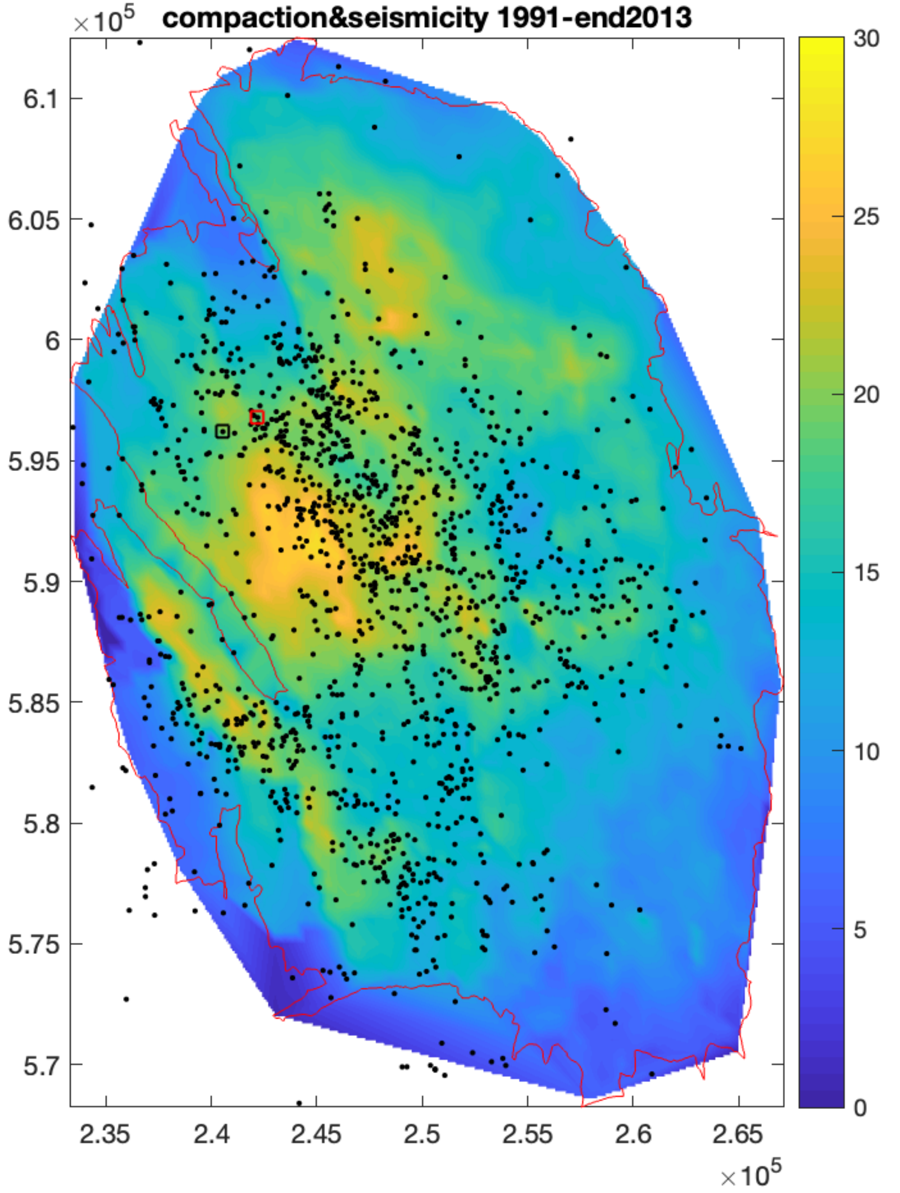

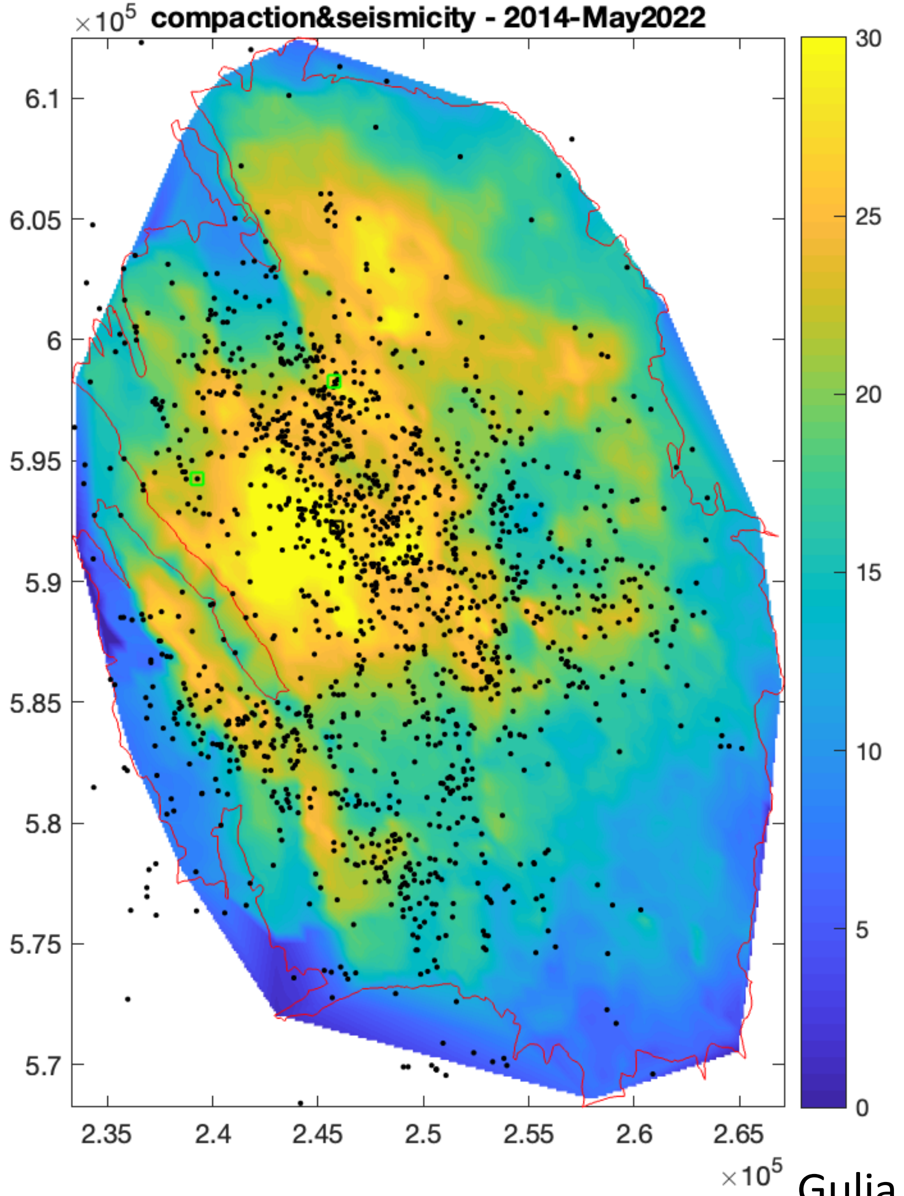

Gulia, in prep.

observations

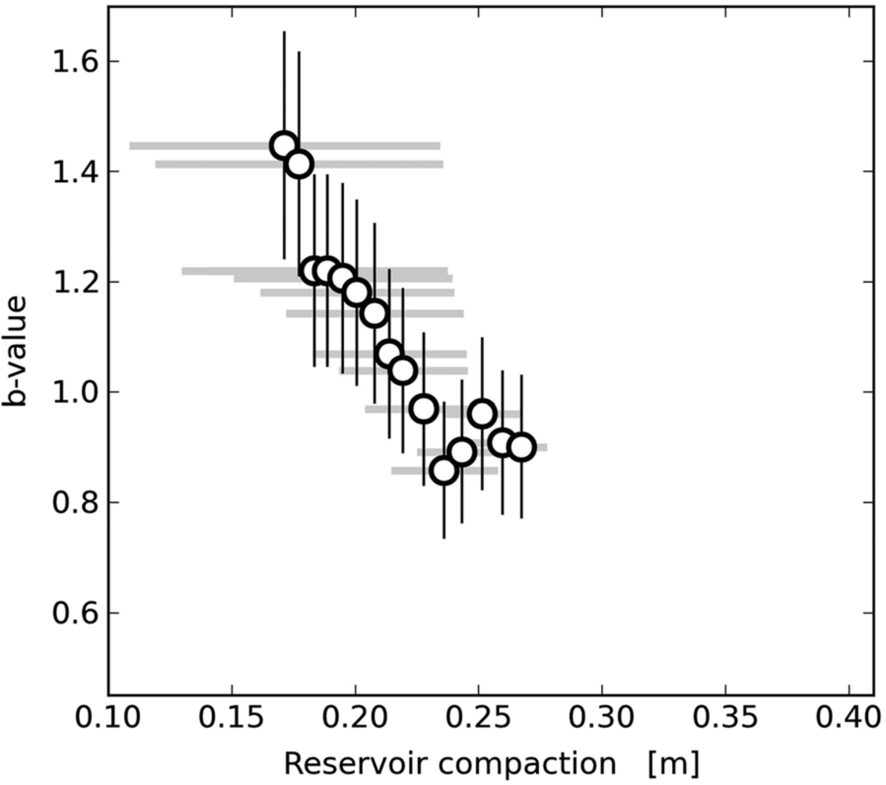

Bourne et a., 2014, JGR

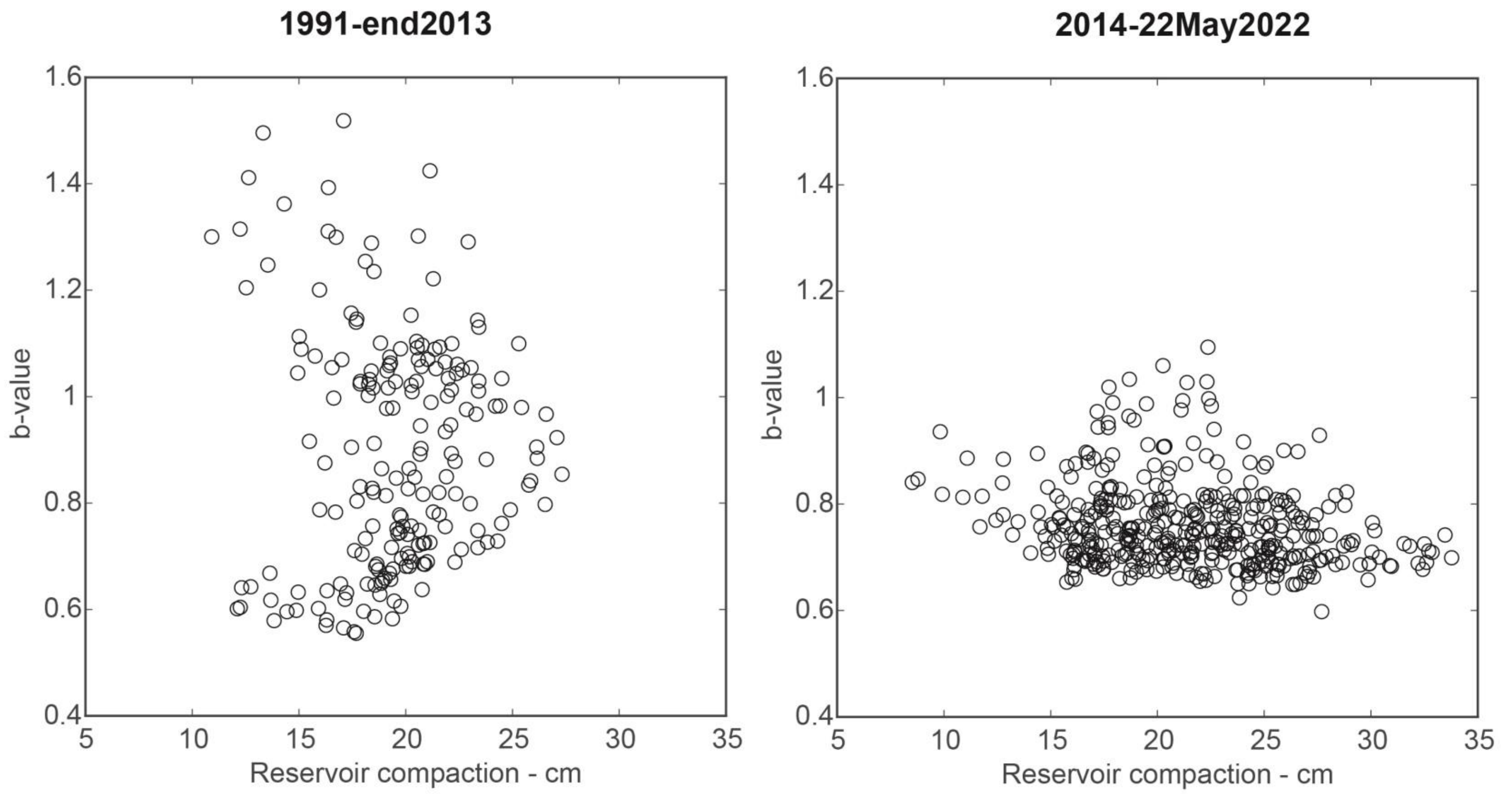

Gulia, in prep.

observations

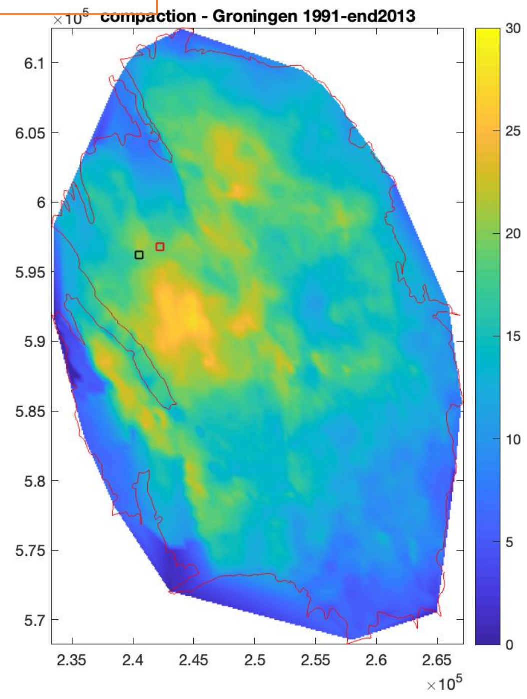

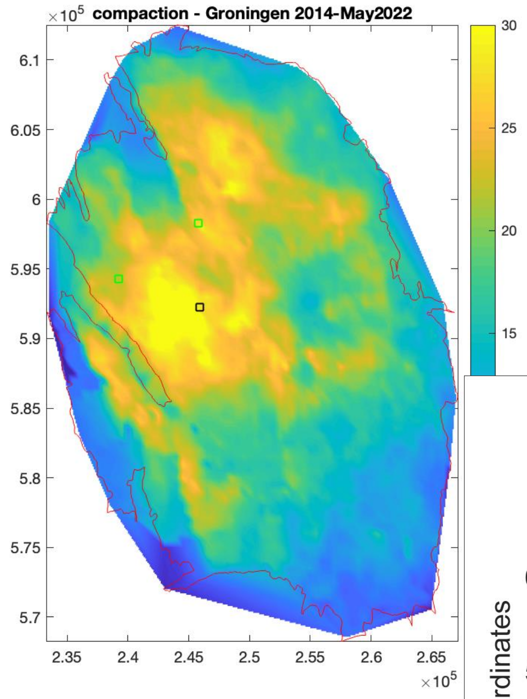

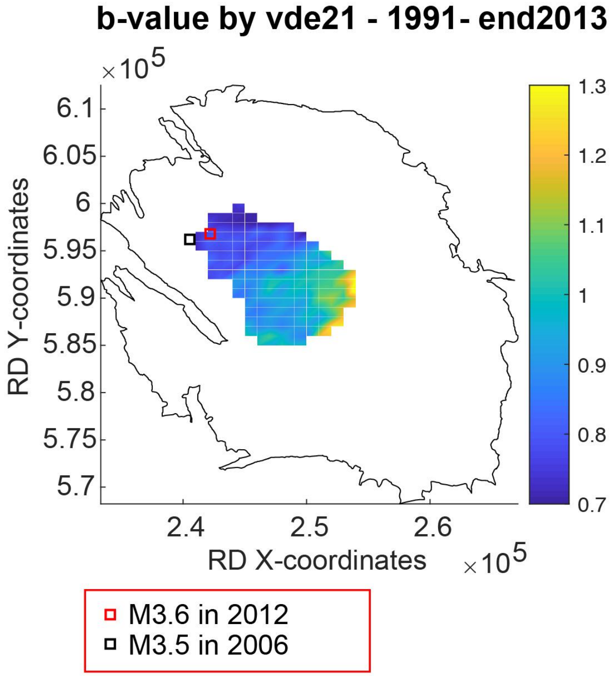

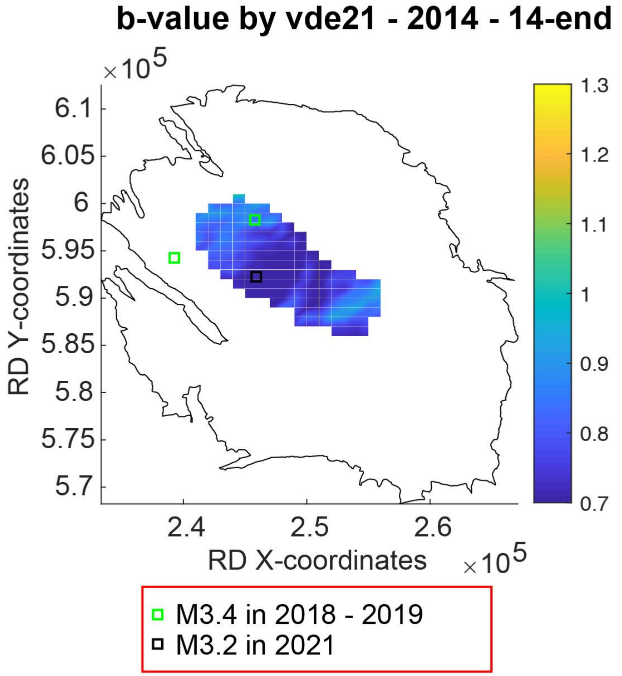

The highest compaction volume encircle the highest b-value's one

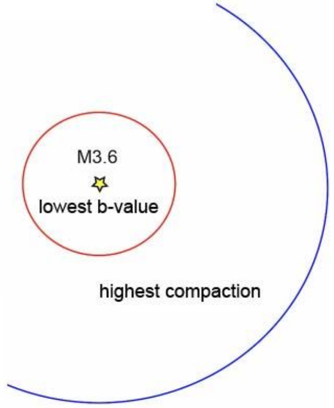

implication for PSHA

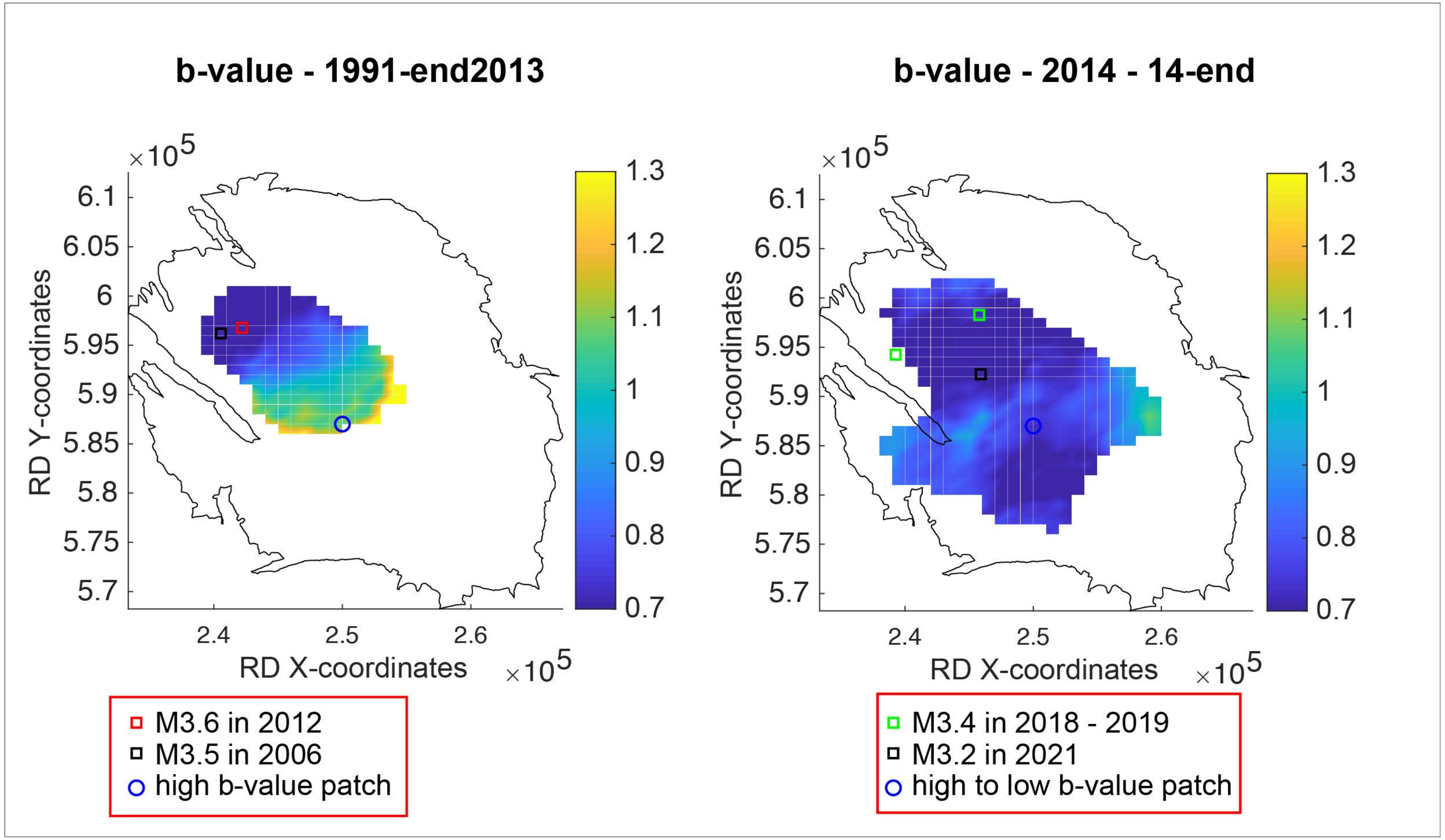

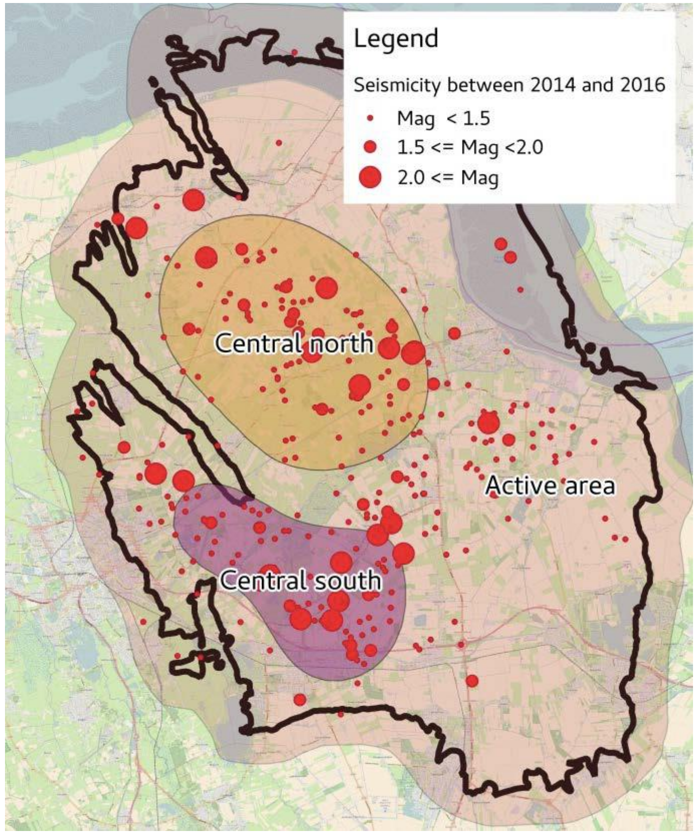

Conclusions

- The variations in production (from 2014) reduced the spatial variation of the b-value in the field
- At present, the field shows a homogenous state-of-the-stress in terms of b-value (homogeneous values)
- No need to adopt different b-values for PSHA
- Need to reassess the correlation between b-value and compaction (the story seems to be more complex…and very interesting: hints for future ruptures?)

An integrated model for stress-based forecasting of induced earthquakes at Groningen - implications for Mmax

Jean-Philippe Avouac & Mateo Acosta

California Institute of Technology

Collaborators

Jonathan Smith, Hadrien Meyer, Elias Heimisson, Hojjat Kaveh
Zachary Ross (*Caltech*)
&
Stephen Bourne (*Shell Global Solutions International B.V.*)

GMG

NSF

Caltech

Objective and Approach

- **Objective:** A robust method for estimating earthquake probabilities for any future scenario of gas extraction at Groningen, transportable to other settings and other applications (e.g., injection, pressure mitigation)

- **Approach:** Development, calibration and validation of an integrated framework for stress-based earthquake forecasting

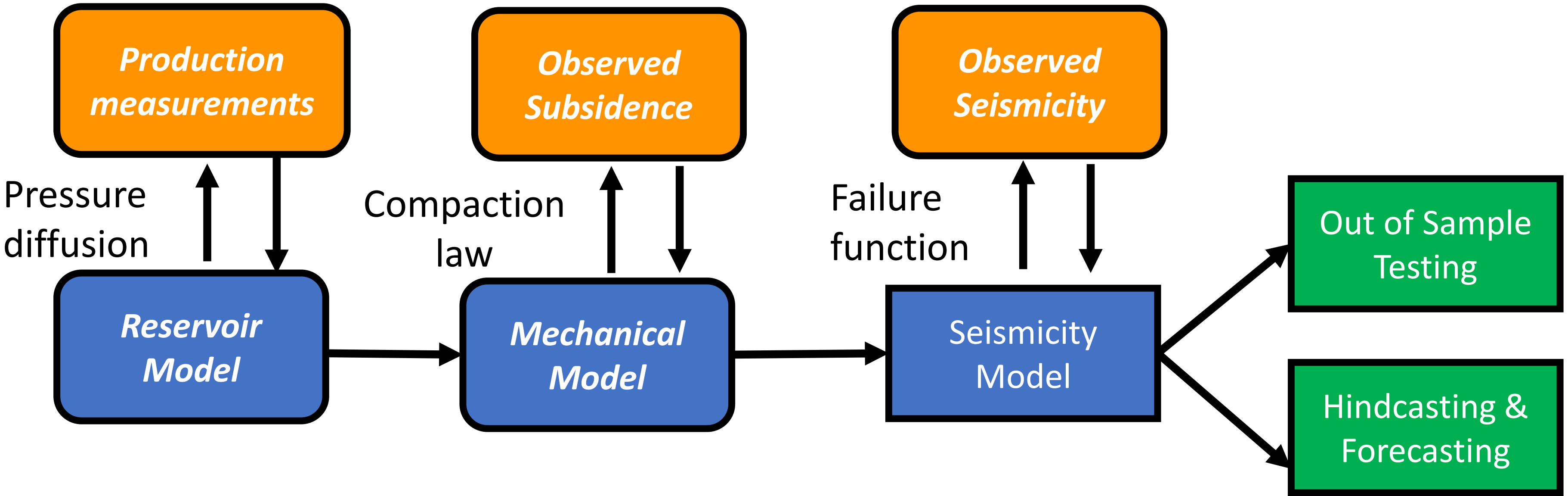

Talk roadmap

- From N, to $E(M_{max})$ and $p(>M)$
- Seismicity- key features (Smith et al, GJI, 2020)
- Stress and strain modeling (Smith et al., JGR, 2019; EPSL, in review)
- Seismicity model (Heimisson et al, 2021; Smith et al., EPSL, in review)
- Reservoir VFE modeling (Meyer et al., GSL, in review)
- $E(M_{max})$ and $p(>M)$.

Relationships between N (>M_c), E(M_{max}) and p(>M)

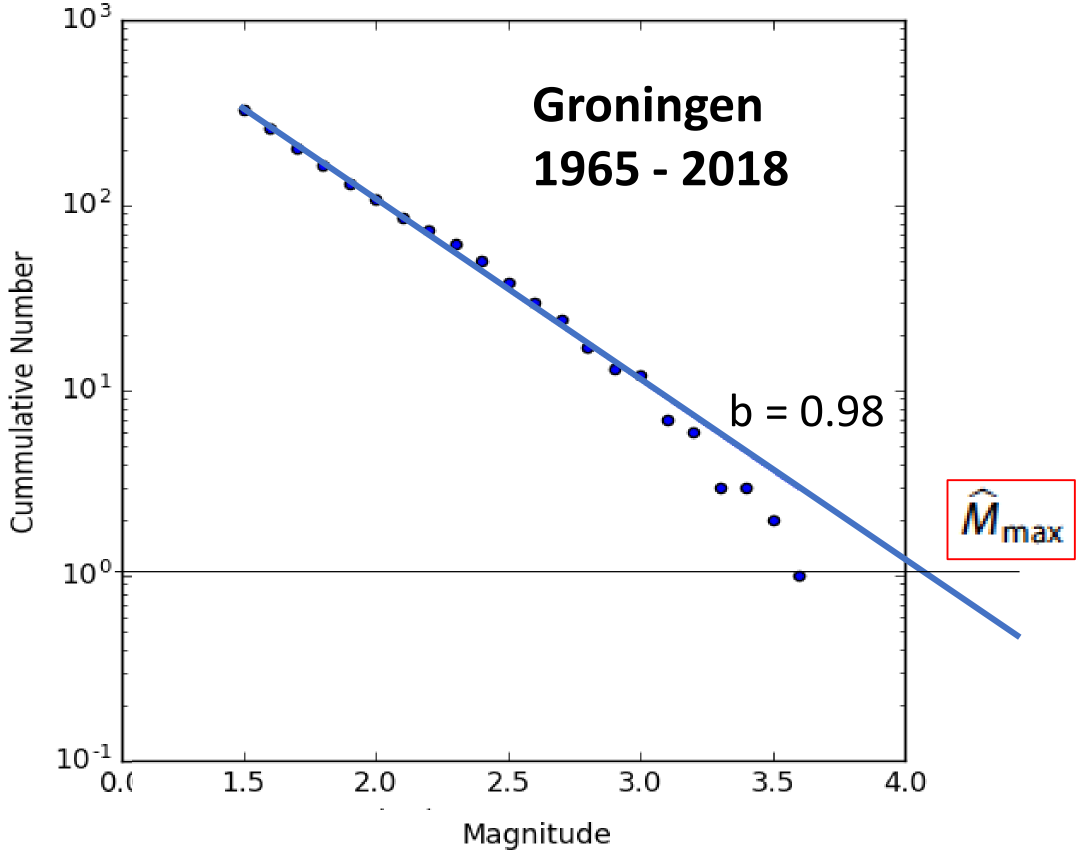

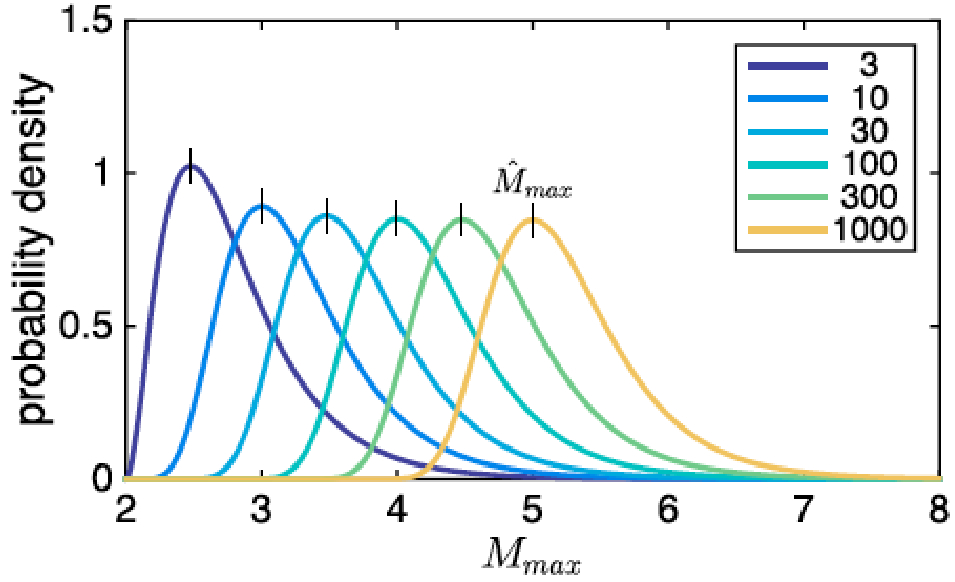

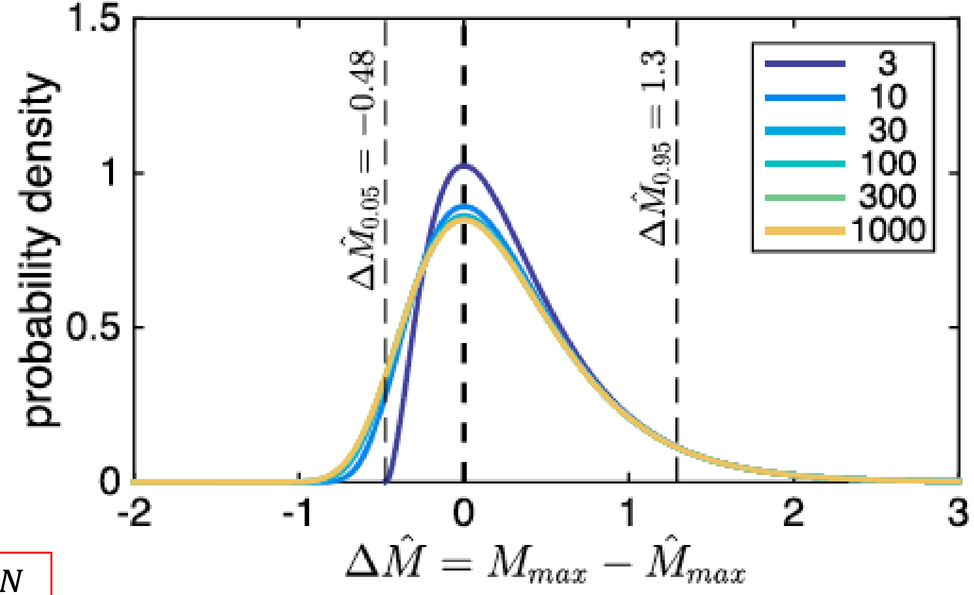

$$\boxed{\widehat{M}_{max} = M_c + \frac{1}{b}\log_{10} N,} \quad (1)$$

$$\widehat{M}_q = \widehat{M}_{max} - \frac{1}{b}\log_{10}\left[N\left(1 - q^{1/N}\right)\right], \quad (2)$$

$$\boxed{p(> M) = 1 - \left(1 - \frac{1}{N}10^{b(M - \widehat{M_{max}})}\right)^N}$$

(van der Elst et al., 2016)

Relationships between N (>M_c), E(M_{max}) and p(>M)

- Estimating earthquake magnitude probability boils down to estimating the **probability distribution of the number of earthquakes, N(>Mc), as a function of time and space, and of the *b*-value of the GR law.**

$$p(>M) = 1 - \left(1 - \frac{1}{N} 10^{b(M - \widehat{M_{max}})}\right)^N$$

-> Two variables need to be estimated: *N(>M, t, x)* and *b*

- Assumptions :
  - Non truncated Gutenberg Richter distribution of iid magnitudes.
  - The physical processes and properties governing the future evolution of the system can be determined from the past.

Seismicity - Key features

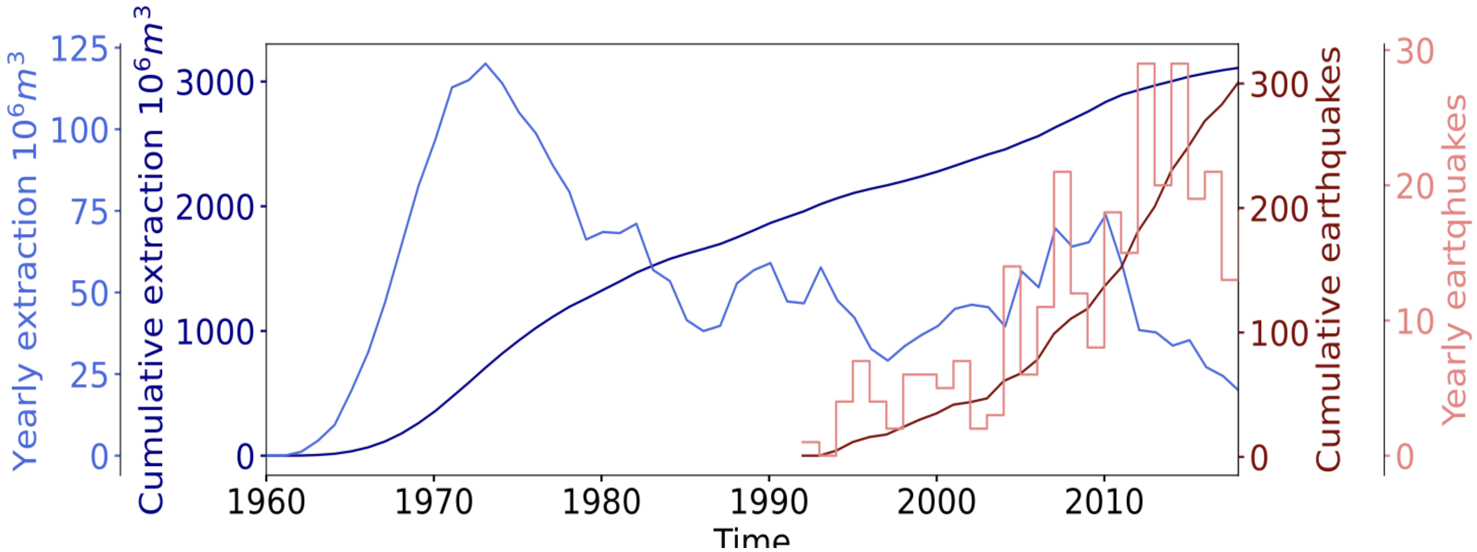

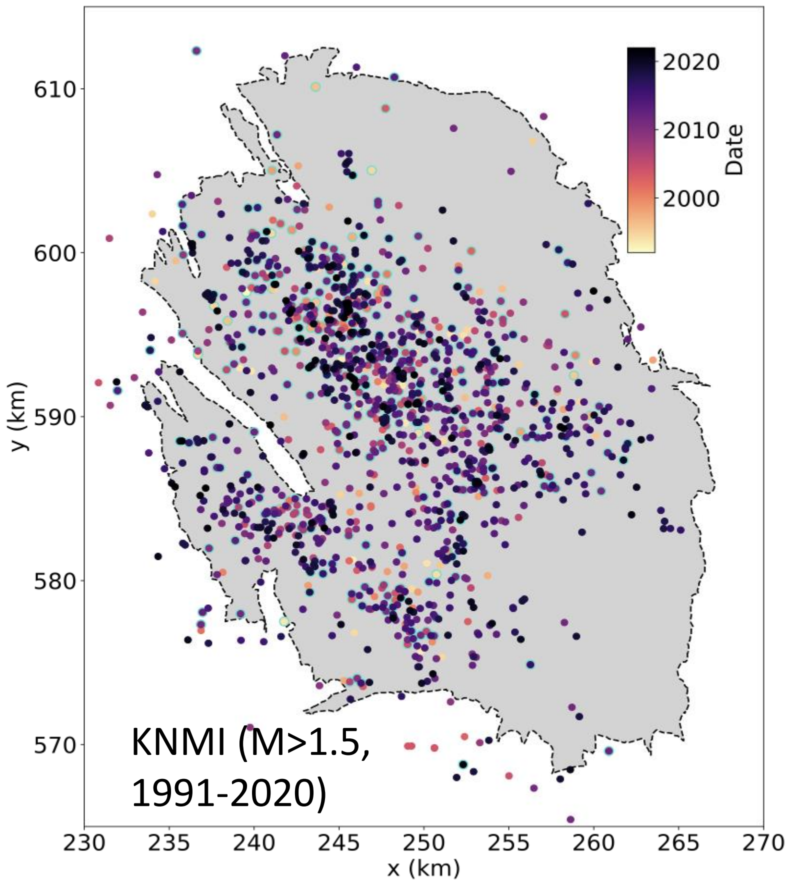

Seismicity - Key features

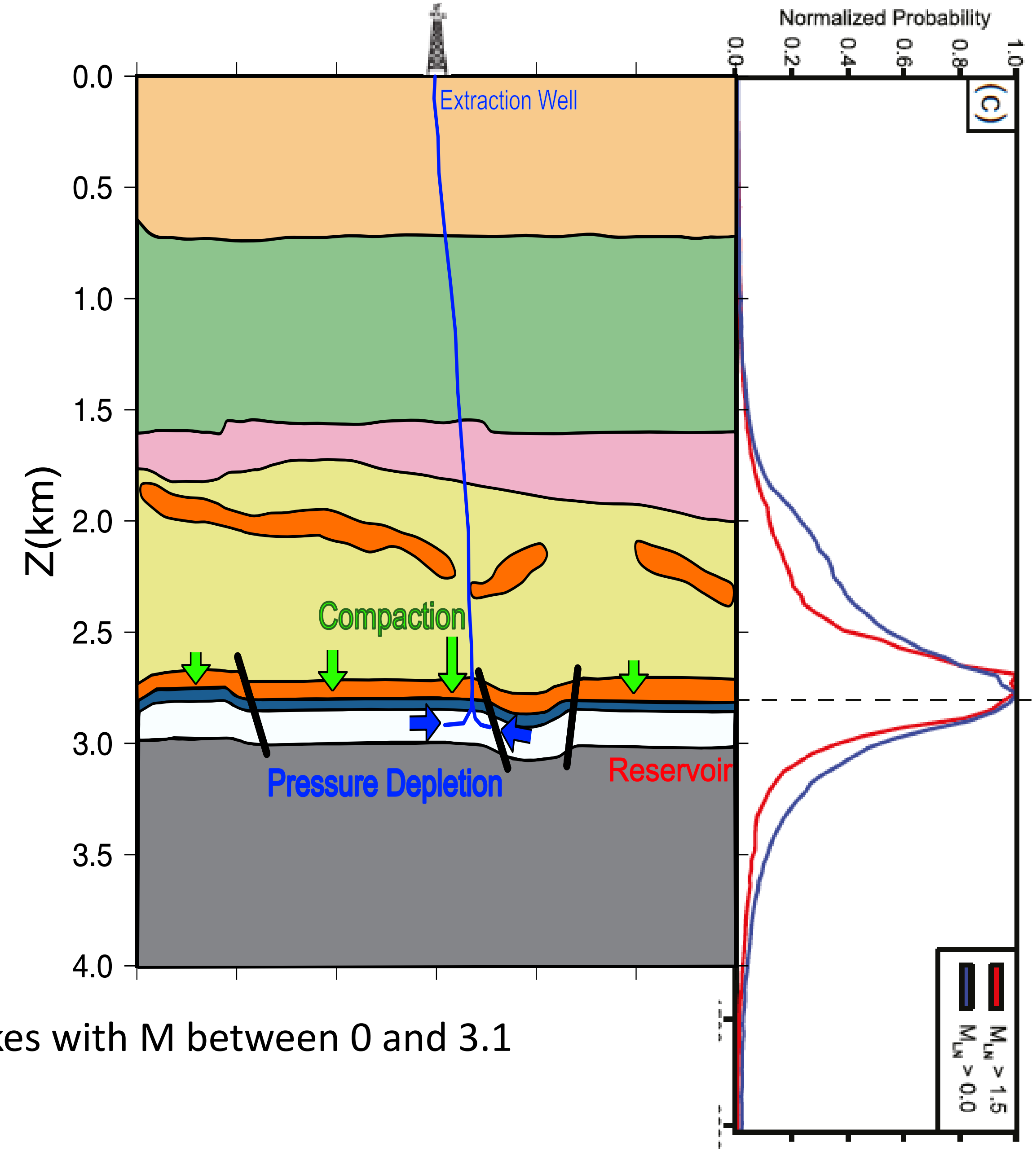

85 earthquakes with M between 0 and 3.1 (2015-2017)

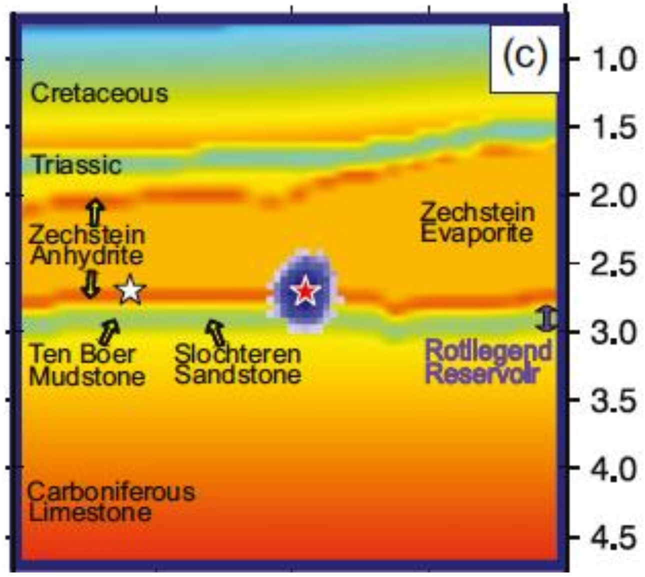

PDF of hypocentral depth determination

Probability of earthquakes

- above the reservoir: 60%
- within the reservoir: 28%
- below the reservoir: 12%

(Smith et al, GJI, 2020)

Seismicity - Key features

Match with faults location and orientation

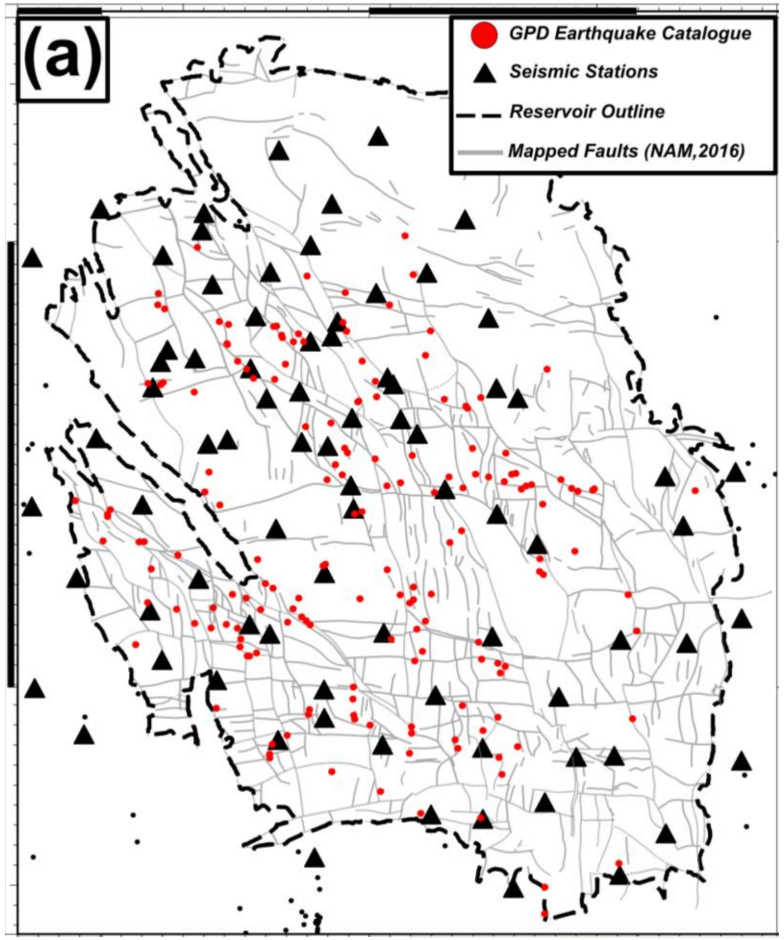

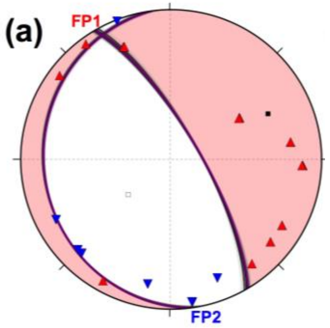

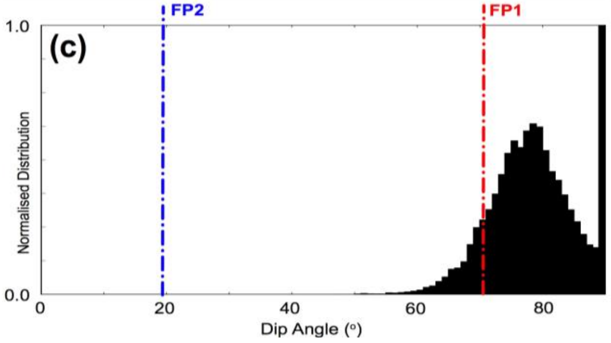

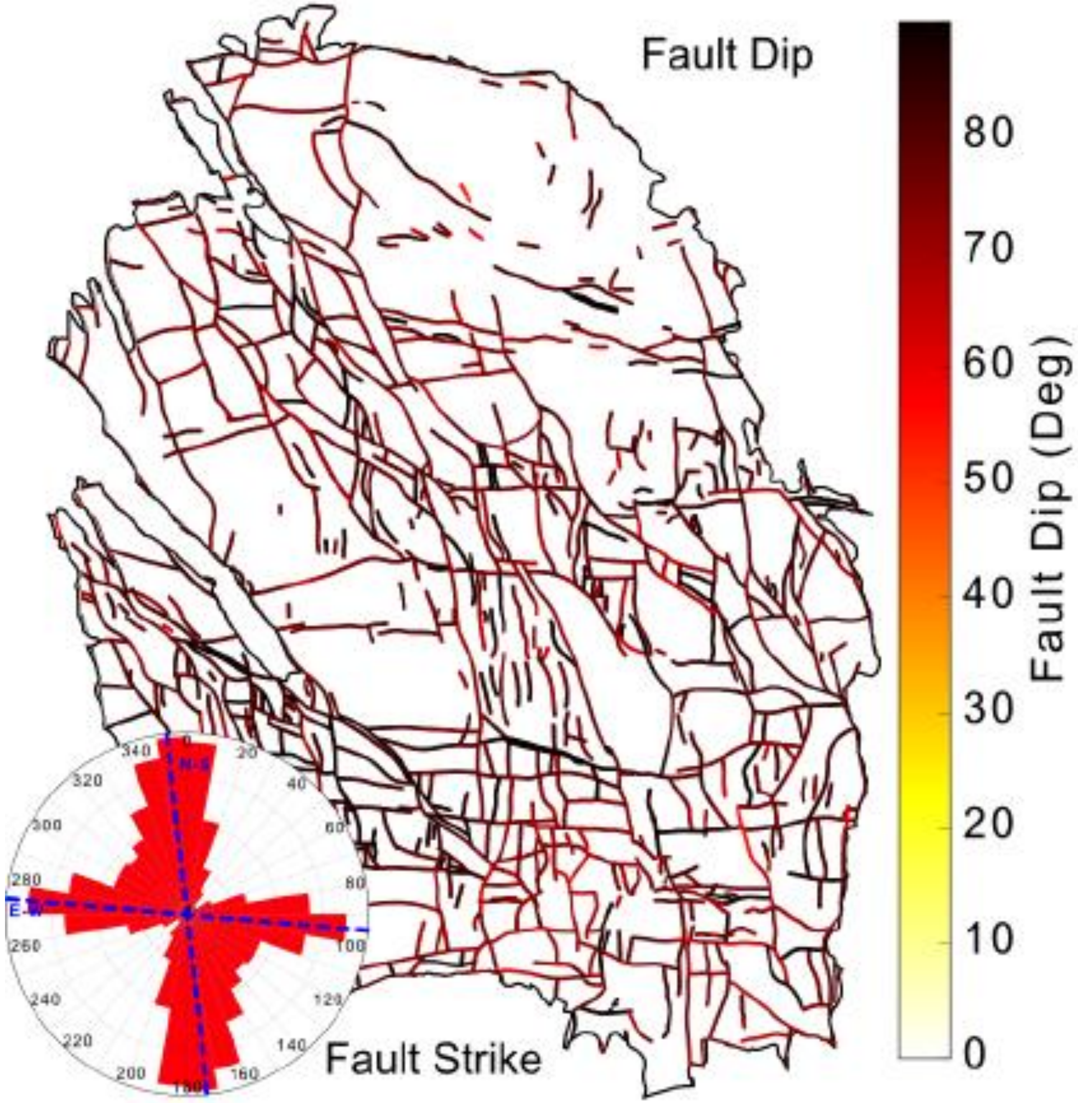

Seismicity - Key features

Magnitude frequency distribution

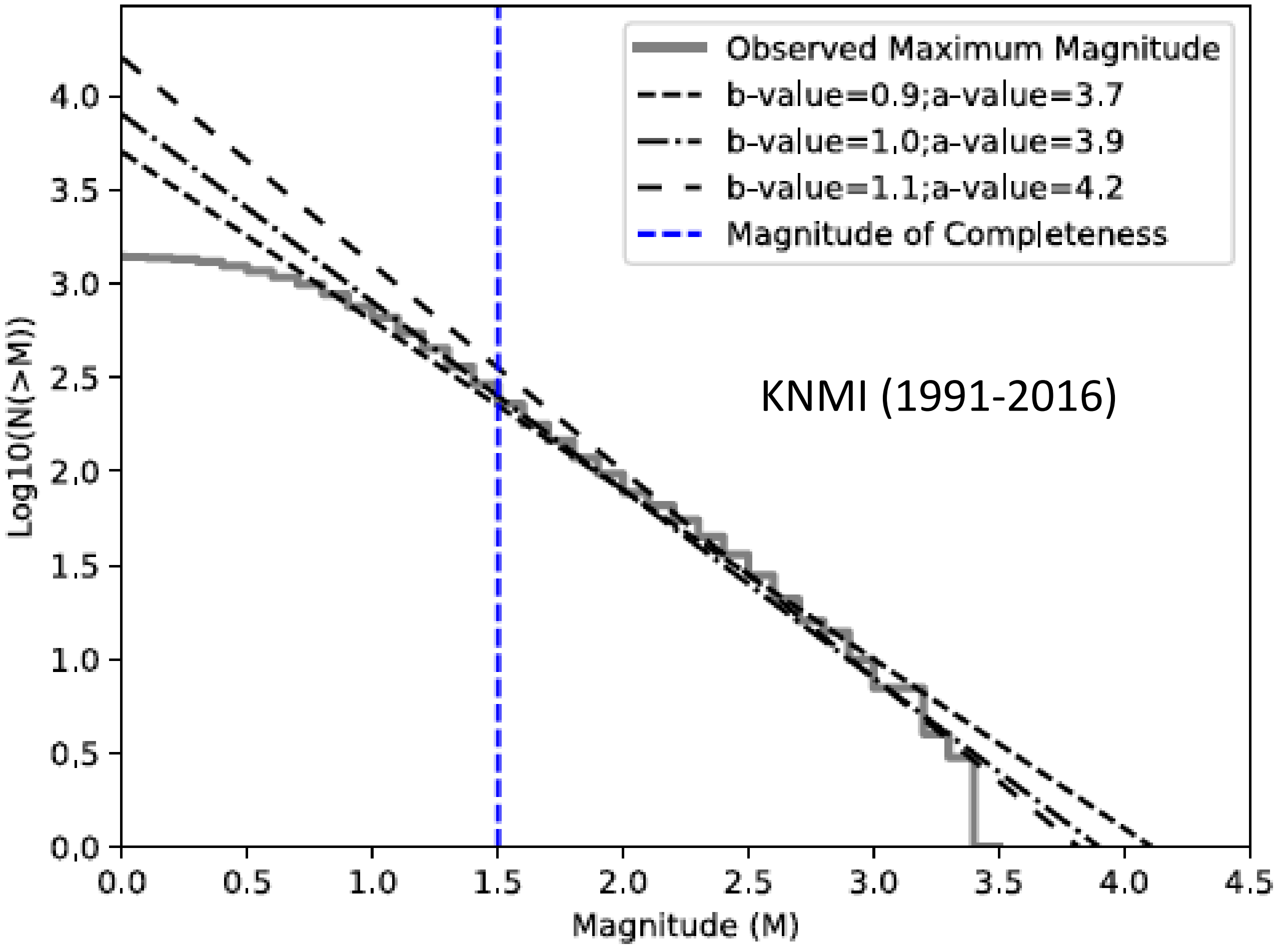

Estimate of b value based on van der Elst (2021) b^+ algorithm (no magnitude cut-off)

***b*-value 1.0 +/- 0.1**

Seismicity - Key features

Searching for clustering and periodicities using the Schuster spectrum (Ader and Avouac, EPSL, 2013)

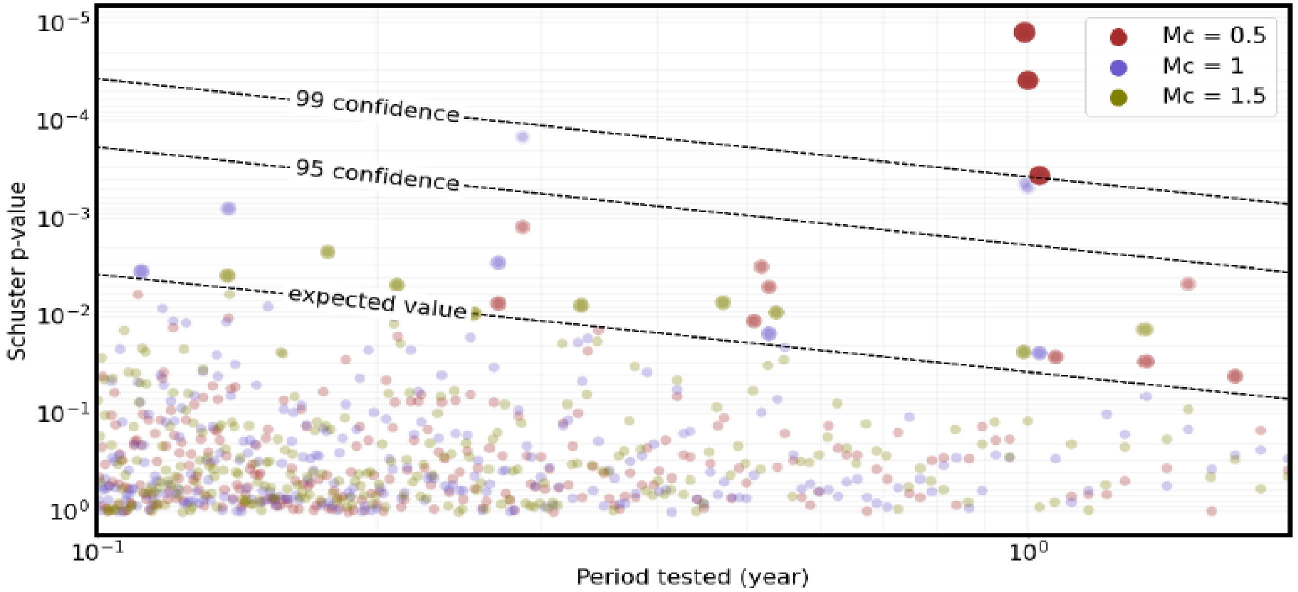

KNMI, 1991-2018

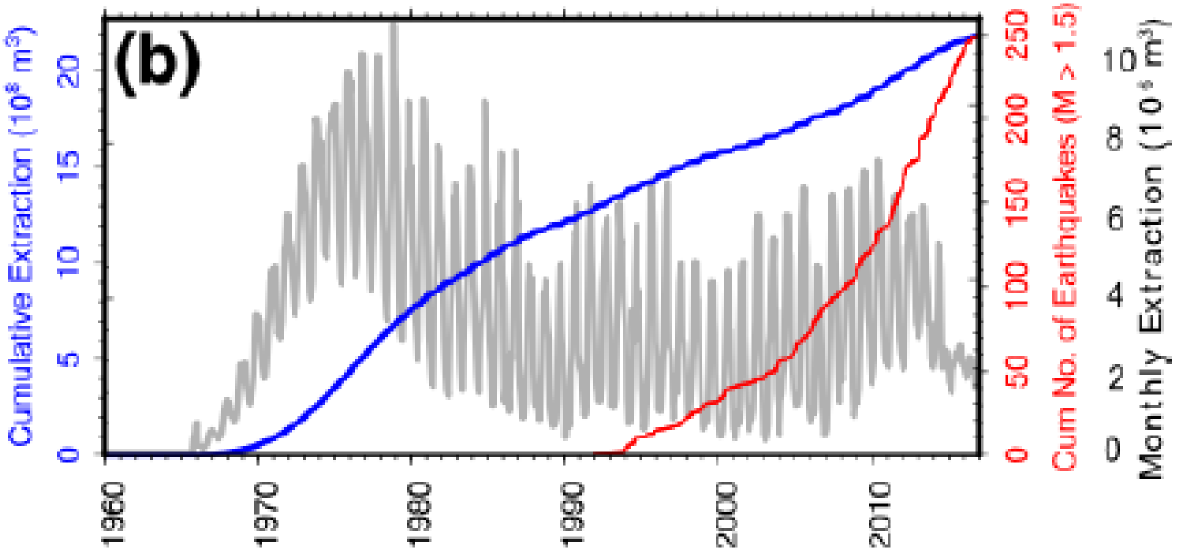

(Mateo Acosta)

Surface Deformation (Leveling, InSAR, GPS)

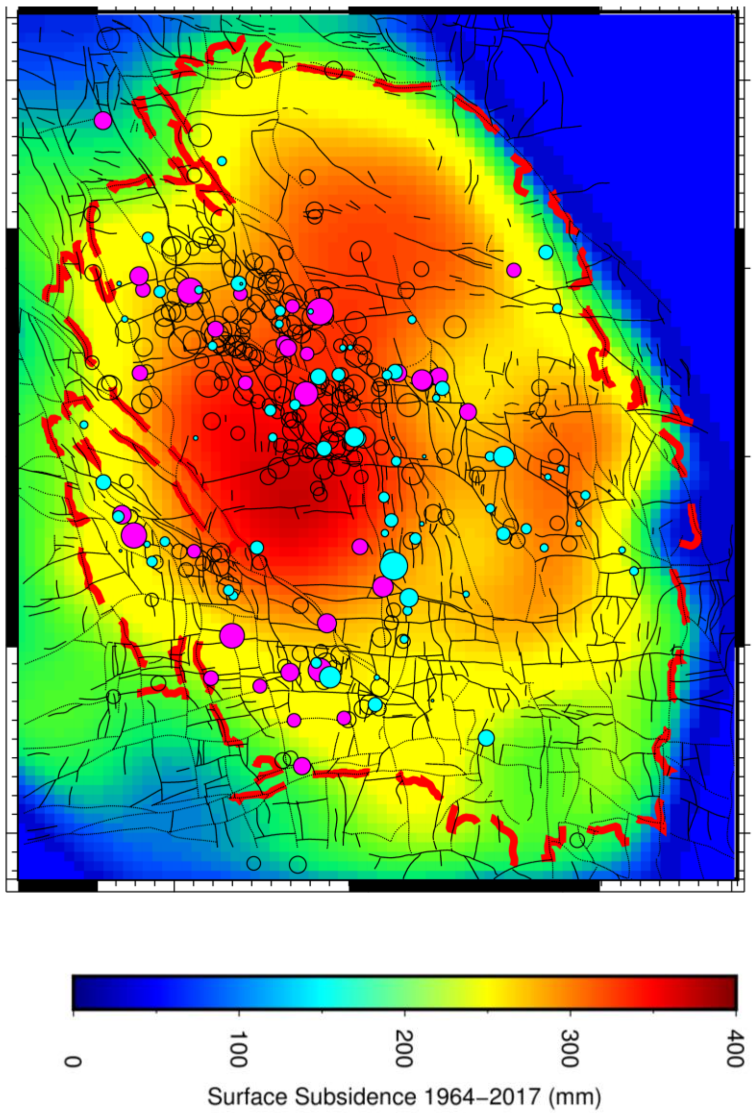

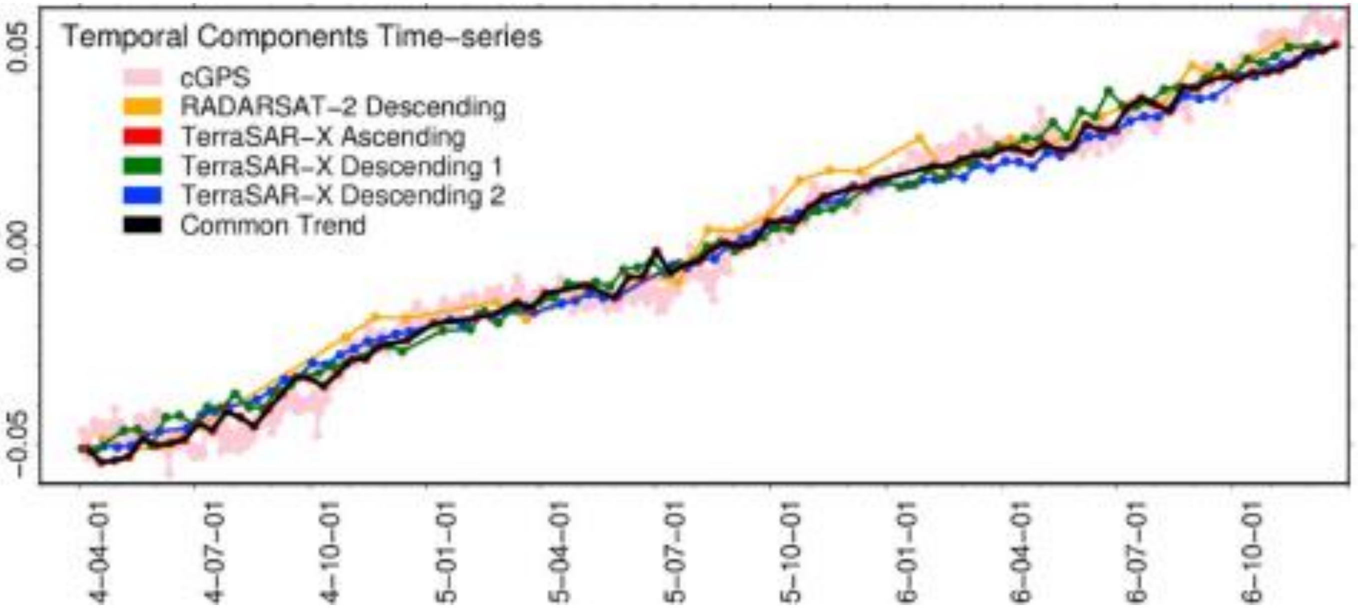

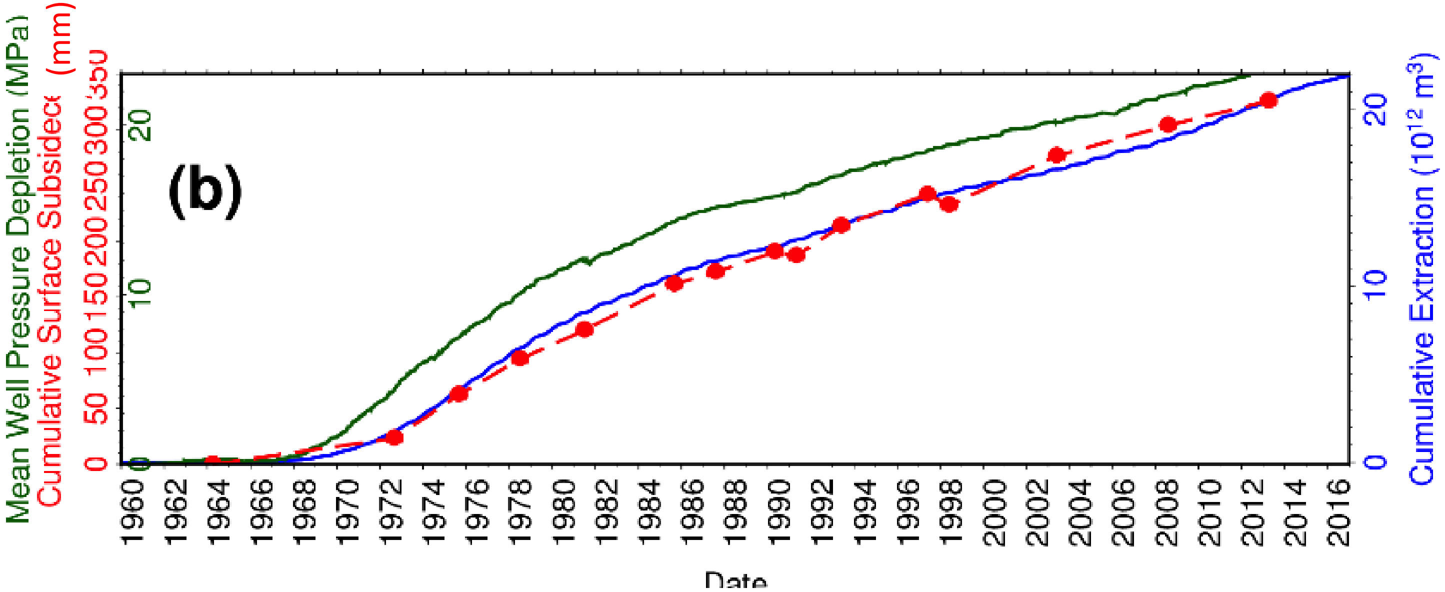

(Smith et al, 2019)

Stress and Strain modeling

Reservoir is decomposed in
Cuboids of 500m x 500m x h

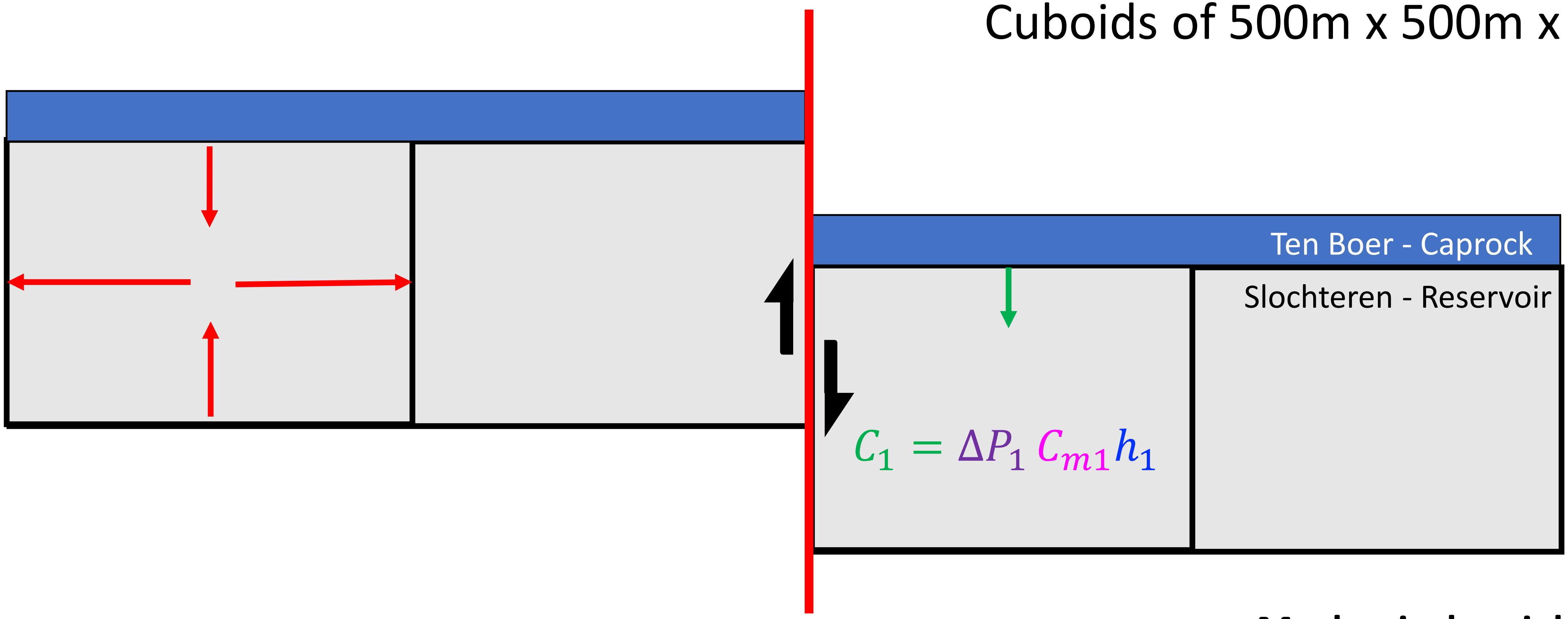

Reservoir: Uniaxial vertical strain+ shear strain
Poroelastic stress

Mechanical variables:

- Compressibility, C_m
- Poisson Coefficient, ν (0.25)
- Biot Coefficient, α (1.0)
- Shear Modulus: G (6 GPa)

Stress and Strain modeling

Analytical Green Functions

- *Nuclei of strain:* Geertsma (1973)
- *Polyhedral inclusions:* Kuvshinov (2008)

Reservoir is decomposed in Cuboids of 500m x 500m x h

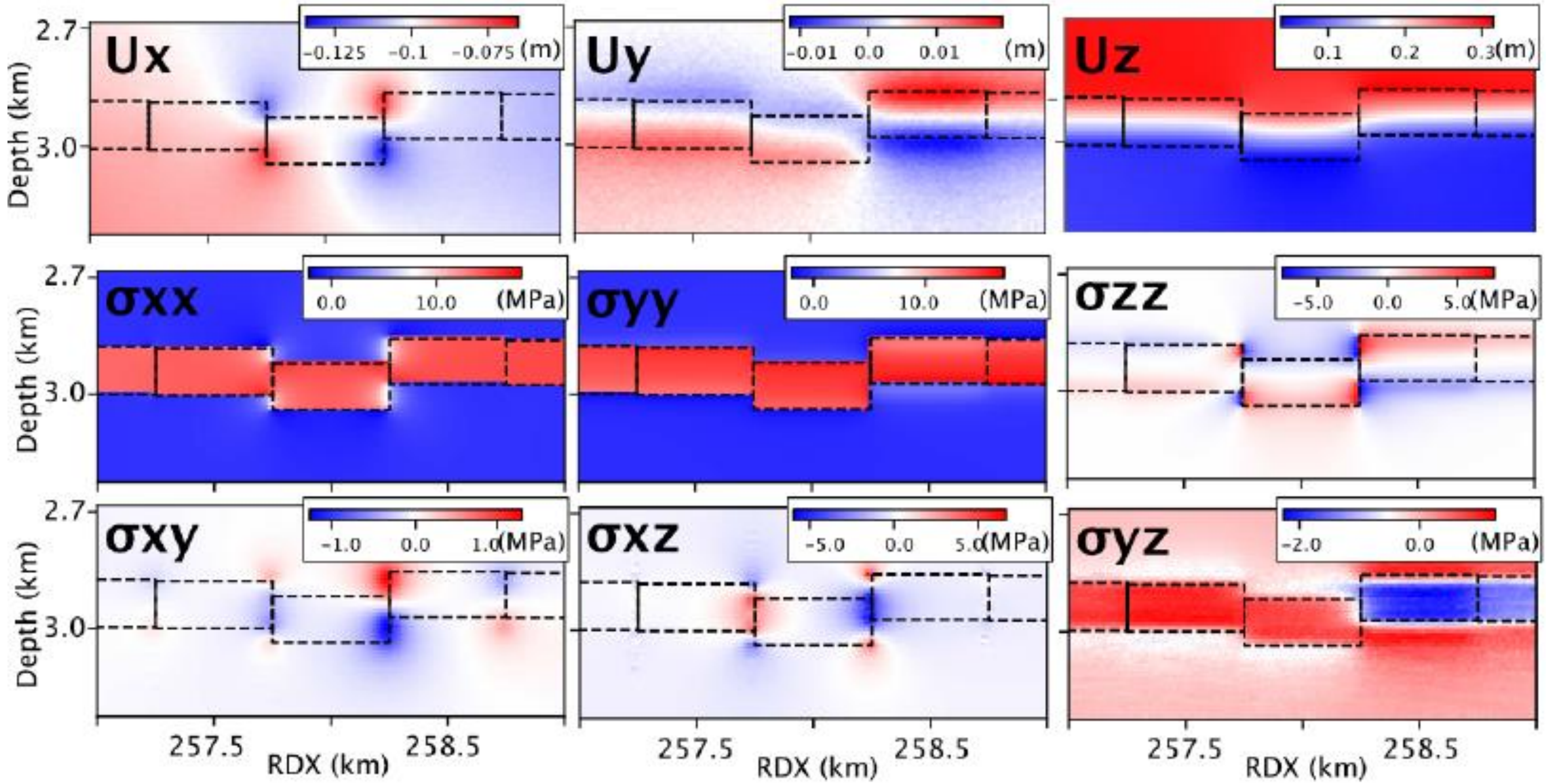

Mechanical variables:

- Compressibility, C_m
- Poisson Coefficient, ν (0.25)
- Biot Coefficient, α (1.0)
- Shear Modulus: G (6 GPa)

(Smith et al., EPSL, in review)

Stress and Strain modeling

Reservoir Compaction from inversion of surface deformation

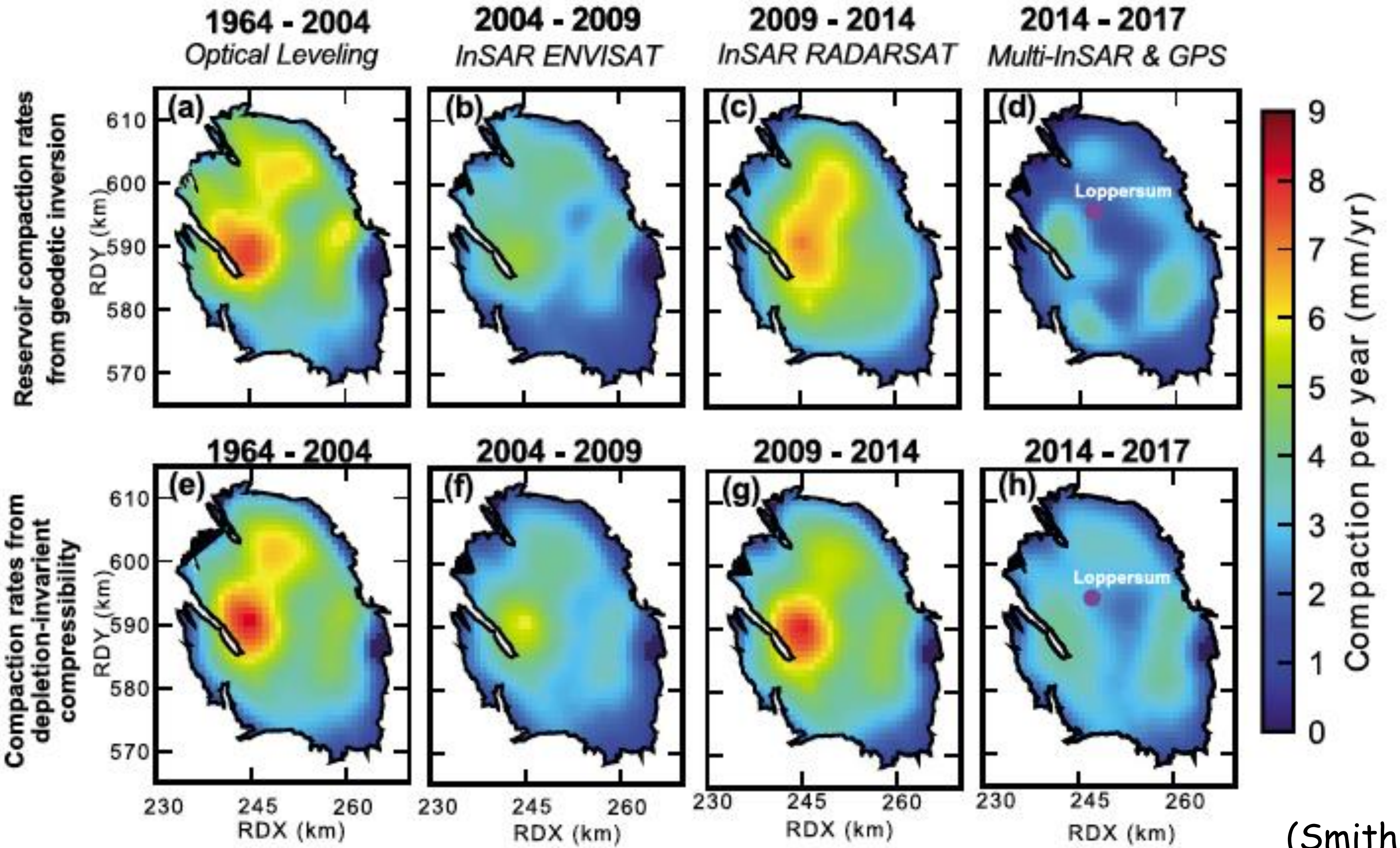

(Smith et al, JGR, 2019)

Stress and Strain modeling

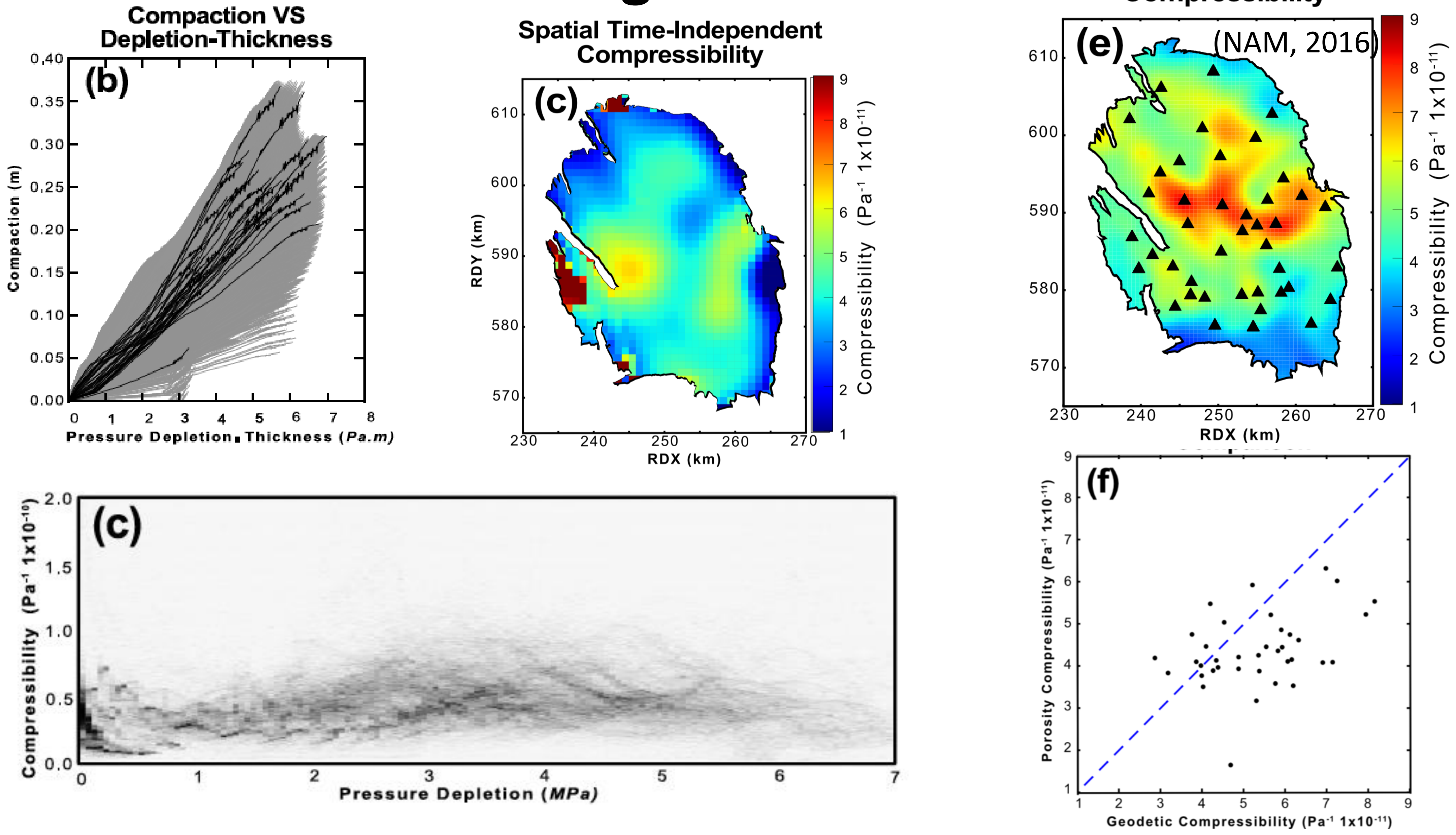

Reservoir Compressibility from Compaction and Pressure Change (Smith et al, JGR, 2019)

Stress and Strain modeling

Comparison of measured and predicted surface deformation

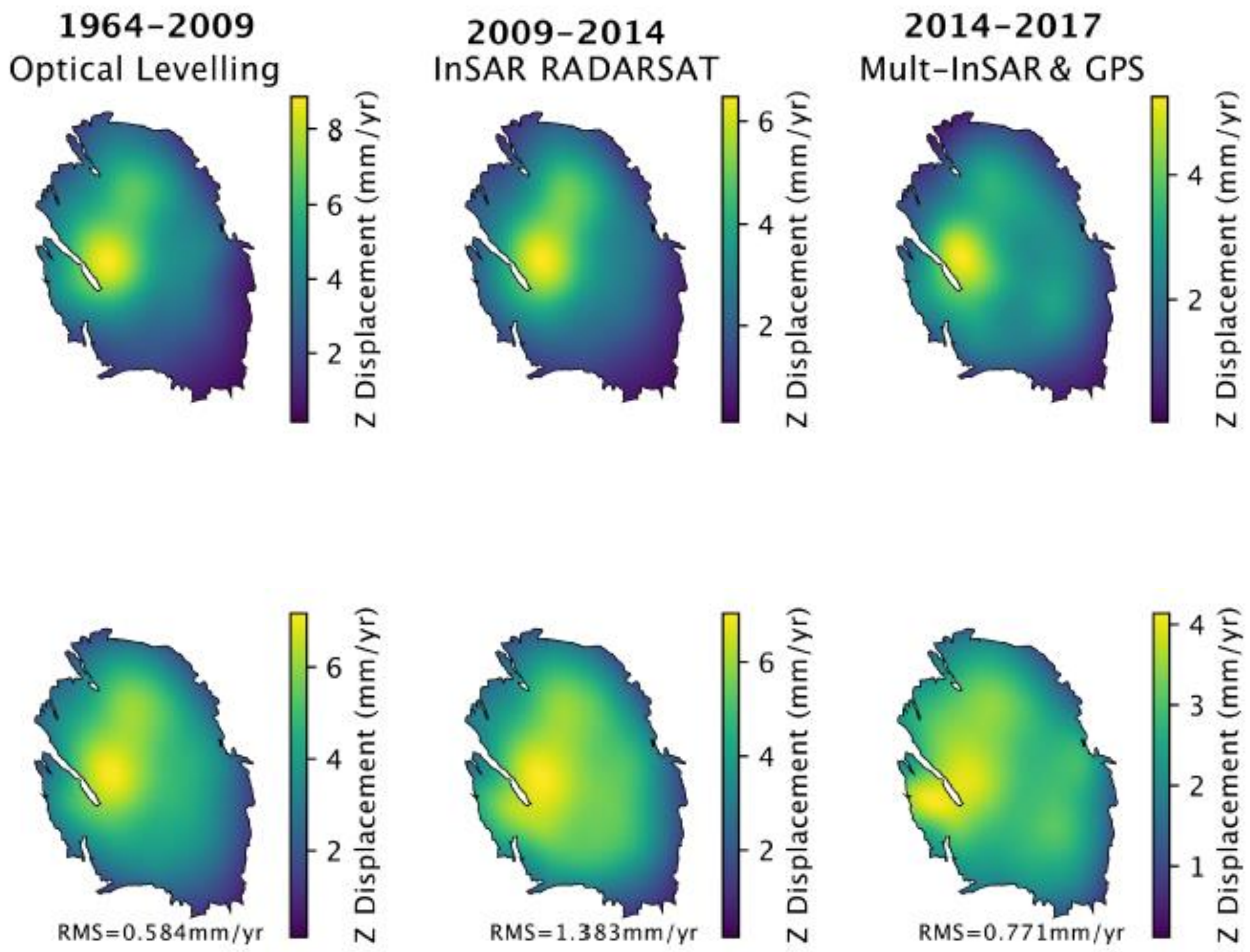

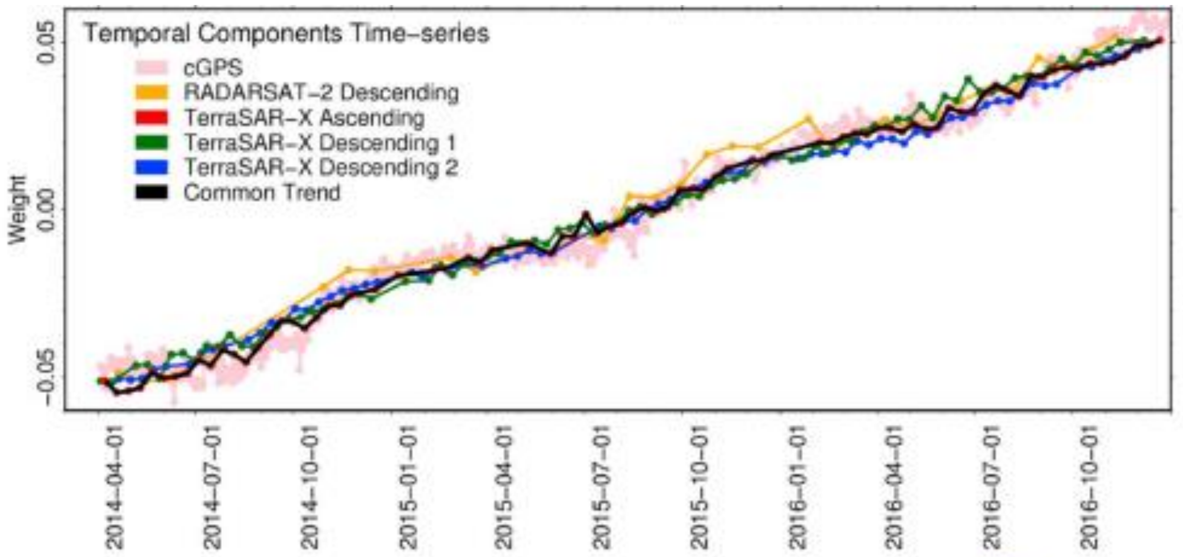

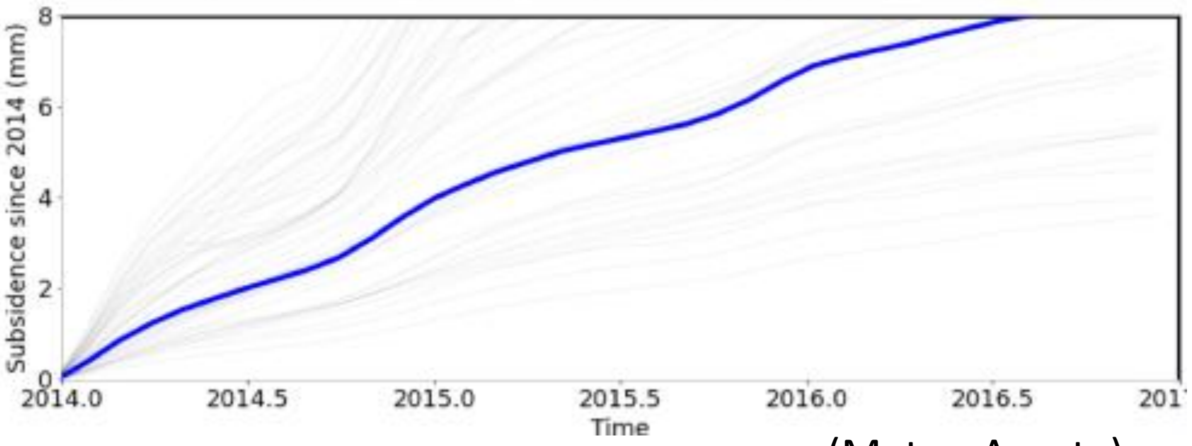

(Mateo Acosta)

(Meyer et al, GSL, in review)

From stress change to seismicity

- Seismicity is assumed to be governed by Coulomb stress changes

$$\boxed{\Delta C = \Delta\tau + \mu(\Delta P - \Delta\sigma_n),}$$

- Earthquake occurred on optimally oriented fault, or on faults with prescribed orientation

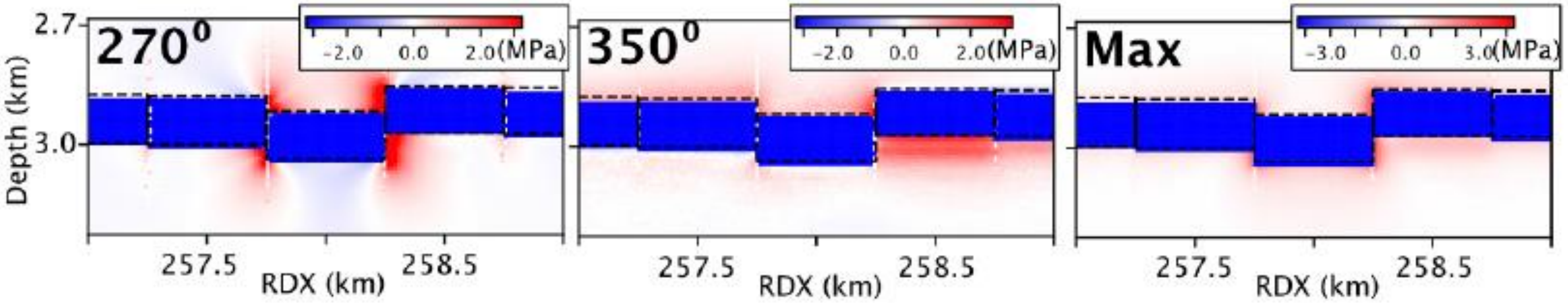

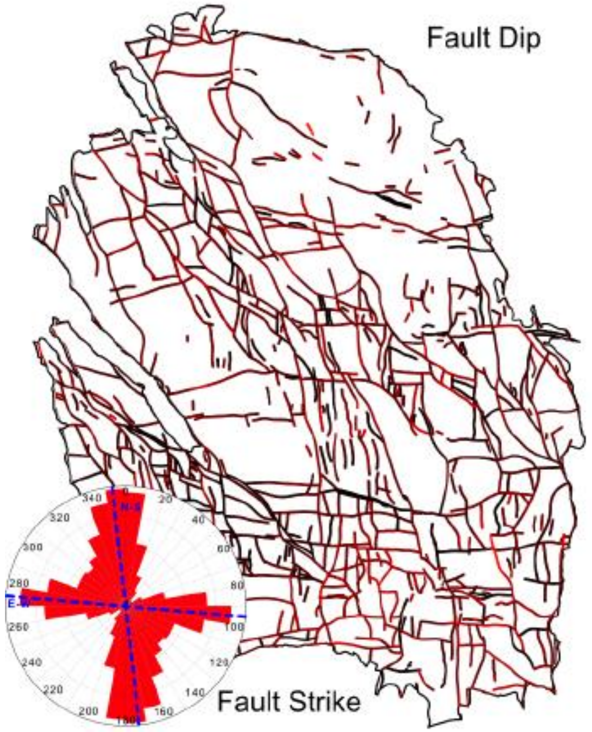

- Earthquakes occur on randomly distributed faults, with uniform probability over the field.

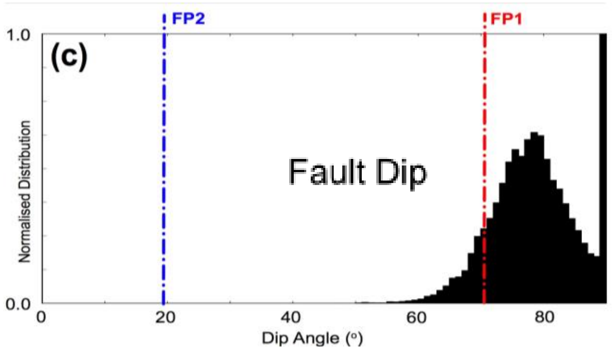

From stress change to seismicity

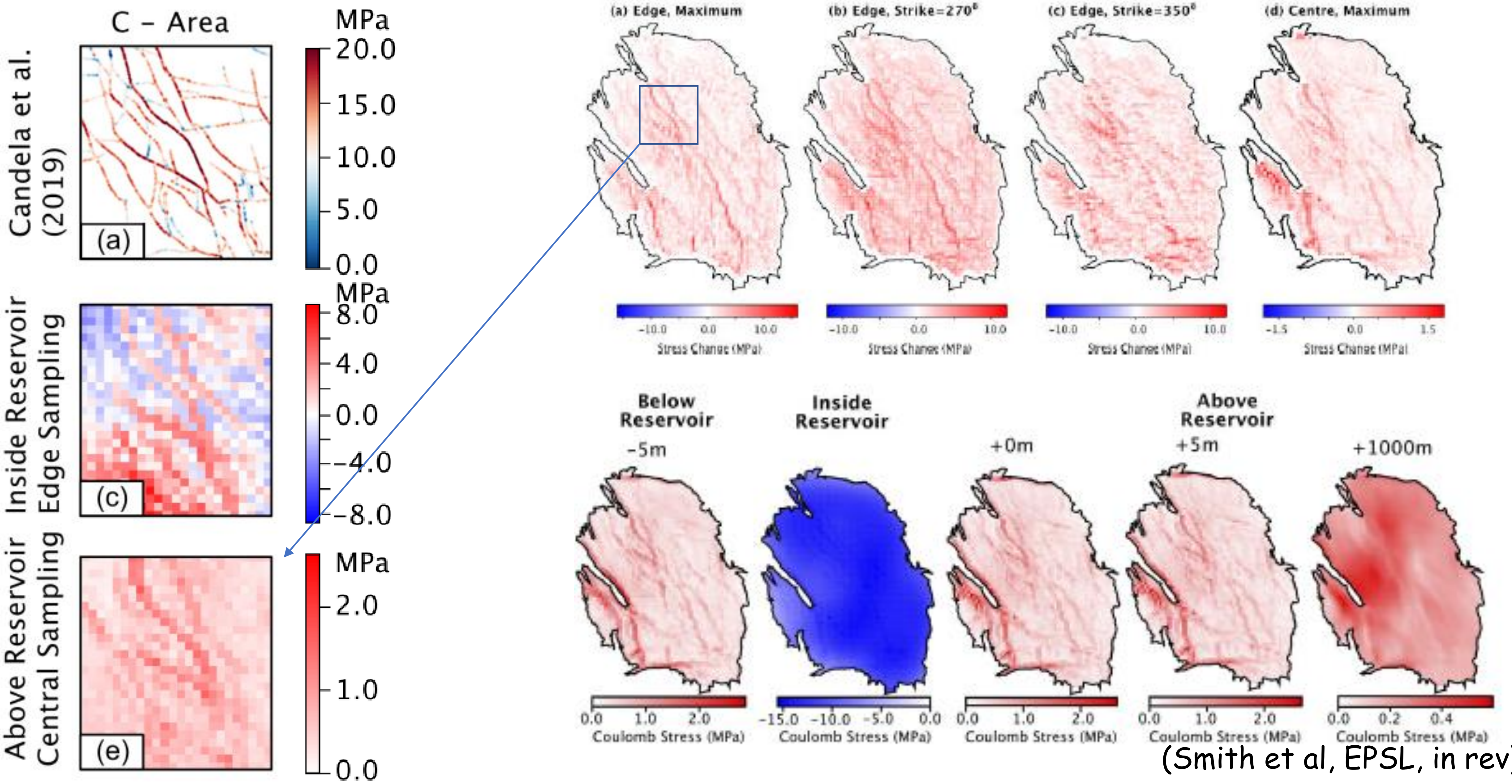

(Smith et al, EPSL, in rev)

From stress change to seismicity

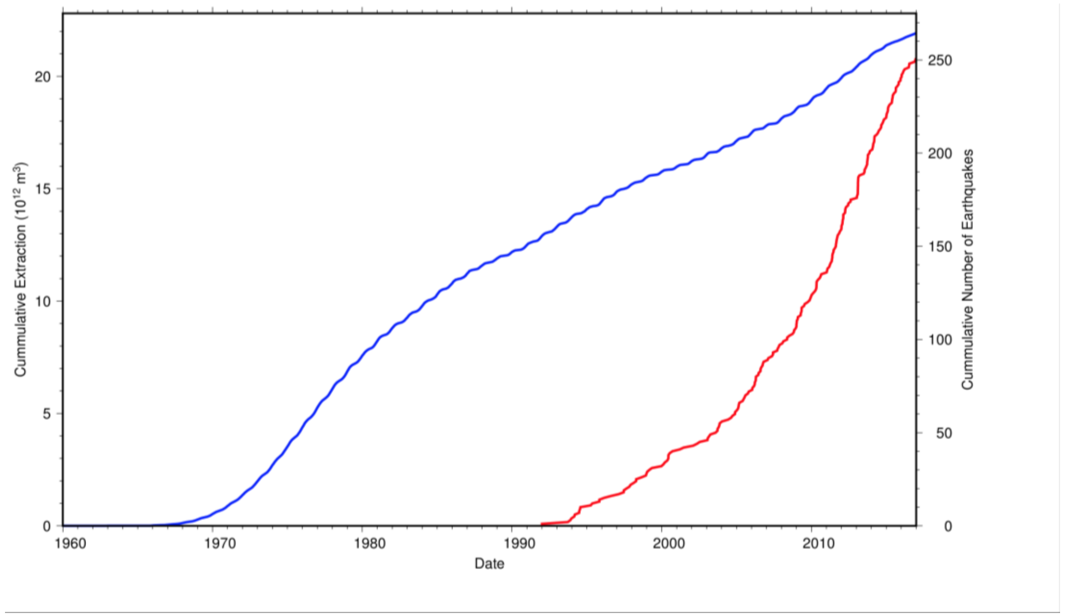

- How to explain the lag?

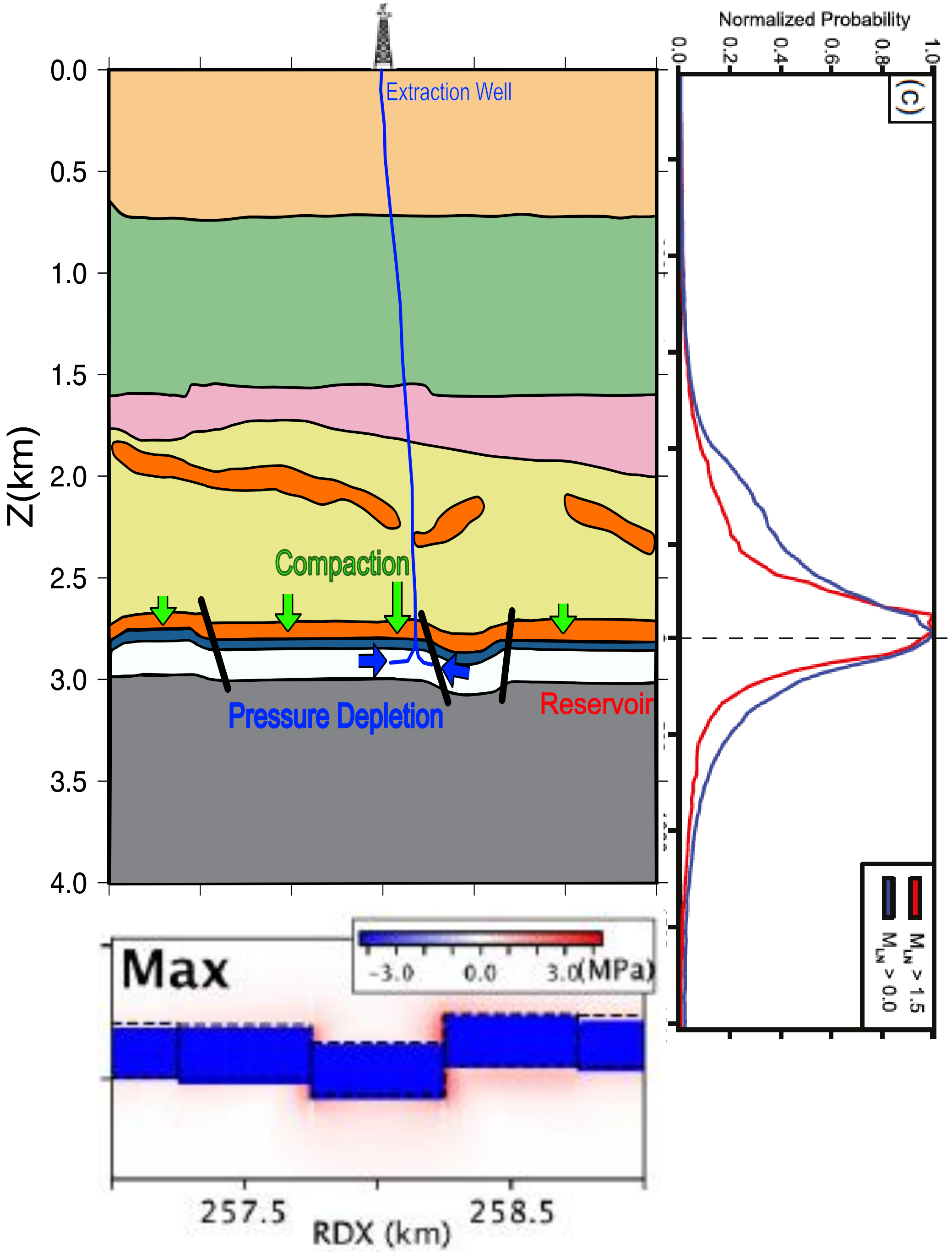

From stress change to seismicity

- **Model 1:** Instantaneous nucleation with stress threshold (Bourne and Oates, 2017; Smith et al., EPSL, in review)

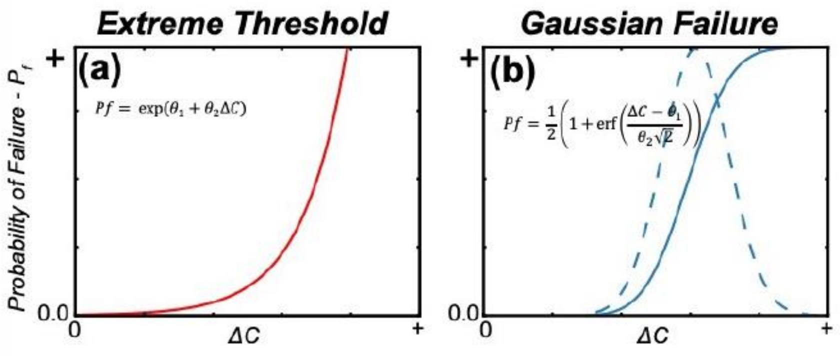

- **Model 2:** Time dependent nucleation governed by rate&state friction (Candela et al, JGR, 2019):

$$\frac{R}{r} = \frac{\exp\left(\frac{\Delta S(t)}{A\sigma_0}\right)}{\frac{1}{t_a}\int_0^t \exp\left(\frac{\Delta S(t')}{A\sigma_0}\right)dt' + 1}$$

(Dieterich, 1994, Heimisson and Segall, 2018)

- **Model 3:** Time dependent nucleation governed by rate&state friction with stress threshold (Heimisson et al, GJI, 2021)

$$\frac{R}{r} = \frac{\exp\left(\frac{\Delta S(t) - \Delta S_c}{A\sigma_0}\right)}{\frac{1}{t_a}\int_{t_b}^{t} \exp\left(\frac{\Delta S(t') - \Delta S_c}{A\sigma_0}\right)dt' + 1} \text{ if } t \geq t_b \qquad \frac{R}{r} = 0 \text{ if } t < t_b$$

(Heimisson et., 2021)

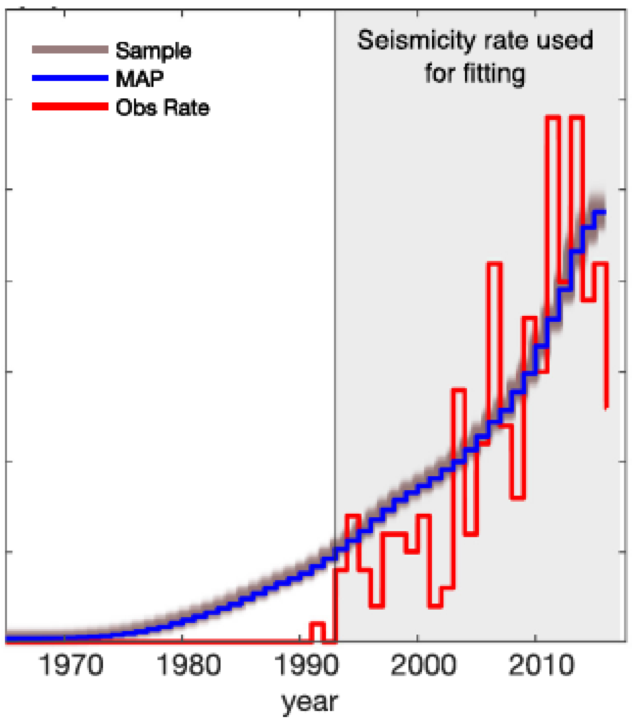

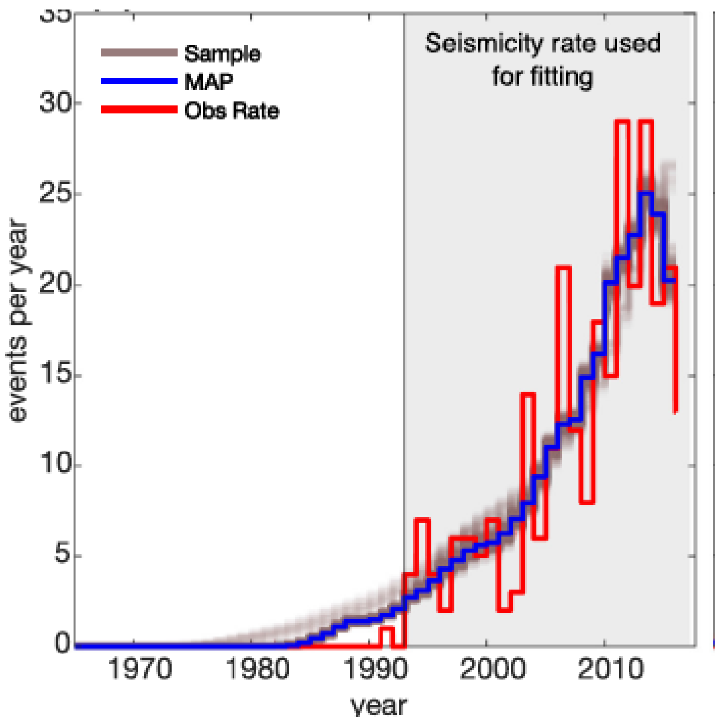

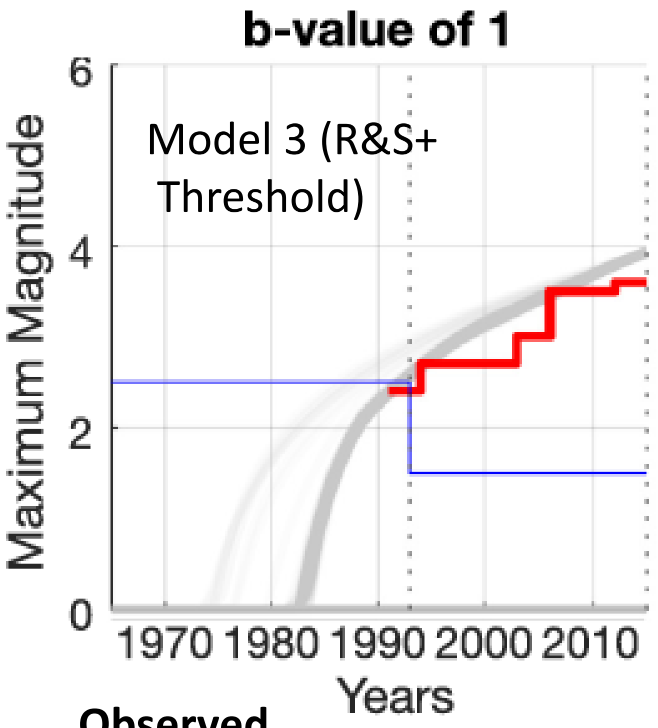

Model 2 (R&S)

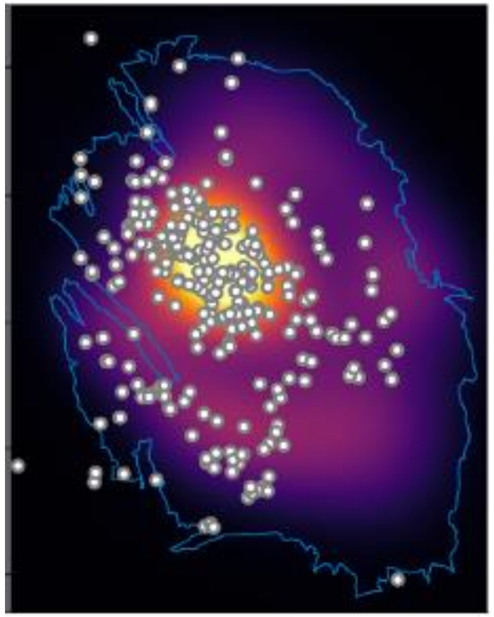

Model 3 (R&S+Threshold)

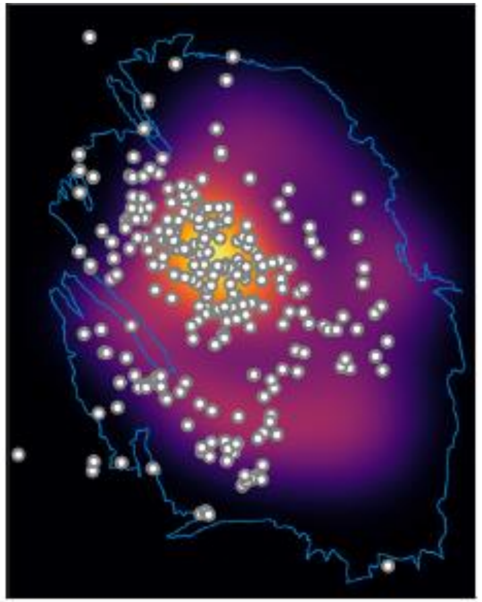

Observed

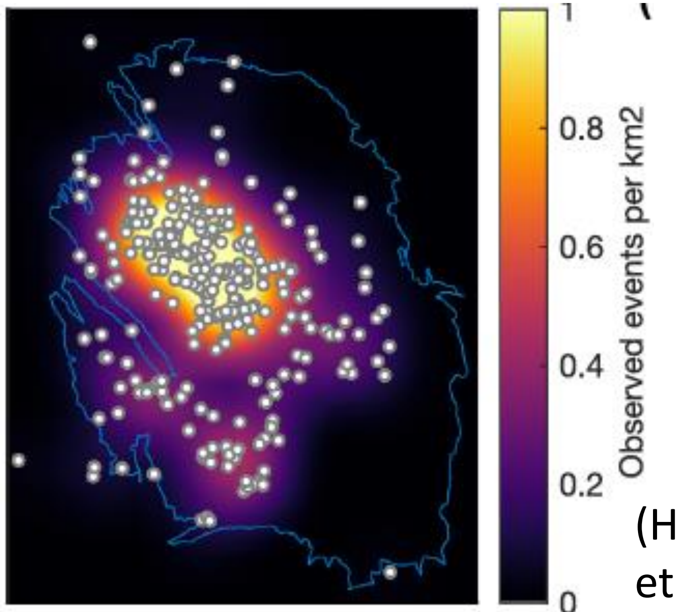

(Heimisson et al., 2021

From stress change to seismicity

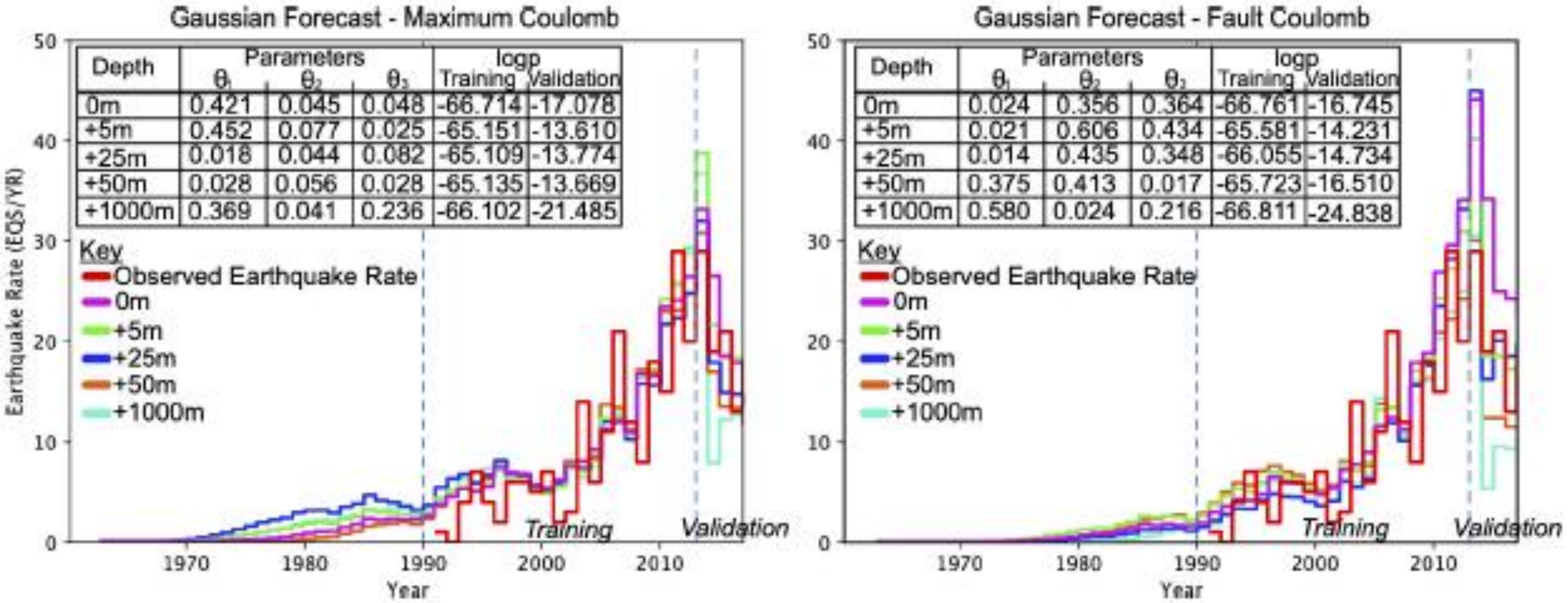

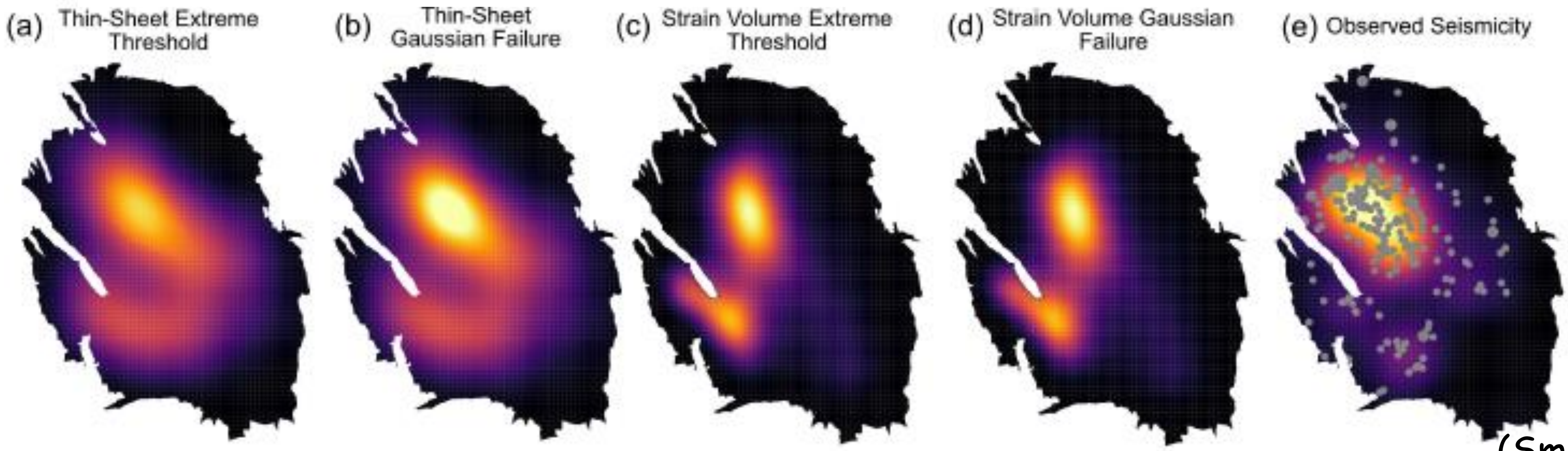

(Smith et al, EPSL, in rev)

Which model is best for forecasting?

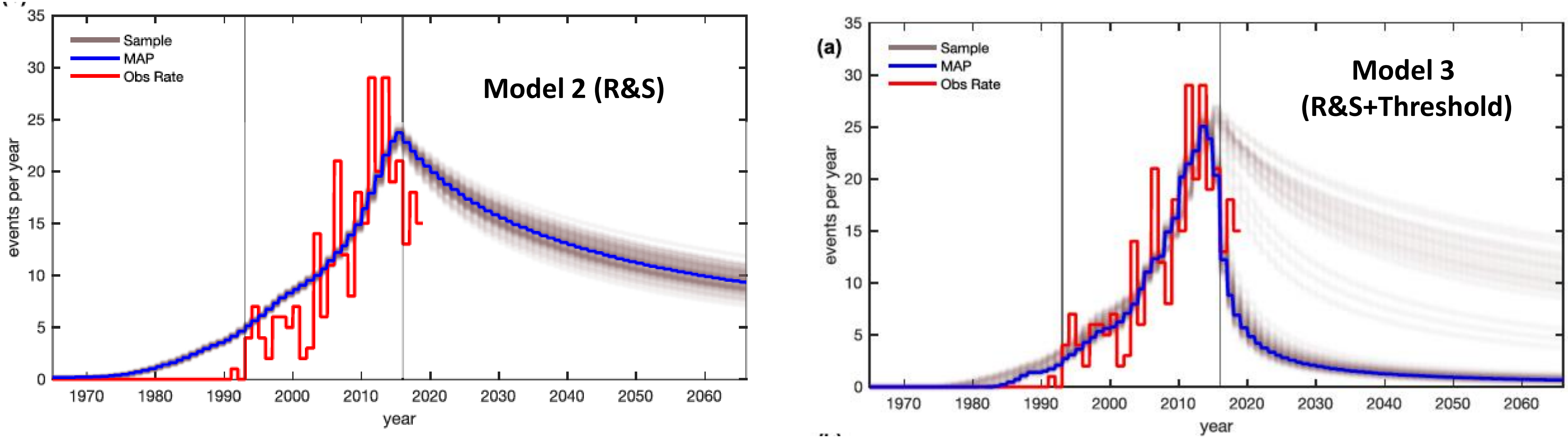

-> Introducing a stress threshold is essential

-> Earthquake nucleation not important at the annual time scale

-> Forecast is independent of stress sampling scheme

(Heimisson et al.,2021)

Seismicity Model- Testing seasonality

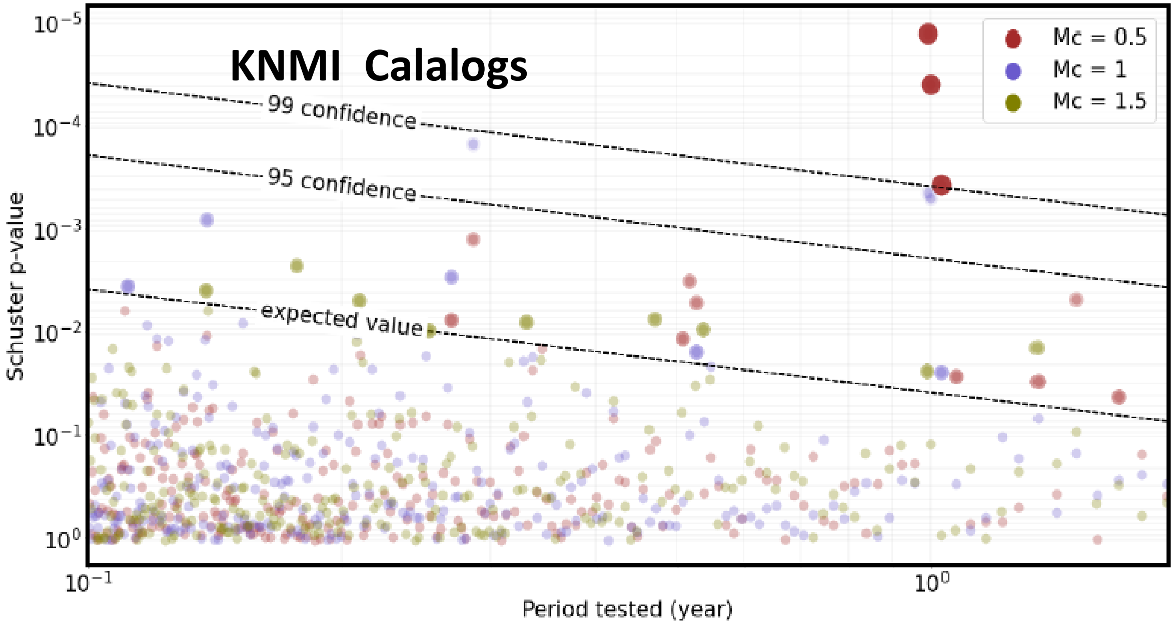

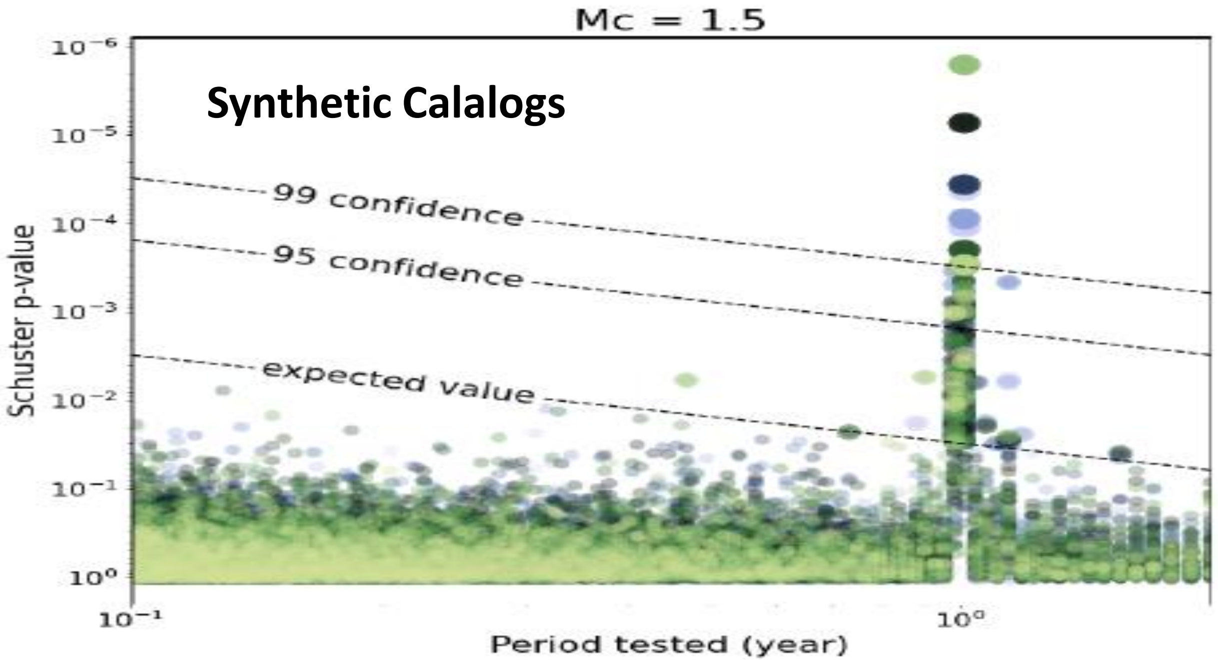

The nucleation process is consistent with the observed (mild) response of he seismicity to seasonal loading.

(Mateo Acosta)

Seismicity model- Out of sample testing

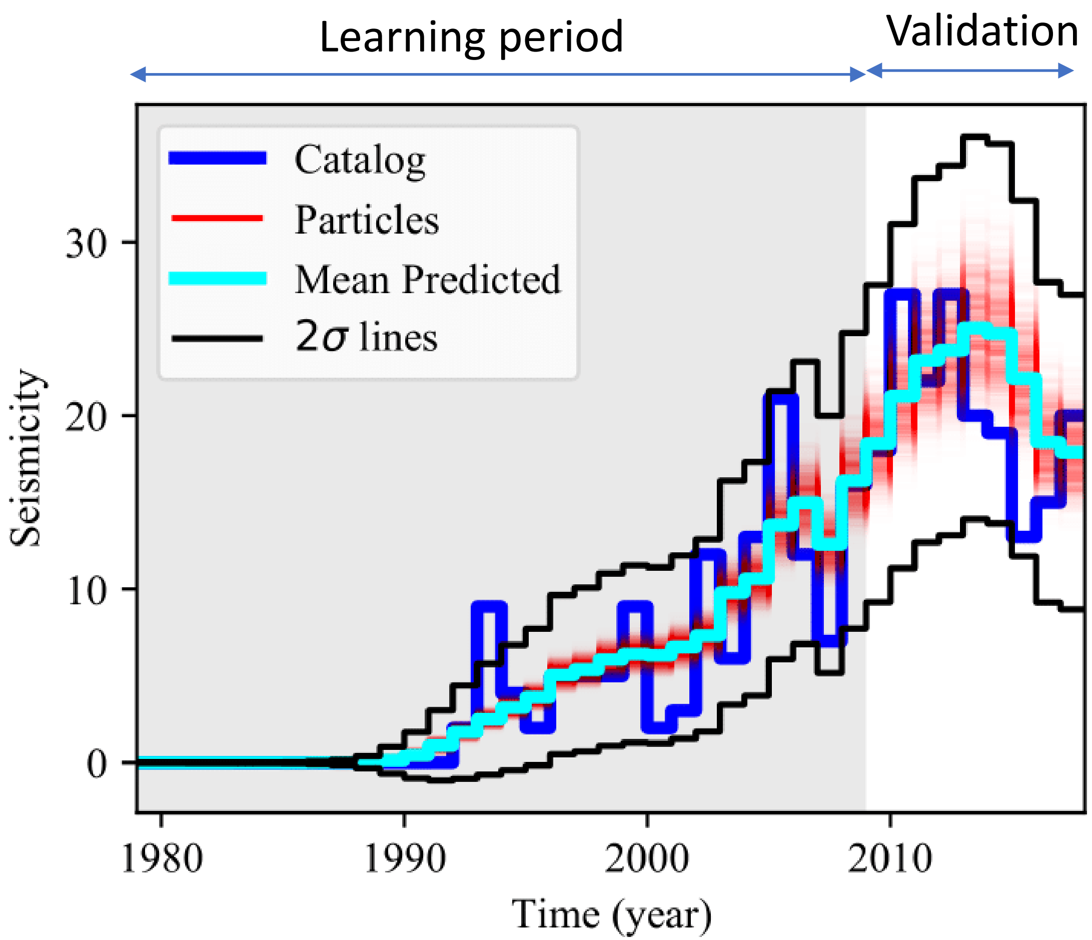

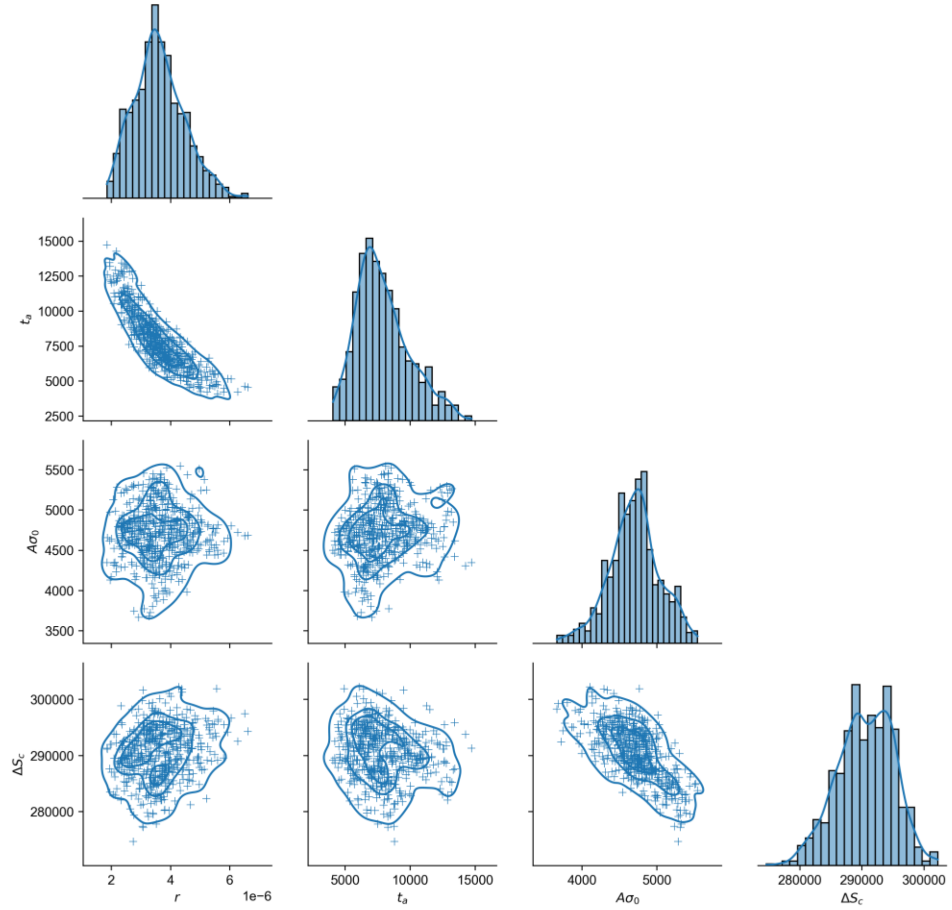

95% confidence interval accounts for:

- stochasticity of EQ occurrence (non-homogeneous Poisson process)
- uncertainties of the nucleation model (R&S + threshold)

Estimation of p(>M)

comparison with observed seismicity

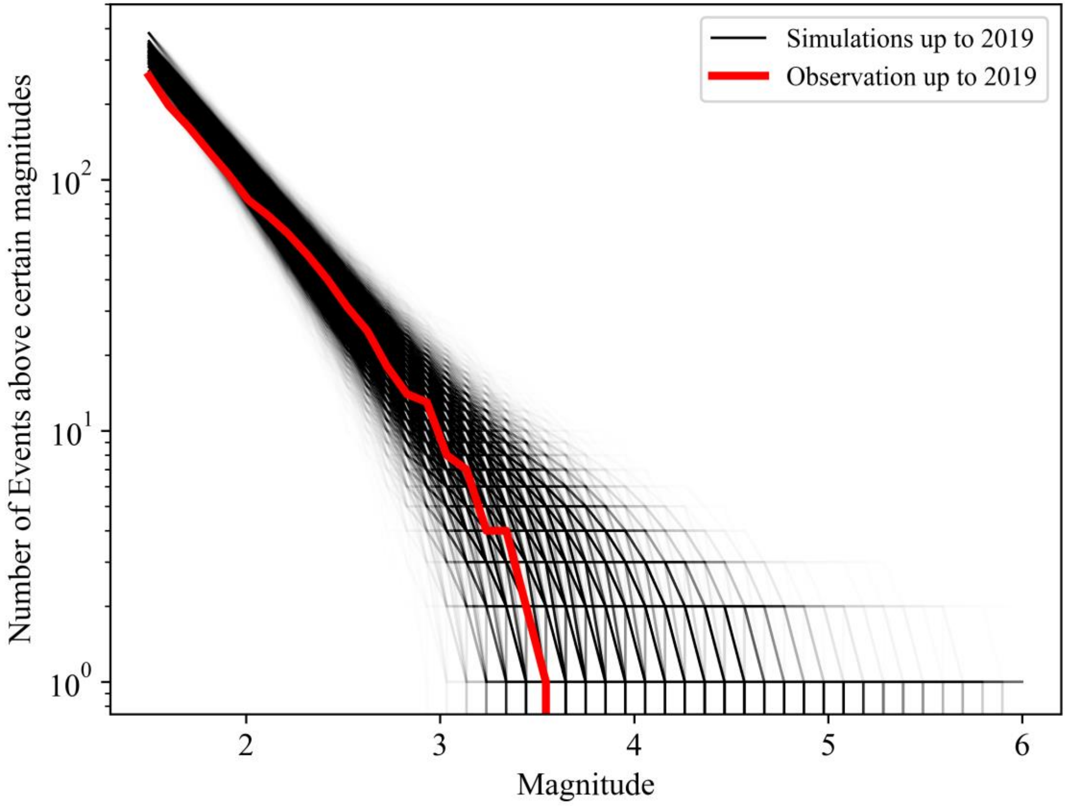

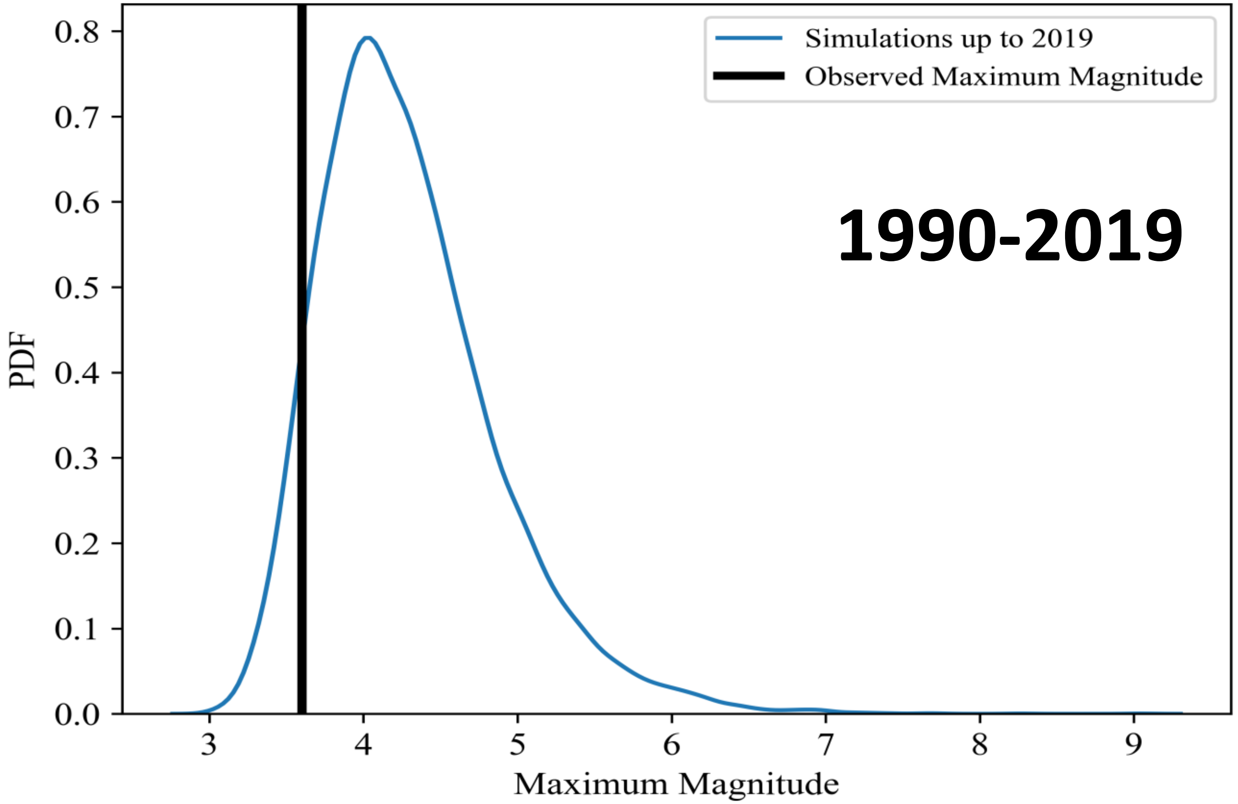

1990-2019

Estimation of p(>*M*)

Given an estimated number of Eqs, ***N***, at time *t*, and ***b***-value:

$$p(>M) = 1 - \left(1 - \frac{1}{N}10^{b(M-\widehat{M_{max}})}\right)^N$$

with $\widehat{M_{max}} = M_c + \frac{1}{b}log_{10}(N)\Big)$

Calculation assumes:

- Non-homogenous Poisson process
- iid distribution of magnitudes, assuming non truncated Gutenberg-Richter law

Calculation accounts for

- pdf of *b*-value
- pdf of predicted *N*
- pdf of EQ magnitudes

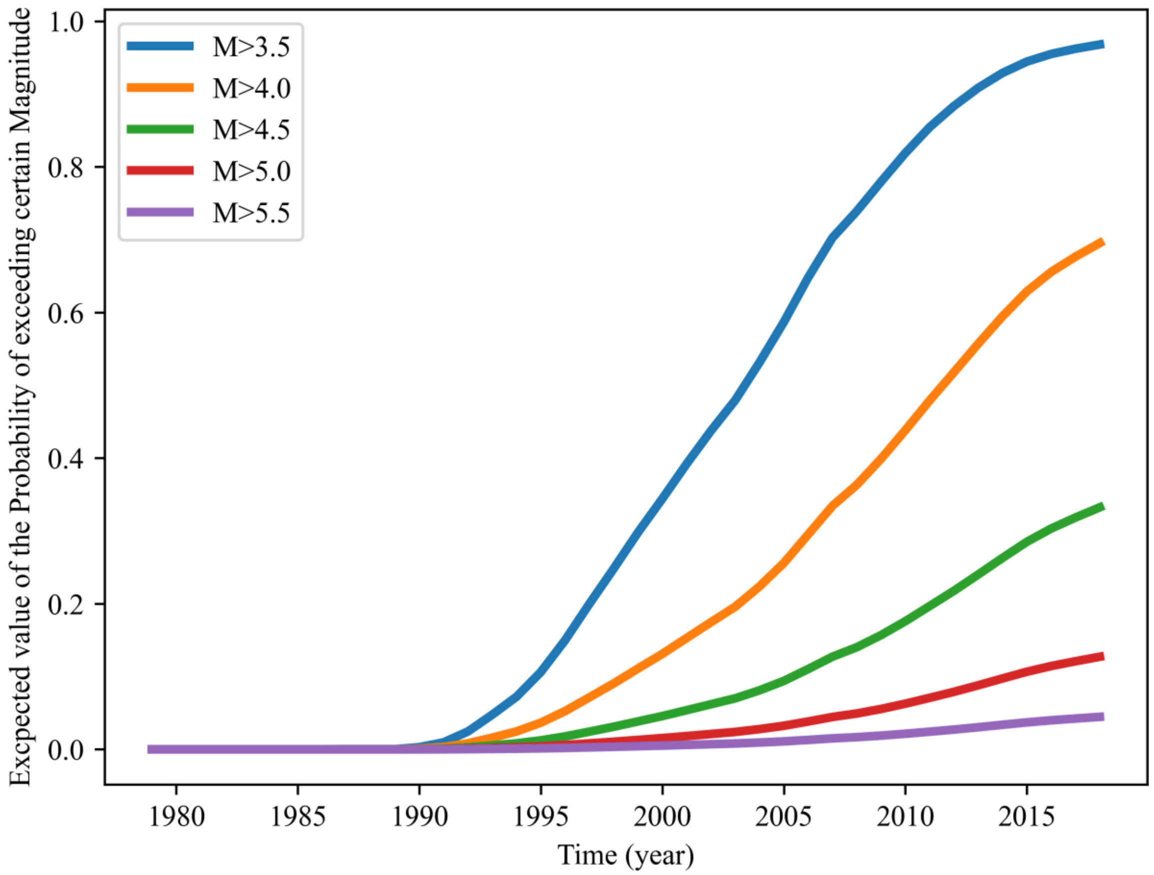

Prospective

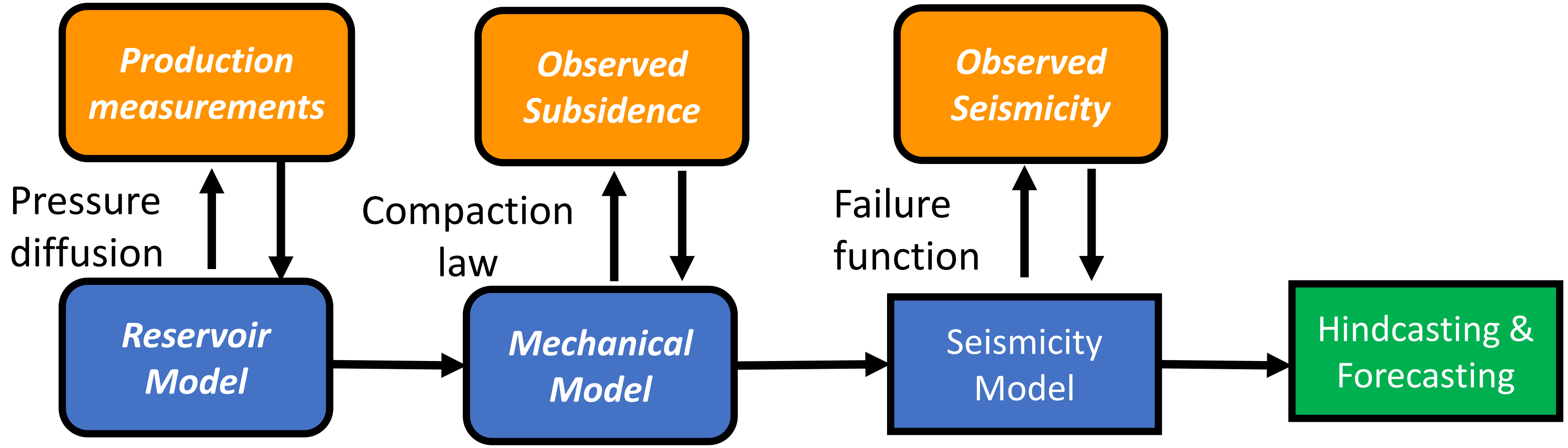

VFE reservoir modeling

(Meyer et al., GSL, in review)

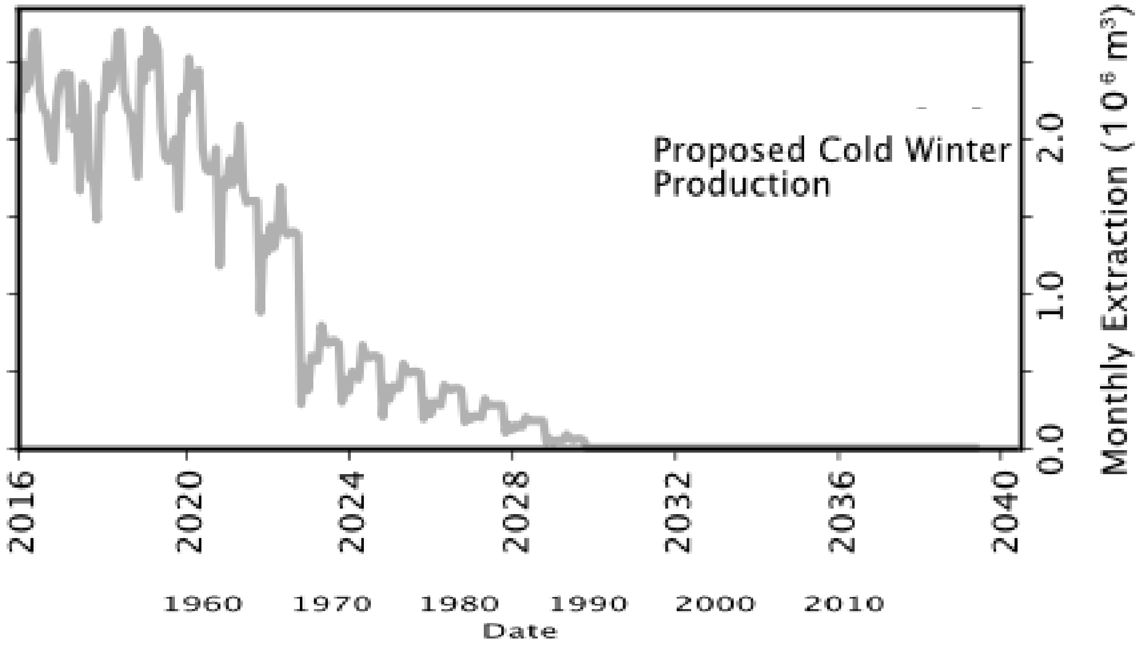

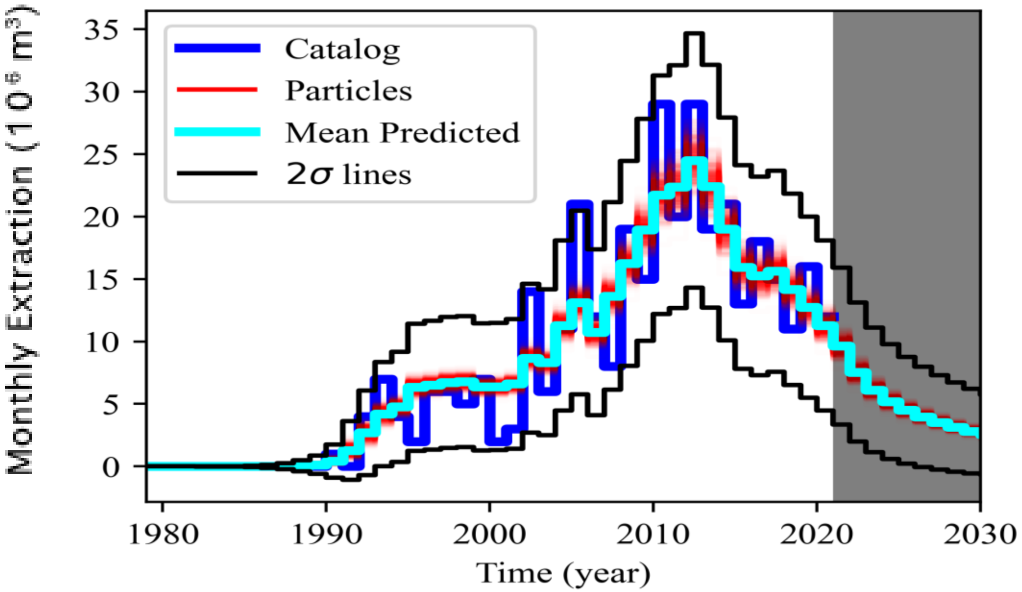

(Mateo Acosta and Hojjat Kaveh)

Prospective

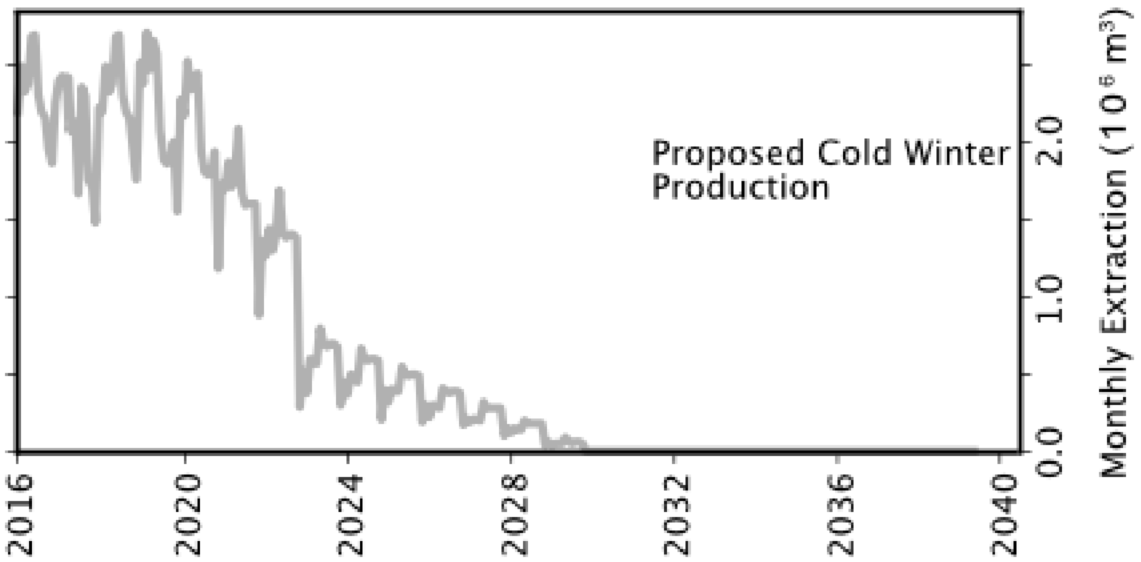

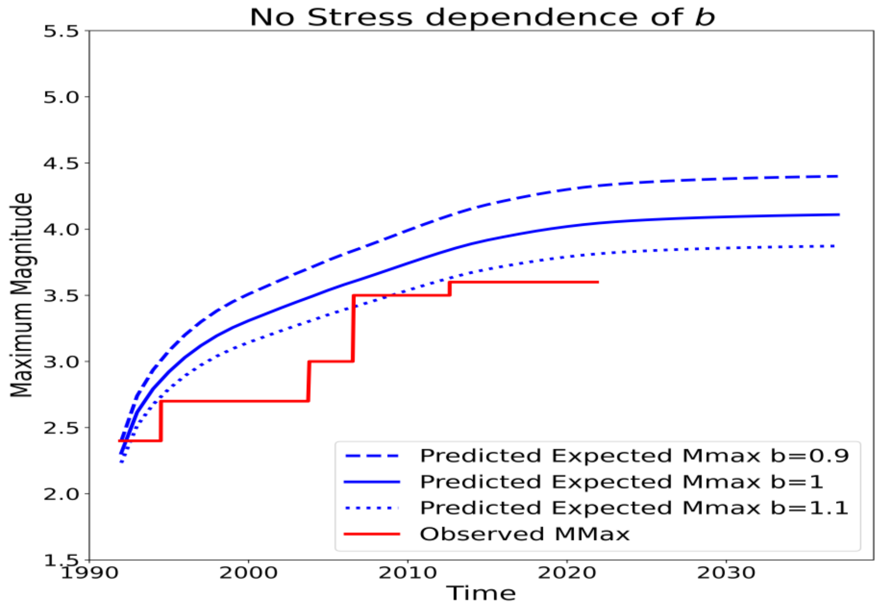

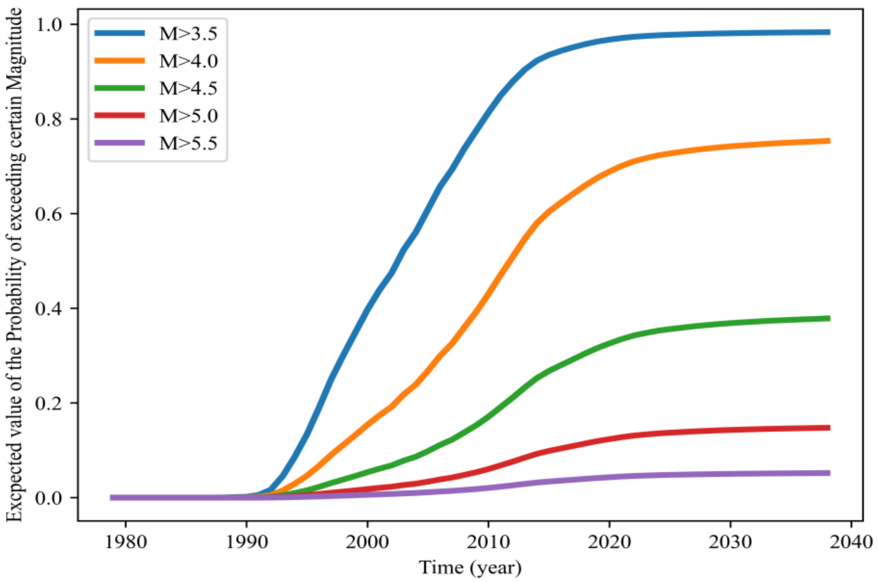

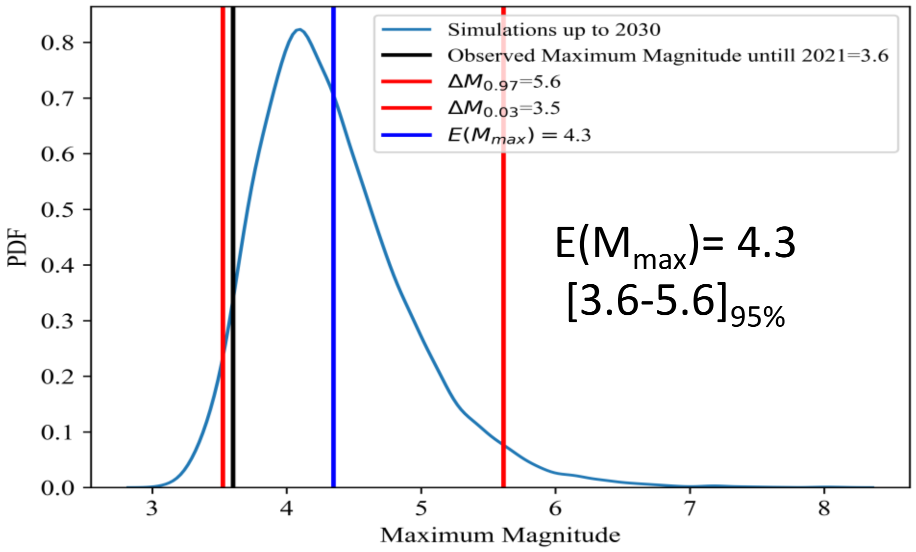

(Mateo Acosta and Hojjat Kaveh)

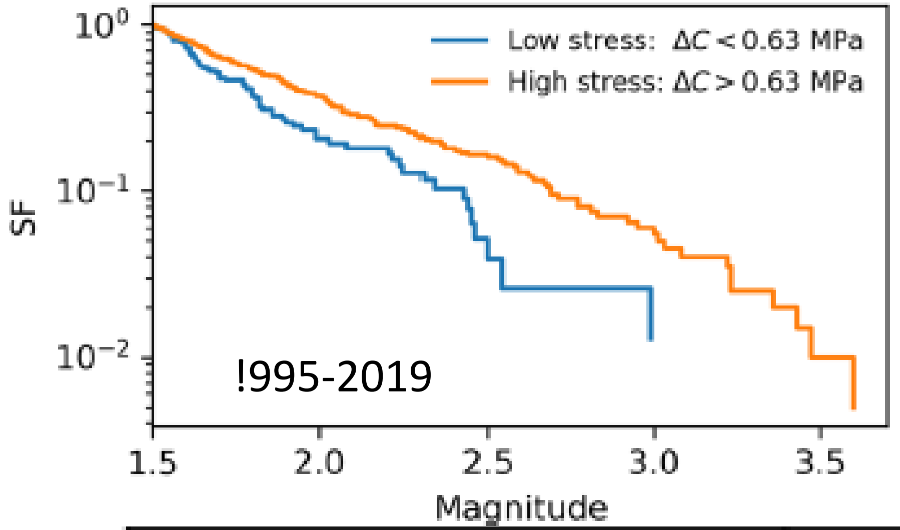

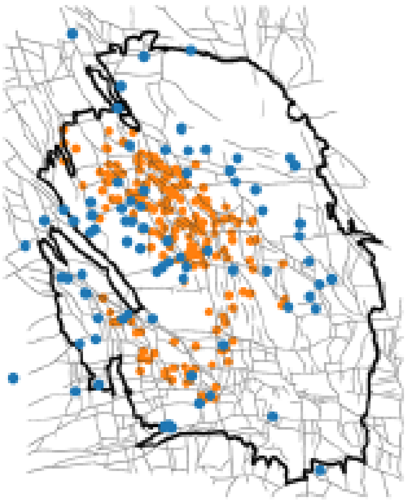

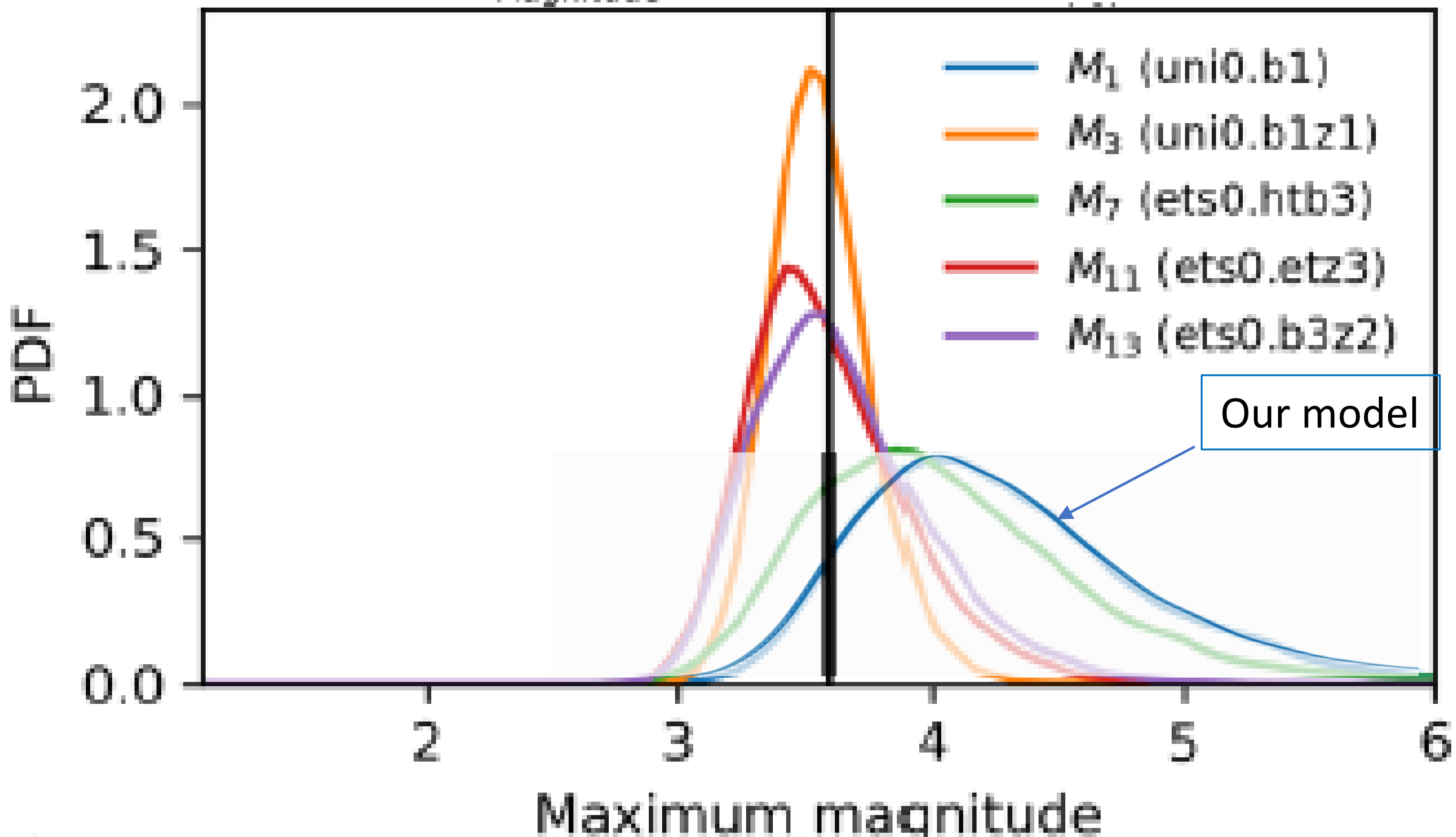

(Bourne and Oates, JGR, 2020)

Conclusions

- A computationally effective integrated model for probabilistic EQ forecasting:
  - A VFE reservoir model calibrated against production data.
  - Spatially variable compressibility calibrated against subsidence observations.
  - Spatially variable stress changes based on reservoir geometry
  - Time dependent EQ nucleation process, with stress threshold.
- Uncertainties on stress estimation, EQ nucleation and EQ stochastic properties can be included.
- Validation from comparison with historical seismicity data.
- E(M_{max}) seems overestimated (tapering? b-value change? estimation bias?)
- *Calibration yields 'effective parameters'.*
  -> forecast is valid as long as calibration conditions apply
- *Seismicity accounts for < 1/100 of the strain needed to explain surface deformation.*
  -> deformation is mostly aseismic. Earthquakes are most probably induced.
  -> the risk of triggered seismicity is not considered in our analysis.

References

- van der Elst, N.J., Page, M.T., Weiser, D.A., Goebel, T.H.W. & Hosseini, S.M., 2016. Induced earthquake magnitudes are as large as (statistically) expected, *Journal of Geophysical Research-Solid Earth,* 121**,** 4575-4590.
- Bourne, S.J. & Oates, S.J., 2017. Development of statistical geomechanical models for forecasting seismicity induced by gas production from the Groningen field, *Netherlands Journal of Geosciences-Geologie En Mijnbouw,* 96**,** S175-S182.
- Smith, J.D., Avouac, J.P., White, R.S., Copley, A., Gualandi, A. & Bourne, S., 2019. Reconciling the Long-Term Relationship Between Reservoir Pore Pressure Depletion and Compaction in the Groningen Region, *Journal of Geophysical Research-Solid Earth,* 124**,** 6165-6178.
- Candela, T., Osinga, S., Ampuero, J.P., Wassing, B., Pluymaekers, M., Fokker, P.A., van Wees, J.D., de Waal, H.A. & Muntendam-Bos, A.G., 2019. Depletion-Induced Seismicity at the Groningen Gas Field: Coulomb Rate-and-State Models Including Differential Compaction Effect, *Journal of Geophysical Research-Solid Earth,* 124**,** 7081-7104
- Smith, J.D., White, R.S., Avouac, J.P. & Bourne, S., 2020. Probabilistic earthquake locations of induced seismicity in the Groningen region, the Netherlands, *Geophysical Journal International,* 222**,** 507-516.
- van der Elst, N.J., 2021. B-Positive: A Robust Estimator of Aftershock Magnitude Distribution in Transiently Incomplete Catalogs, *Journal of Geophysical Research-Solid Earth,* 126
- Heimisson, E.R., Smith, J.D., Avouac, J.P. & Bourne, S.J., 2021. Coulomb threshold rate-and-state model for fault reactivation: application to induced seismicity at Groningen, *Geophysical Journal International,* 228**,** 2061-2072.
- Smith, J.D., Heimisson, E.R., Bourne, S. & Avouac, J.P., *in review,* Stress-based forecasting of induced seismicity with instantaneous earthquake failure functions: Applications to the Groningen Gas Reservoir, *Earth and Planetary Science Letters*
- Meyer, H., Smith, J.D., Bourne, S.J., & Avouac, J.P., *in review,* A integrated framework for surface deformation modeling and induced seismicity forecasting due to reservoir operations, Geol. Soc. Lond., Lyell Collection, in review.

BACK UP SLIDES

An integrated framework for stress-based earthquake forecasting

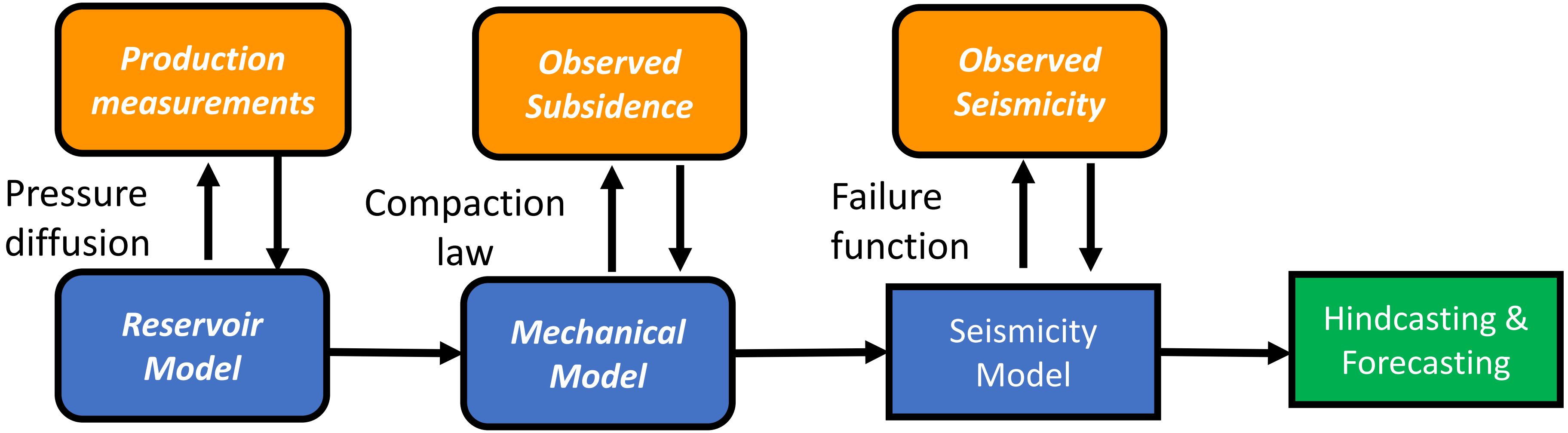

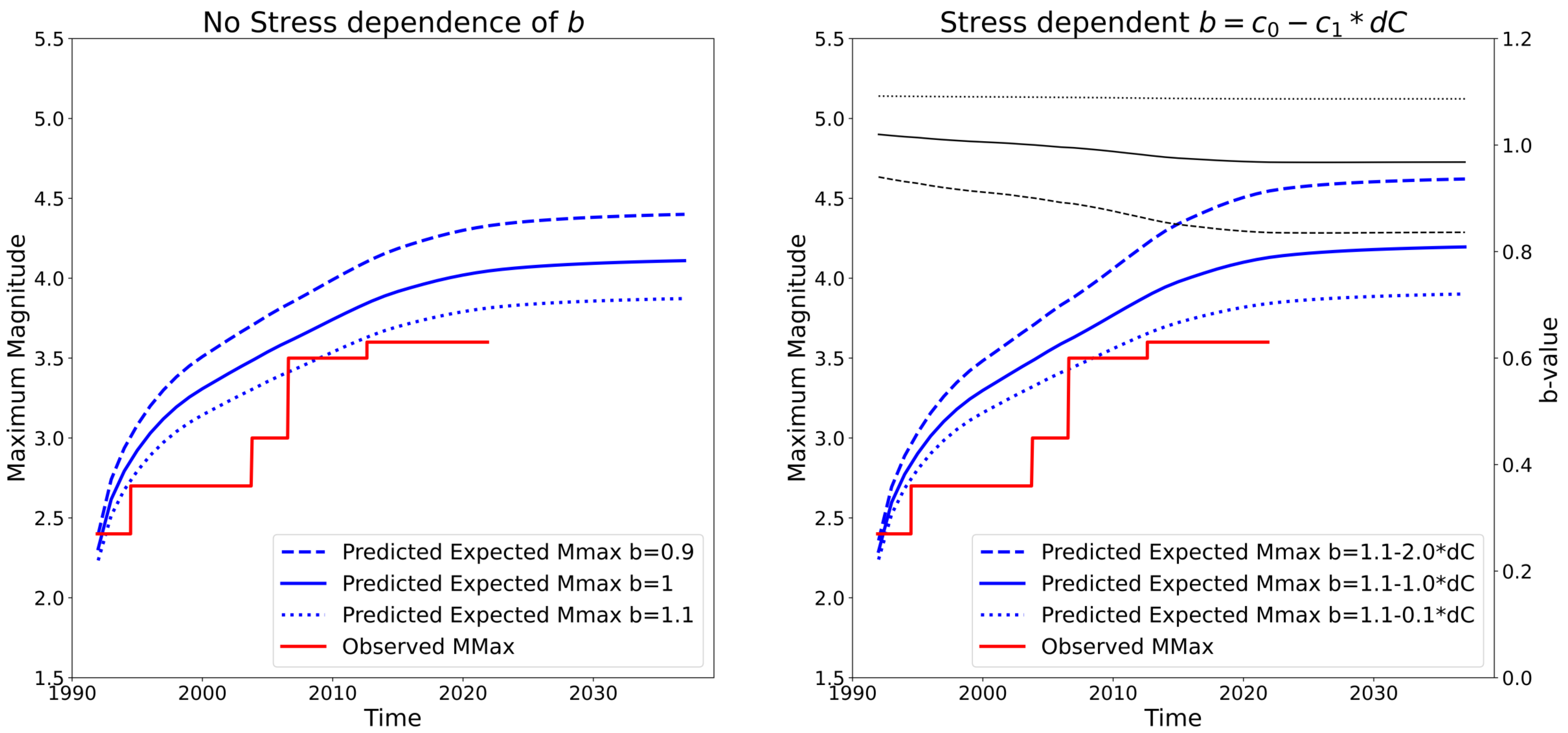

(Mateo Acosta)

VFE Reservoir Modeling

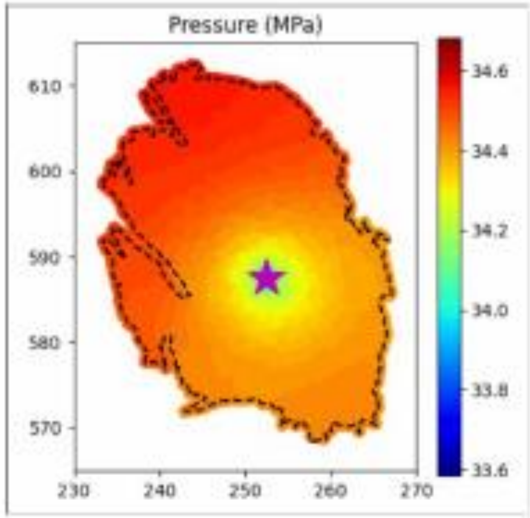

Pressure diffusion

- Vertical Flow Equilibrium (VFE):

Along depth diffusion can be neglected if:

$$R_L = \left(\frac{\Delta x}{\Delta z}\right) \cdot \left(\frac{k_z}{k_x}\right)^{1/2} > 10$$

with Δx the reservoir's horizontal length, Δz the reservoir's thickness, k_x, k_z the horizontal and vertical permeabilities respectively.

In our case, $R_L > 117$, so the 3D problem can be simulated in 2D, allowing computational efficiency.

- $k_x = k$, porosity (ϕ), and gas saturation ($^{gas}_{sat}$) are spatially averaged parameters calibrated with history matching.

- *Fenics* used to solve:

$$\phi \frac{\partial \rho}{\partial p} \cdot \frac{\partial p(x,y,t)}{\partial t} - \nabla\left(\rho \frac{k}{\mu} \nabla p(x,y,t)\right) = \frac{Q(x,y,t)}{^{gas}_{sat} \cdot \Delta z(x,y)}$$

with ρ = fluid density, p = fluid pressure, μ = fluid viscosity, and Q = volumetric flow rate.

(Meyer et al., GSL, in review)

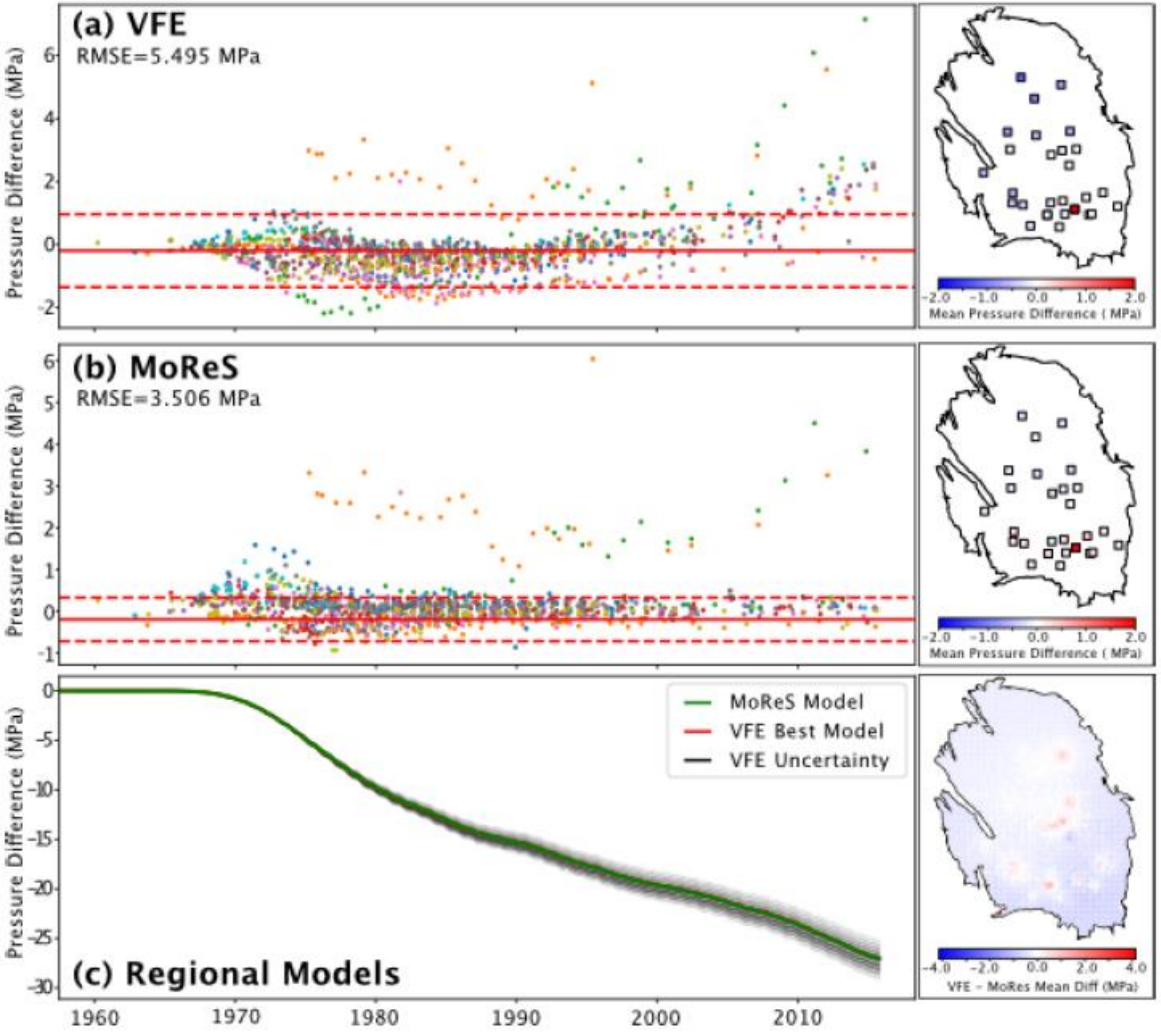

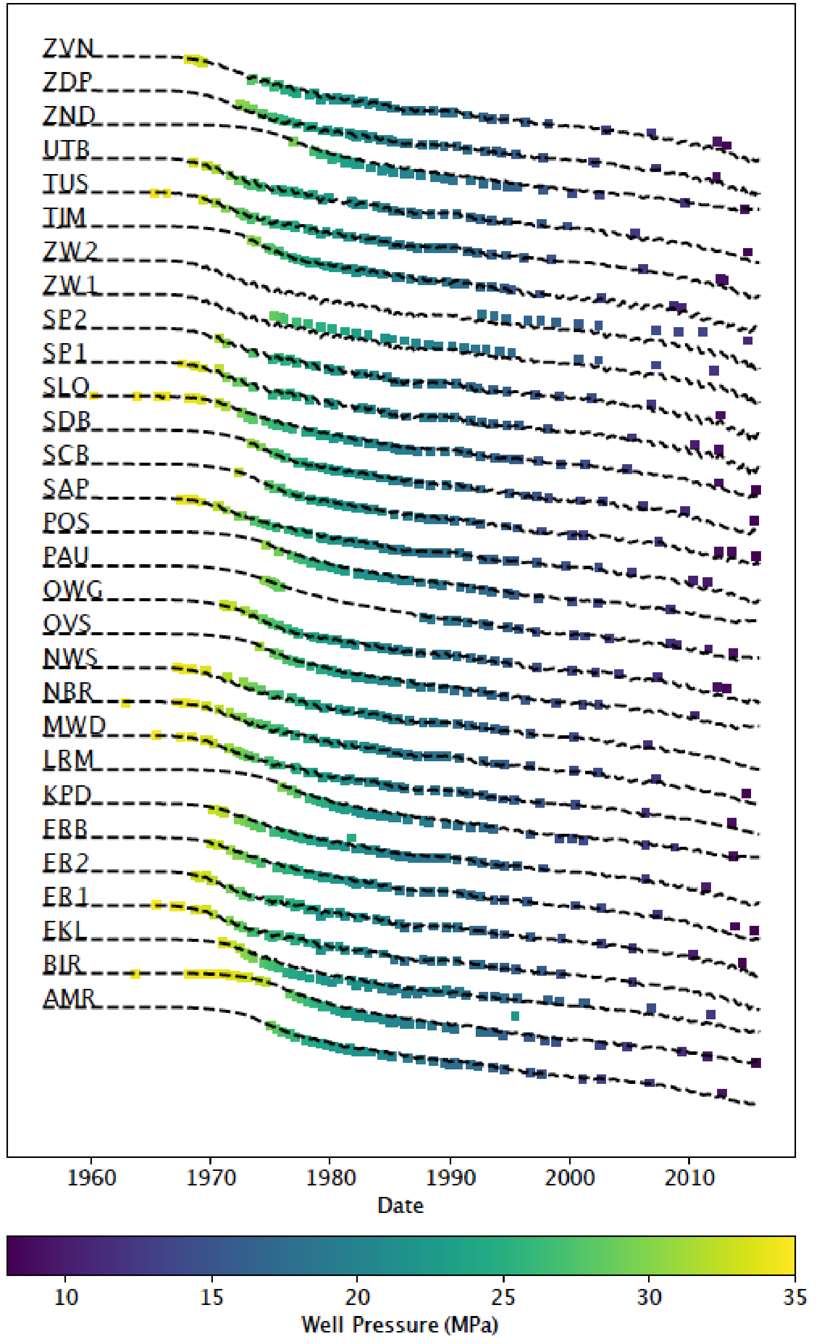

Parameter	Minimum	Maximum	Separation	MAP Value	Standard Deviation
Permeability (m^2)	1×10^{-13}	4.0×10^{-13}	1×10^{-14}	3.1×10^{-13}	6.78×10^{-14}
Porosity	0.1	0.2	0.005	0.185	0.0165
Gas Saturation	0.24	0.35	0.005	0.27	0.0268

(Meyer et al., GSL, in review)

VFE Reservoir Modeling

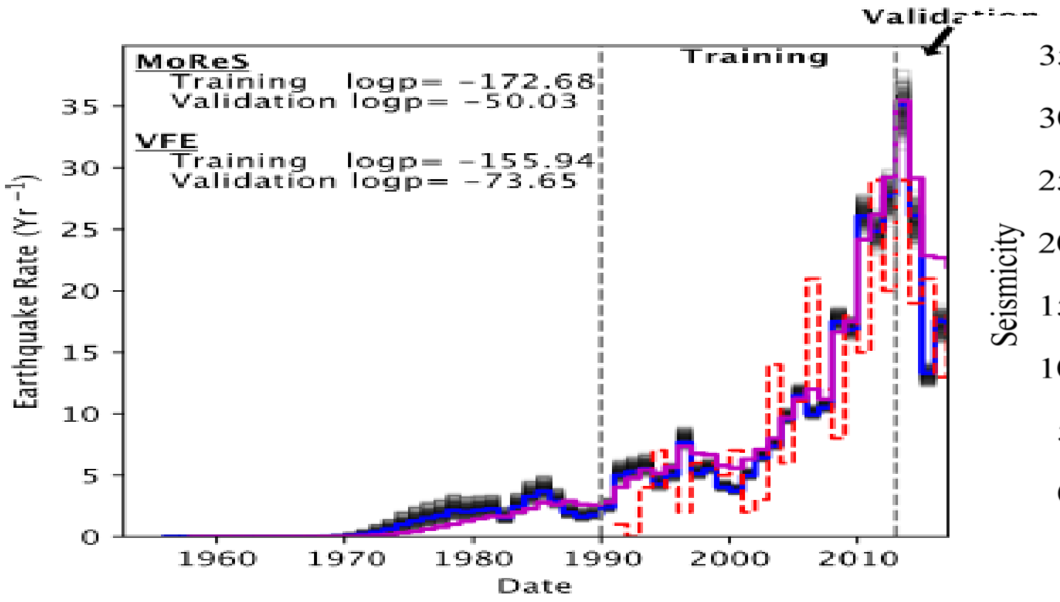

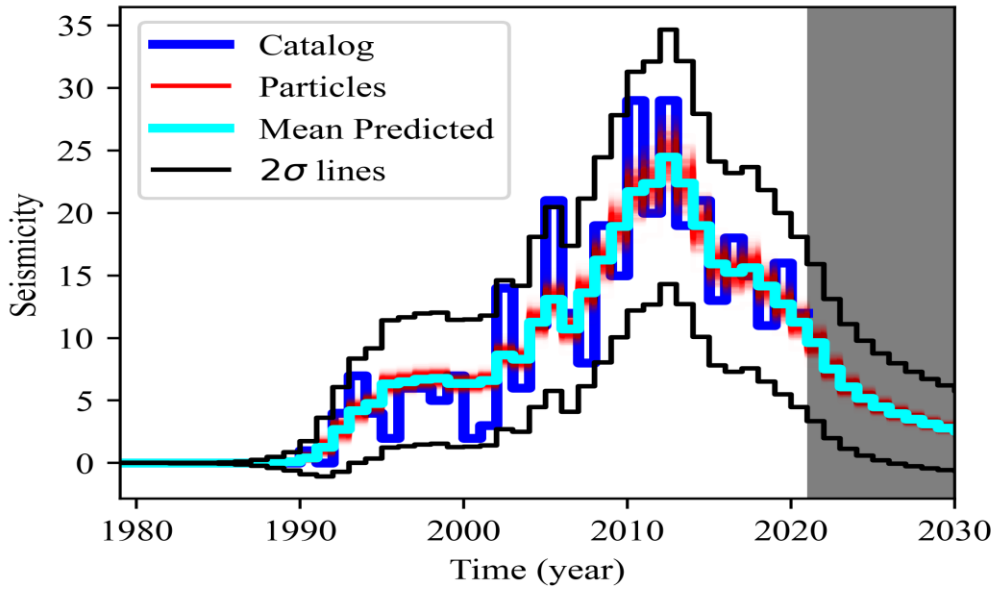

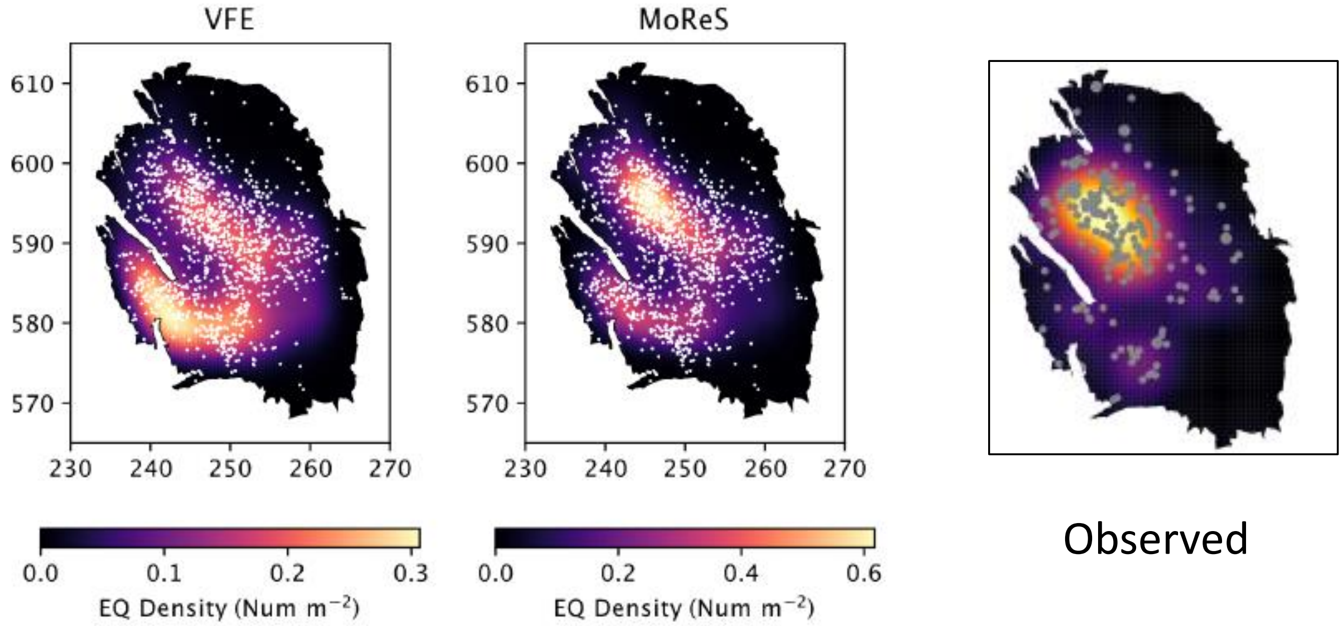

Observed

(Meyer et al., GSL, in review)

(Mateo Acosta and Hojjat Kaveh)

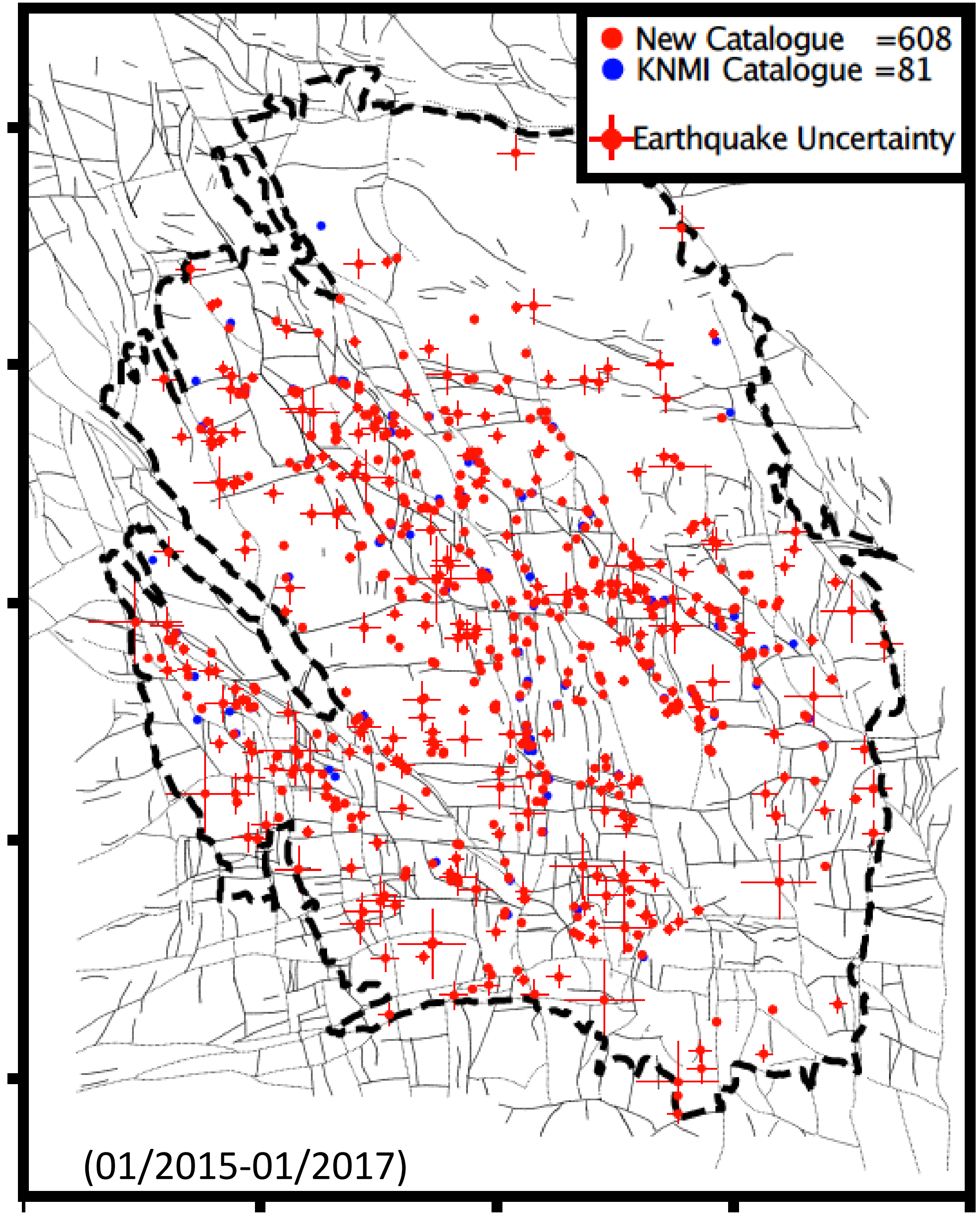
New Catalogue =608
KNMI Catalogue =81
Earthquake Uncertainty
(01/2015-01/2017)

VFE Reservoir Modeling

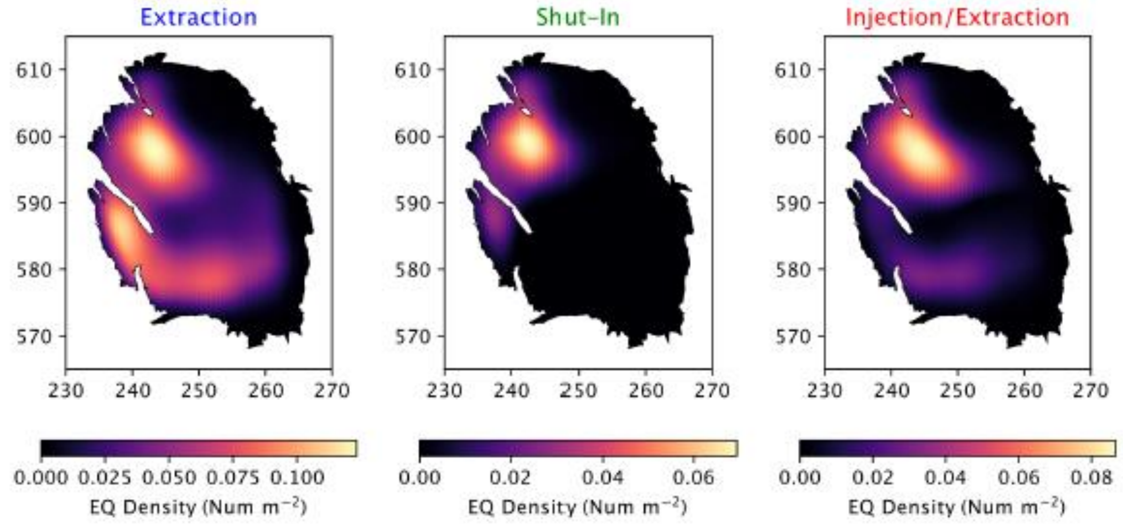

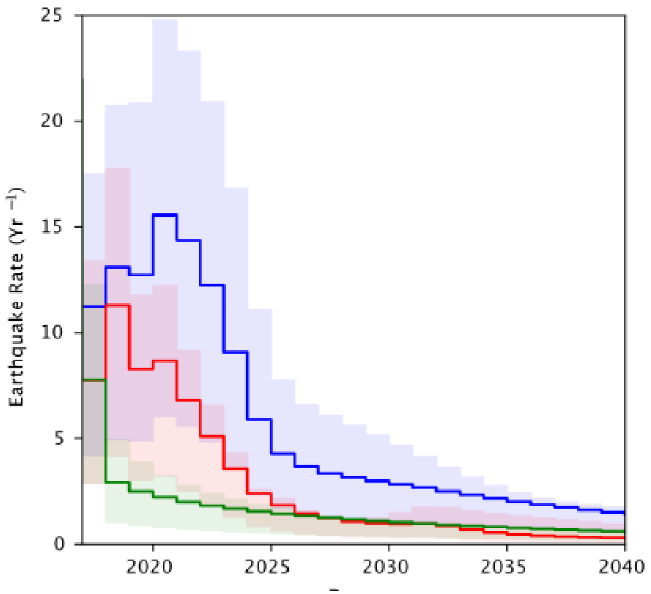

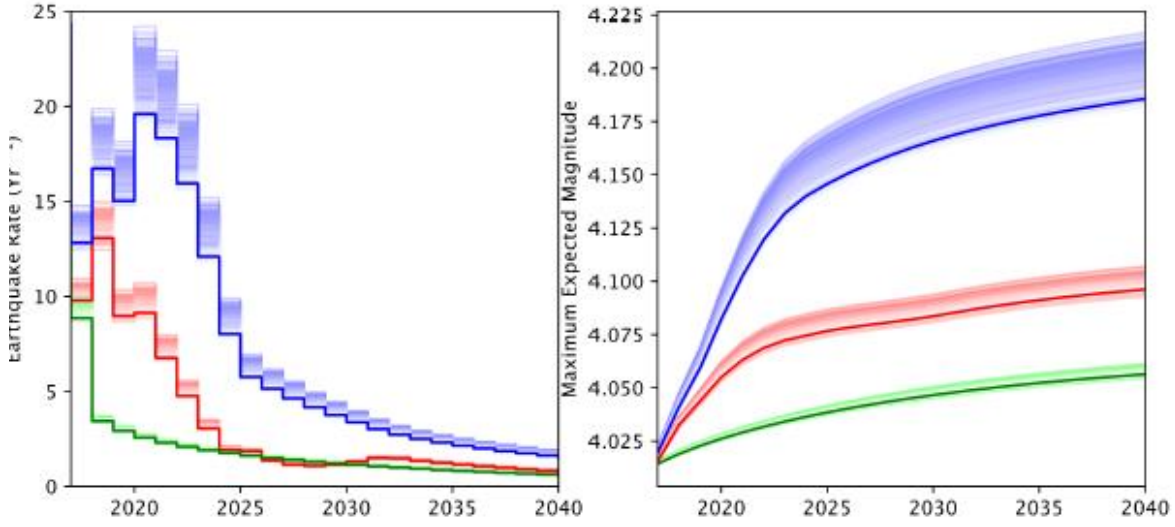

Uncertainies from reservoir modeling

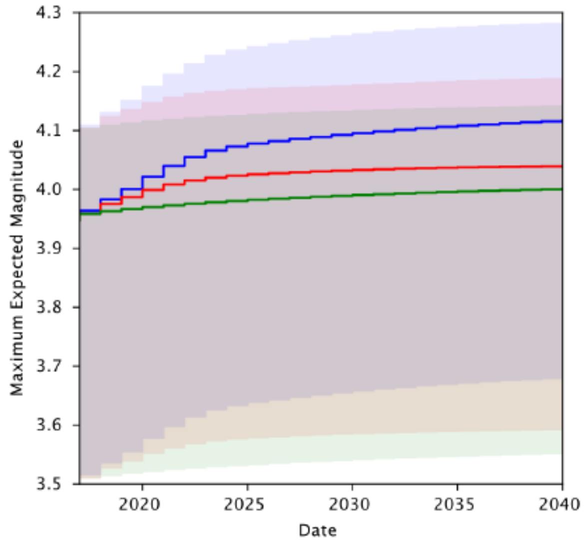

+ Uncertainies from Poisson process

(Meyer et al., GSL, in review)

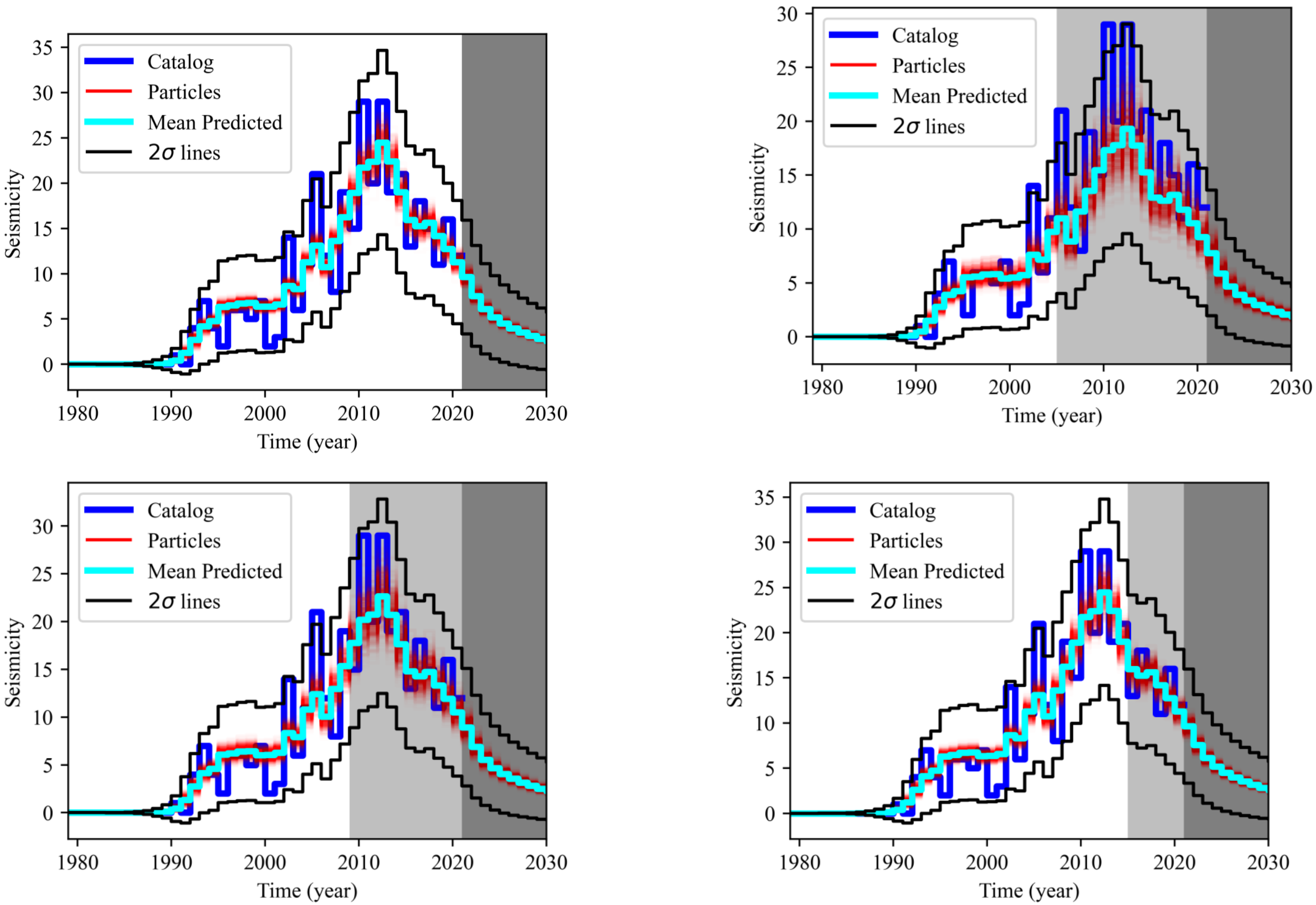

(Hojjat Kaveh)

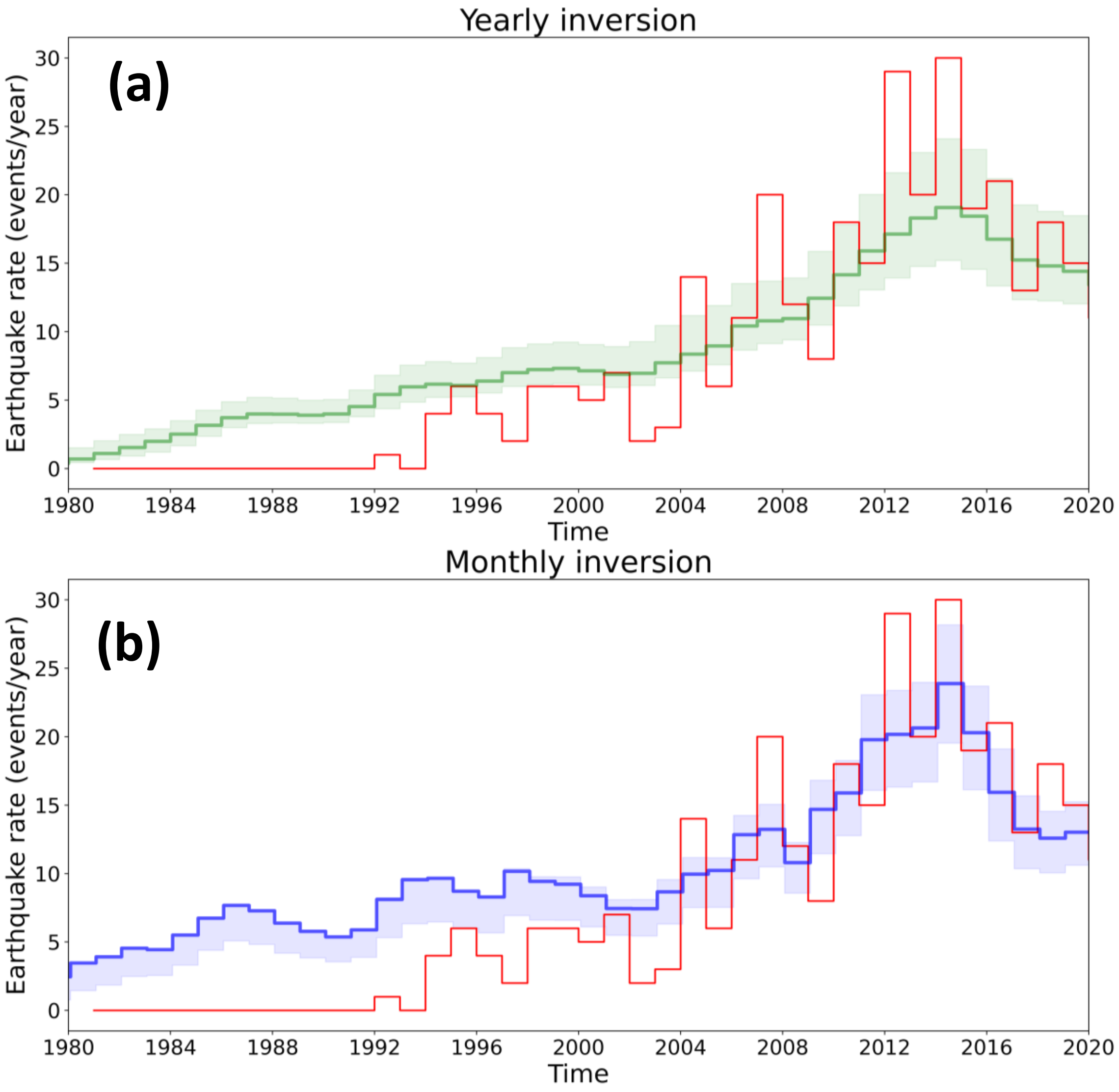

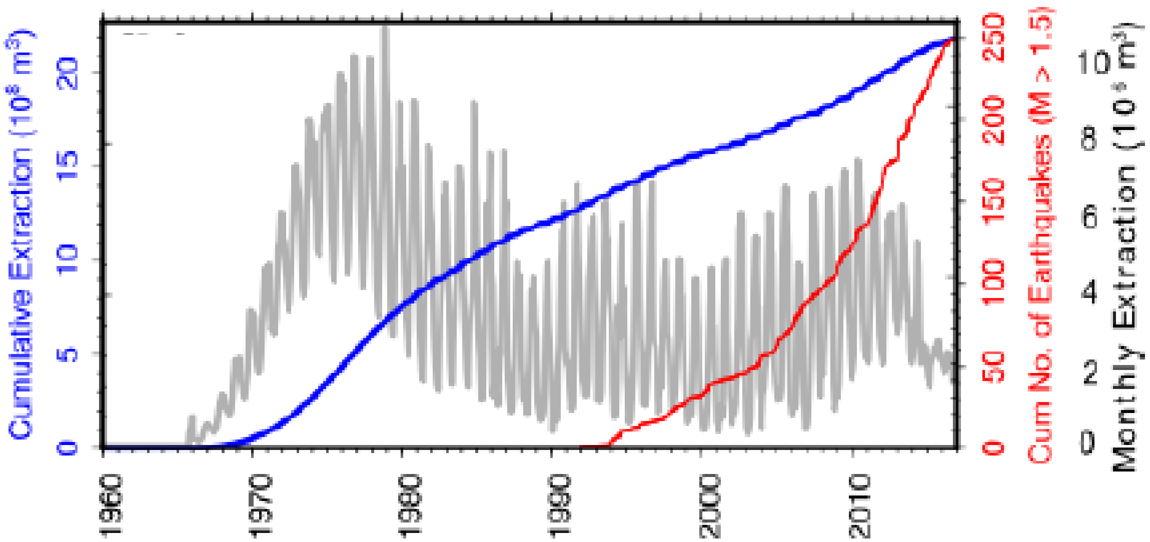

Inversion of seismicity rates using

(a) yearly averaged data (e.g. no seasonal variations),

(b) Monthly averaged data.

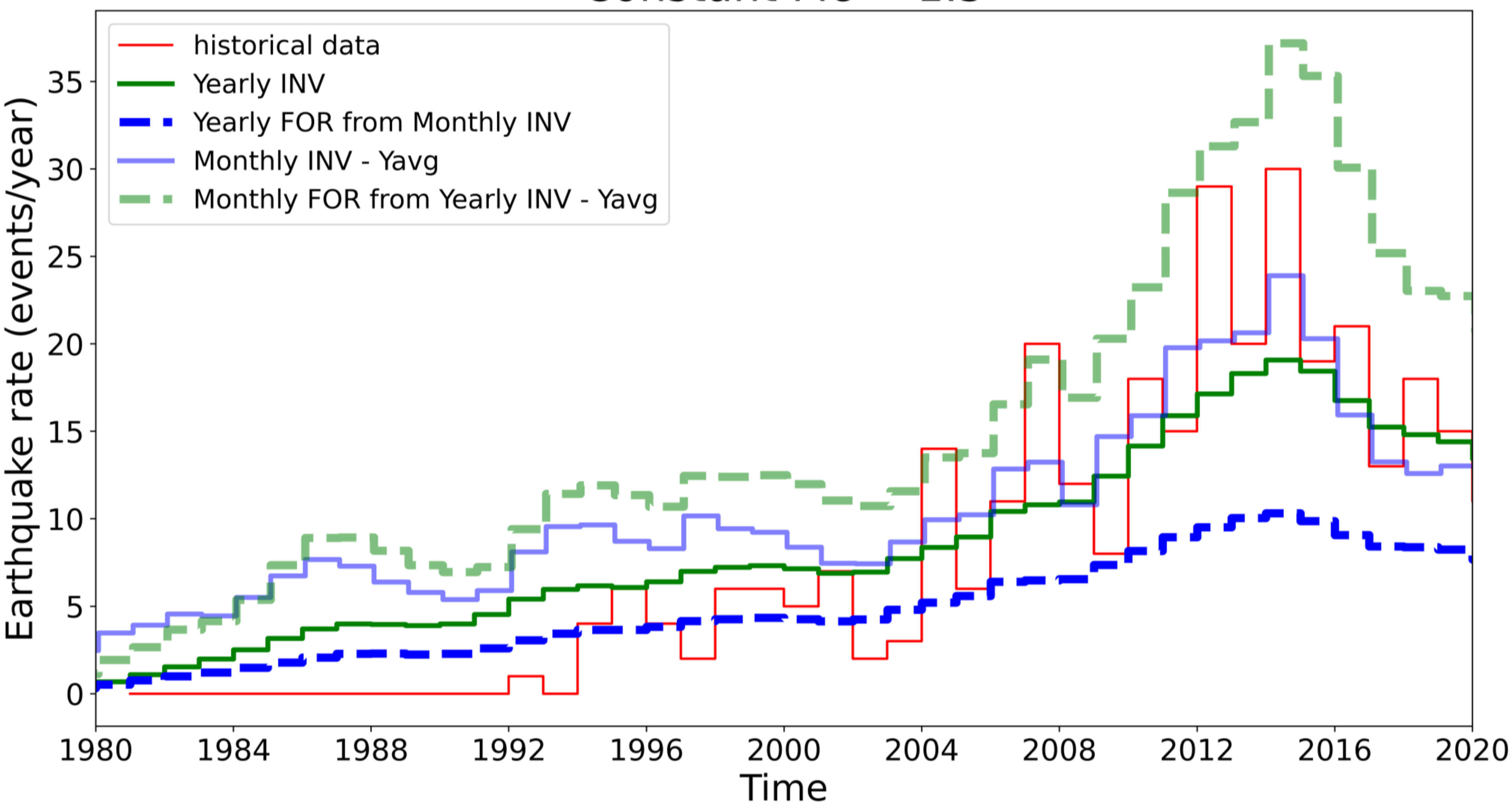

-> Prediction based on monthly rates with parameters derived from yearly inversion (dashed blue line) overestimates the data by 50%+ .

-> Prediction based on yearly rates with parameters derived from monthly inversion (dashed blue line underestimates the data by 50%+.

(Mateo Acosta)

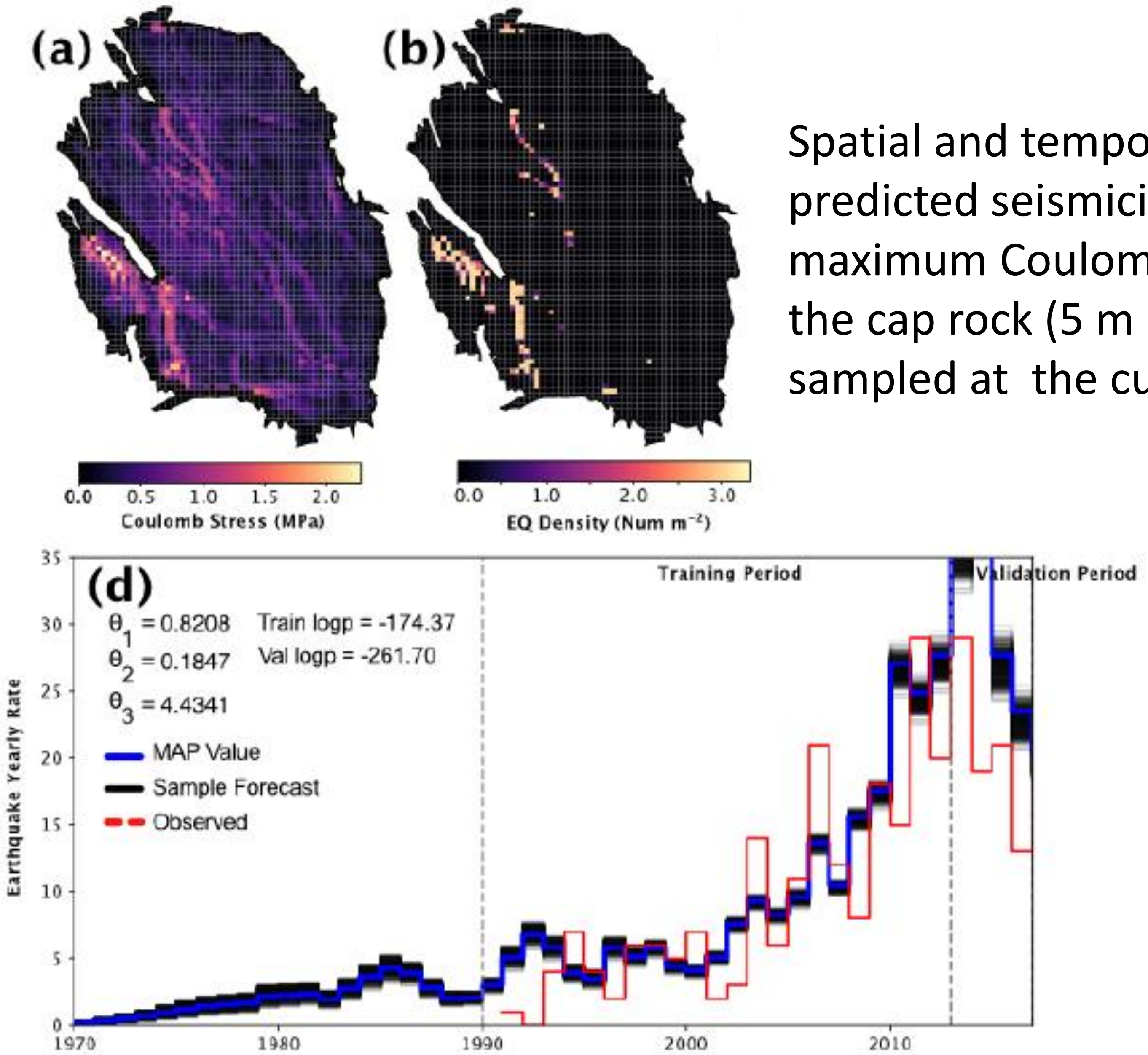

Spatial and temporal variations of predicted seismicity rate based on the maximum Coulomb stress calculated in the cap rock (5 m above reservoir) and sampled at the cuboid centers

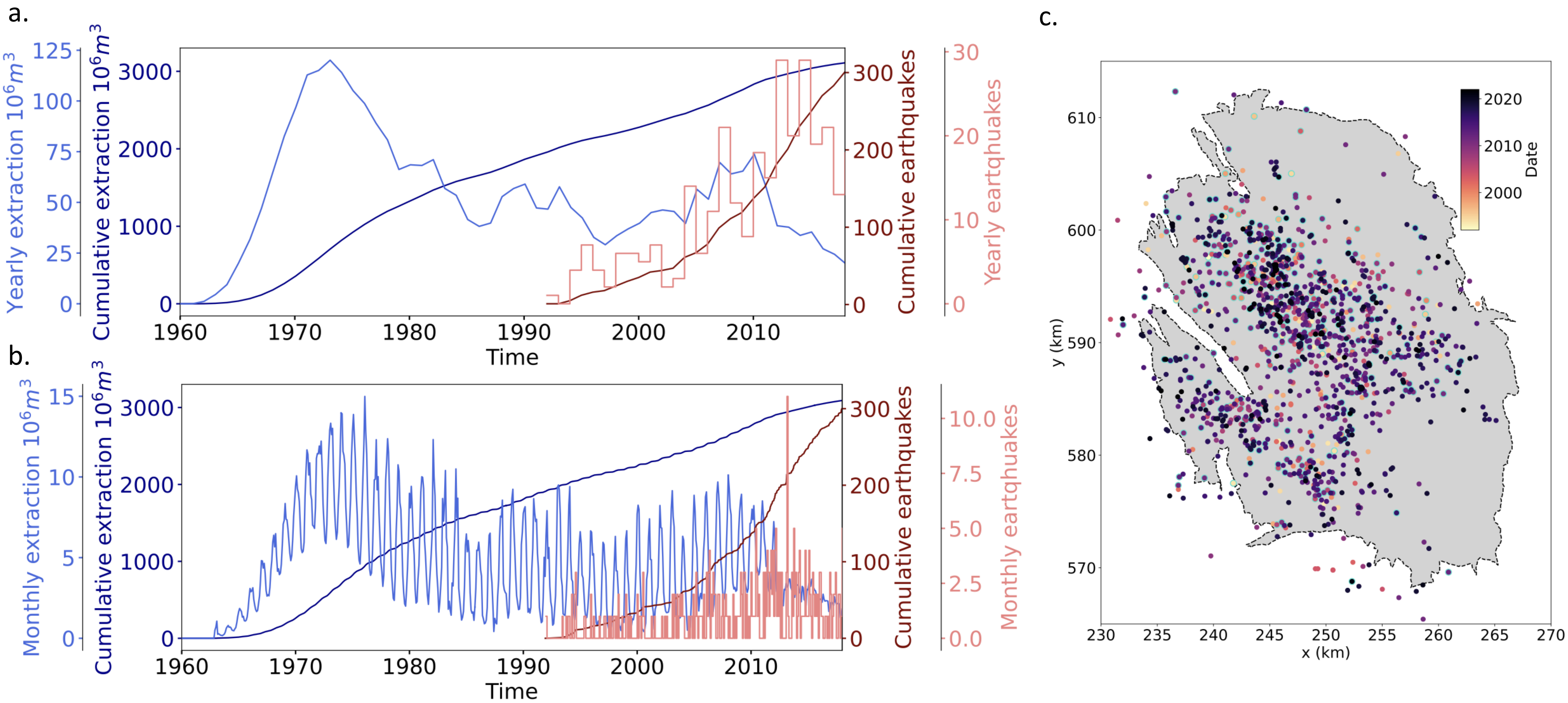

Historic extraction and seismicity. a. Yearly averaged data, extraction rates (light blue), cumulative extraction (dark blue), seismicity rates for M>1.5 (light red), cumulative number of earthquakes with M>1.5 (dark red). b. Monthly averaged data. Same as panel a. c. Top view of the reservoir with all events with M>0 color coded by date. Events with M>1.5 have light blue marker edges. The Catalog is from KNMI.

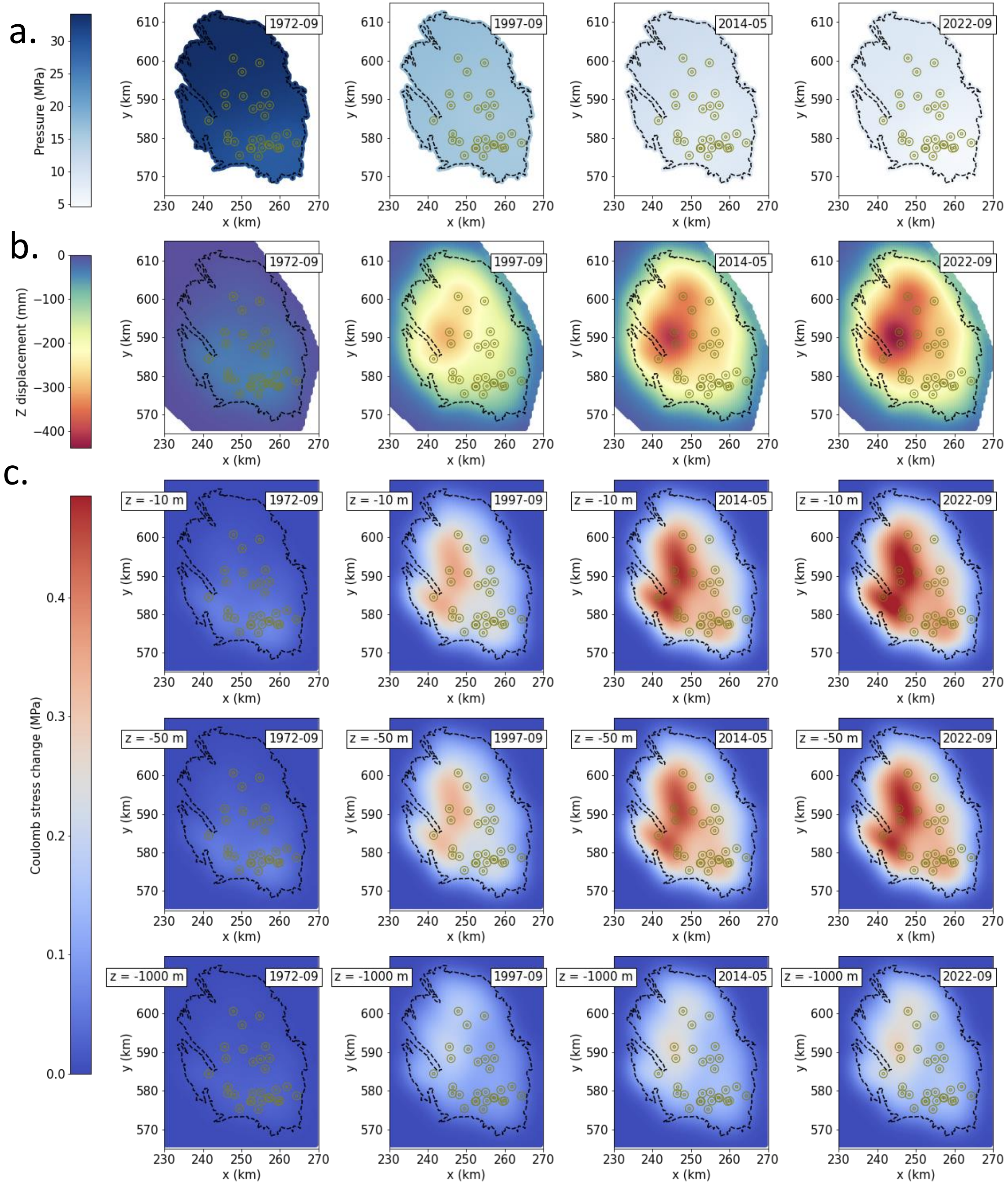

Simulation results using the model of Smith et al., 2019; 2022; and Meyer et al., 2022. a-c. Top view of the reservoir snapshots of different fields over time. a. Fluid pressure simulation. b. Calculated surface subsidence. c. Coulomb stress changes calculated at different depths over the reservoir.

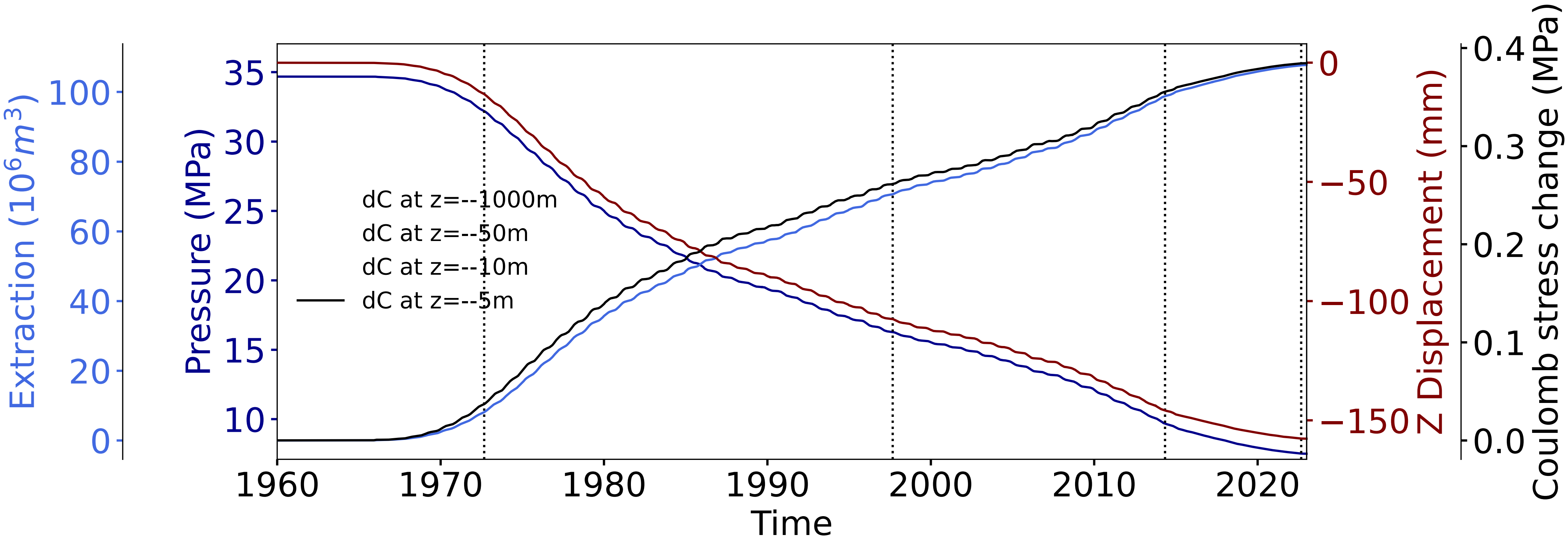

Simulation results using the model of Smith et al., 2019; 2022; and Meyer et al., 2022. a. Evolution of averaged values in the reservoir over time. Cumulative extraction (light blue), Fluid pressure (dark blue), Surface subsidence (red), Coulomb stress changes at different depths in the reservoir (black and gray curves).

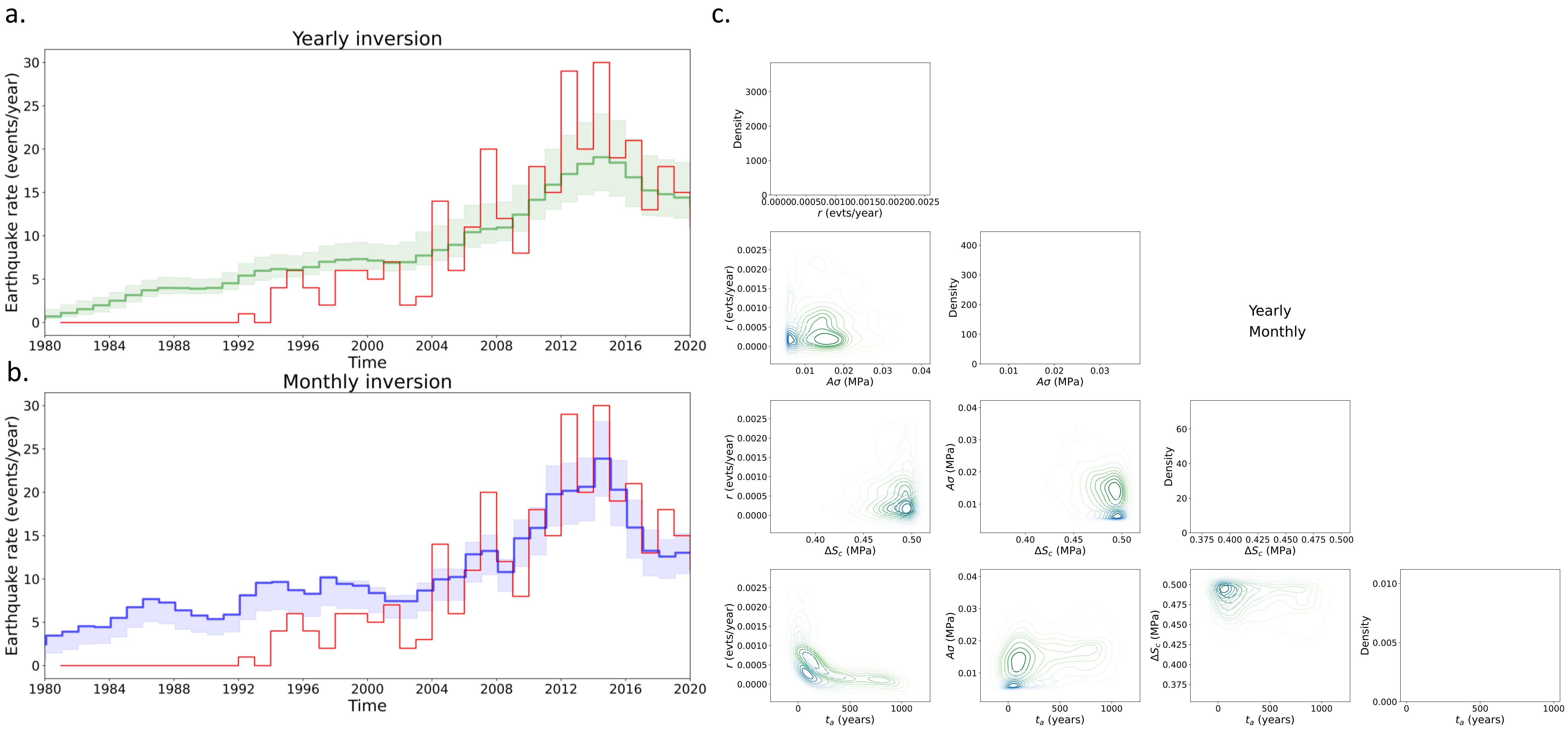

Inversion of seismicity rates using (a.) Yearly averaged data, e.g. no seasonal variations, (b.) Monthly averaged data. c. sows the parameter spaces for the range of models presented in a and b.

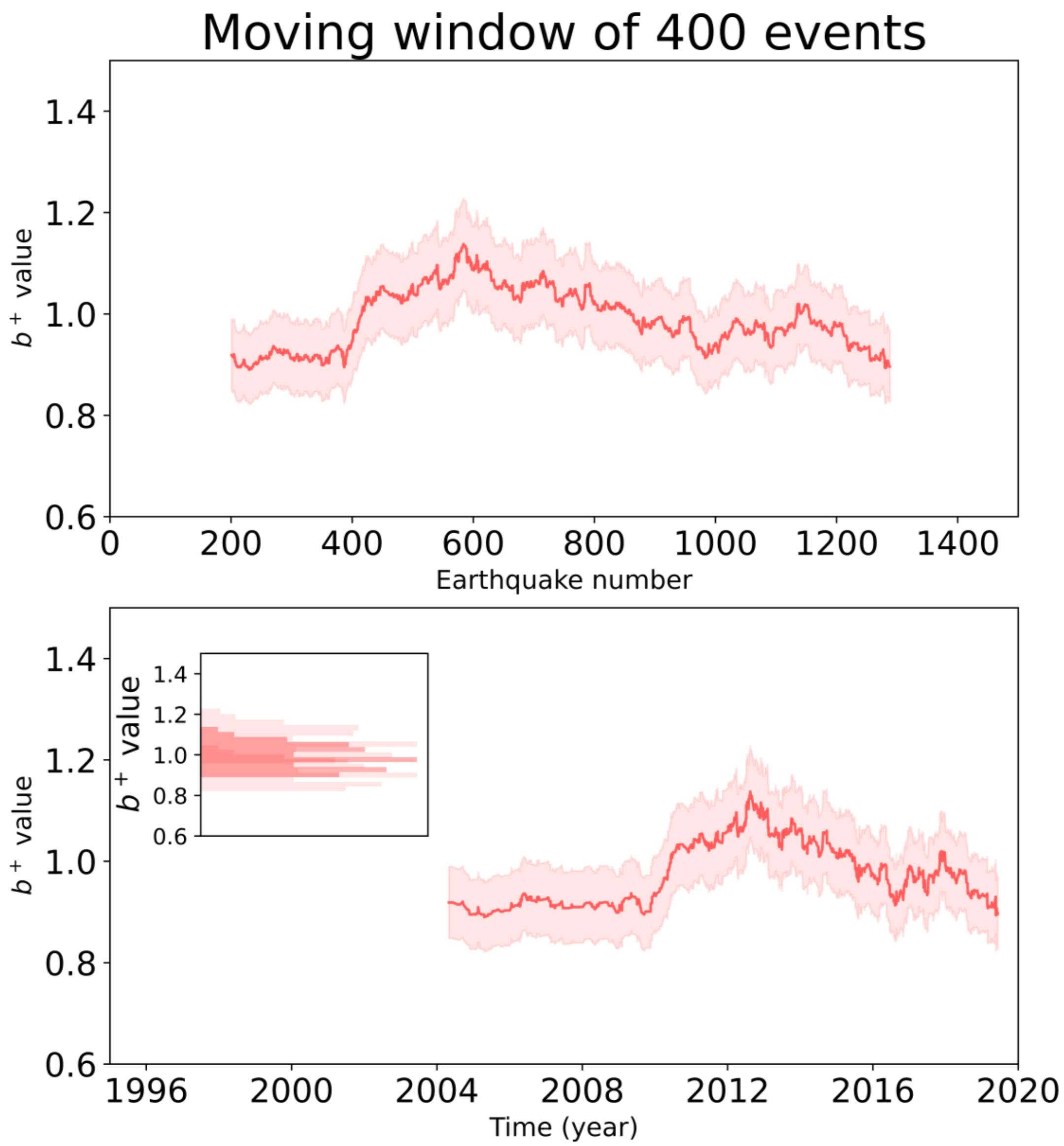

b-positive analysis of the KNMI catalog (from Van-der-Elst, 2021). Top panel shows b-positive for all the events in the catalog function of the total number of events in the KNMI catalog. Bottom panel shows it over time. green and red shaded areas show the uncertainty in the estimation of b-positive. The histograms of b-positive values are shown as insets.

a.

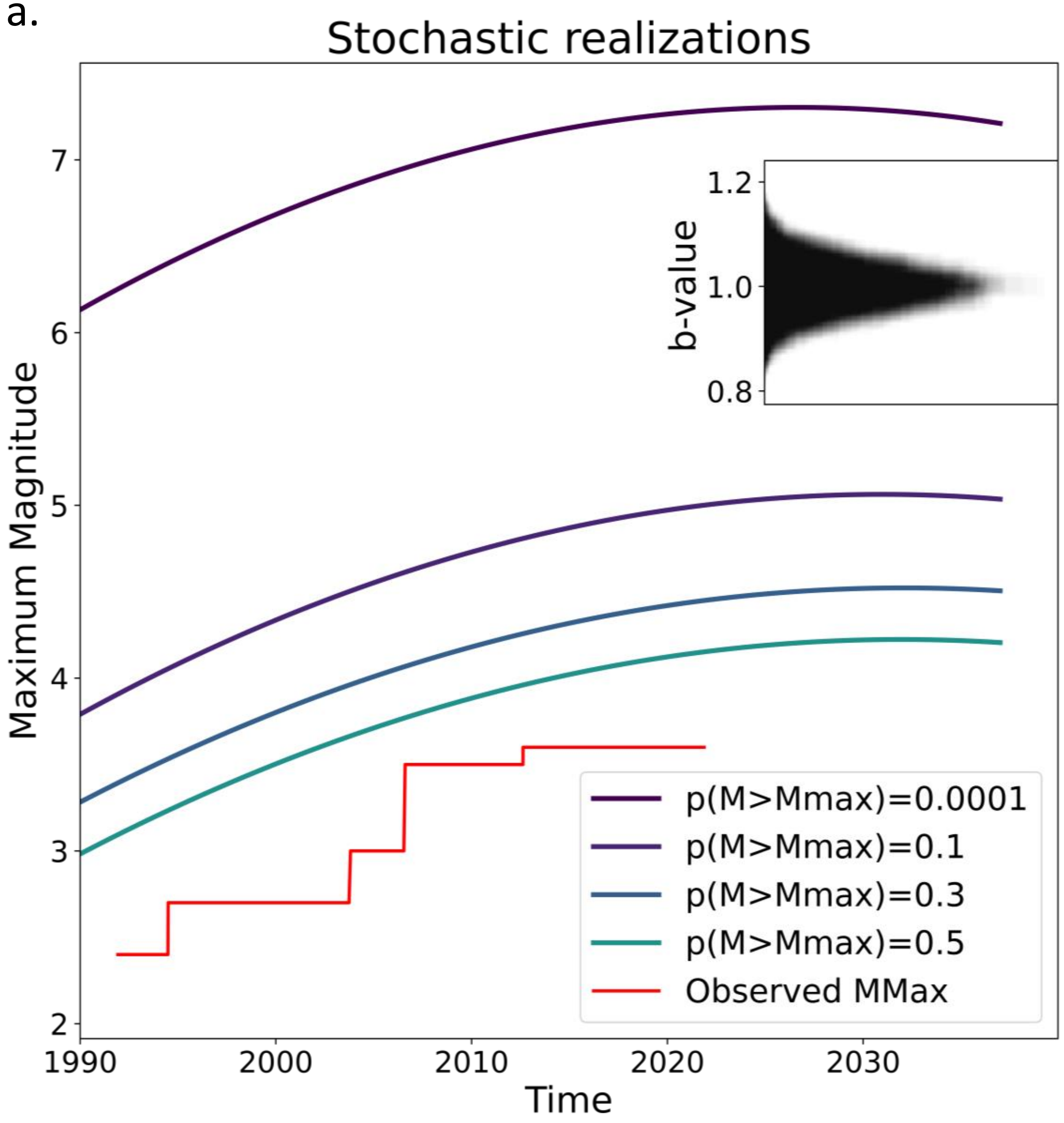

b.

a. Estmation of the maximum magnitude using stochastic realizations of synthetic catalogs with a gaussian distribution of b-values (shown in inset), for a given probability level. b. Probability of exceedance of a given Magnitude (M=4; M=5, M=6) over time using stochastic realizations of synthetic catalogs with a gaussian distribution of b-values. Colors represent density of realizations.

- The cumulated moment released by seismicity accounts for less than 1/100 of the strain needed to explain surface deformation.

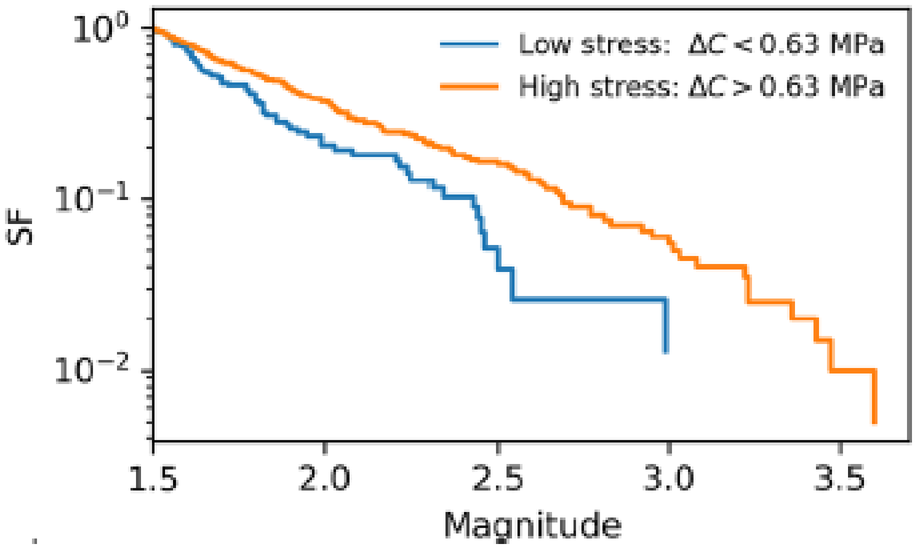

Low stress: $\Delta C < 0.63$ MPa
High stress: $\Delta C > 0.63$ MPa
SF
10^0
10^{-1}
10^{-2}
1.5
2.0
2.5
3.0
3.5
Magnitude

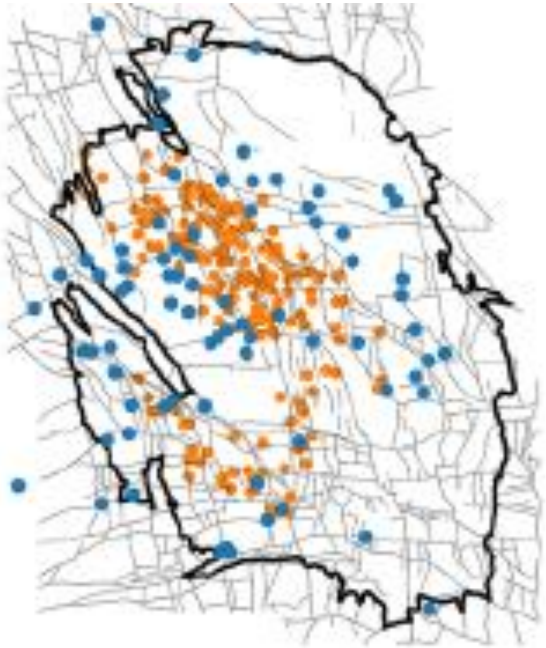

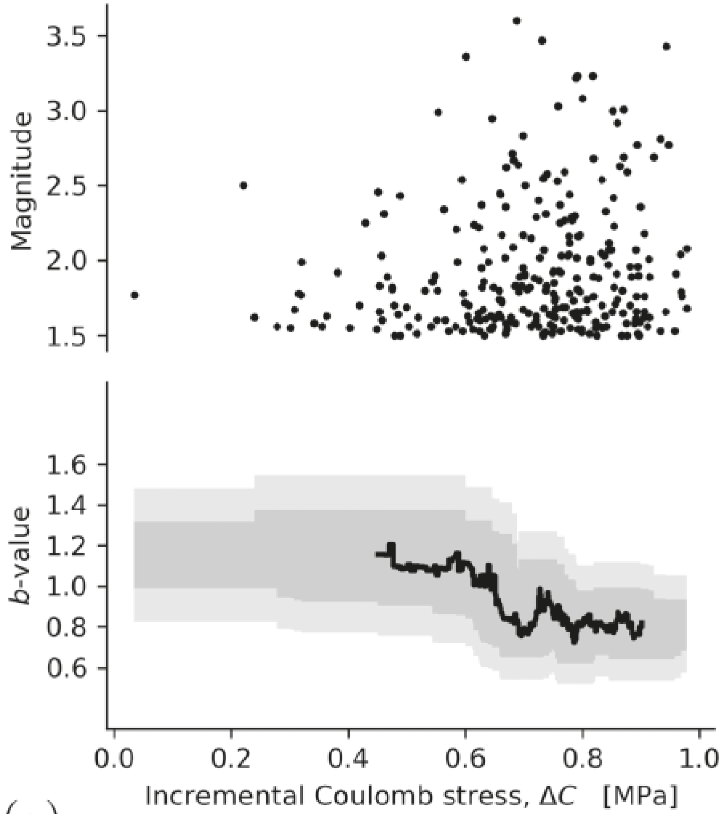

Magnitude
3.5
3.0
2.5
2.0
1.5
b-value
1.6
1.4
1.2
1.0
0.8
0.6
0.0
0.2
0.4
0.6
0.8
1.0
Incremental Coulomb stress, ΔC [MPa]

(a)

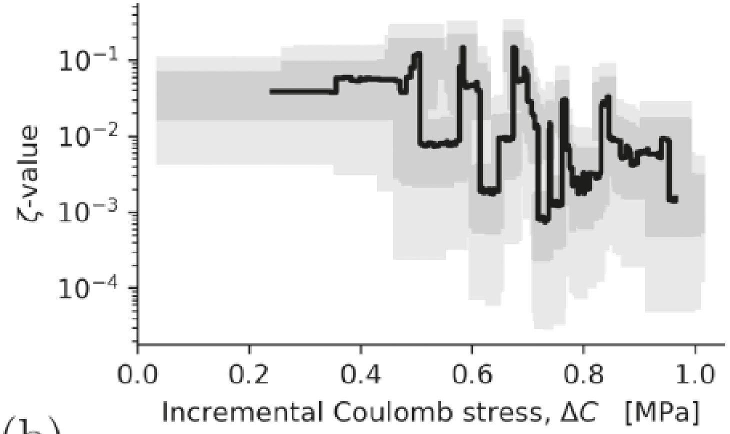

ζ-value
10^{-1}
10^{-2}
10^{-3}
10^{-4}
0.0
0.2
0.4
0.6
0.8
1.0
Incremental Coulomb stress, ΔC [MPa]

(b)

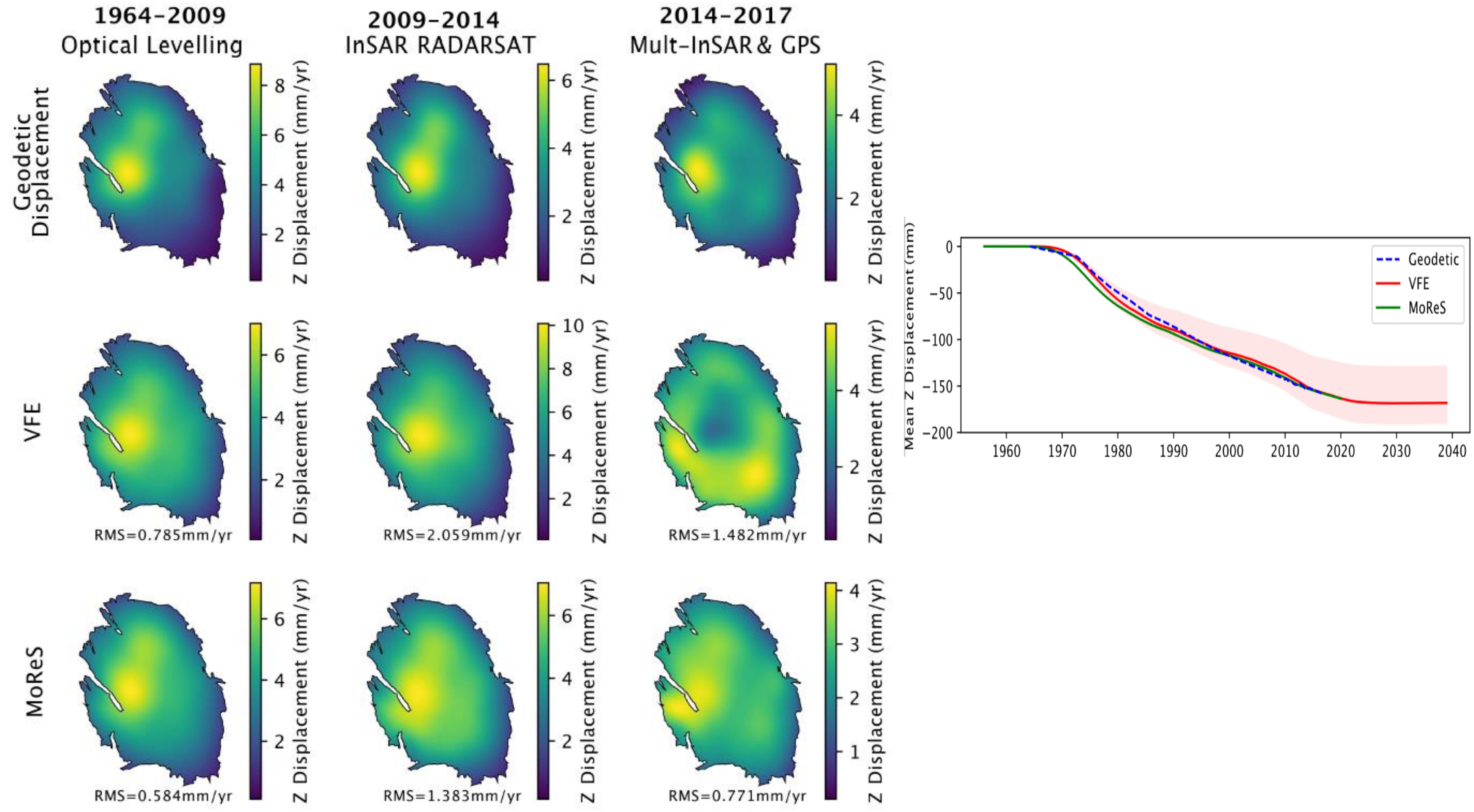

1964-2009
Optical Levelling
2009-2014
InSAR RADARSAT
2014-2017
Mult-InSAR & GPS
Geodetic Displacement
VFE
MoReS
Z Displacement (mm/yr)
RMS=0.785mm/yr
RMS=2.059mm/yr
RMS=1.482mm/yr
RMS=0.584mm/yr
RMS=1.383mm/yr
RMS=0.771mm/yr
Mean Z Displacement (mm)
Geodetic
VFE
MoReS

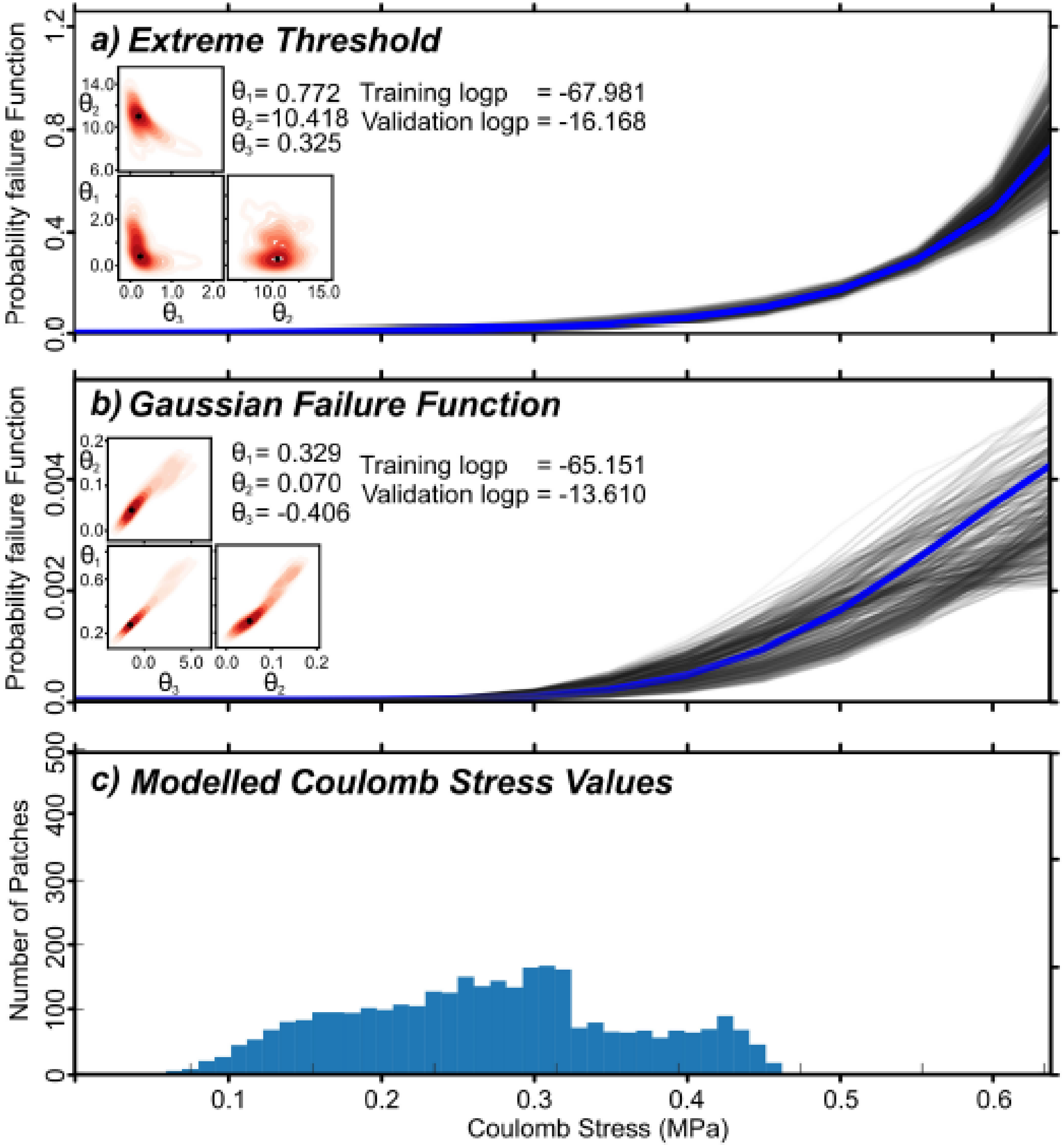
a) Extreme Threshold
θ1 = 0.772
θ2 = 10.418
θ3 = 0.325
Training logp = -67.981
Validation logp = -16.168
b) Gaussian Failure Function
θ1 = 0.329
θ2 = 0.070
θ3 = -0.406
Training logp = -65.151
Validation logp = -13.610
c) Modelled Coulomb Stress Values
Probability failure Function
Number of Patches
Coulomb Stress (MPa)

Groningen Gas Field

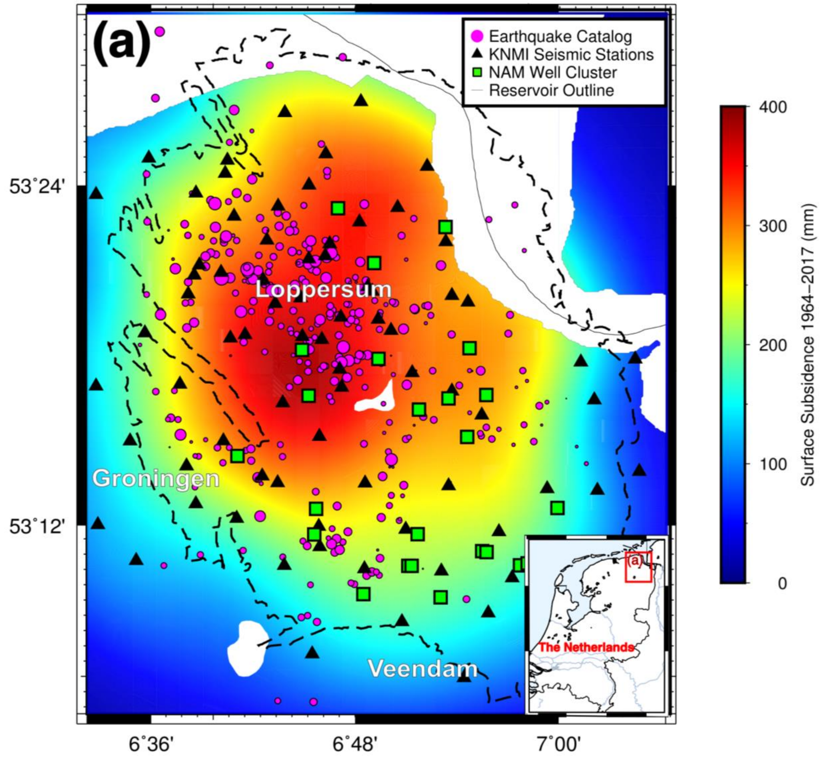

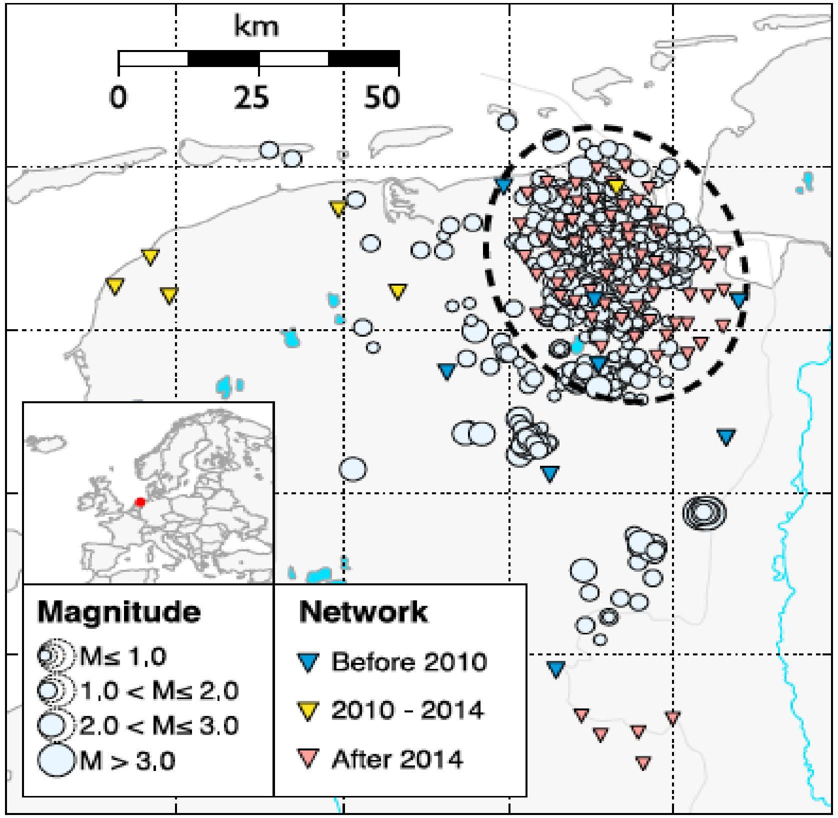

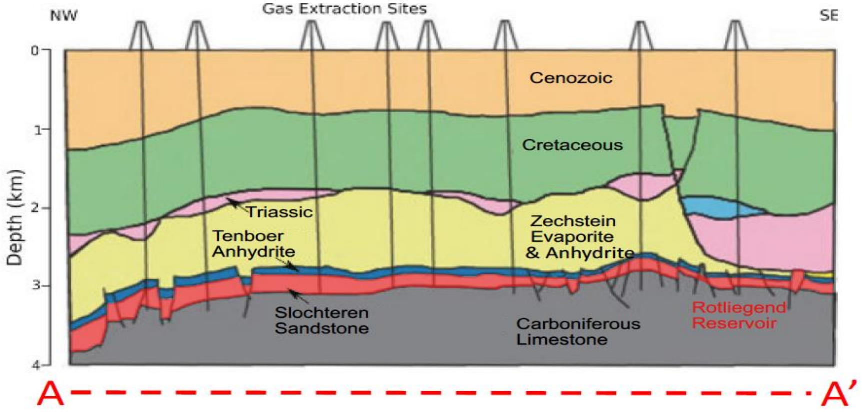

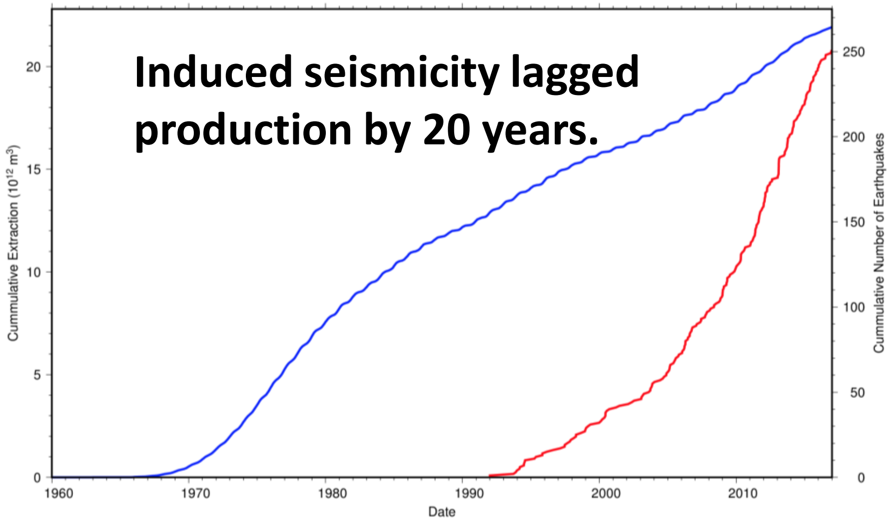

Induced seismicity lagged production by 20 years.

(Smith et al, JGR, 2019)

Failure Forecasting - Failure Function – Instantaneous

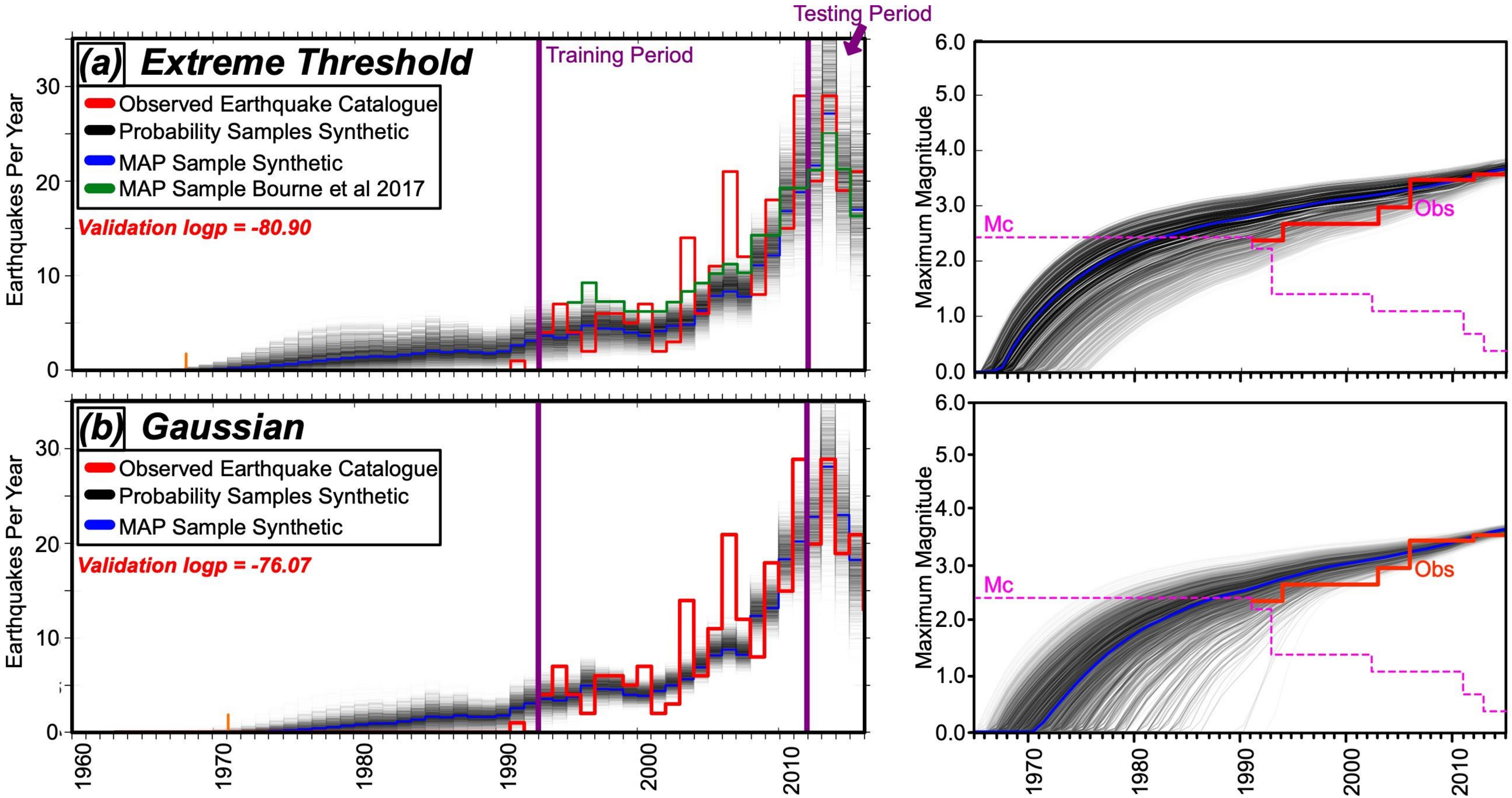

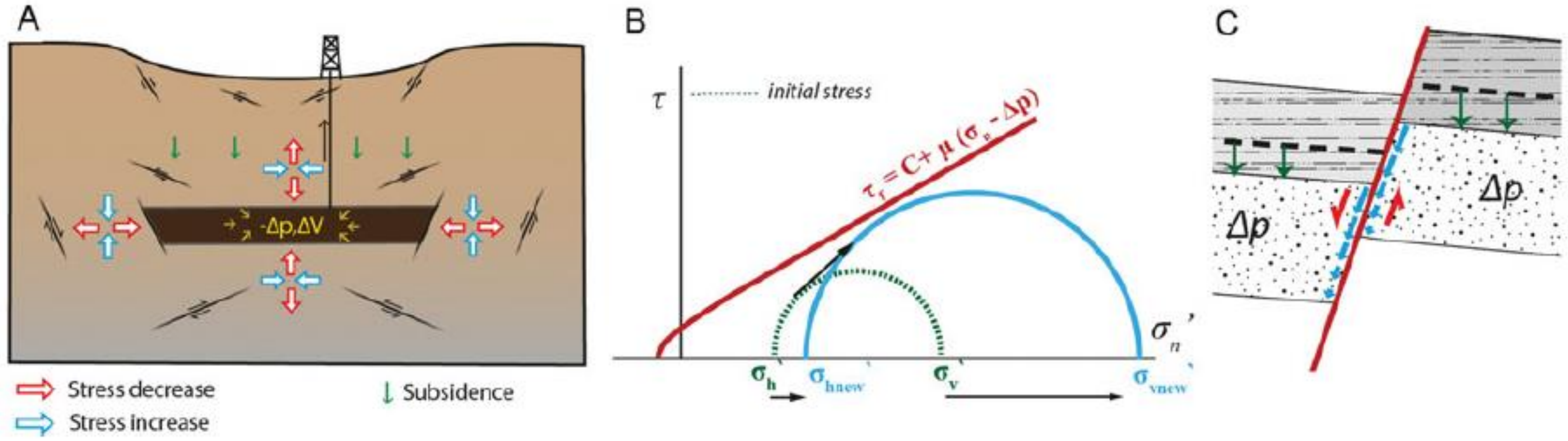

Fig. 2. (A) Illustration of poro-elastic stress changes and promoted faulting mechanisms outside of a depleting reservoir (redrawn after Segall et al., 1998). (B) Effective stress development inside a laterally extensive depleting reservoir undergoing uniaxial compaction, shown for an unstable stress path (arrow). The initial stress state is shown by green dashed semicircle, and the state in depleted reservoir by a blue semicircle. (C) Sketch of differential compaction across a fault.

(Buijze et al., 2017)

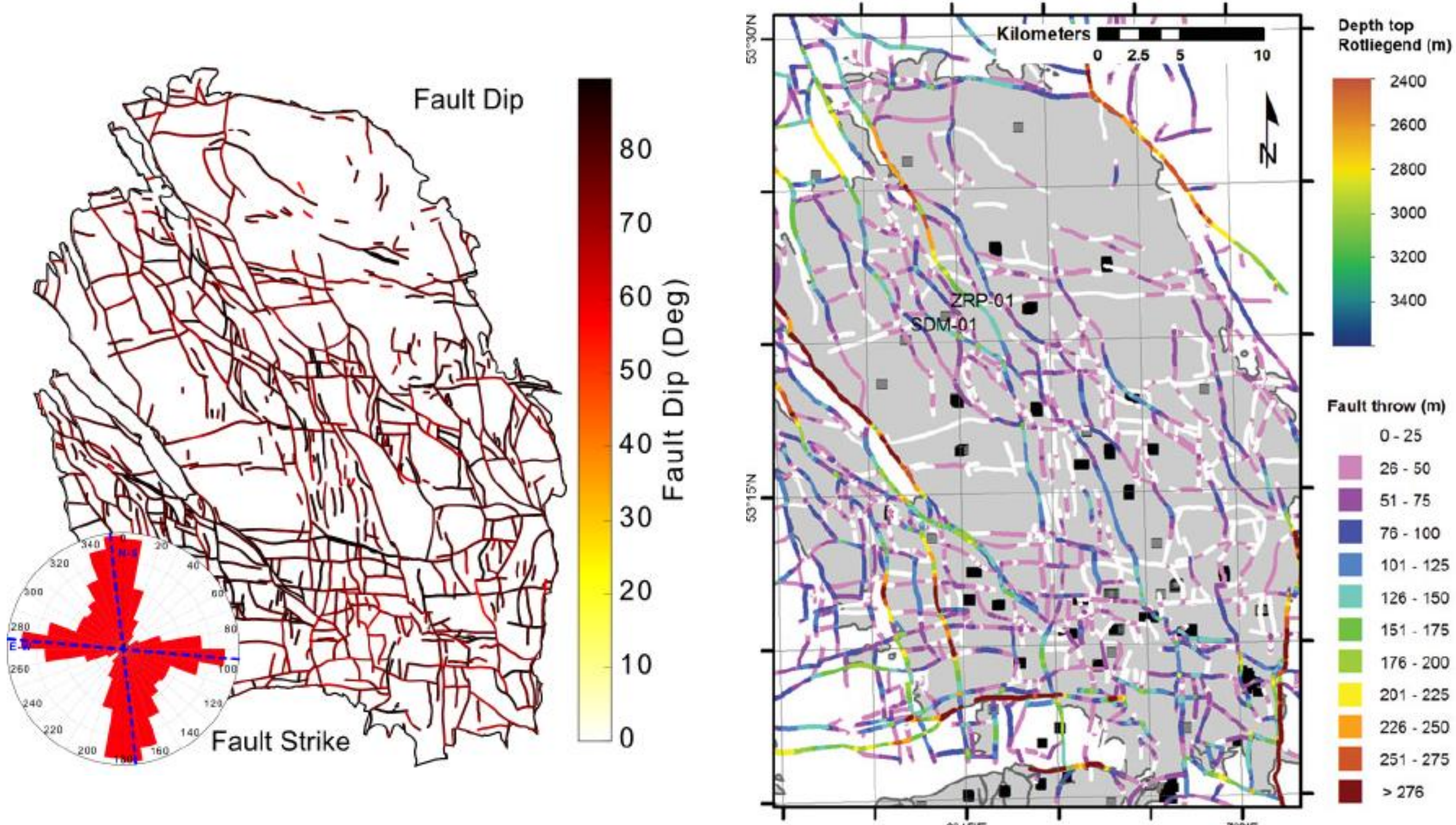

Fault Dip
Fault Dip (Deg)
0
10
20
30
40
50
60
70
80
Fault Strike
N-S
E-W
Kilometers
0
2.5
5
10
53°30'N
53°15'N
6°45'E
7°0'E
ZRP-01
SDM-01
N
Depth top Rotliegend (m)
2400
2600
2800
3000
3200
3400
Fault throw (m)
0 - 25
26 - 50
51 - 75
76 - 100
101 - 125
126 - 150
151 - 175
176 - 200
201 - 225
226 - 250
251 - 275
> 276

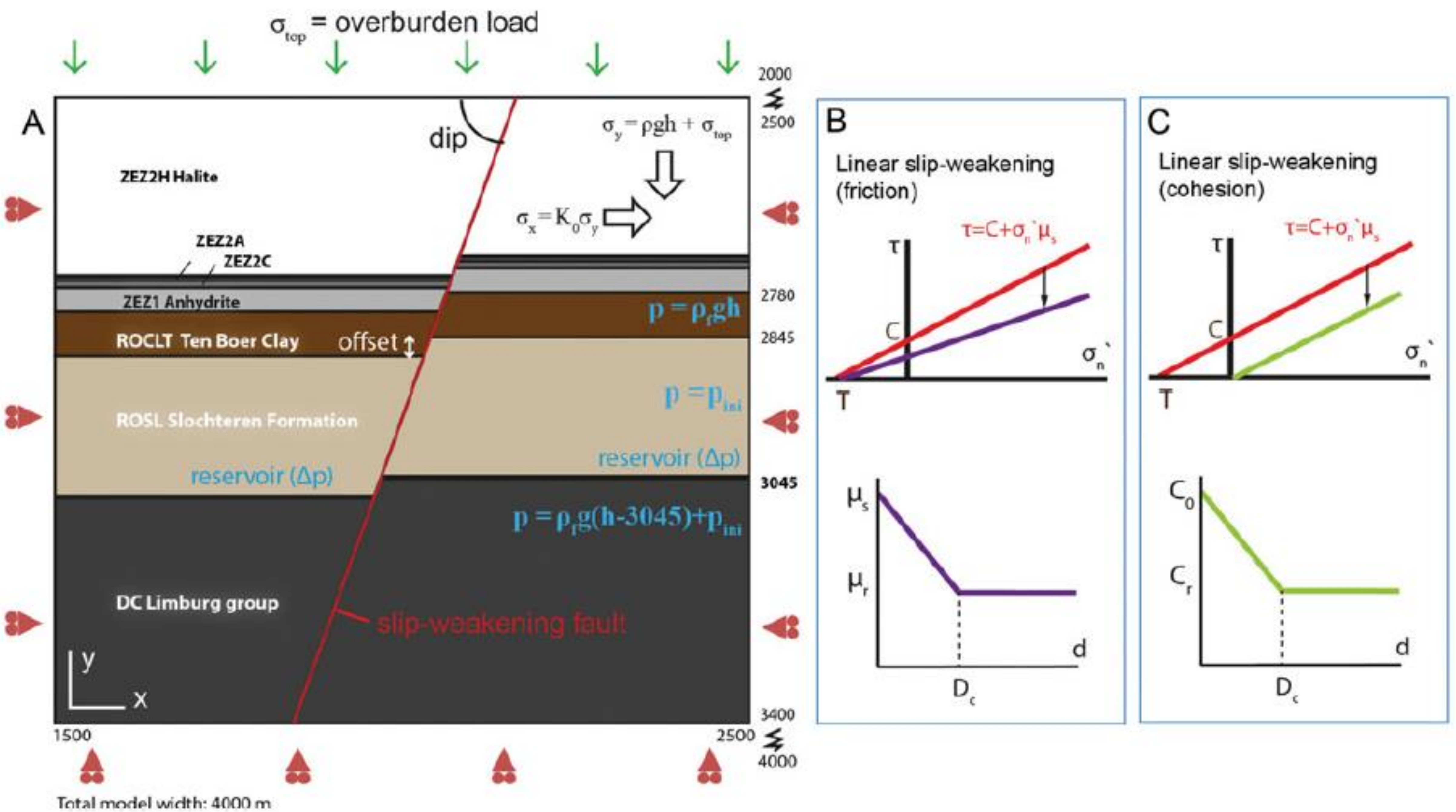

σ_top = overburden load
A
dip
ZEZ2H Halite
ZEZ2A
ZEZ2C
ZEZ1 Anhydrite
ROCLT Ten Boer Clay
offset
ROSL Slochteren Formation
reservoir (Δp)
DC Limburg group
slip-weakening fault
σ_y = ρgh + σ_top
σ_x = K_0σ_y
p = ρ_f gh
p = p_ini
reservoir (Δp)
p = ρ_f g(h-3045)+p_ini
y
x
2000
2500
2780
2845
3045
3400
1500
2500
4000
Total model width: 4000 m
B
Linear slip-weakening (friction)
τ=C+σ_n`μ_s
τ
C
σ_n`
T
μ_s
μ_r
d
D_c
C
Linear slip-weakening (cohesion)
τ=C+σ_n`μ_s
τ
C
σ_n`
T
C_0
C_r
d
D_c

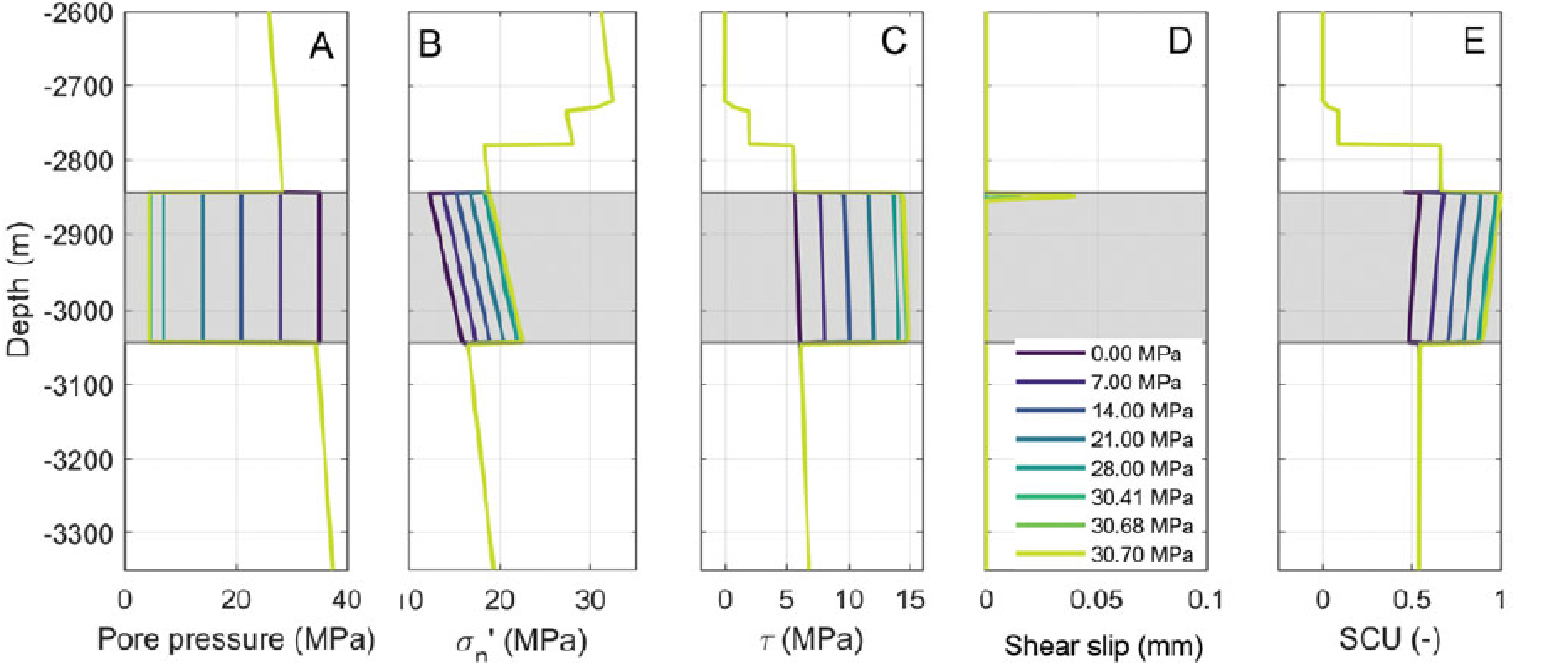

Fig. 11. On-fault results as a function of reservoir depletion Δp (legend of Δp is shown in (D)) on a 0 m offset 70° dipping fault cross-cutting the reservoir. (A) pressure, (B) effective normal stress, (C) shear stress, (D) (aseismic)shear slip, (E) Shear Capacity Utilisation (0 = stable, 1 = sliding occurs). The depth interval of the Slochteren Formation is indicated by the grey area. The coloured lines indicate the amount of pressure decrease.

(Buijze et al, 2017)

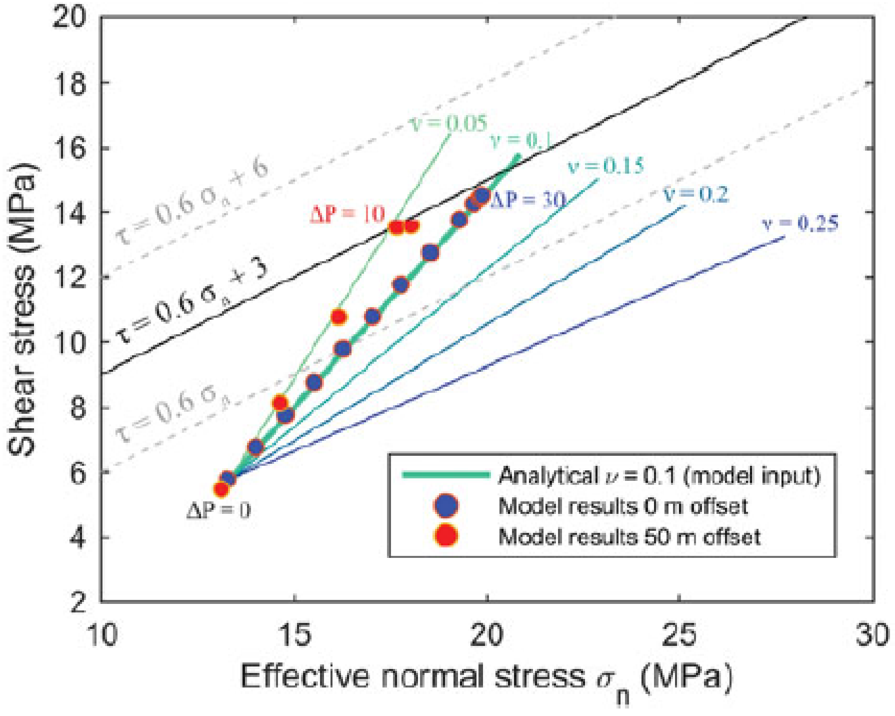

Fig. 12. Stress paths as a function of reservoir depletion at 2900 m depth for the 0 m offset and 50 m offset fault models, and comparison to the analytically calculated stress path for uniaxial compaction in a laterally extensive reservoir depleting from 35 to 0 MPa (initial stresses and pressure, stress ratio $K_0 = 0.72$ and Poisson's ratio $\nu = 0.1$ are same as used in the numerical models). Analytically calculated stress paths for different ν (0.05–0.25) are shown for reference. The failure criterion as used in the numerical models ($\mu = 0.6$, $C = 3$ MPa) is shown in black, and two other failure lines with different C are depicted with grey dashed lines. The stress path for the 50 m offset reservoir is steeper than for 0 m offset due to local stress concentrations along the offset fault.

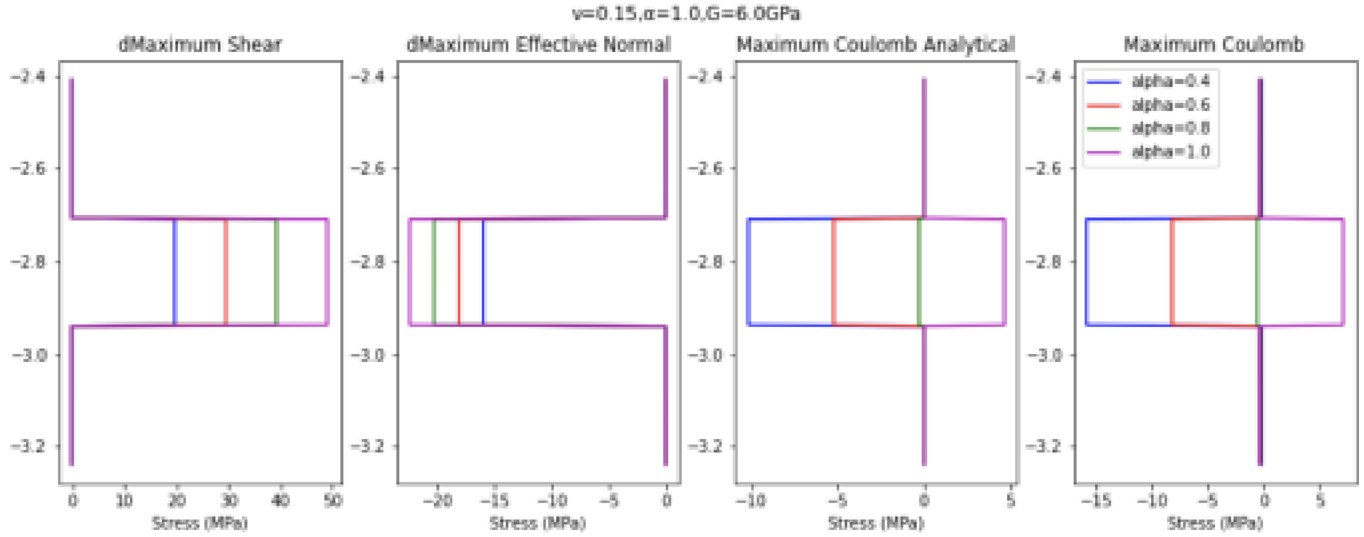

Here ν=0.15, α=1, and μ=0.66 so $\alpha<\alpha_c$

$$\alpha_c = \frac{1-\nu}{1-2\nu}\frac{2\sin\phi}{1+\sin\phi}.$$

Induced Seismicity & Stress Modelling

Analytical – Thin-Sheet (Bourne et al 2018)

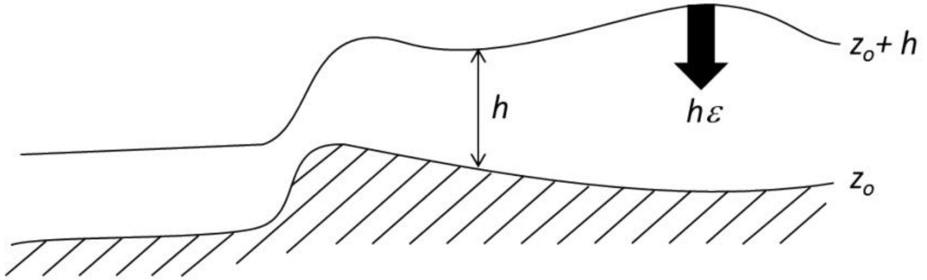

$$\bar{\epsilon}_{xz} = -\frac{\epsilon_{zz}}{2}\left(\frac{\partial z_o}{\partial x}\right) - \frac{\epsilon_{zz}}{4}\left(\frac{\partial h}{\partial x}\right) - \frac{1}{4}\left(\frac{\partial c}{\partial x}\right),$$

$$\bar{\epsilon}_{yz} = -\frac{\epsilon_{zz}}{2}\left(\frac{\partial z_o}{\partial y}\right) - \frac{\epsilon_{zz}}{4}\left(\frac{\partial h}{\partial y}\right) - \frac{1}{4}\left(\frac{\partial c}{\partial y}\right),$$

$$\bar{\epsilon}_{zz} = \epsilon_{zz},$$

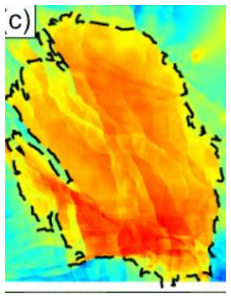

Reservoir Depth

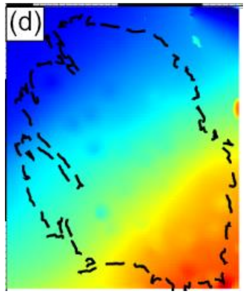

Reservoir Thickness

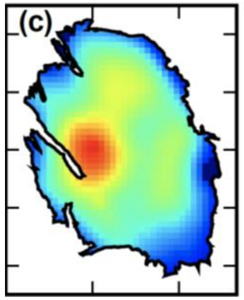

Reservoir Compaction

Semi-Analytical – Strain Volume Smith et al (2021, in review)

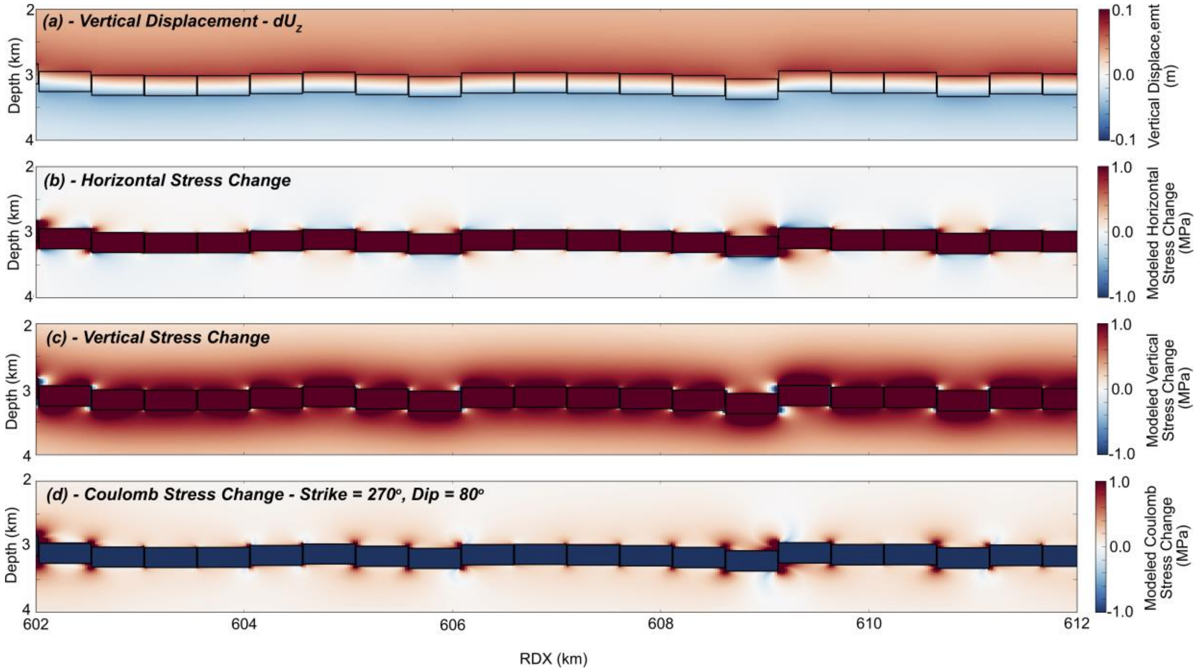

Reservoir Compressibility

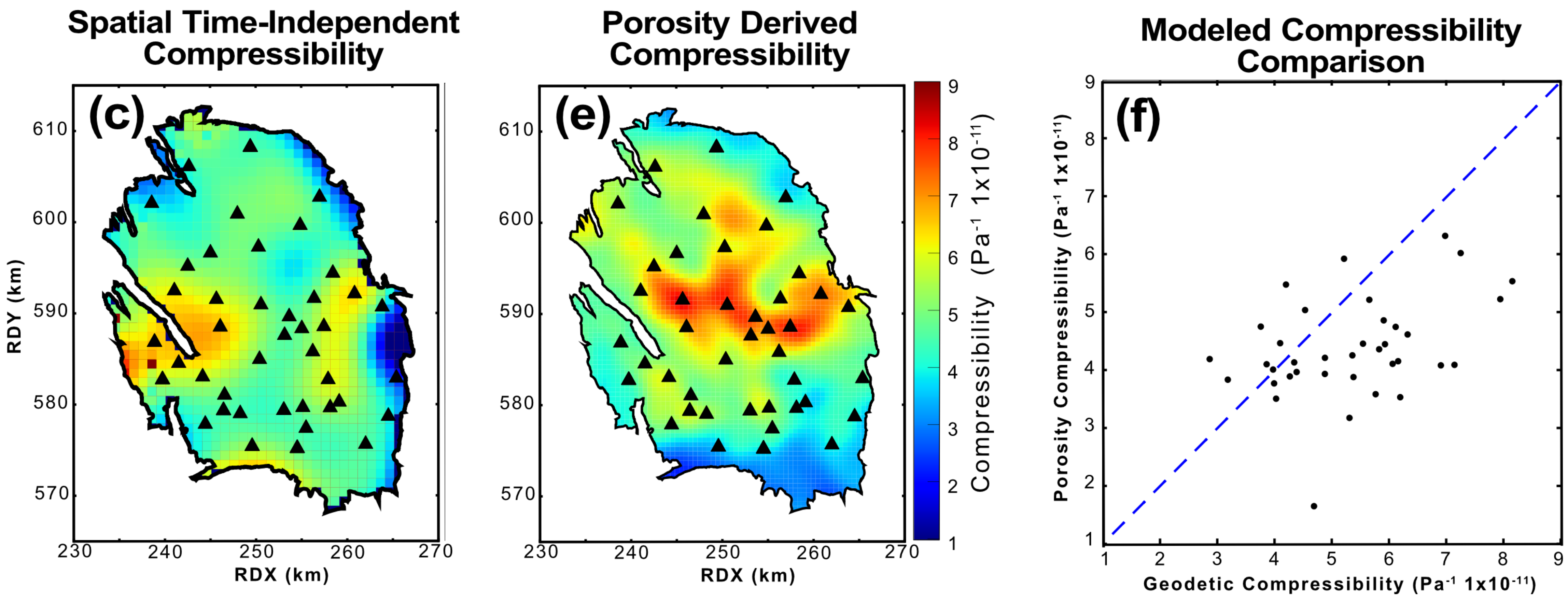

Background & Regional Setting

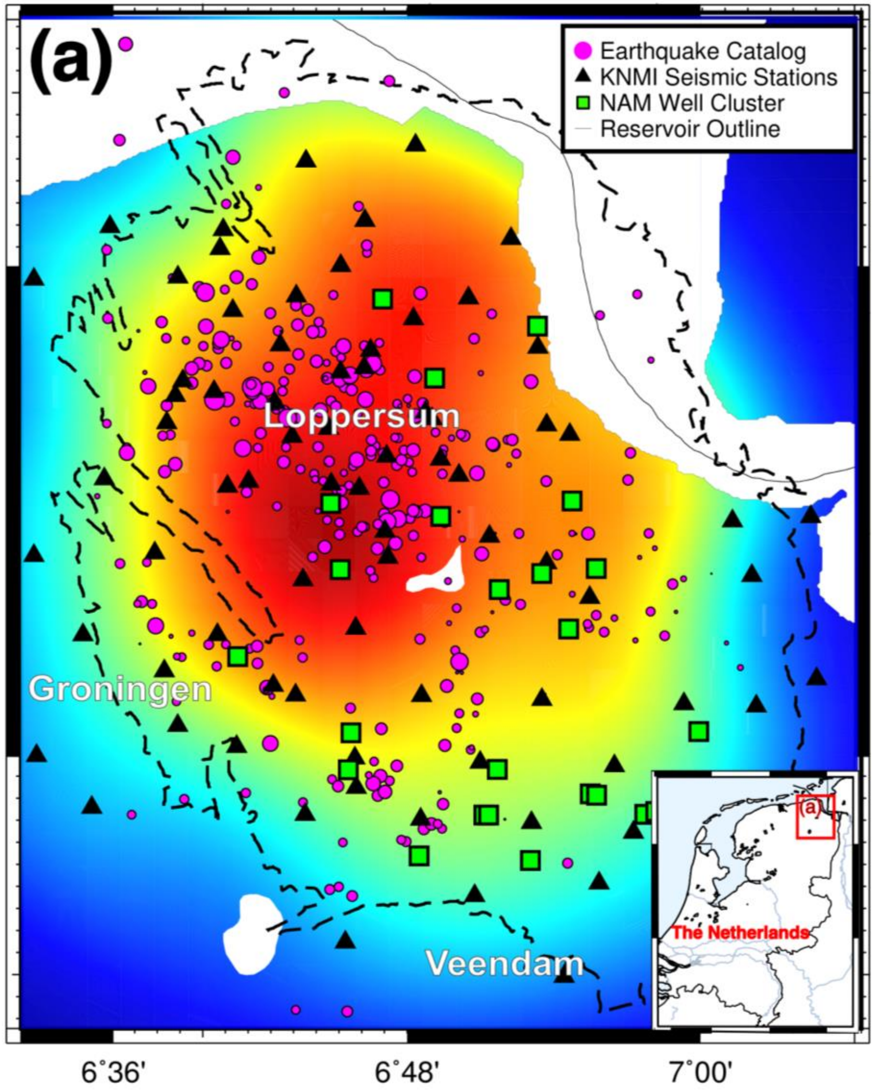

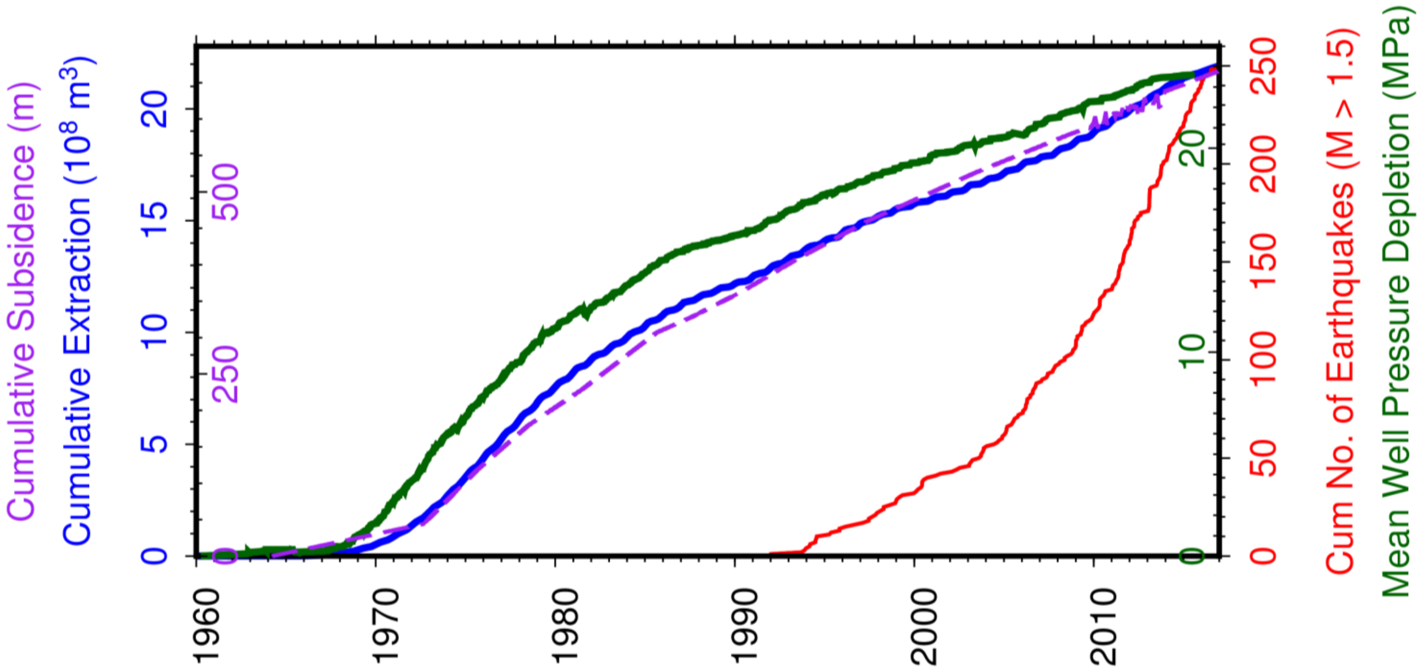

Pressure Depletion Model

- NAM Pressure Depletion Model
  - Pressure distributed to match historic pressure and gas flow measurements
  - Porosity measurements determined at well locations, interpreted for remaining field.

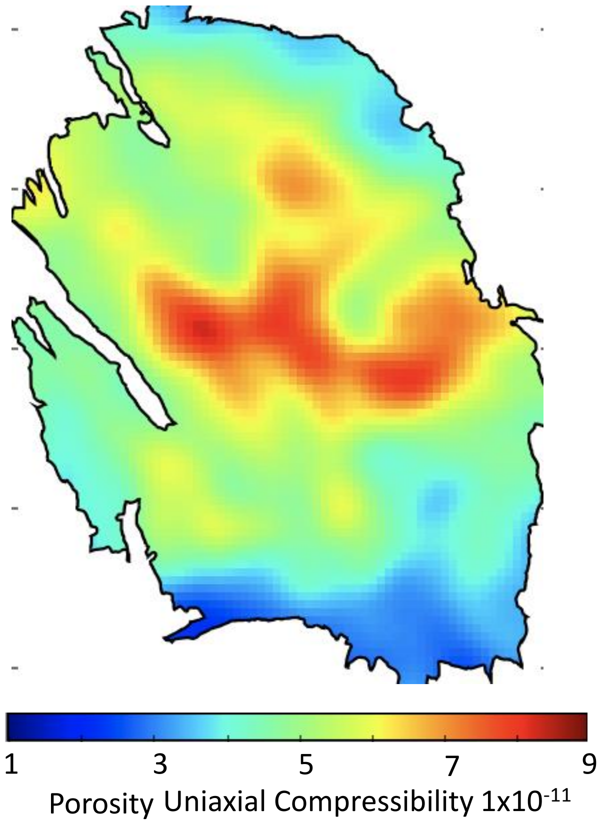

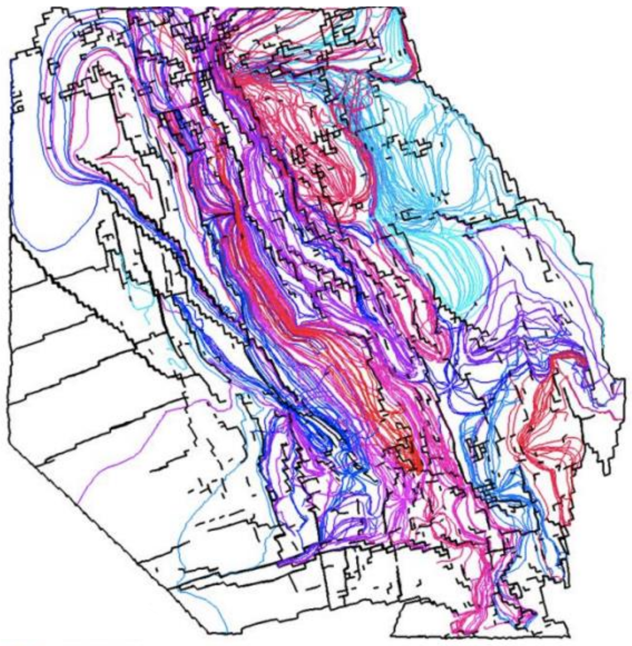

Streamline for drainage time to producer (NAM,2016)

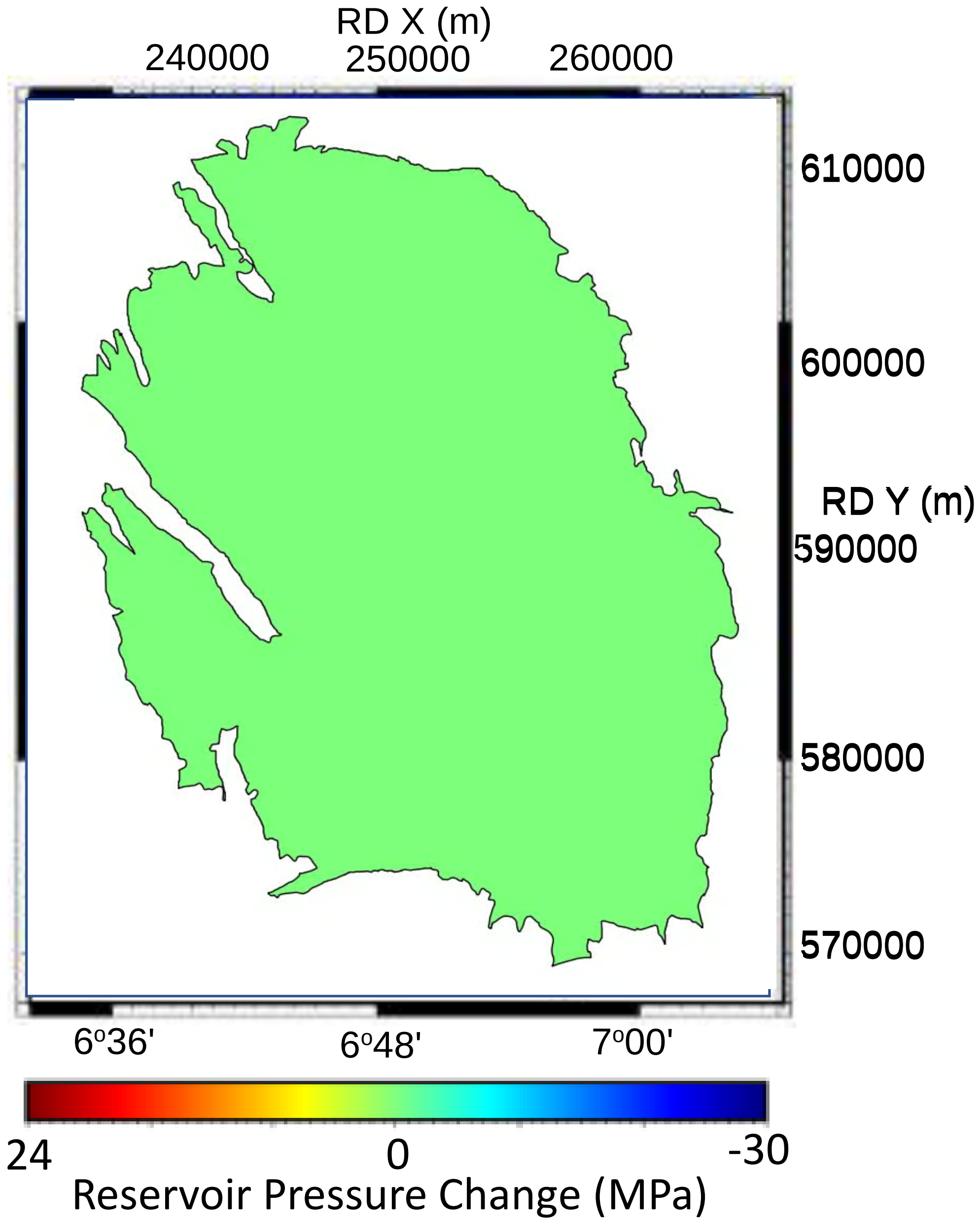

Pressure Depletion, Strain Accumulation & Seismicity – Pressure Depletion

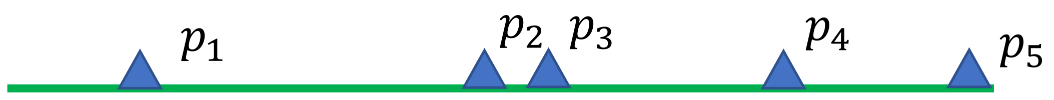

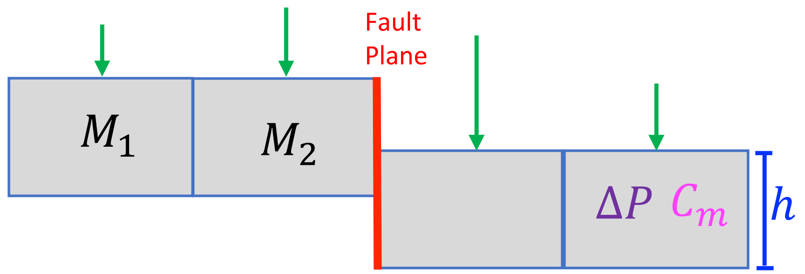

(Geertsma, 1957,
Bourne et al 2015).

$$Compaction = hC_m\Delta P$$

C_m could be time-dependent or time-independent. This will be discussed later in the presentation

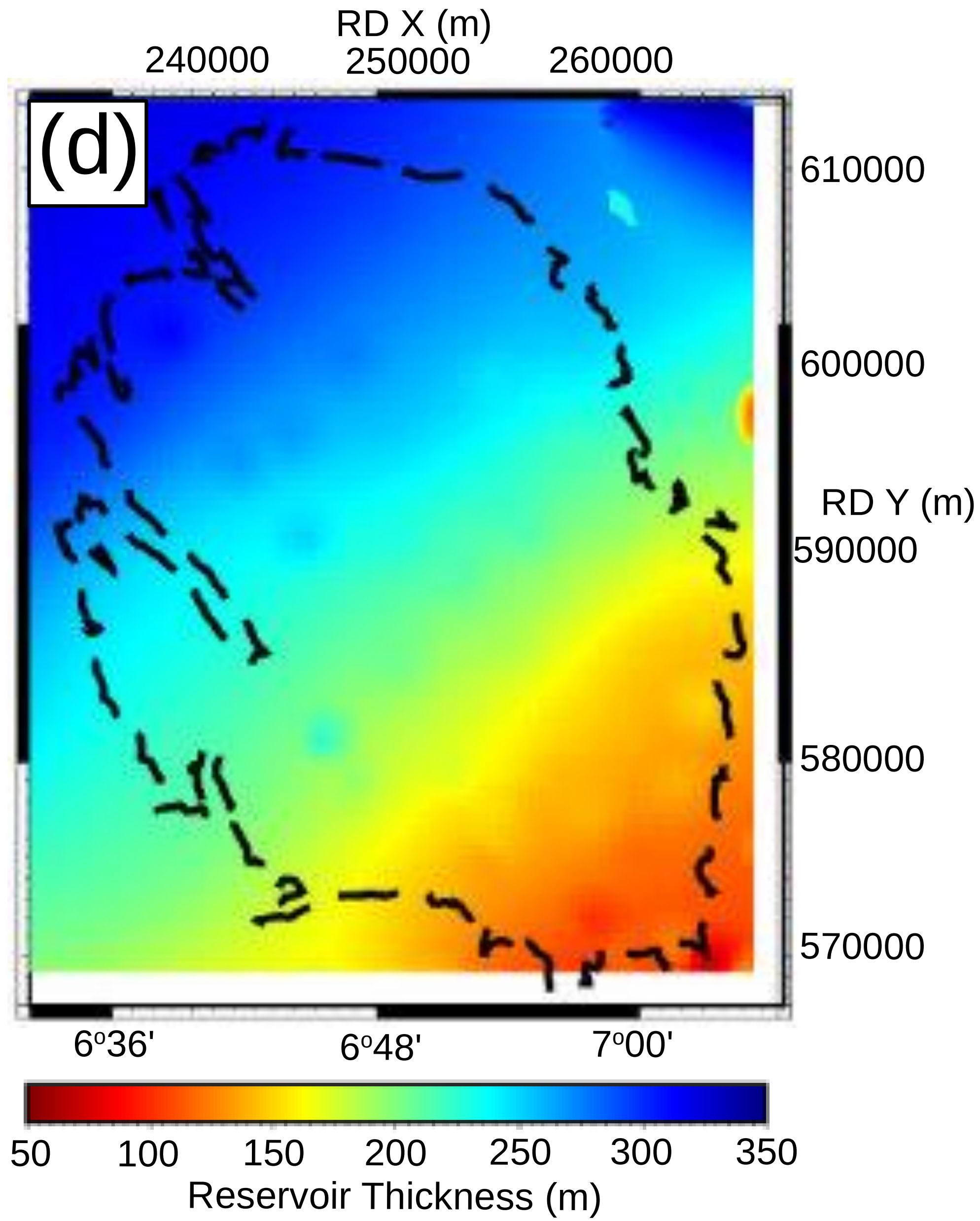

Reservoir Compressibility

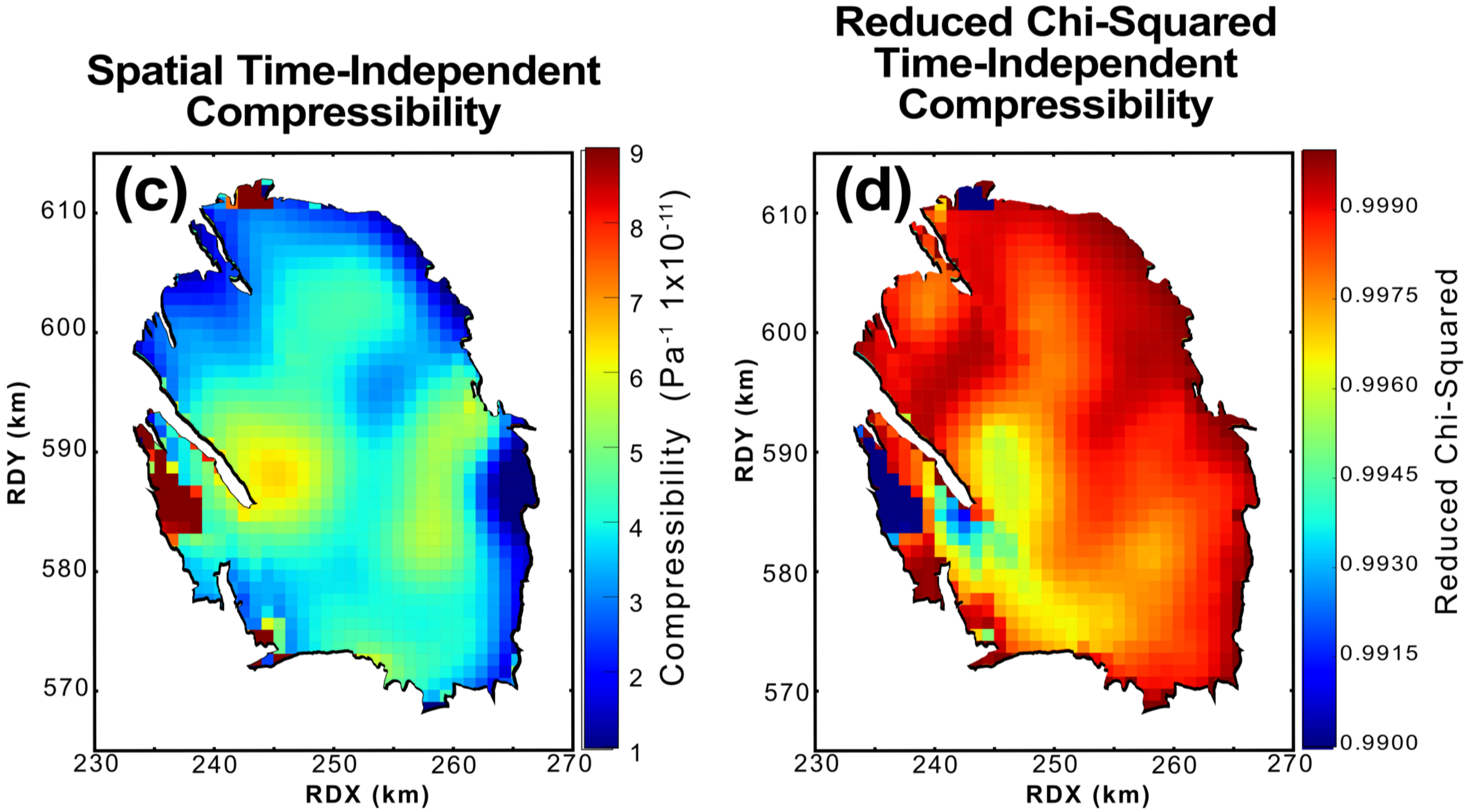

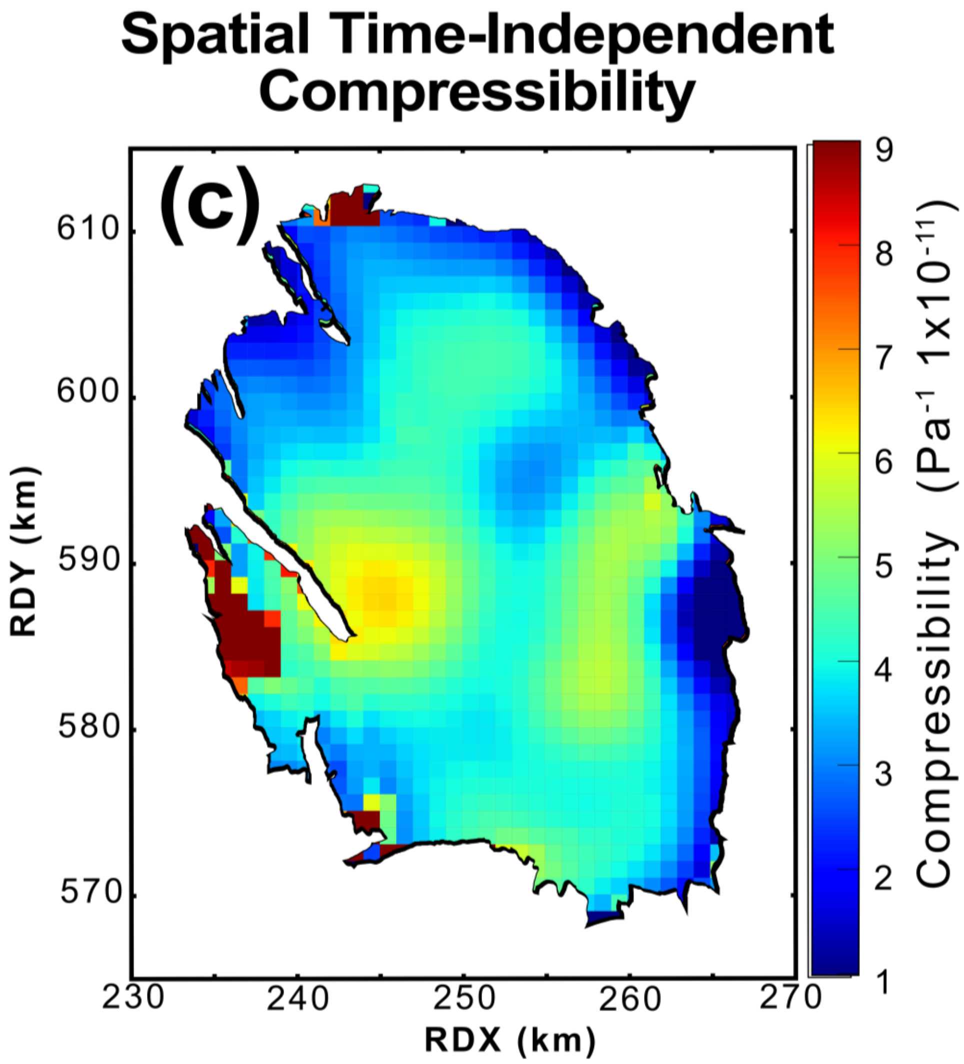

Spatial Time-Independent
Compressibility
(c)
610
600
590
580
570
RDY (km)
230
240
250
260
270
RDX (km)
9
8
7
6
5
4
3
2
1
Compressibility (Pa-1 1x10-11)

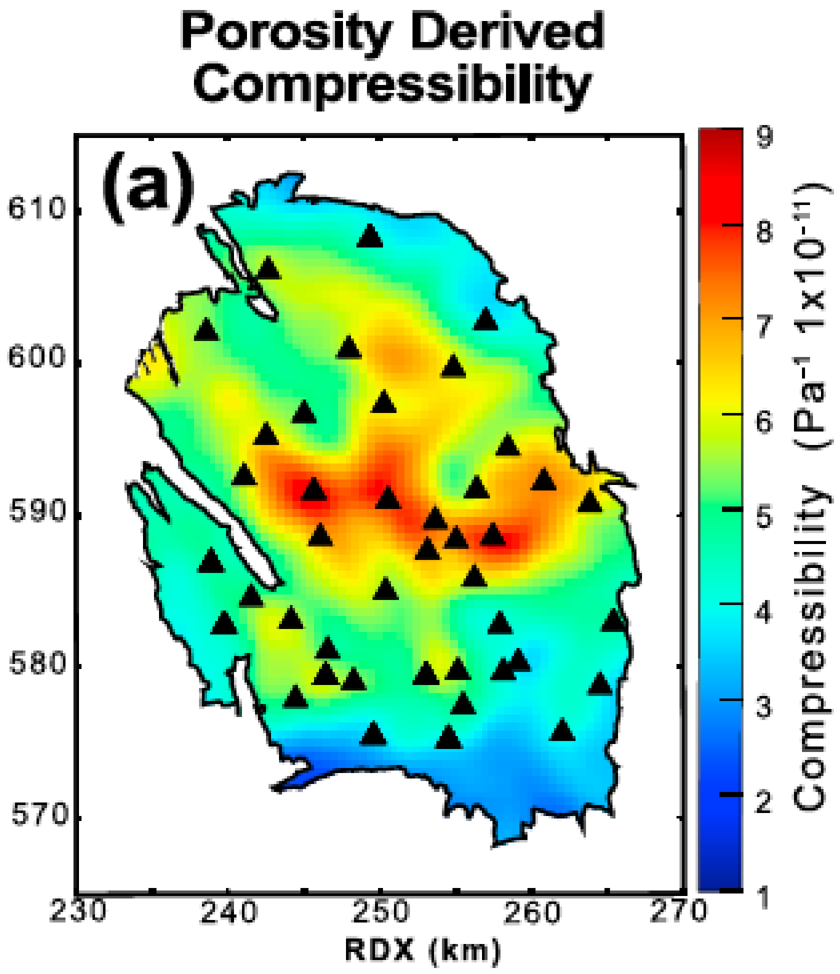

Porosity Derived
Compressibility
(a)
610
600
590
580
570
230
240
250
260
270
RDX (km)
9
8
7
6
5
4
3
2
1
Compressibility (Pa-1 1x10-11)

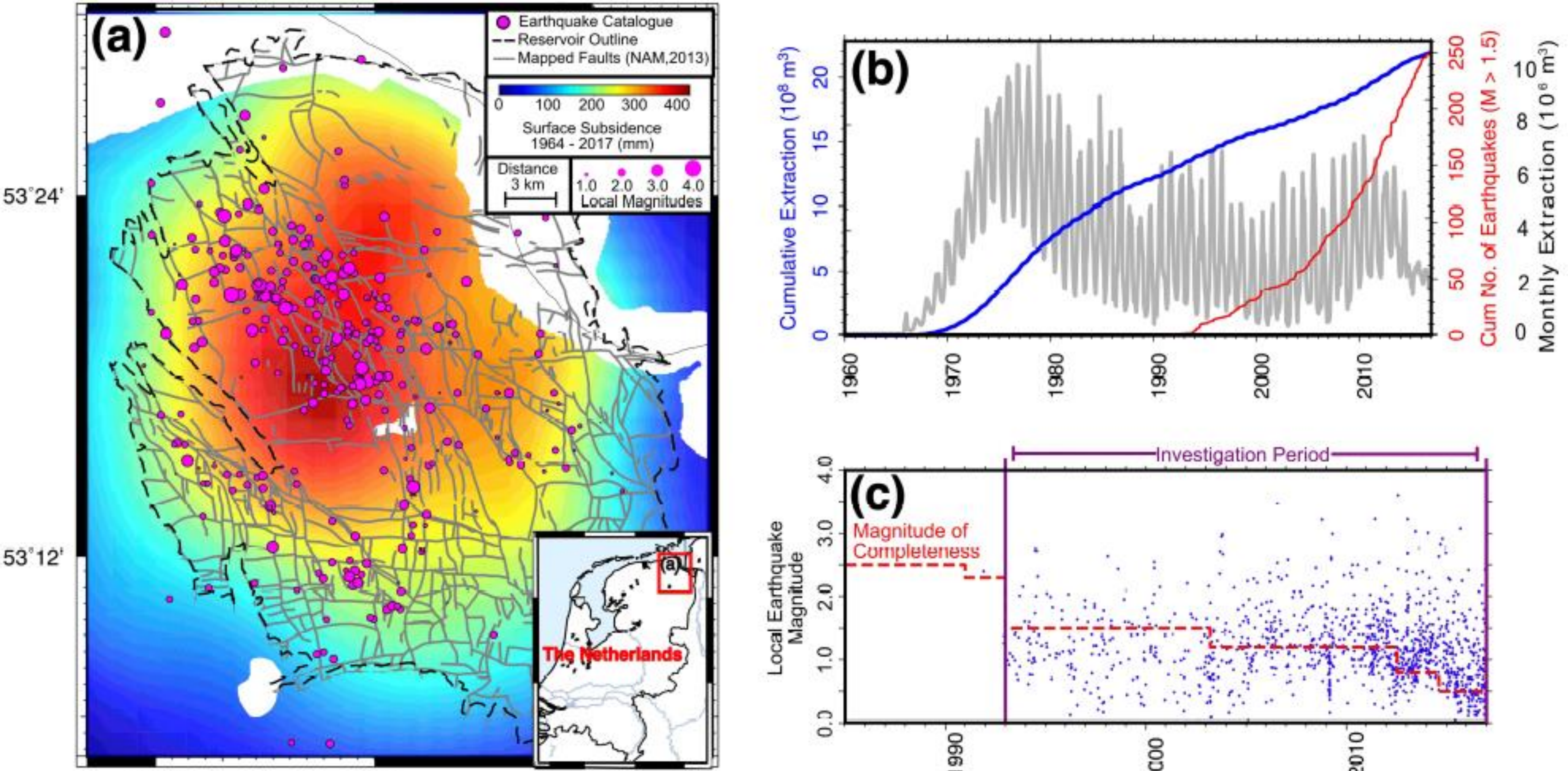
(a)
Earthquake Catalogue
Reservoir Outline
Mapped Faults (NAM,2013)
0 100 200 300 400
Surface Subsidence
1964 - 2017 (mm)
Distance
3 km
1.0 2.0 3.0 4.0
Local Magnitudes
The Netherlands
53°24'
53°12'
6°36'
6°48'
7°00'
(b)
Cumulative Extraction (10^8 m^3)
Cum No. of Earthquakes (M > 1.5)
Monthly Extraction (10^6 m^3)
1960
1970
1980
1990
2000
2010
(c)
Investigation Period
Magnitude of Completeness
Local Earthquake Magnitude
0.0
1.0
2.0
3.0
4.0
1990
2000
2010

$$\tau_f = \mu(\sigma_n - P) + C_0, \qquad \Delta C = \Delta\tau + \mu(\Delta P - \Delta\sigma_n),$$

$$M_{max} = M_c + \frac{1}{b}\log_{10}(N)$$

$$f(\Delta m|N_{tot}) = bln(10) \cdot 10^{-b\Delta m} \sum_{N=N_{min}}^{N_{tot}} \frac{1}{N}\left[1 - \frac{1}{N}10^{-b\Delta m}\right]^{N_{tot}-1}$$

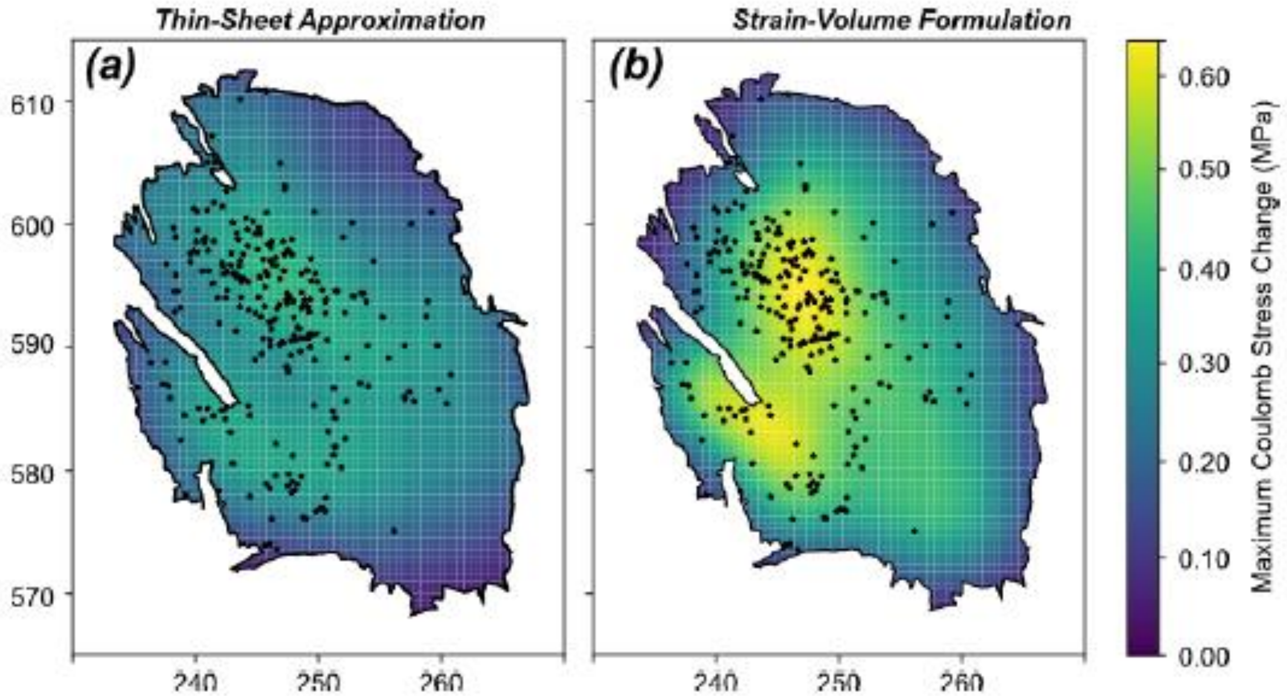

Thin-Sheet Approximation
Strain-Volume Formulation
(a)
(b)
610
600
590
580
570
240
250
260
0.60
0.50
0.40
0.30
0.20
0.10
0.00
Maximum Coulomb Stress Change (MPa)

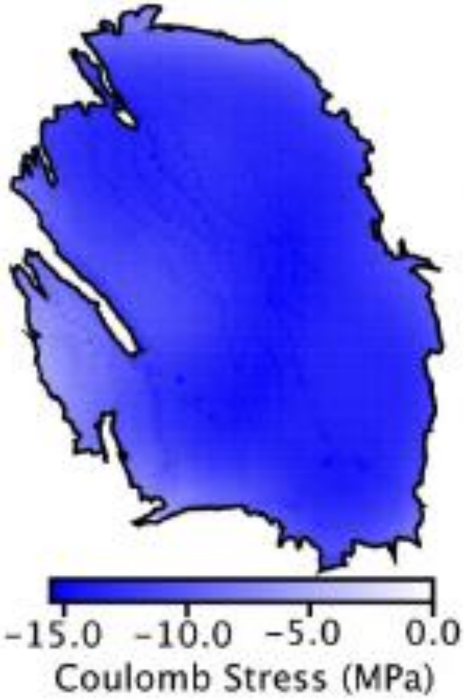

Within the reservoir (n=0.25, Cuboid centers)

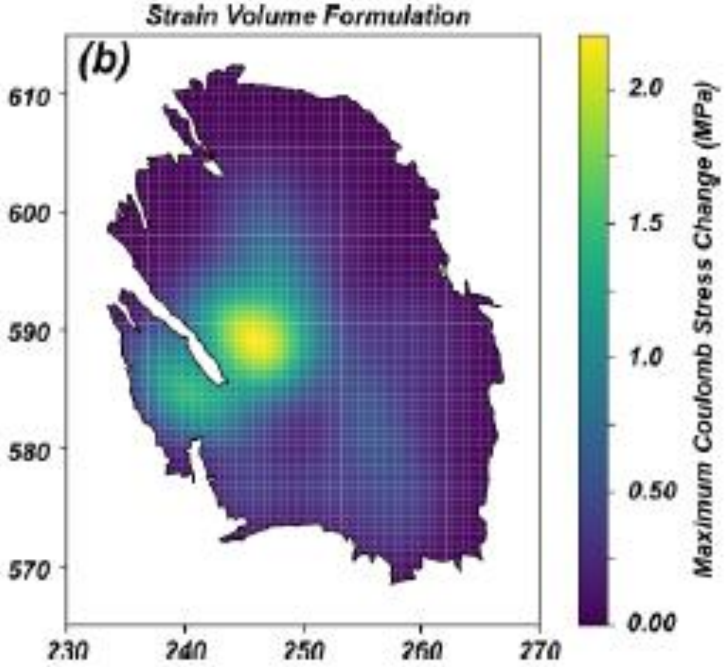

Within the reservoir (n=0.15, Cuboid edges)

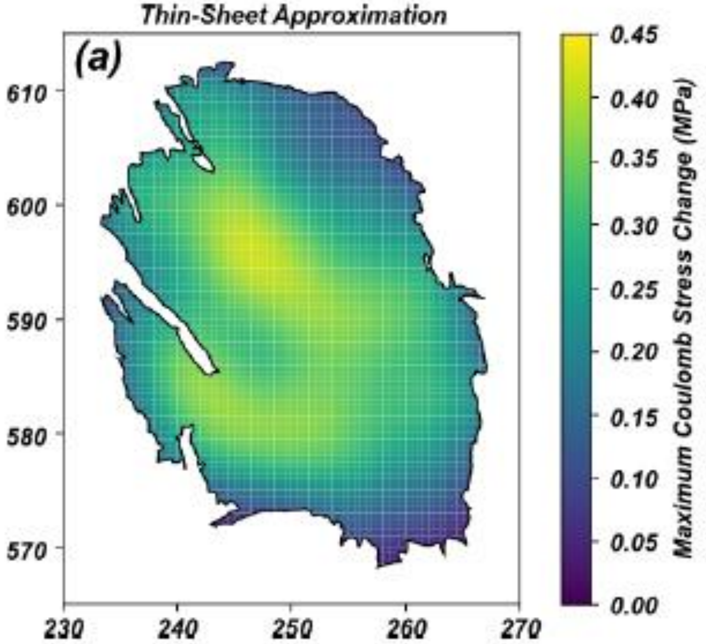

Within the reservoir (n=0.15)

5m above reservoir

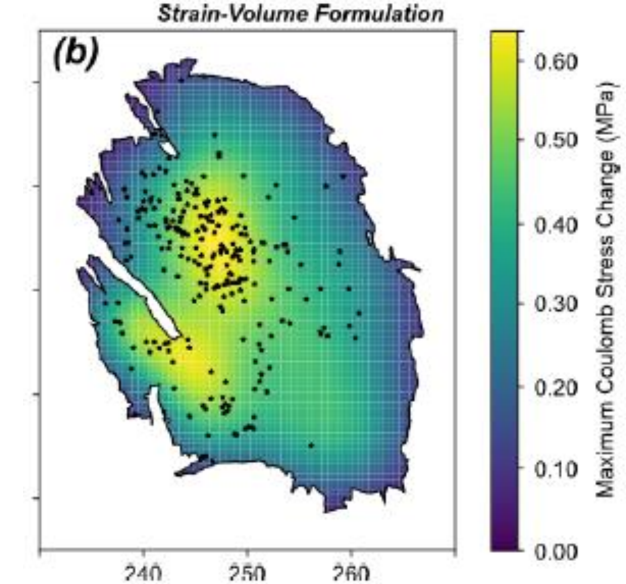

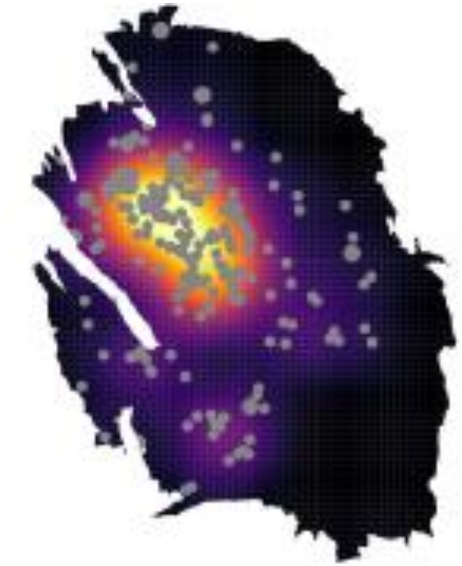

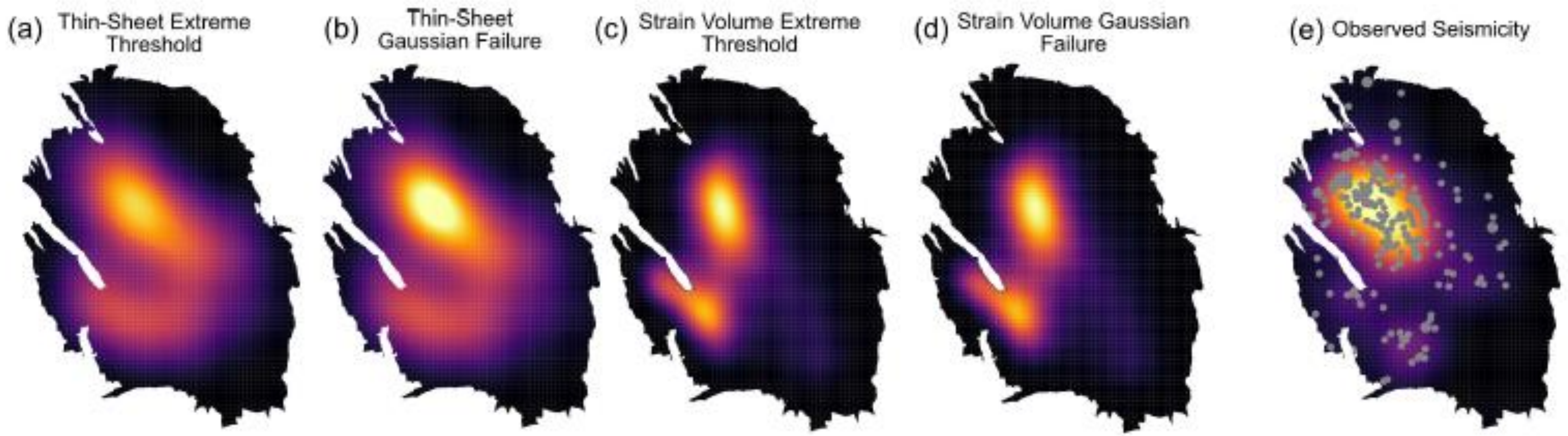

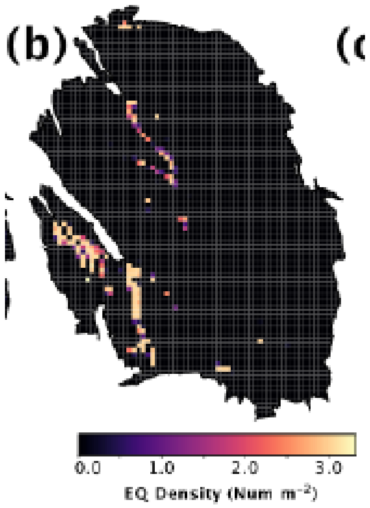

5 meter above reservoir
Cuboid centers
Max Coulomb

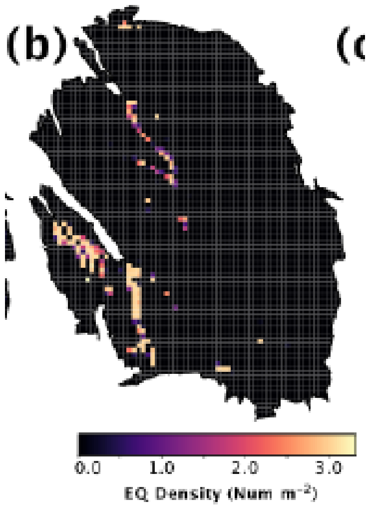

5 meter above reservoir
Cuboid centers
N270E

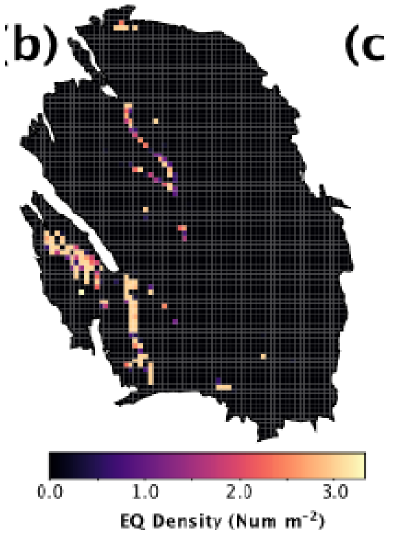

5 meter above reservoir
Cuboid centers
N350E

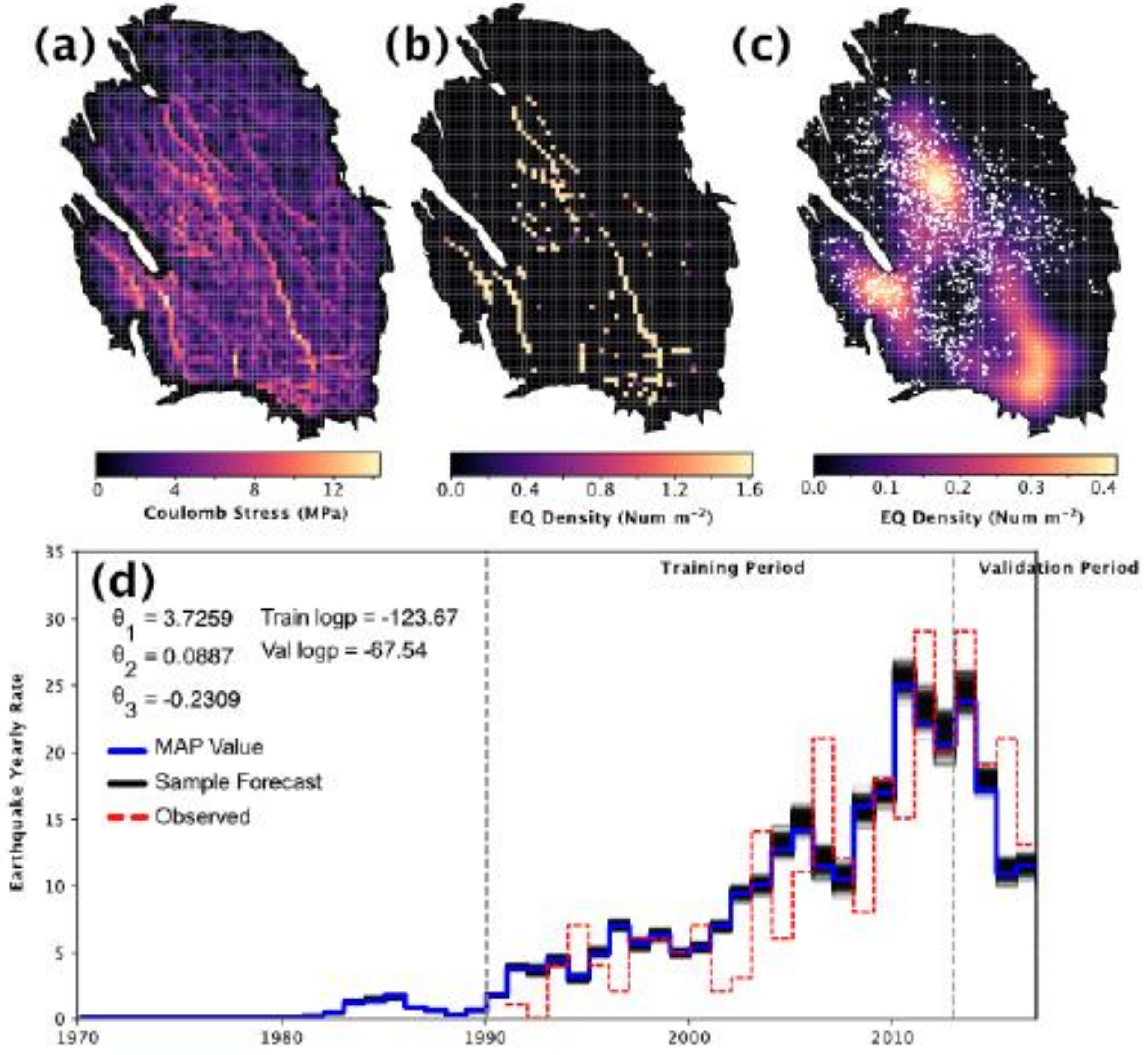

(a)
(b)
(c)
0 4 8 12
Coulomb Stress (MPa)
0.0 0.4 0.8 1.2 1.6
EQ Density (Num m⁻²)
0.0 0.1 0.2 0.3 0.4
EQ Density (Num m⁻²)
(d)
Training Period
Validation Period
θ1 = 3.7259
θ2 = 0.0887
θ3 = -0.2309
Train logp = -123.67
Val logp = -67.54
MAP Value
Sample Forecast
Observed
Earthquake Yearly Rate
0 5 10 15 20 25 30 35
1970 1980 1990 2000 2010

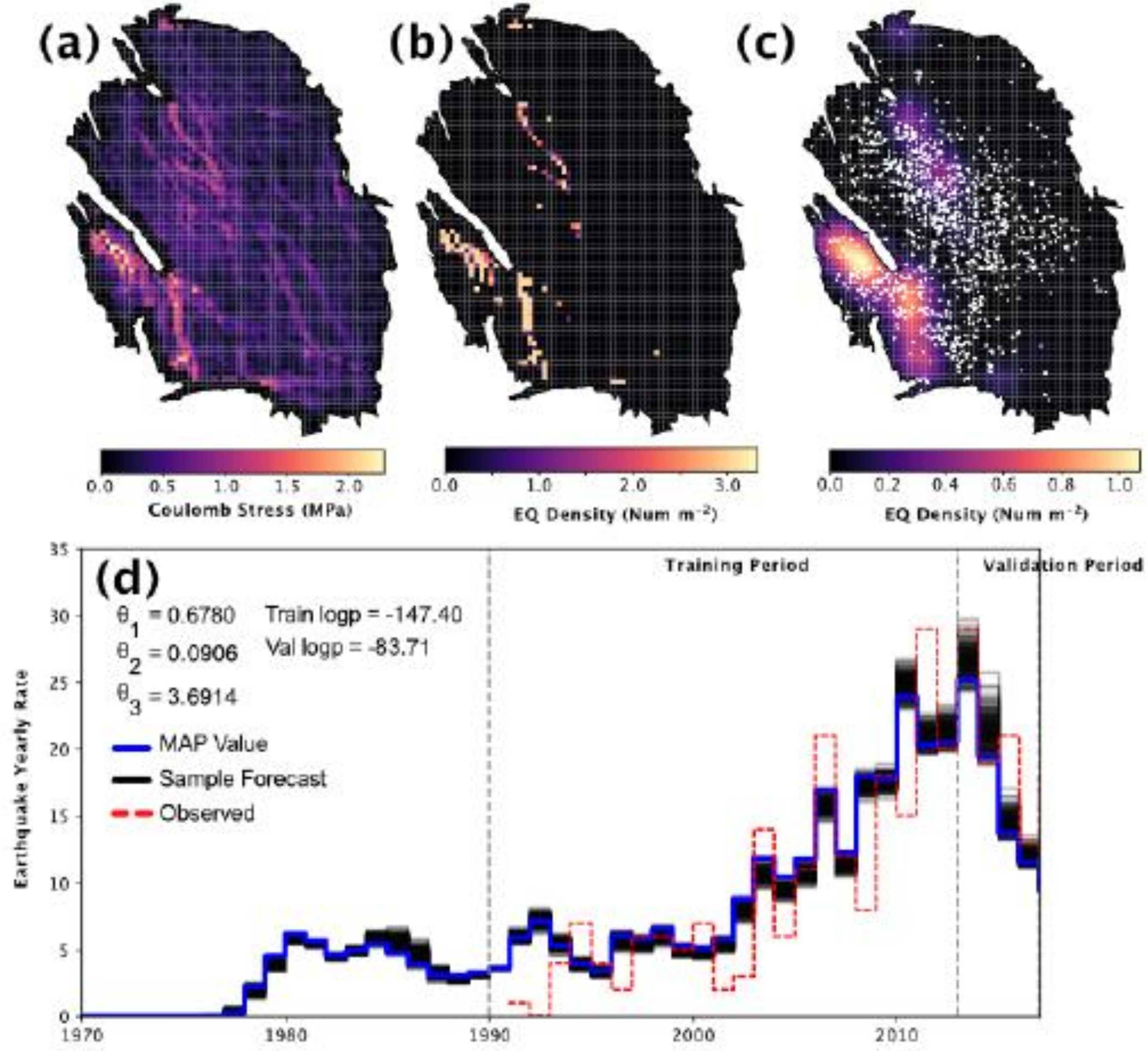

(a)
(b)
(c)
0.0 0.5 1.0 1.5 2.0
Coulomb Stress (MPa)
0.0 1.0 2.0 3.0
EQ Density (Num m⁻²)
0.0 0.2 0.4 0.6 0.8 1.0
EQ Density (Num m⁻²)
(d)
Training Period
Validation Period
θ1 = 0.6780
θ2 = 0.0906
θ3 = 3.6914
Train logp = -147.40
Val logp = -83.71
MAP Value
Sample Forecast
Observed
Earthquake Yearly Rate
0 5 10 15 20 25 30 35
1970 1980 1990 2000 2010

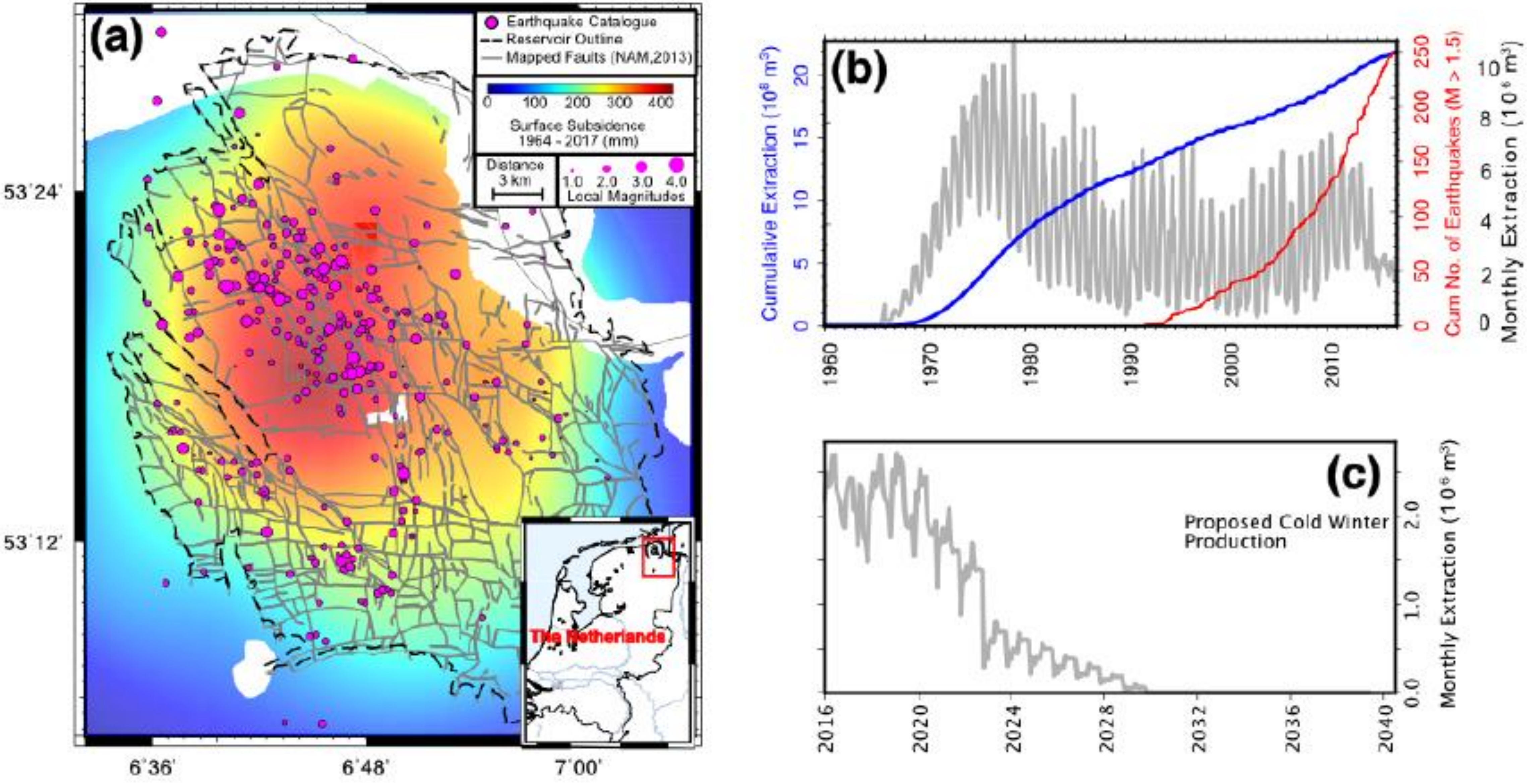

(a)
Earthquake Catalogue
Reservoir Outline
Mapped Faults (NAM,2013)
0 100 200 300 400
Surface Subsidence
1964 - 2017 (mm)
Distance
3 km
1.0 2.0 3.0 4.0
Local Magnitudes
The Netherlands
53°24'
53°12'
6°36'
6°48'
7°00'
(b)
Cumulative Extraction (10^8 m^3)
Cum No. of Earthquakes (M > 1.5)
Monthly Extraction (10^6 m^3)
1960
1970
1980
1990
2000
2010
(c)
Proposed Cold Winter Production
Monthly Extraction (10^6 m^3)
2016
2020
2024
2028
2032
2036
2040

Surface Deformation (Leveling, InSAR, GPS)

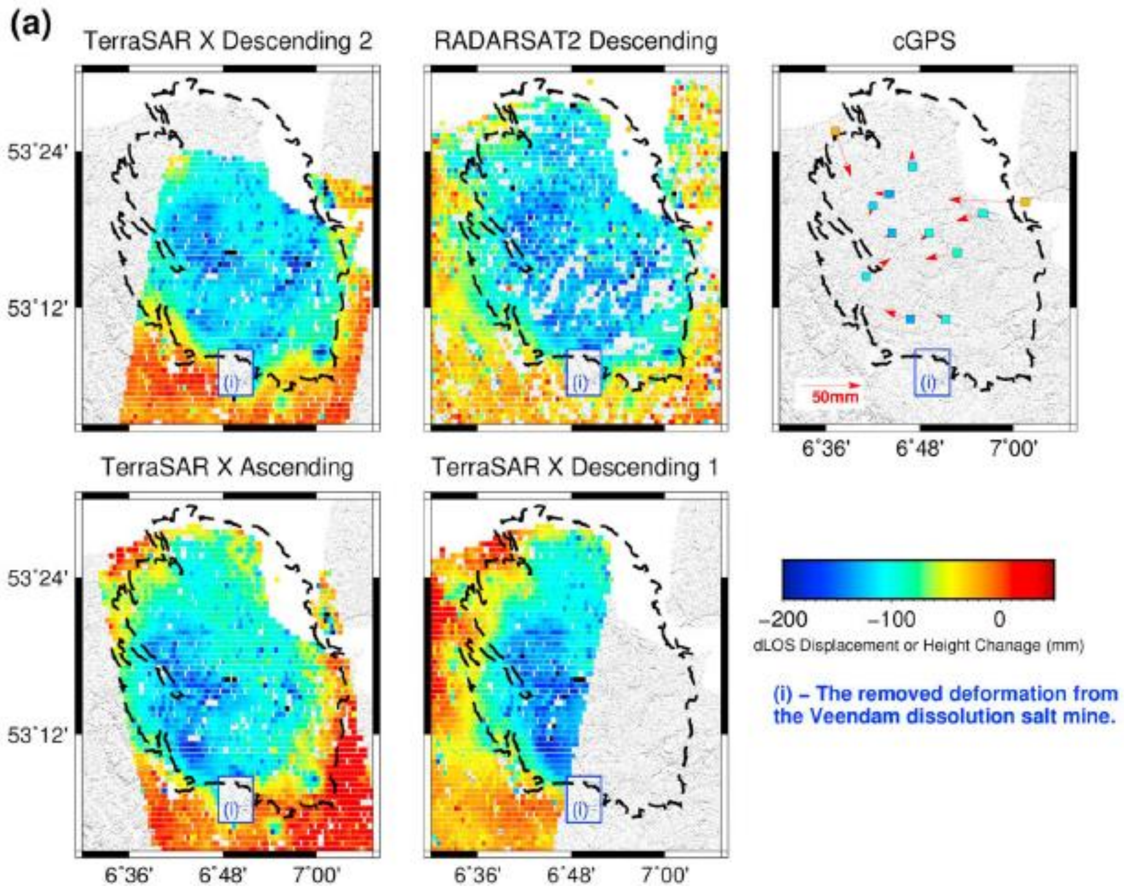

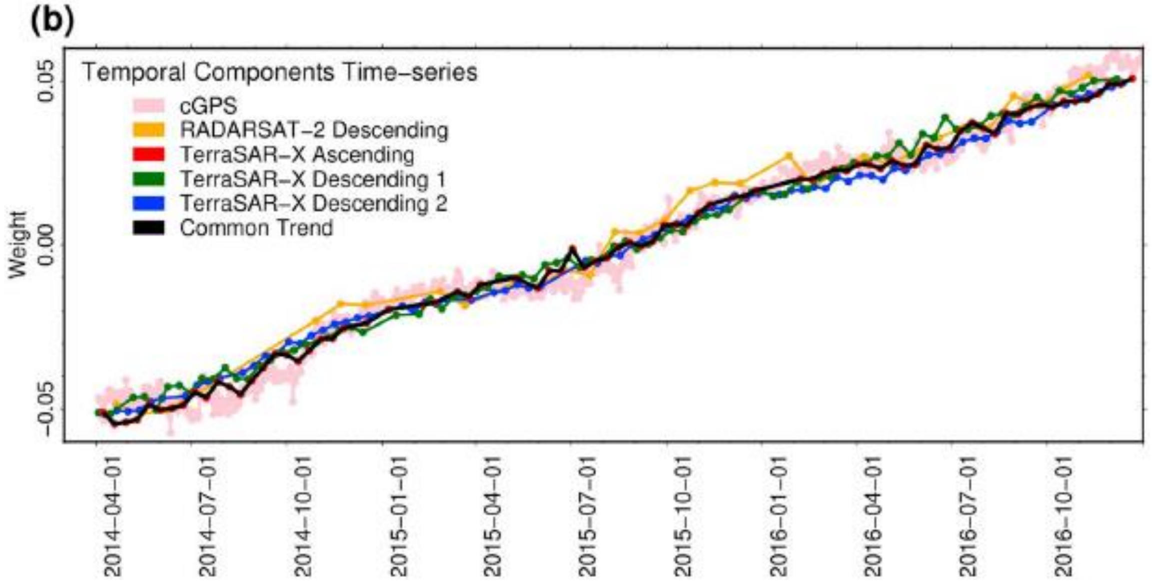

(Smith et al, JGR, 2019)

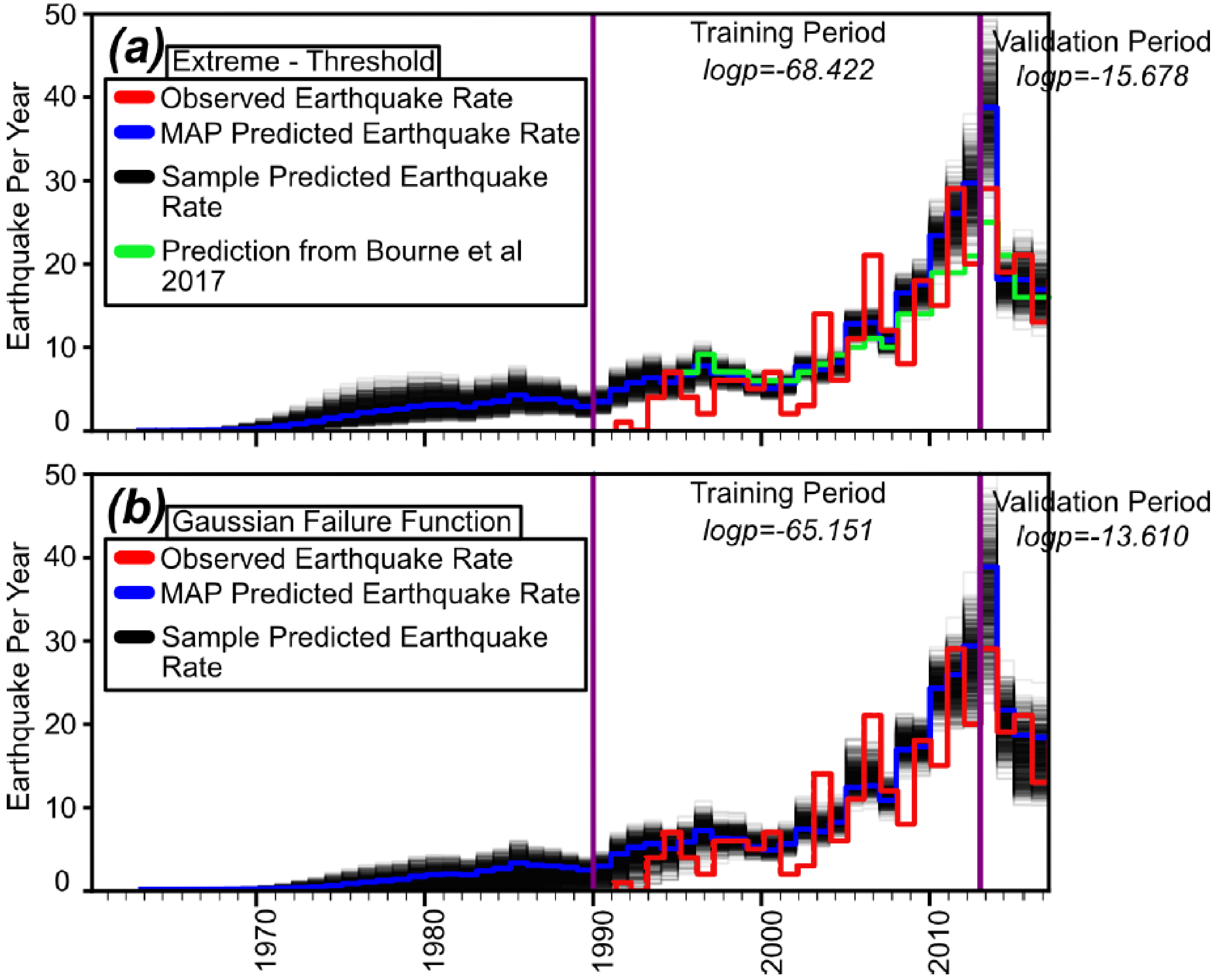

(a)
Extreme - Threshold
Observed Earthquake Rate
MAP Predicted Earthquake Rate
Sample Predicted Earthquake Rate
Prediction from Bourne et al 2017
Training Period
logp=-68.422
Validation Period
logp=-15.678
Earthquake Per Year
0
10
20
30
40
50
(b)
Gaussian Failure Function
Observed Earthquake Rate
MAP Predicted Earthquake Rate
Sample Predicted Earthquake Rate
Training Period
logp=-65.151
Validation Period
logp=-13.610
Earthquake Per Year
0
10
20
30
40
50
1970
1980
1990
2000
2010

Seismicity Forecasting- Synthetic test

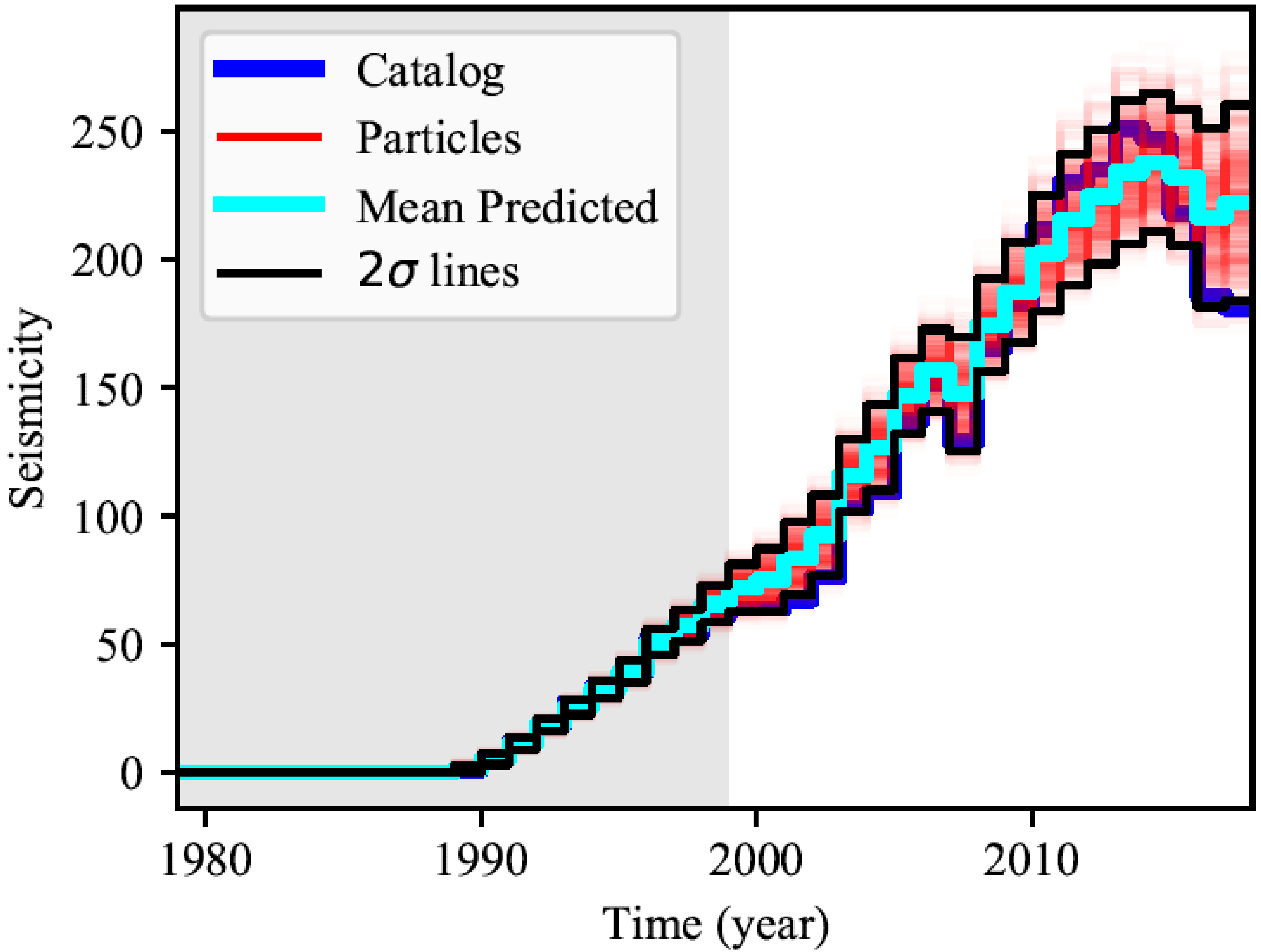

(Hojjat)

Failure Forecasting

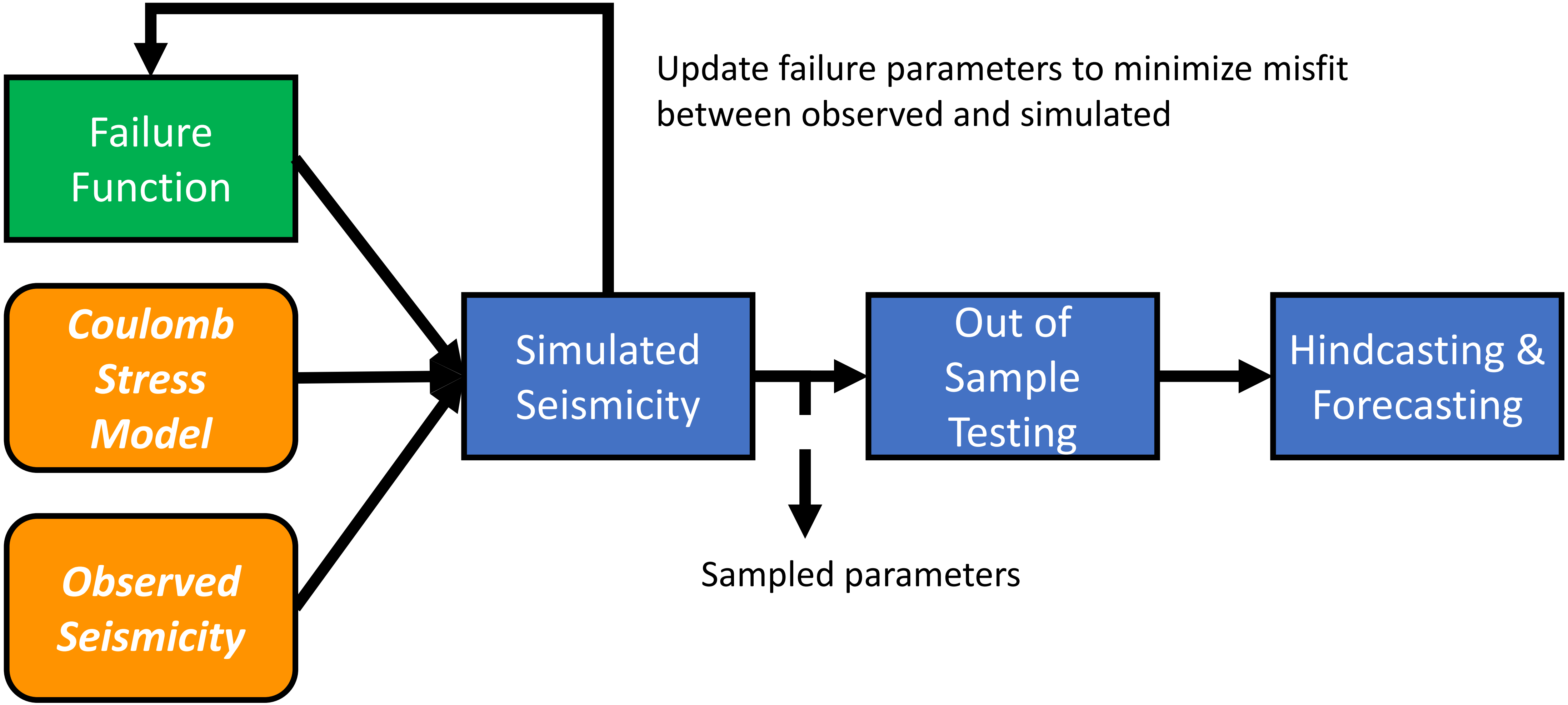

Microseismicity Monitoring – Hypocentral Locations

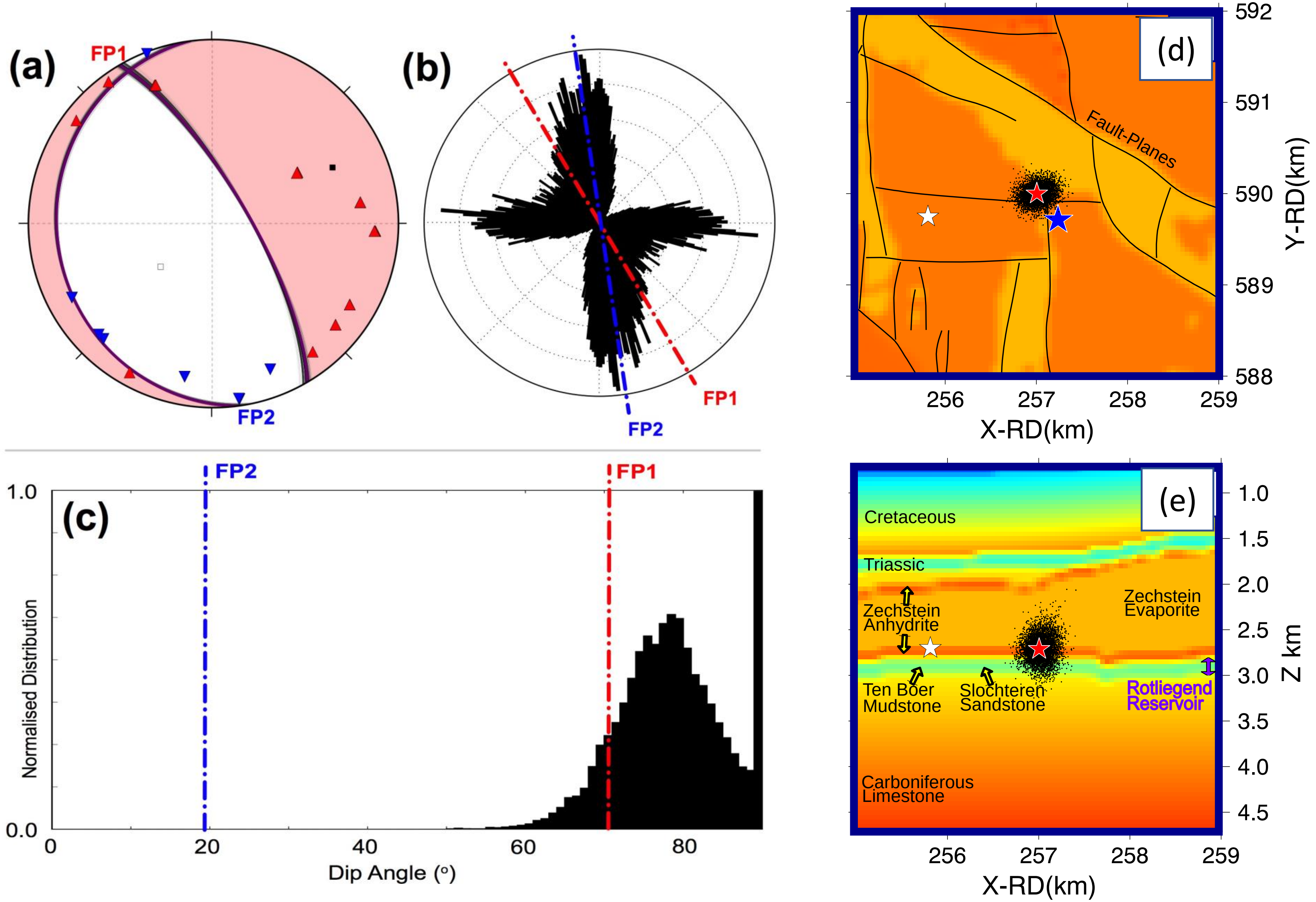

Inference for Extreme Earthquake Magnitudes

How to use and learn from small seismic events

Zak Varty, Jonathan Tawn, Peter Atkinson & Stijn Bierman

M_{max} Workshop, June 2022.

Lancaster University, Shell

Outline

Aim is not only to learn about $M_{\max}$, but also how we approach it.

1. Primer on Extreme Value Theory
2. Learning from Small Magnitude Events
3. Outcomes for Groningen
4. Further Work: Past and Present

A Primer on Extreme Value Theory

Standard Statistical Approaches

- Data = g(Signal, Noise)
- **Aim of Inference:** identify the signal and describe the noise

- Standard methods describe typical values of a process:
  - Linear Regression, t-tests, ANOVA;
  - GLMs, GAMs, Random Forests...
- Fitting and evaluation driven by central values.
  Extrapolate at your own risk!

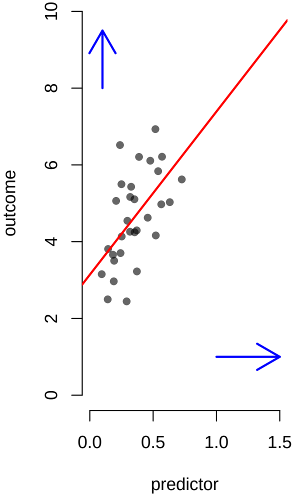

What to do instead: Asymptotically Motivated Model

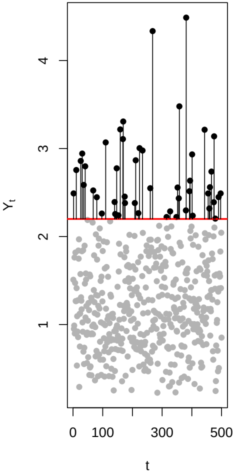

- If we want to model big values then consider only big values.
- Define 'big' as exceedances of some high threshold u.
- In the limit as $u \to \infty$ then the distribution of the suitably rescaled threshold excesses converges to a single probability distribution, **regardless of the initial distribution**.
- Extreme Value Theory tells us that this is the **Generalised Pareto Distribution**.

The Generalised Pareto Distribution

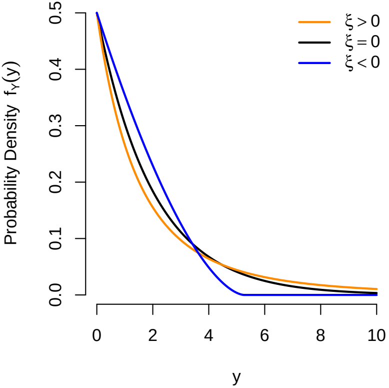

- $\xi = 0$: Exponential distribution $\iff$ GR Law
- $\xi > 0$: Pareto distribution $\iff$ Power Law
- $\xi < 0$: Finite upper endpoint, similar to exponential taper model.

The Generalised Pareto Distribution

Distribution function:

For GPD(σ_u, ξ) exceedances of u

$$F(y) = 1 - \left[1 + \xi \frac{y-u}{\sigma_u}\right]_+^{-1/\xi} \text{ for } y > u$$

where $\sigma_u > 0$ and $x_+ = \max(x, 0)$.

Threshold stability property:

If GPD(σ_u, ξ) above u then for any $v > u$

$$Y - v \mid Y > v \;\sim\; \text{GPD}(\sigma_u + \xi(v-u),\ \xi) \;=\; \text{GPD}(\sigma_v,\ \xi.)$$

Applying EVT to finite samples

- Apply this tractable asymptotic model at finite levels.
- Using assumptions to buy certainty:
  - central limit theorem
  - elastic thin sheet of infinite extent
- Not a spherical chicken in a vacuum, requires only very light assumptions on the original distribution.
- Extends to non-i.i.d. data by having threshold and parameters as a function of time or covariates.

Applications of Extreme Value Theory: Natural Hazards

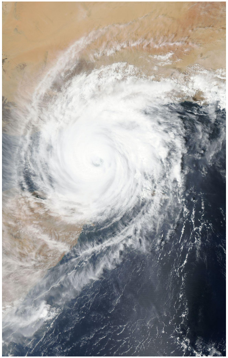

Applications of Extreme Value Theory: Elsewhere

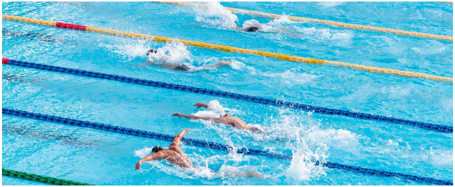

Extreme Value Theory: Summary

- EVT is a mathematically justified means of extrapolation.
- Extreme value models are used as standard across many other disciplines to reflect uncertainty in the tail shape as well as its scale.
- Many intrinsic parallels between EVT and seismicity models:
  - threshold selection $\iff$ magnitude of completion;
  - modelling conditional on being sufficiently large;
  - GPD $\iff$ power law, Gutenberg-Richter, tapered magnitudes.

What can small events tell us about large ones?

Groningen Earthquake Catalogue

Recording:

- Time changing measurement process; more sensors and improved sensitivity.
- Earthquakes missing-not-at-random.
- Rounding to 0.1 M_L.

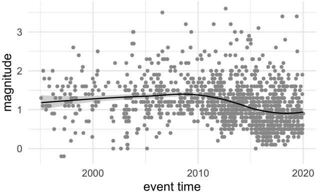

Magnitude of completion $m_c(t)$:

- Smallest magnitude at which earthquake in region is certain to be recorded

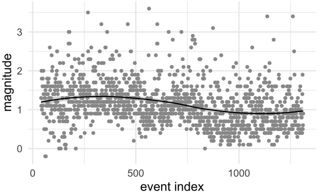

Work in 'event time' and back-transform

Aims of Inference

1. Automate estimation of a time-varying m_c.
2. Estimate and lower $m_c(t)$ from current standard
    - $m_c = 1.45\ M_L$, after 2014 reduced to $m_c = 0.95\ M_L$.
3. Use additional information to **estimate the upper tail of magnitude distribution** - high quantiles and $m_{\max}$.
4. Test consistency with Gutenberg Richter Law.
5. Develop method to handle:
    - trade off in quality of fit vs inference uncertainty
    - rounding
    - non-stationarity
    - informative missingness

Existing Methods & Limitations

Threshold Selection

- Parameter stability plots
- Linearity of magnitude frequency relationship
- PP and QQ plots

- Summaries such as Anderson-Darling
- Rolling quantile

Inference

- Seismic models underestimate epistemic uncertainty
- Roounding and Censoring

New Strategy: Model Structure

- Data $(t_i, x_i) : i = 1, \ldots, n$
- x_i rounded magnitudes, rounding to nearest 2δ
- y_i true magnitudes
- $y_i \in (x_i - \delta, x_i + \delta]$
- event index τ
- threshold (unknown) $v(\tau) \equiv (v_1, \ldots, v_n)$
- $Y_i - u \mid Y_i > u \sim \text{GPD}(\sigma_u, \xi)$ for $u < \min(v_1, \ldots, v_n)$

New Strategy: Model Structure

- Data $(t_i, x_i) : i = 1, \ldots, n$
- x_i rounded magnitudes, rounding to nearest 2δ
- y_i true magnitudes
- $y_i \in (x_i - \delta, x_i + \delta]$
- event index τ
- threshold (unknown) $v(\tau) \equiv (v_1, \ldots, v_n)$
- $Y_i - u \mid Y_i > u \sim \text{GPD}(\sigma_u, \xi)$ for $u < \min(v_1, \ldots, v_n)$

Three cases:

- $x_i > v_i + \delta \implies y_i > v_i$
- $x_i < v_i - \delta \implies y_i < v_i$
- $\mid x_i - v_i \mid < \delta \implies y_i > v_i$ with probability w_i

Likelihood Based Inference

For rounded GPD data and a given threshold $v(\tau)$:

$$\begin{aligned}\ell(\boldsymbol{\theta}|\boldsymbol{x},\boldsymbol{v}) &= \sum_{i=1}^{n} w_i \log \Pr(X_i = x_i | Y_i > v_i, \boldsymbol{\theta}) \\ &= \sum_{i=1}^{n} w_i \log \Pr(\max(v_i, x_i - \delta) < Y_i < x_i + \delta | \boldsymbol{\theta})\end{aligned}$$

where

$$w_i = \frac{\Pr(\max(v_i, x_i - \delta) < Y_i < x_i + \delta | \boldsymbol{\theta})}{\Pr(x_i - \delta < Y_i < x_i + \delta | \boldsymbol{\theta})}.$$

Likelihood Based Inference

For rounded GPD data and a given threshold $v(\tau)$:

$$\begin{aligned}\ell(\boldsymbol{\theta}|\boldsymbol{x},\boldsymbol{v}) &= \sum_{i=1}^{n} w_i \log \Pr(X_i = x_i | Y_i > v_i, \boldsymbol{\theta}) \\ &= \sum_{i=1}^{n} w_i \log \Pr(\max(v_i, x_i - \delta) < Y_i < x_i + \delta | \boldsymbol{\theta})\end{aligned}$$

where

$$w_i = \frac{\Pr(\max(v_i, x_i - \delta) < Y_i < x_i + \delta|\boldsymbol{\theta})}{\Pr(x_i - \delta < Y_i < x_i + \delta|\boldsymbol{\theta})}.$$

Issue: Changing sample size rules out standard model comparison

Measuring Fit: Metric definitions

Calculated on standard exponential scale (threshold invariance and PIT).

$$d_0 = d(q,1) = \frac{1}{m}\sum_{j=1}^{m} |-\log(1-p_j) - Q(p_j)|$$

$$d_0 = d(q,2) = \frac{1}{m}\sum_{j=1}^{m} (-\log(1-p_j) - Q(p_j))^2.$$

- Sequence of probabilities $p_i = i/(m+1)$
- Q is empirical quantile function
- PP methods- much less effective

New Threshold Selection Strategy

For given threshold choice for $v(\tau)$:

- Assess fit using QQ or PP plot
- Use metric to summarise difference between model and empirical - d_0
- Parametric bootstrapped replicates of $X \implies \hat{\theta}_{GPD} \implies Y$
  - Sample size varies (due to rounding)
  - Take expectation over latent Y and $\hat{\theta}_{GPD}$ variables

$\implies$ Output $d = E_{Y,\hat{\theta}_{GPD}|x,v(\tau)}(d_0)$ (subject to Monte Carlo noise)

New Threshold Selection Strategy

For given threshold choice for $v(\tau)$:

- Assess fit using QQ or PP plot
- Use metric to summarise difference between model and empirical - d_0
- Parametric bootstrapped replicates of $X \implies \hat{\theta}_{GPD} \implies Y$
  - Sample size varies (due to rounding)
  - Take expectation over latent Y and $\hat{\theta}_{GPD}$ variables

$\implies$ Output $d = E_{Y,\hat{\theta}_{GPD}|x,v(\tau)}(d_0)$ (subject to Monte Carlo noise)

Automatic selection of $v(\tau)$:

- Parametric $v(\tau)$ with parameters θ_v
- Minimise d over θ_v
- Minimise using grid-search for low dimensional θ_v
- Minimise using Bayesian optimisation methods for higher dimensional θ_v

Parametric Threshold Models

Flat: $\theta_v = (v)$

$$v(\tau) = v.$$

Stepped: $\theta_v = (v_L, v_R, \tau^*)$

$$v(\tau) = \begin{cases} v_L & \text{if } \tau \leq \tau^* \\ v_R & \text{if } \tau > \tau^* \end{cases}$$

Sigmoid: $\theta_v = (v_L, v_R, \tau^*, \gamma)$

$$v(\tau) = v_R + (v_L - v_R)\Phi\left(\frac{\tau^* - \tau}{\gamma}\right)$$

Threshold Selection on Simulated Catalogues

Simulated Catalogue Structure

Censoring methods: (i) hard and (ii) phased. In phased censoring the detection probability of each event is

$$\alpha(y_i, v_i) = \exp(-\lambda[v_i - y_i]_+), \text{ where } \lambda > 0.$$

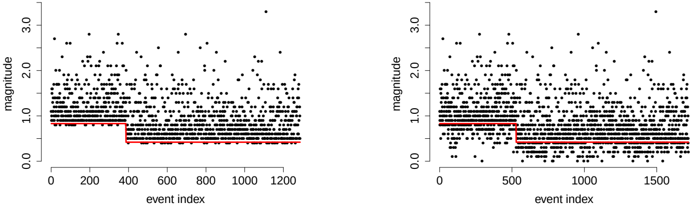

Figure 1: Example simulated catalogues with hard censoring [left] and phased censoring [right] for stepped thresholds of $(v_L, v_R) = (0.83, 0.42)$, shown as a red line, and phasing parameter $\lambda = 7$.

Flat Threshold, Hard Censoring: Single Catalogue

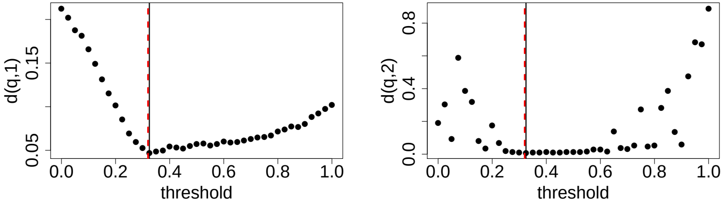

Figure 2: Flat threshold selection on a simulated catalogue. Top row: expected mean absolute [left] and expected mean squared [right] QQ-distances against threshold value. Selected and true thresholds are indicated by solid black and dashed red lines.

Flat Threshold, Hard Censoring: Replicate Results

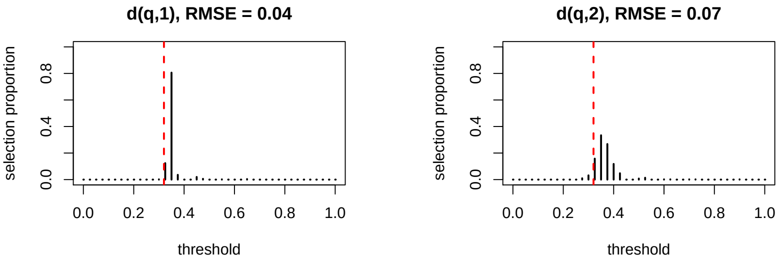

Figure 3: Sampling distribution of threshold selection methods for quantile-based metrics over 500 simulated catalogues with constant threshold and hard censoring. The true threshold is shown by a dashed red line and the root mean squared error (RMSE) for each method is given in plot titles.

Focus now only the absolute error QQ metric

Comparison of Hard and Phased Censoring

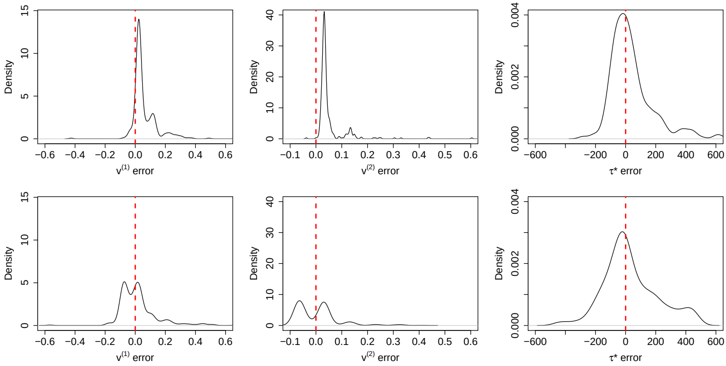

Figure 4: Marginal sampling distributions of errors in the selected values of $v^{(1)}$ (left), $v^{(2)}$ (center) and τ^* (right) for 500 simulated catalogues with change-point type thresholds and hard (top row) or phased (bottom row) censoring.

Application to Groningen Catalogue

Application to Groningen catalogue

Comparing GPD vs Gutenberg-Richter above conservative threshold:

- Conservative threshold: $v_C = 1.45 M_L$
- 311 exceedances
- $\hat{\xi} = -0.018$
- (if rounding ignored $\hat{\xi} = -0.027$)
- Bootstrap 95% CI: $(-0.147; 0.086)$
- Can't rule out Gutenberg-Richter law (Exponential tail)

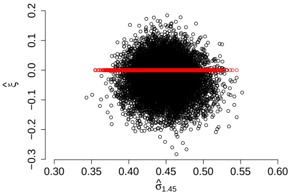

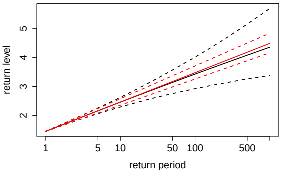

GPD fits well above v_C

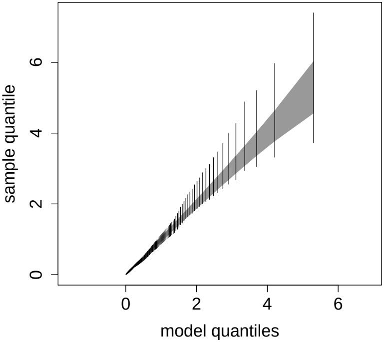

Figure 5: QQ plot for Groningen magnitudes exceeding $1.45\mathrm{M_L}$ under the GPD model. Grey regions show 95% tolerance intervals while vertical lines show 95% confidence intervals on sample probabilities / quantiles. All confidence intervals overlap with the associated tolerance intervals.

Flat Threshold Selection

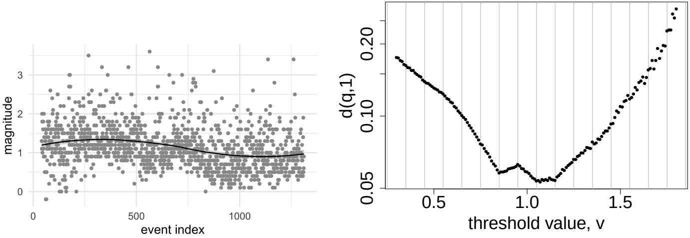

Figure 6: [Left] Data, [Right] Grid search to minimise $d(q,1)$ over threshold values flat threshold. Metric values are shown on log-scale and vertical lines mark the edges of magnitude rounding intervals

- $v_C = 1.45$ is a poor choice
- Two minima of interest

Sigmoid Threshold Selection

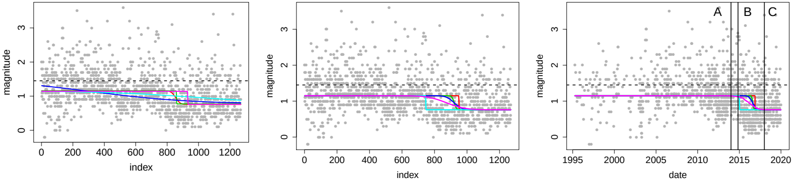

Figure 7: Selected sigmoid thresholds using Bayesian optimisation. [left] Optimising over all thresholds parameters. [centre, right] Optimising over (τ^*, γ) and fixing $(v_L, v_R) = (1.15, 0.76)$ on index- (centre) and natural- (right) timescales. Dates: (A) network development begins, (B) first additional sensors activated, (C) upgrade complete.

Data used above thresholds and value of $d \times 1000$:

- Conservative choice: $n_v = 311$, $d = 91$
- Best flat: $n_v = 627$, $d = 54$
- Best sigmoid: $n_v = 702$, $d = 41$

Benefits of lower threshold

- Lowered $m_c(\tau) \implies$ more data to use
- Better parameter inference
- $\hat{\xi} = -0.069$ 95% CI $(-0.144, -0.008)$
- Excludes zero: weak evidence against Gutenberg-Richter law

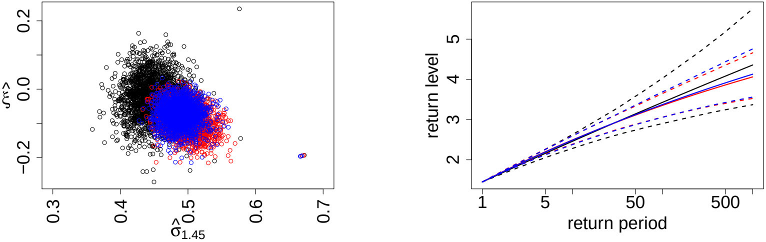

Figure 8: Bootstrap GPD parameter estimates based on exceedances of the conservative (black), flat and sigmoid thresholds [left]. Estimated return levels in M_L and 95% confidence intervals for magnitudes exceeding $1.45M_L$ [right].

Summary

1. The Generalised Pareto Distribution unifies magnitude-frequency relationships, better representing epistemic uncertainty.

2. Including small magnitude events is cost effective and informative.

3. Using a time varying threshold gives evidence of sub-exponential decay.

4. Magnitude-Frequency relationship is described as we approach $M_{\max}$, while properly accounting for uncertainties.

Further Work

- **Does choice of measurement scale matter? ✓**
  Hartog and Bierman investigated robustness to choice of measurement scale.

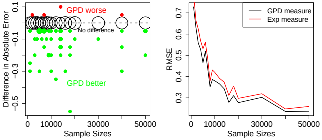

- **Are Exponential margins optimal?**
  Murphy simulation study shows smaller changes can be better.

- **Can we do this without aggregating over space? ✓**
  Murphy extending to spatial threshold selection.

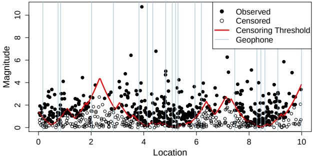

Further, Further Work

- **Can we include stress-dependent magnitudes?**
  More challenging because requires separation of effects.

- **How does this impact prediction?**
  Combining models and propagating uncertainty about earthquake number, rate and size.

- **Can we demonstate effectiveness in other settings?**
  Also useful in more general EVT settings, improved detection common. Suggested applications welcome.

Thank you. Any Questions?

Threshold Selection Paper

Varty, Z., Tawn, J. A., Atkinson, P. M., & Bierman, S. (2021). Inference for extreme earthquake magnitudes accounting for a time-varying measurement process. arXiv preprint arXiv:2102.00884.

Lancaster's EVT Impact

Univariate Extremes

- Optimising the height of all coastal flood protection schemes in the UK, saving £200-300M over 13 years. [link to paper]
- Identified the likely cause of the sinking in 1980 of the MV Derbyshire for the £11M High Court Formal Investigation. [link to paper]
- *Calculated worldwide design standards for bulk carrier hold strength, impacted on the design of 6000 carriers - resulting in many saved ships/lives* [link to paper]

Lancaster's EVT Impact

Multivariate/Spatial Extremes

- *Optimise the structural integrity of over 8% of worldwide offshore oil and gas facilities, saving £80M* [link to paper]
- Developing the widespread flooding scenarios for the UK Government's National Risk Assessment for river + coastal [link to paper]
- Developing spatial flood risk methods for the UK Government's 2016 National Flood Resilience Review:
  e.g., What is probability of a 1 in 100 year event at a site occurring anywhere in UK in a year? [link to paper]

International EVT Impact

- Dutch: Coastal flooding [link to paper]
- US: Hurricanes [link to paper]
- France: Nuclear Safety [link to paper]
- Japan: Earthquake (Annual M_{max} estimation) [link to paper]

Non-Environmental EVT Impact

- Finance: Value-at-risk, portfolio selection [link to paper]
- Sport: rankings across events/records, ultimate performances [link to paper]
- Mortality: Upper bound on Oldest Human Ages [link to paper]

State Supervision of Mines
Ministry of Economic Affairs and Climate

Data-driven Spatiotemporal Assessment of the Event-Size Distribution of the Groningen Extraction-Induced Seismicity Catalogue

Annemarie G. Muntendam-Bos
Associate Professor, TU Delft; Senior Specialist, SodM

Niels Grobbe
Affliate Faculty, University of Hawai'i at Manoa; Specialist, SodM.

Background

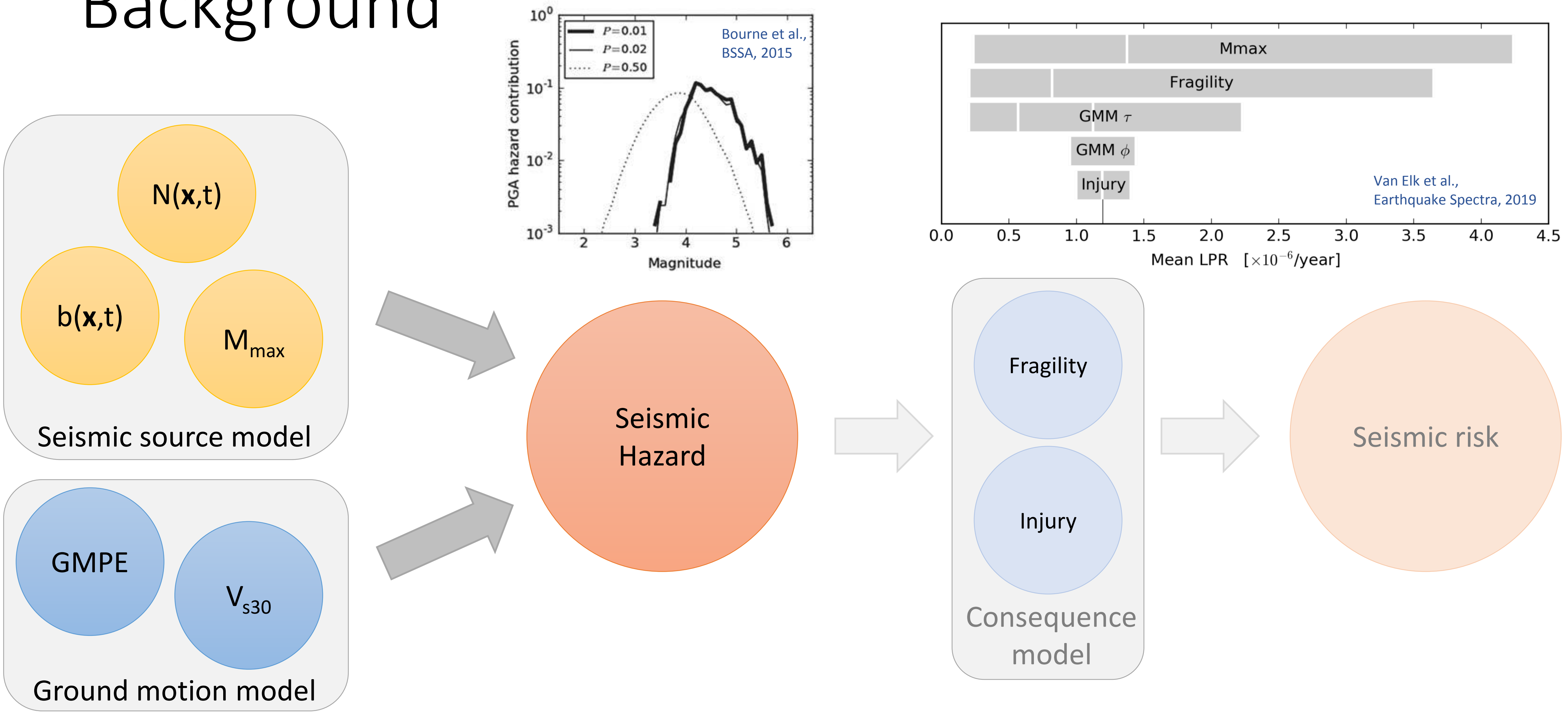

10^{0}
10^{-1}
10^{-2}
10^{-3}
PGA hazard contribution
P=0.01
P=0.02
P=0.50
Bourne et al.,
BSSA, 2015
2
3
4
5
6
Magnitude
Mmax
Fragility
GMM τ
GMM ϕ
Injury
Van Elk et al.,
Earthquake Spectra, 2019
0.0
0.5
1.0
1.5
2.0
2.5
3.0
3.5
4.0
4.5
Mean LPR [$\times 10^{-6}$/year]
N(**x**,t)
b(**x**,t)
M_{max}
Seismic source model
GMPE
V_{s30}
Ground motion model
Seismic Hazard
Fragility
Injury
Consequence model
Seismic risk

Background

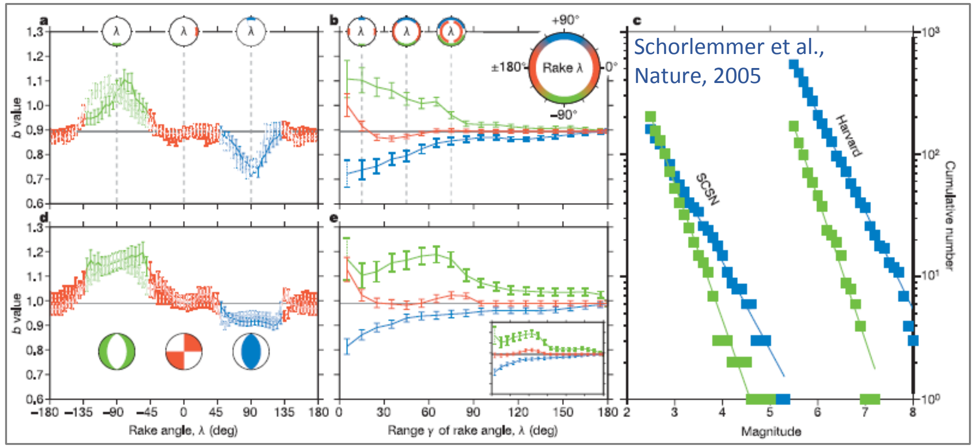

Schorlemmer et al.,
Nature, 2005

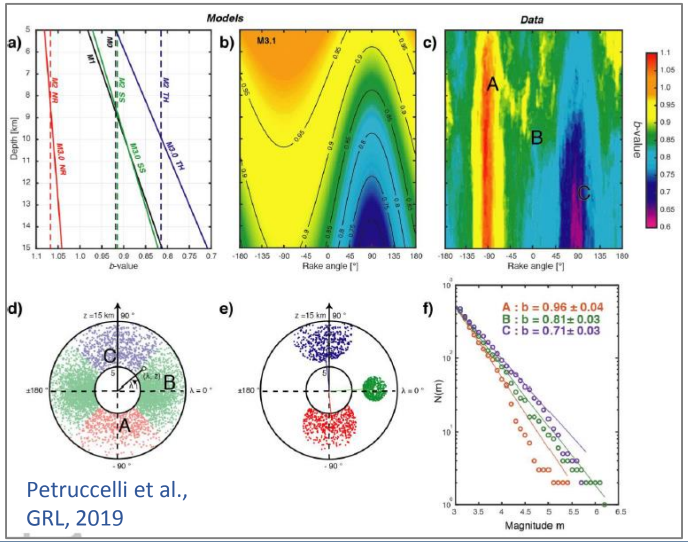

Petruccelli et al.,
GRL, 2019

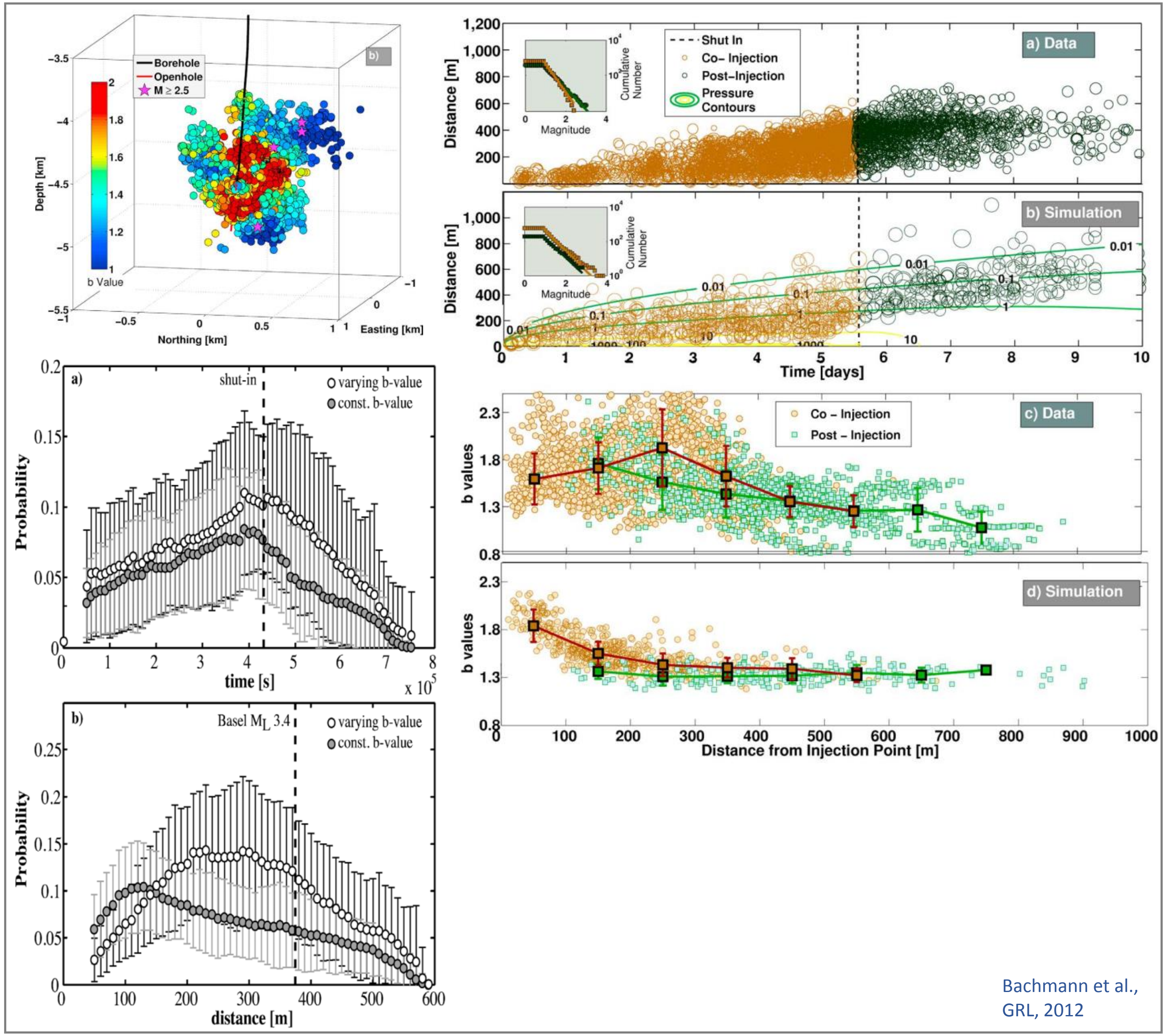

Bachmann et al.,
GRL, 2012

Background

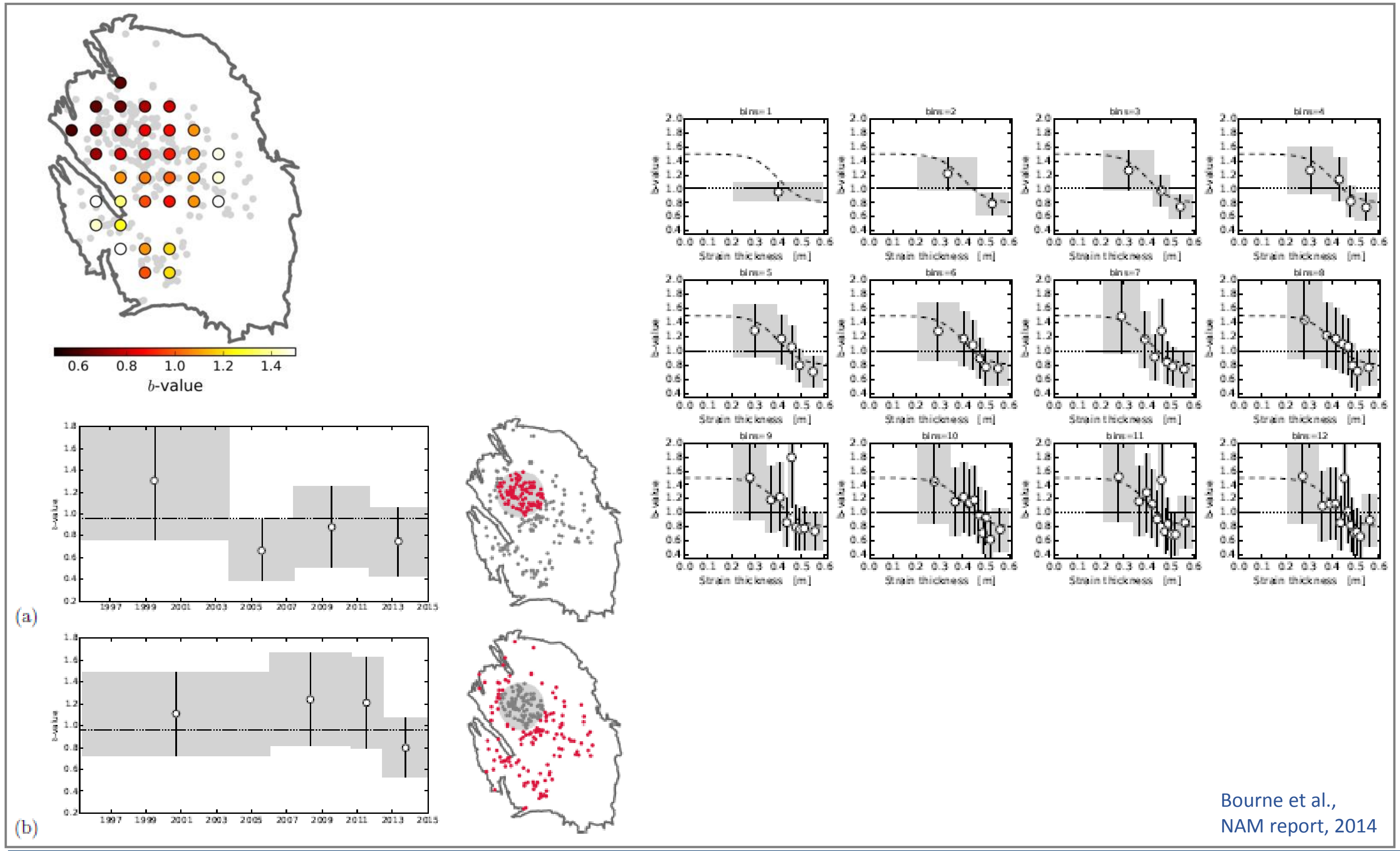

Bourne et al., NAM report, 2014

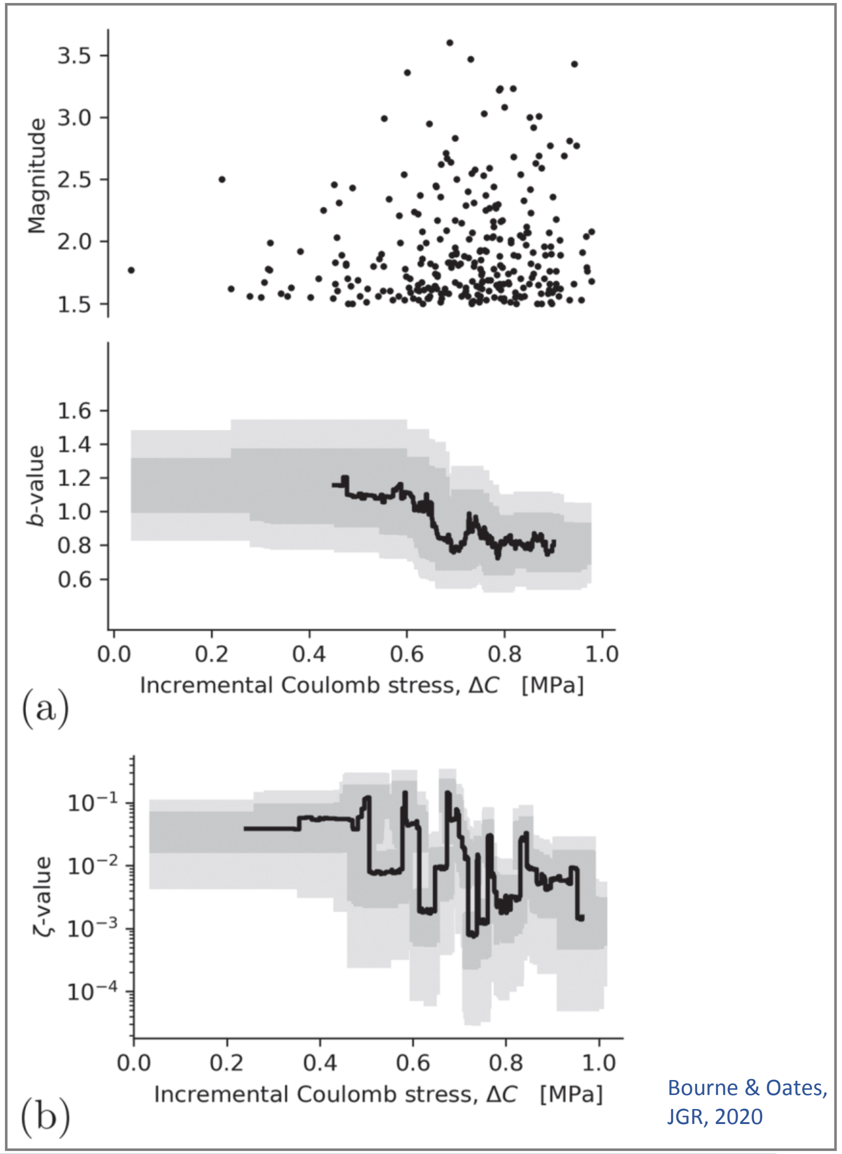

Bourne & Oates, JGR, 2020

Methodology: Penalized likelihood-based method

- Partitioning of the space using a random set of nodes and assign each node its nearest neighbourhood region

  → generates non-overlapping, arbitrarily shaped and sized regions.
  → adding nodes allows for the exploration of smaller scale variations

- Estimate b-value and compute log-likelihood in each region;

- Compute overall log-likelihood of solution by summing the log-likelihoods of all regions;

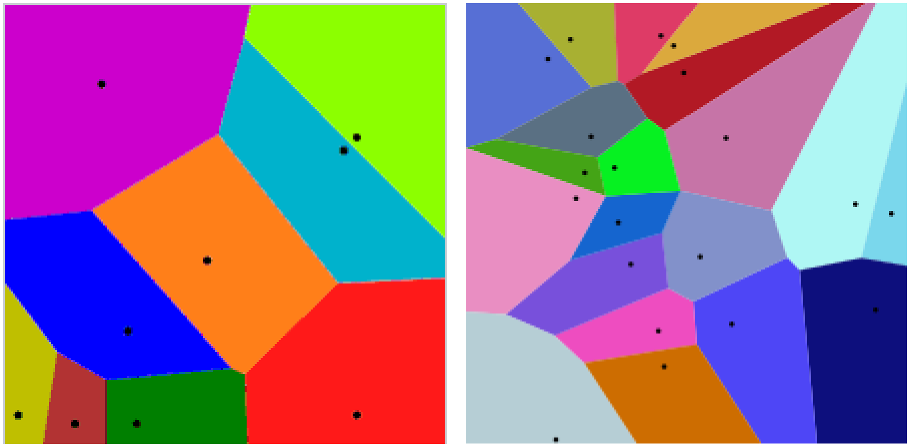

Kamer & Hlemer, JGR, 2015

Methodology: Penalized likelihood-based method

- Compute the Bayesian Information Criterion (BIC) of the solution:

$$BIC = -\log \hat{L} + \frac{k}{2} \log N;$$

- Rank all solutions with $BIC > BIC_{\text{null hypothesis}}$ by their BIC.

- Compute median BIC weighted model of the $BIC > BIC_{\text{null hypothesis}}$ solutions with a max of 1000.

  → representation of the "wisdom of the crowd"-philosophy.

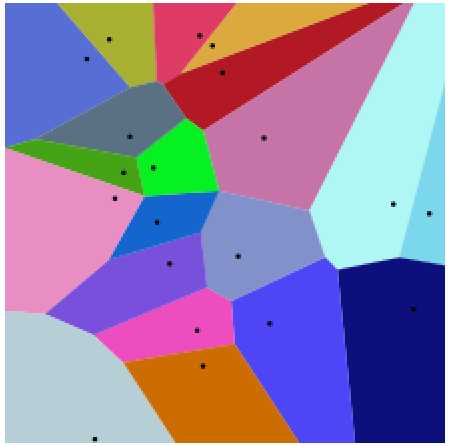

Kamer & Hlemer, JGR, 2015

Methodology: Application to Groningen

1. Derive Mc for full Groningen catalogue (subset KNMI induced seismicity catalogue)
2. Discretize selection space in2.5x2.5km cells (indicated by black corner dots)
3. Select cells with at least two events Ml≥Mc (magnenta dots)
4. Increase number of nodes considered in tessellation from 2-50, performing 2000 random perturbations at each step
5. For each Voronoi cell in each tessellation compute Mc, b-value and log-likelihood
6. Compute tessellation log-likelihood and BIC
7. Compute median model & interquartile range.

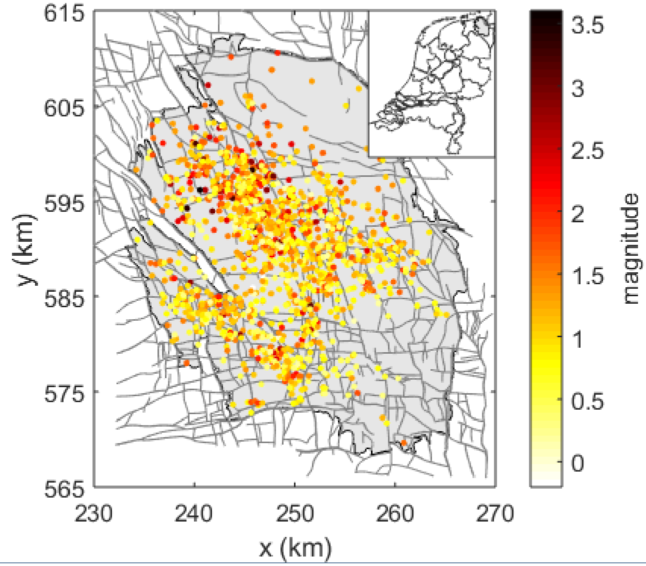

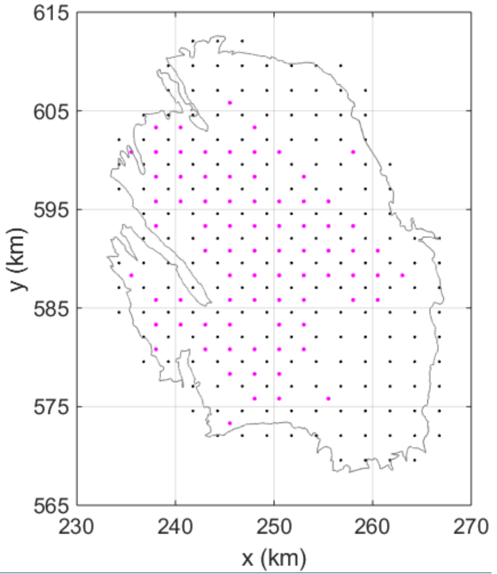

Spatial variations in b-value
Results

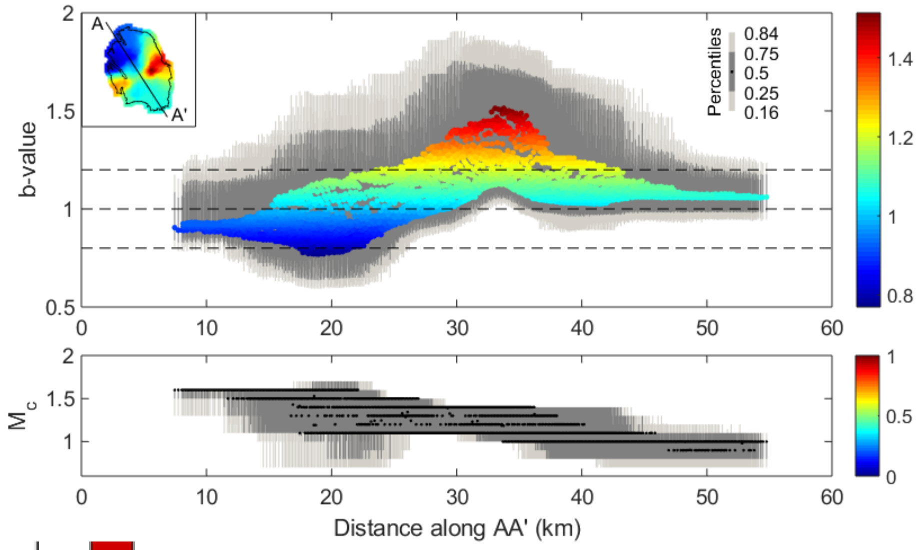

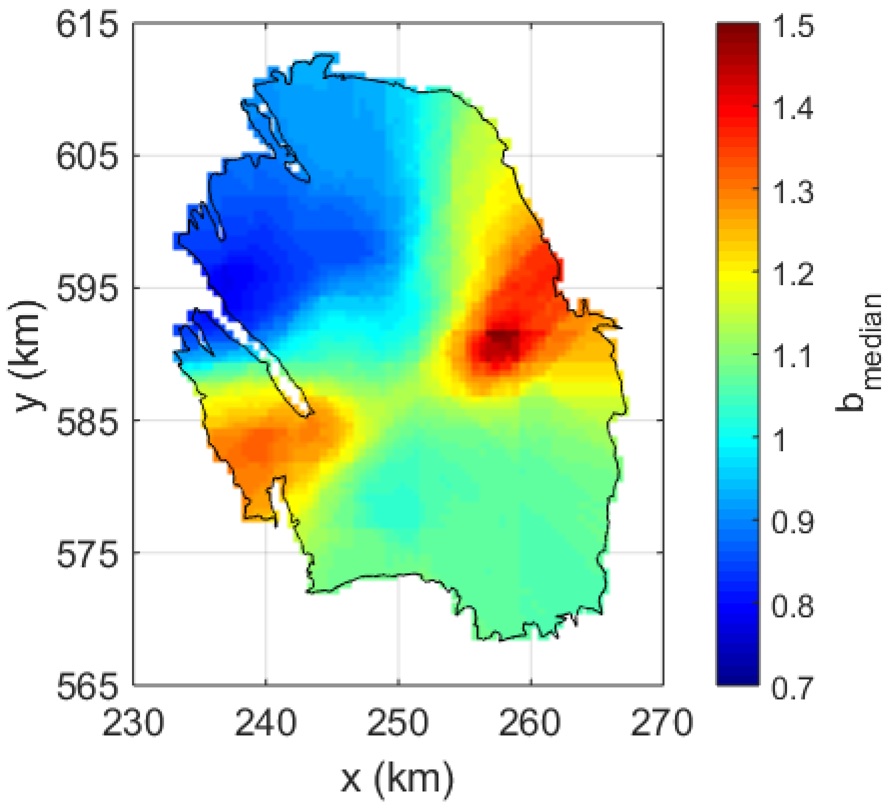

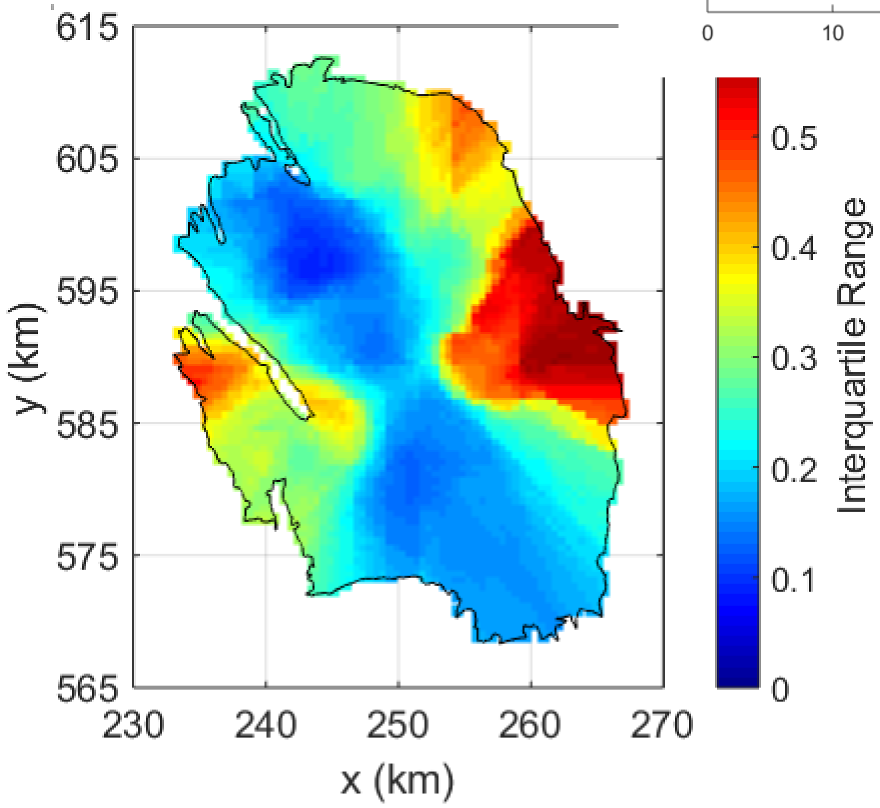

$$b_{null} = 0.95 \pm 0.04$$

Spatial variations in b-value

Validation

1. Two sample, left-tailed t-test:

   Probability that regional b-values are samples of single b-value distribution (null hypothesis) < 5%

2. Corrected Akaike Information Criterion as well as coefficient of variation indicate no bias due to tapering (the relative probability is comparable, or the non-tapered model is favoured)

   The small dataset yields little to no statistical information on the presence of a taper.

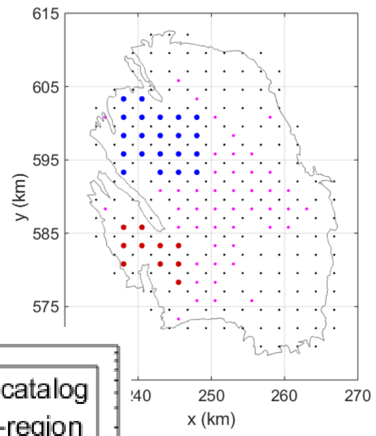

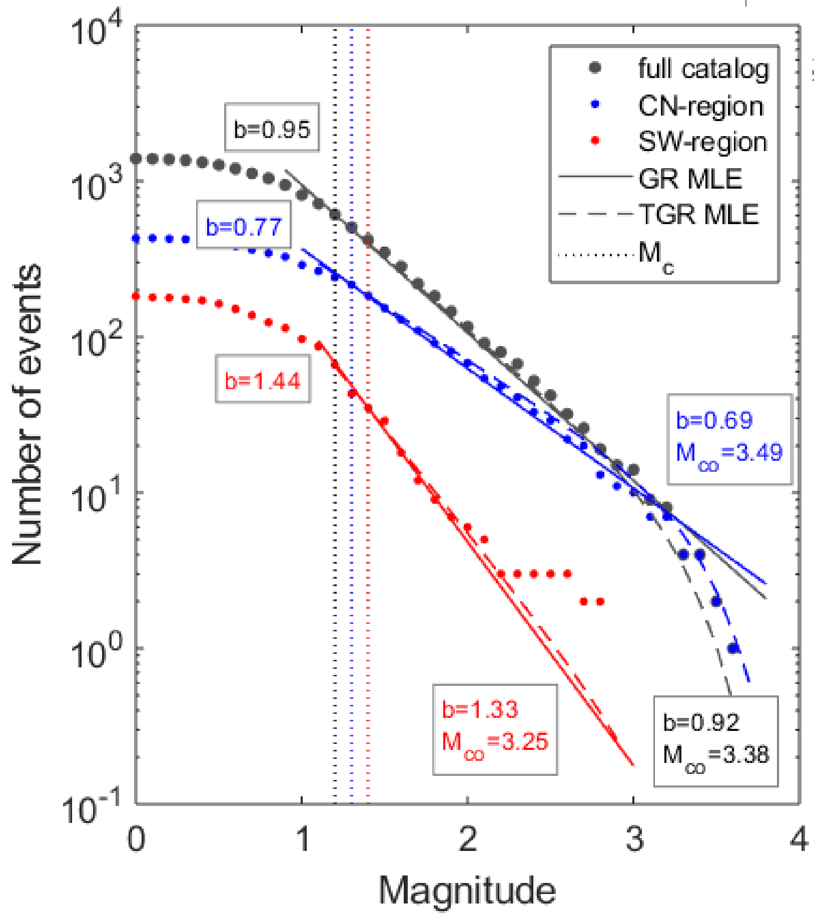

Temporal variations in b-value

Adaptation of spatial approach

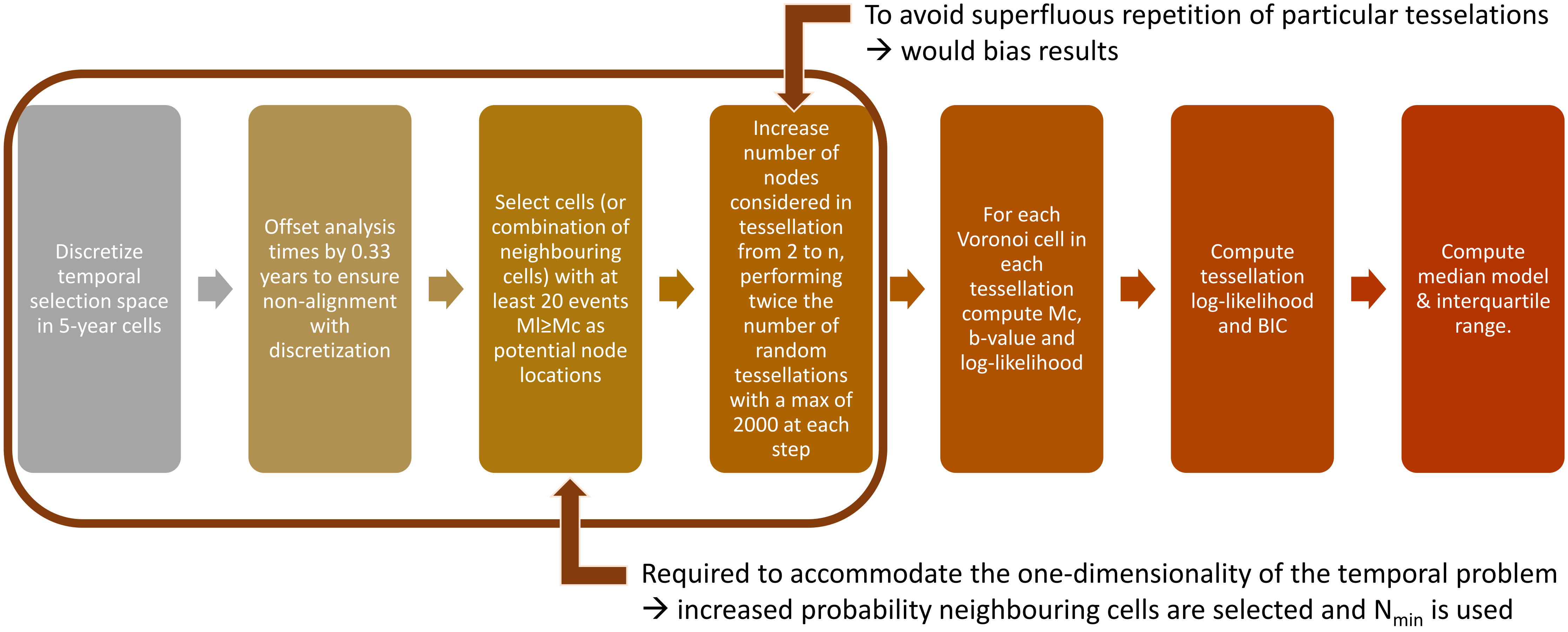

Temporal variations in b-value

Results

- b-value shows minor, statistically insignificant decrease with time; corner magnitude shows statistically insignificant increase with time.
- Significant possitive correlation of b-value with M_c → lowering of M_c due to extension of the network. No indication of a significant bias in (underestimation of) the b-value
- Minor negative correlation with largest event included in the dataset → timing of observed decrease in b-value does not correlate with occurrence of LME's; no bias

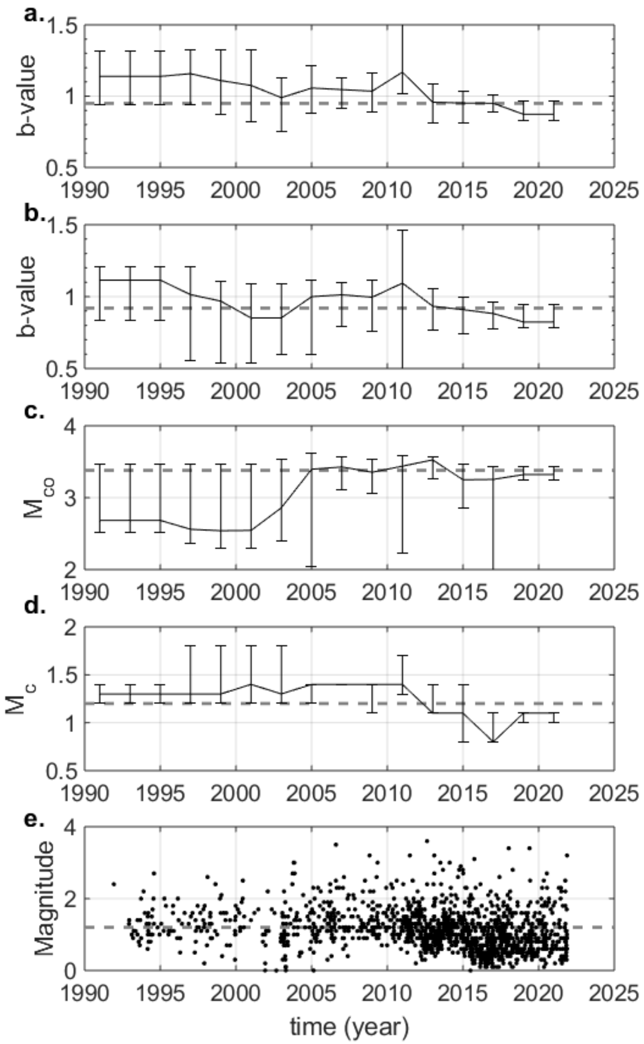

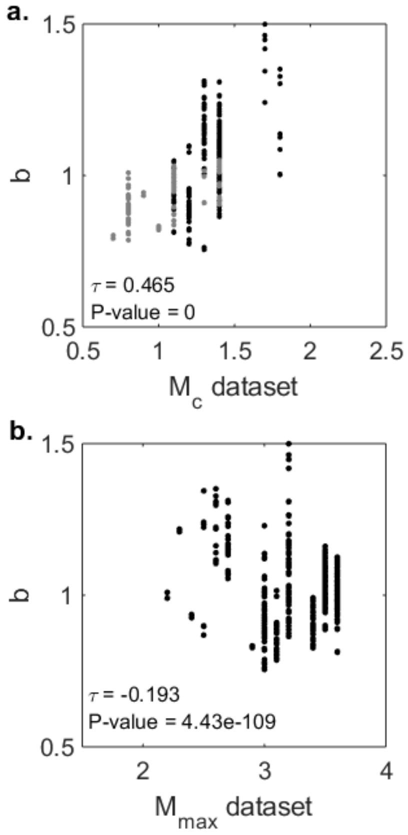

Are the earthquake magnitudes as large as statistically expected?

- Computed the most probable Mmax to be observed (following Van der Elst et al., JGR, 2016)

- In all regions largest magnitude observed increased with time
  → consistent with progressive destabilization of under increasing Coulomb stress due to reservoir depletion.

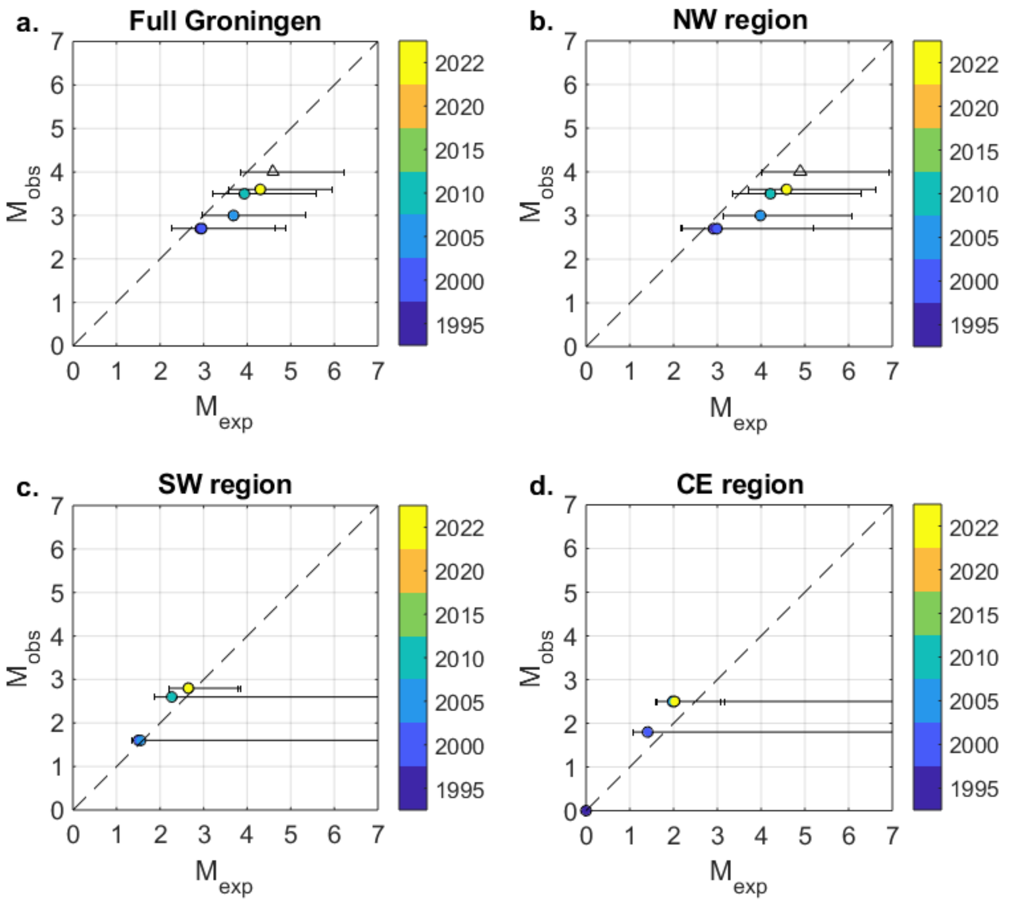

Are the earthquake magnitudes as large as statistically expected?

- Largest magnitude observed in NW-region since 2005 consistently significantly smaller than statistically expected.
- In all other regions and before 2005 are as large as statistically expected.

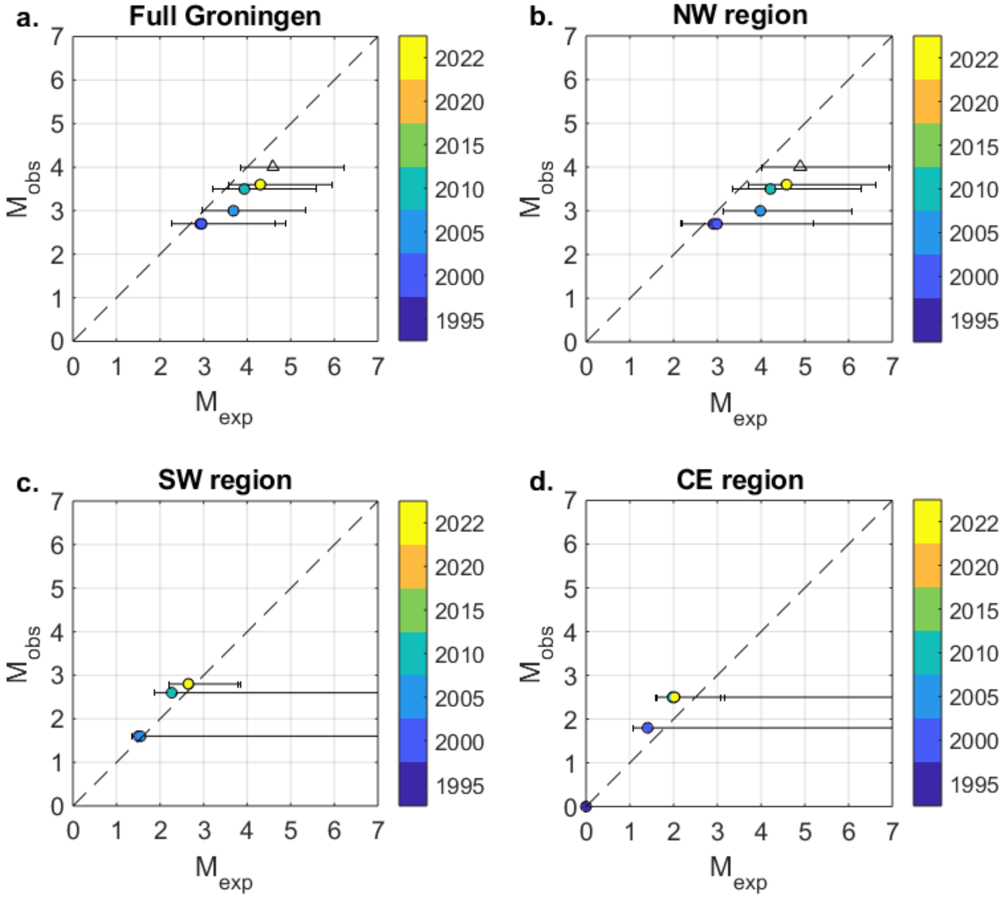

Are the earthquake magnitudes as large as statistically expected?

- M_{obs}^{max} and M_{exp}^{max} can be reconciliated by the occurrence of an increased magnitude event.
- However, even a fictitious $M_l 4.0$ event in the NW region on July 1st, 2022 remains outside the 90% confidence range.

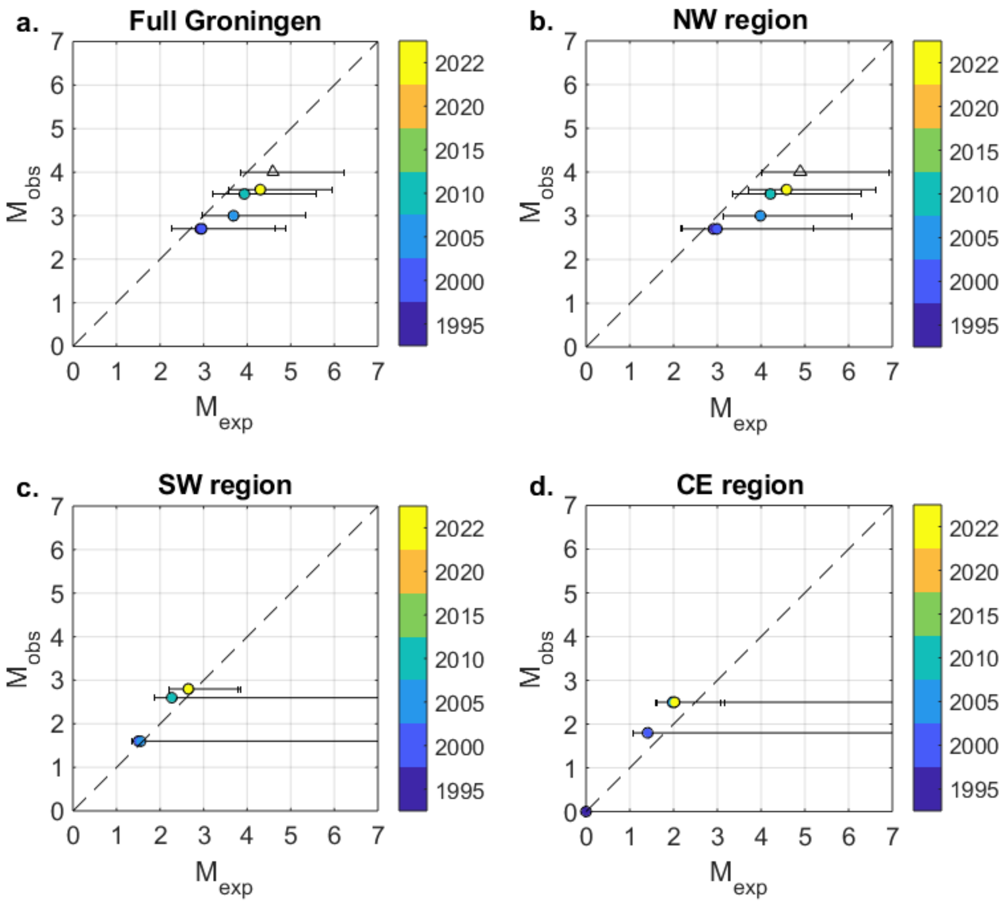

What can we say on Mmax?

- Analysis of NW-region suggests a M_{co}~3.5, bias-corrected M_{co}~3.6
- Would correspond to M_{max}~4.1

- Taking into account large uncertainties → it hints towards the lower end of the current distribution.

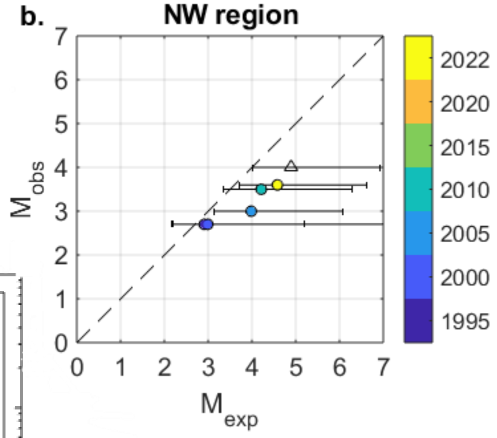

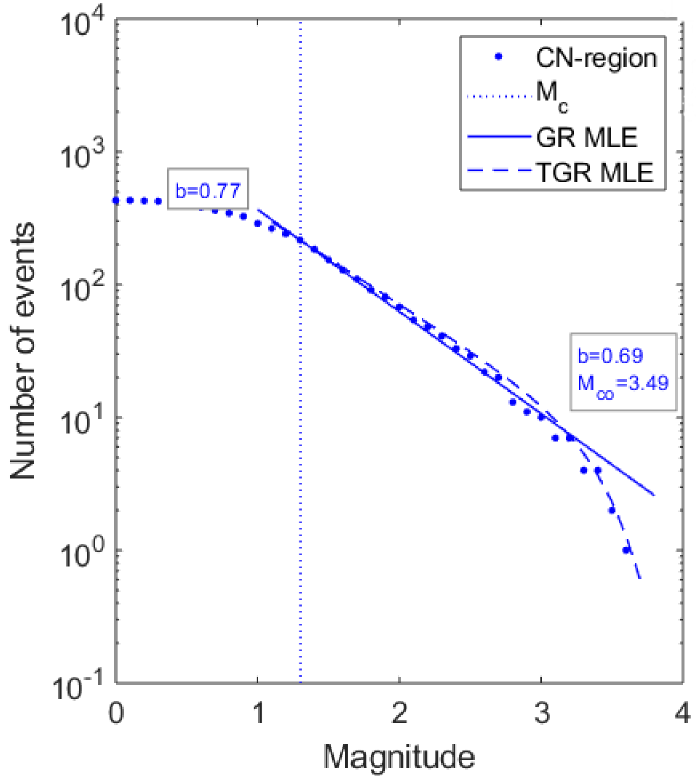

Conclusions

- A clear, statistically significant spatial variation in the b-value:
    - High b-values of ~1.5 in south-western and eastern part of the field;
    - Low b-values of ~0.8 in the northwest of the field.
- No compelling, statistical evidence of temporal variations in the b-value;

- The occurrence probability of the observed larger magnitude events do not scale with the number of earthquakes.
- The results seem consistent with an area-characteristic corner magnitude of 3.6 ($M_{max}{\sim}4.1$)
- Hints towards the lower end of the current distribution

But:
- The dataset for Groningen is very limited and therefore prone to bias.
- This does not disqualify the assessment, but any conclusion on an upper bound should not be inferred based on an assessment of the Groningen dataset alone!

Backup slides

Methodology: Traditional mapping method

Project earthquakes on a planar surface → Grid the surface into equally sized cells → Use the center of each cell as the center of a circle with radius R or an equal-sized (w_b) box →

- If $N_{events}^{circle/box}$ >= N_{min} → compute b-value
- Or increase R/w_b until $N_{events}^{circle/box}$ = $N_{required}$ → compute b-value

→ Assign b-value to location of the cell

Drawbacks:
- b-values of neighbouring cells are inevitably correlated as R/w_b>>D_g → not possible to compute overall log-likelihoods of the solution and compare different solutions.
- Results are sensitive to the choice of the free parameters R/w_b,$N_{\mathrm{required}}/N_{min}$, and D_g;

→ Proper setting of these parameters requires prior knowledge of the spatio-temporal patterns one wishes to resolve (e.g. scale of spatiotemporal variations)

TAPER FROM RECURRENCE RELATIONSHIP TO MMAX

(THE IMPORTANCE OF TAIL DESCRIPTION IN PSHRA)

TNO innovation for life

WORKSHOP OBJECTIVES

1. To clearly define the concept of Mmax in relation to seismicity in the Groningen field and for application in probabilistic seismic hazard and risk analyses.
2. To define a distribution of Mmax values and their associated probabilities, in the form of as discrete logic tree with alternative Mmax values and associated branch weights.
3. To clearly distinguish between induced earthquakes and triggered earthquakes in the formulation of the logic tree, such that the hazard and risk analyses could consider the two types of seismicity separately.
4. To determine if the proposed Mmax distribution is compatible with the existing PSHRA framework for Groningen, including the V6 seismological model and the logic tree.
    1. Can it be implemented? Yes
    2. Does it impact the results of the PSHRA? Yes, but not as much as you may think, and much less than a couple of years ago

TNO'S OBJECTIVES FOR THIS TALK

- To highlight that the context in which Mmax is applied within the Groningen PSHRA has changed considerably since 2016
- To invite discussion on whether that changed context should be accounted for in the workshop results

WHY WE CARE ABOUT EARTHQUAKE MAGNITUDES

And which ones we care about the most

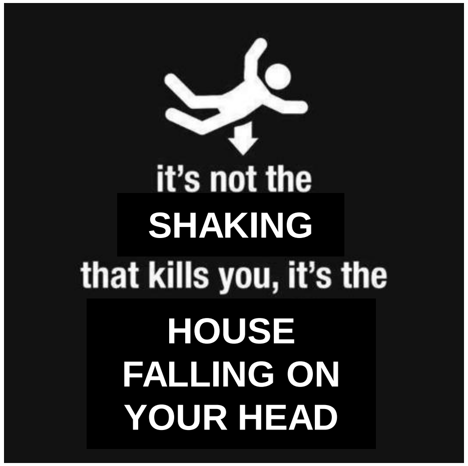

- The risk (of death) usually comes from the rare, but strong earthquakes
- In the case of Groningen, it's from M4.0 and up

Conditional on the 2016 Mmax distribution!

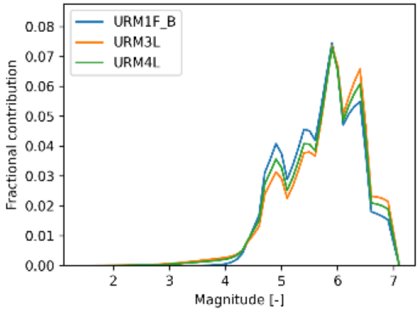

TNO innovation for life

WHY WE CARE ABOUT EARTHQUAKE MAGNITUDES

And which ones we care about the most

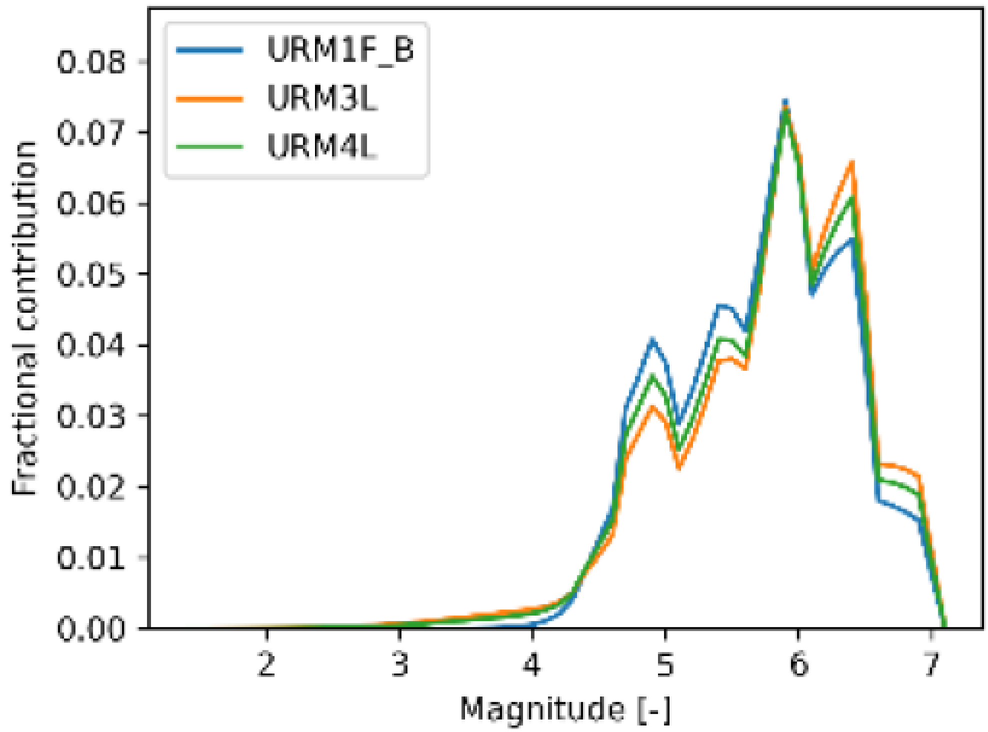

Conditional on the 2016 Mmax distribution!

CONTEXT OF MMAX

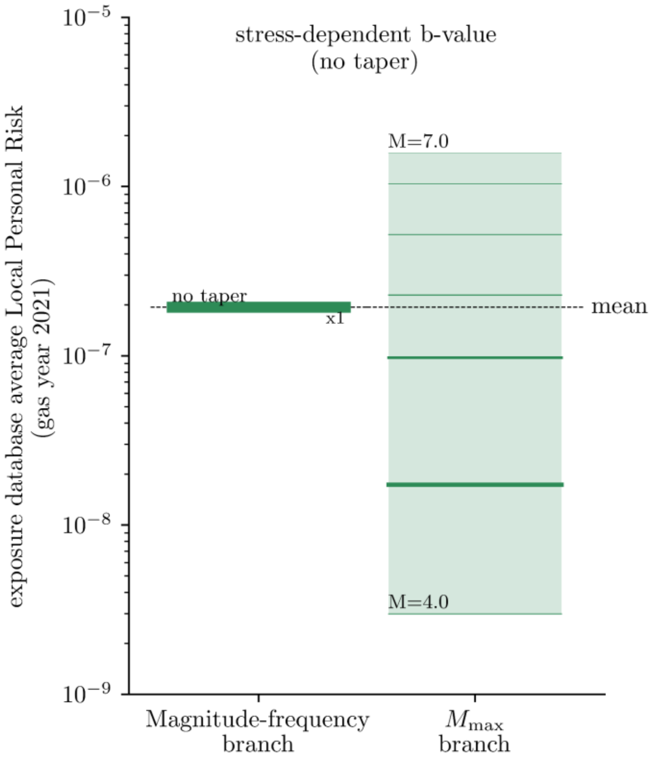

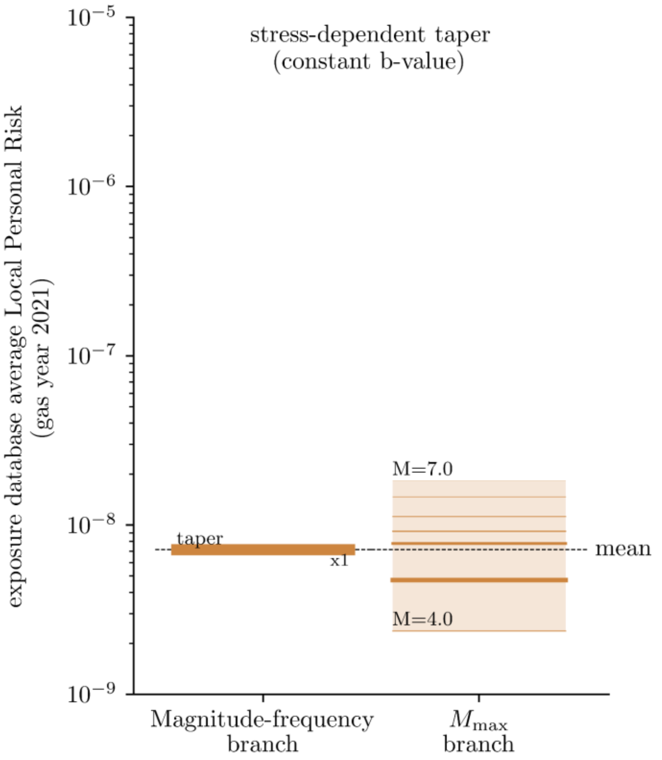

FOCUS OF THIS TALK

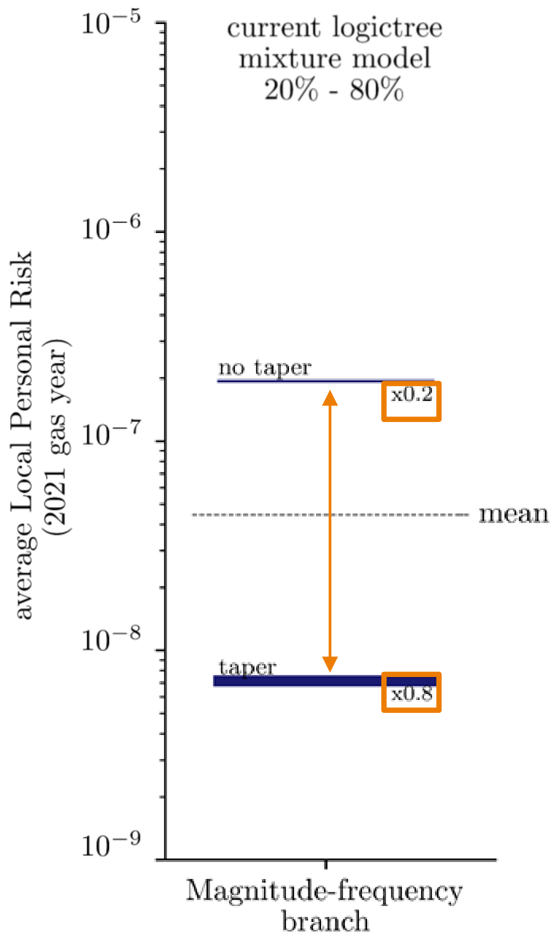

1. Where do these weights come from?
   A statistical analysis that does not appear to be appropriate for assigning weights
2. Where does this gap come from?

Where does that leave the Mmax distribution and its relevance to PSHRA?

FOCUS OF THIS TALK

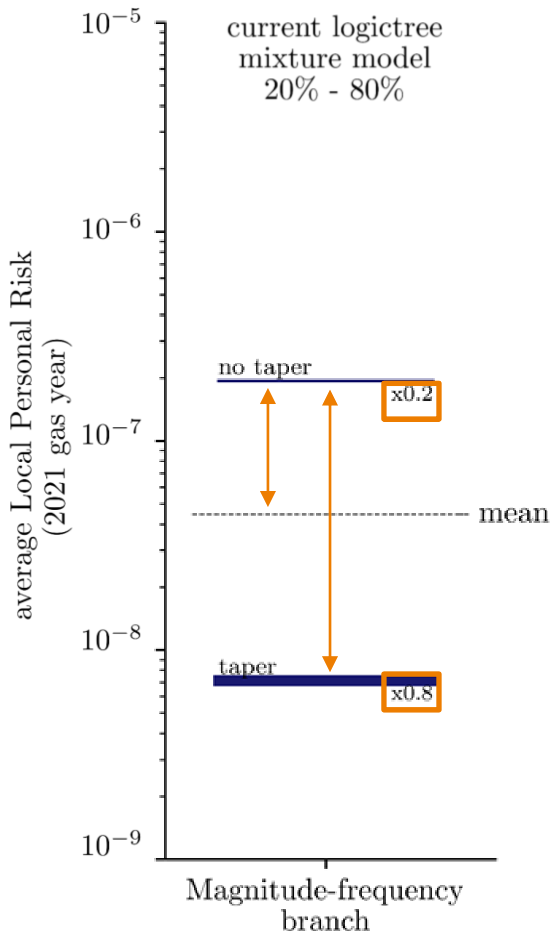

1. Where do these weights come from?
   A statistical analysis that does not appear to be appropriate for assigning weights

2. Where does this gap come from?

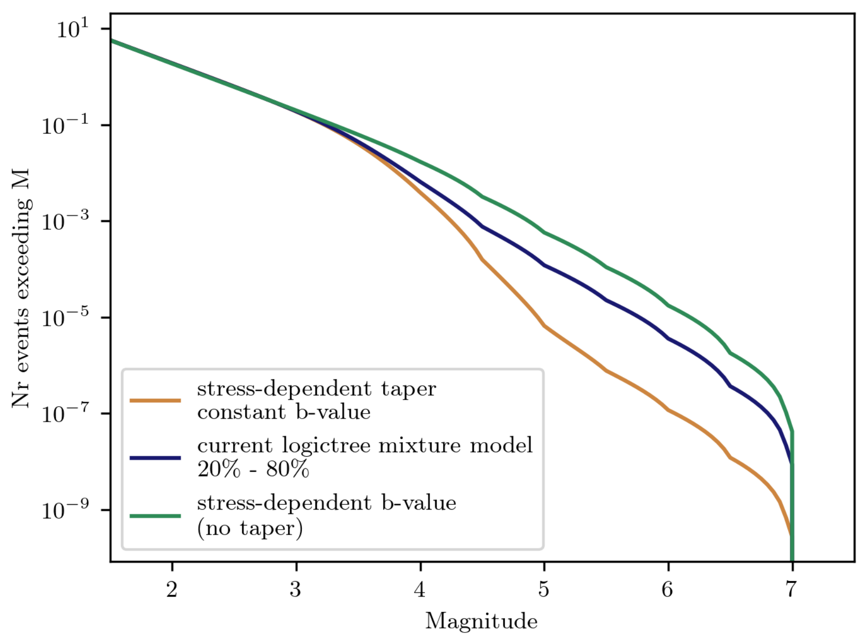

THE G-R MODEL

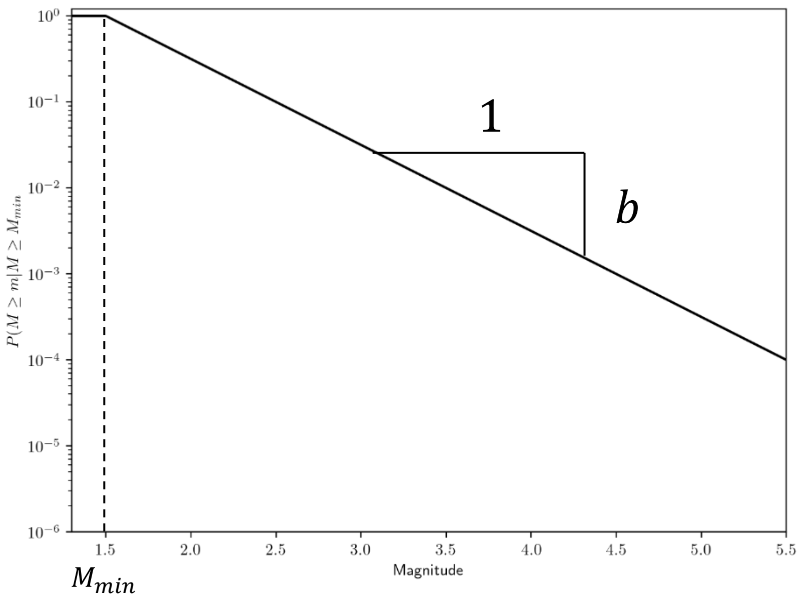

$$P(M \geq m \mid M \geq M_{min}) = 10^{-b(m-M_{min})}$$

THE MMAX-TRUNCATED G-R MODEL

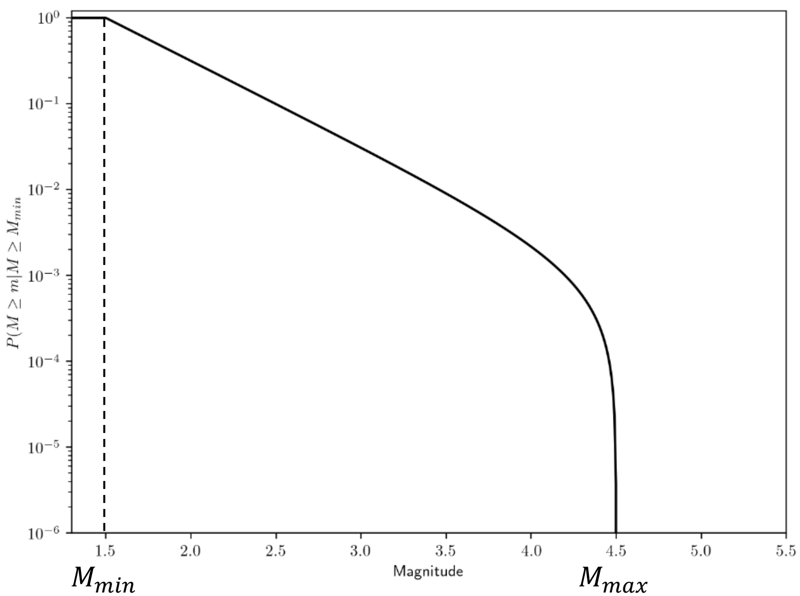

$$P = \frac{10^{-b(m-M_{min})} - 10^{-b(M_{max}-M_{min})}}{1 - 10^{-b(M_{max}-M_{min})}}$$

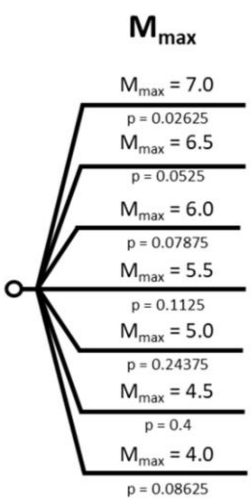

THE TAPER MODEL

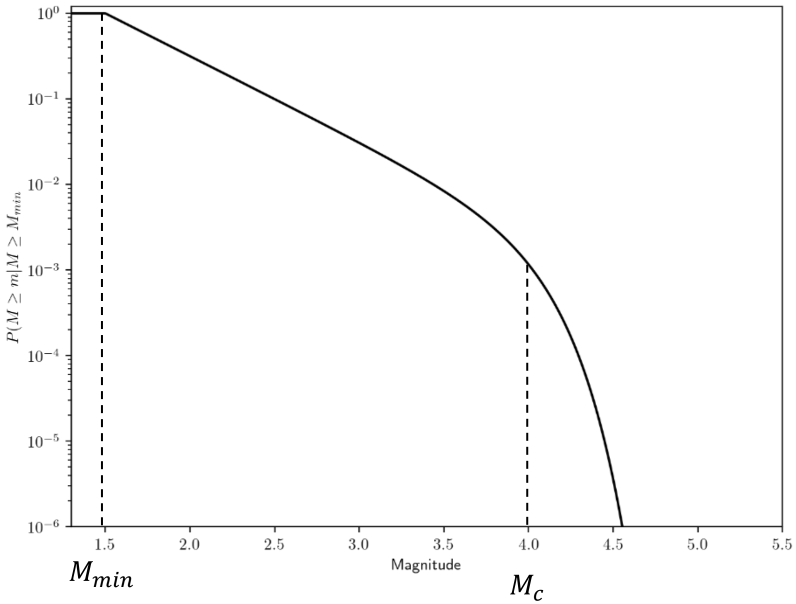

$$P = 10^{-b(m-M_{min})} \times e^{-10^{\frac{3}{2}(m-M_c)}}$$

THE TAPER MODEL

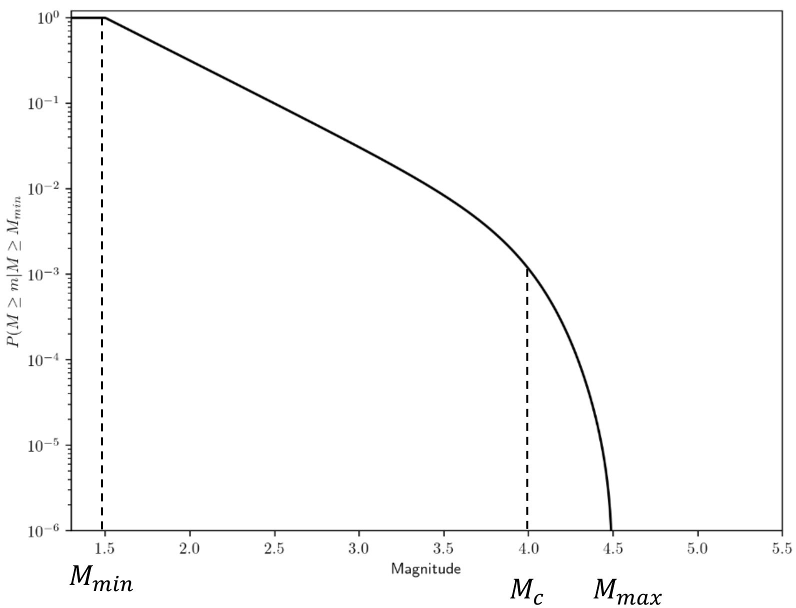

$$P = \frac{10^{-b(m-M_{min})} \times e^{-10^{\frac{3}{2}(m-M_c)}} - T}{1 - T}$$

$$T = 10^{-b(M_{max}-M_{min})} \times e^{-10^{\frac{3}{2}(M_{max}-M_c)}}$$

THE TAPER MODEL

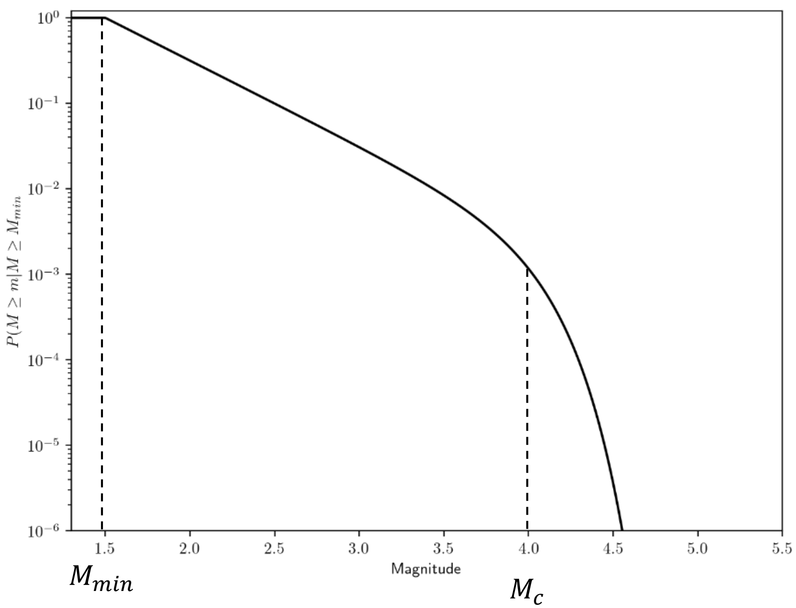

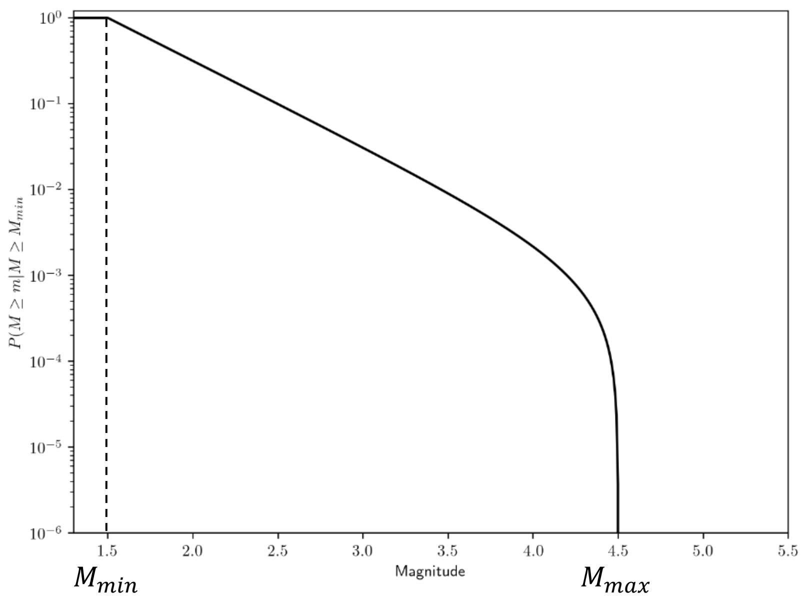

THE TAPER MODEL

JGR Solid Earth

RESEARCH ARTICLE

Stress-Dependent Magnitudes of Induced Earthquakes in the Groningen Gas Field

S. J. Bourne[1] and S. J. Oates[1]

[1]Shell Global Solutions International B.V., Amsterdam, The Netherlands

$$M_c = M_{min} - \frac{2}{3}\log_{10}\zeta$$

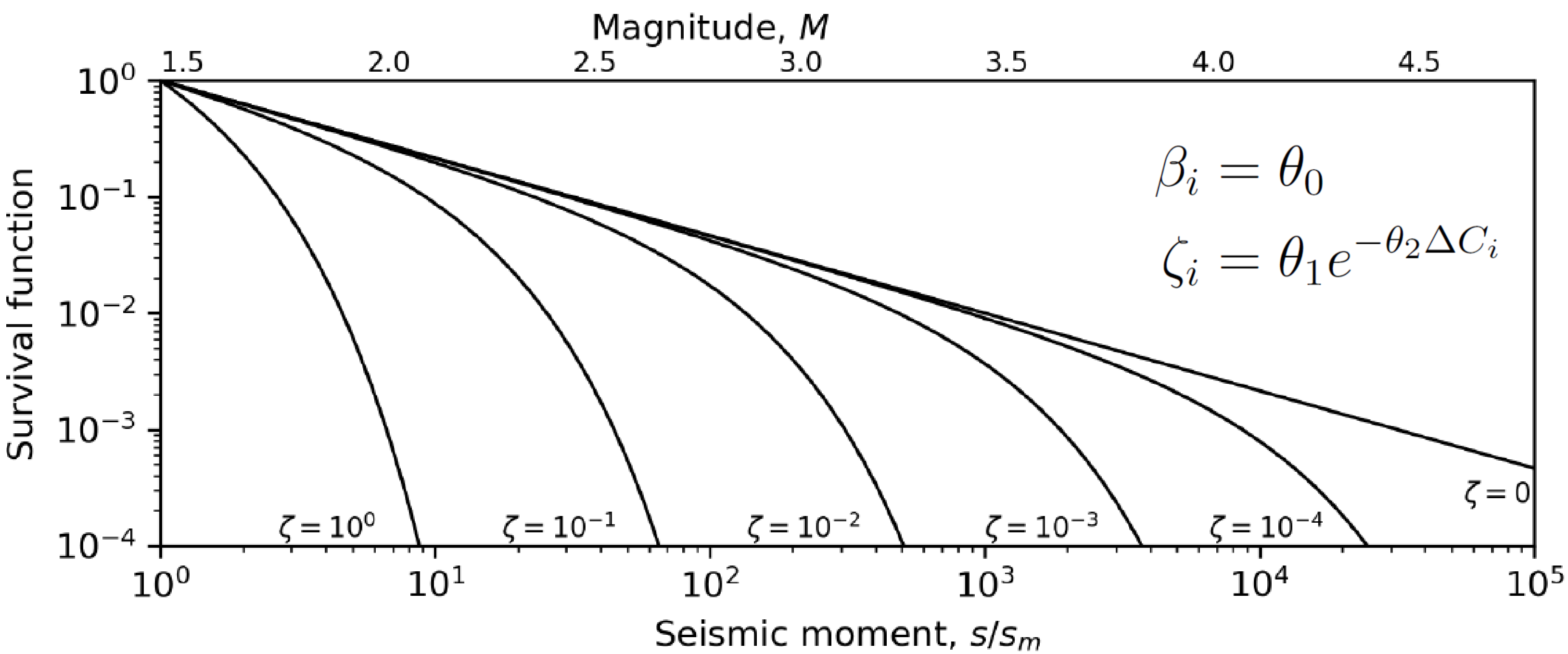

THE TAPER MODEL

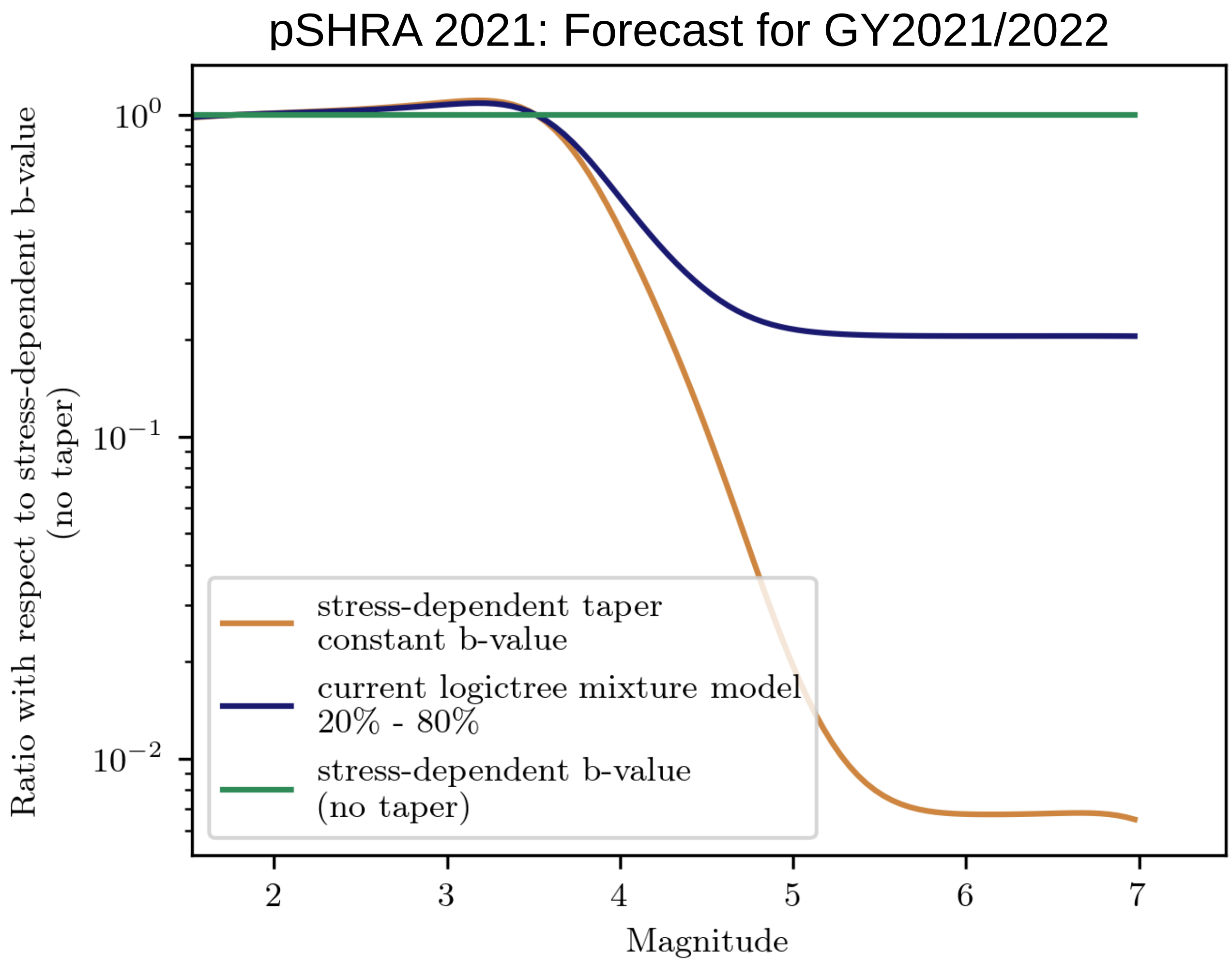

THE TAPER MODEL

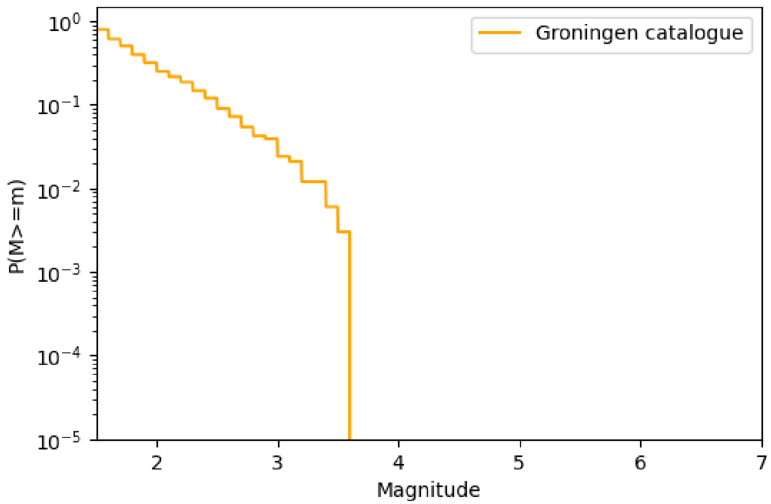

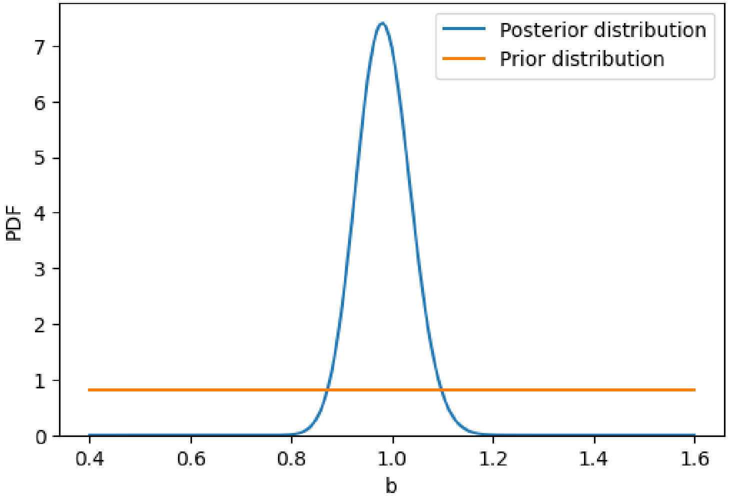

THE TAPER MODEL

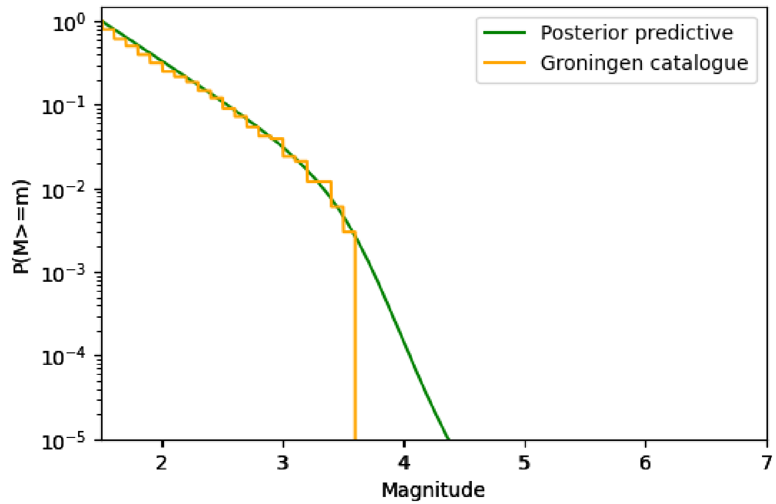

Posterior distribution for taper model

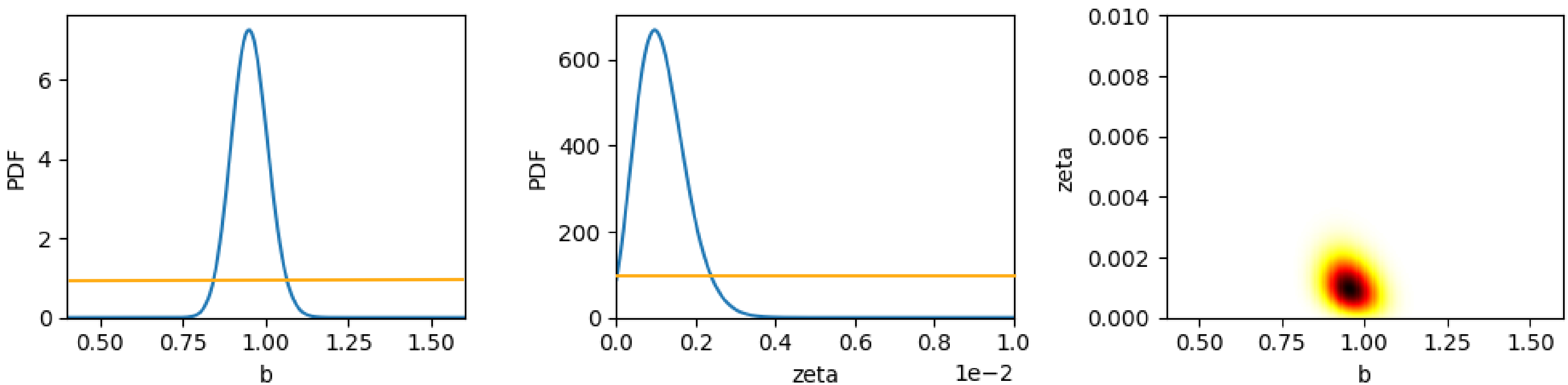

THE TAPER MODEL

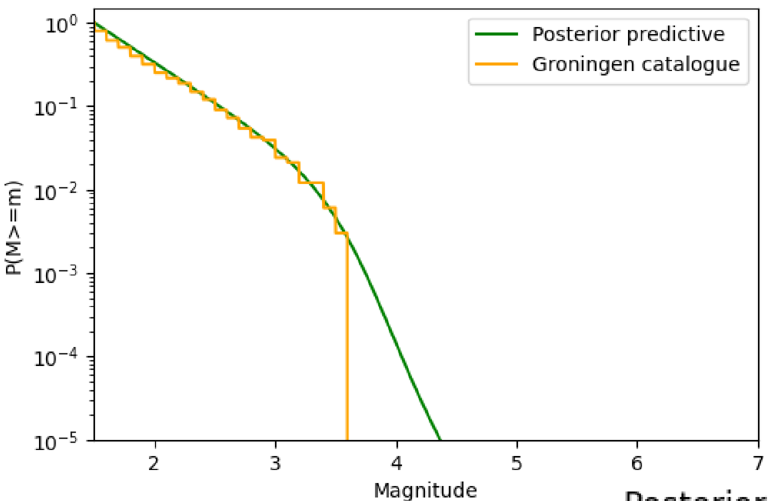

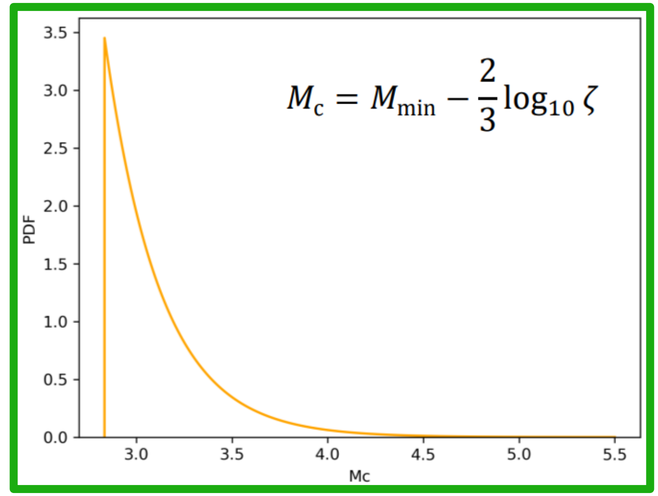

Posterior distribution for taper model

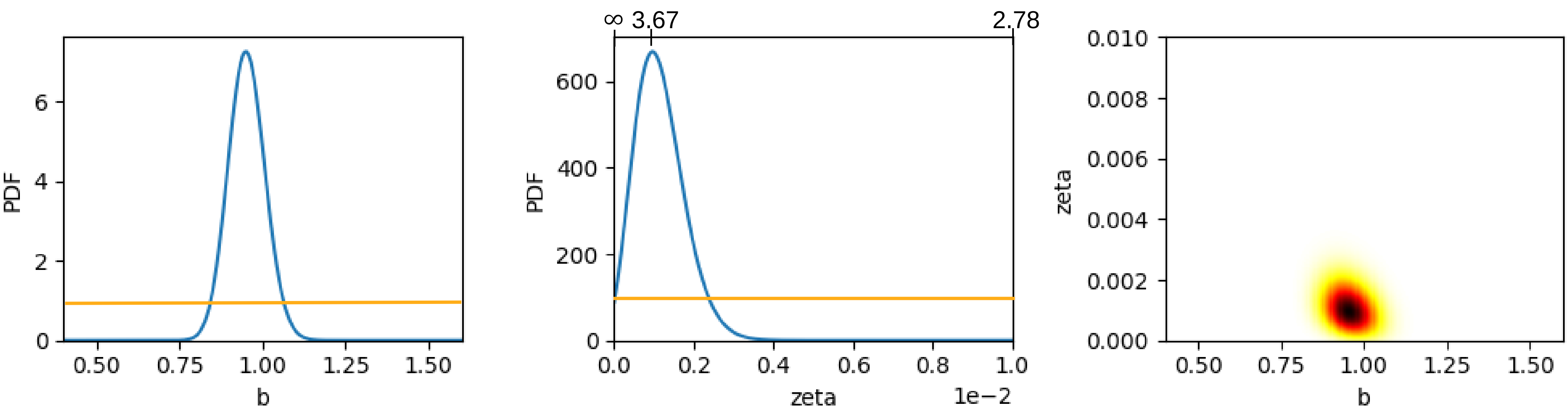

THE TAPER MODEL

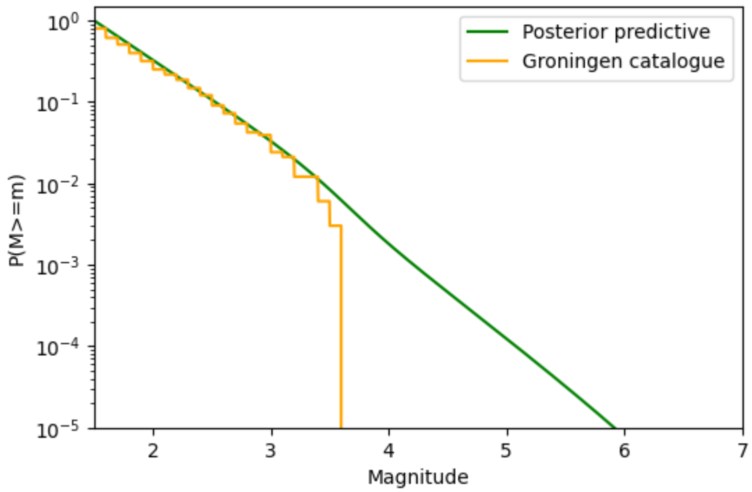

Posterior distribution for taper model

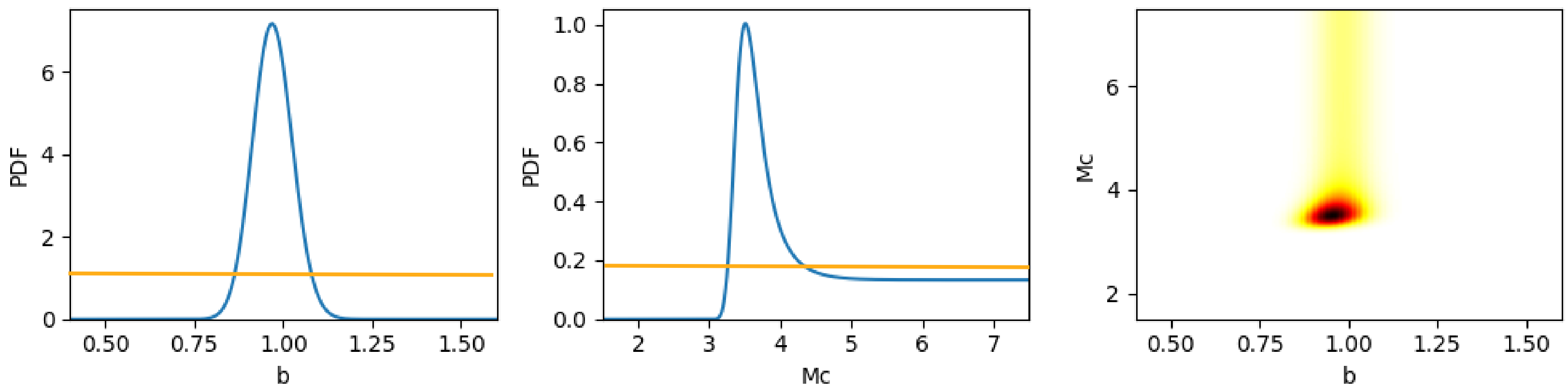

THE TAPER MODEL

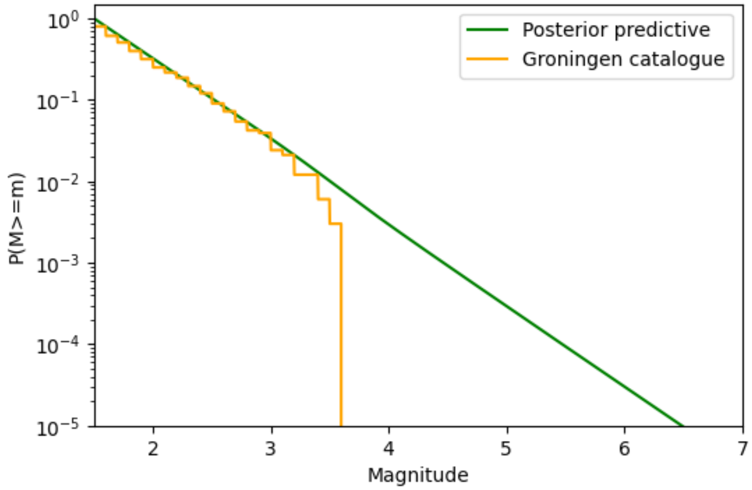

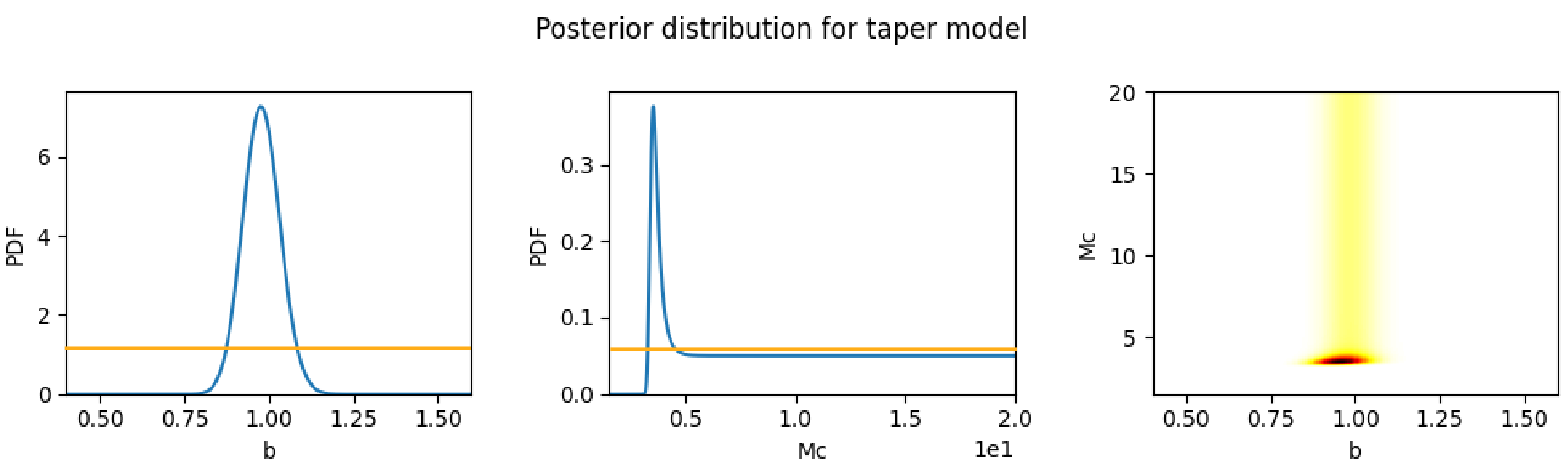

THE TAPER MODEL

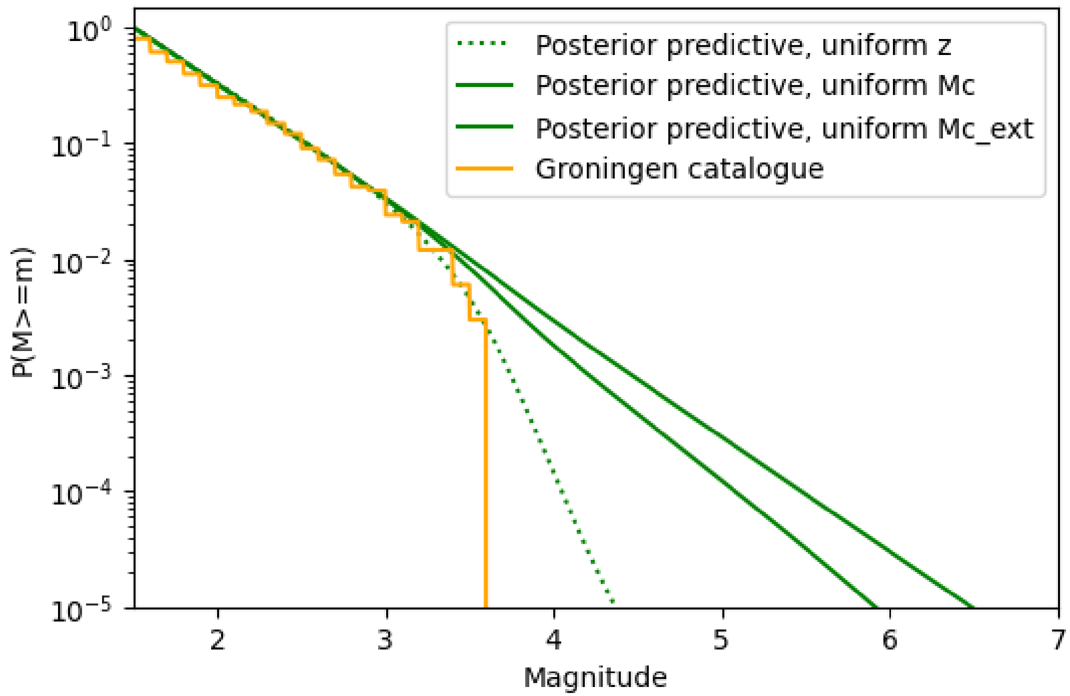

THE TAPER MODEL

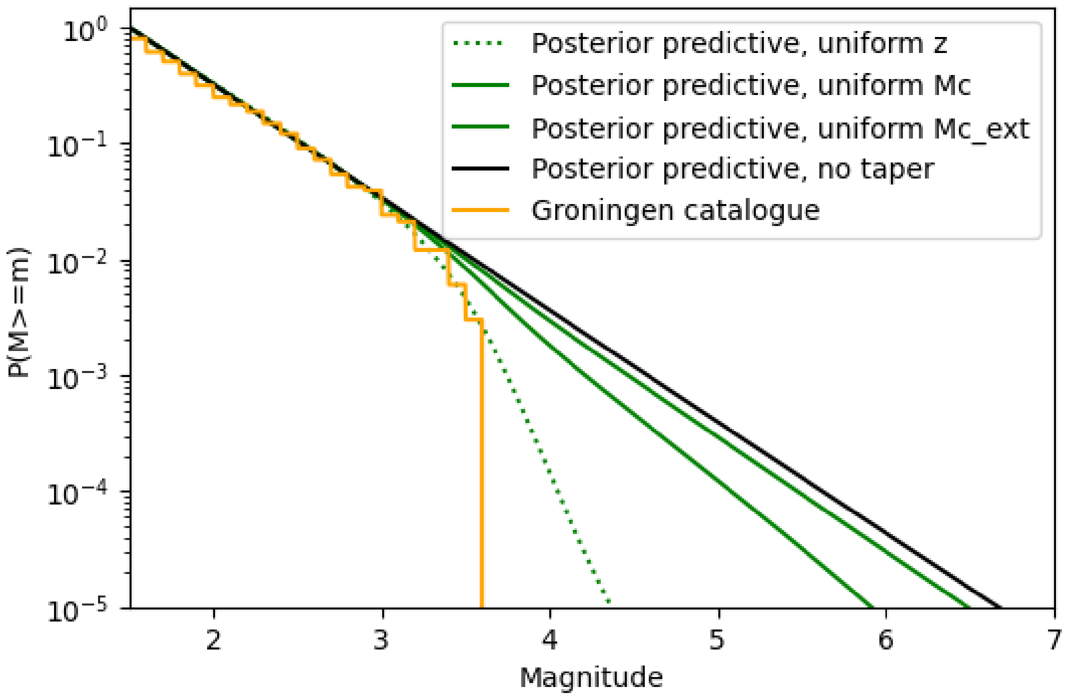

DATA-INFORMED MMAX

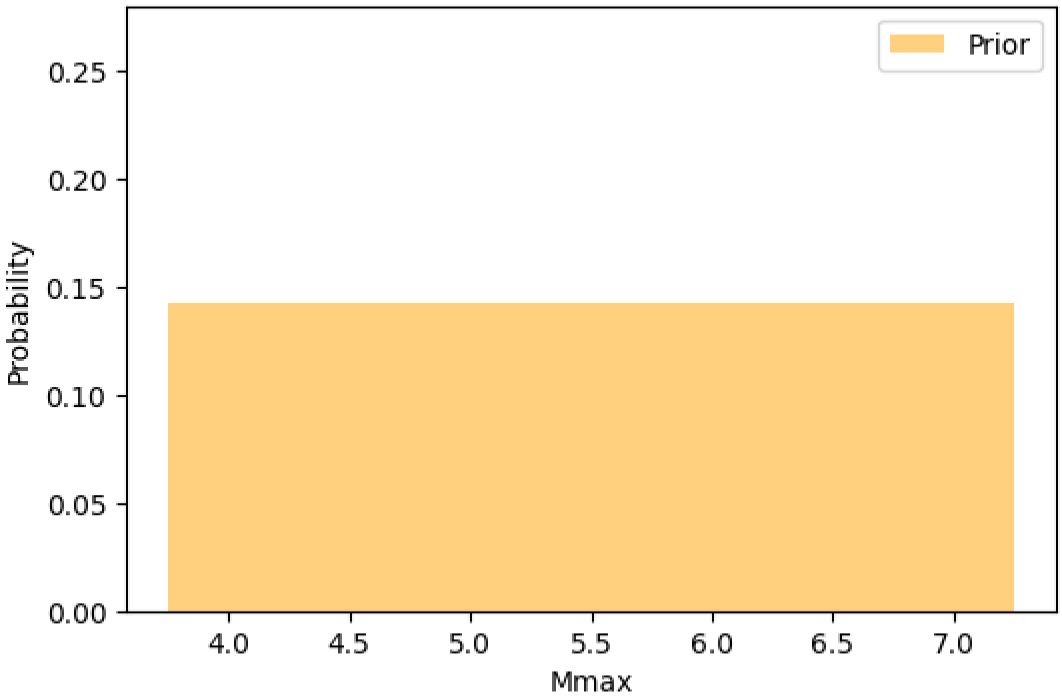

DATA-INFORMED MMAX

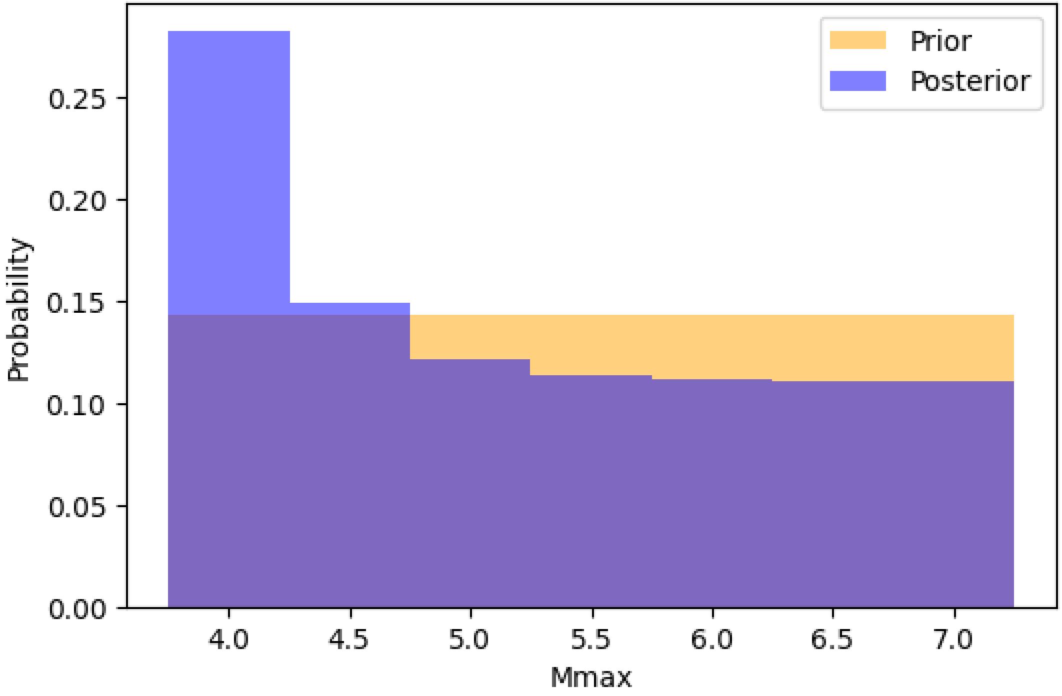

DATA-INFORMED MMAX

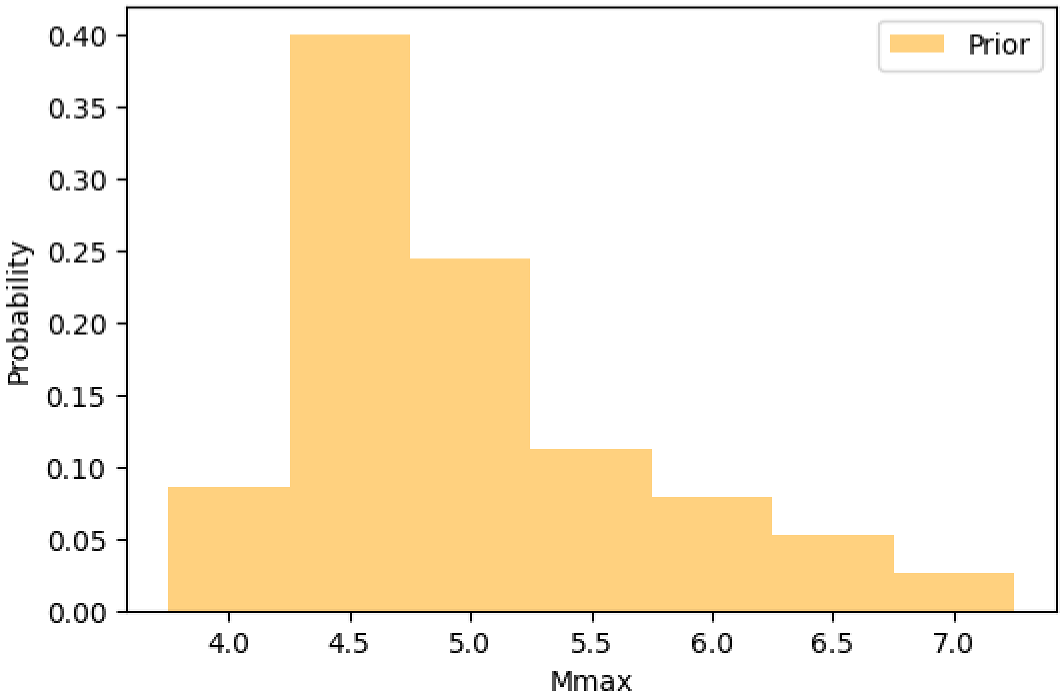

DATA-INFORMED MMAX

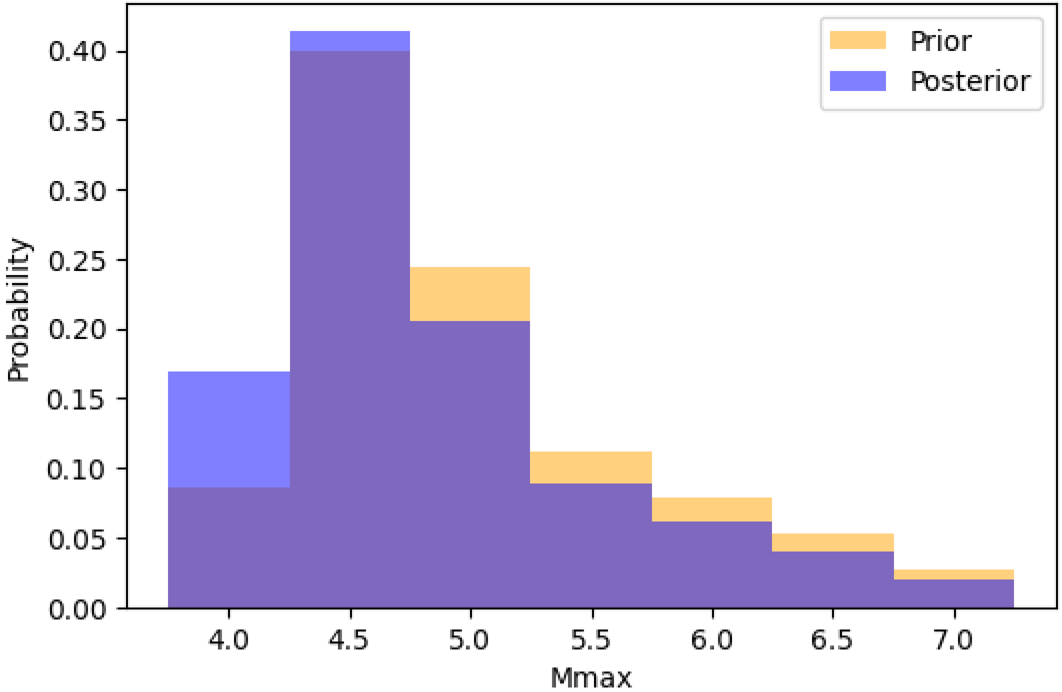

DATA-INFORMED MMAX

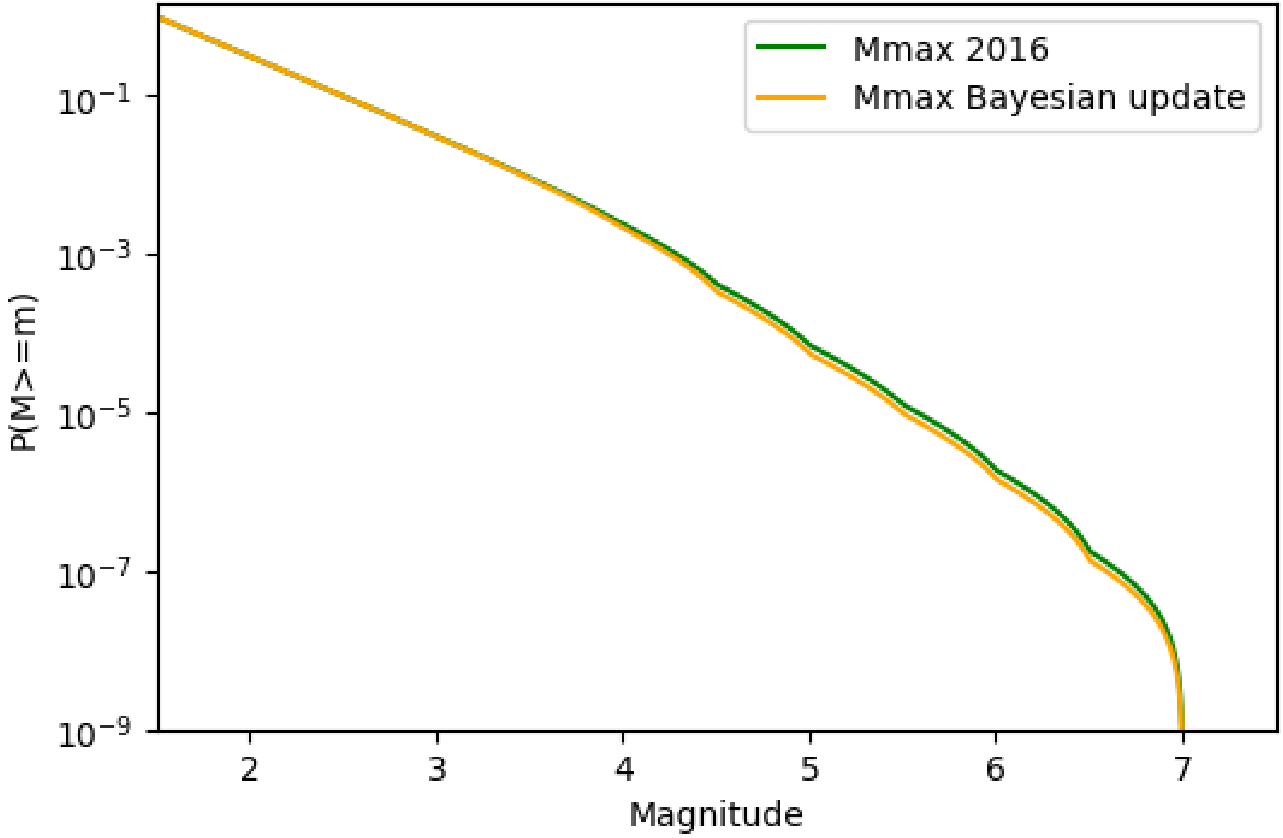

MMAX VS MC

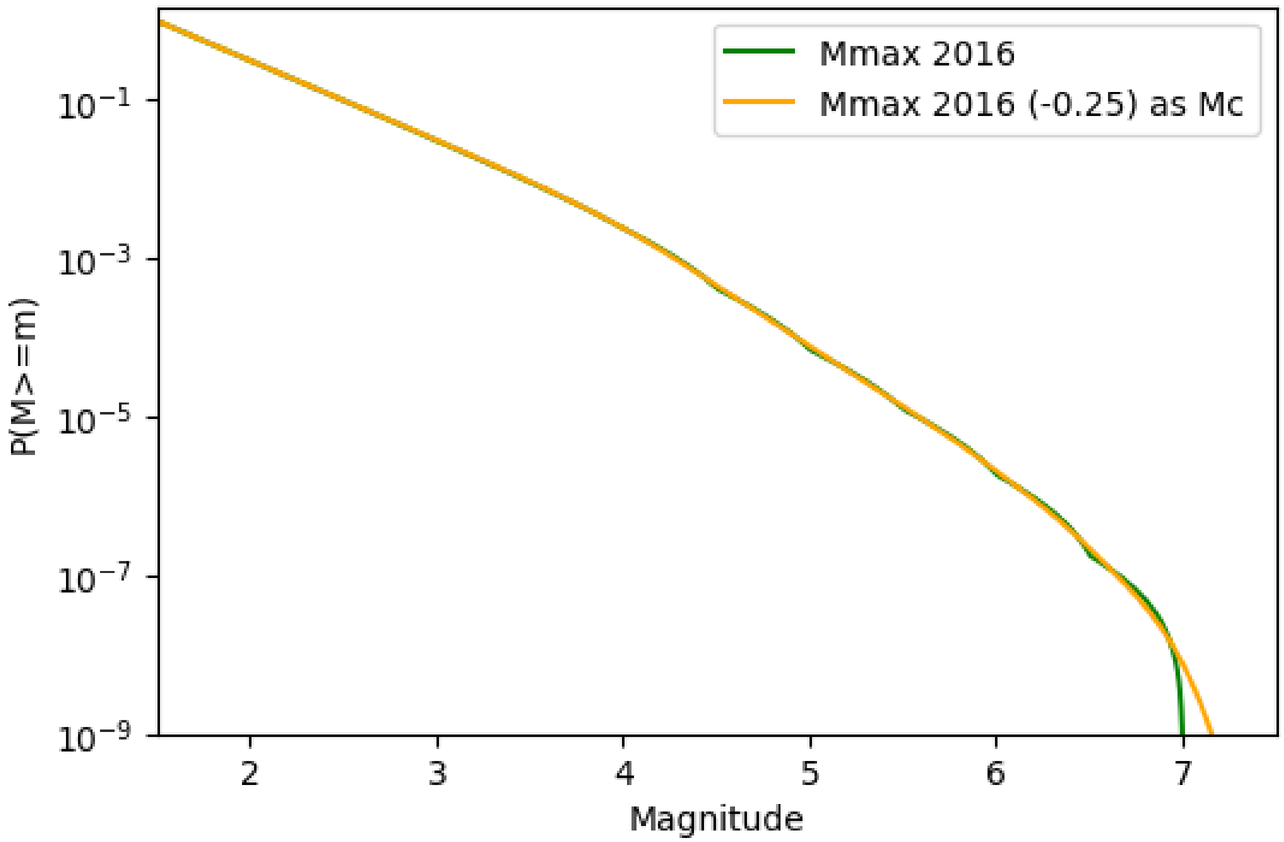
Mmax 2016
Mmax 2016 (-0.25) as Mc
10^{-1}
10^{-3}
10^{-5}
10^{-7}
10^{-9}
P(M>=m)
2
3
4
5
6
7
Magnitude

THE TAPER MODEL

- The posterior predictive FMD is dominated by the chosen prior for the magnitudes beyond the data. These are exactly the same magnitudes that we care about for PSHRA.
- This makes intuitive sense. No data → prior provides (virtually) all the information.
- This is why there is an Mmax panel.
- The taper model's prior distribution has not been subject to expert elicitation or a similar justification process.

FOCUS OF THIS TALK

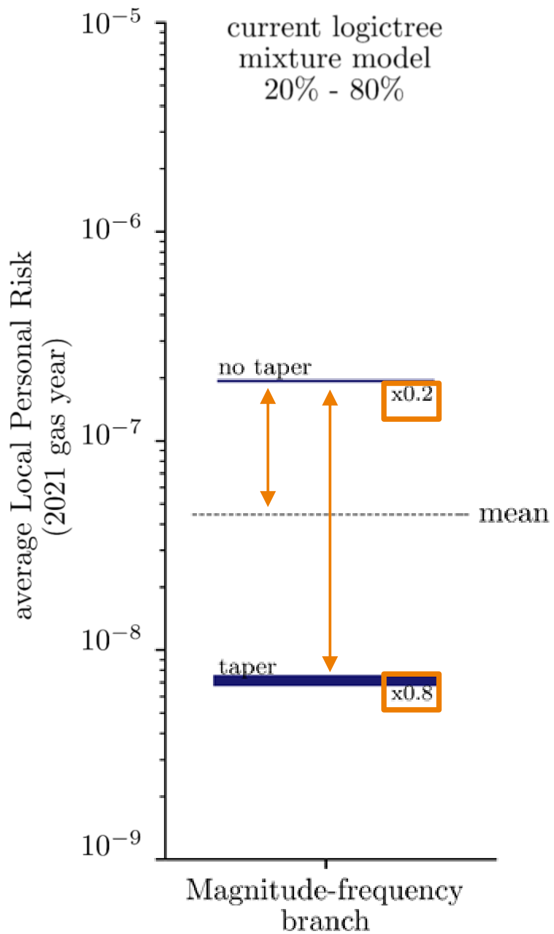

1. Where do these weights come from?
   A statistical analysis that does not appear to be appropriate for assigning weights

2. Where does this gap come from?
   (Mostly) from the chosen prior

Where does that leave the Mmax distribution and its relevance to PSHRA?

IN SUMMARY

- One of the main objectives of this workshop is to determine if the proposed Mmax distribution is compatible with the existing PSHRA framework for Groningen, including the **V6 seismological model** and the **logic tree**.
  - The V6 seismological model introduces a taper (an additional FMD tail modifier) used in conjunction with Mmax.
  - This taper **significantly** lowers the expected rate of high magnitude events
  - The *data-informed* taper model is in fact dominated by the chosen prior
  - The weight assigned to the taper branch is based on a statistical analysis that does not appear to be appropriate for assigning weights

FOOD FOR THOUGHT

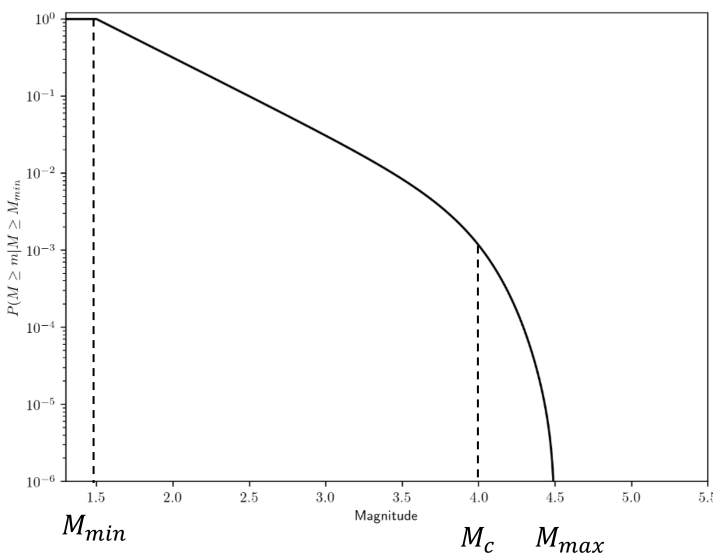

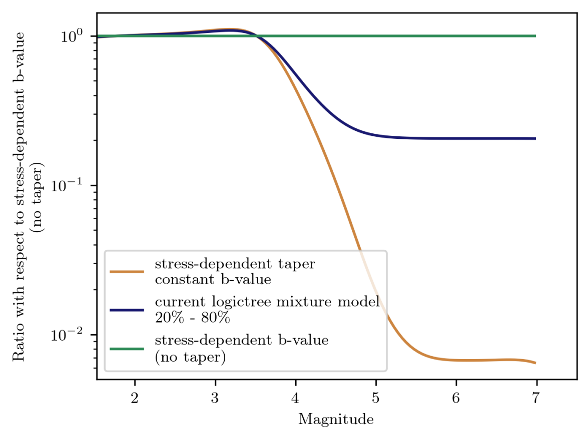

Comments on the Use of the Mmax Distribution for Groningen

[...]

for tectonic faults in a PSHA. For these reasons, the Panel concludes that the Mmax distribution for the Groningen field provided in this document is essentially the same for hazard assessment conducted currently, ten years from now, or at the conclusion of production activities in 2060. However, as is true for all gas field case histories, the distribution is subject to updating in the future if significant new findings occur, such as the occurrence of larger earthquakes at the field, or a change in production or operation mode.

It is suggested that the use of this Mmax distribution in the PSHA be carefully done, given the plans to attach it to the recurrence distributions presented by Bourne. In particular, it is suggested that the development of the earthquake recurrence distributions takes into account that a value of Mmax exists (i.e. the size of the

FOOD FOR THOUGHT: TWO TAIL MODELS

	Mmax	Mc
Tail shape	Hard	Soft
Variations	Static	Dynamic ($f(\Delta C)$)
Prior distribution	Mmax panel 2016	(NAM ?)
Likelihood	Unbounded	Unbounded
Bayesian update	NO	YES
Prior dominated	YES	YES

LOOKING AHEAD

- Is it preferable to have two descriptors (Mmax and Mc) for the tail of the FMD?
- **<u>If</u>** so, should the effort to describe the epistemic uncertainty for these parameters* be limited to just one of them?
- Should these descriptions of epistemic uncertainty be updated in a Bayesian sense? Or are they to be used as effective 'posterior distributions'?
- We would very much appreciate if the Mmax panel could share their insights on this

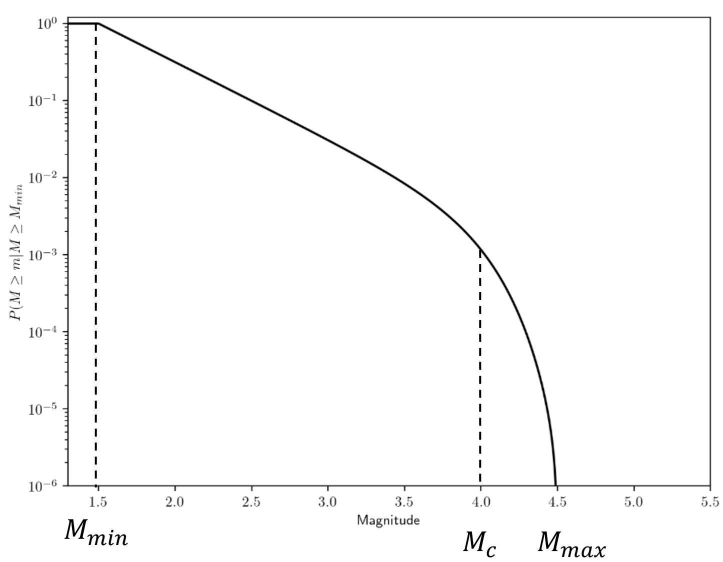

Framework for the Assessment

The Groningen Mmax Panel is charged with developing a distribution of the maximum magnitude (Mmax) for the Groningen natural gas field that is appropriate for use in a probabilistic seismic hazard analysis (PSHA) and subsequent probabilistic risk analyses (PRA). The definition of Mmax is in the context of its common use in seismic source characterization for PSHA (probabilistic seismic hazard analysis). For example, as defined in USNRC (2012a, Chapter 11): Mmax is "the largest earthquake that a seismic source is assessed to be capable of generating. The maximum magnitude is the upper bound to recurrence curves." Mmax, as it is defined for PSHA and used here, is a time-independent upper bound. In general, it cannot be defined from an earthquake catalogue alone or statistical analyses of the catalogue. This is a well-known observation and has been documented for decades. In some cases where a large number of earthquakes have been recorded, it has been suggested that point estimates of Mmax can be made from the catalogue data (e.g. Kijko, 2004). However, assessment of the uncertainty distribution for Mmax from the catalogue data remains problematic without imposing some additional constraints (USNRC, 2012a). As a result, the assessment of Mmax requires expert judgment and the application of physical principles beyond just the earthquake catalogue. The assessment of Mmax is a common assessment and is a


THANK YOU
TNO innovation
for life

New findings on the maximum possible and the maximum expected earthquake magnitude for the Groningen gas field

Gert Zöller

in cooperation with Matthias Holschneider & Sebastian Hainzl

Institute of Mathematics · University of Potsdam

June 15, 2022

Groningen Mmax Workshop II, June 13-17, 2022, Amsterdam

Contents

1. $m_{\max}$: The largest possible earthquake magnitude in a region
   – for all times

   - Estimation of $m_{\max}$: Statistical inference from rare events
   - The statistical model for magnitudes
   - The Groningen case
   - Relation to other statistical models: extreme value theory

2. M_T: The largest expected earthquake magnitude in time T

   - Models for seismicity response to gas production/stress changes: Poisson, Coulomb, rate-and-state dependent friction
   - Results: M_T for different models

Contents

1. $m_{\max}$: The largest possible earthquake magnitude in a region – for all times
    - Estimation of $m_{\max}$: Statistical inference from rare events
    - The statistical model for magnitudes
    - The Groningen case
    - Relation to other statistical models: extreme value theory
2. M_T: The largest expected earthquake magnitude in time T
    - Models for seismicity response to gas production/stress changes: Poisson, Coulomb, rate-and-state dependent friction
    - Results: M_T for different models

General assumptions: $m_{\max}$

1. $m_{\max}$: Physical parameter that depends on the local environment, not on human activity like gas production.
2. $m_{\max}$ is constant, as long as the local physics is constant.
3. No ergodicity assumption (or analogs) used, because the physics is not <u>precisely</u> known.

General assumptions: M_T

M_T ($\leq m_{\max}$): Derived quantity that depends on

- the local physics and
- on human activity (gas production) in the time interval T under consideration.

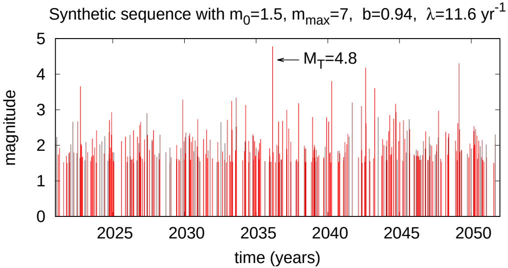

Outline

data 1: earthquake magnitudes $\{m_i\}$

model for magnitudes: $\downarrow$ doubly truncated GR distribution

time independent

estimate FS distribution $F_{b,m_{\max}}(m)$

Outline

data 1: earthquake magnitudes $\{m_i\}$

model for magnitudes: $\downarrow$ doubly truncated GR distribution

time independent

estimate FS distribution $F_{b,m_{\max}}(m)$

$\downarrow$

data 2: gas production / stress data

time model: $\downarrow$ Poisson, Coulomb, rate–state, ...

calculate nr n of EQs until 2052

sample magnitudes from $\downarrow$ GR distribution

time dependent

cdf of M_T : $P(M_T < z) = [F_{b,m_{\max}}(z)]^n$

1. $m_{\max}$: The largest possible earthquake magnitude in a region

Facts on $m_{\max}$

- Earthquakes with $m \approx m_{\max}$ are rare, uncertainties of $m_{\max}$ are high!

Facts on $m_{\max}$

- Earthquakes with $m \approx m_{\max}$ are rare, uncertainties of $m_{\max}$ are high!
- For small samples, the maximum observed magnitude has almost no information on the real $m_{\max}$.

Facts on $m_{\max}$

- Earthquakes with $m \approx m_{\max}$ are rare, uncertainties of $m_{\max}$ are high!
- For small samples, the maximum observed magnitude has almost no information on the real $m_{\max}$.
- Sample size is the critical issue!

Facts on $m_{\max}$

- Earthquakes with $m \approx m_{\max}$ are rare, uncertainties of $m_{\max}$ are high!
- For small samples, the maximum observed magnitude has almost no information on the real $m_{\max}$.
- Sample size is the critical issue! $\rightarrow$ Presentation of Bob Youngs on Monday.

Excercise: Estimate $m_{\max}$ from data

Excercise: Estimate $m_{\max}$ from data

Data (simulated GR law with $b = 0.94$, $m_0 = 1.5$, $N = 359$, $m_{\max} = ?$):

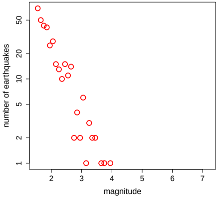

Excercise: Estimate $m_{\max}$ from data

Data (simulated GR law with $b = 0.94$, $m_0 = 1.5$, $N = 359$, $m_{\max} =?$):

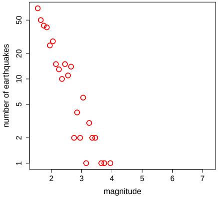

Question: $m_{\max} =?$

Excercise: Estimate $m_{\max}$ from data

Data (simulated GR law with $b = 0.94$, $m_0 = 1.5$, $N = 359$, $m_{\max} = ?$):

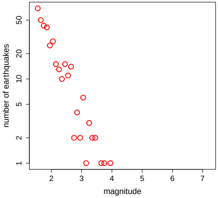

Question: $m_{\max} = ?$

Common guess: $m_{\max} = 5 \ldots 7$ ($m_{\max,\text{observed}} +$ something)

Excercise: Estimate $m_{\max}$ from data

Data (simulated GR law with $b = 0.94$, $m_0 = 1.5$, $N = 359$, $m_{\max} = ?$):

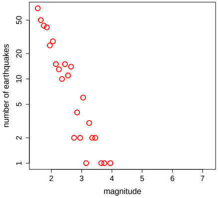

Question: $m_{\max} = ?$

Common guess: $m_{\max} = 5 \ldots 7$ ($m_{\max,\text{observed}} +$ something)

Ground truth: Data stem from a truncated GR law with $m_{\max} = 25$

Excercise: Estimate $m_{\max}$ from data

Data (simulated GR law with $b = 0.94$, $m_0 = 1.5$, $N = 359$, $m_{\max} = ?$):

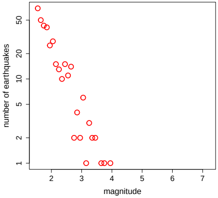

Question: $m_{\max} = ?$

Common guess: $m_{\max} = 5 \ldots 7$ ($m_{\max,\text{observed}} +$ something)

Ground truth: Data stem from a truncated GR law with $m_{\max} = 25$

Lesson: Sparse data do not tell us anything about $m_{\max}$.

Estimation of $m_{\max}$: Statistical inference from rare events

Synthetic earthquake catalogs with $b = 0.94$, $m_0 = 1.5\ldots$

Estimation of $m_{\max}$: Statistical inference from rare events

Synthetic earthquake catalogs with $b = 0.94$, $m_0 = 1.5 \ldots$

$\ldots$ and $m_{\max} = 5.0$

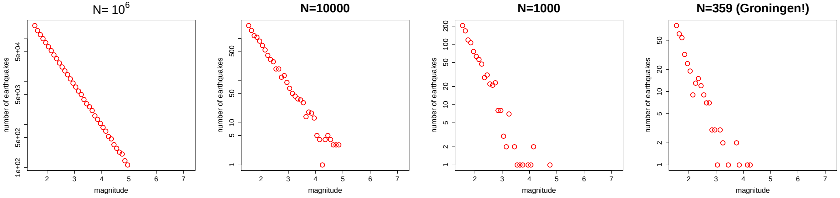

Estimation of $m_{\max}$: Statistical inference from rare events

Synthetic earthquake catalogs with $b = 0.94$, $m_0 = 1.5 \ldots$

... and $m_{\max} = 5.0$

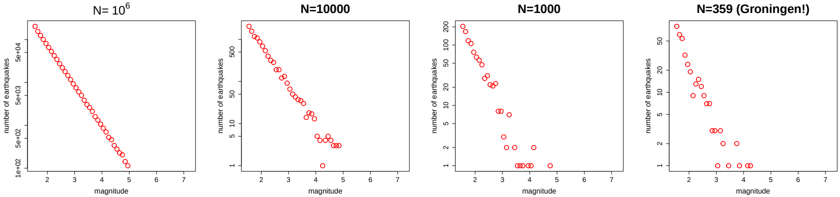

... and $m_{\max} = 7.0$

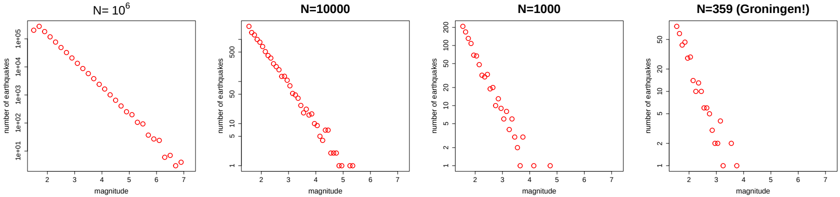

Consequences for the estimation of $m_{\max}$ from sparse data

- Point estimators are not informative, because $m_{\max} = 5$ and $m_{\max} = 7$ (and even $m_{\max} = 25$) are equally likely from a statistical point of view.

- Better: express uncertainties of $m_{\max}$ in terms of confidence intervals.

The statistical model for magnitudes

Gutenberg-Richter law: $\log_{10}(N_{\geq m}) = a - bm$ for $m \leq m_{\max}$

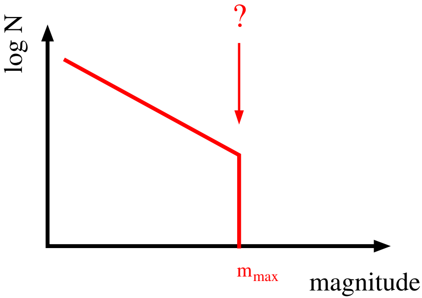

Gutenberg-Richter probability density function for magnitudes

$$f_{b,m_{\max}}(m) = \frac{b10^{-bm}}{10^{-bm_0} - 10^{-bm_{\max}}} \text{ for } m_0 \leq m \leq m_{\max}$$

The earthquake catalog of Groningen

- Time: 12/1991 - 4/2022
- Magnitudes given with one decimal place
- Magnitude of completeness: $m_0 = 1.5$ (Dost et al., 2012)
- Maximum observed earthquake: $\mu = 3.6$ (Huizinge, August 16, 2012)
- Total number of 359 earthquakes with $m \in [1.5; 3.6]$

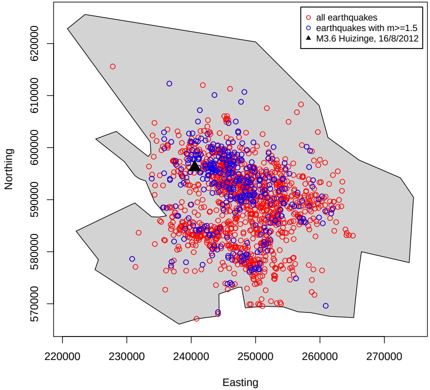

The frequency-magnitude distribution for Groningen

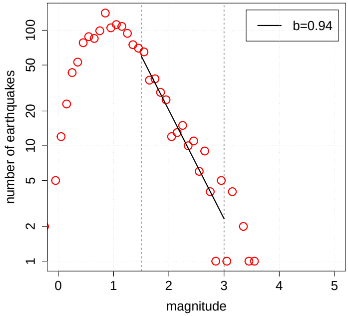

ML estimation of the $b-$value (Page, BSSA 58(3), 1968)

- for $m \in [1.5, 3.0]$
- corrected for rounding errors

$$b = 0.94 \pm 0.05$$

The frequency-magnitude distribution for Groningen

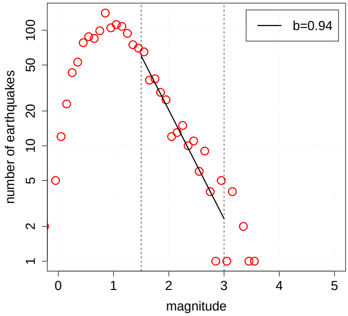

ML estimation of the $b-$value (Page, BSSA 58(3), 1968)

- for $m \in [1.5, 3.0]$
- corrected for rounding errors

$$b = 0.94 \pm 0.05 \qquad (\text{in } 2016: b = 0.95)$$

The confidence interval of $m_{\max}$:

Best confidence interval of $m_{\max}$

$$\mu \leq m_{\max} \leq m_0 - \frac{1}{b}\log_{10}\left[1 + \frac{10^{-b(\mu - m_0)} - 1}{\alpha^{1/n}}\right]$$

(Pisarenko et al., BSSA, 86(3), 1996; Holschneider et al., BSSA, 101(4), 2011)

with

- α: Error probability ($1 - \alpha =$ level of confidence)
- m_0: Lower magnitude threshold
  (=1.5 for Groningen)
- μ: Magnitude of maximum observed earthquake
  (=3.6 for Groningen)
- b: Richter b-value (=0.94)

The confidence interval of $m_{\max}$

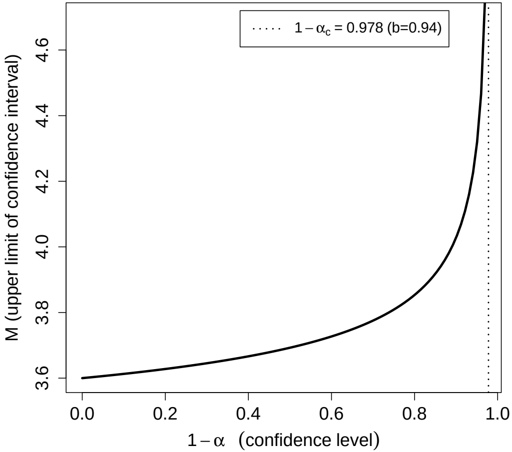

The confidence interval of $m_{\max}$

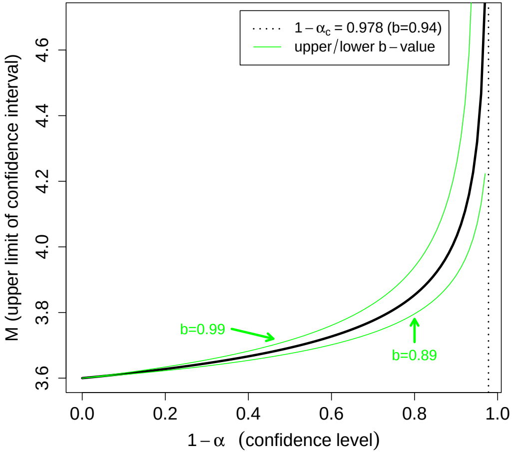

The confidence interval of $m_{\max}$

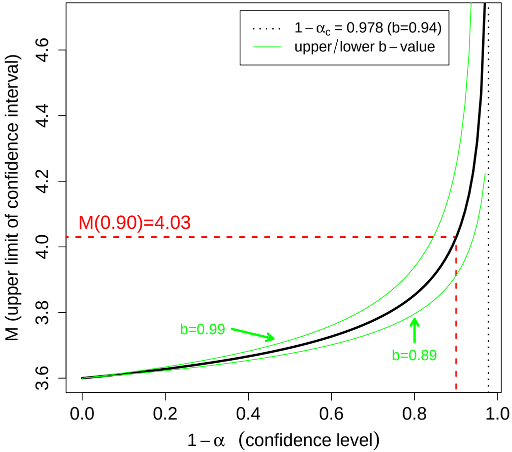

The confidence interval of $m_{\max}$

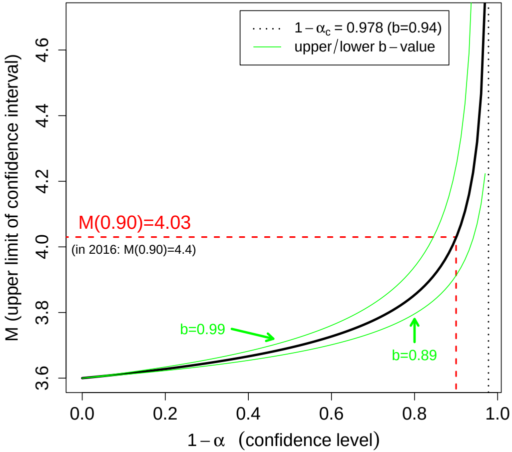

The confidence interval of $m_{\max}$

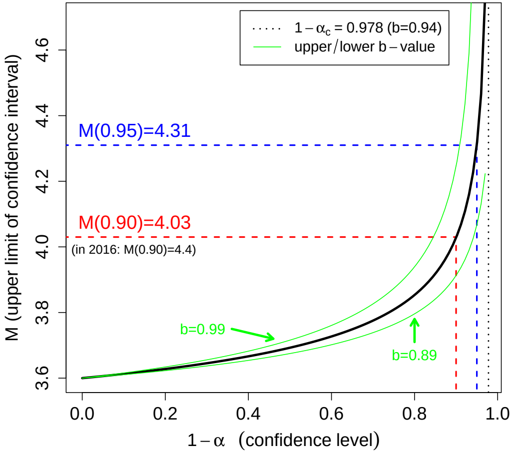

The confidence interval of $m_{\max}$

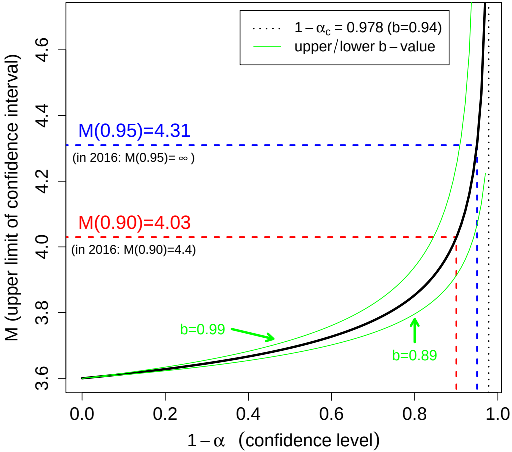

Results for $m_{\max}$

- Frequency-size distribution is stable since 2016.
- Confidence intervals of $m_{\max}$ decrease (with growing catalog size).
- 90% confidence: $3.6 \leq m_{\max} \leq 4.0$
- 95% confidence: $3.6 \leq m_{\max} \leq 4.3$
- $>$ 97.8% confidence: $3.6 \leq m_{\max} \leq \infty$

For practical purposes, one might select the upper bound of the 95% confidence interval:

$$M = 4.3.$$

Relation to other statistical models:

Extreme value theory

Relation to other statistical methods

Remarks on extreme value theory (EVT)

(Zöller, Bull. Seism. Soc. Am., doi: 10.1785/0120210307, 2022)

- EVT studies statistical properties of the largest events in a sample.
- "large event": earthquake with $m > m_t$ ("peak over threshold") with high m_t.
- For distributions fulfilling certain assumptions, the distribution of the largest events ($m > m_t$) can be approximated by the generalized Pareto distribution (GPD)

$$P(x|m_i > m_t) = 1 - \left(1 + \xi \frac{x}{\sigma_t}\right)^{-1/\xi}$$

Relation to other statistical methods

Remarks on extreme value theory (EVT)

(Zöller, Bull. Seism. Soc. Am., doi: 10.1785/0120210307, 2022)

- If a sufficient number of events, say k, close to the truncation point is available, the truncation point can be estimated.

  (Beirlant et al., Extremes 19(3), 2016)

Relation to other statistical methods

Remarks on extreme value theory (EVT)

(Zöller, Bull. Seism. Soc. Am., doi: 10.1785/0120210307, 2022)

- If a sufficient number of events, say k, close to the truncation point is available, the truncation point can be estimated.
  (Beirlant et al., Extremes 19(3), 2016)

- In practical applications, the largest k events in a data set are chosen to estimate the truncation point.

Relation to other statistical methods

Remarks on extreme value theory (EVT)

(Zöller, Bull. Seism. Soc. Am., doi: 10.1785/0120210307, 2022)

- If a sufficient number of events, say k, close to the truncation point is available, the truncation point can be estimated.
  (Beirlant et al., Extremes 19(3), 2016)
- In practical applications, the largest k events in a data set are chosen to estimate the truncation point.
- $k = ?$
  k small: (probably) close to tail, but poor statistics.
  k large: reasonable statistics, but (probably) far from tail.

Relation to other statistical methods

Estimates of $m_{\max}$ for Groningen (Beirlant et al., Nat. Haz. 98, 2019)

- Stable results for $k \geq 75$.

Relation to other statistical methods

Estimates of $m_{\max}$ for Groningen (Beirlant et al., Nat. Haz. 98, 2019)

- Stable results for $k \geq 75$.

However, green points are assumed to be very close to $m_{\max}$.

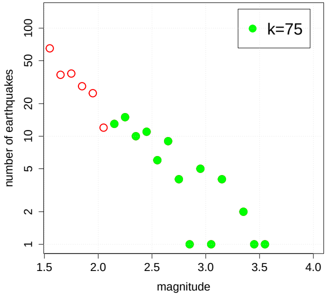

Relation to other statistical methods

Estimates of $m_{\max}$ for Groningen (Beirlant et al., Nat. Haz. 98, 2019)

- $k = 125$

However, blue points are assumed to be very close to $m_{\max}$.

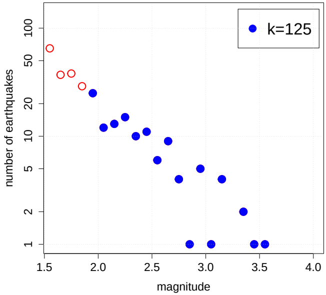

Relation to other statistical methods

Estimates of $m_{\max}$ for Groningen (Beirlant et al., Nat. Haz. 98, 2019)

- $k = 125$ results in $\widehat{m_{\max}} = 3.76$.

However, blue points are <u>assumed</u> to be very close to $m_{\max}$.

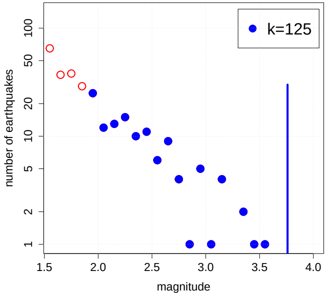

Relation to other statistical methods

Synthetic data: bias estimation

- Step 1: Generate 10.000 synthetic magnitude samples, each with 359 events (Groningen), with given ground truth $m_{\max}$.

Relation to other statistical methods

Synthetic data: bias estimation

- Step 1: Generate 10.000 synthetic magnitude samples, each with 359 events (Groningen), with given ground truth $m_{\max}$.
- Step 2: Estimate $m_{\max}$ using EVT for each sample: $\widehat{m_{\max}}$.

Relation to other statistical methods

Synthetic data: bias estimation

- Step 1: Generate 10.000 synthetic magnitude samples, each with 359 events (Groningen), with given ground truth $m_{\max}$.
- Step 2: Estimate $m_{\max}$ using EVT for each sample: $\widehat{m_{\max}}$.
- Step 3: Compare distribution (histogram) of $\widehat{m_{\max}}$ with ground truth $m_{\max}$.

Relation to other statistical methods

Ground truth $m_{\max} = 4$

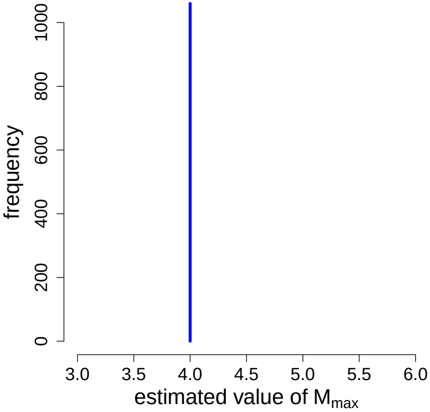

Relation to other statistical methods

Ground truth $m_{\max} = 4$; Histogram: $\widehat{m_{\max}}$

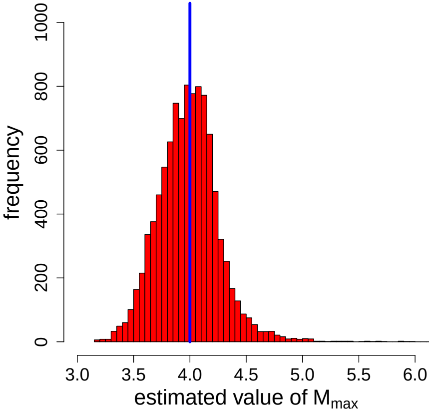

Relation to other statistical methods

Ground truth $m_{\max} = 4$; Histogram: $\widehat{m_{\max}}$; $\mathbb{E}[m_{\max}$ (observed)]

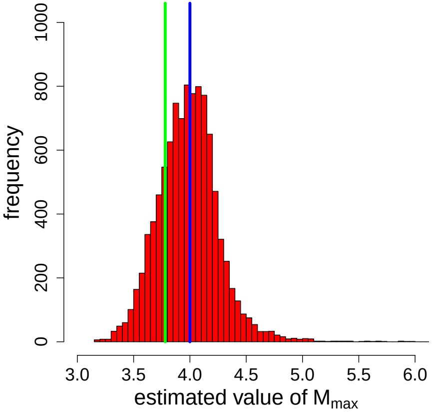

Relation to other statistical methods

Ground truth $m_{\max} = 8$

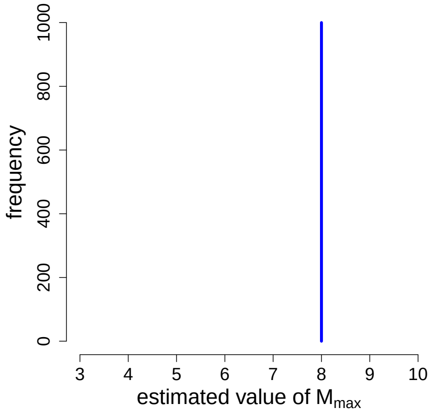

Relation to other statistical methods

Ground truth $m_{\max} = 8$; Histogram: $\widehat{m_{\max}}$

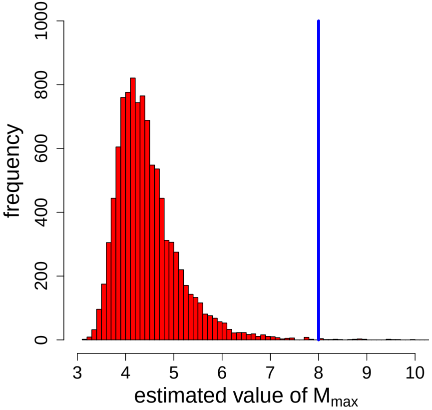

Relation to other statistical methods

Ground truth $m_{\max} = 8$; Histogram: $\widehat{m_{\max}}$; $\mathbb{E}[m_{\max}$ (observed)]

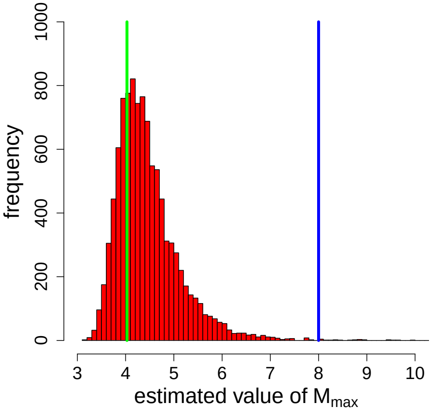

Conclusions on the estimation of $m_{\max}$ with EVT

Relation to other statistical methods

Conclusions on the estimation of $m_{\max}$ with EVT

- EVT estimators assume that the maximum observed events are close to the truncation point of the FS distribution, namely $m_{\max}$.

Conclusions on the estimation of $m_{\max}$ with EVT

- EVT estimators assume that the maximum observed events are close to the truncation point of the FS distribution, namely $m_{\max}$.
- By construction, the method allows only estimations of $m_{\max}$ that are close to the maximum observed earthquake magnitude.

Relation to other statistical methods

Conclusions on the estimation of $m_{\max}$ with EVT

- EVT estimators assume that the maximum observed events are close to the truncation point of the FS distribution, namely $m_{\max}$.
- By construction, the method allows only estimations of $m_{\max}$ that are close to the maximum observed earthquake magnitude.
- Groningen (max. observed magnitude 3.6): $m_{\max} = 5, \ldots, 6, \ldots$ is ruled out by definition.

Relation to other statistical methods

Conclusions on the estimation of $m_{\max}$ with EVT

- EVT estimators assume that the maximum observed events are close to the truncation point of the FS distribution, namely $m_{\max}$.
- By construction, the method allows only estimations of $m_{\max}$ that are close to the maximum observed earthquake magnitude.
- Groningen (max. observed magnitude 3.6): $m_{\max} = 5, \ldots, 6, \ldots$ is ruled out by definition.

Main result of EVT estimator: "Mmax equals Mobs plus an Increment" (Wheeler, USGS Open File Report 2009–1018)

Details in Zöller, Bull. Seism. Soc. Am., doi: 10.1785/0120210307, 2022.

General findings/last Mmax workshop:

Summary on $m_{\max}$ I

General findings/last Mmax workshop:

- All information on $m_{\max}$ is encoded in the b-value and the magnitude μ of the maximum observed earthquake.

General findings/last Mmax workshop:

- All information on $m_{\max}$ is encoded in the b-value and the magnitude μ of the maximum observed earthquake.
- The Bayesian confidence interval is dominated by the prior distribution, not by the observed data.

  (see e.g. Zöller and Holschneider, SRL, 87(1), 132–137, 2016)

General findings/last Mmax workshop:

- All information on $m_{\max}$ is encoded in the b-value and the magnitude μ of the maximum observed earthquake.
- The Bayesian confidence interval is dominated by the prior distribution, not by the observed data.

  (see e.g. Zöller and Holschneider, SRL, 87(1), 132–137, 2016)
- Truncated vs. tapered distribution: makes no difference

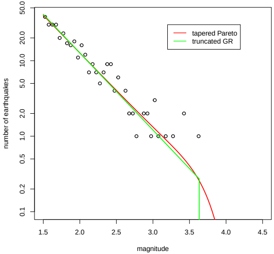

Updates since the last Mmax workshop

Updates since the last Mmax workshop

- The FS distribution (physics) is overall stable. The growth of the catalog results in decreasing uncertainties of $m_{\max}$ estimates.

Updates since the last Mmax workshop

- The FS distribution (physics) is overall stable. The growth of the catalog results in decreasing uncertainties of $m_{\max}$ estimates.
- Probabilistic approach $\rightarrow$ All estimates of $m_{\max}(\geq 3.6)$ can be justified depending on the assumed level of confidence $0, \ldots, 100\%$. However, for practical purposes, it is desirable to provide a specific value:

Summary on $m_{\max}$ II

Updates since the last Mmax workshop

- The FS distribution (physics) is overall stable. The growth of the catalog results in decreasing uncertainties of $m_{\max}$ estimates.
- Probabilistic approach $\rightarrow$ All estimates of $m_{\max}(\geq 3.6)$ can be justified depending on the assumed level of confidence $0, \ldots, 100\%$. However, for practical purposes, it is desirable to provide a specific value:

  For 95% confidence the upper bound of the best confidence interval is

$$M(0.95) = 4.3.$$

2. M_T: The largest expected earthquake magnitude in time T

Why study M_T?

- For purposes of seismic hazard, it might be more interesting to focus on the magnitude M_T of the maximum expected earthquake that occurs in this time period.

Why study M_T?

- For purposes of seismic hazard, it might be more interesting to focus on the magnitude M_T of the maximum expected earthquake that occurs in this time period.
- Groningen: Lifetime of gas field limited, end of gas production is close.

Why study M_T?

- For purposes of seismic hazard, it might be more interesting to focus on the magnitude M_T of the maximum expected earthquake that occurs in this time period.
- Groningen: Lifetime of gas field limited, end of gas production is close.
- M_T can be calculated from the b-value and the earthquake rate (or the a-value), which are accessible from instrumental (short) earthquake catalogs.

Calculation of M_T: The statistical models

1. Magnitudes: Gutenberg-Richter law (limited or unlimited? $m_{\max}$?)

Calculation of M_T: The statistical models

1. Magnitudes: Gutenberg-Richter law (limited or unlimited? $m_{\max}$?)
2. Earthquake rate (time model):

Calculation of M_T: The statistical models

1. Magnitudes: Gutenberg-Richter law (limited or unlimited? $m_{\max}$?)
2. Earthquake rate (time model):

- I. Model based on gas production:

  (see Zöller and Holschneider: BSSA, 106, 2917–2921, 2016)

Calculation of M_T: The statistical models

1. Magnitudes: Gutenberg-Richter law (limited or unlimited? $m_{\max}$?)
2. Earthquake rate (time model):

- I. Model based on gas production:
  (see Zöller and Holschneider: BSSA, 106, 2917–2921, 2016)

- II. Stress-based models:
  (see Richter, Hainzl, Dahm & Zöller: Environ. Earth Sci. 79, 252, 2020)

Calculation of M_T: The statistical models

➤ I. Model based on gas production:

- **Model PP:** Inhomogeneous Poisson process:

  EQ rate $\propto$ gas production rate

  (for whole gas field, no space dependence), no memory (seismicity stops as soon as production stops).

Calculation of M_T: The statistical models

- I. Model based on gas production:

  - **Model PP:** Inhomogeneous Poisson process:

    $$\text{EQ rate} \propto \text{gas production rate}$$

    (for whole gas field, no space dependence), no memory (seismicity stops as soon as production stops).

    $\rightarrow$ Bayesian framework, flat priors, returns distribution of M_T, Bayesian confidence interval.

➤ I. Model based on gas production:

- **Model PP:** Inhomogeneous Poisson process:

  EQ rate $\propto$ gas production rate

  (for whole gas field, no space dependence), no memory (seismicity stops as soon as production stops).

  $\rightarrow$ Bayesian framework, flat priors, returns distribution of M_T, Bayesian confidence interval.

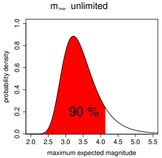

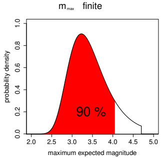

Calculation of M_T: Gas production

Groningen: Gas production vs. earthquake rate

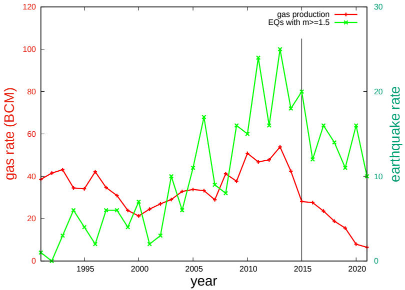

Calculation of M_T: Gas production

Groningen: Future scenario for gas production

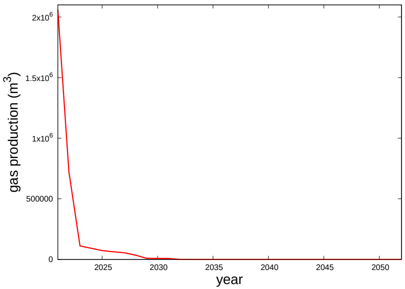

Groningen: Future scenario for gas production
no longer up-to-date :(

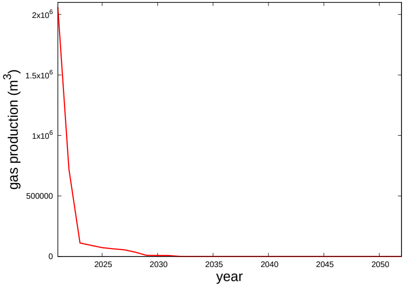

Calculation of M_T: The models

- II. Stress-based models: Coulomb failure stress

Calculation of M_T: The models

➤ II. Stress-based models: Coulomb failure stress

- **Model CFS:** Coulomb failure model: EQ rate $\propto$ Coulomb failure stress at each site, if positive

Calculation of M_T: The models

➤ II. Stress-based models: Coulomb failure stress

- **Model CFS:** Coulomb failure model: EQ rate $\propto$ Coulomb failure stress at each site, if positive
- **Model CFS-AS:** Coulomb failure model with aftershocks: ETAS* model

$$\lambda(t|\mathcal{H}_t) = \underbrace{\mu(t)}_{\propto \text{ EQ rate}} + \underbrace{\sum_{\{j:t_j<t\}} \frac{K \exp[\alpha(m_j - m_0)]}{(t - t_j + c)^p}}_{\text{aftershocks}}$$

* Ogata, J. Am. Stat. Assoc. 83, 1988.

- II. Stress-based models: Coulomb failure stress
  - **Model CFS:** Coulomb failure model: EQ rate $\propto$ Coulomb failure stress at each site, if positive
  - **Model CFS-AS:** Coulomb failure model with aftershocks: ETAS* model

$$\lambda(t|\mathcal{H}_t) = \underbrace{\mu(t)}_{\propto \text{ EQ rate}} + \underbrace{\sum_{\{j:t_j<t\}} \frac{K \exp[\alpha(m_j - m_0)]}{(t - t_j + c)^p}}_{\text{aftershocks}^\dagger}$$

* Ogata, J. Am. Stat. Assoc. 83, 1988.
†ETAS triggering parameters: $c = 0.01$ day, $p = 1.1, K = 0.018, \alpha = 0.8$

Calculation of M_T: The models

➤ II. Stress-based models: Coulomb failure stress

- **Model CFS:** Coulomb failure model: EQ rate $\propto$ Coulomb failure stress at each site, if positive
- **Model CFS-AS:** Coulomb failure model with aftershocks: ETAS* model

$$\lambda(t|\mathcal{H}_t) = \underbrace{\mu(t)}_{\propto \text{ EQ rate}} + \underbrace{\sum_{\{j:t_j<t\}} \frac{K\exp[\alpha(m_j - m_0)]}{(t - t_j + c)^p}}_{\text{aftershocks}^\dagger}$$

$\rightarrow$ CFS parameters: constant in space, estimated by maximum likelihood method.

* Ogata, J. Am. Stat. Assoc. 83, 1988.

†ETAS triggering parameters: $c = 0.01$ day, $p = 1.1, K = 0.018, \alpha = 0.8$

Calculation of M_T: The models

➤ II. Stress-based models: Coulomb failure stress

- **Model CFS:** Coulomb failure model: EQ rate $\propto$ Coulomb failure stress at each site, if positive
- **Model CFS-AS:** Coulomb failure model with aftershocks: ETAS* model

$$\lambda(t|\mathcal{H}_t) = \underbrace{\mu(t)}_{\propto \text{ EQ rate}} + \underbrace{\sum_{\{j:t_j<t\}} \frac{K \exp[\alpha(m_j - m_0)]}{(t - t_j + c)^p}}_{\text{aftershocks}^\dagger}$$

$\rightarrow$ CFS parameters: constant in space, estimated by maximum likelihood method.

$\rightarrow$ Model returns EQ number n for time T.

* Ogata, J. Am. Stat. Assoc. 83, 1988.

† ETAS triggering parameters: $c = 0.01$ day, $p = 1.1, K = 0.018, \alpha = 0.8$

Calculation of M_T: The models

- II. Stress-based models: Rate-and-state dependent friction

Calculation of M_T: The models

➤ II. Stress-based models: Rate-and-state dependent friction

- **Model RS:** Rate-and-state model: seismicity governed by rate-and-state dependent fricition (Dieterich, JGR 99, 2601–2618, 1994)

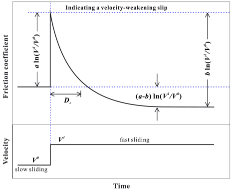

(Figure from Chen et al., JGR 122(12), 2017)

➤ II. Stress-based models: Rate-and-state dependent friction

- **Model RS:** Rate-and-state model: seismicity governed by rate-and-state dependent fricition (Dieterich, JGR 99, 2601–2618, 1994)

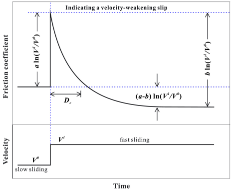

(Figure from Chen et al., JGR 122(12), 2017)

- **Model RS-AS:** Rate-and-state model with aftershocks (ETAS, as for model CFS-AS)

Calculation of M_T: The models

➤ II. Stress-based models: Rate-and-state dependent friction

- **Model RS:** Rate-and-state model: seismicity governed by rate-and-state dependent fricition (Dieterich, JGR 99, 2601–2618, 1994)

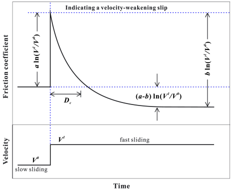

(Figure from Chen et al., JGR 122(12), 2017)

- **Model RS-AS:** Rate-and-state model with aftershocks (ETAS, as for model CFS-AS)

→ RS parameters: independent of space, estimated by maximum likelihood method.

→ Model returns EQ number n for time T.

Calculation of M_T: The models

Stress based models:
forecast of earthquake rates (with 95% confidence ranges)

Stress based models:
forecast of earthquake rates (with 95% confidence ranges)

without aftershocks:

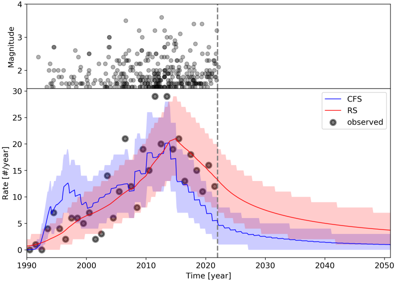

Calculation of M_T: The models

Stress based models:
forecast of earthquake rates (with 95% confidence ranges)

without aftershocks:

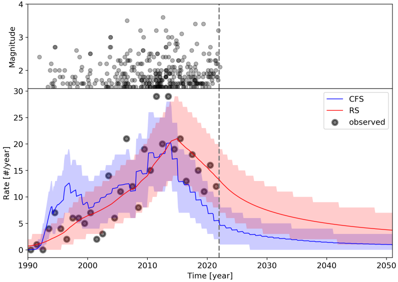

with aftershocks (ETAS model):

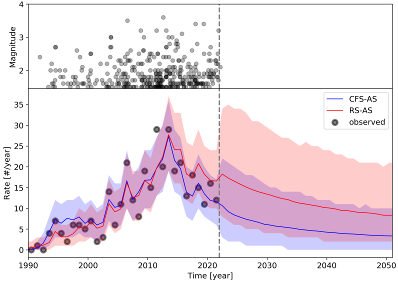

Calculation of M_T: The models

Stress based models:
forecast of earthquake rates (with 95% confidence ranges)

without aftershocks: with aftershocks (ETAS model):

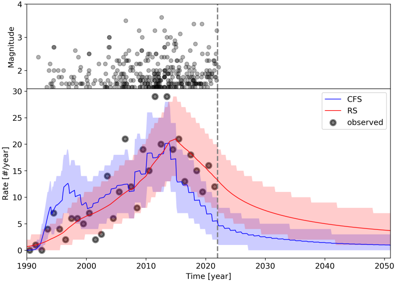

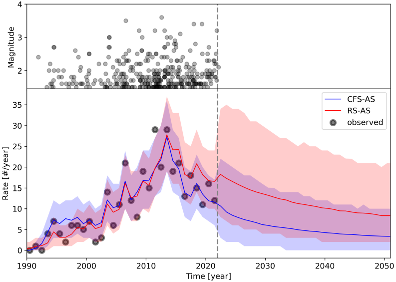

➤ Model comparison: RS fits best to Groningen data.

Calculation of M_T: The models

From EQ numbers to magnitudes:

Calculation of M_T: The models

From EQ numbers to magnitudes:

– model forecasts the number n of future earthquakes.

– sample n random magnitudes, sampled from Gutenberg-Richter distribution $(b = 0.94, m_0 = 1.5, m_{\max} = 4.0/4.3/\infty)$

– $M_T = \max\{m_1, \ldots, m_n\}$

$$P(M_T < z) = [F_{b,m_0,m_{\max}}(z)]^n; \quad F : \mathrm{Gutenberg-Richter\ cdf}$$

Remarks

Remarks

- Time horizon for M_T : 2022-2052; gas production stops in 2032.

Calculation of M_T: The models

Remarks

- Time horizon for M_T : 2022-2052; gas production stops in 2032.
- Model PP: EQs stop in 2032, because EQ rate $\propto$ gas production rate (no memory).

Calculation of M_T: The models

Remarks

- Time horizon for M_T : 2022-2052; gas production stops in 2032.
- Model PP: EQs stop in 2032, because EQ rate $\propto$ gas production rate (no memory).
- Stress-based models have memory (EQs after 2032).

Calculation of M_T: The models

Remarks

- Time horizon for M_T : 2022-2052; gas production stops in 2032.
- Model PP: EQs stop in 2032, because EQ rate $\propto$ gas production rate (no memory).
- Stress-based models have memory (EQs after 2032).
- Three $m_{\max}$ values: 4.0 (90% confidence), 4.3 (95% confidence), ∞ (100% confidence).

Maximum expected earthquake 2022–2052

Ranges for M_T from 2022 to 2052 (95% confidence)

- Model **PP**: $3.1 \ldots 3.2$ (no EQs after 2032!)
- Model **CFS**: $3.9 \ldots 4.8$
- Model **CFS-AS**: $4.0 \ldots 5.2$
- Model **RS**: $4.0 \ldots 5.3$
- Model **RS-AS**: $4.0 \ldots 5.6$

Variability is due to the choice of $m_{\max}$.

Maximum expected earthquake 2022–2052

Ranges for M_T from 2022 to 2052 (95% confidence)

- Model **PP**: $3.1 \dots 3.2$ (no EQs after 2032!)
- Model **CFS**: $3.9 \dots 4.8$
- Model **CFS-AS**: $4.0 \dots 5.2$
- Model **RS**: $4.0 \dots 5.3$ **!!! best fitting model !!!**
- Model **RS-AS**: $4.0 \dots 5.6$

Variability is due to the choice of $m_{\max}$.

Using model RS with $m_{\max} = 4.3$, the maximum expected magnitude until 2052 is

$$M_T = 4.2.$$

Findings for the largest expected magnitude M_T in the time from 2022 to 2052

- Physically motivated models can reproduce the statistical properties of seismicity in Groningen with few (model RS: 3) parameters.
- Model RS based on rate-and-state dependent friction is the best fitting model $\rightarrow$ model PP probably underestimates number and magnitude of future earthquakes.
- Based on given stress data, model RS in comination with a Gutenberg-Richter distribution for magnitudes forecasts the largest expected magnitude until 2052 to be

$$M_T = 4.2.$$

Methodology

1. Use simple and well-accepted models for seismicity.

Methodology

1. Use simple and well-accepted models for seismicity.
2. Provide straightforward uncertainty assessment, even for sparse data.

Methodology

1. Use simple and well-accepted models for seismicity.
2. Provide straightforward uncertainty assessment, even for sparse data.
3. Forecasts benefit from recent successful simulations for Groningen seismicity based on rate-and-state dependent friction.

Results for Groningen (at 95% confidence)

1. Maximum possible magnitude: $m_{\max} = 4.3$.
2. Maximum expected magnitude between 2022 and 2052:
   - $M_T = 3.2$ (based on gas production data).
   - $M_T = 4.2$ (based on stress data).

Results for Groningen (at 95% confidence)

1. Maximum possible magnitude: $m_{\max} = 4.3$.
2. Maximum expected magnitude between 2022 and 2052:
   - $M_T = 3.2$ (based on gas production until 2032).
   - $M_T = 4.2$ (based on stress data).

Results for Groningen (at 95% confidence)

1. Maximum possible magnitude: $m_{\max} = 4.3$.
2. Maximum expected magnitude between 2022 and 2052:
   - $M_T = 3.2$ (based on gas production until 2032).
   - $M_T = 4.2$ (based on stress data).

Thank you!

Slides from 2016: tapered or truncated distribution?

Truncated or tapered: Does it matter?

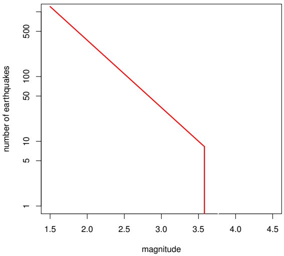

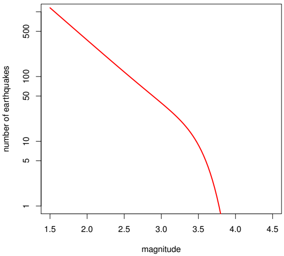

Synthetic Groningen catalog with 10^6 earthquakes

What is the underlying magnitude model?

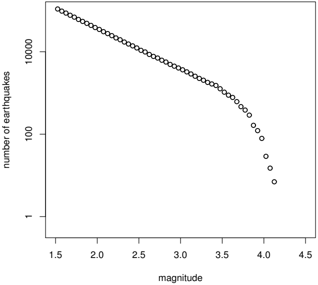

Synthetic Groningen catalog with 10^6 earthquakes

What is the underlying magnitude model?

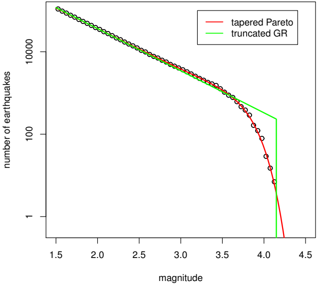

Synthetic Groningen catalog with 10^6 earthquakes

What is the underlying magnitude model?

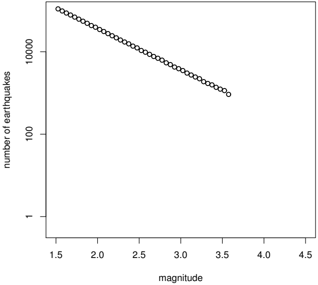

Synthetic Groningen catalog with 10^6 earthquakes

What is the underlying magnitude model?

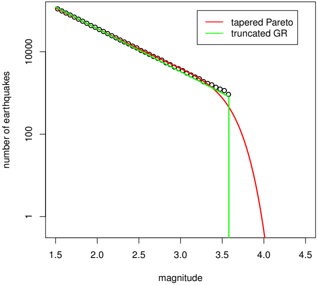

Synthetic Groningen catalog with 261 earthquakes

What is the underlying magnitude model?

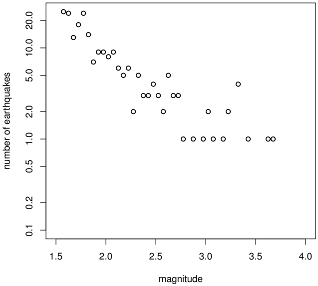

Synthetic Groningen catalog with 261 earthquakes

What is the underlying magnitude model?

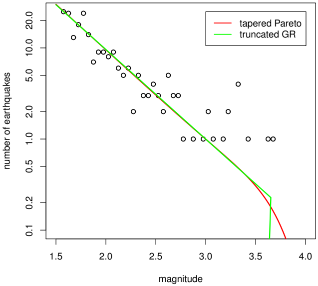

Production Related Seismicity and Probable Maximum Magnitudes in Groningen

N. Boitz and S. Shapiro

Freie Universität Berlin

boitz@geophysik.fu-berlin.de

Motivation and Open Questions

- Which parameters are controlling the maximum magnitude of production induced seismicity?
- Can the LB-concept of injection induced seismicity be applied to production induced seismicity?
- How do changes in pore-pressure and produced gas volumes impact seismicity?

Freie Universität Berlin

Outline

- Part I: Review and application of the Lower-Bound concept
- Part II: Review and application of the Seismogenic Index model

The Gutenberg-Richter law for tectonic seismicity

Frequency Magnitude distribution from Northern California

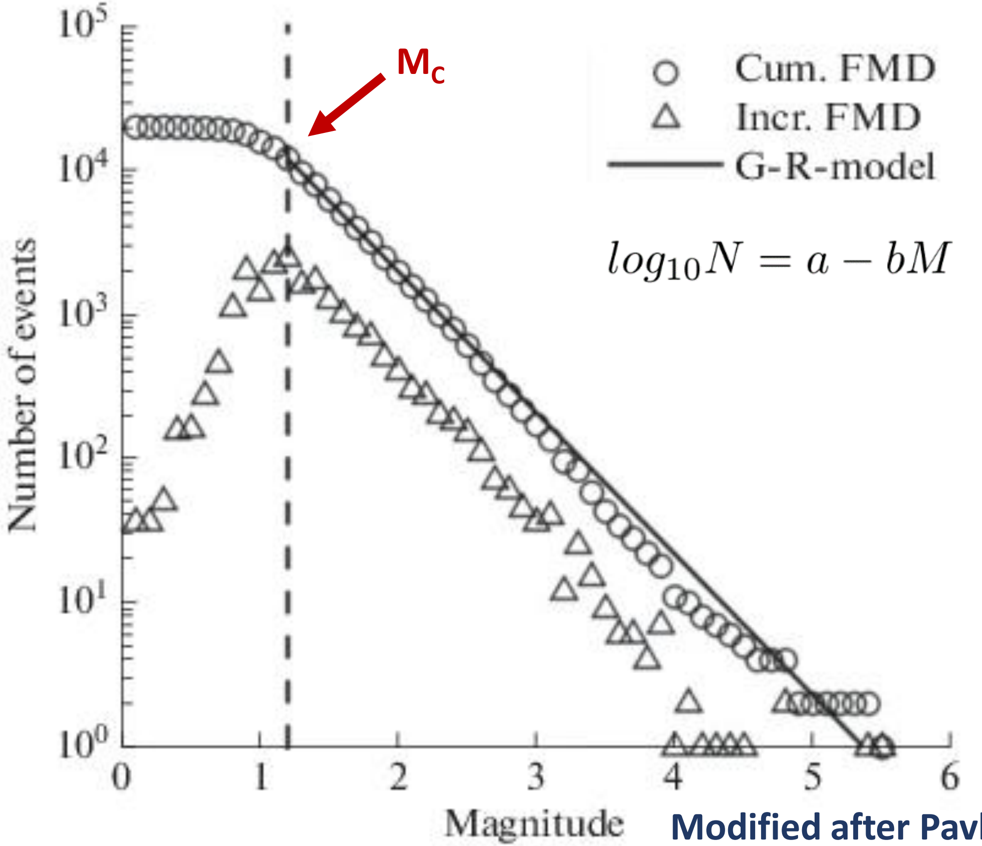

Modified after Pavlenko and Zavyalov, 2022

What are FM distributions for induced seismicity?

Induced seismicity is related to stimulated volume

Stimulated volume can be approximated by an ellipsoid

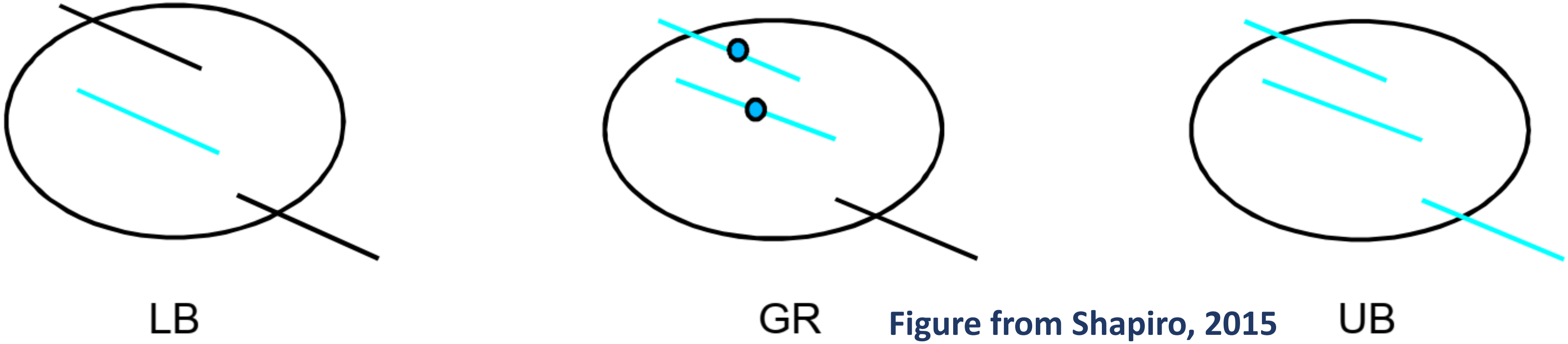

Figure from Shapiro, 2015

The complete rupture surface is within the stimulated volume

The nucleation point is within the stimulated volume, but rupture can propagate beyond

Any part of the rupture touches the stimulated volume

Theoretical concepts of the FM-distribution

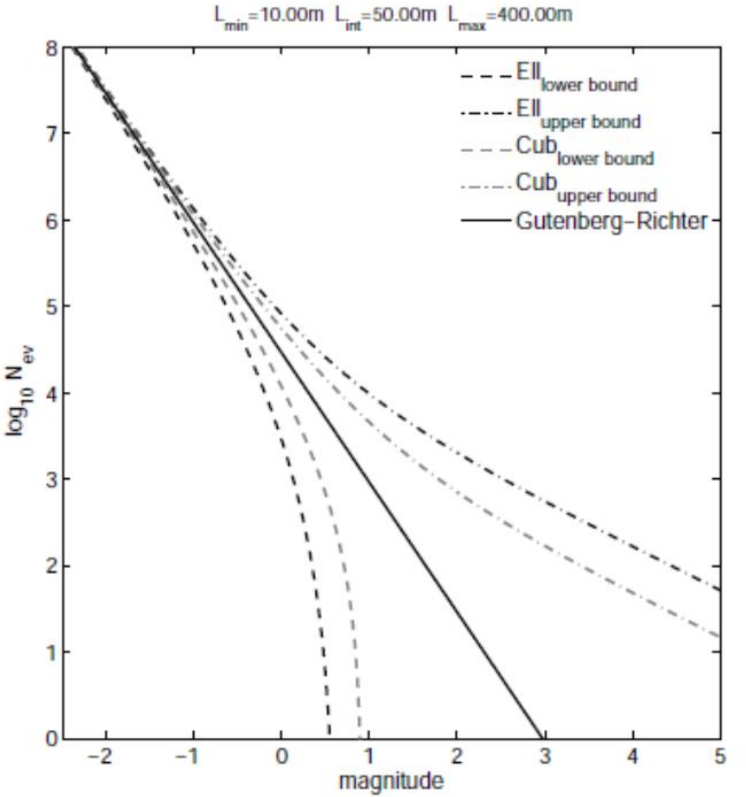

Figure from Shapiro et al. 2013

- **For small magnitude events, LB, GR and UB almost coincide**
- **The LB predicts significant less large magnitude events (asymptotic limit)**
- **GR predicts a linear relationship**
- **UB predicts a higher number of large magnitude events than GR**

Injection induced seismicity follows the lower bound

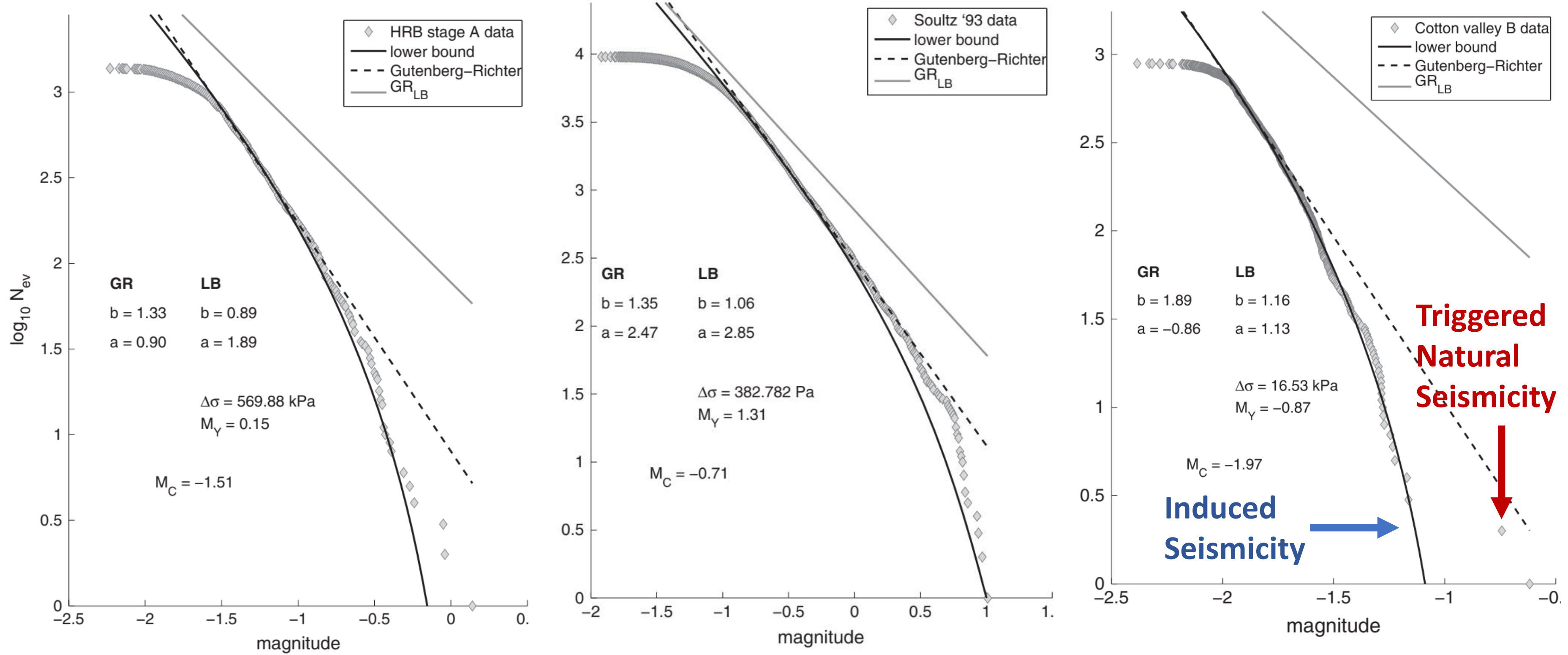

Figures from Shapiro et al. 2013

Injection induced seismicity follows the lower bound

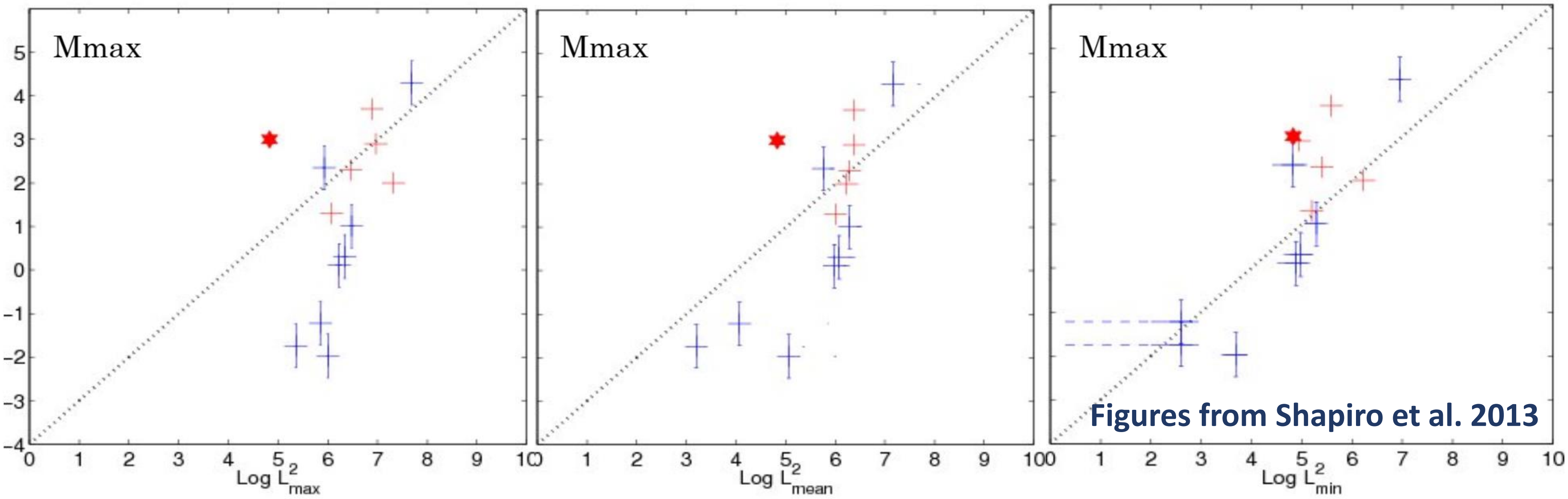

$$M_Y \approx 2log_{10}Y + log_{10}(\Delta\sigma)/1.5 - 6.07.$$

The maximum magnitude depends linearly on the log-length of L_{Min}

Can this concept be applied to production induced seismicity ?

Possible rupture surfaces according to LB

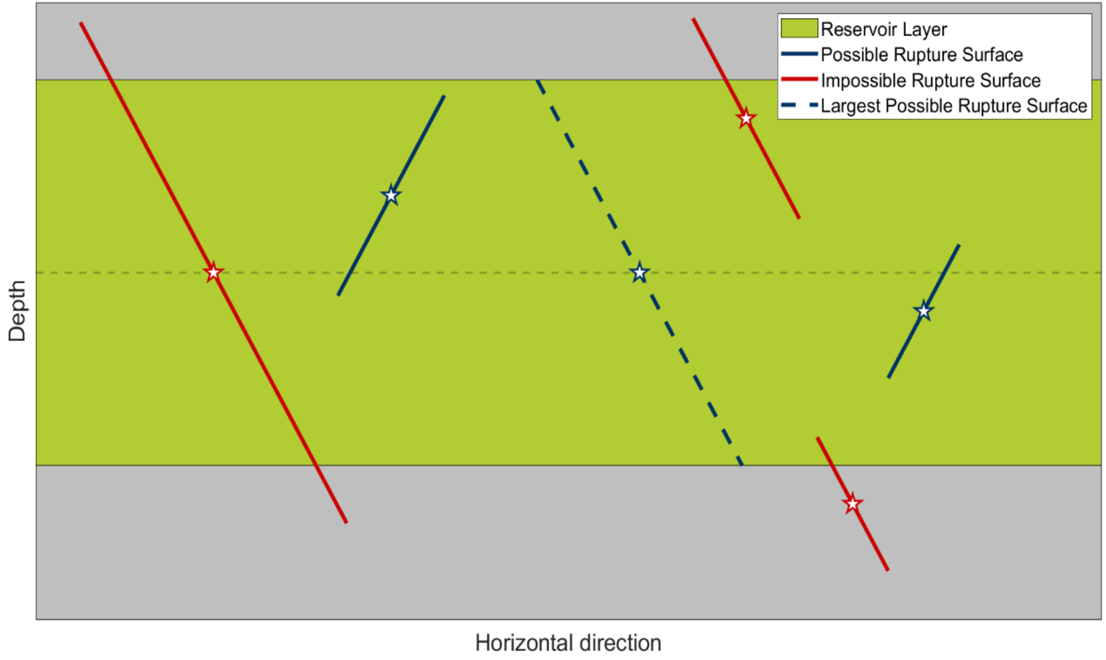

- **We assume a single horizontal layer with an infinite horizontal extend and a given thickness**
- **L_{min} is then given by reservoir thickness**
- **Maximum magnitude theoretically only depends on the reservoir thickness and the stress drop**

$$M_Y \approx 2log_{10}Y + log_{10}(\Delta\sigma)/1.5 - 6.07.$$

What magnitudes can we expect in Groningen?

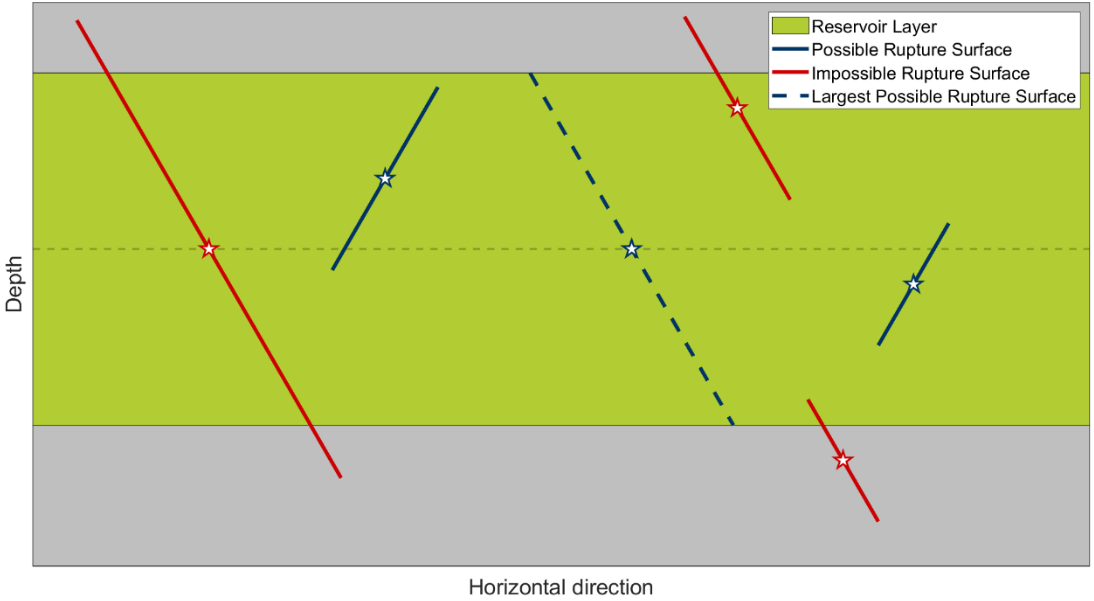

- **Reservoir thickness between (SE=150m and NW = 300m)**
- **Normal faulting tectonics**
- **Maximum observed stress drop in Groningen approx-imately 5MPa**

$$M_Y \approx 2log_{10}Y + log_{10}(\Delta\sigma)/1.5 - 6.07.$$

	X [m]	$\Delta\sigma$ [MPa]	Maximum M_W
Event in SE-part of the reservoir (NF: 30° fault inclination)	173	1	2.41
Event in NW-part of the reservoir (NF: 30° fault inclination)	346	1	3.01
Event in SE-part of the reservoir (NF: 30° fault inclination)	173	10	3.07
Event in NW-part of the reservoir (NF: 30° fault inclination)	346	10	3.67

What magnitudes have been observed in Groningen?

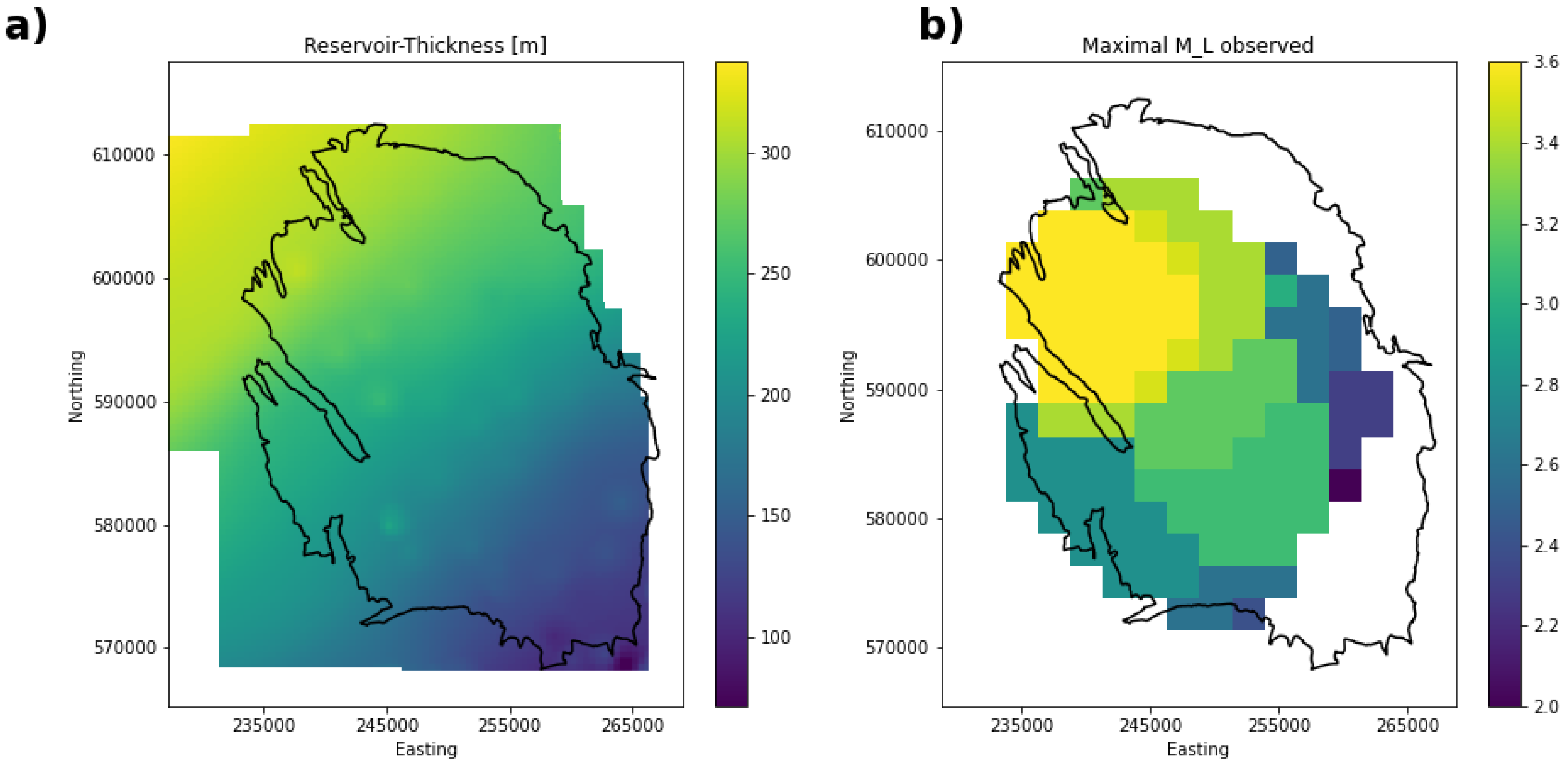

The theoretical estimates are in good agreement with observed seismicity!

Maximum possible magnitude estimates for Groningen

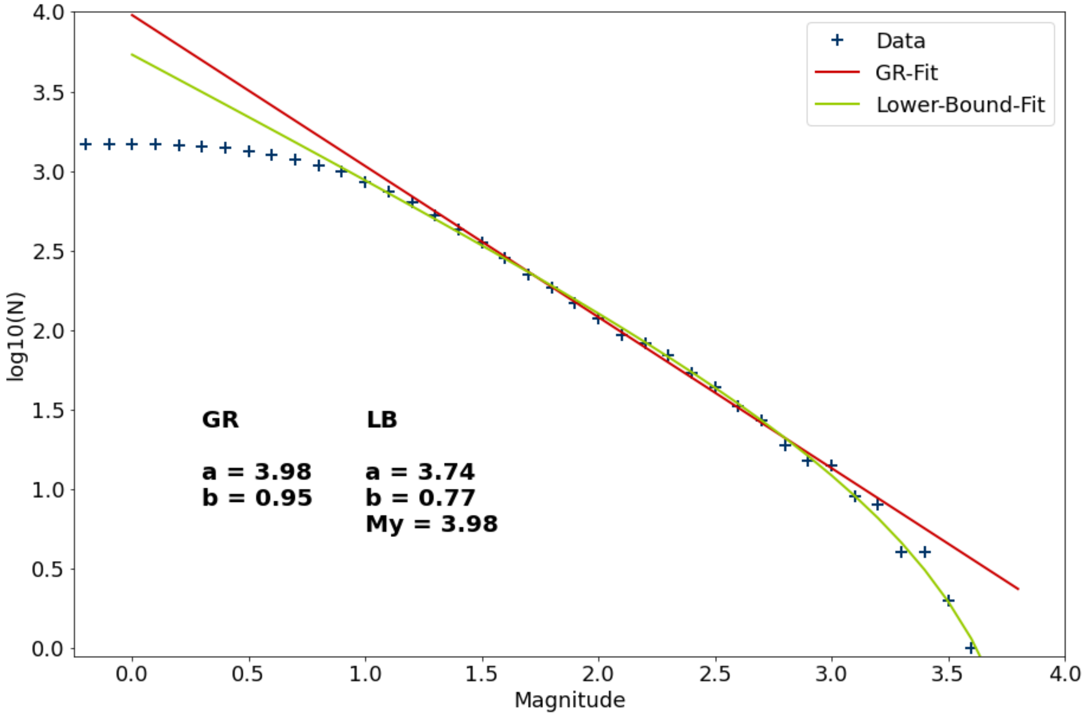

- **Approximate LB-equation for seismicity in a layer**

$$log_{10}N = a - bM + 2log_{10}\left[1 - 10^{\frac{M-M_Y}{2}}\right]$$

- **Lower Bound fits the data significantly better than GR**

- **Maximum possible magnitude for Groningen is M_w = 3.98 (slightly larger than observed M_{max})**

Temporal evolution of LB-parameters

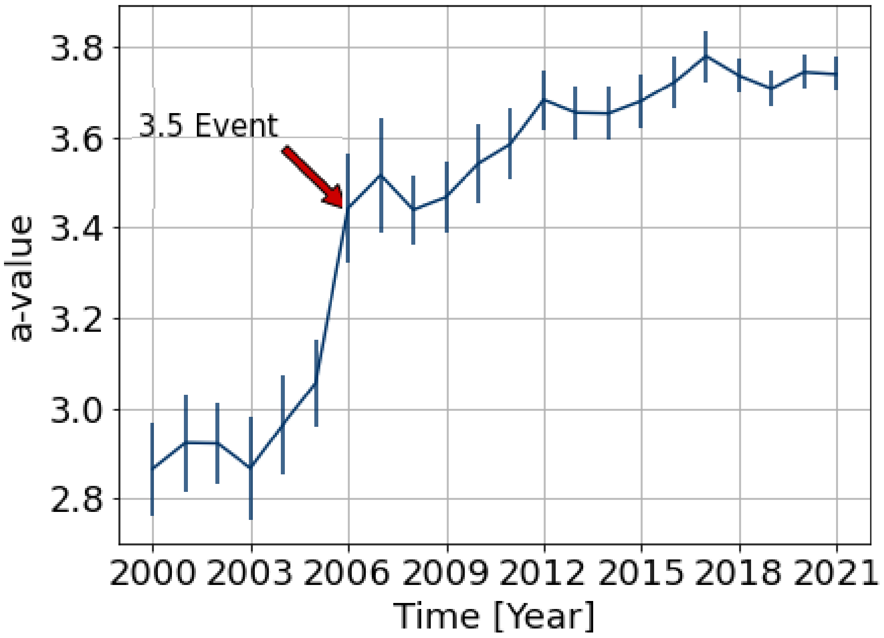

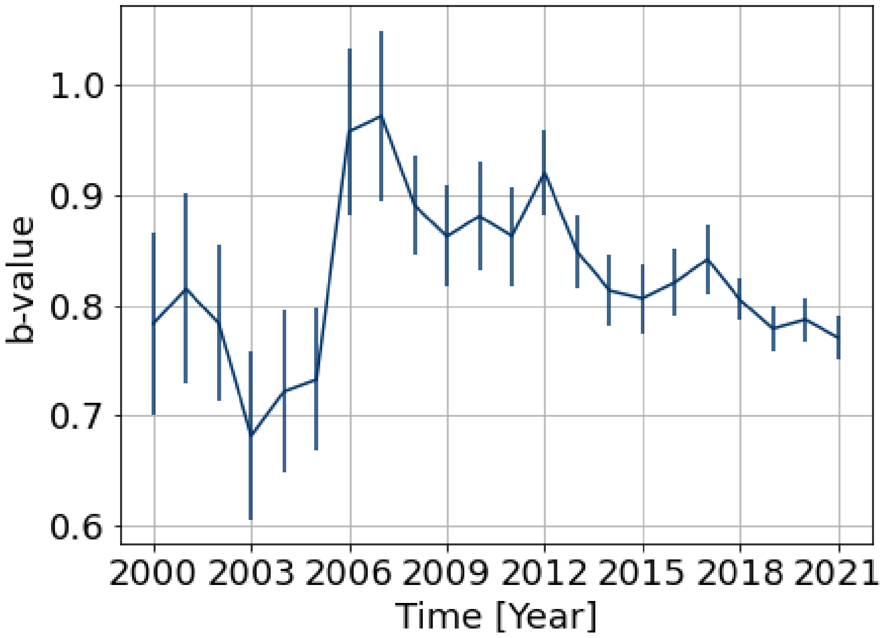

The importance of a correct estimate of the b-value

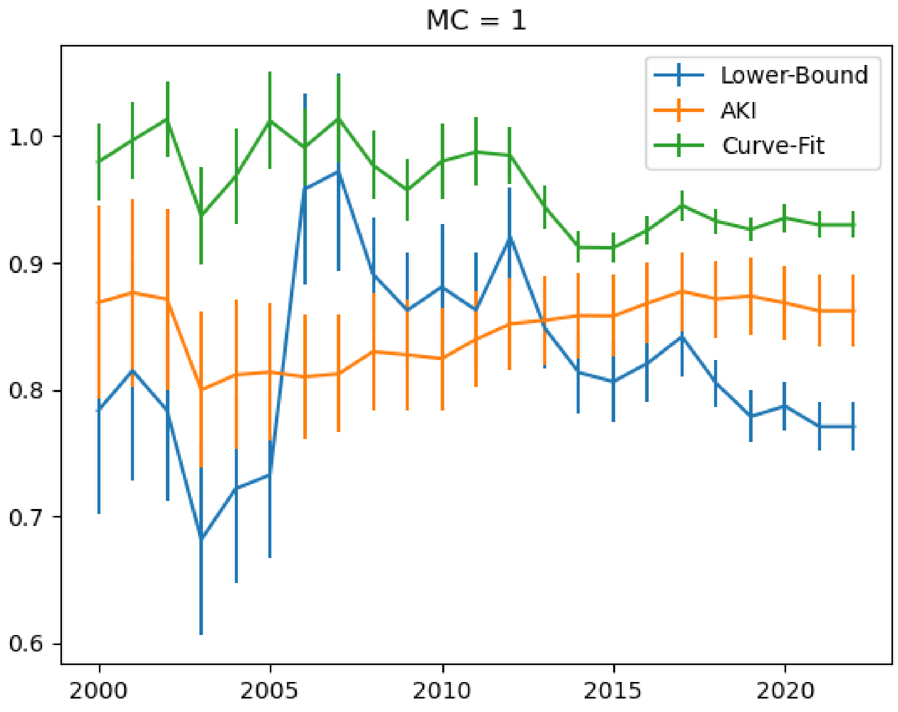

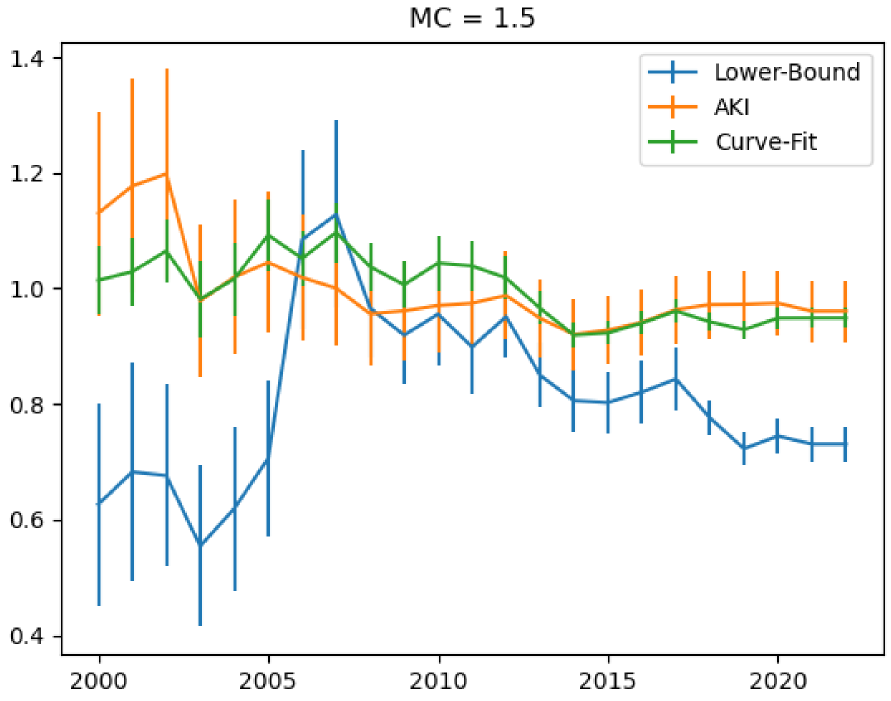

Temporal evolution of LB-parameters

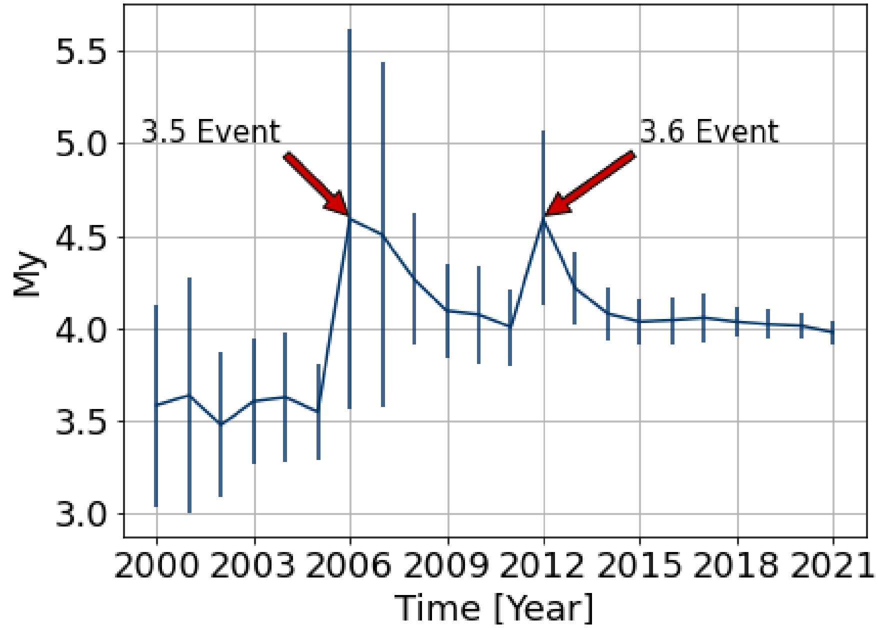

$$M_Y \approx 2log_{10}Y + log_{10}(\Delta\sigma)/1.5 - 6.07.$$

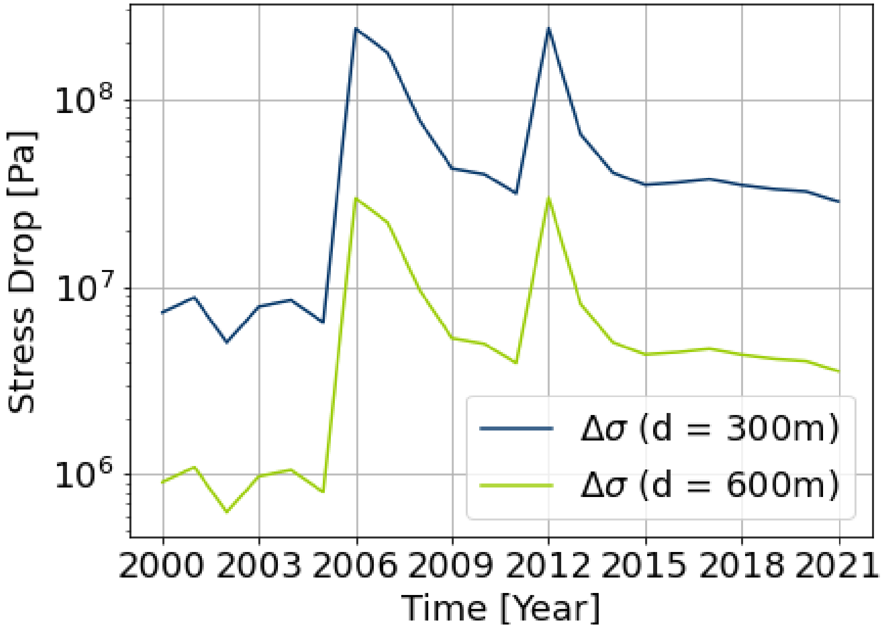

Temporal evolution of LB-parameters

$$M_Y \approx 2log_{10}Y + log_{10}(\Delta\sigma)/1.5 - 6.07.$$

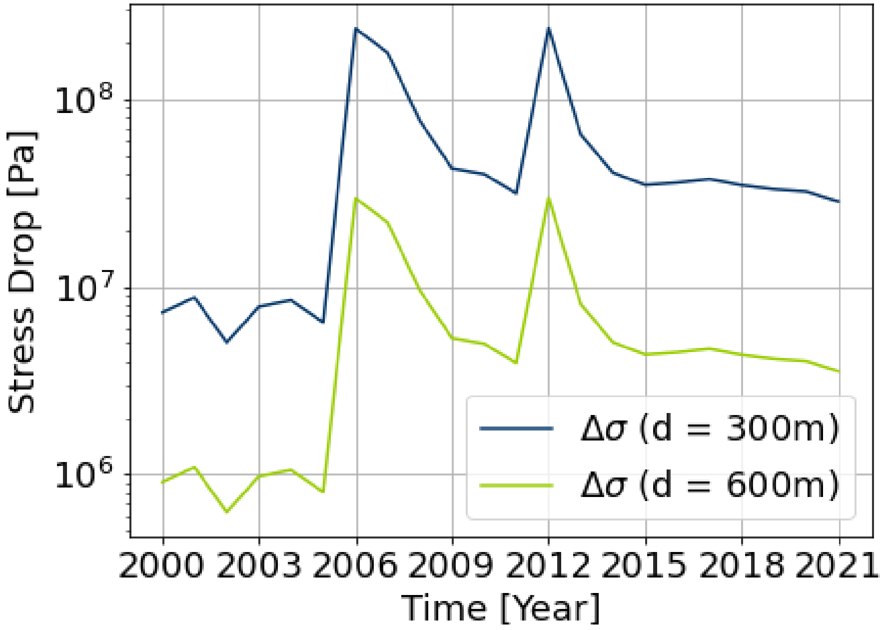

Spatial distribution of observed seismicity

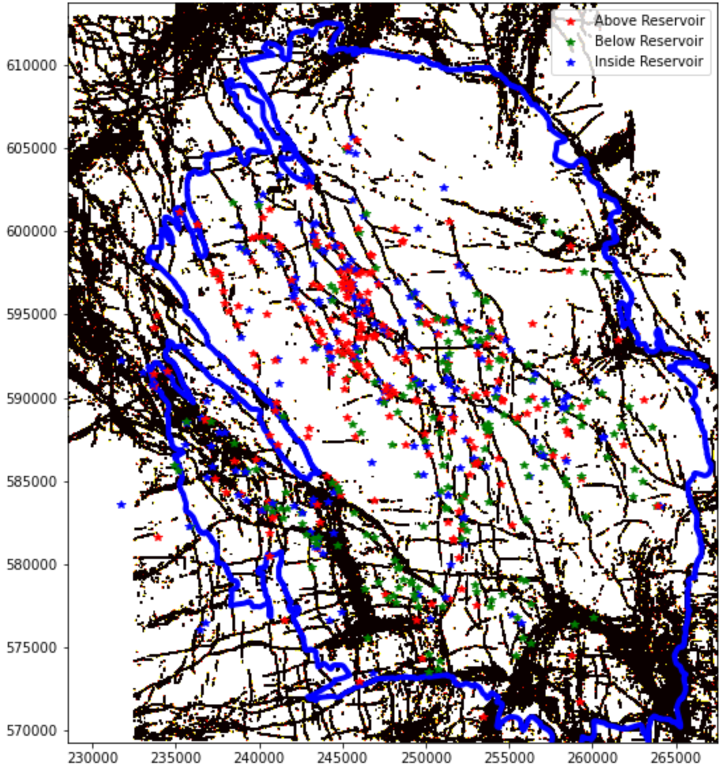

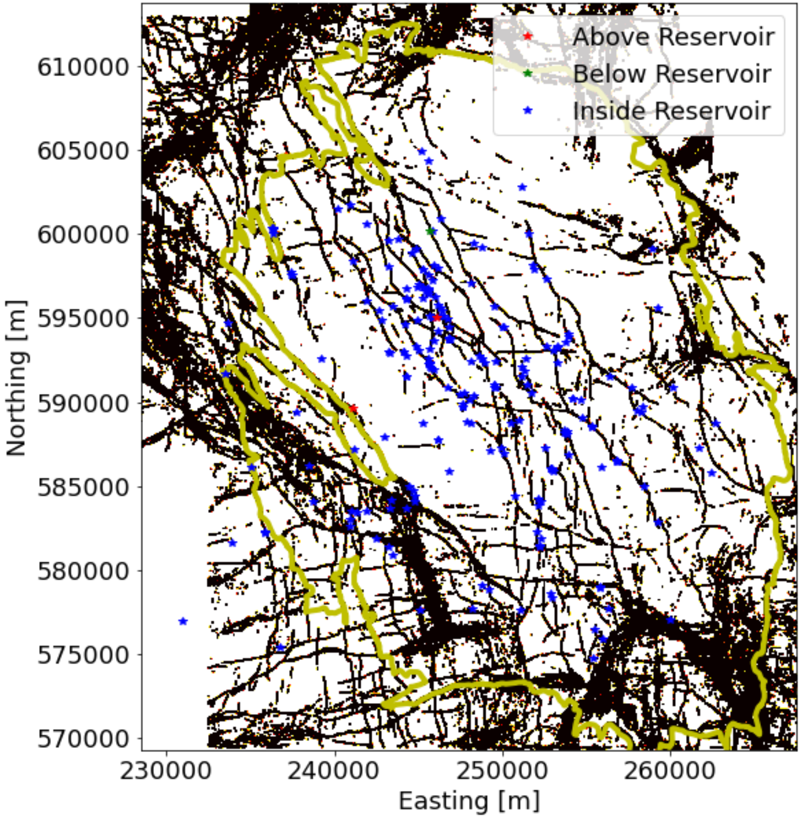

KNMI-EDT Catalog 661 events (2014-2022)

Shell-Catalog (Willacy et al.,(2019)) 224 Events, (2018-2021)

Spatial distribution of observed seismicity

- **KNMI-Catalog (EDT procedure – [Spetzler and Dost, 2017])**
- **661 Events**
- **2014-2022**

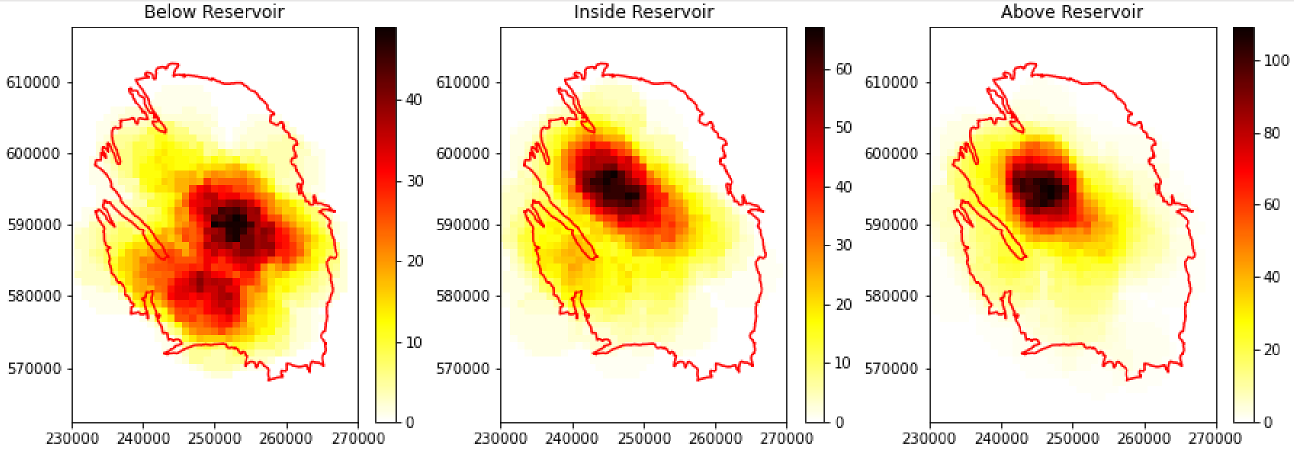

- **Shell-Catalog (Willacy et al. (2019)**
- **224 Events**
- **2018-2021**

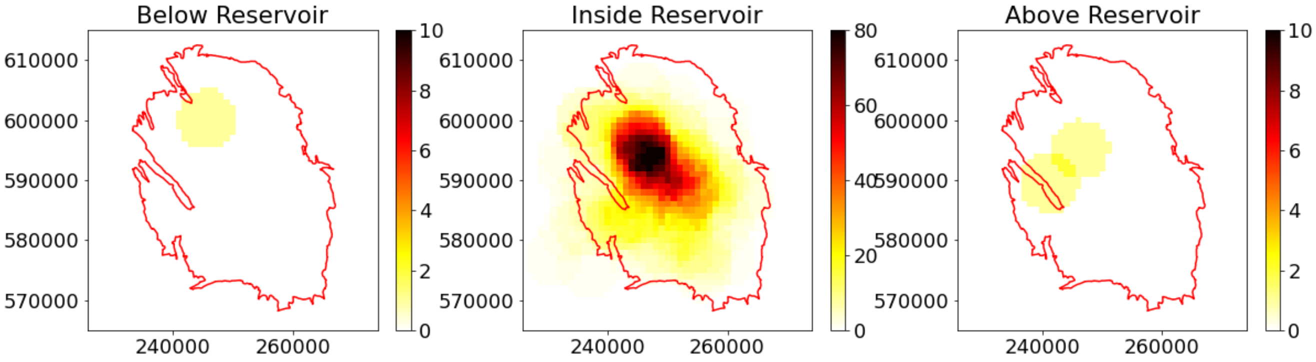

Spatial distribution of LB-parameters: b-value and M_Y

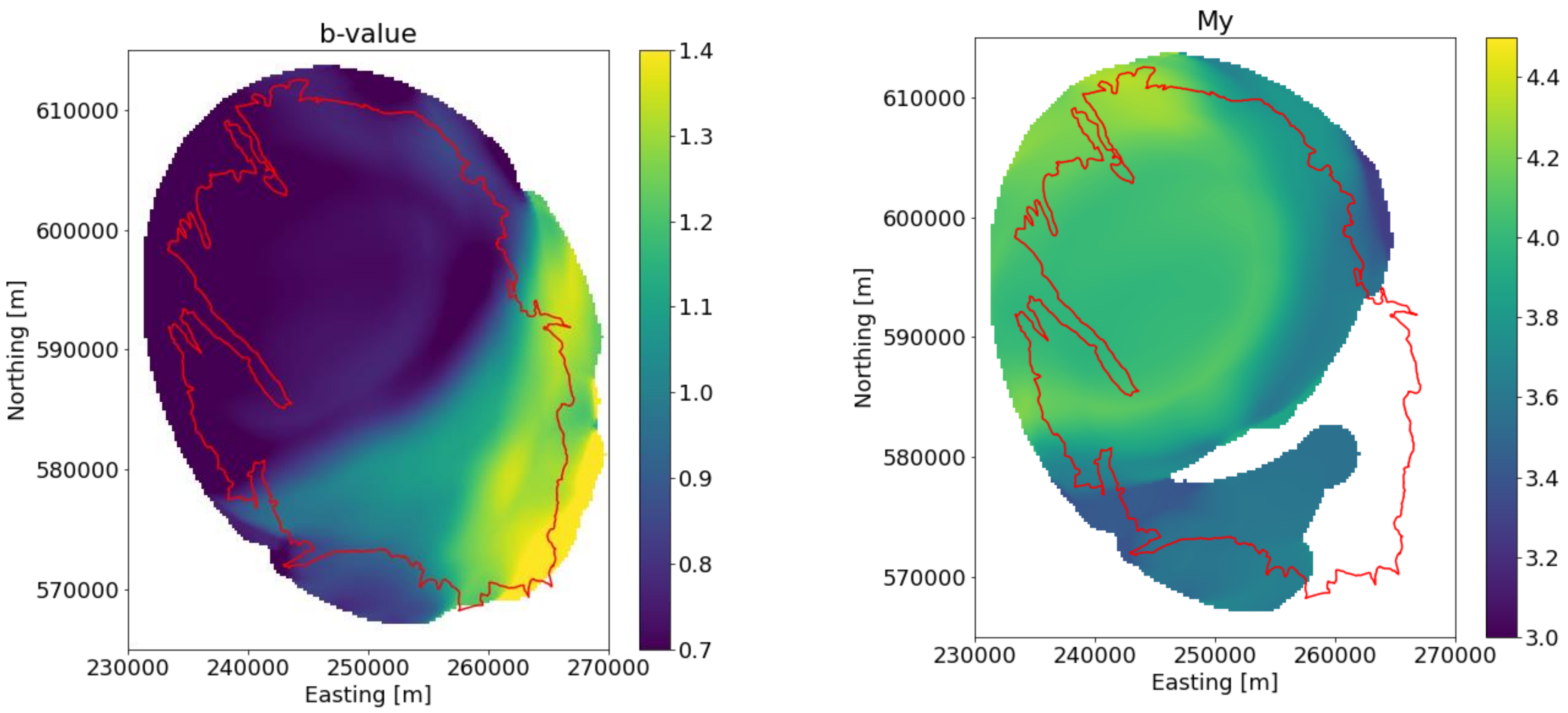

Spatial distribution of **maximum possible** magnitude

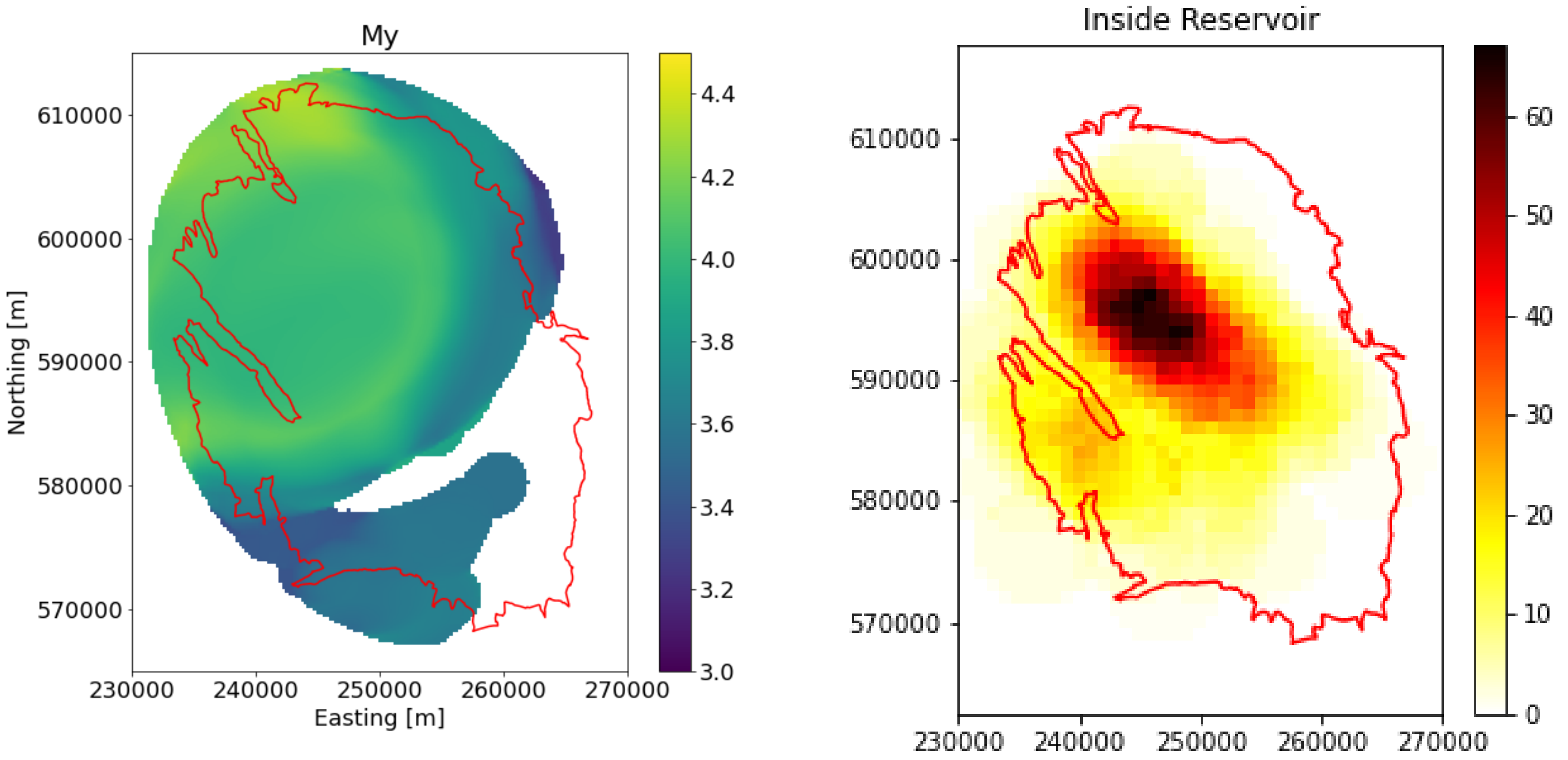

Spatial distribution of maximum possible magnitude

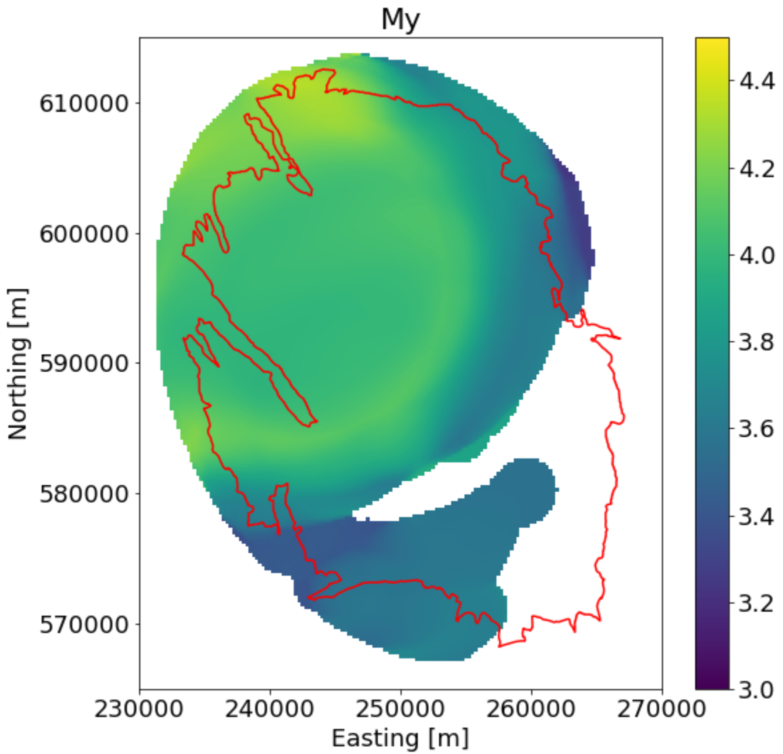

- Overall, M_y is consistent with value for the whole reservoir
- M_y is smaller in domains, where the reservoir is thinner
- This indicates, that M_y is controlled by the reservoir thickness

- Data shows no clear lower-bound for the SE of the field
- Either event density is too small to see LB-effect
- or events may occur mainly below the reservoir and are therefore less controlled by reservoir thickness.

Part II

The Seismogenic Index Model and its Application to Groningen Gas Production and Seismicity

Freie Universität Berlin

GR-law for fluid-induced seismicity – Seismogenic Index

$$\log N_M\,(t) = a(t) - bM$$

$$\log N_M\,(t) = \Sigma + \log Q\,(t) - bM$$

Q(t): Volume of extracted or injected fluid

Σ : Seismogenic Index (a field-site specific quantity for the seismic potential)

Injection-induced seismicity
(Shapiro et al., 2010, The Leading Edge)

$$\log N_M\,(t) = \Sigma + \log Q_{inject}\,(t) - bM$$

Production-induced seismicity
(Shapiro, 2018, JGR)

$$\log N_M(t) = \Sigma + \log Q_{in-situ}(t) - bM$$

$$Q_{in\text{-}situ} = Q_{prod}\,\frac{\rho_{prod}}{\rho_{in-situ}}$$

Seismogenic Index at different field-sites

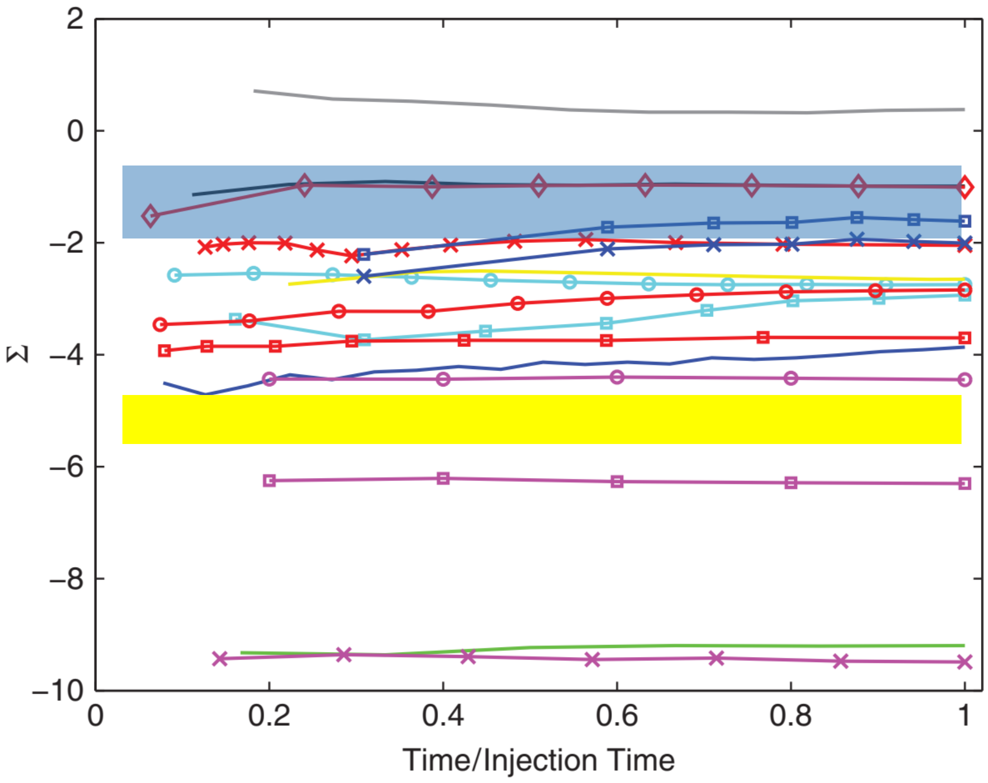

Basel EGS
KTB experiment
Soultz
Cotton Valley
Barnett-Shale
Groningen
Pohang EGS

Figure modified from Shapiro, 2015

Larger Σ in crystalline Rocks, smaller in sedimentary rocks
Σ nearly constant for most cases
Σ for Groningen is rather large for sediments

Generalization of GR-law for induced seismicity

$$\log \mathrm{N_M}(\mathrm{t}) = a(t) - bM$$

$$\log \mathrm{N_M}(\mathrm{t}) = [\,\Sigma_0 + \log \Delta V f(t)\,] - bM$$

$$\log \mathrm{N_M}(\mathrm{t}) = [\,\Sigma_0 + \delta\Sigma(t)] - bM$$

$$\Sigma_0 = a_w + \log \frac{n}{SC_{max}}$$

Reference value for a given field-site

$$\delta\Sigma(t) = \log[\frac{S}{\sin \varphi_f} \int sup\{\Delta FCS(t, \mathbf{r})\} d^3\mathbf{r}\,]$$

Temporal change due to changes in Mohr-Coulomb-Failure stresses

M. Cacace, H. Hofmann & S. A. Shapiro, 2021, Sci. Rep.

The generalized Seismogenic Index Σ_0

$$\Sigma_0(t) = b(t)M + log_{10}N_M(t) - \delta\Sigma(\delta P_p(t))$$

- **$\sum_0$ in Groningen increases until ≈2013 and saturates on a high level for subsequent years**
- **$\sum_0$ relies on an accurate and reliable estimate of the b-value**

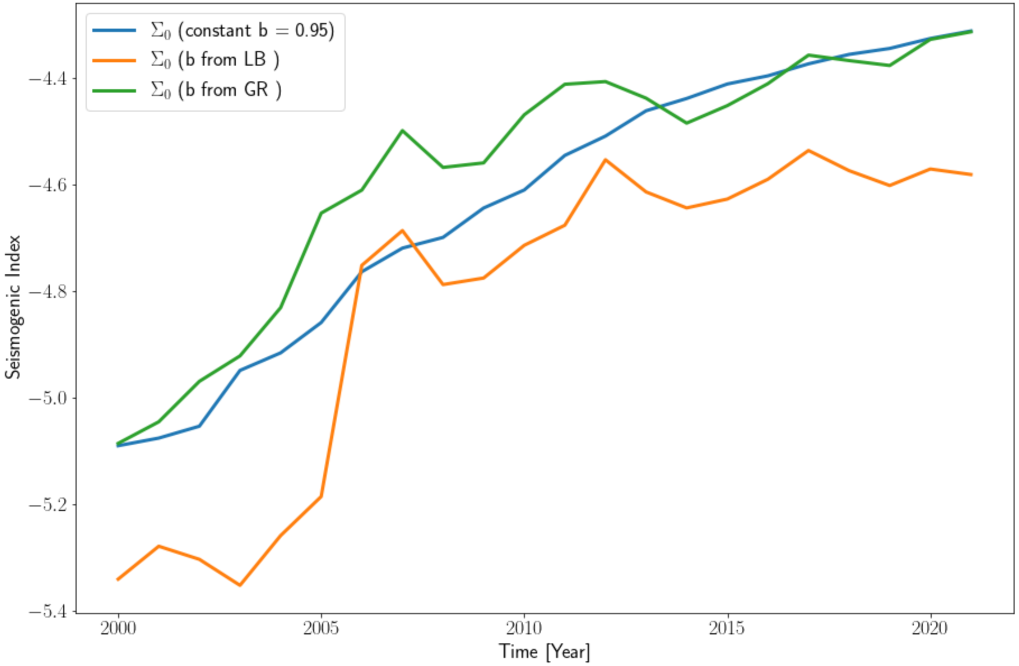

Comparison of LB-parameters, production and SI

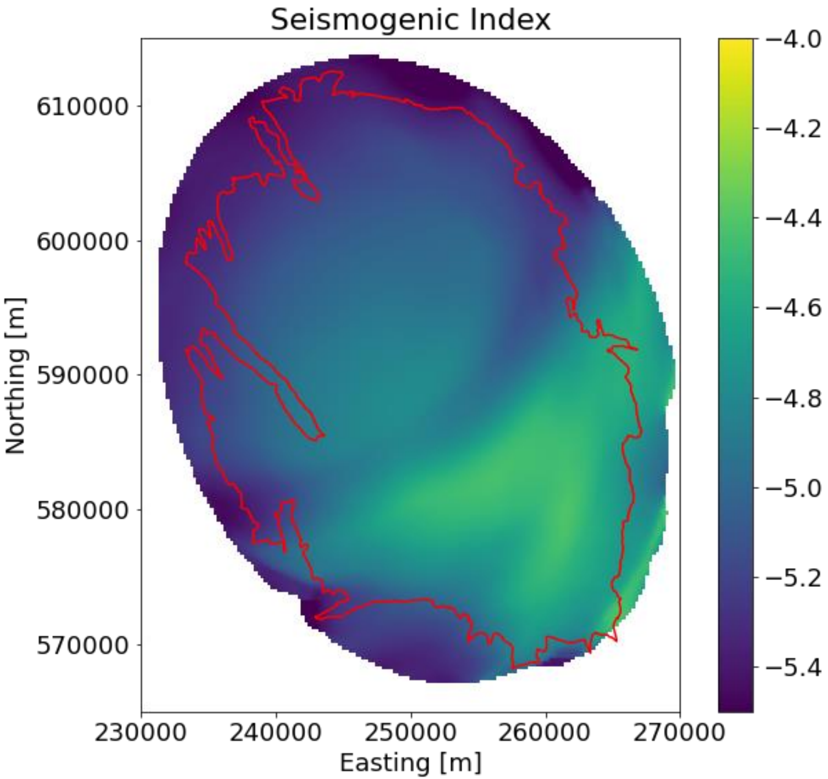

- **b-value, reservoir thickness, and earthquake activity show clear spatial differences**
- **$\sum_0$ is slightly larger in SE part of the field, but no significant variations are observed**

Conclusions

- Lower Bound concept was successfully applied to Groningen seismicity
  - Maximum possible induced magnitude $M_w \approx 4.0$
  - Significant lateral changes and dependance on reservoir thickness
  - Reservoir might be seismologically separated into two parts (NW and SE)
- Seismogenic Index Model
  - Estimation from exact equation for a layer, yields $\sum$ in the range -5.0 to -4.2
  - Corresponds to upper limit for sedimentary rocks
  - Tendency to increase with time until 2013 -> saturation on a rather constant level
  - No significant spatial dependency of Seismogenic index
- What about triggered Large-Magnitude Events?
  - No triggered events have been observed so far, FM-distribution can be accurately described by Lower-Bound concept

We thank the sponsors of the *PHASE* research consortium at Freie Universität Berlin for supporting this research.

Thanks to the organizers of the Mmax workshop for preparing and sharing the data.

Thank you for your attention!

Questions?

Freie Universität Berlin

Appendix

Difference between Moment- and Local Magnitudes

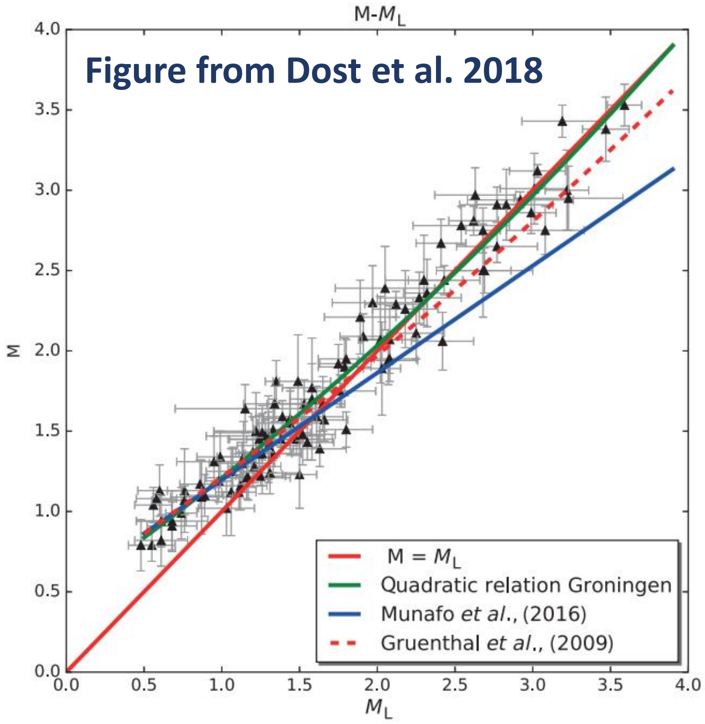

▲ **Figure 7.** Moment magnitude **M** as a function of local magnitude M_L. The proposed quadratic relation is shown in green line (equation 19). The Grünthal *et al.* (2009) relation is shown in red dashed line and the Munafò *et al.* (2016) relation is shown in blue line. Error bars indicate the standard deviation of the magnitudes.

- **Reported magnitudes for Groningen are local magnitudes M_L**
- **Theory was developed for moment magnitudes M_W**
- **Large magnitude events only have a small deviation between M_L and M_W (green and red solid lines)**
- **Only for small magnitudes M_L and M_W significantly**
- **This may affect b-values, but not maximum magnitude estimates**
- **M_L are treated as M_w here**

Depth profile and earthquake depth

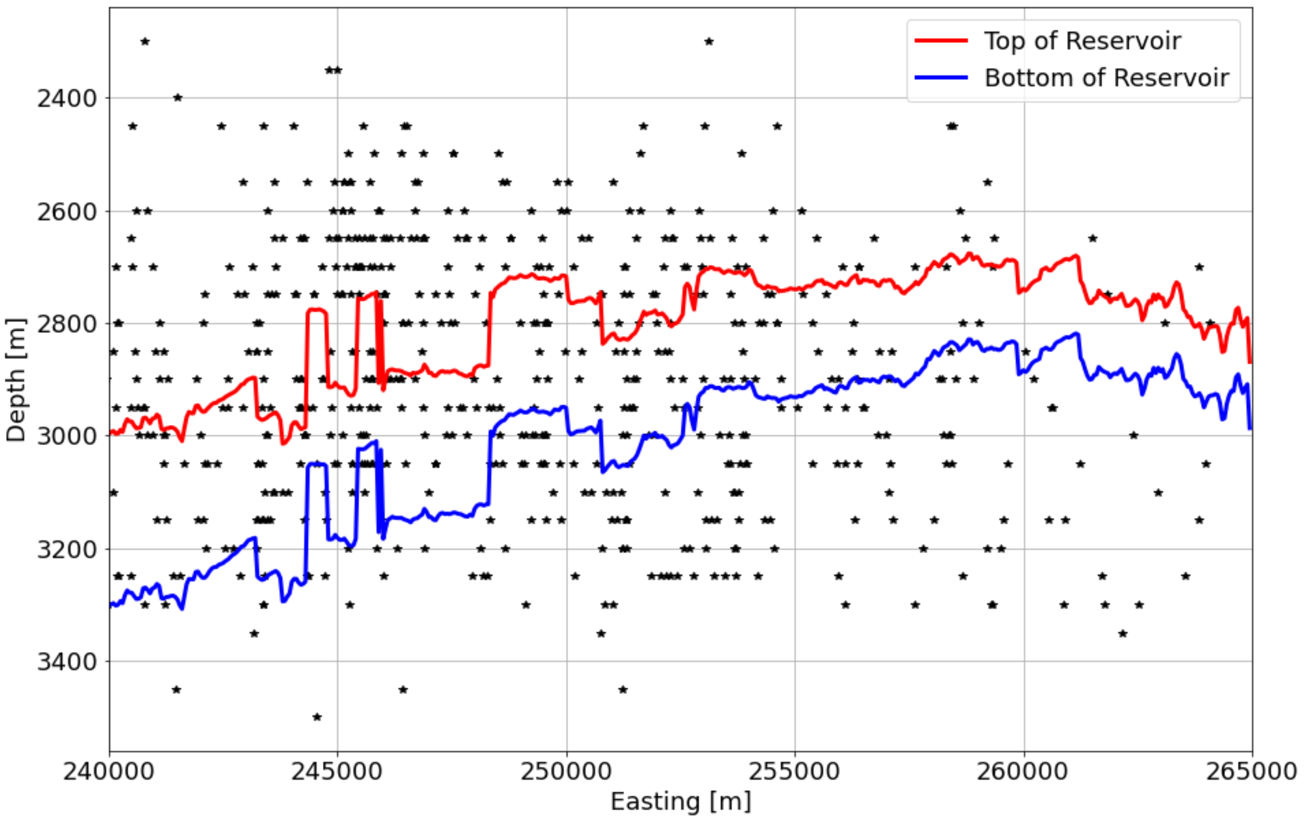

Reservoir top and reservoir thickness

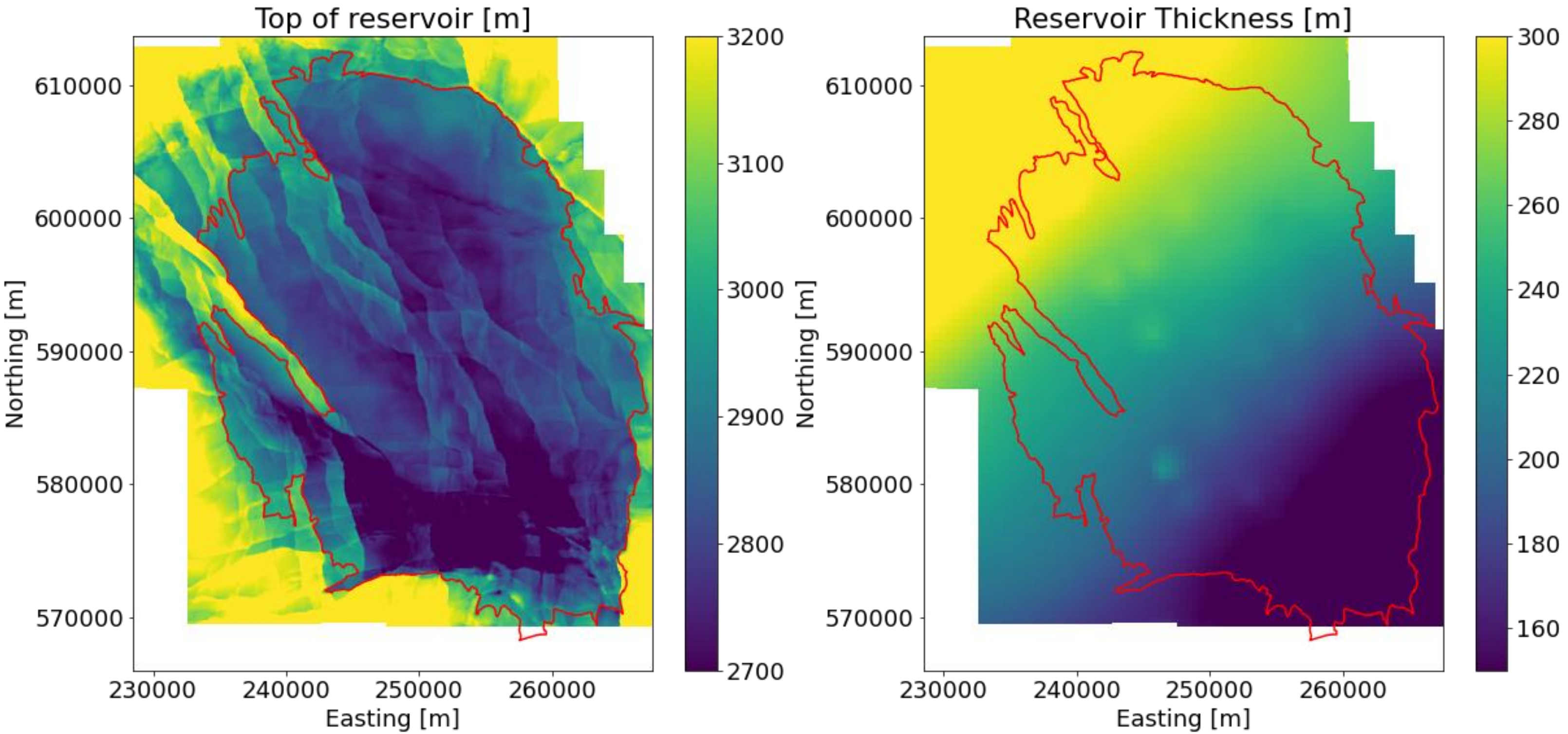

Production or injection in a single layer

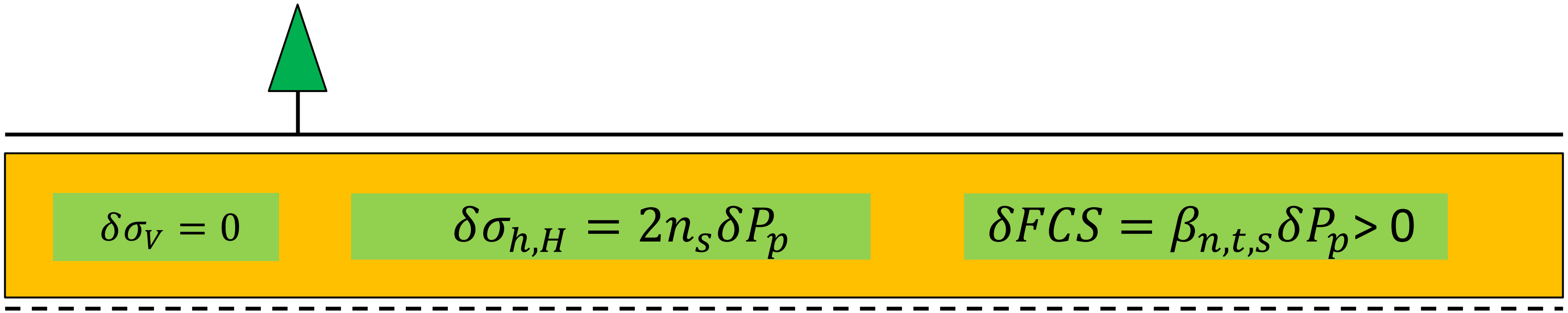

Normal faulting: $\beta_n = \sin\varphi_f(1 - n_s) - n_s$ — **Seismicity by production and injection**

Thrust-faulting: $\beta_t = \sin\varphi_f(1 - n_s) + n_s > 0$

Strike-Slip faulting: $\beta_s = \sin\varphi_f(1 - 2n_s) > 0$

Seismicity only by injection

The poroleastic stress coefficient n_s

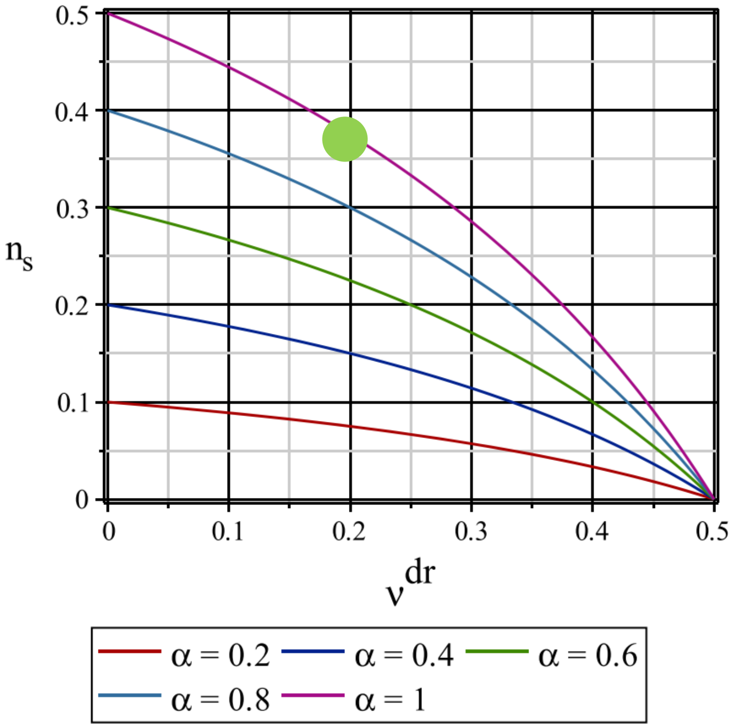

$$n_s = \frac{\alpha(1-2\nu^{dr})}{2(1-\nu^{dr})}$$

$$\alpha = 1, \nu^{dr} = 0.2$$

Values from Bourne and Oates, (2017)

$$n_s = 0.375$$

$$\beta_n = \sin\varphi_f(1-n_s) - n_s$$

$$\delta FCS = \beta_{n,t,s}\delta P_p > 0$$

Destabilization:

$$\boldsymbol{\delta FCS > 0, \delta\Sigma > 0}$$

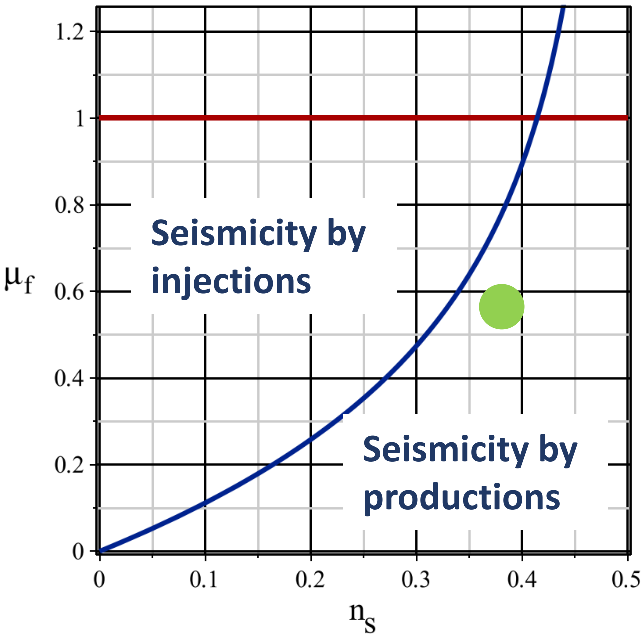

Figures from Shapiro, 2018

Workshop on Maximum Magnitude of earthquakes in Groningen

DAY 4

Thursday 16th June: Proponent models for Mmax

Start	End	Speaker	Presentation
8:30	9:15	David Dempsey*	Proponent assessment for Mmax in the Groningen field
9:15	10:0	Andrzej Kijko*	Proponent assessment for Mmax in the Groningen field
10:00	10:30		*Coffee break*
10:30	11:15	Leo Eisner	Proponent assessment for Mmax in the Groningen field
11:15	12:00	Charles Vlek	Proponent assessment for Mmax in the Groningen field
12:00	13:00		*Lunch*
13:00	13:45	Stephen Bourne	Proponent assessment for Mmax in the Groningen field
13:45	14:45	Loes Buijze	Proponent assessment for Mmax in the Groningen field
14:45	15:15		*Coffee break*
15:15	15:45	Ylona van Dinther	DEEPnl research project on Mmax in the Groningen field
15:45	16:30	All	General discussion

* remote presentation

Physics-based modelling of Mmax at Groningen

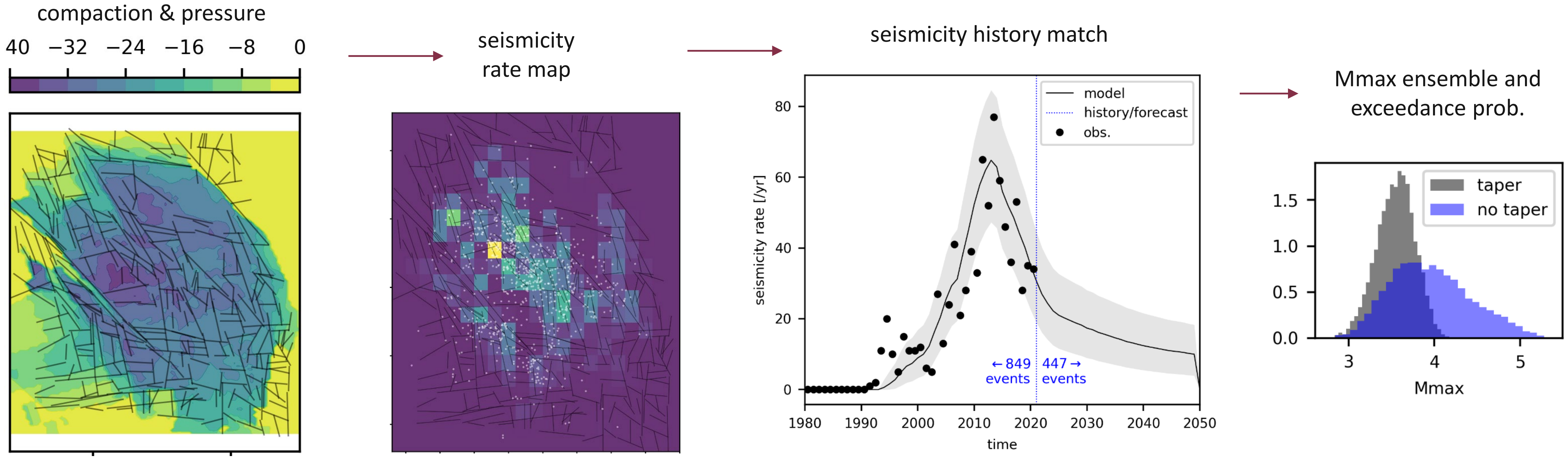

David Dempsey, University of Canterbury

Goals

Express Mmax as an <u>exceedance probability curve</u>.

Dempsey and Suckale (2017)

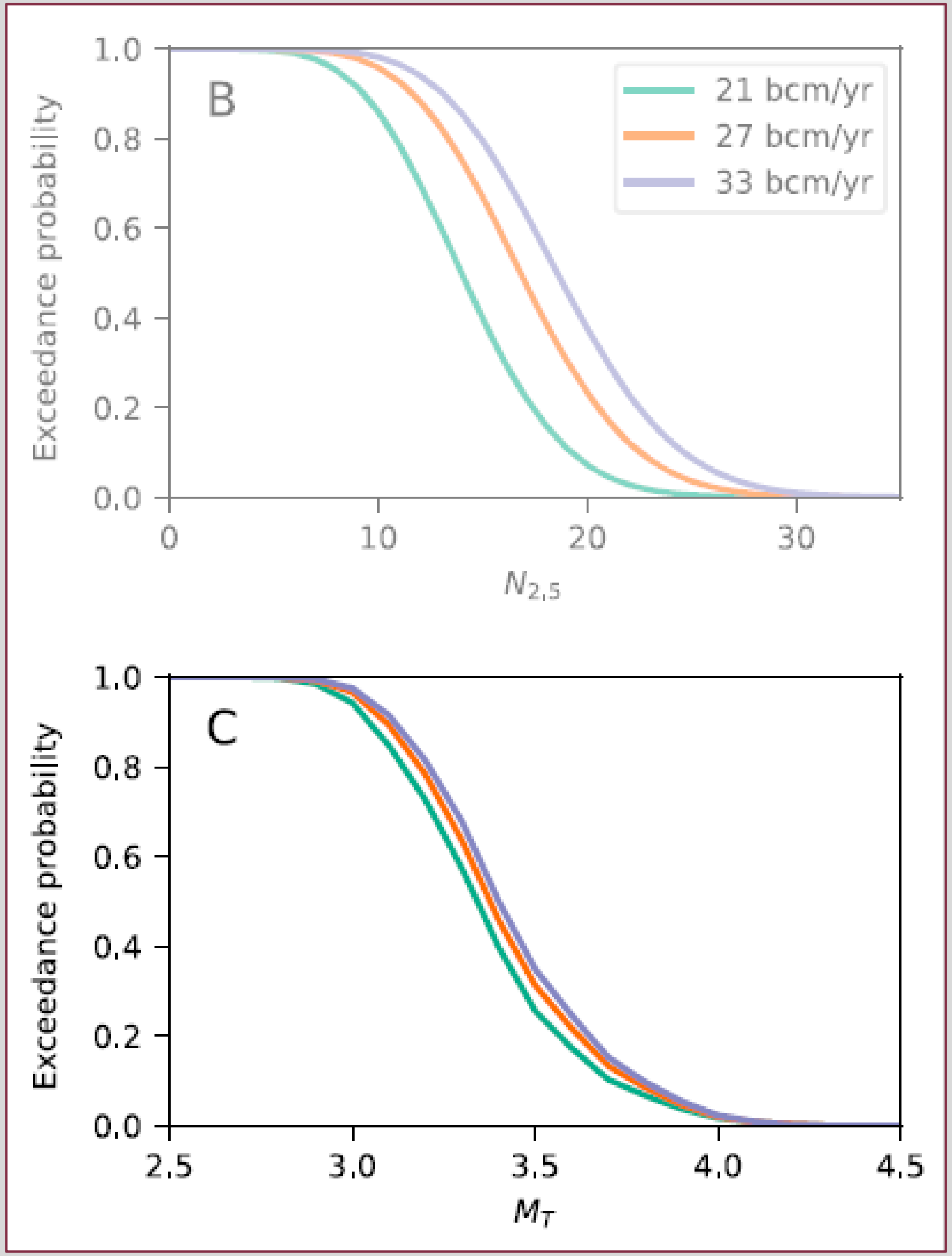

Dempsey and Suckale (2017)

Goals

Express Mmax as an exceedance probability curve.

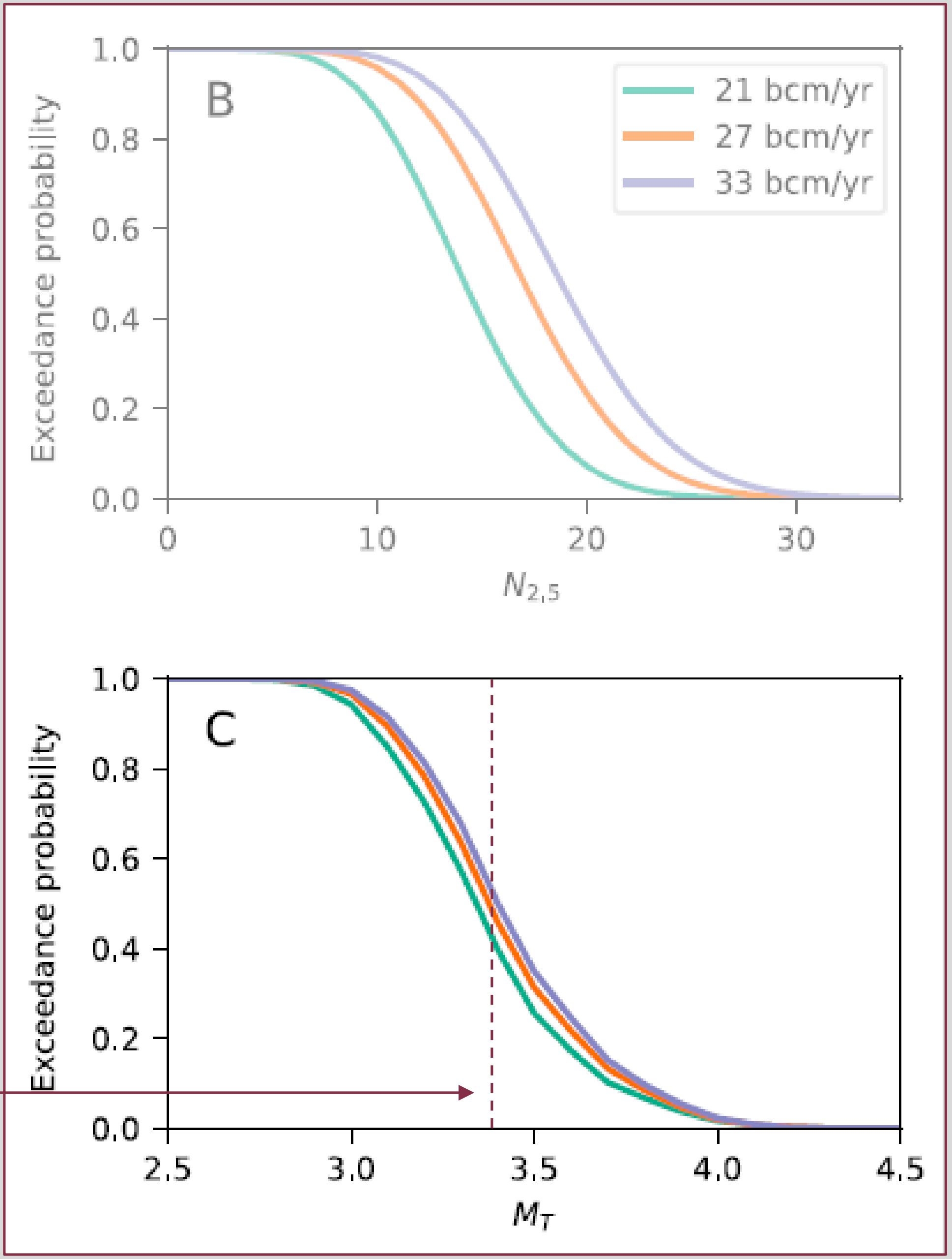

This forecast was published in 2017 for the period 2017-2024.

Mmax 3.4, Jan 2018

Goals

Express Mmax as an exceedance probability curve.

Probability depends on physical forcing applied to reservoir and faults: extraction, depressurisation, compaction.

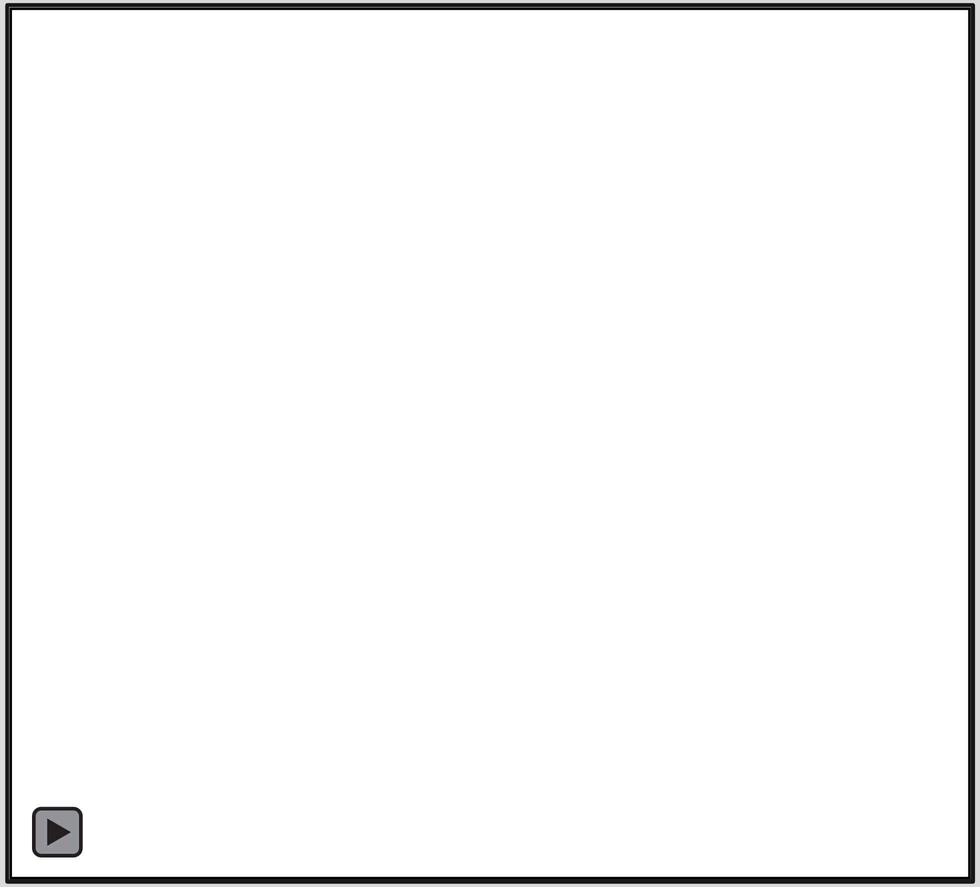

Dempsey et al. (2019)

Goals

Express Mmax as an exceedance probability curve.

Probability depends on physical forcing applied to reservoir and faults: extraction, depressurisation, compaction.

P50*, P95, and P99 values quoted, for select scenarios that span uncertainty.

Scenario	F'cast date	P50	P95	P99
Pressure only MFD w/o taper	2030	3.4	4.6	5.3
	2040	3.6	4.7	5.5
	2050	3.7	4.8	5.6
Pressure only MFD w/ taper	2030	3.3	3.8	4.0
	2040	3.4	3.8	4.0
	2050	3.4	3.8	4.0
Pressure-compaction MFD w/o taper	2030	3.5	4.7	5.4
	2040	3.7	4.9	5.7
	2050	3.9	5.0	5.8
Pressure-compaction MFD w/ taper	2030	3.3	3.8	4.0
	2040	3.5	3.9	4.0
	2050	3.5	3.9	4.0

*PXX = XX% probability that Mmax will be less than or equal to value.

Assumptions and Constraints

Mmax estimated from simulations of depressurisation and compaction.

Deviations from these in future operation of the field may materially alter estimates of Mmax.

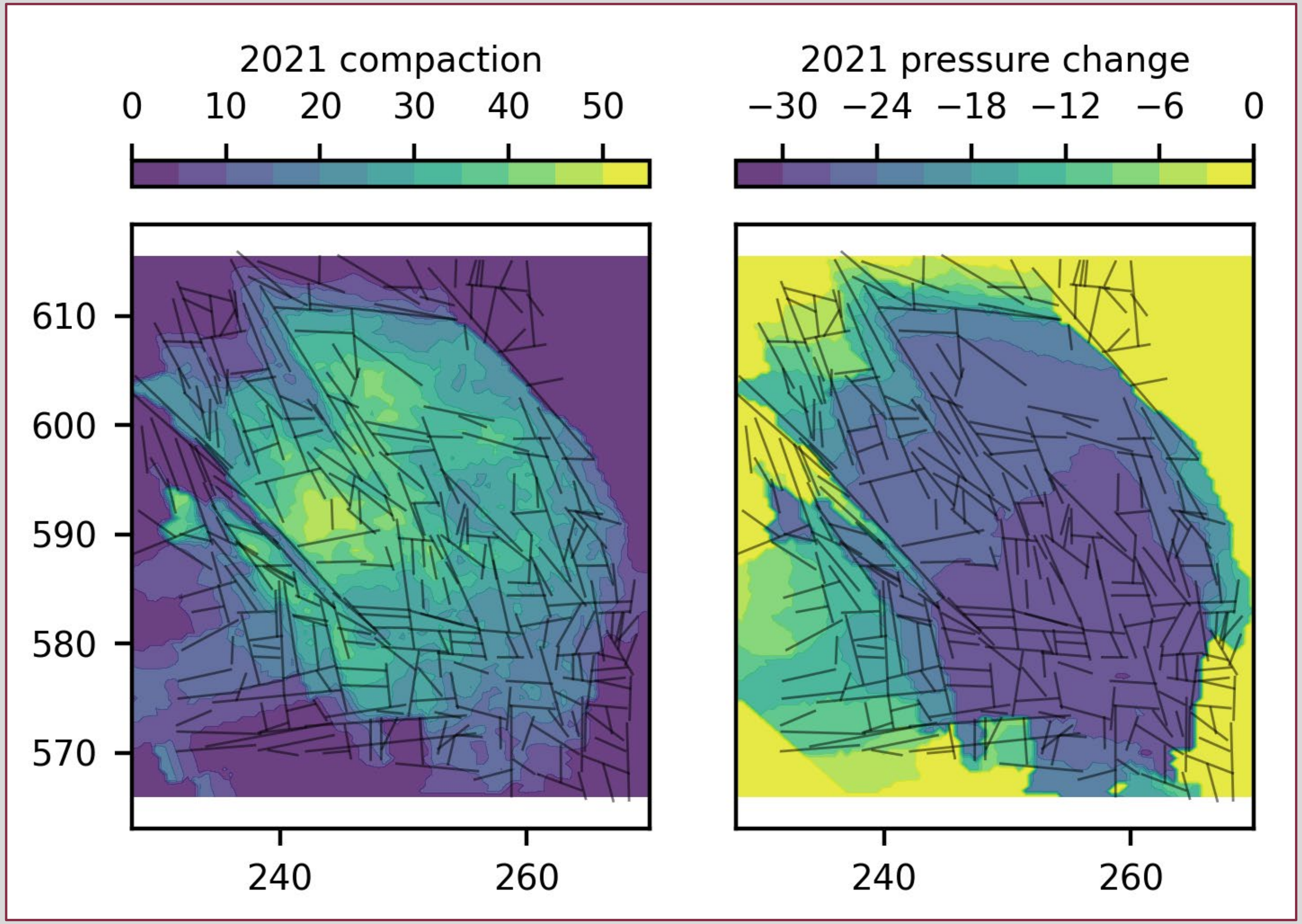

Assumptions and Constraints

Earthquake magnitudes can be parameterized by a Gutenberg-Richter distribution with an exponential taper (e.g., Bourne & Oates, 2020).

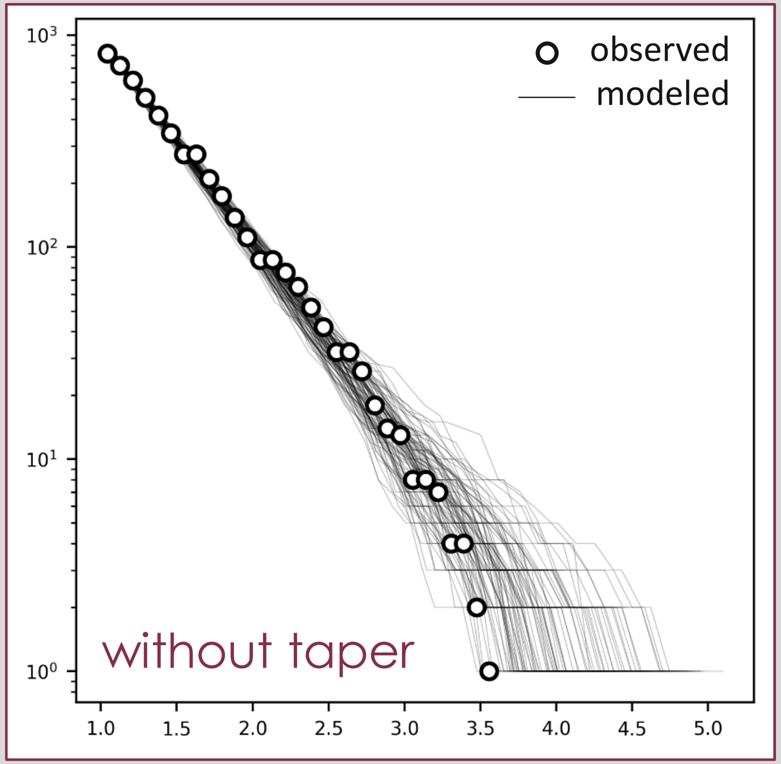

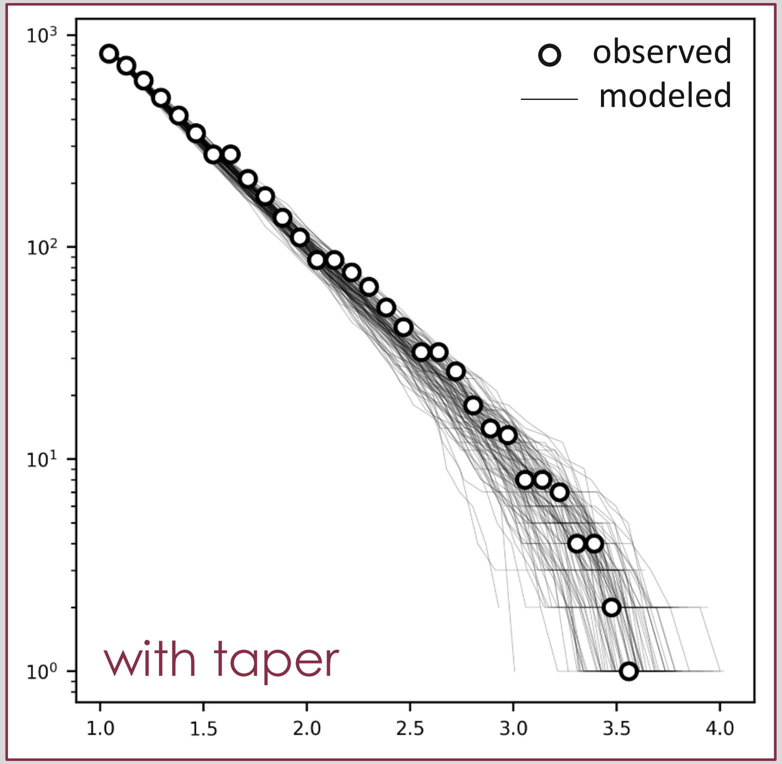

Assumptions and Constraints

Past is a good guide to the future → prioritise models with history match.

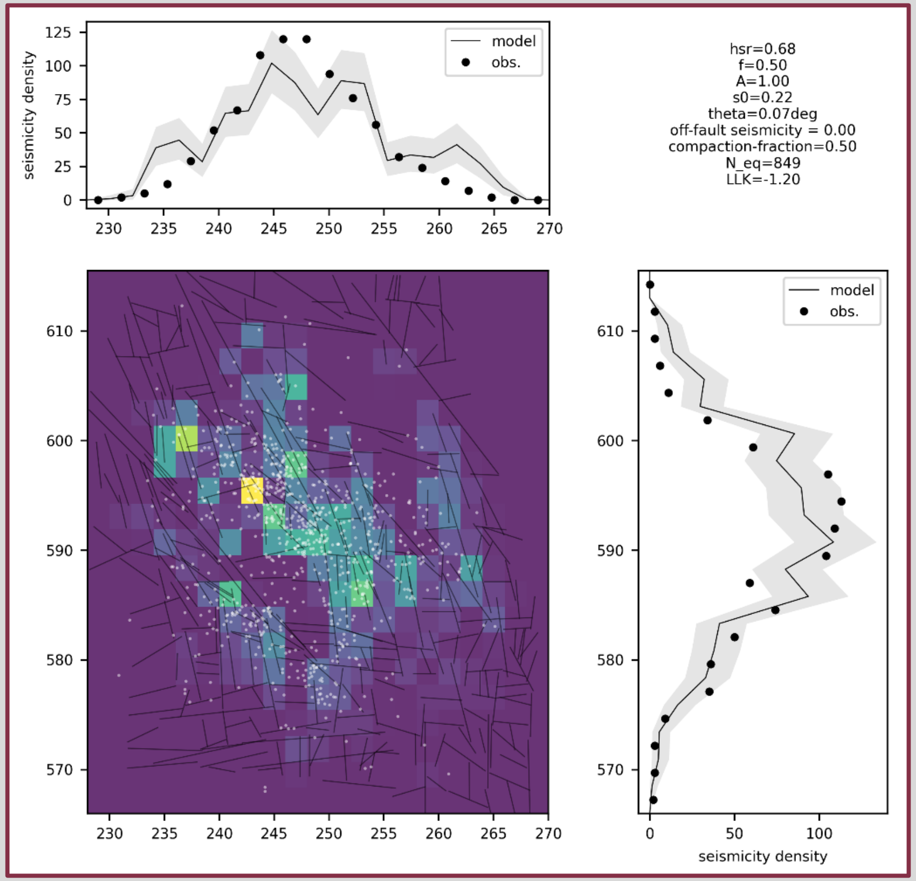

spatial density match

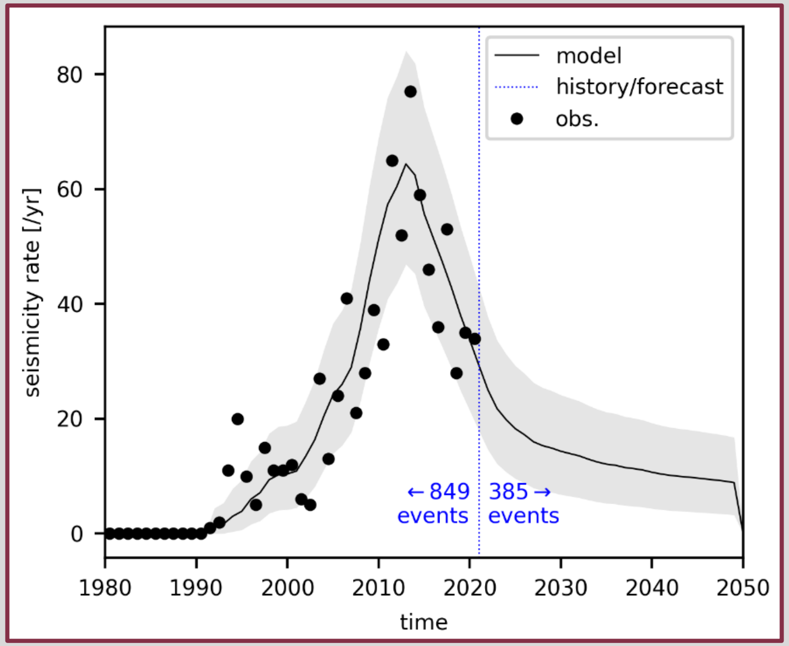

temporal rate match

Assumptions and Constraints

More than one model can fit the data → use a model ensemble.

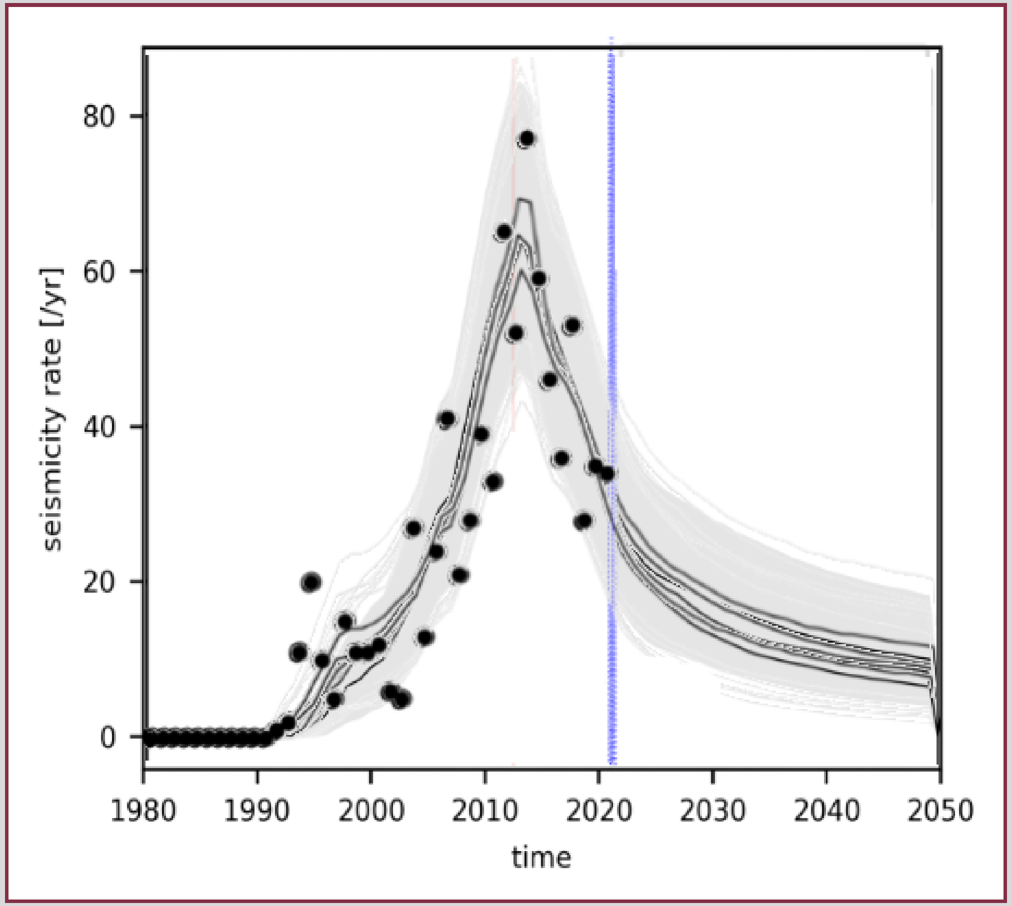

Assumptions and Constraints

Physics not accounted for in model because unnecessary to achieve a good match with the data:

1. Rate and state friction (e.g., Candela et al., 2019).
2. Stress transfer.
3. Aftershocks.
4. Geometric complexity of fault or fault system.
5. Stress dependent frequency-magnitude relation (e.g., Bourne & Oates, 2020).

Assume an extensional stress field. Minimum stress is horizontal, some distance from MC failure.

σ_v

Vertical stress is overburden: $\sigma_v = \rho g z$

Assume an extensional stress field. Minimum stress is horizontal, some distance from MC failure.

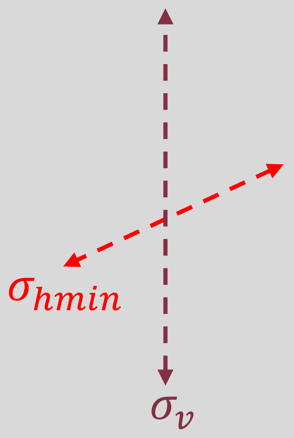

Vertical stress is overburden: $\sigma_v = \rho g z$

Calculate critical MC stress: $\sigma_{crit} = (\sigma_v - p)\left[f + \sqrt{1+f^2}\right]^{-2} + p$
(Jaeger & Cooke)

Min. stress is sub-critical: $\sigma_{hmin} = h(\sigma_v - \sigma_{crit}) + \sigma_{crit}$

Assume an extensional stress field. Minimum stress is horizontal, some distance from MC failure.

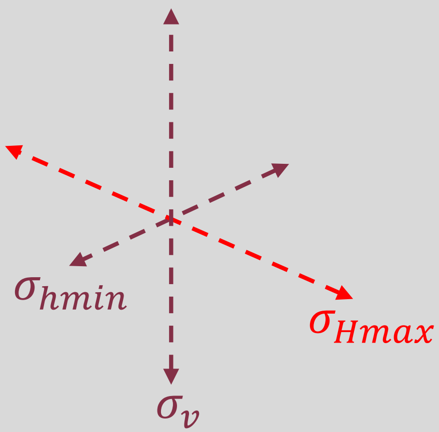

Vertical stress is overburden: $\sigma_v = \rho g z$

Calculate critical MC stress: $\sigma_{crit} = (\sigma_v - p)\left[f + \sqrt{1+f^2}\right]^{-2} + p$
(Jaeger & Cooke)

Min. stress is sub-critical: $\sigma_{hmin} = h(\sigma_v - \sigma_{crit}) + \sigma_{crit}$

Middle stress btw min & max: $\sigma_{Hmax} = H(\sigma_v - \sigma_{hmin}) + \sigma_{hmin}$

Assume an extensional stress field. Minimum stress is horizontal, some distance from MC failure.

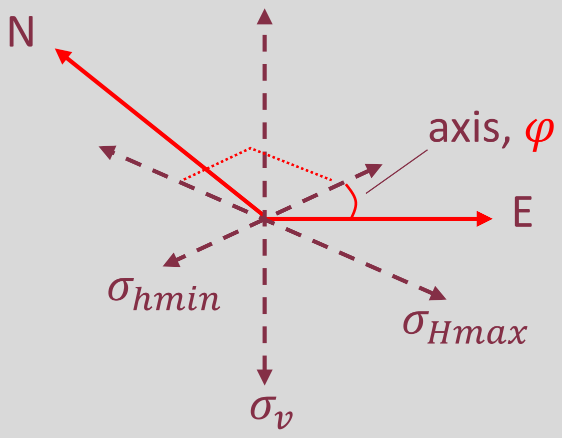

$$\sigma = \begin{bmatrix} \sigma_{hmin} & 0 & 0 \\ 0 & \sigma_{Hmax} & 0 \\ 0 & 0 & \sigma_v \end{bmatrix}$$

$$R = \begin{bmatrix} \cos\varphi & -\sin\varphi & 0 \\ \sin\varphi & \cos\varphi & 0 \\ 0 & 0 & 1 \end{bmatrix}$$

Vertical stress is overburden: $\sigma_v = \rho g z$

Calculate critical MC stress: $\sigma_{crit} = (\sigma_v - p)\left[f + \sqrt{1 + f^2}\right]^{-2} + p$
(Jaeger & Cooke)

Min. stress is sub-critical: $\sigma_{hmin} = h(\sigma_v - \sigma_{crit}) + \sigma_{crit}$

Middle stress btw min & max: $\sigma_{Hmax} = H(\sigma_v - \sigma_{hmin}) + \sigma_{hmin}$

Rotate into coordinate system: $\sigma' = R(\varphi)^T \sigma R(\varphi)$

Stress state is parameterized by $[f, h, H, \varphi]$

Fault approximated as dipping plane whose width varies with reservoir thickness.

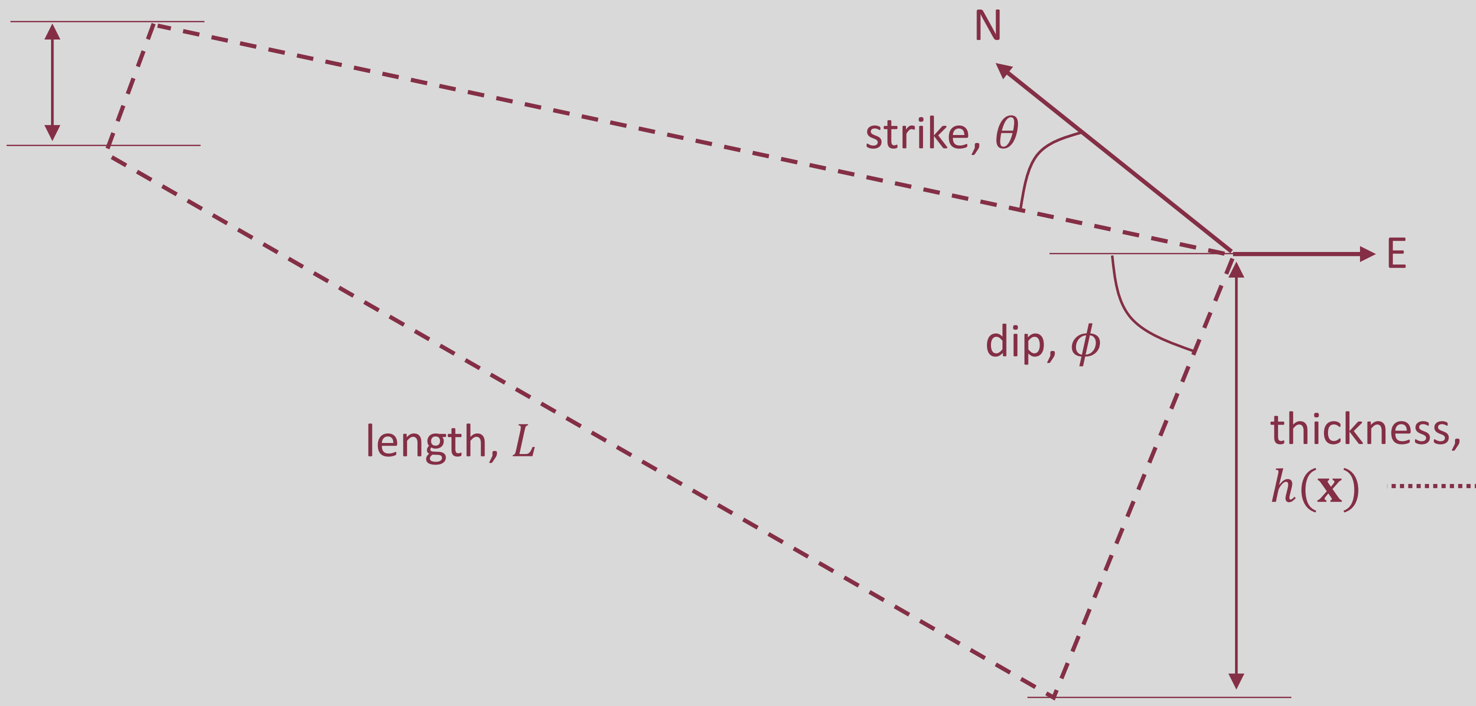

Strikes, lengths and dips from Dempsey and Suckale (2017)

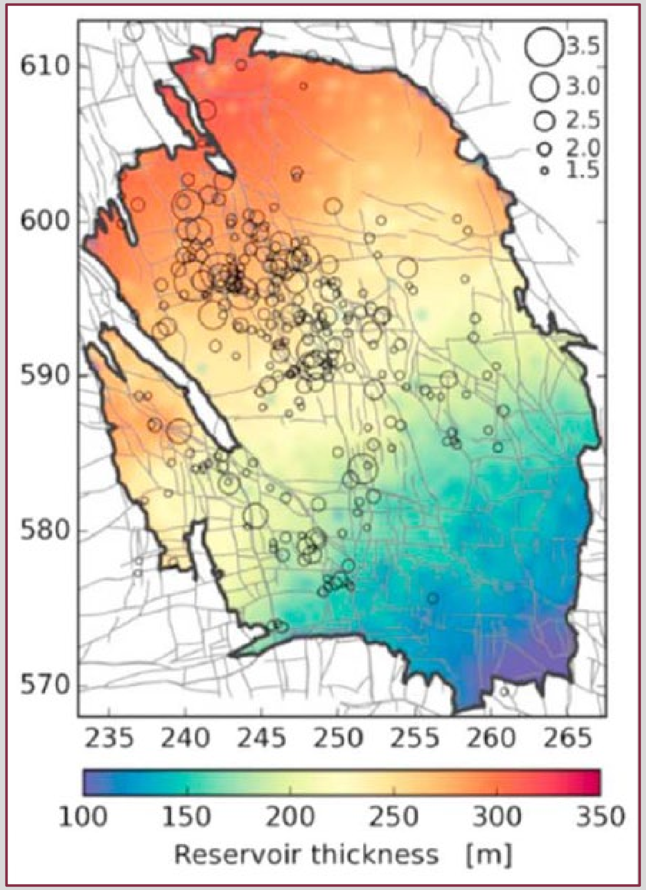

Bourne and Oates (2017)

Shear and normal stresses on fault resolved from regional extensional stress field

Project stress state onto fault.

$$\mathbf{t} = \sigma'\hat{\mathbf{n}}, \qquad \sigma_n = \mathbf{t}\cdot\hat{\mathbf{n}}, \qquad \tau = |\mathbf{t} - \sigma_n\hat{\mathbf{n}}|$$

Compute proximity to failure.

$$CFS_0 = \tau - f(\sigma_n - p)$$

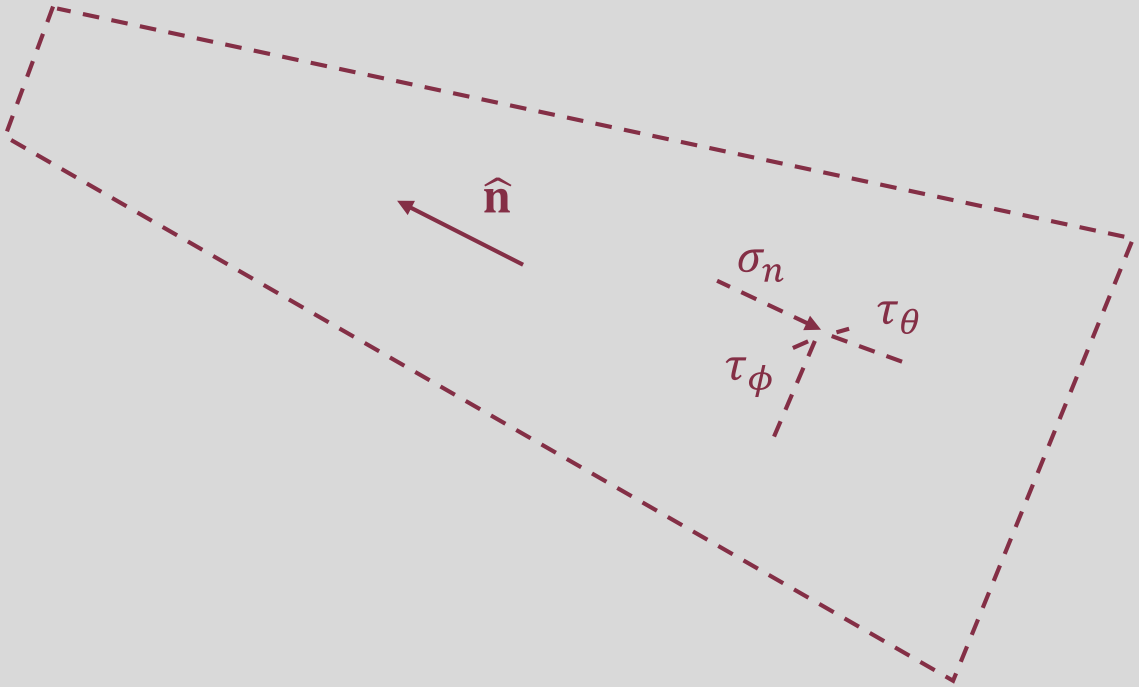

Poroelastic loading model.

Pressure changes induce poroelastic 'stretch' within reservoir, modifying horizontal stresses (Segall & Fitzgerald, 1998).

$\Delta\sigma_{hmin} = \Delta\sigma_{Hmax} = A\Delta p$

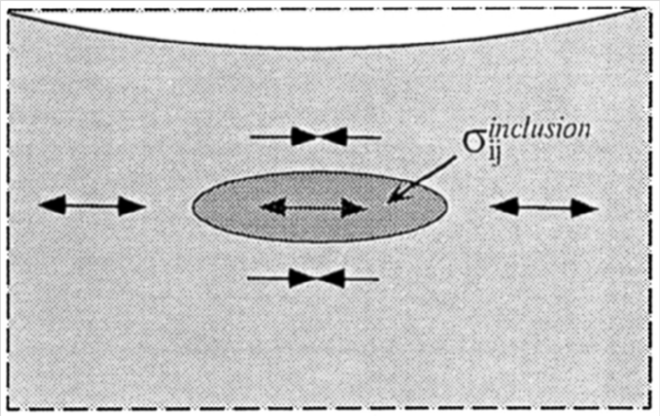

Poroelastic loading model.

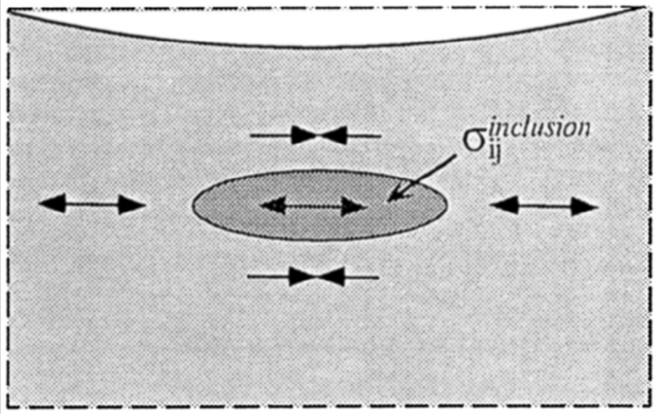

Pressure changes induce poroelastic 'stretch' within reservoir, modifying horizontal stresses (Segall & Fitzgerald, 1998).

$$\Delta\sigma_{hmin} = \Delta\sigma_{Hmax} = A\Delta p$$

Corresponding changes induced in stress field, fault tractions and stability

$$\sigma' \rightarrow \sigma' + \Delta\sigma'$$

$$\mathbf{t} \rightarrow \mathbf{t} + \Delta\mathbf{t}, \qquad \sigma_n \rightarrow \sigma_n + \Delta\sigma_n, \qquad \tau \rightarrow \tau + \Delta\tau$$

$$\Delta CFS = \Delta\tau - f(\Delta\sigma_n - \Delta p)$$

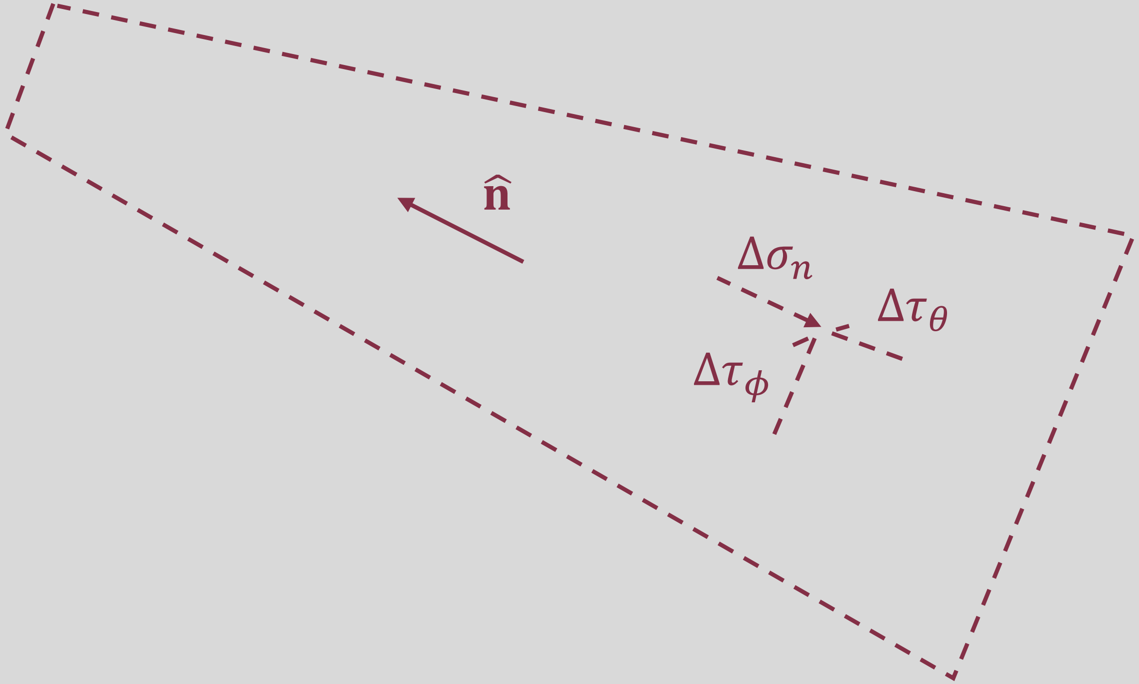

Seismicity model

Fault is active and 'eligible' to nucleate earthquakes when CFS becomes positive

$CFS_0 + \Delta CFS > 0$

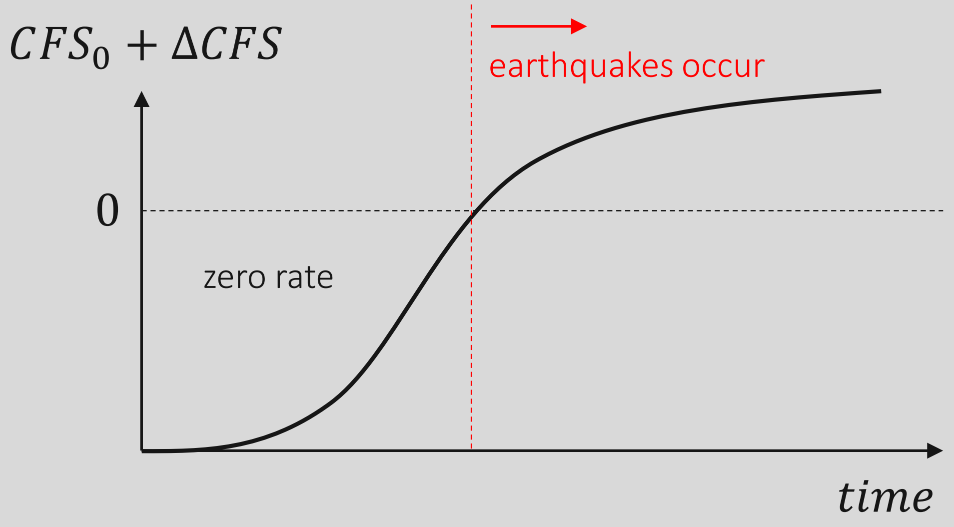

Seismicity model

Fault is active and 'eligible' to nucleate earthquakes when CFS becomes positive

$$CFS_0 + \Delta CFS > 0$$

Earthquake 'rate' is proportional to stressing rate, and fault area

$$\lambda_i \propto \int_A \frac{d}{dt}\,\Delta CFS(\mathbf{x})\; dA$$

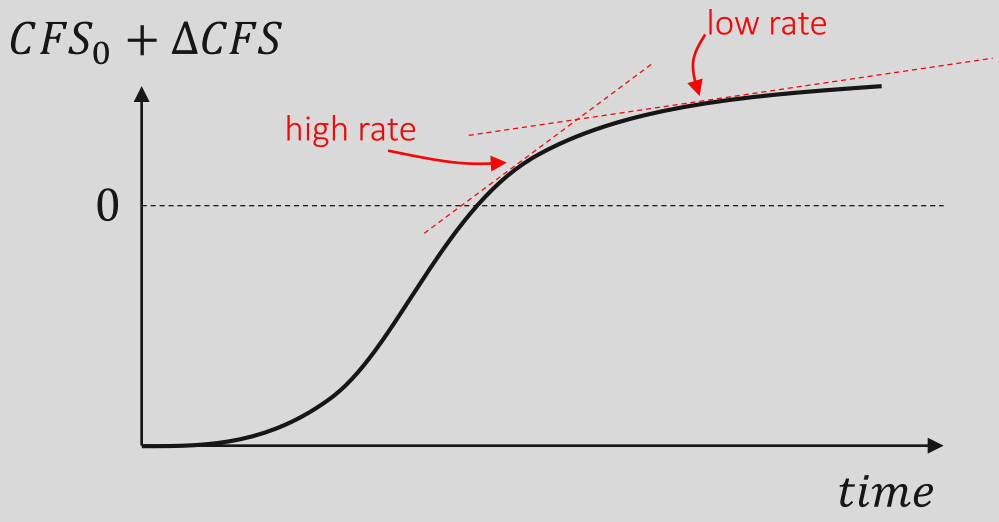

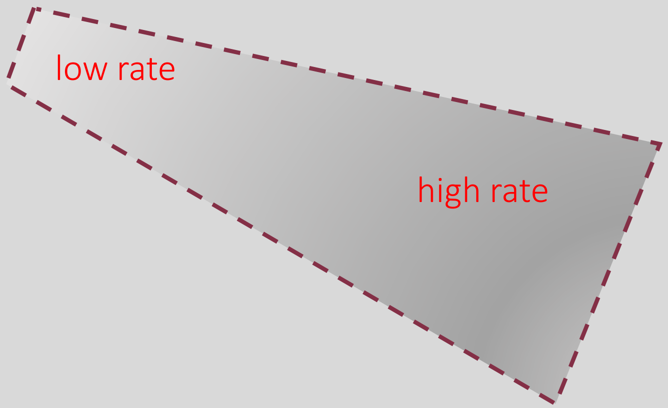

Seismicity model

Fault is active and 'eligible' to nucleate earthquakes when CFS becomes positive

$CFS_0 + \Delta CFS > 0$

Earthquake 'rate' is proportional to stressing rate, and fault area

$$\lambda_i \propto \int_A \frac{d}{dt} \Delta CFS(\mathbf{x}) \, dA$$

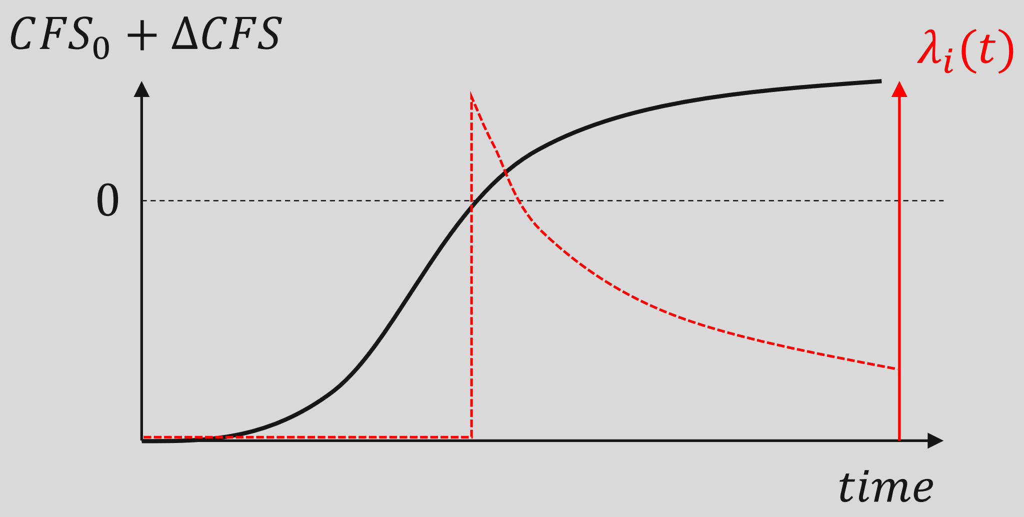

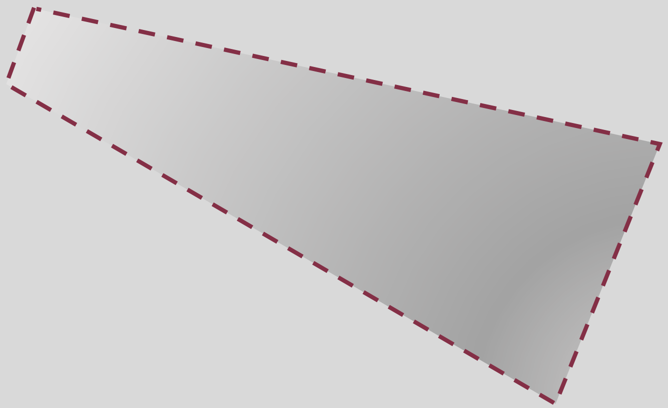

Seismicity model

Fault is active and ‘eligible’ to nucleate earthquakes when CFS becomes positive

$$CFS_0 + \Delta CFS > 0$$

Earthquake ‘rate’ is proportional to stressing rate, and fault area

$$\lambda_i \propto \int_A \frac{d}{dt}\,\Delta CFS(\mathbf{x})\,dA$$

Total EQ rate sum of all faults + off-fault seismicity.

$$\lambda = \sum_i \lambda_i + \chi$$

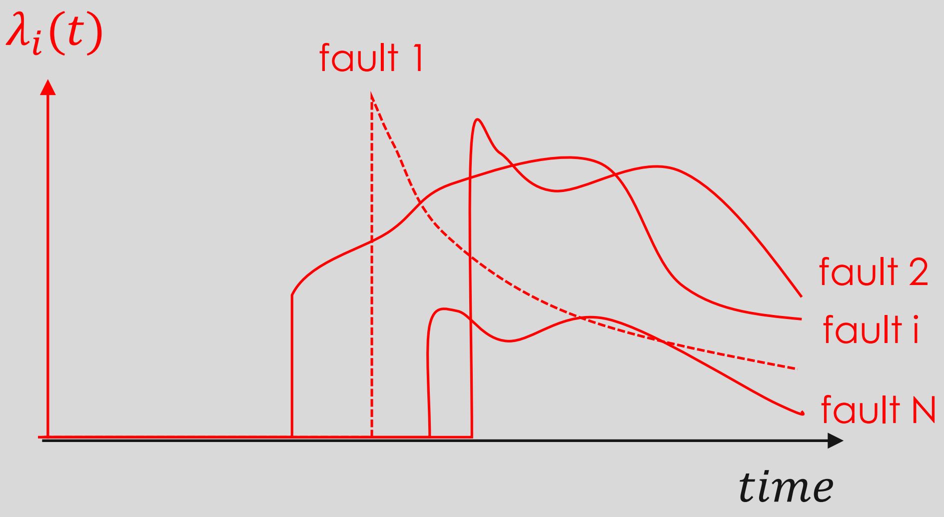

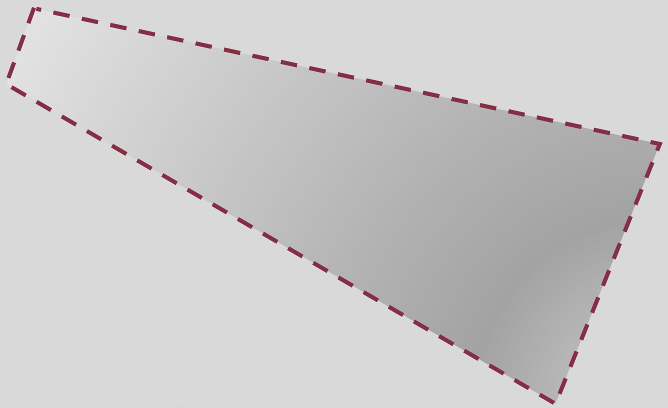

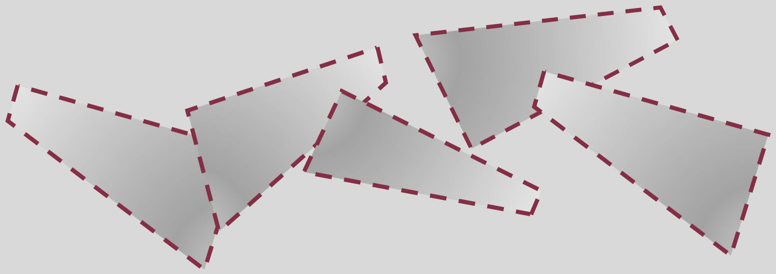

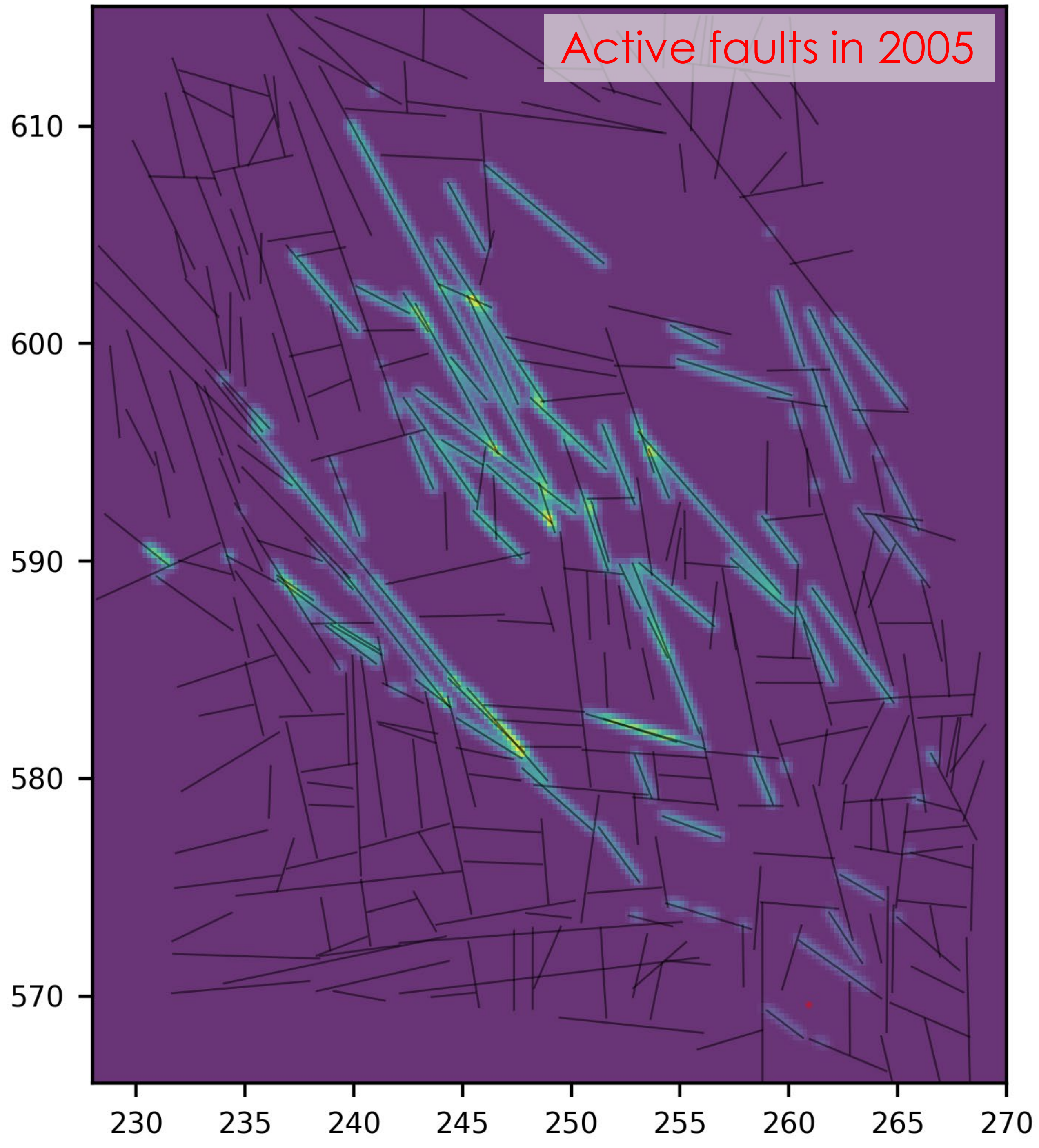
Active faults in 2005
610
600
590
580
570
230
235
240
245
250
255
260
265
270

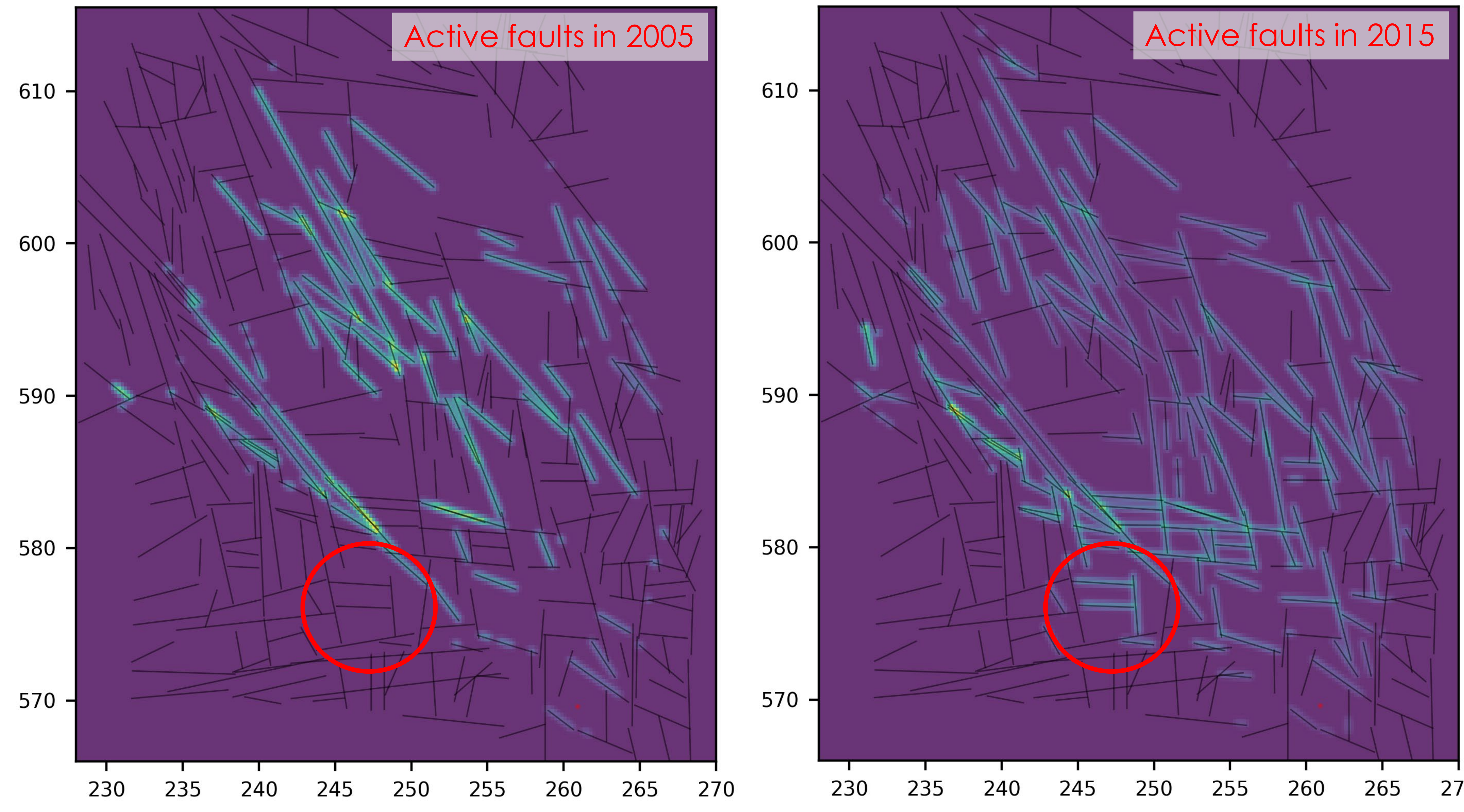

Active faults in 2005
Active faults in 2015
610
600
590
580
570
230
235
240
245
250
255
260
265
270

History match

Models scored using customized log-likelihood for binned seismicity density and rate profiles.

$\hat{\lambda}_t$ = number M ≥ 1 events in a year (whole field)
$\hat{\rho}_x$ = total number M ≥ 1 events in x-slice
$\hat{\rho}_y$ = total number M ≥ 1 events in y-slice

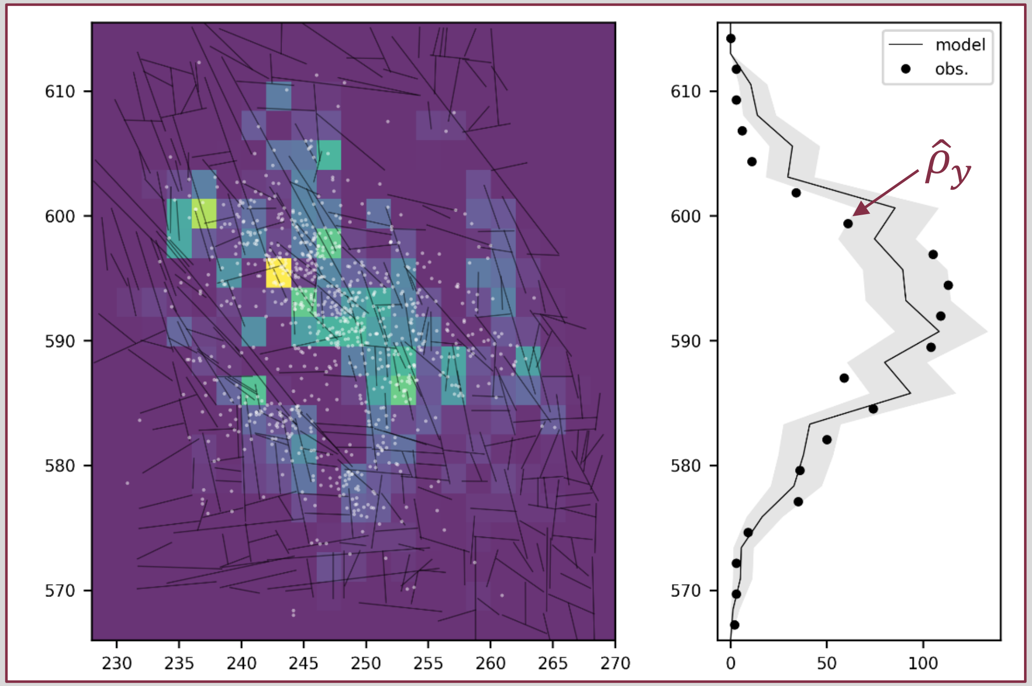

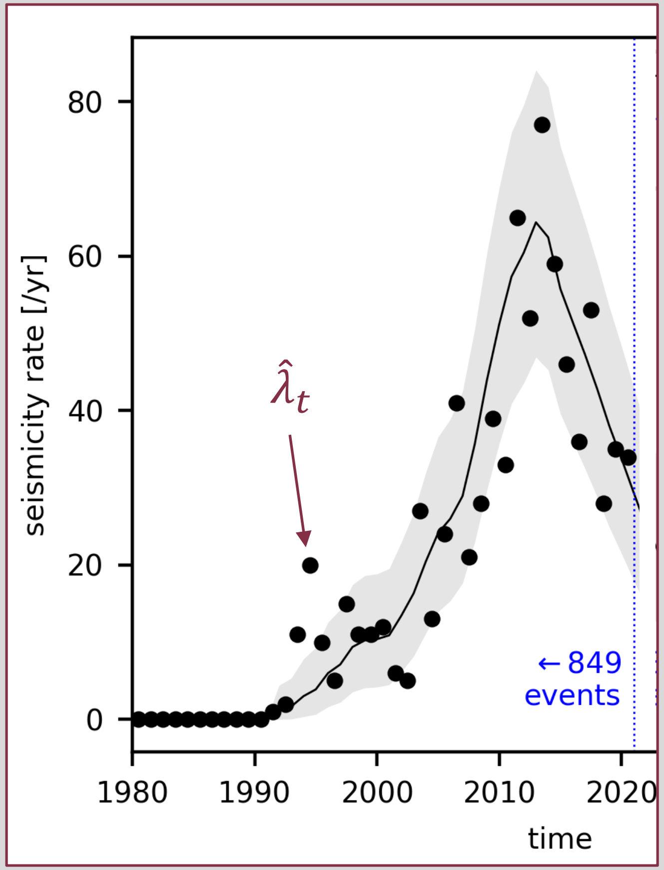

History match

Models scored using customized log-likelihood for binned seismicity density and rate profiles.

$$S = \frac{3}{4}\left(\frac{1}{52}\sum_{1960}^{2012}\frac{\left(\lambda_t-\hat{\lambda}_t\right)^2}{\hat{\lambda}_t}+\frac{1}{9}\sum_{2012}^{2021}\frac{\left(\lambda_t-\hat{\lambda}_t\right)^2}{\hat{\lambda}_t}\right) + \frac{1}{4}\left(\frac{1}{2N_x}\sum_{1}^{N_x}\frac{(\rho_x-\hat{\rho}_x)^2}{\hat{\rho}_x}+\frac{1}{2N_y}\sum_{1}^{N_y}\frac{\left(\rho_y-\hat{\rho}_y\right)^2}{\hat{\rho}_y}\right)$$

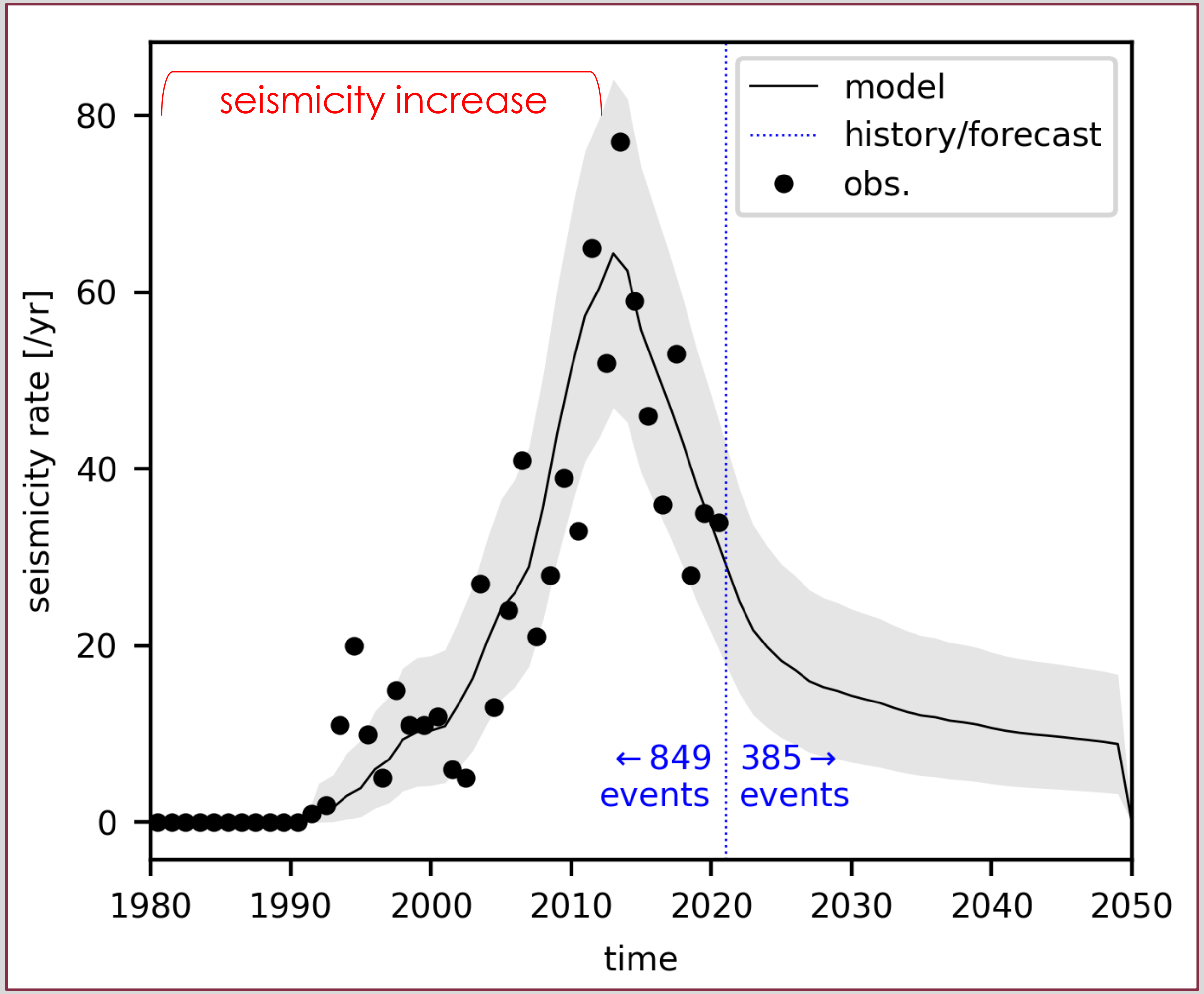

History match

Models scored using customized log-likelihood for binned seismicity density and rate profiles.

$$S = \frac{3}{4}\left(\frac{1}{52}\sum_{1960}^{2012}\frac{(\lambda_t-\hat{\lambda}_t)^2}{\hat{\lambda}_t} + \frac{1}{9}\sum_{2012}^{2021}\frac{(\lambda_t-\hat{\lambda}_t)^2}{\hat{\lambda}_t}\right) + \frac{1}{4}\left(\frac{1}{2N_x}\sum_{1}^{N_x}\frac{(\rho_x-\hat{\rho}_x)^2}{\hat{\rho}_x} + \frac{1}{2N_y}\sum_{1}^{N_y}\frac{(\rho_y-\hat{\rho}_y)^2}{\hat{\rho}_y}\right)$$

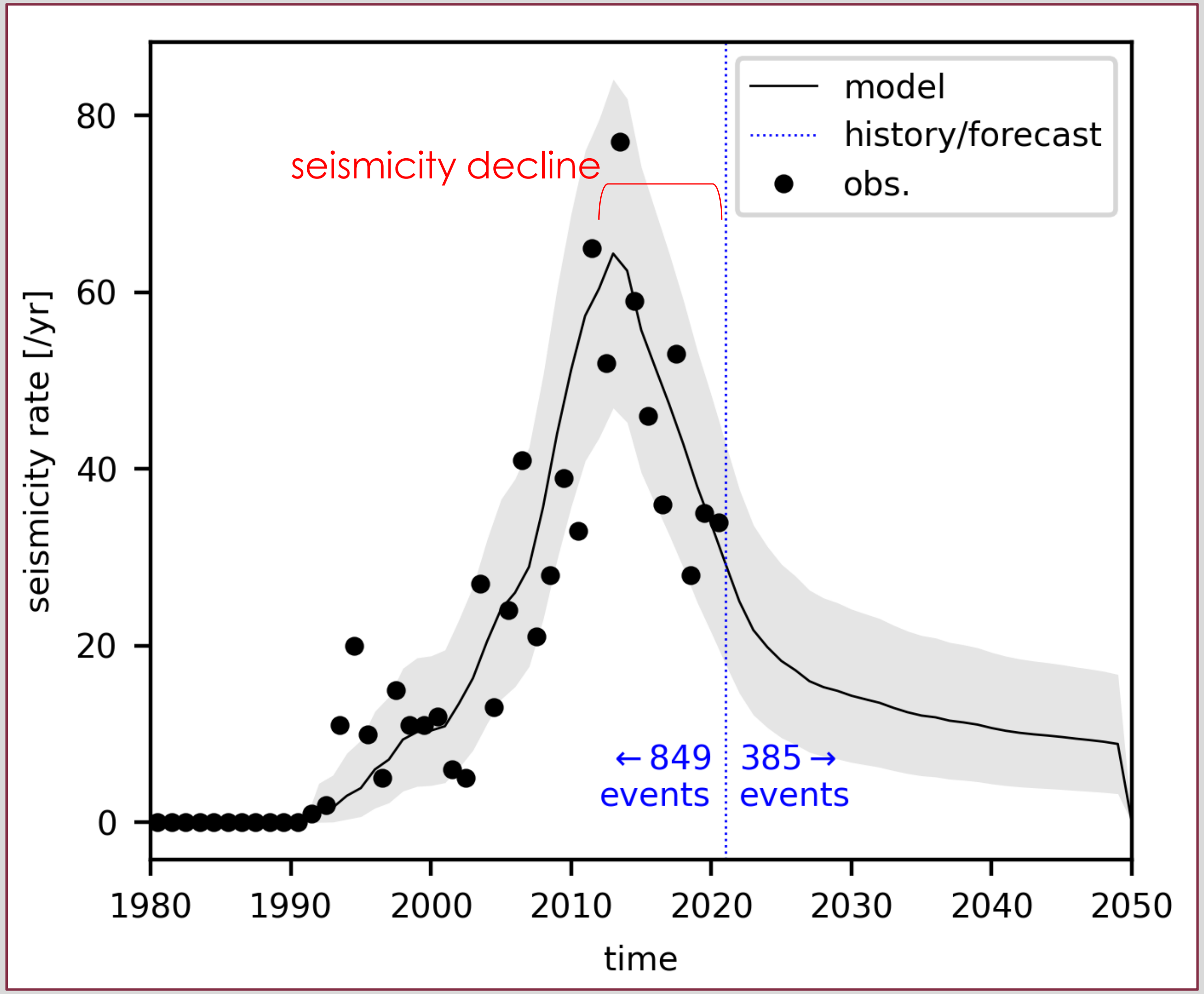

History match

Models scored using customized log-likelihood for binned seismicity density and rate profiles.

$$S = \frac{3}{4}\left(\frac{1}{52}\sum_{1960}^{2012}\frac{\left(\lambda_t - \hat{\lambda}_t\right)^2}{\hat{\lambda}_t} + \frac{1}{9}\sum_{2012}^{2021}\frac{\left(\lambda_t - \hat{\lambda}_t\right)^2}{\hat{\lambda}_t}\right) + \frac{1}{4}\left(\frac{1}{2N_x}\sum_{1}^{N_x}\frac{(\rho_x - \hat{\rho}_x)^2}{\hat{\rho}_x} + \frac{1}{2N_y}\sum_{1}^{N_y}\frac{\left(\rho_y - \hat{\rho}_y\right)^2}{\hat{\rho}_y}\right)$$

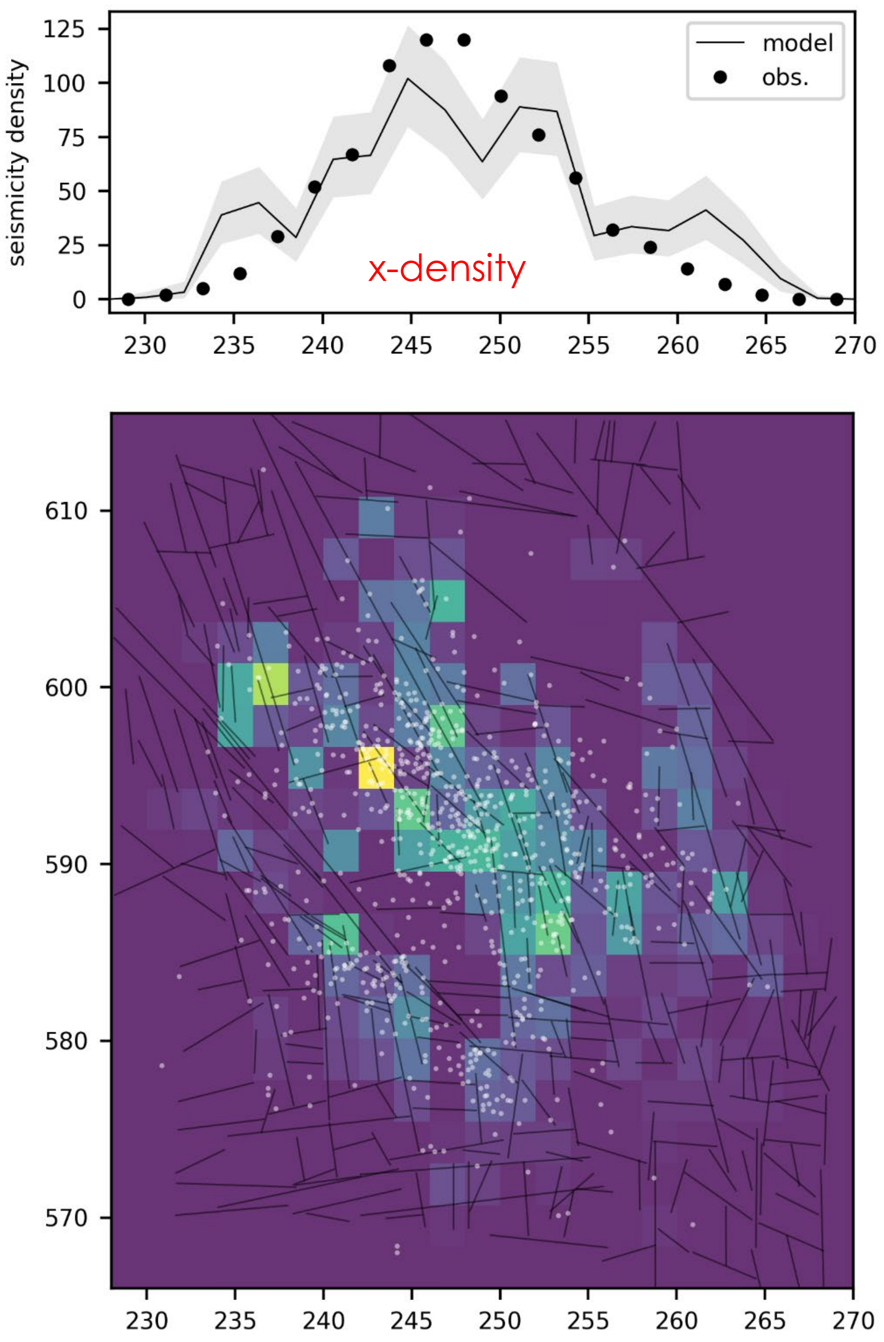

History match

Models scored using customized log-likelihood for binned seismicity density and rate profiles.

$$S = \frac{3}{4}\left(\frac{1}{52}\sum_{1960}^{2012}\frac{\left(\lambda_t-\hat{\lambda}_t\right)^2}{\hat{\lambda}_t}+\frac{1}{9}\sum_{2012}^{2021}\frac{\left(\lambda_t-\hat{\lambda}_t\right)^2}{\hat{\lambda}_t}\right)+\frac{1}{4}\left(\frac{1}{2N_x}\sum_{1}^{N_x}\frac{(\rho_x-\hat{\rho}_x)^2}{\hat{\rho}_x}+\frac{1}{2N_y}\sum_{1}^{N_y}\frac{\left(\rho_y-\hat{\rho}_y\right)^2}{\hat{\rho}_y}\right)$$

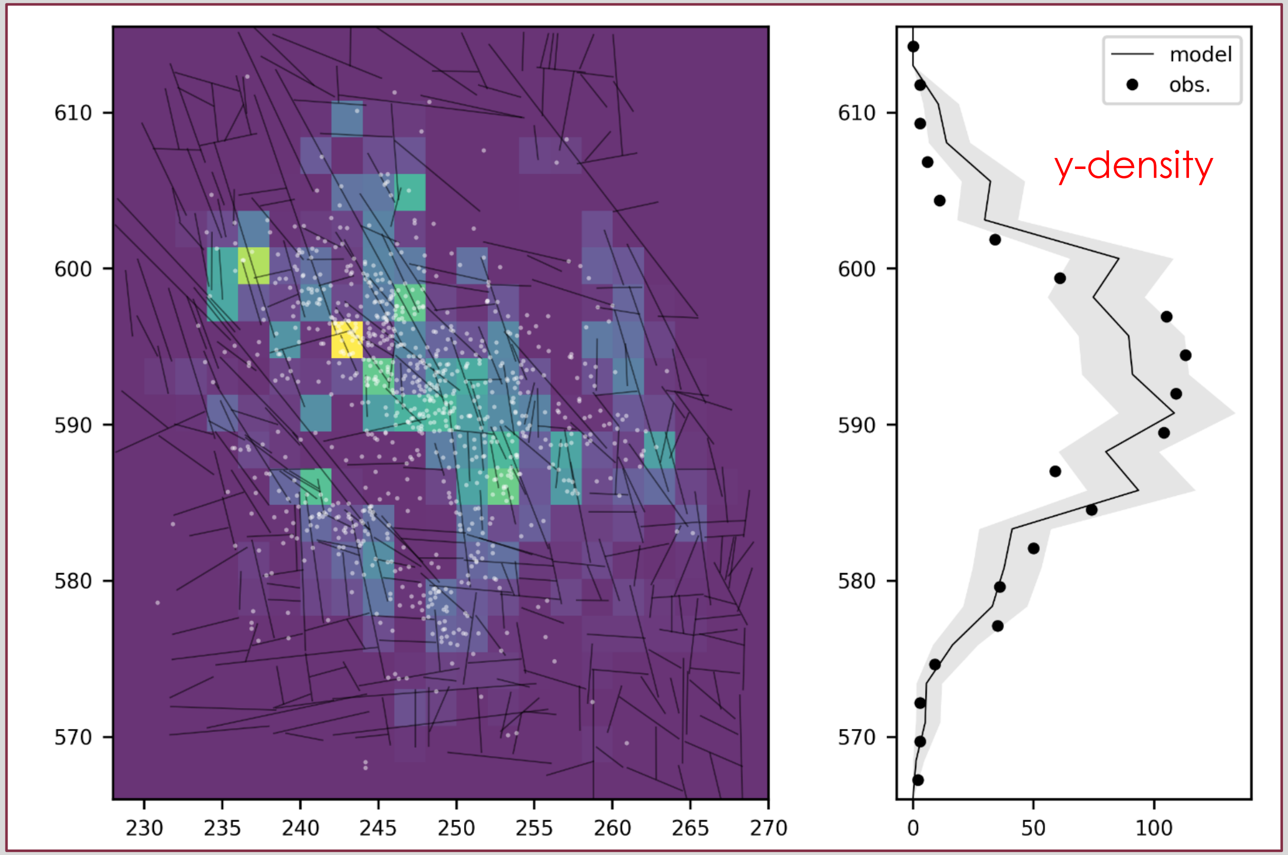

History match

Models scored using customized log-likelihood for binned seismicity density and rate profiles.

$$
\begin{aligned}
S &= \frac{3}{4}\left(\frac{1}{52}\sum_{1960}^{2012}\frac{(\lambda_t-\hat{\lambda}_t)^2}{\hat{\lambda}_t}+\frac{1}{9}\sum_{2012}^{2021}\frac{(\lambda_t-\hat{\lambda}_t)^2}{\hat{\lambda}_t}\right) \\
&+\frac{1}{4}\left(\frac{1}{2N_x}\sum_{1}^{N_x}\frac{(\rho_x-\hat{\rho}_x)^2}{\hat{\rho}_x}+\frac{1}{2N_y}\sum_{1}^{N_y}\frac{(\rho_y-\hat{\rho}_y)^2}{\hat{\rho}_y}\right)
\end{aligned}
$$

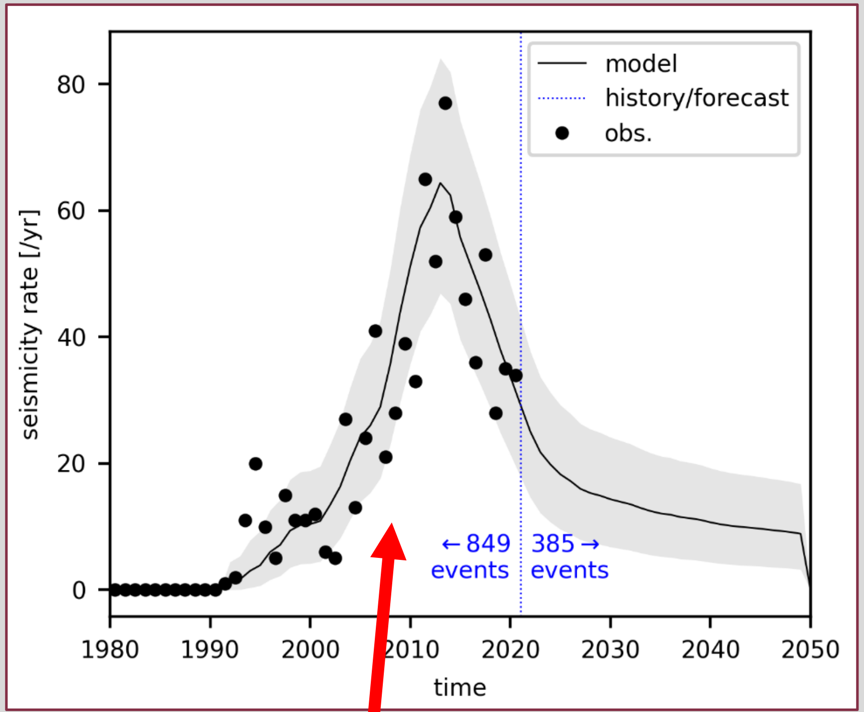

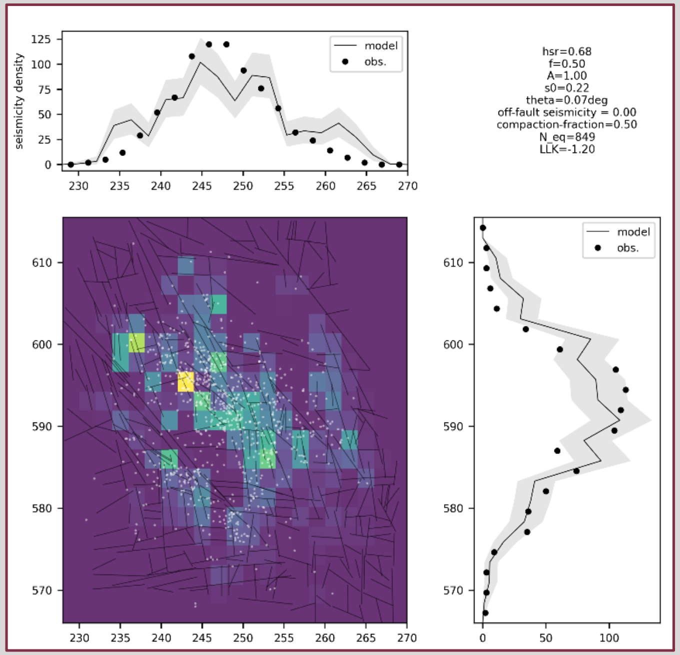

prioritise rate match over density match

History match

Models scored using customized log-likelihood for binned seismicity density and rate profiles.

$$S = \frac{3}{4}\left(\frac{1}{52}\sum_{1960}^{2012}\frac{(\lambda_t - \hat{\lambda}_t)^2}{\hat{\lambda}_t} + \frac{1}{9}\sum_{2012}^{2021}\frac{(\lambda_t - \hat{\lambda}_t)^2}{\hat{\lambda}_t}\right) + \frac{1}{4}\left(\frac{1}{2N_x}\sum_{1}^{N_x}\frac{(\rho_x - \hat{\rho}_x)^2}{\hat{\rho}_x} + \frac{1}{2N_y}\sum_{1}^{N_y}\frac{(\rho_y - \hat{\rho}_y)^2}{\hat{\rho}_y}\right)$$

Use Genetic Algorithm to explore parameter space for models with good scores.

$$[f, h, H, \varphi, A, \chi]$$

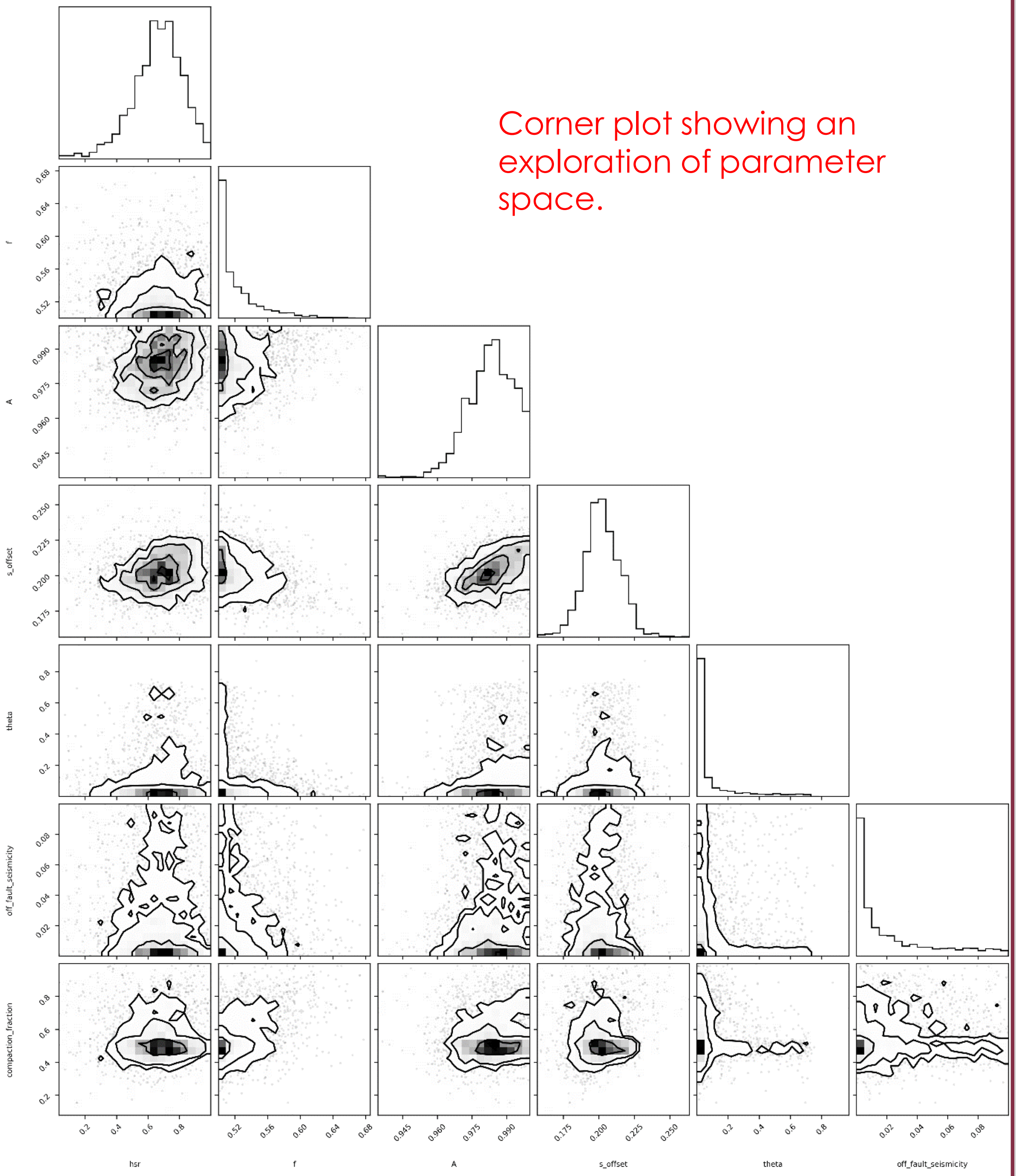

Corner plot showing an exploration of parameter space.

Forecast

1. Predict seismicity rate given simulation of future depressurization.

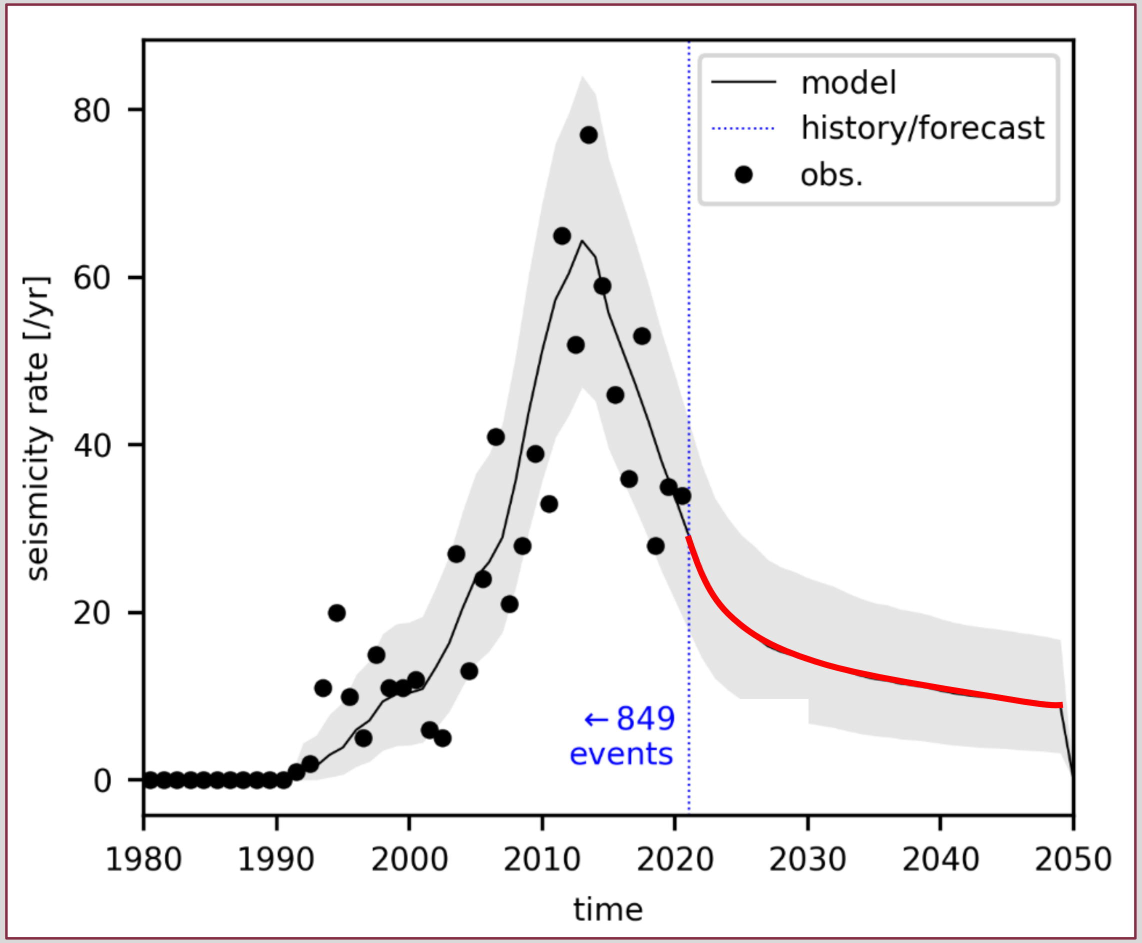

Forecast

1. Predict seismicity rate given simulation of future depressurization.
2. Integrate seismicity rate to predict <u>average</u> total number of earthquakes, $\overline{N}_f$.

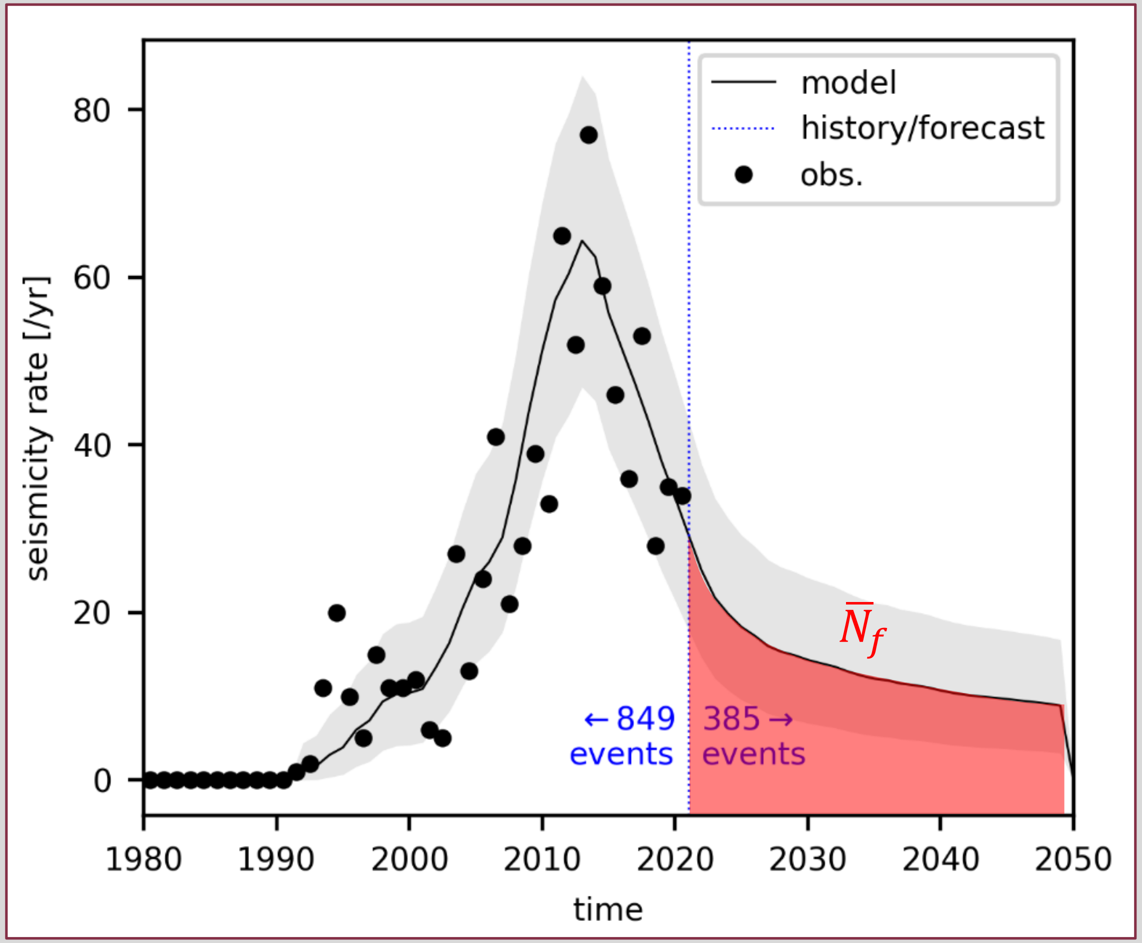

Forecast

1. Predict seismicity rate given simulation of future depressurization.
2. Integrate seismicity rate to predict <u>average</u> total number of earthquakes, $\bar{N}_f$.
3. Poisson sample to predict <u>observed</u> number of earthquakes, N_f.

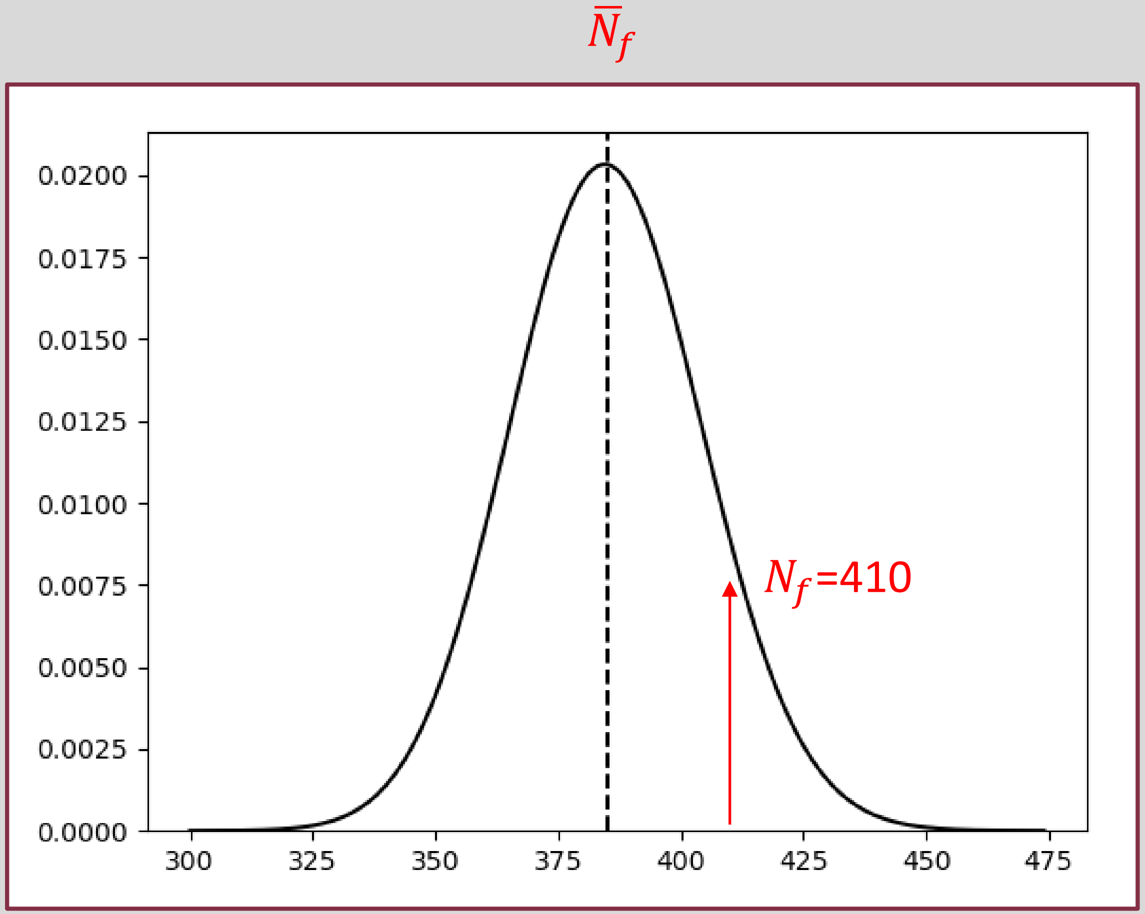

Forecast

1. Predict seismicity rate given simulation of future depressurization.
2. Integrate seismicity rate to predict average total number of earthquakes, $\bar{N}_f$.
3. Poisson sample to predict observed number of earthquakes, N_f.
4. Sample magnitude-frequency distribution N_f times, $[M_1, M_2, \dots M_{N_f}]$
5. Mmax prediction = $\max([M_1, M_2, \dots M_{N_f}])$.

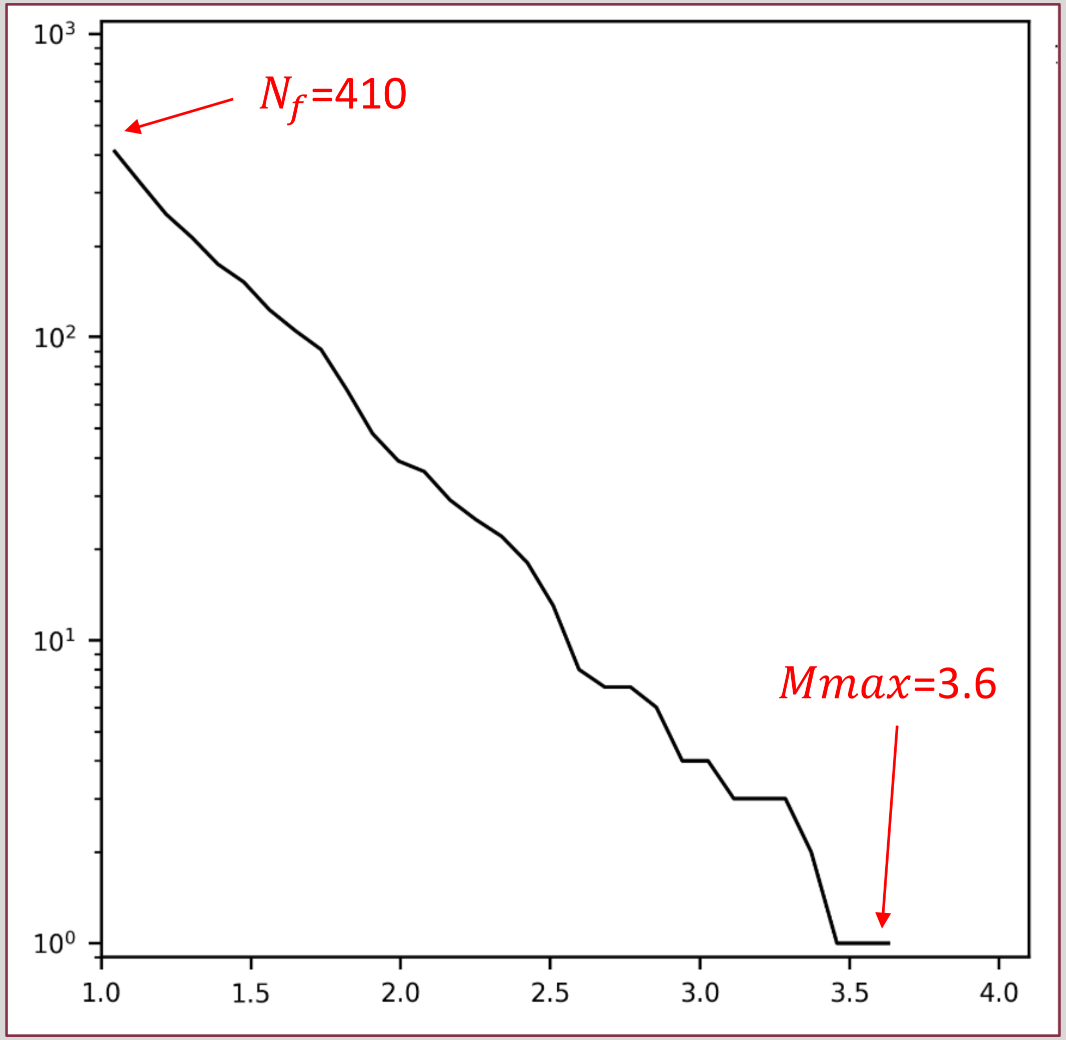

Forecast

1. Predict seismicity rate given simulation of future depressurization.
2. Integrate seismicity rate to predict <u>average</u> total number of earthquakes, $\bar{N}_f$.
3. Poisson sample to predict <u>observed</u> number of earthquakes, N_f.
4. Sample magnitude-frequency distribution N_f times, $[M_1, M_2, \ldots M_{N_f}]$
5. Mmax prediction = $\max([M_1, M_2, \ldots M_{N_f}])$.
6. Compile Mmax distribution by repeating steps 3-5.

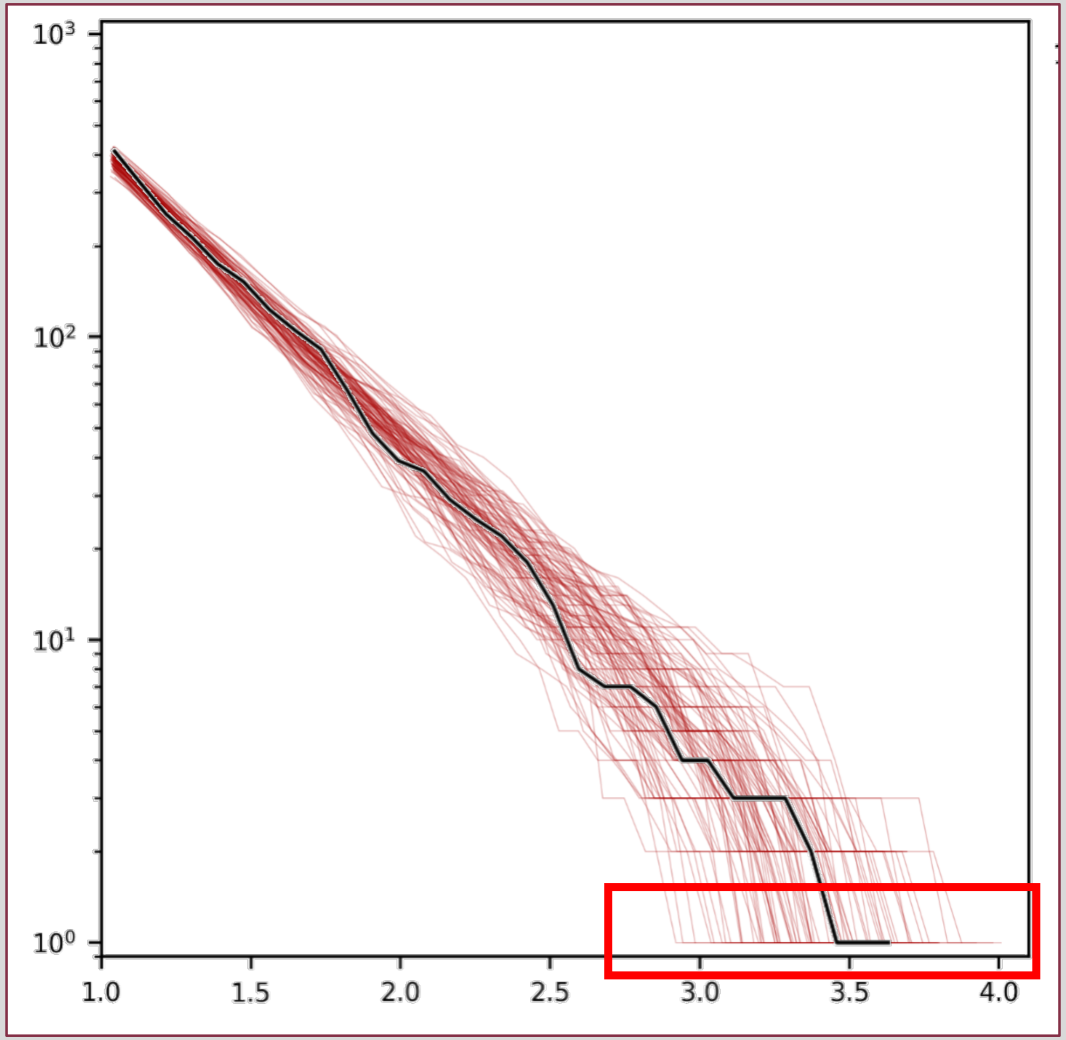

Forecast

1. Predict seismicity rate given simulation of future depressurization.
2. Integrate seismicity rate to predict average total number of earthquakes, $\bar{N}_f$.
3. Poisson sample to predict observed number of earthquakes, N_f.
4. Sample magnitude-frequency distribution N_f times, $[M_1, M_2, \dots M_{N_f}]$
5. Mmax prediction = $\max([M_1, M_2, \dots M_{N_f}])$.
6. Compile Mmax distribution by repeating steps 3-5.

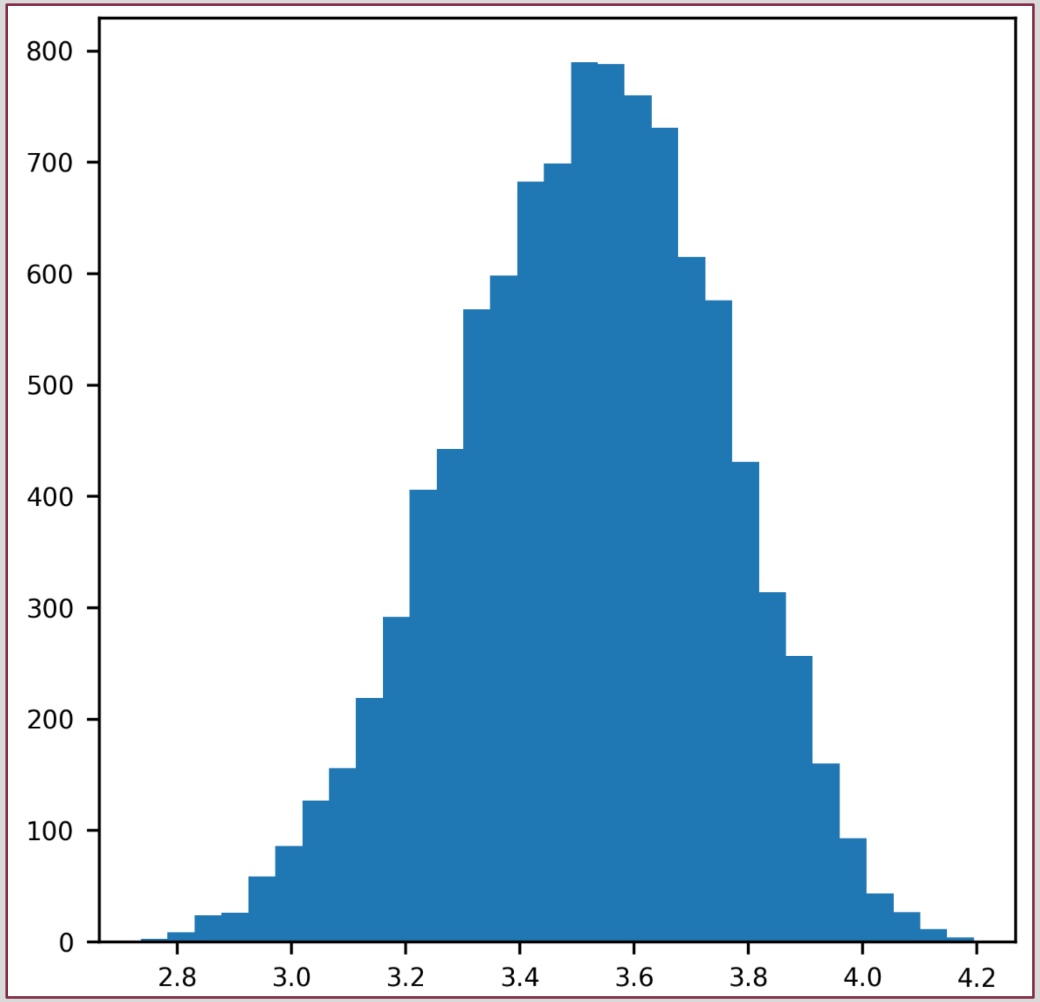

$Mmax$

Forecast

1. Predict seismicity rate given simulation of future depressurization.
2. Integrate seismicity rate to predict average total number of earthquakes, $\bar{N}_f$.
3. Poisson sample to predict observed number of earthquakes, N_f.
4. Sample magnitude-frequency distribution N_f times, $[M_1, M_2, \dots M_{N_f}]$
5. Mmax prediction = $\max([M_1, M_2, \dots M_{N_f}])$.
6. Compile Mmax distribution by repeating steps 3-5.
7. Report percentiles of Mmax distribution.

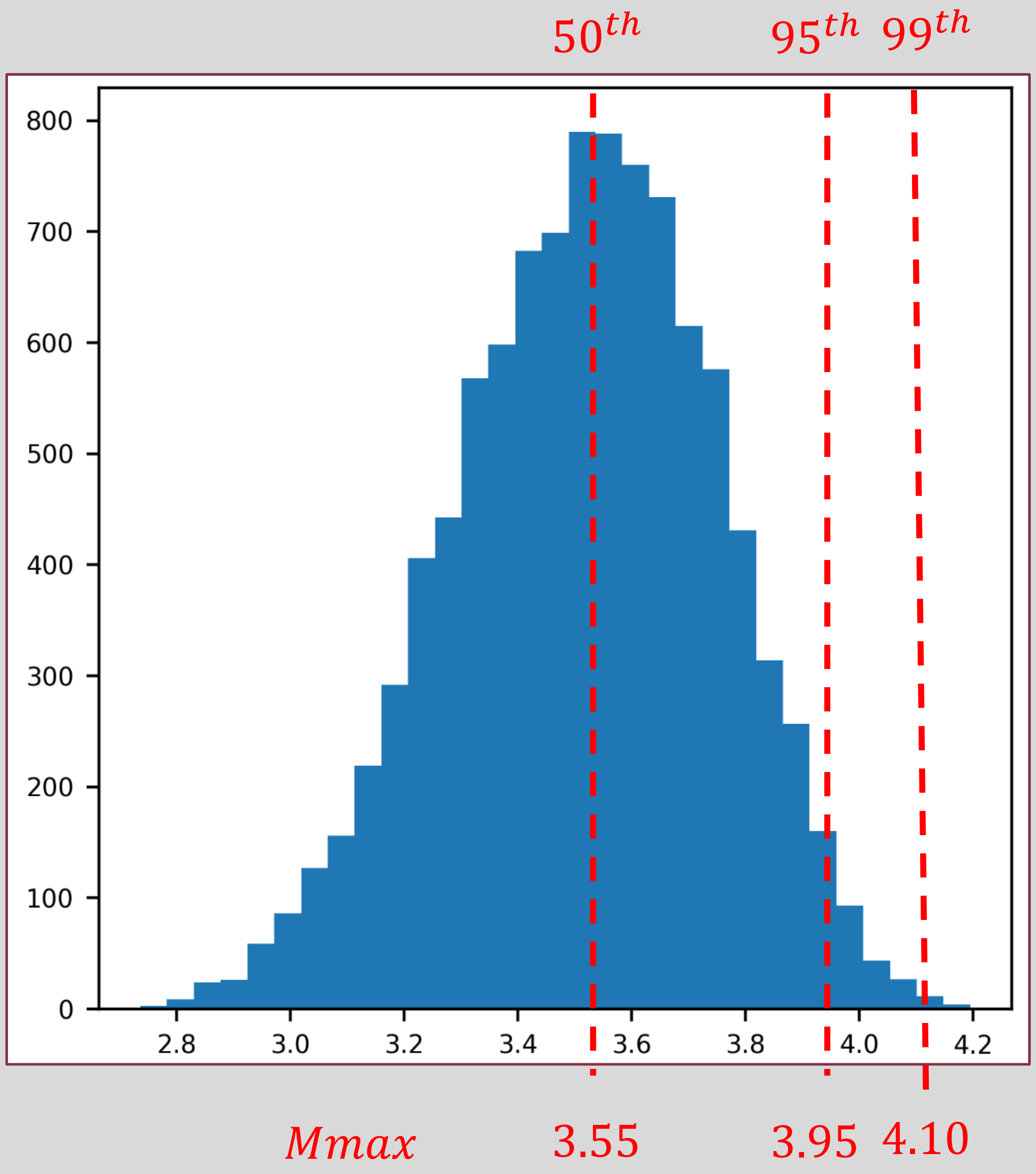

Magnitude-frequency distribution: two scenarios

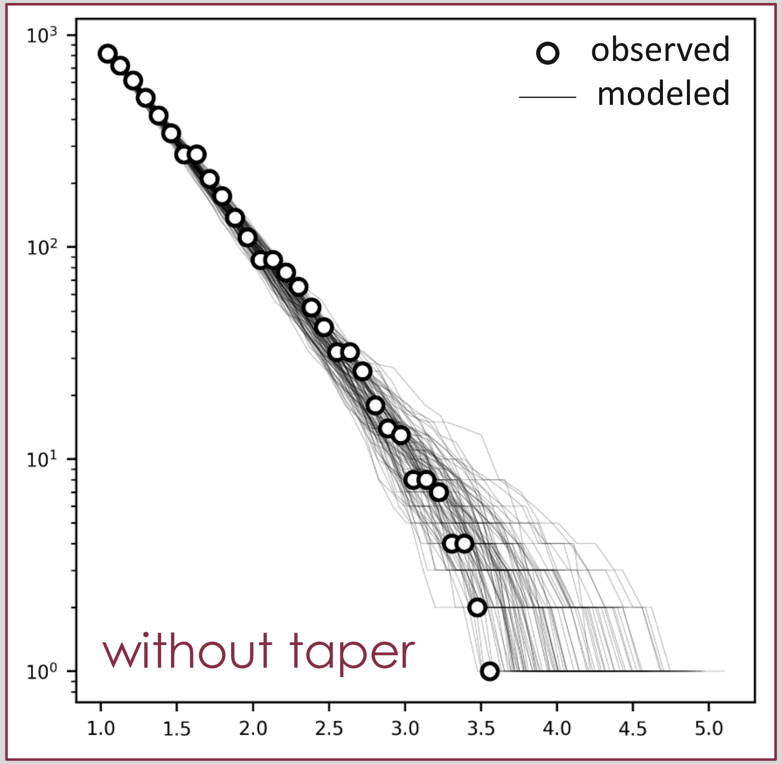

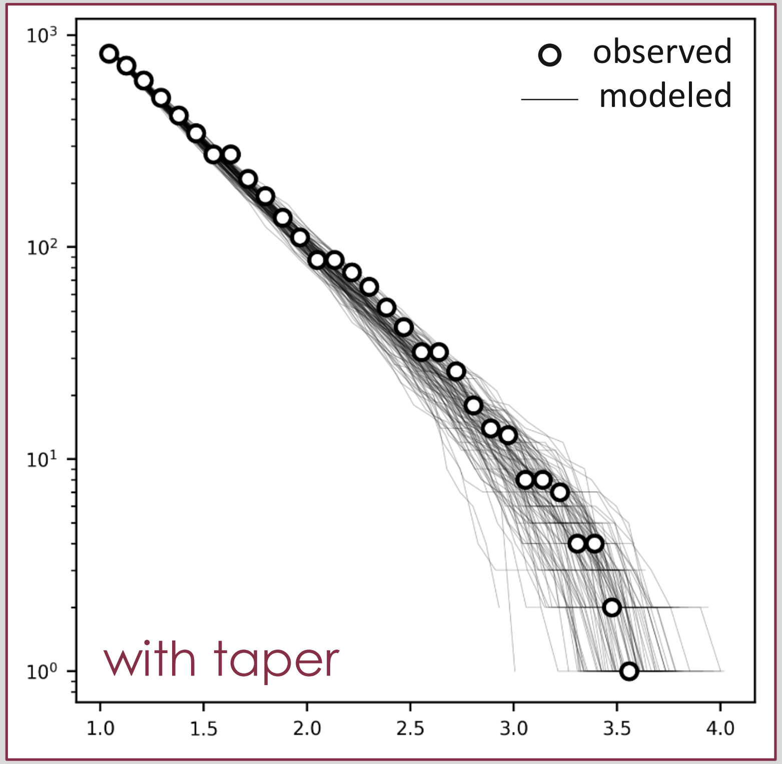

(Bourne & Oates, 2020)

Best model

- overpredicts in the east and southeast
- low friction, f=0.5

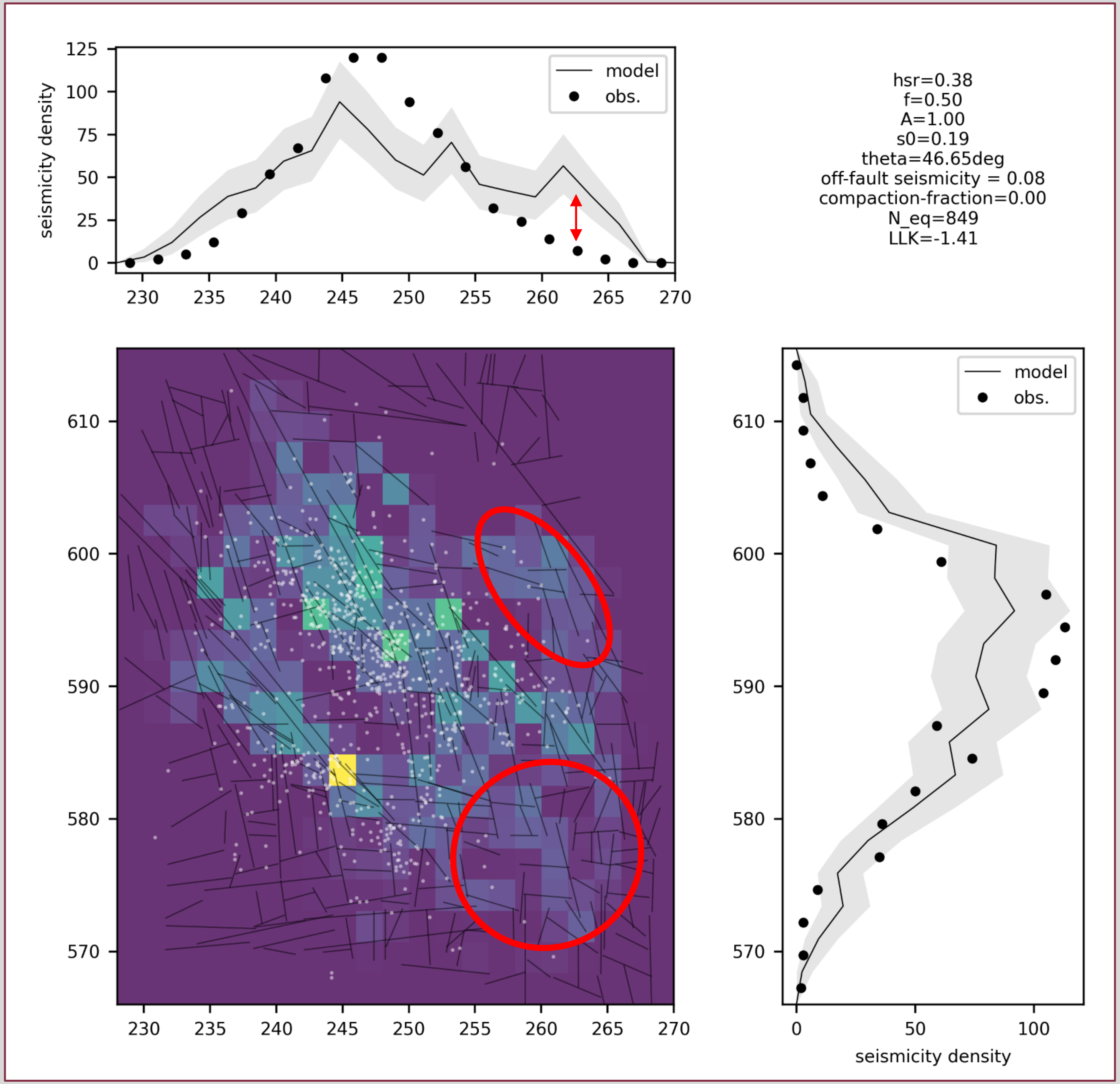

Best model

- overpredicts in the east and southeast
- low friction, f=0.5
- σ_{hmin} oriented NE-SW

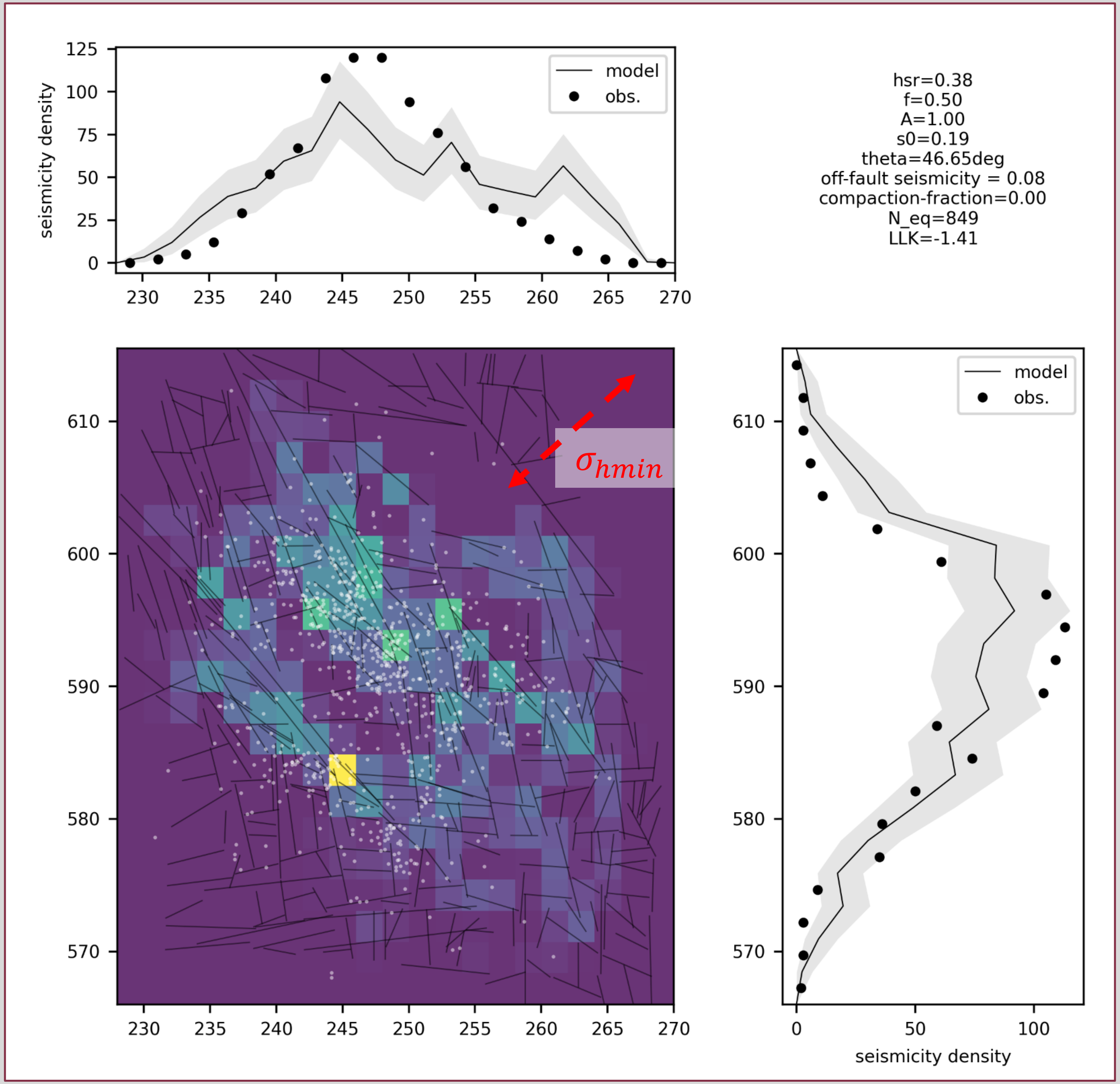

Best model

- overpredicts in the east and southeast
- low friction, f=0.5
- σ_{hmin} oriented NE-SW
- good match to seismicity onset, increase and decline

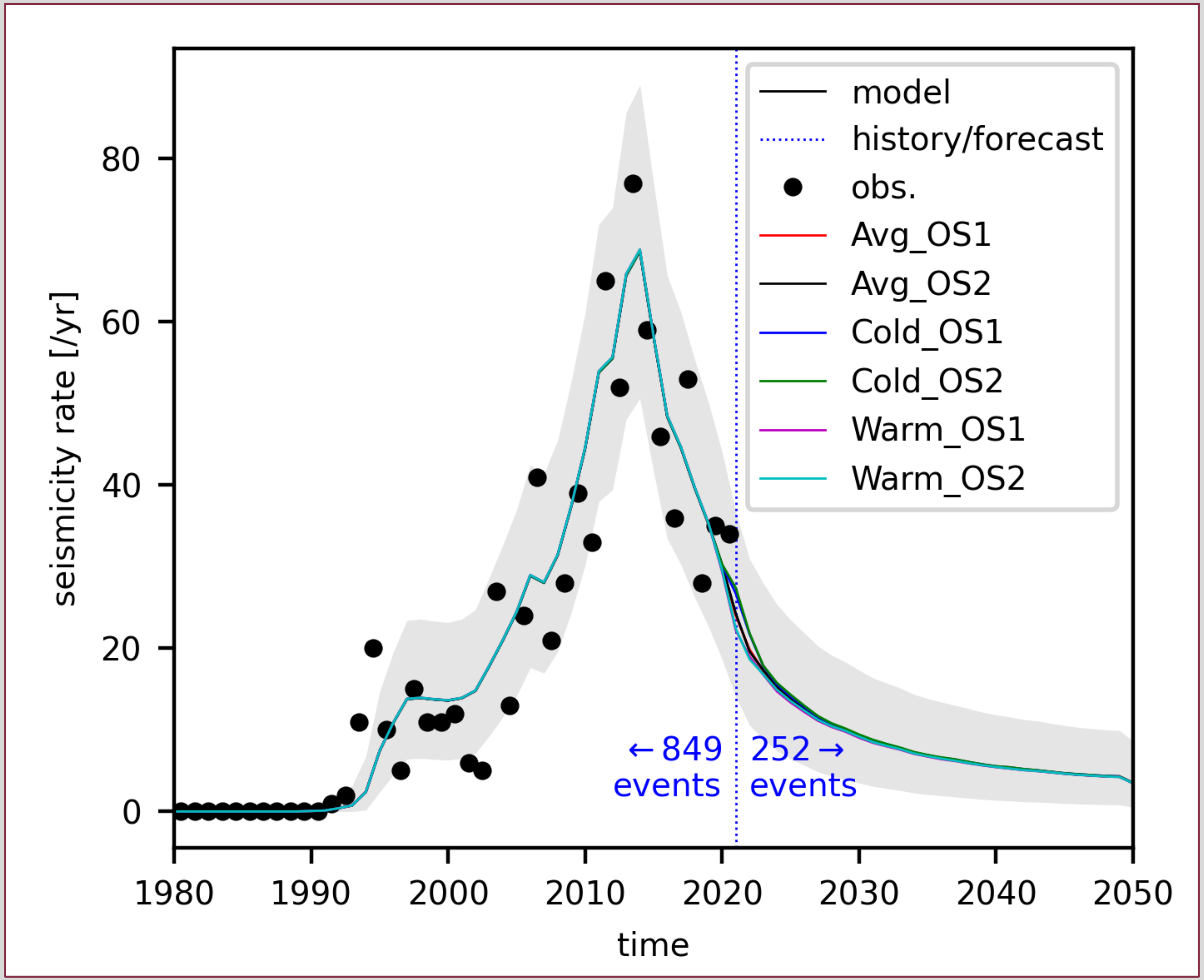

Best model

- overpredicts in the east and southeast
- low friction, f=0.5
- σ_{hmin} oriented NE-SW
- good match to seismicity onset, increase and decline
- 250-270 M ≥ 1 events (out to 2050) depending on scenario

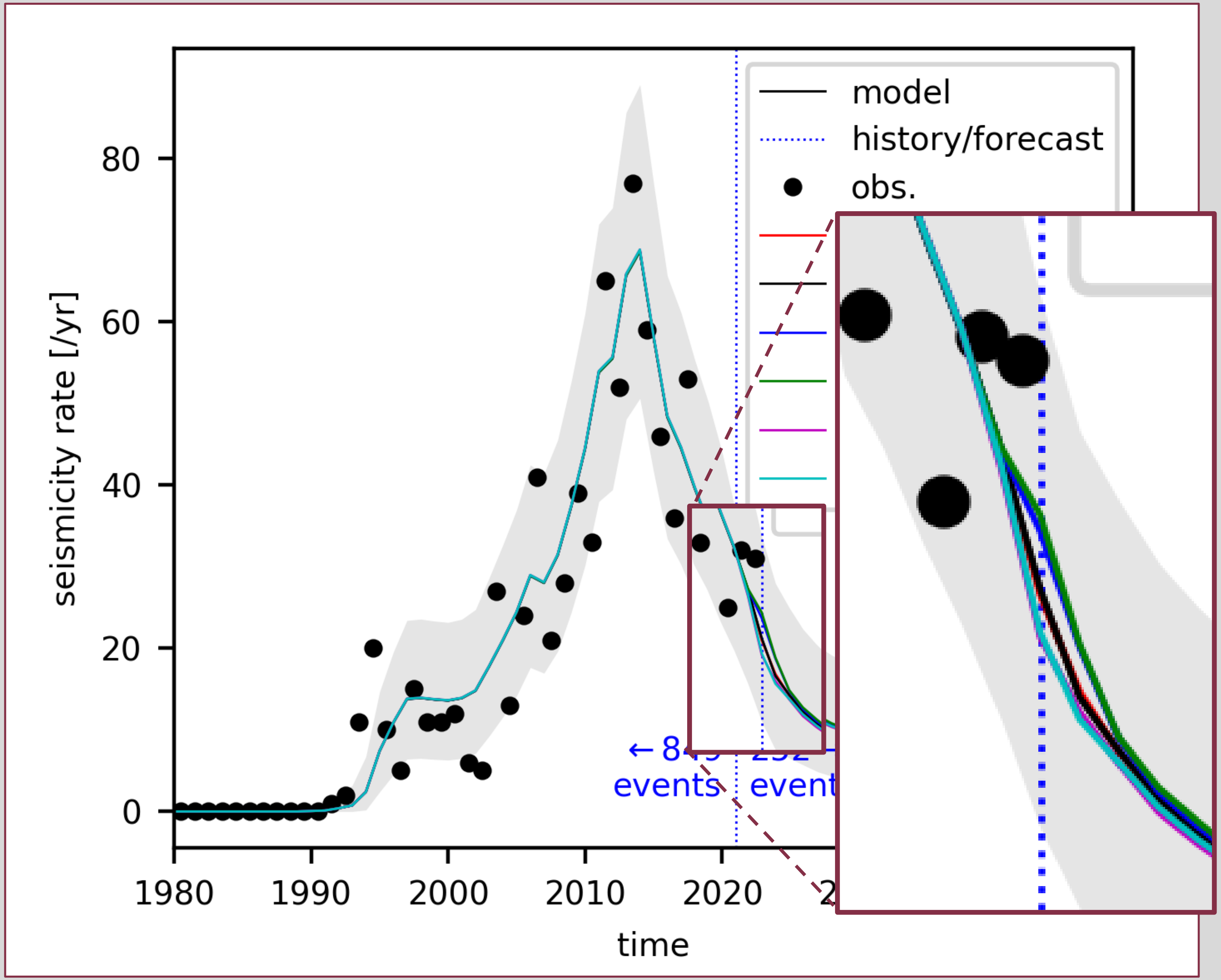

Best model

- overpredicts in the east and southeast
- low friction, f=0.5
- σ_{hmin} oriented NE-SW
- good match to seismicity onset, increase and decline
- 250-270 M $\geq$ 1 events (out to 2050) depending on scenario
- 99^{th} pct Mmax is 4.0 with taper and 5.6 without

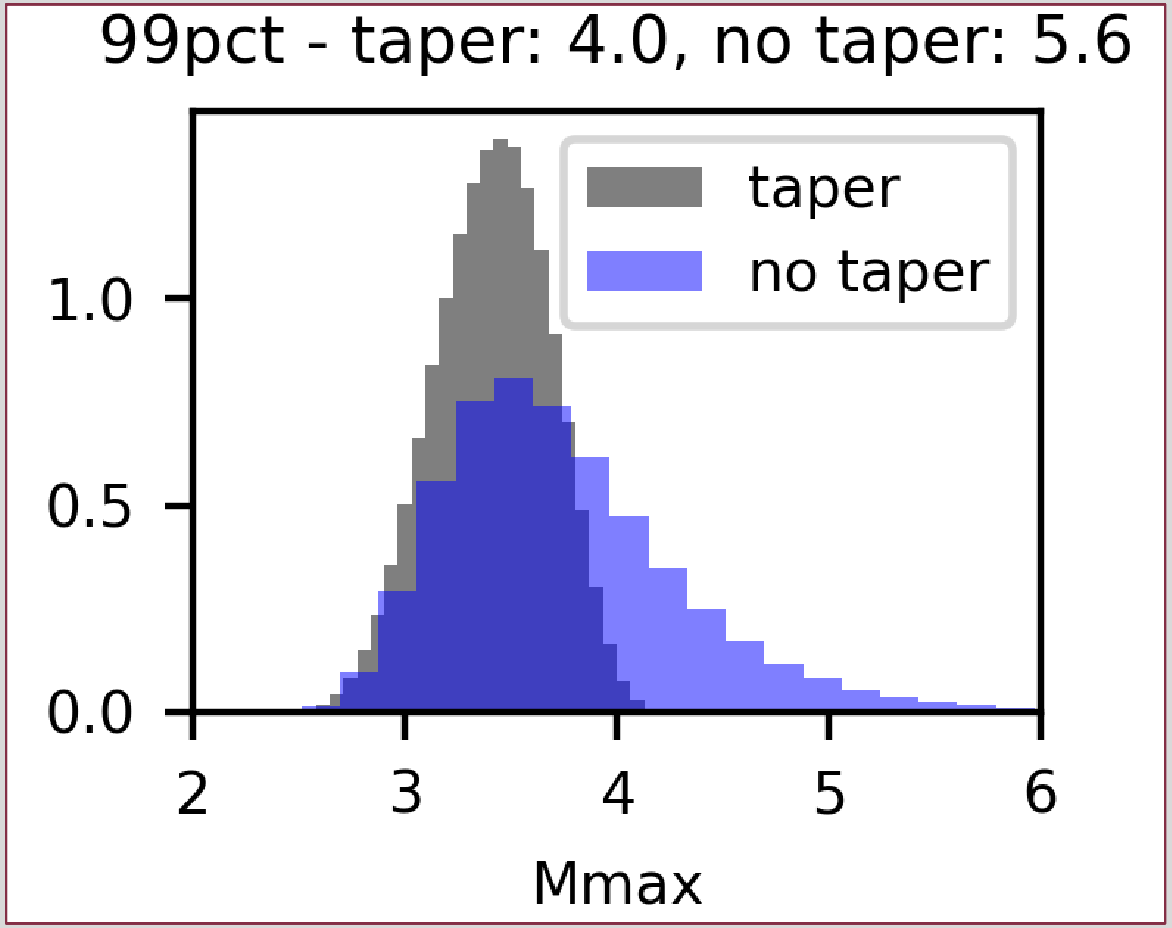

Combined pressure compaction model

Correspondence between compaction and areas of dense seismicity. (e.g.) Bourne and Oates (2017) have argued that compaction, as a proxy for elastic heterogeneity, drives seismicity.

Modify our 'pressure-only' model use a compaction-pressure: mixing fraction, C.

$C \times$

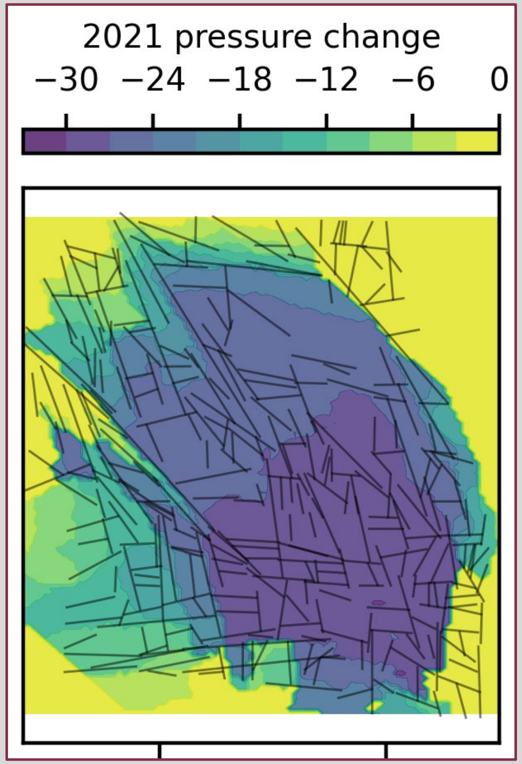

Combined pressure compaction model

Correspondence between compaction and areas of dense seismicity. (e.g.) Bourne and Oates (2017) have argued that compaction, as a proxy for elastic heterogeneity, drives seismicity.

Modify our 'pressure-only' model use a compaction-pressure: mixing fraction, C.

$C \times$

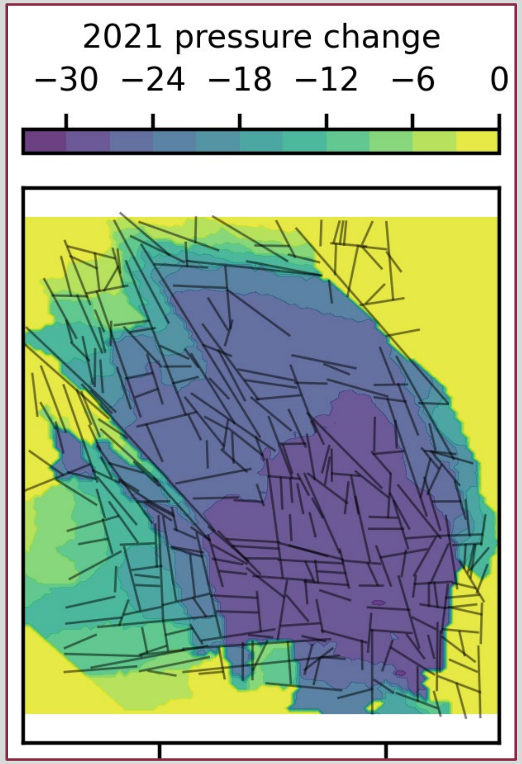

$+ \; (1\text{-}C) \times$

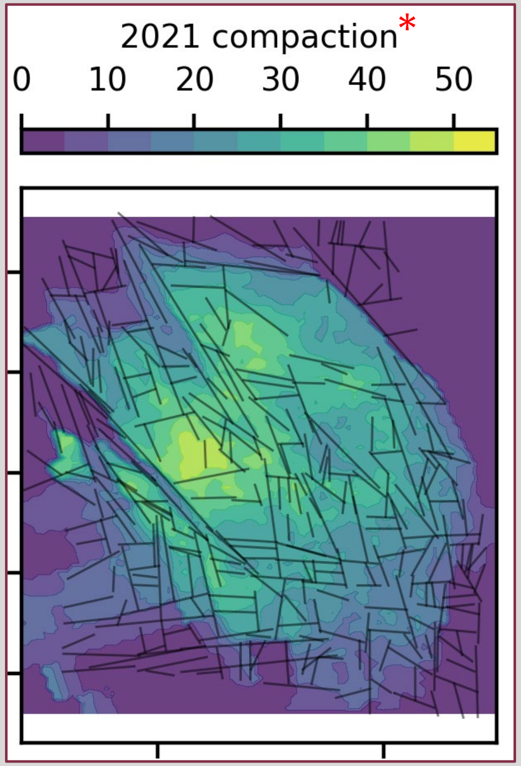

*compaction normalized to have same mean as pressure change in 2021

Combined pressure compaction model

Correspondence between compaction and areas of dense seismicity. (e.g.) Bourne and Oates (2017) have argued that compaction, as a proxy for elastic heterogeneity, drives seismicity.

Modify our ‘pressure-only’ model use a compaction-pressure: mixing fraction, C.

$C \times$

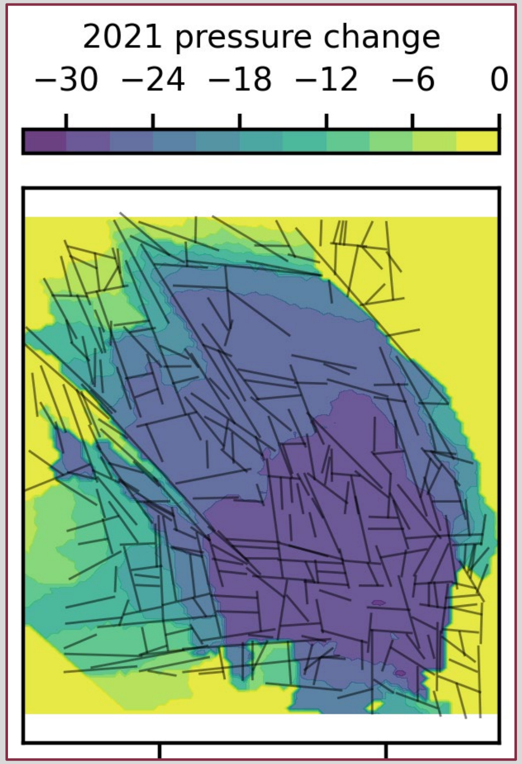

$+ \ (1\text{-}C) \times$

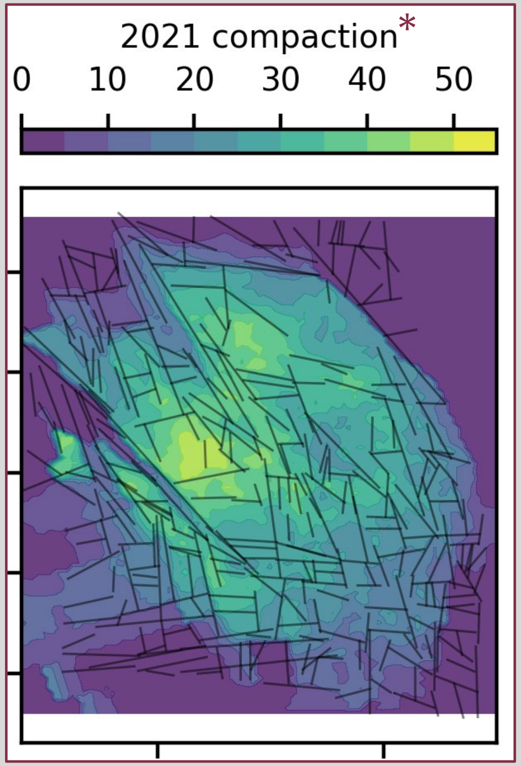

$=$

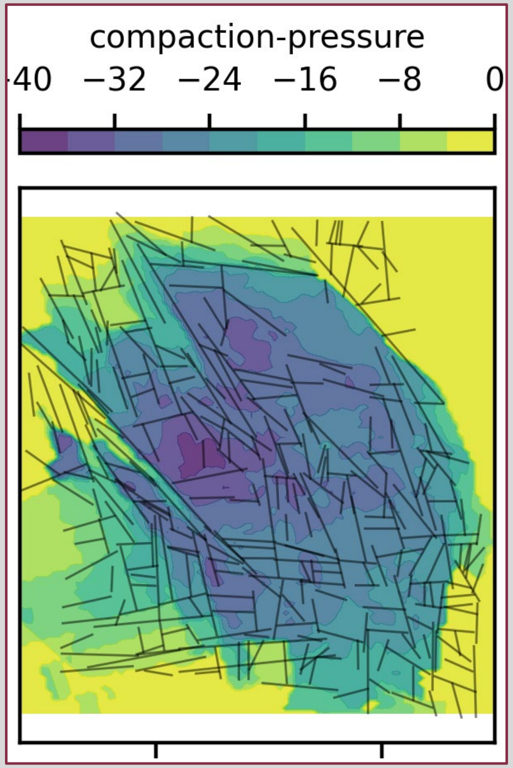

*compaction normalized to have same mean as pressure change in 2021

Best model

- spatial prediction improved
- low friction, f=0.5

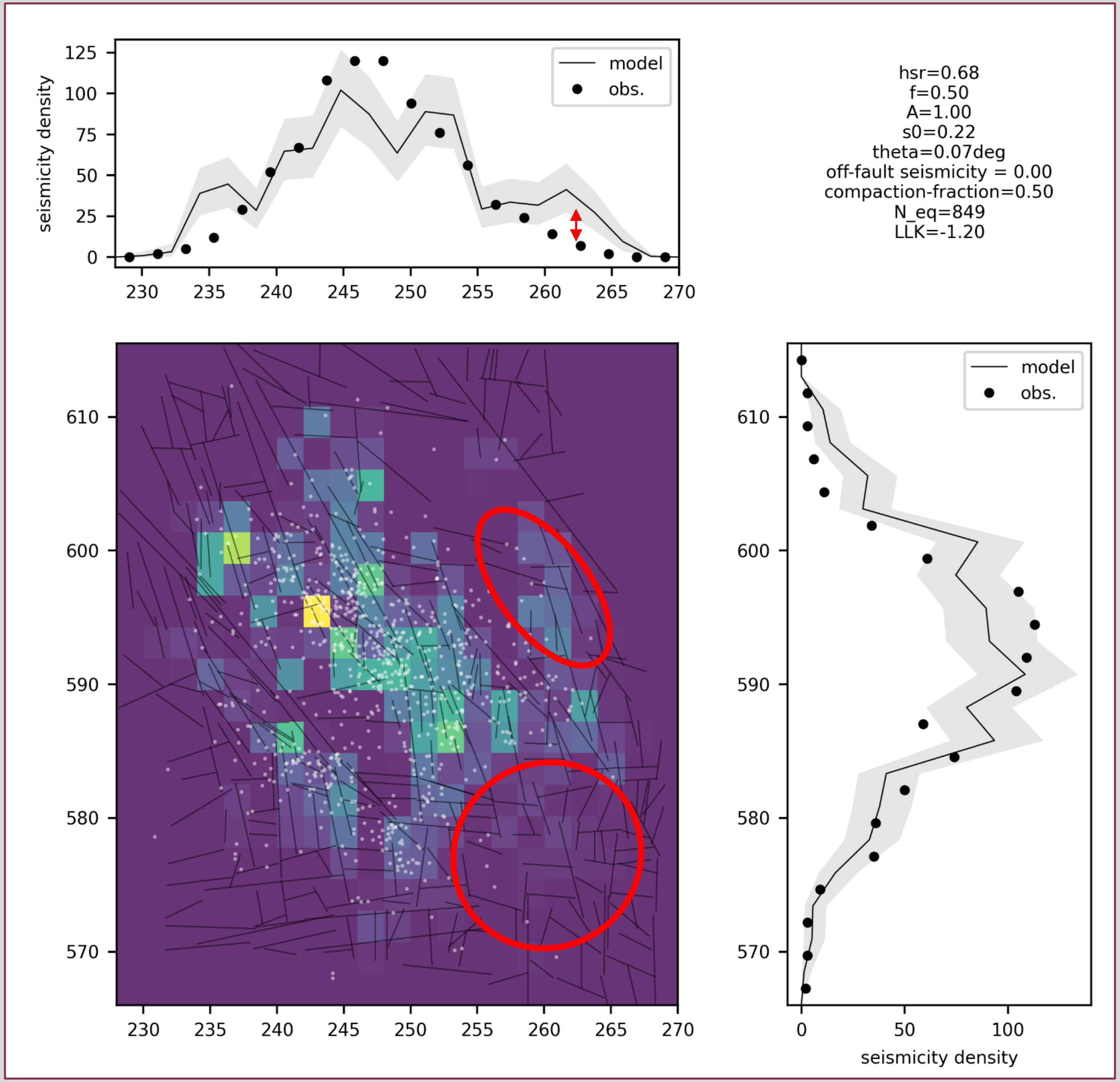

Best model

- spatial prediction improved
- low friction, f=0.5
- σ_{hmin} oriented E-W

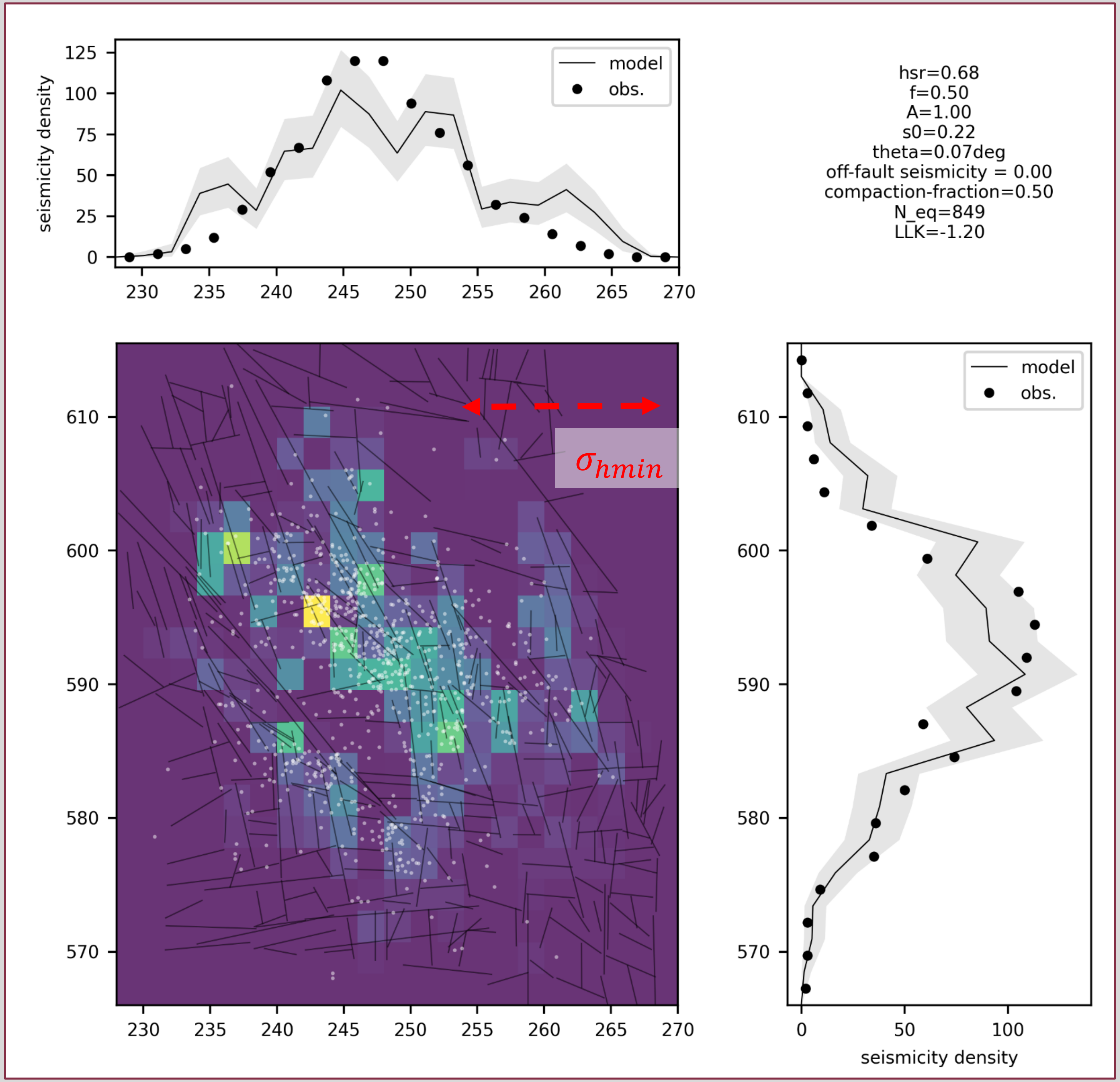

Best model

- spatial prediction improved
- low friction, f=0.5
- σ_{hmin} oriented E-W
- good match to seismicity onset, increase and decline
- 385 M ≥ 1 events (out to 2050)

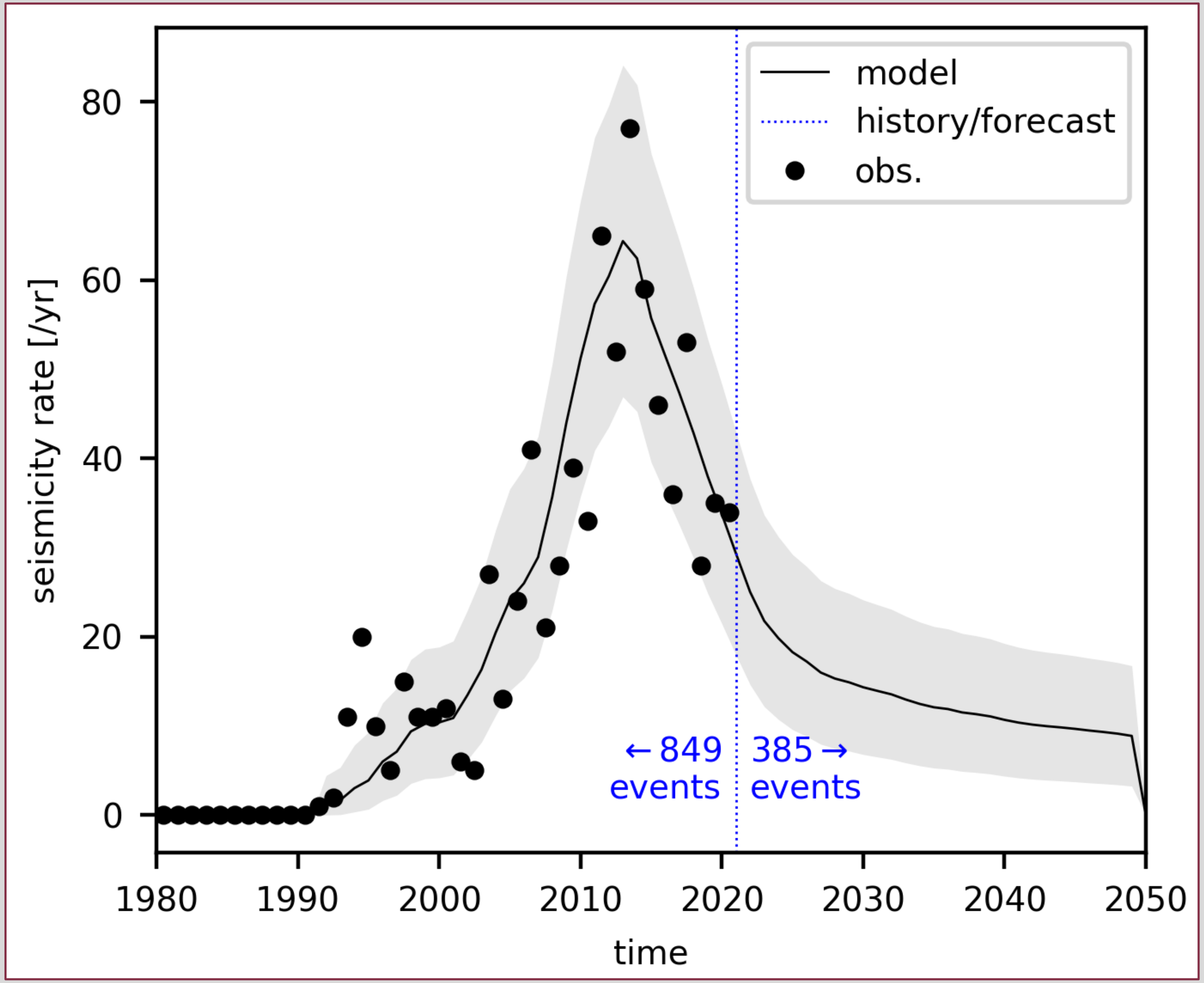

Best model

- spatial prediction improved
- low friction, f=0.5
- σ_{hmin} oriented E-W
- good match to seismicity onset, increase and decline
- 385 M $\geq$ 1 events (out to 2050)
- 99^{th} pct Mmax is 4.0 with taper and 5.8 without

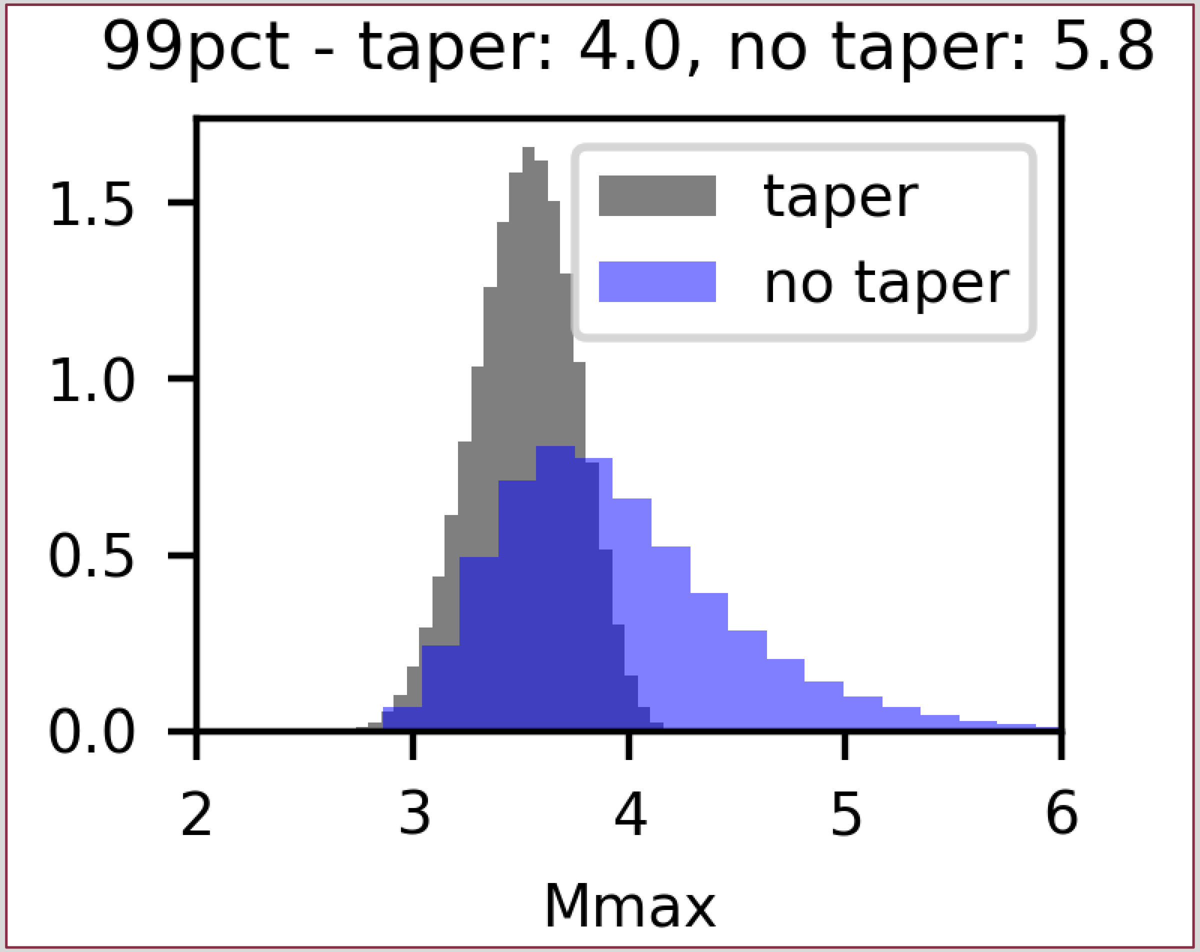

Other good models

- σ_{hmin} oriented 0, 12, 20, 30, 47, 58, 61, 78, 87°
- can always find a model that matches time and space distribution
- all models have same Mmax: 99^{th} pct is 4.0 with taper and 5.8 without

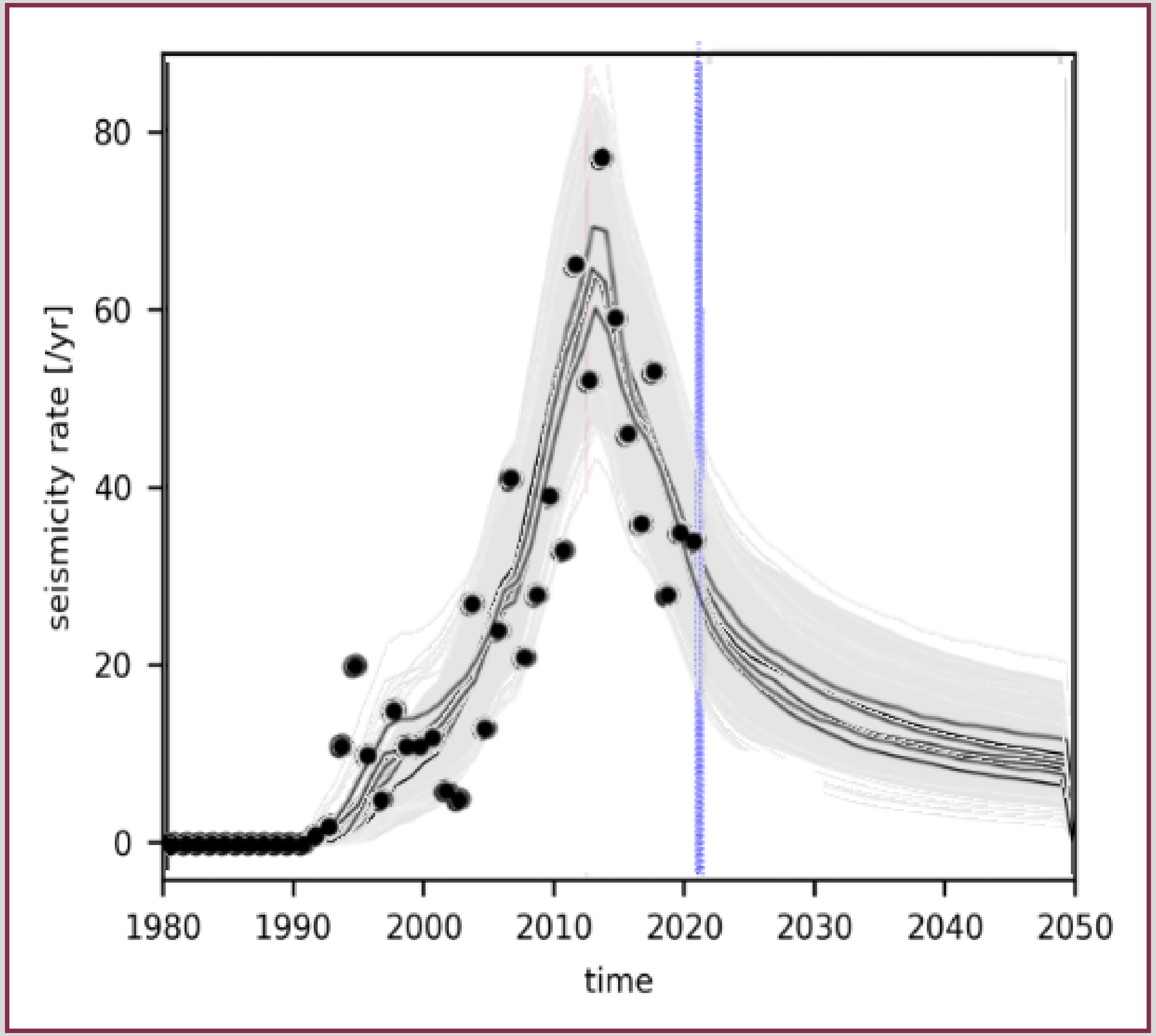

Summary

Major determinant of Mmax is taper of magnitude frequency distribution.

Mmax largely insensitive to other parameters. Because history matching ensures that future is constrained by past.

P99 Mmax ~5.6-5.8 for models without taper and ~4.0 for models with taper.

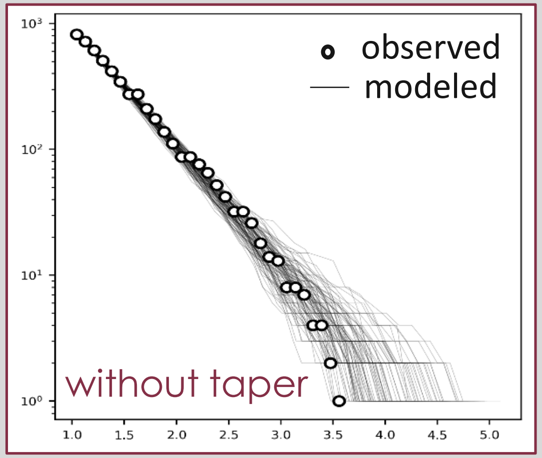

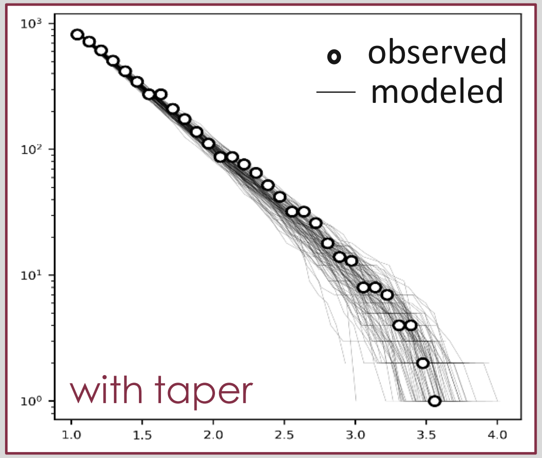

Scenario	F'cast date	P50	P95	P99
Pressure only MFD w/o taper	2030	3.4	4.6	5.3
	2040	3.6	4.7	5.5
	2050	3.7	4.8	5.6
Pressure only MFD w/ taper	2030	3.3	3.8	4.0
	2040	3.4	3.8	4.0
	2050	3.4	3.8	4.0
Pressure-compaction MFD w/o taper	2030	3.5	4.7	5.4
	2040	3.7	4.9	5.7
	2050	3.9	5.0	5.8
Pressure-compaction MFD w/ taper	2030	3.3	3.8	4.0
	2040	3.5	3.9	4.0
	2050	3.5	3.9	4.0

UNIVERSITEIT VAN PRETORIA
UNIVERSITY OF PRETORIA
YUNIBESITHI YA PRETORIA

Estimating the maximal possible magnitude of an anthropogenic seismic event in the Groningen Gas Field

Sensitivity analysis – (sort of)

A. Kijko

University of Pretoria Natural Hazard Centre, South Africa

Groningen Mmax Workshop II

13-17 June 2022, Infinity Building, South Amsterdam, The Netherlands

Contents

The questions I try to answer:

- How stable (reliable, robust) is our Mmax assessment if calculated by different methods and for different time-dependent gas extraction regimes?

- Not all is so rosy as it looks like. What to expect if we will triggered seismicity???

- Conclusions and References

UNIVERSITEIT VAN PRETORIA
UNIVERSITY OF PRETORIA
YUNIBESITHI YA PRETORIA

Background (1)

- Under the province of Groningen lies one of the largest gas fields in the world. The contains ca. 2,800 billion cubic metres of gas. Since 1963, more than 2,000 billion cubic metres of gas has been extracted.

- Despite the economic advantages of the gas extraction on the government finances, there is a severe drawback. Since 1986 the, gas extraction, anthropogenic (man-made) seismicity is observed in the mostly aseismic part of the Netherlands.

- One of the obvious parameters responsible for damage caused by seismic activity is the seismic event's magnitude. So far, the largest seismic event magnitude observed in the GGF is $M_{W.}$=3.6, occurred on 16 August 2012 near the village of Huizinge, municipality of Loppersum. The event caused significant damage to the infrastructure.

Background (2)

- The natural question arise: what is the maximum possible seismic event magnitude Mmax, which can be generated by GGF? Knowledge of such parameter is required by the local authorities, the engineering community, disaster management agencies, environmentalists, and the insurance industry.

What we know ?

- According to study of anthropogenic seismicity that has been recognised since 1929, the largest observed seismic event magnitude caused by oil and gas extraction is 7.3. (Davis *et al*., 2009).
- At the Lacq gas field, France, an event of magnitude ~6.0 was recorded (Bardainne *et al*., 2008).
- In Uzbekistan, in the Gazli aseismic area, two events of magnitude ~7.0 took place.
- Several factors suggest these are the strongest seismic events related to gas extraction from the gas fields.

The questions we ask:

- What is the maximal possible magnitude of an anthropogenic seismic event in the Groningen Gas Field?

  By anthropogenic we understand both: induced and triggered events.

- More precisely, how reliable our assessments of Mmax are? How sensitive they are in relation to the applied assessment techniques and the time-dependent gas extraction regime?

UNIVERSITEIT VAN PRETORIA
UNIVERSITY OF PRETORIA
YUNIBESITHI YA PRETORIA

Sensitivity Analysis. How estimated Mmax depends on time-dependent gas extraction regime?

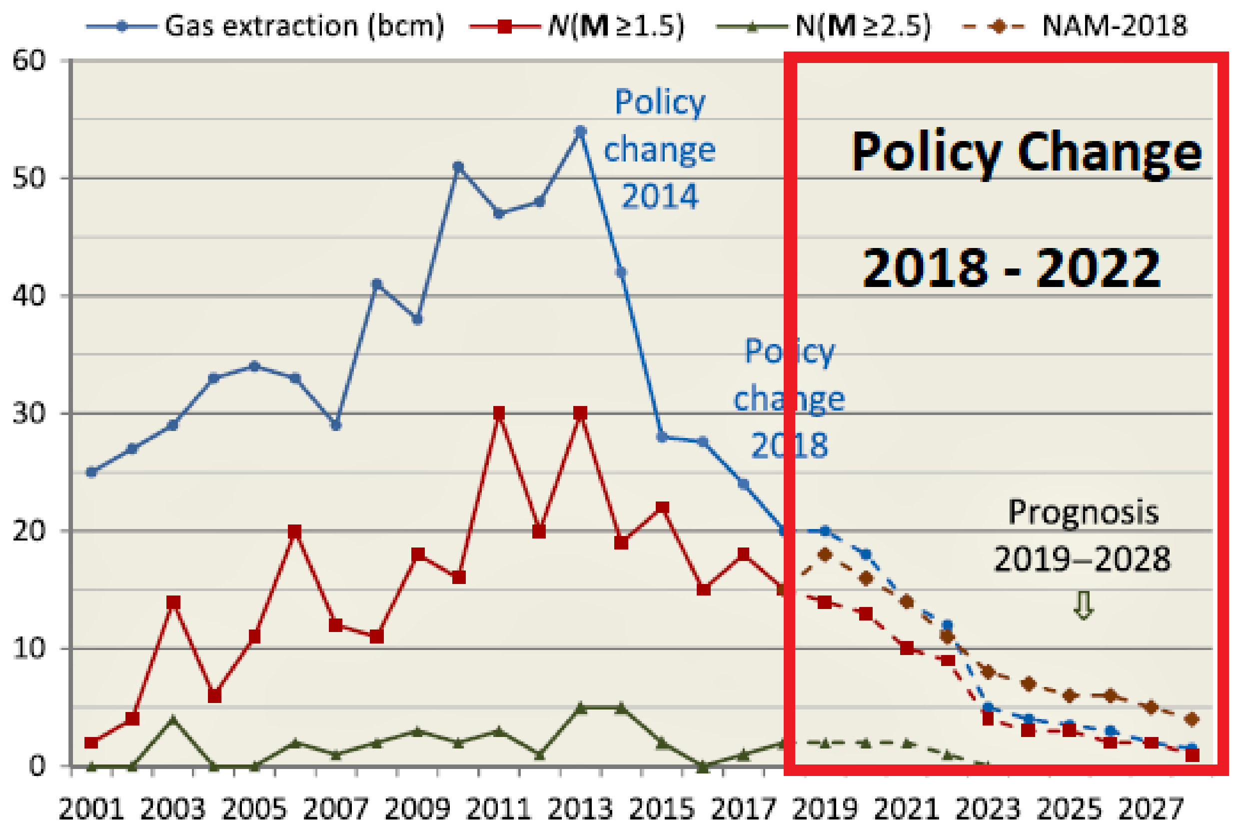

Annual Gas Extraction (Vlek, 2019)

Assessments of Mmax were performed for two catalogues:

(1) Whole catalogue (1991 – 2022)

(2) Recent catalogue (2018 – 2022)

Sensitivity Analysis: Dependence on the Mmax Assessment Technique

1. Non-parametric Gaussian Kernel (NPG)

$$m_{\max} = m_{\max}^{obs} + \Delta,$$

Sensitivity Analysis: Dependence on the Mmax Assessment Technique

2. Non-parametric based on Order Statistics (OS)

$$m_{\max} = m_{\max}^{obs} + \Delta,$$

$$\Delta = \left(m_{\max}^{obs} - (1 - e^{-1}) \sum_{i=0}^{n-1} e^{-i} m_{n-i} \right)$$

Sensitivity Analysis: Dependence on the Mmax Assessment Technique

3. Based on a Few (5) Largest Magnitudes (5L)

$$m_{\max} = m_{\max}^{obs} + \Delta,$$

$$\Delta = \frac{1}{n_0}\left(m_{\max}^{obs} - \frac{1}{n_0 - 1}\sum_{i=2}^{n_0} m_{n-i+1} \right)$$

UNIVERSITEIT VAN PRETORIA
UNIVERSITY OF PRETORIA
YUNIBESITHI YA PRETORIA

Sensitivity Analysis: Dependence on the Mmax Assessment Technique

4. Robson- Whitlock Procedure (RW)

$$m_{\max} = m_{\max}^{obs} + \Delta,$$

$$\Delta = (m_{\max}^{obs} - m_{n-1})$$

Sensitivity Analysis: Dependence on the Mmax Assessment Technique

5. Robson-Whitlock-Cooke Procedure (RWC)

$$m_{\max} = m_{\max}^{obs} + \Delta,$$

$$\Delta = 0.5(m_{\max}^{obs} - m_{n-1})$$

UNIVERSITEIT VAN PRETORIA
UNIVERSITY OF PRETORIA
YUNIBESITHI YA PRETORIA

Sensitivity Analysis: Dependence on the Mmax Assessment Technique

6. Tate-Pisarenko Procedure (TP)

$$m_{\max} = m_{\max}^{obs} + \Delta,$$

$$\Delta = \frac{1 - \exp[-\beta(m_{\max} - m_{\min})]}{n \cdot \exp[-\beta(m_{\max}^{obs} - m_{\min})]}$$

Procedure is straightforward and does not require extensive calculations

Sensitivity Analysis: Dependence on the Mmax Assessment Technique

7. Tate-Pisarenko Compound Procedure (TP-C)

$$m_{\max} = m_{\max}^{obs} + \Delta,$$

$$\Delta = \frac{1}{n\bar{\beta}C_{\beta}}\left(\frac{p}{p + m_{\max}^{obs} - m_{\min}}\right)^{-(q+1)}$$

$$p = \bar{\beta}/(\sigma_{\beta})^2, \qquad q = (\bar{\beta}/\sigma_{\beta})^2$$

Sensitivity Analysis: Dependence on the Mmax Assessment Technique

8. Kijko-Sellevoll Procedure (KS)

$$m_{\max} = m_{\max}^{obs} + \Delta,$$

$$\Delta = \frac{E_1(n_2) - E_1(n_1)}{\beta \exp(-n_2)}$$

$$n_1 = n/\{1 - \exp[-\beta(m_{\max} - m_{\min})]\}, \qquad n_2 = n_1 \exp[-\beta(m_{\max} - m_{\min})]$$

Sensitivity Analysis: Dependence on the Mmax Assessment Technique

9. Kijko-Sellevoll-Compound Procedure (KS-C)

$$m_{\max} = m_{\max}^{obs} + \Delta,$$

$$\Delta = \frac{\delta^{1/q} \exp[nr^q/(1-r^q)]}{\beta} \left[\Gamma(-1/q, \delta r^q) - \Gamma(-1/q, \delta)\right],$$

$$q = (\bar{\beta}/\sigma_\beta)^2$$

Sensitivity Analysis: Dependence on the Mmax Assessment Technique

10. L_1-norm, i.e. fit of CDF of Earthquake Magnitudes (L_1)

- useful when the data are unreliable, and are a mixture of uncertain historic and recent instrumental observations.
- superior to any alternative norm such as least-squares procedure. L_1-norm is robust, since the estimated parameters are insensitive to large outliers (Gentle, 1977; Anderson, 1982).

Sensitivity Analysis: Dependence on the Mmax Assessment Technique

11. Moment Method (MM)

$$m_{\max} = \frac{-3WY + nZ + D^{\frac{1}{2}}}{2\left(nY - 2W^2\right)} + m_{\min}$$

$$D = n^2 Z^2 - 15W^2 Y^2 - 14nWYZ + 12nY^3 + 16W^3 Z,\ \ W = nr_1,\ \ Y = nr_2\ \ \ Z = nr_3$$

The method was introduced by Dixit and Nasiri (2008), however, it is uncommon, as it has been superseded by the Maximum Likelihood Procedure.

Sensitivity Analysis: Dependence on the Mmax Assessment Technique

12. Generalized Extreme Distribution by Alves & Neves (GED)

$$m_{\max} = m_{\max}^{obs} + \Delta,$$

$$\Delta = \sum_{i=0}^{k-1} a_{i,k}\left(m_{n-k} - m_{n-k-i}\right)$$

$$a_{i,k} = -(\ln 2)^{-1}\left(\ln(k+i) - \ln(k+i+1)\right) > 0; \quad k = (\ln(n))^{r}$$

UNIVERSITEIT VAN PRETORIA
UNIVERSITY OF PRETORIA
YUNIBESITHI YA PRETORIA

Sensitivity Analysis: Dependence on the Mmax Assessment Technique

Two Bayesian Mmax assessment Techniques:

- Shift of Likelihood Function & Gaussian Prior

  (i.e. corrected Cornell (1994) procedure)

- Fiduicial Distribution & Gaussian Prior

Sensitivity Analysis

Two catalogues:

- Whole (1991-2022) n=340 events
- Recent (2018-2022) n= 49 events

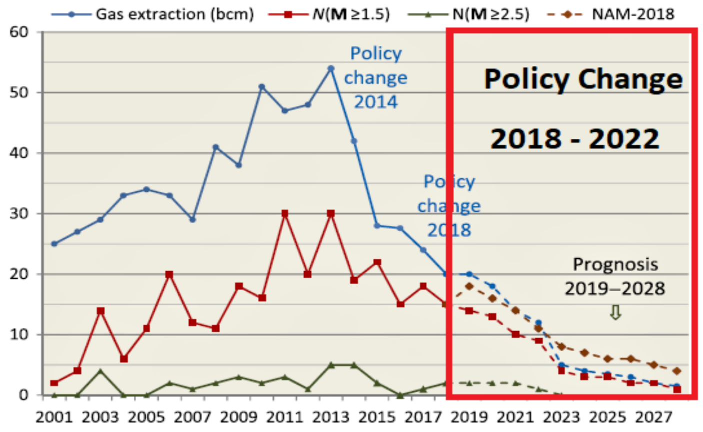

Vlek (2019)

Procedures:

- 12 & 2 Bayesian,
- Mmax(PRIOR) = **3.82±0.25**

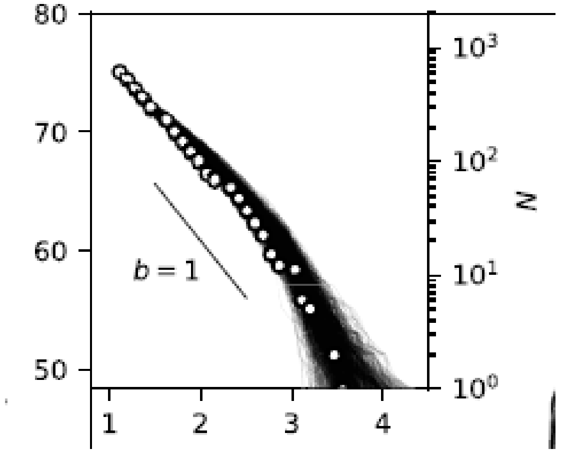

Dempsey & Suckale (2017)

Sensitivity Analysis: Results

Procedure	Whole catalogue	Recent Catalogue	Difference
NPG	3.71 ± 0.15	3.61 ± 0.23	0.10
OS	3.61 ± 0.15	3.54 ± 0.15	0.07
5L	3.66 ± 0.14	3.48 ± 0.14	0.18
RW	3.70 ± 0.24	3.41 ± 0.22	0.29
RWC	3.65 ± 0.17	3.41 ± 0.16	0.24
TP	-	-	
TP-C	3.78 ± 0.21	-	
KS	3.79 ± 0.21	3.93 ± 0.54	- 0.14
KS-C	3.73 ± 0.17	3.80 ± 0.41	0.07
L1	3.72 ± 0.16	-	
MM	3.85 ± 0.27	4.18 ± 0.78	-0.33
GED (Alves & Neves)	3.69 ± 0.13	-	
Bayesian #1 (shift of LF)	3.82 ± 0.24	3.81 ± 0.24	0.01
Bayesian #2 (Fiducial)	3.77 ± 0.19	3.74 ± 0.17	0.03

ERSITEIT VAN PRETORIA
ERSITY OF PRETORIA
BESITHI YA PRETORIA

Sensitivity Analysis – Comments on Results

1. Surprise, surprise, very different procedures provide similar assessments of Mmax. Assessments of Mmax oscillating in the range **Mw 3.7- 4.0**

2. I was expecting that if very limited data will be used (2018-2022, n=49 events), the assessments of Mmax will be vey different. They are different but not dramatically. The non-parametric procedures predict Mmax ~0.2 lower then Mmax estimated by the whole data sets. The parametric and Bayesian procedures predict Mmax the same (**3.7- 4.0)** as calculated by help of whole catalogue.

3. More detailed investigation is required on the effect of slowing down gas exploration. (Does slowing down exploration leads to decrease of Mmax???)

UNIVERSITEIT VAN PRETORIA
UNIVERSITY OF PRETORIA
YUNIBESITHI YA PRETORIA

What about TRIGGERED events???

- It seems that so far the Groningen Gas Field is generating only **the induced** seismicity (???). Based on mining experience in China, Czech Republic, Poland, Canada, South Africa, **extensive mining is triggering the realise of tectonic residual stresses,** observed as very strong seismic events, of magnitude 5-7.

TRIGGERED events – example (South Africa)

1976 Welkom, South Africa ML 5.2

Induced and Triggered Seismicity - Australia

Bi-modal distribution of seismic events, Australia

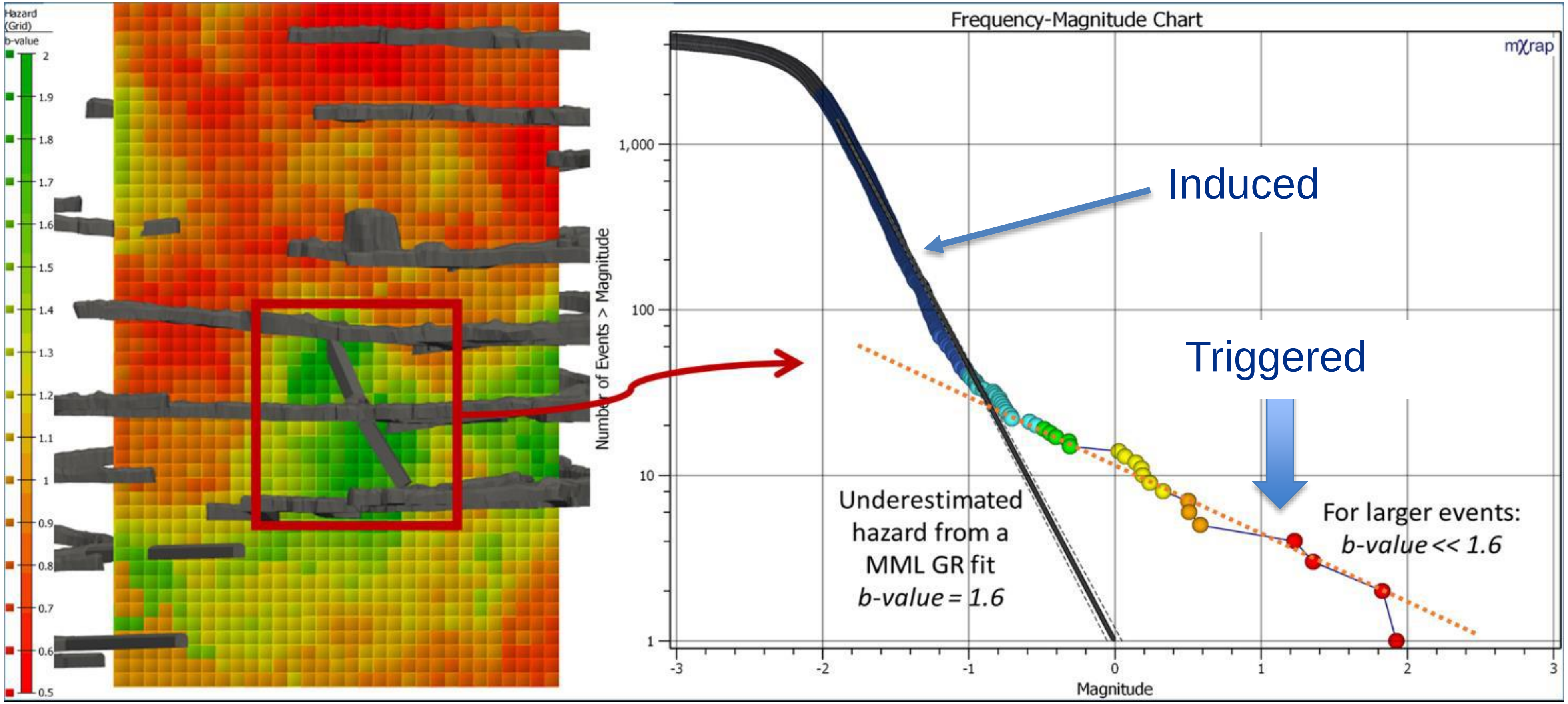

Woodward and Tierney (2017)

Induced and Triggered Seismicity - Poland

Bi-modal distribution of seismic events, Poland

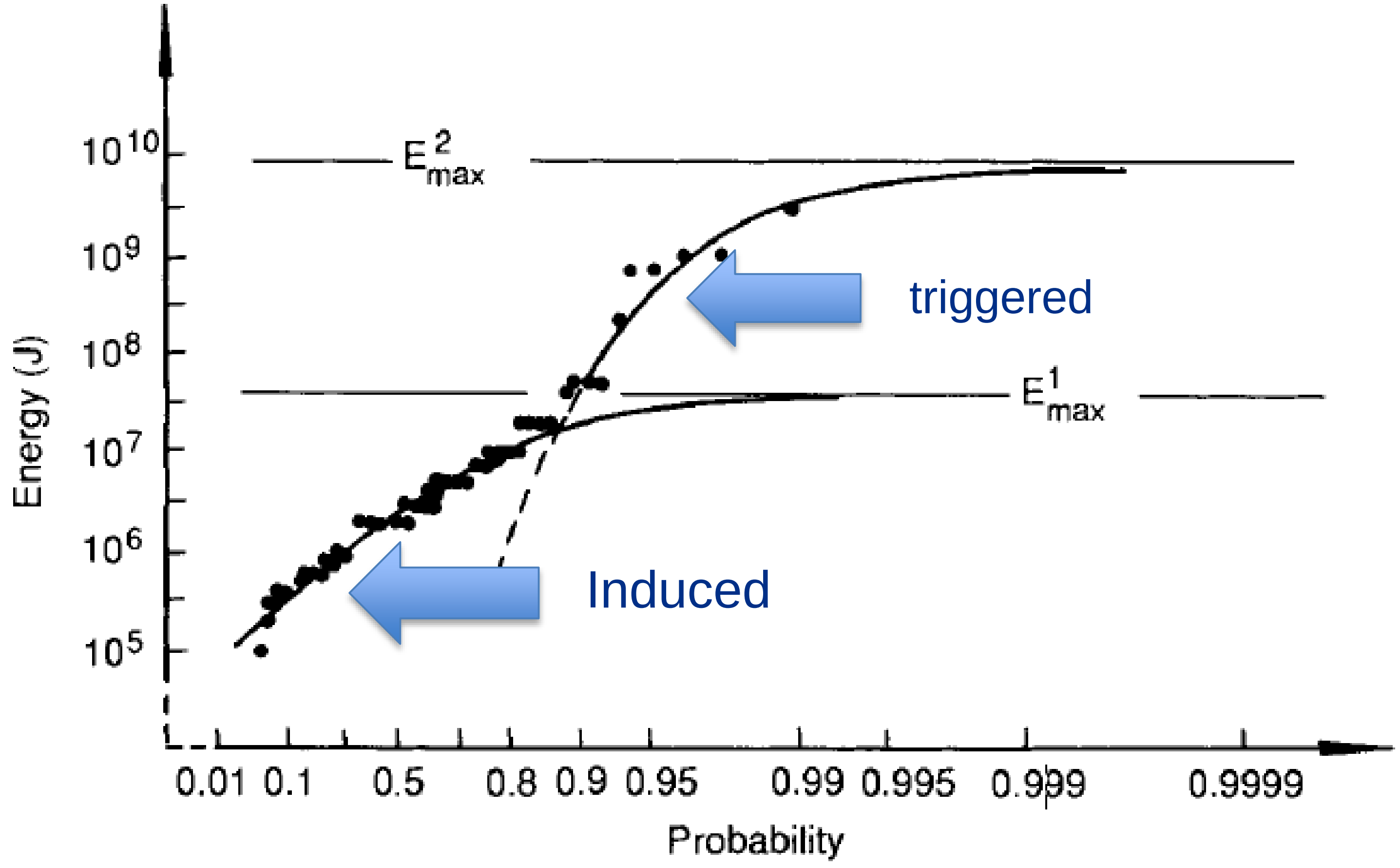

Source: Gibowicz and Kijko, 1994

Triggered seismicity by acid mine water under Johannesburg

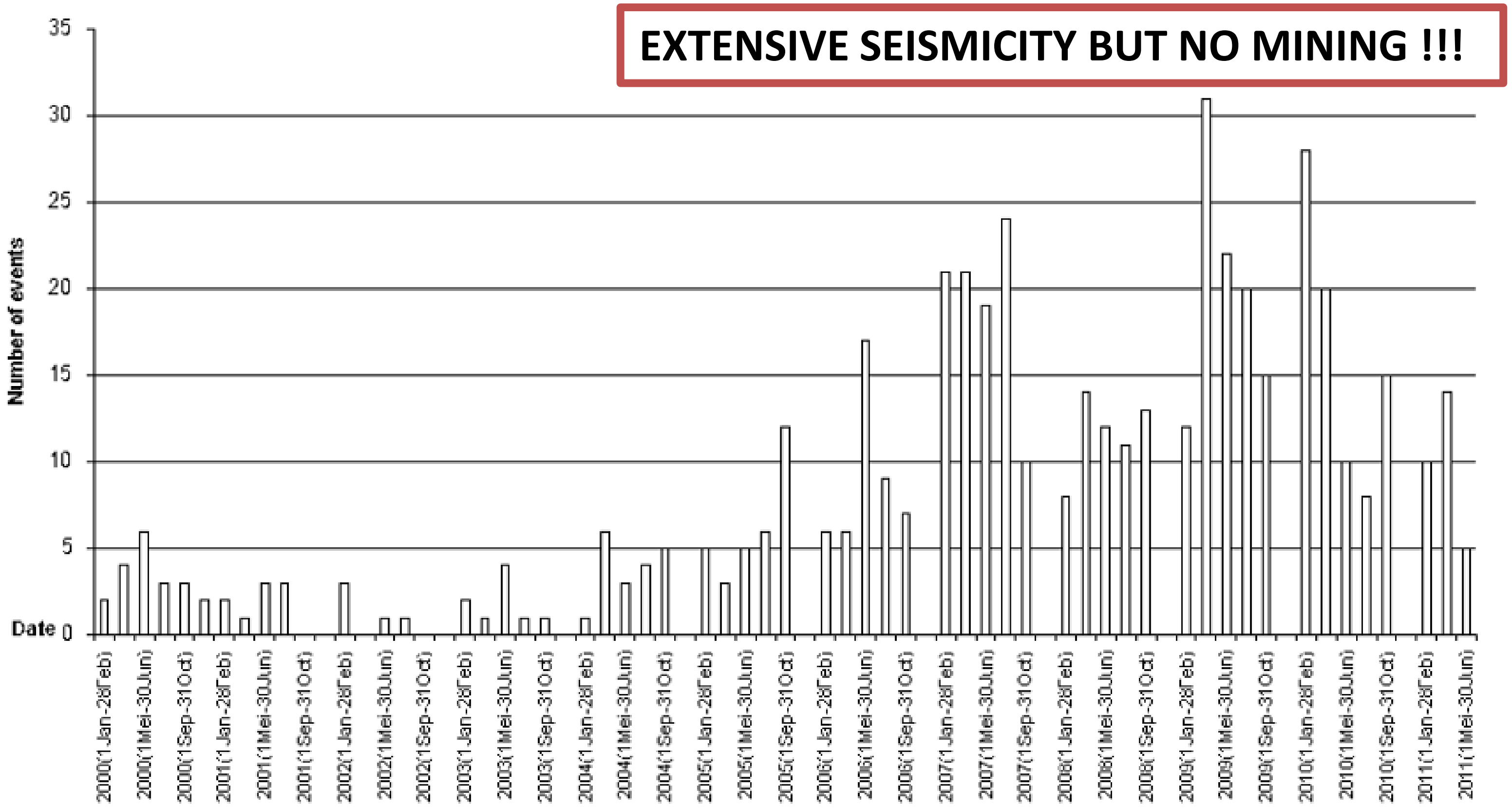

Triggered seismicity by acid mine water under Johannesburg

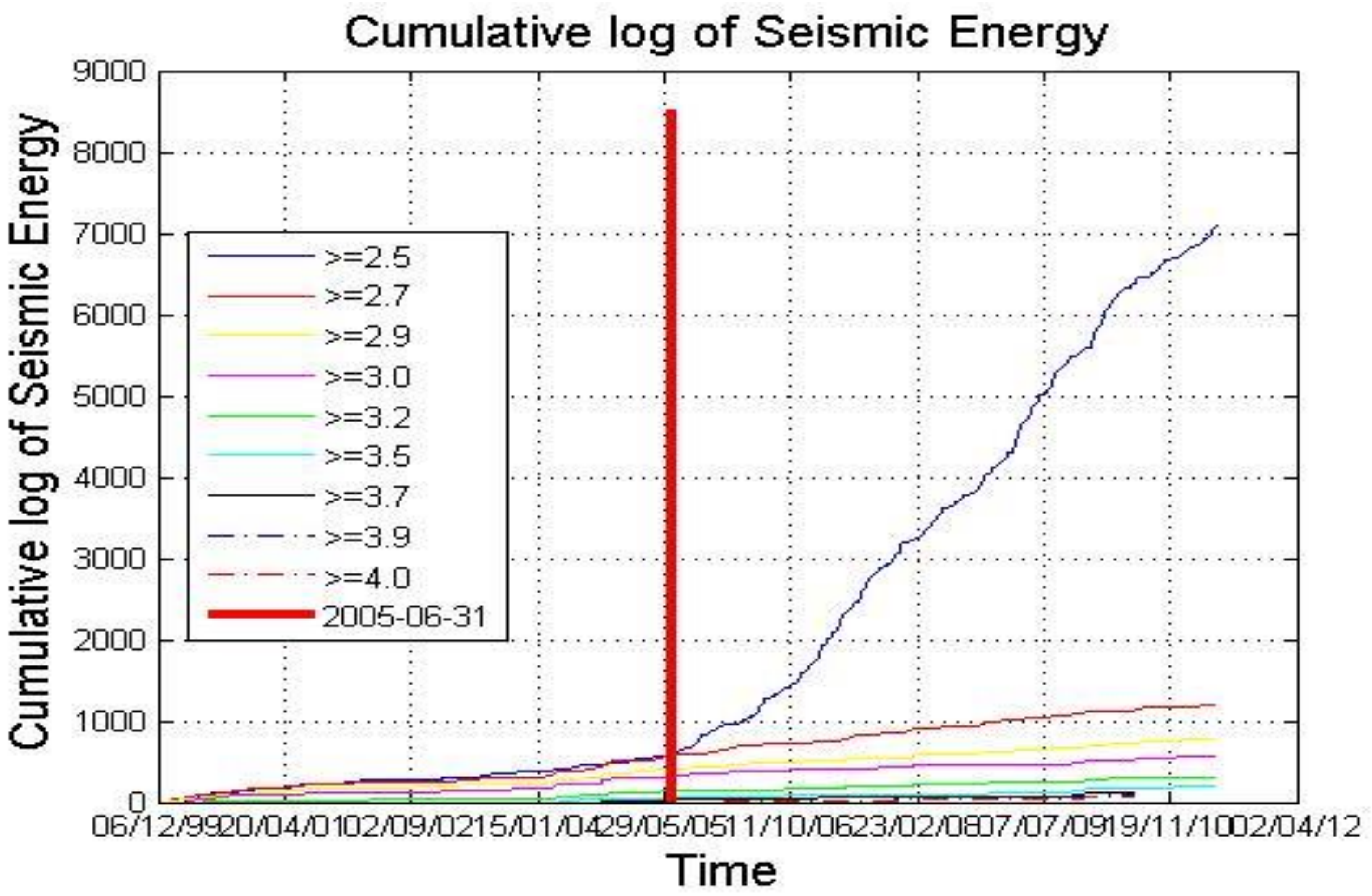

UNIVERSITEIT VAN PRETORIA
UNIVERSITY OF PRETORIA
YUNIBESITHI YA PRETORIA

CONCLUSION:

Seismic hazard and Risk in the the province of Groningen

can NOT be properly estimated without account of potentially triggered seismicity.

Thank you

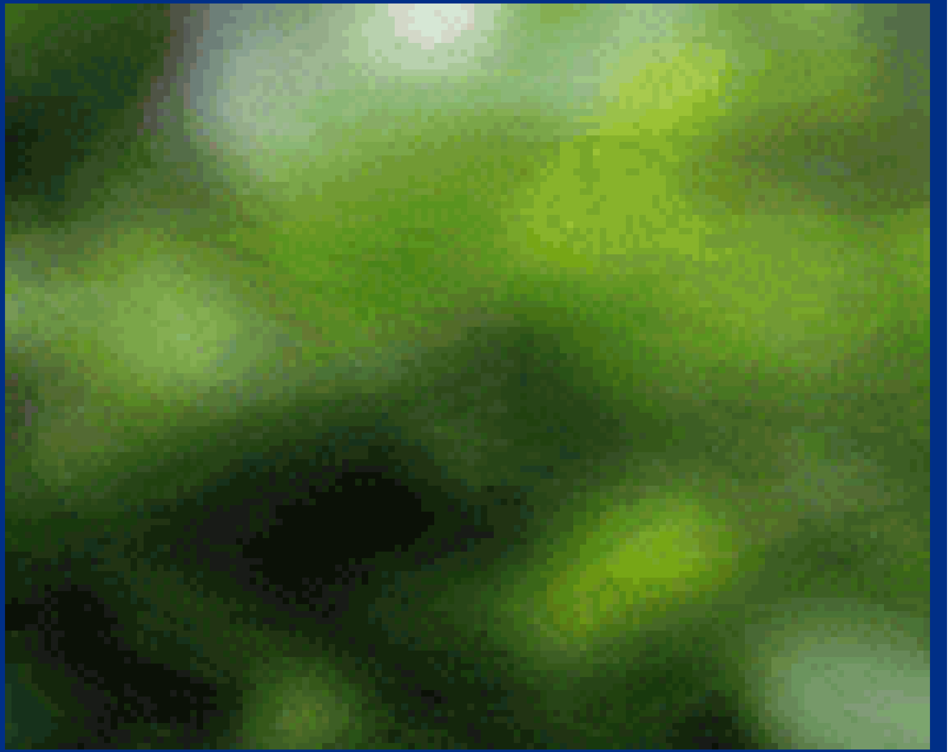

References

Alves, I.F. and C. Neves (2013), Estimation of the finite right endpoint in the Gumbel domain. Statistica Sinica, 24, pp.1811-1835.Beg, M.A. (1982), Optimal tests and estimators for truncated exponential families. Metrica, 29, 103-113.

Anderson, K.R. (1982), Robust earthquake location using M estimates, Phys. Earth Planet. Interiors, 30, 119 130.

Bardainne, T., N. Dubos-Sallée, G. Sénéchal, P. Gaillot and H. Perroud (2008). Analysis of the induced seismicity of the Lacq gas field (Southwestern France) and model of deformation, Geophysical Journal International 172, 1151–1162.

Cooke, P. (1979). Statistical Inference for Bounds of Random Variables. Biometrika, 66: 367-374

Cornell, C. A. (1994). Statistical Analysis of Maximum Magnitudes. In Johnston, A.C., Coppersmith, K.J., Kanter, L.R., and Cornell, C A. (eds), The Earthquakes of Stable Continental Regions — Vol. 1. Assessment of Large Earthquake Potential. California, Electric Power Research Institute, Palo Alto, pp. 5-1–5-27.

Davies, R., G. Foulger, A. Bindley and P. Styles (2013) ’Induced seismicity and hydraulic fracturing for the recovery of hydrocarbons.’, Marine and petroleum geology.

Dempsey, D., and J. Suckale (2017). Physics-based forecasting of induced seismicity at Groningen gas field, the Netherlands, Geophys. Res. Lett. 44, no. 15, 7773–7782, doi: 10.1002/2017GL073878.

Dixit, U.J. and P.N. Nasiri (2008), Estimation of parameters of a right truncated exponential distribution, Statistical Papers, 49, 2, pp.225-236.

Gentle, T.E. (1977), Least absolute values estimation: An introduction, Commun. Statist., B6, 313 328.

Gibowicz, S. J. and A. Kijko (1994). An Introduction to Mining Seismology. Academic Press, San Diego.

Gillian R. Foulgera, M.P. Wilsona, J.G. Gluyasa, B.R. Juliana and R.J. Daviesb (2018). Global review of human-induced earthquakes, Earth-Science Reviews 178 438–514.

References

González, P.J., K.F. Tiampo, M. Palano, P. Cannavo, and J. Fernandez, J., (2012). The 2011 Lorca earthquake slip distribution controlled by groundwater crustal unloading. Nat. Geosci. 5, 821–825. http://dx.doi.org/10.1038/ngeo1610.

Kijko, A. (2004). Estimation of the maximum earthquake magnitude $m_{\max}$, Pure Appl. Geophys. 161, 1-27.

Kijko, A., and G. Graham (1998). Parametric-historic procedure for probabilistic seismic hazard analysis Part I: estimation of maximum regional magnitude mmax. Pure and Applied Geophysics, 152(3), pp.413-442.

Kijko, A. and M. Singh (2011). Statistical tools for maximum possible earthquake magnitude estimation. Acta Geophysica, 59(4), pp.674-

Pisarenko, V. F., A.A. Lyubushin, V.B. Lysenko, and T.V. Golubieva (1996). Statistical Estimation of Seismic Hazard Parameters: Maximum Possible Magnitude and Related Parameters. Bull. Seism. Soc. Am., 86: 691-700.

Vlek, C. (2019). The Groningen Gasquakes: Foreseeable Surprises, Complications of Hard Science, and the Search for Effective Risk (Communication). *Seismo. Res. Lett. 90, 1-71-1077.*

Woodward, K.R. and S.R. Tierney (2017). Seismic hazard estimation using databases with bimodal frequency–magnitude behaviour. Underground Mining Technology 2017 – M. Hudyma & Y. Potvin (eds). © 2017 Australian Centre for Geomechanics, Perth, ISBN 978-0-9924810-7-0. Underground Mining Technology 2017, Sudbury, Canada.

Vermeulen, P. and A. Kijko (2017). More statistical tools for maximum possible earthquake magnitude estimation. Acta Geophys., DOI 10.1007/s11600-017-0048-3.

Next Maximum Event Magnitude using Statistical Methods

Groningen Mmax Workshop II (13-17 June, 2022)

Leo Eisner, Ngoc-Tuyen Cao, Seismik s.r.o.

Outline

Seismik

- Motivation
  - Prior art
  - Why alternative
- Theory
  - Upper Limit Record Breaking - UL
  - Next Expected Record Breaking - NERB
- Application
  - Gas production
  - Hydraulic fracturing (shale)
- Discussion, Conclusions and teaser

Motivation – Traffic Light System

- TLS open questions:

  - Magnitude vs ground shaking
  - How to set the orange/red thresholds?
  - If such threshold is reached, when is it possible to continue?
    - How to handle long term injections such as SWD, geothermal production, production of fluids/gas?
  - What is the strongest event / Maximum Magnitude (M_{Max}) which could be generated?

Prior art – estimating Mmax, M0

- McGarr, 1976

$$\sum M_{TOT} = K\mu|\Delta V|$$

  - ▶ Assumption stress field is adjusted after volume change only through seismic motion

- M_{Max} estimation (e.g. statistical method of Shapiro et al., 2010 or Hallo et al., 2014)

  - ▶ Need *a priori* data:
    - — Historical seismic data, we need apriori estimate b-value
      - • No historical seismicity in some areas
      - • b-value can be high – but that is not valid to infinitely low magnitudes
    - — What part of volume to include:
      - • Which volume to assign? all/separate stages?
  - ▶ Do not account for releasing pre-existing seismic stress (triggering, not inducing)

Seismic hazard assessment in Mines

Mining :

- Induced seismicity common and dangerous
- Need to re-enter mines after large seismic events
- Induced seismicity hazards are required to build underground structures to withstand shaking

- Methodology of hazard assessment based statistics → no physical model
- Mendecki et al. (2012, 2013, 2016) → initially formulated for the Potency (seismic moment divided by shear modulus)
- Prediction of M_{Max} from the earlier record breaking events, M_{Maxo} and the differences between largest observation $\Delta M_{Maxo - i}$
- Two estimates of the next record breaking event:
  - ▶ Upper Limit to the next Record-Breaking event (0 probability it will be exceeded under steady state assumption)
  - ▶ Next Expected Record-Breaking event (most likely next record breaking event)

Estimation of M_{Max} : Upper Limit to the next largest event

Order Statistics (Cooke, 1979):

- Systems driven steadily over long periods
- Record breaking events will be increasing function with decreasing gradient
  - $M_{UL} = M_{Maxo} + (M_{Maxo} - M_{Maxo-1})$
- If not steady – gradient may not decrease – we need to consider previous record breaking events and estimate the upper limit
  - Arbitrary probability distribution of variables (record breaking events)

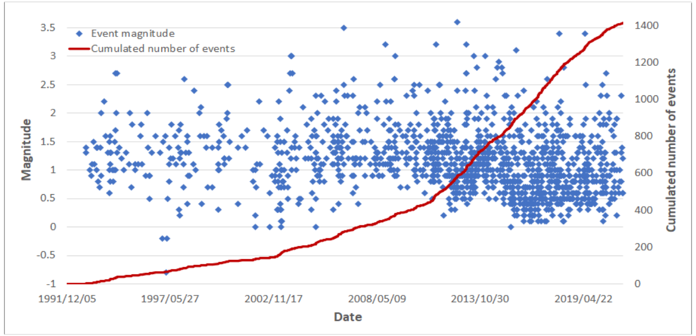

- 2.4 (1991)
- 2.7 (1994)
- 3.0 (2003)
- 3.5 (2006)
- 3.6 (2012)

Estimation of M_{Max} : Upper Limit to the next largest event

Seismik

- **Empirical distribution function based on Order Statistics (Cooke, 1979):**

$$\begin{cases} F_{M_{Maxo}}(M) = i/n, & \text{for } M_{(i)} \leq M \leq M_{(i+1)} \\ F_{M_{Maxo}}(M) = 0, & \text{for } M < M_{Min} \\ F_{M_{Maxo}}(M) = 1, & \text{for } M \geq M_{Maxo} \end{cases}$$

$$dM = M_{i+1} - M_i$$

Decreasing weight of previous records

- **Estimator of the Upper Limit to the next largest event:**

$$M_{UL} = M_{Maxo} + \int_{M_{Min}}^{M_{Maxo}} F^n_{M_{Maxo}}(M)dM = M_{Maxo} + \sum_{i=1}^{n-1} \left(\frac{i}{n}\right)^n \left[M_{(i+1)} - M_{(i)}\right]$$

$$\Delta M_{Max} = 2\Delta M_{Maxo} - \sum_{i=0}^{n-2} \left[\left(1 - \frac{i}{n-1}\right)^{n-1} - \left(1 - \frac{i+1}{n-1}\right)^{n-1}\right] \Delta M_{Maxo-i}$$

Where: n = number of observed jumps

$\Delta M_{Maxo\text{-}i}$ = observed jumps in M

$$M_{RB} = M_{Maxo} + \Delta M_{Max}$$

Estimation of M_{Max}: Record Breaking event – no probability

- Breaking theory:
  - Introduced by Tata (1969) for events that occur randomly
  - Van Aalsburg (2010) or Yoder (2010): application to global earthquakes
  - Mendecki et al. (2012, 2013, 2016): application to induced seismicity in mines

- Record breaking event = event larger (or smaller) than all previous events
  - In a sequence of *independent & identical distributed* variable M_j, $j = 1, 2, \dots, n$, a record breaking high occurs at k if $M_k = max_{j \le k}(M_j)$
  - Probability that a record high (or low) occurs at j is $1/j$

  - Function of the differences of the record breaking events
  - Only the first few differences are significant in estimating the Upper Limit
  - Valid for any underlying probability distribution
  - $\Pr(M_{UL} < M) = 0$

Estimation of M_{Max} : Record Breaking event

- Mendecki et al. (2016) assumed Upper Truncated distribution to adjust the Next Expected Record Breaking event:

  ▸ With $N(\geq M)$, the number of events with magnitude greater than :

  $$N(\geq M) = 10^{\alpha}\left(M^{-\beta} - M_{Max}^{-\beta}\right) \quad \Leftrightarrow \quad \text{Truncated Gutenberg-Richter}$$

  ▸ Probability Density and the Survival Function, with $\Pr(\geq M_{Max}) = 0$:

  $$f(M) = \frac{\beta M^{-\beta-1}}{\left(M_{Min}^{-\beta} - M_{Max}^{-\beta}\right)} \quad ; \quad \Pr(\geq M) = \frac{M^{-\beta} - M_{Max}^{-\beta}}{M_{Min}^{-\beta} - M_{Max}^{-\beta}}$$

  ▸ Using M_{Max} previously determined:

  $$M_{NERB} = \frac{\beta \times \left(M_{Max}^{1-\beta} - M_{Maxo}^{1-\beta}\right)}{(1-\beta)\left(M_{Maxo}^{-\beta} - M_{Max}^{-\beta}\right)} \text{ for } \beta \neq 1 \text{ ; } \quad M_{NERB(k)} = \frac{\ln\left[M_{Max}/M_{NERB(k-1)}\right]}{M_{NERB(k-1)}^{-1} - M_{Max}^{-1}} \text{ for } \beta = 1$$

  ▸ M_{NERB} is not particularly sensitive to changes in $\beta \sim b - value$

Estimation of M_{Max}

Seismik

- **Statistical methods to estimate M_{Max}**
  - work for whatever the type of magnitude: M_W or $M_{L,}$ but must be consistent
  - can be calculated and updated continuously
  - independent of injection volumes

Record Breaking Magnitude (M_{RB}):
  - Record Breaking Theory, Order Statistics of jumps between record-breakings, upper limit of next record-breaking

Next Expected Record Breaking Magnitude (M_{NERB}):
  - Adjustment M_{RB}, assessing Upper Truncated distribution

- **Case study:**
  - Long-term injections (Groningen gas field)
  - Short-term hydraulic fracturing (Cuadrilla)

Case Study

GRONINGEN GAS FIELD

Groningen – Seismic event catalog

- > 30 years of monitoring
  - KNMI seismic catalog of induced events (modified by Bommer, June 2021) : > 1700 events, M_{Maxo} = 3.6 in August 2012
  - Completeness has changed several times with the expansion of the monitoring network, in particular after 2011

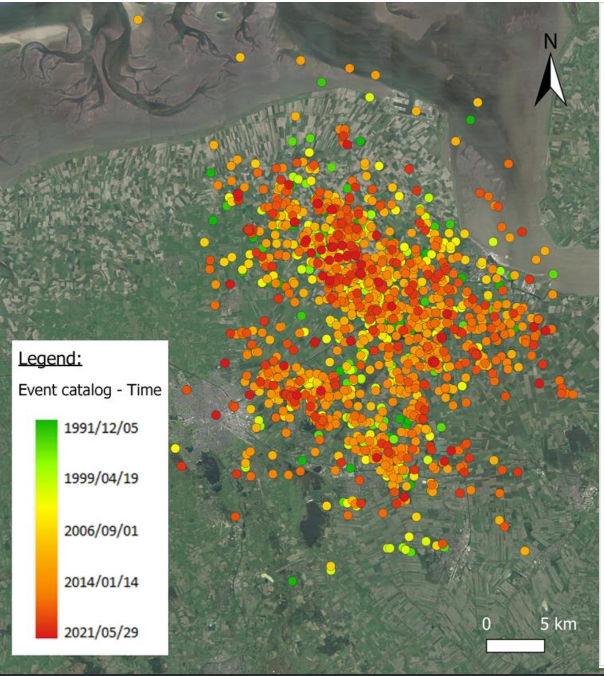

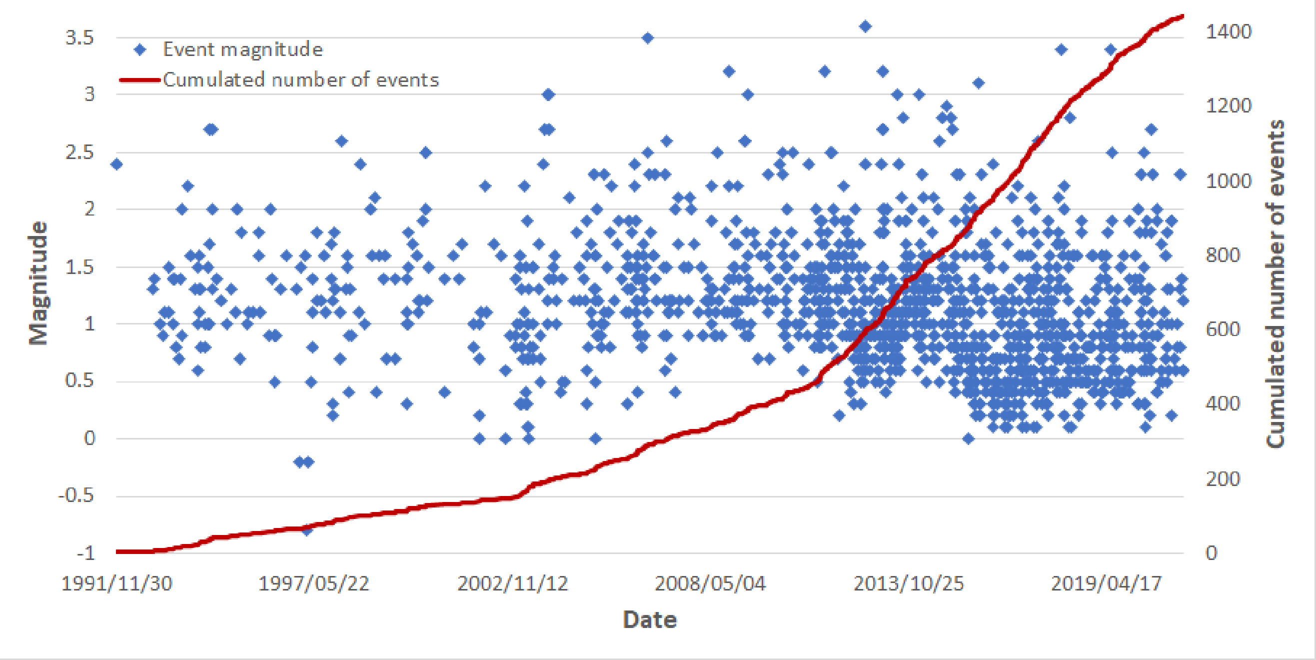

Groningen – Gutenberg-Richter Plot

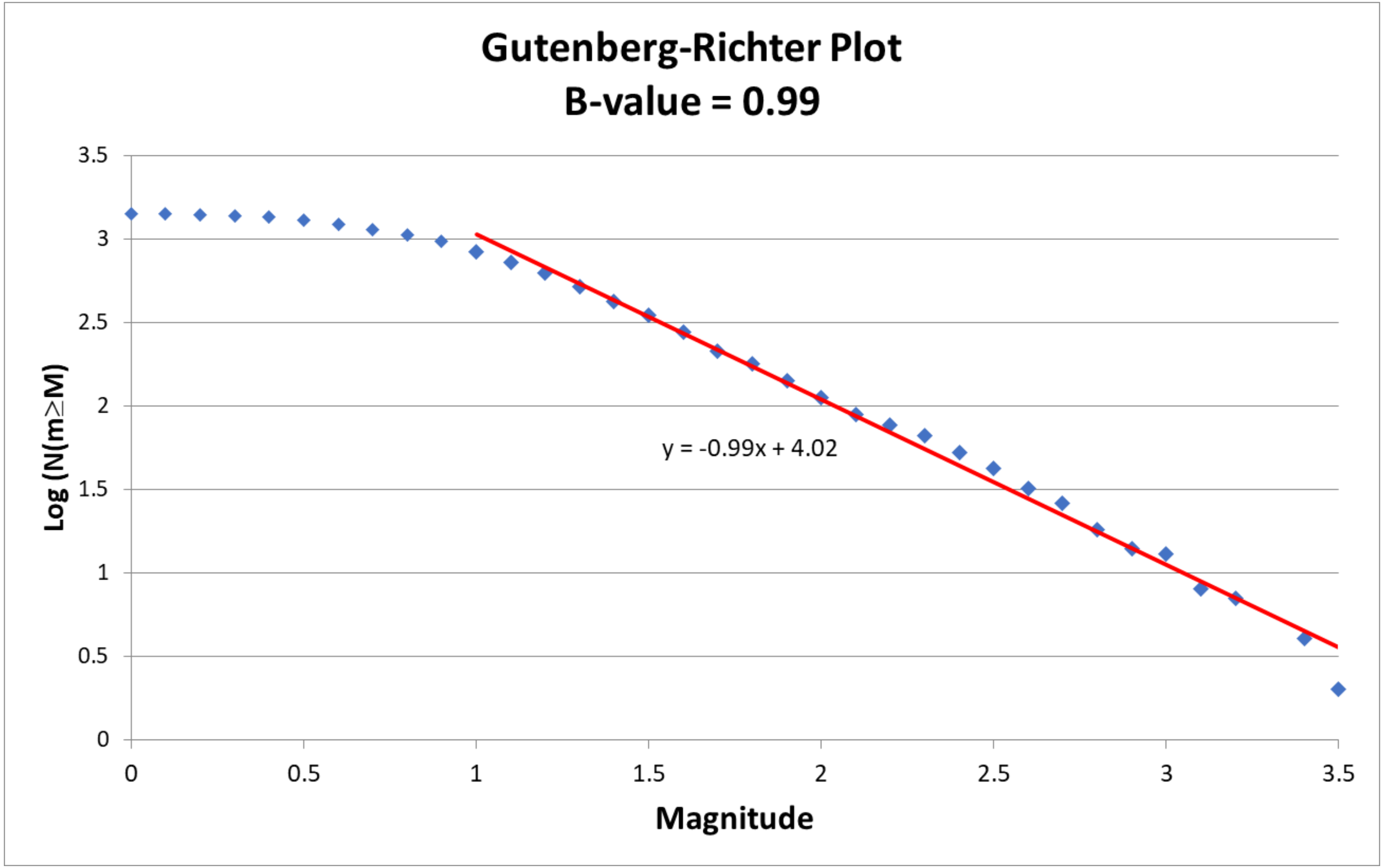

Groningen – Estimation of next M_{Max}

- Taking into account only events with M ≥ 0.9, 1.4 and 2.0, b-value from 0.5 to 2.0

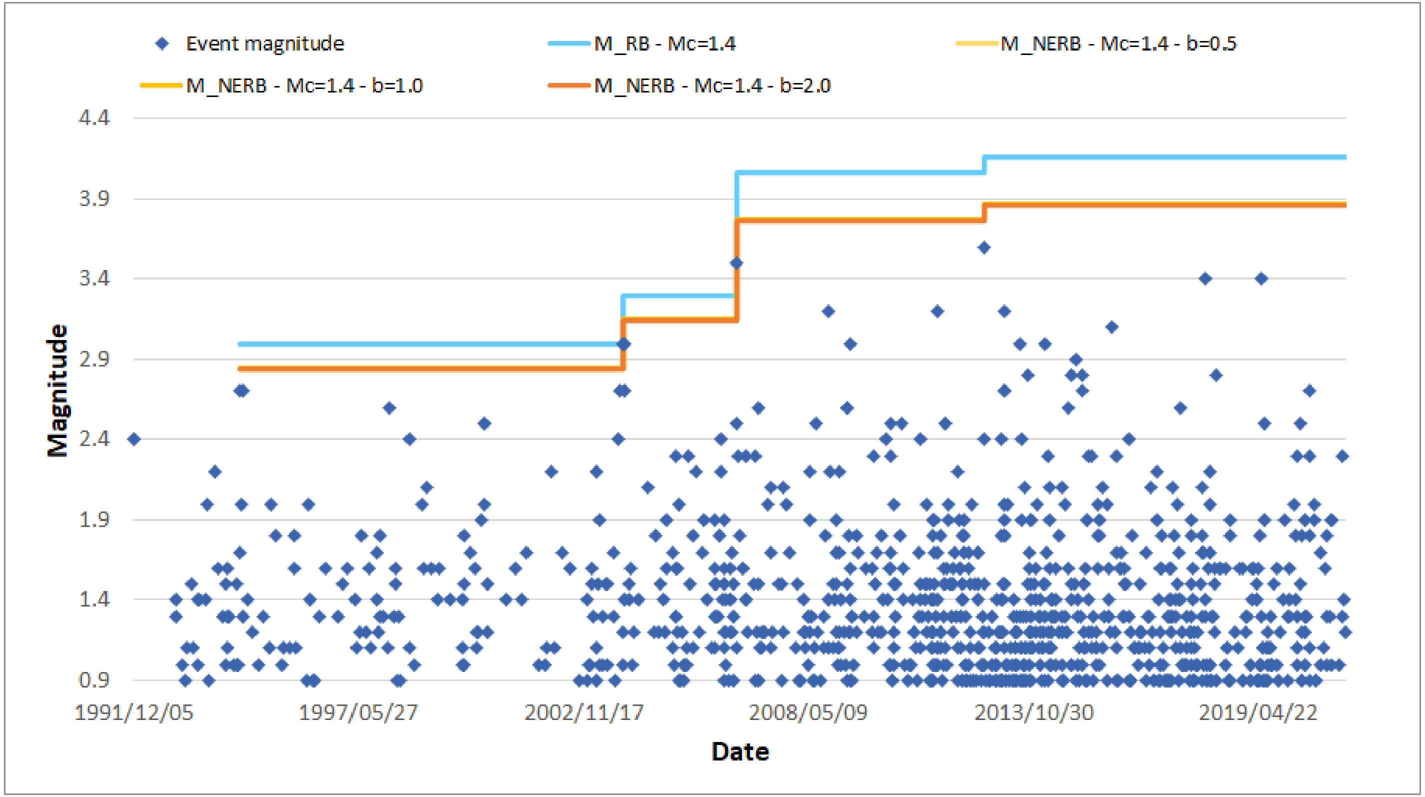

M_{RB}:

- 2 OK
- 1 underestimate by 0.2
- Current estimate at 4.2

M_{NERB} :

- not sensitive to the b-value
- 2 underestimates, 1 over
- Current value at 3.9

Groningen – M_{Maxo} vs Predicted M_{Max}

Seismik

- **Maximum Observed Magnitude M_{Maxo} vs Predicted M_{Max}**

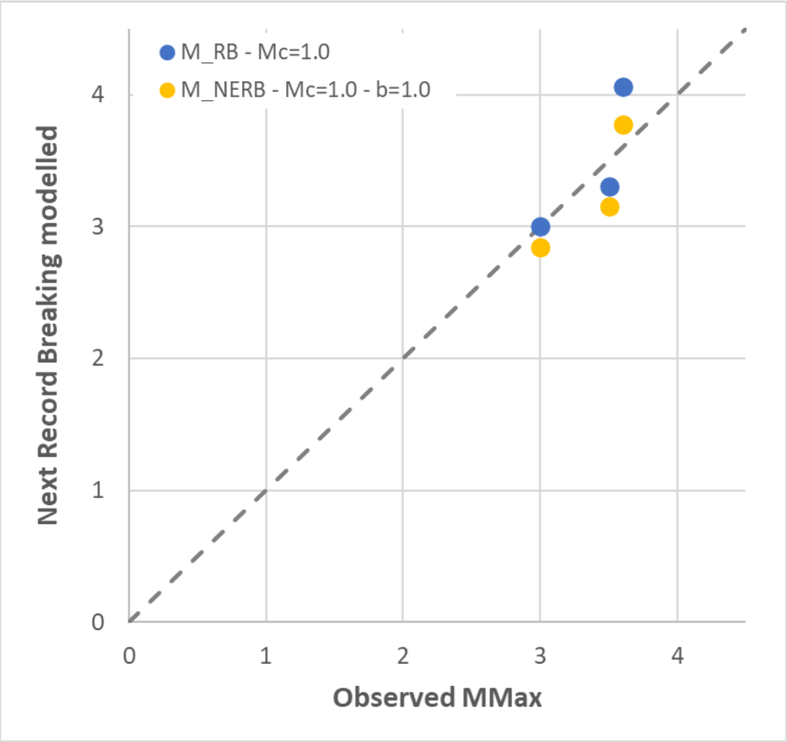

M_{RB}

- Overestimates are not significant – only 0.1 – magnitude error?
- We are missing events before 1991

M_{NERB}

- close to true record breaking

Groningen – M_{Maxo} vs Predicted M_{Max}

Seismik

If we start to monitor in 1992…

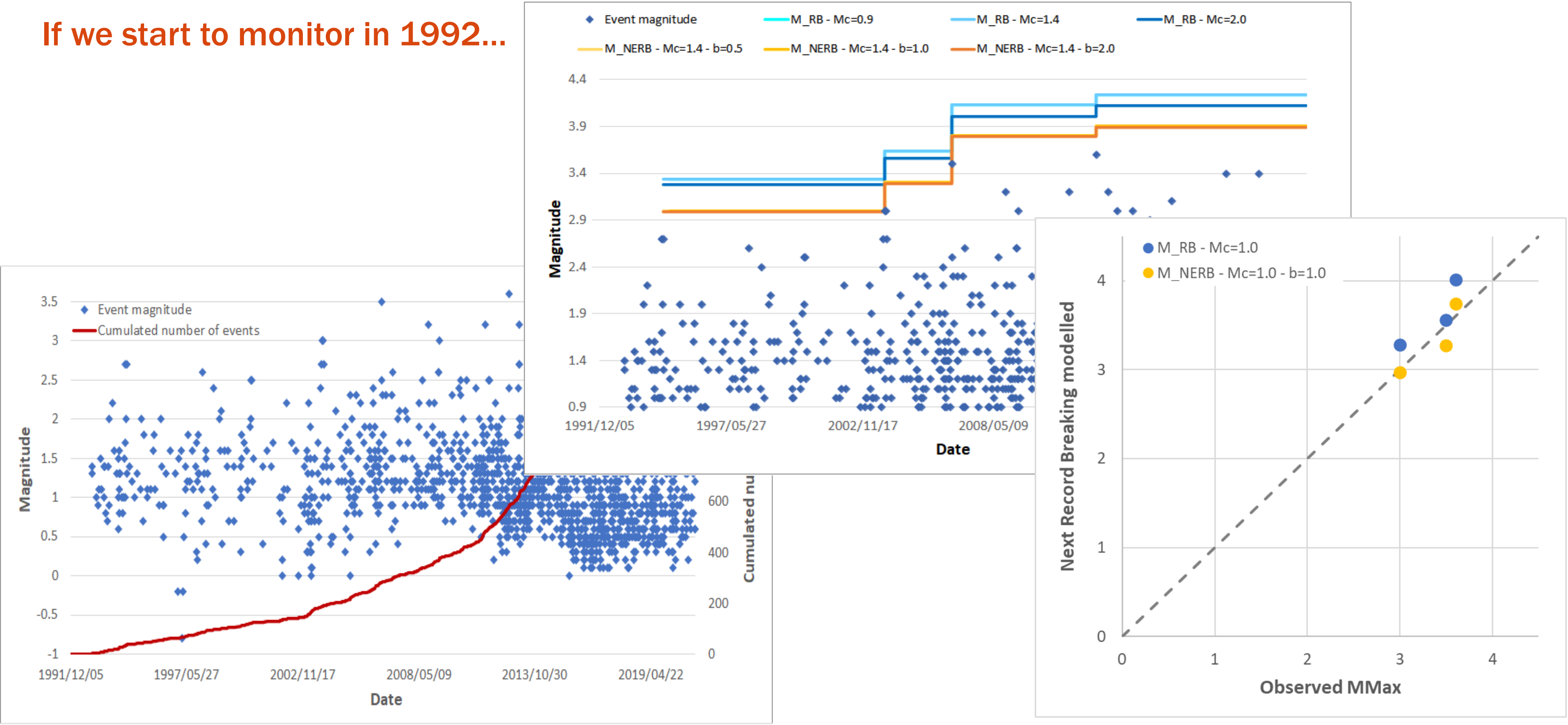

SALT WATER DISPOSAL

National center catalogues

Long term injection since 2012 into very a large reservoir, two areas of injection activity, and seismicity. Events with similar origin times between local network and national center catalogues + events which were probably missed by local network → 994 events (down from >1500 in the area)

- before March 2018: all the magnitude in National center catalog were Local Magnitude, M_L

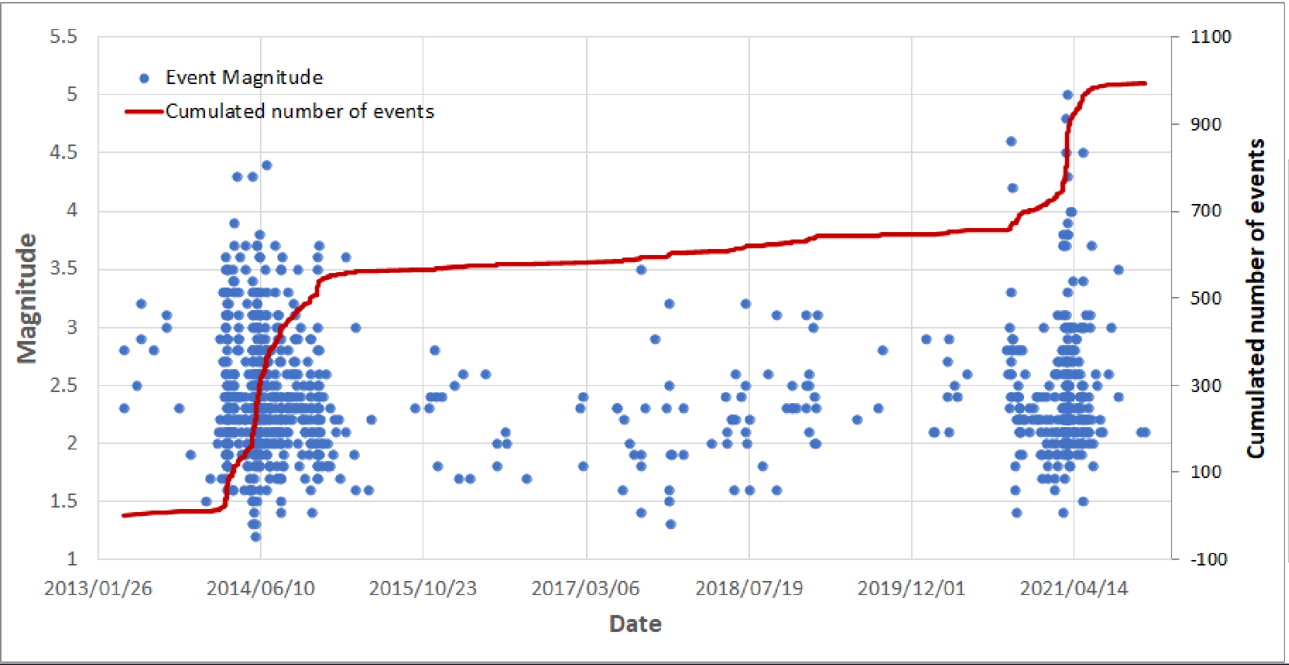

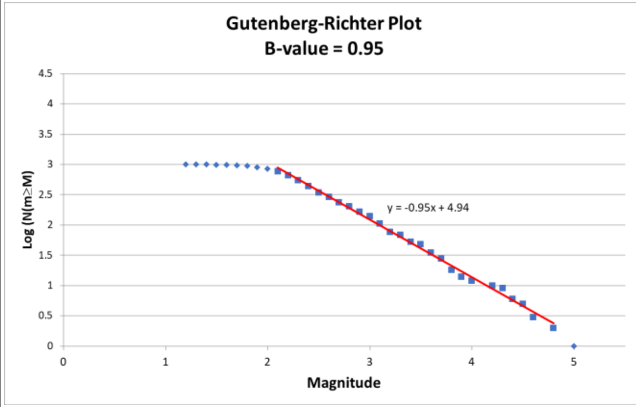

Estimation of next M_{max} for National center catalogue

Seismik

- Using national center catalog & Taking into account only records with M ≥ 2.5, b-value = 0.95

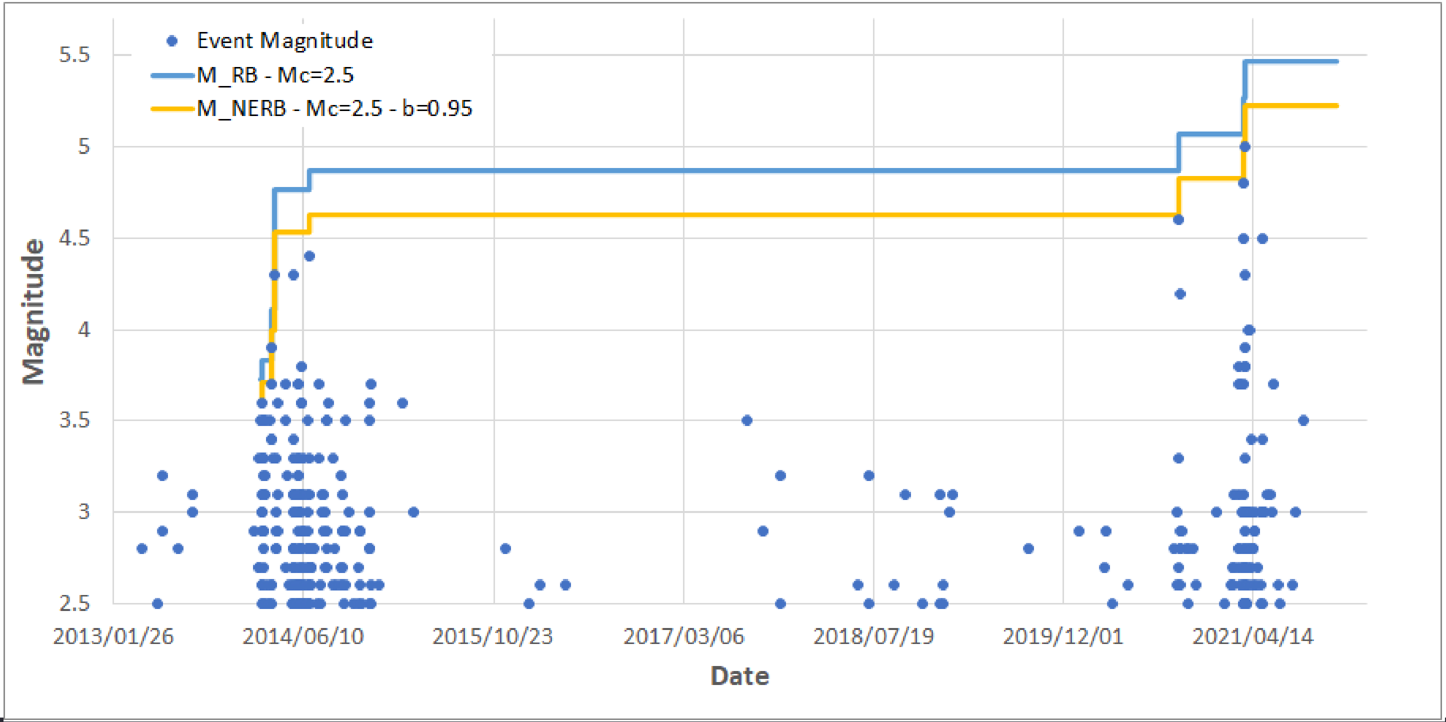

Estimation of next M_{Max}

Seismik

- Using National center catalog & Taking into account only records with M ≥ 2.5, b-value = 0.95
  - Good estimation of the 3 first Record-Breakings
  - Underestimation of the magnitude of the ML 4.3 event

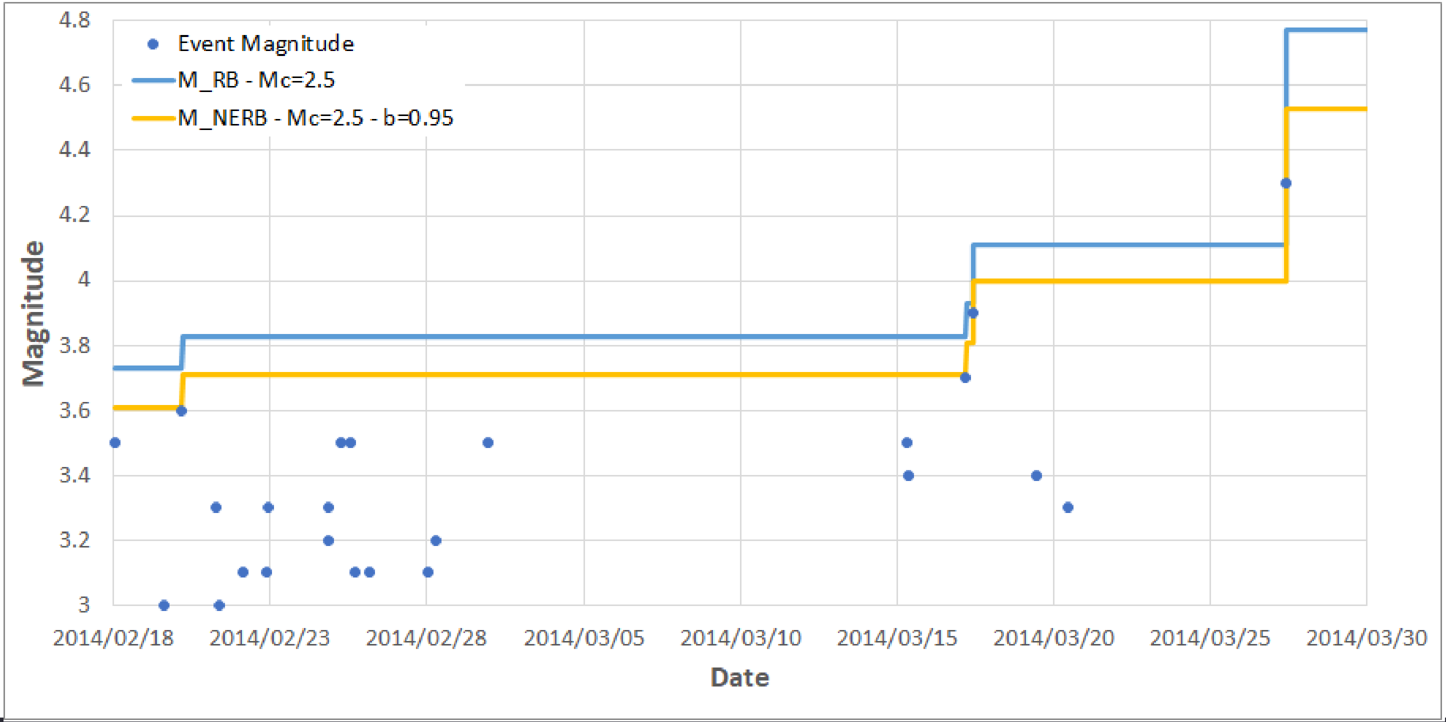

Estimation of next M_{Max}

Seismik

- **Using National center catalog & Taking into account only records with M ≥ 2.5, b-value = 0.95**
  - ▶ Good estimation of the Record-Breakings from 2020-2021

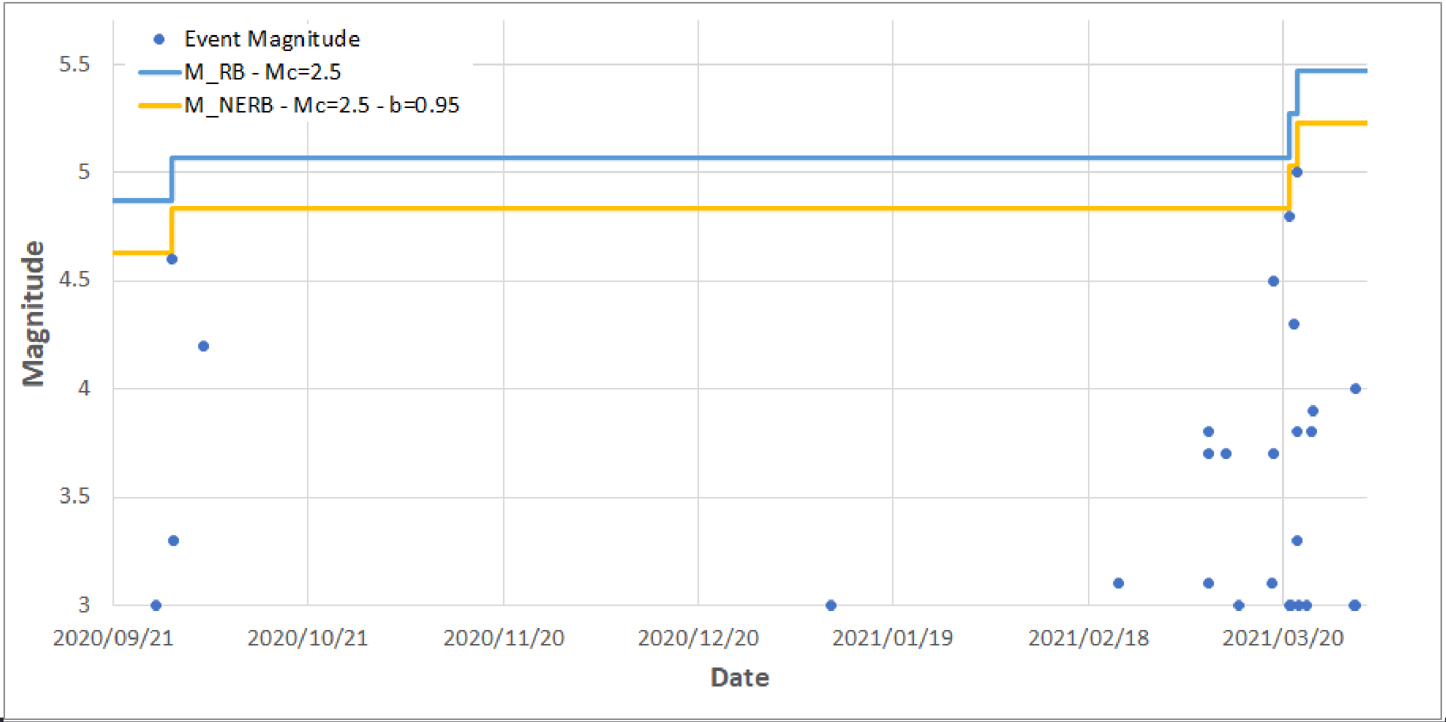

M_{Maxo} vs Predicted M_{Max}

Maximum Observed Magnitude M_{Maxo} vs Predicted M_{Max}

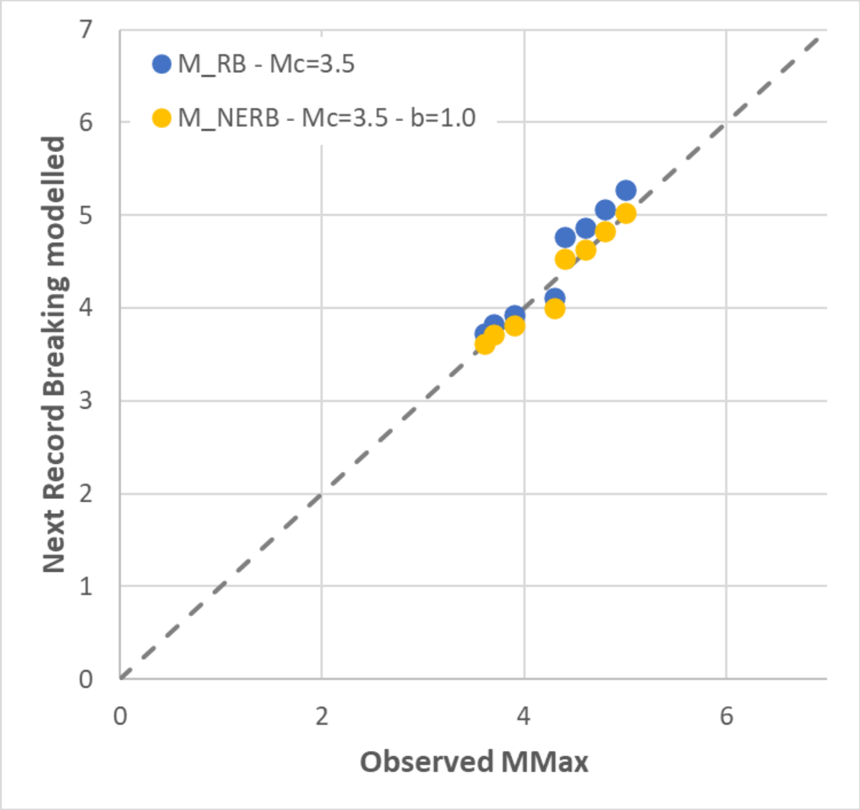

- Good estimate of large events
- One out 7 underestimate by 0.2
- Next expected breaking record is giving very good prediction

Case Study

CUADRILLA - HYDRAULIC FRACTURING - PRESTON NEW ROAD

Cuadrilla – BGS Seismic event catalog

Event catalog from BGS website

- 1 year of monitoring, ~ 200 events, M_{Maxo} = 2.9, in August 2019
- 2 periods of hydraulic fracturing (October-December 2018 & August-September 2019)
- Changes of the monitoring network between the 2 operations

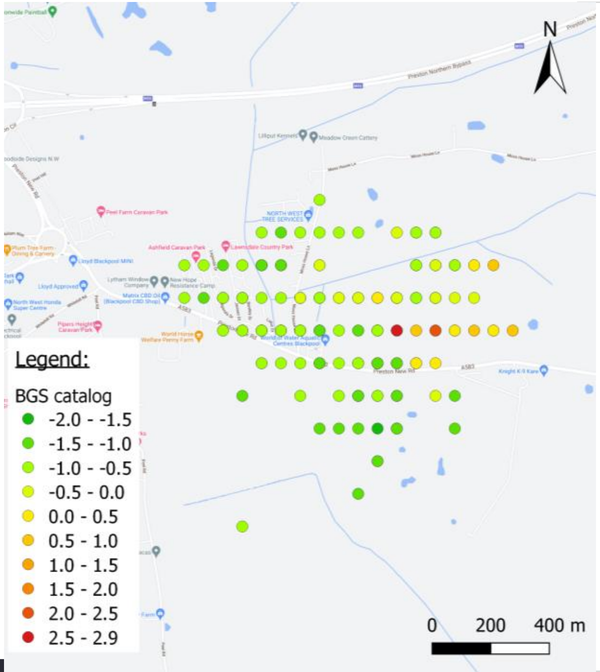

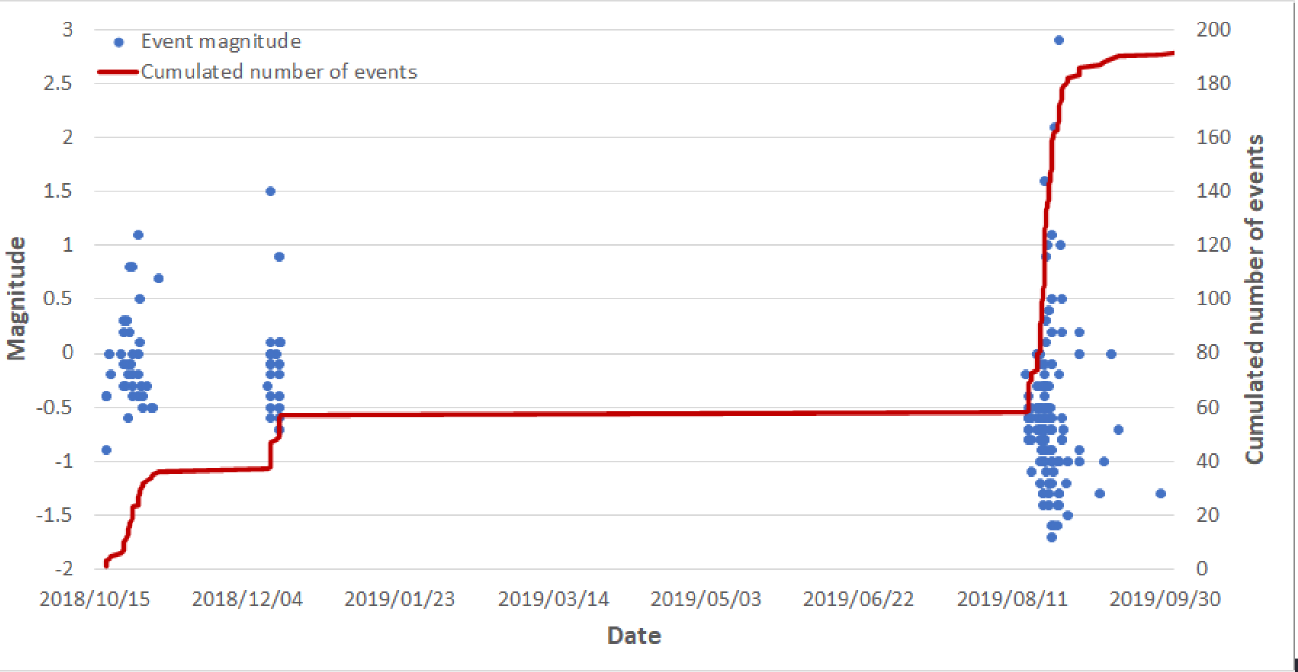

Cuadrilla – BGS – Gutenberg-Richter Plot

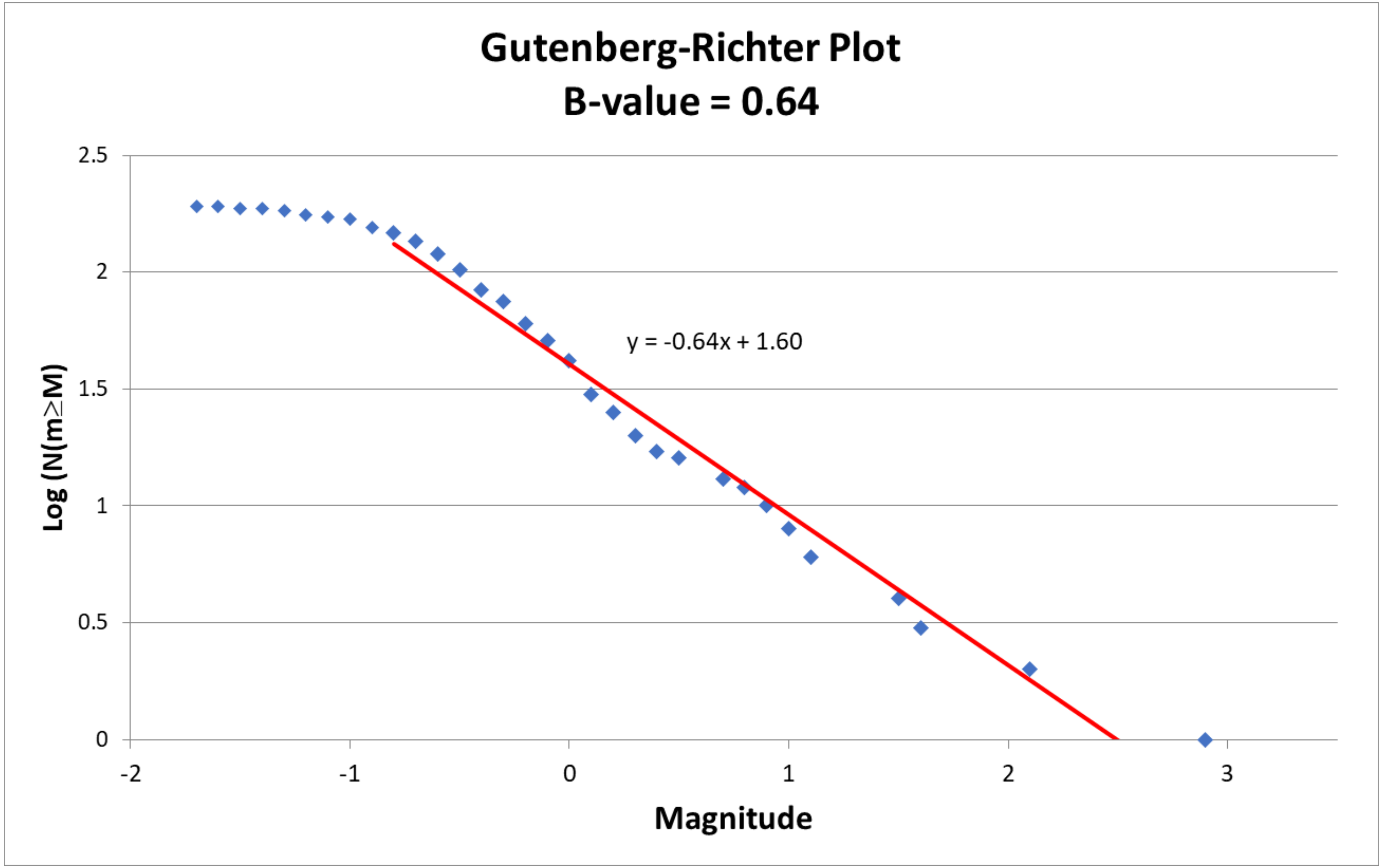

Cuadrilla – BGS – Estimation of next M_{Max}

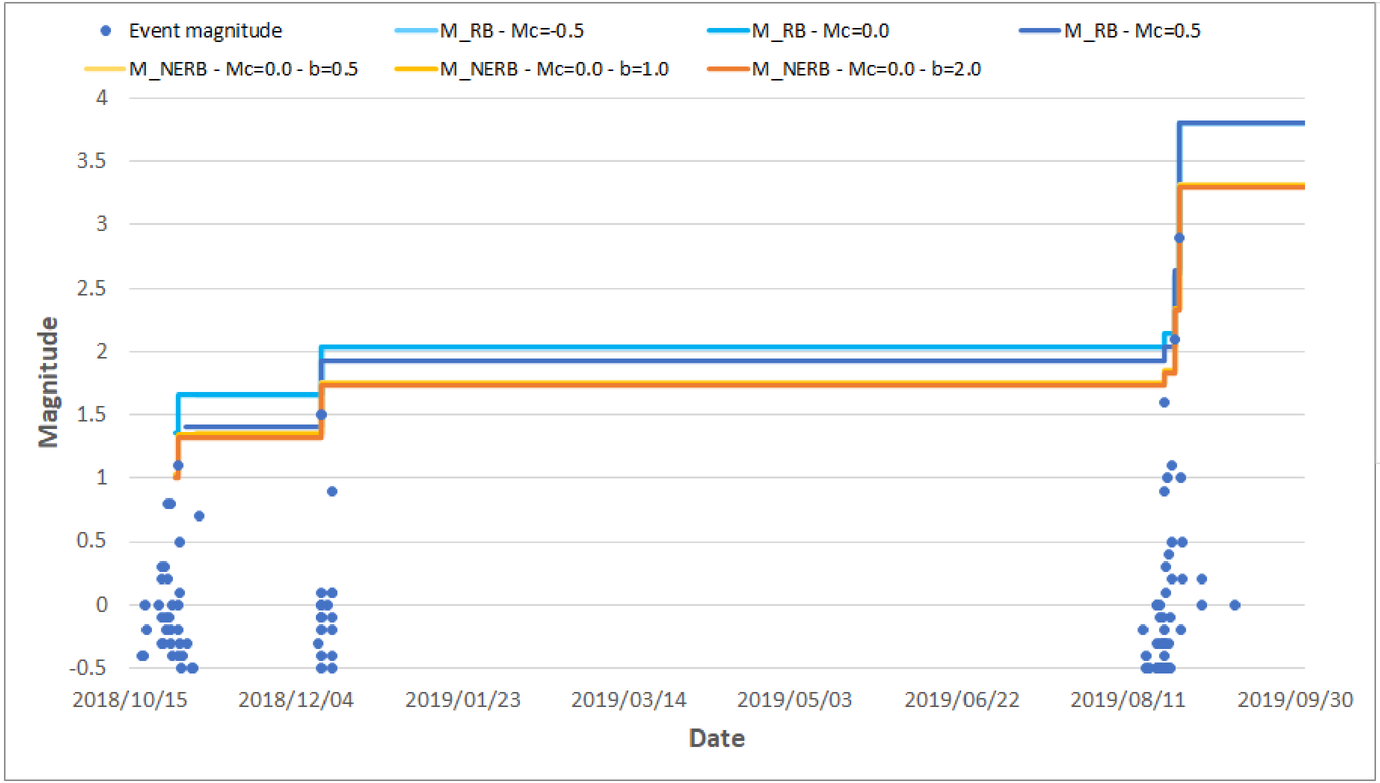

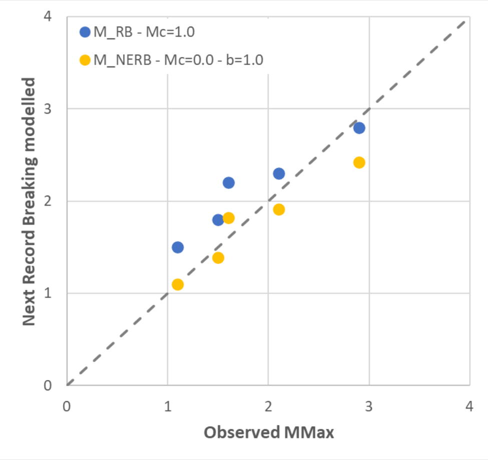

Cuadrilla – BGS – Estimation of next M_{Max}

2018 stimulation

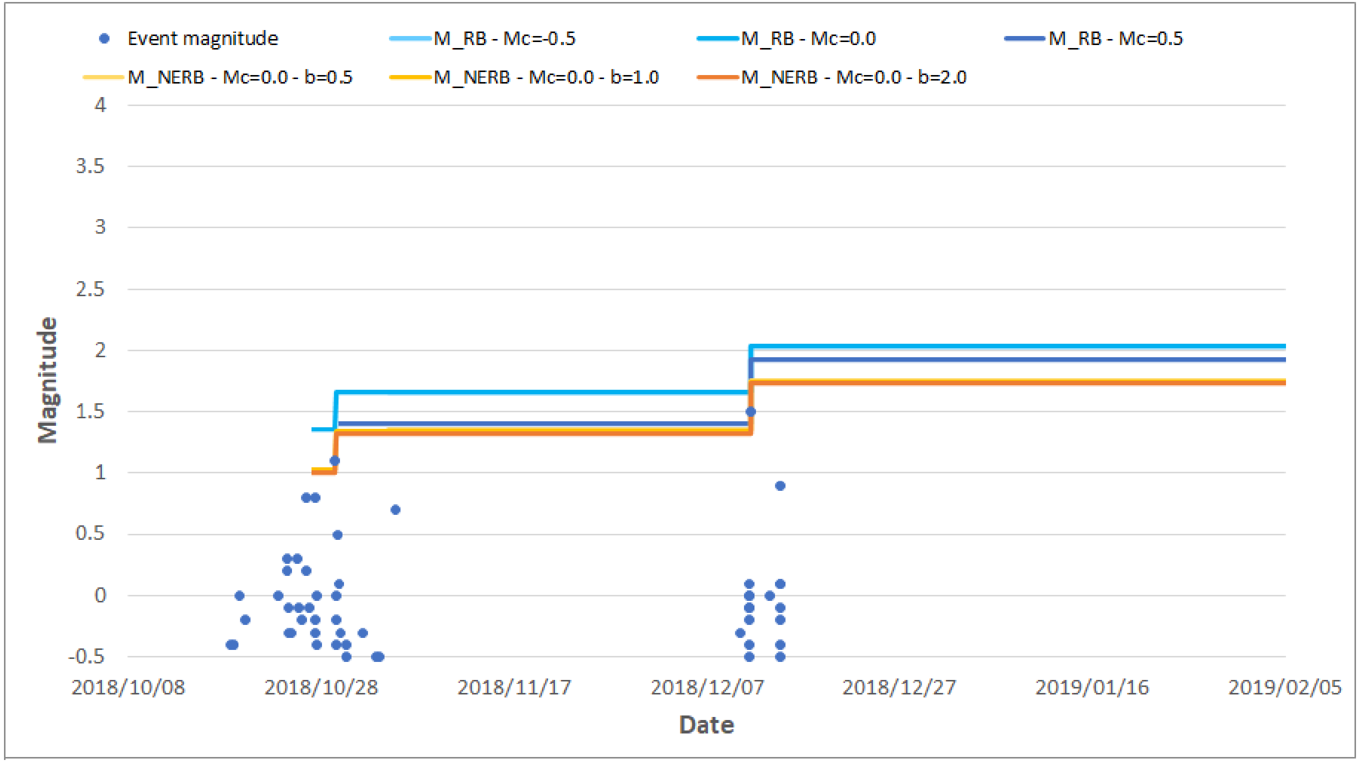

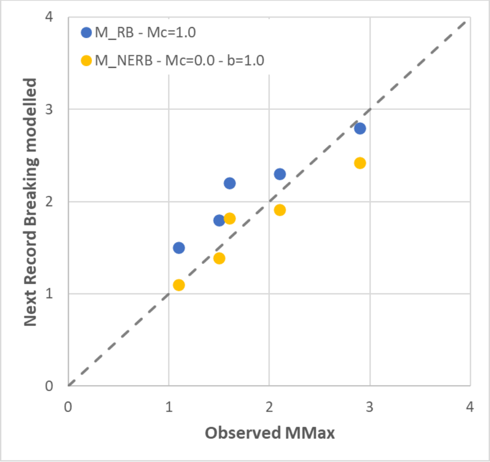

Cuadrilla – BGS – Estimation of next M_{Max}

2019 stimulation

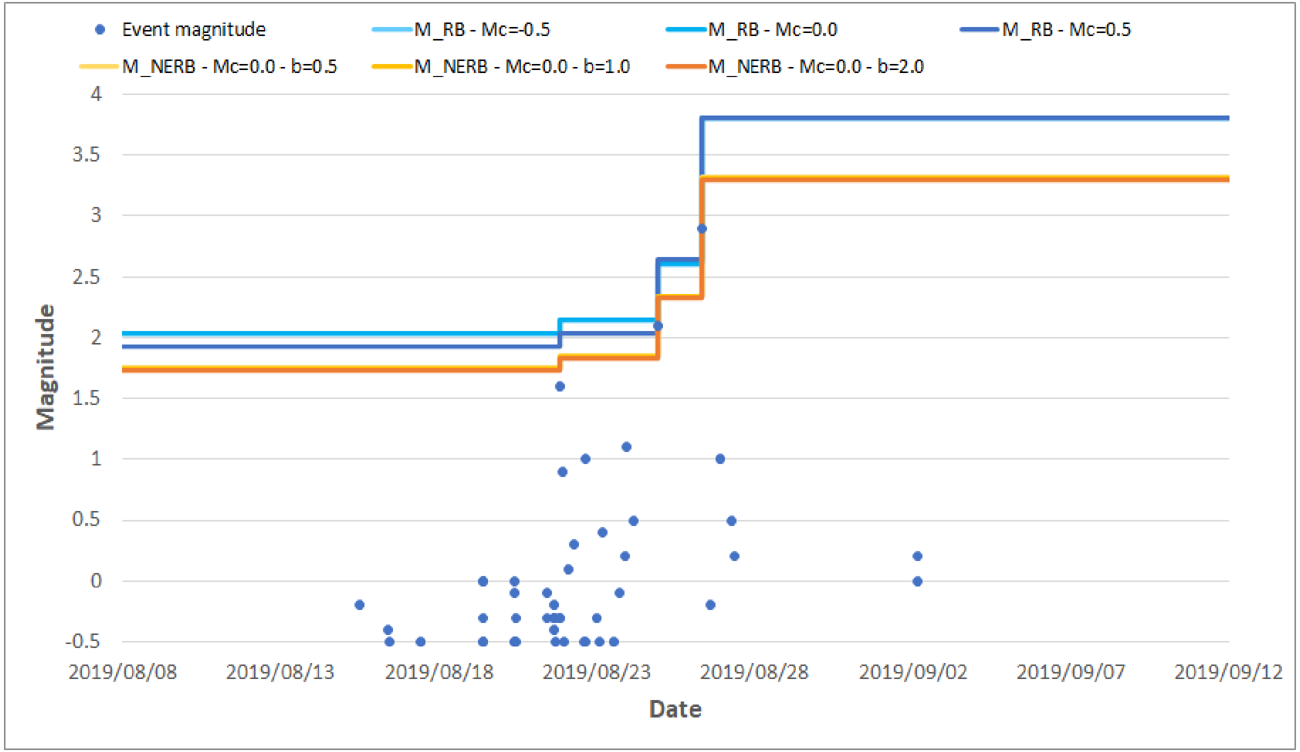

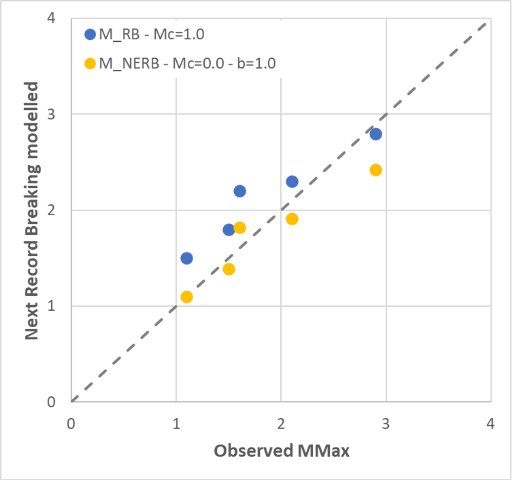

Cuadrilla – extending catalogue to downhole

Seismik

Magnitude issues:

- Downhole event M_W for the majority of events that were not detected by the surface array, combined with M_L provided by the surface array for the larger events
- M_W from downhole stations, lower than the one determined from surface stations
- Limited number of events to build consistent relationship between M_W & M_L

- PNR-1Z
  - Surface stations: detected 54 events, minimum M_L = -0.8
  - Downhole array: detected > 39,000 events, minimum M_W = -3.0

- PNR-2
  - Surface stations: detected 125 events, minimum M_L = -1.5
  - Downhole array: detected > 55,000 events, minimum M_W = -2.5

  + M_W not consistent with PNR-1z stimulations
  + some events not recorded – as strongest event of M_L=2.9 (recording interruptions)

Cuadrilla – OGA Seismic event catalog

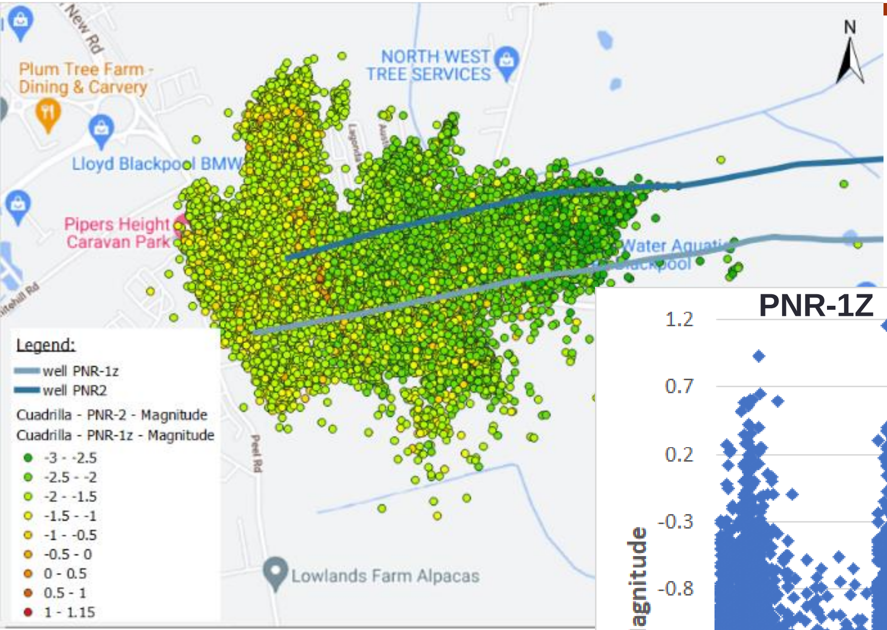

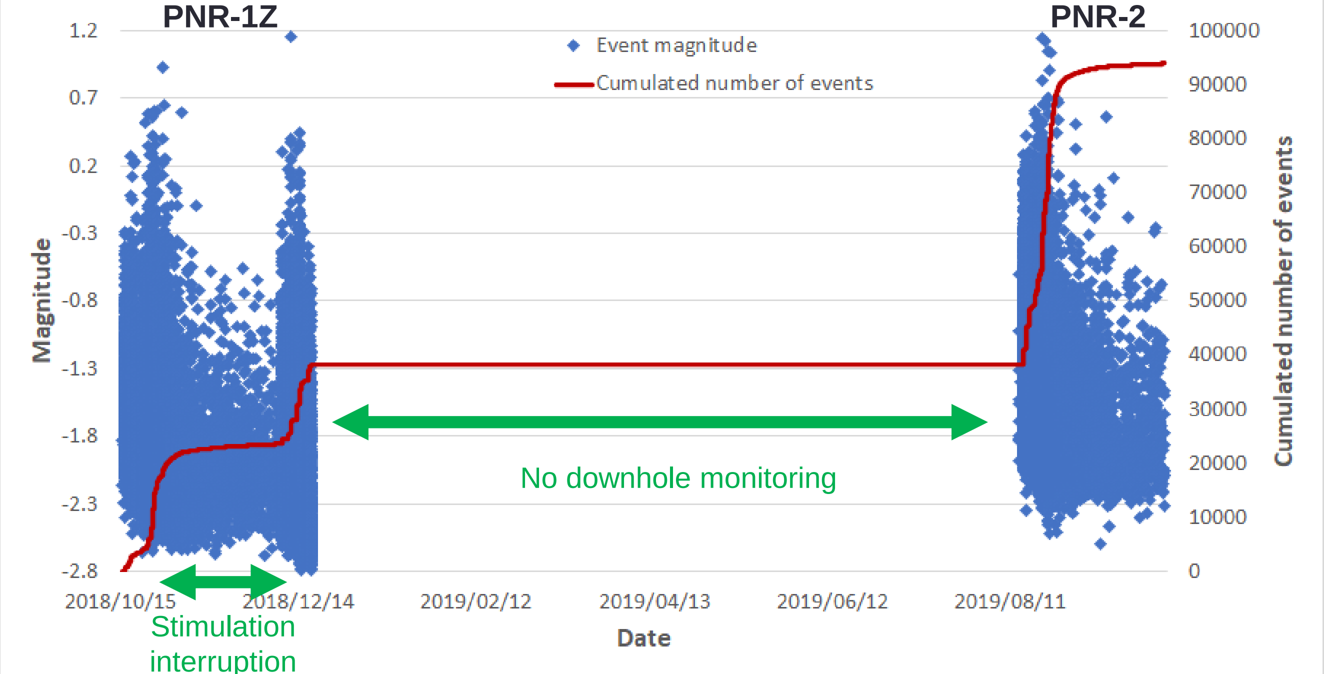

Comparison between BGS and OGA catalogs

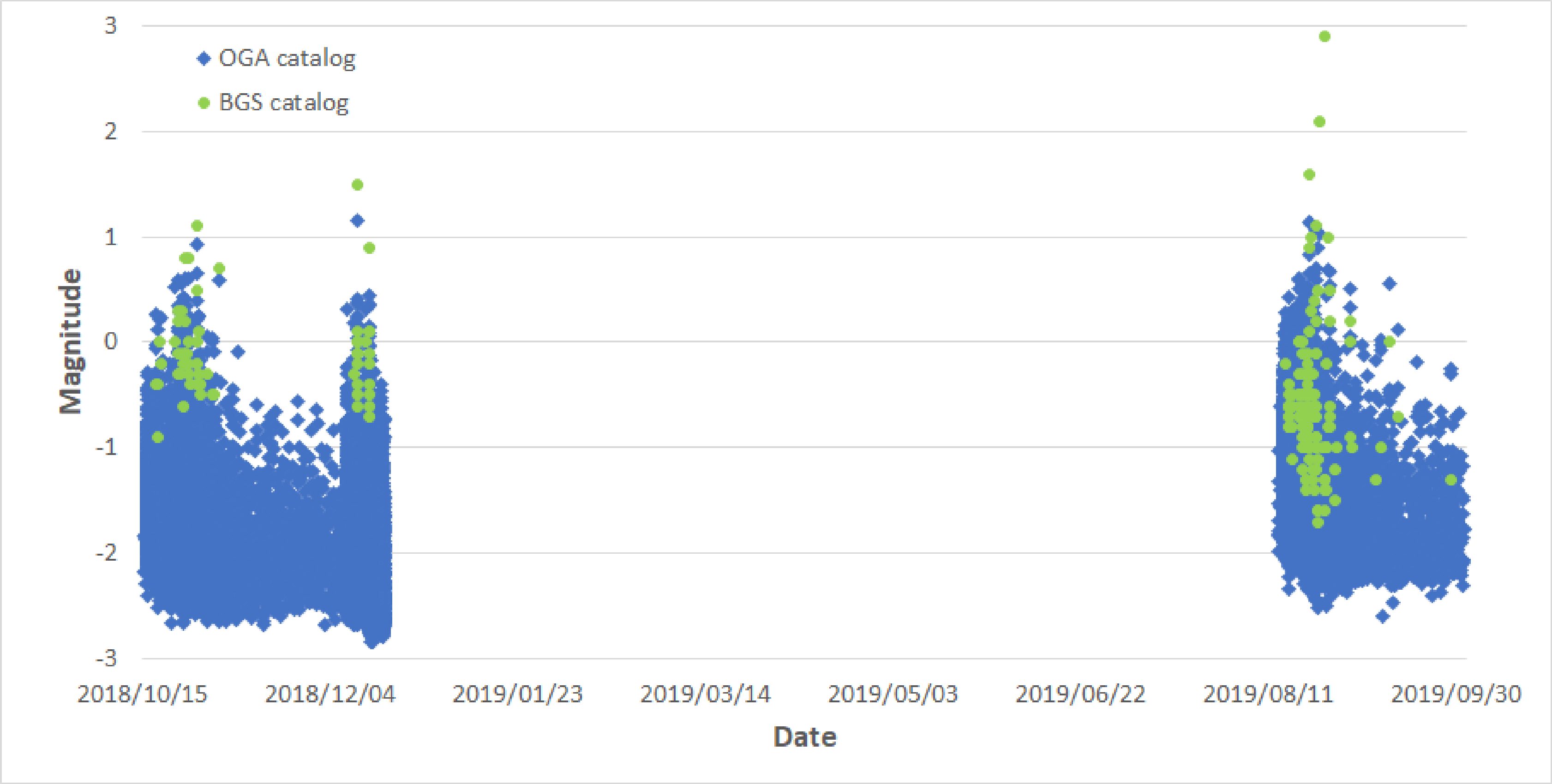

Cuadrilla – OGA – Gutenberg-Richter Plot

Seismik

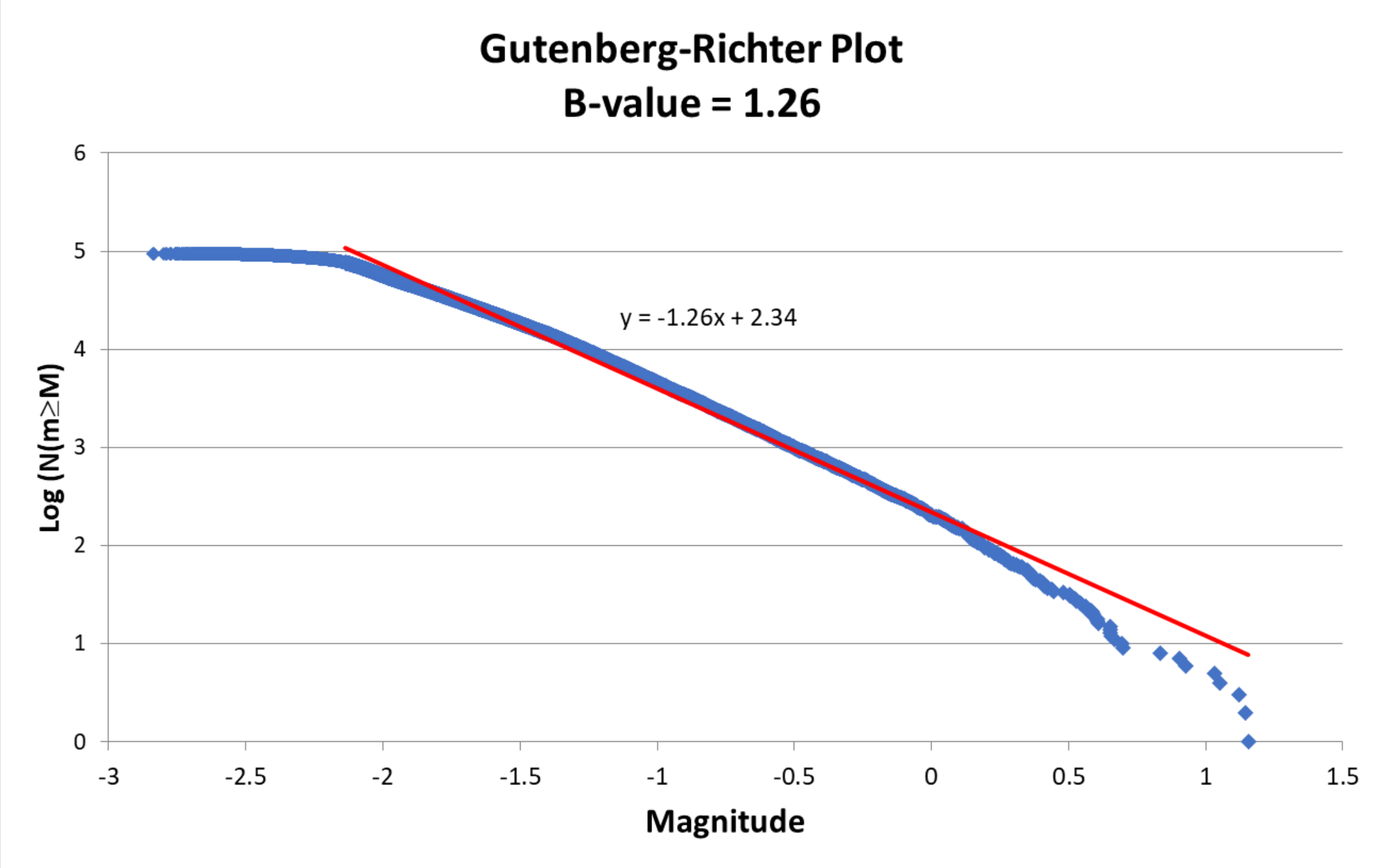

Cuadrilla – OGA – Estimation of next M_{Max}

Taking into account only events with M ≥ -1.5 to M ≥ 0.0, b-value from 0.5 to 2.0

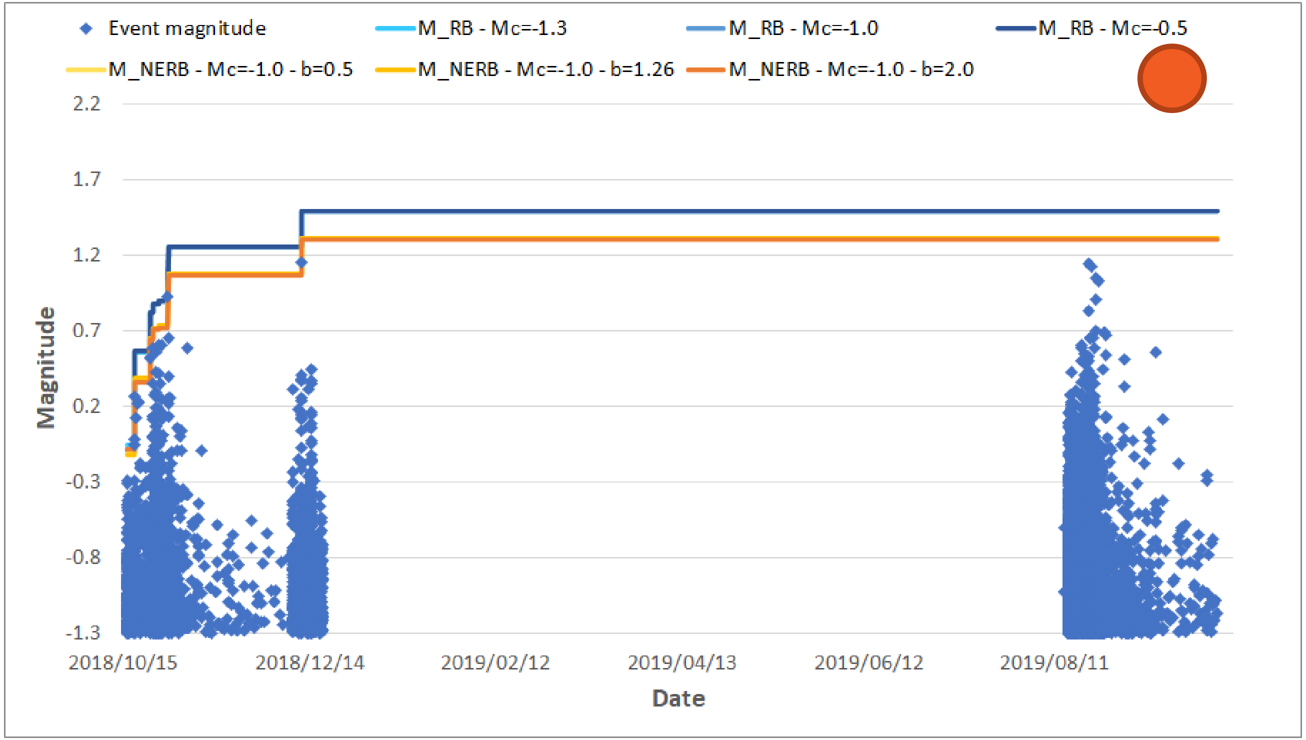

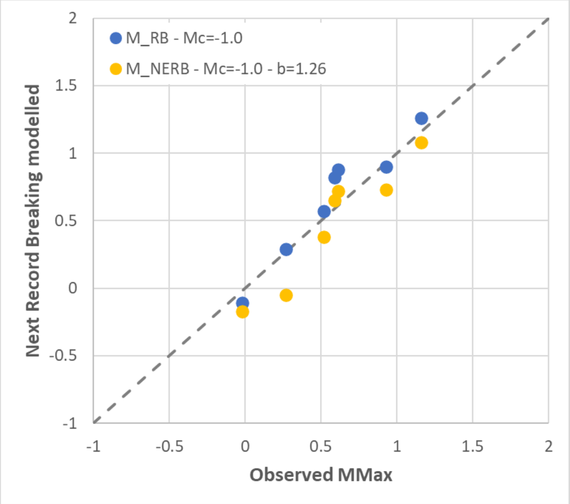

Cuadrilla – OGA – Estimation of next M_{Max}

- Taking into account only events with M ≥ -1.5

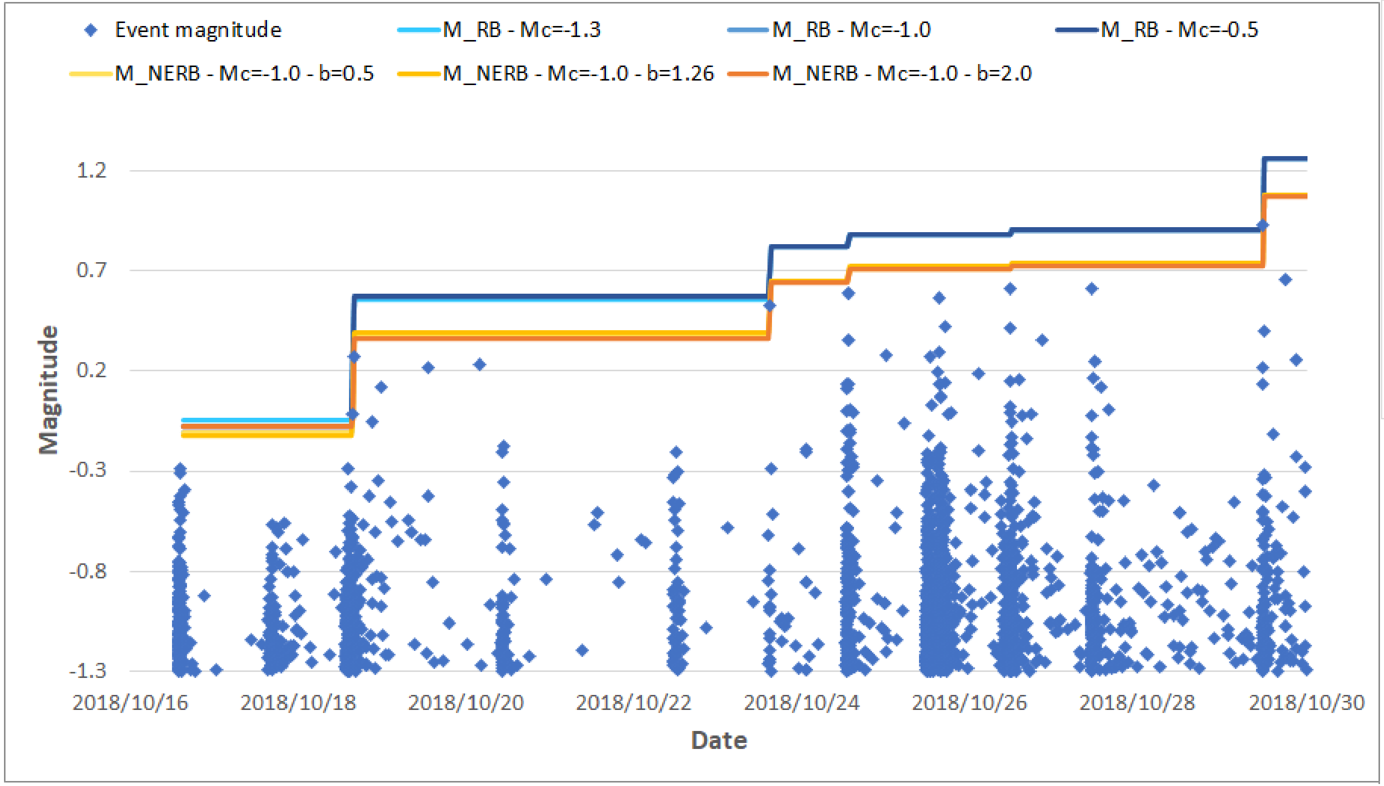

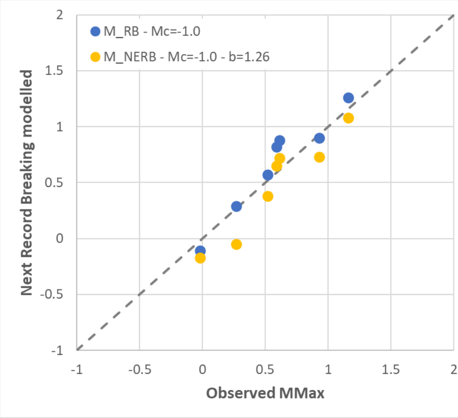

Cuadrilla – M_{Maxo} vs Predicted M_{Max}

- Maximum Observed Magnitude M_{Maxo} vs Predicted M_{Max}

BGS Catalog

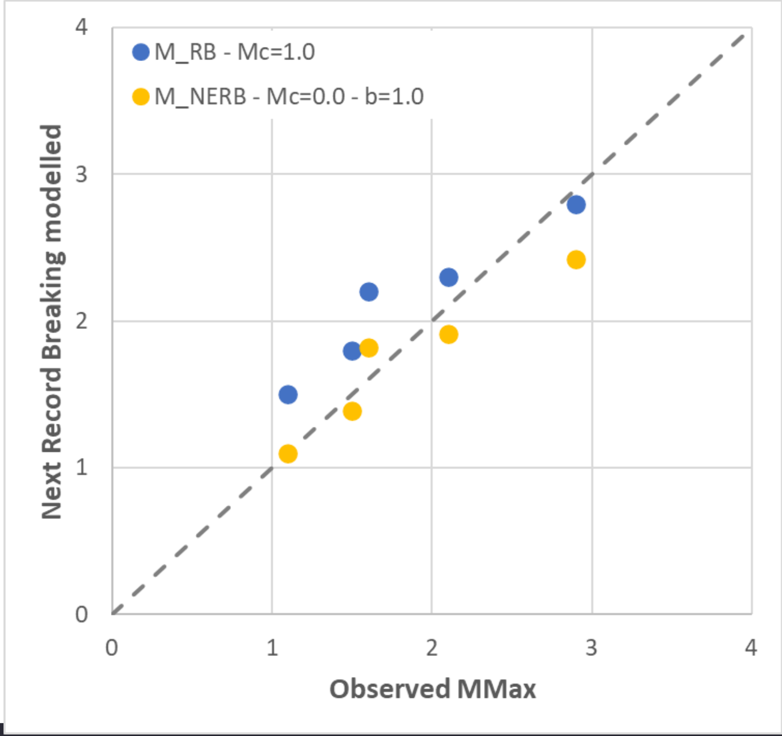

OGA Catalog (includes downhole)

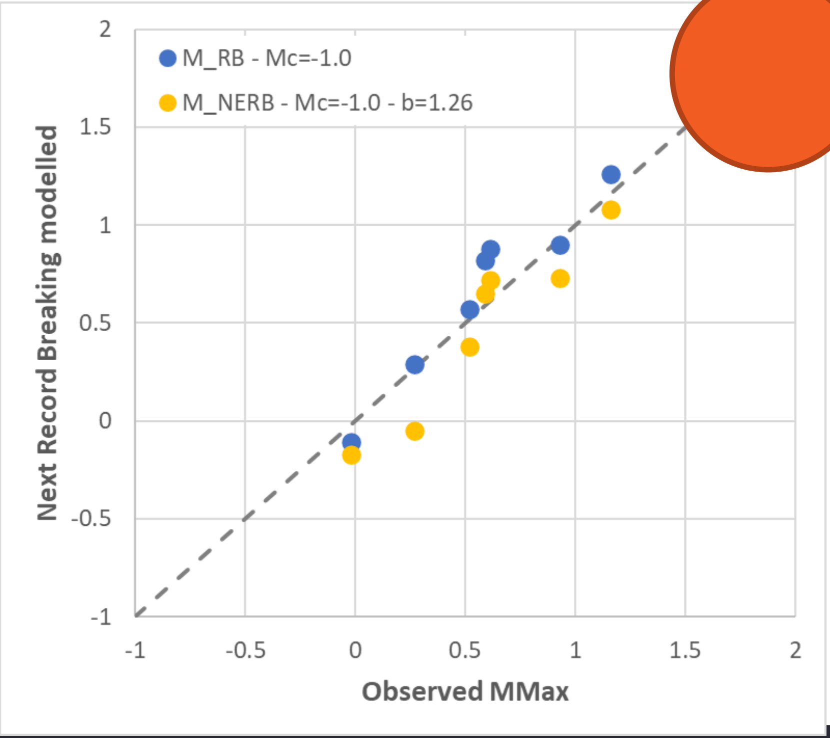

Cuadrilla – M_{Maxo} vs Predicted M_{Max}

- Was the seismicity in 2019 still influenced by the stimulations from 2018?
- We reset the minimum magnitude only for the 2019 stimulation

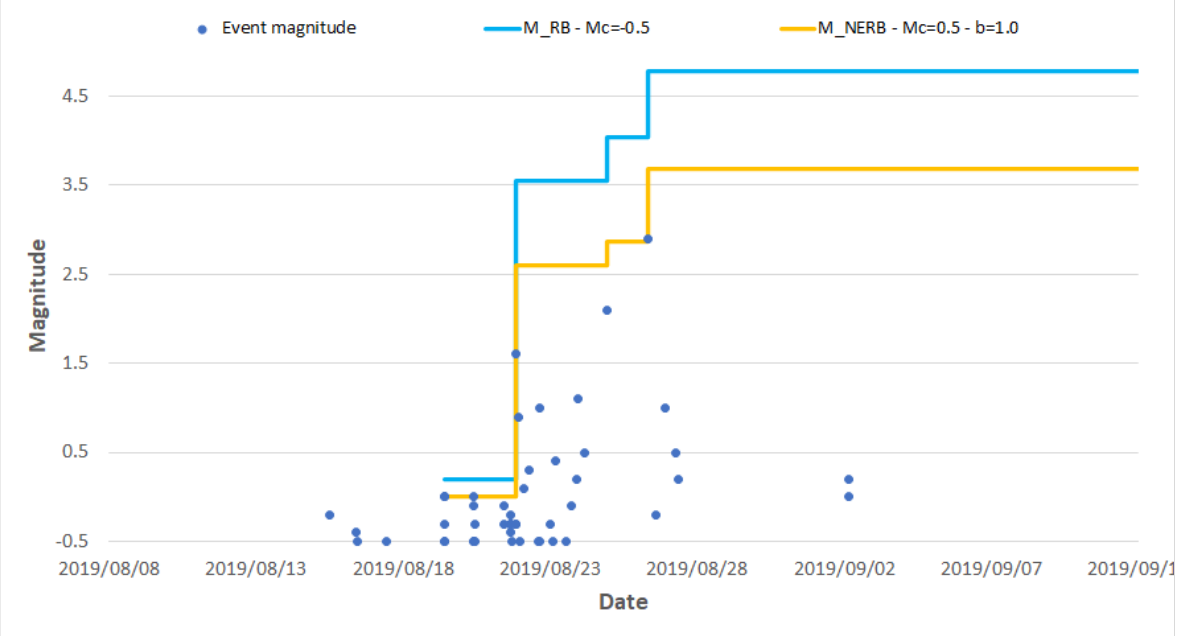

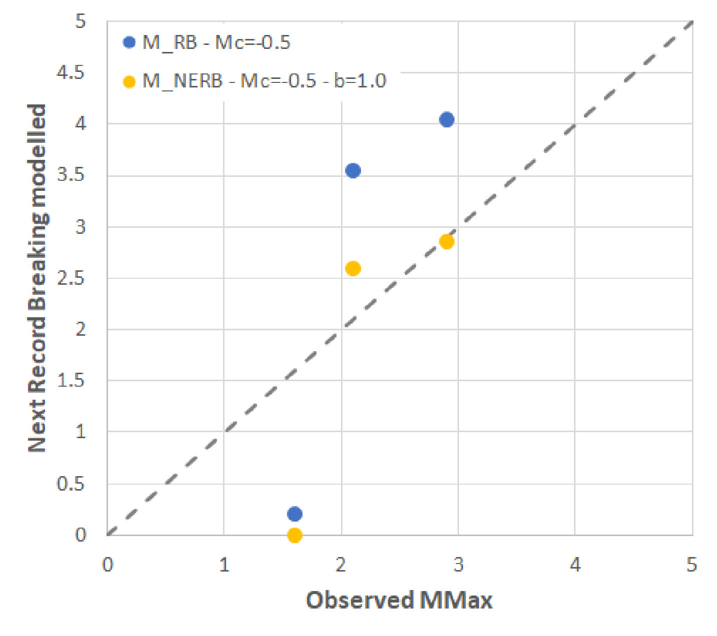

▶ This results in underestimate of the first record breaking event

BGS Catalog

Discussion

- Works OK for Groningen and long term SWD – steady state
  - We would greatly benefit from longer time series in Groningen
  - Template detection can help a lot - PLEASE DO IT – we can detect the start of the seismicity
- We need statistically significant number of breaking events to make initial estimate
  - As low detection threshold as possible early during the monitoring
  - Usually the network is not in place early in the monitoring
  - Downhole and surface monitoring magnitudes are generally not consistent, national network and local network magnitudes can also be inconsistent
- TLS thresholds: it is arbitrary number set apriori by regulator, this method brings science
- Not clear how to generalize this for ground motion thresholds
- Statistical results can be physically impossible (Japan – M_{Br}~10)
- No indication of time of occurrence – extension?

Conclusions

Seismik

- Do not require data like injection faults, stress state, etc, physical model
- Requires seismicity and initial period in which seismicity is recorded to start to make estimates
- Sensitive to self-consistency of the magnitude calculations in the catalogue
  - problem with microseismicity
- Is suitable for magnitudes of Real-time monitoring is possible for TLS – can be the threshold
- Sensitive to magnitude of completeness – especially history of record breaking events
- Insensitive to b-value
- Even one year of pause in hydraulic Fracturing did not reset the clock

Stress constraints: teaser

	Data combinations that allow full stress inversion					
Focal mechanisms	✓	✓	✓	✓	✓	✗
Minimum stress	✓	✗	✓	✗	✓	✗
Vertical stress	✓	✗	✗	✓	✓	✗
HTPF data	✗	2+ HTPF	1+ HTPF	1+ HTPF	✓	6+ HTPF

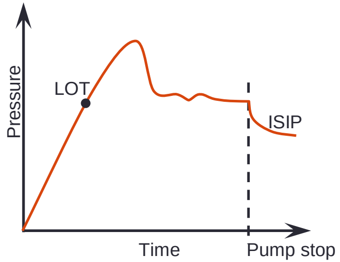

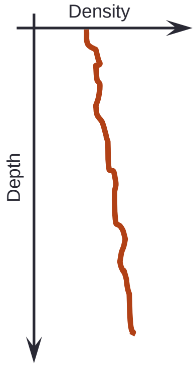

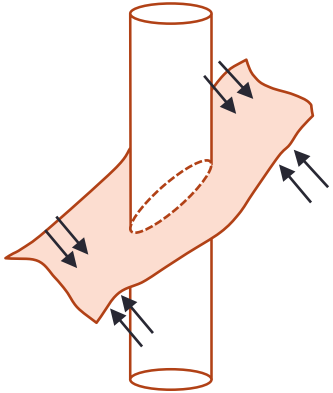

Full stress inversion

Seismik

- Step 1: Gephart & Forsyth

$$misfit: \sum_{i=1}^{N_{mech}} \frac{|\chi_{min}^{(i)}|}{\delta\alpha^{(i)}}$$

$$+ \sum_{i=1}^{N_{htpf}} \frac{|\sigma_i^{(n)} - P_i^{htpf}|}{\delta P_i^{htpf}}$$

$$+ \frac{|\sigma_v - \sigma_{33}|}{\delta\sigma_v} + \frac{|\sigma_3 - P_{ISIP}|}{\delta P_{ISIP}}$$

- Result:
  - approximate stress solution
    - Principal stress magnitudes: $\sigma_1, \sigma_2, \sigma_3$
    - Euler angles: ξ_1, ξ_2, ξ_3
    - Stress gradient: $\alpha_{11}, \alpha_{12}, \alpha_{22}, \rho$
  - fault plane identification

THANK YOU FOR YOUR ATTENTION!

Groningen M_{max} Workshop II (NAM), 13-17 June 2022, Amsterdam, The Netherlands

History and projection of earthquake magnitude-frequency distributions in the Groningen gas field 1991-2031

Charles Vlek

Department of Behavioural and Social Sciences

University of Groningen (RuG), the Netherlands

Draft presentation (June 2022) to be revised in view of workshop discussions and further insights.

Contact: c.a.j.vlek@rug.nl

university of groningen

2. Thirty years of gas extraction and earthquakes in Groningen

[N = number of .., M = magnitude, bcm = billion cubic meters, bcm_{cum} = total-cumulative bcm since 1963]

Per year:

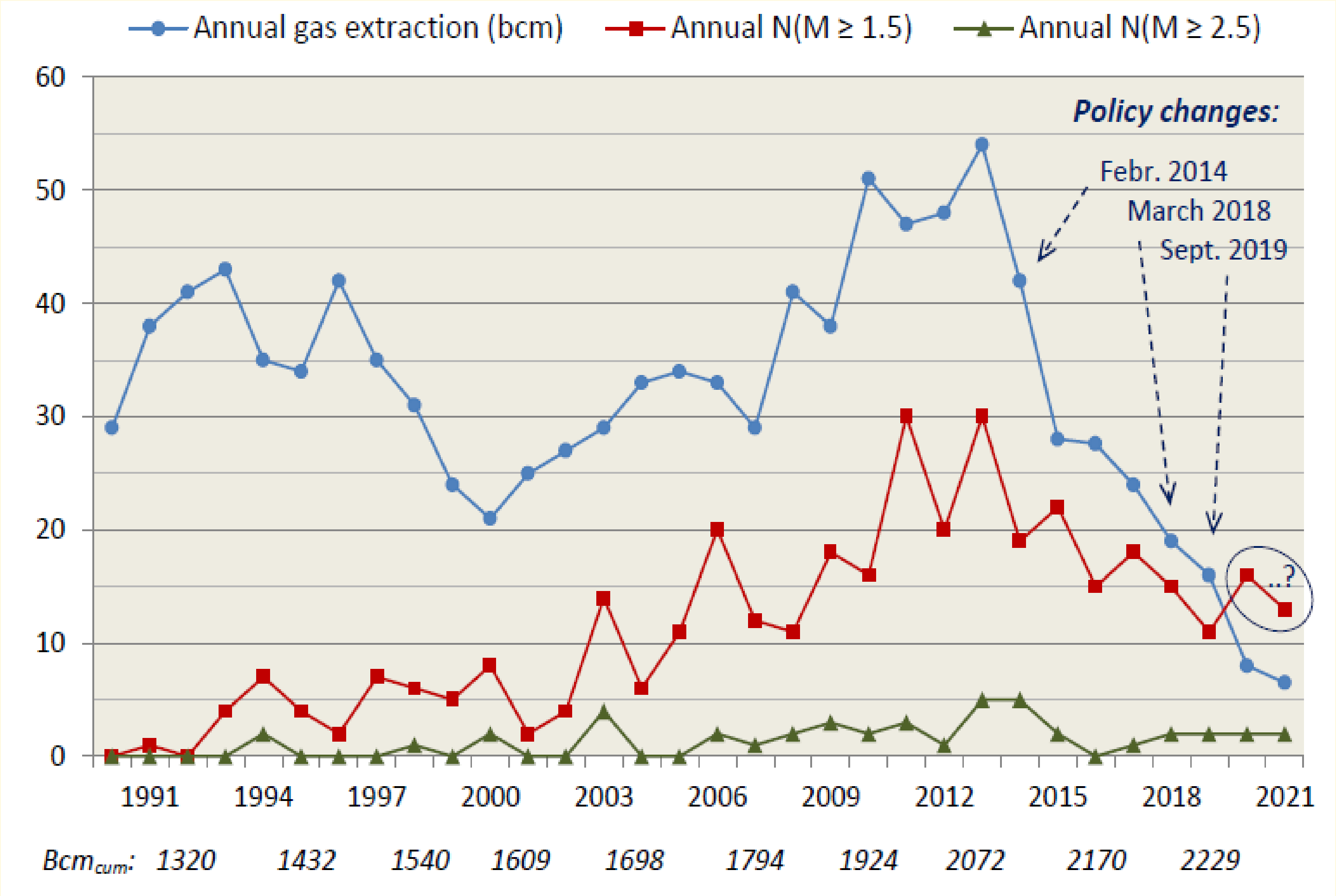

Per two years:

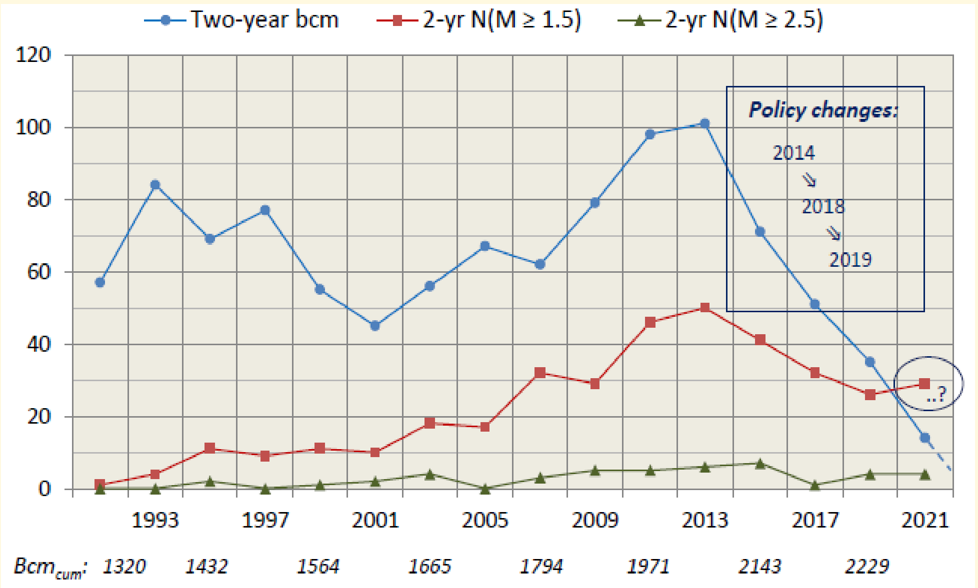

Notes: Groningen gas extraction started in 1963. The first earthquake occurrred in December 1991 (Middelstum, M 2.4).

Policy changes after the Huizinge earthquake (2012, M 3.6) are sketched out in *Appendix 1* (slide 17).

university of groningen

3. A statistical prognosis model for projecting future seismicity: $N(M \geq 1.5)/10$ bcm = $4E\text{-}18 bcm_{cum}^{5.50}$, with $R^2 = 0.72$

Annual N(M ≥ 1.5) per 10 bcm of extraction

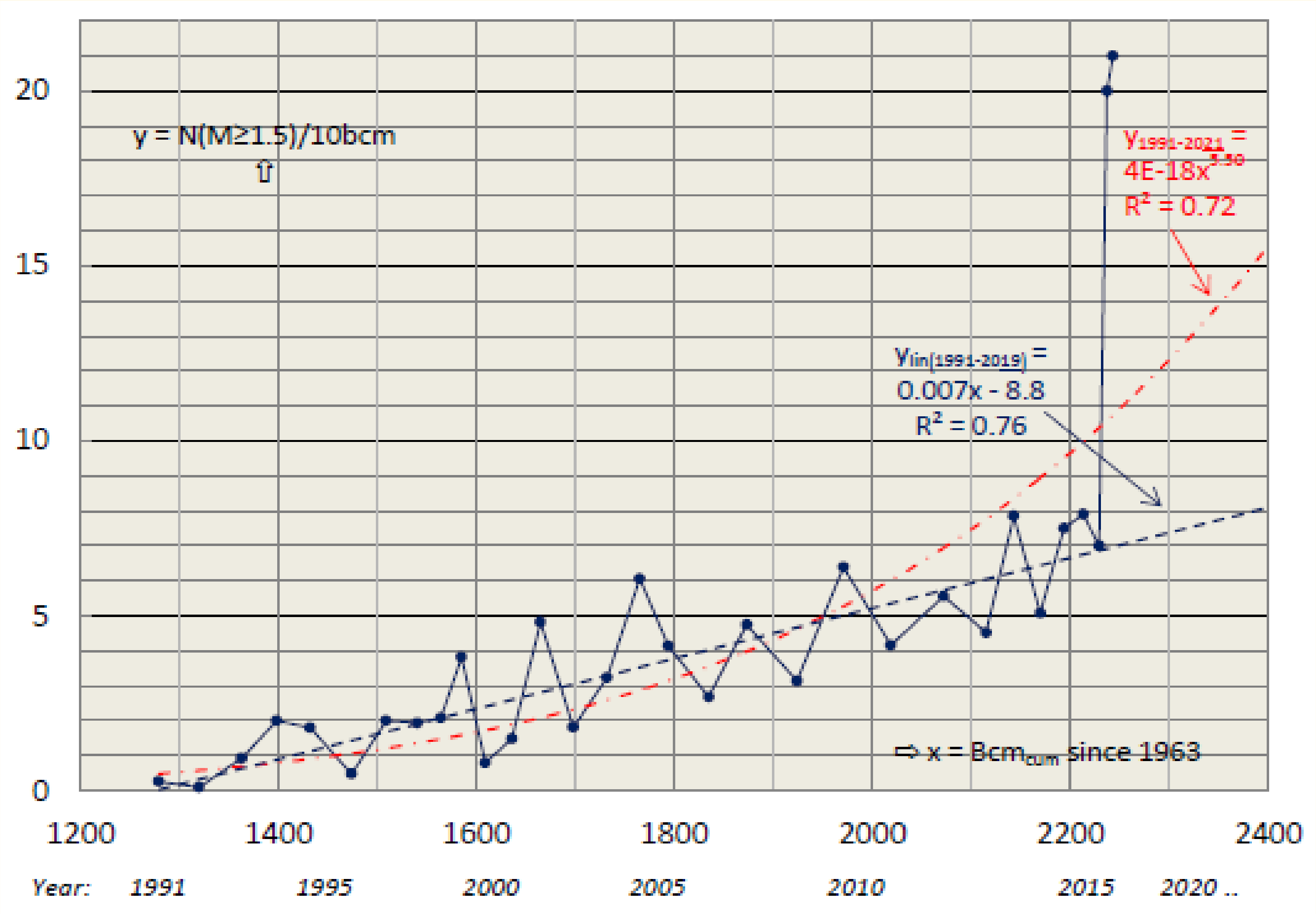

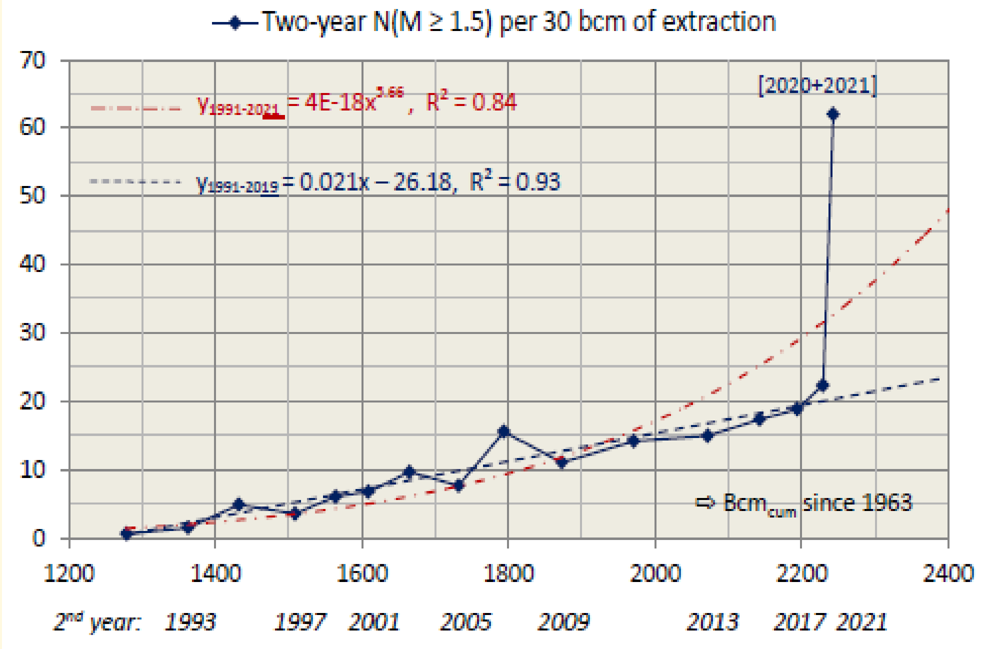

Observation (left graph): The linear statistical trend formula for 1991-2019 is $y_{lin(1991-2019)} = 0.007x - 8.8$, with $R^2 = 0.76$.

The *exponential* trend for 1991-2021 is:

$y = 4E\text{-}18x^{5.50}$, with $R^2 = 0.72$.

[The *linear* trend for 1991-2021 (not shown) has an $R^2 = 0.52$.]

university of groningen

4. During 1991-2021: 366 earthquakes with magnitude M ≥ 1.5, of which 44 (about 12%) with M ≥ 2.5, and 14 with M ≥ 3.0

Fourteen 'maximal' earthquakes with M ≥ 3.0,
all after 1 October 2003, all in the central area of the field

24-10-2003: Hoeksmeer, 3.0	07-02-2013: Zandeweer, 3.2
10-11-2003: Stedum, 3.0	02-07-2013: Garrelsweer, 3.0
08-08-2006: Westeremden, 3.5	13-02-2014: Leermens, 3.0
30-10-2008: Westeremden, 3.2	30-09-2015: Hellum, 3.2
08-05-2009: Zeerijp, 3.0	08-01-2018: **Zeerijp, 3.4**
27-06-2011: Garrelsweer, 3.2	22-05-2019: **Westerwijtwerd, 3.4**
16-08-2012: **Huizinge, 3.6**	16-11-2021: Garrelsweer, 3.2

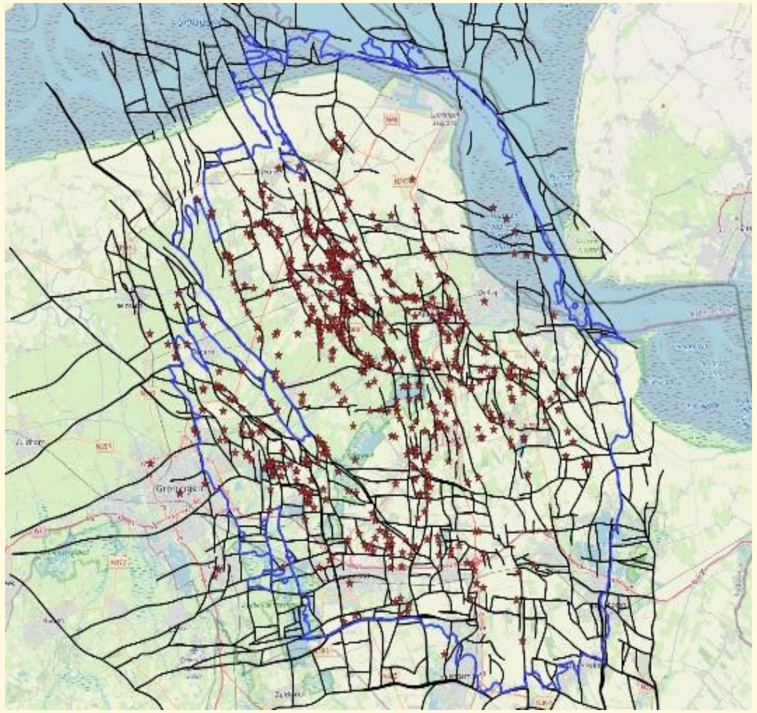

The Groningen field, with red-dotted earthquake locations and blue-lined geological faults (from KNMI, 2022).

Note: **Bold**-printed are policy-changing events

university of groningen

5. With increasing bcm_{cum}, both expert-estimated and empirical values of the maximum earthquake increased

	1992	1993	1998	2004-2012	2013	2016	2022
Bcm_{cum} (1963-) about:	1320	1363	1540	1698-2019	2072	2170	2250
Estimated M_{max} ≈	**3.0**	**3.3**	**3.6-3.8**	**3.9**	**5.0**	**4.0-7.0**	**..?**

	1991-1995	1996-2000	2001-2005	2006-2010	2011-2015	2016-2021
Actual 'M_{max}'	**2.7**[a)]	**2.6**[b)]	**3.0**	**3.5**	**3.6**	**3.4**

[a)] Stedum, 1 July 1994. [b)] 't Zandt, 15 Febr. 1998. See further slide 4.

Observation: Both estimated and actual M_{max} steadily increased, but 'actual' remained significantly below 'estimated'.

Note: From NAM's 'Winningsplan'-2013, p. 39 (transl.): "The statistical trends in the frequency and magnitude of earthquakes indicate that, over time, a gradual increase may be expected in the number of earthquakes and in the maximal magnitude."

university of groningen

6. Estimating a Gutenberg-Richter b-value for three historical magnitude-frequency distributions with about equal N(M ≥ 1.5)

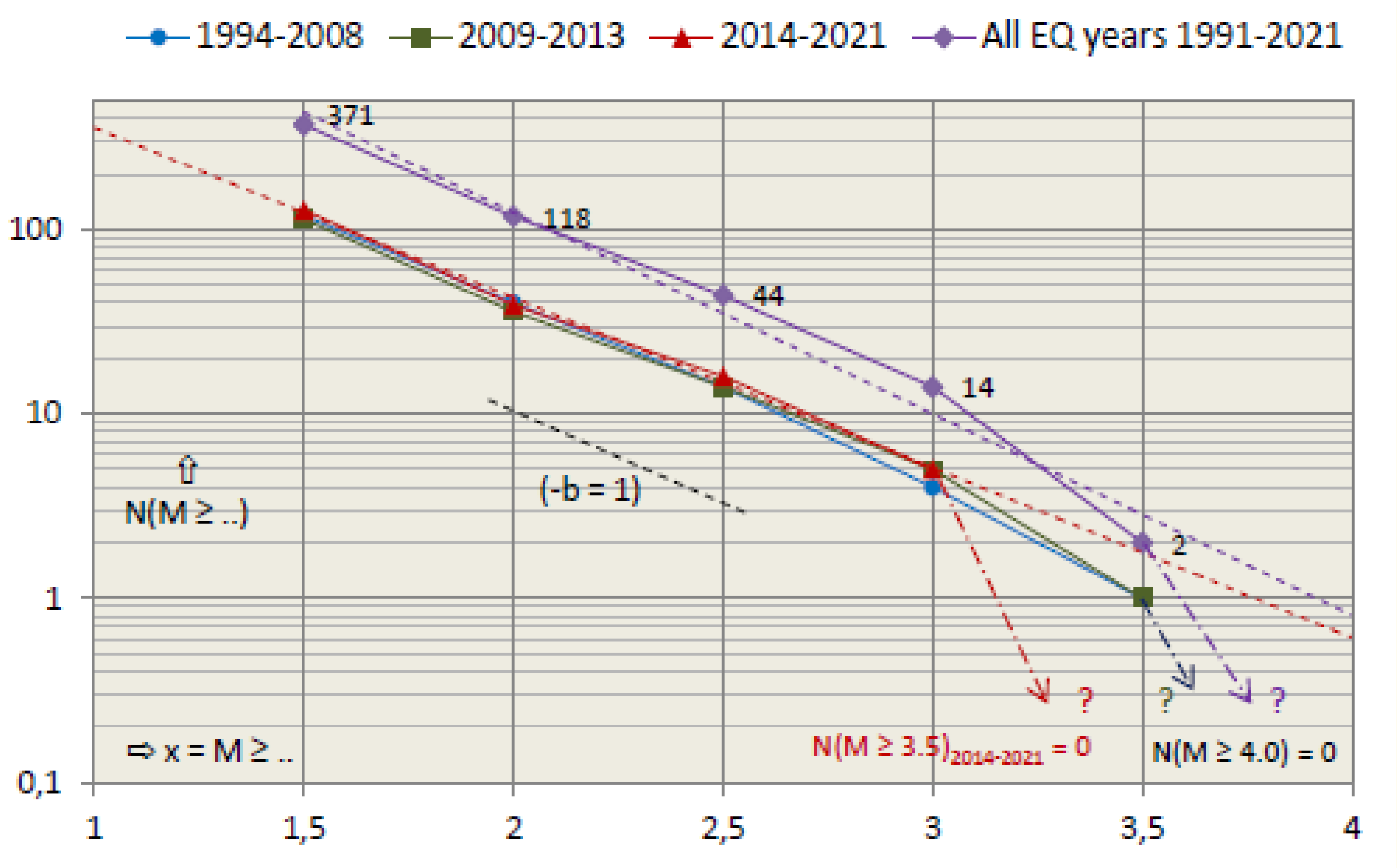

N(M ≥ ..) over 1994-2008 (15 years):
$\log N(M \geq \ldots)_{1994\text{-}2008} = -1.03x + 3.66$, with $R^2 = 0.997$.

N(M ≥ ..) over 2009-2013 (5 years):
$\log N(M \geq \ldots)_{2009\text{-}2013} = -0.99x + 3.58$; $R^2 = 0.999$.

N(M ≥ ..) over 2014-2021 (8 years, + trend line):
$\log N(M \geq \ldots)_{2014\text{-}2021} = -0.93x + 3.49$; $R^2 = 0.997$.

N(M ≥ ..) across all earthquake years 1991-2021:
$\log N(M \geq \ldots)y_{1991\text{-}2021} = -1.09x + 4.28$; $R^2 = 0.98$ (+ trend line).

Dashed arrows indicate that N(M ≥ 3.5) = 0 for 2014-2021, and that N(M ≥ 4.0) = 0 for all years.

Observations: (a) For the three data sets (excl. 'all years'), the Gutenberg-Richter b is rather stable and lies around 0.95.

(b) Absence of events with M ≥ 4.0, or *more* with M ≥ 3.5, indicates the M-F distribution to be truncated around M 3.5-4.0.

university of groningen

7. What happened to total N(M ≥ x) in successive five-year periods after 1996?

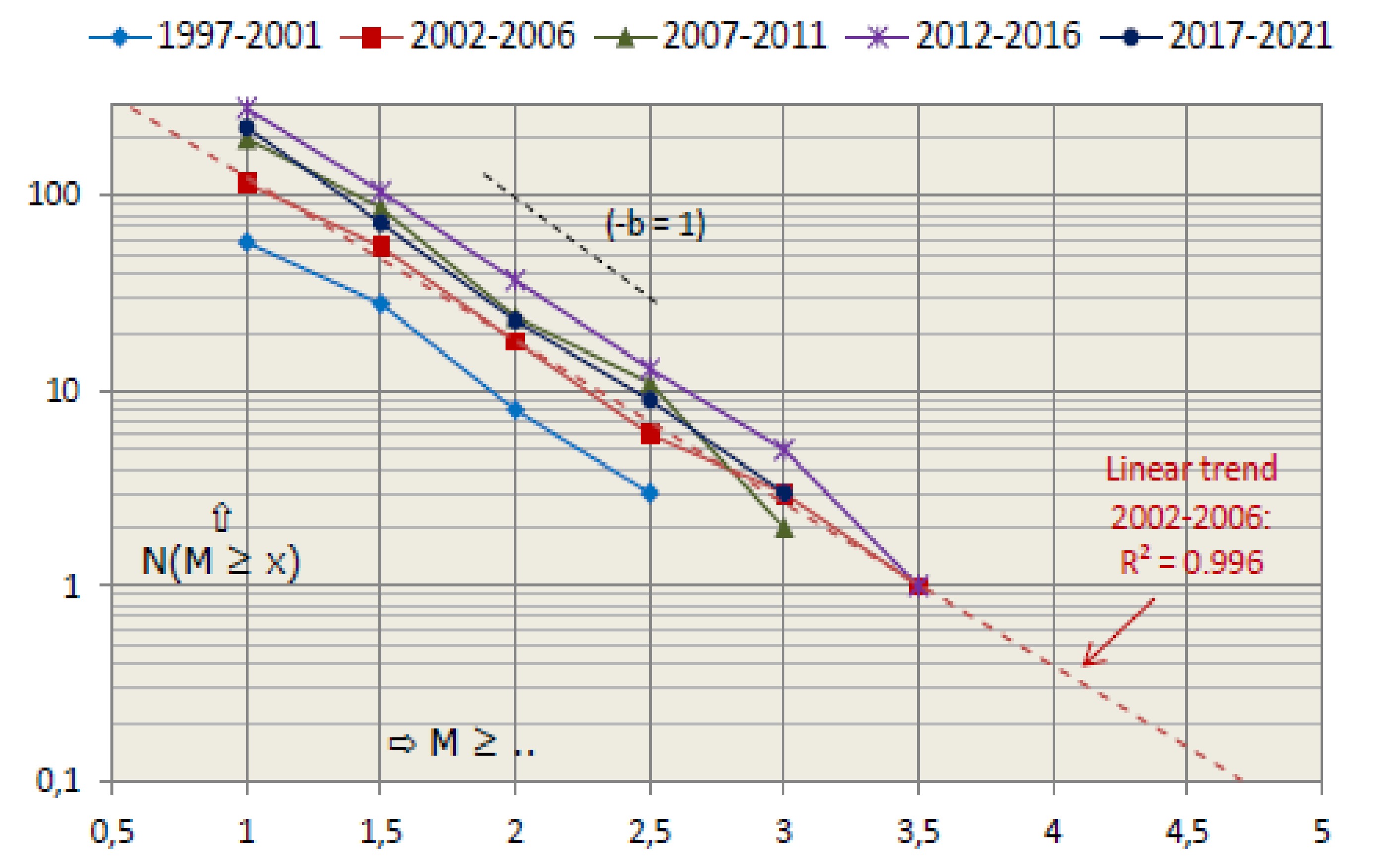

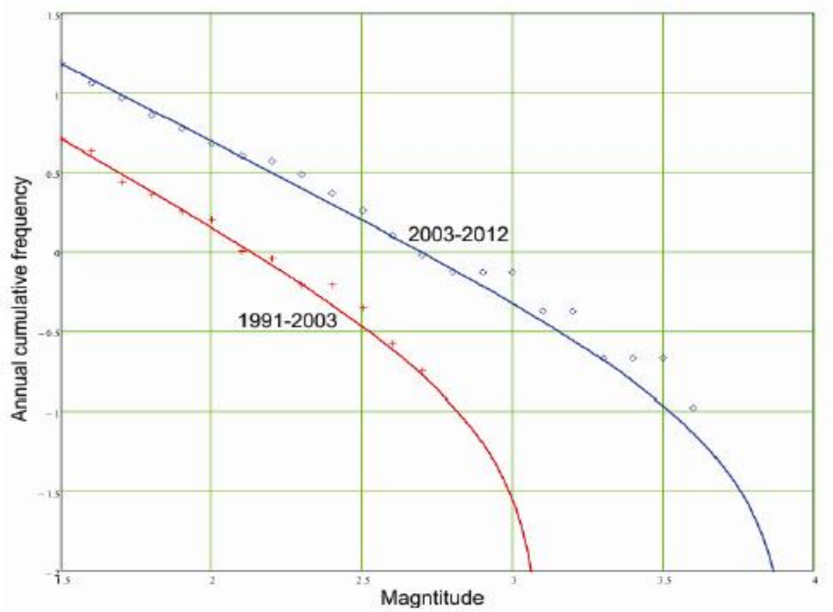

In comparison: M-F diagram from 'Huizinge report' by Dost & Kraaijpoel (2013).

Comment (ChV): How about fitting *straight* trend lines?

Observation: Under total extraction of 156 bcm in 2002-2006, increasing seismicity included the first 3.5 quake (Westeremden, Aug. 2006). Here, the trend towards higher-M earthquakes is clearly visible, with an estimated five-year p(M ≥ 4.0) ≈ 0.4: "Once in 12 years."

Under total extraction of 1999 bcm in 2012-2016, seismic activity was highest, including actual M_{max} = 3.6 near Huizinge (Aug. 2012).

university of groningen

8. Some premises and assumptions for projecting future seismicity in the Groningen field

1. Future earthquake activity, *i.e.* N(M ≥ 1.5), may be projected on the basis of a significant empirical statistical prognosis model (SPM) covering earthquake years 1991-2021.

2. Useful here is the exponential trend formula across 1991-2021 (see slide 3, left graph):

   $$N(M \geq 1.5)/10\ \text{bcm} = 4E\text{-}18\text{bcm}_{cum}^{5.50},$$

   with R^2 = 0.72, implying that 28% of the variance in N(M ≥ 1.5)/10 bcm is unexplained.

3. For assessing N(M ≥ 2.5), N(M ≥ 3.5) and higher-M frequencies, an empirically established Gutenberg-Richter b-value of 0.95 may be applied.

4. The *current* 'Reduce-and-stop' extraction scenario (Sept. 2019) definitely ends in 2023. However, for computing N(M ≥ 1.5)/10 bcm and projecting N(M ≥ 1.5) over 2022-2031, the *initial* Reduce-and-stop scenario (March 2018, running over 2019-2030) may be – adaptively - used, in order to accommodate (or simulate) the expected ten-year effects of on-going reservoir pressure equilibration.

5. In view of recent energy-political challenges, it may be useful to also consider several 'Continue Groningen gas extraction' scenarios, *e.g.* an additional decade of 5, 10 or 20 billion cubic meters per year.

university of groningen

9. Four Groningen gas-extraction scenarios for 2022-2031

Annual bcm in year:	2022	2023	2024	2025	2026	2027	2028	2029	2030	2031	Bcm_{cum}
Reduce-and-stop 2019-2030[a)]	5	5	4	3.5	3	2	1.5	1	1	1	2294
Continue 5 bcm until 2031[b)]	5	5	5	5	5	5	5	5	5	5	2293
Continue 10 bcm until 2031[b)]	10	10	10	10	10	10	10	10	10	10	2343
Continue 20 bcm until 2031[b)]	20	20	20	20	20	20	20	20	20	20	2443

Notes: (a) By following the current, slightly adapted 'Reduce-and-stop 2019-2030' scenario (March 2018), we may (largely?) account for the (about) 10-year effects of on-going reservoir pressure equilibration over 2022-2031.

(b) Extracting 5, 10 or 20 bcm would stop in 2031. Thereafter, another ten years of (significant) reservoir pressure equilibration would presumably occur.

(c) Keeping extraction below 12 bcm/year would (still?) be 'safe enough' (cf. Muntendam-Bos & De Waal, 2013; SodM, 2018).

(d) On June 1, 2022, the Dutch Mining Council advised the minister of EA to prepare for continuing Groningen gas extraction.

university of groningen

10. Actual magnitude-frequency distribution for 2012-2021 and RuG-projected MFDs 2022-2031 for 'Reduce-and-stop 2019-2030'

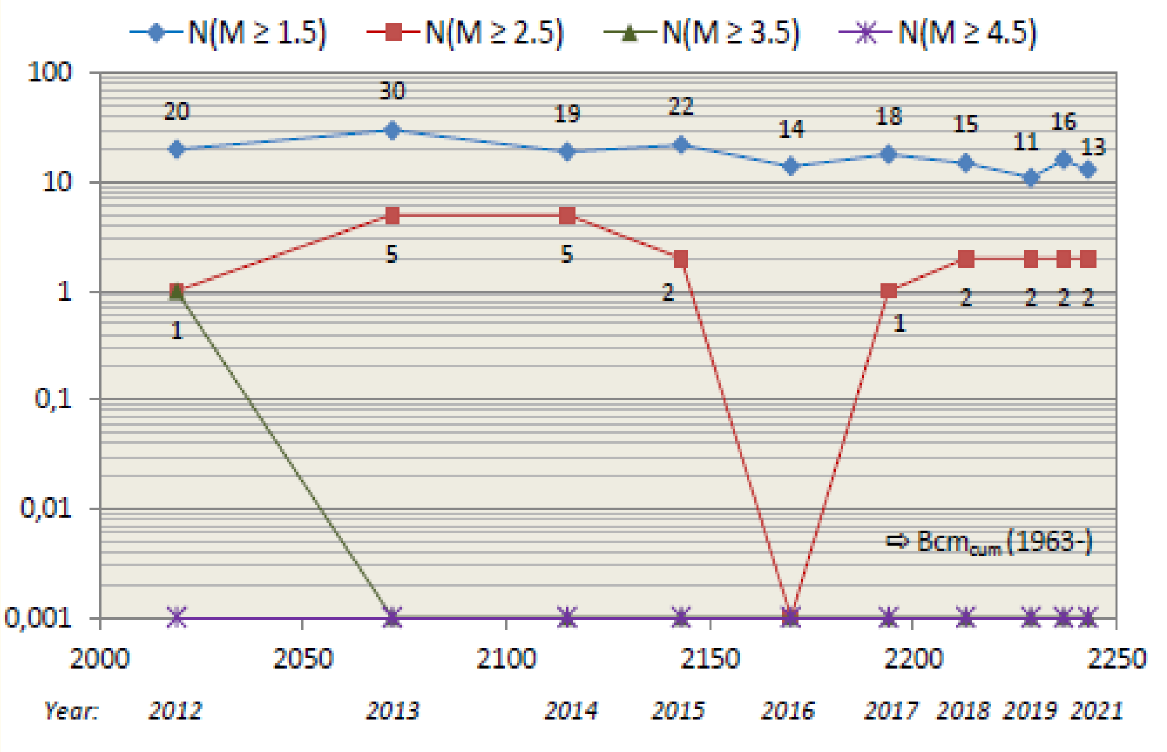

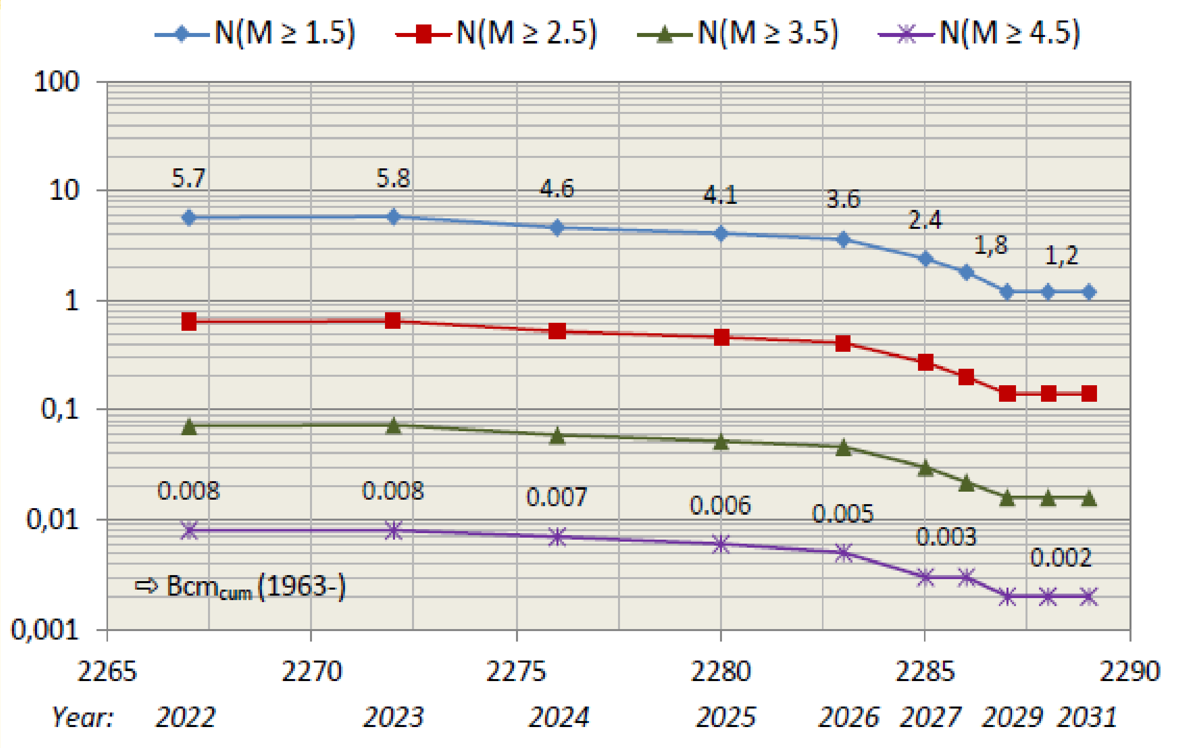

<u>Note</u>: On the log-scale, null occurrences are valued as 0.001.

<u>Observations</u>: (a) *During 2012-2021 (left),* N(M ≥ 1.5) = 178, of which 8 earthquakes reached 3.0 ≤ M ≤ 3.6.

(b) *Over 2022-2031 (right),* RuG-projected magnitude frequencies gradually decline with decreasing extraction (or on-going pressure equilibration). The assumed-constant Gutenberg-Richter b-value makes projected N(M ≥ x)-lines to run parallel.

(c) Any projected M-F distribution (vertical) is time- or compaction-dependent and it differs for, e.g., 2023, 2026 and 2029.

11. For 'Reduce-and-stop 2019-2030': How do the projections from RuG compare to those by NAM-2020 and TNO-2022?

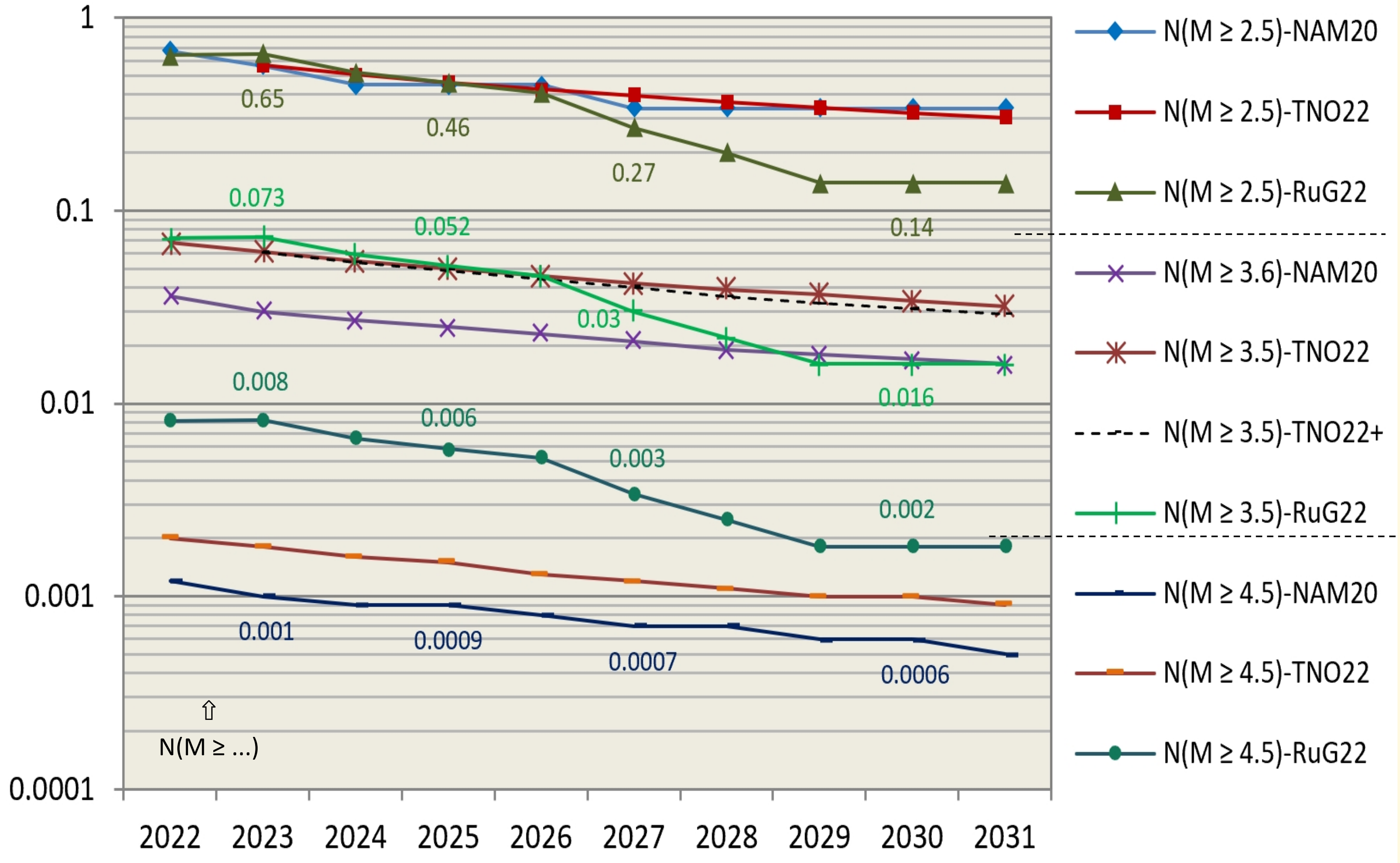

Observations:

1. Any (vertical) MFD is dependent on terminating gas extraction and 10-year reservoir pressure equilibration.

2. Both TNO22 and RuG22 assess the *short-term* probability of M ≥ 3.5 as about 0.07: "once in 14 years".
By 2030, N(M ≥ 3.5) would be between "one in 30 years" (TNO22) and "once in 60 years" (RuG22).

3. Between 0.008 ("once in 125 years") and 0.001 ("1/1.000 years"), N(M ≥ 4.5) is estimated highest by RuG22 and lowest by NAM20.

Note: TNO22+ follows their *preferred* source-model specifications.

university of groningen

12. RuG-projected magnitude-frequency distributions over 2022-2031 for 'Continue 5 bcm/year' and 'Continue 10 bcm/year'

'Continue 5 bcm/year'

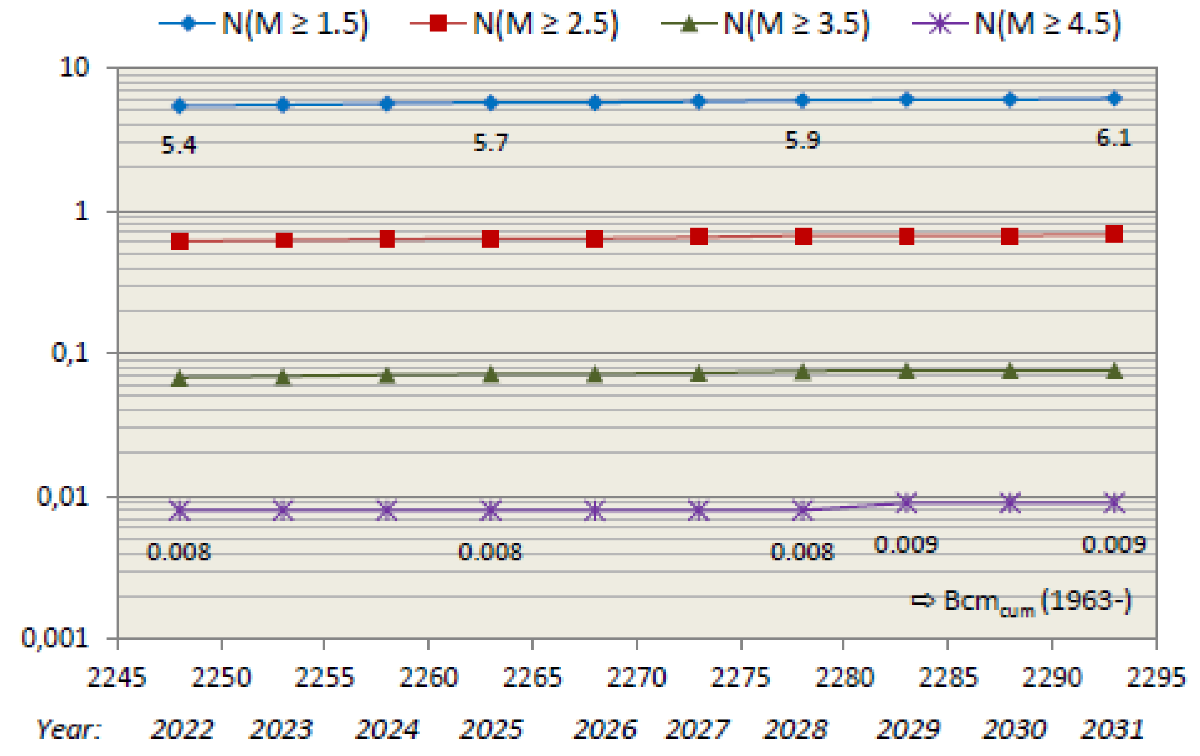

'Continue 10 bcm/year'

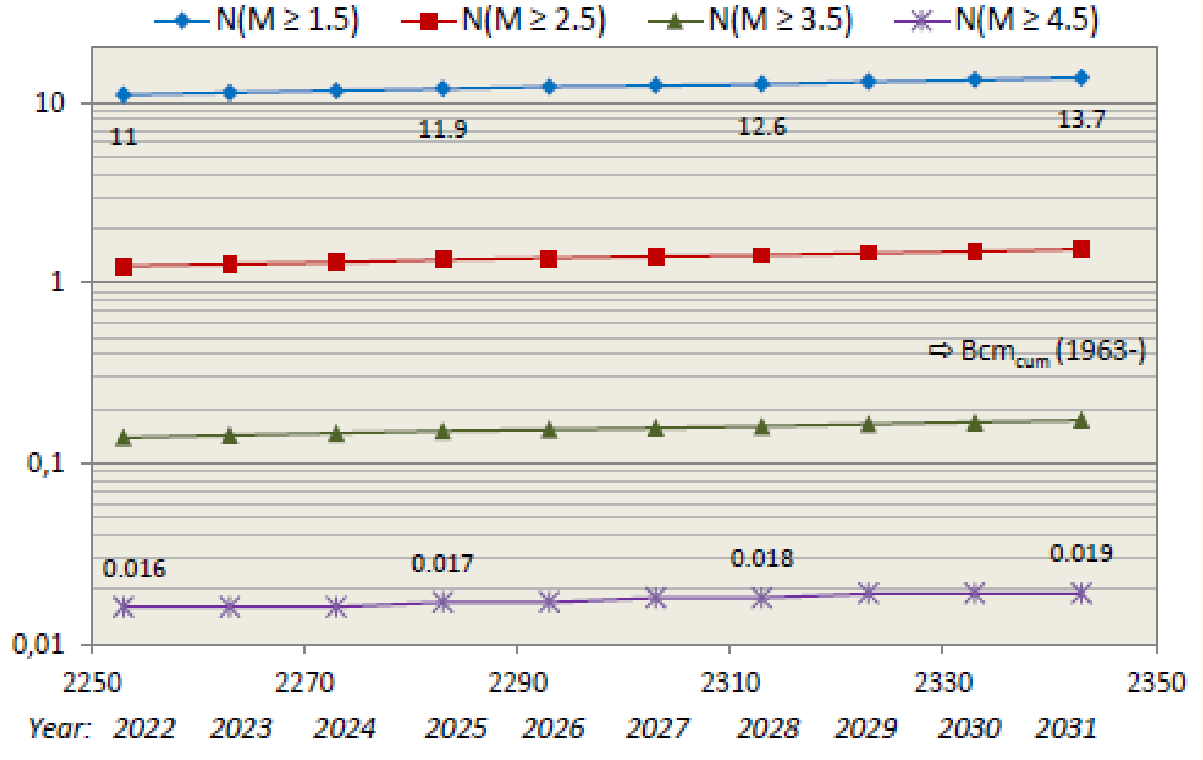

Observations: (a) As extraction continues, earthquake activity goes up again, and less so under 5 than under 10 bcm/year of extraction. (b) Again, any projected M-F distribution (vertical) is time- or compaction-dependent and it differs for different years.

Note: A comparison of RuG-projected MFDs under 10 versus 20 bcm/year is given in Appendix 2 (slide 18).

university of groningen

13. Under the different extraction scenarios, how many events with M ≥ 1.5, 2.5, 3.5 and 4.5 might occur during 2022-’26 and 2027-’31?

RuG-projected *total* number of earthquakes during 2022-2026, ... and during 2027-2031

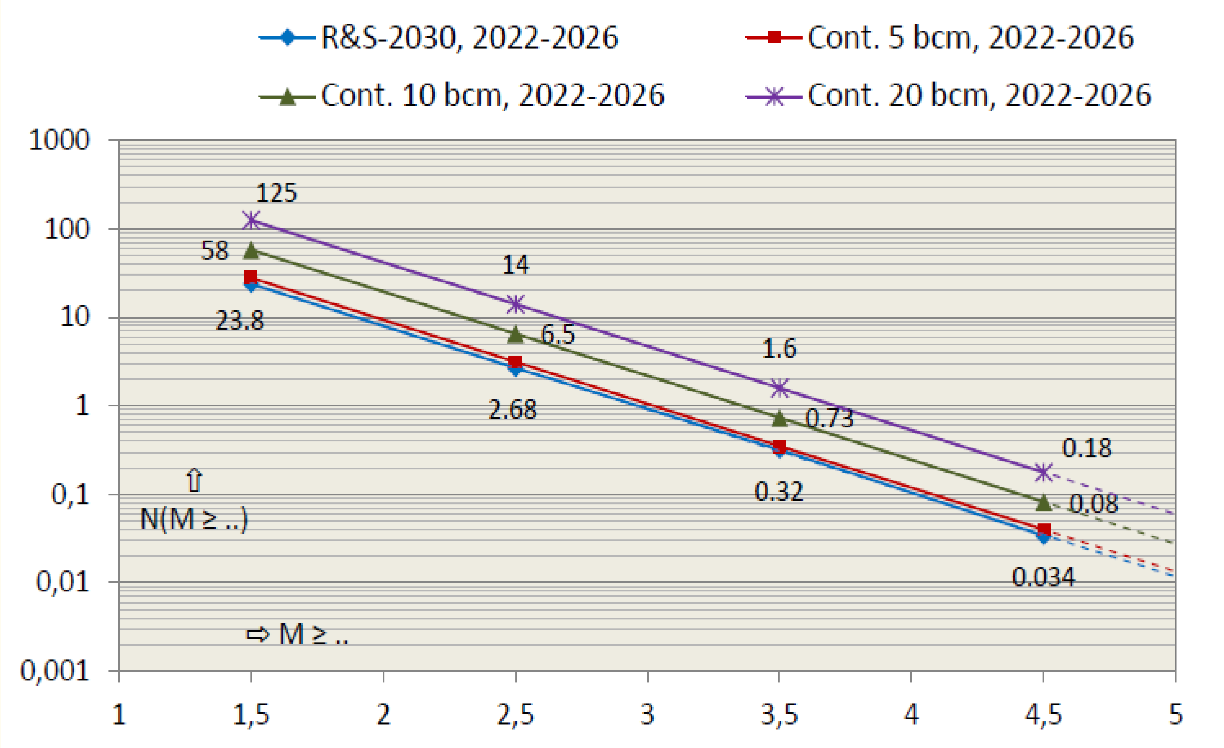

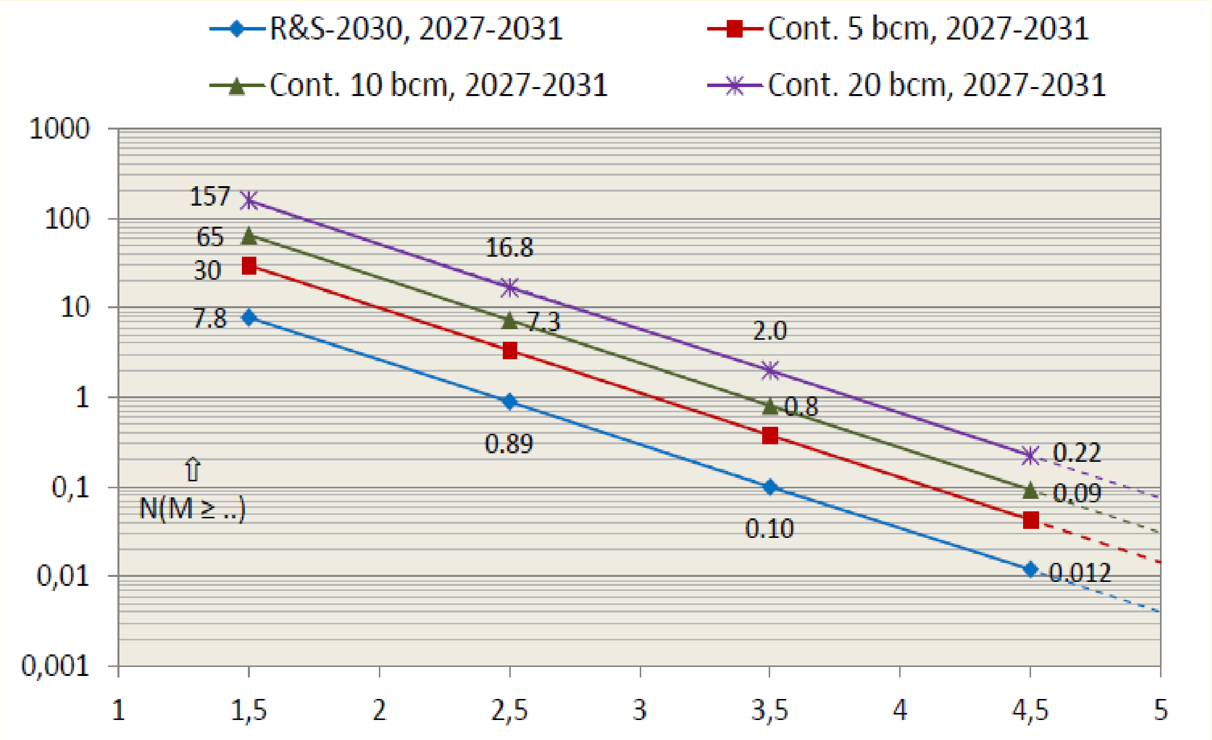

<u>Observations</u>: (a) During 2022-2026, ‘Continue 5 bcm/year’ would not yield more seismicity than (adapted) ‘Reduce-and-stop 2030’.

(b) Any ‘Continue extraction’-scenario would (also) be extended by another ten years of ‘virtual’ extraction due to on-going pressure equilibration effects.

<u>Note</u>: See Appendix 2 (slide 18) for the MFD graph for ‘Continue <u>20</u> bcm/year’.

university of groningen

14. Branches and weights for a logic tree about the (adapted) ‘Reduce-and-stop-2030’ scenario

Four discrete branches (columns) of larger earthquake magnitudes and their associated probabilities (’weights’)

	p(2.5 ≤ M < 3.0)	**p(3.0 ≤ M < 3.5)**	**p(3.5 ≤ M < 4.0)**	**p(4.0 ≤ M < 4.5)**
For 2023	0.430	0.144	0.049	0.016
For 2028	0.133	0.045	0.014	0.005

Note: Probabilities are derived from the numerical data underlying the 2022-2031 RuG-projections pictured on slide 10 (right).

Observation: For ‘branch’ p(3.5 ≤ M < 4.0), a frequentistic interpretation of 0.049 would be: *“Once in about 20 years”. And* 0.014 would mean: *“Once in about 70 years”.* Outstanding assumption: “.. given that the system keeps behaving as it did thus far.”

Obviously: If Groningen gas extraction were to be continued for another decade, the probability values would be significantly higher.

university of groningen

15. Conclusions and suggestions 1-4

1. The present results emerge from:
   a. An exponential statistical 72%-prognosis model over 1991-2021: $N(M \geq 1.5)/10bcm = 4E\text{-}18 bcm_{cum}^{5.50}$,
   b. A stable empirical magnitude-frequency relationship characterized by a Gutenberg-Richter b ≈ 0.95, and
   c. Four extraction scenarios: Stop in 2030 (*incl.* pressure equilibration), versus continue 5, 10 or 20 bcm/year.

2. Both the *exponential* prognosis model (incorporating unexpected 2020 and 2021 seismicity) and a constant Gutenberg-Richter b (also for higher magnitudes) may cause M_{max} assessment to be somewhat 'conservative'.

3. "How many earthquakes with 1.5 ≤ M ≤ 3.5 could still occur?" *My answer to this is:*
   For the (adapted) Reduce-and-stop-2030 scenario – during 2022-2026, N(M ≥ 1.5) ≈ 24 (+/- 28%), N(M ≥ 2.5) ≈ 3 (idem), with a five-year chance of 0.32 ("once in 15 years") that an M ≥ 3.5 might occur.

4. For Bayesian statisticians, 'probability' is a future-oriented personal degree of belief, to be operationalised via a certain willingness to bet on the outcome of a well-defined gamble.
   Thus, as regards M_{max} for the Groningen field, I should be willing to bet you (*e.g.*) three good bottles of wine against one, that *before the end of 2026 no more earthquake with M ≥ 3.5 would occur*.

[And I would bet you 30 to 1 that there would be no M ≥ 4.5]

university of groningen

16. Conclusions and suggestions 5-8

5. From a significant linear earthquake-statistical trend over 1991-2006 (first 16 earthquake years), a 3.6-event like the one near Huizinge in August 2012 could have been foreseen. [Elaboration in Appendix 3, slide 19.]

6. During 2022-2026, a ten-year continuation of extracting 5 bcm/year would hardly or not yield more seismic activity than following the current (adapted) ‘Reduce-and-stop 2030’ scenario (slide 10, right).

7. For Groningers, the ultimate implication of future-seismicity assessment lies in the need for further building reinforcement in order to limit personal-safety risk (which reinforcement is primarily meant to do). Thus:
   a) Under the (adapted) ‘Reduce-and-stop 2030’ scenario, further building reinforcement may no longer be effective for warranting personal safety (although it may help to prevent further material damage).
   b) Under any 10-year continue-extraction scenario (5, 10 or 20 bcm/year), seismic activity would increase again, and further, rapid building reinforcement would be necessary, and it would be the more urgent the higher the annual extraction rate.

8. *However*, if ‘seismic risk’ is to cover probability x severity of:
   - dying,
   - injury,
   - property damage,
   - anxiety,
   - stress,
   - ill health, …

   , then terminating extraction and suppressing earthquake activity may be insufficient to restore ‘safe enough’ living conditions.

university of groningen

17. Appendix 1: After the M 3.6 earthquake near Huizinge (2012), how did extraction go from 54 bcm in 2013 to below 5 bcm in 2022?

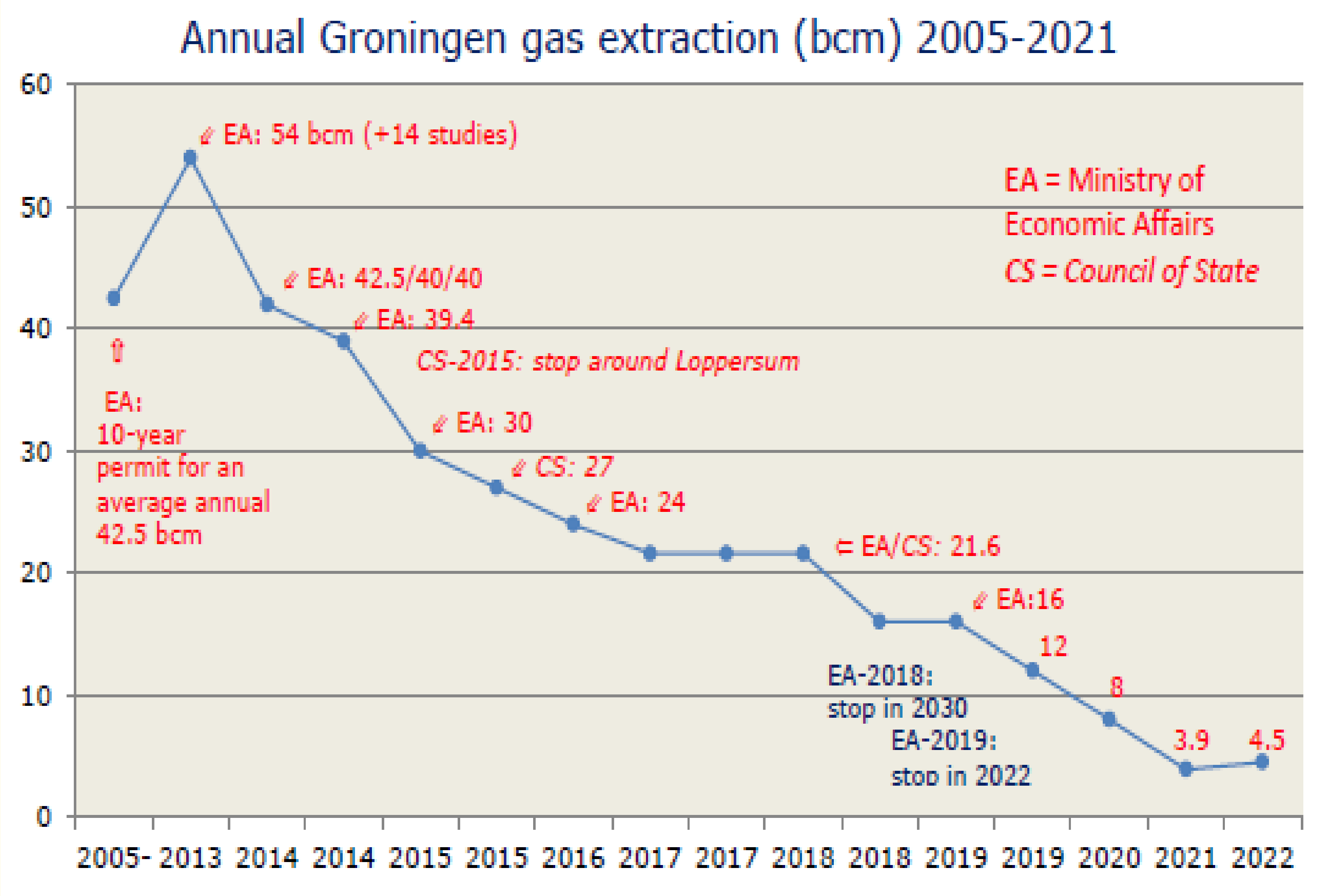

Observations:

The initially modest and later rapid decline in Groningen gas extraction (from 54 bcm in 2013 to 4.5 bcm in 2022) occurred:

- under advisory pressure from the State Supervision of Mines (2013, 2016, 2018),
- under persistent social pressure from residents' representative bodies,
- and via several decisive verdicts by the national Council of State (also weighing the risks of insufficient gas supply).

university of groningen

18. Appendix 2: RuG-projected magnitude-frequency distributions over 2022-2031 for 'Continue 10 bcm/year' versus 'Continue 20 bcm/year'

'Continue 10 bcm/year'

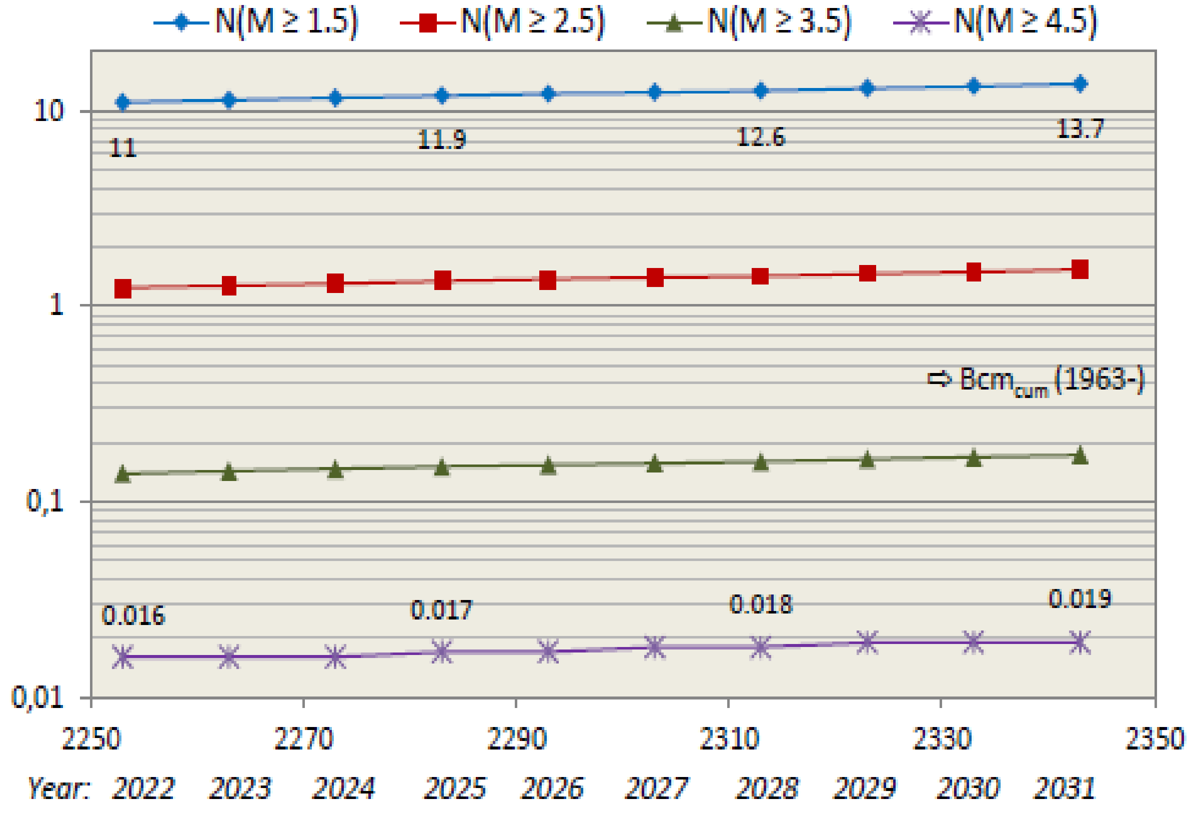

'Continue 20 bcm/year'

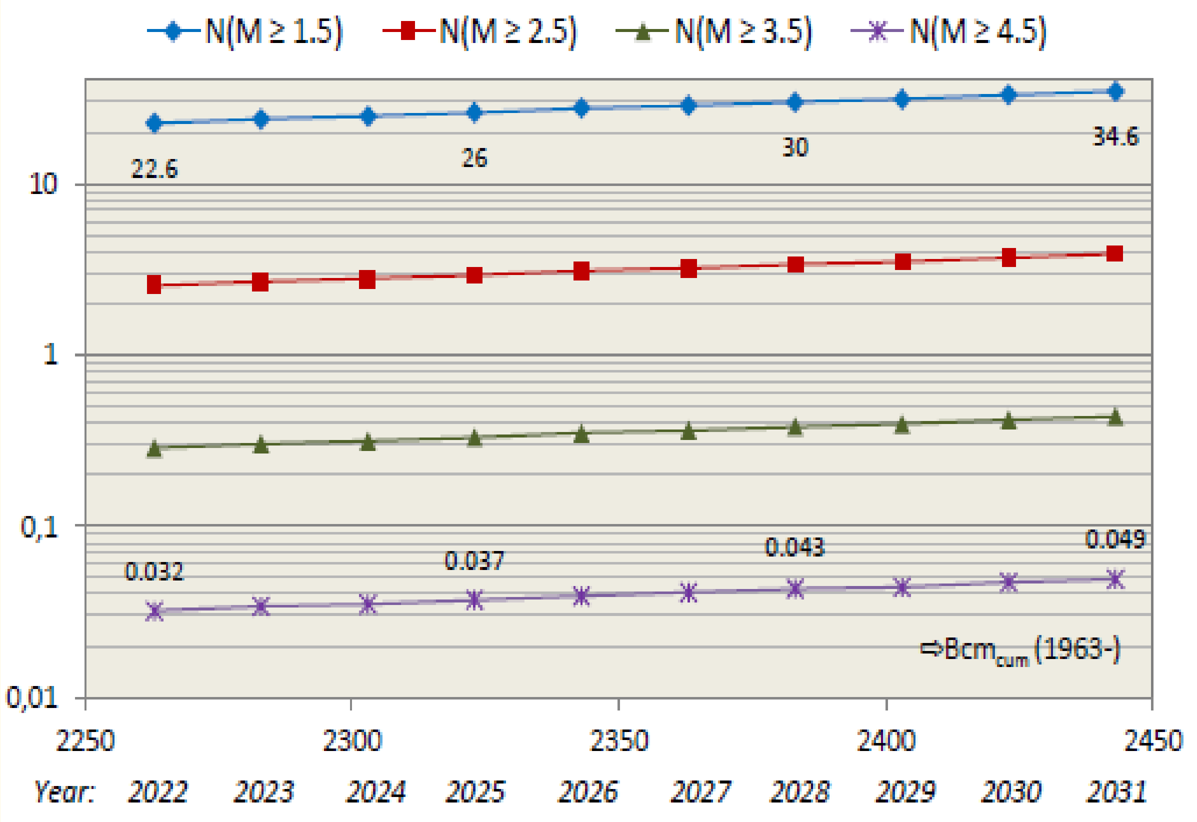

Observation: A sharp increase towards, and ten-year continuation of 20 bcm of annual extraction (right) will lead to significantly greater earthquake activity than under a 10 bcm/year scenario (left), with a projected $N(M \geq 1.5) \approx 23$ in 2023 and an $N(M \geq 1.5) \approx 35$ in 2031.

19. Appendix 3: A 3.6-earthquake like the one near Huizinge in August 2012 could have been foreseen

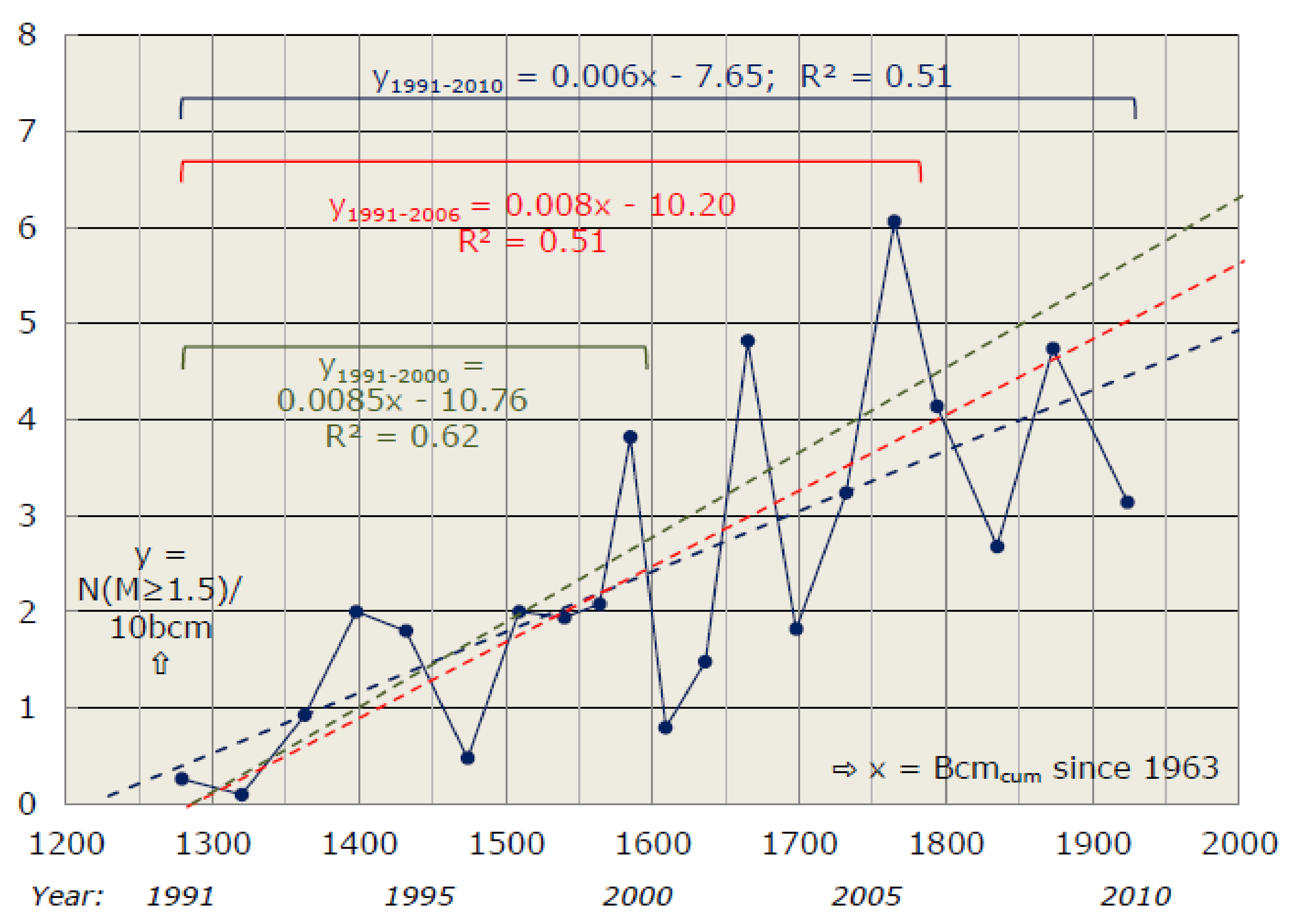

- Considering significant upward trends in N(M≥1.5)/10bcm over 1991-2000, 1991-2006 and 1991-2010,
- and given ongoing (permitted) extraction of at least 40 bcm/year (so that bcm_{cum} would reach 2,000 in 2012),
- a linearly projected N(M≥1.5)/10bcm ≈ 5.5 for 2012, and N(M ≥ 1.5)/40bcm would be 5.5 x 4 ≈ 22.
- Applying a Gutenberg-Richter b-value of 0.95 would then yield an annual N(M ≥ 2.5) ≈ 2.5, while annual N(M ≥ 3.5) ≈ 0.28 ("once per 3.6 years").
- [The first event with M ≥ 3.5 occurred near Westeremden in August 2006, after three years of extracting about 33 bcm/year.]

Note: For all three trends, statistical significance is clear but not impressive...

20. Appendix 4: Some references and other relevances

(excl. well-known papers about estimating M_{max} for the Groningen field)

- Bourne, S.J., Oates, S.J., & Van Elk, J. (2018). The exponential rise of induced seismicity with increasing stress levels in the Groningen gas field and its implications for controlling seismic risk. *Geophysical Journal International,* 213 (3), 1693-1700. https://doi.org/10.1093/gji/ggy084
- Dost, B. & Kraaijpoel, D. (2013). *The August 16, 2012 earthquake near Huizinge (Groningen).* KNMI, De Bilt, January 2013, 26 pp..
- Kühn, D., Hainzl, S., Dahm, T., Richter, G., & Vera Rodriguez, I. (2022). A review of source models to further the understanding of the seismicity of the Groningen field. *Netherlands Journal of Geosciences.* On-line, 12 pp. https://doi.org/10.1017/njg.2022.7
- Mijnraad (2022). *Mijnraadadvies borgen van leveringszekerheid in actuele gascrisis* [Mining Council advice on securing energy supply in actual gas crisis. Den Haag, 24 pp.
- Muntendam-Bos, A.G., & De Waal, J.A. (2013). *Reassessment of the probability of higher magnitude earthquakes in the Groningen gas field. Including a position statement by KNMI.* The Hague, SodM, State Supervision of Mines, 16 January. www.sodm.nl.
- NAM (2013). *Winningsplan Groningen.* [Groningen field production plan 2013, with technical addendum]. NAM, Assen, NL
- NAM (2020). *Seismic Hazard and Risk Assessment Groningen Field; update for Production Profile GTS-raming 2020,* March 2020, by J. van Elk, A.J. Landman, J. Uilenreef & D. Doornhof. Assen (NL): NAM.
- TNO (2022). *Publieke Seismische Dreigings- en Risicoanalyse Groningen gasveld 2022* [Public SHRA 2022]. Utrecht: Report R10517.
- Vlek, C. (2018). Induced earthquakes from long-term gas extraction in Groningen, the Netherlands: statistical analysis and prognosis for acceptable-risk regulation. *Risk Analysis*, 38 (7), 1455-1473. https://onlinelibrary.wiley.com/doi/full/10.1111/risa.12967.
- Vlek, C. (2019). Rise and reduction of induced earthquakes in the Groningen gas field, 1991–2018: Statistical trends, social impacts, and policy change. *Environmental Earth Sciences*, 78, no. 59. https://rdcu.be/bhn68.
- Vlek, C. (2020). *Aardgas, risico's en besluiten: een buitenparlementair onderzoek naar gaswinning-met-aardbevingen in Groningen* ['Natural gas, risks and decisions: an extra-parliamentary inquiry into gas extraction-with-earthquakes in Groningen']. Assen (NL): Van Gorcum, in Dutch. https://www.vangorcum.nl/cultuur-historie/100-359_Aardgas-risico-s-en-besluiten.

Proponent Assessment for M_{max} in the Groningen Field

Stephen Bourne
Shell Global Solutions International

16th June 2022

Tasks Assigned to the Expert Panel

"The expert panel is charged with three [sic] specific tasks:

1. To clearly define the concept of Mmax in relation to seismicity in the Groningen field and for application in probabilistic seismic hazard and risk analyses.

2. To define a distribution of Mmax values and their associated probabilities, in the form of as discrete [sic] logic tree with alternative Mmax values and associated branch weights.

3. To clearly distinguish between induced earthquakes and triggered earthquakes in the formulation of the logic tree, such that the hazard and risk analyses could consider the two types of seismicity separately.

4. To determine if the proposed Mmax distribution [is] compatible with the existing PSHRA framework for Groningen, including the V6 seismological model and the logic tree."

Source: Groningen Mmax Workshop II agenda page 1

What is the definition of M_{max} for Groningen seismicity?

The expert panel's definition of M_{max}

- The definition of Mmax is in the context of its common use in seismic source characterization for PSHA (probabilistic seismic hazard analysis).
- **For example**, as defined in USNRC (2012a, Chapter 11):
  - Mmax is "the largest earthquake that a seismic source is assessed to be capable of generating.
  - The maximum magnitude is the **upper bound to recurrence curves**."
- Mmax, as it is defined for PSHA and used here, is a time-independent upper bound.

Source: Report from the Expert Panel on Maximum Magnitude Estimates for Probabilistic Seismic Hazard and Risk Modelling in Groningen Gas Field 25 April 2016, page 6

What is the Definition of M_{max} for Groningen Seismicity?

A Paraphrased Definition of M_{max}

- The Maximum Possible Magnitude of any earthquake caused by Groningen gas production

Some Consequences

- M_{max} is the upper bound of the magnitude probability distribution
- M_{max} is a finite system limit
- M_{max} is the smallest impossible magnitude
- M_{max} is not the largest historic magnitude
- M_{max} is not the expected maximum magnitude
- M_{max} is not the largest 'credible' magnitude
- M_{max} is not any magnitude with a finite return period
- M_{max} is time-dependent
- M_{max} is not observable, ever

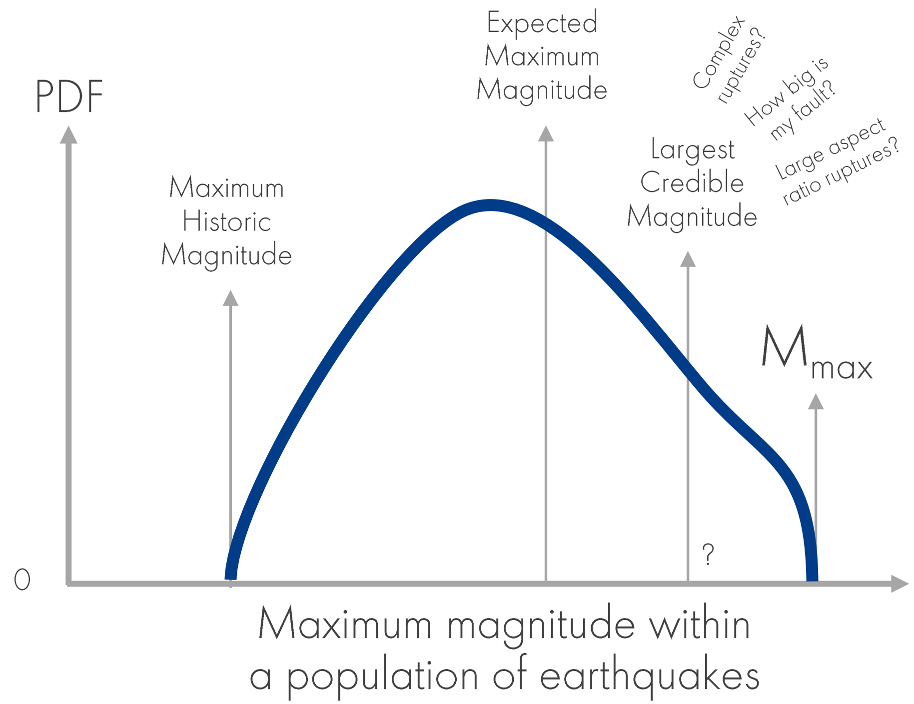

Current M_{max} Distribution Reported by the Expert Panel

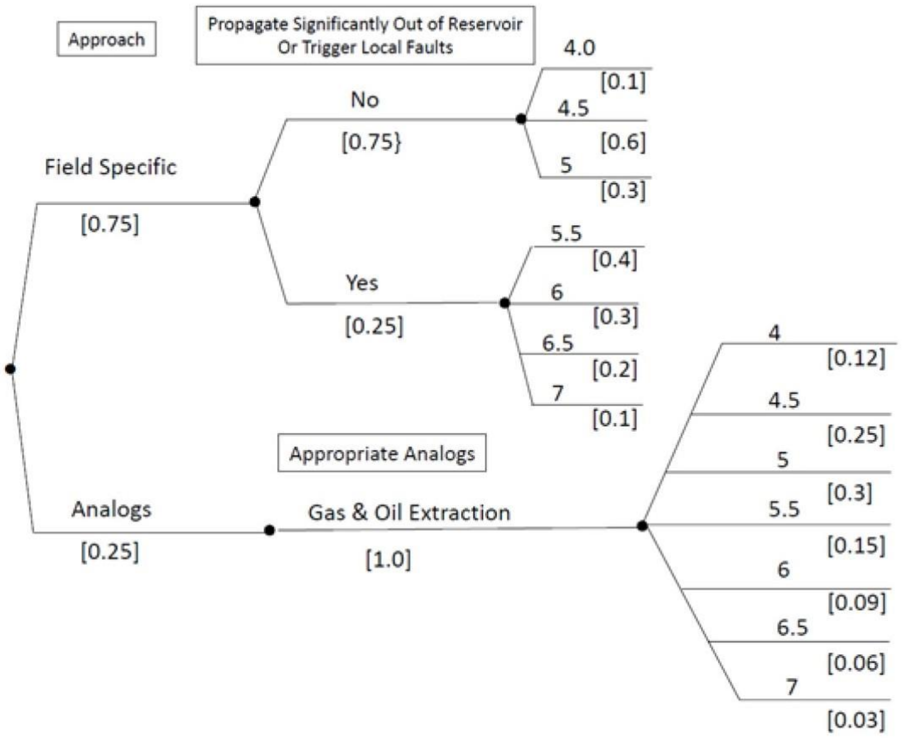

Figure 1. Logic tree showing the major elements of the assessment of Mmax for the Groningen field. Alternative branches are identified at each node and weights are assigned to each branch. The end point for each branch is the estimated maximum magnitude to the nearest half unit and its probability (in brackets).

Source: Report from the Expert Panel on Maximum Magnitude Estimates for Probabilistic Seismic Hazard and Risk Modelling in Groningen Gas Field 25 April 2016, page 6

Current M_{max} Distribution Reported by the Expert Panel

Groningen Reservoir Constrained

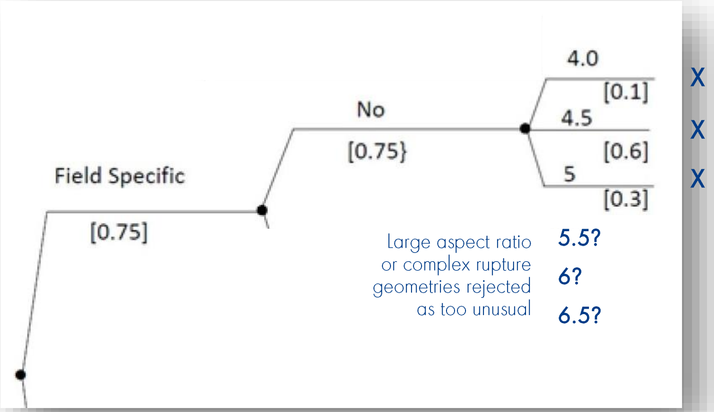

Source: Report from the Expert Panel on Maximum Magnitude Estimates for Probabilistic Seismic Hazard and Risk Modelling in Groningen Gas Field 25 April 2016

Judgements

- "Very few of the field-specific analyses presented at the workshop provided expected maximum magnitude estimates as low as M 4, but Suckale's numerical simulations resulted in magnitudes of M 3.8 to 4.6, depending on various assumptions, and Shapiro reported an M 4.2 from a bounded frequency-magnitude distribution. The Panel assigns a low weight of 0.1 to the Mmax value of M 4 (Figure 1)."
- "The Mmax value of M 4.5 is consistent with several of the field-specific assessments discussed by researchers at the workshop. For example, DeDontney (Exxon) concluded that ruptures lying entirely within the reservoir could result in a magnitude as high as M 4.5. TNO researchers reported an M 4.7, based on a maximum length of 12 km for those faults that have cumulative displacements of 200m or more. A similar magnitude was reported by Van d. Bogen based on dynamic rupture models using the faults with the largest offsets. Zöller reported a range of M 3.6 – 4.7 when the 90% confidence level is used to constrain the uncertainties in b-value."
- "The Panel also notes that length-to-width aspect ratios of 20:1 to 50:1 for dip-slip fault implied by the rupture scenarios presented at the workshop are considered to be very unusual, based on consideration of observed earthquake ruptures. After due consideration of the field-specific results and assuming no significant rupture propagation out of the reservoir, the Panel assigns a weight of 0.6 to M 4.5 and a weight of 0.3 to M 5"

Inconsistent logic?

M_{max} is not the expected maximum magnitude

M_{max} is not the largest 'credible' magnitude

M_{max} is not any magnitude with a finite return period

M_{max} is not any magnitude with a finite return period

Current M_{max} Distribution Reported by the Expert Panel

Groningen Reservoir + Basement

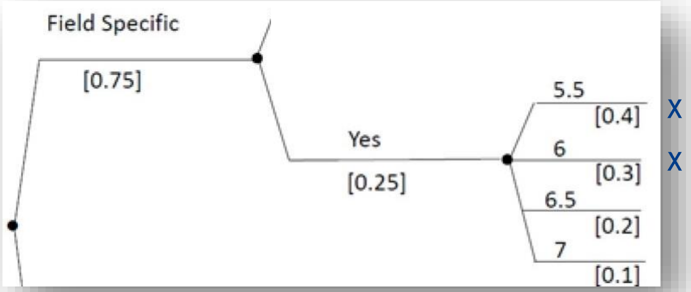

Source: Report from the Expert Panel on Maximum Magnitude Estimates for Probabilistic Seismic Hazard and Risk Modelling in Groningen Gas Field 25 April 2016

Judgements

- "Dost indicated that a magnitude of about M 5.8 results from a fault having dimensions of length 60 km and width of 3 km, which would require significant rupture propagation outside of the reservoir."
- "DeDontney … reported that magnitudes in the range of M 5.5 to 6.5 could result from rupture downdip into the Carboniferous rocks and assuming realistic rupture geometries."
- "Bourne reported that a M 6.5 would result from applying a cumulative strain model to the reservoir assuming all strain is released in a single event and that the strain partitioning factor is assumed to be 1.0, meaning that all strain energy is released seismically. This is considered to be a highly unlikely bounding assumption."
- "Brodsky reported that earthquakes in the range of M 6.5 to 7 have occurred due to triggering faults from induced seismicity."
- In a model where the induced seismicity at the field is assumed to be capable of triggering tectonic faults, it is noted that the maximum magnitude for the seismic source zone that contains all of the Netherlands in the SHARE (Woessner et al. 2013) hazard model is M 6.5 to 7.1."

Inconsistent logic?

→ M_{max} is <u>not</u> the largest 'credible' magnitude

→ M_{max} is <u>not</u> the largest 'credible' magnitude

→ Not a basement rupture

→ M_{max} is <u>not</u> any magnitude with a finite return period

→ Not field-specific

Current M_{max} Distribution Reported by the Expert Panel

Appropriate Analogues

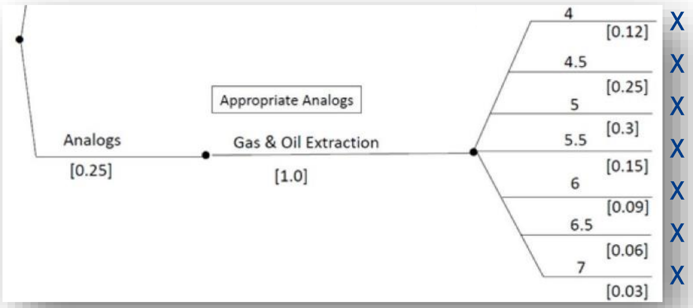

Source: Report from the Expert Panel on Maximum Magnitude Estimates for Probabilistic Seismic Hazard and Risk Modelling in Groningen Gas Field 25 April 2016

Judgements

- "The earthquake occurrences identified as being related to "Gas Extraction" were considered to be analogous to Groningen, as were three earthquake case histories identified as related to "Oil Extraction" without reported injection."
- "The Panel also considered the presentation by Brodsky drawing analogy to the Gazli earthquakes, which reached M 7 and have been interpreted to be associated with gas extraction."
- "The direct assessment is made by considering the maximum observed magnitudes associated with the case histories and considering subjectively the range of magnitudes that should define the Mmax for Groningen in light of the observations."

Inconsistent logic?

M_{max} is not the largest historic magnitude

M_{max} is not the largest historic magnitude

M_{max} is not the largest historic magnitude

M_{max} is an Incomplete Application of Finite Physical Limits to PSHA

Probabilistic Seismic Hazard Analysis

$$\lambda_s(t,T,\mathbf{x}_r,S>s)=\int\int\int \lambda_e(t,\mathbf{x}_s)f_m(M|t,\mathbf{x}_s)f_s(S|t,T,\mathbf{x}_s,\mathbf{x}_r,M)d\mathbf{x}_s dM dS$$

Ground motion exceedance rate	Source occurrence rate	Source magnitude probability density	Ground motion probability density
? Distribution	Poisson Distribution	Exponential Distribution	Log-Normal Distribution
Unbounded	Unbounded	Unbounded	Unbounded
Infinite energy release possible unless occurrence, magnitude and ground motion models are bounded	Infinite energy release possible given $M \geq M_{min}$	Infinite energy release possible given finite λ_e	Infinite energy release possible given finite M
Impose upper bound?	Impose upper bound?	Impose upper bound?	Impose upper bound?
No	**No**	**Yes**	**No**

Any M_{max} Distribution is Compatible With the Seismological Model

Compatible: (of two things) able to exist or occur together without problems or conflict.
– Oxford English Dictionary

Two V6 Seismological Magnitude Models

1. **Pure Power-Law with a Stress-Dependent *b*-value**
   - No upper bound, no inference of M_{max}, no possible incompatibility
   - Posterior magnitude model distribution jointly inferred with the stress model given observed events
   - Any given M_{max} is imposed as an independent distribution by renormalization

2. **Tapered Power-Law with a Stress-Dependent Taper**
   - No upper bound, no inference of M_{max}, no possible incompatibility
   - Posterior magnitude model distribution jointly inferred with the stress model given observed events
   - Any given M_{max} imposed as an independent distribution by renormalization
   - Reduces the influence of M_{max} judgements on the seismic hazard

Reservoir Constrained Ruptures Imply a Taper before any M_{max}

Leonard (BSSA, 2014) for dip-slip events

- Rupture width: log W = F(M) $+ \varepsilon \sigma$ where, e is randomly sampled from Normal(0, 1)
- Width constrained magnitude distribution: $P(>M \mid M>M_{min})\ P(W<W_{max}) = \exp -b^{/}(M\text{-}M_{min})\ \ (1 - \Phi\ (\ (\log W_{max} - F(M)\ )\ /\ \sigma))$

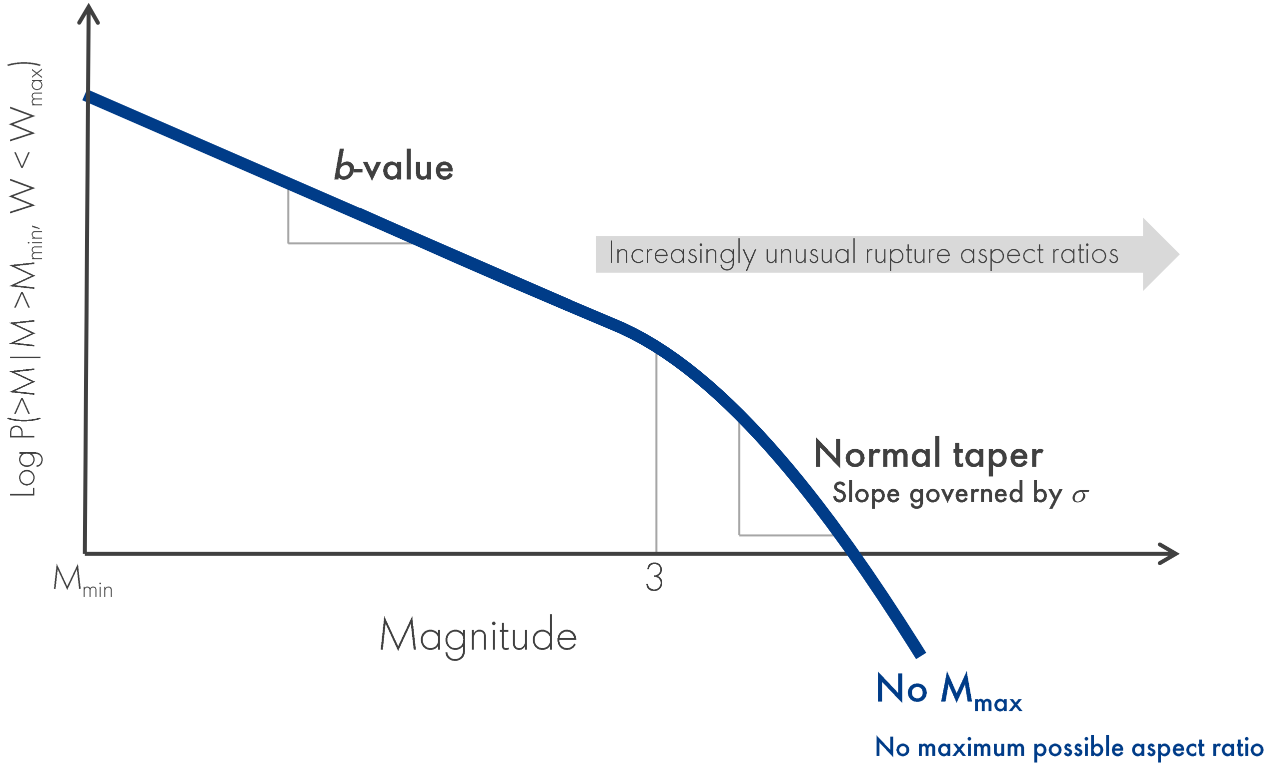

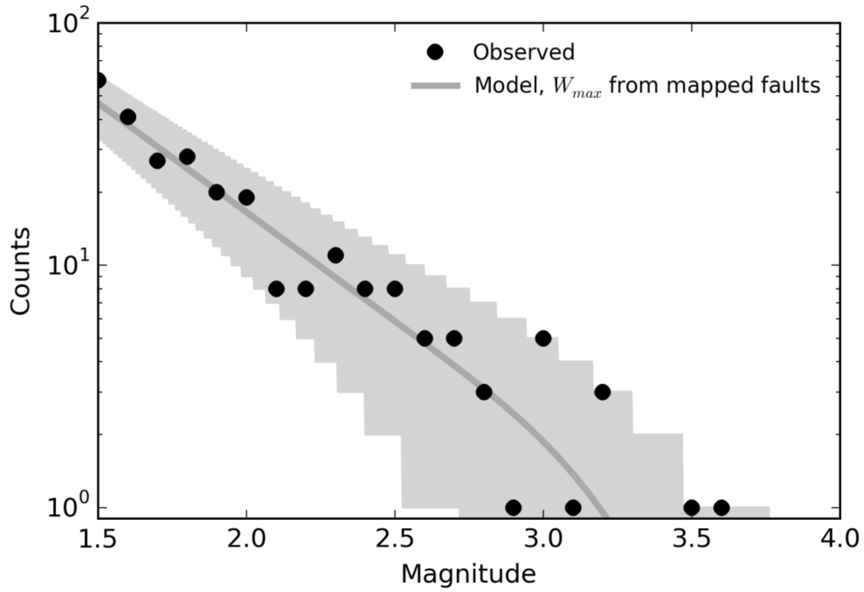

Crustal Constrained Ruptures Imply a Taper before any M_{max}

Leonard (BSSA, 2014) for dip-slip events

- Rupture width: $\log W = F(M) + \varepsilon\,\sigma$ where, e is randomly sampled from Normal(0, 1)
- Width constrained magnitude distribution: $P(>M \mid M>M_{min})\, P(W<W_{max}) = \exp -b'(M-M_{min})\ \left(1 - \Phi\left((\log W_{max} - F(M)) / \sigma\right)\right)$

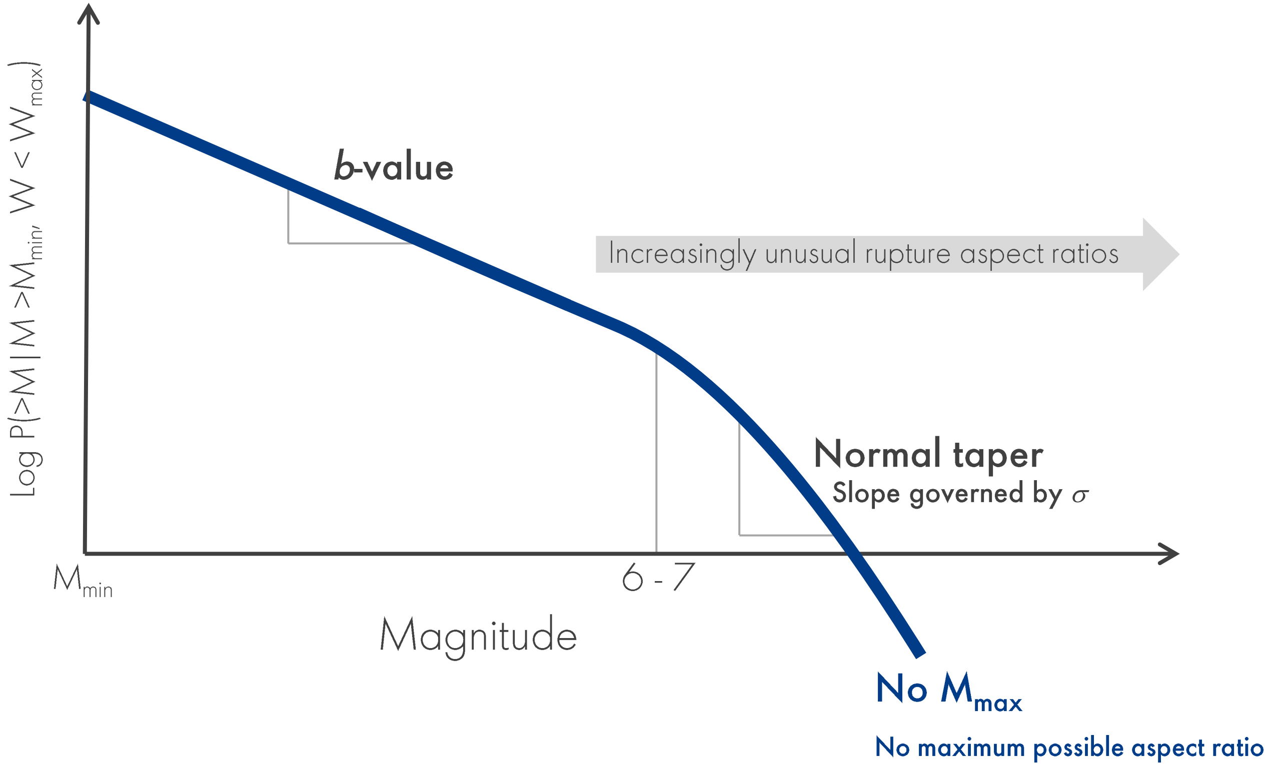

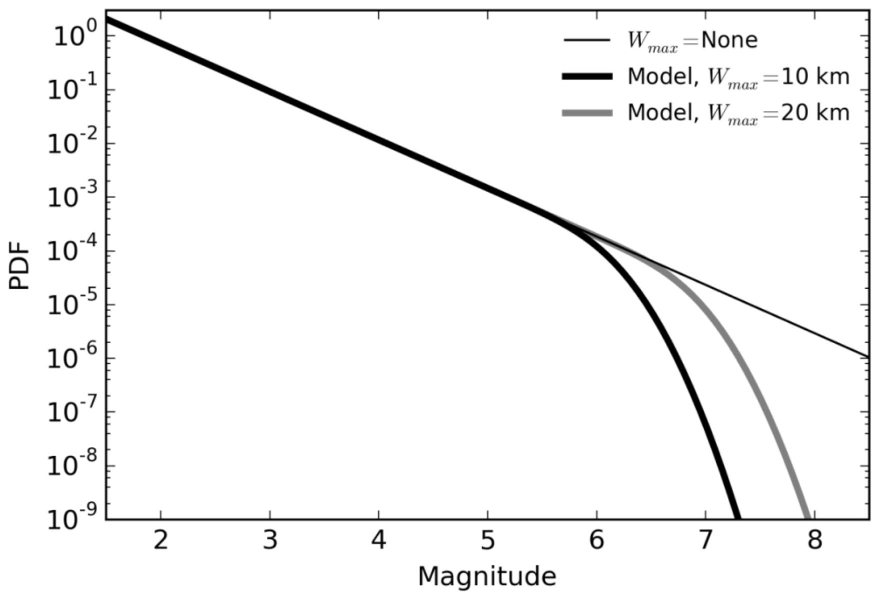

Layer Constrained Ruptures Imply a Taper before any M_{max}

Simple stochastic model of a layer-constrained rupture extent

- Rupture width constraint, W_{max} , eventually implies a 1D rupture geometry

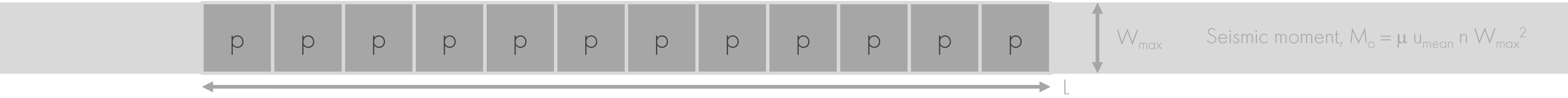

- $Pr(L = n\, W_{max}) = p^n = \exp(n \log p) = \exp(M_o \log p / \mu\, u_{mean}\, W_{max}^2)$ = Exponential taper
- Geometric origin for a stress-invariant Tapered Power-Law distribution (Geometric Taper)
- Compatible with the mechanical origin of a stress-dependent Tapered Power-Law distribution (Mechanical Taper)

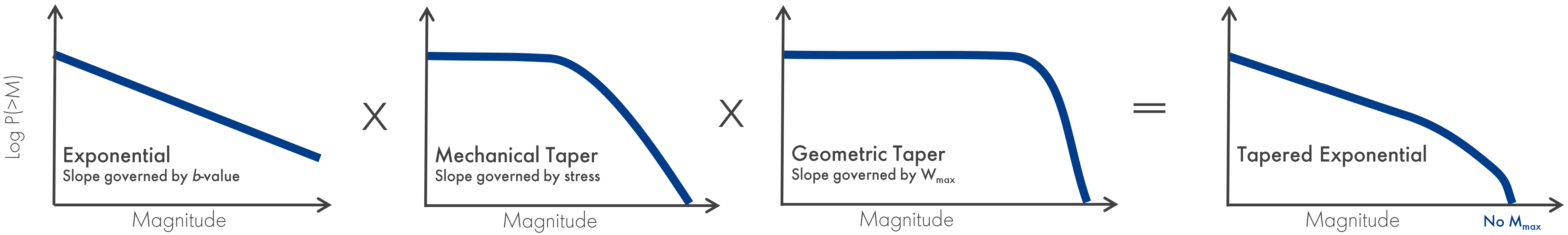

Other Hazards Use Extreme Value Theory Without Needing M_{max}

Some Examples

1. Coastal defence
2. Flood defence
3. Ocean waves
4. Wind loading
5. Tornado risk
6. Wild fire risk
7. Telecommunications traffic
8. Road safety
9. Athletic performance
10. Pipeline corrosion
11. Material strength
12. Equity risks

Extreme Threshold Theory

1. IID stochastic variables
2. Distribution of the maximum of subsets
3. Upper tail is a Generalized Pareto Distribution
4. With or without an upper bound

Source: Coles, S. An Introduction to Statistical Modeling of Extreme Values, 2001, https://doi.org/10.1007/978-1-4471-3675-0

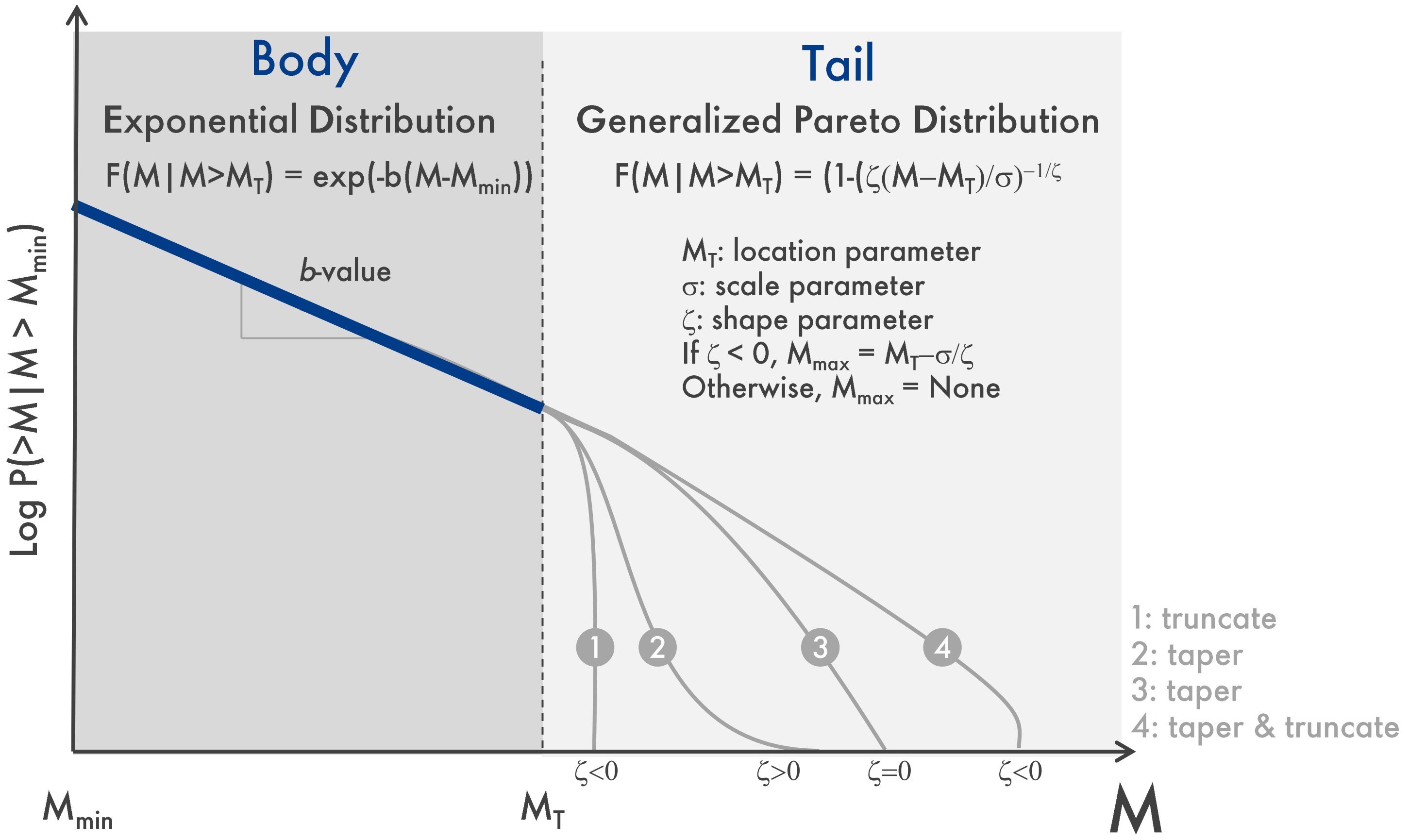

Might M_{max} as an Upper Bound be Unnecessary in PSHA?

An informed skeptic might judge M_{max} estimates to be unnecessary in PSHA because they are based on:

1. an incomplete application of finite physical limits
    1. no upper bound imposed on Poisson distributed event rates
    2. no upper bound imposed on Log-Normal distributed ground motions
2. an inconsistent logic for judging events with infinite return periods
    1. "very usual" fault aspect ratios judged to mean impossible
    2. "highly unlikely" complete release of elastic energy judged to mean impossible
    3. "expected maximum magnitude" judged to indicate the maximum possible magnitude
    4. analogue 'historic maximum' magnitudes judged to be the same as the 'maximum possible'
3. a difficult answer to a difficult question
    1. absence of direct observational evidence to support M_{max} judgements
    2. inability to falsify M_{max} judgements: no early warning of any M_{max} error, any M_{max} exceedance is too late for PSHA
    3. inability to independently replicate M_{max} judgements

Proposal for Updating M_{max} in the Groningen PSHA

Proposal: Incorporate a finite physical limit informed by the observable geological system size

- Replace a finite magnitude limit with a finite rupture height limit
- Replace M_{max} with W_{max} using geometric tapers to represent potential seismogenic thickness limits
- Evaluate the geometric taper given W_{max} using the self-consistent finite-rupture scaling relations from Leonard (2014)
- Redefine M_{max} as the corner magnitude of the geometric taper defined by W_{max} (a soft M_{max})
- The corner magnitude follows as the most-likely magnitude to have a rupture width of W_{max}

Justification

- M_{max} is not observable, W_{max} is observable and supported by simple geometrical/geological observations
- Avoids weak arguments that claim 'highly unlikely' events are impossible. Avoids creating a need for N_{max}, and ε_{max}
- Clearly distinguishes between 'induced' (reservoir) and 'triggered' (basement) seismicity
- W_{max} is time invariant
- W_{max} allows us to "never say never"

Proposal for Updating M_{max} in the Groningen PSHA

Application

- Represent W_{max} as a logic tree to include epistemic uncertainty, compute geometric tapers according to Leonard (2014)

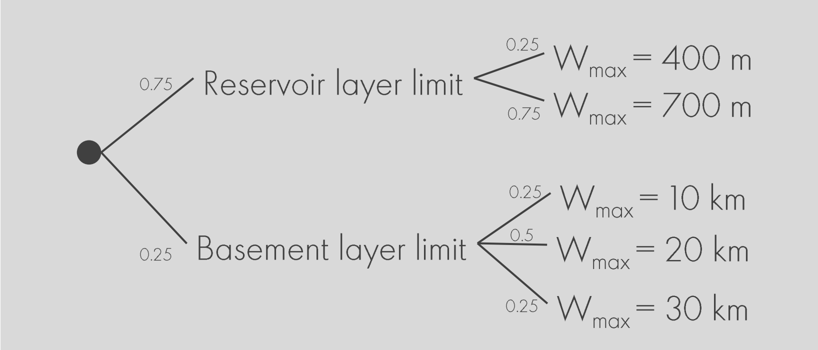

Evidence: Maximum thickness plus offset for faults within 500 m of an epicenter

Evidence: Maximum thickness plus offset for all faults

Evidence: Generic uncertainty: 10 – 30 km (Johnston,1994)

Evidence: Seismogenic thickness for NW-Europe: 20 km (Ward, 1998)

Evidence: Generic uncertainty: 10 – 30 km (Johnston,1994)

- Assign weights based on expert judgement
- Apply this geometric taper in the same manner as the mechanical taper in the seismological magnitude model

Closing Remark 1

The Current M_{max} Distribution Creates a Tapered Bounded Magnitude Distribution

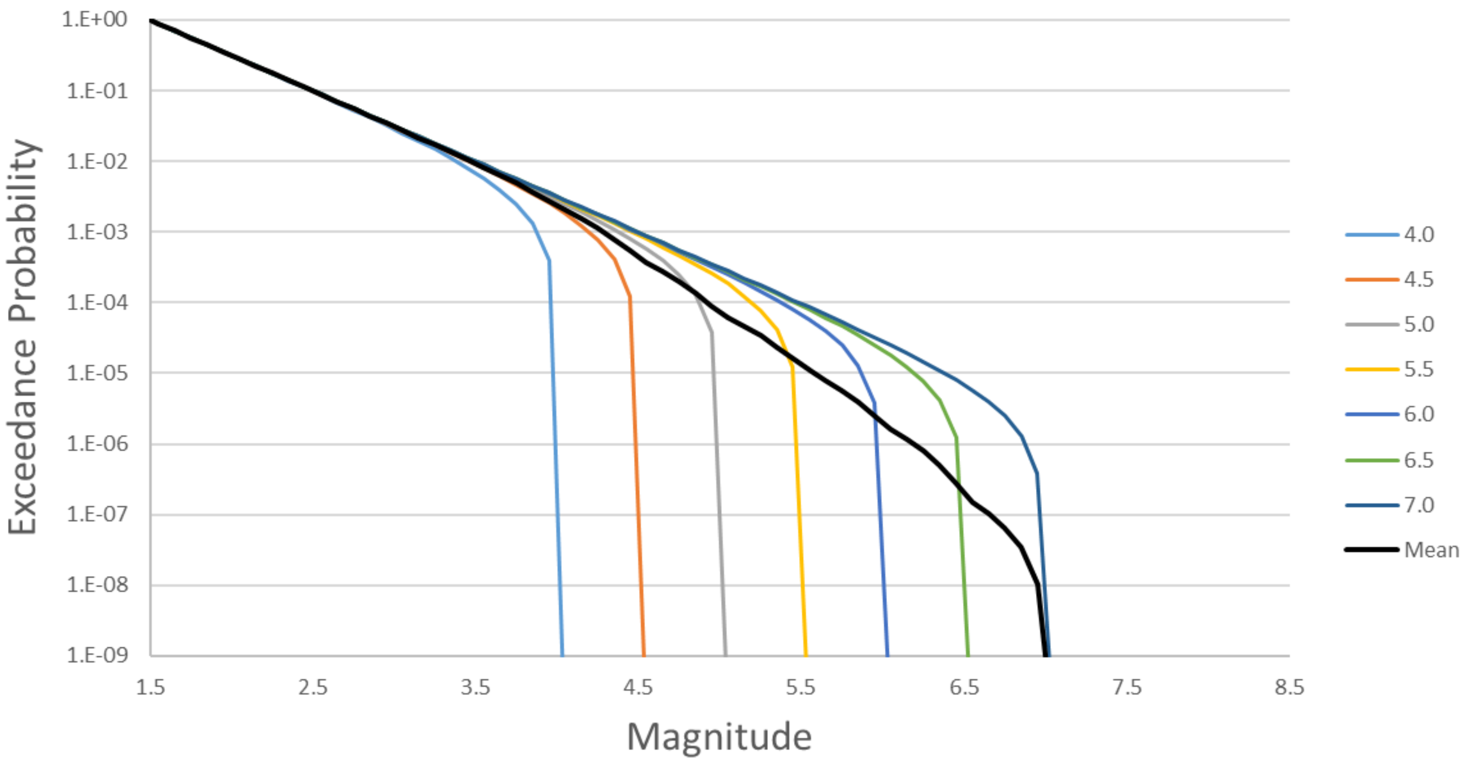

Closing Remark 2

The Proposed W_{max} Distribution Creates a Tapered Unbounded Magnitude Distribution

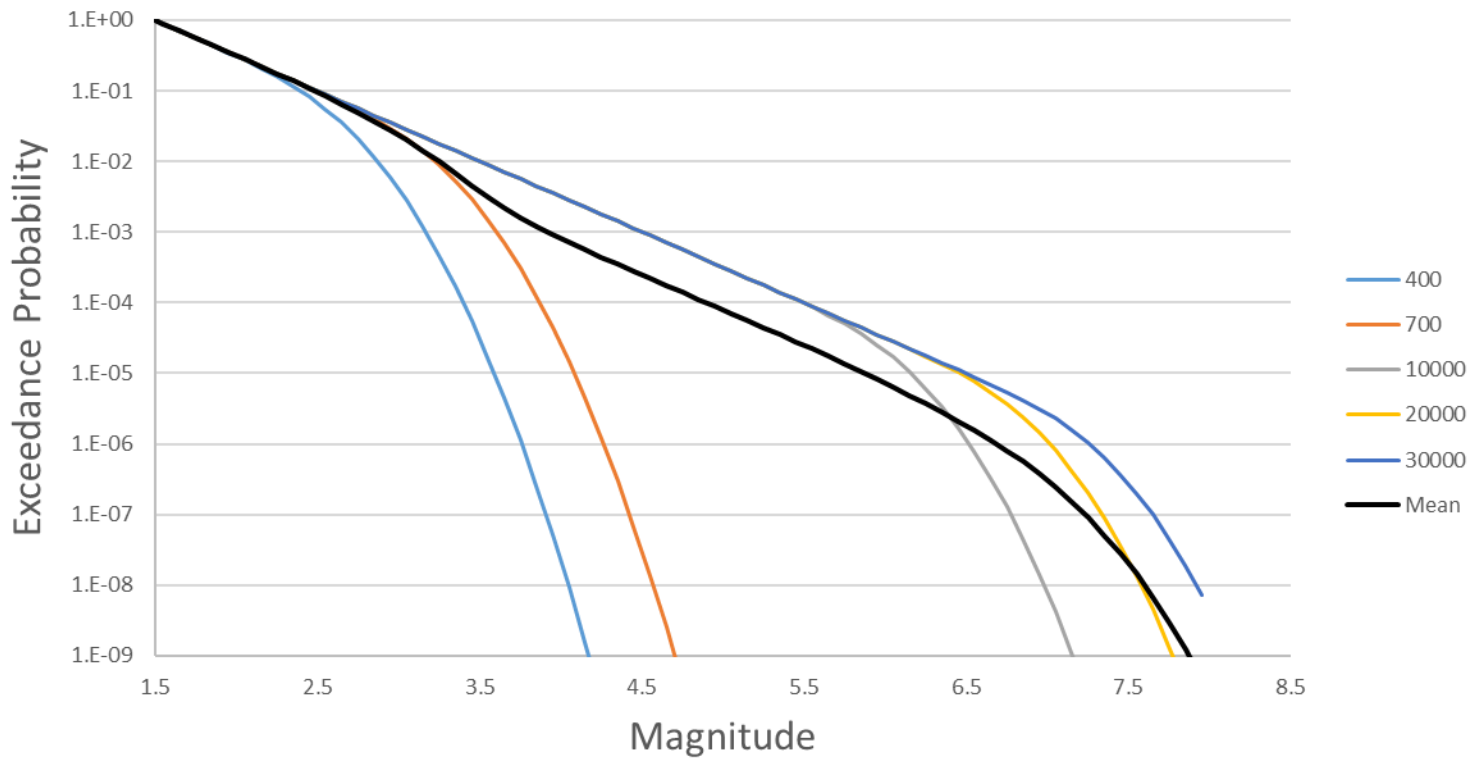

Closing Remark 3
The M_{max} and W_{max} Tapered Magnitude Distributions are Similar

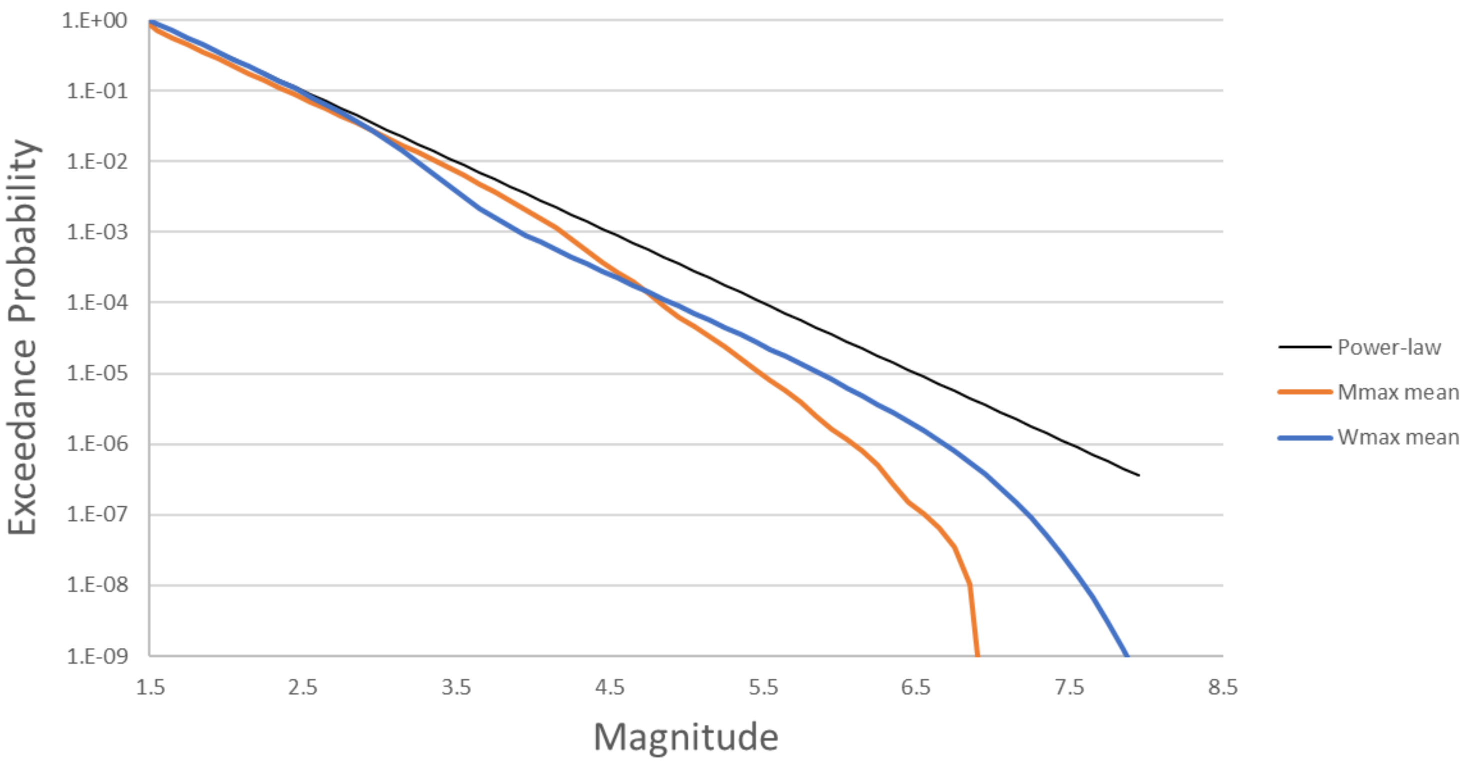

Closing Remark 4

W_{max} can Approximate the Current M_{max} Magnitude Distribution up to max(M_{max}) by including an intermediate W_{max} within the basement

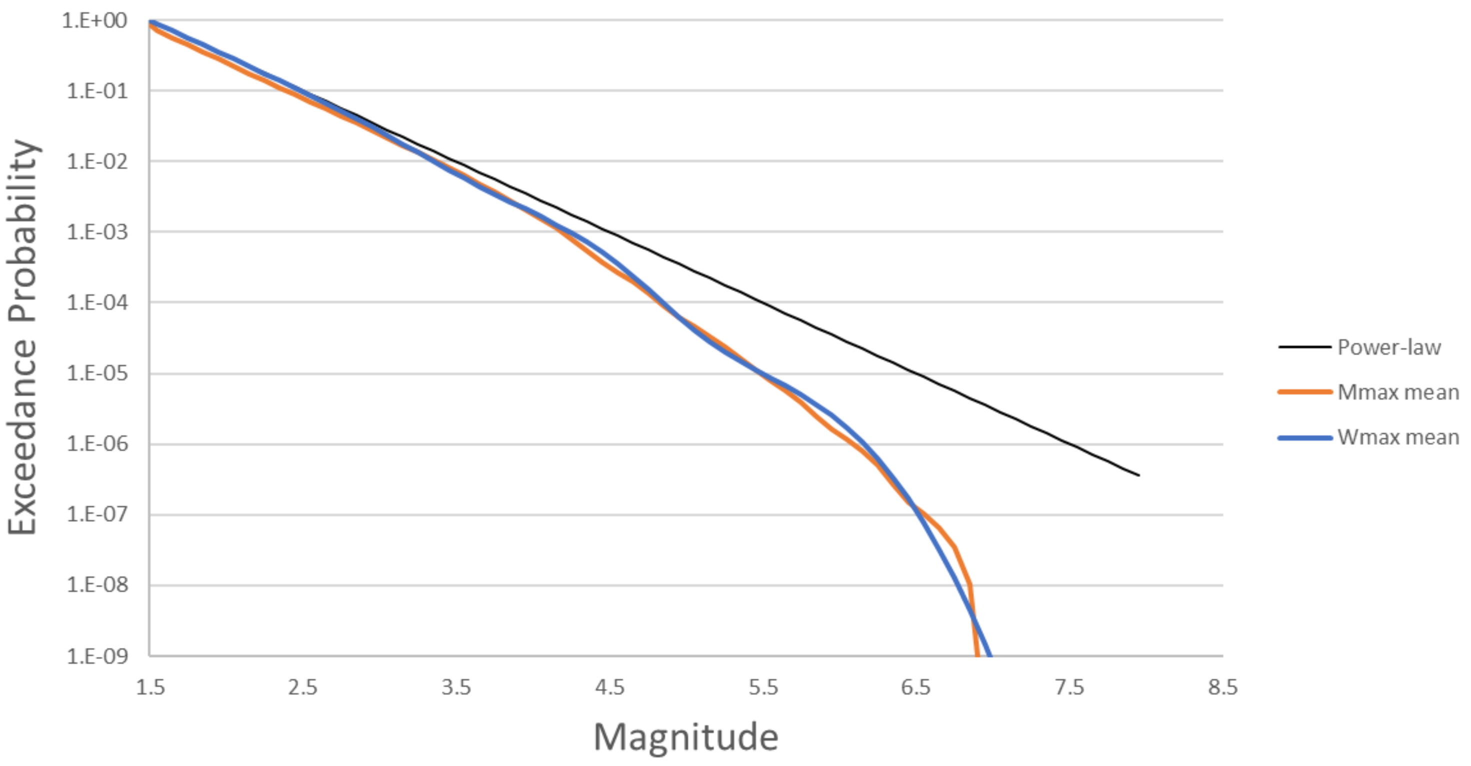

Offer: To Provide an Excel Spreadsheet to the Expert Panel to Facilitate Comparing M_{max} and W_{max} Magnitude Distributions

PHYSICS-BASED CONSTRAINTS ON MAXIMUM MAGNITUDES IN THE GRONINGEN FIELD

LOES BUIJZE[1], HUIHUI WENG[2], PABLO AMPUERO[2]

[1] APPLIED GEOSCIENCES, TNO [2] ÙNIVERSITÉ COTE D'AZUR NICE

ACKNOWLEDGEMENTS

- 2011 – 2015 Applied Geosciences, TNO (Geological Survey of the Netherlands)
- 2015 – 2020 PhD at Utrecht University, Applied Geosciences TNO
  - Project: Rupture modeling & Lab-field validation, Prof. CJ Spiers
  - UU project “Studies on fault (re)activation and dynamic friction and failure behavior” funded by NAM BV.
- 2020 – current: Applied Geosciences, TNO
  - Geomechanics Team

Thanks to many people for discussions, advice, guidance and help during these years: Chris Spiers, André Niemeijer, Ronald Pijnenburg, Luuk Hunfeld, Jianye Chen, Jan van Elk, Clemens Visser, Rob van Eijs, Rick Wentinck, Peter van den Bogert, Brecht Wassing, Sander Osinga, Thibault Candela,…

TNO innovation for life

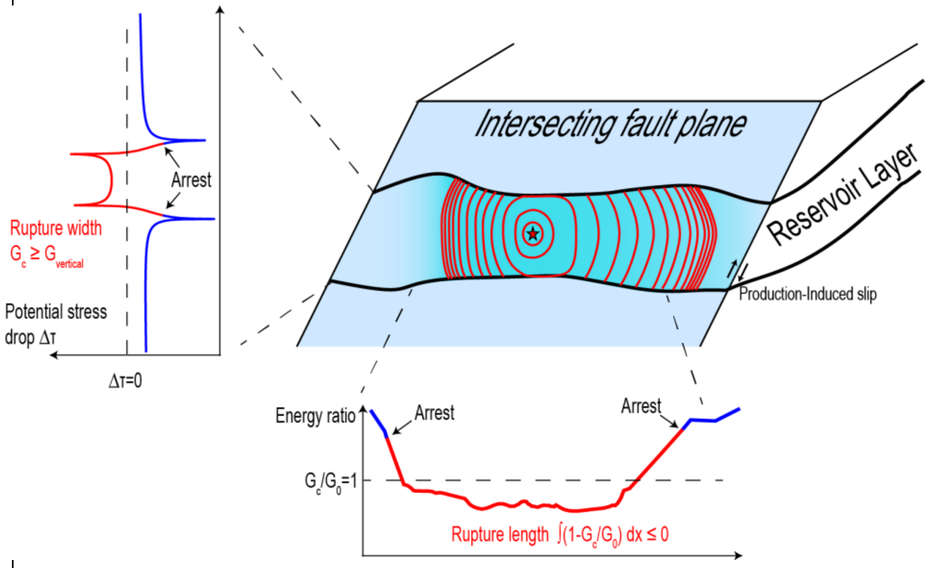

Efficient dynamic rupture modeling includes:

- Combined along-dip 2D LEFM and along-strike 2.5D LEFM
- Fault friction constrained by lab and seismological observations
- Groningen fault network geometry
- Models of fault stress induced by reservoir depletion

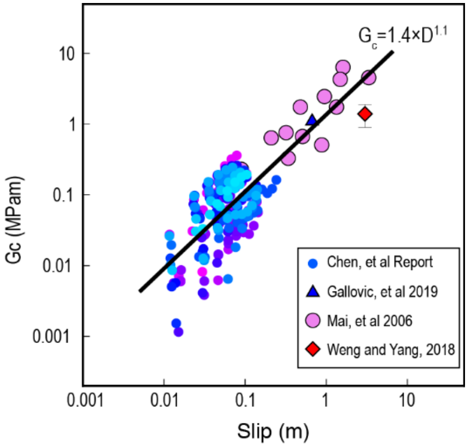

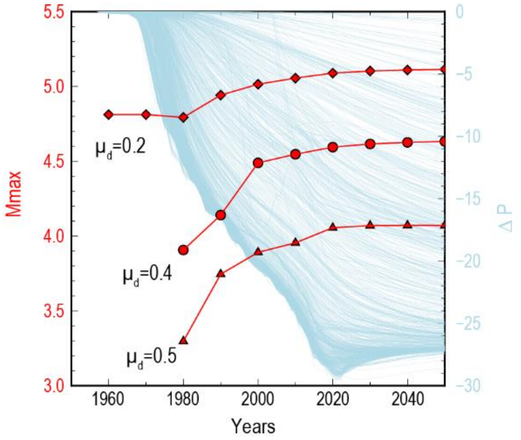

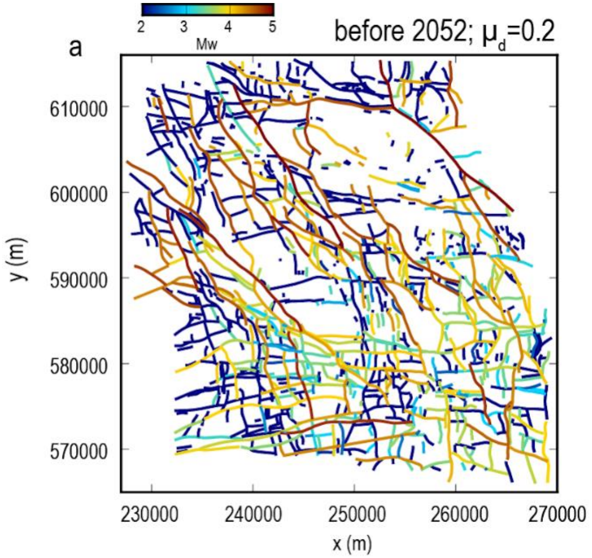

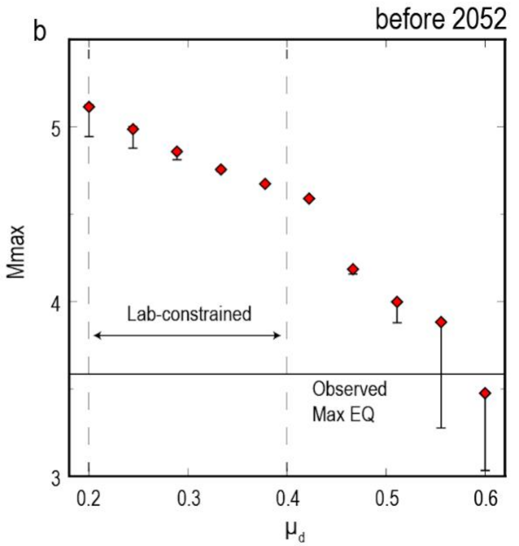

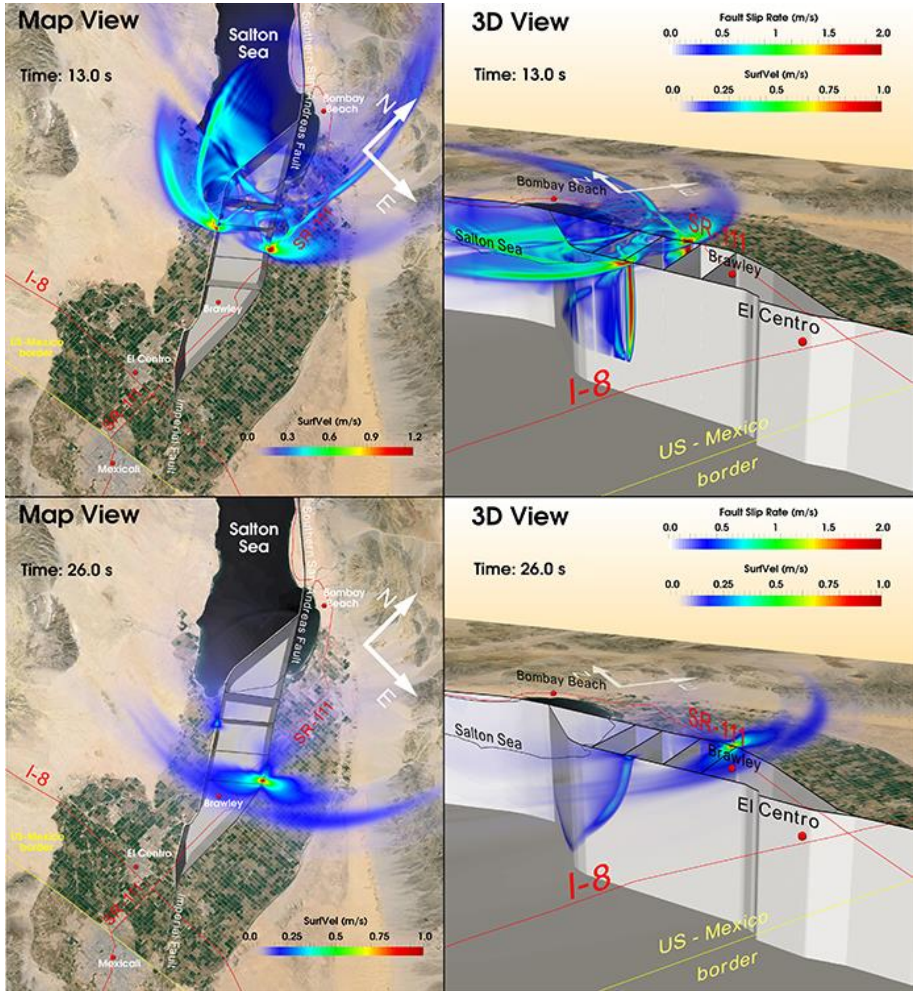
Map View
Salton Sea
Time: 13.0 s
Bombay Beach
Brawley
El Centro
I-8
SurfVel (m/s)
Mexicali
3D View
Time: 13.0 s
Fault Slip Rate (m/s)
SurfVel (m/s)
Bombay Beach
Salton Sea
SR-111
Brawley
El Centro
I-8
US - Mexico border
Map View
Salton Sea
Time: 26.0 s
3D View
Time: 26.0 s

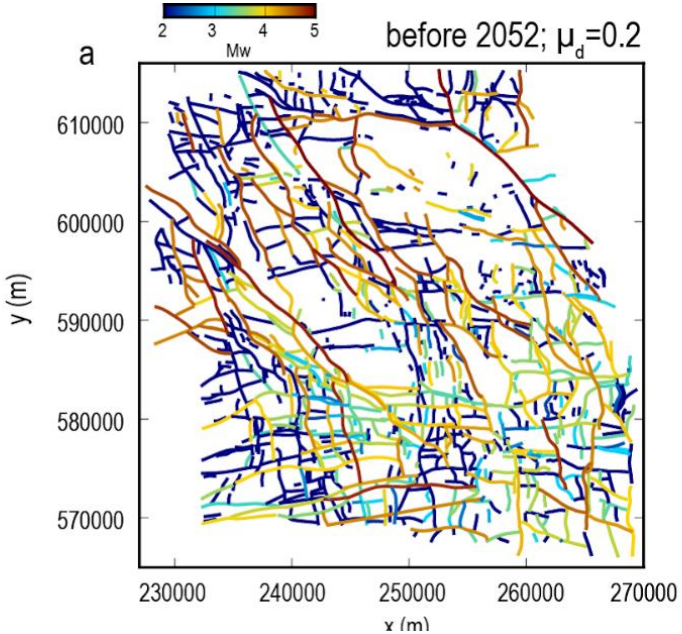
a
Mw
2 3 4 5
before 2052; μd=0.2
y (m)
610000
600000
590000
580000
570000
230000
240000
250000
260000
270000
x (m)

TOWARDS FAST 3D GEOMECHANICAL MODELING

Galis et al (2017, 2019)

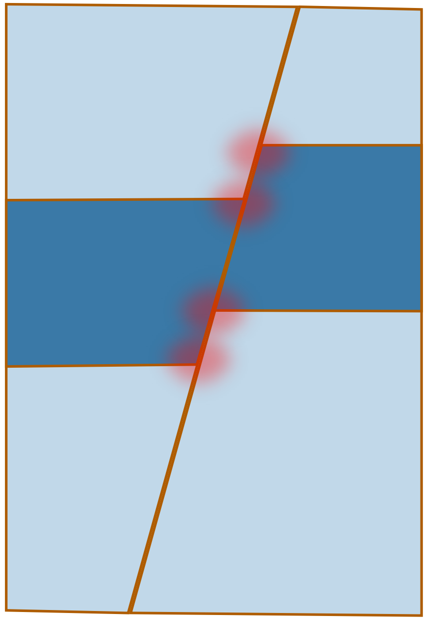

2D

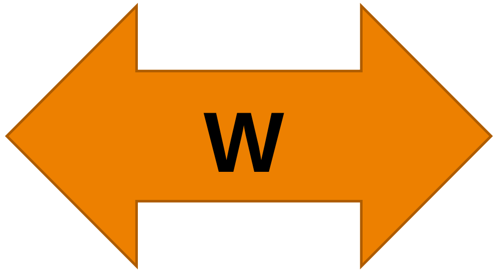

2.5D

Weng and Ampuero (2019, 2020)

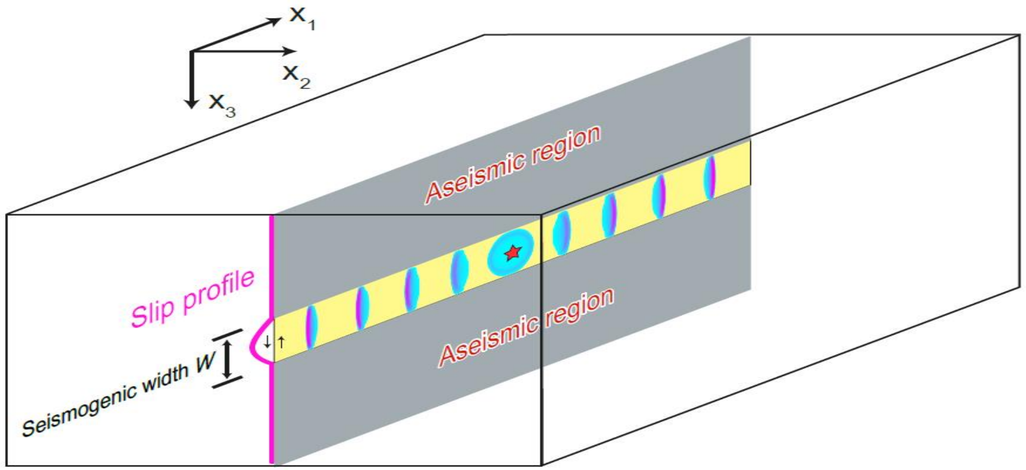

3D

Rupture arrest, Mmax

Needs:
Map of faults and offsets, reservoir thickness, pressure changes
Stressing rates
Material strength: Gc vs D relation

Constraint on Mmax from available stress and rupture dynamics. Not: modeling of catalog, events

OUTLINE

- Part I Applying LEFM elongated rupture theory to Groningen for MMax
  - Fast field-scale 2.5 D model for evaluation of Mmax
  - Key ingredients: initial stress and stress change,
  - Results & sensitivities
- Part II Rupture propagation into the Carboniferous
  - 2D, added complexity
  - Along-dip rupture length W, potential propagation into Carboniferous

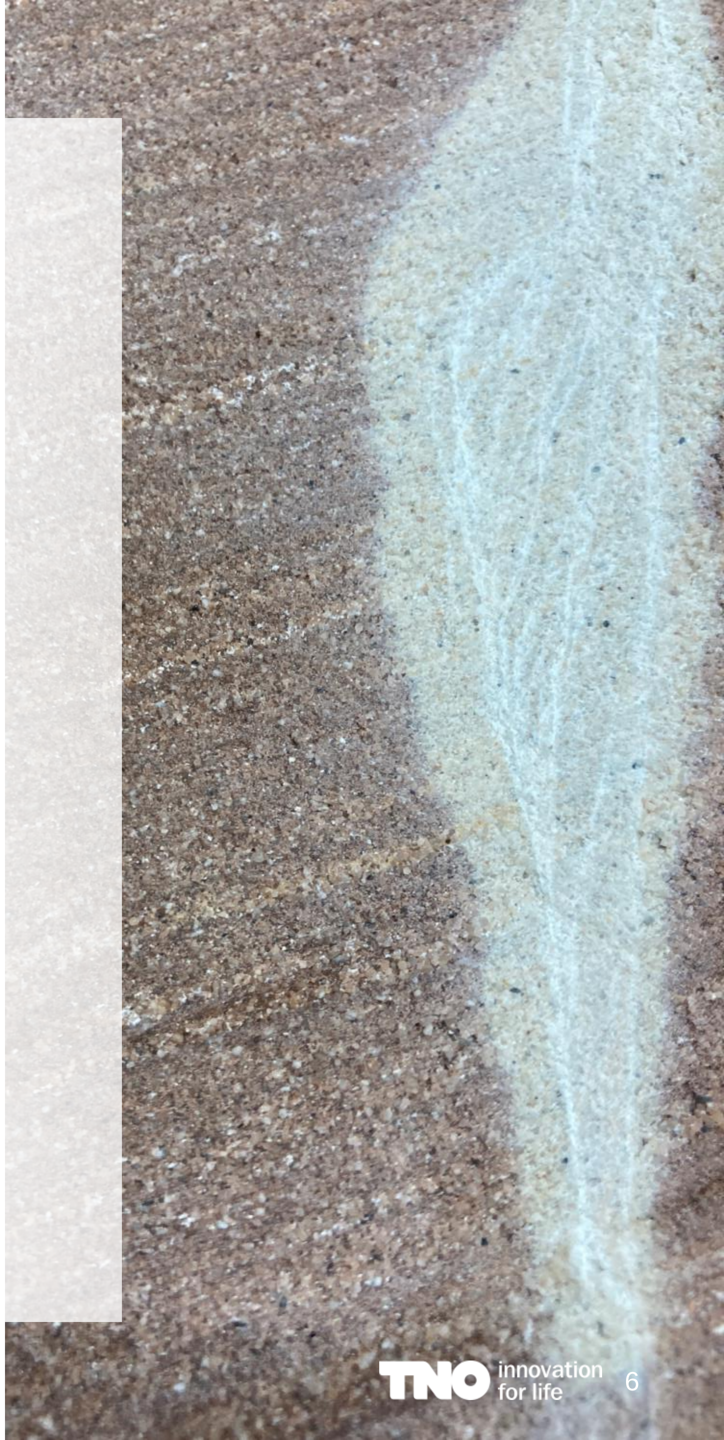

FAULT STRIKE, DIP, THROW

- NAM, 2017,
- > 1000 faults
- Represented by >35,000 pillars
- At each pillar top depths of main litho-stratigraphic units are known, as well as dip and dip azimuth

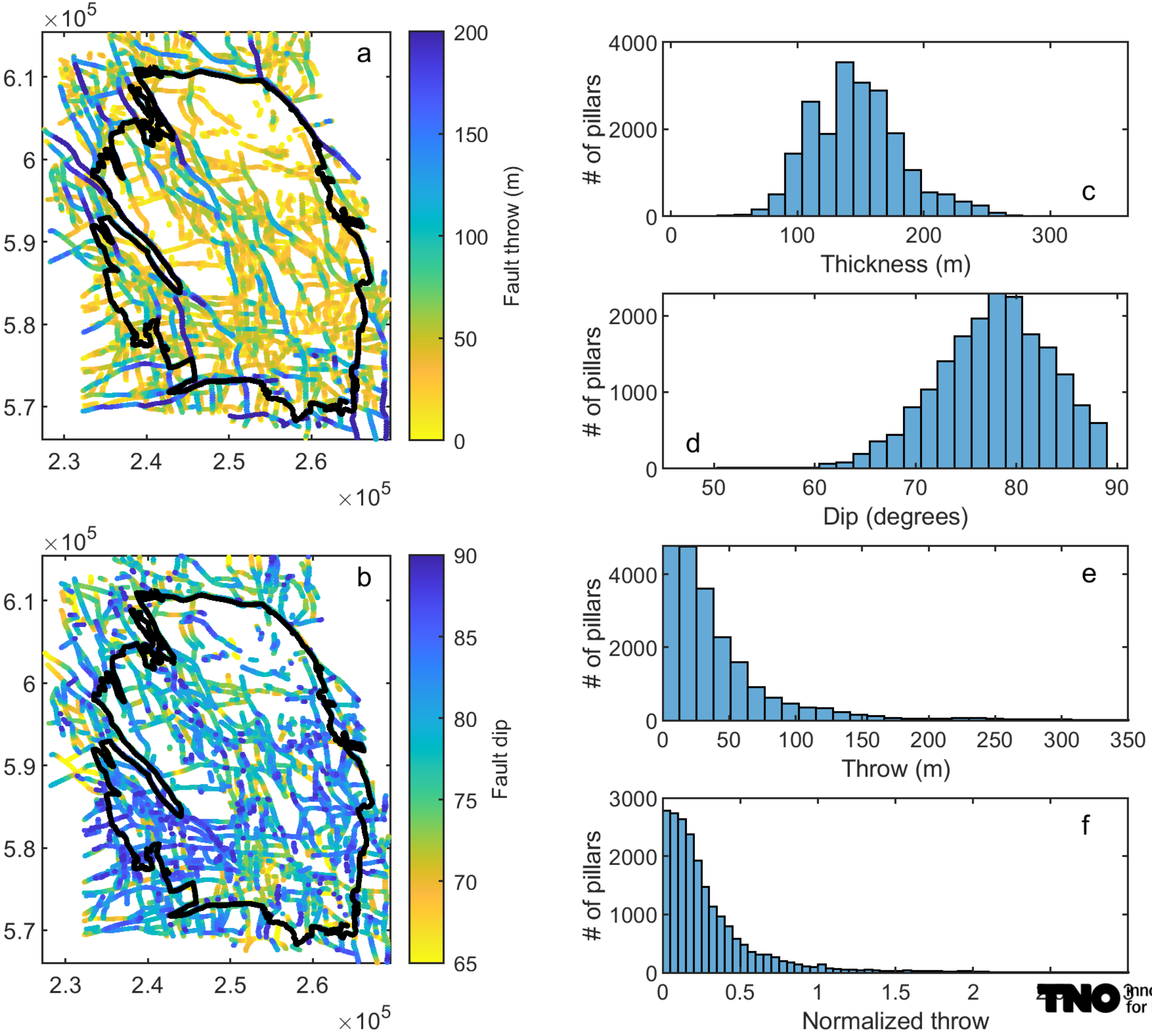

2D CROSS-SECTIONS FOR STRESS COMPUTATION

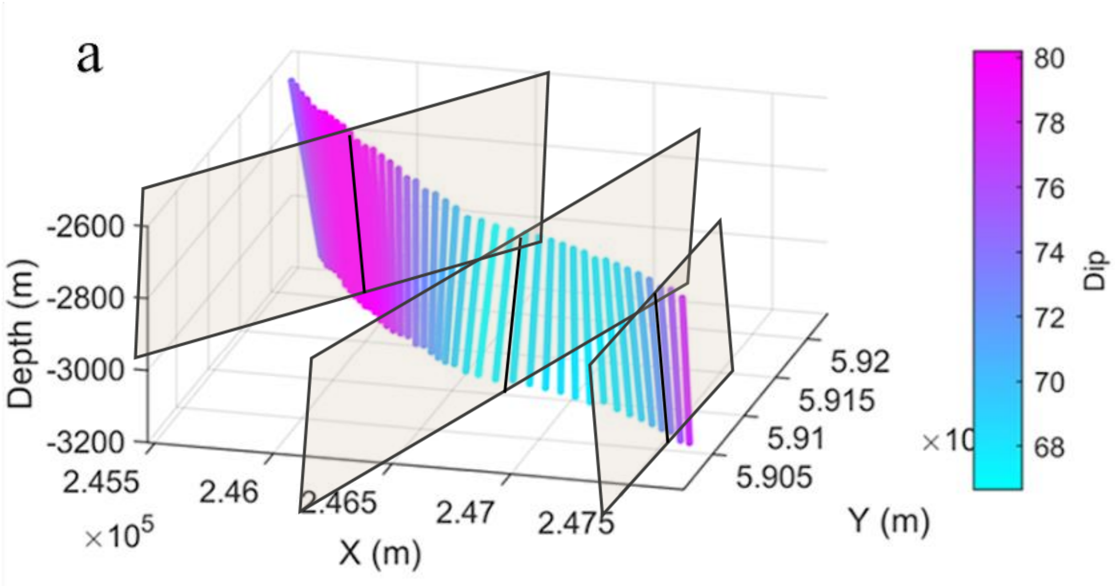

INITIAL STRESS

› F

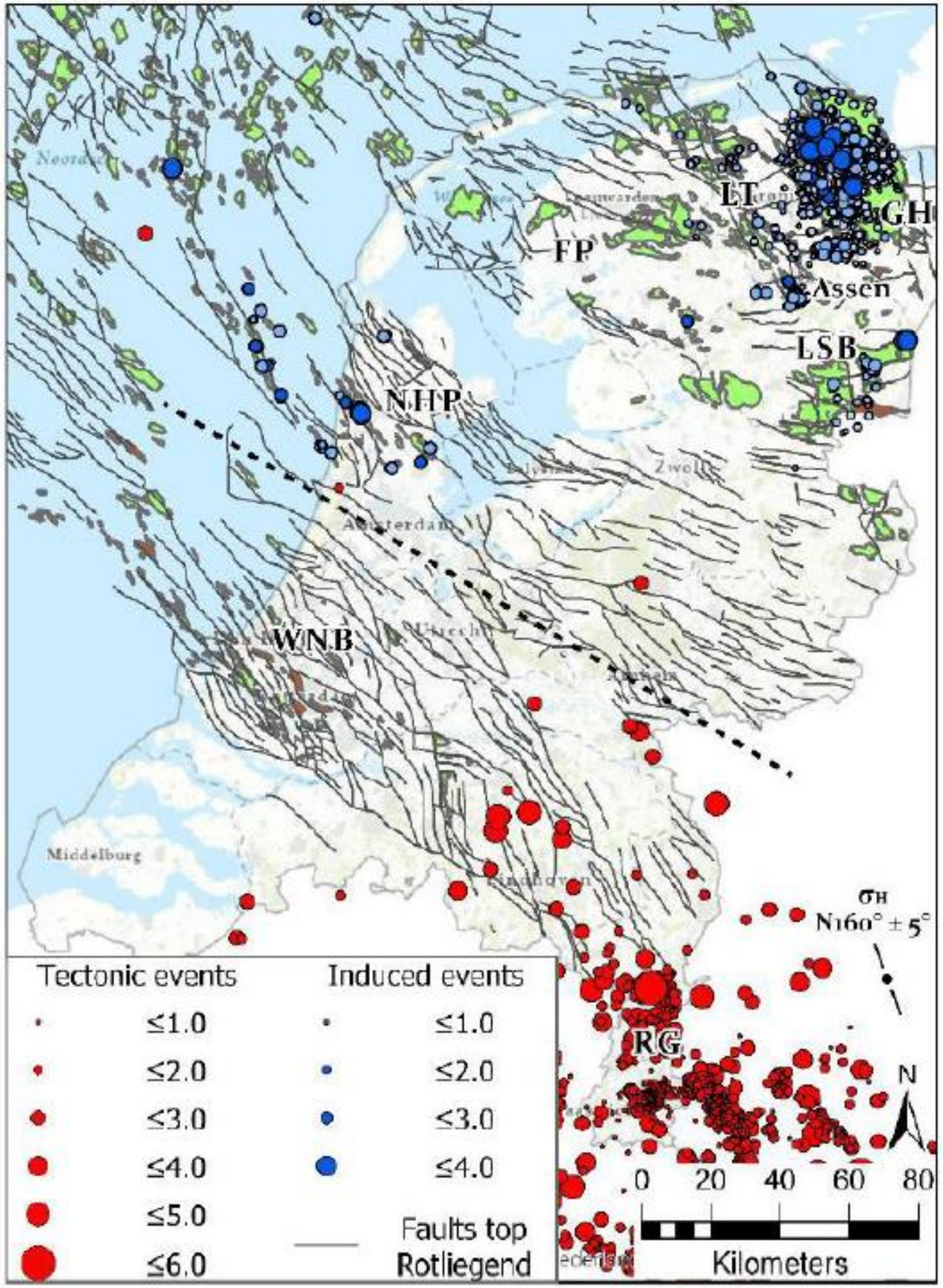

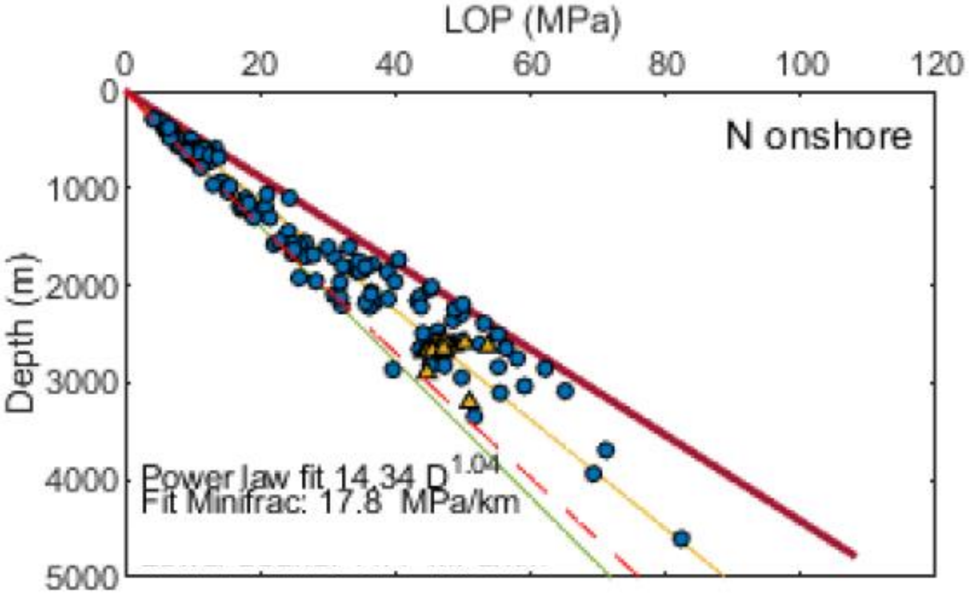

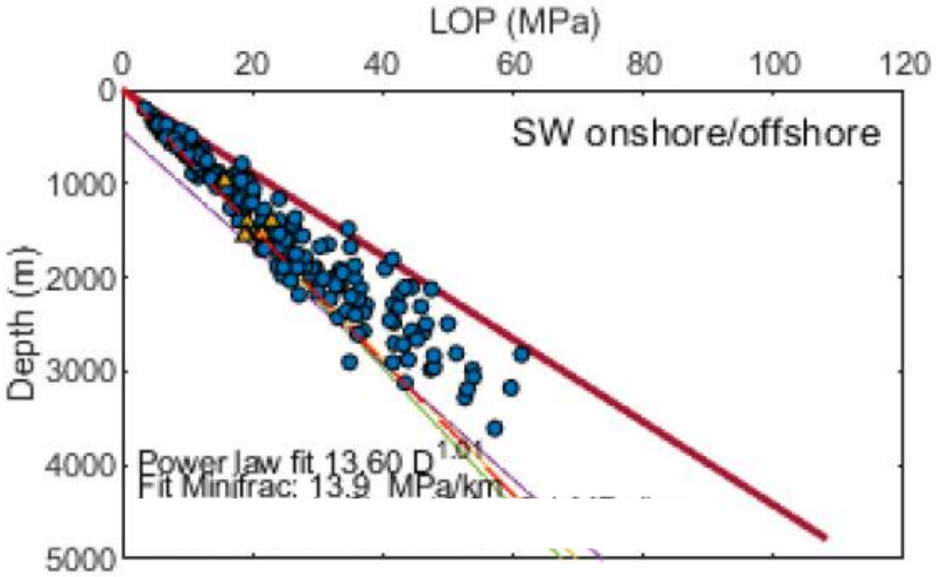

tion

MINIFRAC MEASUREMENTS IN NEARBY ROTLIEGEND FIELD

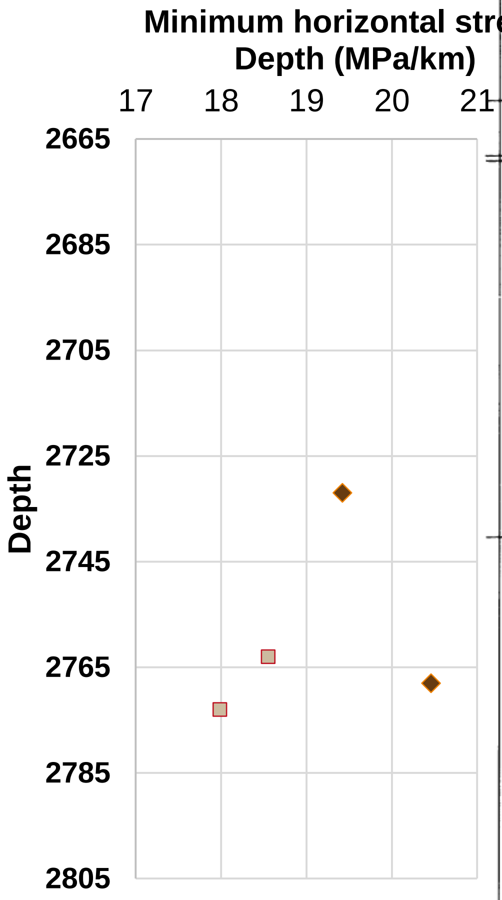

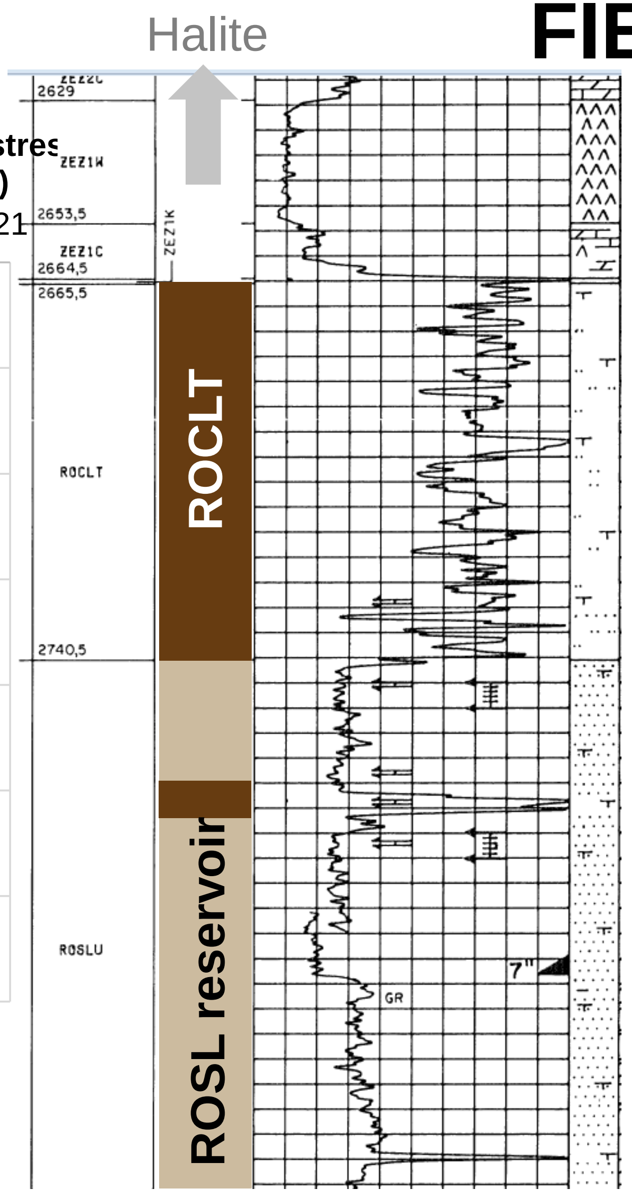

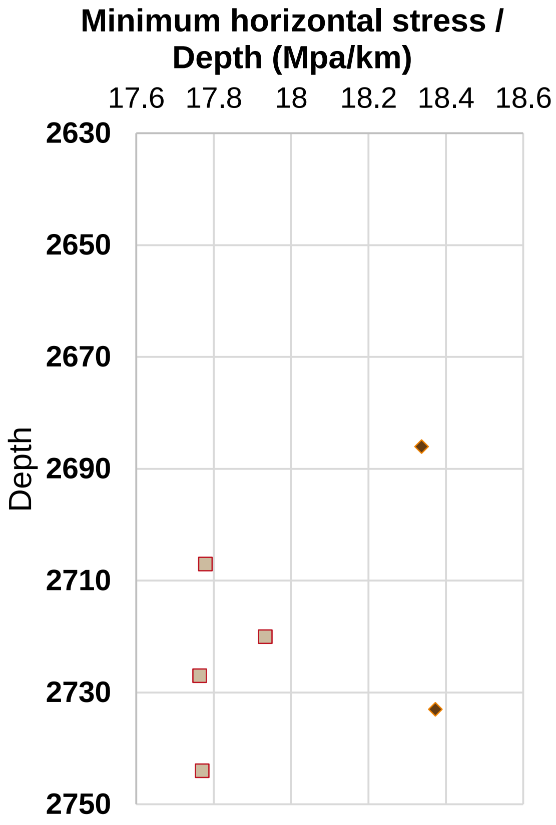

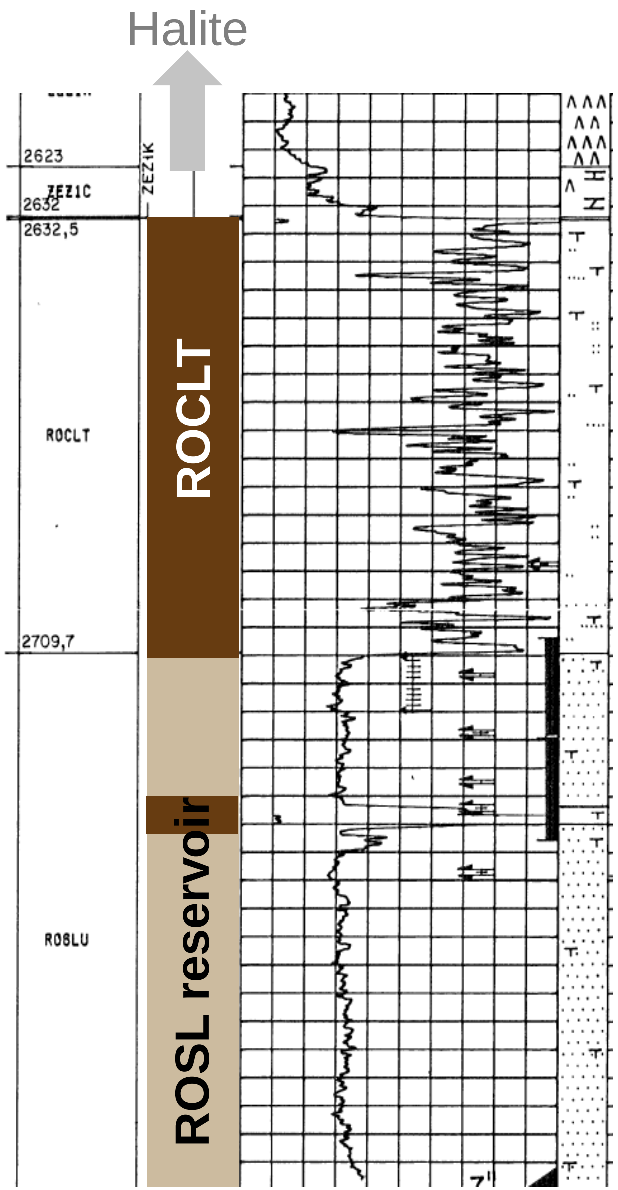

PRESSURE CHANGES

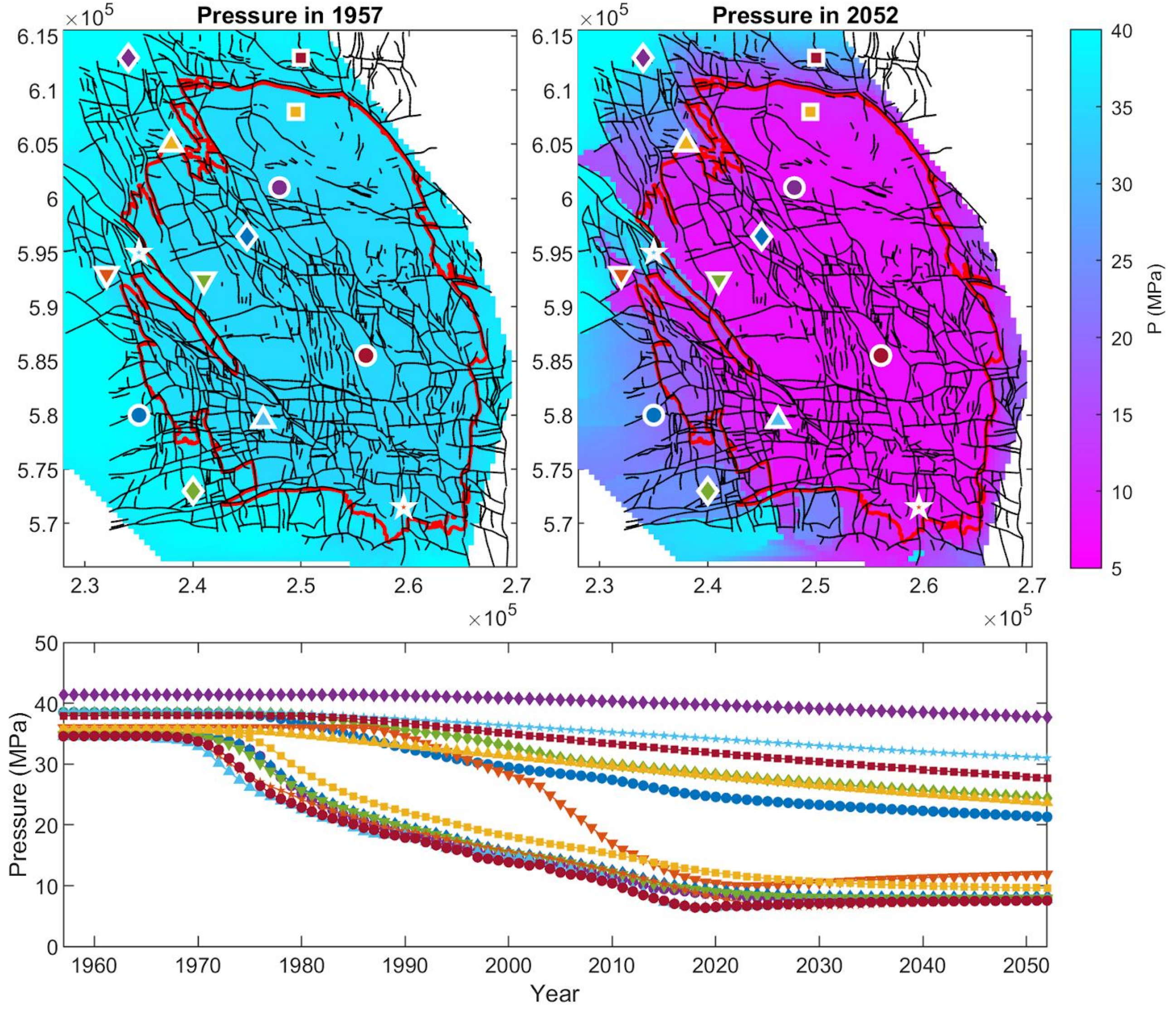

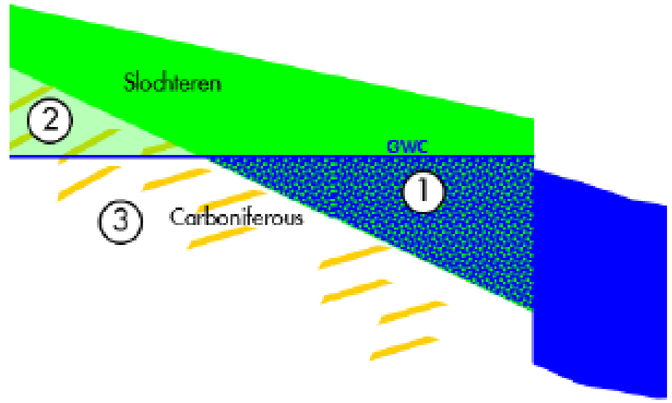

Figure 2-1: Schematic representation of new model elements

V6 pressure model: depletion Carboniferous

Hydraulic diffusivity computed from depletion of Carboniferous in V6 reservoir model

→ 1e-8 – 1e-6

POROELASTICITY FOR BEGINNERS

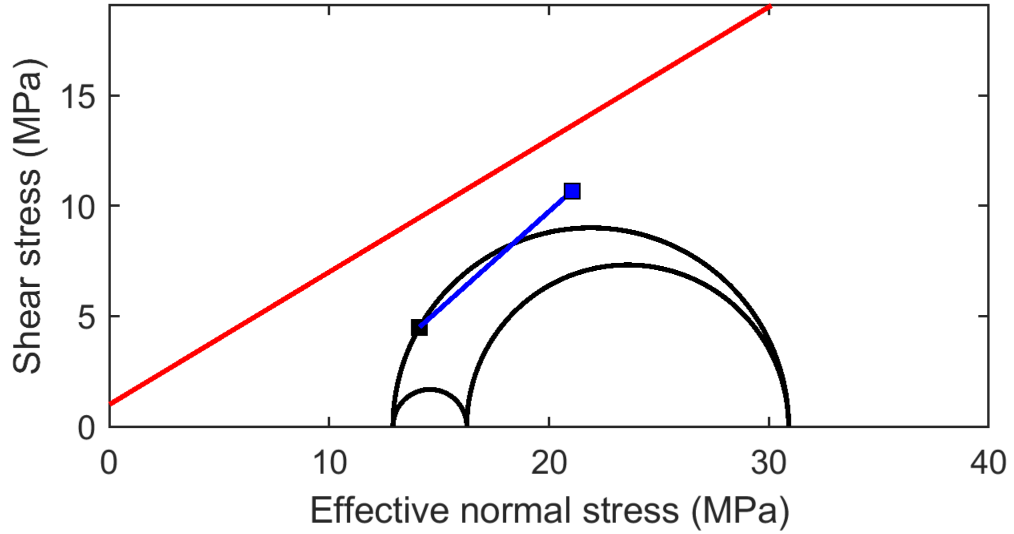

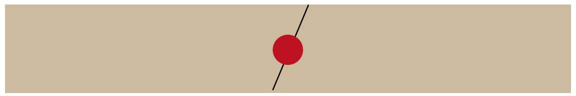

$$\frac{\Delta\sigma_h}{\Delta P} = \gamma_h = \frac{\alpha(1-2\nu)}{(1-\nu)}$$

$$\frac{\Delta\sigma_v}{\Delta P} = \gamma_v = 0$$

Largest stress change in the reservoir

γ_h field estimates: 0.5 – 0.8

For α = 1, v → 0.15 – 0.3

Laterally extensive reservoir (e.g. Segall 1989, Hettema 2000, Soltanzadeh& Hawkes)

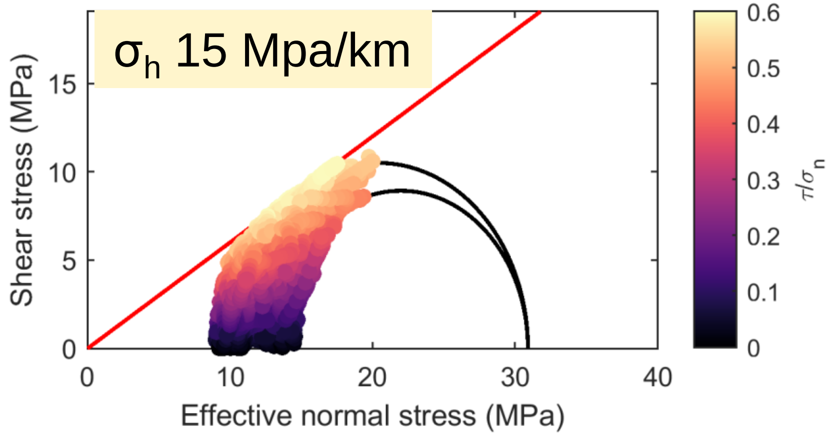

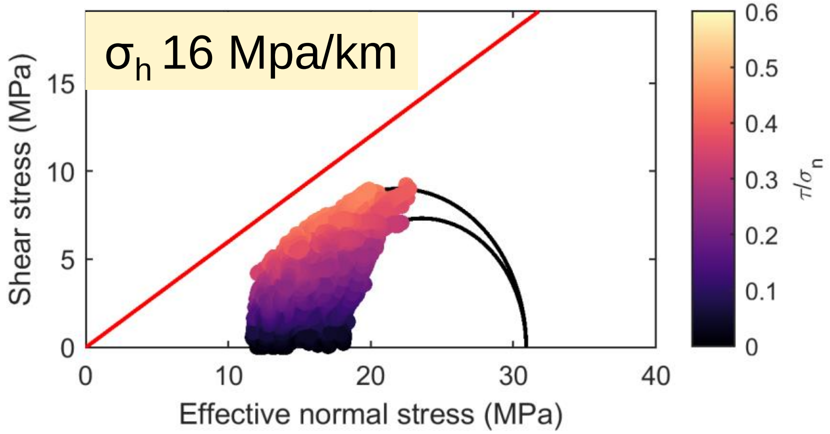

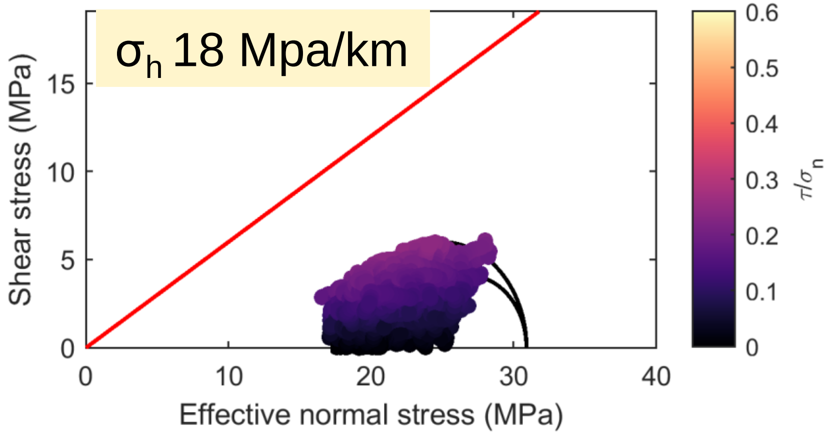

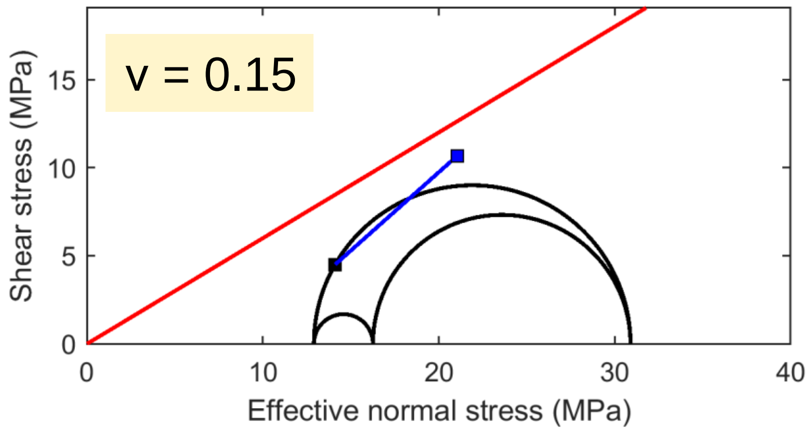

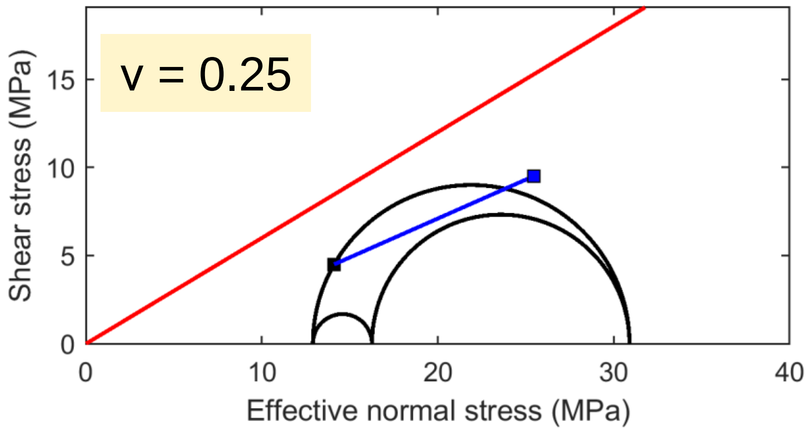

TNO innovation for life

ELASTOPLASTICITY?

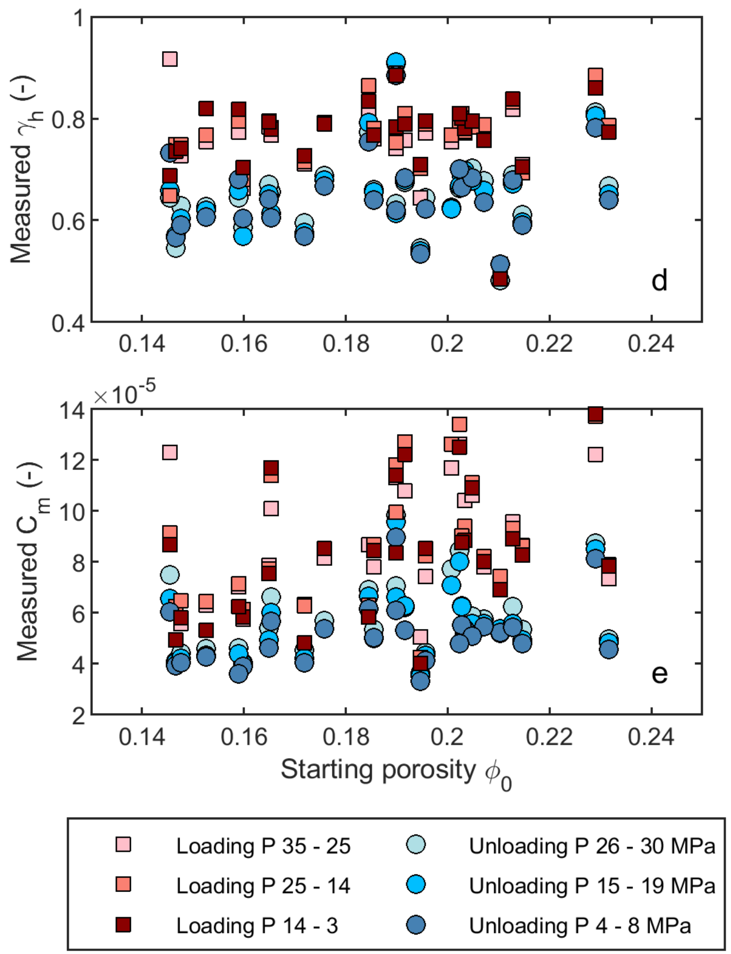

Hol et al., 2018

- Although 50% of strain is inelastic, stress path is near-linear at reservoir stress
  - Hol et al., 2018, Pijnenburg et al., 2018, 2019
- We can use the loading stress path parameter as first order estimate
- Porosity-dependent stress path and Young's modulus

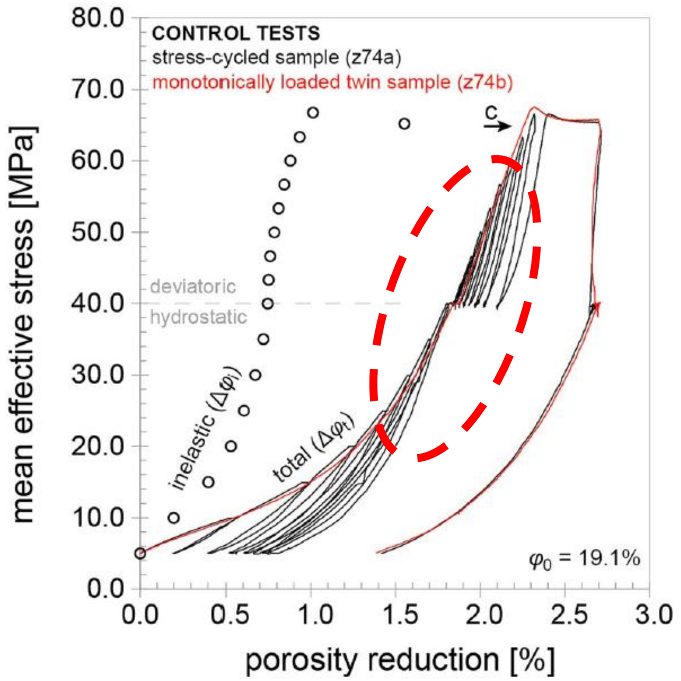

FAULT OFFSET CAN LEAD TO A STEEPER STRESS PATH

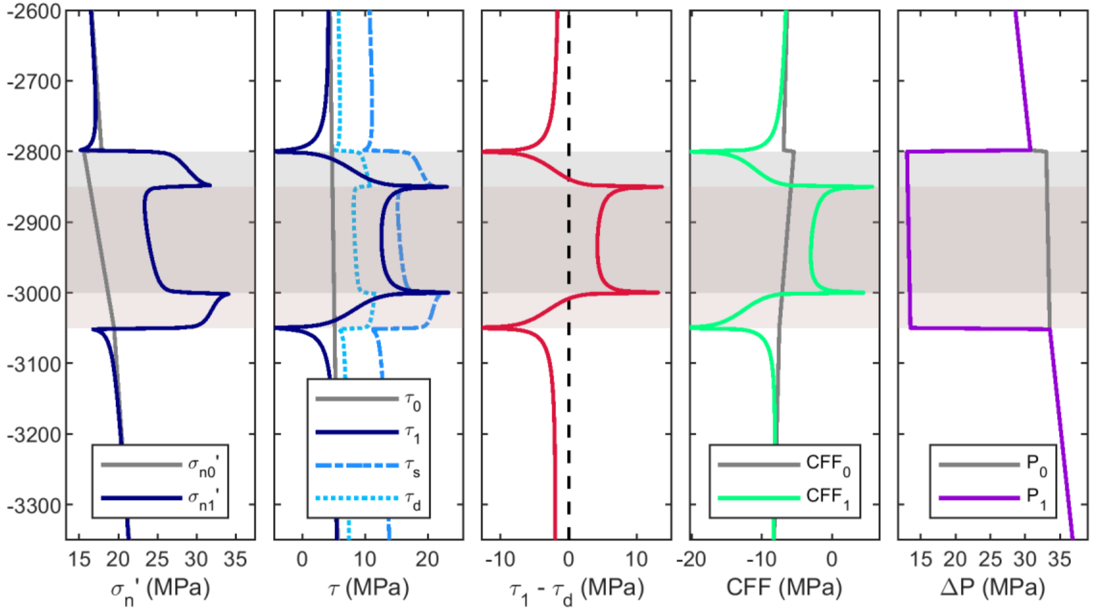

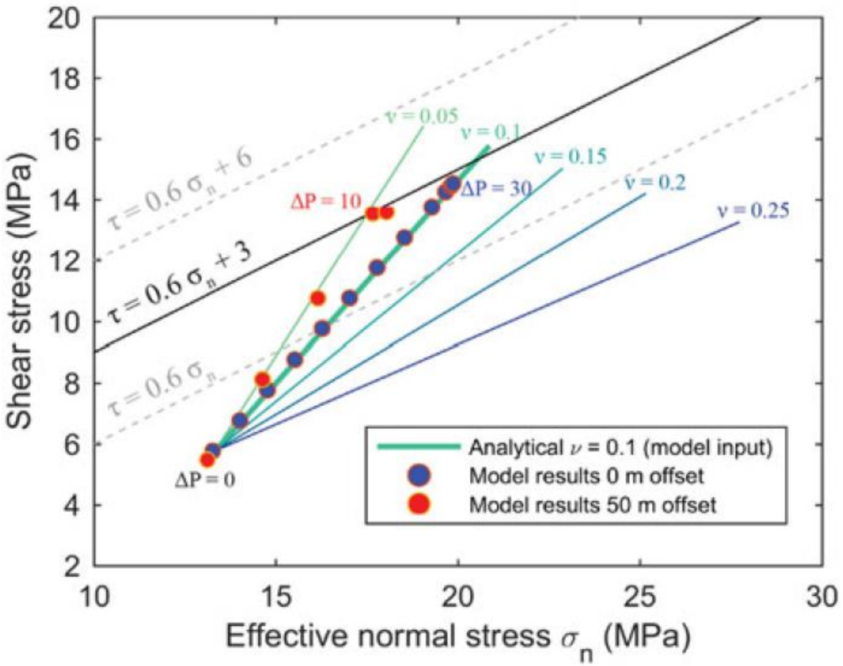

STRESS CHANGES DUE TO DEPLETION

- Stress calculation through analytical solutions
  - Jansen et al. 2019, Lehner, 2019, Wu et al., 2020
- Solutions adjusted to incorporate diffusion, single-sided depletion, aseismic slip during nucleation
  - Buijze et al., 2022
- Stress benchmarked against 3D stress calculation

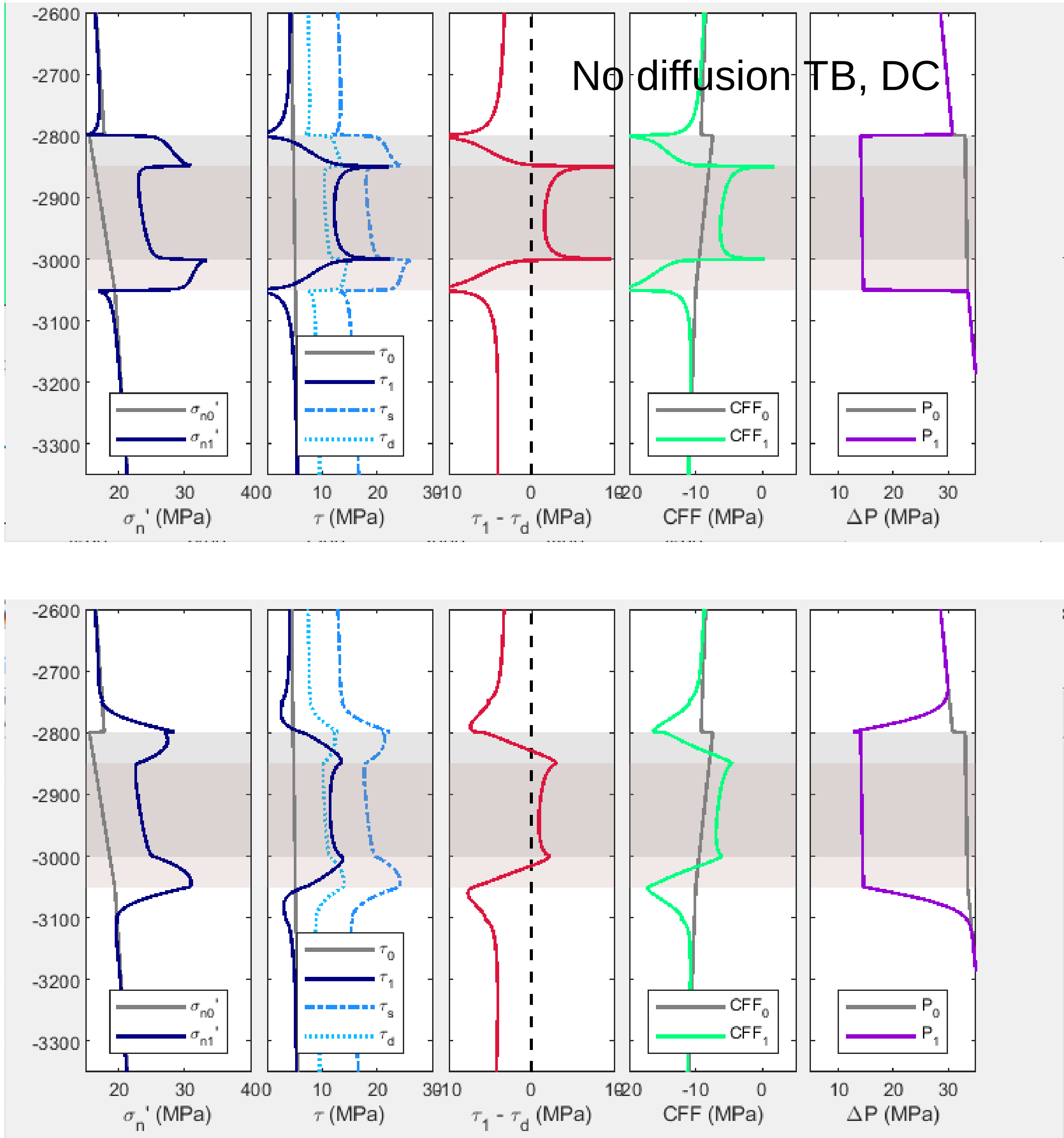

EXAMPLE STRESS CHANGES ALONG-STRIKE

- Elongated band of elevated Δτ at reservoir-reservoir juxtaposition
- Bands of lower Δτ above and below reservoir

- Strong effect of fault dip and throw

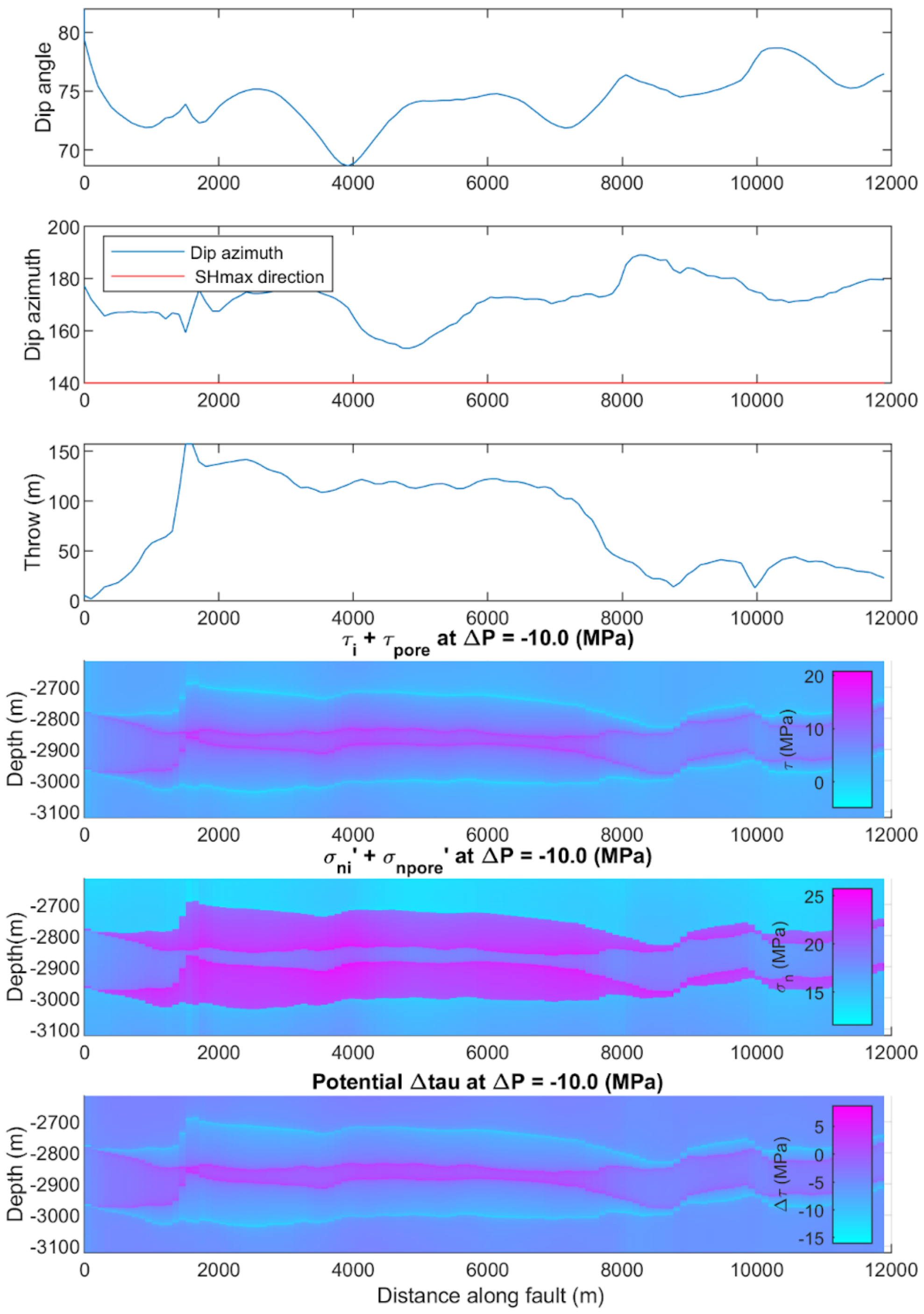

SLIP WEAKENING AND GC SCALING

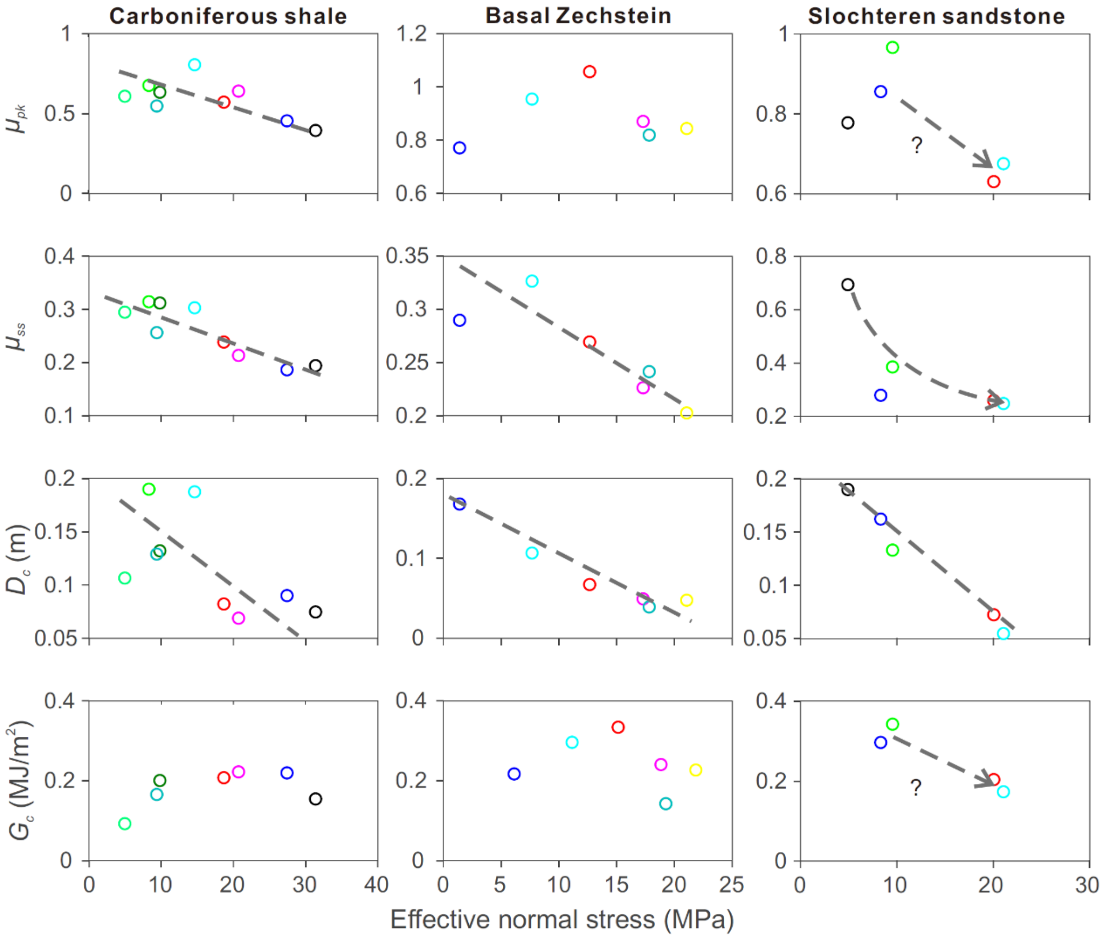

Chen et al., submitted

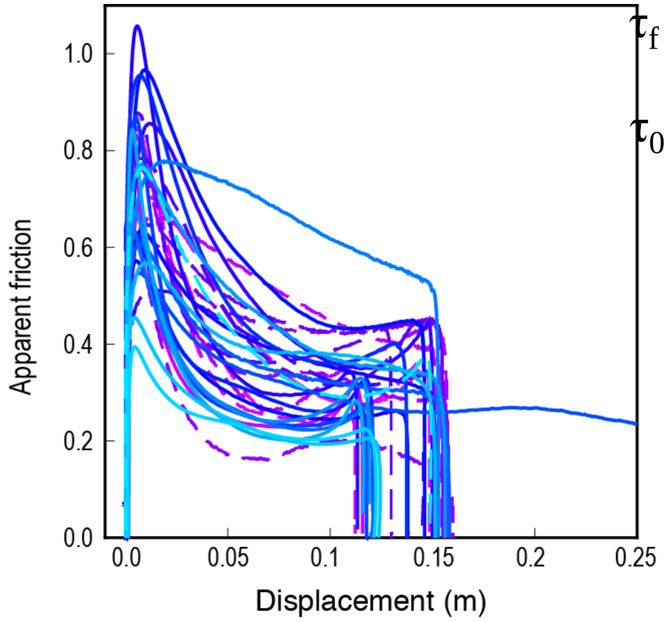

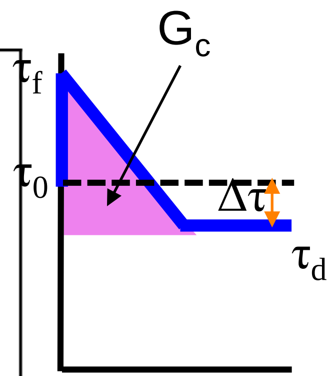

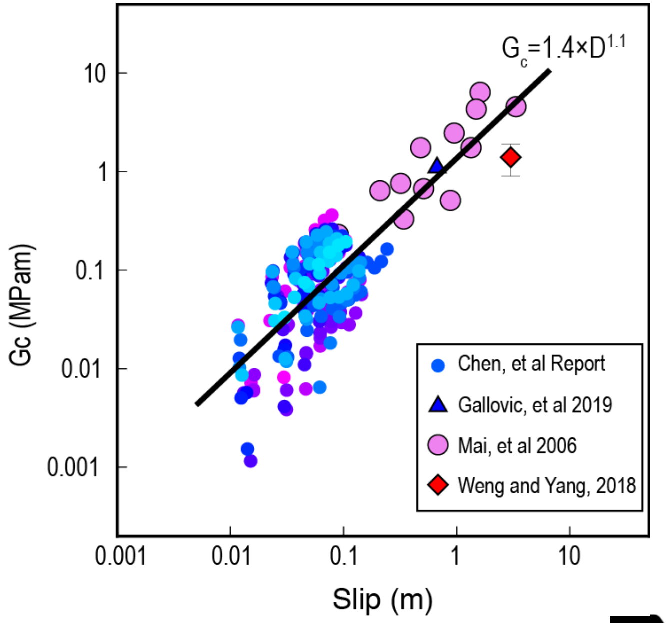

LEFM THEORY ALONG-DIP AND ALONG-STRIKE RUPTURE

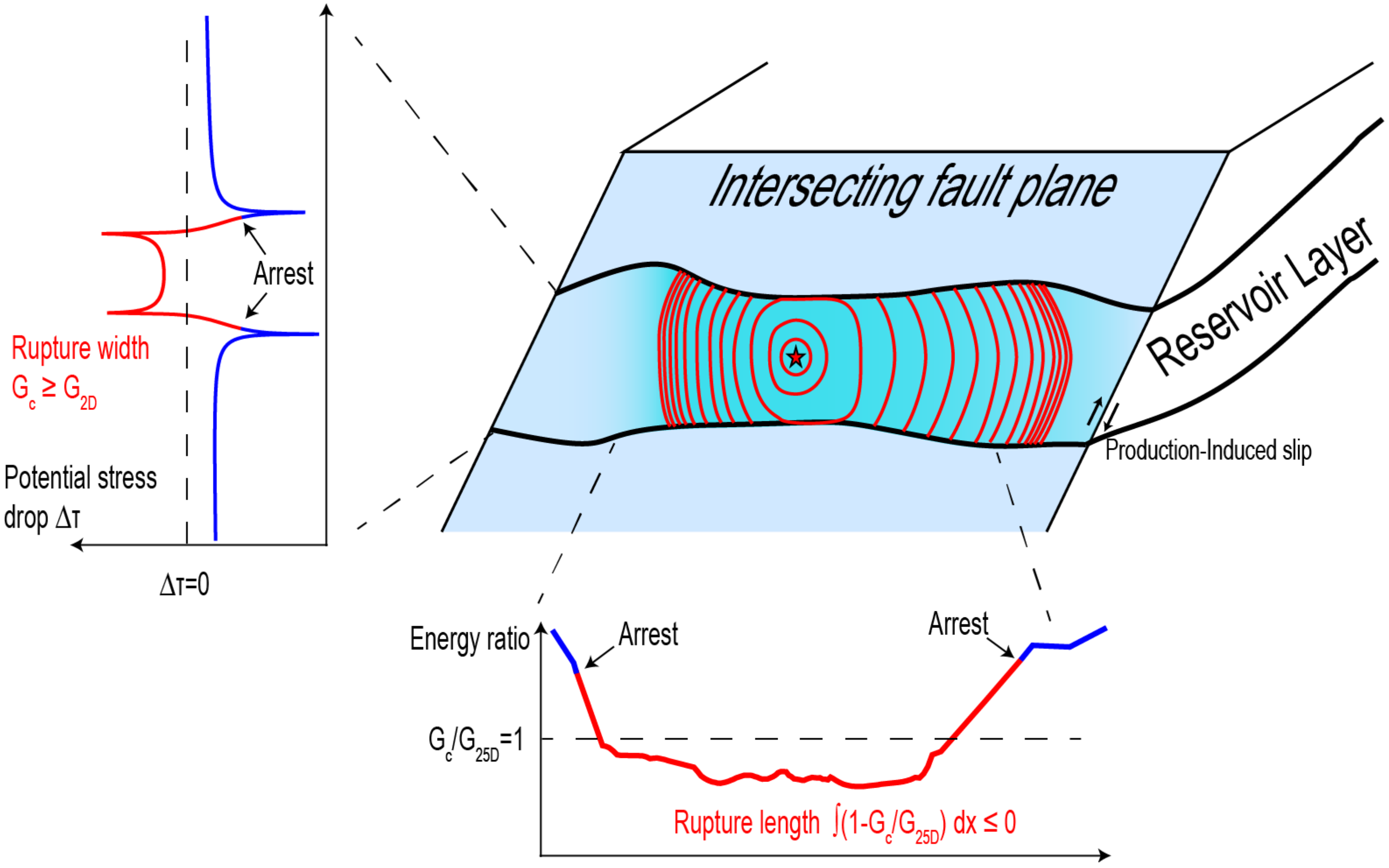

- Rupture size & stress drop computed in 2 steps
- 1: Determine along-dip rupture width W
  - E.g. Ripperger, 2007, Galis, 2015, Buijze, 2020
- 2: Compute average G_0 and Δτ over W
- 3: Compute rupture potential and arrest along-strike
  - Weng & Ampuero, 2019
- At different depletion times

RESULTS 3D MODELLING: DEFAULT

- Mu_d = 0.3

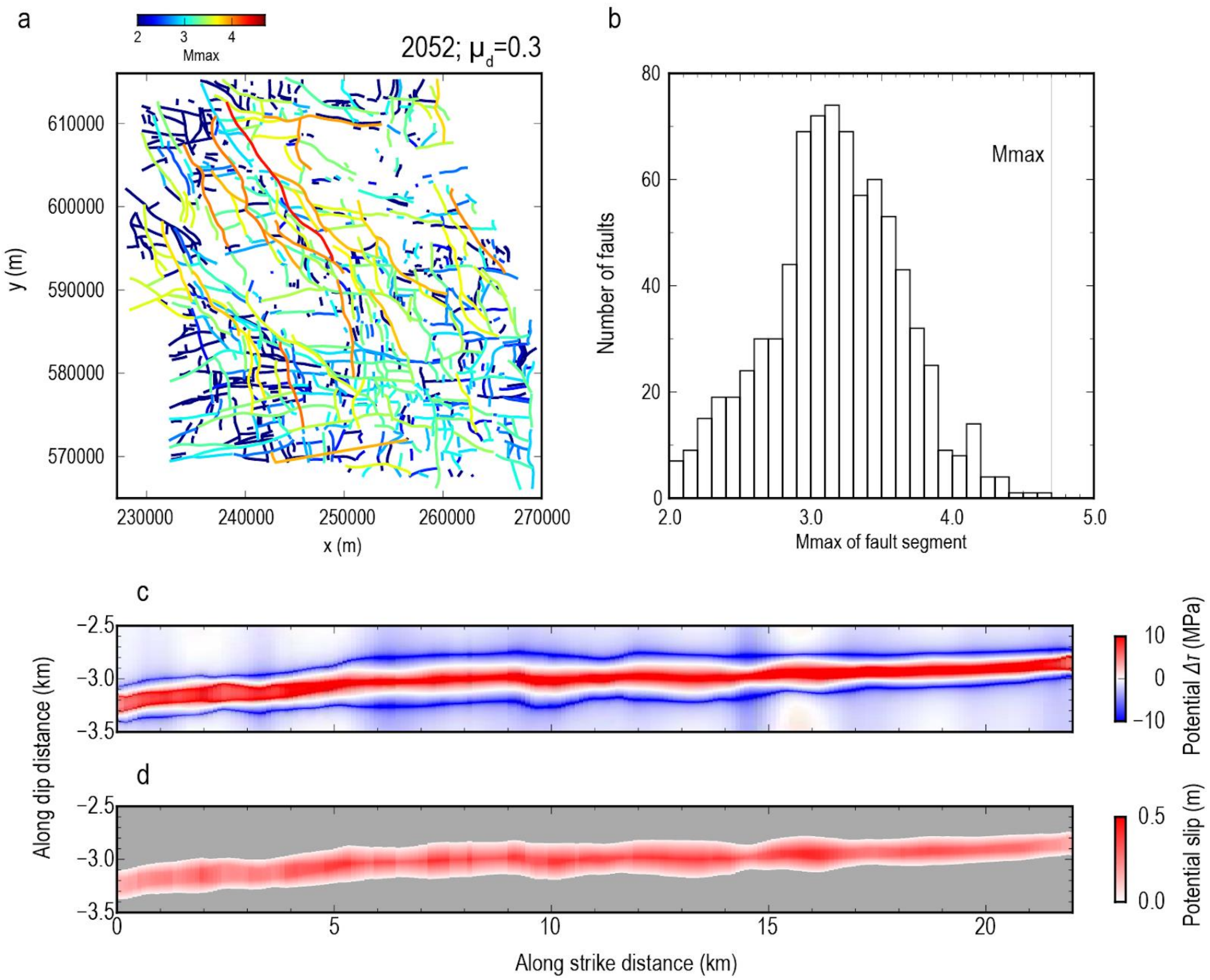

MMAX WITH TIME

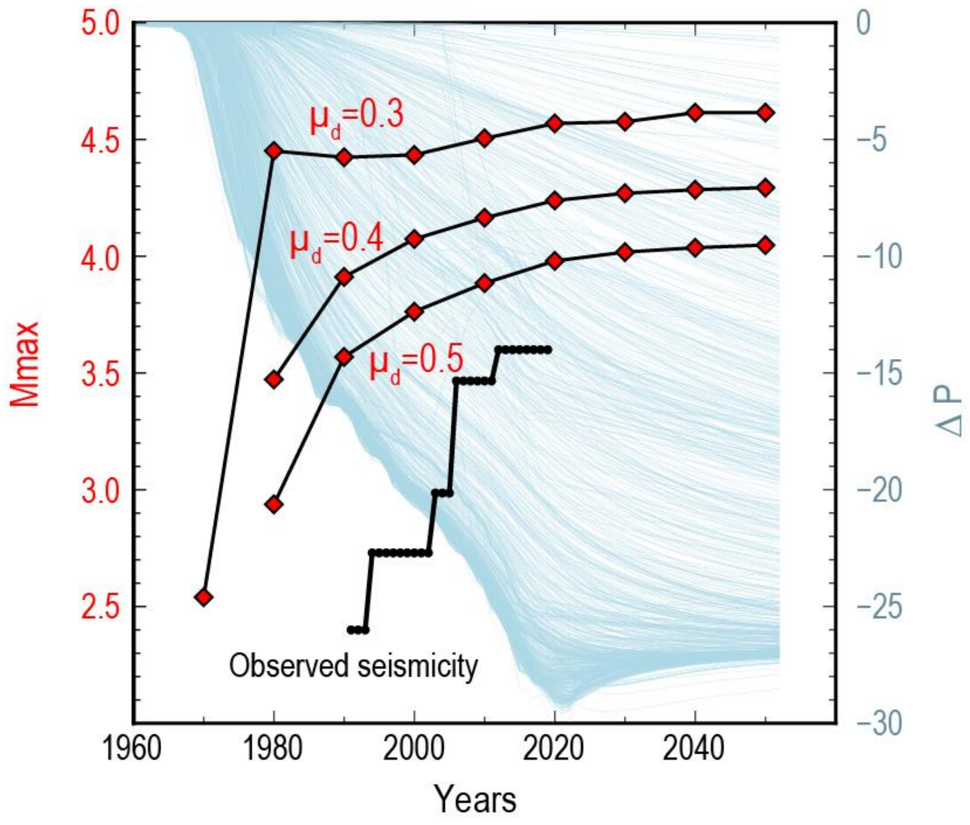

- Saturates as max fault area in reservoir becomes stressed
- Mainly determined by largest faults
- Dependency on mu_d and horizontal stress gradient

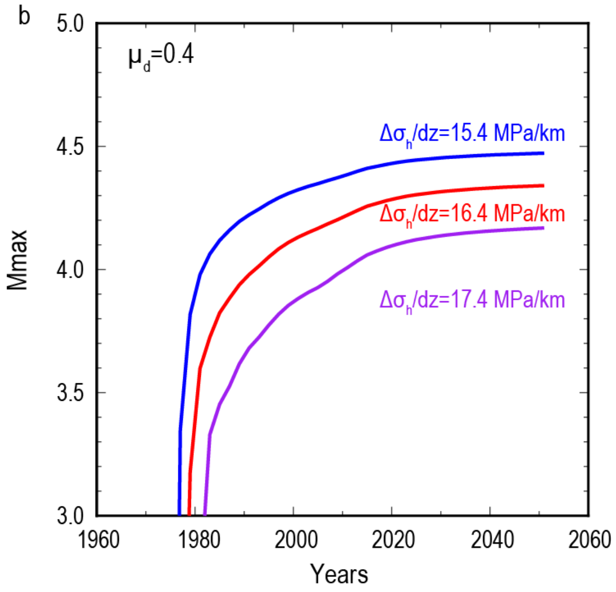

MAGNITUDES IN TIME AND SPACE

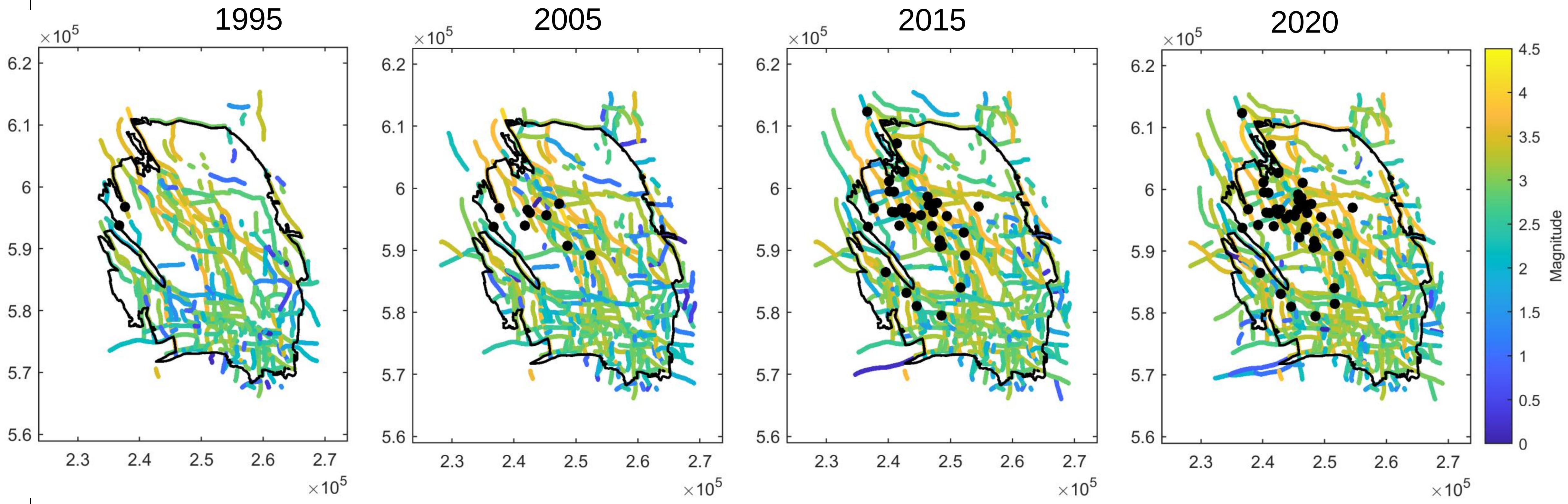

- Black dots: observed M > 2.5
- Enough stress build-up at onset of seismicity. NB sensitive to shmin

SPATIAL VARIATIONS

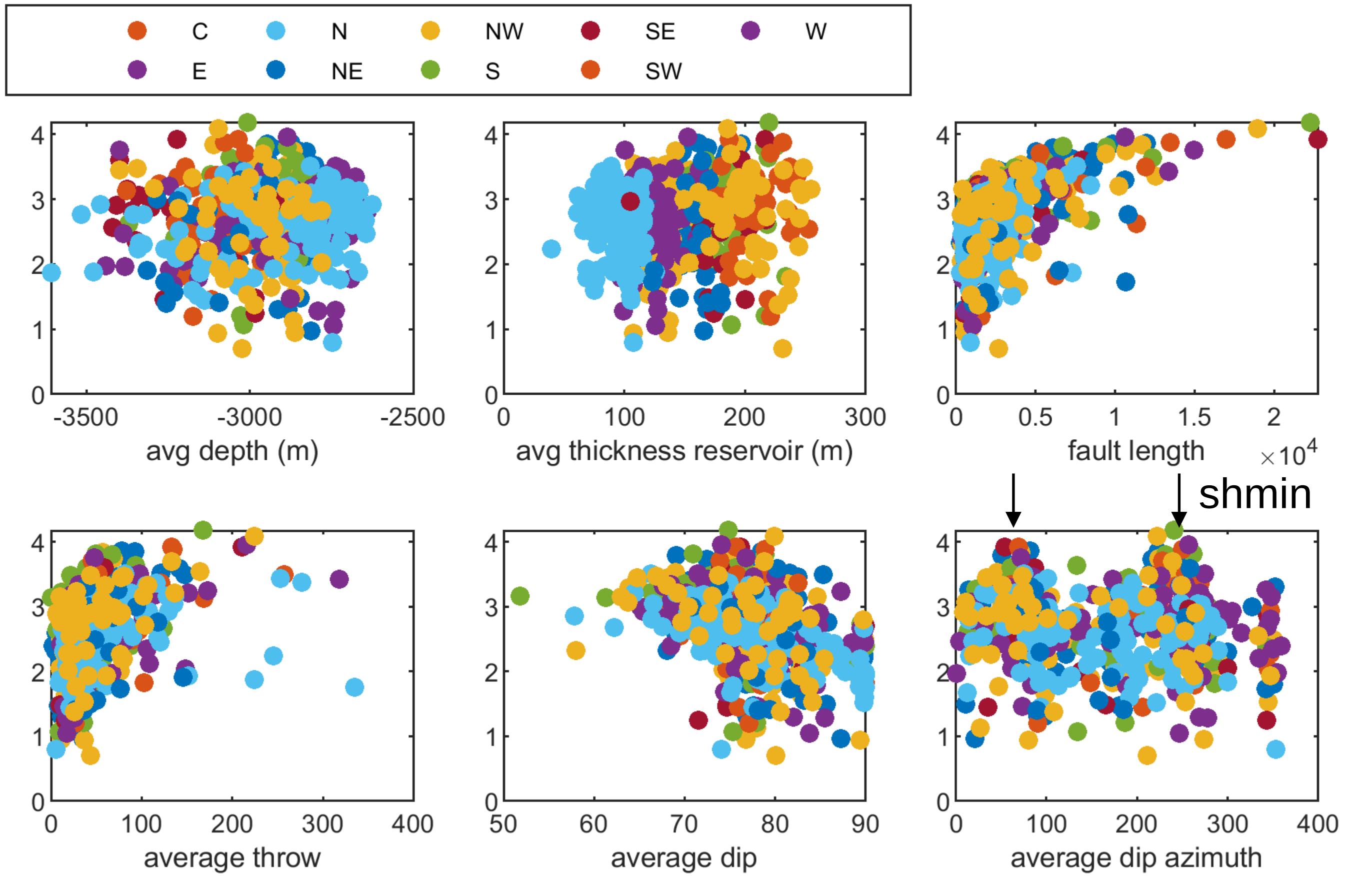

Magnitude increases (mildly) with fault length, dip, thickness, throw. Clear effect of SH.

NW faults well aligned in stress field

Relatively thick part of reservoir

SENSITIVITY ANALYSIS

- K0 = shmin/sv

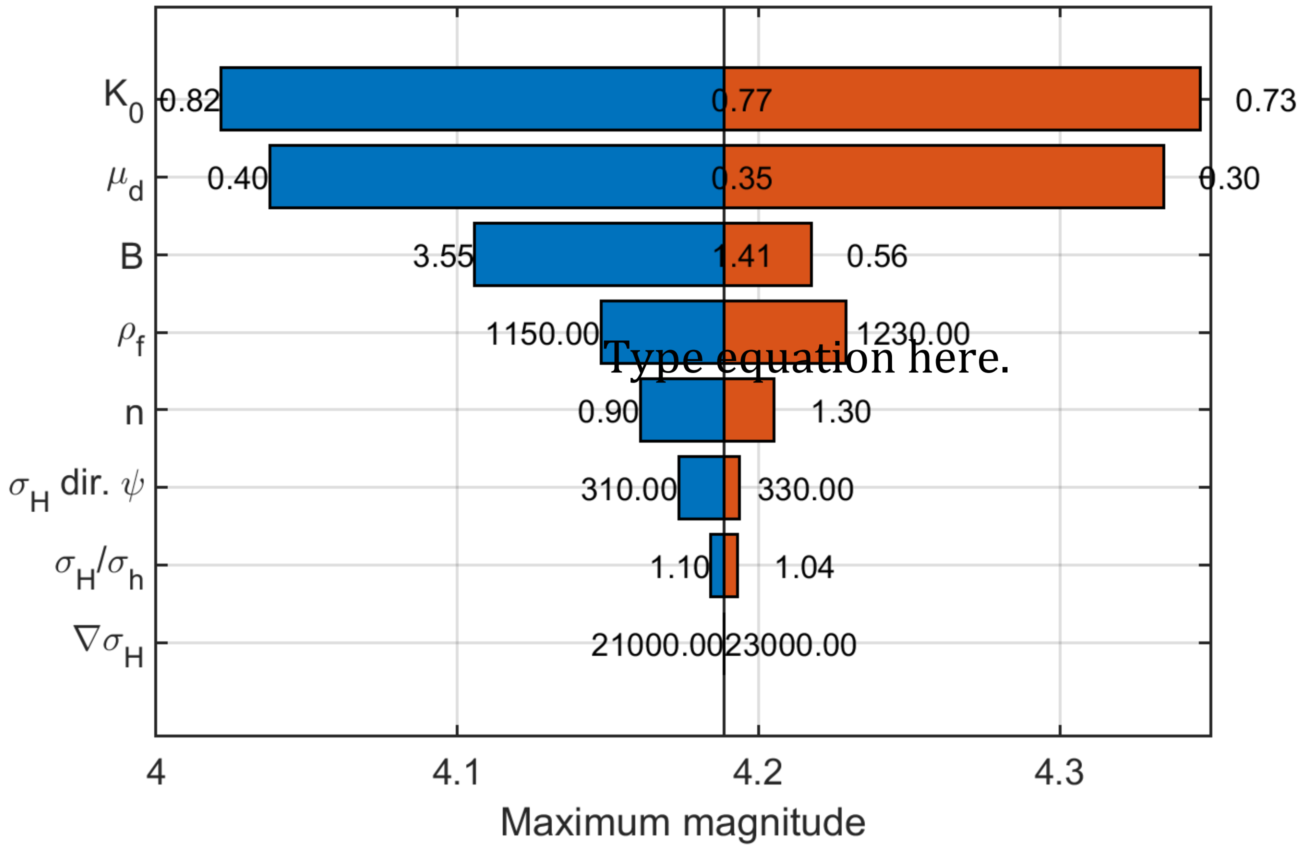

EFFECT OF DIFFUSION

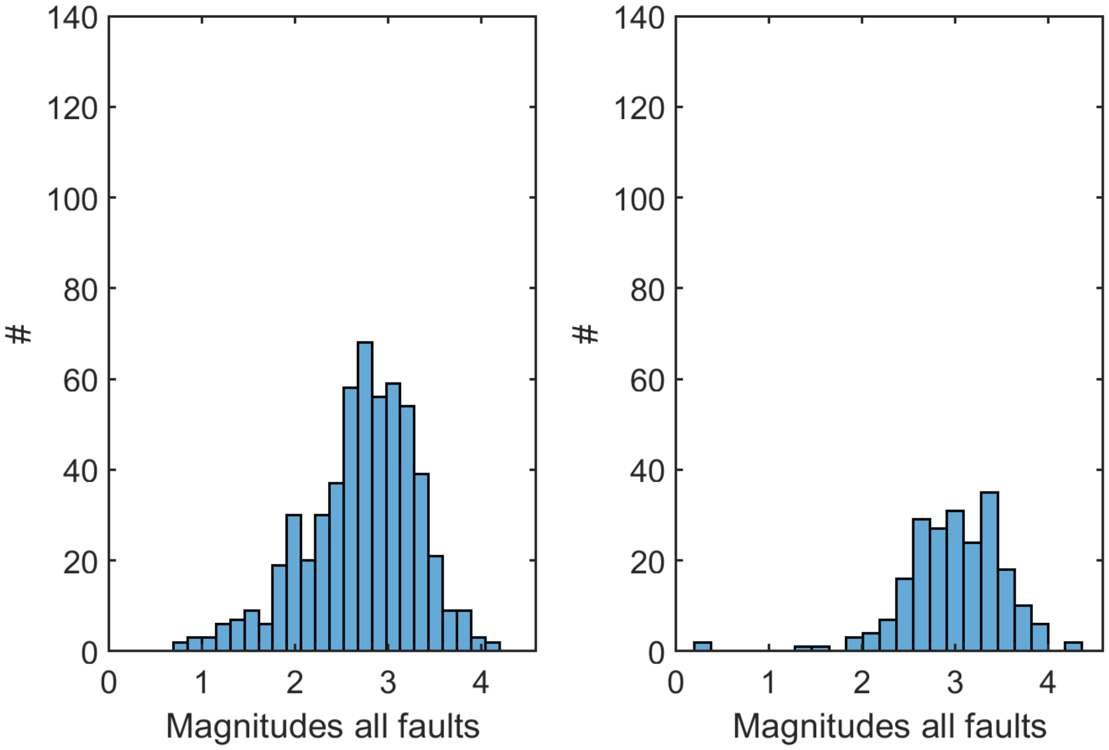

- Less faults reactivated, but similar magnitude range

PART II: WHAT IS THE POTENTIAL FOR RUPTURE TO GROW BEYOND THE RESERVOIR DEPTH INTERVAL?

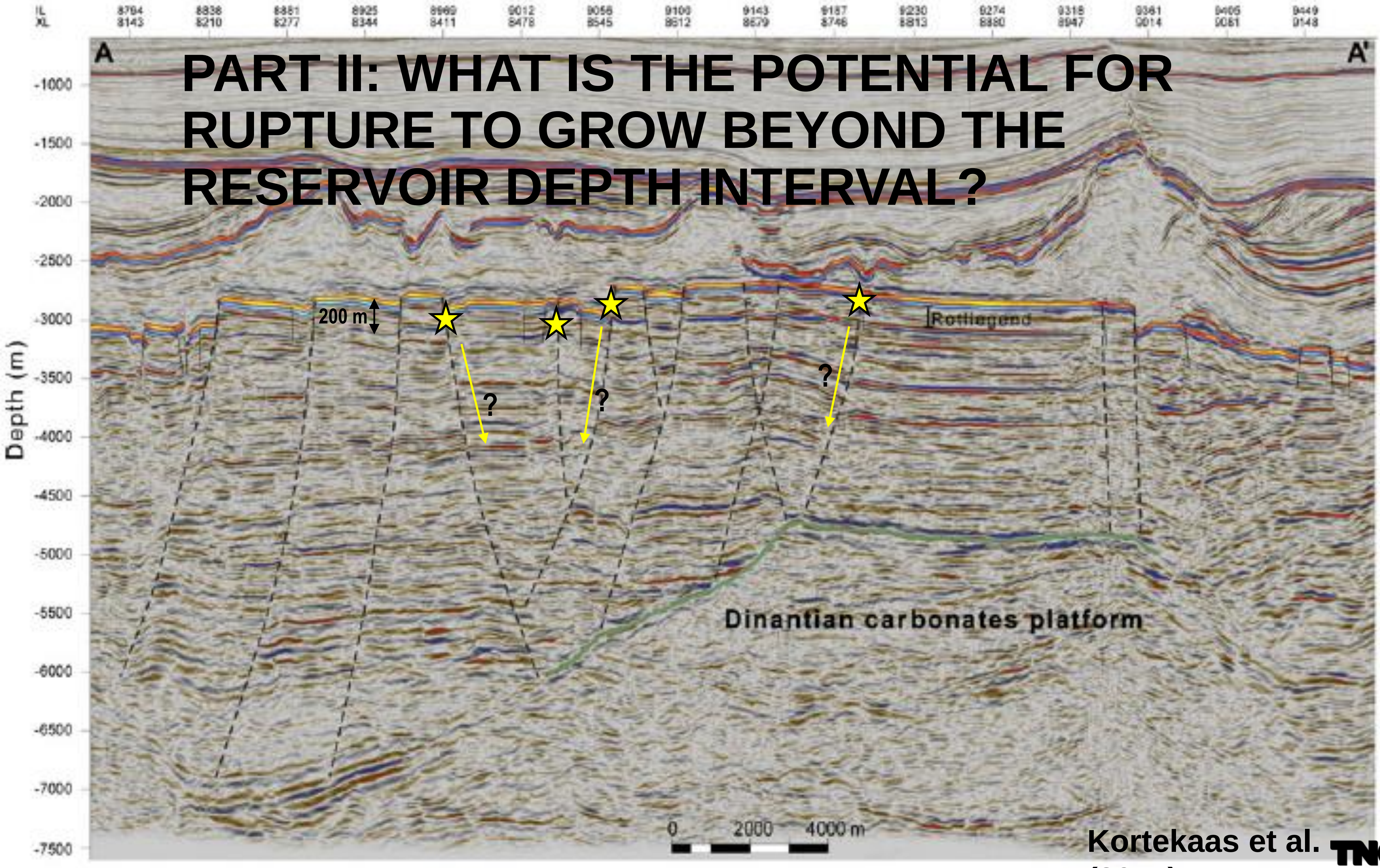

Kortekaas et al. (2017)

Ref. presentation Clemens Vissers

2D MODEL GEOMETRY
LITHO-STRATIGRAPHIC UNITS

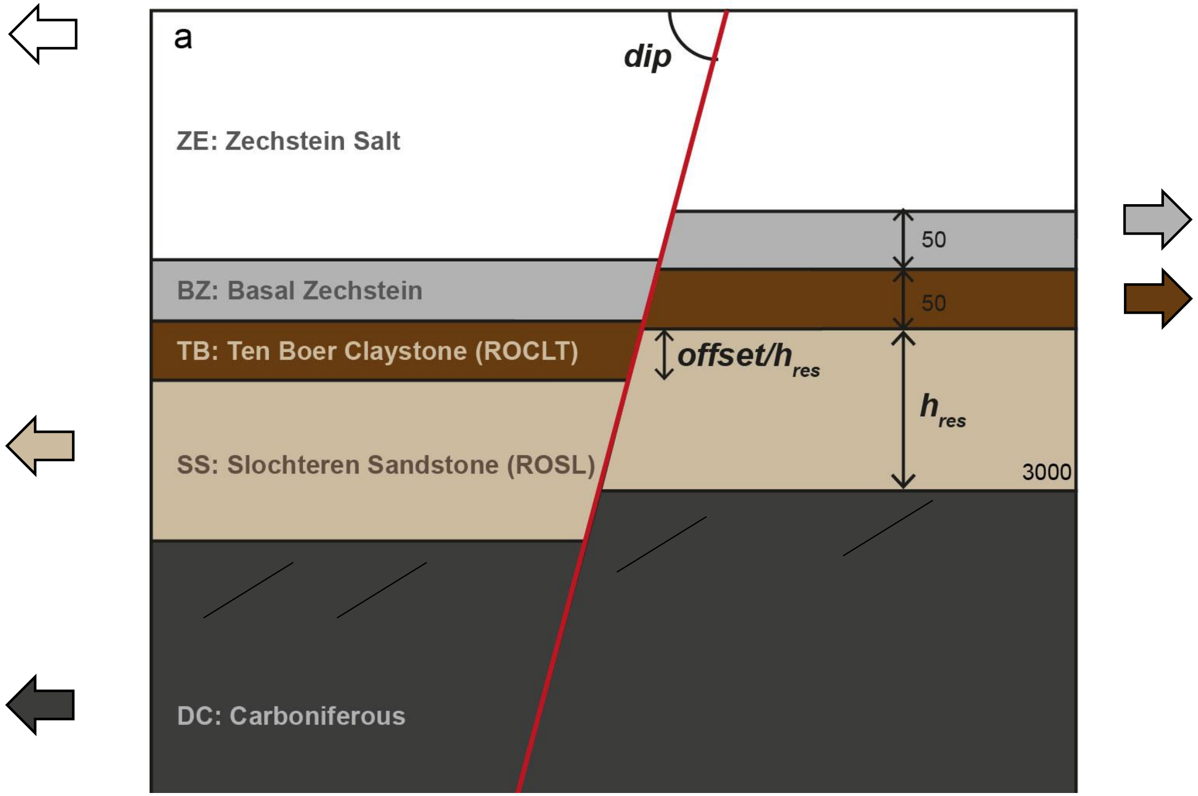

PART II: 2D MODEL POTENTIAL FOR RUPTURE PROPAGATION CARBONIFEROUS

- Along-dip rupture using fracture mechanics
- 0.1 s per simulation, 1000,s of simulations
- Include more complexity:
  - Heterogeneous initial stress
  - Diffusion
  - Various nucleation criteria
  - Aseismic slip

- Quantify the potential for propagation into Carboniferous
- Stochastic modeling, sampling from prescribed distributions

SV gradient	21.3 – 23.3 Mpa/km
Sh gradient	16 – 18 Mpa/km
SH/Sh	1.07
μ_s	0.65 +- 0.05
μ_d	0.3 +- 0.05
D_c	0.005 – 0.01

TNO innovation for life

MONTE CARLO SIMULATION 2D
50,000 REALIZATIONS SAMPLED FROM GRONINGEN FAULT MODEL

	No diffusion	Diffusion
Reactivated %	32%	11%
Propagation DC % of total	1.1 - 3%	0.6%
Propagation DC % of reactivated	4.2%	5.9%

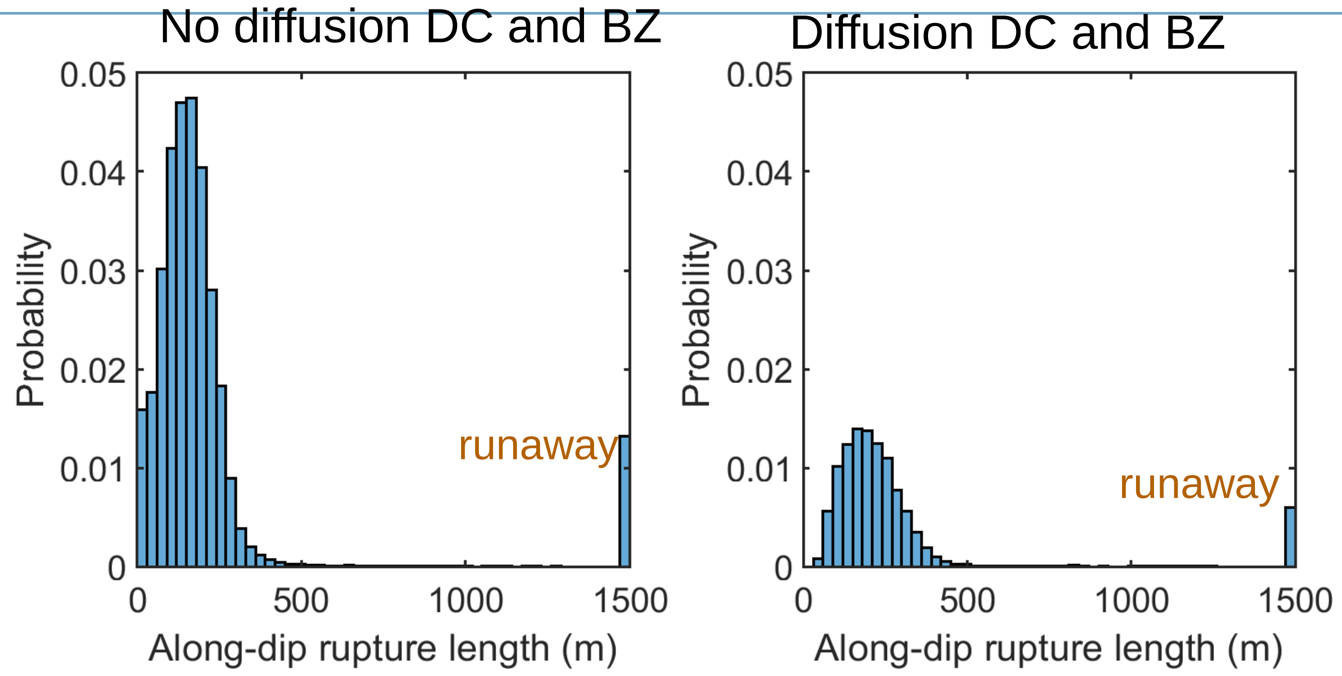

MODELED STRESS DROPS

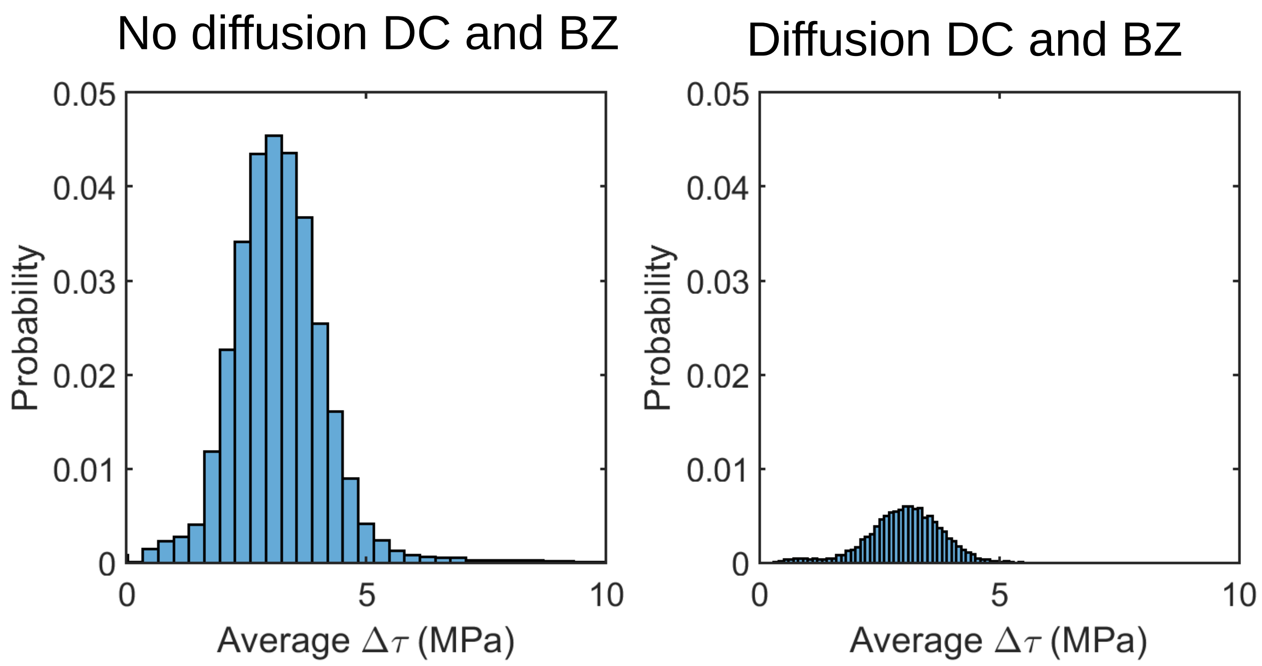

- Difference between shear stress before and after rupture.

RUNAWAY

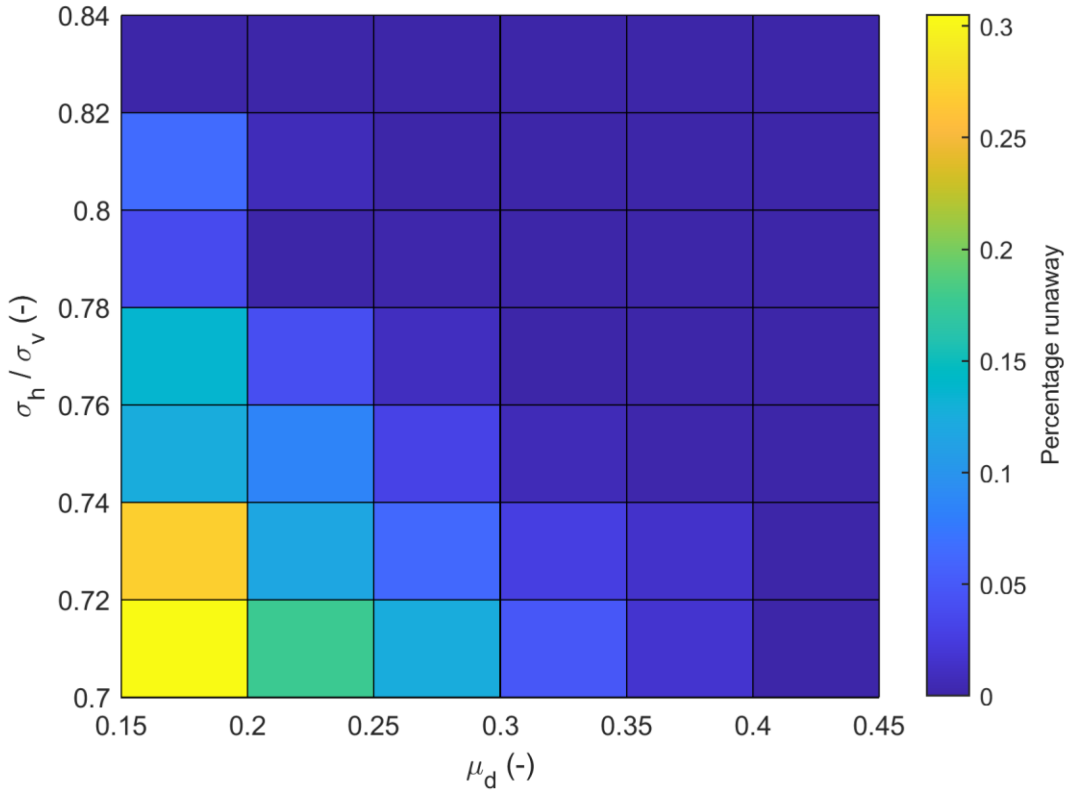

- Runaway down-dip strongly depends on mu_d and shmin/sv

CONLUSIONS & OUTLOOK

- Rupture remains confined to the near-reservoir interval
- But ruptures can have (very) large aspect ratio’s
- Magnitude is largely governed by the areas of the largest faults
- Mmax ~4.1 – 4.5

- Potential for propagation into the underburden a few %
  - (Current logic tree branch Carboniferous -> 25%)

- Outlook:
  - 3D Model may not be suitable to run 1,000,000s of simulations for statistics
  - But fast enough to run 100 – 1000s of simulations to evaluate physics-based control on tail events
  - Needs to be combined with nucleation criterion

Constraining the maximum magnitude in Groningen

through 3D multi-physics, data-driven modelling

PhysMmax

Vincent v.d. Heiden (UU), T. Ulrich (LMU Munich), H. Weng (Côte D'Azur),
Y. van Dinther (UU), J.D. van Wees (UU),
A. Gabriel (LMU Munich), J.P. Ampuero (Côte D'Azur), L. Buijze (TNO),
T. Candela (TNO), L. Matenco (UU), L. v.d. Wiel (UU),
From InFocus: M. Li (UU), A. Niemeijer (UU)

Contact me at y.vandinther@uu.nl

Objective

- Determine a probabilistic **physics-based** Mmax due to gas extraction in Groningen within a realistic fault network

  - Physics to go beyond what data can tell us → critical for Mmax

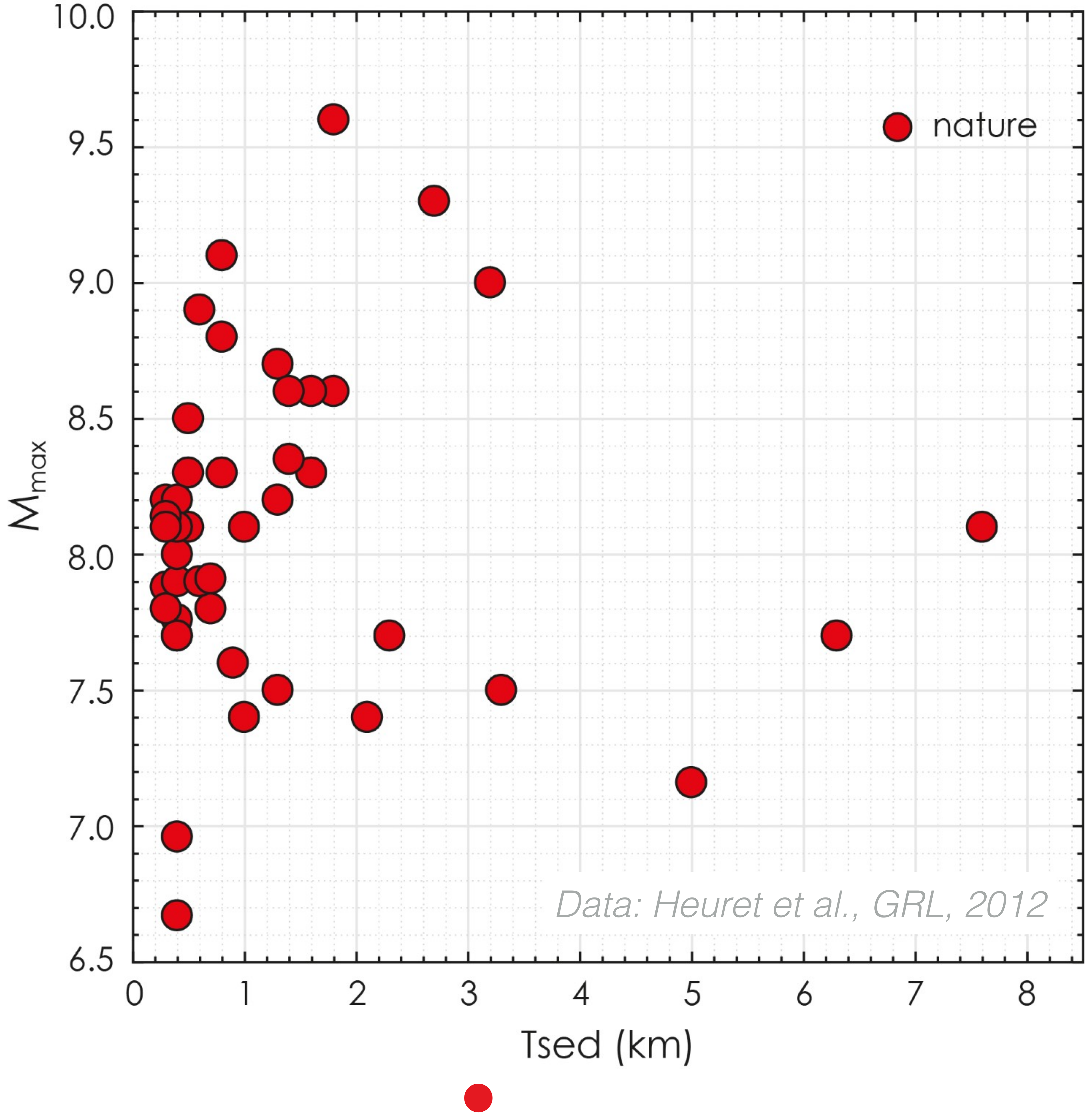

= subduction segment

Objective

- Determine a probabilistic **physics-based** Mmax due to gas extraction in Groningen within a realistic fault network
  - Physics to go beyond what data can tell us → critical for Mmax

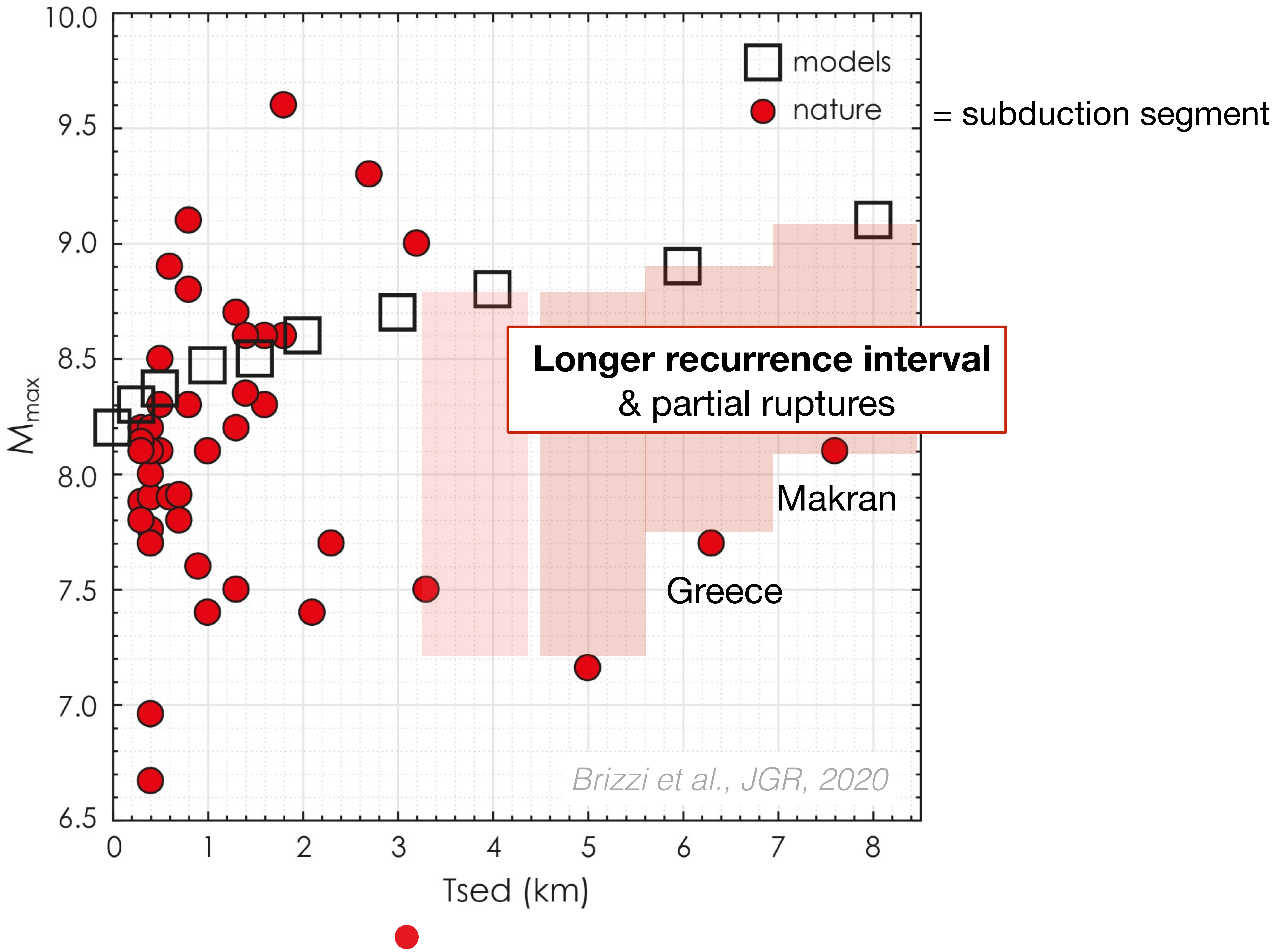

Physics-based Mmax estimates for natural seismicity …

- … go beyond data to identify relations between Mmax and sediment thickness in subduction zones *(Brizzi et al., JGR, 2020)*
- … predicted new, yet verifiable relations between Mmax and convergence rate in orogens *(Dal Zilio et al., EPSL, 2018)*

Thermo-Mechanical models (TM)

- Based on 2D finite-difference with marker-in-cell code

- **Input**
- Initial geometry and temperature
- Tectonic parameters
- Material parameters rock types

- **Tectonic output**
- Geometry
- Distribution physical parameters
  - Velocity, temperature, pressure
  - Viscosity, stress, fluid pressure

Conservation of mass, momentum and heat

Visco-elasto-plastic rheology

Δt = 1000 years

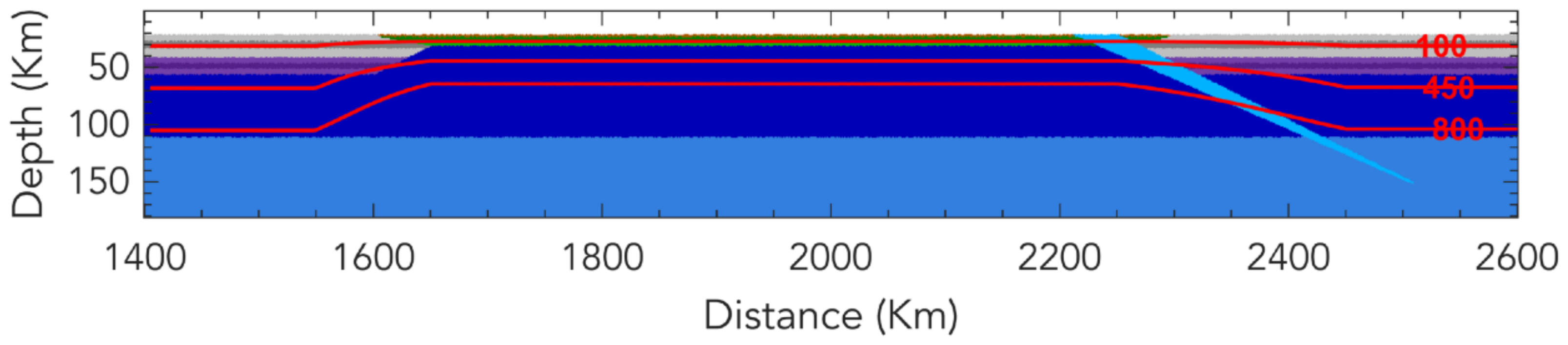

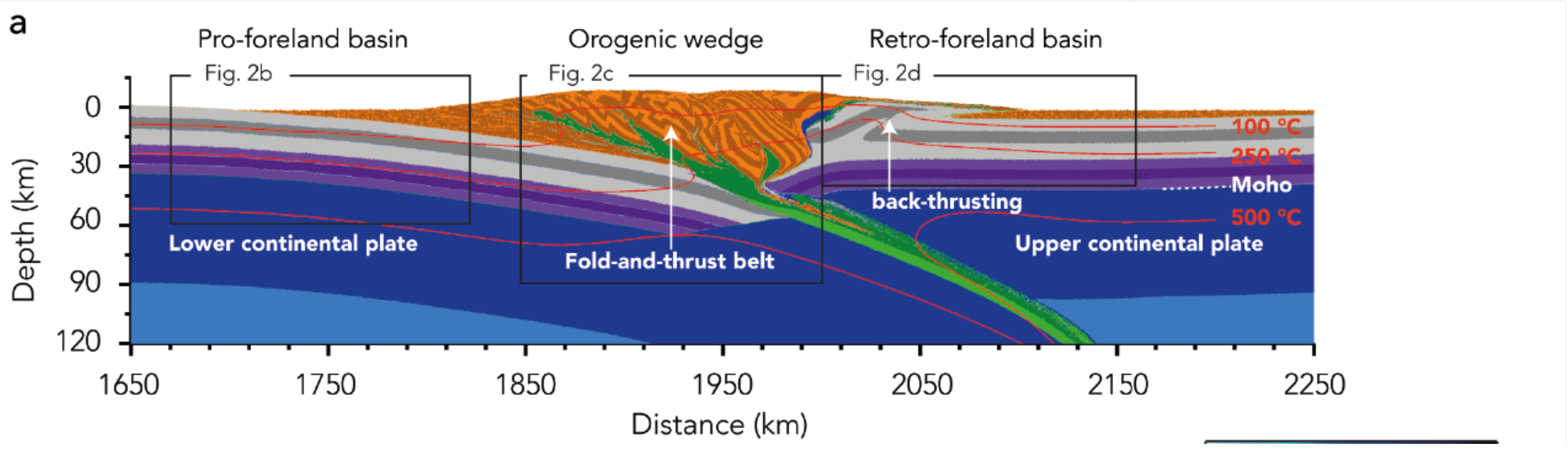

Geodynamic → Seismicity

Seismo-Thermo-Mechanical models (STM)

- Based on 2D finite-difference with marker-in-cell code

- **Input**
- Initial geometry and temperature
- Tectonic parameters
- Material parameters rock types

- **Tectonic output**
- Geometry
- Distribution physical parameters
  - Velocity, temperature, pressure
  - Viscosity, stress, fluid pressure

- **Seismicity output**
- Event nucleation, propagation, arrest

Conservation of mass, momentum and heat
Visco-elasto-plastic rheology

+ inertia
+ strongly rate dependent friction

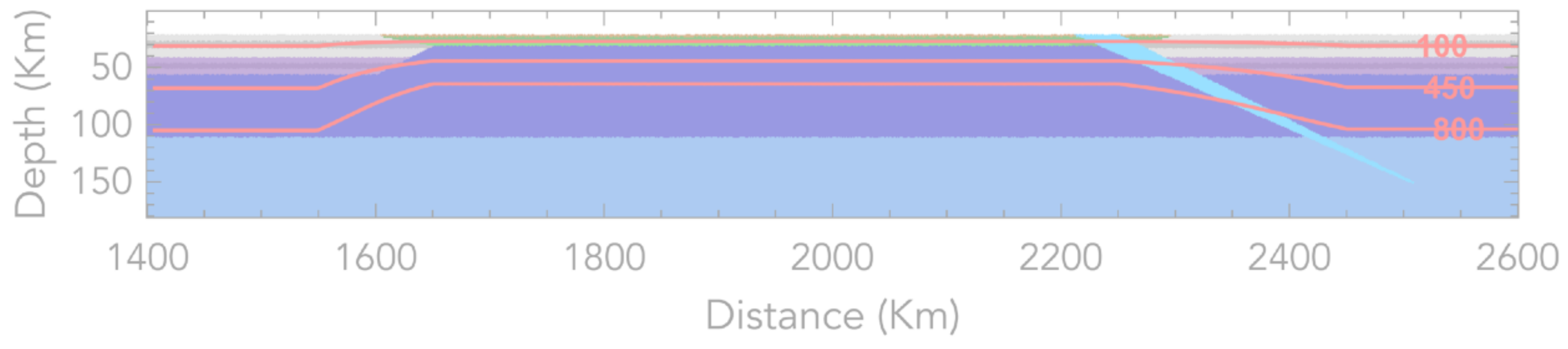

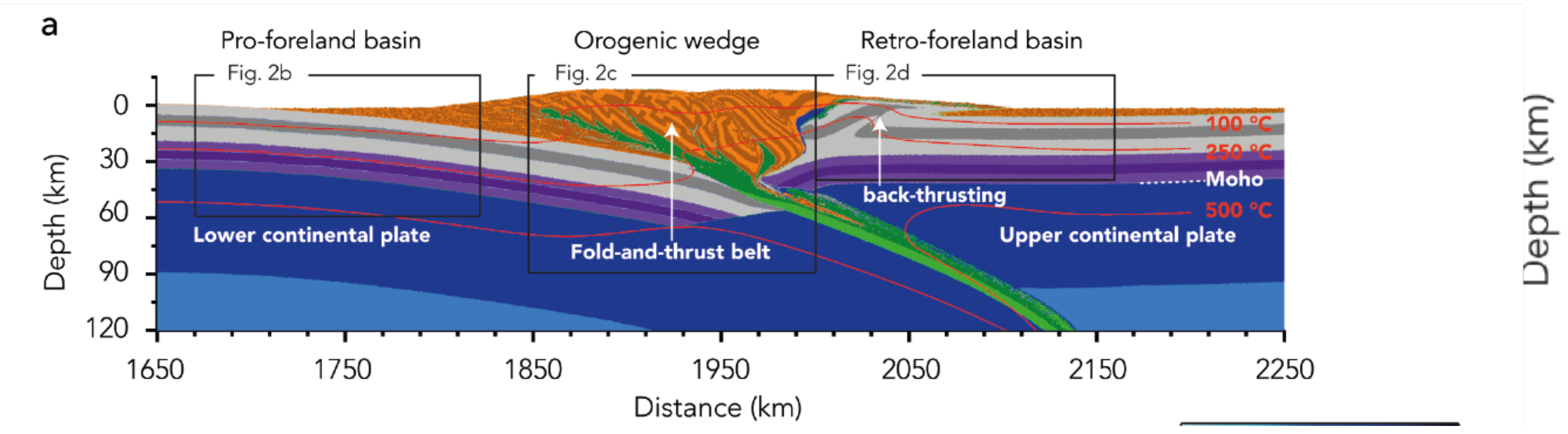

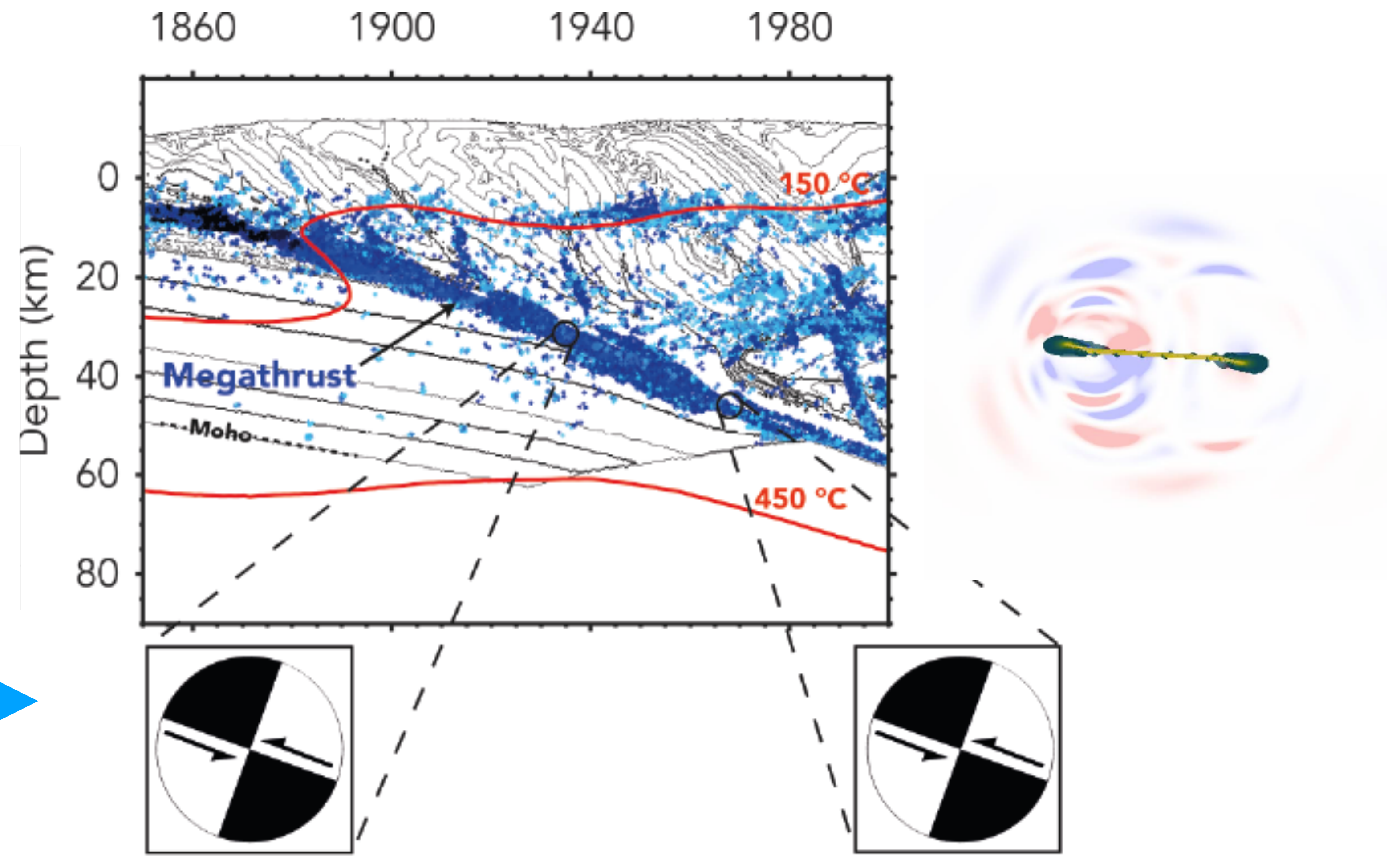

Geodynamic
Seismicity

New verifiable relation between convergence velocity and Mmax collisional orogens

Instead of taper rather a characteristic behaviour

Relation and magnitude for varying convergence rate agree with regional observations

- Why is this so? Is it an artifact of a limited observational time window?
- Faster penetration of cooler temperatures to larger depths → larger brittle area → larger and relatively more larger events

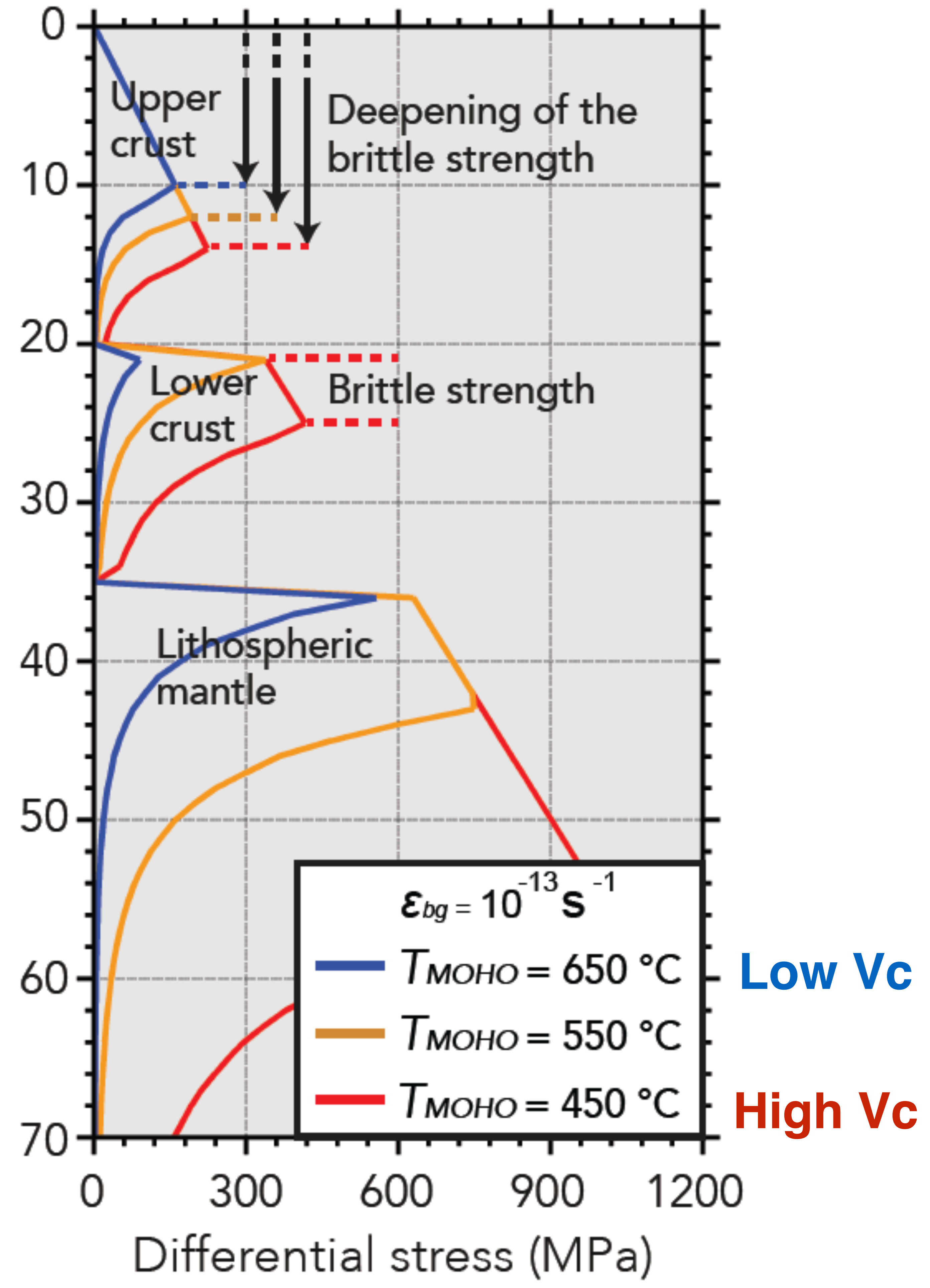

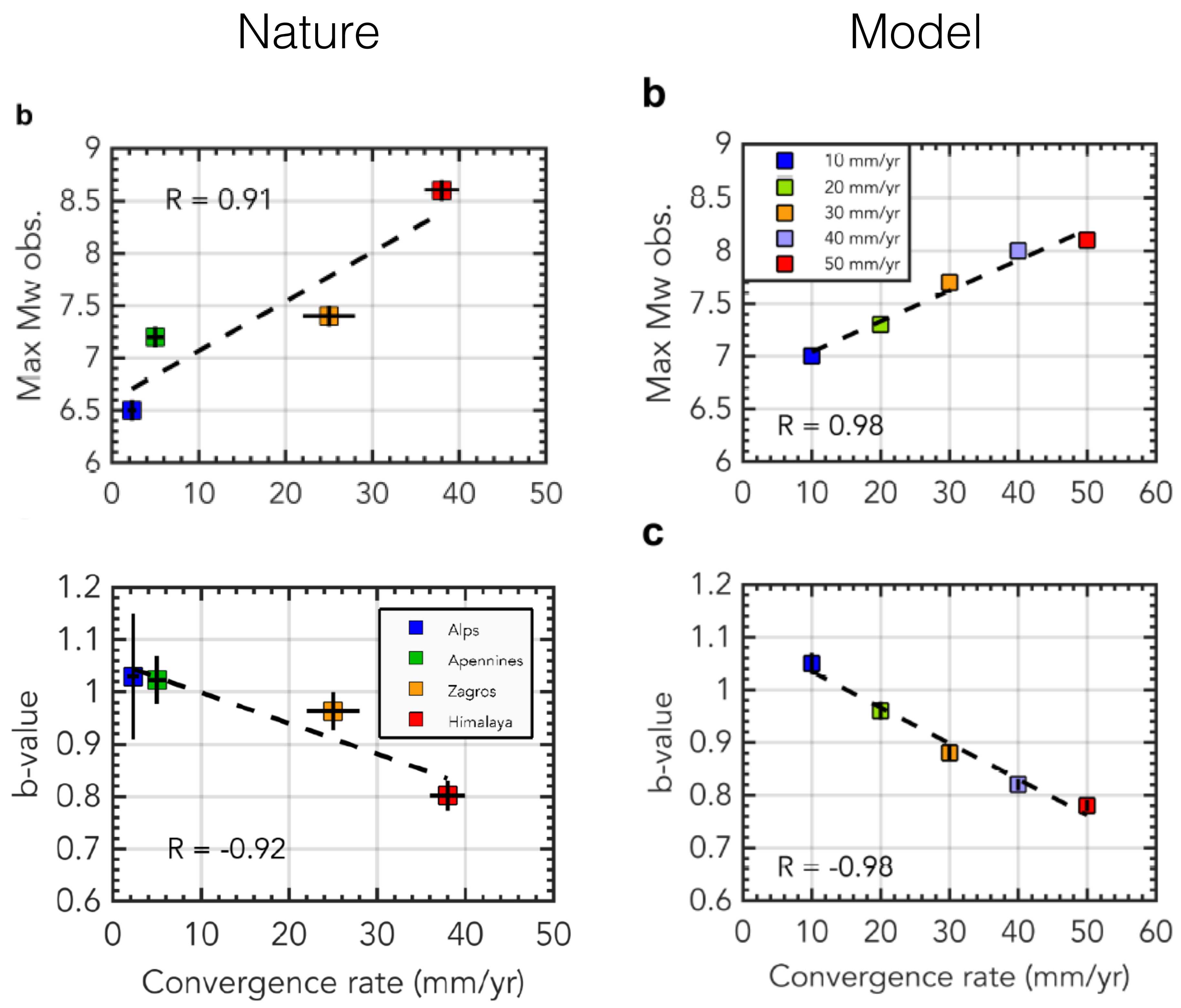

Convergence velocity *Vc* in collisional orogens

- Instead of a taper rather a characteristic behaviour due to dominance of a large mega thrust

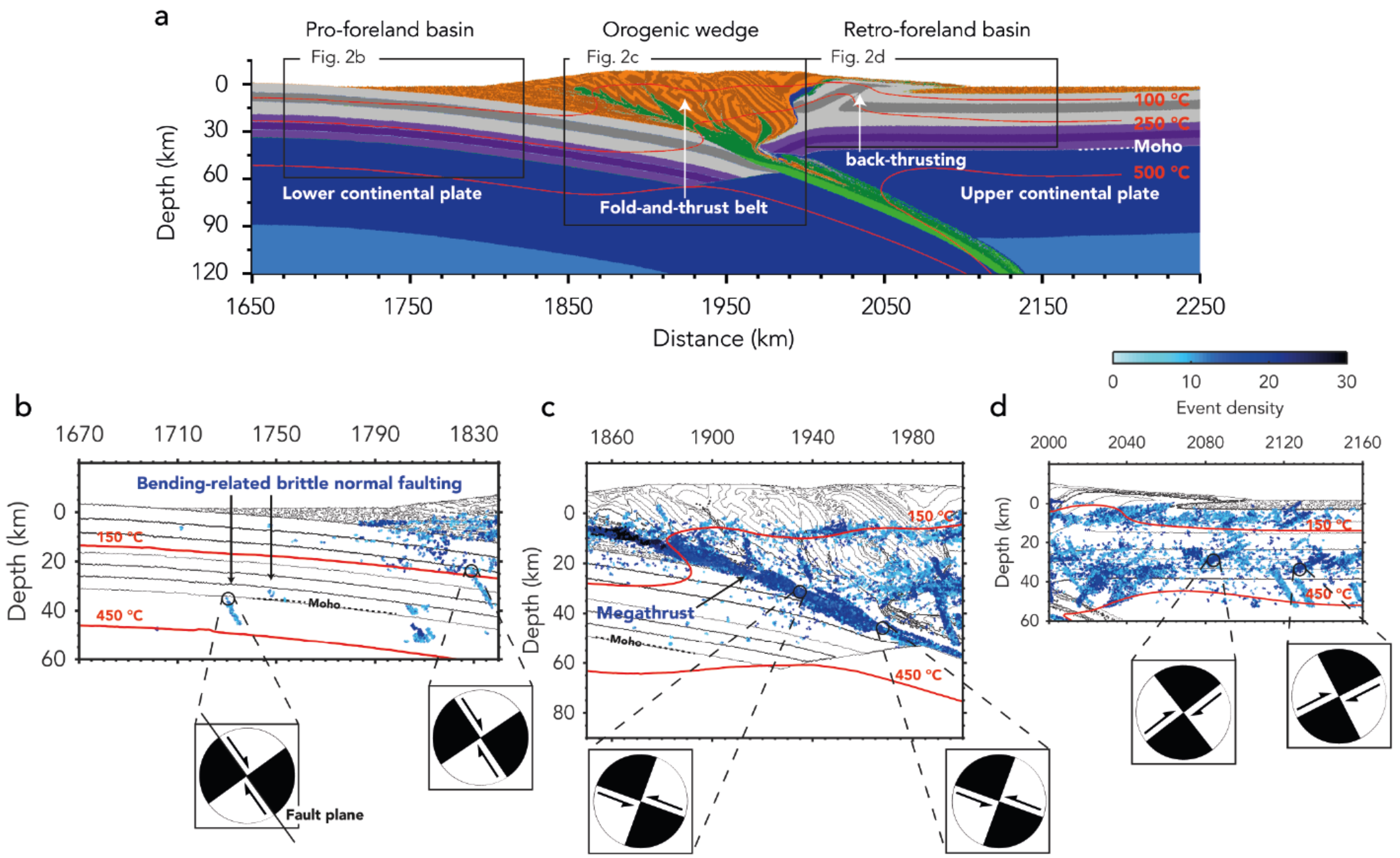

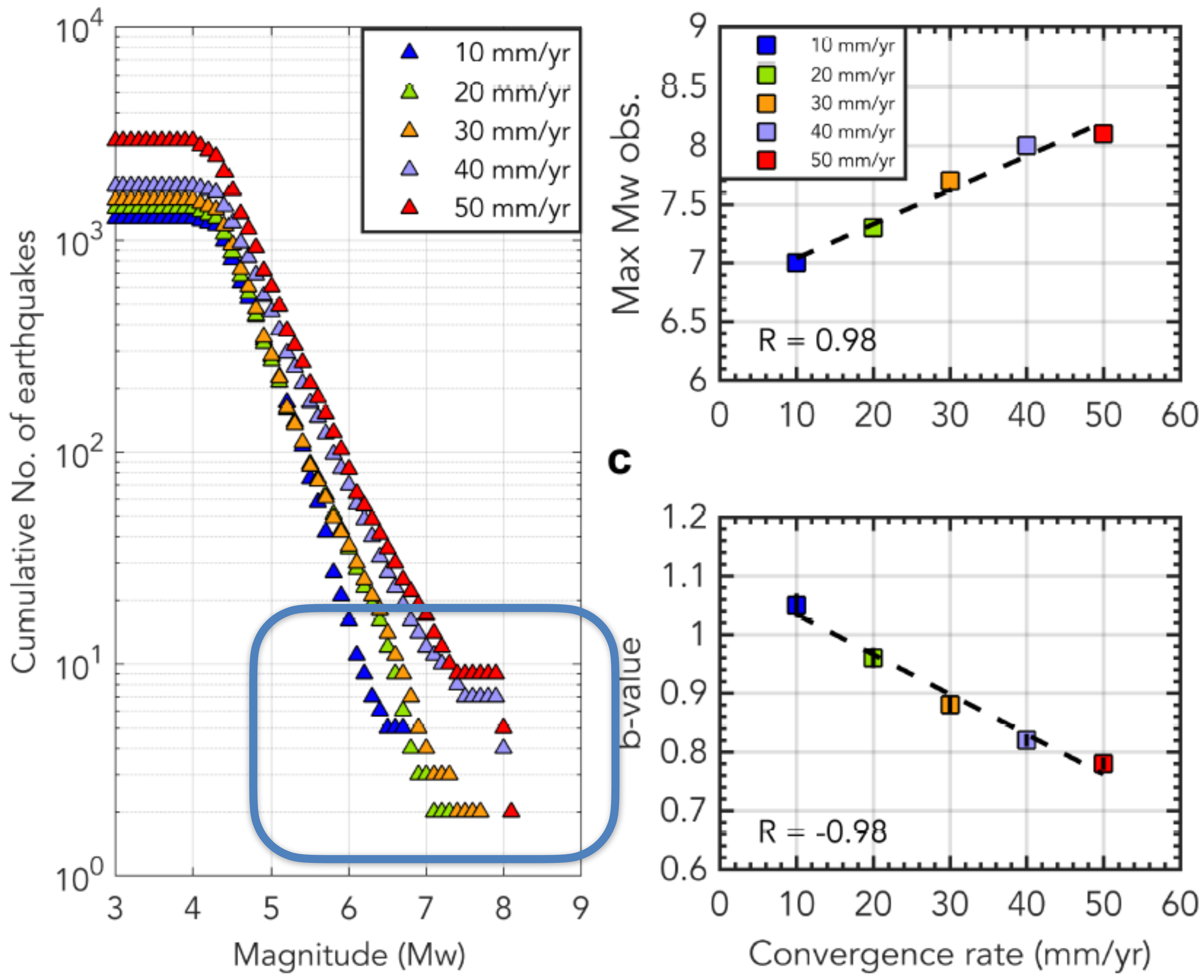

Mmax tapers? No

Natural vs. induced seismicity

- Key difference is loading of fault stresses, but fault slip processes remain the same → Learn from natural earthquakes!
  - Different parameters and scales introduce (large) changes in importance of processes for fault slip

Loading

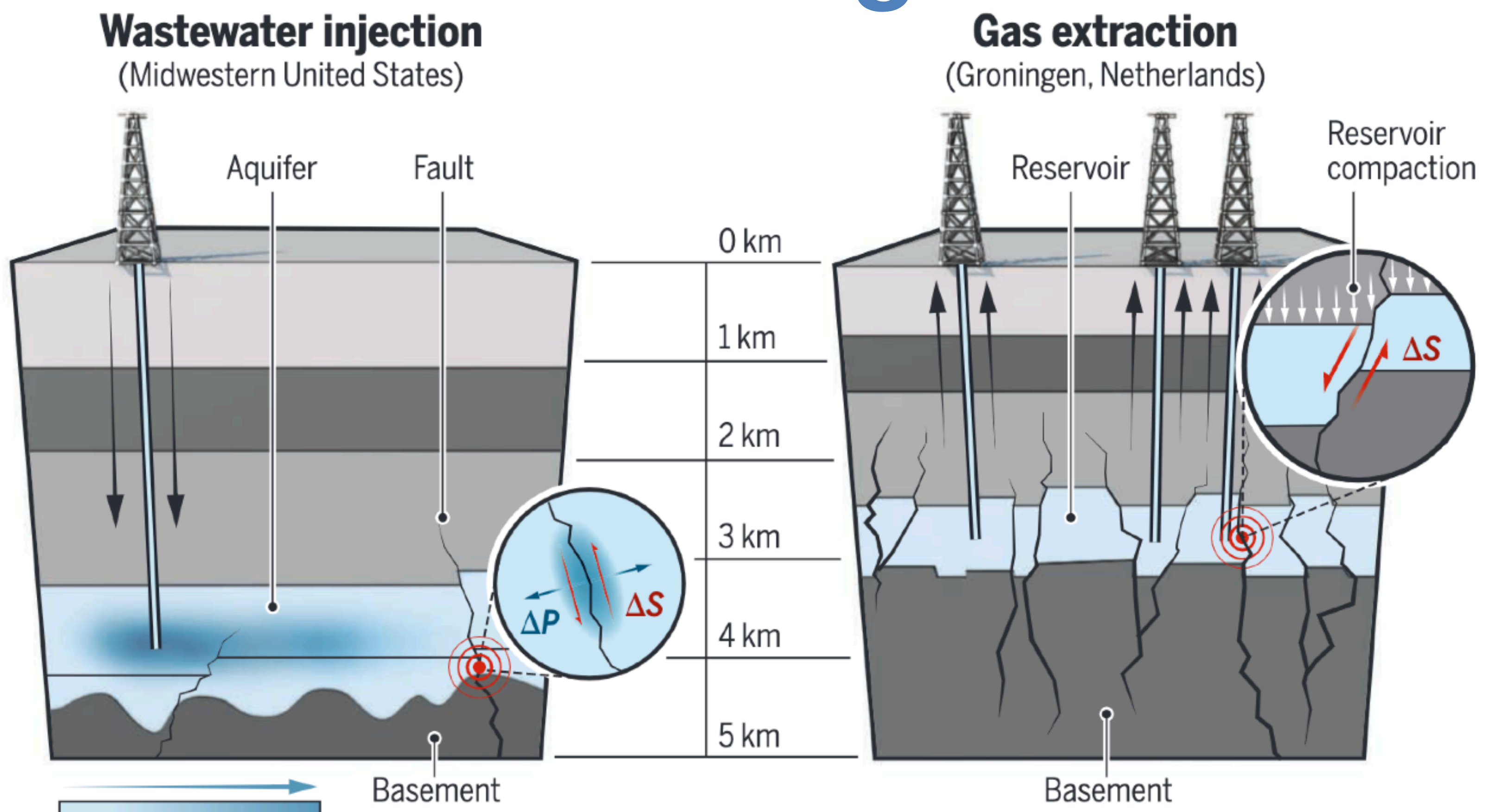

Candela et al., Science, 2018

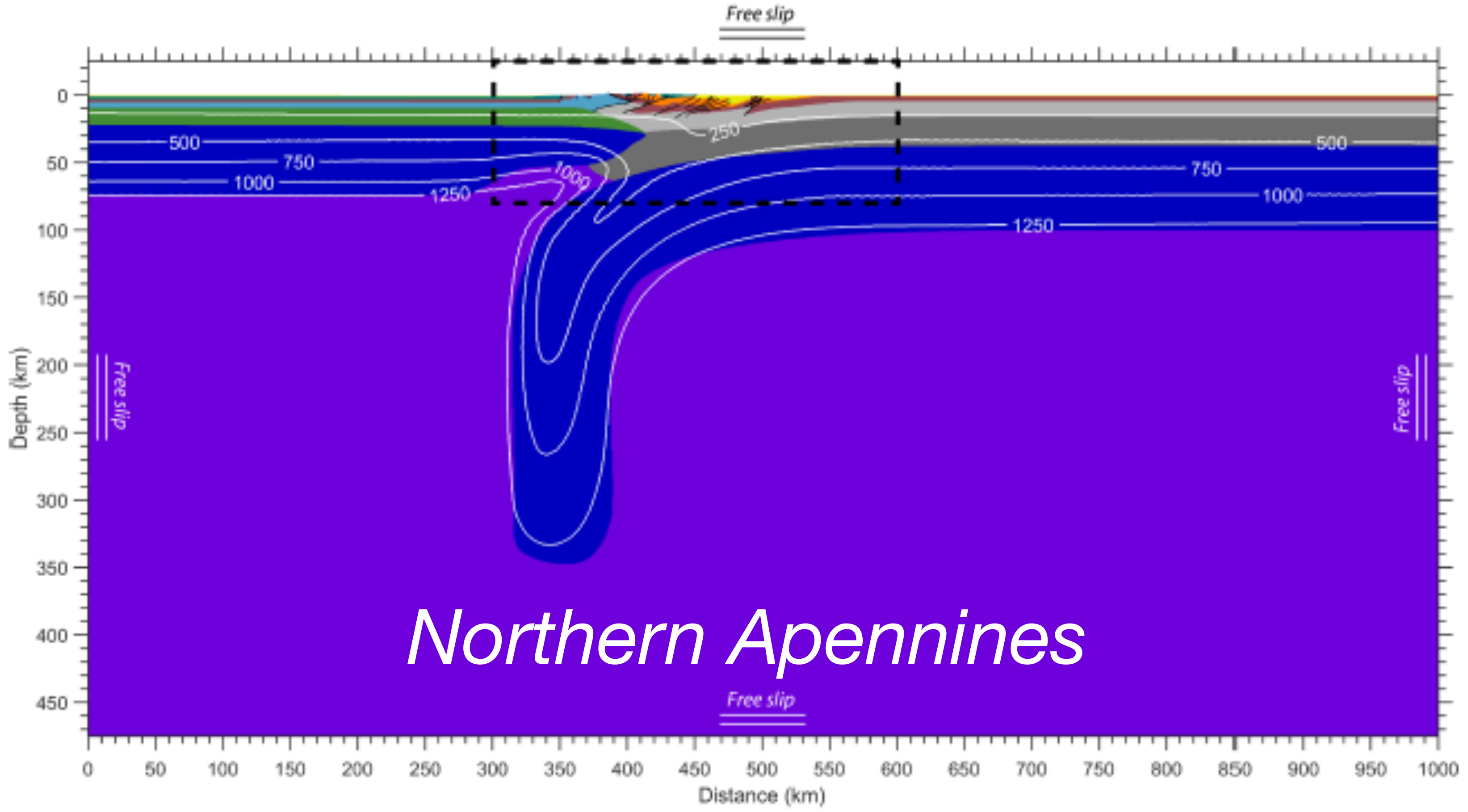

D'Acquisto et al., TP, 2020

Stress

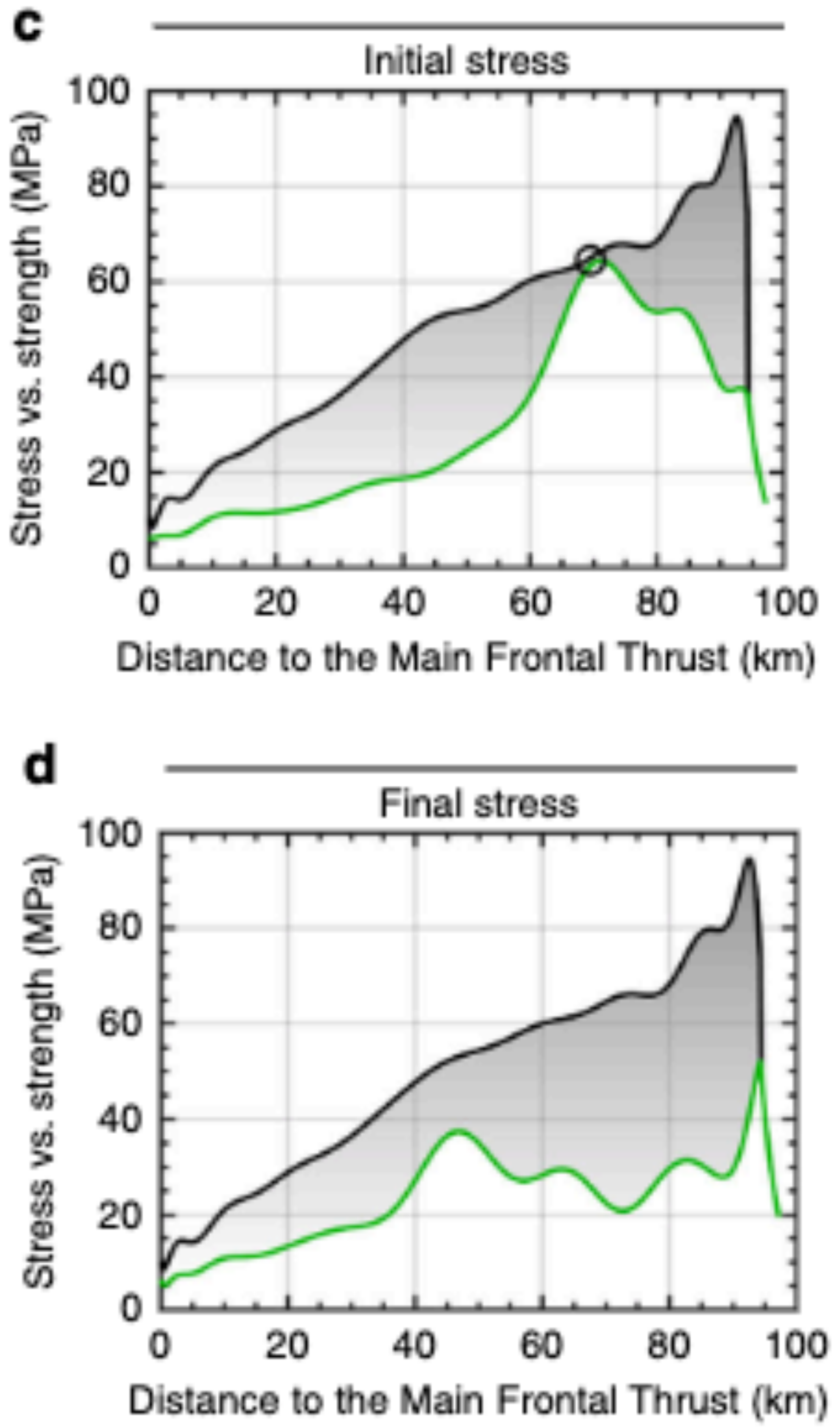

Dal Zilio et al., Nat. Comm., 2019

Slip

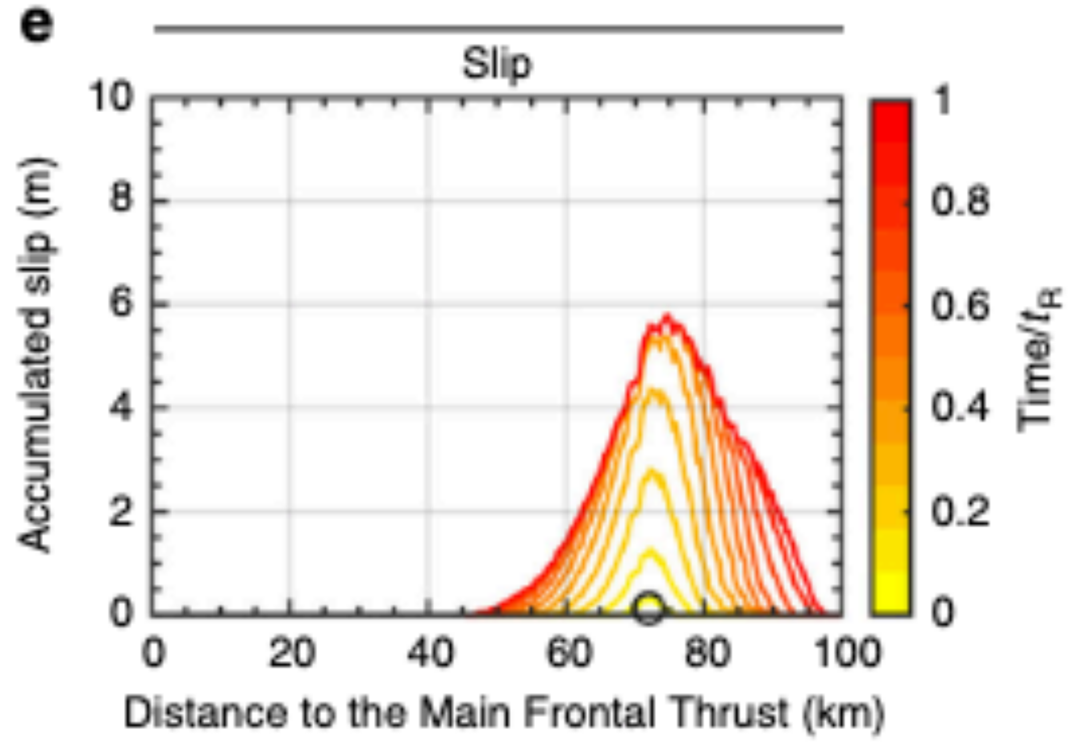

- Depth (and hence shaking levels)

Objective

- Determine a physics-based Mmax accounting for
  - 2.5D finite-width dynamic rupture propagation **across single, planar faults** in complex Groningen fault network
  - Using Linear Elastic Fracture Mechanics (LEFM)

- **>> Take this to the next level …**

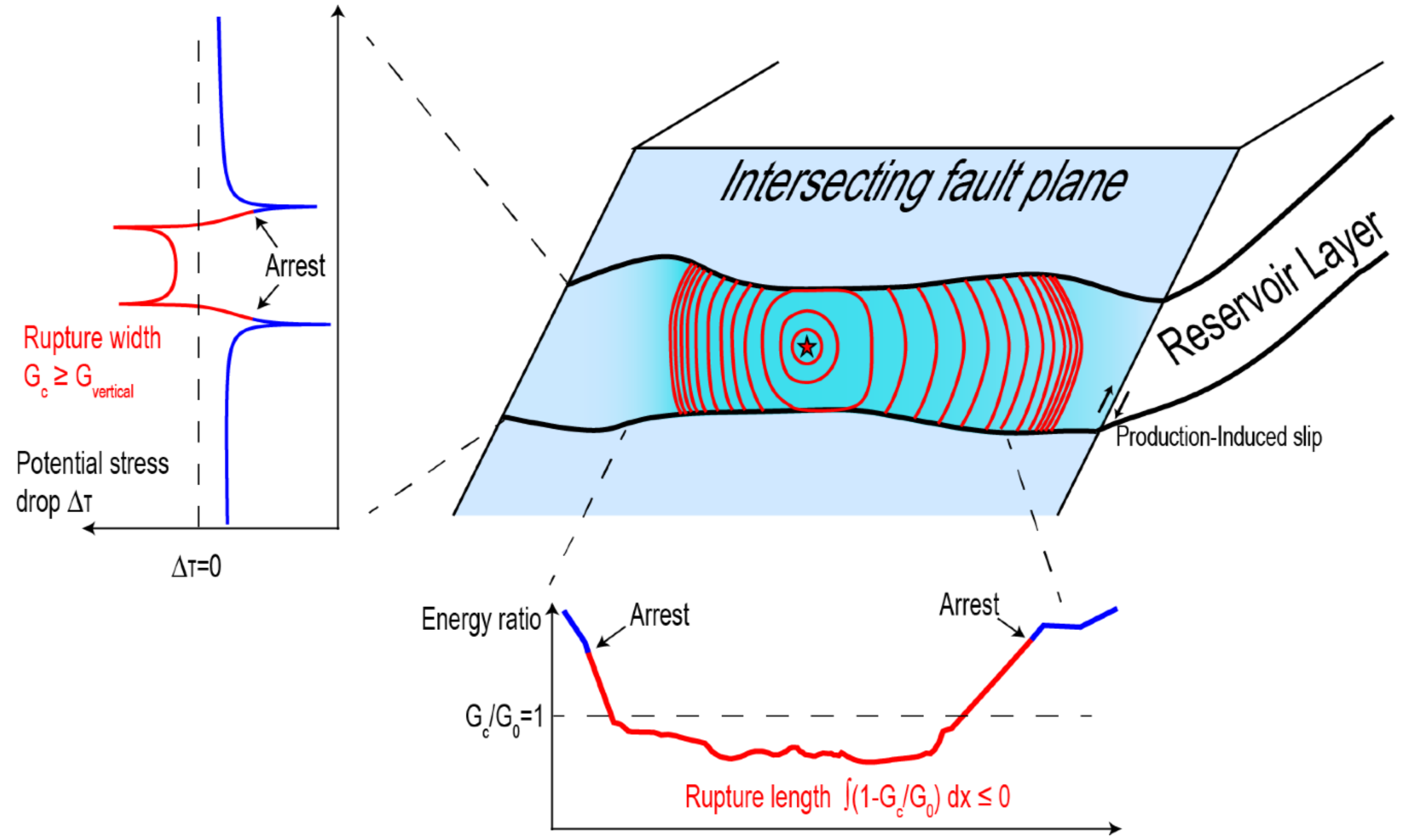

Weng & Ampuero, JGR, 2019

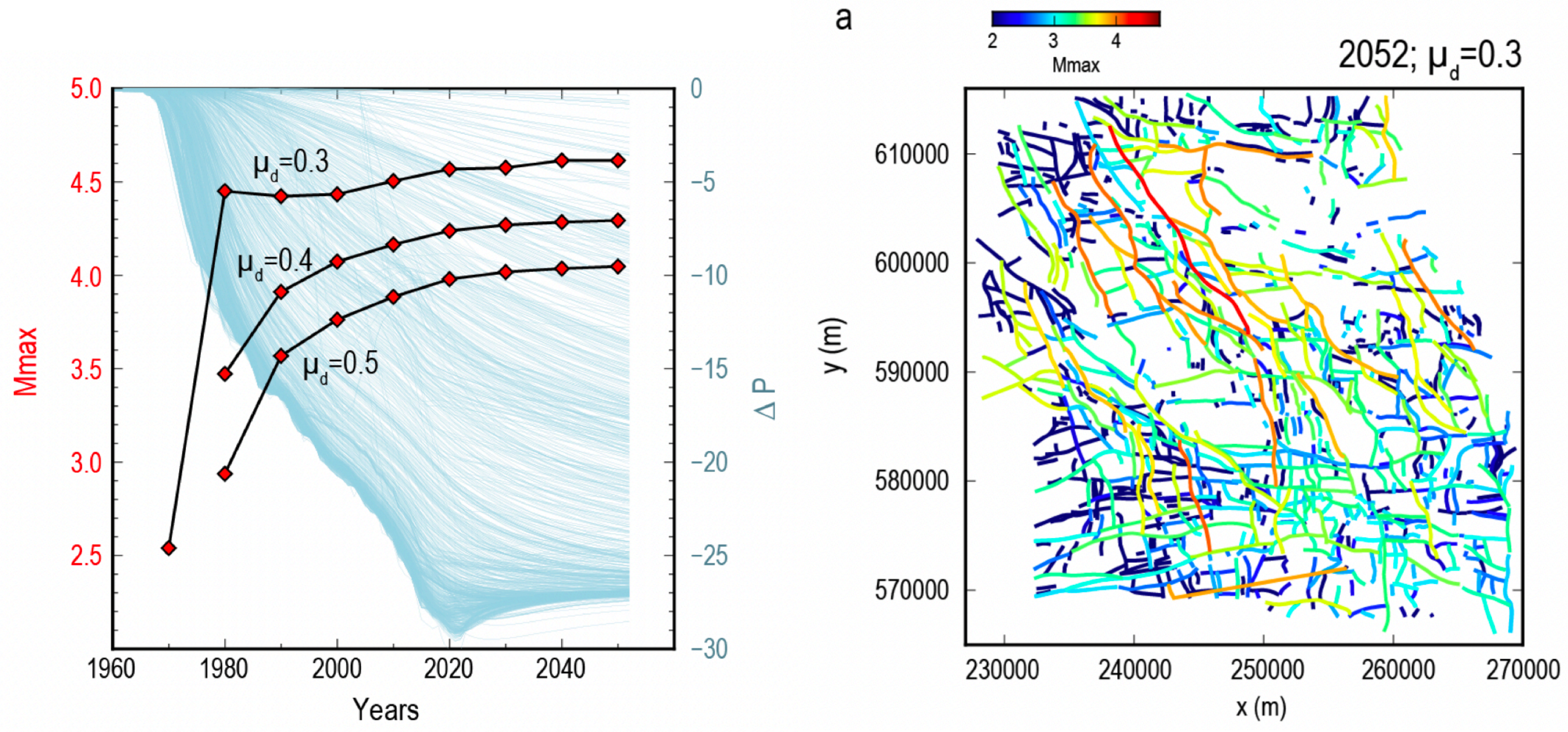

Weng et al., Mmax report, 2022

Objective

- Determine a physics-based Mmax accounting for (or testing)
  - 2.5D finite-width dynamic rupture propagation across single, planar faults in complex Groningen fault network
  - Improved fault model
  - Improved probabilistic pre-stresses
  - Fault roughness during rupture
  - Multi-segment faults
  - Seismic wave reflections
  - Improved probabilistic strength evolution
  - Second-generation earthquakes

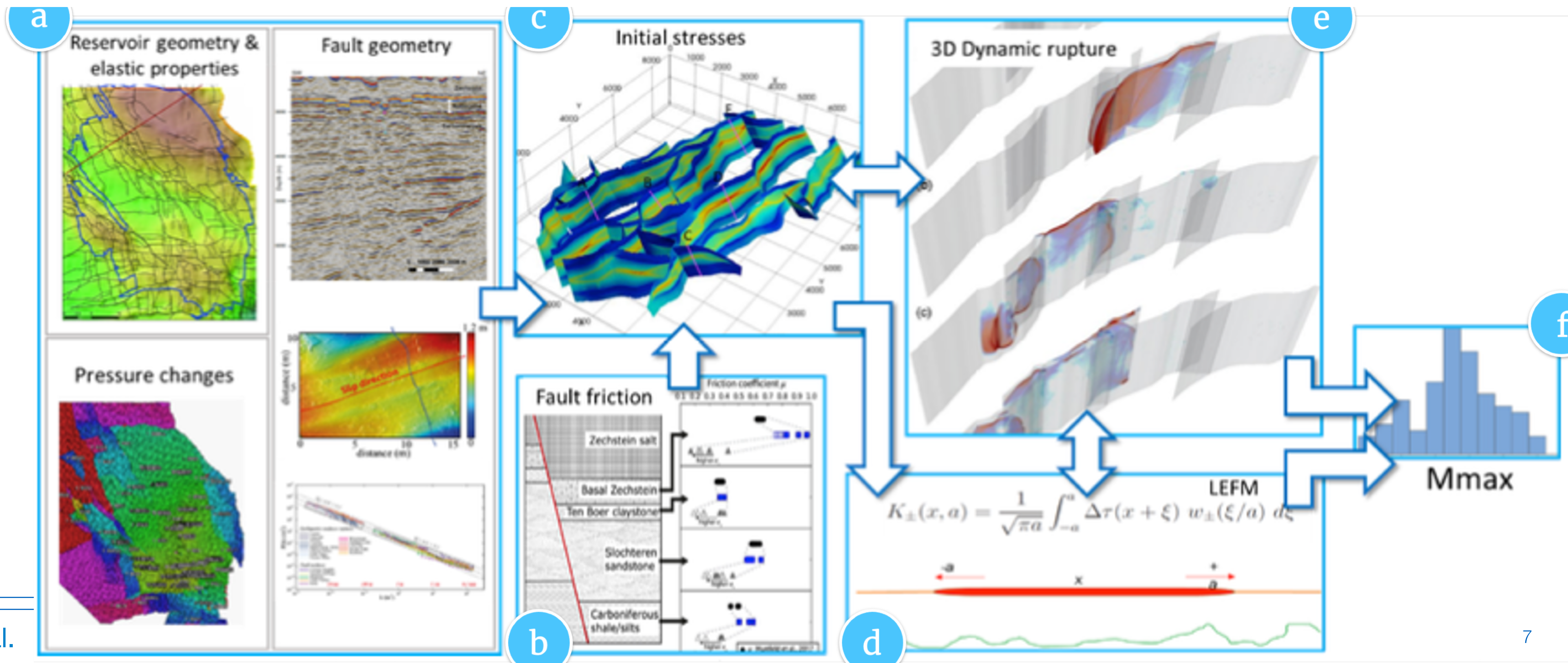

Objective

- Determine a physics-based Mmax accounting for (or testing)
  - 2.5D finite-width dynamic rupture propagation across single, planar faults in complex Groningen fault network
  - **Improved fault model**
  - Improved probabilistic pre-stresses
  - Fault roughness during rupture
  - Multi-segment faults
  - Seismic wave reflections
  - Improved probabilistic strength evolution
  - Second-generation earthquakes

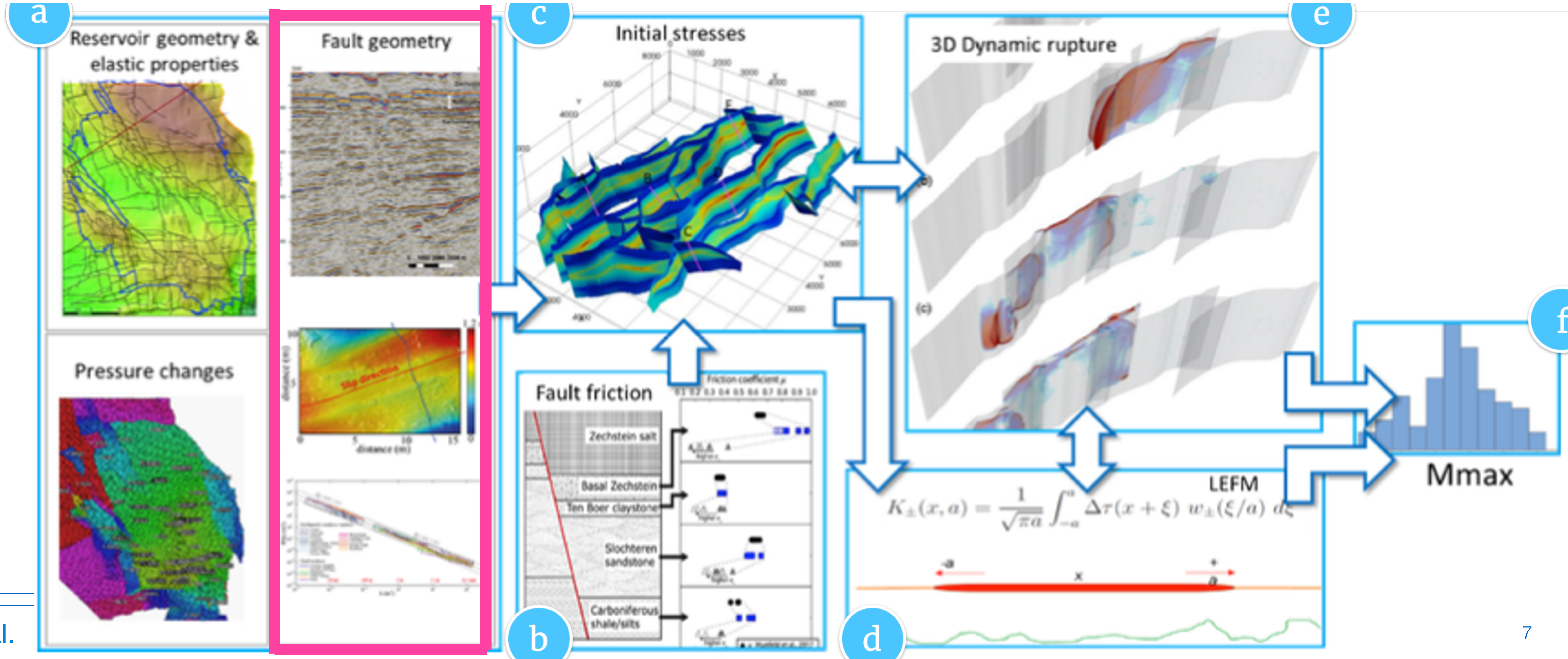

Improving fault geometry

- New fault models from ant tracking look comparable in map view, but miss coherent kinematics in cross-sections
  - Solution lies in kinematic mapping and steering attributes such as ant-tracking

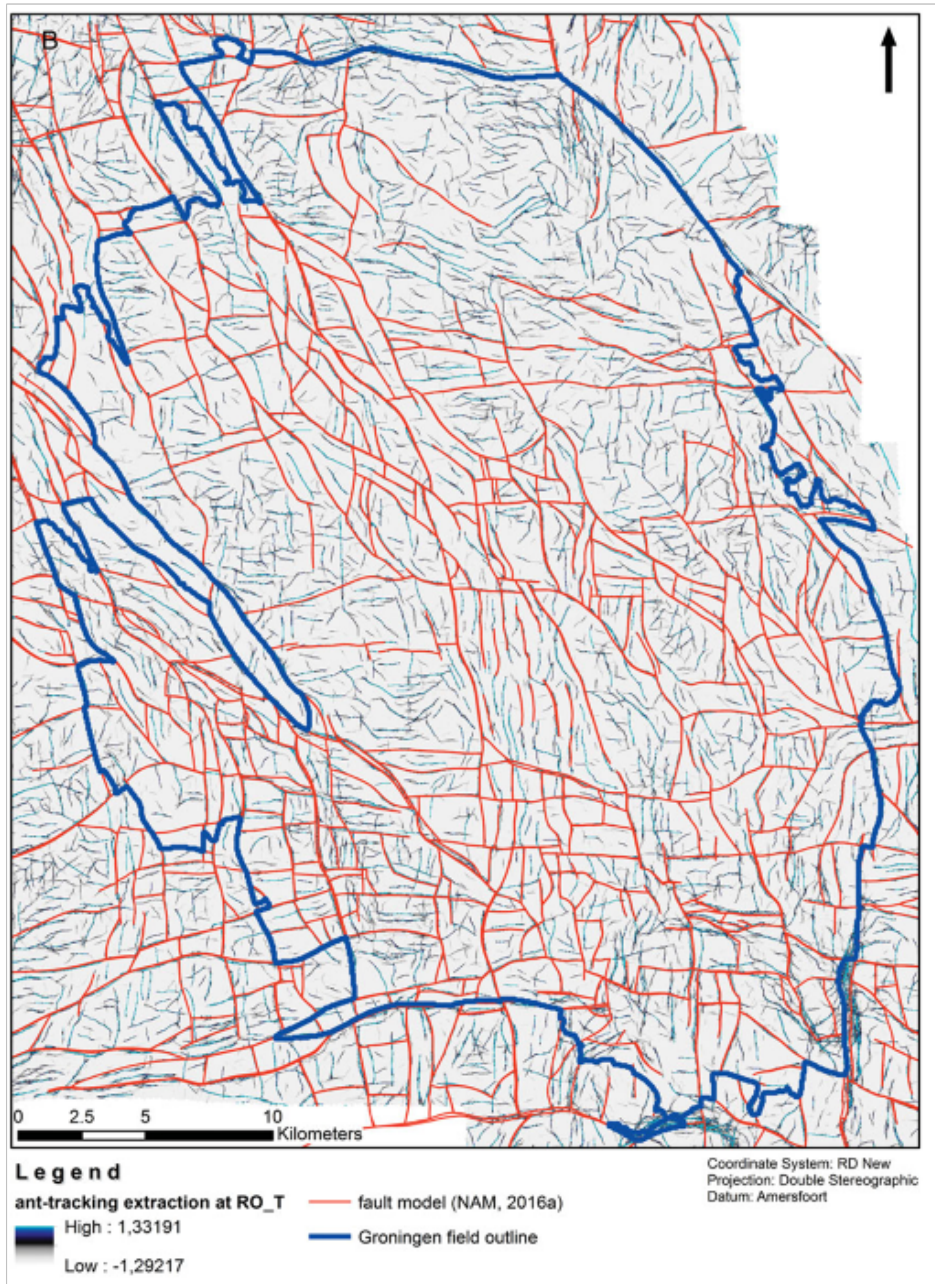

Kortekaas & Jaarsma (2017)

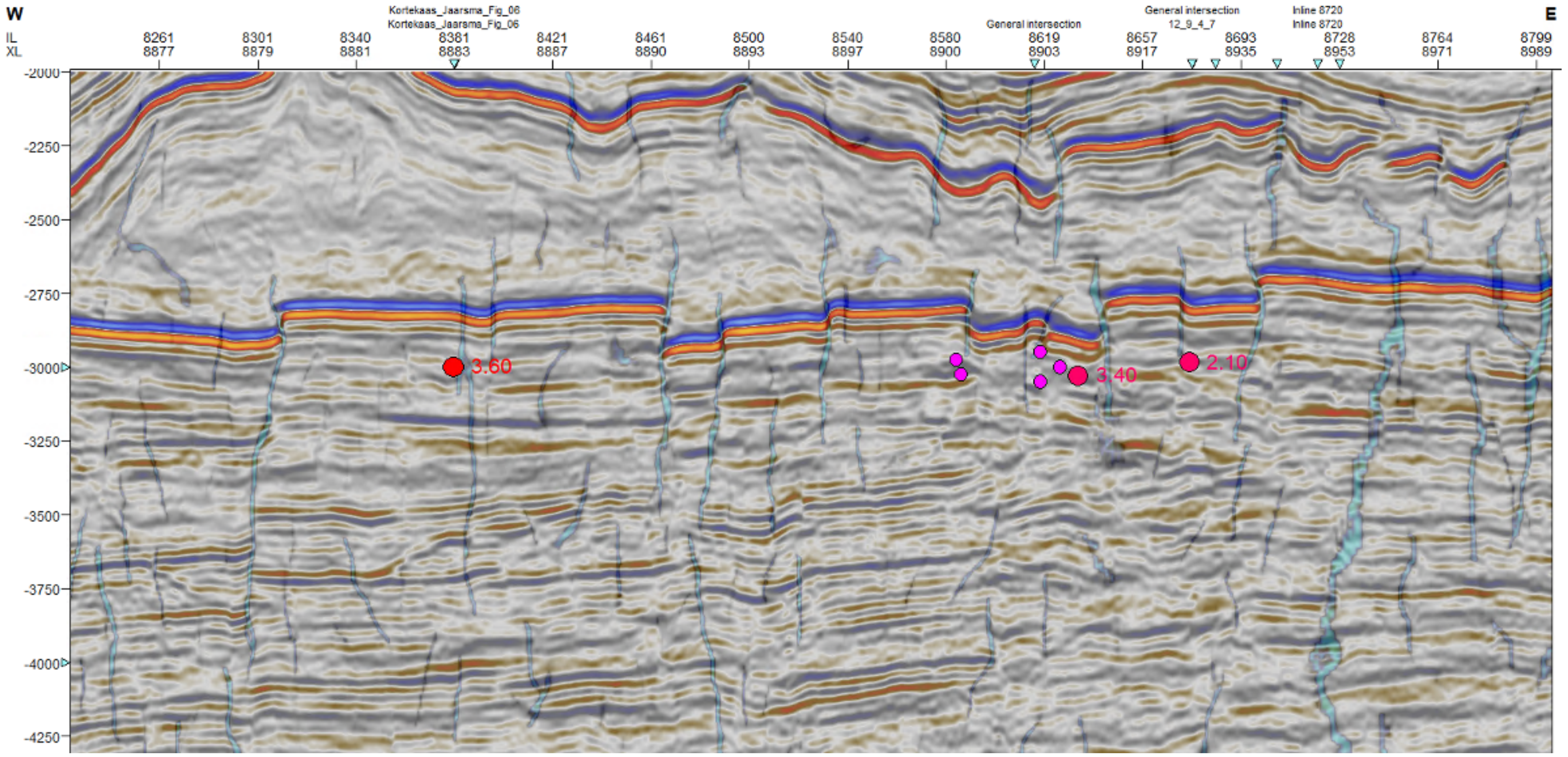

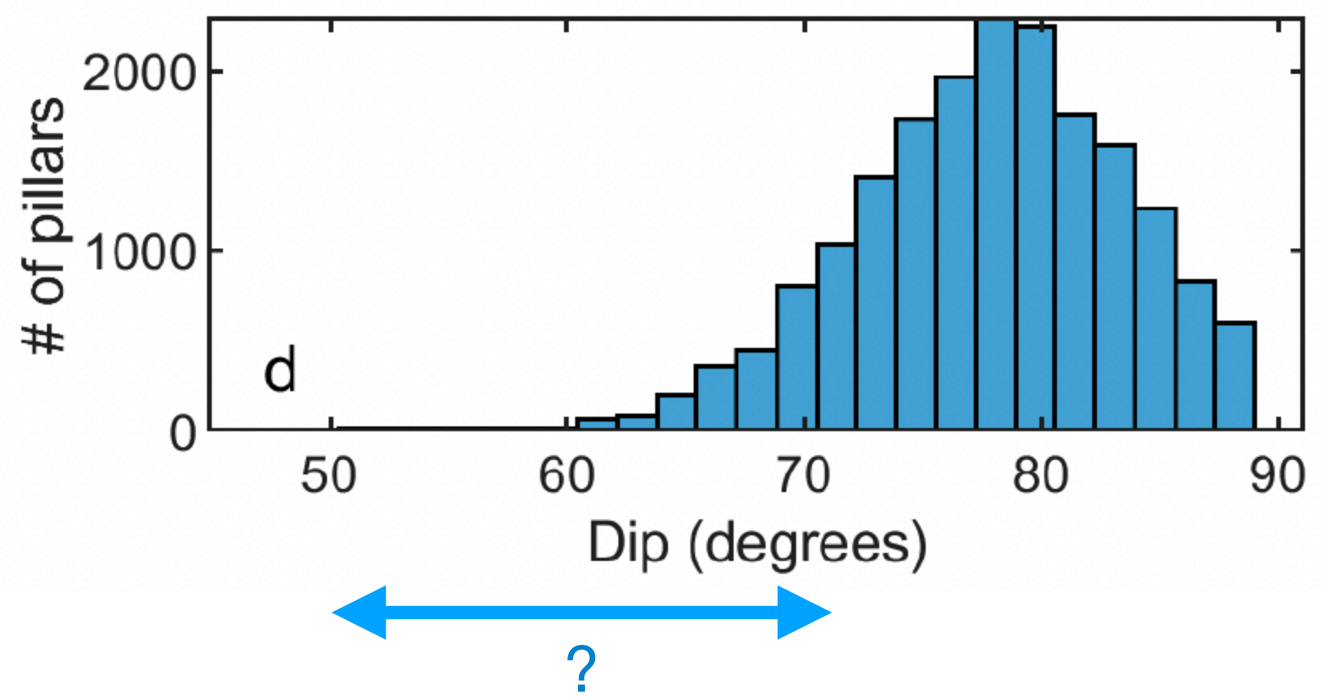

Objective

- Determine a physics-based Mmax accounting for (or testing)
  - 2.5D finite-width dynamic rupture propagation across single, planar faults in complex Groningen fault network
  - Improved fault model
  - **Improved probabilistic pre-stresses**
  - Fault roughness during rupture
  - Multi-segment faults
  - Seismic wave reflections
  - Improved probabilistic strength evolution
  - Second-generation earthquakes

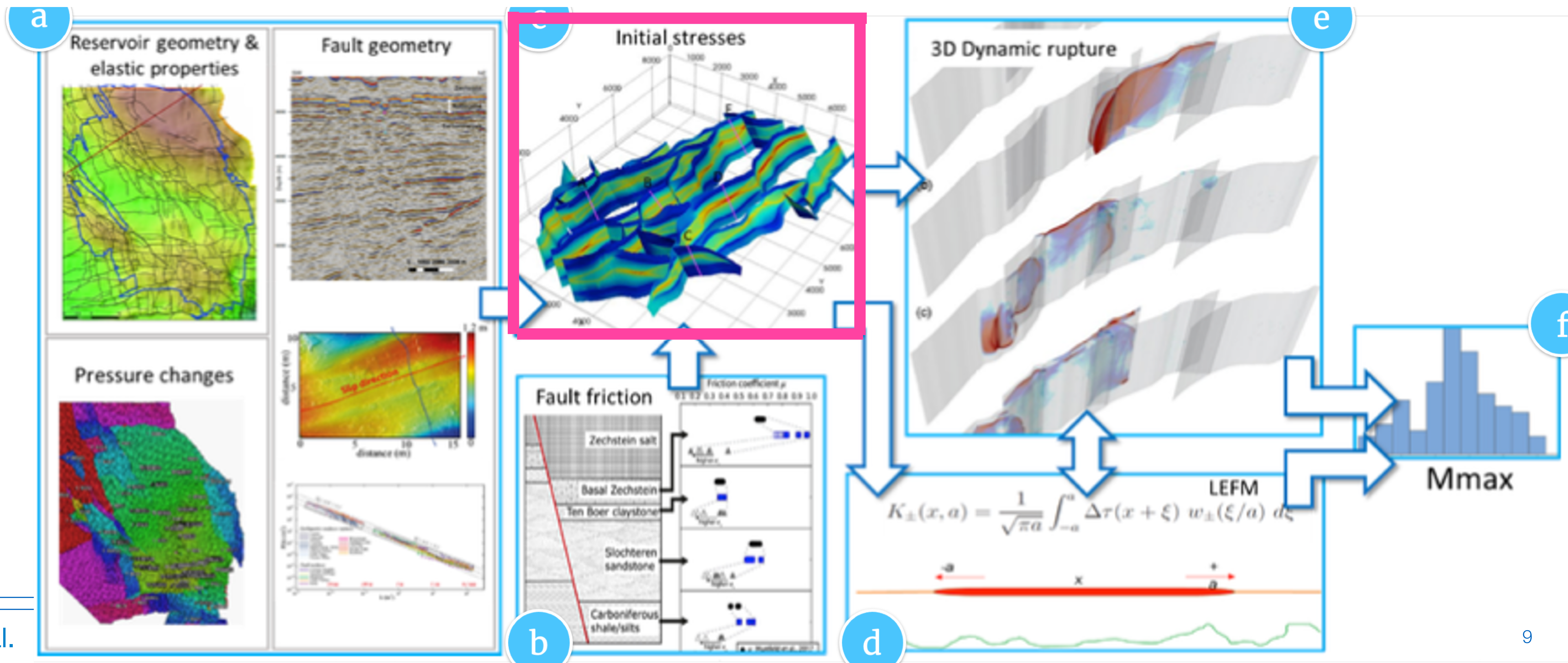

Improved fault stresses

- Build upon improved fault geometry and a probabilistic representation thereof
- 2D Jansen et al. (2019) ok for towards 3D, but for fault intersections

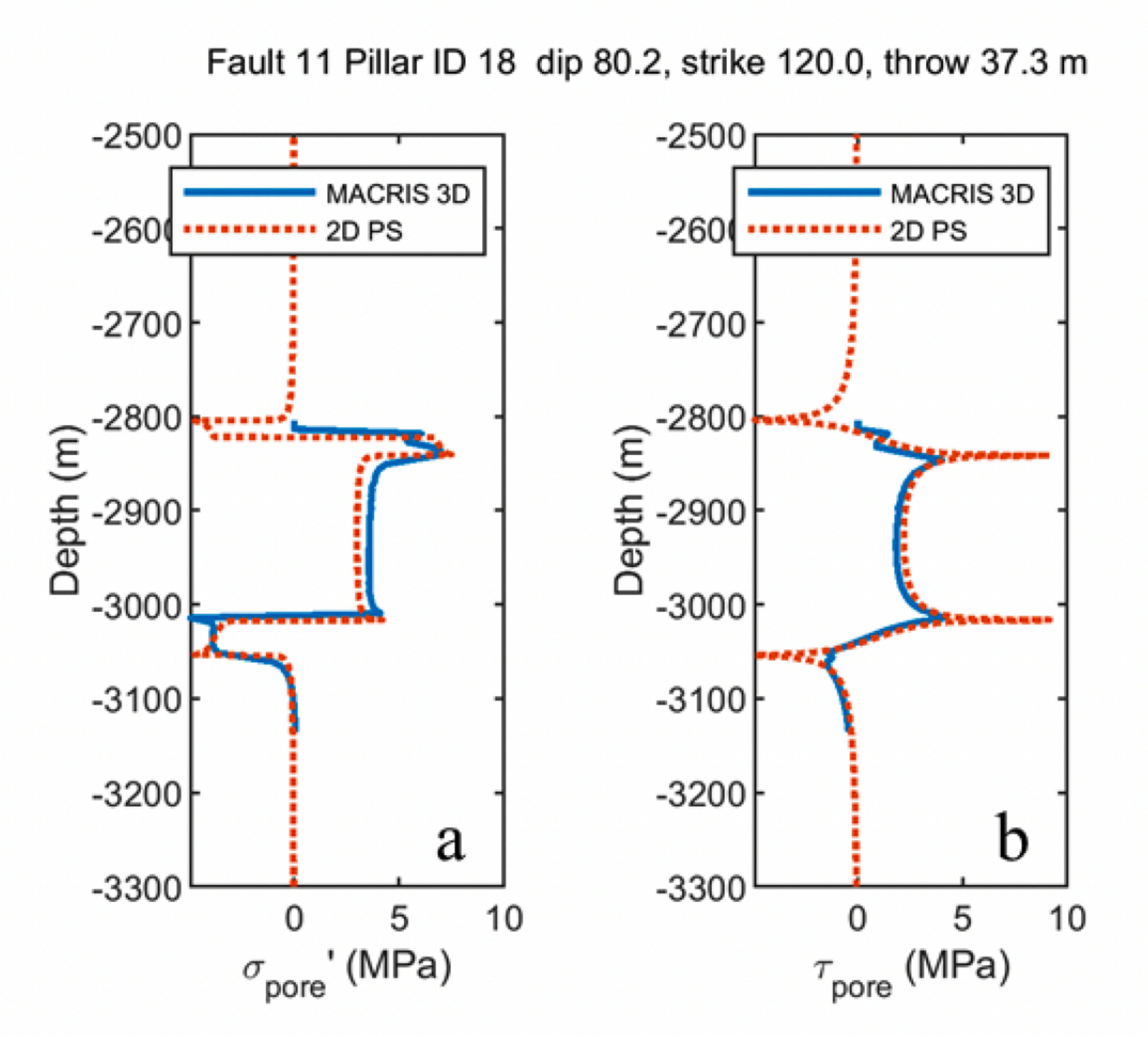

Weng et al., Mmax report, 2022

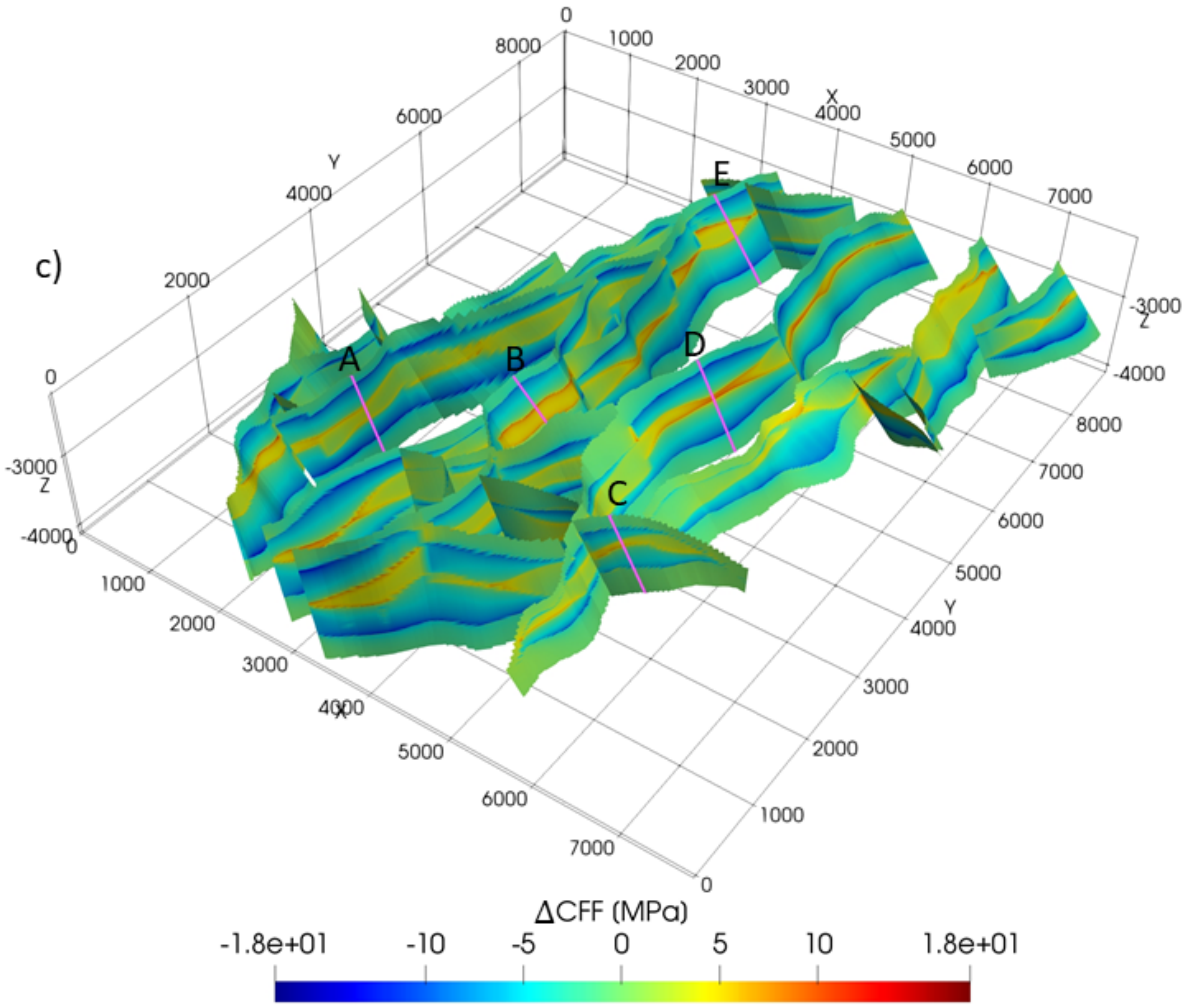

van Wees et al.., 2019; Candela et al., 2019, 2021

Objective

- Determine a physics-based Mmax accounting for
  - 2.5D finite-width dynamic rupture propagation across single, planar faults in complex Groningen fault network
  - Improved fault model
  - Improved probabilistic pre-stresses
  - **Fault roughness during rupture**
  - Multi-segment faults
  - Seismic wave reflections
  - Improved probabilistic strength evolution
  - Second-generation earthquakes

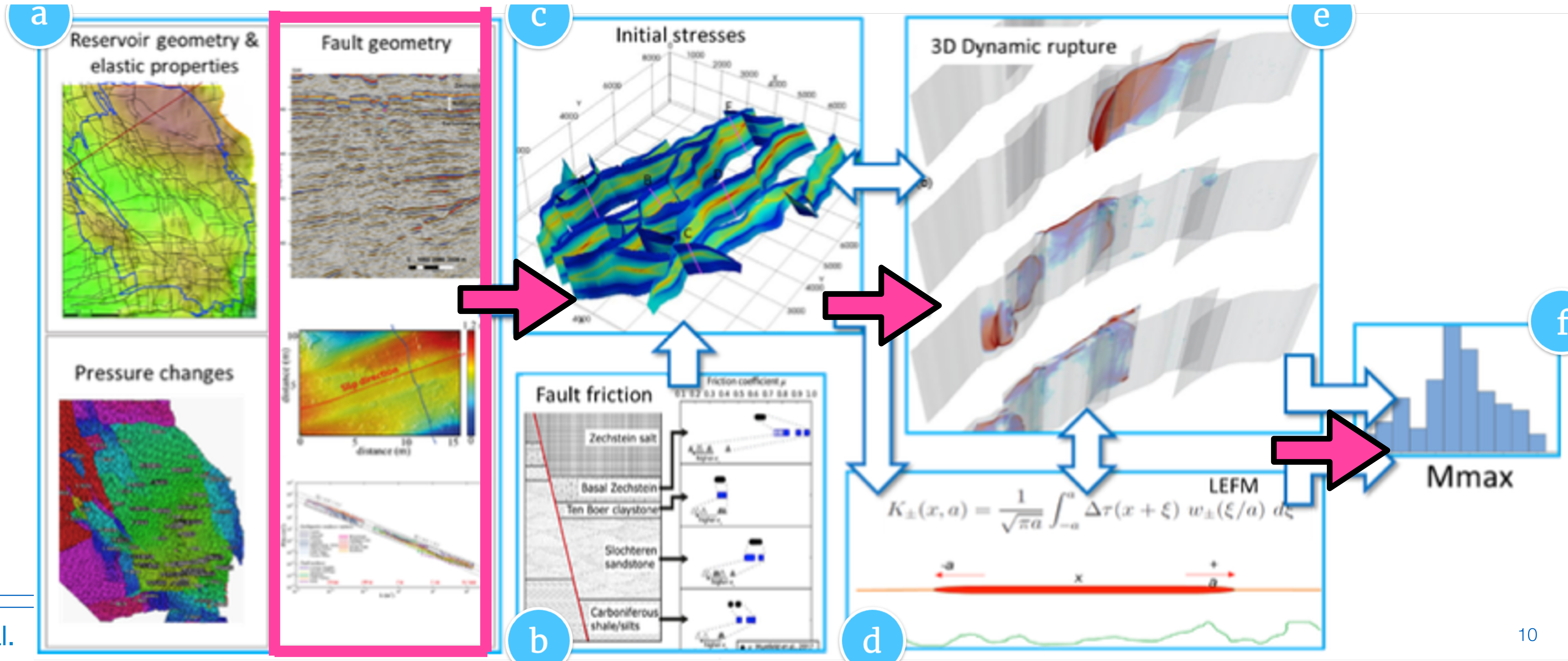

Improved single fault geometry

- Study role fault geometry
  - Improvements of kinematic consistency (and dip issue)
  - Listric faults in underburden
- Study role roughness (e.g.,jogs), jogs, roughness

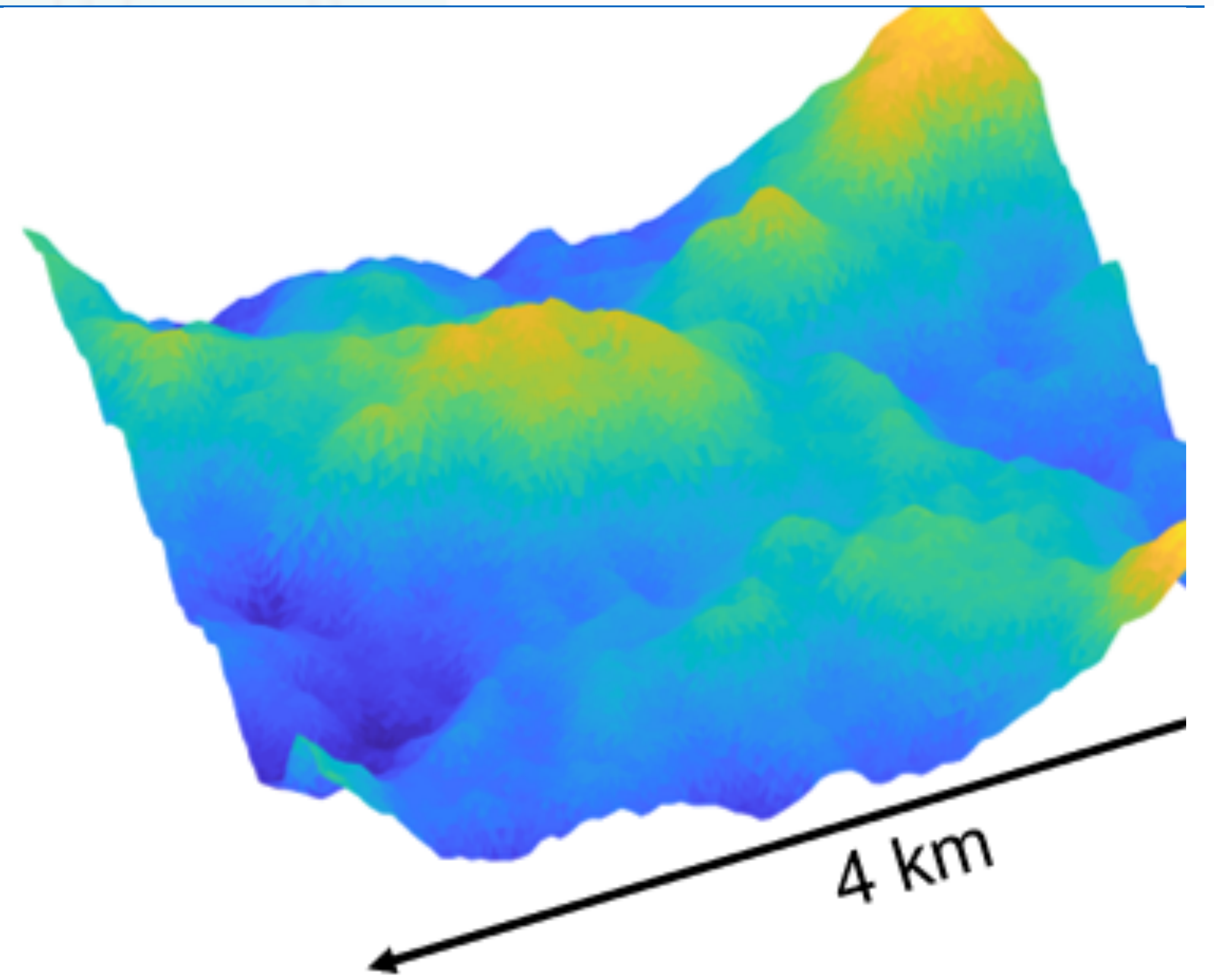

- Loes showed importance of fault geometry for stress loading
- Yet miss impact dynamic rupture (Ulrich, PhD thesis, 2021) → needs enhancement in LEFM?

Objective

- Determine a physics-based Mmax accounting for
  - 2.5D finite-width dynamic rupture propagation across single, planar faults in complex Groningen fault network
  - Improved fault model
  - Improved probabilistic pre-stresses
  - Fault roughness during rupture
  - **Multi-segment faults**
  - **Seismic wave reflections**
  - Improved probabilistic strength evolution
  - Second-generation earthquakes

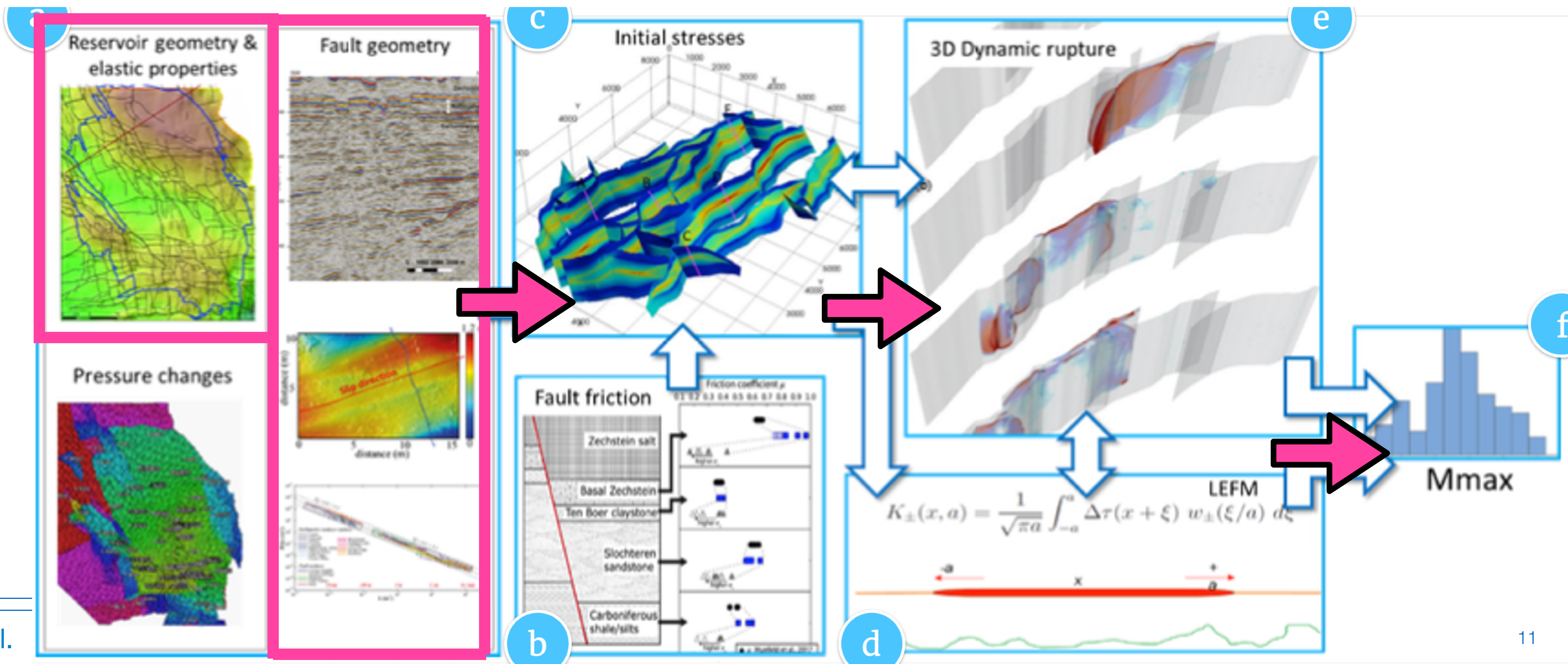

Multi-segment faults

- Recent high-resolution seismological observations suggest (large) earthquakes can jump to adjacent and intersecting faults

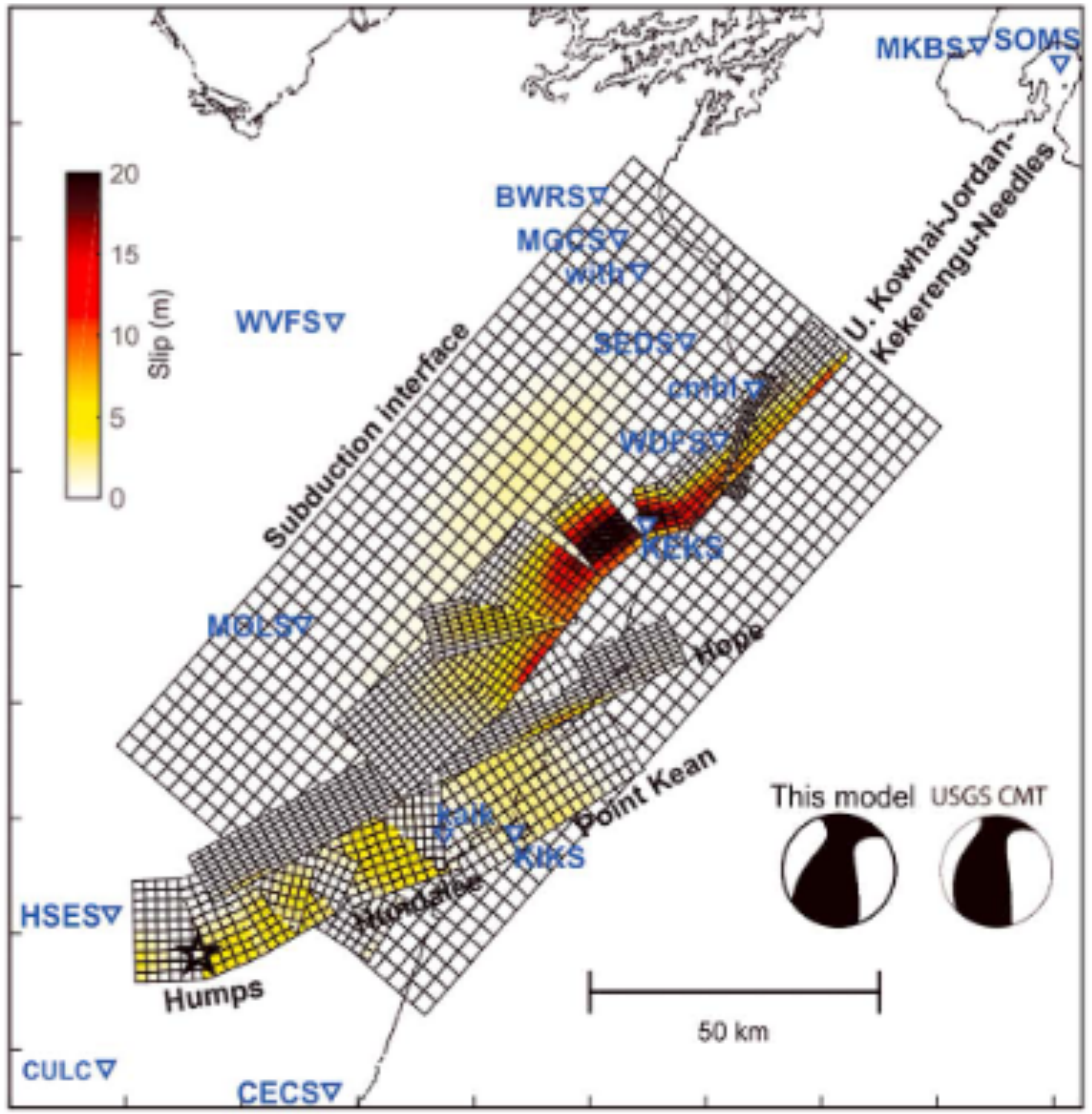

Clark et al., EPSL, 2017

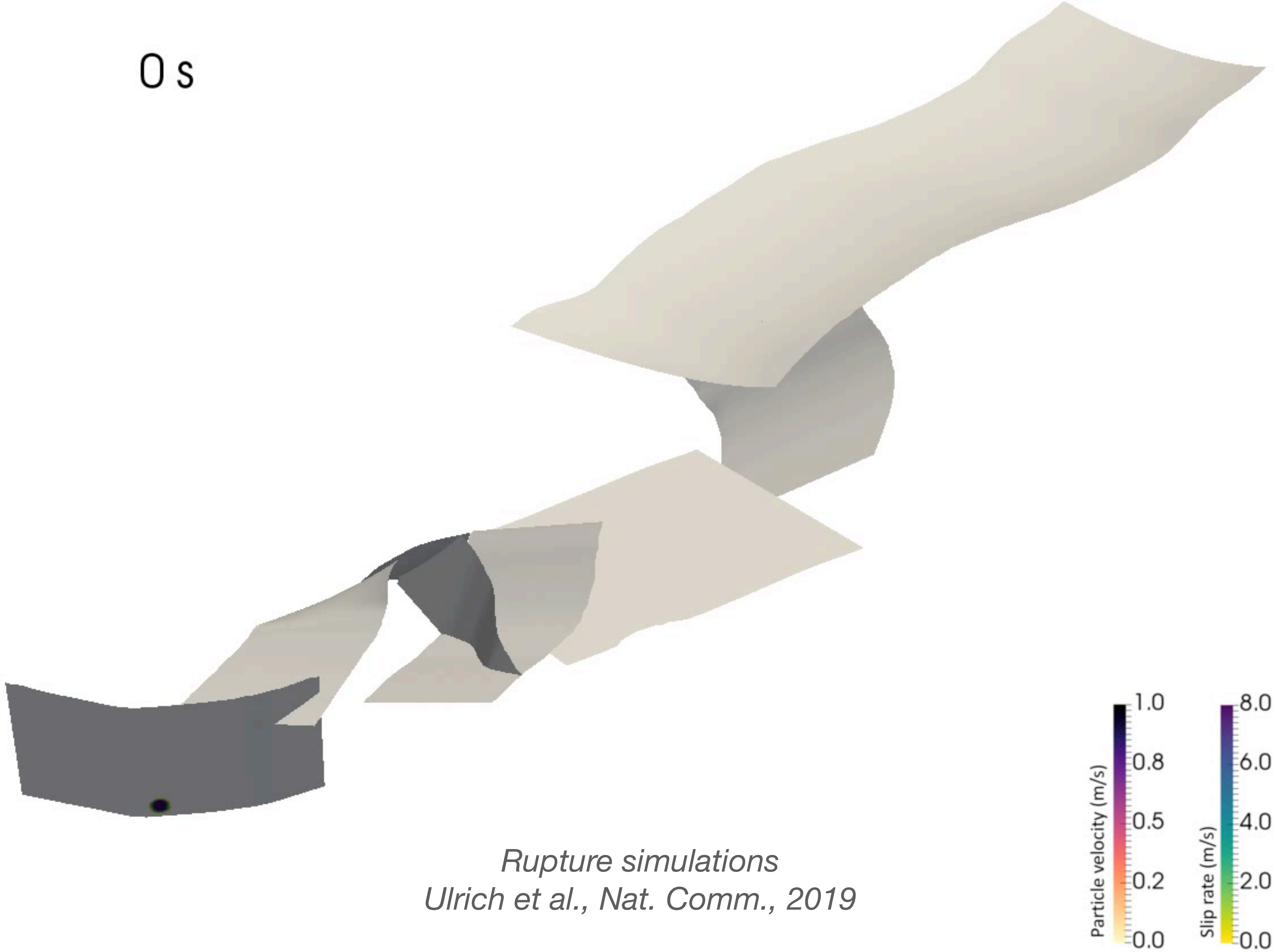

Rupture simulations
Ulrich et al., Nat. Comm., 2019

Multi-segment faults

- Recent high-resolution seismological observations suggest (large) earthquakes can jump to adjacent and intersecting faults
  - Run dynamic rupture simulations to push for largest magnitudes relevant for Mmax in Groningen

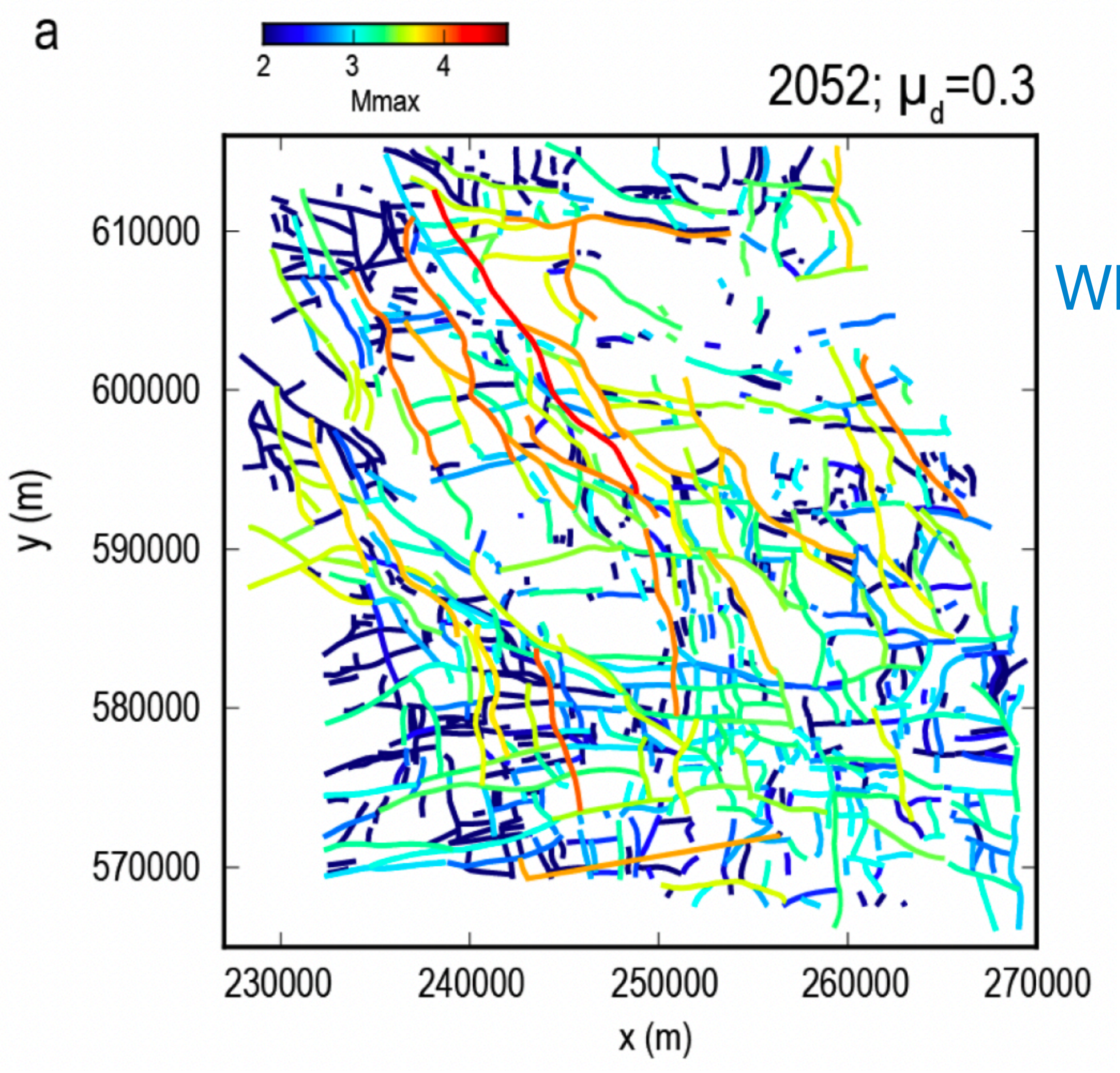

LEFM
Weng et al., Mmax, 2022

What to run?

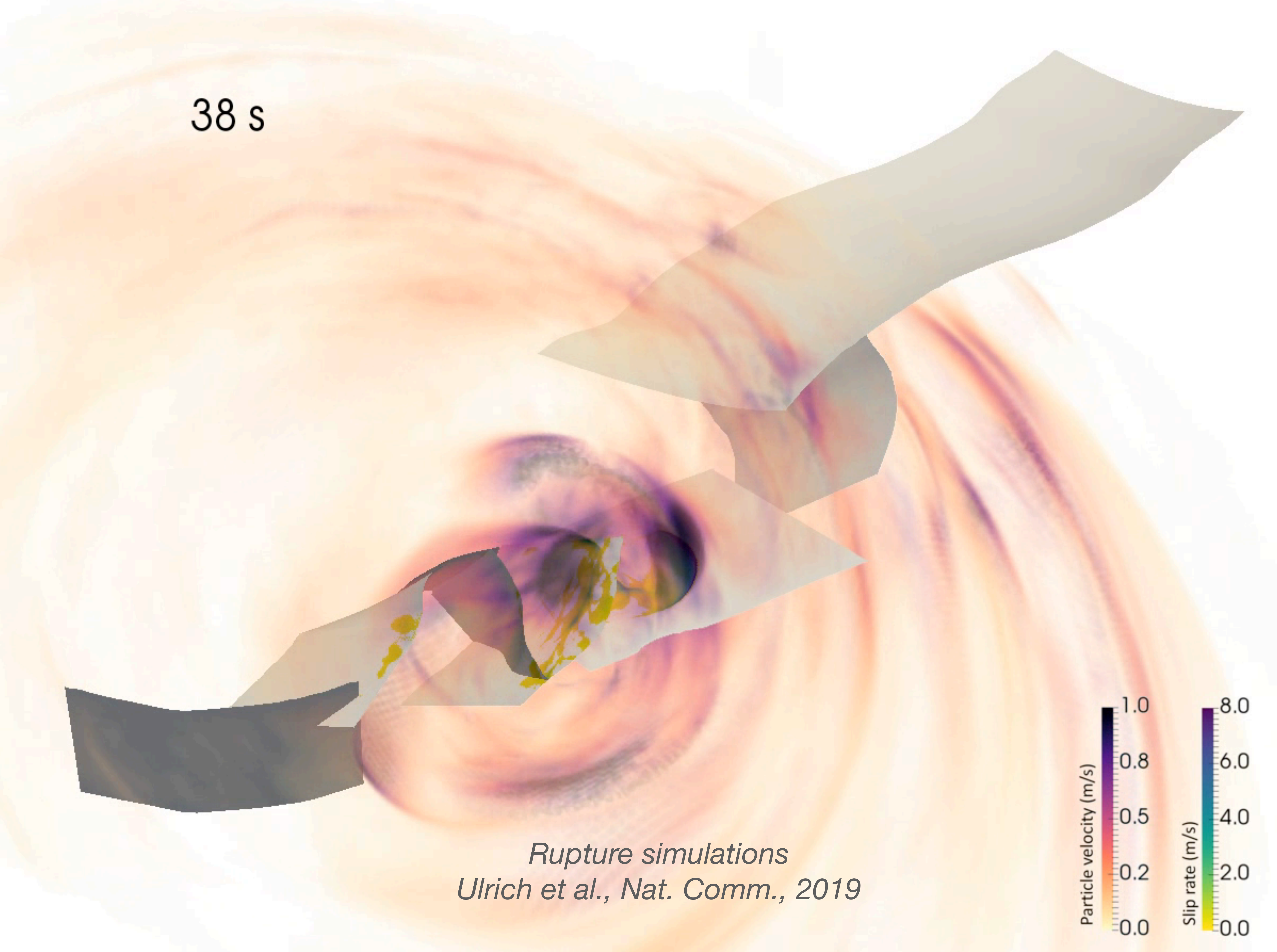

Rupture simulations
Ulrich et al., Nat. Comm., 2019

Multi-segment faults

- Recent high-resolution seismological observations suggest (large) earthquakes can jump to adjacent and intersecting faults
  - Run dynamic rupture simulations to push for largest magnitudes relevant for Mmax in Groningen
  - Extend and validate LEFM results to multi-segment faults *(inspiration from e.g., Kaneko et al., 2010; Weng & Ampuero, 2019; Michel et al., 2021)*

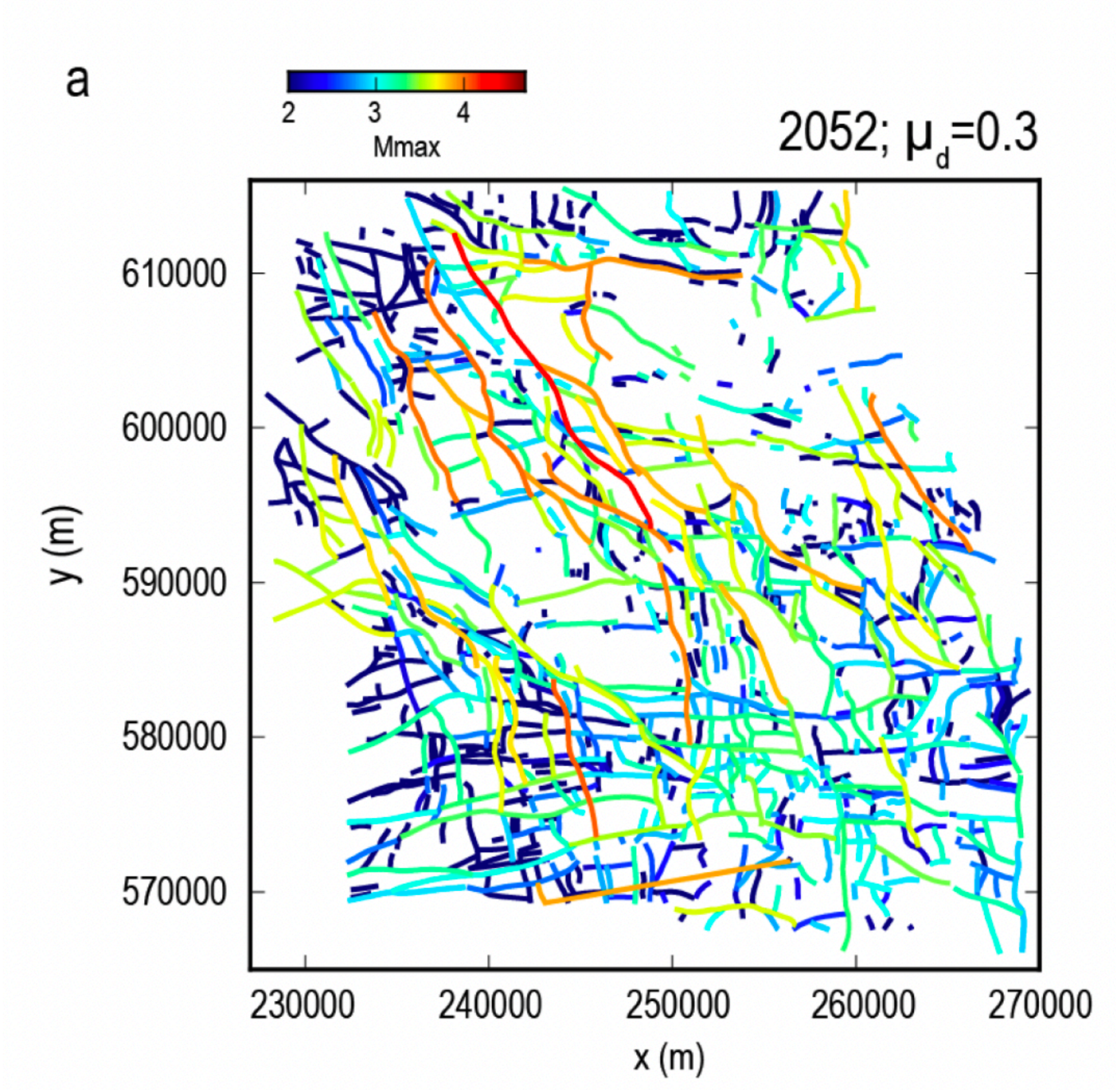

LEFM
Weng et al., Mmax, 2022

Update:
How?
Correct?

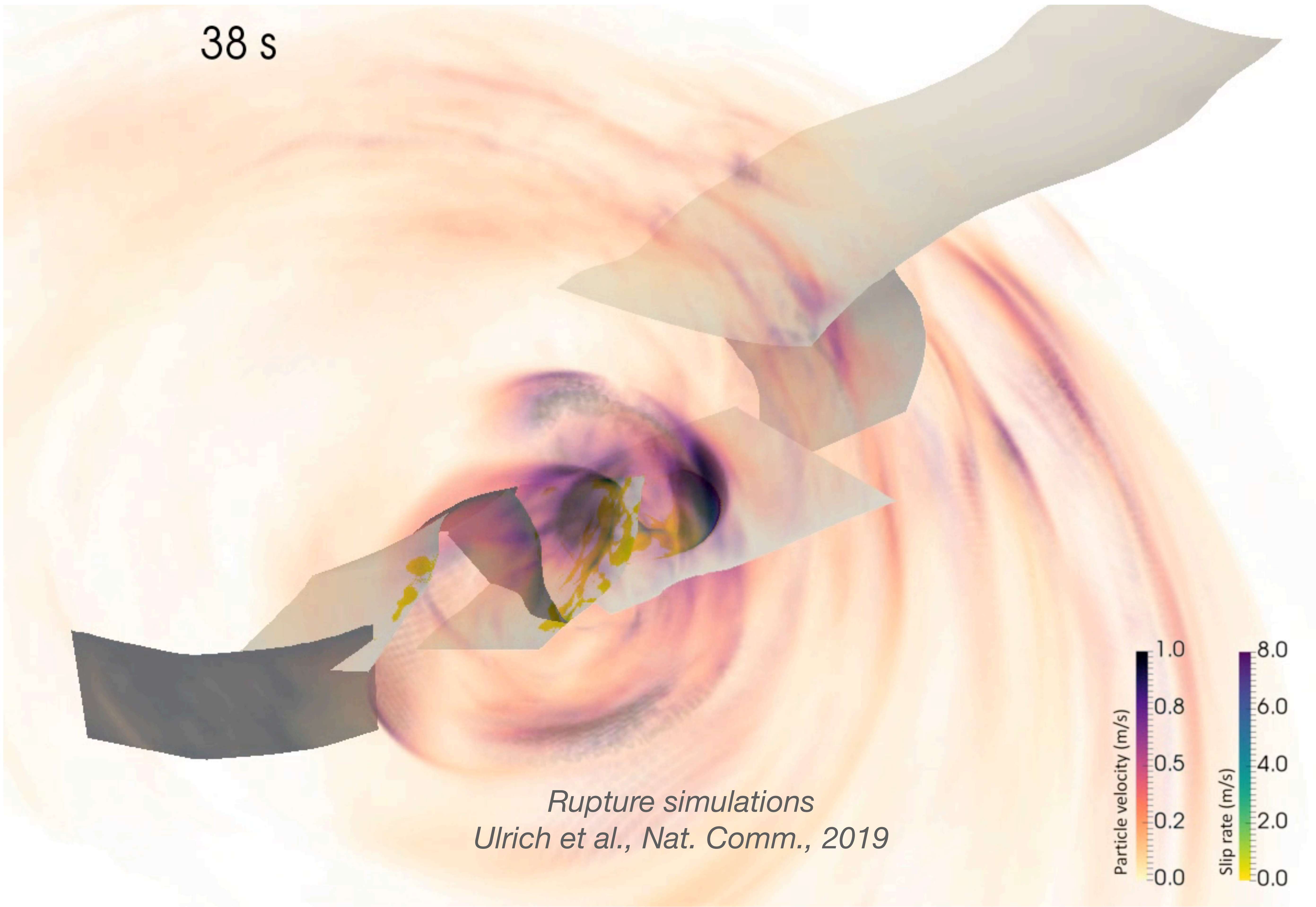

Rupture simulations
Ulrich et al., Nat. Comm., 2019

Dynamic earthquake rupture simulations

- Using High Performance Computing code SeisSol *(e.g., Breuer et al., IEEE, 2016)*
- Validated for branching, normal and rough faults through Southern California Earthquake Center *(Pelties et al., GMD, 2014)*

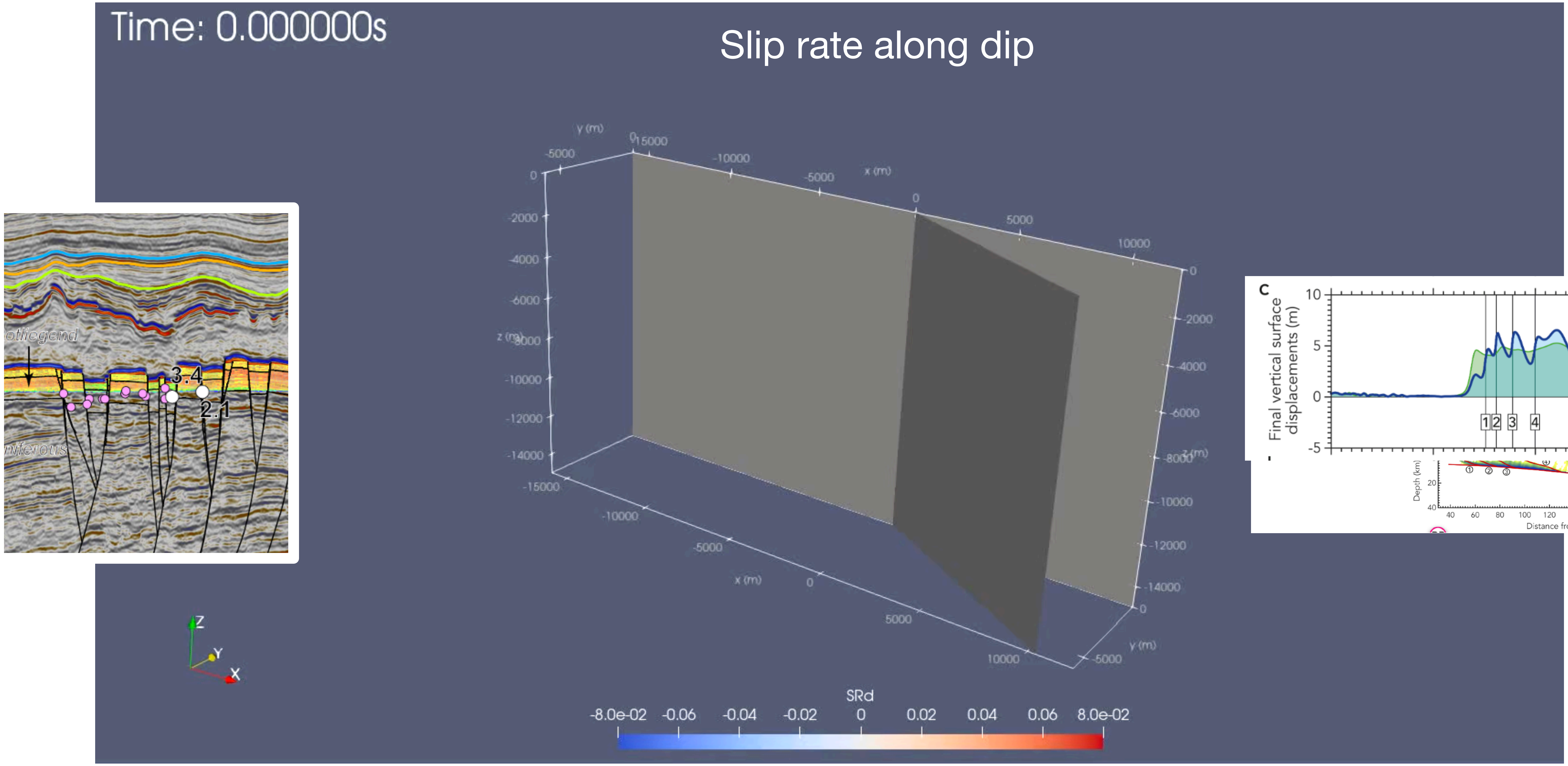

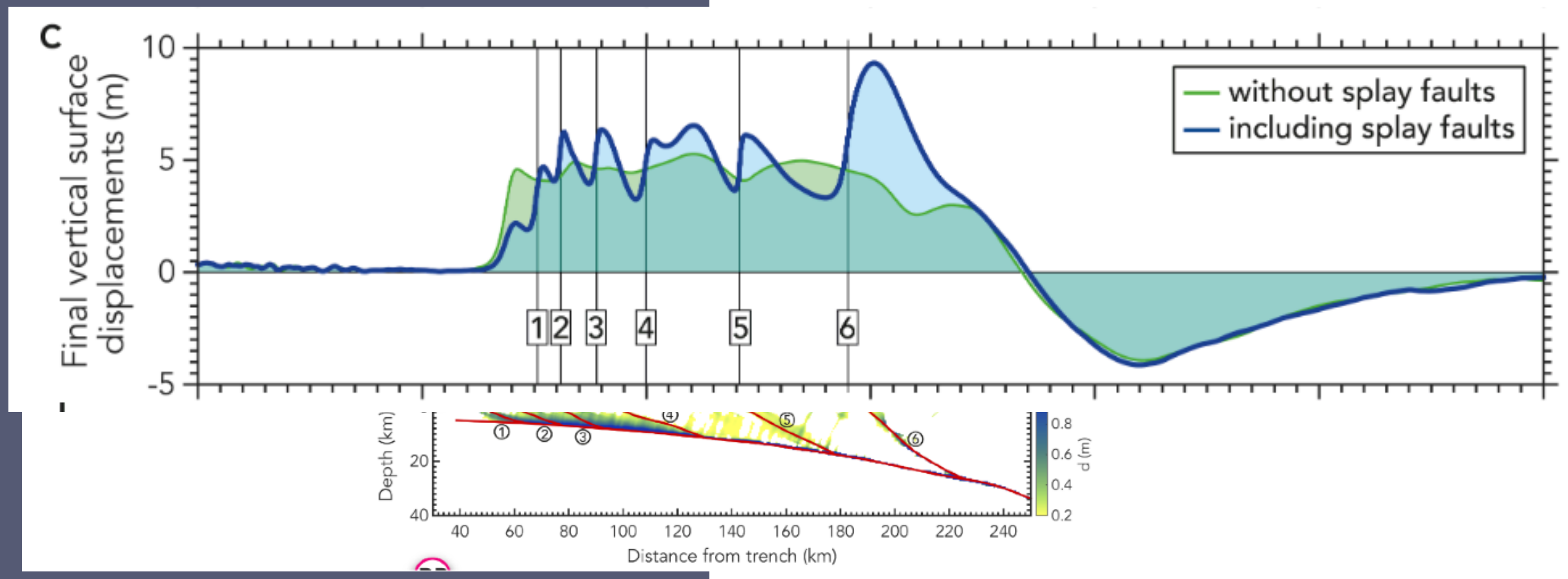

van Zelst et al., JGR, 2019, 2022:
- 2-3x more slip in wedge
- Splay fault activation

Extended and validated to gas extraction in Groningen

- 3D SeisSol results are in good agreement with 2D results from Buijze et al., JGR, 2019
  - Slightly less slip *(agrees with e.g., Li et al., JGR, 2022 and Weng et al., Mmax report)*

2D
By L. Buijze 2019

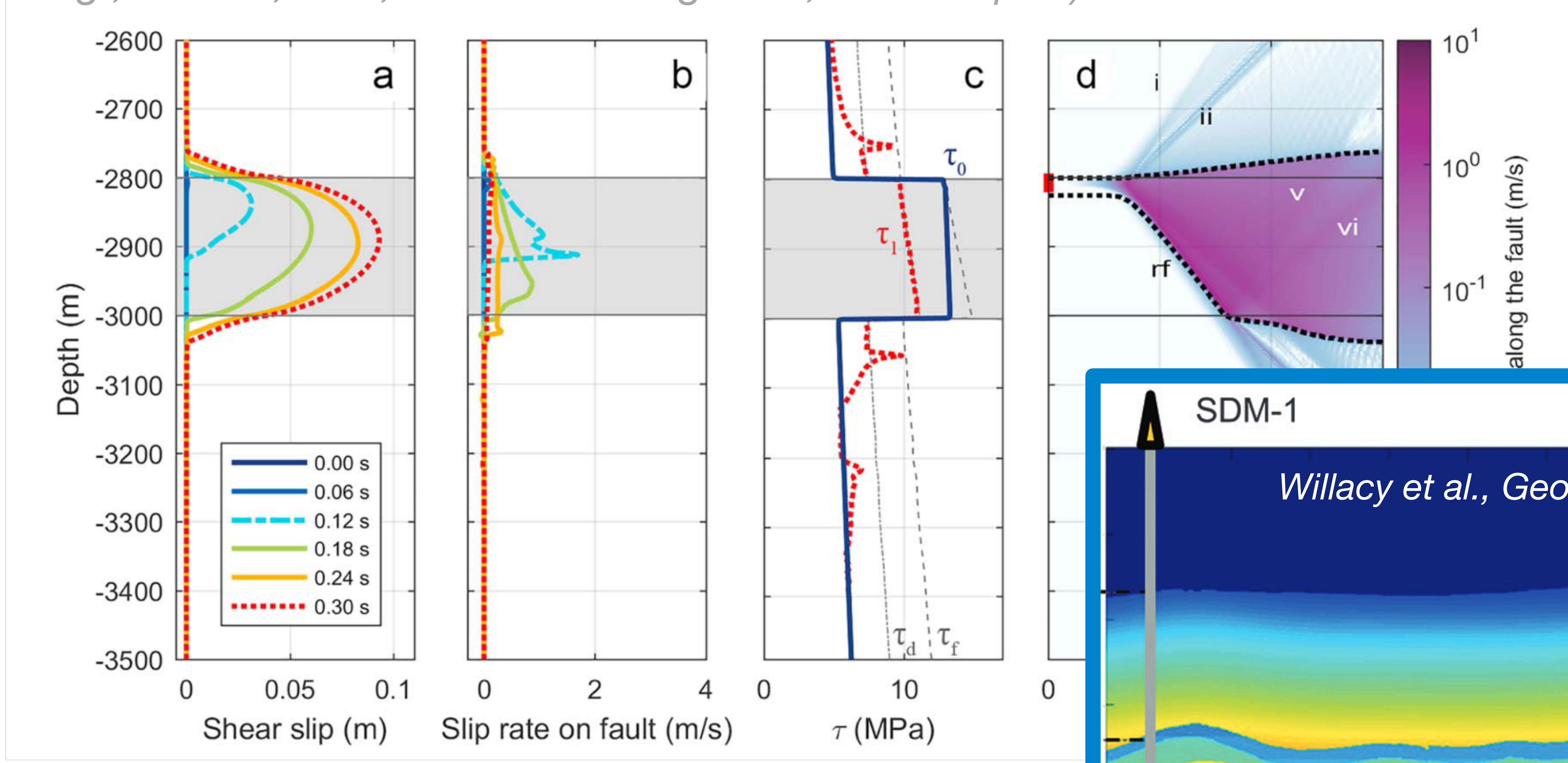

3D
Using SeisSol

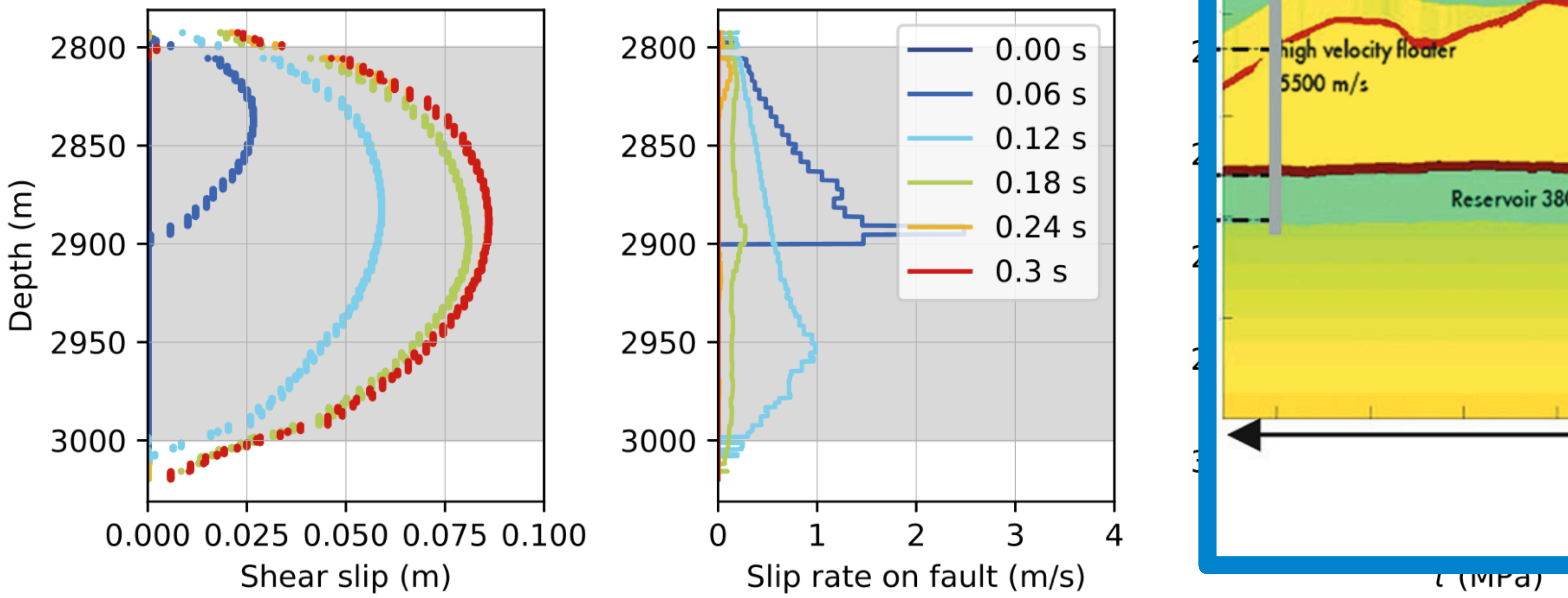

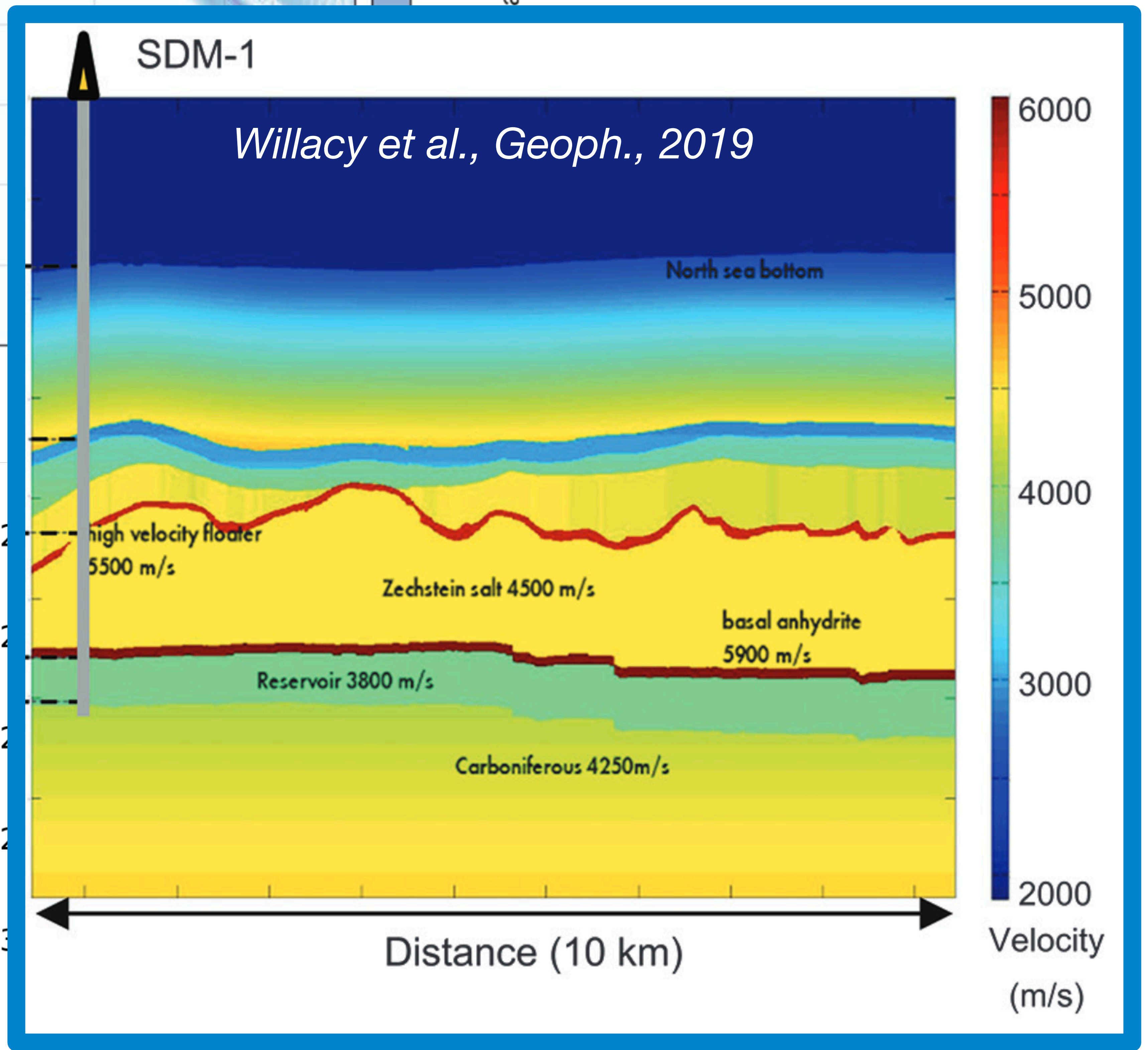

Seismic wave reflections reduce M_{max} on single faults through reservoir

- Reflections enhance stopping phase and reduce slip rates and slip

without
impedance
contrast

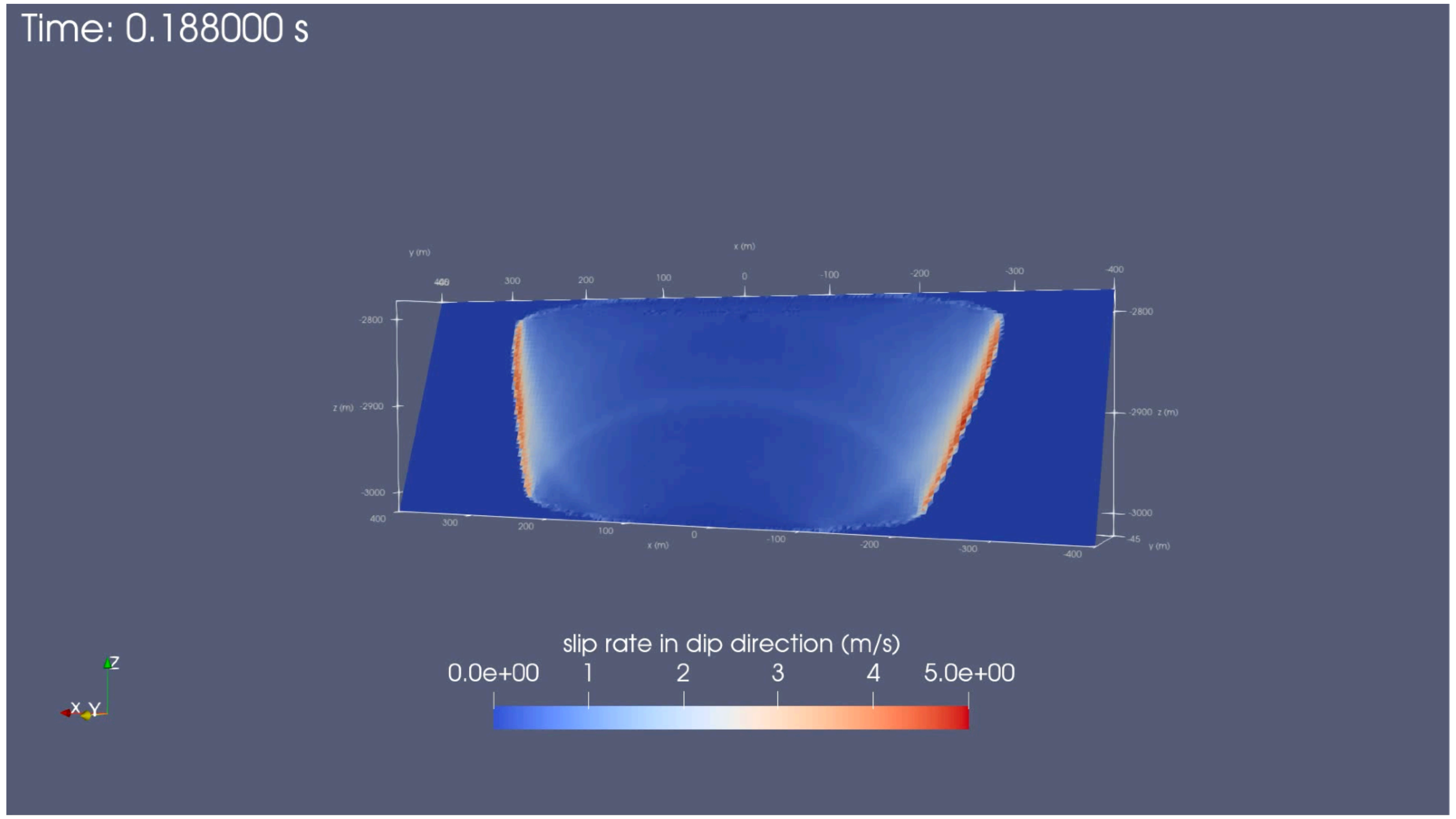

M_W = 3.22

with
impedance
contrast

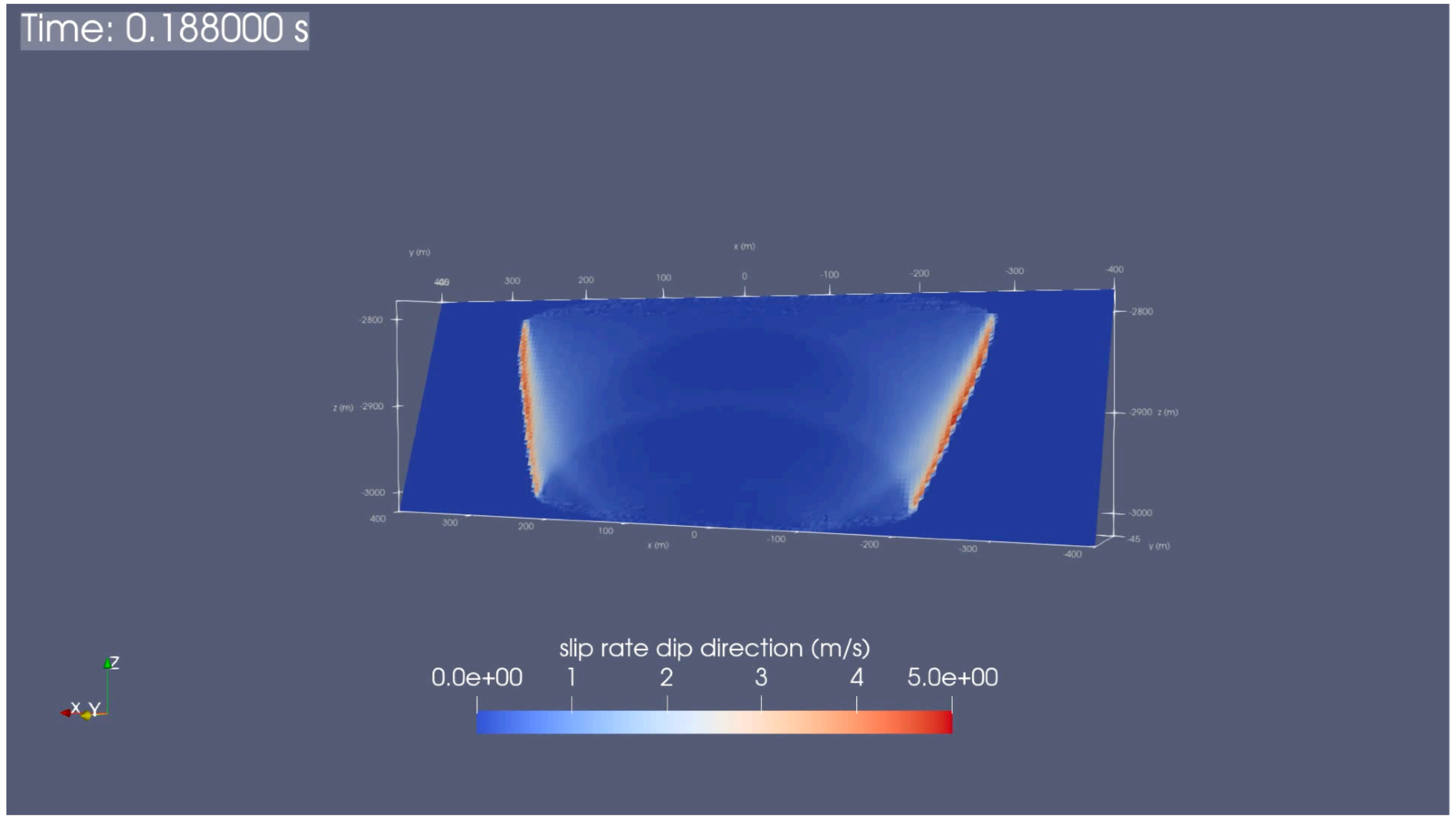

M_W = 3.09

Caution: Fresh and thus preliminary

Seismic wave reflections reduce M_{max} on single faults through reservoir

- Reflections enhance stopping phase and reduce slip rates and slip

without
impedance
contrast

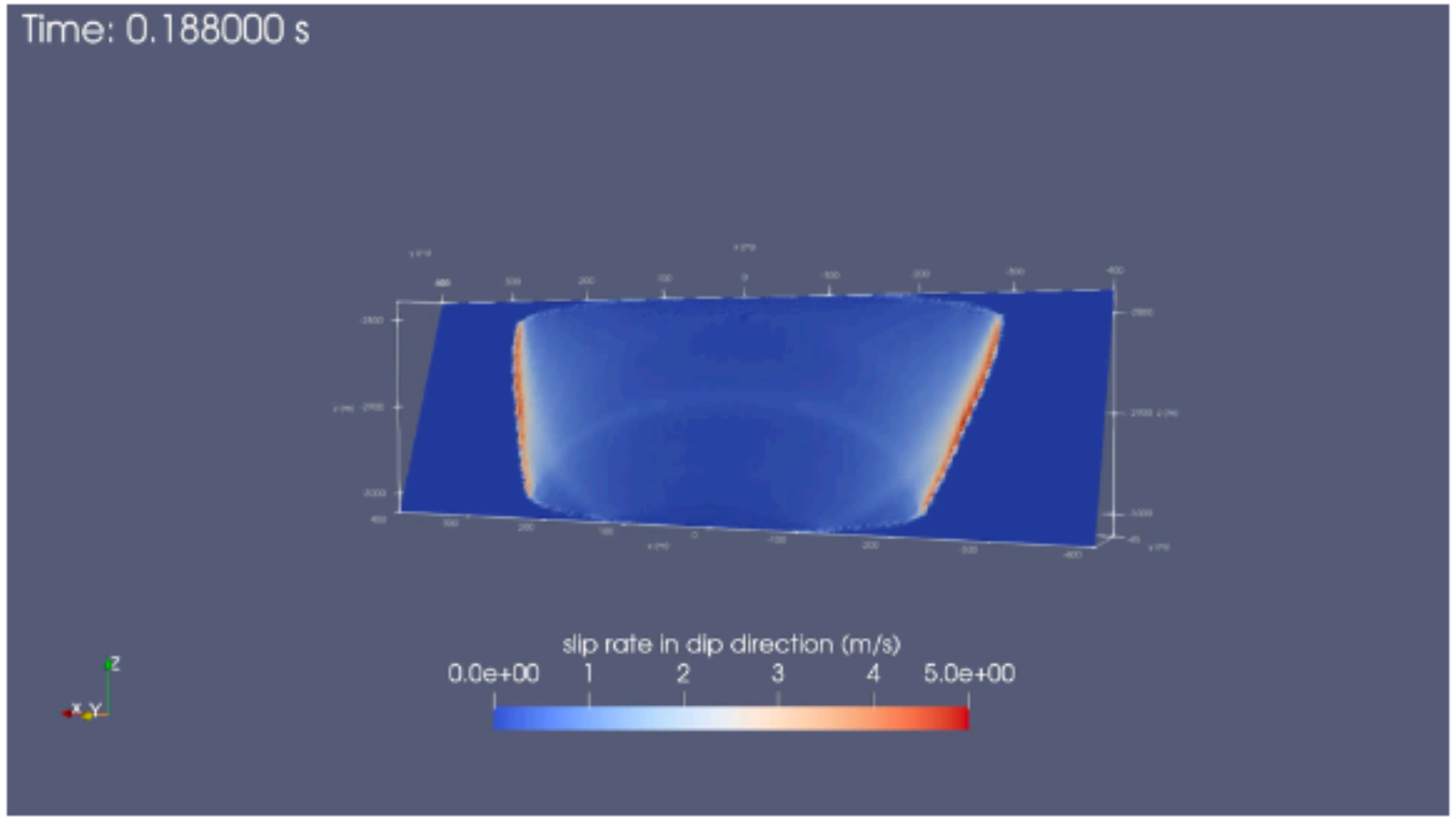

$M_w = 3.22$

with
impedance
contrast

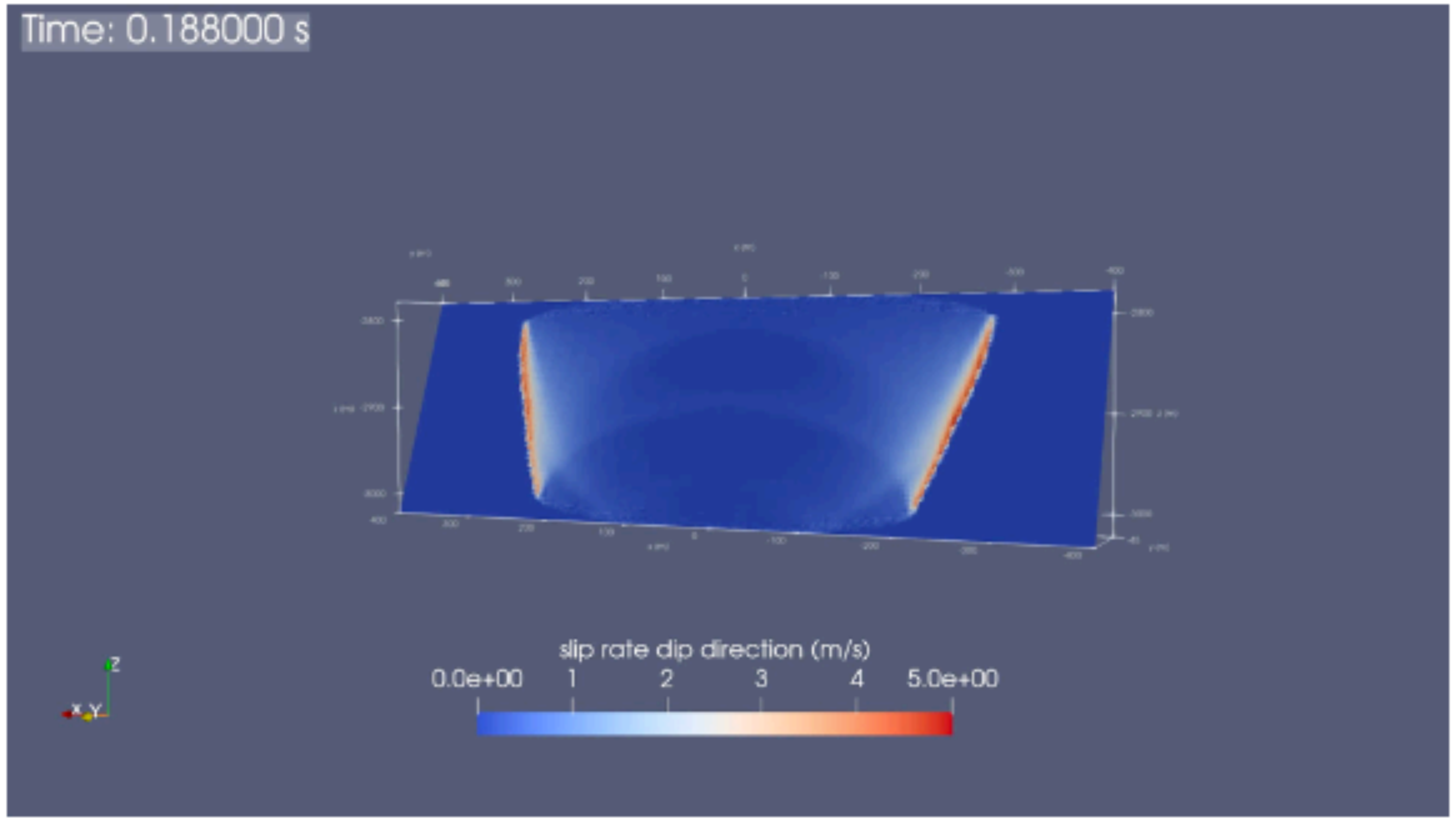

$M_w = 3.09$

Caution: Fresh and thus preliminary

Seismic wave reflections reduce M_{max} on single faults through reservoir

- Reflections enhance stopping phase and reduce slip rates and slip

without impedance contrast

$M_w = 3.22$

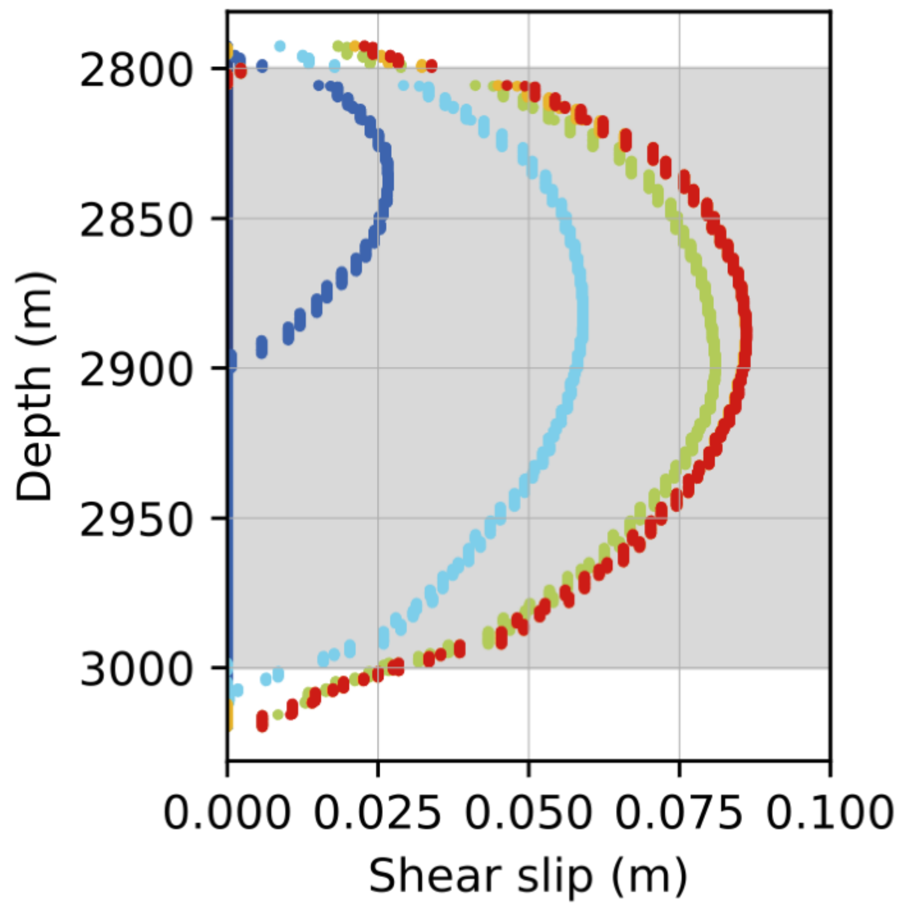

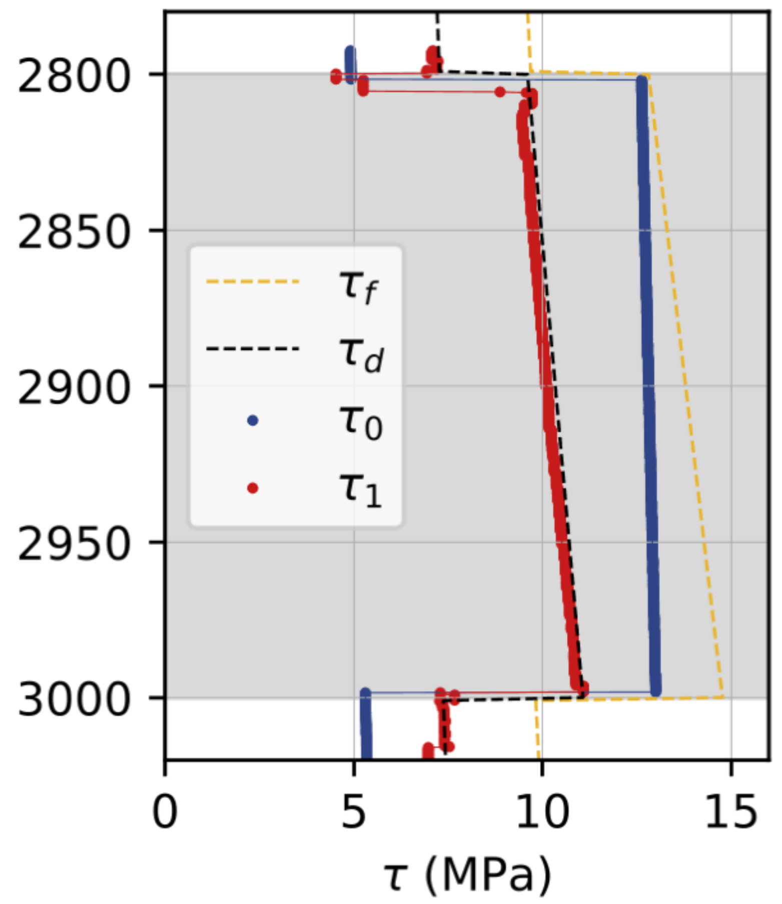

ρ (kg/m³)	μ	λ
2400	6.5217e+09	2.7950e+09
2400	6.5217e+09	2.7950e+09
2400	6.5217e+09	2.7950e+09

Buijze et al., JGR, 2019

with impedance contrast

$M_w = 3.09$

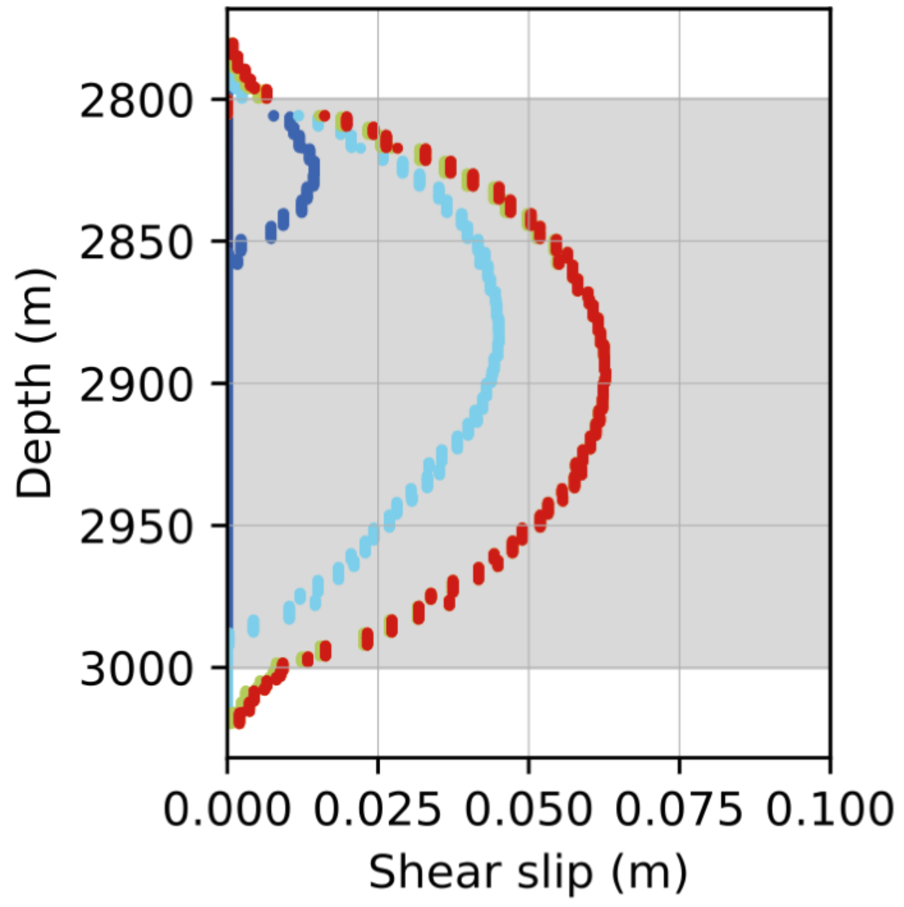

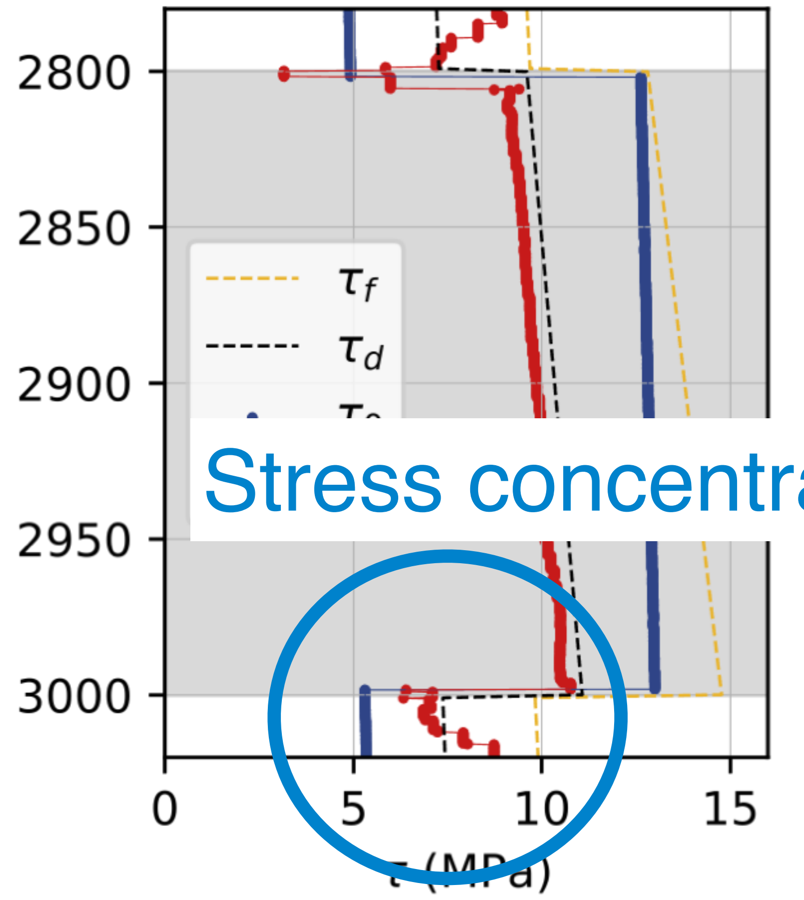

Stress concentration enhances rupture propagation into under burden?

2810	2.95e+10	3.89e+10
2400	6.5217e+09	2.7950e+09
2650	1.45e+10	1.76e+10

Groningen Velocity Model 2017 (Romijn et al.)

Objective

- Determine a physics-based Mmax accounting for (or testing)
  - 2.5D finite-width dynamic rupture propagation across single, planar faults in complex Groningen fault network
  - Improved fault model
  - Improved probabilistic pre-stresses
  - Fault roughness during rupture
  - Multi-segment faults
  - Seismic wave reflections
  - **Improved probabilistic strength evolution**
  - **Second-generation earthquakes**

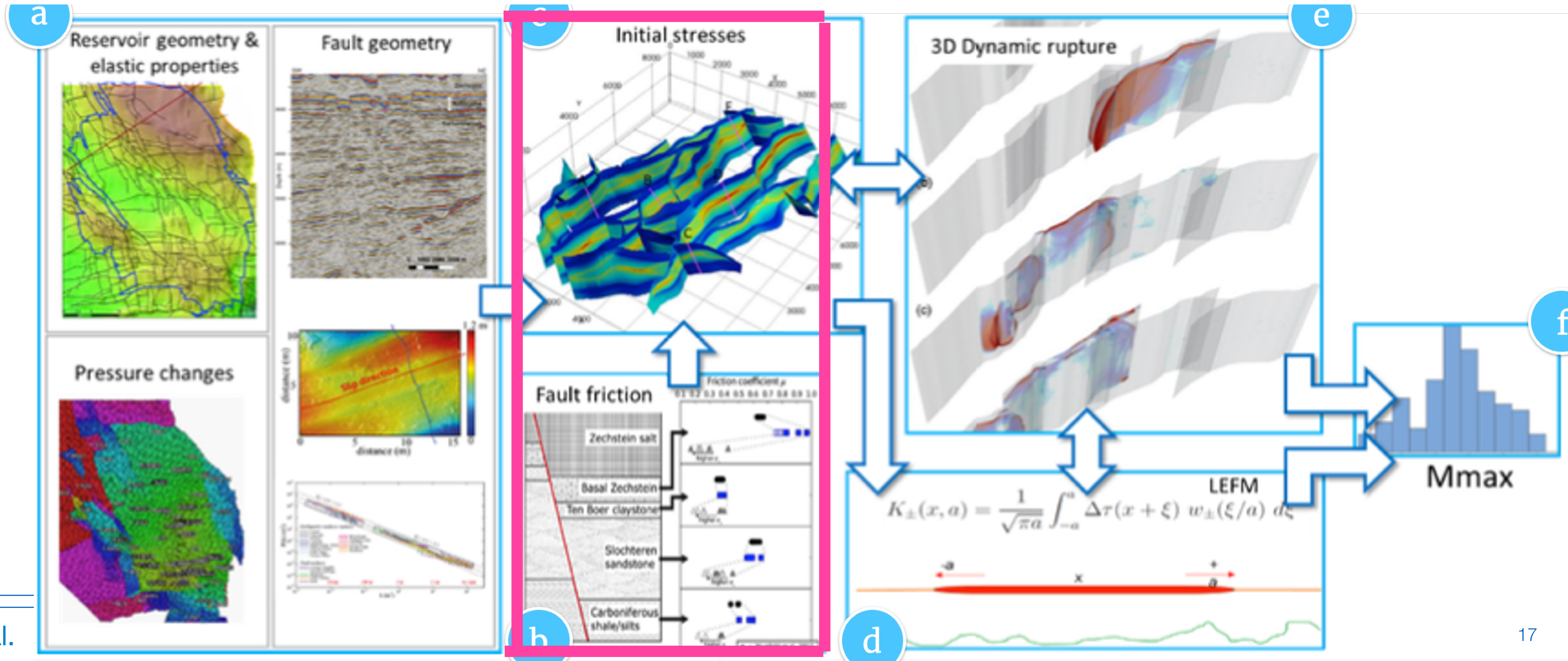

Can second-generation earthquake propagate further into under-burden?

- Answer depends on RSF parameters

Improved fault strength

- Impact of a low dynamic friction is and will be assessed *(Weng et al., Mmax report, 2022)*
- A note on applicability of rate-and-state friction data (and a stress threshold in *Heimisson et al., GJI, 2022*)
  - Lab experiments show velocity-strengthening for reservoir sand stones at slow rates
  - Theoretically means nucleation is not readily possible, so how can we explain earthquakes?

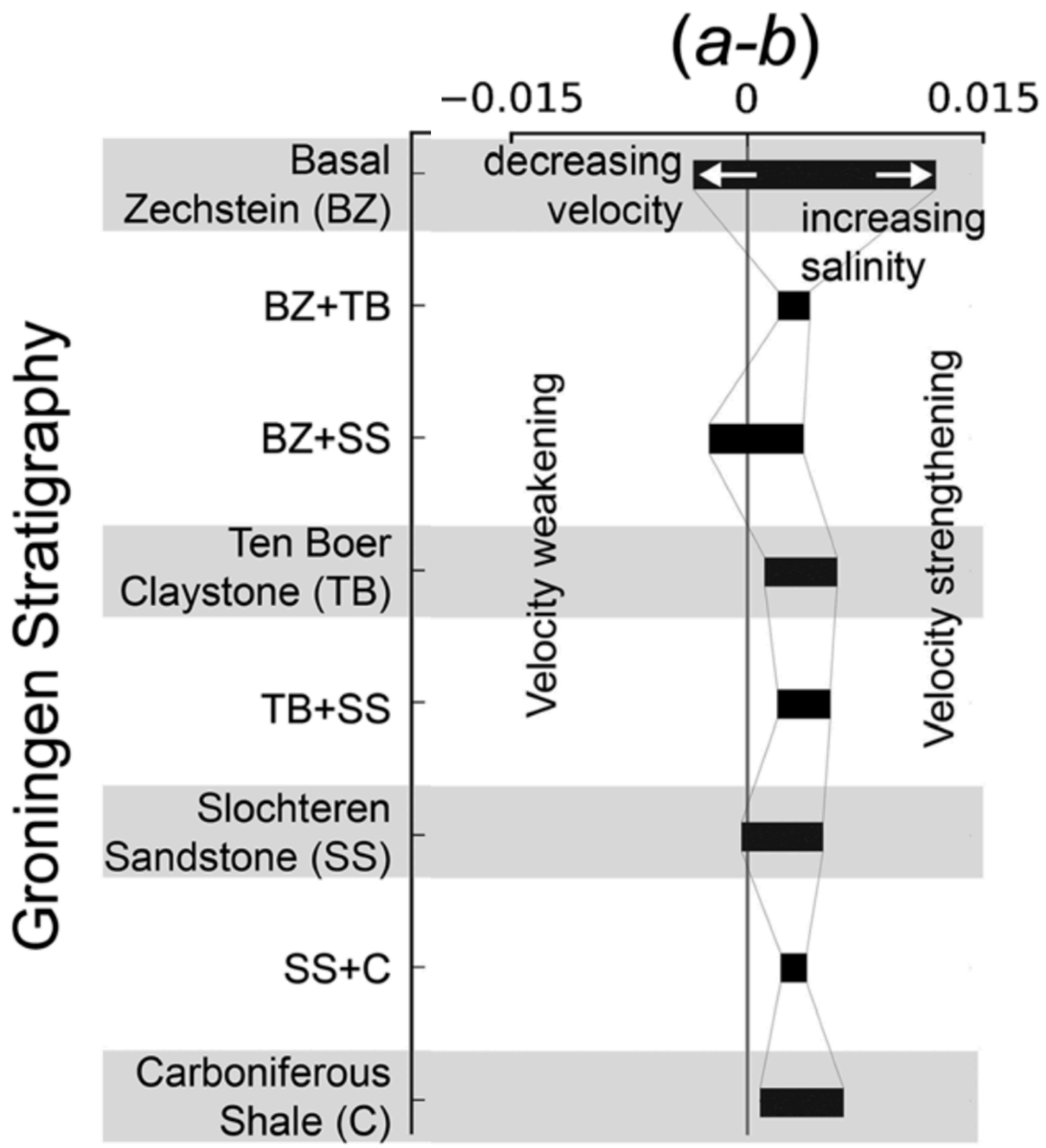

Hunfeld et al., JGR, 2017

Improved fault strength

- Impact of a low dynamic friction is and will be assessed *(Weng et al., Mmax report, 2022)*
- A note on applicability of rate-and-state friction data (and a stress threshold in *Heimisson et al., GJI, 2022*)
  - Lab experiments show velocity-strengthening for reservoir sand stones at slow rates
  - Theoretically means nucleation is not readily possible, so how can we explain earthquakes? **Healing of state variable**

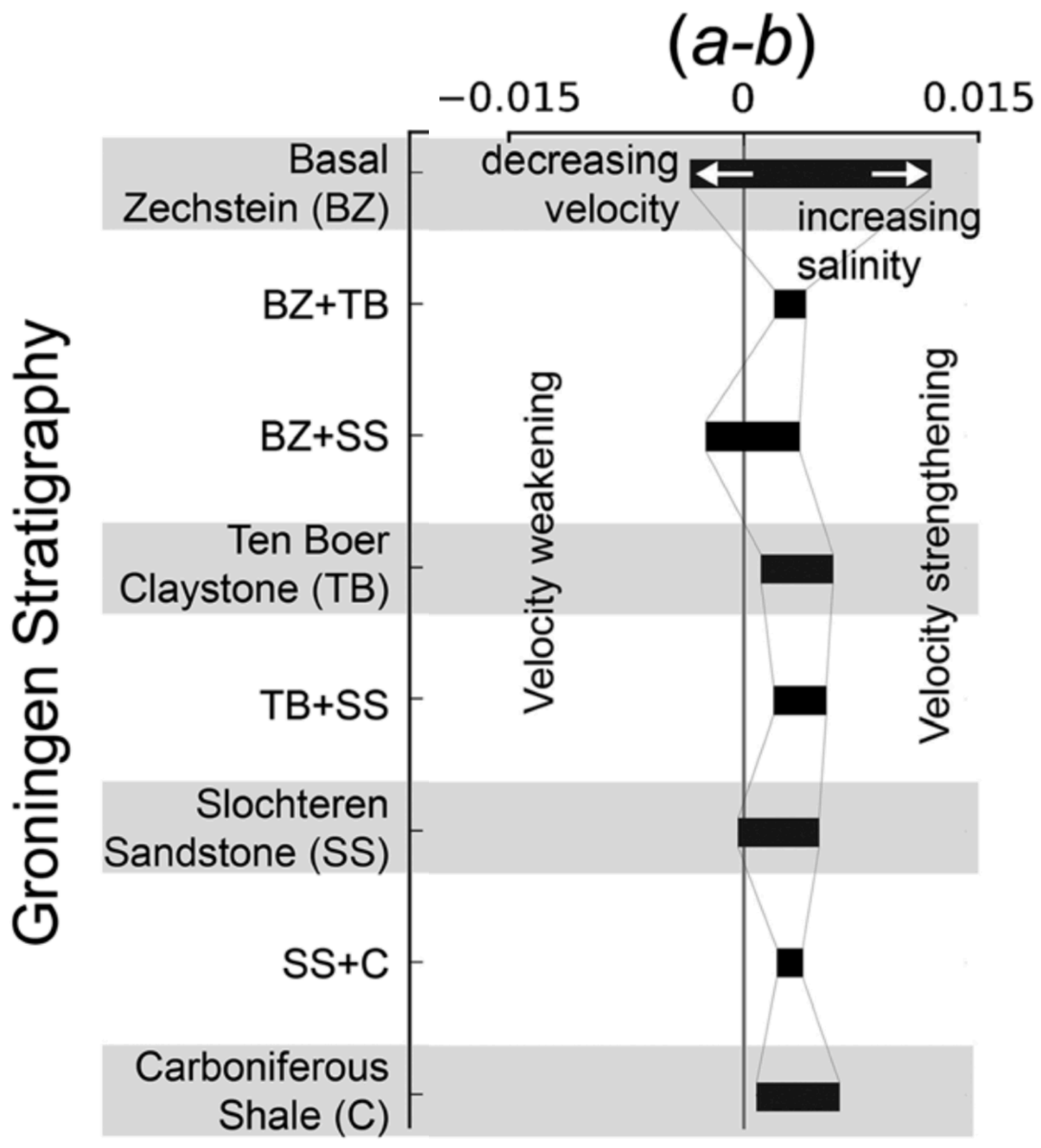

Hunfeld et al., JGR, 2017

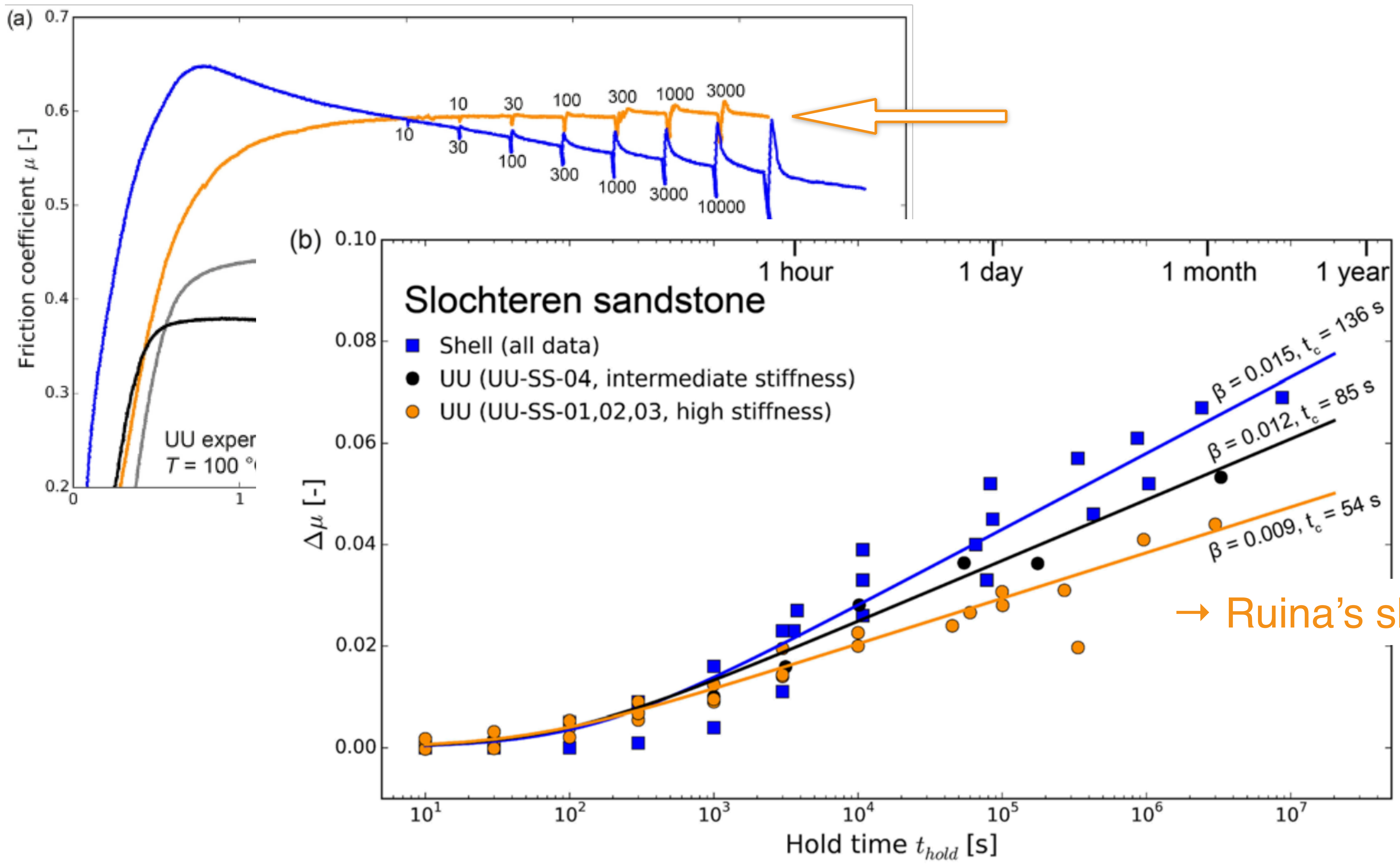

→ Ruina's slip law

Hunfeld et al., JGR, 2020

Earthquakes can occur under velocity-strengthening friction

- 0D Spring-block slider simulations

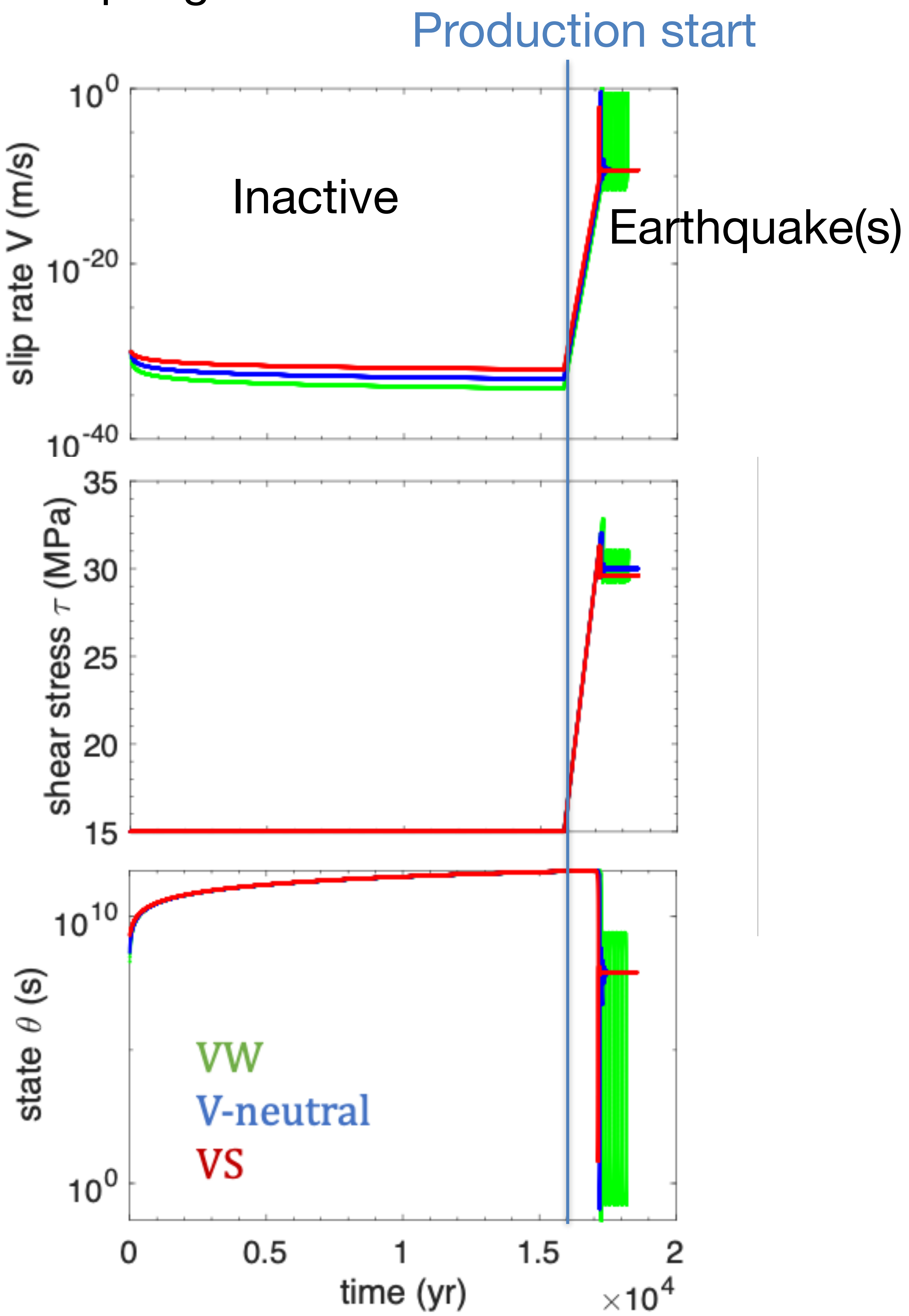

Earthquakes can occur under velocity-strengthening friction

- 0D Spring-block slider simulations

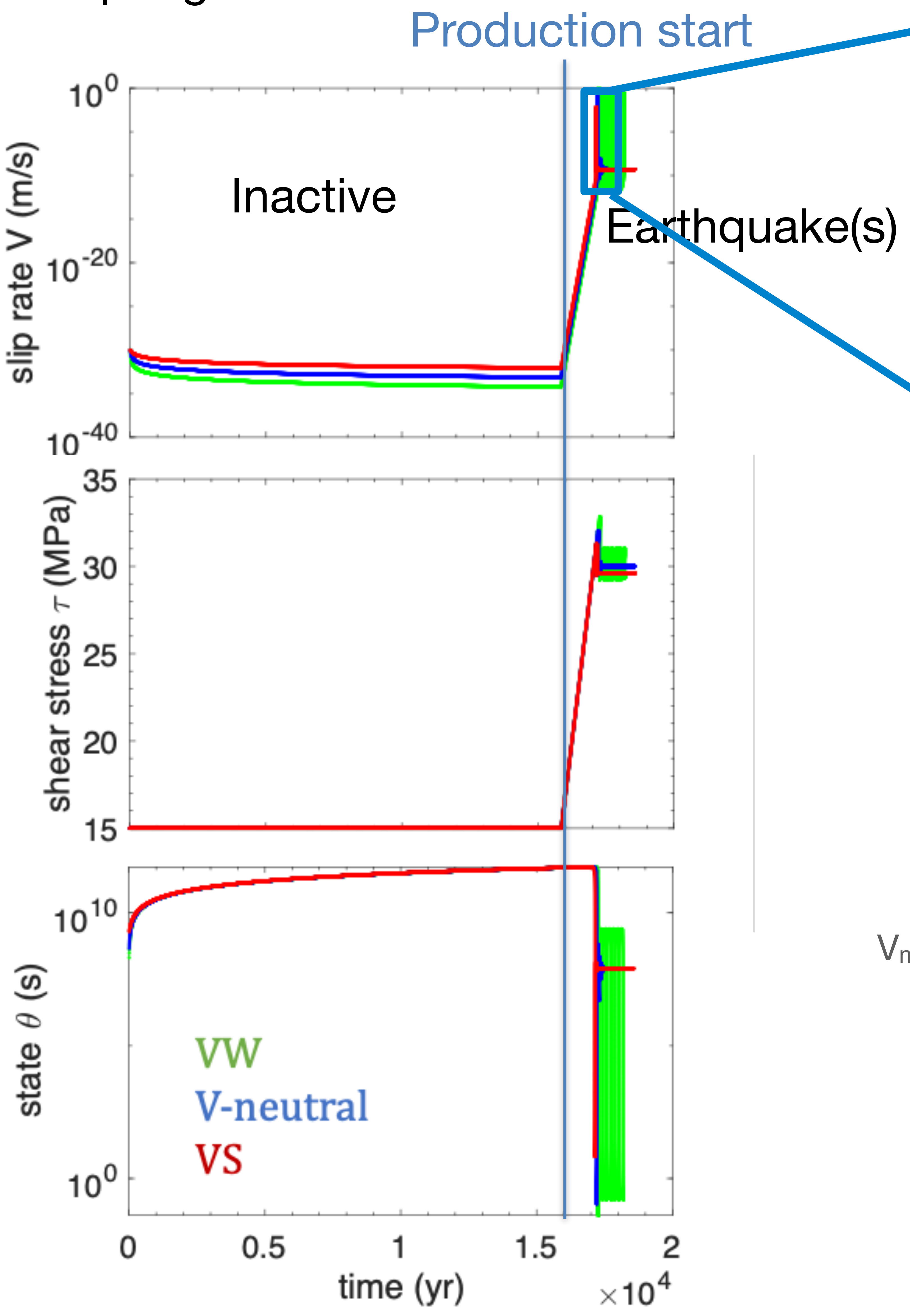

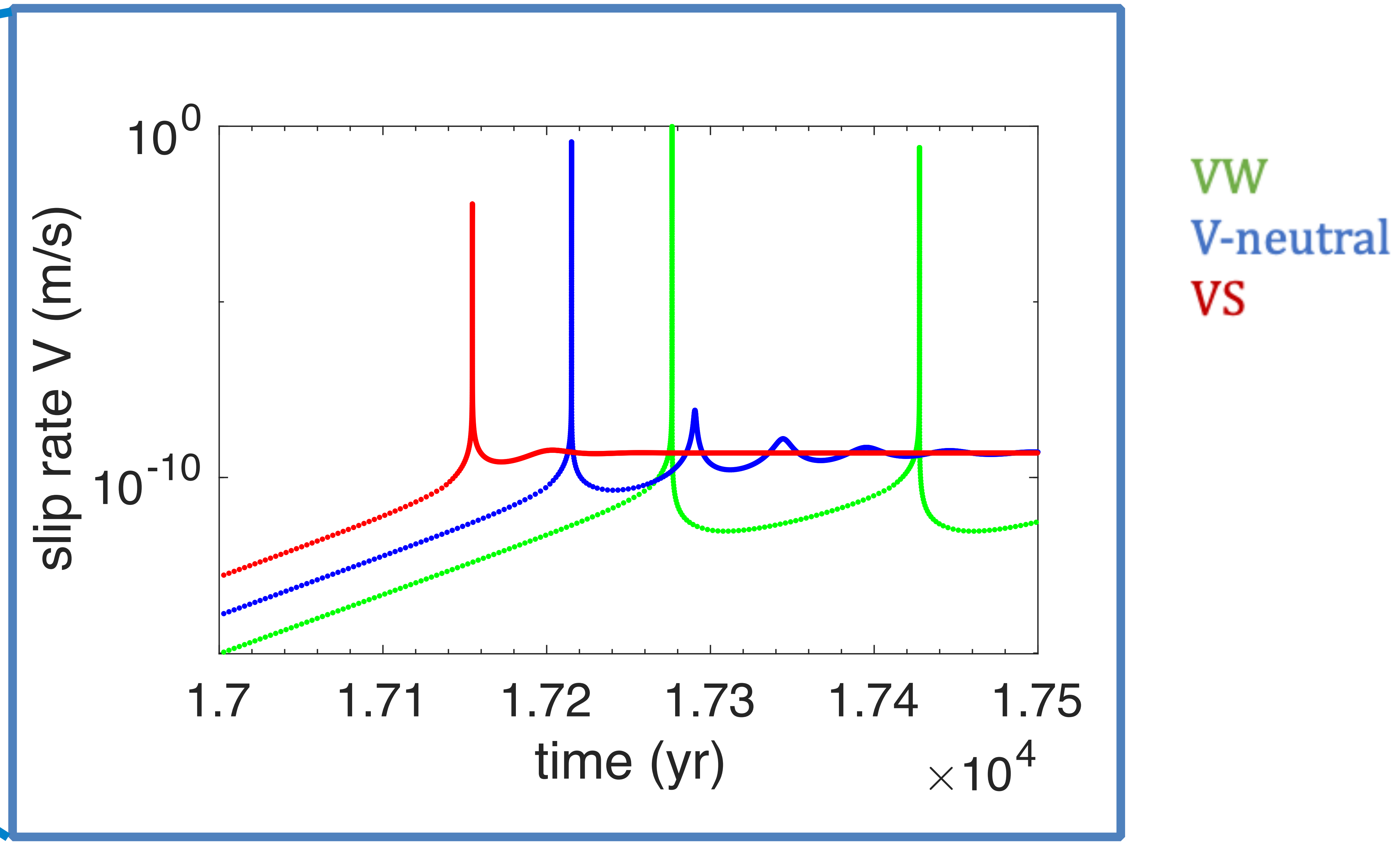

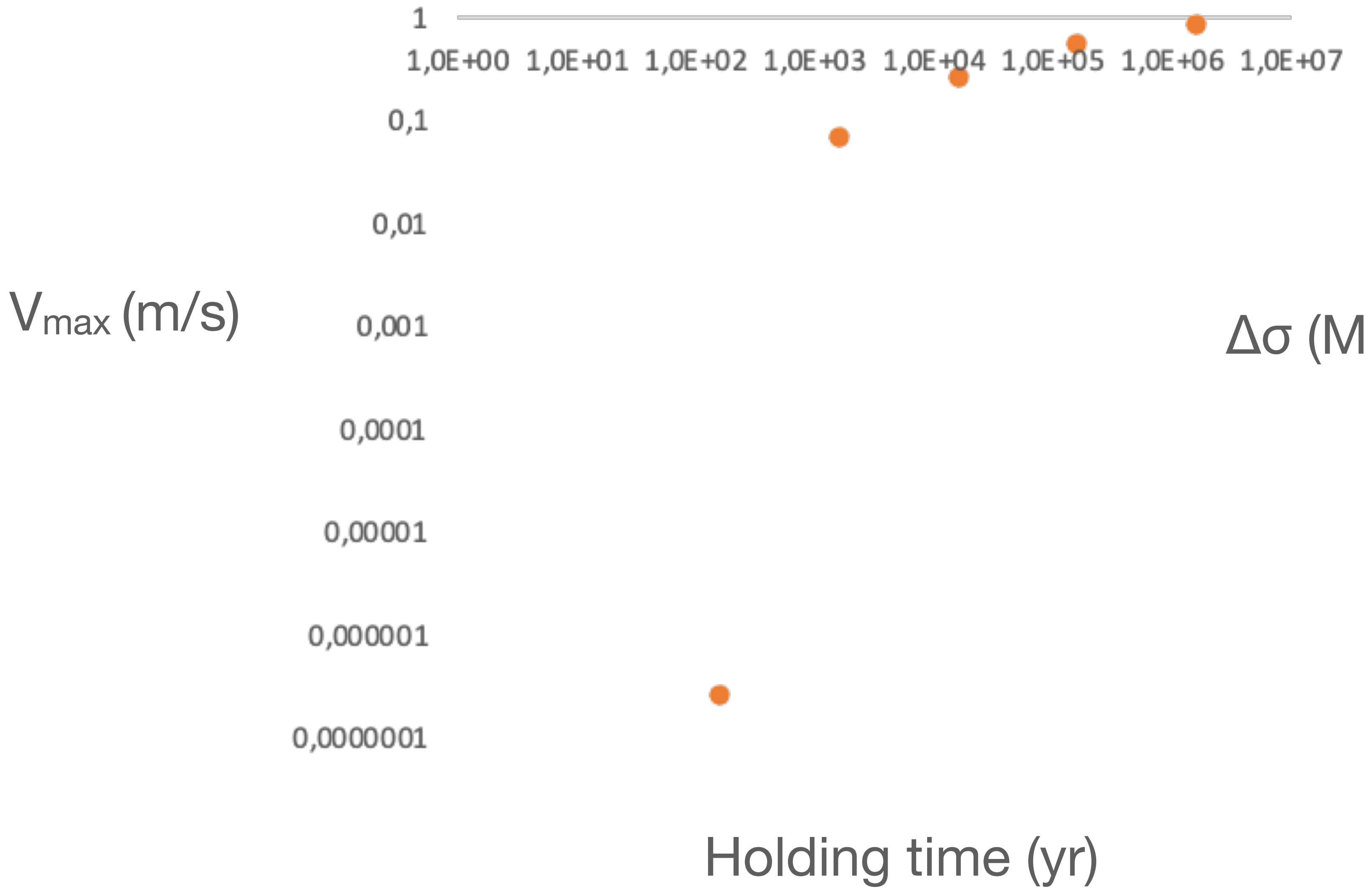

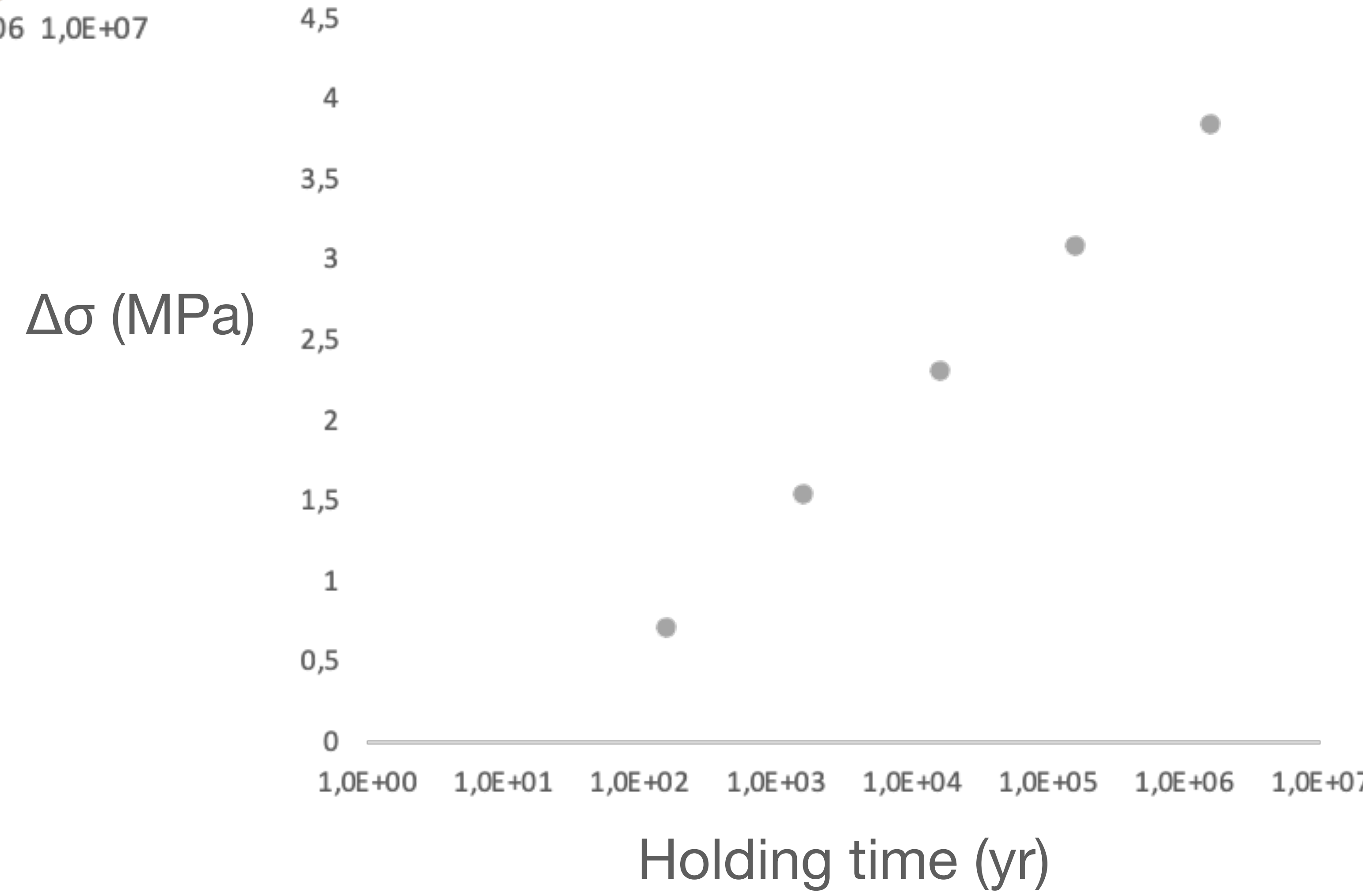

Earthquake rupture in 2D Groningen setting on velocity-strengthening faults

- “Nucleation” at top of reservoir
- Rate-and-state friction theory and laboratory results can explain induced seismicity in Groningen (no need to involve more)
- — Stress theshold impact — what state use in Hemissinon?
- Does not impact estimated propagation or arrest

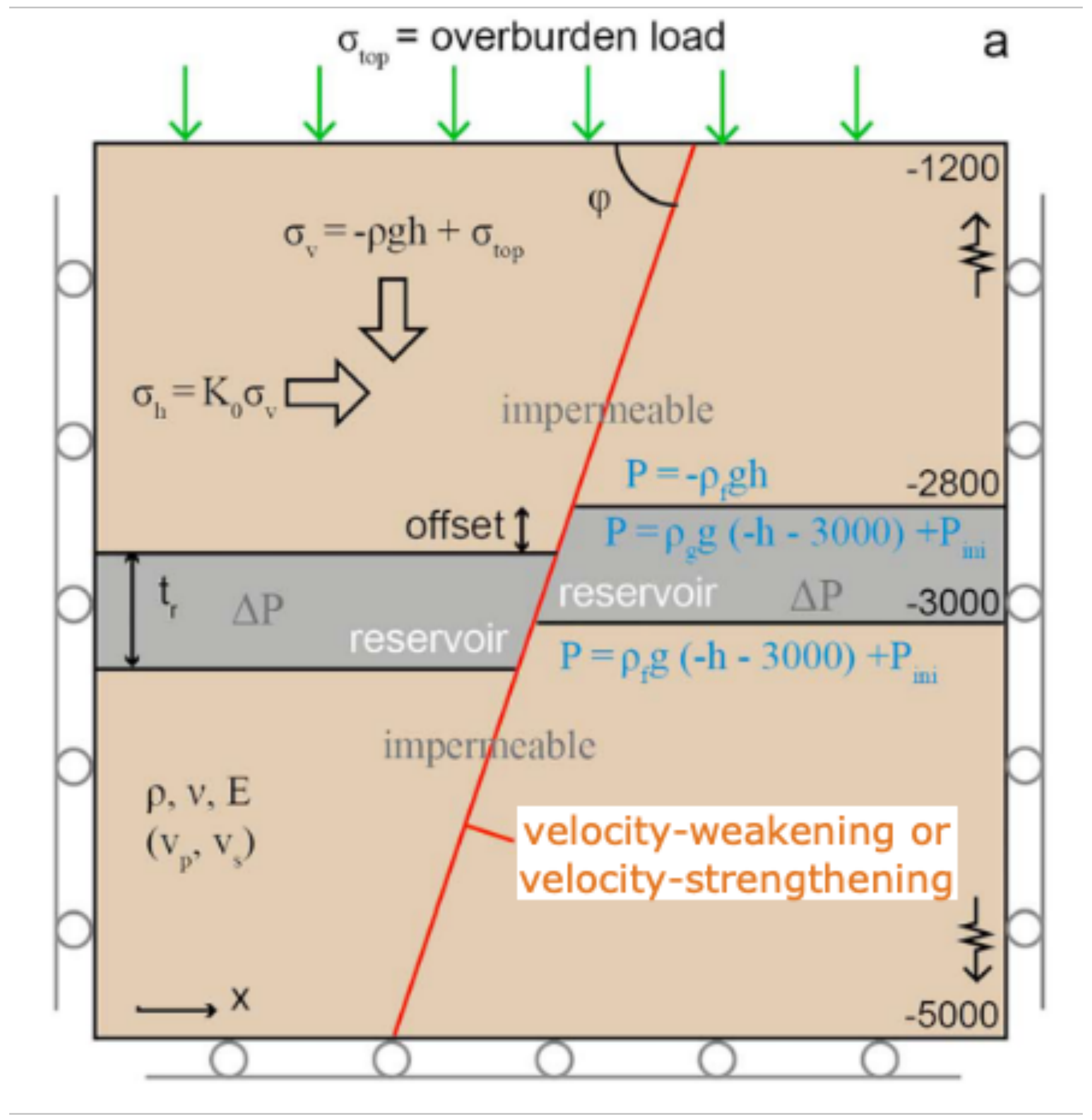

Adapted from Buijze et al., JGR, 2019

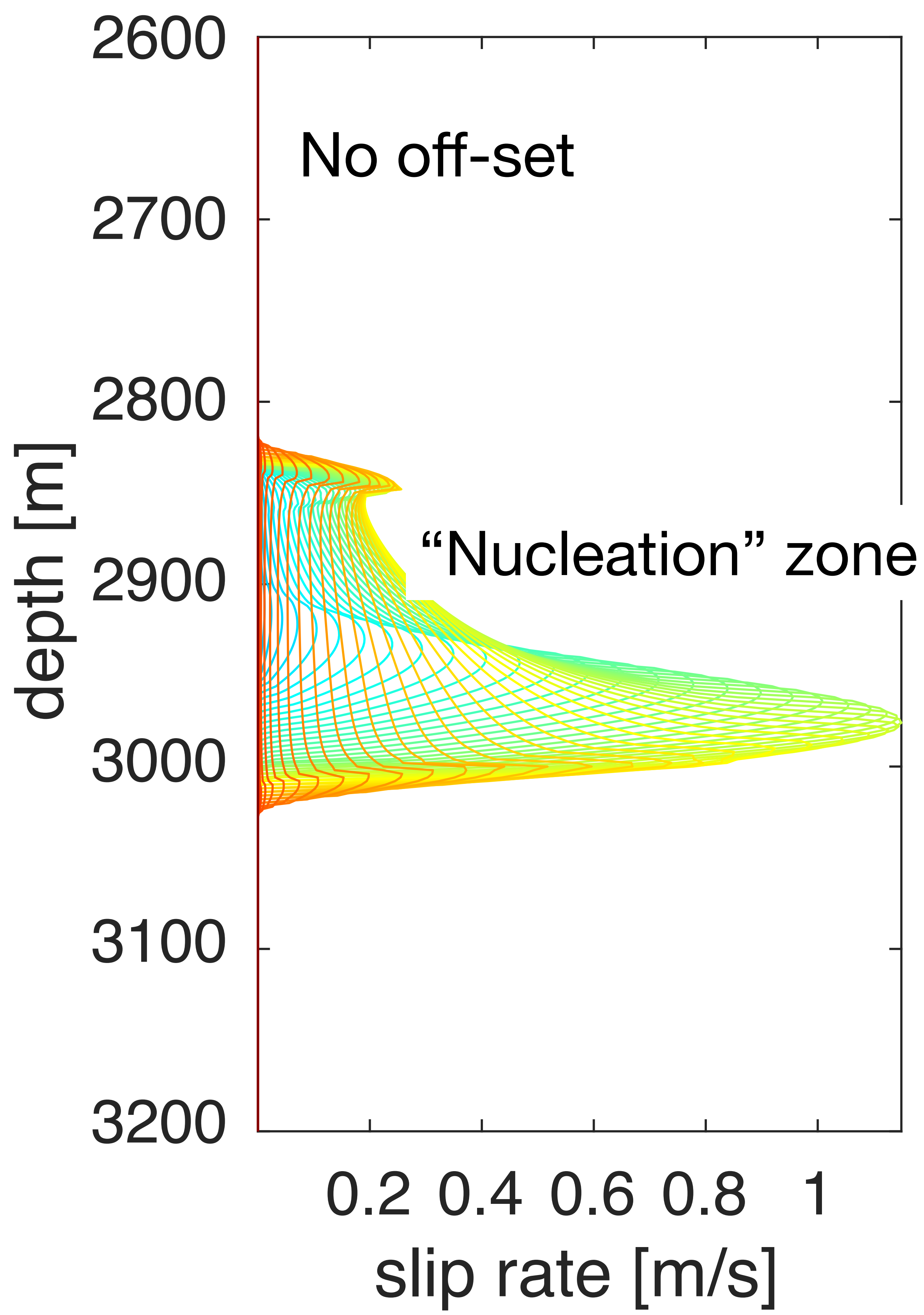

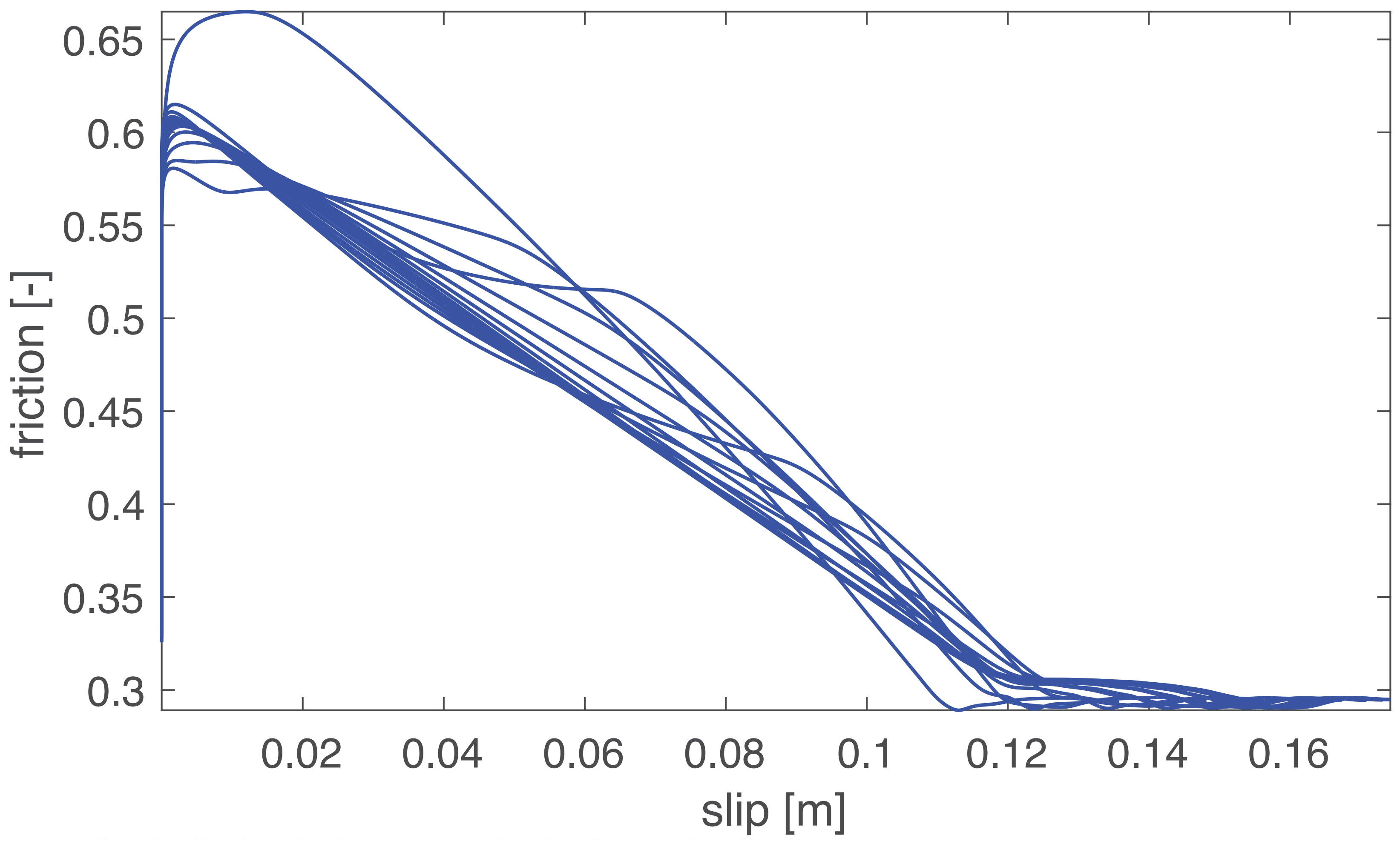

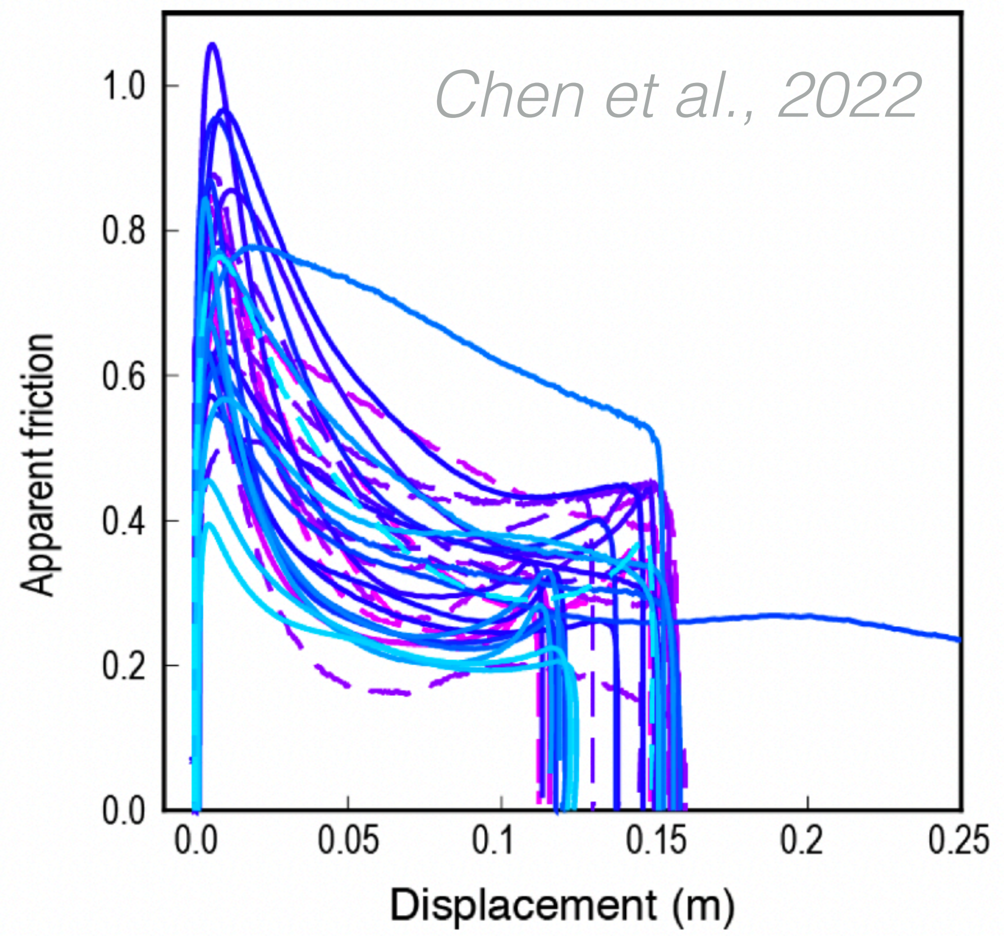

Earthquake rupture in 2D Groningen setting on velocity-strengthening faults

- “Nucleation” at top of reservoir
- Rate-and-state friction theory and laboratory results can explain induced seismicity in Groningen (no need to involve more)
- — Stress theshold impact — what state use in Hemissinon?
- Does not impact estimated propagation or arrest of first earthquakes → shown results hold

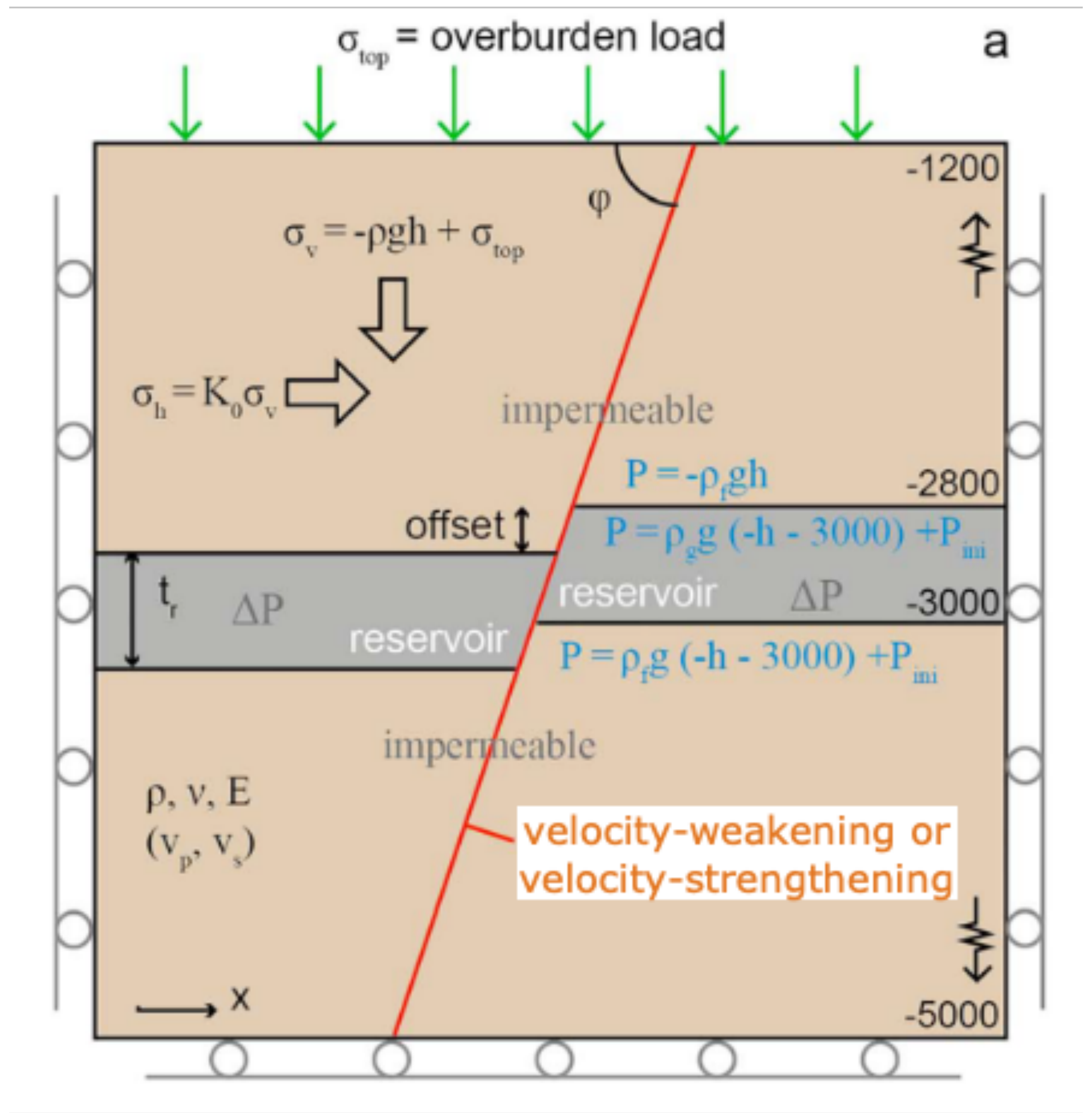

Adapted from Buijze et al., JGR, 2019

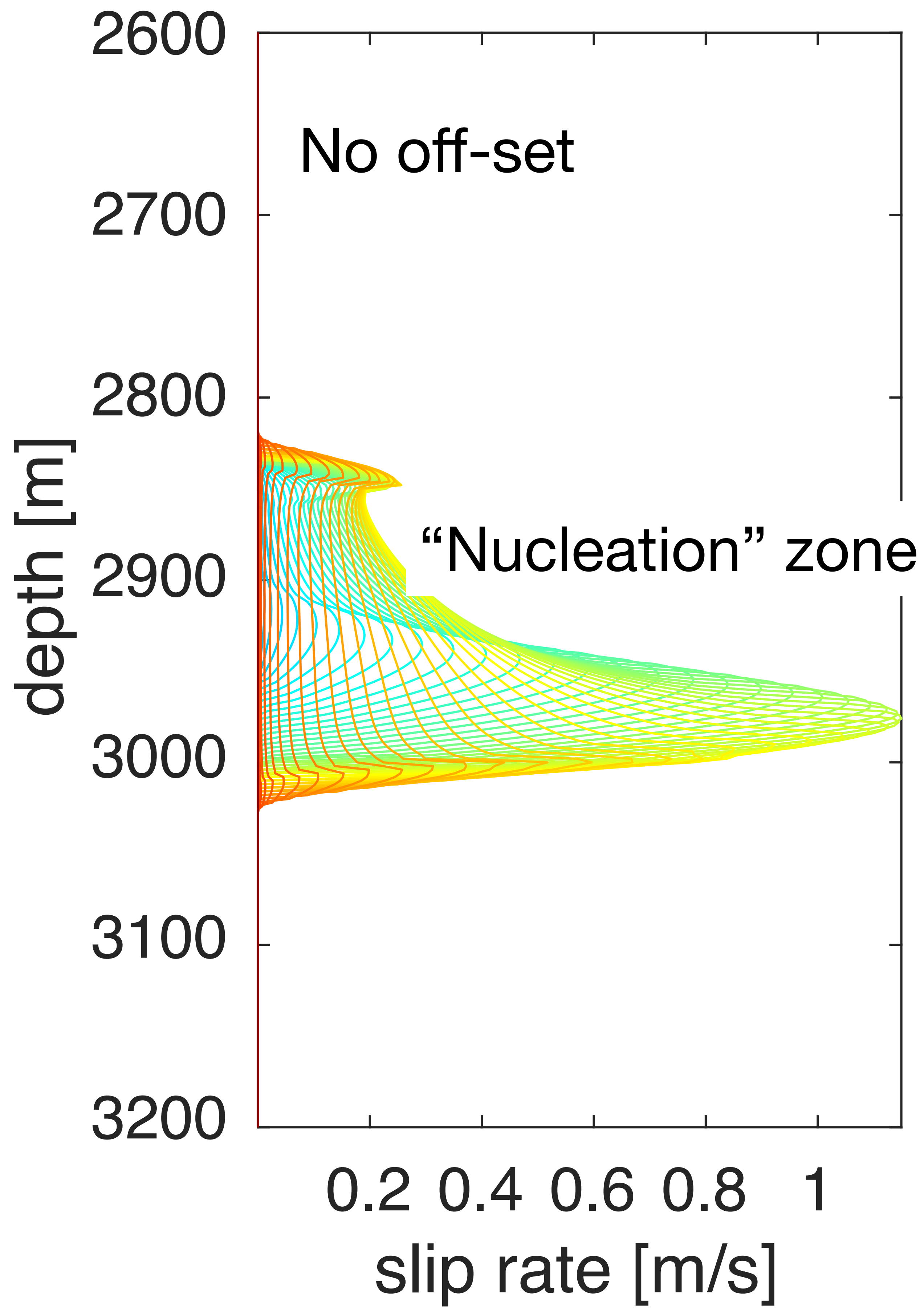

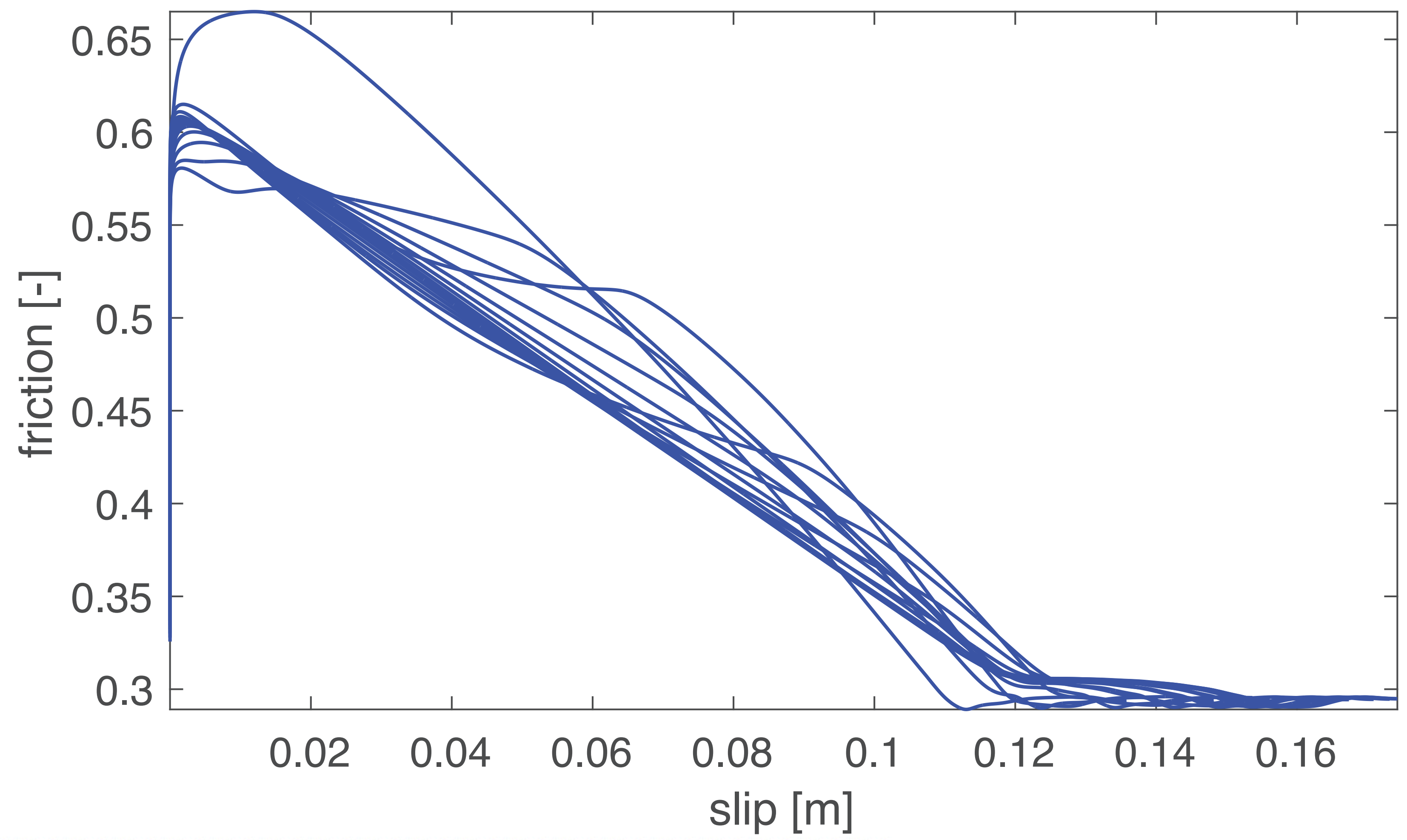

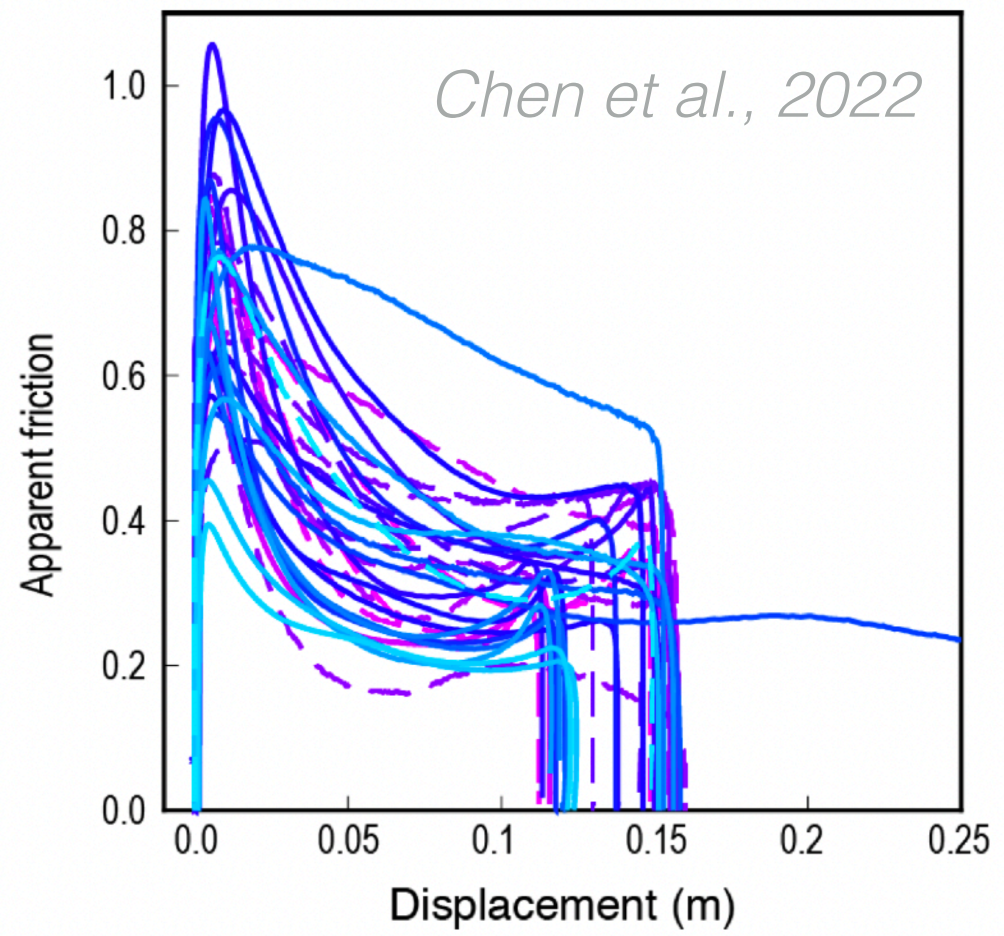

Can second-generation earthquake propagate further into under-burden?

- However, may impact estimated parameters or consequences of what happens next (i.e., Mmax)
  - Answer depends on rate-and-state friction parameters

If indeed velocity-strengthening
→ no next earthquake → barrier

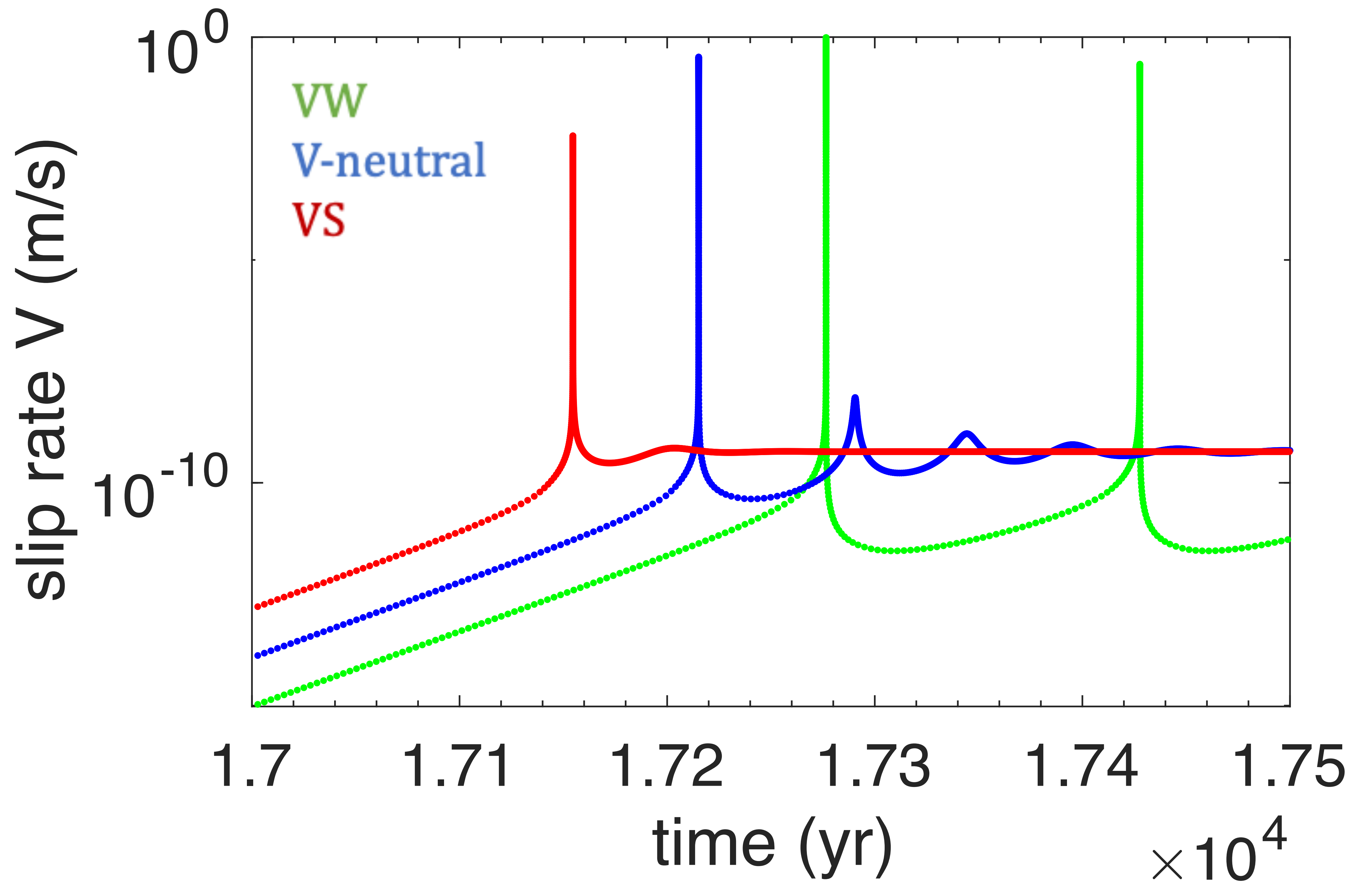

If mix gives velocity-weakening
→ next takes longer and not much further

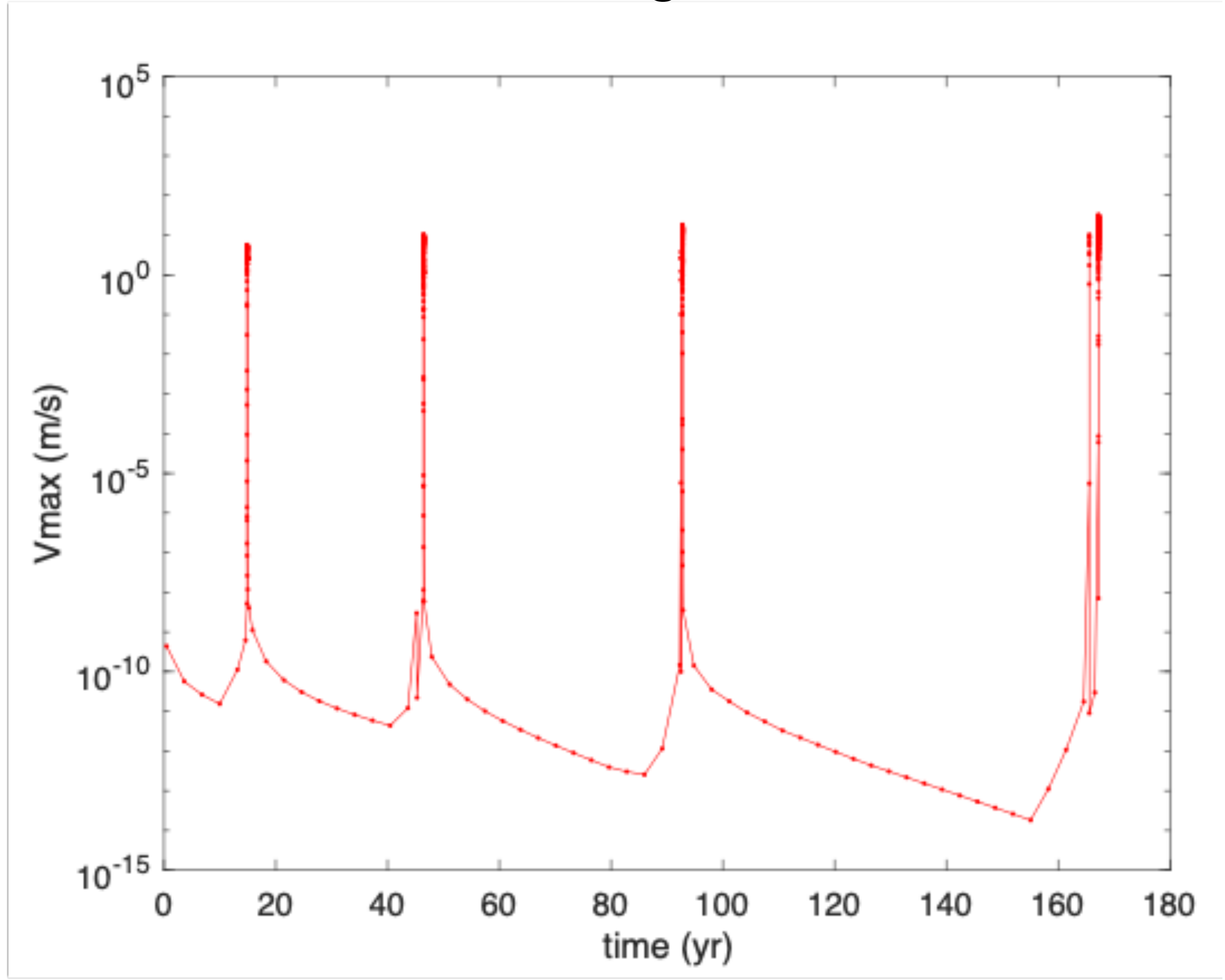

- Neither suggests (strong) reasons to worry

My preliminary proponent assessment

- Excellent, state-of-the-art LEFM work → use!
- Smaller Mw due to single fault roughness and reflections
- Larger Mw due to potential jumps across fault network
- → in end?

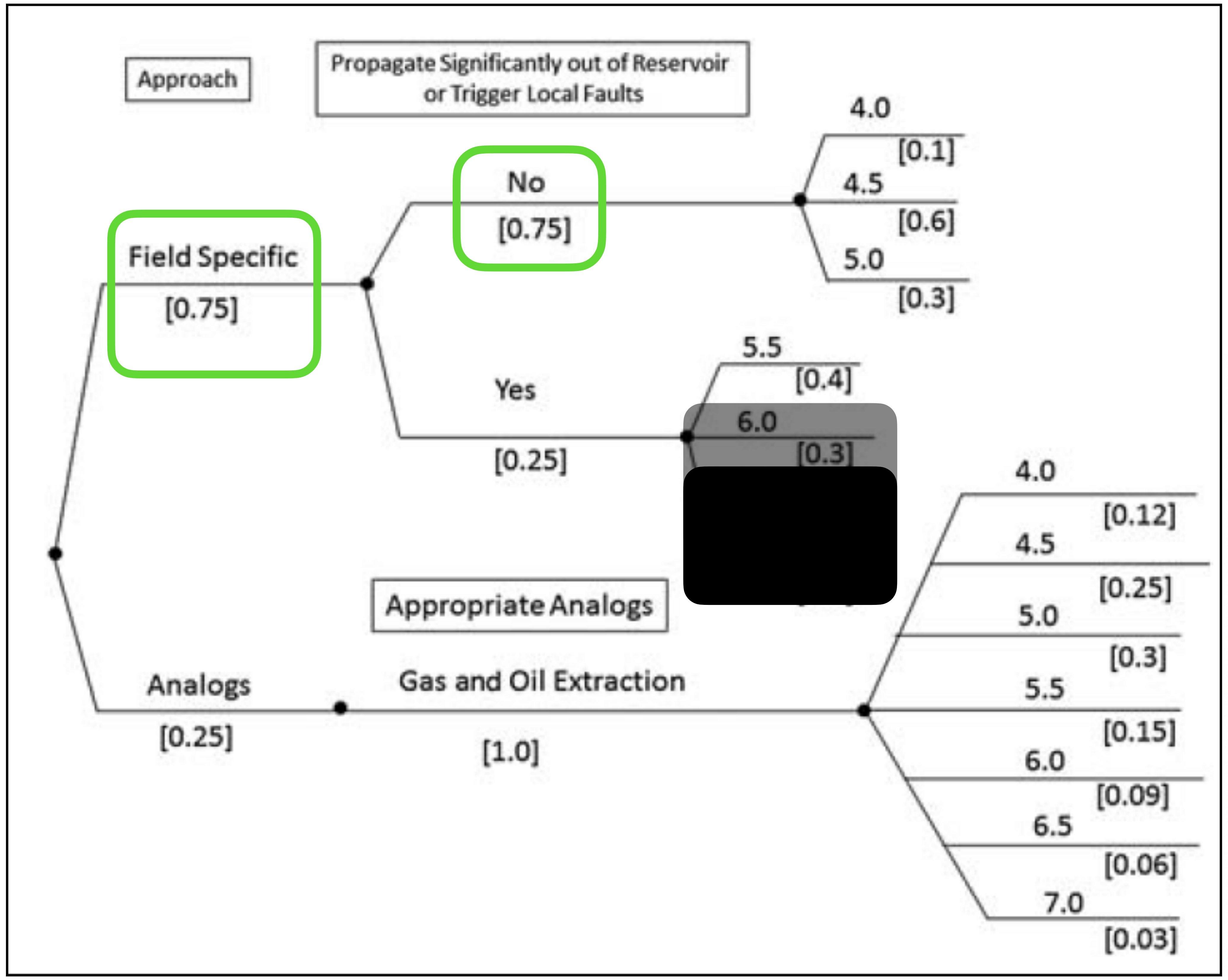

Bommer & van Elk (comment in BSSA, 2017)

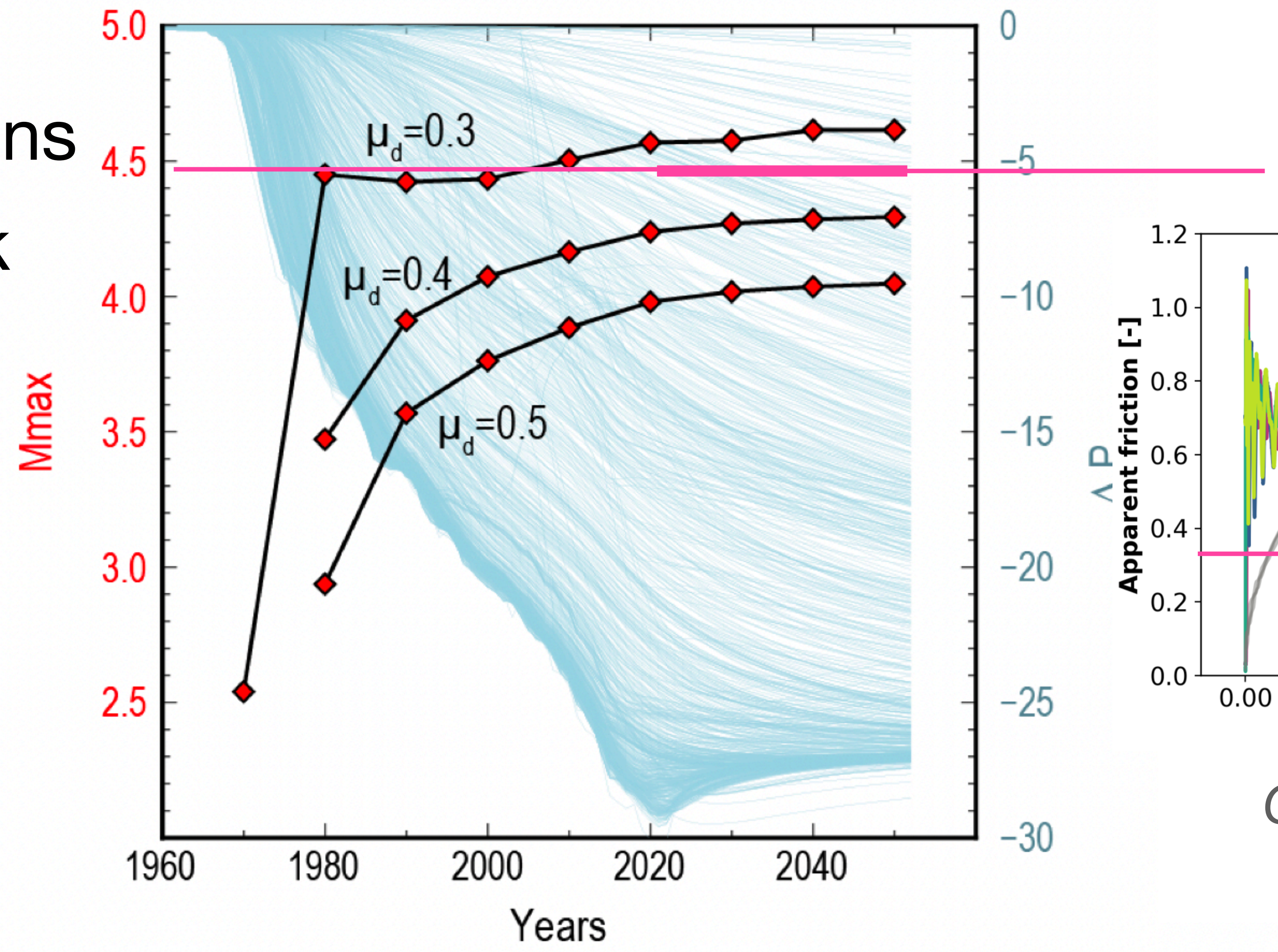

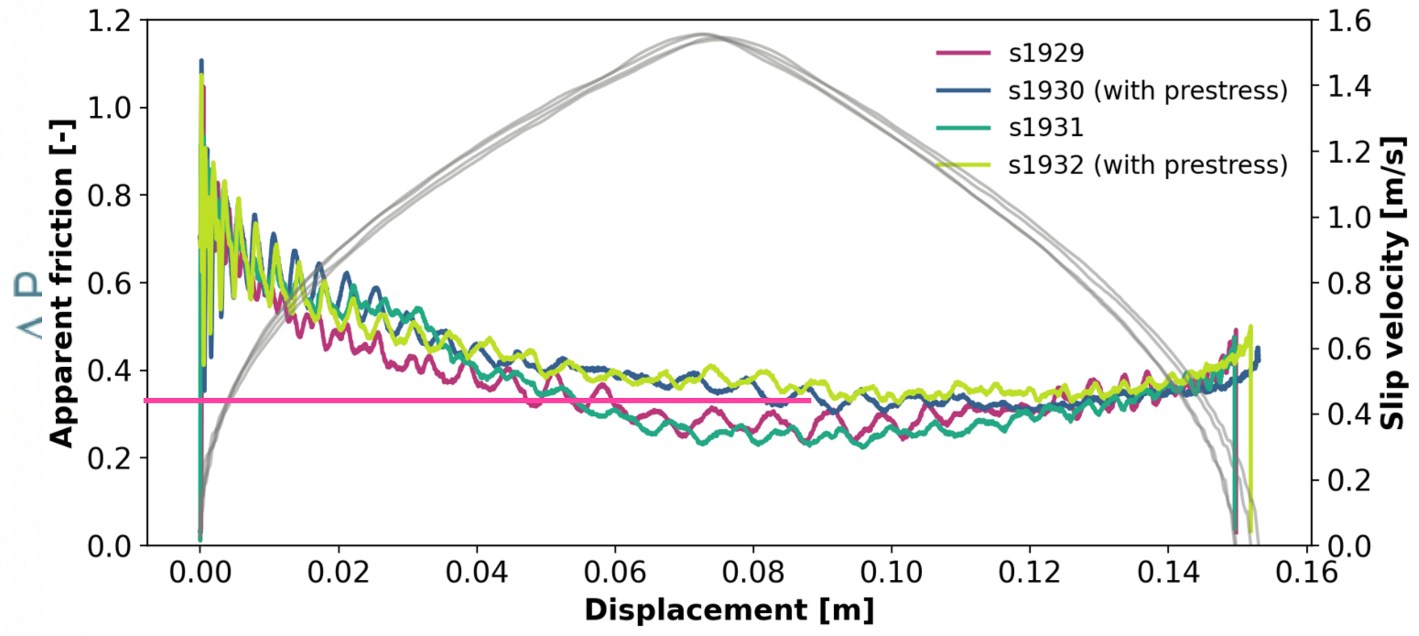

Chien-Cheng et al., results April 2022

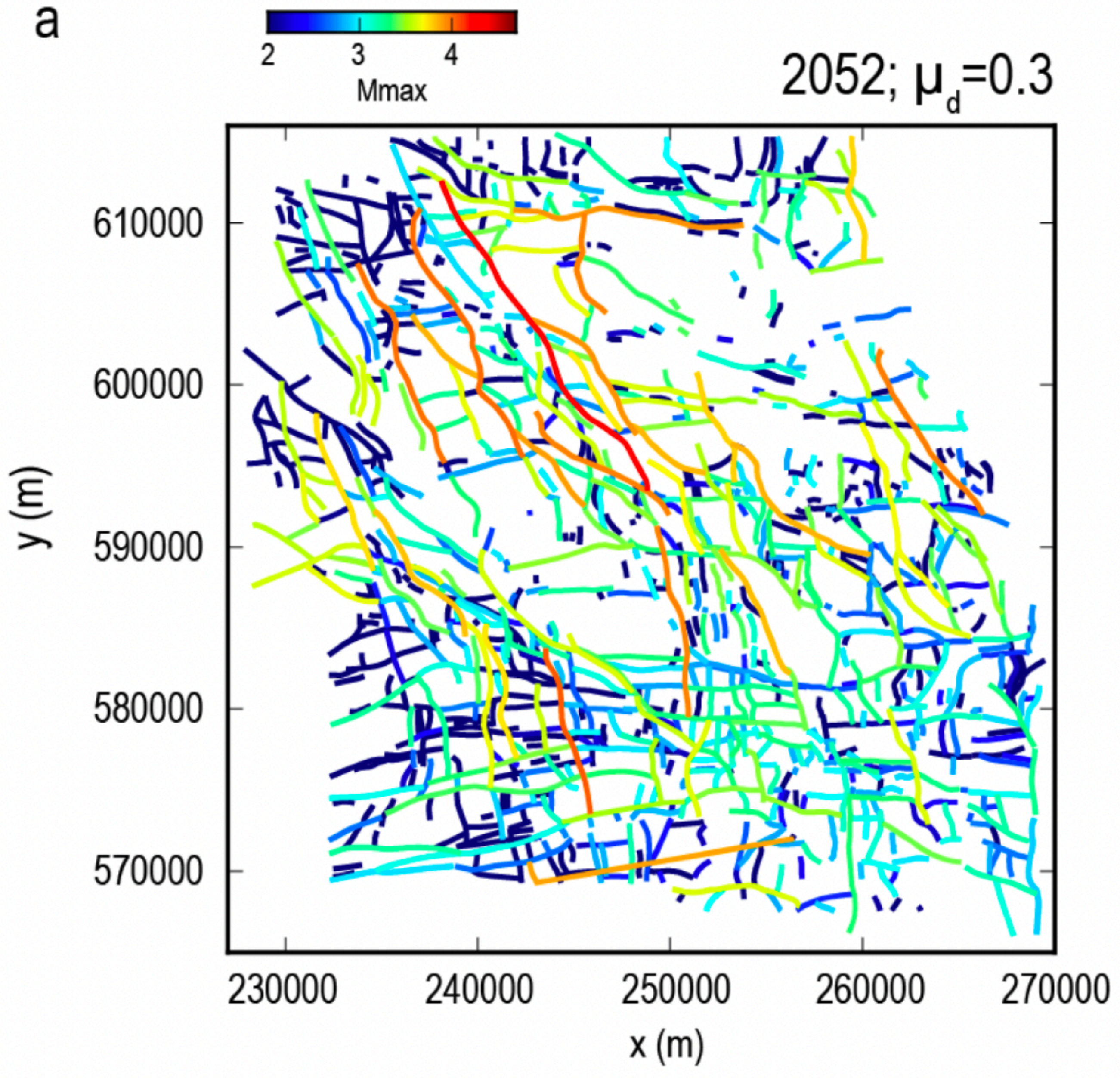

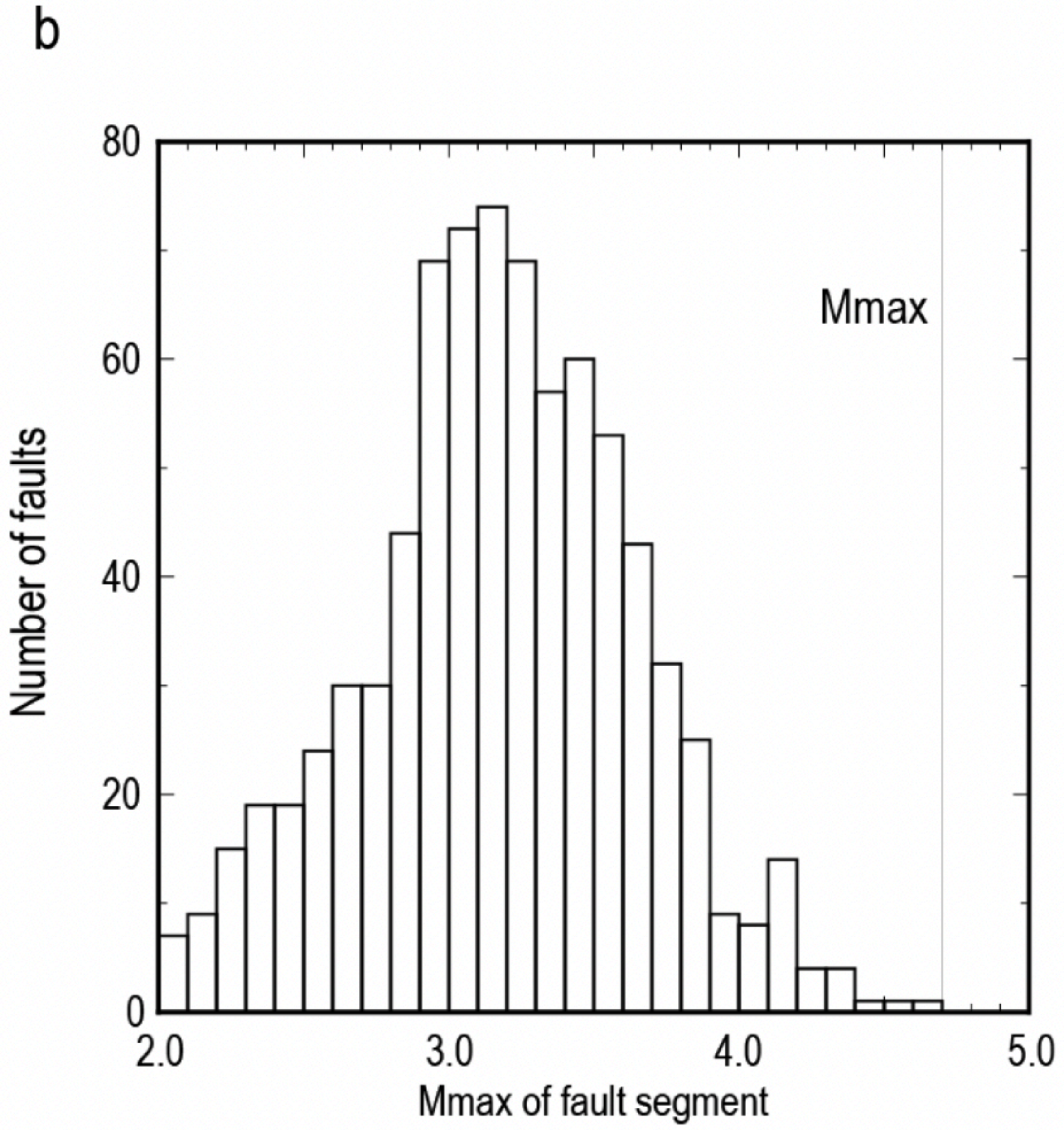

Conclusions

- Proponent assessment (Mmax ± 4.5):
  - Physics-based proposal LEFM is excellent
    - State-of-the-art of international earthquake physics with 1st order processes included

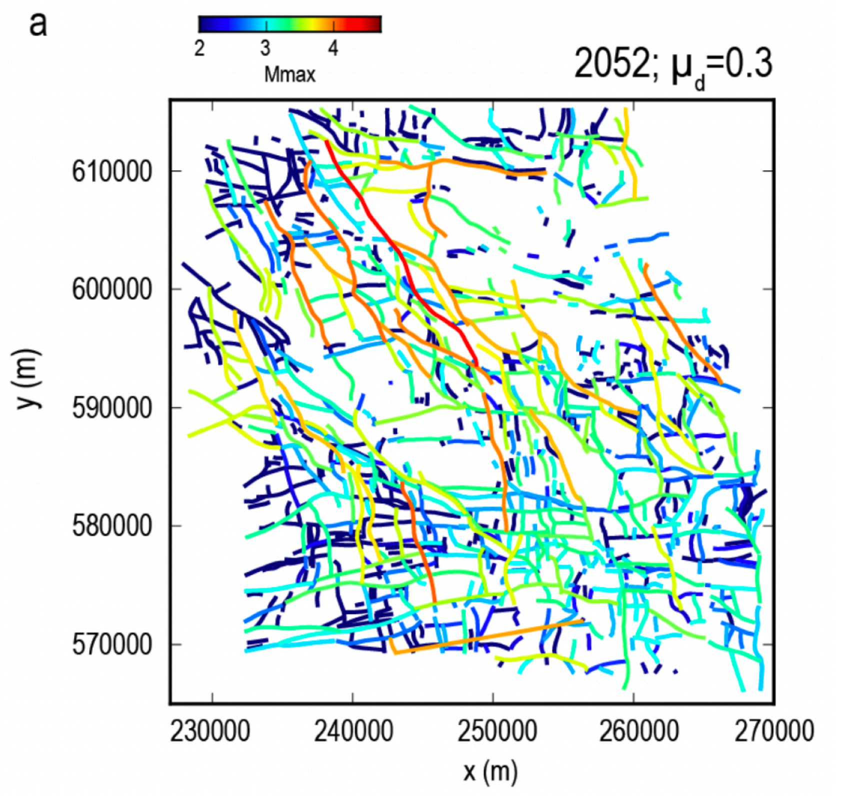

- We take this to the next level to include potential 1st and 2nd order processes, which may be critical for Mmax in Groningen
- To do so combine and advance various state-of-the-art approaches
  - Faults → stresses & strength → dynamic rupture → LEFM → P(Mmax)

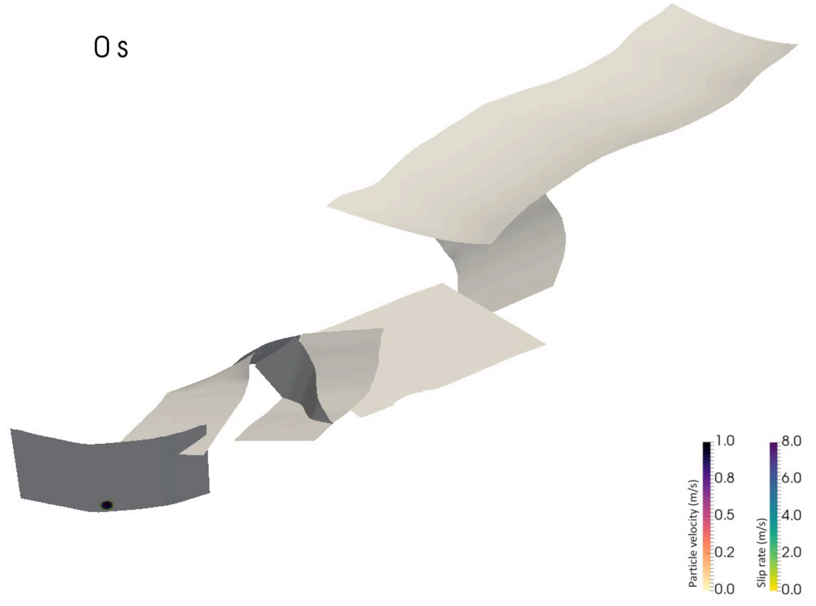

- Also useful for future physics-based PSHA in natural and other induced seismicity settings

- Inspiration from workshop → contact us with outstanding problems, data …